C52.23:
969/v.1

A UNITED STATES
DEPARTMENT OF
COMMERCE
PUBLICATION

U.S. DEPARTMENT OF COMMERCE
Environmental Science Services Administration

COLLECTED REPRINTS—1969

Volume I

ATLANTIC OCEANOGRAPHIC
AND METEOROLOGICAL LABORATORIES
PACIFIC OCEANOGRAPHIC LABORATORIES

U. S. DEPARTMENT OF COMMERCE
Maurice H. Stans, Secretary

ENVIRONMENTAL SCIENCE SERVICES ADMINISTRATION
Robert M. White, Administrator
RESEARCH LABORATORIES
Wilmot N. Hess, Director

Collected Reprints—1969
Volume I

ATLANTIC OCEANOGRAPHIC AND METEOROLOGICAL LABORATORIES
PACIFIC OCEANOGRAPHIC LABORATORIES

ISSUED SEPTEMBER 1970

Atlantic Oceanographic and Meteorological Laboratories
Miami, Florida 33130

Pacific Oceanographic Laboratories
Seattle, Washington 98105

For sale by the Superintendent of Documents, U. S. Government Printing Office, Washington, D. C. 20402
Price $4.25

U. S. Depository Copy

FOREWORD

Knowledge of the ocean and its processes develops slowly. It is the result of the work of many researchers in this country and throughout the world. To be useful, however, each new increment of knowledge must be disseminated so that the other workers will know of it and be able to build upon it.

Because the published results of the scientific and technical work of ESSA's Atlantic Oceanographic and Meteorological Laboratories and Pacific Oceanographic Laboratories are scattered through the literature, they are being brought together in a series of annual publications. These publications provide to researcher and to interested layman alike a convenient summary of the results of the work of these two Research laboratories of the Environmental Science Services Administration of the U. S. Department of Commerce.

This volume, the fourth in the series, holds the published papers for the year 1969.

Harris B. Stewart, Jr.
Director
Atlantic Oceanographic and
Meteorological Laboratories

TABLE OF CONTENTS

Volume I

GENERAL

1. Dietz, Robert S., and Robert F. Dill, 1969, Down into the sea in ships: Sea Frontiers, 15, No. 1, 2-9.

2. Maul, George A., Precise echo sounding in deep water: ESSA Tech. Rep. C&GS 37, Jan.

3. Stewart, Harris B., Coastal zone management conference statement: in Hearings, Committee on Merchant Marine and Fisheries, H. R. 91 Congress, 1st Session Ser. No. 91-14, 107-111.

4. Stewart, Harris B., Biscayne Bay as a natural resource: in Hearings, Committee on Merchant Marine and Fisheries, H. R. 91 Congress, 1st Session Ser. No. 91-14, 193-197.

5. Stewart, Harris B., Oceanography and the U. S. Merchant Marine: U.S. Naval Inst. Proc. 95, No. 10/800, 68-77. 1969, U. S. Naval Inst.

MARINE GEOLOGY AND GEOPHYSICS

6. Bassinger, B. G., O. E. DeWald, and G. Peter, Interpretation of the magnetic anomalies off Central California: J. Geophys. Res. 74, No. 6, 1484-1487.

7. Brier, Chester, Robert Bennin, and Peter A. Rona, Preliminary evaluation of a core scintillation counter for bulk density measurement in marine sediment cores: J. Sedimentary Petrology 39, No. 4, 1509-1519.

8. Bush, Sam A., and Patricia A. Bush, Isostatic gravity map of the eastern Caribbean region: Transactions - Gulf Coast Association of Geological Societies, XIX, 281-285.

9. Bush, Sam A., and Patricia A. Bush, Trincomalee and associated canyons, Ceylon: Deep-Sea Res. 16, 655-660.

10. Dietz, Robert S., Ocean basins and lunar seas: Oceans 2, 1, 7-15.

11. Dietz, Robert S., Ocean floor in the decade ahead (5th Ann. Meeting Marine Technol. Soc., Miami, Fla., June): Marine Technol. Soc J. 3, No. 5, 68-69.

12. Dietz, Robert S., Primitive earth: A marine geologist's appraisal: The Primitive Earth Symp., Miami Univ., Oxford, Ohio, special publ. D1-D11.

13. Dietz, Robert S., Book review of "History of the Earth's Crust" ed. R. Phinney, Princeton Univ. Press: J. Marine Technol. Soc., 3, No. 5, 30.

14. Dietz, Robert S., Robert Fudali, and William Cassidy, Richat and Semsiyat domes (Mauritania): Not astroblemes: Geol. Soc. Am. Bull., 80, No. 7, 1367-1372.

15. Dietz, Robert S., and Knebel, Harley J. First deep sea sounding: Sea Frontiers 15, No. 4, 212-218.

16. Erickson, Barrett H., and Paul J. Grim, Profiles of magnetic anomalies south of the Aleutian Island Arc: Geol. Soc. Am. Bull., 80, No. 7, 1387-1390.

17. Grim, Paul J., Heat flow measurements in the Tasman Sea: J. Geophys. Res. 74, No. 15, 3933-3934.

18. Grim, Paul J., SEAMAP deep-sea channel: ESSA Tech. Rept. ERL 93-POL 2, Jan.

19. Grim, Paul J., and Barrett H. Erickson, Fracture zones and magnetic anomalies south of the Aleutian trench: J. Geophys. Res. 74, No. 6, 1488-1494.

20. Grim, Paul J., and Frederick P. Naugler, Fossil deep-sea channel on the Aleutian abyssal plain: Science 163, No. 3865, 383-385.

21. Harbison, Reginald N., Possible morainal deposits in the Gulf of Maine: Maritime Sediments, 5, No. 1, 19-21.

22. Keller, George H., Book Review of "Marine Geotechnique": Marine Geol., 7, No. 2, 176-181.

23. Keller, G. H., Radioisotopes and Oceanography: Isotopes and Radiation Tech. 6, No. 4, 376-381.

24. Malloy, R. J., and G. F. Merrill, Vertical crustal movement associated with the Prince William Sound, Alaska, earthquake: The Prince William Sound, Alaska, Earthquake of 1964 and Aftershocks II, Part C, U. S. Government Printing Office, 329-338.

25. Malahoff Alexander, and Barrett H. Erickson, Gravity anomalies over the Aleutian Trench: E⊕S, Trans, Am. Geophys. Union 50, No. 10, 552-555.

26. Mathewson, Christopher C., Bathymetry of the north insular shelf of Molokai Island, Hawaii, from surveys by the USC&GSS McArthur, Data Report No.14, HIG-69-21, Sept.1969.

27. Peter, George, and O. E. DeWald, Geophysical Reconnaissance in the Fulf of Tadjura: Deep Sea Research, Geol. Soc. Am. Bull., 80, 2313-2316.

28. Peter, G., and R. Lattimore, Magnetic structure of the Juan de Fuca-Gorda Ridge area: J. Geophys. Res. 74, No. 10, 586-593.

29. Rona, Peter A., Linear "lower continental rise hills" off Cape Hatteras: J. Sedimentary Petrology 39, No. 3, 1132-1141.

30. Rona, Peter A., 1969, Comparison of continental margins of eastern North America at Cape Hatteras and northwestern Africa at Cape Blanc: Am. Assoc. Petroleum Geologists Bull. 54, No. 1, 129-157.

31. Rona, Peter A., Middle Atlantic continental slope of United States: Deposition and erosion: Am. Assoc. Petroleum Geologists Bull. 53, No. 7, 1453-1465.

32. Rona, Peter A., Possible salt domes in the deep Atlantic off Northwest Africa: Nature, 224, No. 5215, 141-143.

33. Sproll, Walters, and Dietz, Robert S., Morphological continental drift fit of Australia and Antarctica: Nature, 222, No. 5191, 345-348.

METEOROLOGY

34. Anthes, Richard A., Numerical experiments on ring convection and effect of variable resolution of cellular convection: ESSA Tech Memo ERLTM-NHRL No. 86, June.

35. Carlson, Toby N., Hurricane genesis from disturbances formed over Africa: Mariner's Weather Log, 13, No. 5, 197-202.

36. Carlson, Toby N., Some remarks on African disturbances and their progress over the tropical Atlantic: Monthly Weather Rev. 97, No. 10, 716-726.

37. Carlson, Toby., Synoptic histories of three African disturbances that developed into Atlantic hurricanes: Monthly Weather Rev. 97, No. 3, 256-276.

38. Chase, P., A note on drawing probability sectors: Monthly Weather Rev. 97, No. 8, 602-603.

39. Gentry, R. Cecil, Project STORMFURY: WMO Bull., XVIII, No. 3, 146-154.

40. Gentry, R. Cecil, Project STORMFURY: Bull. Am. Meteorol. Soc. 50, No. 6, 404-409.

41. Koss, Walter J., Note on the accumulated error in the numerical integration of a simple forecast model: Monthly Weather Rev. 97, No. 12, 896-901.

42. Miller, Banner I., Hurricane: in McGraw-Hill Yearbook of Science and Technology, McGraw-Hill, New York, 193-196.

43. Miller, Banner I., Experiment in forecasting hurricane development with real data: ESSA Tech. Memo. ERLTM-NHRL 85, Apr.

44. Rosenthal, Stanley L., Experiments with a numerical model of tropical cyclone development. Some Effects of radial resolution: ESSA Tech. Memo. ERLTM-NHRL 87. Aug.

45. Rosenthal, Stanley L., Numerical experiments with a multilevel primitive equation model designed to simulate the development of tropical cyclones. Experiment 1: ESSA Tech. Memo. ERLTM-NHRL 82, Jan.

46. Staff, Office of the Director, National Hurricane Research Laboratory, "Project STORMFURY" Annual Report, 1968.

47. Sheets, Robert C., Some mean hurricane soundings: J. Appl. Meteorol. 8, No. 1, 134-146.

48. Sugg, Arnold L., and Robert L. Carrodus, Memorable hurricanes of the United States since 1873: ESSA Tech. Memo. WBTM-SR-42, Jan.

49. Hebert, Paul J., and Banner I. Miller, Hemispheric circulation and anomaly patterns observed when tropical storms reach hurricane intensity: ESSA Tech. Memo. WBTM-SR-46, May.

TABLE OF CONTENTS

Volume II

EXPERIMENTAL METEOROLOGY

50. Brier, G. W., and Joanne Simpson, Tropical cloudiness and rainfall related to pressure and tidal variations: Quart. J. Roy. Meteorol. Soc. 95, No. 403, 120-147.

51. Holle, Ronald L., The efect of rainfall on cloud condensation nuclei from vegetation fires over South Florida during spring droughts: ESSA Tech. Memo. ERLTM-AOML 4, Oct.

52. Johnson, H. M., and Ronald L. Holle, Observations and comments on two simultaneous cloud holes over Miami: Bull. Am. Meteorol. Soc. 50, No. 3, 157-161.

53. Lettau, Bernard, The transport of moisture into the Antarctic interior: Tellus XXI, No. 3, 331-340.

54. Lettau, Bernard, Wind structure in the equatorial maritime friction layer: Ann. der Meteorol. NF No. 4, 30-34.

55. Oort, Abraham H., and Albion Taylor, On the kinetic energy spectrum near the ground: Monthly Weather Rev. 97, No. 9, 623-636.

56. Sax, Robert I., The importance of natural glaciation on the modification of tropical maritime cumuli by silver iodide seeding: J. Appl. Meteorol. 8, No. 1, 92-104.

57. Simpson, Joanne, Cloud building and breaking: Medical Opinion & Review 5, No. 10, 39-58.

58. Simpson, Joanne, On some aspects of sea-air interaction in middle latitudes: in Deep Sea Res. 16, 233-261.

59. Simpson, Joanne, and Victor Wiggert, Models of precipitating cumulus towers: Monthly Weather Rev. 97, No. 7, 471-489.

60. Simpson, Joanne, and William L. Woodley, Intensive study of three seeded clouds on May 16, 1968: ESSA Tech. Memo. ERLTM-APCL 8, May.

61. Simpson, Joanne, William L. Woodley, Howard A. Friedman, Thomas W. Slusher, R. S. Scheffee, and Roger L. Steele, An airborne pyrotechnic cloud seeding system and its use: ESSA Tech. Memo. ERLTM-APCL 5, Feb.

62. Woodley, William L., Precipitation results from a pyrotechnic cumulus seeding experiment: ESSA Tech. Memo. AOML 2, Aug.

63. Woodley, William L., and Alan Herndon, A rain gage evaluation of the Miami reflectivity-rainfall rate relation region: ESSA Tech. Memo. ERLTM-AOML 3, Sept.

64. Woodley, William L., A. Herndon, and R. Schwartz, Large-scale precipitation effects of single cloud pryotechnic seeding: ESSA Tech. Memo. ERLTM-AOML 5, Nov.

65. Woodley, William L., and Jose Partagas, Radar and photographic documentation of convective developments on May 16, 1968: ESSA Tech. Memo. ERLTM-APCL 7, April.

66. Cantilo, Luis M. H., and William L. Woodley, Cloud photogrammetry from air-borne time-lapse photography. Preprint No. 105-52, 105th Techn. Conf. Soc. of Motion Picture and Television Eng., April 20-25, Miami Beach, Florida.

* Simpson, Joanne, Modification experiments on tropical cumulus clouds, Paper presented at Cloud Weather Modification and Cloud Physics Conf., Tbilisi, Georgia, USSR, May.

* Woodley, William L., The effect of air-borne silver iodide pyrotechnic seeding on the dynamics and precipitation of supercooled tropical cumulus clouds: A dissertation submitted to the Graduate School of Florida State Univ. in partial fulfillment of the requirements for the Degree of Doctor of Philosophy.

---

* Reprints not available.

PHYSICAL OCEANOGRAPHY

67. Byrne, Robert J., Field occurrences of induced multiple gravity waves: J. Geophys. Res. 74, No. 10, 2590-2596.

68. Cartwright, David, Walter Munk, and Bernard Zetler, Pelagic tidal measurements: EOS Trans., American Geophys. Union, 50, No. 7, 472-477.

69. Hansen, Richard T., Charles J. Garcia, Shirley F. Hansen, and Harold G. Loomis, Brightness variations of the white light corona during the years 1964-67: Solar Phys. 7, 417-433.

70. Hansen, Richard T., Shirley F. Hansen, and Harold G. Loomis, Differential rotation of the solar electron corona: Solar Phys. 10, 135-149.

71. Laird, Norman P., Anomalous temperature of bottom water in the Panama Basin: J. Marine Res. 27, No. 3, 355-357.

72. Laird, N. P. and T. V. Ryan, Bottom current measurements in the Tasman Sea: J. Geophys. Res. 74, No. 23, 5433-5438.

73. Larsen, J. C., Long waves along a single step topography in a semi-infinite uniformly rotating ocean: J. Marine Research 27, No. 1, 1-6.

74. McAlister, E. D., and William McLeish, Heat transfer in the top millimeter of the ocean: J. Geophys. Res. 74, No. 13, 3408-3414.

75. Nelson, Raymond M., The potential application of remote sensing to selected ocean circulation problems: in Oceans from Space, Gulf Publishing Co., Houston, Texas 38-45.

76. Ostapoff, Feodor, A fourth brine hole in the Red Sea?: in Hot Brines and Recent Heavy Metal Deposits in the Red Sea, Ed. Egon T. Degens and David A. Ross, Springer-Verlag, New York, 18-21.

77. Reed, R. K., Deep water properties and flow in the Central North Pacific: J. Marine Res. 27, No. 1, 24-31.

78. Shaw R. P., and Courtine D. F., Diffraction of a plane acoustic pulse by a free orthogonal trihedron (3-D Corner): J. Acoustic Soc. Am. 46, No. 5, 1382-1384.

79. Shaw, R. P., and Bugl P., Transmission of plane waves through layered linear viscoelastic media: J. Acoustic Soc. Am. 46, No. 3, 649-654.

80. Sokolowski, T. J., and M. H. Manghnani, Adiabatic elastic moduli of vitreous calcium aluminates to 3.5 Kilobars: J. Am. Ceramic Soc. 52, No. 10, 539-542 (also HIG 287).

81. Smith John A., Bernard D. Zetler, and Saul Broida, Tidal modulation of the Florida current surface flow: Marine Technol. Soc. J. 3, No. 3, 41-46.

82. Wunsch, C., D. V. Hansen, and B. D. Zetler, Fluctuations of the Florida current inferred from sea level records: Deep Sea Res. 16, Suppl. 447-470.

83. Zetler, B. D. Tides, 1-74 to 1-81, Tide Forecasting, 11-109 to 11-113, and 11-119: in Handbook of Ocean and Underwater Engineering, © North American Rockwell, Inc., McGraw-Hill Inc. New York.

84. Zetler, Bernard D., Computer applications to tide and current analysis in the Coast and Geodetic Survey: Proc. Symp. on Tides organized by the Intern. Hydrographic Bureau, Monaco, 28-29 April 1967, 75-77.

85. Zetler, Bernard D., Shallow water tide predictions: Proc. Symp. on Tides organized by the Intern. Hydrographic Bureau, Monaco, 28-29 April 1967, 163-166.

86. Zetler, Bernard D., Tide-talk: monthly column, GO Boating Miami, January through October.

Reprinted from Sea Frontiers Vol. 15, No. 1, 2-9.

Down into the Sea in Ships

By ROBERT S. DIETZ
Atlantic Oceanographic Laboratories
Environmental Science Services Administration
and
ROBERT F. DILL
Marine Environment Division
Naval Undersea Warfare Center, San Diego

RECALLING THE EXTENSIVE debugging and tedious preparation when diving with Jacques Piccard and his bathyscaph *Trieste* off Italy more than a decade ago, many have been skeptical that the new generation of Deep Research Vehicles (DRV's) are really ready to do useful routine work in probing the ocean floor. So was Robert Dietz when invited by the Naval Undersea Warfare Center of San Diego to be a co-observer with Robert F. Dill for two dives in the Gulf of California with Westinghouse's *Deepstar 4000*. This caution proved unnecessary, as the whole operation clicked off with clock-like precision—two five-hour dives in two days without a hitch.

Early on the morning of January 22, 1968, Dill and Dietz slithered into the egg-shaped, yellow submarine. The pressure hull is so jammed with equipment that it was like crawling into the works of some giant Swiss watch.

An articulated crane, actually a modified back-hoe, deftly lifted the sub off the deck and, with the care given an egg, carefully set it down on the sea's mirror surface. As *Deepstar* is retained by a nylon tagline, a skin diver inspected her, tripped the release, and within a minute or two the dive commenced. Once below the surface, the dancing rays of sunlight flickered out, daylight quickly faded to deep green twilight and then to absolute blackness. All buffeting by the waves ceased as the serene realm of inner space was entered. For those poor sailors who get a queazy feeling when someone waves good-bye from dockside, DRV diving is the way to go—stability prevails, no roll, no pitch, and no yaw.

Deepstar has an unusual mode of descent. It is usually done "dead stick" rather than under power. Purposely weighted eccentrically, it spirals down backwards, making two turns per minute and sinking 1,000 feet each fifteen minutes. This allows excellent viewing. The mid-water creatures slowly swing

RISING FROM THE DEPTHS *with the crew of three still aboard,* Deepstar 4000 *is snatched aboard the mother ship by an articulated crane, which looms like a giant preying mantis. (Ron Church)*

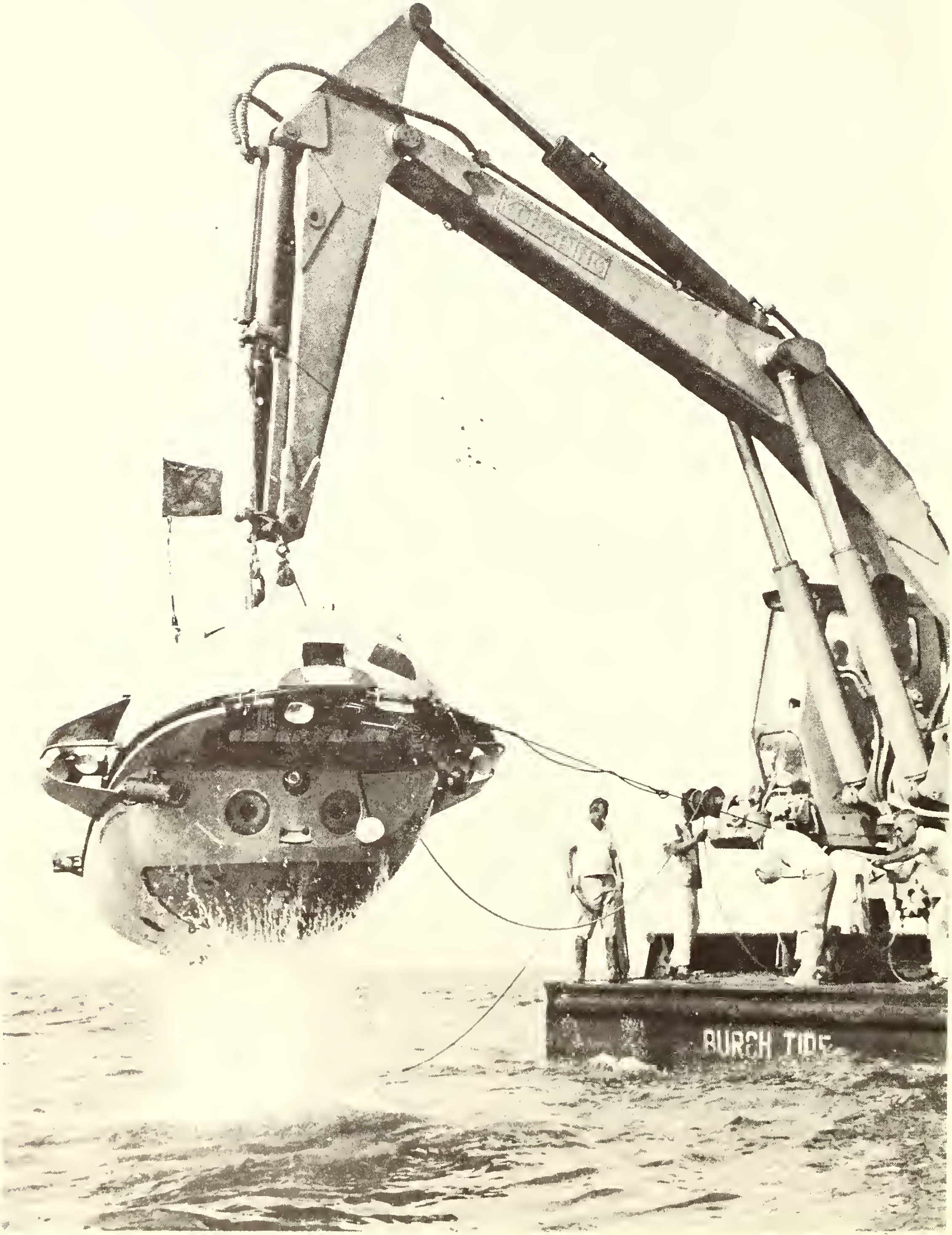
BURCH TIDE

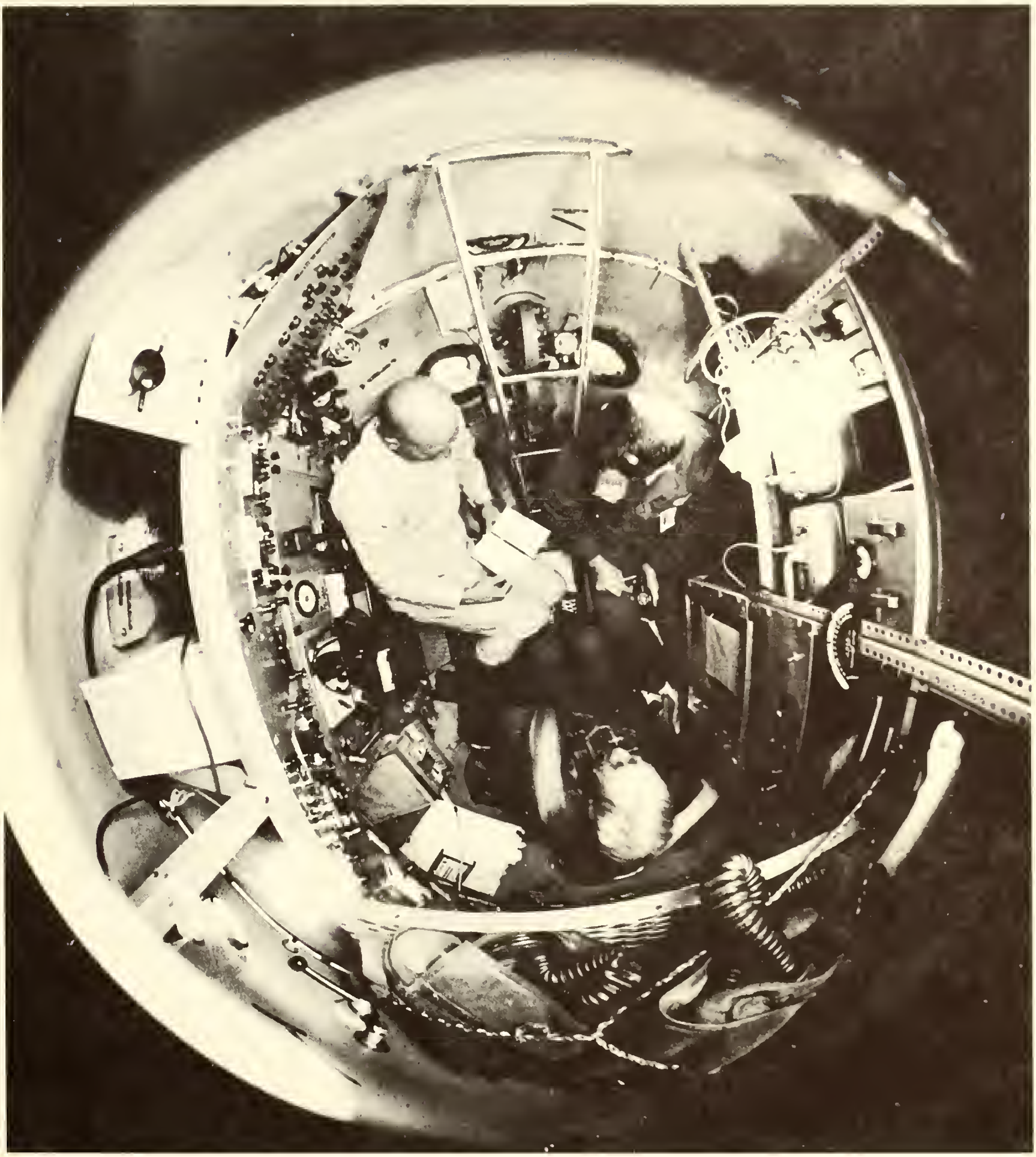

by, seeming to spiral helically upward. But, more importantly, it conserves power and permits a touchdown directly beneath the launch point. This is especially useful when trying to land at a site that has been previously selected after a brief echo-sounder survey. Once the *Deepstar* is 100 feet off the bottom, as revealed by its own echo sounder or by the bottom suddenly looming into view, a 200-pound weight is dropped so that the DRV

Fish-eye view *of the compact interior of Westinghouse's* Deepstar 4000. *(Ron Church)*

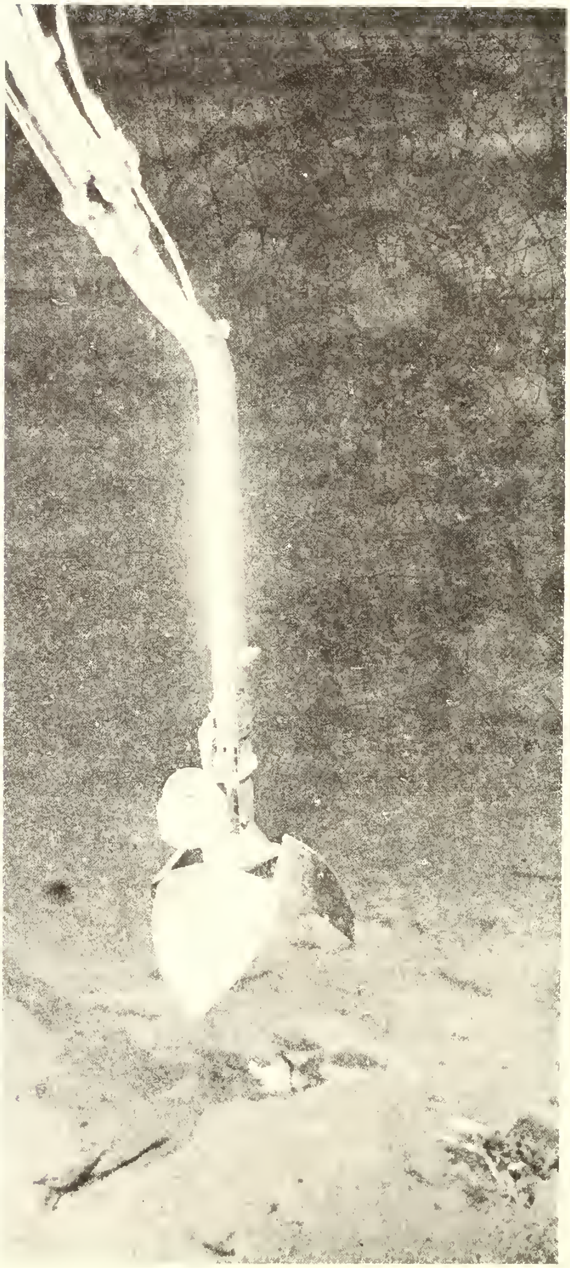

Prehensile arm *of* Deepstar 4000 *reaches down to grasp a gastropod while a shrimp remains close by. Such samples of biota and rocks are stored in a small "vest pocket" outboard of the capsule until the submarine returns to the surface. (Robert F. Dill)*

levels off, as it is then neutrally buoyant. A slow descent for the remaining distance to the bottom is done under power. In the cruising mode, one may then fly a few feet off the bottom, touching down now and then to carefully observe some benthic animal or break off a rock sample with the hydraulic claw.

Should any water leak in, a possible emergency measure might have been to drink it. But our best assurance was in our pilot, Ron Church, for here was a man who could "keep his cool." (He is one of the few skin divers who have actually photographed a shark attack. While tending a wave-recording meter off Wake in 1958, a white-tipped shark twice attacked his colleague, Jim Stewart, the diving officer of the Scripps Institution of Oceanography, who almost lost his arm.)

The target on these two dives was the axis of submarine canyons, deep gashes that cleave the continental slopes of the world. Two were investigated, Los Friales and Palmas in the Gulf of California. Once on bottom, *Deepstar* attempted to wend its way up the axis toward the shore-end head. This proved to be an ambitious task, only partially achieved, as these canyons are rugged and tortured domains.

LEFT: LUSH GROWTH *of siliceous sponge, ophiuroids, anemones, and hybroids cover the thinly bedded Pliocene wall rock in Las Palmas Canyon, Baja California.*

RIGHT: 90° CONTACT *between the fill and wall rock is typical of areas swept by periodic strong currents. The heavy cover of organisms indicates abundant food is provided by canyons channeling organic material from the euphotic zone into the deep sea.*

FAR RIGHT: STEEPLY DIPPING BEDS *of thin shale mark a large fault that cuts across the canyon. (Robert F. Dill)*

Although their ultimate origin remains obscure, these canyons are today being actively eroded by processes acting beneath the sea. They can hardly be drowned and dead river canyons, for they appeared as freshly cut as any river canyon on the nearby land. Tumbled debris and fresh rock scars were on all sides.

Canyons Like Glacial Valleys

In detail submarine canyons are quite unlike land canyons. There is an absence of the fine rivulet sculpturing seen on land but, instead, there are plunging swales and debris-filled, U-shaped floors reminiscent of a moraine-glutted glacial valley. This is evidence of recent slides, slumps, and other mass movements. Large, lenticular, sandy silt bodies were also a prominent aspect of the underwater scene. Some of these formed tail dunes piled up on the down-slope lee of large blocks of wall rock that had fallen into the canyon axis. Such features could perhaps attest to turbidity current flows, rivers of mud which, from time to time, cascade down the canyon axis impelled by gravity like a stream of mercury, or maybe another type of unknown bottom current. There is much yet to be learned about what really goes on in these mystifying canyon heads and these dives only open the door to solving their true origin. But this was not the main purpose of these dives. It was to study how sediment moves into the deep sea from land. Canyons are one of the main avenues down which sediment travels and they play an important role in controlling sediment distribution patterns on the sea floor. Knowing what happens on today's sea floor helps us understand what happened in the ancient continental sea in which the marine sediments we now find on land were deposited.

Whether or not the undersea realm is a silent world one would never learn aboard *Deepstar*, as there is so much

self noise. The echo sounder pings, the hydraulic systems whirr, the inverter whines, and the underwater telephone (UQN) crackles with the white noise of static even on standby. But amidst this cacaphony, a periodic sputtering coming from the outside can still be sorted out. This is a friendly noise—the outboard motor of *Searchtide's* skiff "flying top cover" and keeping acoustic surveillance. This small boat was christened *Ratspeed* not in mock affection or in deference to her habit of scampering about, but simply because this name is *Deepstar* spelled backwards.

Abyssal Animals Pay No Heed

The bottom was rich in life attesting to the nutrient-rich waters of the Gulf. Most striking were the numerous shrimp and the Lilliputian fish fauna of brotulids and rat-tails, 3 or 4 inches long. They were spread out in one-species domains within which each animal seems to have his own territory of perhaps 1 square yard. Curiously none of these abyssal animals were "spooked" by *Deepstar*, being oblivious to our presence. Occasionally schools of squid flashed by attracted by our powerful lights. We missed the friendly sable fish so common off California, which in sleek droves like to bathe in the lights of a DRV. They even poke their noses against the view port as though the bathynauts were goldfish in a bowl. The denizens of the deep are a friendly lot with but few exceptions, perhaps most notably not the shy octopus, but rather the broad-billed swordfish, *Xiphias gladius*. Although usually regarded as a surface dweller, this fish has "buzzed" *Deepstar* and even rammed other DRV's at depths as great as 2,000 feet. (See "Broadbill Swordfish in Deep Water," *Sea Frontiers,* Vol. 14, No. 4, July-August, 1968.) DRV's are revealing much new information about the depth range of so-called surface animals. From the

Diving Saucer in a canyon nearby, Joseph Curray of Scripps Institution of Oceanography noted a green turtle at 600 feet and aboard *Aluminaut* off Florida a bottle-nosed dolphin, *Tursiops truncatus,* was seen at 600 feet.

No strong currents were encountered, but neither was the water ever completely still. The most rapid flow was estimated to be about two-tenths of a knot, which was not sufficient to cause observable rippling or erosion of the bottom. In some areas, however, there was clear evidence that some earlier movements had been caused by strong currents. Such domains are covered with smoothed-over or decayed ripple marks that have not yet fully disappeared.

Maintaining Position in the Dark

The benthic fauna reacts to the current regime in a curious manner. The shrimp and fish are oriented upstream much as birds on land face into the wind. This is perhaps to be expected for animals that rest on the bottom, such as the shrimps and the tripod fish, *Bathypterois*. But what about the rat-tails and brotulids which hover just off the bottom and hold station, exactly offsetting the bottom current? One can understand how a trout maintains position in a tumbling mountain stream, for he can fix his position visually. But in the perpetual inky blackness of the abyss eyes are of no avail. For some of these hoverers, a fine trailing thread could be detected which seemed to be designed to provide tactile contact with the bottom. But this is at most a partial answer to this mystery, for any fish had no such "sounding line" or were much too high off the bottom to use such a detector. Perhaps they have some sort of "sixth sense" within their lateral line which provides intelligence on the precise whereabouts of the bottom.

Both of these dives were terminated by ascents up the sheer side walls of the submarine canyons, cliffs 500 feet

FAR LEFT: A 5-FOOT GRANITE BLOCK *forms an erratic in the sediment fill of the canyon at a depth of 3,000 feet. The large scour depression around the block is evidence of periodic strong bottom currents. The gorgonian coral attached to the rock is oriented to the prevailing current direction. (Robert F. Dill)*

LEFT: TRIPOD FISH, Bathyterois bigelowi, *and* RIGHT: RAT-TAIL FISH, Coryphaenoides acrolepis, *were photographed on an earlier dive of* Deepstar 4000. *(Ron Church)*

and 800 feet high, respectively. The rocky walls were mostly thinly-bedded mudstone lying in a horizontal attitude and probably of late Tertiary age. Such strata do not outcrop on the nearby land. Little is known for sure about their origin, but it is surmised that they may be beds laid down in a localized deep basin formed in the Miocene or Pliocene about 5 to 15 million years ago when the Gulf of California first opened up. The Gulf appears to be a giant gore created by rifting as the deep earth's mantle spread laterally from a newly-formed, "misplaced" mid-ocean rise, an extension of the East Pacific Rise. This is, in turn, but a tail on the great, worldwide oceanic rift system which runs for 20,000 leagues under the sea.

So ended *Deepstar 4000* Dives 342 and 343, each to 3,300 feet (deeper than Bebee's record half mile down) and lasting about five hours. DRV diving is certainly high adventure, but it is a credit to Westinghouse and the *Deepstar* team that they made the whole operation look easy. Over the years Dietz and Dill have made dives in *Kuroshio, Trieste, Archimede, Diving Saucer,* and *Aluminaut,* but never before with such ease. It would seem that the *Deepstar* team did this sort of thing almost every day—and, with over 400 dives in the eighteen months prior to these dives, they really do.

It is not sufficient to remotely probe the ocean with samplers and geophysical sensors. To gain full insight it is necessary to enter the medium and grapple intimately with the sea. The new generation of DRV's offer this capability. Their advent is ushering in a new era in oceanography.

U.S. DEPARTMENT OF COMMERCE
Maurice H. Stans, Secretary
ENVIRONMENTAL SCIENCE SERVICES ADMINISTRATION
Robert M. White, Administrator
COAST AND GEODETIC SURVEY
Don A. Jones, Director

ESSA TECHNICAL REPORT C&GS 37

Precise Echo Sounding in Deep Water

GEORGE A. MAUL

ROCKVILLE, Md.
January 1969

List of Symbols

d	draft of the transducers
Mn	weighted mean
Sv	sounding velocity
T	time
Vs	velocity of sound
$\bar{V}s$	average velocity of sound within a standard oceanographic layer
Vs_0	velocity of sound at the surface
Z	depth in meters
Z_0	surface
ΔZ	thickness of a standard oceanographic layer
Z_c	computed depth
Z_s	echo-sounder depth
Z_t	true depth

List of Abbreviations

ADI	Automatic depth input
DAS	Data Acquisition System
db	decibels
fm/s	fathoms per second
kHz	kiloHertz (cycles per second × 10^3)
m/s	meters per second
NBES	Narrow-Beam Echo Sounder
PDR	Precision Depth Recorder
TVG	Time-varied-gain

UDC 551.46.082:531.719.35
551.46. Oceanography
.082 Instruments for measuring depth and pressure
531.719. Instruments for measuring length and depth.
.35 Echo sounding.

UNITED STATES GOVERNMENT PRINTING OFFICE ● WASHINGTON: 1969

For sale by the Superintendent of Documents, U.S. Government Printing Office
Washington, D.C., 20402 - Price 25 cents

Precise Echo Sounding in Deep Water

LT. CDR. GEORGE A. MAUL, USESSA

USC&GS ship *Discoverer*, ESSA, Norfolk, Va.

ABSTRACT

The advent of narrow-beam stabilized echo sounders and shipboard digital computers is revolutionizing bathymetry measurements in the deep ocean. New and more precise procedures for obtaining and correcting depth measurements are described, and the application of these methods aboard the USC&GS ship *Discoverer* is presented.

EQUIPMENT

The United States Coast and Geodetic Survey ship *Discoverer* is equipped with a Narrow-Beam Echo Sounder (NBES) designed and built by the Harris ASW. Division of General Instrument Corp. The performance specifications were provided the corporation by the Coast and Geodetic Survey. Among the specifications was that this echo sounder is to project a 12 kHz narrow sound beam to be effectively $2\frac{2}{3}$ degrees total beam (3 db down). The sound beam is gyro stabilized to ±1 degrees of the local gravity vertical within the limitations of ±10 degrees pitch and ±20 degrees roll. The depth resolution is ±1 fathom at 4000 fathoms. The sounding is displayed on a digital display to the nearest whole fathom, as well as on the conventional analog readout, a McKiernan-Terry Corp. Mark XV Precision Depth Recorder (PDR). The digital display of the NBES aboard the *Discoverer* was adjusted to provide an automatic correction for the average draft of the transducers.

The Data Acquisition System (DAS) of the USC&GS ship *Discoverer* is a Westinghouse Prodac 510 processor utilizing a UNIVAC 1218 computer. The system is designed to collect, process, display, and store environmental data such as bathymetry, gravity, magnetics, wind speed and direction, and air and surface water temperatures; control data such as ship's course and speed, and position; and on-station data which includes water temperature, salinity, and velocity of sound as a function of depth.

OPERATING PROCEDURE

Prior to departure on a cruise, anticipated values of the velocity of sound are provided to the Coast and Geodetic Survey by the National Oceanographic Data Center. Computations are made from historical data using the empirical equation of W. D. Wilson.[1]

The values provided to the ship are divided into applicable geographic zones. As the survey progresses from zone to zone, the values of the velocity of sound are changed to conform with the particular area of operations. An example of the geographic zones for a project is shown in figure 1.

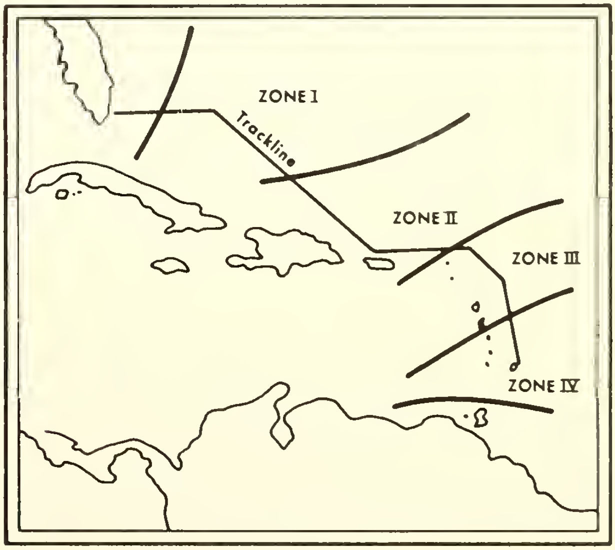

FIGURE 1.—Geographic zones for velocity corrections. Corrections to soundings, as read from the sounding instrument, are changed as the trackline progresses from zone to zone.

---

[1] Wilson, W. D., Equation for speed of sound in seawater *Journal of the Acoustical Society of America*, Vol. 32, p. 1357, 1960.

NARROW-BEAM ECHO SOUNDING[2]

In this paper, the term *sounding* means the uncorrected reading of the echo sounder; *depth* means the vertical distance from the water surface to the bottom. The term *automatic depth input* as used in the description of the data acquisition system means *automatic sounding input.*

The narrow-beam echo sounder projects a signal at a repetition rate which is a function of the depth. If the water depth is in the range of 0-400 fathoms, a signal is projected once every second; if the depth is 400-800 fathoms, the signal is projected every 2 seconds, etc. This echo sounder is designed to receive the projected signal before the next sound burst is triggered.

The first wave form of the returning sound pulse that exceeds a preset threshold level is used to measure the elapsed traveltime of the projected signal. The time count, which began with the trigger pulse, is stopped when the trend of the amplitude of this wave form is reversed (see fig. 2). The elapsed time is converted to fathoms and is displayed on the digital readout.

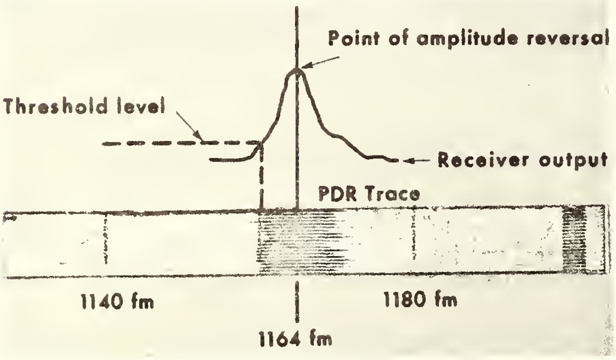

FIGURE 2.—Superposition of the oscilloscope trace of the detected, filtered, and amplified receiver output over a section of PDR trace.

The mark on the precision depth recorder begins after the returning signal exceeds a preset threshold level, but before the amplitude is reversed, and lingers past the point of amplitude reversal until the threshold level is again reached. This produces a mark on the graphic recorder which varies from light to dark to light again as the signal passes. The change in density is not discernable to the eye. This implies that the digital sounding is not necessarily coincident with the leading edge of the mark on the recorder. This is illustrated in figure 2.

The difference in digital and analog values depicted in figure 2 was taken from a test conducted aboard the *Discoverer*. The 3-fathom draft correction was subtracted from the digital value prior to the comparison. The apparent difference in soundings may be due to many factors among which are bottom slope, paper distortion, and instrumental error. It should be recognized that a 1-fathom difference will occur if the time from the threshold to amplitude reversal is 2.5 milliseconds.

The digital value, with the draft correction, is automatically read into the data acquisition system when automatic depth input (ADI) is initialized. For the sake of continuity, the digital readings are used to obtain soundings whenever the narrow-beam echo sounder is in operation.

The narrow-beam echo sounder is a gated instrument. The gating switch is divided into ranges of 400 fathoms. This provides coordination with the scales on the precision depth recorder. If this switch is set at a range less than the sounding, the digital readings become erratic. If the setting is greater, the digital readings remain correct; however, the signal-to-noise ratio will decrease. A time-varied-gain (TVG) effectively provides greater receiver sensitivity with increasing depth.

The echo sounder gating provides positive identification of the correct 400-fathom multiple, hence scale checks on the precision depth recorder are not necessary with the narrow-beam echo sounder operation. Scale checks may be easily accomplished on the Narrow-Beam Echo Sounder–Precision Depth Recorder by switching to the 0- to 4000-fathom scale on the graphic recorder; the gain on the Precision Depth Recorder usually must be reduced during this operation.

The recording procedure is as follows: At the prescribed intervals, the sounding is read from the echo sounder digital display, and written on the graphic recorder trace for cross reference on the appropriate time mark. If automatic depth input is initialized in the data acquisition system, the sounding record is checked as the survey progresses. Manual entry requires check scanning at a later time.

DATA REDUCTION

Reduction of the soundings is accomplished by the data acquisition system on a real-time basis. The reading of the echo sounder is entered into the system either manually or automatically; manual entry is necessary when operating conditions require the manual override of the time-varied-gain. After processing for the velocity of sound, the depth is displayed on a Nixie tube readout, printed on the hydrographic and geophysical report typeouts, and stored on magnetic tape.

---

[2] *Technical Manual*, Narrow-Beam Echo Sounder, Volume 1, System Description, General Instrument Corp.

Definitions of sounding velocity[3] and echo sounder depth[4] are now in order. Sounding velocity (Sv) is the weighted mean (Mn) of the velocity of sound (Vs) with depth (Z); that is, integrated velocity from the surface to the stated depth. Echo sounder depth (Z_s) is the sounding the instrument will read in a water column whose sounding velocity is not identical with the instrumental velocity of 800 fathoms per second.

The computer corrects the sounding for acoustic velocity in the following manner: The entered reading of the echo sounder is converted to time by dividing by the instrumental velocity of 800 fathoms per second. The computer then searches a listing of sounding velocity versus echo sounder depth; a linear interpolation is performed between the tabulated values for the applicable sounding velocity. The corrected depth is calculated by multiplying the sounding velocity by time.

The sounding velocity may be derived from the basic equation for the weighted mean[5] of any parameter:

$$Mn=\frac{\sum_{i=1}^{i=n} X_iQ_i}{\sum_{i=1}^{i=n} X_i} \qquad (1)$$

where Q_i is any variable and X_i is the interval over which Q_i is applicable.

In order to determine the mean velocity from the surface to a stated depth, it is assumed that linearity exists between the point sources of the data as shown in figure 3.

Consider the case of Z_i to Z_{i-1}, the mean velocity can be written:

$$\frac{Vs_i+Vs_{i-1}}{2}=\bar{V}s_i=Q_i$$

The bounded interval over which this value applies is:

$$Z_i-Z_{i-1}=\Delta Z_i=X_i$$

Z_i must always be greater than Z_{i-1}.
Substituting into equation (1):

$$Mn=\frac{\sum_{i=1}^{i=n} \Delta Z_i\bar{V}s_i}{\sum_{i=1}^{i=n} \Delta Z_i}=Sv_n \qquad (2)$$

The denominator when expanded:

$$\begin{aligned}\sum_{i=1}^{i=n} \Delta Z_i &= \Delta Z_1+\Delta Z_2+\Delta Z_3+\ .\ .\ .+\Delta Z_n\\ &= Z_1-Z_0+Z_2-Z_1+Z_3-Z_2+\ .\ .\ .+Z_n-Z_{n-1}\\ &= -Z_0+(Z_1-Z_1)+(Z_2-Z_2)+\ .\ .\ .+Z_n\\ &= -Z_0+Z_n\end{aligned}$$

but Z_0, the surface $=0$,
therefore

$$\sum_{i=1}^{i=n} \Delta Z_i=Z_n$$

Rewriting (2)

$$Sv_n=\frac{\sum_{i=1}^{i=n} \bar{V}s_i\Delta Z_i}{Z_n}$$

$$=\frac{1}{Z_n}\sum_{i=1}^{i=n} \bar{V}s_i\Delta Z_i \qquad (3)$$

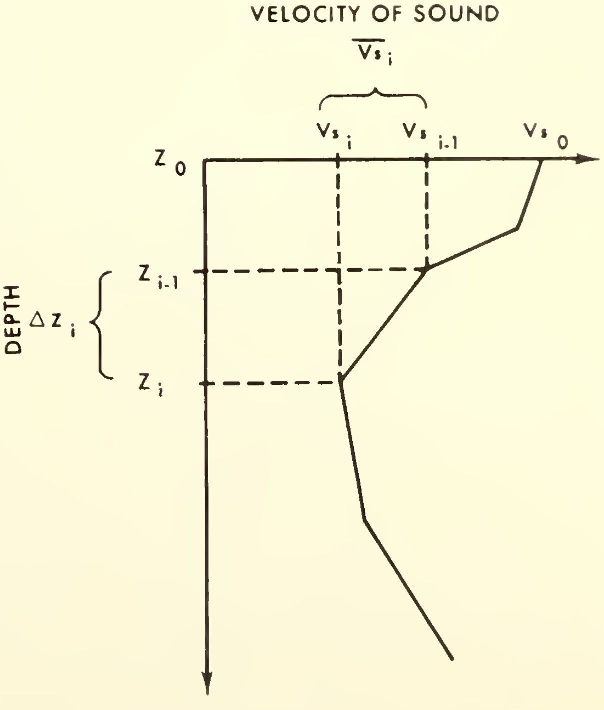

FIGURE 3.—Point to point distribution of velocity of sound versus depth.

---

[3] Sverdrup, H. U., Johnson, M. W., and Fleming, R. H., *The Oceans*, Prentice-Hall, Englewood Cliffs, N. J., p. 79f, 1942.

[4] Ryan, T. V., and Grim, P. J., "A New Technique for Echo Sounding Corrections," *International Hydrographic Review*, Vol. XLV, No. 2. pp. 41-58, 1968.

[5] James G., and James, R. C., Editors, *Mathematics Dictionary*, Van Nostrand, Princeton, N. J., p. 380, 1949.

The summation is from $Z=0$, the surface, to $Z=n$, the depth to which the integration is desired. The function Vs is continuous on the closed interval $0 \leq Z_i \leq Z_n$, hence the definite integral exists, and the equation may be written:

$$Sv=\frac{1}{Z}\int_0^Z \bar{V}sdz \qquad (4)$$

The integral is evaluated numerically by means of the trapezoidal rule. The entering arguments of Vs and Z are the tabulated values at the standard oceanographic depths. The standard oceanographic depths are enumerated in appendix 1. The average velocity of sound ($\bar{V}s$) is calculated for the standard oceanographic layers. An example of these calculations is shown in appendix 1. A graphic illustration of sounding velocity, velocity of sound, and instrumental velocity is shown in figure 4.

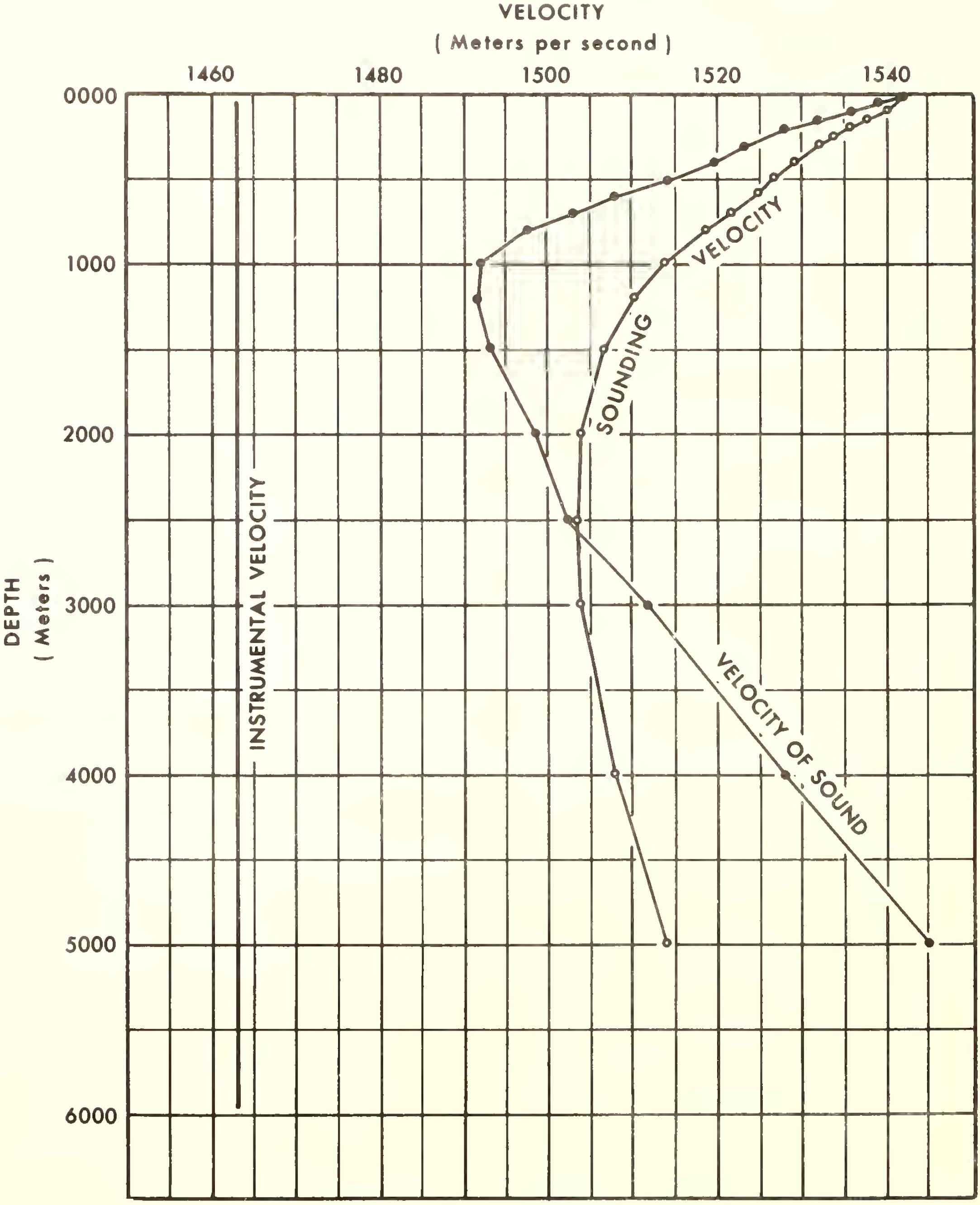

FIGURE 4.—Velocity as a function of depth.

Computer programming of sounding velocity is accomplished by substituting into equation (3) the expressions for Vs_i and ΔZ_i above, and developing the following algorithm:

$$Sv=\frac{1}{2Z_n}\sum_{i=1}^{i=n}(Z_i-Z_{i-1})(Vs_i+Vs_{i-1}). \qquad (5)$$

The echo sounder depth (Z_s) is derived from the basic equation: Distance = time (T) × speed. For an instrument calibrated for a standard speed of sound in sea-water of 800 fathoms per second:

$$Z_s=T\times 800 \text{ fm/s}$$

$$=T\times 1463.04 \text{ m/s} \qquad (6)$$

The metric conversion is based on the U.S. Survey Foot which by definition equals 1200/3937 meter exactly.

True depth[6] (Z_t) has the same relationship to time:

$$Z_t=T\times Sv \qquad (7)$$

Solving the simultaneous equation for echo sounder depth:

$$Z_s=\frac{Z_t\times 1463.04}{Sv} \qquad (8)$$

The sounding velocity in equation (8) is the applicable value for the true depth. These calculations are shown in the example in appendix 1.

An example of the computer listing for the calculations in appendix 1 is shown in appendix 2. A gradient is applied to best fit the historical data beyond the deepest tabulated value.

The original data acquisition system programming would not allow the numerical value of the depth to exceed the value of the sounding velocity in the listing. Effectively this meant that the gradient had to be linear from 1500 meters to the bottom. The data acquisition system software was changed to correct this situation.

The use of sounding velocity computations is a computer application of the basic method of hand corrections outlined in Pub. 20-2, Hydrographic Manual.[7] Sounding velocity computations have been used aboard the USC&GS ship *Discoverer* since she went into operation in July 1967. The refinement of interpolating with echo sounder depth as the entering argument, as suggested by Ryan and Grim,[8] is now in effect.

LIMITATIONS IN SHOAL WATER

The procedure of adding the draft of the transducers to the echo sounder depth prior to processing the soundaug for acoustic velocity will introduce an error in shoal water. It is desired to keep all errors less than 1/2 of 1 percent of the depth. That is:

$$0.5\%=\%\text{ error}=\frac{Z_c-Z_t}{Z_t}\times 100 \qquad (9)$$

where Z_c is the computed depth. The true depth and the computed depth may be written in the following form:

$$Z_t=\left[\frac{Z_s}{1463}\times Sv\right]+d \qquad (10)$$

$$Z_c=\frac{Z_s+d}{1463}\times Sv \qquad (11)$$

where d is the draft of the transducers in meters.

Substituting equations (10) and (11) into equation (9) and solving for echo sounder depth, it can be stated that an error that exceeds 1/2 of 1 percent of the depth will be introduced if:

$$Z_c\leq d\left[200-\frac{294063}{Sv}\right] \qquad (12)$$

Consider the case of a Class I Oceanographic Survey Vessel whose draft is approximately 6 meters. If the sounding velocity is a rather high 1542 meters per second, an error that exceeds 1/2 of 1 percent of the depth will be introduced when the fathometer depth equals 55.8 meters (30.5 fathoms).

Due to signal blanking, the narrow-beam echo sounder is not usable in depths less than 40 fathoms. Furthermore, current project instructions require the use of a shoal water echo sounder in depths less than 100 fathoms. Hence, the narrow beam sounder coupled with the data acquisition system will not, under even these extreme conditions, inadvertently introduce this error.

FUTURE REFINEMENTS

Many of the refinements suggested by Ryan and Grim[9] in area surveys recognize the fact that off-line postsurvey processing is necessary. On-line, real-time processing depends on the use of historical data. This is an obvious shortcoming of the *Discoverer*'s methods. It must be recognized, however, that a practical limit may have been reached with the present state-of-the-art that warrants additional equipment and processing uneconomical.

---

[6] "True depth" is understood to mean precise in the theoretical sense; the accuracy of the value is not implied.

[7] Jeffers, K. B., *Hydrographic Manual*, Publication 20-2, U.S. Coast and Geodetic Survey, Washington, D.C., p. 182 ff, 1960.

[8] Ryan, T. V., and Grim, P. J., Op. cit. note 4.

[9] Ibid.

A compiler language program for the Westinghouse Prodac 500 of the sounding velocity and fathometer depth is given as appendix 3. This program can be adopted to provide on-station, real-time, calculation of these parameters for multisensor data input, as well as off-line processing of historical data or Nansen cast data. The addresses in the program were arbitrarily chosen and will have to be changed for use with the present data acquisition system on-station programs; the scale factors (B4 for velocity of sound, and B0 for depth) conform to the scaling in the present system on-station program. This scaling satisfies the accuracy of the data input.

CONCLUSION

This report represents a cohesion of ideas into a working system. The equipment and methods presented will reduce the labor of processing, and improve the accuracy of deepwater soundings.

APPENDIX 1

Z_t	Vs	ΔZ	$\bar{V}s$	$\Delta Z \times \bar{V}s$	$\Sigma \Delta Z \times \bar{V}s$	$Sv = \frac{\Sigma \Delta Z \times \bar{V}s}{Z_t}$	$Z_s = \frac{Z_t \times 1463.04}{Sv}$
0	1542.0					(1542.0)	0
		10	1542.1	15421			
10	1542.2				15421	1542.1	9.5
		10	1541.9	15419			
20	1541.6				30840	1542.0	19.0
		10	1541.2	15412			
30	1540.7				46252	1541.7	28.5
		20	1539.8	30796			
50	1538.8				77048	1541.0	47.5
		25	1538.2	38455			
75	1537.5				115503	1540.0	71.3
		25	1536.6	38415			
100	1535.8				153918	1539.2	95.0
		50	1533.7	76685			
150	1531.6				230603	1537.4	142.7
		50	1529.8	76490			
200	1527.9				307093	1535.5	190.6
		50	1526.4	76320			
250	1524.8				383413	1533.7	238.5
		50	1523.9	76195			
300	1523.0				459608	1532.0	286.5
		100	1521.2	152120			
400	1519.5				611728	1529.3	382.7
		100	1516.8	151680			
500	1514.1				763408	1526.8	479.1
		100	1510.8	151080			
600	1507.6				914488	1524.1	576.0
		100	1505.2	150520			
700	1502.7				1065008	1521.4	673.1
		100	1500.0	150000			
800	1497.3				1215008	1518.8	770.6
		200	1494.6	298920			
1000	1492.0				1513928	1513.9	966.4
		200	1491.8	298360			
1200	1491.6				1812288	1510.2	1162.5
		300	1492.3	447690			
1500	1493.0				2259978	1506.7	1456.5
		500	1495.6	747800			
2000	1498.3				3007778	1503.9	1945.7
		500	1500.2	750100			
2500	1502.2				3757878	1503.2	2433.2
		500	1507.0	753500			
3000	1511.7				4511378	1503.8	2918.7
		1000	1519.7	1519700			
4000	1527.7				6031078	1507.8	3881.3
		1000	1536.2	1536200			
5000	1544.7				7567278	1513.5	4833.3

NOTE: Z_t is the standard oceanographic depth in meters. Vs and Sv are in meters per second.

APPENDIX 2

Interpolation		Computer Listing
Sv	Z_s	*DVP*[1]
1542.0	0	1542/0000/
1541.0	47.5	1541/0048/
1540.0	71.3	1540/0071/
1539.0	100.3	1539/0100/
1535.0	203.9	1535/0204/
1532.0	286.5	1532/0286/
1529.0	394.3	1529/0394/
1527.0	471.4	1527/0471/
1524.0	579.6	1524/0580/
1521.0	688.1	1521/0688/
1519.0	763.1	1519/0763/
1514.0	962.4	1514/0962/
1510.0	1179.3	1510/1179/
1507.0	1481.7	1507/1482/
1504.0	1928.2	1504/1928/
1503.2	2433.4	1503/2433/
1504.0	2966.8	1504/2967/
1508.0	3914.7	1508/3915/
1513.0	4749.5	1513/4750/

$$\text{Gradient}=\frac{V_2-V_1}{Z_2-Z_1}$$ G/+.00599/

$$=\frac{1513.5-1507.8}{4833.3-3881.3}$$

$$=+0.00599$$

---

[1] The computer listing will accept integers only for the values of sounding velocity and echo-sounder depth. To minimize error, interpolations for integer values of sounding velocity are performed; only values of echo-sounder depth are rounded to the nearest meter.

The program will accept up to nineteen points in the form of four-digit numbers. The left column of the computer listing is the sounding velocity; the right column is the depth. The gradient is applied at depths greater than 4750 meters.

APPENDIX 3

Address	Instruction		Remarks
33333	ELC	1234	arbitrary non-zero constant
33334	JLZ	3344	
33335	STZ	3410	clear register
33336	STZ	3411	Do
33337	STZ	3412	Do
33340	STZ	3413	Do
33341	ELC	0	
33342	ENB	3341	
33343	STB	3333	3333 ELC 0
33344	ENL	3411	Vs_{i-1} scaled B4
33345	JLZ	3367	
33346	ADD	6010	$+Vs_i$ scaled B4
33347	STL	3414	Vs_i+Vs_{i-1}
33350	ENL	6011	Zi scaled B0
33351	SUB	3410	$-Z_{i-1}$ scaled B0
33352	JLN	3402	
33353	JLZ	3402	
33354	MPL	3414	$\times Vs_i+Vs_{i-1}$
33355	ADA	3412	$+\Sigma$
33356	STU	3413	$\Sigma(Z_i-Z_{i-1})(Vs_i+Vs_{i-1})$ scaled B4
33357	STL	3412	
33360	ELC	2	
33361	MPL	6011	$\times Z_i$
33362	STL	3416	$2Z_i$
33363	ENL	3412	
33364	ENU	3413	
33365	DIV	3416	$\div 2Z_i$
33366	STL	3415	$=Sv$ scaled B4
33367	ENL	6010	
33370	STL	3411	new Z_{i-1}
33371	ENL	6011	
33372	STL	3410	new Vs_{i-1}
33373	ENL	3415	
33374	RSL	4	
33375	STL	3420	$=Sv$ scaled B0
33376	ELC	2667	$2667_8=1463_{10}$
33477	MPL	6011	$\times Zi$
33400	DIV	3420	$\div Sv$ scaled B0
33401	STL	3417	$=Z_s$ scaled B0
33402	1000		STOP

Program Input Addresses

36010	Vs_i scaled B4	input from the multisensor during on-station operations
36011	Z_i scaled B0	

List of Mnemonics

Mnemonic	Meaning
ELC	Enter AL with constant Y
JLZ	Jump on (AL) zero to Y
STZ	Set (Y) to 0
ENB	Enter B with (Y)
STB	Store (B) in Y
ADD	Add (Y) to (AL)
STL	Store (AL) in Y
ENL	Enter AL with (Y)
SUB	Subtract (Y) from (AL)
JLN	Jump on (AL) negative to Y
MPL	Multiply (AL) by (Y)
ADA	Add (Y+1, Y) to (A)

Mnemonic	Meaning
STU	Store (AU) in Y
ENU	Enter AU with Y
DIV	Divide (A) by (Y)
RSL	Right shift (AL) by k positions

Where AL is the lower accumulator
AU is the upper accumulator
A is the AU and AL (36 bit word)
B is the B register
(Y) is the contents of Y
Y is the address

3

COASTAL ZONE MANAGEMENT CONFERENCE

HEARINGS

BEFORE THE

SUBCOMMITTEE ON OCEANOGRAPHY

OF THE

COMMITTEE ON
MERCHANT MARINE AND FISHERIES
HOUSE OF REPRESENTATIVES

NINETY-FIRST CONGRESS

FIRST SESSION

ON

The Washington, D.C., Conference on the Organization, Utilization, and Implementation of the Coastal Zones of the United States, Including the Great Lakes

---

October 28, 29, 1969

Serial No. 91-14

Printed for the use of the
Committee on Merchant Marine and Fisheries

U.S. GOVERNMENT PRINTING OFFICE
37-487 WASHINGTON : 1969

Next, Dr. Harris B. Stewart, Director of the Atlantic Oceanographic Laboratory, in ESSA.

STATEMENT OF DR. HARRIS B. STEWART, JR., DIRECTOR, ATLANTIC OCEANOGRAPHIC LABORATORIES, ESSA

Dr. Stewart. Thank you, Dr. Fye.

The immediate ocean shoreline, the Continental Shelf, our estuaries and harbors, and the Great Lakes constitute what is now called the coastal zone.

But the term today connotes much more than a mere geographic area. This is the area where some 75 percent of our population is concentrated, so it is also the area where not only the sea and the land meet, but—more importantly—where the sea and man meet.

Thus the coastal zone is where the demand for recreational facilities is greatest, where the major water transportation routes terminate in our great port cities, where our greatest concentrations of municipal and industrial wastes accumulate, and where the specter of pollution looms the largest.

The coastal zone is where many of our commercial and sport fish spend at least a part of their life cycles, and where our first halting steps toward mariculture are taking place. It is where our major marine petroleum resources are found. It is the locus of our coastal shipping and the terminus of our transoceanic shipping.

It is where many of us want to live, or at least go for vacation. It is where we can get cheap coolant water for our powerplants, and where we can bulkhead and fill to make expensive real estate that can be sold at a profit.

It is also the location where many of our wetlands, marshes, mangrove swamps, and coastal ecological niches are being singled out for the establishment of conservation areas.

Our coastal zone is all of these things, and that is where the problem lies. Each of these is a legitimate use of our coastal zone, but as the activity in each of these use areas increases, it eventually reaches a point where it is out and out in conflict with another use. We have already reached this point in most of the populated portions of our coastal zone.

I might add parenthetically that again it is a problem of the interrelationship between man and the sea. It is a people problem.

Garrett Hardin in his article on "The Tragedy of the Commons" that appeared in Science last December—volume 162, pages 1243–1248, December 13, 1968—provided the sociological framework for this problem.

If I may be allowed to put his discussion in my own words, it runs something like this: If a common pasture will support 100 head of cattle, and each of 10 herdsmen has one cow each pastured there, there is no problem. If each herdsman increases his own herd to 10 cows, the commons is then supporting its 100 head, or all it can without degrading the total resource.

Then one of the herdsmen stops and thinks and decides that if he adds one cow to his own herd of 10, the worth of his own holdings will be increased by 10 percent, but his share of the costs resulting from the degradation of the commons by adding only one cow over the 100 the commons can support is only 1 percent, so it is some 9 percent to his advantage to add that one cow. Other herdsmen get the same idea, and cow after cow is added until the commons is totally destroyed.

The same situation holds for our coastal zone. Take, for example, the use of our coastal zone for the disposal of industrial and municipal wastes. So long as there are few people and few industries using the coastal zone as a self-flushing disposal system, there is no real problem.

Then the number increases. The cost for the individual plant to process its waste before disposing of it harmlessly into the coastal zone is many times more than that plant's share of the overall social costs of the ensuing degradation of the receiving waters, which, of course, is shared equally by all coastal zone users.

Thus, our coastal zone, like Hardin's commons, is doomed, unless some means is found to halt this relentless march toward destruction.

The coastal zone authority concept proposed by the Commission on Marine Science, Engineering, and Resources is one method of controlling this otherwise destructive process.

I believe that the establishment of such coastal zone authorities should be primarily a State or regional responsibility, and that the role of the Federal Government is mainly one of providing support to the State—both financial support and support in the acquisition of the basic understanding of the coastal zone environment on which valid judgments on coastal zone uses must ultimately be based.

I reiterate, the really essential part, and one of the major roles of the Federal Government, is to provide the basic understanding of the coastal zone requirements.

Before getting into the research requirements, there is one other point that I would like to make. There are two alternative costs related to the coastal zone: The cost of doing something, and the cost of doing nothing.

It is my contention that the cost of doing something, although an immediate cost, is considerably less than the eventual costs to society of doing nothing—it is the "Tragedy of the Commons" exemplified.

The real problem, it seems to me, is that we as a people are prone to defer the immediate costs because they are immediate. The unavoidable result is that we eventually are forced to pay the much greater costs of cleaning up the mess that we were unwilling to pay the relatively small costs to avoid in the first place.

The requirements for coastal zone research, therefore, are related first to the need for the environmental understanding on which sound decision on coastal zone use can be made, and secondly to the need to provide this understanding now at considerably less cost than the costs related to some future attempts to make up for our shortsightedness in not doing it now.

When it comes to the requirements for research in the coastal zone, the differences between the traditionally basic research activities of the universities and private institutions and the more mission-relevant, mission-oriented, or applied research missions of the Federal laboratories become less distinct.

I have always objected to the artificial distinction between "basic" and "applied" research, for one man's basic is another man's applied.

In the coastal zone, the problems are so numerous and diverse that almost any research leading to a better understanding of the complex processes operating there is by definition relevant to the equally complex problem of coastal zone management.

So I would find it difficult, really, to separate out discrete and unique research roles for the universities and for the Federal laboratories. This is one of the many areas where the universities and the Federal laboratories must work together for their mutual benefit.

The problems of the coastal zone and the research needs were described by the Commission's Panel on Management and Development of the Coastal Zone, and are published as part III of volume I of the Commission's panel reports This document contains important information for anyone concerned in any way with the coastal zone.

Although we have learned a great deal about the coastal zone, much additional information is needed.

The research effort should be aimed at "understanding" this Nation's coastal zone. This means an adequate understanding of the dynamics of estuarine circulation, the advection and the diffusion, the water budget, the movement of sediment as it relates to channel filling and deepening and to coastal erosion and deposition, the life histories of the organisms that populate our coastal zone, and their very complex interrelationships with the highly variable coastal zone environment, the basic physics of shoaling and breaking waves and of longshore and rip currents, the development of inundating storm surges related to intense coastal storms, the coastal runup of tsunamis, the movement of hurricanes, the capability of coastal zone waters to receive wastes without undesirable side effects (it is really how much of what can be introduced where for how long a time without creating more problems than it solves), the ocean-atmosphere interactions, and the land-sea interactions.

It is only with an understanding of the coastal zone as a highly complex and highly variable ecosystem that we can predict what the overall effect will be of man's proposed changes to that system.

It does not matter if we contemplate a channel deepening for deeper draft ships, bulkheading and filling for a new shipping terminal or real estate development, a new causeway to an offshore island, a new marina, a new powerplant to use coastal waters for cooling, a new park, a wildlife refuge established, a mariculture area set aside, an additional sewer outfall constructed, or any of a number of other uses to which we put our coastal zone. It really does not matter what we contemplate. The sine qua non for sensible value judgments for the use of the coastal zone is a basic understanding of the zone itself. For it is only with this understanding that we can predict the effects of the changes we contemplate.

I might add parenthetically here the need for what I would like to call legal research and development, legal R. & D. In effect, this is preventive maintenance. This is doing the legal research work in the coastal zone now to avoid the lawsuits that could come up later on.

I also might add that we should look at the coastal zone as a total man environment system, and we must do the research work relating to the interaction of man and his activities with this coastal environment.

It is to the Federal laboratories that we must look for that part of this fundamental understanding that relates to the mission of the agencies for which they carry out research.

Twenty-four Federal departments, administrations, agencies, bureaus, commissions, councils, and offices have, as a part of their missions, responsibilities related to the coastal zone. The agencies are listed by the Panel on Management and Development of the Coastal Zone, in their report ("Panel Reports of the Commission on Marine Science, Engineering, and Resources," vol. 1, pt. III, pp. III–81 to III–105).

I believe these groups should be encouraged to carry out mission-relevant coastal zone research. Coordination will, of course, be necessary to assure that research results are shared with other researchers, that major problem areas do not go unstudied, and that the concentration of several research activities in the geographically restricted coastal zone does not result in an undesirable duplication of effort. In summary:

1. Any research in the coastal zone can be considered as applicable to the basic requirement of understanding the coastal zone as a complex ecosystem.

2. The universities and the Federal laboratories do not have unique roles, but must work together to further this understanding.

3. The cost of doing something now is much less than the ultimate cost of doing nothing.

4. Future value judgments on the uses of our coastal zone must depend for their validity on a basic understanding of the area as a total system.

5. The coastal zone research work of the various Federal laboratories must be adequately supported and adequately coordinated to insure that the several efforts are all working cooperatively toward the same goal of coastal zone understanding, an absolute essential for coastal zone management.

The problems related to the coastal zone constitute what is probably the major marine science problem facing the United States today.

In an era when the socially relevant problems are the ones that get the attention and support, it behooves the Nation's oceanographers to direct at least a portion of their attention to problems in this category.

For the Federal laboratories, it is essential that their research relate to the missions of their parent agency. For many of the Federal agencies this means research in the coastal zone, and a vigorous program of coordinated coastal zone research is absolutely essential if our estuaries, harbors and near-shore areas are not to become part of "The Tragedy of the Commons."

Thank you.

Dr. **Fye.** Thank you, Dr. Stewart.

Next we will hear from Dr. Robert Abel, of the sea-grant program.

Biscayne Bay as a Natural Resource

(An address before the Zoological Society of Florida, October 6, 1969, by Dr. Harris B. Stewart, Jr., Director of ESSA's Atlantic Oceanographic and Meteorological Laboratories, Miami, Fla.)

Biscayne Bay is a beautiful, busy, bountiful, and booming bay. It extends some forty miles along the southeast Florida coast from Dumfounding Bay and the Interama site on the north to Card Sound and Arsenicker Keys on the south. On the west it is bounded by expensive homes, a busy port, the heart of a major city, more homes, public beaches, and a long stretch of red and black mangroves. On the east, Biscayne Bay is bounded by the wall-to-wall hotels and condominiums of Miami Beach, by Virginia Key and Key Biscayne, and by the string of beautiful keys from Soldier Key on the north through Ragged Keys, Sand Key, and Elliott Key, to Totten and Old Rhodes Keys at the south end of Biscayne Bay. I have come to know the bay intimately only during the past two years, but I have come to love it. Because I love it, I am terribly concerned for its future; for its future is our future, is Dade County's future. I predict in all confidence that if we, the people, allow the overall use of our bay to continue to develop unplanned as it has for the past forty years, our children and grandchildren will be living with an unattractive, azoic, concrete bounded, open cesspool. This is not an exaggeration. Boston Harbor two hundreds years ago was one of the truly beautiful estuaries in America, and the early accounts of New York harbor and the Hudson River estuary are beautiful to read. But look at these harbors today! And look at Baltimore Harbor, look at the Potomac River at Washington, look at Norfolk and Charleston harbors. You have seen them, you know what I am talking about without my having to go into details of open sewers, oily waters, no swimming, no fishing, unsafe boating, and waterfront areas of rotted piers and slums. We have not reached this stage yet, but only because we are younger. Give us time and the same disinterest, and we will be just like all the others. It is a slow and inexorable process nurtured by the selfish interest of short-sighted man himself. If the process continues unchecked here, the end result will be the same. It is only through the actions of man that the process continues, so it must be through the actions of man—albeit more enlightened man—that the process can be checked.

Before going any farther, I would like to set some groundrules establish what the physicists call the boundary conditions. First, although I am a federal civil servant, I left my ESSA hat out in the lobby and am speaking tonight only as a concerned Dade County oceanographer and a member of our Zoological Society of Florida. Secondly, I would like to establish in your minds my own personal position on "conservation", for the militant conservationist—even the quiet conservationist—plays a major role in what I call the Biscayne Bay syndrome. Of all the endangered species, I consider Homo sapiens as the most important. Wildlife refuges should be established and maintained inviolate—not for the animals themselves, but so that *man* can enjoy them, so that *man* can know that they still exist in their natural habitat and derive pleasure therefrom. Mine is a man-oriented view of conservation. When it comes to Biscayne Bay, I consider conservation of the natural environment as one of many uses to which the bay will be put, one of the many conflicting and multiple uses of the bay. It is not the *ne plus ultra* that many would consider it, but rather it is one more of the many uses, and it must be carefully balanced with the other demands when value judgments on the utilization of this resource are being considered. "Conservation", like "motherhood", has to many become an inviolate concept. I can think of nothing worse for the world than unrestricted motherhood. Overpopulation is probably the greatest problem facing mankind today. Conservation should be put in the same category. It should be looked at objectively, dispassionately, and stripped of the unenlightened blind emotionalism with which it is too often associated. A third boundary condition is my own personal bias—prejudice, if you will. I happen to love Biscayne Bay and want to see its use go for the greatest possible good for the greatest number of people.

Tonight I would like to outline briefly the problems that if unsolved will eventually result in the destruction of Biscayne Bay as probably our greatest natural resource in Dade County. I will also offer what I consider the best present solution to this problem. It is a major problem and will take a major solution. It is a problem created by the actions of people, and it will take the action of people to solve it.

The present problem with Biscayne Bay, the same problem that has gone unresolved in most of the other bays along our Atlantic seaboard, is that the bay is what the resource economists call a "resource held in common" and one on which ther are many—and often conflicting—demands. Let me give you some examples of these conflicting uses. If the pleasure-boat operators prefer not to have holding tanks for sewage on their boats but to use the bay as a convenient sewer, those who like to swim can not use for our marina slips where people live on boats as areas for swimming. If you doubt me, look over the side of the piers at any of the big marinas on Biscayne Bay. If you elect to have a big area set aside as a National Monument, you can't expect to build hotels, homes, and condominiums there. If you want to save all the red mangroves, you can't dredge and fill the area for an industrial seaport. If you want a causeway to join up a few islands, you can't sail through it. If you want to aside an area for mariculture, you can't water-ski through it. If you want the power required for a fast-growing metropolitan area and use bay-water to cool the generating equipment, you must be prepared to have some warm water put back into the bay. If you don't feel up to paying for proper sewage treatment, the bay is an economical toilet that flushes itself in a half-hearted way twice a day, but swimming, fishing, and the aesthetic resource may suffer. A thriving industrial seaport is important to the economic base of the community, but this involves dredging and filling and getting rid of the spoil. If spoil is spread over the shallows where many of our commercial and sport fish spend at least part of their life cycles, then these nursery grounds diminish and the fish population diminishes accordingly. If you want to live on the water you may have to bulkhead and fill in some of the mangrove areas. If you want to dump raw sewage, you can't swim. If you want to preserve the whole bay in its pristine condition, you can't do anything at all, and so it goes. These, then, are the problems related to the multiple and often conflicting uses of Biscayne Bay.

I would like to take a look at one of these conflicting uses of the bay in some detail. One of the great resources of Biscayne Bay may in fact be that it is a big hole in the ground, a self-flushing system, and a fine place to get rid of the waste material that we do not want to live with on land. You can spit in the bay, and the bay will probably never know the difference. Two people, a hundred people, could do the same, and the bay would still be essentially unpolluted. So the question is not "yes" or "no," but rather, "how much" of "what", "where", and "when", and "for how long". Answers to these questions have not been attempted, so the normal course of action by inconsiderate man is just to keep on pouring the waste materials into the bay until the effects become so bad that man himself objects to the results and tries to clean it up. Usually by that time it is too late, the reaction is an irreversible one, and one more bay becomes useful only as an open sewer. This certainly is one use to which the bay *can* be put, but I doubt that we are willing to pay the social price for using Biscayne Bay uniquely used for getting rid of our municipal and industrial wastes.

We are, however, well along on just that road. I understand from Dr. William Fogarty of the University of Miami that of Dade County's 90-plus sewage treatment plants, less than five were putting out what is termed "acceptable effluent" during a recent inspection. I might add, parenthetically, that the big City of Miami treatment plant on Virginia Key is one of the best. If you fly over the offshore outfall discharge area and look down, you will see that the water coming out of the outfall is actually cleaner and clearer than the brownish bay water coming out of Government Cut. I also understand from Dr. Fogarty that Snake Creek, Snapper Creek, and the Coral Gables Waterways are too polluted even for swimming. But let me put some numbers on this. Sanitary engineers use as one measure of pollution what they call the "most probable number" or MPN. This refers to the number of enteric organisms—human origin—in a water sample. The upper limit for "safe" swimming is an MPN of about 1000. Dr. Fogarty has routinely measured 16,000 in Coral Gables, in Snapper Creek, and in Snake Creek—sixteen times the upper safe limit—not for drinking, but just for swimming. Near one point of discharge from a treatment plant, he measured an MPN of 16 million, or 16 thousand times the upper safe swimming limit! Fishkills have been reported in the local press, and a boat trip up any of these waterways will prove that the situation is bad. There are those in the local government who are working hard to correct this. There are good pollution control laws on the books—some of the best in the nation—but unless they can be enforced, they are of little use, and the effluent continues to pour into our once beautiful creeks and waterways and eventually into Biscayne Bay. When did you last go swimming in the Miami River? There are those in the city today who can remember when the swimming in that river was great.

The spectre of pollution hangs over Biscayne Bay, and I maintain that the major reason is voter apathy. "The County should do something" is the recurring cry, but YOU are the County. These are your waterways, your creeks and rivers, your bay. Pinellas County is now some 90 per cent sewered. It happened in a relatively short time, and it happened only because the people were willing to become involved. I must admit, however, that the real driving force there was the women. County officials were elected or defeated on the basis of their stand on this one issue. Bond issues were pushed and voted through. They got what they felt was needed, but only by becoming involved, working for what they needed, and seeing that it was accomplished. We can do this in Dade County. It will take a lot of work by a lot of dedicated people, but it can be done if the people will rise up *en mass* and demand that it be accomplished. The Zoological Society of Florida can and should play an important role in this "popular uprising".

Getting rid of the wastes of a busy metropolitan complex is just one of the many and conflicting uses to which our bay is being put. The thermal effects of the Turkey Point power plant coolant water discharge is—both literally and figuratively—a "hot" issue right now. You notice that I say "thermal effects" rather than the more popular term "thermal pollution", for my contention is that until we know exactly what the effects are, we are pre-judging the case by calling it "pollution". This use of the bay is another conflicting use. A new seaport has recently been proposed for southern Dade County, and a study by the Bechtel Corp. has been released. A bridge-causeway joining Fisher Island to Virginia Key has long been in the planning stages, and the recently announced plans for the development of Fisher Island have brought this plan to the forefront again. The New Port of Miami has a 25-year development plan that calls for eventual use of Lumas Island as the eastward extension of the Port. The deepening of the ship channel to Dodge Island has long been pushed as a needed improvement. The location of the bulkhead line is still in contention. A large National Monument for the southern part of Biscayne Bay is well along on the road to realization. The City and County have this spring agreed to set aside some 162 acres on Virginia Key as a marine science park, and this will include the dredging of a channel into an oceanographic small-boat marina north of the Marine Stadium. The new Miamarina at the north end of Bayfront Park is nearing completion. The bulkheading of the south side of Dodge Island is on the books, and I am sure that there are other plans afoot for Biscayne Bay about which I do not know. The point here is that things are happening in Biscayne Bay. They will continue to happen. Change is not bad *per se*, but haphazard changes to Biscayne Bay carried out within the present framework for effecting such changes could be disasterous. As of today, dictated primarily by the unenlightened apathy of the residents of Dade County, the use of the bay will continue to go to the group with the most money, the most political "pull", or the group that shouts the loudest. It could result in anything but what I like to call "the greatest good for the greatest number of people."

Let me assume that the problem has been adequately stated, that you realize that unless something is done a great natural resource will little by little be whittled away until it becomes a liability rather than a great natural asset. The question then becomes "What can be done about it?".

I would like to approach answering this question in two ways. First, what has happened elsewhere and what is being done at the Federal level; and secondly, what should we do here in Dade County.

San Francisco Bay is farther down the road than we are here, so a look at San Francisco Bay today may well be a look at Biscayne Bay in the future. What has happened there? In the mid-nineteenth century San Francisco Bay with its marshlands covered some 680 square miles. Extensive bulkheading and filling has reduced this to little more than 400 square miles today. Of the 280 miles of shoreline, only about ten miles are open for public access. The boundary lines of nine counties and 32 cities extend into the bay, about 22 per cent of the bay has been sold by the state into private ownership (mainly the shallow areas where filling is easiest), and 23 per cent has been granted by the state to cities and counties—generally with filling in mind. In brief, the bay was steadily being used up, the pollution was bad and getting worse, and the bay itself was under the control of an incredible number of separate jurisdiction and private ownerships. California did two things. It appointed a San Francisco Bay Conservation and Development Commission—an interesting juxtaposition of two terms that are so often in dire conflict—and a San Francisco Bay-Delta Water Quality Control Program. The San Francisco Bay Plan has recently been published, and it is a truly fine document. Even now the State is working out the methods whereby this plan might be implemented. But San Francisco waited until it was too late—or almost too late. We here still have time—but not much!

At the Federal level, Management of the Coastal Zone has popped to the surface in Washington circles as the major marine problem with which this country is now faced. Although various agencies, groups, organizations, panels, committees, and individuals have long been preaching the importance of the coastal zone, it took an adroitly worded report to bring the whole effort into proper focus. Public Law 89-454 authorized in 1966 the establishment of a Commission on Marine Science, Engineering and Resources. The President appointed a distinguished Commission under the Chairmanship of Dr. Julius Stratton, Chairman of the Ford Foundation. Their extremely thoughtful, technically sound, and nationally relevant report entitled *Our Nation and the Sea* was published last January and received wide acclaim. Chapter 3 of the main volume is entitled "Management of the Coastal Zone" and presents a succinct summary of the more detailed report of the Panel on Management and Development of the Coastal Zone. This latter report, contained in Volume I of the published Panel Reports of the Commission, should be read by everyone concerned in any way with the problems of the coastal zone. The response to this report has been broad-based and enthusiastic. Senators Magnuson of Washington and Hart of Michigan have recently introduced Senate Bill 2802 known as the Coastal Zone Management Act of 1969 which would encourage through federal support the establishment of Coastal Zone Authorities at the State level. On the 28th and 29th of this month the House Merchant Marine and Fisheries Committee is holding a series of panel discussions on the problems of the coastal zone and the need for such Coastal Zone Authorities. So the Federal government is concerned, is involved, and can be looked to for support for locally-generated initiatives.

Finally, what should we be doing here? Presently we are doing very little. Local conservationists are tooling up to shoot down any attempts to get a new seaport in South Dade County. People are beginning to listen to Dr. Fogarty, Paul Leach, and others who are screaming about our levels of pollution. Florida Power and Light is fighting for some means to cool its Turkey Point generators, and the problems related to land acquisition for the Biscayne National Monument are far from solved. But there is no overall Biscayne Bay Plan, no Biscayne Bay Policy Board, and very little concern for Biscayne Bay as a total physical, biological, ecosystem. The one exception here is the University of Miami's Institute of Marine Sciences of its newly-formed School of Marine and Atmospheric Sciences. Operating with funding from the Sea Grant College Program administered by the National Science Foundation, the Institute of Marine Sciences is preparing for a complete study of Biscayne Bay.

Therefore, my first recommendation for preventing the total destruction of Biscayne Bay is based on the valid assumption that in order to make truly meaningful value judgments on the future use of the bay, we must first understand how the bay works as a complex physical and biological system. To this end, there should be provided every available assistance to the University of Miami in its efforts to understand Biscayne Bay. The study should entail total community commitment. Local elements involved in any way should plan to work with the University. This would entail County and City planning Departments and other relevant local government agencies. It would entail the local representatives of State agencies, including the Department of Natural Resources, Department of Air and Water Pollution Control, Department of Community Affairs, the Commission on Marine Science and Technology, and the Board of Trustees of the Internal Improvement Trust Fund. At the Federal level, it would include the local representatives of the Federal Water Pollution Control Administration, Corps of Engineers, Coast Guard, Geological Survey, Bureau of Commercial Fisheries, Bureau of Sport Fisheries and Wildlife, and the Environmental Science Services Administration. But most important would be the many local people with particular involvement in Biscayne Bay. I am thinking of the developers, the conservationists, the sanitary engineers, the marine engineers, the lawyers, the fishermen (both sport and commercial), the boat manufacturers, the shipyard operators, and all the rest. The study must be primarily a scientific and technical study with the major amount of work being carried out by the appropriate scientists and technicians. However, to be truly meaningful, the study must be followed by a plan for the effective conservation and development of Biscayne Bay; and if this plan is to be at all meaningful, it must have the involvement of all the various user groups I have just mentioned. Every user and potential user and every relevant agency (federal, state, and local) must be involved from the very beginning. Without this total community involvement, the study—no matter how good—may well receive the stigma of the 'I-wasn't-involved-so-it's-no-good' attitude that so often follows the publication fo studies carried out by a single group. My first recommendation, then, is for the complete community involvement in a detailed study of Biscayne Bay as a total system. My second recommendation is for the formal establishment by the County Commission of a Biscayne Bay Conservation and Development Commission patterned after the successful San Francisco Bay Conservation and Development Commission. Let's be frank. The problem of the management of our coastal zone is a problem of national scope and importance. Something *will* be done about it. I personally feel that it is highly preferable to have this "something" initiated at the local level and in response to local requirements rather than to sit back until the State or the Federal government forces some program on us that may have little relevance to our own particular coastal zone problems. By the same token, the initiation of a local Biscayne Bay Conservation and Development Program would serve as a prototype of comparable programs elsewhere and could very possibly attract both State and Federal support for our efforts here.

As I said earlier, Biscayne Bay is a beautiful, busy, bountiful, and booming bay. If we want our major natural resource in Dade County to be something of which future generations can be proud, we must not wait until it is too late to do anything about it. The time is now. I would like to conclude with a quotation by Theodore Roosevelt: "The Nation behaves well if it treats the natural resources as assets which it must turn over to the next generation increased and not impaired in value. * * * Conservation means development as much as it does protection."

Reprinted from U.S. Naval Inst. Proc.
Vol. 95, No. 10/800, 68-77. © 1969

Oceanography and the U. S. Merchant Marine

By Harris B. Stewart, Jr.

Reminiscent of the plight of Androcles' lion is the unhappy state of the former monarch of world shipping—now crippled by a whole paw-full of such thorns as the staggering in-port costs of loading and discharging cargo. An altogether unlikely Androcles, oceanographic research, might pluck out this thorn—and many of the other festering economic barbs as well.

The United States is beset with many problems related to our use of the sea as a highway for international commerce. It would be presumptuous to think that increased knowledge of the sea deriving from an active program of oceanographic research would remove all these problems. It would not. However, oceanography can make significant contributions to the alleviation of many of these problems through providing the knowledge of the sea that will permit its more efficient—and hence less costly—use for transportation. Cost is the major factor that has resulted in the present difficulties in which the ocean transportation industry in this country now finds itself. Many of these costs can be reduced by the use of the knowledge that will become available as we learn more about the sea in general and more about those specific aspects of it which have a direct bearing on its use as the major intercontinental highway.

Our projected dependence upon imports of strategic material is frightening. For example, the United States is now self-sufficient only in coal, molybdenum, phosphate, and magnesium. Even lumber and petroleum have shifted from net exports to net imports within the last few years, and we are notably deficient in asbestos, tin, manganese, iron ore, cobalt, nickel, chromite, lead, and zinc. Already we are 100 per cent dependent on foreign sources for tin, quartz crystal, industrial diamonds, and amosite asbestos, and our dependence on foreign imports is increasing steadily for many other essential raw materials.

In view of the future needs of the United States which require a continuing and increasing influx of the world's raw materials, and considering the apparently waning ability of U. S. flag vessels to meet these demands,

the importance to the United States of oceanographic research, or any other type of research that might materially assist in revitalizing the marine transportation industry cannot be overstated. The problem is clear, and it can be expected to get worse rather than better unless new knowledge and new ideas are generated and applied to the task of improving the whole field of oceanic transportation.

The fact that increased oceanographic research might be of considerable benefit to the transportation industry has been stated many times in the past. On numerous occasions, it has been used as one of the several justifications for increased support of oceanography by the Federal government. The period of tacit acceptance of sweeping generalities is past, however, and the time has come to spell out in some detail just how oceanography can be of benefit.

Ship Design. Even though there is some tendency now to design faster merchant ships—the 20-knot Mariners are the outstanding example—a real incentive to design ships for optimum speeds would result if freight rates were varied to recognize the value of speed of delivery.

It might be possible, under a policy of varying freight rates, to have a certain number of express ships much as the land and air transportation systems have air freight, rail express, and parcel post. Realizing that faster ships will have to be built, the ship designers have already come to the oceanographers asking for information that is not yet available.

For example, from the oceanographers and the statisticians are needed the data to develop an integrated theory of the strains and motions to which a ship is subjected in a seaway. On the basis of such a theory, ships can be better designed for the environment in which they have to operate. It is the waves that produce the major strains suffered by a ship and, therefore, must be taken into account in the earliest design stage. Similarly, it is the sea itself that causes the heavy slamming and the emergence of the propeller, both of which produce dangerous vibrations which must also be considered in the design stages. In addition, the loss of speed to be expected in heavy weather must be considered in the design for the fuel consumption and power requirements. The various oscillations induced into a ship by the waves she encounters must be considered in designing for freeboard, stability, and general ship safety. Yet, adequate statistical wave data from the open sea are not now available. There is not even sufficient wave information to allow the ship designers to know how realistic are the wave conditions which they create in their test and model basins.

The U. S. Maritime Administration has recently advanced the idea of designing ships specifically for certain limited trade routes so that construction costs may be reduced by building ships to withstand the waves to be expected only along one particular route. Yet, there is not now adequate data available on wave conditions at sea even to distinguish the wave characteristics of various ocean areas—if indeed there are typical differences.

Recent basic research work on the hydrodynamics of porpoises holds great potential for developing means to reduce the skin friction and hence increase the efficient speed of submarines. This work may produce major improvements in the design of future commercial as well as military undersea vehicles.

The future of undersea commercial transportation should not be overlooked, and the design of cargo-carrying submarines is already being considered. Plans for a nuclear-powered submarine cargo ship have already been presented before the Royal Institution of Naval Architects in London. This ship, appropriately nicknamed *Moby Dick*, was designed to carry iron ore from northern Canada to Britain at speeds of 25 knots at depths of 250 to 350 feet. Under the northern ice-fields, speed would be reduced to about 15 knots. There is more to such ships than merely building them. The designers, for example, say that submarine freighters probably could not be justified on economic grounds at speeds of less than 25 knots. They would probably be used for special trades in which surface vessels would be limited to seasonal operations, as in the Arctic. The availability of shorter routes using under-ice movement contributes to the appeal of the commercial submarine. The polar route between London and Tokyo, for example, is only 6,300 miles in contrast to 11,200 by the conventional surface route. From Honolulu to London, the

Unless otherwise credited, all photographs courtesy of ESSA

Ice in inland and coastal waters presents a very real hazard to shipping. The USC&GS Ship *Marmer,* on a current measuring survey, works her way carefully through the ice floes in the Hudson River.

Continual improvement in the coverage and quality of marine charts is essential. An officer and a chief on board a hydrographic survey ship plot and check offshore soundings in the ship's plotting room.

under-ice polar route would save nearly 3,000 miles.

Ship Routing. The knowledge of any system has reached a high level of sophistication when future actions of that system can be accurately predicted; and, conversely, if the aim is prediction, a large body of knowledge about the system must be developed. A case in point is the prediction of sea surface conditions. If the causes of waves, the mechanisms for the growth and decay of waves, the movement of waves, and the effect of waves on ships were completely known, and if the distribution of these causes were known and predictable, it would be possible to predict the waves which any ship would encounter along any given route. Ships could then be routed along an optimum time track or routed for maximum comfort or safety.

To some extent this is already possible on the basis of the rather limited knowledge available. The Naval Oceanographic Office has prepared wave forecasts for a number of tows of heavy equipment that were extremely sea-sensitive. The Texas Tower radar stations were towed into position on the basis of recommended route and predicted wave conditions. The movement of the large rocket boosters from New Orleans to Cape Canaveral is also governed in part by a similar service provided by oceanographers. In 1956, the Navy Hydrographic Office initiated the Navy's ship routing service with a total of 34 experimental routes. Presently the Navy is provided with about 1,600 optimum tracks per year. The Maritime Administration and some commercial steamship operators have also used the Least Time Track principle to reduce the time of vessels at sea. Savings in steaming time have been recorded at 8 hours for a 3,000-mile trip and 13 to 15 hours for a trip of 5,000 miles. The ship-routing technique is still in its infancy, however.

There are other advantages to accrue to the shipping industry from intelligent routing procedures. Safety and comfort may in some instances be as important economically as speed. The minimizing of heavy weather damage to ships, cargo, and personnel would amount to substantial savings annually to the shipping industry. In one recent year, four ships totalling 30,118 gross tons were total losses, owing solely to weather damage, and 822 ships sustained partial damage from the effects of bad weather. Cargo losses from weather damage run well into the millions of dollars annually.

For a ship whose operating costs at sea run $3,000 per day, a saving of 12 hours on a transoceanic crossing amounts to a saving of $1,500 on that trip alone. Considering the number of ships operating at any given time and the number of crossings such ships might make, the potential savings to the maritime industry from a perfected ship-routing program would run into many millions of dollars annually. To this should also be added the savings resulting from minimizing the cargo losses and ship repairs resulting from weather damage.

Port Facilities. The major portion of the cost-to-the-shipper of goods carried by oceanic transport is absorbed in the port areas particularly in the process of loading and discharging his cargo between the ship and the land. These in-port costs have been estimated at over half of the total shipment bill. The seaborne part of an overseas shipment is the most economical form of transportation known to man. The real need is for more efficient transfer between the ship and the shore. Quick port turnaround is extremely important, too, primarily because U. S. ships cost more to build and operate than do their foreign counterparts. Marine transportation and the U. S. public ultimately would benefit from such improvements, because of the increase in the nation's imports and exports that might be expected if the cargo-handling costs could be reduced. Such reductions would also make higher sea speeds more logical.

Improved predictions for tidal currents in narrow channels and constricted harbors, improved nautical charting techniques, incorporation of radar "pictures" in harbor chart atlases, improved harbor construction based on more accurate predictions of the resulting changes in bottom silting conditions, development of schemes for preventing or dissipating such natural hazards as fog and ice, all of these could result from an increased effort in oceanographic research. These would all contribute to more efficient operation and hence lower costs in existing harbors, whereas what is most needed is a whole new approach to the major harbor problem of reducing the cargo-handling costs and turnabout time.

Harbors in most cases are crowded, and the maneuvering of large ships in the constricted waterways and turning basins is a slow and difficult process at best.* Strong tidal currents, shoaling waterways, slips almost always at right angles to the current and prevailing wind, and channel lights masked by a strong background of city lights are but a few of the hazards that the captain of an oceanic ship must encounter. Normally, the docking of a large ship in a typical harbor is such a demanding task that local pilots are brought aboard to conn the ship to her berth.

The oceanographers could well team up with the marine engineers in a concerted study to devise an entirely new approach to the problem of transferring bulk cargo from the sea to the land. One possible solution has already been used successfully by the oil companies. At many places they use offshore buoys through which their cargoes are discharged through sea-bottom pipelines to the shore. It is quite possible that floating terminals could be used for other types of cargo. Ores, grains, and oil would be particularly amenable to this type of offshore terminal. As "containerization" and other types of "cargo utilization" are developed, so, too. should be the methods of handling the cargo by means other than the conventional harbor techniques.

The formation of ice in the extreme northern and southern harbors has been a definite detriment to marine transportation in these areas. In Greenland, Sweden, and Canada, recent trials with the so-called "bubbler" system have definitely shown that the technique works. This involves laying pipes on the bottom of a harbor and pumping compressed air through the pipes which are perforated along their length. The rising air bubbles create a vertical circulation which carries the warmer bottom water to the surface, raising by a fraction of a degree the temperature at the very surface where the ice first forms. Additional applied research in this area might well increase the open port time for many of the world's high-latitude harbors.

---

* *See* T. L. Lewis, "Canals and Channels, A Look Ahead," August 1967 Proceedings, pp. 33–43; D. J. Flood, January 1968 Proceedings, pp. 109–110.

All the developments in faster and better ocean transportation are efforts wasted if the ships doing the job have to waste half of their time in inefficient ports. Oceanographic research can contribute much to the solution of this problem.

Navigation and Strandings. Traditionally, the ship captain has entertained a fear of running aground. The Loss Book of the Liverpool Underwriters' Association shows that these fears are still well founded, for in one year alone, 68 ships ran aground and were lost. This amounted to a loss of 280,732 gross tons of shipping. Partial losses owing to the same cause were sustained by 925 ships. Yet, the threat of running aground is only a part of the problem related to the navigation of ships on the high seas. In the 19th century, Matthew Fontaine Maury realized the importance of wind and current information to the captains of sailing ships;* but with the advent of steam, ships were able to roam the seas with little need to consider the currents and wind. Now that submarines are operating in all seas, and with the possible future development and use of cargo-carrying submarines, noted earlier, it is necessary that we learn more of the subsurface currents that can have a marked effect on the movement of such submerged freighters. If we wait until these undersea ships are a reality, it will be too late.

For example, the Great Circle distance from New York to Gibraltar is 2,805 nautical miles. If there were no current at all, a submarine traveling at 20 knots could make the trip in 140 hours. With a three-knot current moving in the same general direction, the transit time would be some 18 hours less. If the current were opposing at the same rate, the transit time would be some 18 hours more, for a total saving of a day-and-a-half in the passage of a submarine between New York and Gibraltar. This presupposes that the

Improved harbor facilities demand more accurate tidal predictions. Two officers of the ESSA Commissioned Corps run a line of levels to tie in a tide gauge with bench marks of known elevation on the land.

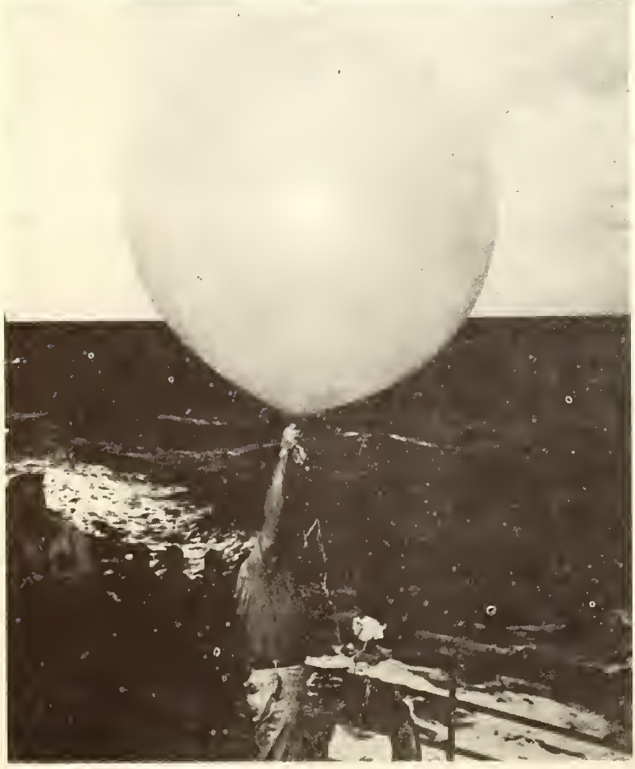

Weather observations at sea provide data that ESSA's meteorologists use in preparing marine forecasts for the transportation industry. A Weather Bureau meteorological technician launches a radiosonde balloon from the USC&GS Survey Ship *Explorer* in the Caribbean

---

* *See* A. C. Brown, "The *Arctic* Disaster, Maury's Motivation," January 1968 PROCEEDINGS, pp. 78–83.

Such buoys as this prototype for measuring oceanic and atmospheric characteristics, placed in a global network, will one day give oceanographers and meteorologists data needed to improve sea state and marine weather forecasts.

Part of the solution to the problems created by marine boring and fouling mechanisms rests on the ability of marine biologists—two examine samples from the cod end of a plankton net just recovered from a night tow—to determine the life histories of the organisms.

skipper would know at exactly what depth he could encounter a three-knot current that would assist him. The Cromwell Current, an undercurrent in the Equatorial Pacific, has been clocked at these speeds, and a comparable current in the Atlantic has recently been measured at half this speed. At present, these are the two major subsurface oceanic currents that are known to oceanographers as potentially important in submarine navigation. Probably others exist but have yet to be discovered. That such currents are present has occasionally been shown by observations of the movement of submarines. It is up to the oceanographers to measure and chart such subsurface currents so that when the submarine freighter is a reality, we shall have the environmental data that will make these vehicles profitable.

The status of accurate charting of the ocean bottom is sufficiently bad that the hydrographers of the world are actually embarrassed about it. Nautical charting along the coasts of the major maritime nations is in fair shape, but there exist no accurate charts of over 95 per cent of the ocean.* The aircraft pilot operating under visual flight regulations is able to look out of his window and see rivers, mountain ranges, canyons, and hills, and by these locate himself by the method known as piloting. In simpler words, this merely means looking and seeing where you are. With very few exceptions, this technique is not available to the marine navigator because the knowledge of the submarine landscape is too meager for him to use. The area of submarine canyons, which indent the continental slope off Georges Bank, some 100 miles east of Cape Cod, is one of the few exceptions. A series of steep submarine canyons lies athwart the major sea lane between Europe and New York. These canyons have been accurately charted by the U. S. Coast and Geodetic Survey of ESSA and are shown on the navigational charts of the area. As trans-oceanic shipping approaches the area, the normal procedure is to switch on the echo sounder. As the bottom trace shows that the ship has crossed the first canyon, the navigator checks the maximum depth of crossing. By reference to his chart, he is able to get an accurate fix on his location, for the canyon axis gives him a check in one direction, and the point of axis-crossing is neatly defined by the maximum depth to give him a check in the other direction. As he crosses the next of the series of canyons, the procedure is repeated to give a second fix, and he has not only a firm check on his course, but also on his speed of advance. Fixes of this sort are independent of the cloud cover that prohibits star fixes and of the sky wave problem, precipitation static, and occasionally poor transmission that sometimes interfere with obtaining good positions from electronic positioning systems. Once the entire ocean has been adequately charted, this same piloting technique can be used to help the ocean navigator locate himself.

---

* *See* C. N. G. Hendrix, "The Depths of Ignorance," May 1968 PROCEEDINGS, pp. 32–45.

Considerable portions of the coasts of this, and other countries, still need to be surveyed by accurate methods. Studies need to be made of the possible use of depth contours in addition to, or as replacements for, the traditional spot soundings on nautical charts. The use of relief portrayal of bottom configuration should be studied, so that the best means of navigation by bottom topography may be developed. Charts or related publications may well be improved by showing more and better information on currents and possibly even weather. For all of these items, continued and expanded oceanographic research is a prerequisite. Such fields as current delineation by aerial photography and airborne and satellite radiation thermometry, improved soundings by stabilized narrow-beam transducers and by lateral sounding equipment to cover a wider area, and greater area coverage by carefully planned oceanic surveys, all will contribute to better navigation through better charting of currents and bottom topography.

Better navigation will mean fewer strandings and less loss of ships and cargo, it will mean faster transit times resulting from better underway track control, and it may even mean fewer losses from collisions resulting from poor navigational control. Collisions alone caused the total loss of 14 ships amounting to 60,843 gross tons, and a partial loss of 1,804 ships during one recent, although not typical, year.

Fouling, Corrosion, and Boring. The fouling and corrosion of ship hulls and the ravages of boring organisms have been a "calamitas navium," as the Swedish botanist, Carolus Linnaeus, referred to them, since man first took to the sea. The ancient Carthagenian and Phoenician ship owners were beset with the problems of fouling and boring organisms, and they routinely charred the bottoms of their ships and painted them with pitch as protective measures. In the 3rd century B.C., Archimedes of Syracuse sheathed the bottoms of his ships with lead, fastened with copper bolts to prevent their destruction by the insidious boring organisms. During the American Revolution, the introduction of copper sheathing for wooden ship hulls did much to slow down the damage of marine borers, but these creatures are still with us and still doing millions of dollars worth of damage each year.

This source of ships' bottom fouling is probably the most direct organic threat to the world's merchant fleets today. Freedom from corrosion and fouling means a smoother hull. This in turn means less frictional resistance and hence less power requirement, with a resultant demand for less fuel for the same speed. This in turn means lower costs to the ship operator.

The costs related to fouling of ships' hulls have been well documented. A study by the Bureau of Ships in the early stages of World War II was carried out on ten destroyers. It was found that the use of galvanic cathode protection systems to offset electrolytic action corrosion resulted in maintenance savings of $10,000 to $20,000 per destroyer per overhaul. Similarly, a study by Arthur D. Little, Inc., showed that fouling by barnacles and other organisms can so reduce the speed developed at a given engine power that in order to maintain shipping schedules, fuel consumption must be increased by 50 per cent. Actually the fouling organisms on ships' hulls are not only the well-known barnacle, but also commonly include the hydroids, algae, calcareous worm tubes, and sea squirts. The larval stages normally attach themselves to the hull while the ship is in port, and unless detached by friction when the ship is underway, they remain in place to grow and thereby to reduce, measurably, the efficient operation of the ship.

In earlier times, it was not uncommon for a ship to have her bottom encrusted to a thickness of 8 or 9 inches, adding 300 tons or more to her original weight. More recently, dry-docking has reduced the maximum growth that most ships can expect; but after 6 to 8 months at sea, growths 2 to 3 inches thick and weighing upwards of 100 tons can be expected. It has been conservatively estimated that the annual cost to U. S. shipping, from fouling alone, runs upwards of $100,000,000.

Some advances in reducing the costs owing to fouling have been made in recent years. For example, compositions that give off toxic ions of copper or mercury can actually poison organisms within one millimeter of a ship's hull, and studies have shown that ships should be repainted at regular intervals, based upon the effectiveness of the original paint, the season of the year, and the "foulness" of the ports visited. Plastic hulls have recently been used by the Coast Guard with great success in their 40-foot utility boats. Fiberglass-reinforced plastic hulls constructed in 1951 and 1952 have been used in the extremely acid environment of Houston Harbor for almost seven years. It was found that the average hull maintenance costs were only $814 with the plastic hulls, as opposed to more than ten times that amount for steel boats and over seven times that amount for wooden boats.

Oceanographic research can definitely contribute to the reduction in costs incurred as a result of marine fouling. Practical anti-fouling methods must rest on a complete understanding of the whole life history of the particular species of organisms involved. Only then can we hope to know the weak points where their growth can be effectively inhibited. It is especially noteworthy that the major fouling of ships' hulls occurs not while the ship is underway in the open ocean but rather while she is in port. This is another valid reason for the development of port facilities that will allow a quicker turnaround time.

A graduate of Princeton University, Doctor Stewart served in the U. S. Army Air Force from 1942 to 1946 and was Hydrographic Engineer with the Persian Gulf Expedition in 1948–1949. He has participated in a number of oceanographic expeditions, including the 1960 *Explorer* Expedition, the 1964 *Pioneer* Expedition, and the 1968 *Discoverer* work off Barbados. He was Chief Oceanographer and Deputy Assistant Director of the U. S. Coast and Geodetic Survey from 1957 until the formation of ESSA in 1965. Since then, he has been Director of ESSA's Atlantic Oceanographic and Meteorological Laboratories.

Three families of boring organisms are responsible for the largest part of the great destruction wrought each year to wharves, piers, ferry slips, and other terminal facilities composed wholly or in part of wood. These are the *Teredinidae*, *Pholadidae*, and *Limnoria.* Probably the most destructive are *Teredo* and *Bankia* of the *Teredinidae.* These are the so-called "shipworms" and may grow to a length of more than 5 feet, while attaining a diameter of only one inch. Although they look like worms, they actually are a species of mollusk.

A single species of boring organism which attacked a large wharf in Boston Harbor did more than $3,000,000 worth of damage, and in 1946, the Brielle Bridge over the Manasquan River in New Jersey completely collapsed as a result of the activities of marine borers in the center pier supports.

A frequently quoted figure for the annual destruction of marine facilities by the action of boring organisms is $50,000,000, a figure first presented in a 1948 report. By 1957, the American dollar losses owing to the activities of marine wood borers amounted to $500,000,000, with the total cost to the U. S. Navy alone amounting to $50,000,000 annually.

Considerable progress has already been made in the fight against the destruction caused by these marine organisms. Pressure creosoting has been one of the best deterrents to date. As an example of the effectiveness of this treatment, the piles and timbers for the Sausalito ferry slip in San Francisco Bay were pressure-treated with creosote in 1898. When these same pilings were removed some 59 years later, they were still in useable condition. In the same general area, wharf installations on Treasure Island were seriously damaged by *Limnoria*, and a fender system, built of untreated eucalyptus during World War II, was so badly damaged by these boring organisms that it was totally unfit for use within five years.

Oceanographic research to date has shown that the organisms responsible for this destruction are to varying degrees sensitive to salinity, temperature, the food supply, current action, pollution, dissolved oxygen concentration, pH, and the amount of dissolved H_2S in the water. The research into the life cycles and limiting factors of these organisms must continue, for it is in the results of research that the solution to this problem must lie. There are two costs related to this problem: the cost of doing nothing, and the cost of doing something. We know that the former is expensive; considerable savings could result from the latter.

Corrosion of ships ranks with fouling and boring in over-all costs to the U. S. shipping industry. The Socony-Vacuum Oil Company has estimated that the corrosion bill for a fleet of 20 tankers amounts to $1,000,000 per year, or $50,000 per tanker per year. The cost for any individual tanker depends on the trade routes on which it operates, the type of cargo carried, the ballasting, and the frequency and method of cleaning. A typical tanker, in coastwise service after eight years of operating with mixed cargoes, normally must have the top 18 feet of all cargo bulkheads renewed at a cost of about $250,000 for an average cost of $1,300 per voyage. The lower bulkheads need to be replaced every four years involving corrosion cost of between $50,000 and $75,000 per year for replacement of steel alone. Additional costs include $3,000 to $8,000 per day during the time the ship is laid up for repairs.

Some advances have already resulted from marine corrosion research. Anti-corrosion paints using mineral pigments have been developed for steel. These include the long-famous red lead, as well as the zinc or lead chromate paints, and paints made with iron oxide, titanium oxide, or aluminum flakes. Steels with copper or phosphorus have been found to be more resistant to corrosion than ordinary steel, and the addition of silicon, chromium, and the various nickel-copper alloys also increases the resistance to marine corrosion. Cathodic protection has also proven to be of considerable use in the prevention of corrosion. In Britain, for example, it has been estimated that an unprotected tanker might last 12 years, after which the hull would have to be renewed at a cost of about $1,200,000. Cathodic protection of the same ship over 17 years costs $165,000 for a total saving of over a million dollars.

The corrosion problem is far from solved, and the costs to the American shipping industry from corrosion alone amount to an estimated $50,000,000 per year. Marine chemical research, long neglected in this country, might well discover some new technique for reducing these losses.

From all of this, the final conclusion to be derived is that the best approach to solving these problems is a concerted effort in both basic and applied oceanographic research. This research should be coupled with that being carried out by the ship designers, coastal engineers, and industrial engineers who have long been involved in these very problems. A vigorous program of oceanographic research can help point the way to the development of a U. S. merchant fleet that can regain its rightful place among the maritime nations of the world.

Reprinted from Journal of Geophysical Research
Vol. 74, No. 6, 1488-1494.

JOURNAL OF GEOPHYSICAL RESEARCH VOL. 74, NO. 6, MARCH 15, 1969

Interpretation of the Magnetic Anomalies off Central California

B. G. BASSINGER, O. E. DEWALD, AND G. PETER

ESSA Atlantic Oceanographic Laboratories, Miami, Florida 33130

Magnetic total intensity observations off the coast of California to 133°W delineate additional offsets of the magnetic anomaly lineations not previously reported. The lack of topographic expression of the minor magnetic anomaly offsets suggests that either the sedimentary cover masks small displacements or the source of the magnetic anomalies lies in the deeper part of the oceanic crust. A distinct change in amplitude, wavelength, and trend of the magnetic lineations occurs at approximately 124°20′W. This change coincides with a hiatus in the pattern of the magnetic lineations and supports the contention that the process of sea-floor genesis was episodic rather than a continuous event.

INTRODUCTION

As part of the ESSA Coast and Geodetic Survey contribution to the Upper-Mantle Project, shipborne magnetic total intensity observations were made in the area of the offshore extension of the U. S. TransContinental Geophysical Survey. The measurements were made primarily along east–west track lines spaced at intervals of approximately 18 km between 35°N and 30°N, extending westward to 133°W. Control for the track lines was maintained by satellite navigation.

The residual anomaly map presented by *Lattimore et al.* [1968] extends seaward the more closely spaced observations, reported by *Mason and Raff* [1961]. Figure 1 shows both maps combined. The good agreement between the two maps is illustrated by the close match of the contour lines in the area of junction. Because of closer track line spacing and better anomaly definition, the *Mason and Raff* [1961] map was preferred in the coastal area to the map presented by *Lattimore et al.* [1968].

DISCUSSION

The pattern of magnetic anomaly lineations and their worldwide distribution has been demonstrated by *Pitman et al.* [1968], *Dickson et al.* [1968], and *Le Pichon and Heirtzler* [1968]. These authors interpret the origin of the magnetic anomaly lineations in accordance with the hypothesis of *Vine and Matthews* [1963]. Recent interpretations of global tectonics, based on the distribution of the magnetic lineations, by *Morgan* [1968] and by *Le Pichon* [1968] assume that sea-floor spreading is the consequence of crustal opening caused by the rotation of individual crustal blocks. By using the data presented by *Ewing and Ewing* [1967] and by *Ewing et al.* [1968], *Le Pichon* [1968] modified the geomagnetic time scale discussed by *Vine* [1966] and *Heirtzler et al.* [1968] and presented the global spectrum of magnetic lineations in terms of episodic sea-floor spreading. The difference in the time span of sea-floor spreading between the *Le Pichon* [1968] estimation and the earlier time scale is only 17 m.y. This duration is arrived at by retarding the rate of spreading and finally completely stopping it at anomaly 5 (magnetic anomalies numbered after the system of *Pitman et al.* [1968]). The pause in spreading at anomaly 5 is estimated to have lasted 10 m.y. It is assumed by *Le Pichon* [1968] that a major reorganization of spreading took place at the Mesozoic-Cenozoic boundary (anomaly 32) and at the Miocene-Pliocene boundary (anomaly 5). *Menard and Atwater* [1968] assumed five reorganization events, based on the change of strike of the fracture zones in the northeast Pacific. An independent study by *Peter et al.* [1969] suggests two changes in the direction and speed of crustal spreading: the first occurred between anomalies 22 and 24 and the second between anomalies 5 and 7. The new data off California support the idea of an

Copyright © 1969 by the American Geophysical Union.

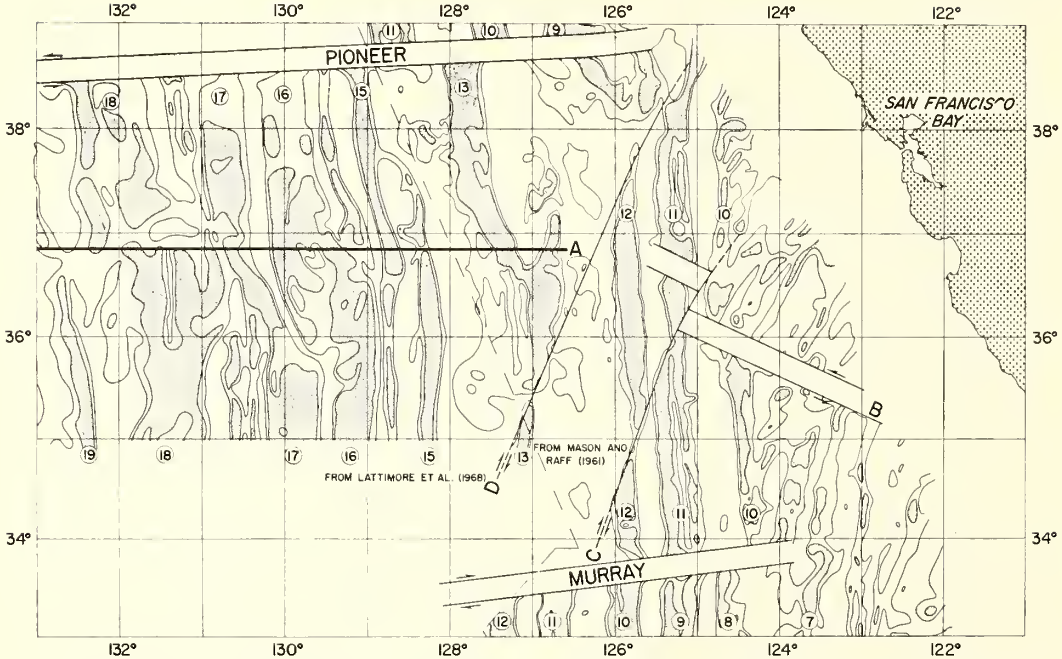

Fig. 1. Magnetic anomaly map showing major faulting. The 0- and 100-gamma contours are shown, with the stippled areas indicating anomalies greater than 100 gammas. Magnetic anomalies are numbered after the system of *Pitman et al.* [1968].

episodic crustal generation and its reorientation in direction at the beginning of a new episode.

The region investigated (Figure 1) can be divided into two separate zones at approximately 124°20′W: the western zone is characterized by north–south oriented anomalies with high amplitude and long wavelength and the eastern zone by northeast–southwest oriented anomalies with lower amplitude and shorter wavelength. Within both zones, small-scale faulting is indicated by the systematic displacement of the anomaly bands. The trend of faulting of the magnetic structures is different in the two zones, and a given fault appears to be restricted to one of the zones with the exception of fault B, which apparently extends west of fault C, based on bathymetric data and distortion of the double-anomaly character of anomaly 11. Even the Murray fracture zone appears to terminate near the boundary of these two zones.

The magnetic anomaly lineations have been numbered in accordance with the system of *Pitman et al.* [1968]. The easternmost lineation that can be clearly identified between the Pioneer and Murray fracture zones is anomaly 11. Anomaly 10, apparently forming the border between the two zones, loses its characteristic shape and wavelength as a high-amplitude, broad, double anomaly. Its width and amplitude are reduced (particularly north of fault B in Figure 1) where the northeast–southwest-trending anomalies abut sharply against it. South of the Murray fracture zone the sequence is more continuous: anomalies 9, 8, and 7 are present, followed by the small-amplitude, short-wavelength anomalies shown on the standard profile of *Pitman et al.* [1968]. Between the Pioneer and Murray fracture zones, however, the singular character of the anomalies east of anomaly 10 does not appear to be associated with the double-anomaly character of anomalies 9, 8, and 7. The lineations that abut anomaly 10 seem to be intermediate in character between the short-wavelength anomalies east of anomaly 7 in the northeast Pacific and anomalies 9, 8, and 7.

Data published by *Le Pichon* [1968] and by *Peter et al.* [1969] indicate that, in the northeast Pacific, one of the reorganizations in the direction of crustal spreading took place between anomalies 5 and 7. If the anomalous magnetic pattern between the Pioneer and Murray fracture zones is related to a reorganization of crustal spreading, it represents a deviation from the standard northeast Pacific pattern as well as from the global magnetic pattern.

Discrepancies in the orderly succession of the magnetic anomalies were noted by *Raff* [1962] immediately south of the Murray fracture zone and by *Keller and Peter* [1968] in the western South Pacific. In the latter case it was suggested that the magnetic pattern was influenced by the possible extension of the Austral seamount chain. From the data available, it appears that, since the discontinuities occur in different parts of the magnetic pattern, these disturbances reflect only the influence of local geology, rather than being related to global changes in sea-floor spreading. Between the Pioneer and Murray fracture zones the disturbed pattern may be related to the reorganization of the spreading pattern between anomalies 5 and 7, but in this particular area the tectonic trends and forces that were related to the new cycle of spreading apparently distorted part of the older crust (between anomalies 11 and 7) that was formed during the previous spreading epoch. A combination of the nearness of the continent and the movements of crustal blocks may be responsible for this local tectonic development. As an explanation, one may use the same argument as *McManus* [1965] and *Peter and Lattimore* [1969], who inferred, on the basis of the similarity of the structural trends on the coast and in the bathymetric and magnetic trends at sea, that the Blanco fracture zone and the general deformation of the area off the Washington-Oregon coast most likely are related to the late Tertiary coastal orogeny.

Fault B in Figure 1 is in alignment with numerous other left-lateral faults onshore. It also appears to offset the bathymetric contour lines [*Lattimore et al.*, 1968] at the base of the continental slope in a left-lateral sense. From these relationships, one may also infer that the late Tertiary and Pleistocene orogeny off the California coast [*Taliafero*, 1951; *Oakeshott*, 1966] also affected the adjacent sea floor or that the fault systems of central California and those of the adjacent sea floor are related to the late Tertiary tectonic activity along the East Pacific rise, which is considered to be in Baja California, southeast of this area.

Although some seamounts lie along the trend of the magnetic expression of fault B (this displacement of magnetic anomalies was first noted by *Mason and Raff*, [1961]) and although minor left-lateral offsets of the bottom contours are evident, there is no obvious topographic expression along faults A, C, and D. Seismic reflection data also fail to provide reliable correlation with these faults. (Weeks and Lattimore, in preparation).

Faults C and D appear to be normal strike-slip faults that extend between the major fracture zones. Fault B may be a transform fault [*Wilson*, 1965], but, if the short-wavelength anomalies belong to a new phase of spreading with an original transform fault, there is no reason why anomalies 10 and 11, which presumably belong to an earlier spreading phase, should be offset. Since fault B offsets both the short-wavelength inshore anomalies and anomalies 10 and 11, it is probably another strike-slip fault caused by differential block motion. By realigning anomaly 12 along fault C, it is apparent that fault B offsets anomaly 11 and apparently stops before it reaches anomaly 12.

The line representing fault A (Figure 1) was drawn along the approximate median of a zone, which suggests both clear breaks and gradual distortion of the anomaly pattern. These dislocations of the magnetic lineations are unusual when compared with normal displacements in the oceanic crustal area. Because the distortions of the magnetic lineations along fault A are intermixed with clear offsets and because the sense of distortion is in agreement with that expected where drag would occur along a left-lateral strike-slip fault, it is possible that fault A is another strike-slip fault.

It is generally assumed that the source of the magnetic lineations lies within layer 2 of the oceanic crust. Considering, however, the lack of correlation of the bathymetry with fault A and the fact that the sediment cover of this area is very thin (less than 200 meters, according to Weeks and Lattimore, in preparation), either the offsets occurred before the deposition of the sediments, or the primary source of the magnetic lineations lies in the deeper part of the crust, as suggested by *Peter and Lattimore* [1969]. In the latter case, offsets of the magnetic anomalies do not necessarily reflect the offsets of the entire crustal column, and small offsets may not even reach to the top of layer 2. The deeper offset of the 'magnetic crust' may be compensated along horizontal shear planes within the upper parts of the crust. The combination of offsets and distortions of the magnetic lineations may represent the manifestation of this proposed compensation.

REFERENCES

Dickson, G. O., W. C. Pitman, III, and J. R. Heirtzler, Magnetic anomalies in the South Atlantic and ocean floor spreading, *J. Geophys. Res., 73*, 2087, 1968.

Ewing, J., and M. Ewing, Sediment distribution on the mid-ocean ridges with respect to spreading of the sea floor, *Science, 156*, 1590, 1967.

Ewing, J., M. Ewing, T. Aitken, and W. J. Ludwig, North Pacific sediment layers measured by seismic profiling, in *The Crust and Upper Mantle of the Pacific Area, Geophys. Monograph 12*, pp. 147–173, American Geophysical Union, Washington, D. C., 1968.

Heirtzler, J. R., G. O. Dickson, E. M. Herron, W. C. Pitman, III, and X. Le Pichon, Marine magnetic anomalies, geomagnetic field reversals, and motions of the ocean floor and continents, *J. Geophys. Res., 73*, 2119, 1968.

Keller, G. H., and G. Peter, East–west profile from the Kermadec trench to Valparaiso, Chile, *J. Geophys. Res., 73*, 7154, 1968.

Lattimore, R. K., B. G. Bassinger, and O. E. DeWald, Magnetic map from the coast of California to 133°W longitude, *Misc. Geol. Invest. Map I-531A*, U. S. Geological Survey, 1968.

Le Pichon, X., Sea-floor spreading and continental drift, *J. Geophys. Res., 73*, 3661, 1968.

Le Pichon, X., and J. R. Heirtzler, Magnetic anomalies in the Indian Ocean and sea-floor spreading, *J. Geophys. Res., 73*, 2101, 1968.

McManus, D. A., Blanco fracture zone, northeast Pacific Ocean, *Marine Geol., 3*, 429, 1965.

Mason, R. G., and A. D. Raff, A magnetic survey off the west coast of North America, 32°N to 42°N, *Bull. Geol. Soc. Am., 72*, 1259, 1961.

Menard, H. W., and T. Atwater, Changes in direction of sea floor spreading, *Nature, 219*, 463, 1968.

Morgan, W. J., Rises, trenches, great faults, and crustal blocks, *J. Geophys. Res., 73*, 1959, 1968.

Oakeshott, G. B., San Francisco Bay area: Its geologic setting, *Geotimes, 11*, 11, 1966.

Peter, G., and R. K. Lattimore, Magnetic structure of the Juan de Fuca Gorda ridge area, *J. Geophys. Res., 74*(2), in press, 1969.

Peter, G., B. H. Erickson, and P. J. Grim, Magnetic structure of the Aleutian trench and northeast Pacific basin, in *The Sea*, vol. 4, edited by A. Maxwell, Interscience, New York, in press, 1969.

Pitman, W. C., III, and D. E. Hayes, Sea-floor spreading in the Gulf of Alaska, *J. Geophys. Res., 73*, 6571, 1968.

Pitman, W. D., III, E. M. Herron, and J. R. Heirtzler, Magnetic anomalies in the Pacific and sea-floor spreading, *J. Geophys. Res., 73*, 2069, 1968.

Raff, A. D., Further magnetic measurements along the Murray fault, *J. Geophys. Res., 67*, 417, 1962.

Taliafero, N. L., Geology of the San Francisco Bay counties, in *Geol. Guidebook, San Francisco Bay Cnty., Calif. Div. Mines Bull. 154*, 117, San Francisco, Calif., 1951.

Vine, F. J., Spreading of the ocean floor: New evidence, *Science, 154*, 1405, 1966.

Vine, F. J., and D. H. Matthews, Magnetic anomalies over oceanic ridges, *Nature, 199*, 947, 1963.

Wilson, J. T., A new class of faults and their bearing on continental drift, *Nature, 207*, 343, 1965.

(Received September 13, 1968;
revised November 20, 1968.)

Reprinted from Journal of Sedimentary Petrology
Vol. 39, No. 4, 1509-1519.

7

JOURNAL OF SEDIMENTARY PETROLOGY, VOL. 39, NO. 4, P. 1509-1519
FIGS. 1-4, DECEMBER, 1969

PRELIMINARY EVALUATION OF A CORE SCINTILLATION COUNTER FOR BULK DENSITY MEASUREMENT IN MARINE SEDIMENT CORES[1,2]

CHESTER BRIER,[3] ROBERT BENNIN,[4] AND PETER A. RONA[5]
Hudson Laboratories of Columbia University,
Dobbs Ferry, New York 10522

ABSTRACT

A core scintillation counter which measures transmitted gamma radiation was applied to determine wet bulk density of cores of marine sediment sealed in plastic liners. A preliminary evaluation indicates that two principle problems affecting accuracy of the bulk density determination are: (1) The radioactive source emits random radiations, which must be treated statistically to determine the dependence of counting accuracy on number of counts. (2) The Compton mass attenuation coefficient, which must be known in order to calculate density from scintillation counts, varies significantly with sediment composition and water content.

INTRODUCTION

A core scintillation counter, similar in principle to that described by Evans (1965), was evaluated for the measurement of bulk density in water-saturated cores of marine sediment contained within plastic liners (fig. 1). The core scintillation counter is a device which measures the transmission of radiation from a controlled radiogenic source (cesium^{137}) through a sediment core; bulk density of the sediment is derived by counting radiation that has passed through the core. The transmission method has been used with soils (Vomocil, 1954; Bernhard and Chasek, 1955; van Bavel, *et al.*, 1957), rock cores (Harms and Choquette, 1965; Evans, 1965), and unconsolidated sediment (McHenry and Dendy, 1964; Wilson, 1967; Preiss, 1968).

This paper outlines some preliminary findings in the application of the core scintillation counter to bulk density determination in marine sediment, which we did not find adequately developed in the literature. In particular, the paper considers two problems:

1. Statistical limitations inherent in the data owing to the random nature of the radioactive source.
2. Variations in Compton mass attenuation coefficients (μ) of different sediment-water mixtures.

STATISTICAL LIMITATIONS IMPOSED BY RANDOM RADIOACTIVE SOURCE

Principle

The core scintillation counter evaluated herein is similar in principle to that described by Evans (1965). In operation, a core of water-saturated marine sediment inside a sealed plastic liner is placed between a radioactive source (Cs^{137}, gamma-ray energy level 0.66 mev) and a scintillator (fig. 1). Each gamma ray that passes through the sediment core and strikes the scintillator causes a flash of light. The flash of light is detected by a photomultiplier. The output of the photomultiplier is amplified, detected, and counted for a fixed time interval. The number of counts is related to the density of the core material.

Because the gamma-ray output from the radioactive source is random, the data obtained are subject to the statistical limitations inherent in any random-sampling process. Because the sampling (counting) period is long relative to the duration of any one event (one gamma ray), and the events are independent of each other, gamma rays emitted from the radioactive source can be represented by a Poisson distribution (Laning & Battin, 1956).

For the discrete Poisson distribution the standard deviation σ is $\sqrt{m}$, in which $m = VT$.

m = Average number of events
V = Rate at which the events occur (number of counts/sec)
T = Interval of time measurement (sec.)

When the number of discrete samplings taken for purposes of averaging is large, the distribu-

---

[1] This work was supported by the Office of Naval Research under Contract Nonr-266(84). Reproduction in whole or in part is permitted for any purpose of the United States Government. It is Hudson Laboratories of Columbia University Contribution No. 351.

[2] Manuscript received February 28, 1969.

[3] Present address: Naval Research Laboratory, Washington, D. C.

[4] Present address: Environmental Protection Administration, New York.

[5] Present address: ESSA Atlantic Oceanographic and Meteorology Laboratories, Miami, Fla.

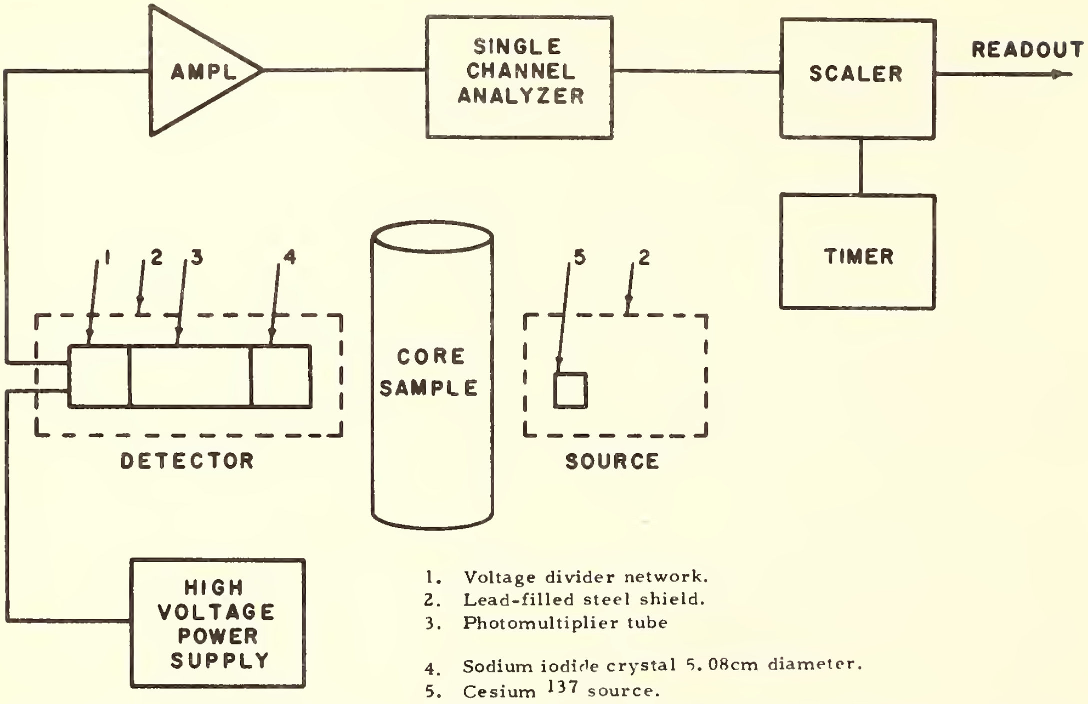
AMPL
SINGLE CHANNEL ANALYZER
SCALER
READOUT
TIMER
1
2
3
4
CORE SAMPLE
5
2
DETECTOR
SOURCE
HIGH VOLTAGE POWER SUPPLY
1. Voltage divider network.
2. Lead-filled steel shield.
3. Photomultiplier tube
4. Sodium iodide crystal 5.08cm diameter.
5. Cesium 137 source.

FIG. 1.—Schematic diagram of the core scintillation counter. Gamma rays from a cesium^{137} source pass through core sample in plastic liner tube, are received by a sodium-iodide crystal and photomultiplier tube, and are displayed on the scaler. Sample attenuates gamma rays according to the bulk density of solid and fluid phases present.

tion may be approximated by the normal or Gaussian distribution having the same mean and variance.

For any sampling process that is approximated by a Gaussian distribution there is the probability that an error greater than one standard deviation will occur for approximately 32% of the data. In terms of the scintillation counter, this means that for a given number of counting periods in a homogeneous material, approximately two-thirds of the counts will be within one standard deviation of the average value, and one-third of the counts will be greater than a standard deviation.

Experimental Verification

To verify experimentally the limitations imposed by the random sampling process, several homogeneous materials were scanned by the scintillation counter. Each sample material was 6.31 cm in diameter. Twenty counting intervals of 10-sec duration each were used for each sample.

The following data were tabulated for each material: (1) average value of the counts for the 20 intervals, and (2) percent deviation from the average for each interval.

A curve of percent deviation vs. the number of counts obtained for each interval was then plotted (fig. 2). From this information it is now possible to observe the effects of random sampling and the resolution capabilities of the system.

In Table 1 it is seen that the average number of counts obtained for an air sample is approximately 17,317. The standard deviation expected for this discrete sampling is

$$\sqrt{17310} = \pm 131 \text{ counts.}$$

The variation from the average $= 131\ (100)/17310 \cong 0.75\%$.

If many points are plotted to obtain a continuous distribution and if a Gaussian distribution applies, then approximately two-thirds of the data should be within a standard deviation or within 0.75% for the air sample. Thus, for the air sample approximately two-thirds of 20 or about 13 or 14 points should have a deviation of 0.75% or less. The same applies for samples other than air which are listed in Table 1 and presented in figure 2. The close agreement between the expected and observed numbers of points experimentally verifies the probability model and demonstrates that the distribution is near Gaussian.

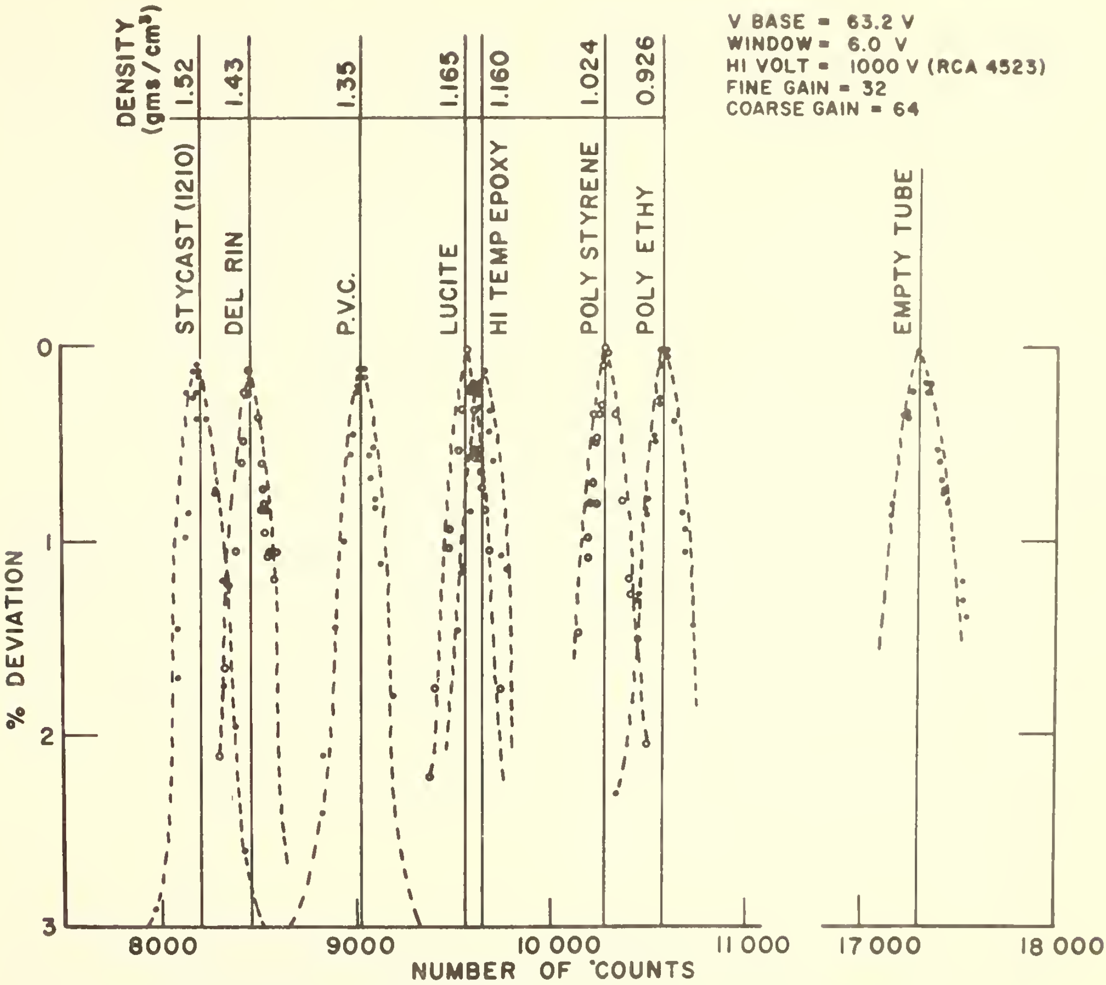

FIG. 2.—Number of counts measured on the core scintillation counter is plotted against percent deviation from the average for each counting interval for samples of different density.

Counting Accuracy

The counting accuracy of the core scintillation counter, in percent deviation from the mean number of counts for a given sample, can be improved by increasing the sampling period or by taking a greater number of samples. For the Gaussian process the number of counts is within $\pm 3\sigma$ of the mean count 99.5% of the time (ITT

TABLE 1.—*Variations in number of counts from different materials*

Material	Air	Poly-ethylene	Poly-styrene	Epoxy	Lucite	PVC	DelRin	Stycast 1210
* Average Value (N)	17317	10581	10280	9651	9577	9034	8467	8212
Std. Deviation ($\sqrt{N}$)	131	102.5	101	98	97.7	95	92	90.6
% Std. Deviation ($\sqrt{N}(100)/N$) expected	0.75	0.97	0.984	1.015	1.02	1.05	1.09	1.1
No. of Points $\geq \sqrt{N}(100)/N$ observed	14 13	14 14	14 14	14 11	14 15	14 15	14 16	14 13
Specific Gravity		0.926	1.02	1.16	1.16	1.35	1.43	1.52

* Taken for 20 observations.

Data, 1961). If the counting accuracy desired is to be $\pm x$ percent of the mean value and if this accuracy is to include almost all the possible statistical variations expected, then the following equations apply:

$$3\sigma = xm$$

or

$$3\sqrt{m} = xm$$

where

m = mean value of counts
x = percent deviation from m
σ = std. deviation = $\sqrt{m}$.

For example, to insure 1 percent accuracy 99.5% of the time (3σ of the counts) requires that the approximate number of counts to be taken through a core section equal $9/(0.01)^2 = 90{,}000$. Thus a minimum of 90,000 counts is required to insure a 1 percent accuracy 99.5% of the time. Table 2 shows the number of counts required to obtain different percentages of deviation about the mean value m 99.5% of the time.

Resolution of Densities

Consider now the problem of deciding if the difference between two counts is statistically significant. Following our consideration of counting accuracy, the simplest method is to compare the difference between the two counts with the square root of each count. If the difference exceeds three times the square root of the count, then a difference actually exists or a rare event has occurred.

For example, let us assume that 1% counting accuracy is desired and that approximately 10,000 counts occur during one counting interval. For 1 percent accuracy we must obtain the sum of nine counting intervals or approximately 90,000 counts. The expected deviation for the accuracy we desire $= \sqrt{90{,}000} = \pm 300$ counts. Note that $10{,}000 = 3\%$ accuracy. We require 3σ to locate 99.5% of the points, $= 3(300) = (900)$. If the number of counts in an adjacent section of the core is 90,900 the difference is 900 counts and there is more than a 99.5% chance that a significant difference exists. A review of figure 2 and Table 1 indicates the degree of separation that was obtained for various materials using only 3% accuracy (approximately 10,000 counts for each point).

If the curves of figure 2 are interpolated toward the 3 percent deviation line, it is observed that two different materials, PVC (density 1.35) and Stycast (density 1.52) may easily be resolved with 3% accuracy and still account for approximately 99.5% of the total points taken. It is also seen that the separation of DelRin (1.43) and Stycast (1.52) can be resolved to within 1% of their mean values but this separation can only be "guaranteed" for two out of three samples or for approximately 66% of the total points taken.

Thus it is seen that the question of resolution of materials depends on the number of counts taken in each sample. The closer the densities of adjacent materials, the greater the number of counts that must be taken to insure a given accuracy.

TABLE 2.—*Minimum number of counts required for specified accuracy 99.5 percent of the time*

Accuracy (percent deviation from the mean number of counts for $\pm 3\sigma$)	Minimum Number of Counts
1	90,000
2	22,500
3	10,000
4	5,630
5	3,600

VARIATION IN COMPTON MASS ATTENUATION COEFFICIENTS

Evaluation of Data

The number of counts is related to the density by the following equation:

$$\rho = \frac{1}{\mu d} \mathrm{Ln} \frac{N_0}{N} \qquad (1)$$

where

ρ = density (gm/cm^3)
μ = Compton mass attenuation coefficient (cm^2 gm^{-1})
d = thickness of material (cm)
N_0 = number of counts in air or water (reference)
N = number of counts obtained for a given material.

In order to utilize Eq. (1) it is necessary that the Compton mass attenuation coefficient μ remain reasonably constant for the various materials to be scanned, or that we know which value of μ to use.

The Compton mass attenuation coefficient, which depends on the gamma-ray energy and the nature of the absorber, is (Evans, 1965)

$$\mu = \sigma_e \frac{Z}{A} N(\mathrm{cm}^2\ \mathrm{gm}^{-1}) \qquad (2)$$

where

σ_e = average collision cross section in cm^2/electron (energy dependent)
N = number of atoms/mole in the absorber
A = atomic weight of the absorber in gm/mole

Z = number of electrons/atom (atomic number)

The work done by Evans (1965) indicates that many homogeneous rock specimens exhibit a reasonably constant Compton mass attenuation coefficient for the constant gamma-ray energy level of the Cs^{137} source used. However, this may not be the case for cores taken at sea where the relative proportions of different sediment compositions and water content vary. Values from Evans (1965) indicate about a 4% variation in μ related to the composition of common minerals:

Mineral	μ
Quartz	0.074
Feldspar	0.074
Shale (Clay)	0.076
Limestone	0.077

Some trial calculations are presented to show the variation in μ for different mixtures of silicon and water. The mass attenuation coefficient for water (Evans, 1965) at an energy level of 0.66 mev (Compton effect region) is approximately 0.082 cm^2/gm. The Compton mass attenuation coefficient for silicon was obtained by interpolation using the Compton mass attenuation coefficient of a nearby element and the relationship:

$$\mu_1 = \mu_2 \frac{A_2}{A_1} \frac{Z_1}{Z_2} = 0.0695$$

where

Z = Atomic number

A = Atomic weight

$\mu_2 = 0.078$ for Al (Evans, 1965).

Assuming a homogeneous mixture of water and silicon, the overall Compton mass attenuation coefficient μ_x for a mixture is given by

$$\mu_x = \mu_1 w_1 + \mu_1 w_2 + \cdots + \mu_n w_n$$

where μ and w are the Compton mass attenuation coefficient and fraction by weight, respectively, of those elements that make up the mixture.

The calculated variation in Compton mass attenuation coefficients for a core of silicon and water (fresh) whose water content varies 25%, 50% and 65% by weight of the total (33%, 100%, 185% water content to dry weight) is as follows:

$$25\%\ H_2O\ 75\%\ Si\ \mu_{mix} = 0.082(0.25) + 0.0695(0.75) = 0.0726$$

$$50\%\ H_2O\ 50\%\ Si\ \mu_{mix} = 0.082(0.5) + 0.0695(0.5) = 0.0758$$

$$65\%\ H_2O\ 35\%\ Si\ \mu_{mix} = 0.082(0.65) + 0.0695(0.35) = 0.0776$$

The calculations indicate that a 40% variation in water content by weight of the total (152% variation in water content to dry weight) in a water-silicon mixture will produce a 6.5% variation in μ. Actual measurements of water content by percent of dry weight in the upper 14 cm of 22 marine sediment cores by Richards (1962, Table 3) range between about 40% and 175%. Variation of water content along the length of a core may be nonlinear. Richards and Keller (1962) show a 75% variation of water content to dry weight along the 3 meter length of one core related to changes of sediment particle size.

The variation in μ with water content is largely determined by the amount of hydrogen present. For most elements which have protons and neutrons μ is roughly independent of atomic number Z because $Z/A \approx 0.45 \pm 0.05$ (Chappell, 1956; Berry, 1961). For hydrogen which has one proton and one electron but lacks a neutron $Z/A \approx 1$. The difference, in Z/A between hydrogen and most other elements significantly affects the value of μ in Eq. (2).

Limitations of a Calibration Curve

The construction of a calibration curve using various materials to determine N_0/N and the directly measured densities (mass/volume) of these same materials can introduce serious errors.

TABLE 3.—*Table of densities* ($gm\ cm^{-3}$)

Material	Directly Measured*	Handbook of Chemistry and Physics	Dupont Polychemicals Dept.	Alcoa
Polyethylene	0.926	0.92		
Polystyrene	1.02		1.06	
Nylon	1.12	1.09–1.14		
Lucite	1.16	1.16–1.2	1.19	
Polyvinylchloride	1.35	1.2–1.7	1.33–1.36–1.39	
Teflon	2.16	2.1–2.3	2.14–2.15	
Magnesium	1.69	1.79–1.83	1.81	
Aluminum (6061)	2.65			2.702
Titanium	4.63	4.5		

* These values were used for plotting figure 3.

TABLE 4

Material	1.27 cm thick		6.31 cm thick		Directly measured density gm cm^{-3} from Table 3
	Average	N_0/N	Average	N_0/N	
Air	15938	1	15771	1	
Polyethylene	14460	1.102	9787	1.61	0.93
Lucite	14174	1.125	8883	1.775	1.16
PVC	14087	1.131	8319	1.895	1.35
Magnesium	13534	1.178	7099	2.22	1.69
Teflon	13239	1.205	6032	2.218	2.16
Aluminum	12580	1.27	4736	3.33	2.65
Titanium	10787	1.48	2068	7.61	4.63

A "calibration curve" was prepared using various homogeneous materials. Density (mass/volume) was directly measured and compared against some published values as indicated in Table 3. These same materials were examined by the core scintillation counter and values of N_0/N determined for each sample. The data are tabulated in Table 4 and plotted in figure 3.

Equation (1) will yield a line with slope $\Delta y/\Delta x = 1/\mu d$ when density (P) vs. N_0/N is plotted. Thus, by measuring $\Delta y/\Delta x$, it is possible to determine μ if d is constant by solving for μ as follows:

$$\mu = \frac{\Delta x}{\Delta y} \cdot \frac{1}{d}$$

When N_0/N vs. ρ was plotted on a semilog graph a straight line resulted (fig. 3) which means that the slope is not constant. Because the diameters of the sample materials were constant the variation in slope is attributed to variations in the Compton mass attenuation coefficient (μ) of the various samples used.

For example, the slope $\Delta y/\Delta x$ about $N_0/N = 2$ in figure 3 is approximately

$$\frac{1.57 - 1.35}{\ln 2.1 - \ln 1.9} = 2.2 \text{ gm/cm}^3.$$

The diameter of the core was 6.35 cm; μ evaluated about the point $N_0/N = 2$ is as follows:

$$\mu = \frac{\Delta x}{\Delta y} \cdot \frac{1}{d} = \frac{1}{2.2 \text{ gm/cm}^3 (0.35 \text{ cm})} = 0.0716 \text{ gm/cm}^2.$$

By the same procedure the mass attenuation co-

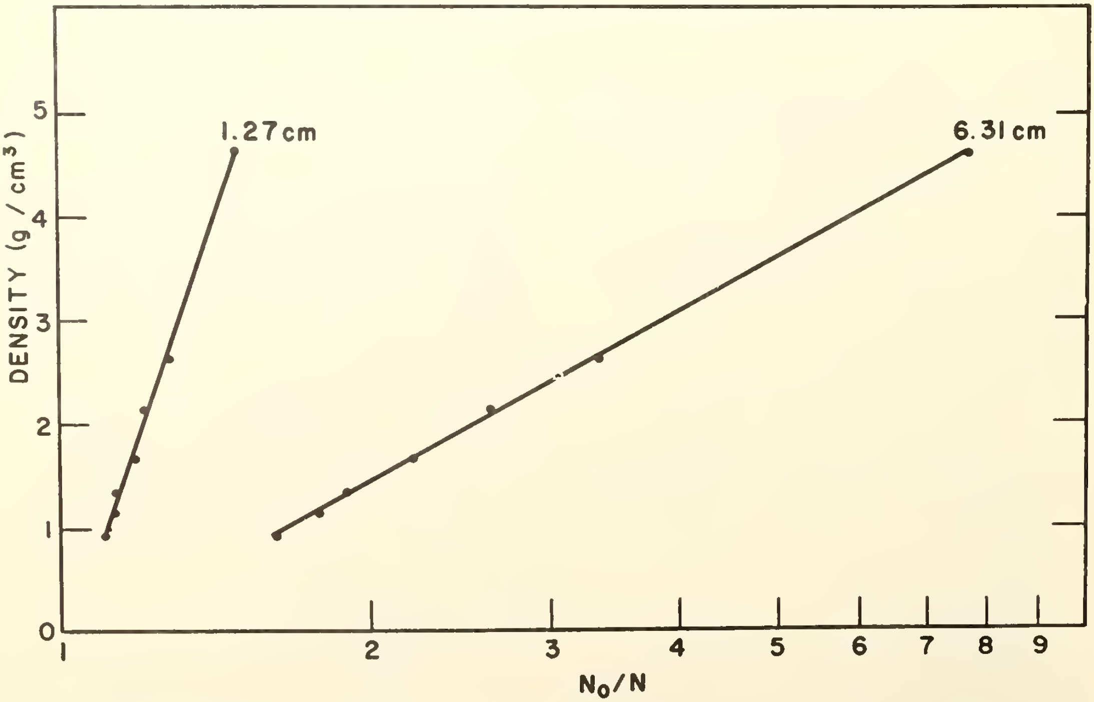

FIG. 3.—Two calibration curves are constructed by plotting number of counts measured by the core scintillation counter against independently known densities of six samples in 1.27 cm and 6.31 cm diameters.

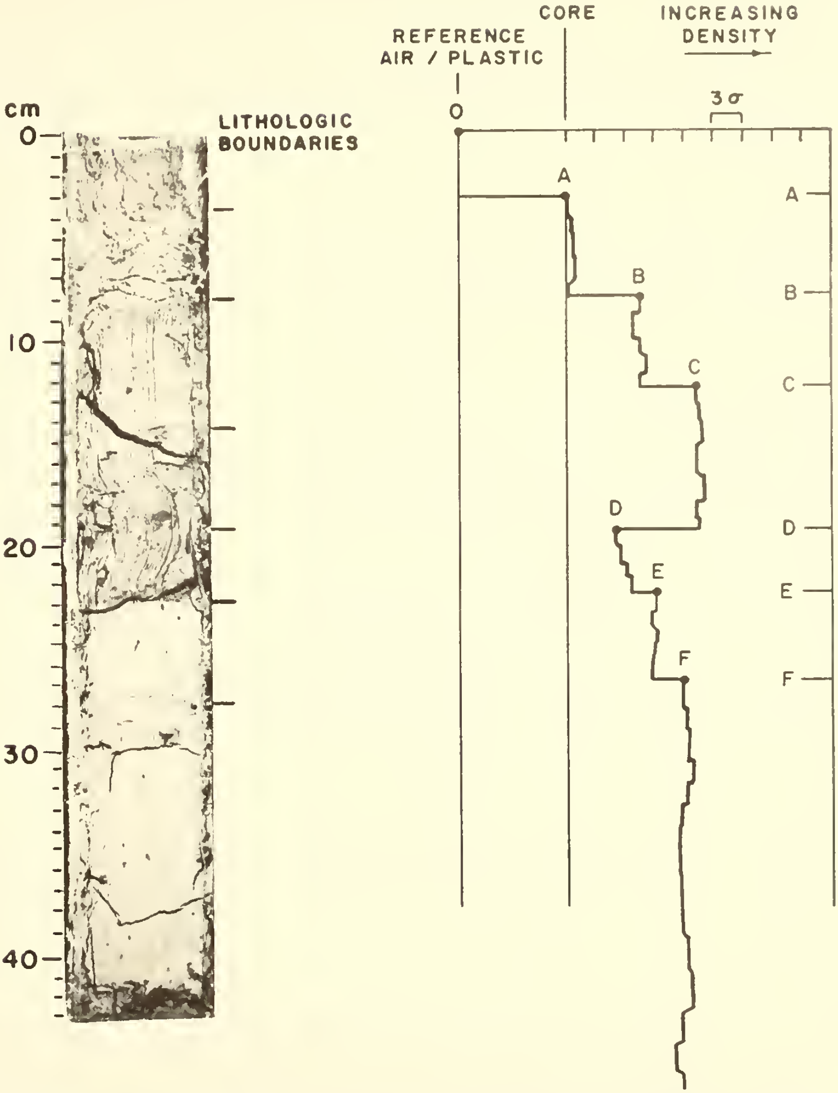

FIG. 4.—Representative analog printout from the core scintillation counter along a photograph of the corresponding sediment core. Bulk density transitions in the core detected by the core scintillation counter are indicated at A, B, C, D, E, F. Lithologic boundaries are also indicated. The magnitude of total statistical variation attributable to the random nature of the radioactive source is shown (3σ).

efficient μ evaluated about the point $N_0/N=4$ is as follows:

$$\mu = \frac{\Delta x}{\Delta y}\cdot\frac{1}{d} = \frac{\ln 4.15 - \ln 3.85}{(3.22 - 3.04)(6.35\text{ cm})} = \frac{0.0750}{0.18(6.35)}$$
$$= 0.0656\text{ gm/cm}^2.$$

Thus it is seen that the mass attenuation coefficients of materials used to construct the sample calibration curve vary. The use of a calibration curve of this type implies one variable, a variation in density, with μ and d constant so that a unique N_0/N is associated with a unique density. Use of a calibration curve where both μ and N_0/N vary as in the sample calibration curve will introduce unknown errors in the determination of density.

Use of a calibration curve constructed from materials of known density to determine unknown densities from measurement of N_0/N is limited by the following conditions: (1) diameter d of the core to be measured should not vary (2) Compton mass attenuation coefficient μ of the core to be measured should remain reasonably constant, and (3) Compton mass attenuation coefficient μ of the samples used to construct the calibration curve should be similar in value to those to be measured because the density is dependent on both μ and N_0/N which may vary independently.

TABLE 5.—*μ assumed constant = 0.076 cm^2 gm^{-1} (after Evans, 1965). d measured = 6.58 cm.*

Core #	Interval below top cm	N_0/N	ln (N_0/N)	$1/\mu d$	Core scintillation counter density ρ_s (μ assumed constant) gm cm^{-3}	Measured wet bulk density ρ_m gm cm^{-3}	Calculated μ from measured wet bulk density cm^2 gm^{-1}
196-2	8.0	$\frac{336208}{174681}=1.925$	.654	1.999	1.307	1.423	.0698
196-2	26.7	$\frac{336208}{166814}=2.015$	.700	1.999	1.399	1.386	.0767
196-2	62.9	$\frac{336208}{170669}=1.970$	.678	1.999	1.355	1.380	.0746
196-3	17.4	$\frac{334037}{159684}=2.092$	.739	1.999	1.477	1.403	.0800
196-3	56.4	$\frac{334037}{153658}=2.174$	.777	1.999	1.401	1.424	.0823
196-3	87.3	$\frac{334037}{153268}=2.179$	.779	1.999	1.557	1.51	.0784
196-4	14.0	$\frac{334422}{162041}=2.064$	.726	1.999	1.451	1.279	.0862
196-4	49.0	$\frac{334422}{153287}=2.182$	.780	1.999	1.559	1.416	.0837
196-4	65.5	$\frac{334422}{151530}=2.207$	.791	1.999	1.581	1.499	.0801
196-8	11.5	$\frac{332631}{162345}=2.049$	.717	1.999	1.433	1.436	.0758
196-8	26.0	$\frac{332631}{161910}=2.054$	.720	1.999	1.439	1.398	.0782
196-8	65.0	$\frac{332631}{151504}=2.196$	.785	1.999	1.569	1.489	.0801

TABLE 5—(*continued*)

Core #	Interval below top cm	N_0/N	ln (N_0/N)	$1/\mu d$	Core scintillation counter density ρ_s (μ assumed constant) gm cm^{-3}	Measured wet bulk density ρ_m gm cm^{-3}	Calculated μ from measured wet bulk density cm^2 gm^{-1}
196-9	21.5	$\frac{334933}{157617}=2.124$	.754	1.999	1.507	1.401	.0817
196-9	44.0	$\frac{334833}{155256}=2.157$	.768	1.999	1.535	1.398	.0834
196-9	63.0	$\frac{334833}{156557}=2.104$	.760	1.999	1.519	1.396	.0827
196-10	12.1	$\frac{338224}{165793}=2.040$	.714	1.999	1.427	1.582	.0685
196-10	45.3	$\frac{338224}{160311}=2.110$	.746	1.999	1.491	1.487	.0770
196-10	79.9	$\frac{338224}{156592}=2.160$	.770	1.999	1.539	1.486	.0787
196-12	17.5	$\frac{334721}{165808}=2.019$	.701	1.999	1.401	1.417	.0751
196-12	38.0	$\frac{334721}{163980}=2.041$	.714	1.999	1.427	1.419	.0764
196-12	55.5	$\frac{334721}{157897}=2.120$	.752	1.999	1.503	1.482	.0771
196-12	65.6	$\frac{334721}{154552}=2.166$	.773	1.999	1.545	1.497	.0784
196-12	91.5	$\frac{334721}{153848}=2.176$	.777	1.999	1.553	1.519	.0777
196-13	44.0	$\frac{335850}{159033}=2.112$	.747	1.999	1.493	1.460	.0777
196-13	81.0	$\frac{335850}{158867}=2.114$	.749	1.999	1.497	1.346	.0845

Measurement of Density with Assumed Constant Compton Attenuation Coefficient

Recognizing that μ varies as a function of sediment composition and water content, it remains impractical to determine a separate μ for each sediment core or sample within a core. Therefore, we made a series of core scintillation counter measurements on which we assumed a constant μ in solving Eq. (1).

The cores were scanned to simultaneously obtain a printed readout and the analog record of the gamma energy passing through the core (fig. 4). A scan rate of 45 mm/min was selected to obtain the optimum overlap for the size of the source/detector aperture and the count rate. The scan rate was sufficiently slow to avoid crossing a possible density horizon without detection. At sections along the core, where possible changes were indicated by a sudden change in the count rate, a notation was made on the core and the analog record. These points are shown as distinct deflections representing either a statistical variation inherent in the energy source or a discrete density horizon within the sedimentary column (fig. 4).

To verify these changes in the count ratio and to establish a 99.5% certainty that these points were within the 1% accuracy, a long count rate was made at each of the observed deflections. For the N_0/N ratio or the counts ratio, 20 counting intervals each of approximately 10-sec duration were taken through the air in the plastic core holder above the water sediment interface. This scan established the count rate of the energy source for a given time period and served as a calibration for each particular core. The subsequent scan down the core is normalized to this count for the density calculation.

To calculate bulk density from Eq. (1), a Compton mass attenuation coefficient μ as described by Evans (1965) was assumed. This μ, which depends upon the gamma-ray energy and the nature of the absorber, is assumed to remain constant for typical geologic materials present in deep sea cores. These calculations yielded the results indicated in Table 5.

Comparison of Core Scintillation Counter Bulk Density with Directly Measured Bulk Density

Direct density measurements were made at intervals in the cores corresponding to the core scintillation counter (μ assumed) measurements as an independent check of accuracy. The cores were split longitudinally and samples were extracted using a 20 cm^3 syringe at the points of deflection noted in the core scintillation counter analog record. The volume of the extracted sample could be read to about ± 0.5 cm^3 on the syringe. The samples were immediately weighed on a Mettler analytical balance to determine wet bulk density (Lambe, 1951). We estimate errors in volume determination up to about 10% as a result of such factors as the presence of voids and the small volume sampled.

Discrepancies in wet bulk density as great as about 0.1 gm cm^{-3} ($\pm 6\%$) were found between core scintillation counter (μ assumed) and direct density measurements (Table 5). The discrepancies in density are the same magnitude as the inaccuracies in measurement of sediment volumes used in the direct density determinations. To compare directly measured density with core scintillation counter sediment bulk density, the accuracy of the direct measurements must be improved.

Calculation of Mass Attenuation Coefficient from Direct Density Measurement

An attempt was made to calculate independently the Compton mass attenuation coefficient (μ) for each sample by substituting the directly measured density and the corresponding measured ratio N_0/N in Eq. (1) and solving for μ (Table 5). The Compton mass attenuation coefficient (μ) derived by this method varies up to about ± 0.010 cm^2 gm^{-1} ($\pm 3\%$) from the μ assumed after Evans (1965). The discrepancy between the calculated and assumed values of μ may be attributed to real variations in sediment composition and water content in the sediment core. Our direct density determinations are not sufficiently accurate to unambiguously determine the variations in μ which we know to exist from considerations of variations in composition and water content.

SUMMARY

A preliminary evaluation was made of two problems encountered in the application of a core scintillation counter to determine wet bulk density in marine sediment cores.

A relationship was derived between the number of scintillation counts obtained in a given material and resolution of densities between adjacent materials. Resolution between different materials depends on the number of scintillation counts taken (fig. 2; Table 2). The statistical deviation of counts about the mean value is inversely proportional to the number of counts.

In order to calculate bulk density from core scintillation counter measurements, the Compton mass attenuation coefficient μ of the sample material measured must be known. In wet marine sediment cores nonlinear variations in water content as much as 152% of dry weight along the length of the core will result in about

6.5% variation in μ which will affect bulk density calculations based on an assumed constant μ in the first decimal place. Assumption of a constant μ in wet marine sediment samples is liable to introduce significant errors in bulk density determinations by the core scintillation counter and imposes limitations on the use of calibration curves.

ACKNOWLEDGEMENTS

The evaluation of the core scintillation counter was undertaken at the request of Dr. John E. Sanders. Dr. C. S. Clay and Dr. T. E. Pochapsky provided valuable advice on physical principles in the operation of the core scintillation counter. Mr. Royce Young and Dr. B. Harris provided helpful engineering advice. Mr. Thomas Farrell provided mechanical engineering support throughout the project. The manuscript was constructively reviewed by Dr. Burton P. Fabricand, Dr. John E. Sanders, and Dr. David Sternberg of Hudson Laboratories.

REFERENCES

Bernhard, R. K., and Chasek, M., 1955, Soil density determination by direct transmission of gamma rays: Am. Soc. Test. Mater. Proc., v. 55, p. 1199–1223.

Berry, P. F., 1961, Gamma-ray attenuation coefficients: Nucleonics, v. 19, p. 62.

Chappell, D. G., 1956. Gamma-ray attenuation: Nucleonics., v. 14, p. 40–41.

Evans, H. B., 1965, GRAPE—A device for continuous determination of material density and porosity: Soc. Prof. Well Log Analysts 6th Am. Symp., v. 2, 25 p.

Harms, J. C., and Choquette, P. W., 1965, Geologic evaluation of a gamma-ray porosity device: Soc. Prof. Well Log Analysts 6th Am. Symp., v. 2, 37 p.

I.T.T. Reference Data for Radio Engineers: Fourth Edition, July 1961, Stratford Press Inc., N.Y., p. 981–990, p. 1117.

Lambe, T. W., 1951, Soil testing for engineers. New York, Wiley, 165 pp.

Laning, J. H., Jr., and Battin, R. H., 1956, Control systems engineering. McGraw-Hill Book Co.

McHenry, J. R., and Dendy, F. E., 1964, Measurement of sediment density by attenuation of transmitted gamma rays: Soil Sci. Soc. America Proc., v. 28, p. 817–822.

Preiss, K., 1968, Non-destructive laboratory measurement of marine sediment density in a core barrel using gamma radiation: Deep-Sea Res., v. 15, p. 401–407.

Richards, A. F., 1962, Investigations of deep-sea sediment cores. II. Mass physical properties: U.S. Navy Hydrographic Office, Technical Report 106, 146 p.

———, and Keller, G. H., 1962, Water content variability in a silty clay core from off Nova Scotia: Limnology and Oceanography, v. 7, p. 426–427.

Van Bavel, C. H. M., Underwood, N., and Ragar, S. R., 1957, Transmission of gamma radiation by soils and soils densitometry. Soil Sci. Soc. America Proc., v. 21, p. 588–591.

Vomocil, J. A., 1954, In situ measurement of soil bulk density: Agric. Engng. St. Joseph, Mo., v. 39, p. 651–654.

Wilson, B. F., 1967, A. E. C. nuclear sediment density probe: A. E. C., ORO-622.

8 Reprinted from Transactions of the Gulf Coast Association of Geological Societies, 281-285, Vol. XIX.

ISOSTATIC GRAVITY MAP OF THE EASTERN CARIBBEAN REGION

SAM A. BUSH
Environmental Science Services Administration
Atlantic Oceanographic and Meteorological Laboratories
Miami, Florida

PATRICIA A. BUSH
Environmental Science Services Administration
Atlantic Oceanographic and Meteorological Laboratories
Miami, Florida

ABSTRACT

Thirty-nine newly reduced gravity stations are incorporated with other published and unpublished data to produce a Pratt-Hayford isostatic gravity map of the Antilles Islands and Venezuelan Basin. Negative and Positive isostatic anomaly belts of the West Indies island arc are delineated.

INTRODUCTION

The historical development of the theory of isostasy and descriptions of diverse isostatic hypotheses are presented by a number of authors (Lyustikh, 1957, Heiskanen and Vening Meinesz, 1958). The two most prominent hypotheses are those of Airy and Pratt. A modification of the latter by Hayford and Bowie (1912) is the basis for the Pratt-Hayford system of isostatic reduction and that which is discussed here.

The Pratt-Hayford hypothesis assumes that topography projecting above sea level has material of relatively low density lying directly below it; the higher the surface, the lower the density. The reverse holds true for the oceans; the deeper the basin, the greater the density of the underlying material. Complete equilibrium (depth of compensation) exists at some uniform depth measured from the solid surface. The depth of compensation assumed for the computations of isostatic reductions in the present paper is 113.7 km.

Partially formulated on exiguous gravity information, varying hypotheses have been proposed by a number of authors (Vening Meinesz *et al.*, 1934; Hess, 1938; Ewing and Worzel, 1954; and Lagaay, 1968) to explain the origin of the West Indies island arc (Fig. 1). The isostatic reduction of thirty-nine additional gravity stations by the authors (Table I) provides data to supplement existing anomalies for the compilation of an isostatic gravity map of the Antilles Islands and Venezuelan Basin (Fig. 2).

METHODS

Mean estimates of topography and bathymetry were made from the latest available charts of the area using templates based on the tables of Hayford and Bowie (1912). A three per cent scale agreement was maintained between templates and chart reading areas.

Compensation and topographic corrections for land compartments, zones A thru O, were taken from Hayford and Bowie (1912). Special topographic and compensation reduction tables for sea stations (Swick, 1942) were used to make corrections for bathymetric readings in zones A thru O. To avoid cumulative errors due to large depth variations, these corrections were tabulated by compartment in units of 10^{-5} cm/sec^2. Corrections for numbered zones 18 thru 11 were obtained according to procedures described by Swick (1942). Numbered zones 10 thru 1 were corrected by interpolations from topographic-isostatic world maps (Heiskanen and Nuotio, 1938). When permissable, interpolated corrections from nearby stations were used for distant zones (Swick, 1942).

No corrections were applied for the gravitational effect of the relatively thin mass between the spheroid and geoid; this indirect effect is comparatively small, especially in ocean areas (Lambert, 1966).

Total isostatic corrections were computed in units of 10^{-4} cm/sec^2, but final gravity anomaly values are rounded to the nearest milligal (Table I).

Accuracy estimate of the corrections to theoretical gravity for the effects of topography and compensation is difficult to make. Template readings of mean bathymetry and/or topography are complicated by uncertainties in station positioning, scale, quality of available charts, and human error. Other possible sources of error are in the acceptance of the assumed mean surface density, the depth of compensation, and the interpolations of corrections for distant zones to the antipodes. Assuming a density of 2.67 gm/cm^3 and a compensation depth of 113.7 km (Hayford and Bowie, 1912), the Pratt-Hayford corrections appearing in Table I have a probable error of ± 2 milligals.

SUMMARY

The theory of isostasy is accepted by most scientists, but no one system of isostatic reduction has been adopted. Although the Pratt-Hayford system of isostatic reduction is not universally accepted, a great number of gravity observations in the Caribbean region have been reduced by this classical method. The anomalies appearing on the gravity map (Fig. 2) incorporate these data with additional stations isostatically reduced by the authors.

ACKNOWLEDGMENTS

Grateful thanks are given to Donald A. Rice for furnishing unpublished U. S. Coast and Geodetic Survey data, to Robert K. Lattimore for furnishing preliminary data from a USC&GSS DISCOVERER cruise, and to Jacob A. Duerksen for earlier discussions.

REFERENCES

Ball, M., C. G. A. Harrison, P. R. Supko, W. Bock, and N. J. Maloney, 1969, Marine geophysical measurement on southern boundary of the Caribbean Sea: submitted to Geol. Soc. America.

STATION IDENT.	STATION SOURCE*	YEAR	LATITUDE	LONGITUDE	STATION DEPTH or ELEVATION (meters)	OBSERVED GRAVITY ** (gals)	THEORETICAL GRAVITY BY INTERNATIONAL FORMULA 1930 (gals)	CORRECTION to THEORETICAL GRAVITY FOR TOPO. & COMP. (gals)	ANOMALY FREE-AIR (mgals)	ANOMALY PRATT-HAYFORD ISOSTATIC*** (mgals)
374-210	1	1947	12°16′N	73° 25′W	-2770	978.132	978.282	-.0388	-150	-111
376-212	↓	↓	11 34	70 45	- 34	.190	.256	+.0216	- 66	- 88
378-214	↓	↓	12 25	70 41	- 79	.326	.287	+.0502	+ 39	- 11
380-216	↓	↓	13 07	70 38	-1223	.266	.314	+.0390	- 48	- 87
381-217	↓	↓	13 22	70 42	-2858	.226	.324	-.0260	- 98	- 72
382-218	↓	↓	13 36	70 39	-4009	.236	.334	-.0661	- 98	- 32
386-222	↓	↓	12 27	67 52	-2950	.168	.288	-.0605	-120	- 60
388-224	↓	↓	11 54	67 53	-1656	.302	.268	-.0050	+ 34	+ 39
390-226	↓	↓	11 15	67 54	-1210	.218	.245	-.0147	- 27	- 12
391-227	↓	↓	10 48	67 54	- 235	.211	.230	+.0142	- 19	- 33
392-228	↓	↓	10 23	65 40	- 74	.155	.216	+.0195	- 61	- 80
393-229	↓	↓	10 46	65 40	-1337	.152	.229	-.0316	- 77	- 45
394-230	↓	↓	11 10	65 40	- 196	.255	.242	+.0465	+ 13	- 34
396-232	↓	↓	11 52	65 37	-2576	.227	.267	-.0551	- 40	+ 15
398-234	↓	↓	12 21	65 39	-4133	.138	.285	-.0816	-147	- 65
400-236	↓	↓	12 27	64 01	-3082	.241	.288	-.0587	- 47	+ 12
402-238	↓	↓	12 07	63 38	- 455	.359	.276	+.0595	+ 83	+ 24
404-240	↓	↓	11 44	63 12	- 732	.209	.262	+.0258	- 53	- 79
406-242	↓	↓	11 27	62 47	- 87	.327	.252	+.0442	+ 75	+ 31
408-244	↓	↓	11 14	62 19	- 95	.237	.244	+.0359	- 7	- 43
410-246	1	1947	10 53	61 50	- 108	.188	.233	+.0270	- 45	- 72
849	2	1949	12 39	62 21	-2910	.208	.296	-.0536	- 88	- 34
850	2	1949	12 19	61 28	- 50	.398	.283	+.0864	+115	+ 29
115	3	1954	17 44	64 40	+ 27	.696†	.527	+.1503	+169	+ 19
2217-28	4		17 56	64 44	-3902	.426	.537	-.0625	-111	- 48
2218-29	↓	1954	18 00	64 44	-3519	.422	.541	-.0496	-119	- 69
2322-7	↓	1955	15 37	62 55	-1986	.421	.422	+.0088	- 1	- 10
2325-9	4	1955	13 37	59 55	- 901	.389	.335	+.0649	+ 54	- 11
563	5	1962	15 01	62 37	-2419	.369	.395	-.0083	- 26	- 18
582	5	1962	15 00	63 26	-1204	.447	.394	+.0491	+ 53	+ 4
179/1230	6	1968	12 01	60 46	-2170	.214	.272	-.0338	- 58	- 24
180/0000	↓	↓	11 37	60 13	-1902	.130	.258	-.0173	-128	-111
/0145	↓	↓	11 29	60 05	-1335	.193	.253	+.0078	- 60	- 68
/0216	↓	↓	11 27	60 03	-1483	.186	.252	+.0008	- 66	- 67
/0732	↓	↓	12 08	59 55	-1125	.207	.276	+.0338	- 69	-103
/1013	↓	↓	12 44	59 37	-1158	.204	.299	+.0469	- 95	-142
180/1053	6	1968	12 51	59 30	- 518	.258	.304	+.0846	- 46	-131
158	7	1969	10 54	65 19	+ 1	.289†	.233	+.0471	+ 56	+ 9
161	7	1969	11°00′N	64° 23′W	+ 1	978.276†	978.236	+.0427	+ 40	- 3

* See Reference;
1. Ewing, M., *et al.*, (1957)
2. Bruins, G. J., *et al.*, (1960)
3. Shurbet, L. G., *et al.*, (1956)
4. Worzel, J. L., (1956)
5. Caputo, M., *et al.*, (1964)
6. ESSA, Ship Discoverer (preliminary data, this paper).
7. Ball, M., *et al.*, (1969)

** Values are referred to 980.118 gals (Potsdam System) at Commerce Building Base, Wahington, D. C.

***Depth of compensation, 113.7 km.

† Corrected for elevation; vertical gradient +0.3086 mgals/m.

Table I. Principal facts at gravity stations.

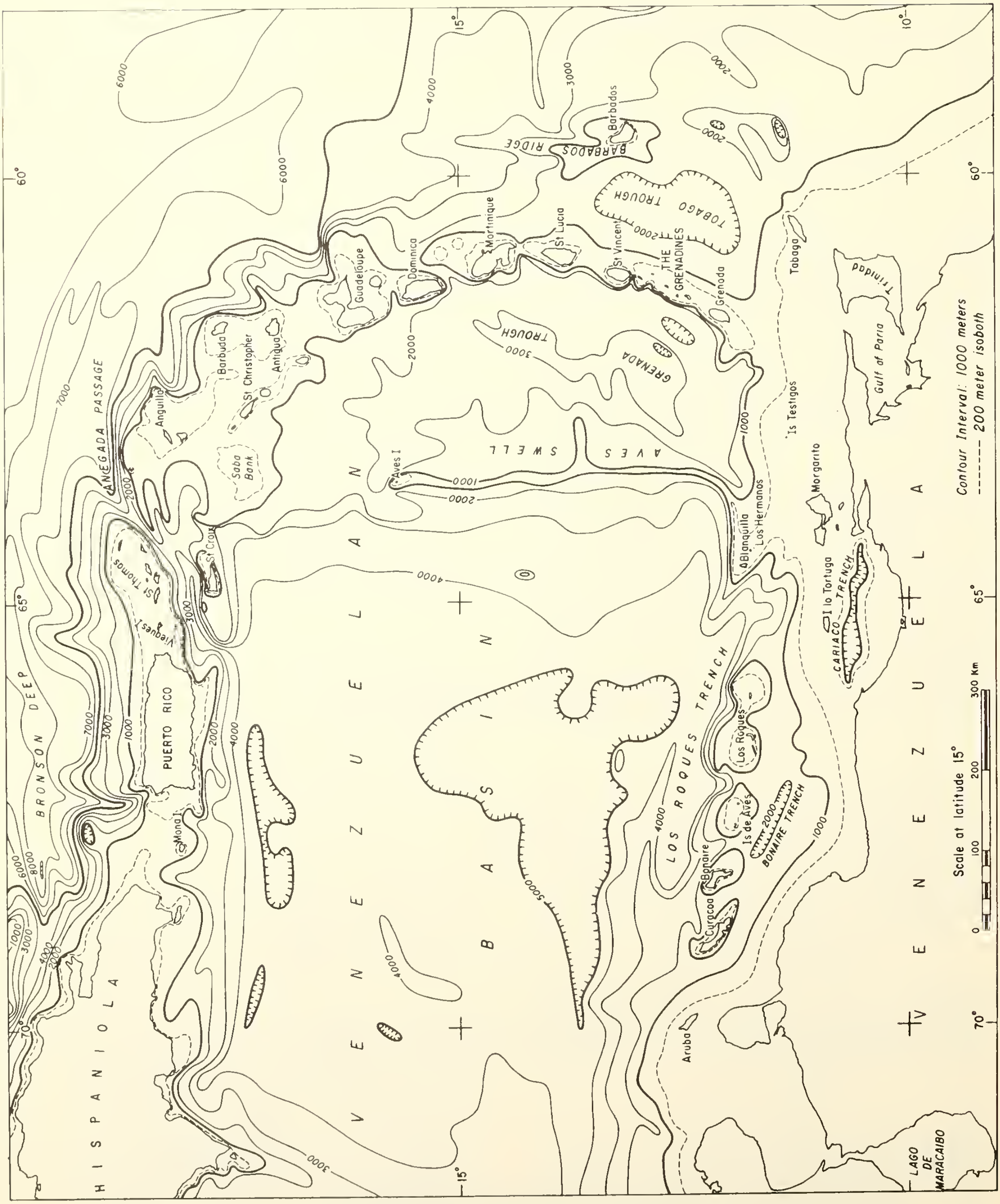

Figure 1. Location and generalized bathymetric map of the Antilles Islands and Venezuelan Basin.

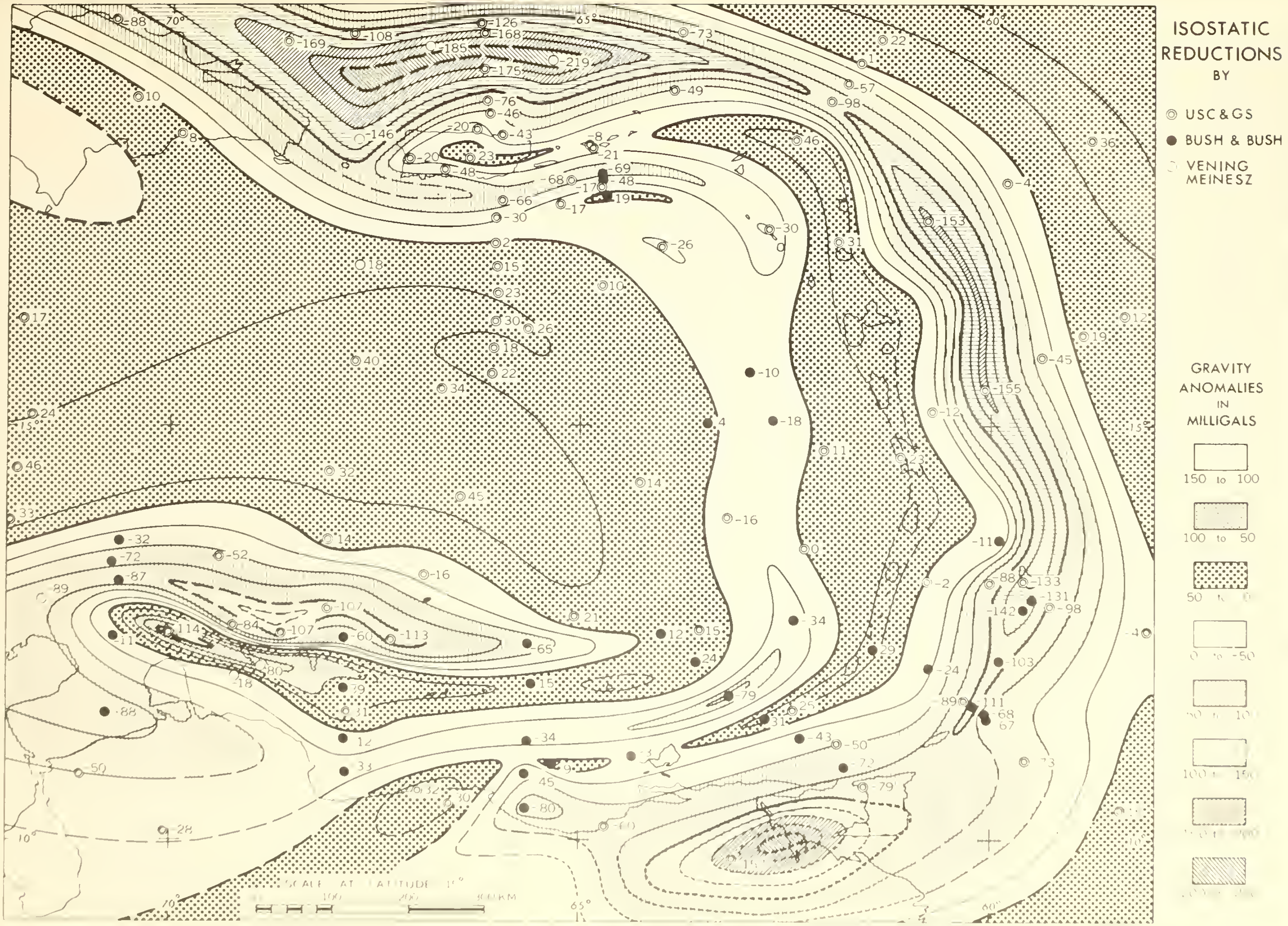

Figure 2. Pratt-Hayford isostatic gravity map of the Antilles Islands and Venezuelan Basin. Depth of compensation. 113.7 km. Short dashed contours are from an unpublished *USC&GS* Map. Long dashed contours are inferred. *USC&GS* isostatic reductions are for gravity observations from the following 1936-1937 Barracuda cruise (Ewing, 1957); 1953 Diablo and 1954 Conger III cruises, 1938 expedition of the Netherland's H.M.S. O 12, 1928 West Indies expedition of the U.S.S. 21, Hispaniola -Puerto Rico and Venezuela (*C&GS* files). Bush and Bush: see Table I. Vening Meinesz (1948) 1926 cruise of the Netherland's H.M.S. K XIII with indirect effect removed.

Bruins, G. J., R. Dorrestein, H. J. A. Vesseur, G. Bakker, and L. Otto, 1960, Gravity expeditions at sea, 1948-1958: Vol. V, Part I. Netherlands Geod. Comm., Delft, 111 p.

Caputo, M., R. Masada, M. Helfer, and C. L. Hager, 1964, Gravity measurements in the Atlantic, Pacific and Indian Oceans, May 1962–August 1963 (R/V ARGO): Inst. of Geophys. and Planetary Sci., UCLA, Interim Report.

Ewing, M., and J. L. Worzel, 1954, Gravity anomalies and structure of the West Indies, Part 1: Geol. Soc. America Bull., v. 65, p. 165-174.

—— and G. L. Shurbet, 1957, Gravity observations at sea in U. S. submarines Barracuda, Tusk, Conger, Argonaut and Medregal: In: A. van Weelden (editor), Geodenkboek, F. A. Vening Meinesz., N. V. Boek-en Kunstdrukkerij, V/H mouton and Co., 'S-Gravenhage 1957, p. 49-115.

Hayford, J. F., and W. Bowie, 1912, The effect of topography and isostatic compensation upon the intensity of gravity: Spec. Pub. No. 10, U. S. Dept. of Commerce, Coast and Geodetic Survey, p. 5-129.

Heiskanen, W., and U. Nuotio, 1938, Topographic-isostatic world maps of the effect of the Hayford zones 10, 9, 8, and 7 to 1: Publ. Isos. Inst. IAG, Helsinki, No. 3.

—— and F. A. Vening Meinesz, 1958, The earth and its gravity field: McGraw-Hill Book Co., New York, 453 p.

Hess, H. H., 1938, Gravity anomalies and island arc structure with particular reference to the West Indies: Proceedings, American Philosophical Society, v. 79, I, p. 71-96.

Lagaay, R. A., 1968, The gravity field of the Southern Caribbean: Abst., Symposium on investigation and resources of the Caribbean Sea and adjacent regions, Willemstad, Curacao, p. 29.

Lambert, W. D., 1966, The isostatic reduction of gravity data and its indirect effect: In: Orlin (editor) Gravity anomalies: unsurveyed areas, Amer. Geophys. Union, Geophys. Mon. 9, p. 81-84.

Lyustikh, E. N., 1957, Isostasy and isostatic hypotheses: Geophysics Institute, Acad. Sci. USSR, Transactions 38:165 translated by Consultants Bureau, New York and published by American Geophysical Union, Soviet Research in Geophys., v. 2, 1960, p. 3-45.

Shurbet, G. L., J. L. Worzel and M. Ewing, 1956, Gravity measurements in the Virgin Islands: Geol. Soc. America Bull., v. 67, p. 1929-1936.

Swick, C. H., 1942, Pendulum gravity measurements and isostatic reductions: Spec. Pub. No. 232, U. S. Dept. of Commerce, Coast and Geodetic Survey, p. 65-75.

Vening Meinesz, F. A., 1948, Gravity expeditions at sea, 1923-1938, Vol. IV: Netherlands Geod. Comm., Delft, 233 p.

—— J. H. F. Umbrgrove, and Ph. H. Kuenen, 1934 Gravity expeditions at sea, 1923-1932, Vol. II: Netherlands Geod. Comm., Delft, 108 p.

Worzel, J. L., 1965, Pendulum gravity measurements at sea, 1936-1939: New York, John Wiley and Sons, 422 p.

Deep-Sea Research, 1969, Vol. 16, pp. 655 to 660. Pergamon Press. Printed in Great Britain.

SHORTER CONTRIBUTION

Trincomalee and associated canyons, Ceylon

Sam A. Bush* and Patricia A. Bush*

(*Received* 25 *March* 1969)

Abstract—Trincomalee and associated canyons conform to Ceylon's geological structure. Trincomalee Canyon crosses the insular shelf and slope with a general northeast trend similar to the strike of charnockite-khondalite series found on the island. Deviations in the canyon's strike result from joint planes and tectonic deformation. Two secondary canyons which also trend northeast align with north and south contact zones of Wanni gneisses and charnockite–khondalites.

INTRODUCTION

As part of the 1964 International Indian Ocean Expedition, the USC & GSS *Pioneer* conducted a detailed bathymetric and geophysical survey over Trincomalee and two associated canyons (Fig. 1).

Trincomalee Canyon was first noted in 1908 when Somerville discussed several deep and narrow notches in the submarine plateau off the east coast of Ceylon (Adams, 1929a). Shepard (1963) published an inshore bathymetric map and described a branching, rock-walled canyon with heads in Trincomalee Harbor and Koddiyar Bay. Data collected by the *Pioneer* in 1964 were used by Shepard and Dill (1966) to expand Shepard's earlier compilation.

GEOLOGY

Rocks of the Koddiyar Bay area (Fig. 2) consist of biotite gneiss basement rock overlain by charnockite–khondalite series and Wanni gneisses. Khondalites are metamorphic rocks that have been intruded by charnockites. The younger Wanni gneisses outcrop both northwest and southeast of the charnockite–khondalite series. Adams (1929a, b) and Coates (1935) place the Wanni gneiss and charnockite–khondalite ages as Early Precambrian. Afanassyev, Borisovich and Shanin (1964) reported K–Ar whole rock ages approximating 800 million years for charnockites on Ceylon, but Aswathanarayana (1968) substantiates the Early Precambrian. Using Rb–Sr methods, he dates one group of charnockites as older than 2100 million years and mentions a younger group (1660 ± 250 million years).

In the vicinity of Koddiyar Bay, Wanni gneiss and charnockite–khondalite formations strike northeast with strong evidence of folding. According to Coates (1935) a road between the towns of Nilaveli and Trincomalee crosses the strike of two charnockite–khondalite ridges. The first ridge, 6 km wide, lies just south of Nilaveli, and the second, 1 km wide, lies immediately north of Trincomalee. At these two localities the dips are nearly vertical, but decrease southeast of Trincomalee until a northwest–southeast anticlinal arch can be seen at Dutch Point (Fig. 2). Southeast of Dutch Point the dip returns to nearly vertical (Coates, 1935).

Reversal in dip and outcropping of younger Wanni gneisses on northwest and southeast sides of the charnockite–khondalite series indicates the existence of a northeast trending synclinal fold with its axis in Koddiyar Bay.

BATHYMETRY

Within the area of this investigation the dominant feature is northeast trending Trincomalee Canyon (Figs. 2 and 3). Two of its principal heads are located in Koddiyar Bay and a third in

[*] Environmental Science Services Administration, Atlantic Oceanographic Laboratories, Miami, Florida 33130.

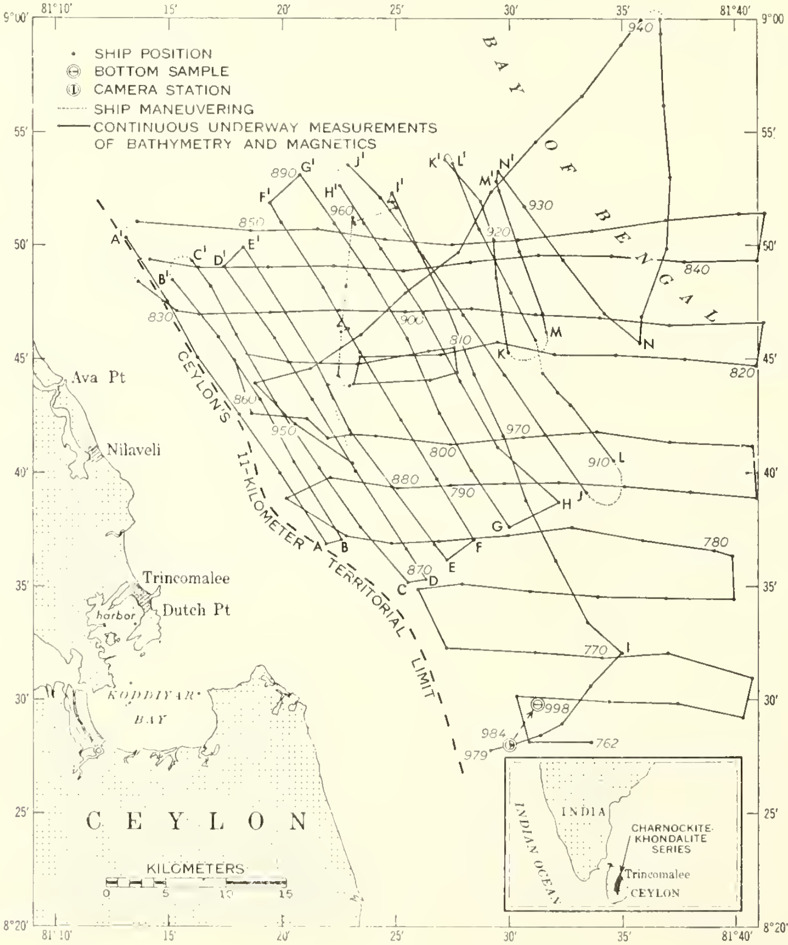

Fig.1. Index chart showing a section of track run by USC & GS Ship *Pioneer*. Positioning was established by astronomical fix, but track was adjusted on the basis of bathymetric (PDR) crossings. Broken line with arrow indicates direction and drift of underwater camera.

Trincomalee Harbor. Two tributaries enter the canyon from the south. On the broad ridge northwest of Trincomalee Canyon a northeast trending sea valley originates (Fig. 2). The valley bends east, is deflected by a rise in bottom topography (Fig. 3, profiles K–K′ to N–N′), and continues northeast parallel to Trincomalee Canyon.

Northwest of and parallel to Trincomalee Canyon is a canyon herein named North Trinco Canyon* (Figs. 2 and 3). Three northeast trending tributaries cross the insular slope and debouch into it from the west. A shoreward projection of North Trinco Canyon aligns with the northern contact zone of Wanni gneiss and charnockite–khondalite.

Southeast of and parallel to Trincomalee and North Trinco canyons is another canyon herein named South Trinco Canyon* (Figs. 2 and 3). One east and two northeast trending tributaries originate on the insular slope and debouch into it from the west. A shoreward projection of South Trinco Canyon aligns with the southern contact zone of Wanni gneiss and charnockite–khondalite.

*The authors have named the features to the north and south of Trincomalee Canyon, respectively North and South Trinco canyons. A town, harbor and submarine canyon named Trincomalee now exist within the same small geographical area, so these names are given a shortened form in keeping with the modern trend toward brevity.

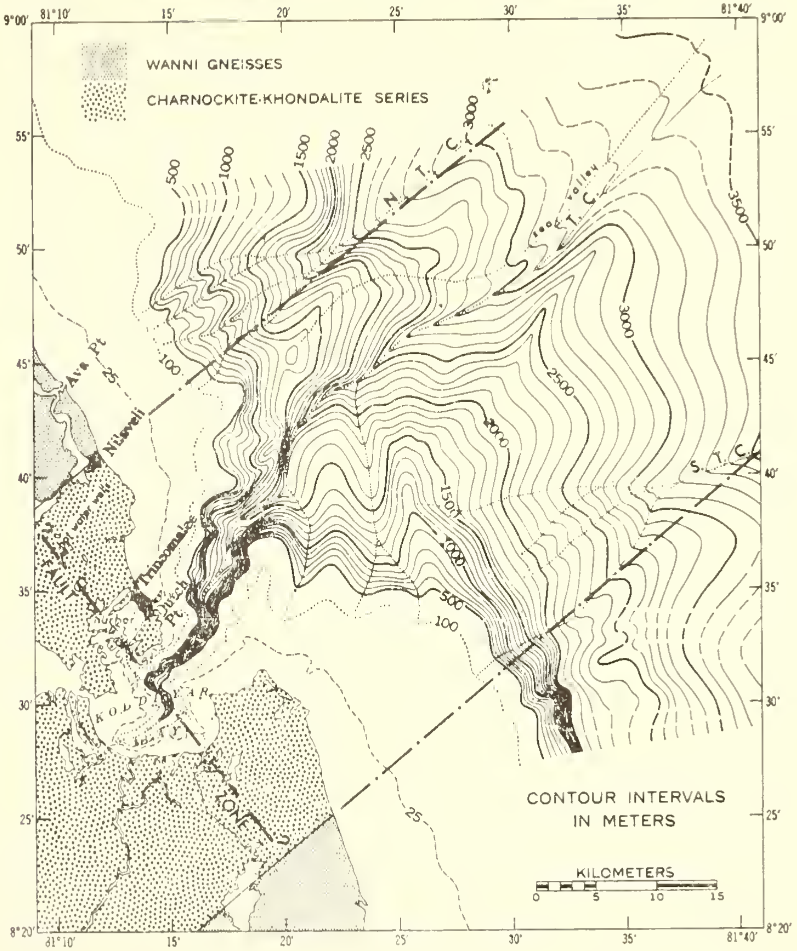

Fig. 2. Bathymetric chart contoured from PDR soundings (corrected) of the USC & GS Ship *Pioneer*. Data shoreward of Ceylon's territorial limit (Fig. 1) compiled from H. O. 3689. Dotted lines show axes of North Trinco Canyon (N.T.C.), Trincomalee Canyon (T.C.), South Trinco Canyon (S.T.C.), their tributaries, and a sea valley. Dot-dashed lines show assumed contact zones of Wanni gneisses and charnockite–khondalites. Light dashed contour lines are over areas containing fragmentary data. Heavy dashed line is the projection of Trincomalee Canyon's northwest–southeast trending segment and possible fault zone. Lengths, average gradients, and maximum wall heights of North Trinco, Trincomalee, and South Trinco canyons are respectively: 29 km, 100 m/km, 900 m; 59 km, 54 m/km, 1560 m; 28 km, 107 m/km, 350 m.

MAGNETICS

A Varian nuclear precession magnetometer recorded continuous total intensity measurements of the earth's magnetic field. The nearest magnetic observatory located near Bombay, India, furnished magnetograms which indicated such a slight diurnal variation that it has been disregarded in this study. Because of the small geographic extent encompassed by the survey, a constant of 40,450 gammas was assumed to be the value for the earth's main field (U.S. Naval Oceanographic Office, 1966). Removing this constant from total field values and contouring the resultant field (Fig. 4) leaves a gentle gradient varying from − 50 gammas in the southeast to − 300 gammas in the northwest.

Elongation of the magnetic trends along the projected contact zones of Wanni gneisses and charnockite–khondalites suggests a continuation of these rock series on to the insular slope.

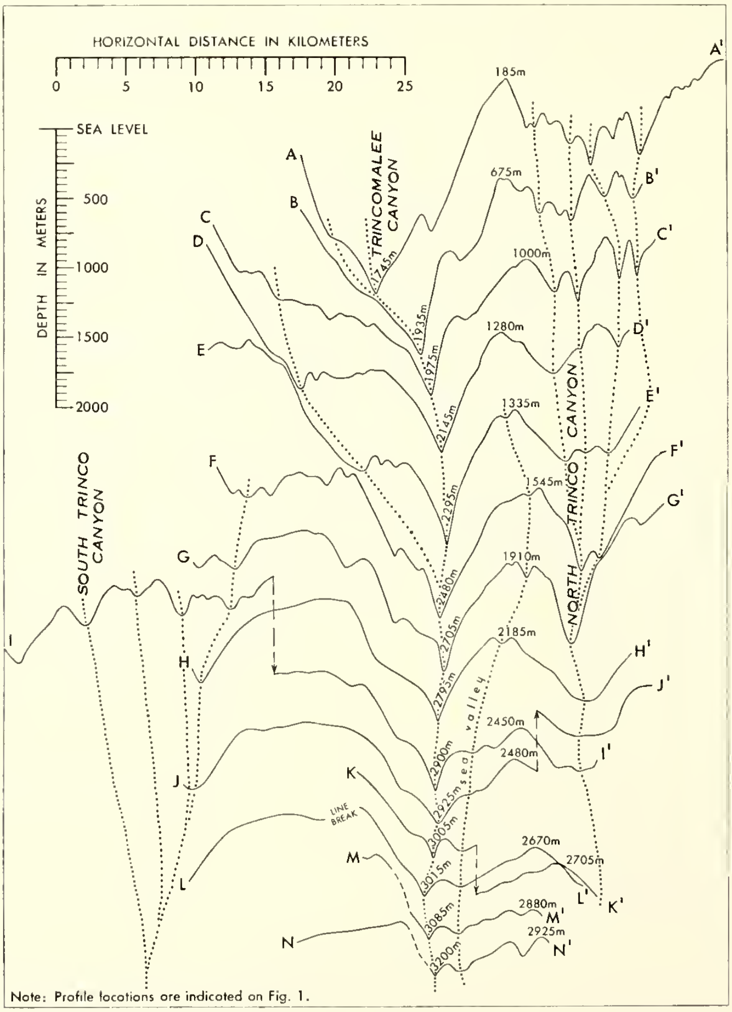

Fig. 3. Bathymetric profiles of Trincomalee and associated canyons. Vertical exaggeration is 10:1. Axes of canyons, their tributaries, and a sea valley are shown by dotted lines based on USC & GS Ship *Pioneer's* PDR data and their interpretation (Fig. 2). Broken lines with arrows indicate where profiles are broken to keep them in proper perspective (Fig. 1).

BOTTOM PHOTOGRAPHY AND DREDGING

One camera lowering was made at ship's position 984 (Fig. 1). Bottom photographs revealed a flat bottom which appeared to be composed of fine-grained sediments. As the camera drifted across the insular shelf it crossed over a rock outcrop and detritus (Fig. 5). Seaward from the talus, photographs of the bottom appear similar to the flat bottom shown landward from the outcrop. Near ship's position 998 (Fig. 1) the camera passed over an extremely steep slope (International Indian Ocean Expedition, U.S.C. and G.S. Ship *Pioneer*—1964. 1965, Vol. 1). At this location the camera was retrieved, and a chain dredge was lowered over the side. The dredge haul recovered "eight chunks of medium-grained saccharoidal dark green to black igneous rock," (International Indian Ocean Expedition, U.S.C. and G.S. Ship *Pioneer*—1964. 1965, Vol. 2).

The field description of these rocks suggests a similarity to rocks found in the Koddiyar Bay area by Coates (1935).

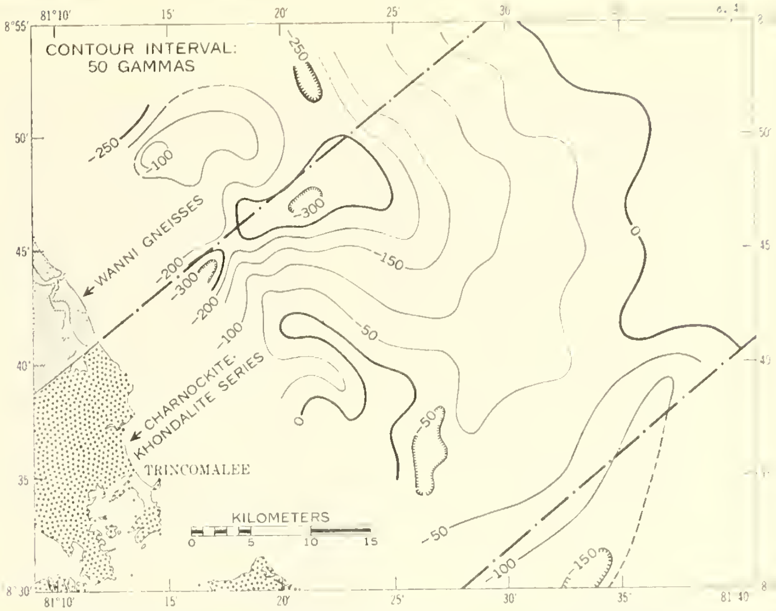

Fig. 4. Residual magnetic field off northeast Ceylon. Dot-dashed lines indicate projected contact zones of Wanni gneisses and charnockite–khondalites. Note elongation of magnetic trends along lines of projection.

DISCUSSION

The epeirogenic history of Ceylon has been positive with some minor oscillations. The last major uplift was pre-Miocene (Krishnan, 1953) when, according to Adams (1929a) the island was raised approximately 460 m above sea level. Ensuing peneplanation formed the present coastal plains which were incised before their submergence in the Miocene sea (Adams, 1929a). During this period of erosion, Trincomalee Canyon was probably cut along the axis of a synclinal fold and served as the major flume for denudation. Submergence was followed by a positive movement that raised the present insular shelf up to or slightly above sea level (Adams, 1929a). North and South Trinco were likely cut during this emergent period. Subsequent oscillations returned Ceylon to its present elevation. Feeder channels cutting across the shelf into North and South Trinco canyons were presumably buried during the depositional cycle following the last glacial stage of the Pleistocene. Trincomalee Canyon remained open because of its greater width and steeper gradient.

Like the major rock units of this area, Trincomalee Canyon has a general northeast strike. In Koddiyar Bay the axis of its main head trends northeast approximately 4 km, abruptly turns 90° northwest for a distance of 3 km, and again bends 90° northeast. The canyon's two remaining heads are in alignment with a landward projection (Fig. 2) of the northwest-southeast striking 3 km segment of Trincomalee Canyon. The northwest projection crosses a quartzite ridge (Shepard and Dill, 1966) and aligns with a series of hot water wells and lakes (U.S. Hydrographic Chart 3689, 1949). The southeast projection aligns with a river mouth and series of lakes. It seems plausible that this lateral offset in Trincomalee Canyon's axis is the result of a major fault. Sharp bends which alter the northeasterly course of Trincomalee Canyon as it crosses the insular shelf are probably due to structural control. According to Adams (1929a) the rivers on Ceylon frequently cross quartzite ridges along joint planes so it seems reasonable to assume that joint planes may have deflected Trincomalee's path.

North and South Trinco canyons are very similar in structure. With one exception their tributaries trend northeast and enter their respective canyons from the west. Both canyons strike northeast parallel to Trincomalee Canyon, and both canyons are apparently cut along Wanni gneiss and charnockite–khondalite contact zones.

That surface geology on Ceylon continues across the insular slope is established by (1) agreement of major rock unit strikes with submarine canyon trends; (2) alignment of North and South Trinco canyons with contact zones of Wanni gneisses and charnockite–khondalites; (3) alignment of the broad ridge between North Trinco and Trincomalee canyons with the 6 km wide quartzite ridge between Nilaveli and the town of Trincomalee; (4) elongation of magnetic trends along Wanni gneiss and charnockite–khondalite contact zones; (5) rock outcrops on the insular shelf; and (6) rock type recovered from the insular slope.

Acknowledgements—We are indebted to the officers and men aboard the USC & GS Ship *Pioneer* and to members of the Atlantic Oceanographic Laboratories. We are particularly grateful to Dr. H. B. STEWART, JR. for the loan of his personal field notes and to Mr. R. K. LATTIMORE for his manuscript edits.

REFERENCES

ADAMS F. D. (1929a) The geology of Ceylon. *Can. J. Res.* **5**, 425–465.

ADAMS F. D. (1929b) The geology of Ceylon. *Can. J. Res.* **6**, 467–510.

AFANASSYEV G. D., I. V. BORISOVICH and L. L. SHANIN (1964) On the K–Ar age of certain rocks of the Indian peninsula and the Isle of Ceylon. *Dokl. sov. geologov. na 22-i sessii Mezhdunar. geol. Kongr.* Izd-vo Akad. Nauk SSSR.

ASWATHANARAYANA U. (1968) Precambrian geochronology of peninsular India and Ceylon; a reinterpretation. *Bull. geol. Soc. India* **5**, 63–64.

COATES J. S. (1935) The geology of Ceylon. Section B, Zoology and Geology. (*Spolia Zeylancia*). *Ceylon. J. Sci.* **19**, part 2, 101–191.

KRISHNAN F. N. I. (1953) The structural and tectonic history of India. *Mem. geol. Surv. India* **81**, 80–81.

INTERNATIONAL INDIAN OCEAN EXPEDITION, 1965, Vol. 1.

INTERNATIONAL INDIAN OCEAN EXPEDITION, 1965, Vol. 2.

SHEPARD F. P. (1963) Submarine canyons. In: *The Sea*, M. N. HILL, ed. Wiley, New York, **3**, pp. 480–506.

SHEPARD F. P. and R. F. DILL (1966) *Submarine canyons and other sea valleys.* Rand McNally & Co., pp. 203–204.

U.S. DEPARTMENT OF COMMERCE, ENVIRONMENTAL SCIENCE SERVICES ADMINISTRATION (1965) International Indian Ocean Expedition, USC & GS Ship *Pioneer*—1964. U.S. Govt. Printing Office, **1**, 53–58.

U.S. DEPARTMENT OF COMMERCE, ENVIRONMENTAL SCIENCE SERVICES ADMINISTRATION (1965) International Indian Ocean Expedition, USC & GS Ship *Pioneer*—1964. U.S. Govt. Printing Office **2**, 169.

U.S. NAVAL OCEANOGRAPHIC OFFICE (1966) The total intensity of the earth's magnetic force. Chart 1703, 3rd edition.

U.S. NAVY HYDROGRAPHIC OFFICE (1949) Approaches to Trincomalee. Chart 3689, 2nd edition.

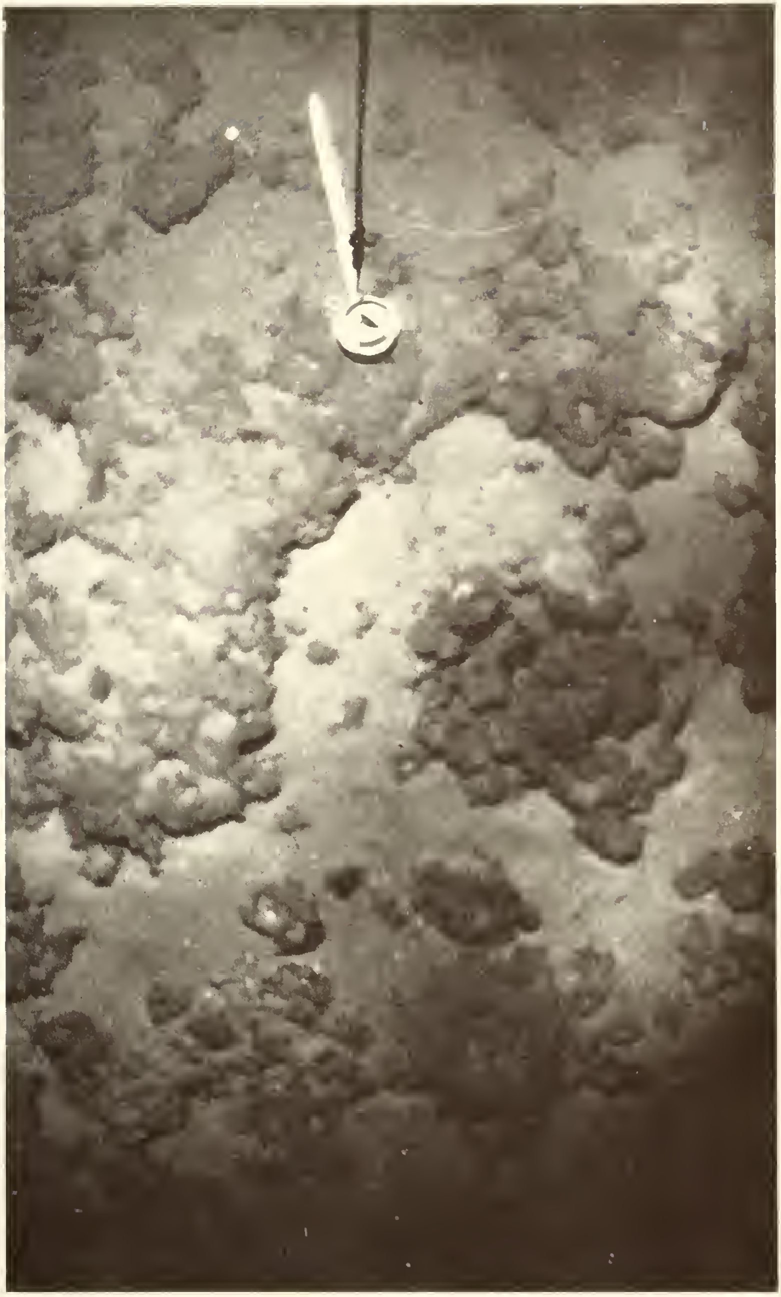

Fig. 5. Bottom photograph of rock out-crop and talus. General location shown on Fig. 1.

Reprinted from Oceans Vol. 2, No. 1, 7-15.

OCEAN BASINS AND LUNAR SEAS

NASA

Lick Observatory

by Robert S. Dietz

As we know from gazing at the moon, even with naked eye, the lunar surface displays dark and light realms. From early times, Man has tried to relate the dark lunar regions to earth's own ocean basins.

Aristotle, whose views held sway for two millenia, proposed the bizarre notion that the moon was a perfect mirror reflecting the earth's features. Thus, he supposed the dark regions on the lunar disk were a miniaturized view of all the world's oceans.

In May 1609, Galileo pointed the first telescope (of his own invention) toward the moon and saw the lunar surface more clearly than anyone before. At variance with Aristotelian philosophy, he observed that the moon is not smooth, but covered with craters, mountains and dark, flat basins.

In his *Sidereus Nuntius* (Venice 1610) Galileo recorded these first impressions: "I feel sure that the surface of the Moon is not perfectly smooth, free from inequities and exactly spherical as a large school of philosophers considers...but that, on the contrary, it is full of inequalities, uneven, full of hollows and protuberances just like the Earth itself."

When hearing of this discovery, conservative philosophers of the day allowed that this might be so but added that these irregularities must be, in turn, covered by a transparent or crystalline layer which filled all the cavities and made the surface of the moon perfectly smooth after all. Galileo retorted with an answer precisely suited to the merit of this argument. "Let them be careful. For if they provoke me too far, I will erect on their crystalline shell invisible crystalline mountains ten times as high as any I have yet described."

It remained for the astronomer Kepler several years later to clearly identify the dark regions as seas and the light areas as uplands or continents. He wrote: *"Do maculus esse maria, do lucidas esse terras."* ("The dark areas I take to be seas, the light areas I take to be uplands.") His use of the term *maria* (Latin for seas; singular—mare) persists to this day, with the dark lunar basins bearing interesting names that indicate weather or states of mind, such as Mare Imbrium (Sea of Storms); Mare Humorum (Sea of Vapors); Mare Tranquilitatis (Sea of Tranquility); Mare Crisium (Sea of Crisis); and Mare Serenitatis (Sea of Serenity).

Kepler believed there was a lunar hydrosphere forming seas and also that there were lunar inhabitants. At least certain craters he attributed to the result of their labors.

Following Kepler, other astronomers for the next century or so thought the maria to be water-filled depressions entirely like earth's ocean basins. With the advent of more powerful telescopes, it soon became evident that the maria are dry. It was probably Schroeter (about 1800) who finally consigned any concept of a lunar hydrosphere to limbo by his discovery that the maria surfaces are not perfectly smooth but covered with numerous, sinuous ridges and crevices (rilles).

But the idea persists even yet that the maria may be fossil oceans that somehow dried up—or at least that the maria originated in the same manner as the ocean basins on earth. There are, in fact, some suggestive similarities between maria and ocean basins. Both are vast depressions in planetary crusts; both are floored with a dark deposit presumed to be the volcanic rock basalt; and both have smooth expanses as compared to the rugged upland terrane.

We will not have to wait long to acquire fresh insight about the lunar seas, for an astronaut from the United States is scheduled to land on the moon this month. When astronauts return lunar rock samples to earth for analysis, one wonders what their composition will be. Are the smooth floors of maria made up of sedimentary layers deposited in some now dessicated ancient sea? Is the dark coloration of the maria due not to basalt but to dispersed organic matter—the dead husks of bygone life? Will fossils of archaic life be discovered? Man will only know for sure by exploring there, but in the interim we can speculate reasonably about the nature of these lunar seas.

While the similarities between maria and ocean basins are intriguing and suggestive, they hardly prove that these two gross features of the moon and earth are of similar origin. In fact, more searching analysis suggests that the maria and the ocean basins actually offer a study in contrasts.

Perhaps the chief lesson we can learn from any foray into comparative planetology is that the moon and the earth are now wholly dissimilar bodies. Without pursuing the subject in detail, let us briefly examine three aspects in which maria differ markedly from ocean basins: there is no general interconnection between the maria; their depths in the lunar crust differ rather than being uniform; and, unlike the earth's ocean basins and continental masses which are counterbalanced, the maria are underlain by heavy rock masses that are out of balance with the lunar uplands.

Before discussing these contrasts, I should point out that certain other dissimilarities may not be meaningful in that they are secondary rather than fundamental aspects of ocean basins. For example, one nearly universal aspect of our ocean basins that would be strikingly revealed were they drained of water is the shallow, flat shelf that fringes all the continents. Although some selenographers (selenologists are scientists who specialize in studying the moon—selenographers deal expressly with its surface features) have described shelves around many of the maria, any such interpretation is farfetched, and actually we can discern no convincing examples on the lunar surface. However, this dissimilarity is not significant, because continental shelves are a secondary aspect of ocean basins created by the interaction of the sea's surface with the continental block.

A dry ocean basin would not have any continental shelves. It is entirely conceivable that a celestial body could have an ocean basin without any water—now or in the past. The earth would have ocean basins even if it had no hydrosphere; the creation of the oceanic basins and their filling with water are separate matters. The presence of water is just an incidental aspect of ocean basins, proving only that water runs downhill seeking its own level. If the lunar maria were, in fact, once filled with water, we should be able to discern a fossil continental shelf dating from the time they dried up. No such shelves are present, which must mean that no large amount of water ever covered the moon. But, again, this argument does not exclude the possibility that lunar maria might be genetically similar to the ocean basins.

Aristotle supposed the moon to be a mirror reflecting the earth's features, the dark regions being the images of the world oceans.

Returning now to the question of contrasts, the first basic difference between earth and moon is the universality of our ocean basin. Although geographers speak of many oceans, all, in fact, interconnect into a worldwide ocean basin above which the continental plateaus rise as isolated islands. Excluding the shelves and all of the semi-continental oceanic regions above ocean depths of 2,000 meters (about 1,100 fathoms), the true oceanic realm still covers 60 percent of the earth. It is the ocean floor that is typical of the earth's surface, not the continental regions.

In contrast, the moon is dominated by the light colored zones (variously called uplands, terra, or the continental regions). The maria mostly are not interconnected, but generally are isolated by uplands into which these basins appear to have been punched. Maria cover only one third of the moon's nearside, while Lunar Orbiter satellites have shown its backside to be free of maria of any importance. The orientation of the moon with most maria always facing toward earth probably results from these basins being heavy. The moon is, of course, gravitationally trapped in orbit by the earth and makes exactly one rotation on its axis for each revolution about earth. Originally the moon was nearer earth and rotated more rapidly, but tidal friction in the earth's oceans slowed the moon's spin until it ultimately became "locked in" with its heavy hemisphere (for there the gravitational pull is greater) always facing earthward.

The second significant contrast is that the floors of the maria have differing levels, while the ocean floor throughout the various oceans has a common level. (A popular opinion prevails that the Atlantic Ocean is shallower than the Pacific. Such a difference does show up on some hypsometric—pertaining to the measurement of elevation—tables and graphs showing ocean levels. It arises when the broad continental shelves of the Atlantic are included as ocean basin features; these are geologically part of the continent. If you consider the basins alone, there is no large difference between the Atlantic and Pacific Oceans.)

If we compare the hypsographic curves for the earth and moon, we find that the earth is characterized by two levels. The continental level averages 500 meters (about 1,650 feet) above sea level and the ocean floor, 4,120 meters (approximately 13,400 feet) below sea level. Thus, the earth has a bimodal (two-group) distribution of land levels separated by the abrupt continental slopes. The hypsographic curve of the moon reveals no such preferential levels, as the maria vary in depth, with Mare Imbrium and Mare Humorum being the deepest.

The hypsometric curves reveal fundamental properties of both celestial bodies. A bimodal distribution for the earth is consistent with the fact that the ocean basins are free of continental-type rock (sial or, loosely speaking, "granite") and are essentially areas where the earth's crust is missing and the upper mantle is exposed. In loftier terms, the earth

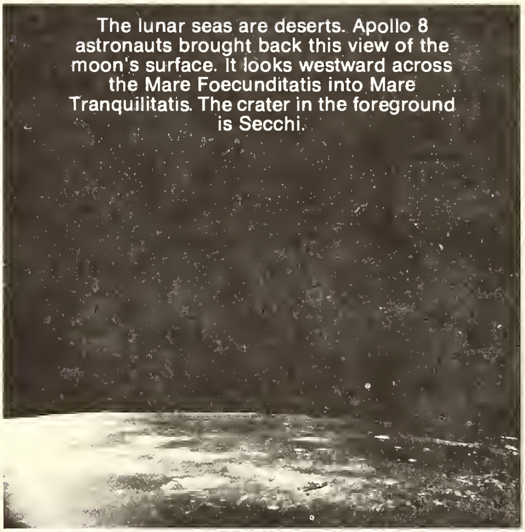
The lunar seas are deserts. Apollo 8 astronauts brought back this view of the moon's surface. It looks westward across the Mare Foecunditatis into Mare Tranquilitatis. The crater in the foreground is Secchi.

NASA

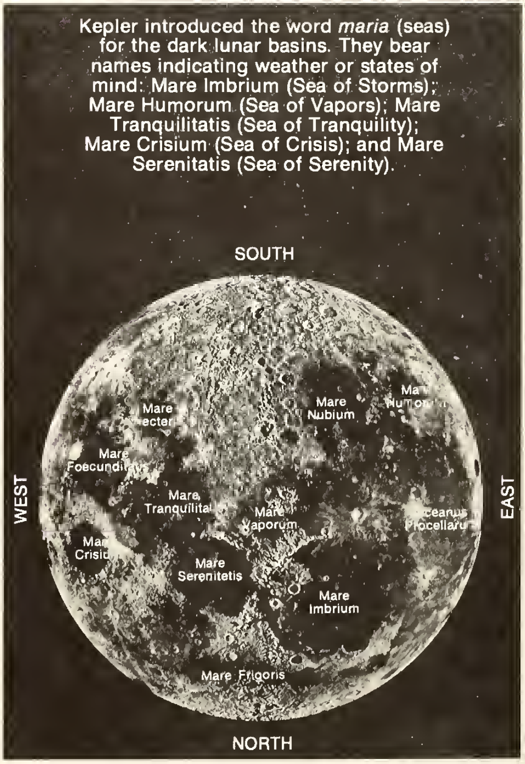
Kepler introduced the word *maria* (seas) for the dark lunar basins. They bear names indicating weather or states of mind: Mare Imbrium (Sea of Storms); Mare Humorum (Sea of Vapors); Mare Tranquilitatis (Sea of Tranquility); Mare Crisium (Sea of Crisis); and Mare Serenitatis (Sea of Serenity).

Lick Observatory

Science is now quite certain that the continents have rifted and drifted apart in the last few percent of geologic time.

has a discontinuous sialic layer with granitic rock being confined to the continental plateaus. This makeup can be likened to an egg with the shell removed from two thirds of its surface, exposing the albumin (egg white).

In contrast, the moon must not be so layered. It, instead, must be fairly homogeneous to at least a considerable depth. If any deep second layers (corresponding to earth's mantle) were responsible for the development of the maria depressions, their existence would show up in the moon's hypsometric curve as a preferred basin level. Almost certainly the moon has no mantle and probably not even a core, which means it is most likely a homogeneous, or undifferentiated, body.

The maria differ from ocean basins in another way. Our ocean basins lie deep because they are underlain by heavy rock layers, above which the lighter continents actually float like icebergs. The two realms exist in a nice state of balance or, as scientists say, "in isostatic equilibrium without any large gravity anomalies."

Such a balance is not true for the lunar maria. National Aeronautics and Space Administration (NASA) scientists P. M. Muller and W. L. Sjogren recently found that the maria reveal large, positive, gravity anomalies, which mean that they are underlain by heavy rock that sits above its level of gravitational balance. If a lunar equivalent to the earth's mantle existed, the maria would sink even deeper.

These heavy mass concentrations, or mascons, are found beneath the centers of all of the five, nearside, ringed maria (Imbrium, Serenitatis, Crisium, Nectaris, and Humorum). They were detected as perturbations in the orbits of the Lunar Orbiter satellites around the moon. The NASA scientists suggest that these mascons may be the remnants of the asteroids which originally created the maria. In other words, they suggest that these anomalies may be the remnants of the cosmic cannonballs—nickel-iron meteorites as much as 100 kilometers in diameter—that struck in bygone aeons.

Although many scientists, including myself, do not agree with Muller's and Sjogren's simplistic interpretation of mascons, there is rather universal agreement that the lunar maria are indeed explosion basins created catastrophically by the impact of large cosmic bodies. If errant meteorites, asteroids or comet heads have struck the moon, how has the earth escaped this bombardment? Cannot the ocean basins be accounted for in the same manner? Such an interpretation is conceivable, but, as I explain later, it is highly unlikely.

There are at least two ways to account for earth not bearing evidence of a cosmic bombardment comparable to the moon's. Much of the moon's pocked surface may have resulted from its sweeping up bodies not in solar orbit but in earth orbit as "micro-satellites," moonlets, or a ring around the earth like that around Saturn.

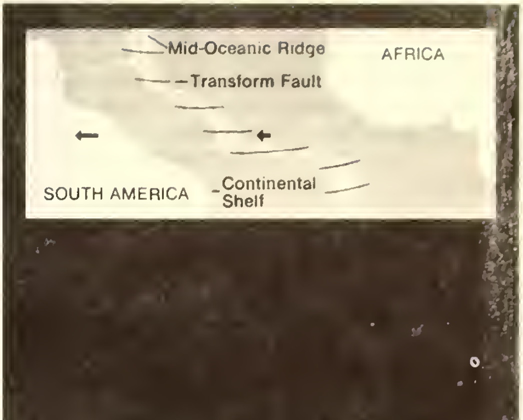

The mid-Atlantic ridge is part of a world-straddling geologic feature. New ocean floor appears along the crest of the ridge and spreads down the slopes. In the process, the continents float, like icebergs, on the denser crustal layer, slowly drifting apart. The hypothesis implies that at some earlier time, the continents must have been in contact. It seems that Africa and Antarctica have remained relatively fixed, while South America and the mid-oceanic ridge have migrated westward. The other continental masses have shifted similarly away from their earliest positions. (After *Heezen and Tharp* [1965].)

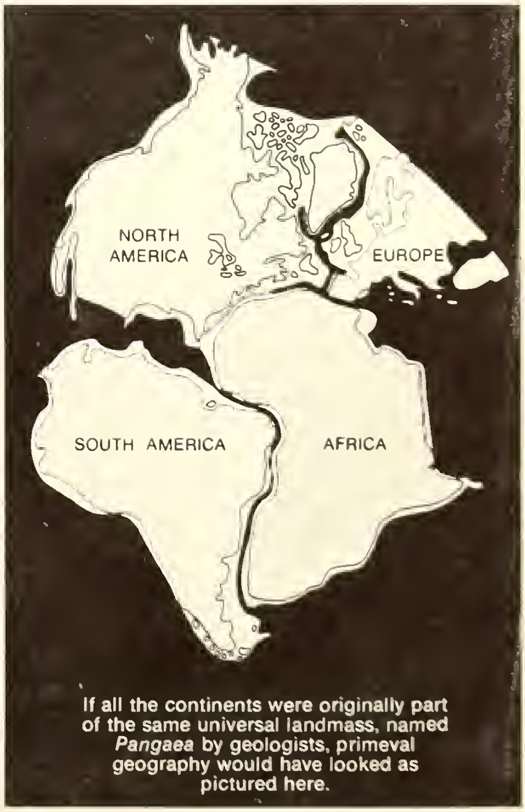

If all the continents were originally part of the same universal landmass, named *Pangaea* by geologists, primeval geography would have looked as pictured here.

Tom Cardamone for Fortune February 1969

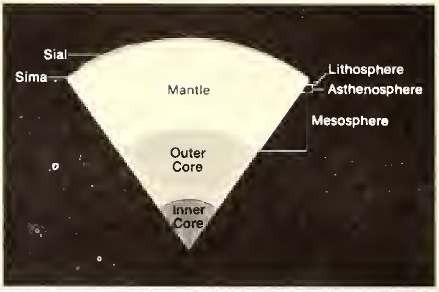

The makeup of the earth comprises three principal zones—the *core*, the *mantle* and the *crust*. The ratio of masses for the three regions is 20:79:1. (After *Isacks, Oliver, and Sykes* [1968].)

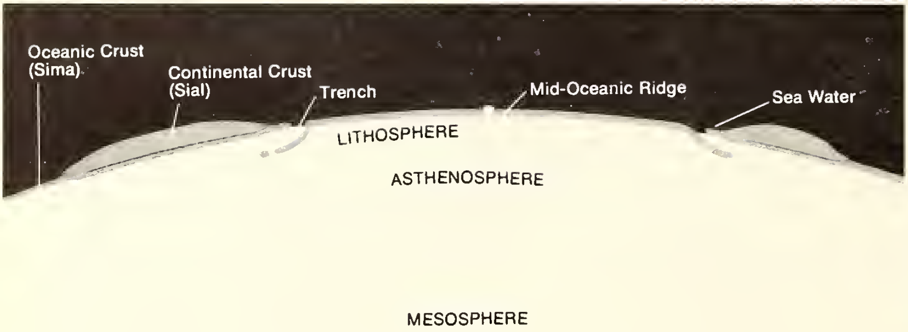

The shells forming the earth are dynamic. Convective circulation high in the mantle (asthenosphere zone) transports the topmost region of the mantle as well as the crust. The landmasses are buoyed along on the spreading lithosphere. (After *Isacks, Oliver, and Sykes* [1968].)

The moon has been slowly receding from the earth and as its rotation slowed, it may have been struck by such cosmic debris along the way. More likely, however, the maria are exceedingly ancient basins formed by impact explosions very early in terrestrial history—more than three billion years ago. There are virtually no rocks on earth of that vintage that have not been thoroughly reprocessed since then. Thus, there is no readable geologic record of the first one and one half billion years of earth history.

Unlike the earth, the airless, waterless, and structurally inert moon undergoes little change, so that lunar features formed aeons ago remain intact. The moonscape is a museum of ancient landforms.

The idea that asteroid impacts sculptured our own ocean basins is not without its devotees. I once published such a speculation, but only to suggest that this occurred during the first, or lost, aeon of earth's history. It seemed evident to me then, as now, that the ocean basins as they now exist allow no such interpretation. But, *if* an original, universal crust once existed after the initial cooling of a molten earth, then this crust might have been pierced and fractured during the early sweepup of celestial debris.

Nearly all earth scientists, however, now believe in the so-called Urey earth model. It conjectures that the earth accreted from a dust cloud of small particles and never, in fact, melted; no original crust ever formed. Hence, any speculation about the fragmentation of an early crust is unnecessary. (Curiously, a possible exception to this camp may be Nobel Laureate Harold Urey himself. At least, in Vienna recently he told me that he was not so sure of his cold earth model after all.)

Certainly, if an object as big as the 800-kilometer diameter of Ceres—the largest asteroid discovered in space—were to strike the earth, a gaping scar as big as the Pacific Ocean would be blown out. However, it seems equally clear to geologists that such an event has never happened in readable geologic history. The ocean basins, as we see them now, are quite young geologically—one or two hundred million years old at most. Catastrophism on so huge a scale could not have formed them within Phanerozoic time (the last 600 million years) while the complex higher metazoan forms of life have existed. If it had, the slender skein of evolution would have suffered discernibly with, perhaps, all life snuffed out.

In the realm of catastrophism, the inverse of the Pacific basin being formed by impact is the classical view that this great depression is the scar left when solar tidal forces physically extracted the moon's mass from the earth.

This durable myth still pervades literature, although scientists have discredited it since the 1930's. The concept that the moon is the daughter of the earth refuses to die and recently has enjoyed some renewed advocacy among scientists. Its persistence in popular print I can only ascribe to its poetic beauty rather than its scientific merit. Scientific hypotheses, like cats, seem to enjoy nine lives.

Scientists are now quite certain that the earth's hydrosphere is not primitive but has been continuously squeezed or "sweated" out of the planet's interior by volcanism and hot springs.

Some water must reach the moon's surface in the same manner, but lunar gravitation is only one sixth that of the earth, allowing any free water to escape rapidly to space to be captured ultimately by the earth or the sun. However, John Gilvarry, an astrophysicist, takes exception to this standard belief and has calculated that water can stay on the lunar surface for as long as one billion years. He argues that the maria were once water-filled oceans in which primitive forms of life such as algae evolved. He ascribes the dark color of the maria not to volcanic rock, as is usually supposed, but to sedimentary deposits that would owe their dark coloring to an admixture of organic matter—remnants of these early life forms. Such a speculation, however, seems rather bizarre to most selenologists.

Although as yet we have no rock samples from the moon, we do have three crude analyses of the lunar surface rock from the Surveyor soft landings. Two were made on the maria and one on the uplands near the rayed crater Tycho. A radioactive source irradiated the lunar surface, a suitable detector recorded the energy of alpha and proton particles, and the spacecraft then transmitted the results back to earth. These analyses seem to rule out the possibility that the moon's surface is composed of meteoritic rock, ultrabasic rock, or granite. Instead, the maria seem to be a basic volcanic rock common on earth—namely, basalt. The upland soil has a similar composition, although with a relatively small content of the iron-group elements, hence it is somewhat more granitic.

A decade ago the belief was widespread that the ocean floor was a primitive surface and that it had remained essentially undisturbed and pristine since its formation. This idea stimulated some scientists to see similarities between the ocean floor and the lunar surface.

In 1962, in the *Bulletin of the Geological Society of America*, geologist P. A. Chenowith drew comparisons, for example, between: the Madeira Abyssal Plain in the central Atlantic Ocean and Mare Crisium; the Romanche Trench, which slices through the Mid-Atlantic Ridge, and the lunar Alpine Valley; the Mid-Ocean Canyon of the Atlantic and the rilles that traverse the surfaces of the maria; and the seamounts and the lunar mountains. Chenowith concluded his paper with the statement: "Perhaps, when we can study at close range the geology of the lunar surface and the sea floor, we will find that they are as closely alike in detail as they now appear in general." In the ensuing years there has been profound progress in undersea and lunar exploration. Geophysical theory has kept pace, with the result that scientific consensus now realizes the ocean floor and the moon's surface are wholly dissimilar. It now would take great imagination to draw even vague comparisons. It has been largely demonstrated that the ocean floor is a realm of more active tectonism (the deformation process that produces geologic features) than the continents. We now know the ocean floors are young terrane, no more than 200 million years old (formed within the last three percent of geologic time).

We need only to look at the marginal continental slopes of the world's oceans to realize their newness. These rugged and abrupt slopes, standing 5,500 meters high, are incised by submarine chasms as deep as the Grand Canyon. This very ruggedness is the hallmark of youth. By contrast, a topography of old age would show degraded, gentle slopes which in the sea would taper gradually toward the abyssal ocean floor. To account for youthful margins, we do not need a catastrophic genesis but some evolutionary and steady state mode of ocean basin development that renews the ocean margins.

The moon, then, is quite unlike the earth, and the lunar "seas" bear no relationship to our ocean basins. The circular maria are explosion basins—scars where great asteroids or comet heads struck aeons ago. These holocausts were of such great energy that they triggered the flow of molten rock from the moon's interior, like blood from a wound, which then filled these saucer-shaped depressions with lakes of dark lava. You can still see the explosion rays scoring the face of the moon clearly around Mare Imbrium. The maria were born full-blown in virtual instants of time!

The story of our ocean basins is much more complex. We have been able to piece together only recently an acceptable account of their evolution, and even this remains tentative and fragmentary.

To begin with, the earth must have been much like the moon for the first billion years after it accreted as a cold body from a solar dust cloud. Although the moon has apparently remained a primitive body, the earth underwent a dramatic change about 3½ billion years ago—perhaps in part because our planet is sufficiently larger than the moon that heat generated within by decay of the radioactive elements potassium, thorium and uranium could not readily escape. The earth started to differentiate into what are its present component layers—the core, mantle and crust. It was no longer merely a homogeneous rock in space.

Very likely there was an initial core-forming event when heavy, liquid iron sank toward the planet's center to form the core and left a cleansed mantle. At the same time, light sialic components rose to the surface to form a proto-crust. Water and gases were squeezed out, creating an atmosphere and a hydrosphere.

The mantle's bulk is by far the largest of the earth's three solid domains; thus, it most closely resembles the chondritic, stony meteorite rock that accreted to form the protoplanet. The ratio of the masses of the core, the mantle and the crust is curiously like that of the main components of the present atmosphere—oxygen, nitrogen and argon—which is 20:79:1. The sialic crust on which we live is as exceptional as is the argon in the atmosphere.

Although this geologic differentiation probably proceeded more quickly at first, it apparently has continued until the present, for we still can witness new crust being created in the formation of mountain ranges. The intruding granite batholiths that contribute to mountain building must be, in part, juvenile substance. (Batholiths are very large subterranean masses of igneous rock which have no clearly definable floors.)

A critical question is: Did the granitic crust ever become a completely encircling layer that formed an unbroken skin around the earth? In all probability, the answer is no. Through the action of convection cells in the mantle, the granitic substance piled up into one or two initial rafts of sialic "scum." The mantle, even though solid, behaves as a quasi-liquid or highly viscous material and undergoes slow creep. It was never necessary, then, for there to have occurred some catastrophic event to account for the ocean basins. these "depressions" have existed from the planet's beginning. Precisely speaking, they are not really basins but rather the normal surface of the earth, above which the continents have been built. Continents are protuberances above the true surface of the earth, instead of the ocean basins being depressions within the earth's outer shell.

About 200 million years ago, in the era when dinosaurs flourished, the thermal regime of the upper half of the mantle became unstable: slow convection, or overturn, commenced. This, in turn, impressed stresses upon the earth's outer shell so that it broke up into a group of rigid plates. These plates

The moon is quite unlike the earth, and the lunar "seas" bear no relationships to our ocean basins.

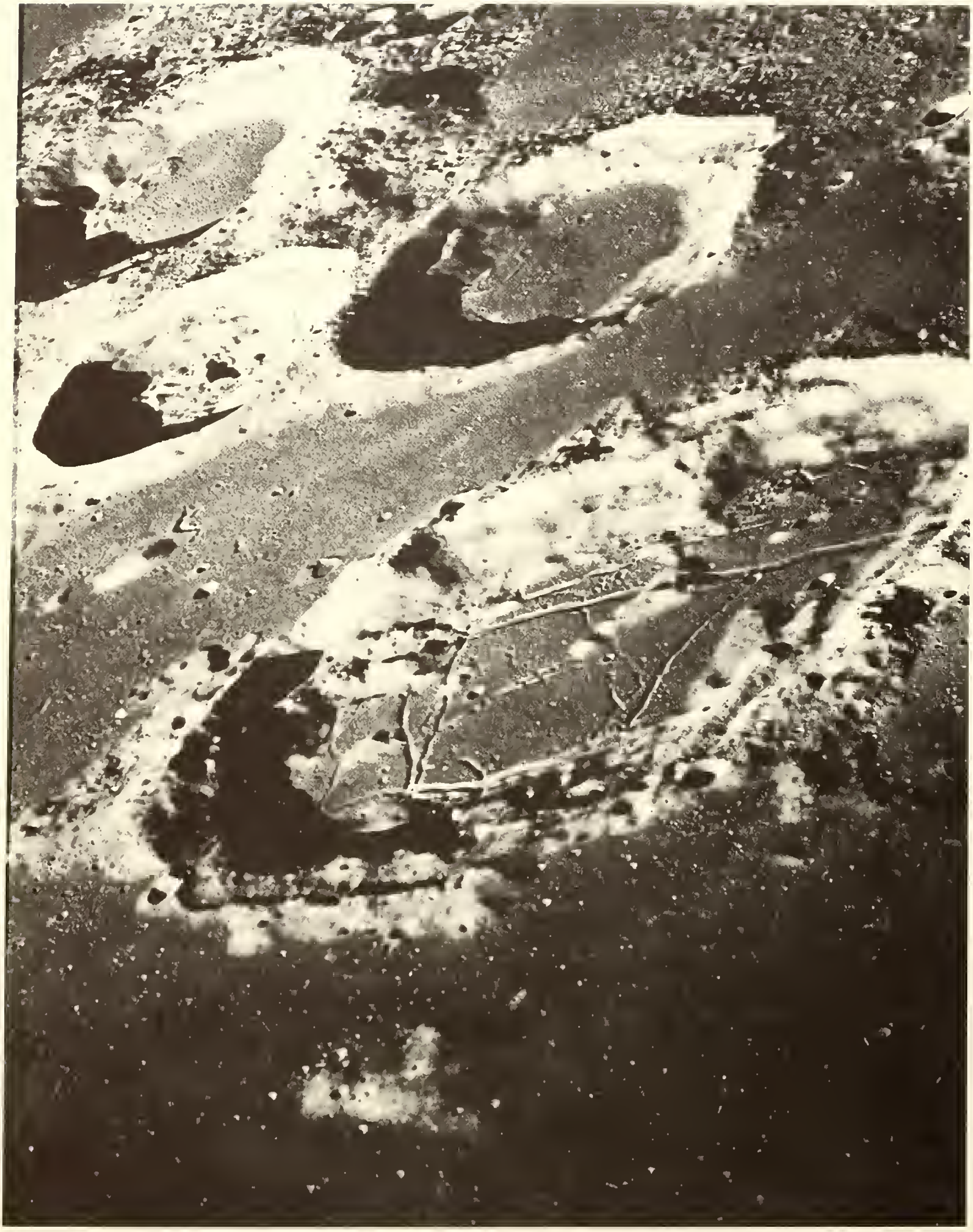

NASA

In contrast to the tectonically active earth, the moon is an inert, frozen orb. The moonscape is a museum of ancient landforms. Less than a decade ago, geologists drew comparisons between the mid-oceanic ridge and lunar rilles. The ridges are young features of active volcanism. The rilles, like this one on the floor of Mare Foecunditatis, are old, lifeless scars.

The earth's outer shell has broken into a group of rigid plates.

According to the plate theory—and more and more evidence indicates it is accurate—new crust is born along the mid-oceanic ridges (dashes) and older crust descends into the trenches or pushes up into mountains (solid lines). The rift system extends as ridges and transform faults (dots) all around the globe. The plates bounded by these features maintain a constant area, and the planet's diameter grows neither larger nor smaller. (After *Sykes* [1968], *Heezen and Tharp* [1965].)

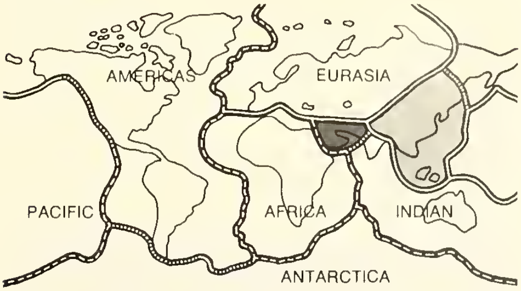

seem to be about 100 kilometers thick, or much thicker than the continental layers, which extend only down to the Moho—the boundary between the continental sial and the upper mantle.

Subsequently, these plates have moved apart at rather steady rates with the result that mantle rock and hot lava continually well up to fill the opening suture. The process created the world-encircling, mid-oceanic ridge. Its central rift marks the locus of the pulling apart that extends over a serpentine course of nearly 100,000 kilometers and resembles the seam on a tennis ball.

In the past 60 million years a swath of new oceanic crust, or *sima*, 500 to 1,500 kilometers wide has formed and spread down both slopes of the mid-oceanic ridge. The rate of spreading has been so rapid that about one-third of the oceanic crust has been emplaced during this geologically brief span of time.

Science has obtained this information only very recently—within the past decade or less. The mid-oceanic ridge is entirely hidden and all but inaccessible beneath the sea except where it breaches the surface of the North Atlantic Ocean as the island of Iceland.

This concept of sea-floor spreading suggests that these rigid crustal plates are in constant, relative motion. Like a conveyor belt, they have a zone where new crust is born (mid-oceanic rifts) and another where it is destroyed by descending along trench zones, or sinks, into the mantle. The uptake in the sinks probably offsets exactly the generation of new crust, so that the plates maintain a constant area and the earth's diameter grows neither larger nor smaller. The boundaries of the "belts" are marked by great fault zones, or *megashears*. The force that shifts these plates must be thermal convection cells in the upper region of the mantle. However, no one has yet made an exact correlation between the plates and the convection cells. The movement of the plates seems to conform to the overall motion of the quasi-plastic upper mantle.

Our modern world appears to be divided into six major plates which are moving with respect to each other. These blocks are as follows: *North America and South America*, including the Atlantic Ocean out to the mid-oceanic rift; a *Eurasian block*, limited to the west by the North Atlantic mid-oceanic rift, to the east by the Pacific trenches and to the south by the Mediterranean trenches; an *African block*, including not only Africa but also the surrounding sea floor out to the mid-oceanic rifts in the South Atlantic and the Indian Oceans and limited on the north by the Mediterranean trenches; a *Pacific block*, including all of the Pacific Ocean, except for that portion east of the East Pacific Rise; an *Indian-Australian-New Zealand block*, covering the intervening ocean regions; and, finally, an *Antarctica block* comprising not only Antarctica but also the ocean floor out to the surrounding mid-oceanic rift.

The blocks are all defined and limited by one of three earth structures: *trenches*, which are zones where crust disappears; *mid-oceanic rifts*, where new crust is born; or large *transform faults*, of which the well-known San Andreas fault is a fine example. Along western North America, for example, the American crustal block is limited off western Mexico by the East Pacific Rift which enters North America through the Gulf of California. This rift then transforms into the San Andreas fault that extends to the Gulf of Alaska where a series of transform faults finally connects with the great Aleutian trench and, thereby, with the remainder of the Pacific trench system.

Although scientists are now quite certain that the continents have rifted and drifted apart in the last few percent of geologic time, many aspects of the breakup remain a puzzle. The impression and usual assumption are that both Africa and Antarctica have remained fixed in position with respect to the earth's rotational axis for the past 100 million years—or since Africa split away from the remainder of the supercontinent of Gondwana (the southern continents plus India).

For South America to move westward from Africa and open up the South Atlantic Ocean, at least two of three elements (Africa, the Mid-Atlantic Ridge, and South America) must have migrated, because the mid-oceanic rift, the axis of the spreading, remains midway between the two continents. It seems that both South America and the mid-oceanic ridge have migrated westward. This translation is now checked by the Peru-Chile trench, a zone of crustal convergence, unless this, too, is being overridden and pushed to the west.

It is more difficult to prove that something has disappeared from the earth than that something new has arrived. Nonetheless, it seems quite certain that an amount of crust equal to that being born is disappearing into a globe-girdling trench system that is discernible mainly around the Pacific, but which probably exists in other, hidden regions such as beneath the Himalayas.

Ten years ago, when I coined the term "sea-floor spreading" and helped establish this general concept, for which we are indebted mainly to Dr. Harry Hess of Princeton University, the evidence for this conveyor-belt action of the earth's outer shell came from indications that the trench system was a realm of crustal uptake. Now the weak point in the concept lies in our imperfect understanding of the role of the trenches. The mid-oceanic ridges today provide the really convincing evidence. Most of us are sure, however, that the trenches are the uptake ends of the crustal conveyor-belt system.

The early configuration of the continents remains obscure. Most geologists are now certain that major continental rifting and drifting began about 200 million years ago. It continues to this day, with earthquakes along the margins of these moving blocks punctuating this slow shifting of a few centimeters per year.

Possibly all of the land was formerly one universal landmass, which geologists term *Pangaea* (meaning universal land). Or there may have been two supercontinents, *Laurasia* (North America and Eurasia) in the northern hemisphere and *Gondwana* in the southern hemisphere.

One reason to suspect the two-continent configuration existed is that when we sum up the total areas of these two hypothetical supercontinents (using the now scattered parts of which they were once composed), the two would have had identical areas of almost exactly 100 million square kilometers each. This equivalency is understandable if both continents were born from the mantle in opposite hemispheres. Surprisingly, there is growing evidence to suggest that these two supercontinents collided in mid-Paleozoic time, prior to the major drift event in the mid-Mesozoic era, temporarily joining Africa to the eastern margin of the United States.

The work of earth scientists who have recently mapped the directions and field strengths of the magnetic properties trapped in abyssal rock has convincingly demonstrated that crust is being generated. In their mapping, linear magnetic anomalies, in mirror image, parallel the mid-oceanic ridge system on both flanks of the ridge. The anomalies form broad bands, like zebra stripes, of normally and reversely magnetized extrusions of basalt. The basalt trapped the signature of the earth's ancient magnetic field when these lavas froze. We now know that the earth's magnetic poles have flip-flopped, with north becoming south and vice versa about every half-million years. This phenomenon makes it possible to read the record of generation of new oceanic crust as though the sea floor were a magnetic tape recorder. We know, for example, that spreading began actively in the North Atlantic at least 70 million years ago, but in the Antarctic Ocean between Australia and Antarctica only about 40 million years ago.

It follows from sea-floor spreading that the continents have been passively carried along like so many icebergs. They float on a lithosphere set into motion by gigantic convection cells within the upper mantle. Spreading has dispersed the continents to their present, scattered positions on the globe. The Atlantic and Indian Oceans are new rift oceans, while the continents have encroached upon the Pacific, the remnant of an even larger ancient ocean. Thus, in most general terms, we can account for the pattern of ocean basins and continents on the earth today.

In summary, the lunar maria and the ocean basins are worlds apart, a study in contrasts. The moon is a primitive body which will give us some clue as to how the earth probably looked 3½ to 4½ billion years ago, for this record is forever lost on our planet. The moon is virtually a dead rock in space, and its surface largely records only exogenic (external or cosmic) events plus pseudo-volcanic occurrences which the larger of these great impacts have triggered.

The earth is perhaps unique among the planets in showing crustal spreading. The moon shows no surface structure like the earth's trench system, the mid-oceanic ridge system, cordilleras of folded mountains or large crustal transform faults. Any crustal offsets should be especially evident if present on the moon, for the circular craters form an excellent reference grid that evidently has been fixed through time and not sheared. Photos from the Mariner fly-by mission have revealed Mars to be covered with craters much like the moon, although erosion has somewhat subdued them. Among the terrestrial, or inner, planets, the earth is the largest and probably is of just the critical size for gravitational forces to reduce the mantle's strength so that it undergoes quasi-liquid creep or flow.

The geology of the earth's surface has been molded by internal processes, especially by an active, thermally convective upper mantle which has given rise to sea-floor spreading. Volcanism, earthquakes, mountain-making and trenches are all expressions of this sea-floor spreading, which is the *primum mobile* of geotectonism, the deformation of earth's crust.

The Man in the Moon is dead and his expression has changed but little over the aeons. In contrast, Mother Earth is much alive and the earth's surface, including the positions of all the continents, has been completely reordered since the age of the dinosaurs.

NASA

Reprinted from Marine Technological Society Journal
Vol. 3, No. 5, 68-69.

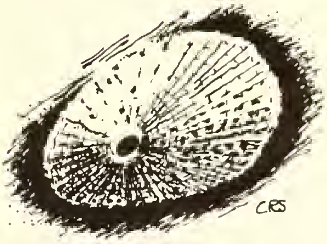

OCEAN FLOOR IN THE DECADE AHEAD

Robert S. Dietz
ESSA, Atlantic Oceanographic Lab.
Miami, Florida

Past is prelude – so we can best presage the decade ahead by recalling trends and advances since 1960, or better since the end of World War II, remembering the accelerating pace of technology. I propose to discuss here the marine geology and geophysics of the ocean floor in the decade ahead. The sea bed is the world's great *third surface*, the others of course being the land and the sea surfaces. It is in the nature of things that these surfaces are more important than the volumes or 'spheres' which make up our earth for it is on the surfaces that the main energy exchanges take place.

Sea floor spreading and the new global tectonics

In the present decade we have witnessed a great breakthrough in the understanding of ocean basin evolution based upon the concept of sea floor spreading with its corollaries of transform faulting, continental drift and rigid plate tectonics – together comprising what has been termed the new global tectonics. Over the years we have seen tectonic models come and go, but I believe that with this concept, whereby new oceanic crust is generated at mid-ocean ridge and resorbed into the mantle at trenches, we have achieved a model which will be elaborated upon but not discarded over the next decade. The new model implies that all ocean floors are new and that about one third of the ocean floor has been renewed (resurfaced with new crust) in the past 70 million years alone. It means, too, that the ocean floor is a window to the earth's upper mantle – and this is where the geologic action is.

With this workable model of the earth's crustal evolution, we will see academic science and its application to technology drawing ever closer together. With better science we will be able to make predictions with confidence. By 1980 I suppose, for example, that we will have achieved a clear understanding of the earthquake mechanism whereby it will be possible to predict earthquakes with considerable accuracy.

Deep Research Vehicles

Although they now play but a minor role in producing scientific results, DRV's in the decade ahead will become increasingly important in opening up the ocean floor. In 1965 with ONR support I joined Jacques Piccard in initiating the Navy's first deep submergence effort with the *Trieste* making 26 dives in the Mediterranean. At the turn of the decade, I was fortunate in being topside while the *Trieste* dove seven miles down in the Challenger Deep, the deepest hole in the deepest ocean. Since these "early days" we have seen the development of an impressive array of American DRV's. It has been peculiarly an American success story, paced largely by industry. Unlike the much-publicized race to the moon, the Soviets never got off the ground (or, rather, beneath the sea) in this sector of technology.

Unfortunately, at present the scientific utilization of DRV's is in the doldrums. There is only about 30 percent usage of the available vehicles. Potential users in industry in the scientific community (other than the Navy) lack the funds to use these expensive facilities. Recently it was proposed that the government through ONR block fund three million dollars to subsidize the use of DRV's by oceanographers, but this funding has failed to materialize to date. Clearly some governmental support is needed to get the DRV program moving and to promote its use by scientists such that sophisticated instrumentation will eventually be placed aboard these vehicles. When this occurs, the DRV program should gain momentum. In this next decade the dream of oceanographers to go down *into* the sea in ships should be realized. We will pierce the veil of the ocean surface which heretofore has reflected only the sky.

Deep-Sea Drilling Project

At this point in time, we should take special notice of the Deep-Sea Drilling Project (JOIDES) now coring in the western Pacific out of Hawaii. By any measure, the Deep-Sea Drilling Project has already been an outstanding success. We all now should realize that it is the way the defunct Mohole Project should have gone in the first place.

We may list among its accomplishments within the Atlantic Basin the following: The

Deep-Sea Drilling Project proved for the first time the feasibility of drilling in the oceanic realm – at depths up to 20,000 feet. It showed that salt domes, cap rock, and sulphur can form at abyssal depths and that oil and gas can be generated and can accumulate there. It drove the age of the oldest rocks it recovered from the oceans back to the late Jurassic and indicated that significant older sediments are likely to be found with deeper drilling. It has tended to confirm sea floor spreading and the youth of ocean basins. It demonstrated the wide occurrence of turbidites in the deep ocean and resulted in a discovery of a widespread Eocene chert blanket in the North Atlantic (Layer "A"). It is worth noting, in passing, that the really significant accomplishments of this project have not relied on any new science. Instead, the precise age determinations and the environmental interpretations achieved are being provided by the most classic of the classical disciplines of geology – that of paleontology.

I understand that there is under consideration a proposal to extend this project with National Science Foundation support. I anticipate, and certainly hope, that the drilling of the deep ocean floor for scientific purposes prospers during the coming decade.

New Methods

A science is only as good as its instruments. In the current decade we have witnessed some important breakthroughs in geophysical instrumentation which have created a revolution in our understanding of ocean basins. One of these is the towed magnetometer. It has revealed large anomalies in the total field of the ocean floor forming stripped patterns. These combined reversals of the polarization of the earth's field have not only confirmed the concept of sea floor spreading, but have quantitized it. The ocean floor has been a magnetic tape recorder as new crust has been created and moved outward from the mid-ocean rifts. The growth of the ocean floor can be measured like so many tree rings.

Secondly, continuous seismic reflection profiling which has given us a sort of X-ray radiographic view of the sedimentary layers on the ocean floor to the depth of a few kilometers. The technique also clearly differentiates between turbidite layers and pelagic sediments. Due to this technique, we are developing a knowledge of the sedimentary basins on the sea floor which is superior to that which we have on the continents. With more powerful sound sources in the coming years we should be able to obtain reflection profiles down to the Moho discontinuity.

Another breakthrough has been satellite navigation which is perhaps the most significant development in navigation since the invention of the chronometer by John Harrison. The precise positions achieved make true oceanic surveys feasible for the first time. In the next decade we should see much sophistication of the echo sounding and related techniques such as will, for example, permit a broad swath of the ocean floor to be surveyed by a fanshaped array of narrow beam projectors and a bathymetric map simultaneously drawn up of the ocean floor. By 1980 we should have made impressive strides in the total mapping of the ocean basin.

Manpower Requirements

Oceanography has been widely publicized with the result that enthusiasm for the field has grown more rapidly than its financial base. Even some of the observed growth of oceanography has been fictitious, as it has depended upon an expansion of the definition of the term.

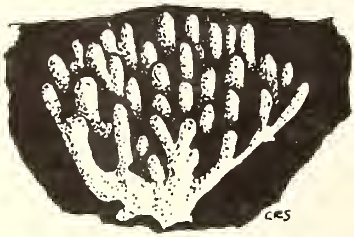

University curricula in oceanography has been greatly expanded, but unless the present manpower ceilings in government laboratories are eased, the prospects for employment in this sector at least are dim at present. Hopefully, this is a temporary condition.

In the long run, I suppose the demand for oceanographers to study the ocean floor will remain reasonably brisk. Perhaps the main reason is that the ratio of professionals to technicians and support personnel in industry, in government and at research centers will continue to increase. The universities today appear to be turning out more than enough marine geologists to satisfy current demand. However, there is a great dearth of marine geophysicists and marine engineers – a gap that promises to open up further in the coming years.

Ocean Floor Resources

Beyond the shelves, whose geology is simply an extension of continental geology, the picture of ocean floor resources is not bright. The ocean floor clearly has no potential as a storehouse of minerals like the Canadian Shield and other Archean terranes. By the sea floor spreading concept, we know that the oceanic crust is a first differentiate of the mantle's peridotite. It is composed of the common volcanic rock called basalt – and the ocean floor variety (tholeiite) is of a remarkably uniform and, resource-wise, uninteresting type. The ocean crust, like Hawaii and Iceland, have little potential for mineral resources. Geologists would be much happier if, as many predicted, the sea floor had turned out to be underlain by the early crust of the earth. There is some promise, of course, in the phosphate and manganese nodules, and their associated trace elements, that have been colloidally precipitated on the ocean floor, but it seems doubtful that these will be exploited by 1980. The greatest potential lies in the great prisms of young post-mid-Mesozoic sediments which comprise the continental rises, as they offer an enormous potential for gas and oil when technology can be advanced sufficiently to be able to tap them. In the interim any political move to prevent the movement of the oil industry offshore, for reasons such as the recent Santa Barbara oil spill, would stifle developments for years to come.

"Blue sky" predictions abound as to the sea's "unlimited resources." Unrestrained by practical considerations, artists create drawings which have that certain dream-like quality. Brochures show undersea cities frequented by men-fish and midget submarines zooming through crystal clear water. But, in realism, the ocean is murky and so is its future. Science cannot compete with science fiction.

By 1980 the problems of this world will no longer be those of man against nature but rather of man against man. In this context we will have to strike up a symbiotic relationship with the ocean rather than simply exploiting it. We will also need a workable body of international law for we cannot proceed under the dictum that he who rules the waves, waves the rules.

The ocean's recoverable resources are finite and severely constrained by energy requirements for extracting them. The oceans are mostly blue but this is the desert color of the sea indicating a dearth of the nutrient salts or fertilizing phosphate and nitrates. The ocean offers no cornucopia of food or mineral resources on the scale needed to cope with the population explosion. In any event, the human spirit will not burn brightly in a world where there is standing room only. Let us not deceive the people into believing that "inner space" is their ace-in-the-hole.

Reprinted from The Primitive Earth Symp., Miami Univ., Oxford, Ohio, Special publication., D1-D11.

PRIMITIVE EARTH: A MARINE GEOLOGIST'S APPRAISAL - Robert S. Dietz

It's a great pleasure to be here today and to see this fine new geology building. Let me say, at the outset, that we have heard a lot of bizarre ideas so far today. I will not disappoint you by agreeing with anyone. Our disagreement may be an example of Theobold's law which says "Nature is usually wrong."

Over the past decade or two the earth's age has increased at an alarming rate--of something like a million years each week. As of yesterday, the quotation on the earth's age was 4.5 billion years, but today I don't know. I can only assure you, that when I finish this talk, the earth will be exactly one microcentury older.

I would like to discuss the primitive earth in terms of the ocean floor which dominates this planet; the deep ocean basins covering 3/5 of its entire surface. I would like to speak in terms of what has been termed "the new global tectonics"; that is in terms of sea floor spreading, transform faulting, rigid crustal block tectonics and continental drift. Figure 1 is a simplified diagram of the spreading concept; i.e. the conveyor belt model of the earth with the mantle being active. The mantle, of course, composes the large bulk of the earth (some 80%) and is much like the original substance of the earth; the original chondritic substance. The core composes another 20%, and the sialic continents, which I will call the crust, just a mere 1%. In other words, the crust is just about as rare as the argon in the atmosphere. It is a special substance.

Although geologists differ in our view, we do have one point of agreement. It is that the mountains, the earthquakes and all of the tectonic processes we witness are not Acts of God. On the contrary, it seems to be the work of the Devil.

We have learned (figure 3) in recent years that the oceans are very young domains. It was hoped some years ago that, with the Mohole, we might discover the Archean, the earliest aeon, beneath the sea. The ocean floor would then provide a complete section of the earth back into early Precambrian times. We now know that such will never be found; that in fact the sea floor is a very young domain. These seamounts of the mid-Pacific (figure 3) were first thought to be by Hesse, Precambrian in age but, when dated, they turned out to be Cretaceous. In fact, whenever we go back into the geologic history of ocean floors, we draw a blank after only about 150 million years ago, or latest Jurassic. We have dredged some 500 pre-Holocene samples from the ocean floor none of which goes back beyond 150 million years. So it is a young domain.

The oldest rocks we know of on earth are about 3.5 billion years old. As the earth is 4.5 aeons old, we have a lost aeon for which we have no geologic record. We can envision that, perhaps, the early earth was like the moon before the earth's heart had warmed up. The lunar surface gives us some feeling for the early appearance of the earth with no continents and with no ocean basins. The lunar maria do not appear to be ocean basins; they appear to be large extrusive lopoliths. The moon is sort of a layman's version of a planet; simply a rock in space with no internal activity. In the earth, however, we have an active mantle which is the prima mobile of earth tectonics.

In terms of the new global tectonics (figure 4), we must concern ourselves with the mid-ocean rise, which encircles the earth and which is thought to be the center of upwelling or spreading; the opening up part of the earth where new crust is being generated while the trenches are the take-up part of this conveyor belt system. In this model as now envisioned by Lamont and Princeton workers--and I believe correctly--the earth's crust appears to consist of a thick lithosphere, some 100 kilometers thick, and the crustal blocks rotate relative to each other in a conveyor belt-like fashion. New crust is being generated in the mid-ocean rises and descending into the trenches. The rigid lithosphere is entrained only in a secondary sense by the thermal convection cells of the earth's mantle.

This (figure 5) simply shows the concept from a recent paper by Isachs and others of the lithosphere as being 100 kilometers thick. It moves into a trench zone as the downward part of this conveyor belt. A decade ago at least my conviction about sea floor spreading was based upon the "take-up" of oceanic crust in trenches but now the best evidence for a conveyor belt ocean floor comes from the generation of new crust at the mid-ocean rises.

We have learned that the ocean is an entirely new domain, quite unlike the earth, and the section is entirely new. The oceanic rocks are different and the ocean basin windows into the earth's upper mantle. From the ocean floor we can learn something about the early earth, because it offers us a new view of global tectonics. As already noted, the ocean floor is quite young, and we cannot learn much about the early earth by the rocks of the ocean floor themselves but only by using this window into the earth--a vast Moholicic surface, so to speak--2/3 the size of the earth, to learn more about the inner workings of this big clock of ours and to see how it ticks.

I would like to pass from the ocean floor itself and view the continents (figure 6) in terms of the new global tectonics to show how we might use this new insight to understand the continents themselves. Continents, in my view, represent the primitive elements, and we must study them to see the primitive rocks of the earth. To explain this, I will delve into the question of geosynclines. Indeed these seem to be not only the precursors of mountains, but also the basic building blocks of the continents themselves. You will recognize this as the tectogene concept of geosynclines (a common concept, especially in days gone by but not accepted today) as to how geosynclines are the precursors to mountains.

More commonly today (figure 7) is the concept of what we may call the "Kay-type" geosyncline. Like the last, it is an ensialic geosyncline laid down upon sial, upon the granitoid crust of the earth (the type of geosyncline which Dr. Clifford prefers), and showing the two basic elements of these geosynclinal provinces; the miogeosyncline and the eugeosyncline, and in turn the other elements, the tectonic borderland and the offshore island arc.

Next (figure 8), I would like to point out that it is possible to perform certain surgery on this geosynclinal concept, and throw out certain elements which have been inferred to exist, but, in fact, are erosional realms and at least do not now exist in the field. We take the miogeosyncline and the eugeosyncline, using the same elements as in the previous diagram, and then place a continental slope between the two sedimentary prisms and drop down the eugeosyncline in the fashion shown. This is, of course, gross surgery, but I think the patient survives.

Figure 9 is a revised version of figure 8 to show it in terms of an actualistic model, whereby now the miogeosyncline becomes a continental terrace prism. We have added the continental slope, the boundary between the sial and sima, everywhere in evidence around the world; the eugeosyncline is laid down as a turbidite prism ensimatically, laid down on the ocean floor as a continental rise, as a great prism of turbidites.

If we look at the East Coast today (figure 10), we have this sort of picture, from Heezen, and therefore my version is what one might call an actualistic model. This would be the situation off Cape Hatteras. Only recently have we realized the vast size of these eugeosynclinal prisms--these continental rise prisms; how important they are; how large they are; and how they must play some role in geologic history. They are all post-Jurassic in age, but of enormous size. This represents great erosion of the continents. Now, the continents can't stand up to all this erosion unless there is some way to return this material to the continents; somehow to feed back this lost substance so as to rebuild the continents through geologic time. It is evident that we have had dry land at least since the latest Silurian when the first vascular plants, the psilophites, first evolved. The continents have retained subaerial free-board ever since, thus we have been able to preserve the continental massifs as subaerial bodies.

Again, just to show these prisms (figure 11) and their vast importance in the marine geologic realm, this illustrates these fringing prisms we term the continental rises which we see in the oceans today.

This (figure 12) is an example of a modern turbidite such as those comprising these prisms. You can recognize the usual fossils: Canis vulgaris and the good 5¢ cigar.

If we look at this in terms of the world today, we see here an example of, say, Japan or the Aleutian arcs. We see ocean floor going down, we see the collapsing prism and we see entrained the collapsed prism. Here you would expect a high dynamic, high load metamorphism but low temperature on the oceanward side. This would change to high thermal and low load metamorphism on the landward side. I think you see this today in arcs such as Japan.

In a time sequence diagram, we can offer a model like this, (figure 13). In the bottom panel this prism is collapsed, and you have intrusion of this prism by partial fusion of material going down into the mantle. As Dr. Kennedy pointed out, there is an awful lot of tholeiitic basalt in the world but it still isn't what continents are composed of. They are composed mainly of granitoid rocks, I believe. It takes a lot of geology to make granite. You can generate these tholeiitic basalts in the mid-ocean regions quite properly, but then you must reprocess these in some way. You must translate them by conveyor belt, to the continental margins into trenches, and have the hyperfusibles come off as grandiorites and andesites and intrude the folded prisms to account for the development of truly sialic continents. Also, by this same process, small pods are broken off which are pieces of ocean floor; serpentine and peridotite. These pods are incorporated into the eugeosynclinal prism, and you will see that if you break these off, the granites are always younger than the sediments. They intrude the sediments as was discovered in Canada in the last century by Andrew Lawson.

We cannot look to granites for primitive material in view of the generally accepted cold earth hypothesis, but perhaps we can look to the ultrabasic pods which are invariably older than the sediments in which they are contained.

We can look at the earth, then, in terms of an accretionary regime in which I would disagree with all of these curves, but draw one which was first quite rapid then tailing off. The accretionary amount would be on the order of 10 or 15% since the beginning of the Phanerozoic, but that is only 600 million years ago and this is only 10% of geologic time or 15%, so it is more or less linear. This is a diagram (figure 14) of the Appalachian region to show how one would incorporate a prism and how this appearance of accretion is real. This is an accordian model of the earth rather than a layer-cake model.

This (figure 15) is similar, but refers to all of North America, showing the new Phanerozoic elements on either side. It shows these new accretionary belts on either end of the United States as truly accretionary elements. They would be if they were laid down ensimatically on the ocean floor. We would date these as less than 800 m.y. by Professor Hurley's break in the dating sequence.

If we take out a deep slice out of the earth, from say Ohio (figure 16), we find this general sequence of the cratonic-cover beds which are largely undisturbed. Below this we pass into the basement complex commonly called the Archean, but this term is a tectonic facies rather than a time unit. Collapsed continental rises form this cratonized basement complex which contain the intrusive granites. These granites intrude older sediments which, in turn, contain ultrabasic pods. Since there probably is no such thing as ultrabasic magma--i.e. no such thing as peridotite magma--these would always have been cold and not melted and would represent the most primitive material we can hope to find on earth. So, if we wish to look for the primitive crust of the earth, we should look for it in this context. We should not look for the ocean floor, we should not look to the granites which are younger than the meta-sediments and we should not look to the sediments. Instead we should look to the ultrabasic pods. If we look back to the oldest cratonic nuclei, the oldest areas of Manitoba, Rhodesia, Karelia, within these old nuclei we will find ultrabasic pods. Perhaps this material will be most like the original chondritic substance of which, presumably, the earth was made.

I would tend to go along with the idea of accretion being real along path A'-B'-C' (figure 17) rather than a path of a withdrawal and reworking of the continent with time (A-B-C). Much of the accretion must have occurred very early, especially around 2.7 eons ago. At this time there was already a sizable core which was circulating, because we have rocks of this age containing fossil (remnant) magnetism. If they have this, then the earth already should have had a magnetic field, which in turn means the earth's core was magneto-hydrodynamic. That, perhaps, was the initial big event in continent formation, but this has progressed with time.

Looking back (figure 18) from the primitive earth, I think we start with the small cratons and we add to them by this sea floor spreading and add belts to either side. Through the course of time, we build them up into larger and larger cratonic units through earth history.

Reviewing this thought somewhat (figure 19), if we started with a tectogene and collapsed the crust, we would end up with a smaller continent. Also, if we lay down a eugeosyncline ensialically on the edge of a continent, when we collapse it, the continent becomes smaller. Under this view, if you collapse the continental rise, even though the earth contains fold belts, this does not mean that the continents have become smaller. The continents grow larger with time if you add fold belts. Now, of course, you must add new material as well as reprocess the old material carried from the continents. We must add a certain amount of juvenile material to make the continents grow. You do this through having mid-ocean tholeiitic basalt reworked by partial fusion into granites and other silicic rocks which have the necessary buoyancy to become continents.

If we look back into early mid-Ordovician time, we have a picture like this (figure 20), adapted from Kay but not quite in his terms. It shows no island arcs, etc., but instead broad continental shelves and continental rises. These would be later accreted to the continent to make it grow as we see it today.

If we cut a section (figure 21) out of North America, we see accretionary belts, the Appalachian, the Grenville, etc. I would go along here with Hurley in saying that if we drilled down into the earth by a bore hole, the date we got at the top would be the same as the date we got down at the bottom. This is not a layer cake view of the basement of continents but rather an accordian-like picture.

This (figure 22) is also an accordian-like picture which I propose for a contrast with a standard model. I simply show this to wonder if continents were plastered on the bottom and if the continents had not been rifted and drifted and if they had not been accreted, why do they have continental slopes? The continents do have abrupt boundaries, which we call the continental slopes. If a continent were plastered with new substance on the bottom you would expect it to tail out some way. You would not have the abrupt edges to the continental masses, and this is a fact of life we must live with and explain. This is explainable in terms of accretion, because by plastering things on the side, by making a new orogene, by making a new fold belt on the side of a continent, you can generate from time to time a new continental slope. Also by rifting it and by modifying this rift, we can also generate a continental slope of the Atlantic type. By accretion we can generate one of what we might call a margin of the Pacific type.

This (figure 23) is to show that we have a certain ratio of continents to ocean basins on the earth today. The ratio of sial by volume to sea water is about 4.5 to 1 in the present earth; the deep oceans are essentially 5 kilometers deep. In terms of isostasy one can balance this out and you can indeed show that the thickness of continents is a function of the depth of the ocean. The continents must be approximately 7 times as thick as the ocean is deep. This is a very basic fact of geology, and if you tamper with the size of earth, if you expand it or contract it, you raise havoc with the earth. If one assumes, along with Warren Carey, that the earth has doubled in area since the Paleozoic, one derives figures requiring the crust to have been, maybe, 70 kilometers thick in the Paleozoic, and you have to infer that 35 kilometers have been eroded from the continental cratons since that time which is patently ridiculous. On the other hand, this ratio of 4.5 controls the total area of continents, not their geographic form or distribution. It controls only their total area as being two-fifths of the earth, essentially 200 million square kilometers.

We can change this ratio (figure 24) and we can infer that there was a different ratio than 4.5, but one can still show that there would still be continents and ocean floor. The point here is that we have these continents which are sea-level bodies. Now, if we collapse continental rises, the thickness of these rises, which grow to be about 40,000 feet thick, is controlled isostatically by the depth of the ocean plus isostasy. Then, by collapsing these continental rises, you insure that you have a mass sialic rock which will reach sea level, and continents do reach sea level. We have no right to assume that continents always reached sea level because we know there are other forms on earth, the mid-ocean rises, which never reach sea level except in Iceland. The continents invariably reach sea level, so we must also live with this fact as well as the fact that they have abrupt boundaries; that is, that continents attain some dry (subaerial) freeboard. If they grow much higher, of course, they are quickly eroded down to sea level, are ultrapeneplained, and remain at sea level. There is no easy way to submerge a continent once it is above sea level, but getting it up to that level in the first place is an important aspect of geologic history. You can tamper with this ratio (4.5:1) and assume that it wasn't God-given, and make it less or greater, and you end up with an ocean 4 kilometers deep and the continents become 28 kilometers thick and cover 24% of the earth. If we halve this ratio, we had ratios of 4.5:1 to 2.5:1.

If we go the other way (figure 25) and double this, we have 9 parts to 1. We also change the configuration of the earth, only the total area of continents, and we change the depth of the ocean floor to 7.3 and the area of continents to 60% rather than 40% of the earth. So, we can tamper with this amount of ocean water; the volume of the ocean must be more or less conservative. We can have it grow slowly with time. We can stand having it grow at most a meter per million years, which would be linear since the oceans are 4.5 kilometers deep and the earth is 4.5 eons old. But, perhaps, it is a bit less than linear and we're squeezing out water and adding sial at some rate less than that whereby the ocean is growing a bit deeper with time, but the continents can stand that and maintain their free-board, and we can expect continents which exist through time in these terms.

Figure 26 points out that we do have these two separate crustal columns--the continental segment and the oceanic segment--which are isostatically in balance, and we do have an abrupt transition between these two levels, and that the ocean floor is in a sense a window into the earth's upper mantle. These abrupt margins must be fitted into any satisfactory model of earth evolution. By our process of accretion of continental rises, we can in fact do this.

Let me now turn to the subject of continental drift. First, let me agree with Dr. Hurley that the drift in the last 150 million years perhaps is a unique event, at least in its great scale. At least we must have had sparse drift prior to that time. We can largely account for fragmentation for the continents as we see them today in terms of this Mesozoic rifting and drift. We now have some six continents (figure 27) and some other micro-continents plus sub-continents like India and New Zealand. The continents would be a lot more fractured and broken up if we did not restrict this drift as a unique event in recent time. Why this suddenly has occurred beginning in the Jurassic, I don't know. Perhaps the mantle became "restless" in some way as a result of warming up to the point where this new type of global tectonics took over. There is sort of a basic thesis here. It is that we can't understand the primitive earth in terms of the global tectonics of the last 150 million years--sea floor spreading, transform faulting, continental drift and the conveyor-belt crustal motion. This may be an entirely new aspect of the earth. Prior to this time, we may have to deal with other concepts of what tectonism and mountain-building were like.

Let's take a look (figure 28) at this jig-saw puzzle of drift for a moment, just touching on one facet of it. This is the closing of the Atlantic by Bullard et al. with which you doubtlessly are all acquainted. It shows the fit, not only of Africa into South America, but also of Africa into North America. I would like to emphasize this a bit, because I wonder about whether it should be questioned; that is, the fit of Africa into North America. Certainly the fit between Africa and South America must be valid. The evidence for drift, I think, is rather overwhelming these days, and you will recall from Hurley's diagram that there are discordant elements between Africa and South America but, in contrast, between Africa and North America there are these parallel or concordant fold belts. Now, if you were to collapse the Pacific today you would end up with concordant fold belts in Japan and in California, but this wouldn't necessarily mean drift or that they were ever together; it only means parallel evolution of marginal geosynclines which fringe ocean basins. But we do have these two large supercontinental cratonic elements which we call the Gondwana, the southern hemisphere group, and Laurasia, the northern hemisphere group.

This is another fit (figure 29) which I recently made with Walter Sproll which fits very well with Professor Hurley's geological diagram in Scientific American. It places Antarctica against Australia. This is based on a computerized fitting of the isobaths which is even better than the South America-Africa fit. The total overlap and underlap fit is only about the size of the state of Illinois.

This shows our fit (Sproll and Dietz) of Africa into North America. I'm really undecided as to whether this illustration is valid (figure 30) or not and perhaps the Atlantic has in fact closed and opened again, because there is some evidence that this is valid, but other evidence that we really don't need it geologically. Perhaps the lack of the fact that we don't need it geologically really explains why North American geologists have been sort of non-drifters. They haven't needed this fit. I wonder about it myself. I am inclined to agree with J. T. Wilson's belief that the North Atlantic was originally open but that it closed in the mid-Paleozoic and then opened again in the mid-Mesozoic.

Now, if we look at all of the earth (figure 31), we see that much of it is below sea level. This shows the total amount of earth which one may regard as continental, i.e. sialic. Regarding all of the earth down to the 1,000 fathom isobath as sialic, you end up with 40% of the earth being sialic or continental, and 60% being ocean basins. The ratio of continents to ocean basins is 60:40 not 70:30 as usually quoted.

If you sum the total areas up (figure 32) of the total area of what we presume to have been Gondwana and what we presume to have the elements of Laurasia, you end up with these two supercontinents, each being about 101 million square kilometers. In other words this means that Gondwana and Laurasia were of the same size. This perhaps suggests that they may have evolved separately from opposite hemispheres of the earth.

For a primitive earth in terms of drift reconstruction, there are two options (figure 33). One is to go back to a Pangaea, a universal continent merging all the continents together and accepting the North Africa bulge to North America fit as correct. It is the only line of contact between these two opposing regions of the earth within the drift theory. Alternately we can go back to another sort of model and look at the earth in a primitive fashion as being composed of two elements; Gondwana and Laurasia. If sea floor spreading was in process in early time, there could be, perhaps, a mid-ocean rise along an equatorial belt, and the continents then could be placed near the poles where they would be stable and not under any disruptive influence. They would be subject to accretion but not to destruction such as continents are experiencing today. The modern continents are eroding at a rate whereby North America would be ultra-peneplained 12 times during the Cenozoic alone. We are losing continental substance at a catastrophic rate. We have two terms in geology: orogenesis, meaning mountain-making, and continent-making. Earthquakes and so forth are constructive mechanisms so far as geology is concerned, although they may be catastrophic to man's culture. We gain more land; we gain more sial. On the other hand, when we have pyrogenesis, so-called continent building of which the Colorado plateau is an example, we expose great areas of the continent, of the sialic block, to erosion, and we actually degrade continents and we lose substance at an enormous rate. Here, in a sort of stable picture of the earth, with the continents being over convergent zones, the earth would have a minimum erosion and maximum construction. It is evident that we need to have the continents stay with us through geologic times, since we still have them. They are a fact of life and we have to explain why we still have dry continents on the earth today.

This (figure 34) pertains to my last point. The Colorado plateau is an example of epeirogenesis. We thought at one time this high plateau represented a thickening of the sialic layer. Now we recognize that it seems to be related to some kind of tumescence of the earth's mantle. A great mass of rock is being exposed to erosion, the continents are being degraded today by such epeirogenesis.

In terms of the new global tectonics, we would explain this in terms of the mid-ocean rise running under western North America and causing this tumescence of the mantle and in turn up-arching the continent to form the great Rocky Mountain arch. Now, this again is explaining things in terms of new global tectonics which doesn't necessarily apply prior to the pre-mid-Mesozoic. Epeirogenesis, as we now know it, may be a modern thing. Certainly, the history of the earth has been typically one of ultra-peneplanation. We see examples in the cyclothem sedimentation of the Pennsylvanian where a small rise of sea level of some feet causes incursion of the sea as much as 500 miles. Last June I had the pleasure of going down the Colorado in a rubber boat and seeing the world's largest outcrop. Wonderful unconformities occur within the section. There, also you have this impression of ultra-peneplanation. There are no paleo-Grand Canyons in the geologic section today. There are small valleys, etc., and minor knolls and so forth, but you don't really see any evidence of epeirogenesis on a scale which would cause such great canyons in the past. Otherwise, how could we maintain the cratonic cover we now have, not only of the Paleozoic but of the Precambrian in parts of the earth today. We must believe in the historic stability of the earth, by and large. Also we must maintain the freeboard of continents and the depth of the oceans as conservative aspects of the world.

There is another type of mountains today--the Himalayan type (figure 35) where you have the impingement of one block of the piece of Gondwana which hit a piece of Laurasia throwing up the Himalaya Mountains and causing a slab of sial which is not 35 kilometers thick but 70 kilometers thick, and you have the ramparts of the Himalayas which are 15,000 feet high. In other words, here you have a mountain range which is as high as the oceans are deep, high as the continental slope, and this presumably is for the same reason; that you have a double continental thickness and therefore by isostasy you have here what you might regard as a continental slope here on land. This is very special sort of mountain range which is again related to drift and a type of mountain range which might not apply to earth prior to the mid-Mesozoic, something which would not happen unless we had drift and if we had no drift we wouldn't have this type of enormous mountain range in the geologic past.

The Himalayan Mountains (figure 36) tower above all the other mountains of the world (from Life books). The Himalayas, as a high block, stand alone. They form enormous mass of rock which is related to the impingement of two sialic blocks--a type of mountain range which is uniquely related to the new global tectonics. Did such mountains exist in the Paleozoic and earlier?

In figure 37 we see a gold mine in South Africa showing some fragile sedimentary structures very well preserved in the two billion year old Witwatersrand Series. This is an example of one of the cratonic cover beds which have existed of the Precambrian, which are of great extent like the Dubuant of Canada, the Athabasca, the Transval Series, and the Bambui of Brazil, which have existed since the Precambrian. These have been regarded in the past as being Eocambrian or Infracambrian; very close to Cambrian age, but when we date them we find them, in many cases, to be very old. The Bambui of Brazil is an example which I visited a couple of years ago--a carbonate series 300 meters thick covering an area the size of Texas which is shown on the 1960 map of Brazil as being Silurian. This is based on the presence of a Favosites, but this Favosites probably is just cone-in-cone structure. This is the only "fossil" in the series, so very likely this is another example of a great well preserved cratonic cover bed which is Precambrian in age, and perhaps even well back in the Precambrian. This bespeaks of the great tectonic stability of the cratons. If we do preserve these, I don't see how we can (by Dr. Clifford's model) periodically orogenize the crust, other than to intensely deform it at its margins. Once the cratons are formed and chelatonized they appear to be stable. The cover beds and the continents remain largely undisturbed and maintain a freeboard which puts them at sea level, or very close to sea level, whereby they can be preserved over geologic time.

Thus, in summary, in terms of the new global tectonics, we must look at the primitive world a bit differently. We tend to rely upon the uniformitarianism. But, these processes of the new global tectonics, perhaps, do not apply to the earth prior to the Mesozoic. We must get a new set of rules for early geologic time and not look too closely at the world today to try to understand the Paleozoic and the Precambrian world in terms of the types of global tectonics which then applied. Secondly, we have this concept of permanency, a word with a very fine ring to it, but it means different things to different people. In terms of the classic concept of the earth, we had permanency of continents in a geographic outline and in a fixed position.

However, under these new tectonics, under drift, we do away with some aspects of permanency which are dear to geologists, but we bring in other aspects of permanency. In other words we can maintain the volume of ocean basins. The ocean basins per se can be as old as the earth, but the ocean floor can, in turn, be new. You can renew the floor but maintain the ocean basins. By drifting continents you can maintain the volume of ocean basins and in turn maintain depth of the oceans and maintain the freeboard of the continents as being constant through time. You can roughly maintain the total area of continents by slow accretion, linear at most; you can add something to their size and you can return the sediments carried in to the oceans. You can further process the tholeiitic basalt and make sialic material and make continents grow in a slow and orderly way but in a pattern which, I think, is consistent with geologic history. So we give up certain aspects of permanency and accept others.

So finally, let me show this concretion (figure 38) and conclude my fish story by saying our conversations with the earth are always one-sided since the earth does not speak. The earth is mute; however, rocks never lie in spite of Theobold's law and eventually, I presume, we will learn the truth about this by more rigorous laboratory methods and by better field work, and we will know whether we have caught a fish or not (figure 39).

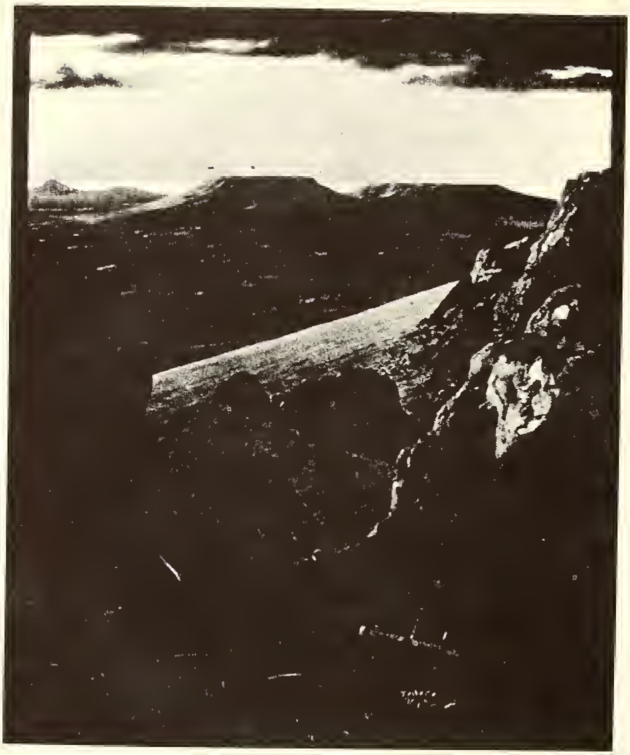

Figure 1

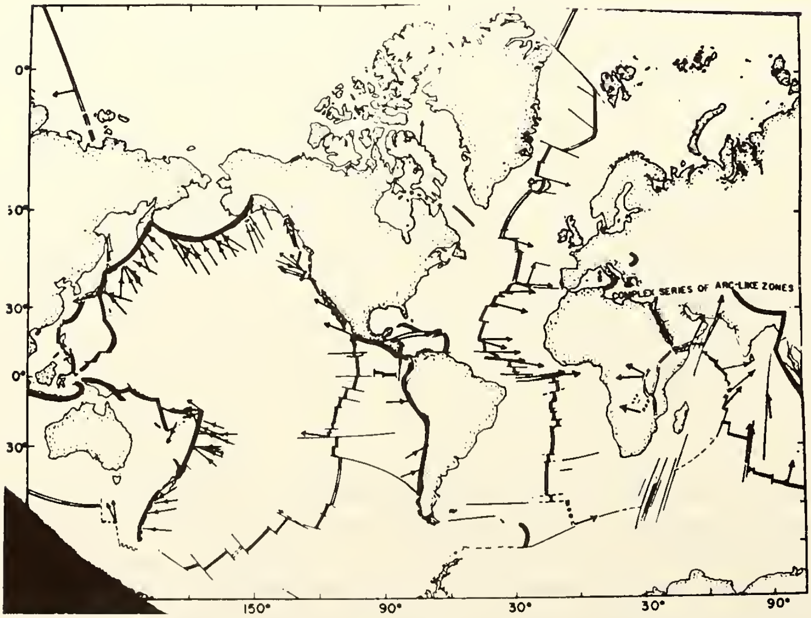

Figure 2

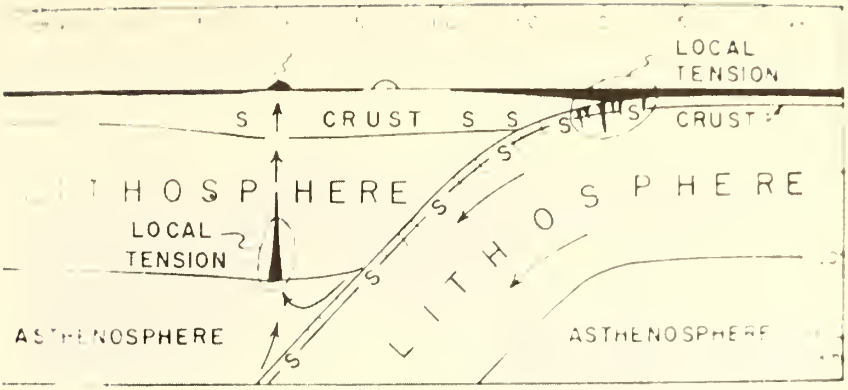

Figure 3

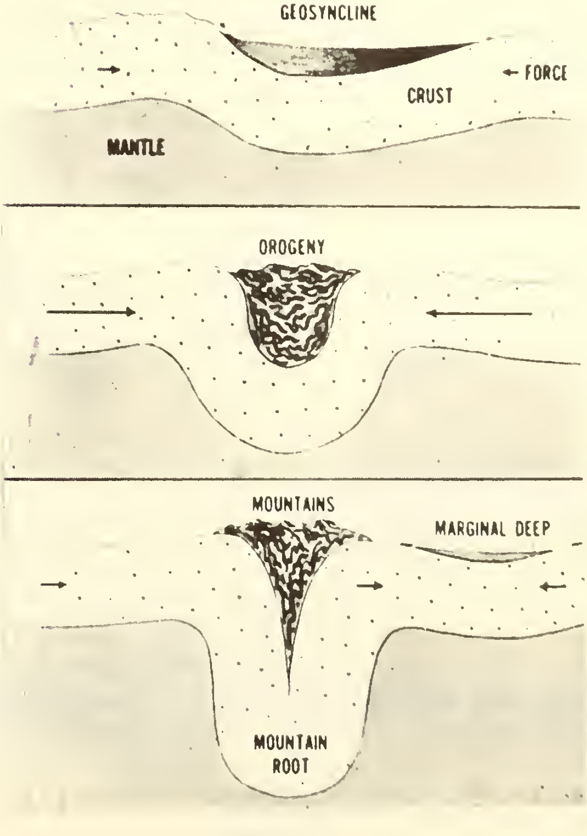

Figure 4

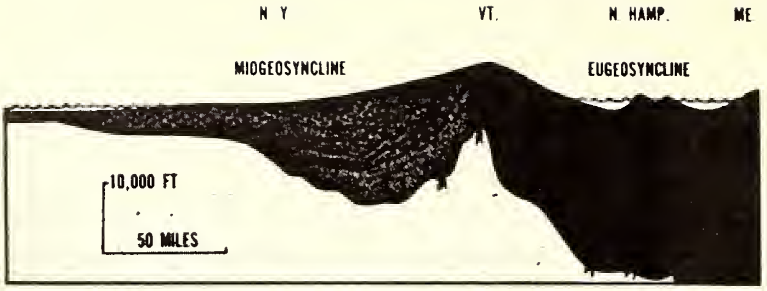

Figure 5

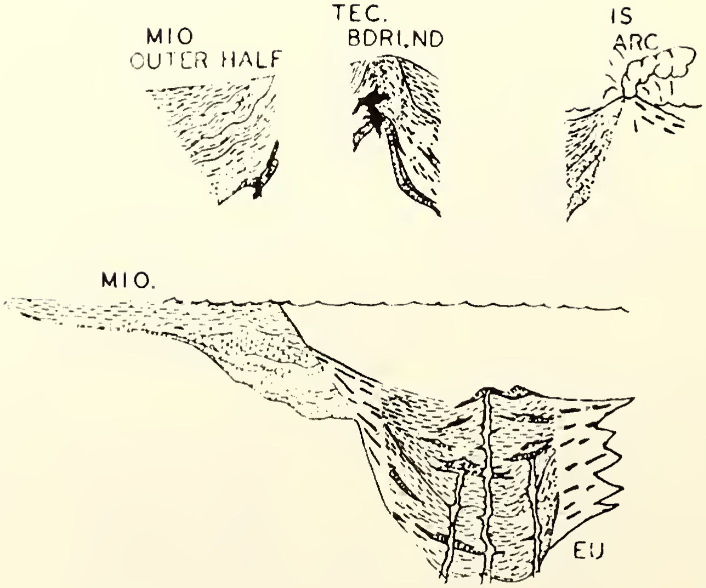

Figure 6

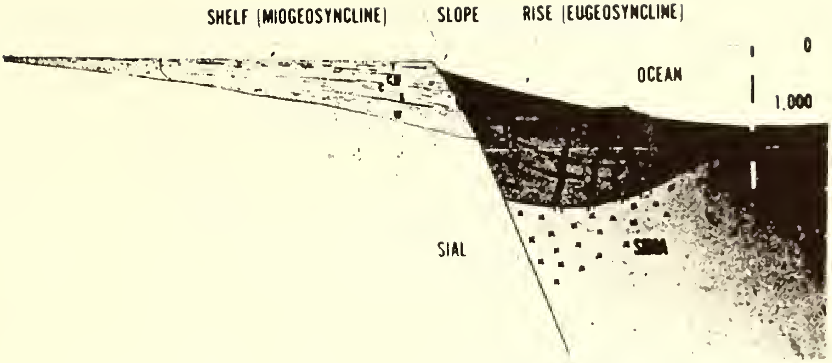

Figure 7

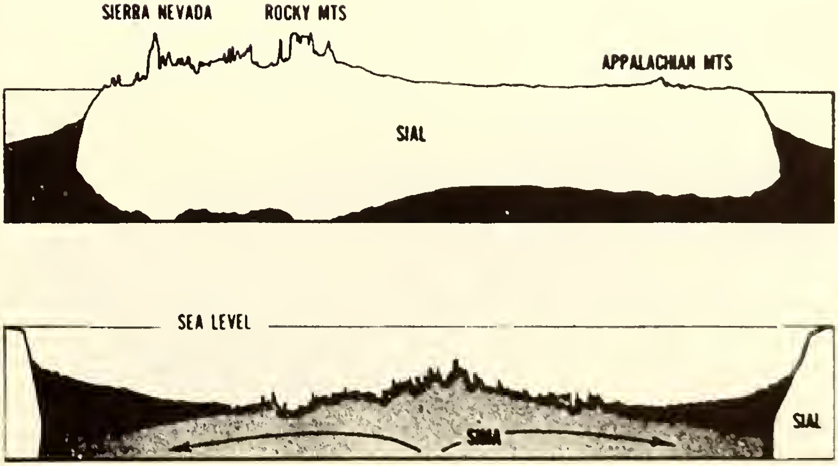

Figure 8

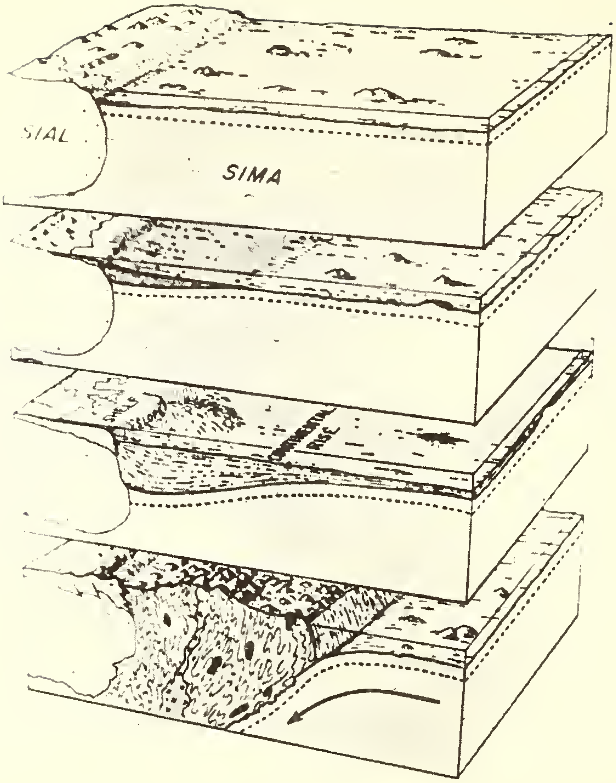

Figure 9

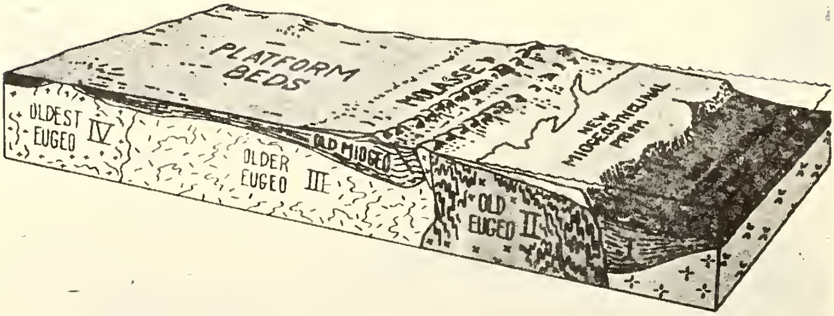

Figure 10

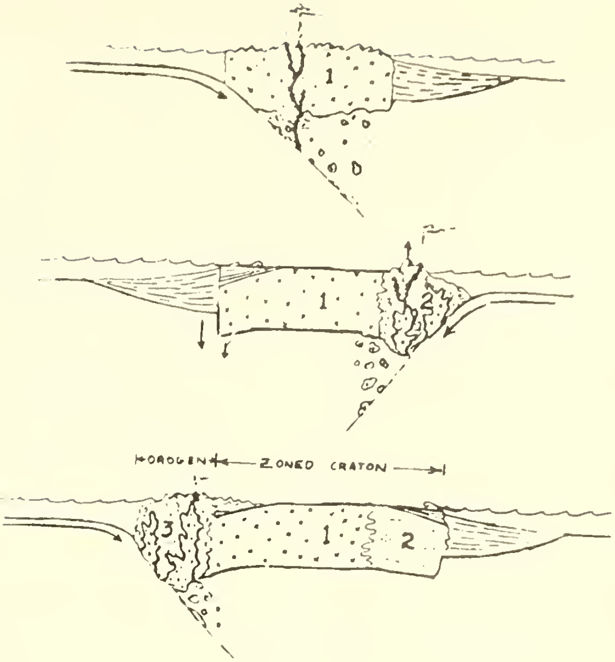

Figure 11

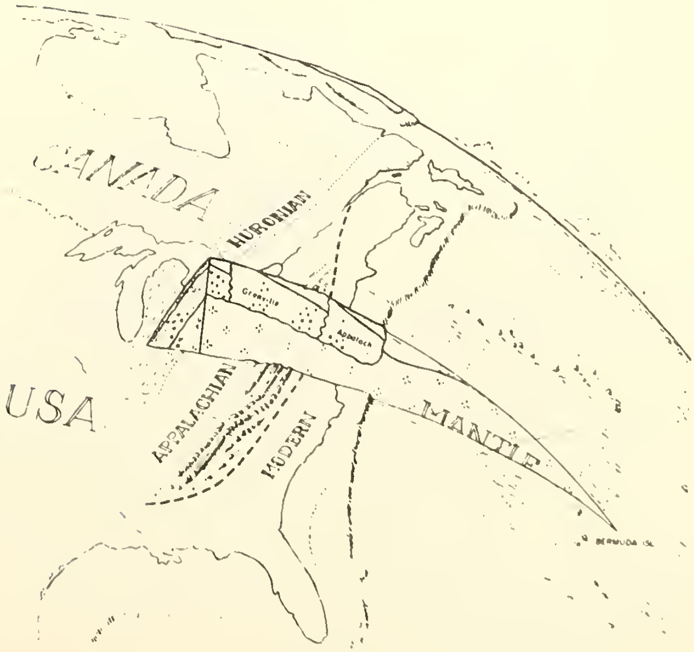

Figure 12

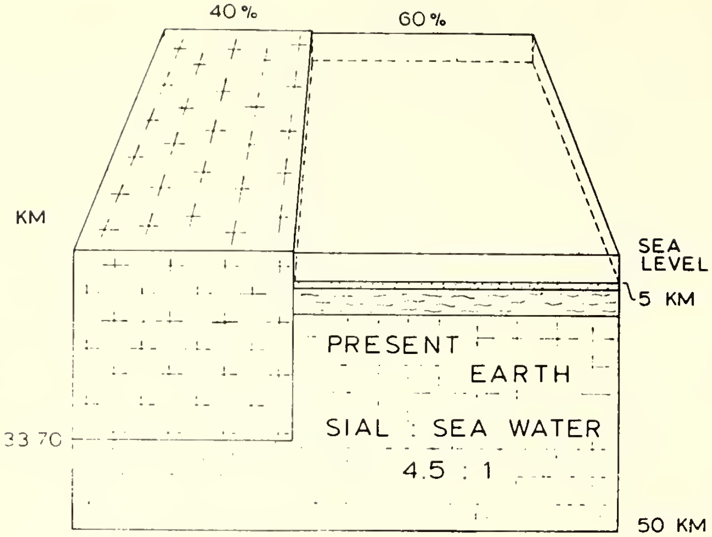

Figure 13

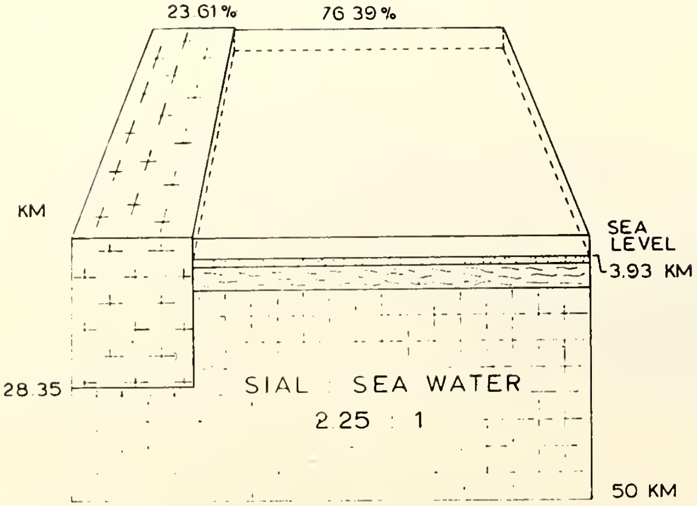

Figure 14

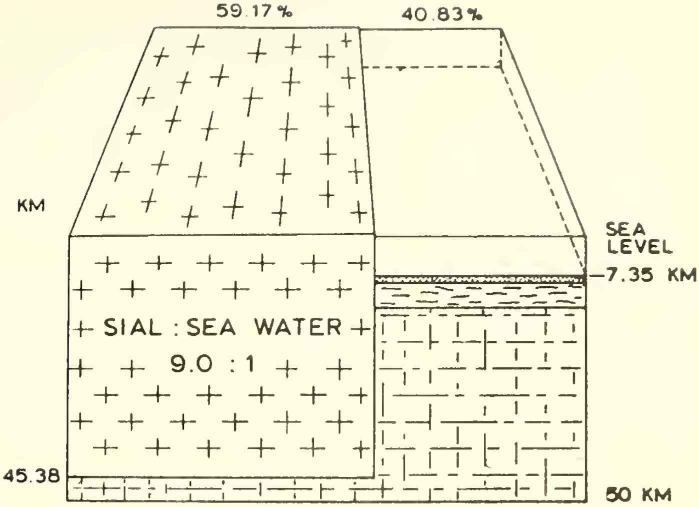

Figure 15

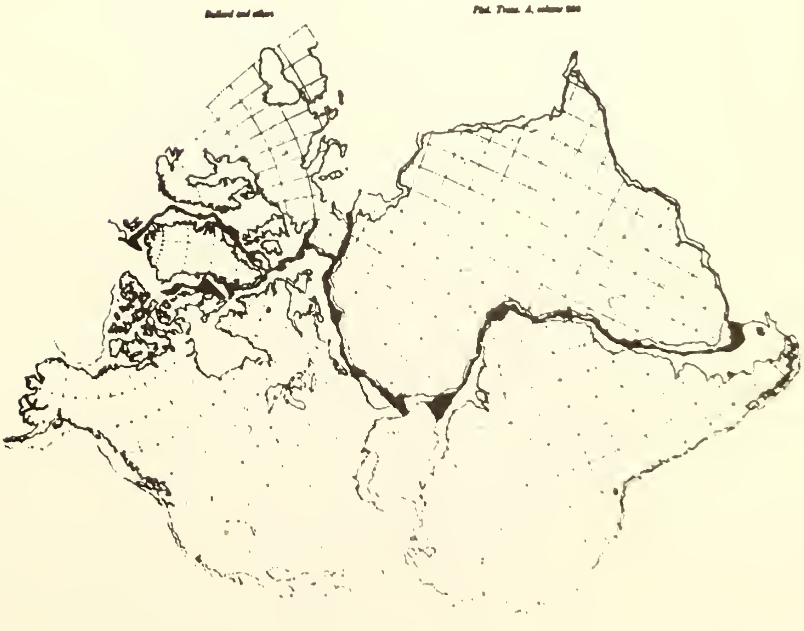

Figure 16

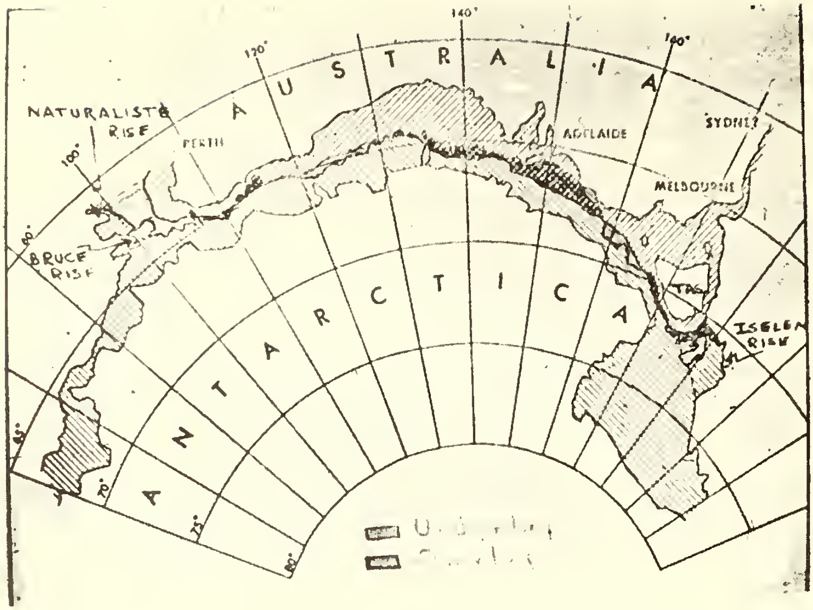

Figure 17

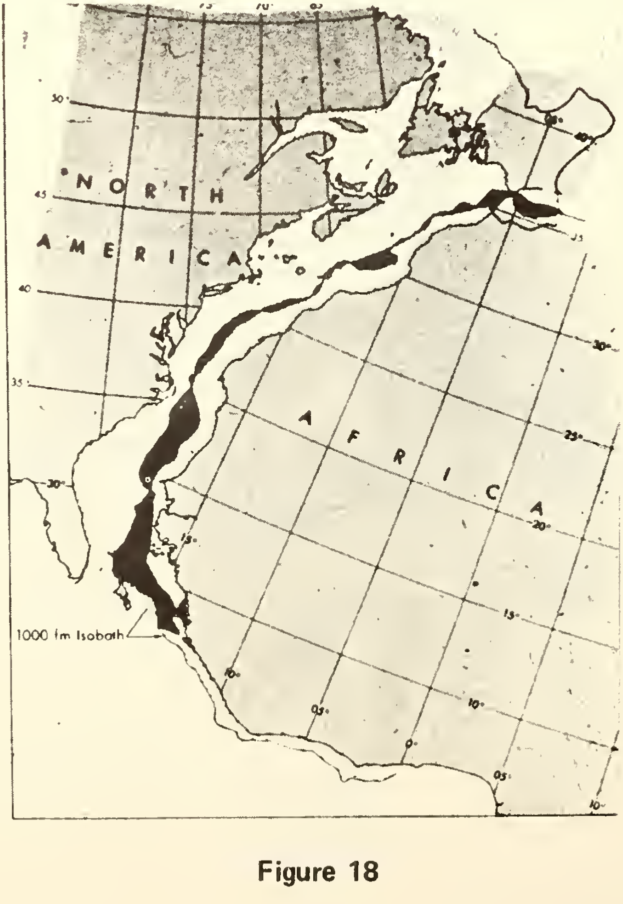

Figure 18

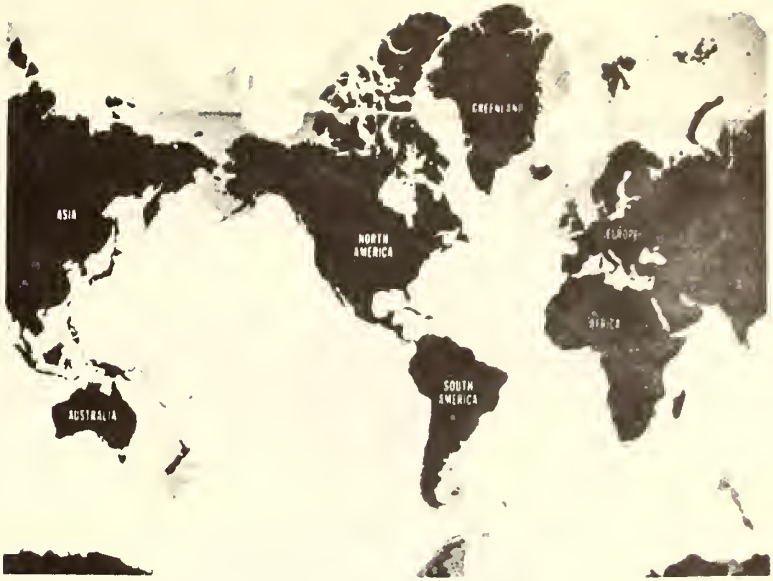

Figure 19

Table I. Equal Areas of Laurasia and Gondwana[1]

Laurasia[2]		Gondwana	
Eurasia	70.49 x 10^6 km^2	Africa[4]	37.80 x 10^6 km^2
North America	35.39 x "	Australia and New Guinea	13.31 x "
	105.88 x "	New Zealand	2.59 x "
India	- 5.19 x "	Antarctica	16.91 x "
		South America	22.36 x "
			92.97 x "
		India	+ 5.19 x "
		Himalayan overlap	+ 2.44 x "
	100.69 x 10^6 km^2		100.6 x 10^6 km^2
	or 100.7 x 10^6 km^2		[illegible] x 10^6 km

Figure 20

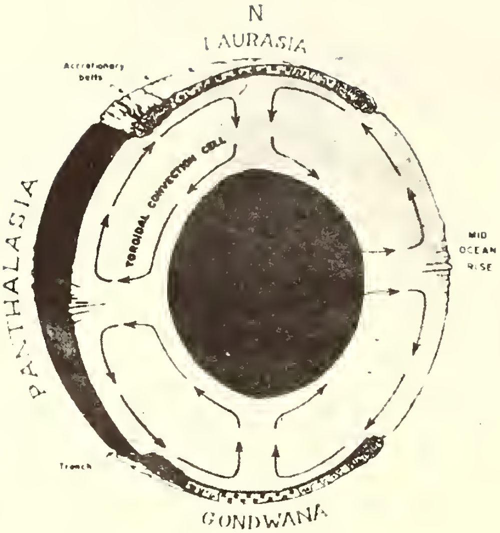

Figure 21

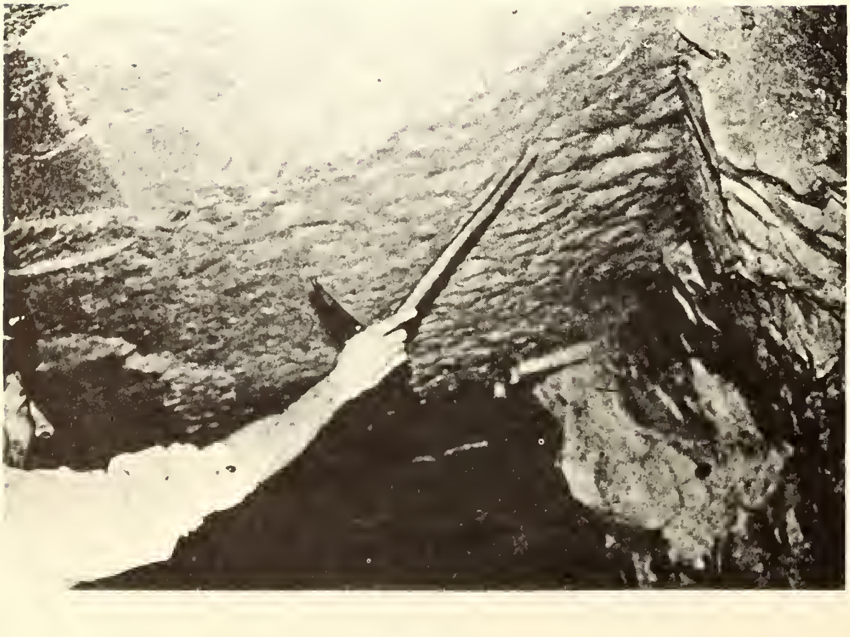

Figure 22

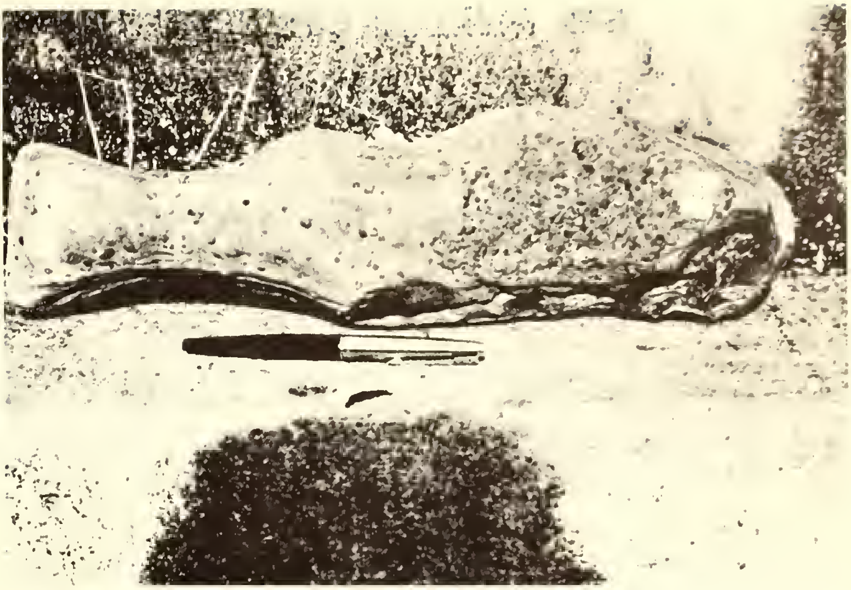

Figure 23

13 Reprinted from Marine Technological Society Journal
Vol. 3, No. 5, 30.

BOOK REVIEWS

THE HISTORY OF THE EARTH'S CRUST

Edited by
Robert A. Phinney
Princeton Univ. Press,
1968, 244 p., $12.50

Robert S. Dietz

ESSA, Atlantic Oceanographic and
Meteorological Laboratories
901 South Miami Ave.
Miami, Florida 33130

The book presents 17 papers presented at a NASA-Columbia University-sponsored symposium held in late 1966, so, considering the rate of change in earth science, it is already somewhat out of date. Also, the title "The History of the Earth's Crust" is also something of a misnomer, as the papers are all, in fact, directed toward the question of continental drift. The main sections of the book treat (1) the rheology and chemistry of the upper mantle, (2) the evidence from the continents, and (3) the evidence concerning drift from the ocean basins.

Concerning the ocean floor, which presumably is the primary interest of MTS members, this particular group of papers treat the paleomagnetism of sediment cores (the magnetic reversals which are recorded in deep-sea cores are now providing an important new method of geochronology back to four million years ago, providing an independent check of micropaleontologic results); general aspects of sea floor spreading; seismological evidence for sea floor spreading, transform faulting and continental drift; heat flow from the ocean floor; and the magnetic "zebra stripe" anomalies which parallel many mid-ocean ridges and which provide evidence for the growth of new oceanic crust by sea floor spreading like so many tree rings. It seems that the ocean floor anomalies (the magnetic reversal method) is now providing even stronger evidence for drift than the remnant magnetism of certain rocks, especially basalts which behave as fossil magnets giving orientation and latitude, but not longitude, for continents in the geologic past (polar magnetic method).

Although two authors question continental drift, the book as a whole gives rousing support to crustal plates which behave as conveyor belts, generating new crust at mid-ocean ridges and resorbing oceanic, but not continental, crust in trenches. An outstanding paper is that of F.J. Vine on the magnetic anomalies associated with the mid-ocean ridges which displays color plates of the magnetic reversal patterns associated with the Reykjanes Ridges near Iceland and of the more complex region off the northwestern United States and Canada. The evidence seems clear that new oceanic crust is being constantly created by dike injections along the ridge rift.

It would seem that the new global tectonics involving rigid crustal plates and sea floor spreading is remarkably successful in explaining the geologic nature of the real earth. Without doubt, the sea floor spreading concept works and, although modifications will certainly be made, it is here to stay. The book is highly recommended to anyone who would like to learn more about this modern revolution in earth science. And it is the ocean floor which has provided the key.

Reprinted from Geological Society of America Bulletin
Vol. 80, No. 7, 1367-1372.

ROBERT S. DIETZ *Environmental Science Services Administration, Atlantic Oceanographic Laboratories, Miami, Florida*
ROBERT FUDALI *Smithsonian Institution, Washington, D. C.*
WILLIAM CASSIDY *University of Pittsburgh, Pittsburgh, Pennsylvania*

Richat and Semsiyat Domes (Mauritania): Not Astroblemes

Abstract: The 38-km-diameter Richat Dome, in central Mauritania, has been widely regarded as a possible astrobleme. Our field examination of the structure and subsequent petrographic study of the critical rock types failed to reveal a single feature attributable to shock processes. We, therefore, dismiss an impact origin for this structure. It must, instead, be endogenic. The same conclusion applies to the much smaller, associated, Semsiyat Dome.

Introduction

In March 1968, we examined two geologic structures of considerable interest to meteoriticists in the Adrar region of central Mauritania, Africa—the Richat and Semsiyat Domes. These structures have been widely regarded as possible astroblemes (ancient meteoritic impact scars) and are listed as such in several bibliographies on this subject (for example, Freeburg, 1966).

Interest in the Richat Dome has been heightened recently by a well-publicized Gemini photo, no. S-65-34670, on which the dissected dome appears as probably the most striking earth structure so far photographed from near space—a giant bullseye vaguely reminiscent of Mare Orientale on the Moon (Pl. 1). A NASA publication on the Gemini results lists it as a suspected impact feature (Anonymous 1967).

The purpose of our expedition was not to achieve any full understanding of Richat Dome, which is a structure of considerable complexity. We did feel, however, that shock metamorphic effects should be readily observable if the Dome were the root structure of a large impact crater. Our purpose was to determine whether or not such shock metamorphic features were present.

Acknowledgments

We gratefully acknowledge the financial support for the expedition of the Barringer Crater Company, headed by Brandon Barringer, and are particularly indebted to Paul and Dorothy Barringer, whose participation and assistance was invaluable in easing diplomatic and logistics problems. We also wish to express our deep appreciation to Max Deyneux, whose extensive geologic and geographic knowledge of the Adrar region made our field work less tedious and much more rewarding.

For a portion of his expenses, Cassidy also wishes to thank the University of Pittsburg's fund for space research provided by the Sarah Mellon Scaife Foundation and by Lt. General and Mrs. Richard K. Mellon.

General Geologic Setting of Richat

The Richat Dome was first described by Richard-Mollard (1948; 1952) and further elaborated upon by Monod (1952; 1954). The coordinates of its center are lat 21° 4′ N. and long 11° 22′ W. It forms a circular topographic depression about 38 km in diameter at the edge of a very extensive plateau composed of a flat-lying sedimentary sequence capped by the Chinguetti Sandstone of lower Paleozoic age. The lower part of the sequence, well exposed in the dome, consists of a series of upper Precambrian and lower Paleozoic, miogeosynclinal-facies rocks (carbonates, cherts, sandstones, quartzites, and slightly metamorphosed siliceous shales). As now sectioned by erosion, the dome consists of a series of annular rings, like the cut through an onion, with the quartzites forming ring ridges and the softer rocks forming toroidal depressions (which, incidentally, provide easy access to all parts of the structure). The dips of the beds increase toward the center to an average maximum of 20° to 25° (although dips as great as 35° are attained locally). Beyond these maximum values, the dips abruptly decrease as the center is approached. The central "eye" is occupied by a flat-lying limestone and a very subordinate amount of flat-lying meta-arkose. This central "eye" is immediately encircled by a discontinuous, massive ridge of chert and chert breccias, forming the so-called Guelb er Richat.

There has been at least minor igneous activity. Small dolerite dikes or sills outcrop at several locations within the structure. And a rather enigmatic rock type, termed analcimolite (Bardossy and others, 1963) occurs in several areas near the central Guelb. Although there is room for argument here, we interpret these rocks as zeolitized volcanic tuffs.

Radial and tangential faults are present in the outer parts of the structure, but are by no means pervasive. Additionally, in the northern part of the structure, we found a well-developed fault system which is apparently unrelated to the structural doming. Curiously, the system strikes N. 30° E., which is the trend of a straight line joining Richat with two other circular features of uncertain origin—Tenoumer and Temimichat—lying 300 and 400 km to the northeast, respectively.

Evidence Suggestive of Impact

Several lines of evidence have been advanced in favor of a meteoritic origin for Richat:

(1) Highly circular *endogenous* structures of this size are very unusual. With considerable justification, astrogeologists have come to regard all such structures as possible astroblemes until proven otherwise.

(2) The purely vertical uplift occurs in a region of flat-lying sedimentary rocks with few other structural disturbances of undisputed terrestrial origin within several hundred kilometers.

(3) Cailleux and others (1964) point out that the drainage pattern is directed inward rather than outward, as it should be if inherited from an original geomorphic dome. Such a pattern would, however, be expected if Richat were the root structure of a crater.

(4) There are rather extensive outcrops of brecciated cherts and quartzites immediately outside the central "eye." Impact breccias are, of course, a characteristic feature of astroblemes.

(5) Cailleux and others (1964) reported the presence of coesite in one of these brecciated quartzites.

(6) Aouelloul, a small crater of undoubted impact origin (Chao and others, 1966a; 1966b) is located 150 km to the southeast.

Results of the Present Investigation

The results of our investigation can be stated as follows: (1) no structural evidence for cryptoexplosive activity, (2) no megascopic evidence of shock metamorphism, and (3) no microscopic evidence of shock metamorphism in the rocks examined. These points are discussed in some detail below.

(1) Impact structures should show evidence of a natural explosive event. Because of the point application of an intensive force, and because shock waves are rapidly damped, an impact structure typically reveals a central "megabreccia" of highly disturbed beds which have been rotated and upthrown, and this distortion rapidly dies out radially outward. Further, astroblemes of this size have a so-called damped-wave aspect, that is a domal center surrounded by a structural depression. At Richat we found no case for the application of any sudden impulsive force. There is no evidence of what might be termed "geologic overkill." There is no megabreccia. No strata are overturned or even vertical. In fact, a flat-lying limestone and meta-arkose occupy the central "eye." Both appear normal in all respects and have not been subjected to any intense tectonism. The structure has the form of a simple dome and lacks any hint of any annular structural depression beyond the uplift. The entire dome is remarkably intact; only minor radial faulting was noted and some outward displacement of beds, which may be ascribable to gravitation slippage after domal uplift. All in all, the tectonic style at Richat best fits a history of slow vertical uplift.

(2) We observed no dikes or pods of injection breccia or pseudotachylite-like material. We did note rare, radial sandstone dikes, which we interpret as sedimentary fillings of open joints.

Of much greater significance is the absence of the conical shock fractures termed *shatter cones*, which have been found in about 20 other putative astroblemes (Dietz, 1968). The fine-grained, homogeneous carbonates and quartzites of Richat should have preserved this type of fracturing especially well. Such rocks are widely exposed within Richat, but our extensive search revealed no sign of this useful field-shock criterion. There is some evidence that shatter coning is related to the development of an elastic precursor shock wave and is formed over a limited range of shock overpressures—roughly from 20 to 80 kb (Johnson and Talbot, 1964). Hence, for large astroblemes shatter coning may be absent from the central eye, but well developed farther out. Shatter coning at the 35-km-diameter, well-exposed La Malbaie (or Charlevoix) structure of Quebec offers an instructive comparison, for it is of a size almost as large as Richat. This shock fracturing is a pervasive aspect of the central regions of this astrobleme; it is found in the central eye and out to ranges of 14 km from ground zero. However, the best development of shatter cones is not at the central point of greatest shock, Mont des Eboulements, but at about 7 km from this central peak where the plastic wave apparently had attenuated to the extent that the combination of strong elastic compression and rapid tensional release was optimal for their formation (Robertson, 1968).

We searched all regions of Richat without finding shatter cones. One horizon of cone-in-cone structure, which has been confused elsewhere with shatter coning (but which actually bears little resemblance), was noted. In view of the excellent outcrop exposures and the pervasive engulfment of the shocked rocks in astroblemes by shatter cones, their total absence is strong evidence against an impact origin for Richat.

(3) The past few years have seen the development of some very useful microscopic criteria indicative of shock metamorphism. Among the most diagnostic are: planar features (fracture sets lying along unusual crystallographic directions) in the mineral grains—shocked quartz, feldspar, and carbonates show these features especially well; optical isotropism of quartz and feldspar (maskelynite) without melting; and kink-banding in mica (Short, 1966). Twenty-eight thin sections of eleven rock types were examined carefully for any such features, and the results were completely negative. The rocks included all those most likely to show such features. Particular attention was paid to the chert and quartzite breccias.

Two of the quartzite breccias were collected from the same general area that Cailleux and others reported as the site of their coesite-bearing, shattered sandstone. Our specimens appear to be simple tectonic breccias, caused by slippage between adjacent rock units during the updoming. They do not correspond to the specimen description given by Cailleux and others. Our specimens consist almost entirely of quartz grains which uniformly display well-rounded nuclei and well-developed overgrowths. The rocks are very clean; there is little or no fine-grained material; the breccia fragments are essentially in place and are identical to the groundmass. The quartz grains are uniformly intact, showing neither random fracturing nor planar features.

The absence of planar features does not preclude the presence of coesite in these rocks since the minimum shock pressure necessary to produce planar features is about 50 kb, while coesite may form at pressures as low as about 20 kb (Short, 1966). However, at 20 kb shatter cones should form in the rocks, and the quartz grains should show extensive shattering.

The central nest of chert breccia is a remarkable aspect of Richat, and its origin would seem to be rather critical to the Richat problem. These breccias are highly variable over very short distances, principally with respect to the size and crystallinity of the chert fragments, the crystallinity of the groundmass chert, and the amount of quartz in the groundmass. All contain detrital quartz grains in the cherty groundmass. Some have only a trifle, some so much that the groundmass appears to be a quartzite in hand specimen. Rarely, both extremes may be found in the same thin section. No fractures or planar features are present in the quartz. All of these chert breccias are polymict breccias in the sense that the angular fragments are clearly different from the groundmass and cannot be derived from it, even though there is evidence of in-place fracturing for some fragments (some pieces could be fitted back together). They, therefore, *cannot* be tectonic breccias. Texturally, it appears that the quartz in the groundmass is being replaced by chalcedony. The groundmass shows no evidence of fracturing, grinding, or other disturbance, which suggests it had not lithified at the time of brecciation. On the basis of our examination, we suggest tentatively that these rocks may be pseudobreccias in the sense that they assumed their present configuration prior to complete lithification, perhaps as a result of the lithification process itself, which would involve the differential shrinkage of lenses and pods of pure silica gel in a mass of silica gel and quartz. But aside from speculation about the true origin of these chert breccias, and more to the point of this investigation, we are certain that these breccias are not shock breccias of the type formed by cosmic impacts.

Summary and Conclusions

During our careful field and laboratory examination of rocks exposed in the Richat Dome, we failed to find any of the features which should have been present, if the dome were the root structure of an impact crater. Other than for the minor presence of problematical rhyolite tuffs, there is neither evidence for explosive activity nor the application of any shock imprint.

It may be argued that Richat is a deep root structure of an impact crater and that all evidence of impact metamorphism has been removed by erosion. However, the amount of erosion this theory would require is excessive. Available data indicate that rather severe shock effects can be expected beneath an impact crater to depths which are about one-fifth the crater diameter (Baldwin, 1963). Less severe effects, such as shatter-coning, would extend even deeper. Thus, for a feature the size of Richat, we would expect to find evidence of shock to a depth of at least 10 km below the original surface. Removal of all shock features, then, requires at least 10 km of erosion of an area which has shown exceptional crustal stability, such as the flat-lying, undisturbed Precambrian and Paleozoic sediments, for half a billion years. Clearly there has been no significant tectonism or uplift, or both, since the formation of the dome. And since the maximum uparching of the dome can be no more than 3 to 4 km (Cailleux and others, 1964), it appears to be the upper limit to the amount of rock removed by subsequent erosion.

We conclude that the total lack of shock metamorphic effects is significant and that Richat is *not* an astrobleme, but is endogenous in origin. We note that both Richard-Mollard and Monod assigned an endogenic origin to Richat. The latter regarded it as a probable laccolith, but another possibility is that it is structural in response, for example, to tumescence of the upper mantle. Geophysical surveys might do much to explain its origin. Regional gravity and magnetic anomalies for the region have been assembled by Rechenmann (1965–1966), and these show no unusual anomalies. However, the critical control lines in the Adrar region may have skirted Richat only.

What of the other arguments favoring an impact origin? Except for the reported coesite, we regard them as either circumstantial or specious, or both. An endogenous origin for a large, highly circular dome requiring the application of purely vertical forces, in an area conspicuously lacking in any other tectonic features, is unusual, but is not impossible. The centripetal drainage pattern is not superimposed. It has clearly developed subsequent to peneplanation and is entirely normal for the present topographic configuration. The proximity of an undisputed meteorite crater—Aouelloul—has no significance, because the two events are quite unrelated in time. Aouelloul is a slightly eroded, bowl-shaped depression with a raised rim. It is probably Quaternary in age. Richat is an ancient geologic structure which has been peneplaned and then resculptured to its present configuration, which displays 100 m, or so, of local relief.

We have not yet attempted to separate coesite from the brecciated quartzites. We hope to do so in the near future. But even if coesite is present, we see no reason to change our conclusions. The complete absence of even minor grain fracturing in the quartz breccias compels us to reject a shock wave origin for that coesite. Coesite is stable at pressures of 20 kb or so, and it is possible that local intergrain stress concentrations may exceed this figure in certain tectonic environments which are characterized by strong shear stresses. Alternately, pressures lower than 20 kb may suffice to produce coesite in high-stress environments. Recent experiments have shown, in fact, that coesite can be synthesized metastably at confining pressures as low as 5 kb in samples which are simultaneously subjected to high-strain rates (Green, 1968). Should the presence of coesite in these rocks be confirmed, we would regard it as the first documented occurrence of this mineral resulting from normal, near-surface endogenous processes.

Semsiyat Dome

The flat-lying beds of the Mauritanian Adrar are disturbed by another dome, Semsiyat, 50 km west southwest of Richat's center, at lat 21° 0′ N. and long 11° 50′ W. Only 5 km across, it is much smaller than Richat, but of the same tectonic style, so that it may be fairly regarded as a *petit frére* of this great dome. Although it shows clearly from the air, it is barely perceptible on the ground. The quaquaversal dips of the annular beds are too low to measure in the field. The dome occurs on a flat plateau and the structure itself has a relief of only a few meters. The central "eye" is slightly depressed as is an outer "race track."

The direct evidence bearing on the origin of this structure is not nearly as clear-cut, as is the case for Richat. Primarily, this is due to the very poor exposures and the greater effect of weathering on those rocks which are exposed. There are, for example, no outcrops at all in the central "eye." During a one-day field reconnaissance, we found no shatter cones nor did we see any other structures or rock types suggestive of shock processes. A few pieces of badly weathered chert breccia were found as float in the central "eye." No quartzite breccias were found. There was no microscopic evidence of shock metamorphism in the quartzites we examined.

Taken alone, the evidence is far from conclusive. Nevertheless, the close structural similarity and areal proximity to Richat leads us to believe, in the absence of any evidence to the contrary, that the origins of the two structures are closely related. We conclude, therefore, that Semsiyat is also endogenous in origin and is not an impact feature.

Relationship to Three Modern (?) Meteorite Craters

French workers have tended to associate the Richat and Semsiyat domes with three modern (only slightly eroded) craters of central Mauritania—Aouelloul, Tenoumer, and Temimichat-Gallaman—which are aligned along a trend of N. 30° E. and over a distance of 500 km. This trend also passes just west of Semsiyat and skirts the eastern side of Richat. There can be no common time of genesis of these two groups of features, as Richat and Semsiyat are clearly ancient peneplaned and exhumed structures of at least pre-Neogene age. One may still argue that they all are endogenic and developed along a common fault line, but we are inclined to believe that the presence of Richat and Semsiyat along this lineation is fortuitous. Because of its impact glass, Aouelloul seems certainly to be a meteorite crater, and we suspected that Tenoumer and Temimichat-Gallaman may possibly be as well, although associated meteorites are unknown. Their lineation is suggestive of a possible triple impact event. Monod and Pomerol (1966) suggested that Tenoumer is a volcanic crater based upon associated lava dikes. However, a sample of this "lava" obtained by us at Dakar from the Bureau for Research in Geology and Mines has been the subject of restudy by Bevan French, who has found shocked inclusion of country rock of the type commonly associated with impact craters. Hence, this "lava" appears to be an impactite which tends to identify Tenoumer as a meteorite crater (B. French, personal commun.).

References Cited

Anonymous, 1967, Earth photographs from Gemini III, IV, and V: Natl. Aeronautics and Space Agency Spec. Pub. 129, p. 29.

Bardossy, G., Monod, T., and Pomerol, C., 1963, Decouverts d'analcimolites d'origine endogene dans les Richat (Adrar mauritanien): Acad. Sci. Comptes Rendus, 256, no. 9, p. 3934–3936.

Baldwin, R. B., 1963, The Measure of the Moon: Chicago, Univ. Chicago Press, 488 p.

Cailleux, A., Guillemaut, A., and Pomerol, C., 1964, Presence de coesite, indice de hautes pressions, dans l'accident circulaire des Richat: Acad. Sci. Comptes Rendus, 258, no. 22, p. 5488–5490.

Chao, E.C.T., Merril, C. W., Cuttitta, F., and Annell, C., 1966a, The Aouelloul crater and the Aouelloul glass of Mauritania, Africa (Abs.): Am. Geophys. Union Ann. Trans., v. 47, no. 1, p. 144.

Chao, E.C.T., Dwornik, E. J., and Merrill, Celine W., 1966b, Nickel-iron spherules from Aouelloul glass: Science, v. 154, p. 759–765.

Dietz, R. S., 1968, Shatter cones in cryptoexplosion structures, p. 267–285 *in* French, B. and Short, N. *Editors*, Shock metamorphism of natural materials, Baltimore, Mono Press, 646 p.

Freeburg, J., 1966, Terrestrial impact structures—a bibliography: U.S. Geol. Surv. Bull. 1220, 91 p.

Green, H. W., 1968, Metastable growth of coesite in highly strained quartz aggregates (Abs.): Am. Geophys. Union Trans., v. 49, no. 4, p. 753.

Johnson, G., and Talbot, R., 1964, A theoretical study of the shock wave origin of shatter cones: MS thesis, Air Force Inst. Tech., Wright Patterson AFB, Ohio, 92 p.

Monod, T., 1952, Les accidents crateriformes ou circulaires: French West Africa Div. Mines Bull., 15, tome 1, p. 166–194.

——— 1954, Sur quelques accidents circulaires ou crateriformes du Sahara Occidental: Internat. 19th Geol. Congr. Comptes Rendus, pt. 20, p. 85–93.

Monod, Th., and Pomerol, C., 1966, Le cratere de Tenoumer (Mauritanie) et ses laves: Soc. Géol. France Bull., ser. 7, 8, p. 165–172.

Rechenmann, J. (and **Y. Crenn and Rechenmann**), 1965–1966, Catalogue of gravimetric and magnetic stations of West Africa: Office de la Recherche Scientifique et Technique Outre-Mer Geophys. Papers, nos. 5, 6.

Richard-Mollard, J., 1948, Boutonniere du Richat en Adrar Mauritanien: Acad. Sci. Comptes Rendus, v. 227, p. 142–143.

——— 1952, La pseudo-boutonniers du Richat: French West Africa Div. Mines Bull. 15, tome 2, p. 391–401.

Robertson, P. B., 1968, La Malbaie structure—A Paleozoic meteorite impact scar: Meteoritics, v. 4, no. 2, p. 89–112.

Short, N. M., 1966, Shock processes in geology: Jour. Geol. Education, v. 14, no. 4, p. 149–166.

MANUSCRIPT RECEIVED BY THE SOCIETY, DECEMBER 2, 1968

Reprinted from Sea Frontiers Vol. 15, No. 4, 212-218.

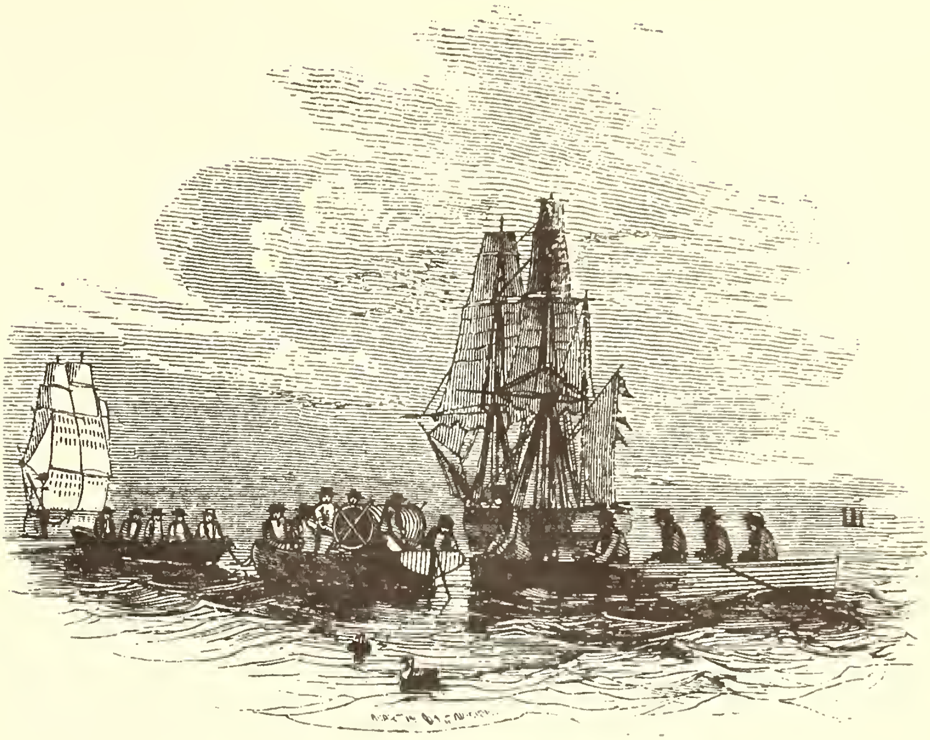

First Deep-Sea Sounding

By Robert S. Dietz and Harley J. Knebel
Environmental Science Services Administration
Atlantic Oceanographic and Meteorological Laboratories
Miami, Florida

On the 3rd of January [1840], at latitude 27°26'S., longitude 17°29'W., the weather and other circumstances being propitious, we succeeded in obtaining soundings with two thousand, four hundred twenty-five fathoms of line, a depression of the bed of the ocean beneath its surface very little short of the elevation of Mount Blanc above it." By this laconic account, Sir James C. Ross reported the first abyssal sounding from any ocean. It was made from H.M.S. *Erebus,* which, along with H.M.S. *Terror,* was participating in the British Antarctic Expedition, the results of which are

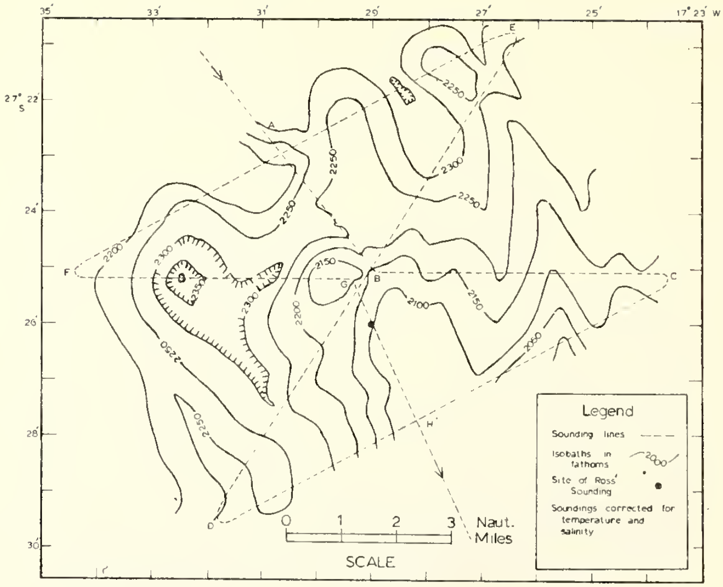

From small boats *(left) sailors lower hemp line and cannonball plummet to make the first abyssal sounding. This drawing accompanied Ross's original account of this voyage. Above is a bathymetric survey of the Ross sounding site as made by USC&GSS* Discoverer *in January, 1968.*

reported in *A Voyage of Discovery and Research in the Southern and Antarctic Regions, 1939-1943.*

Many years earlier (in 1818) Sir John Ross, commanding H.M.S. *Isabella* and exploring Baffins Bay for the purpose of "inquiring into the Possibility of a Northwest Passage," had recovered bottom mud from depths of 1,000 fathoms (73°37'N.; 77°25'W.) and 1,050 fathoms. Although this also was a remarkable accomplishment, it was not truly a deep-sea sounding, because the deep oceans have an average depth of 2,555 fathoms, or more than 2½ miles.

Ross made several fruitless attempts to obtain oceanic soundings while passing through the tropics en route to the Antarctic. These were, of course, made with long hemp lines, since sonic methods and even the use of thin piano wire had not yet been devised. Ross's repeated failures were principally due to the lack of a proper kind of line, but these failures served to point out what type was actually needed. Accordingly, Ross made up a line (stranded hemp?) on board of "three thousand six hundred fathoms or, rather more than four miles in length fitted with swivels to prevent it unlaying in descent, and strong enough to support a weight of seventy-six pounds."

Since it is not feasible to "feel" bottom at oceanic depths, Ross identified bottom by a decrease in the rate of pay-out of line from a free-spooling reel. Each 100 fathoms of the 3,600-fm. line was marked so that the rate-of-pay-out could be timed. This enormous reel was then placed in one of the ship's small boats and set free from the mother ship. This permitted oarsmen to maneuver the small boat in such a way as to offset currents and windage so as to keep the sounding line straight up and down. The oceans are so deep that even with a free-running line nearly an hour passed before Ross's 76-lb. plummet reached bottom.

Ross's Sounding Survives

Ross's sounding is still retained on modern charts (e.g., U. S. Navy Hydrographic Office Chart 5761), but it reads 2,426 fm. instead of 2,425 fm. Admiral G. S. Ritchie, the British Hydrographer, has written us that the sounding by Ross first appeared on Admiralty Chart No. 2203 in 1853 as 2,426 fm. and has been recorded as such ever since. However, no evidence can be found in the records of the Hydrographic Department as to why one fathom was added to Ross's measurement. We suppose that this is a calligraphic error, for a poorly handwritten "5" may have been transcribed as a "6." Certainly there is no justification for unrounding Ross's sounding considering the many inaccuracies involved in obtaining it.

Curiously, the position of Ross's sounding on modern charts is slightly at variance with that given by Ross. Presumably, this is also the result of a creeping error in transcription from one collection sheet to another without reference to the original source. The position of a sounding printed on a chart is, by convention, taken as a point at the geometric middle or, for a sounding such as 1,234 fathoms, between the 2 and the 3 and halfway up. It would seem that chart makers should return to Ross's values on their future charts. Certainly the first deep-sea sounding deserves special consideration.

"Bottomless" Soundings in Error

In the 1850's Lt. Matthew Fontaine Maury, the father of oceanography, formalized Ross's rate-of-pay-out method in his so-called Law of the Plummet's Descent. The method was prescribed for U. S. Navy ships after several doubtful ultra-deep soundings were duly reported to the Depot of Charts, the Navy's predecessor to the modern Naval Oceanographic Office. Maury was aware that deep undercurrents could induce "swigging forces upon the bight," which would cause a line to run out forever or, since sounding lines are of finite length, until the bitter end spooled off and disappeared beneath the surface. Even so, Maury recorded on his early Atlantic charts depths, now known to be fictitious, of 34,000, 39,000, 46,000, and even

A TOKEN LOWERING *with a cannonball is made by Captain Lorne Taylor of ESSA ship* Discoverer *at the site of James Ross's first abyssal sounding. (ESSA)*

7

50,000 feet with bottom contact unattained. It would seem that some naval officers, instead of determining the depth of the ocean, were attempting to answer the waggish question, "How long is a piece of string?"

In 1859 Maury wrote that successful soundings could not be made from a large vessel, presumably due to windage. Instead, "it was necessary that a boat should be lowered, and the trial be made from it; the men with their oars keeping the boat from drifting, and maintaining it in such a position that the line should be 'up and down' the while." It was pointed out earlier that Ross also used this method to maintain a zero line angle.

A Rugged Seascape

Since literally millions of soundings are now taken each year, it seemed appropriate to ask the USC&GSS *Discoverer* (while en route from Recife, Brazil, to Tristan da Cunha) to make brief, but precise, soundings at Ross's site. This is located in the South Atlantic Ocean on the western flank of the Mid-Atlantic Ridge, roughly halfway between the lower halves of South America and Africa. Accordingly, a brief survey was made over a 47-

THE CANNONBALL *that was lowered as a commemorative gesture at the site of Ross's sounding is held by Robert S. Dietz (left) and Harley J. Knebel. The arrow marks the site location in the South Atlantic.* (Miami Herald)

square-nautical-mile area in the vicinity of lat. 27°26'S., long. 17°29'W. Positions were maintained by dead reckoning with respect to reliable five-star celestial fixes so that the accuracy is probably within one nautical mile or so. Any greater accuracy is probably not critical since Ross's fix cannot be regarded as precise because of the time drift in his chronometer and the type of navigational devices used a century ago. The survey was laid out in a butterfly or hourglass pattern and the soundings were recorded on a Precision Depth Recorder set at 800 fm/sec. The soundings were corrected for salinity and temperature variations in sea water.

The bathymetric map resulting from the *Discoverer*'s survey shows the relief of the area to be bold and rugged; steep, isolated peaks separated by deep, V-shaped depressions are common. The northwestern half of the region has a mean depth greater than 2,200 fm. (4,023 m.); the southeastern half is shallower. The absolute relief observed along the sounding lines was 404 fm. The depth at Ross's sounding site is 2,100 fm. (3,843 m.), rounded to the nearest 5 fm. The maximum depth (2,400 fm.; 4,392 m.) in the survey area was found in a hole in a broad depression in the northwestern sector. Approximately 3.5 nautical miles separate these two locations. The Ross site occurs within the western flank province of the Mid-Atlantic Ridge, which accounts for the rugged relief. With this irregular sea-floor topography, substantial variations in depth can be recorded in small horizontal distances.

Ross a Trifle Deep

The precise position of H.M.S. *Erebus* at the time Ross made his historic sounding is uncertain. Today, even with the most sophisticated type of navigation, there are inherent errors. It is doubtful that Ross obtained an accuracy comparable to modern standards. Even if his position was exactly that which he recorded, the change in depth within 1 mile could have been more than 100 fm. It would be meaningless to speculate about the exact location of the first abyssal sounding. Nonetheless, it is interesting to compare the depth that Ross obtained with that which we obtained at his documented position. Ross's measured depth is about 325 fm. greater than ours. This amounts to an error of about 15 per cent, an error which could be introduced by a line angle of about 30°. If, however, we select the maximum depth within the area, then Ross's sounding is only 25 fm. more than ours and is in error by only 1 per cent. A line angle of 9° would account for this difference.

We cannot determine with any certainty the reason for Ross's sounding being overly deep, but two possibilities stand out: That the moment of bottom contact was not immediately recognized and that Ross's position was in error by 5 miles or more. We can probably rule out line angle as contributing to his excess depth for, as noted earlier, he obviated this problem by the use of a small boat with oarsmen. Most likely slowness and difficulty in recognizing first bottom contact was the reason as Ross, for his next sounding, used a plummet weighing 540 pounds—a sevenfold increase.

A Cannonball Lowered

In commemoration of Ross's historic sounding, a cannonball was lowered over the side in the vicinity of Ross's site. This iron ball is one recovered by divers in the Florida Keys and is believed to have come from an old Spanish wreck possibly three centuries old. Our original intent was to attempt to duplicate Ross's sounding by the historic technique of Maury, who prescribed cannonballs of either 32 lbs. or 68 lbs. as plummets. However, as our cannonball weighed only 12 lbs., it would not have been an effective plummet. Therefore, only a token lowering was made.

The exact nature of Ross's plummet is not known, but in his case it was probably not a cannonball, for his instructions from the Lord High Admiral read: "In the event of England being involved in hostilities with any other power during your absence, you are clearly to understand that you are not to commit any hostile act whatever; the expedition under your command being fitted out for the sole purpose of scientific discoveries, and it being the established practice of all civilized nations to consider vessels so employed as exempt from operations of war."

Little was known about oceanic depths prior to Ross's sounding. Among laymen, the oceans were generally regarded as bottomless. An estimate by the astronomer Laplace, based upon a deduced relationship between ocean depth and tide wave velocity, placed the abyssal depth at 12 miles. Other scientists had argued from an intuitive feeling that oceans were as deep as mountains are high. As Ross showed, this is more or less correct, although it takes a tall seamount to reach the surface of the ocean.

In revisiting this site, a hydrographic milestone was recognized and a bit of oceanographic history was relived. With Ross's sounding, the mirror that until then reflected only the sky would never be quite the same.

CHANGE OF ADDRESS

Members are requested to advise us six weeks prior to change of address.

Reprinted from Geological Society of America Bulletin,
Vol. 80, p. 1387-1390.

BARRETT H. ERICKSON
PAUL J. GRIM
Pacific Oceanographic Research Laboratory, Environmental Science Services Administration, Seattle, Washington

Profiles of Magnetic Anomalies South of the Aleutian Island Arc

Abstract: Characteristic features of linear magnetic anomalies south of the Aleutian Island Arc are illustrated by a series of closely spaced anomaly profiles. Within the area the anomalies change trend at the "Great Magnetic Bight," are offset at several fractures zones and terminate where they intersect the Aleutian Trench.

Oceanic crust that is thought to have formed from ascending mantle materials and spread away from oceanic rises is characterized by a recognizable pattern of linear magnetic anomalies (Vine and Matthews, 1963; Heirtzler and others, 1968). Studies based on the geographical distribution of this pattern, the orientation of fracture zones, and seismological observations have suggested that the earth's surface is comprised of large mobile blocks of crust bounded, where they interact with one another, by major tectonic features—rises, fracture zones, and island arc structures or belts of folded mountains (*see*, for example, Isacks and others, 1968). According to this hypothesis, the blocks spread apart from oceanic rises, slide past one another along fracture zones, and converge at island arcs where oceanic crust is thrust downward and destroyed.

A unique opportunity to examine the effects of an island arc structure on adjacent oceanic crust and on its characteristic magnetic anomaly pattern is afforded by data from detailed magnetic and bathymetric surveys of a large area south of the Aleutian Island Arc (Fig. 1). Studies based on these measurements have shown that the northward-trending anomaly pattern in the northeast Pacific Ocean swings westward just south of the eastern part of the Aleutian Islands (the "Great Magnetic Bight" described by Elvers and others, 1967) and continues westward to be offset by two fracture zones and to disappear where it intersects the Aleutian Trench. In this note we present a set of detailed magnetic anomaly profiles (Pl. 1) that illustrates the characteristic features of the anomalies and the changes that occur at their intersection with the Aleutian Trench. This material complements a more extensive discussion presented elsewhere (Grim and Erickson, 1969).

The magnetic measurements used in preparing the profiles were taken by the U.S. Coast and Geodetic Survey ships PIONEER, SURVEYOR, and OCEANOGRAPHER between 1961 and 1968 as part of ESSA's SEAMAP project (Peter and Stewart, 1965). The tracklines (Fig. 1), spaced at about 18.5 km, (10 n.m.) were controlled by Loran-C navigation. Satellite navigation was employed on the OCEANOGRAPHER in 1968.

Total magnetic field measurements, made with a proton precession magnetometer, were sampled and digitized at appropriate intervals, normally 5 minutes. No corrections were made for diurnal variations. With the use of a computer, positions were determined for each measurement and the "regional" magnetic field, calculated with the GSFC 9/65 set of spherical harmonic coefficients (Hendricks and Cain, 1966), was removed. The residual values, the magnetic anomalies, were then displayed as a sequence of north-south profiles with an x-y plotter. This sequence of profiles is shown in Plate 1. The geographic position of each profile is represented by the base of the shaded positive areas (*see* inset, Pl. 1). The anomalies, plotted with positive values to the west and negative to the east, are labeled according to the system of Pitman and others (1968). The two prominent peaks

Geological Society of America Bulletin, v. 80, p. 1387–1390, 1 fig., 1 pl., July 1969

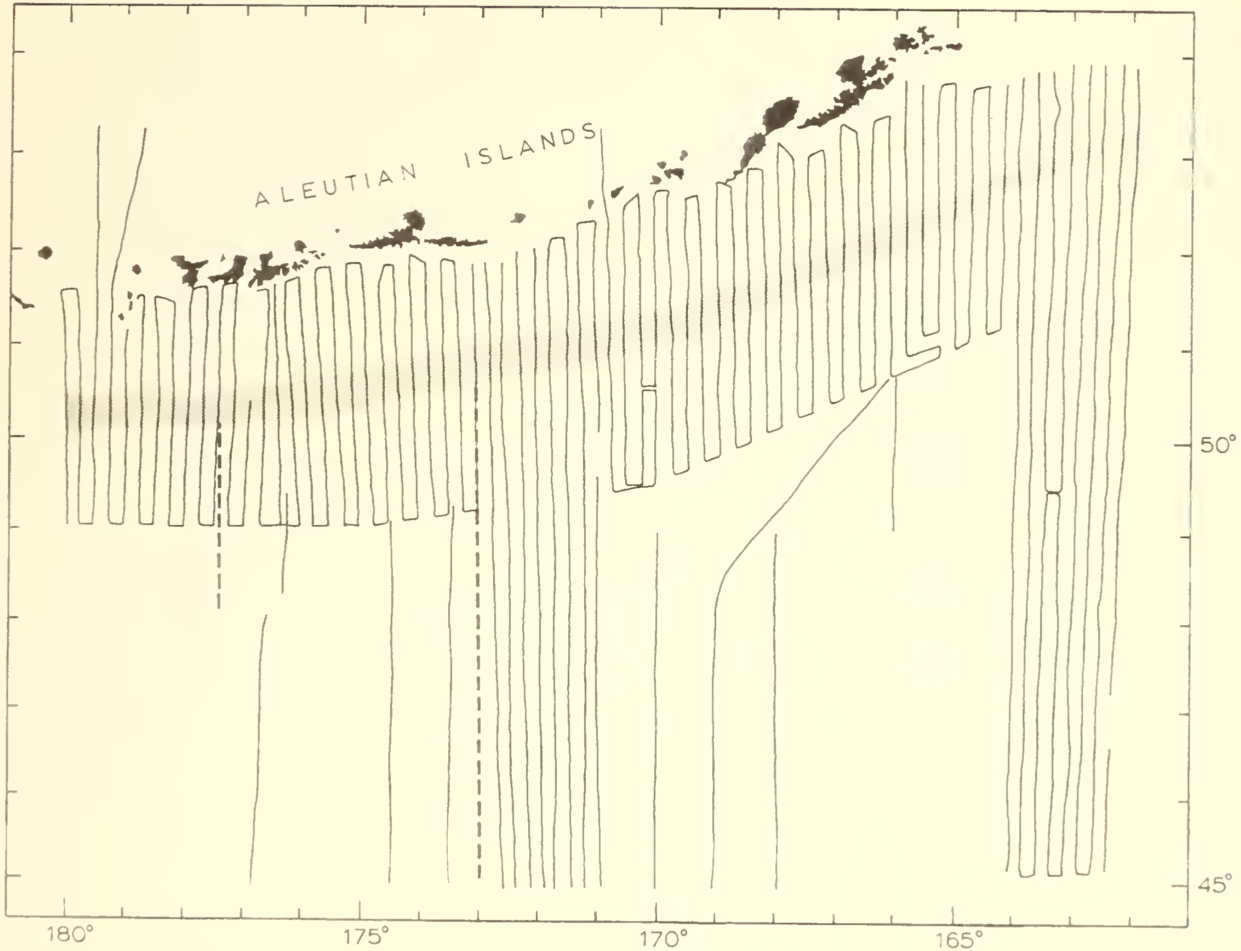

Figure 1. Index chart for the magnetic anomaly profiles shown in Plate 1. Aleutian Trench depths greater than 6400 meters are shaded. Dashed lines represent the locations of the Amlia and Adak fracture zones.

in this region, that lie on either side of anomaly 32, have been designated 32A and 32B.

The continuity of the anomalies and the persistency of the characteristic profile shapes are clearly demonstrated by Plate 1. Near 163° W., a portion of the "Great Magnetic Bight" is shown by the change in trend of anomalies 32A and 32B. The Amlia and Adak Fracture Zones (Hayes and Heirtzler, 1968; Grim and Erickson, 1969) interrupt the continuity of the anomalies at 173° W., and 177° 30′ W., where the pattern is offset left laterally. Near 168° W., a small fracture zone may be indicated by the offset of anomaly 32A. Over the Aleutian Trench the anomaly field is generally smooth and increases northward toward the island arc where shorter wavelength variations are observed as the water shoals. The anomalies encounter the Aleutian Trench at a small angle and die out over, or just beyond, the north wall. West of the Amlia Fracture Zone, the amplitudes of anomalies 25 through 27 are noticeably less than those observed farther east.

More extensive descriptions of the magnetic anomalies and fracture zones in this area and discussions of their relationship to concepts of sea-floor spreading can be found in Pitman and Hayes (1968) and Peter and others (1969), in addition to those references previously cited.

References Cited

Elvers, D. J., Mathewson, C. C., Kohler, R. E., and Moses, R. L., 1967, Systematic ocean surveys by the USC&GSS PIONEER 1961–1963: ESSA Operational Data Report C&GS DR-1, 19 p.

Grim, P. J., and Erickson, B. H., 1969, Fracture zones and magnetic anomalies south of the Aleutian Trench: Jour. Geophys. Research, v. 74, no. 6, p. 1488–1494.

Hayes, D. E., and Heirtzler, J. R., 1968, Magnetic anomalies and their relation to the Aleutian Island arc: Jour. Geophys. Research, v. 73, no. 14, p. 4637–4646.

Heirtzler, J. R., Dickson, G. O., Herron, E. M., Pitman, W. C., III, and Le Pichon, L., 1968, Marine magnetic anomalies, geomagnetic field reversals, and motions of the ocean floor and continents: Jour. Geophys. Research, v. 73, no. 6, p. 2119–2136.

Hendricks, S. J., and Cain, J. C., 1966, Magnetic field data for trapped-particle evaluations: Jour. Geophys. Research, v. 71, no. 1, p. 346–347.

Isacks, B., Oliver, J., and Sykes, L. R., 1968, Seismology and the new global tectonics: Jour. Geophys Research, v. 73, no. 18, p. 5855–5899.

Peter, G., and Stewart, H. B., Jr., 1965, Ocean surveys: The systematic approach: Nature, v. 206, p. 1017–1018.

Peter, G., Erickson, B. H., and Grim, P. J., 1969, Magnetic structure of the Aleutian Trench and northeast Pacific basin, in The Sea, v. 4: Interscience Publishers, in press.

Pitman, W. C., III, and Hayes, D. E., 1968, Sea-floor spreading in the Gulf of Alaska: Jour. Geophys. Research, v. 73, no. 20, p. 6571–6580.

Pitman, W. C., III, Herron, E. M., and Heirtzler, J. R., 1968, Magnetic anomalies in the Pacific and sea-floor spreading: Jour. Geophys. Research, v. 73, no. 6, p. 2069–2085.

Vine, F. J., and Matthews, D. H., 1963, Magnetic anomalies over oceanic ridges: Nature, v. 199, p. 947–949.

MANUSCRIPT RECEIVED BY THE SOCIETY JANUARY 22, 1969

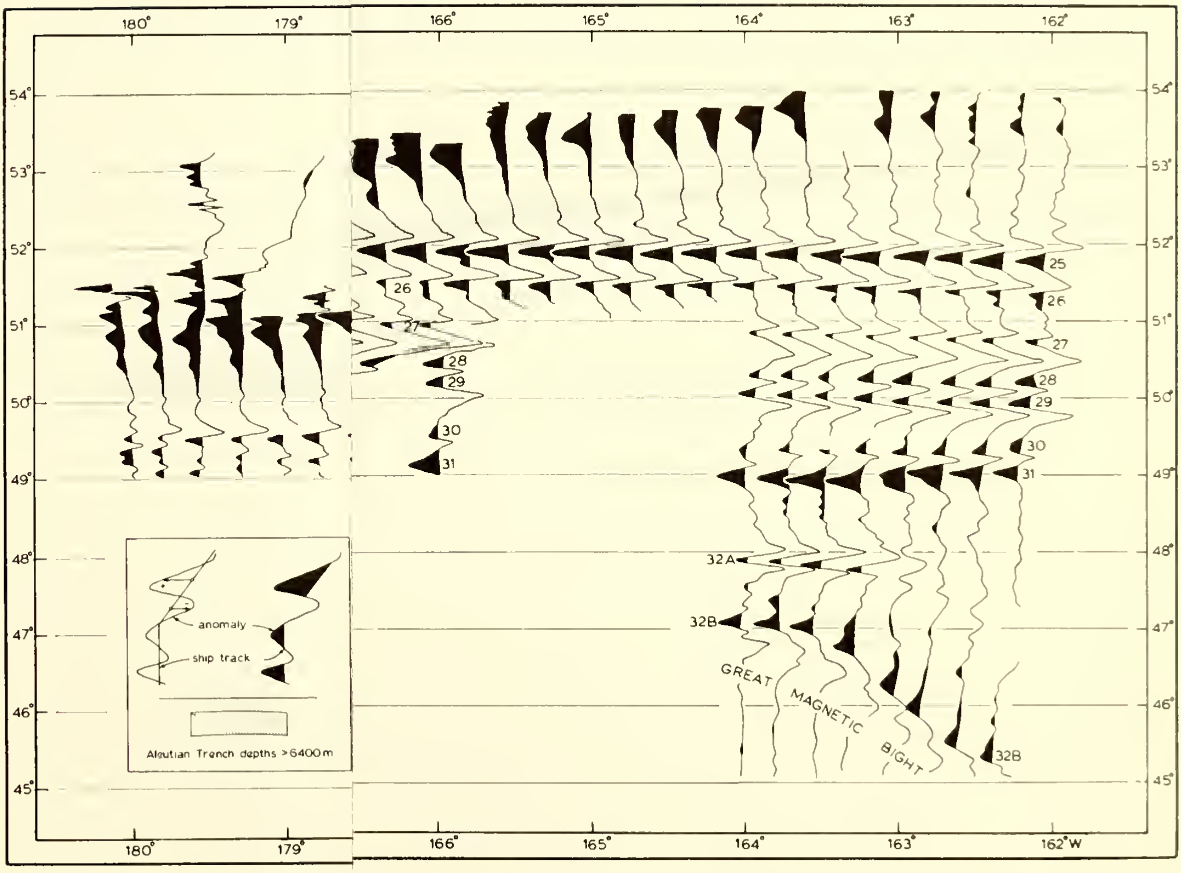

ERICKSON AND GRIM, PLATE 1
Geological Society of America Bulletin, v. 80, no. 7

in this region, that lie on either side of anomaly 32, have been designated 32A and 32B.

The continuity of the anomalies and the persistency of the characteristic profile shapes are clearly demonstrated by Plate 1. Near 163° W., a portion of the "Great Magnetic Bight" is shown by the change in trend of anomalies 32A and 32B. The Amlia and Adak Fracture Zones (Hayes and Heirtzler, 1968; Grim and Erickson, 1969) interrupt the continuity of the anomalies at 173° W., and 177° 30′ W., where the pattern is offset left laterally. Near 168° W., a small fracture zone may be indicated by the offset of anomaly 32A. Over the Aleutian Trench the anomaly field is generally smooth and increases northward toward the island arc where shorter wavelength variations are observed as the water shoals. The anomalies encounter the Aleutian Trench at a small angle and die out over, or just beyond, the north wall. West of the Amlia Fracture Zone, the amplitudes of anomalies 25 through 27 are noticeably less than those observed farther east.

More extensive descriptions of the magnetic anomalies and fracture zones in this area and discussions of their relationship to concepts of sea-floor spreading can be found in Pitman and Hayes (1968) and Peter and others (1969), in addition to those references previously cited.

References Cited

Elvers, D. J., Mathewson, C. C., Kohler, R. E., and Moses, R. L., 1967, Systematic ocean surveys by the USC&GSS PIONEER 1961–1963: ESSA Operational Data Report C&GS DR-1, 19 p.

Grim, P. J., and Erickson, B. H., 1969, Fracture zones and magnetic anomalies south of the Aleutian Trench: Jour. Geophys. Research, v. 74, no. 6, p. 1488–1494.

Hayes, D. E., and Heirtzler, J. R., 1968, Magnetic anomalies and their relation to the Aleutian Island arc: Jour. Geophys. Research, v. 73, no. 14, p. 4637–4646.

Heirtzler, J. R., Dickson, G. O., Herron, E. M., Pitman, W. C., III, and Le Pichon, L., 1968, Marine magnetic anomalies, geomagnetic field reversals, and motions of the ocean floor and continents: Jour. Geophys. Research, v. 73, no. 6, p. 2119–2136.

Hendricks, S. J., and Cain, J. C., 1966, Magnetic field data for trapped-particle evaluations: Jour. Geophys. Research, v. 71, no. 1, p. 346–347.

Isacks, B., Oliver, J., and Sykes, L. R., 1968, Seismology and the new global tectonics: Jour. Geophys Research, v. 73, no. 18, p. 5855–5899.

Peter, G., and Stewart, H. B., Jr., 1965, Ocean surveys: The systematic approach: Nature, v. 206, p. 1017–1018.

Peter, G., Erickson, B. H., and Grim, P. J., 1969, Magnetic structure of the Aleutian Trench and northeast Pacific basin, in The Sea, v. 4: Interscience Publishers, in press.

Pitman, W. C., III, and Hayes, D. E., 1968, Sea-floor spreading in the Gulf of Alaska: Jour. Geophys. Research, v. 73, no. 20, p. 6571–6580.

Pitman, W. C., III, Herron, E. M., and Heirtzler, J. R., 1968, Magnetic anomalies in the Pacific and sea-floor spreading: Jour. Geophys. Research, v. 73, no. 6, p. 2069–2085.

Vine, F. J., and Matthews, D. H., 1963, Magnetic anomalies over oceanic ridges: Nature, v. 199, p. 947–949.

MANUSCRIPT RECEIVED BY THE SOCIETY JANUARY 22, 1969

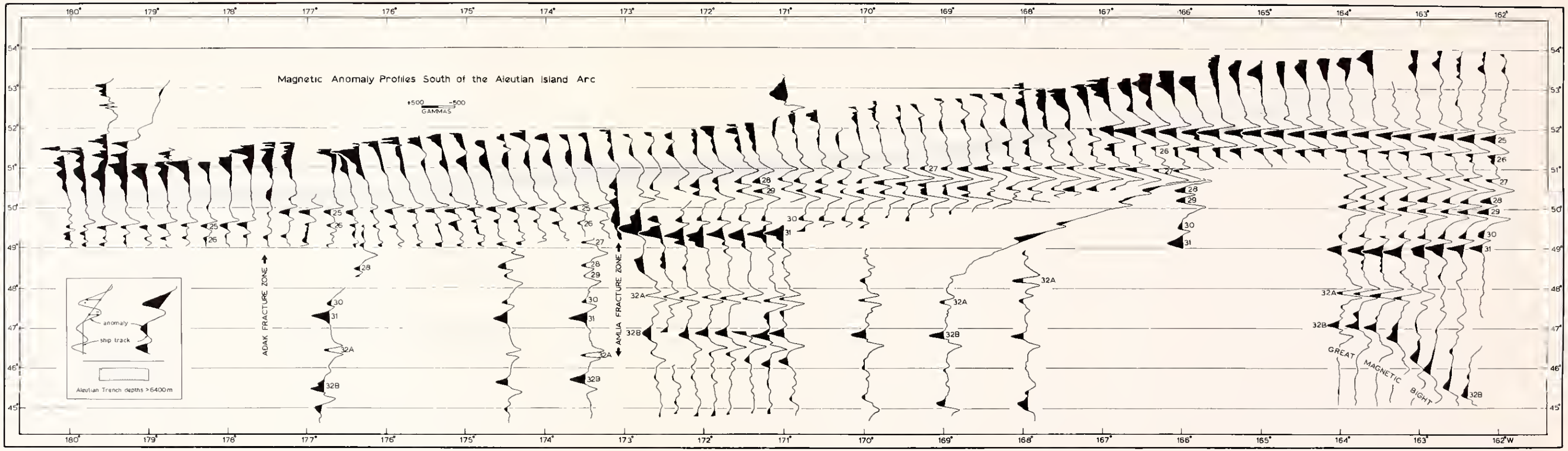
Magnetic Anomaly Profiles South of the Aleutian Island Arc
+500 -500
GAMMAS
180° 179° 178° 177° 176° 175° 174° 173° 172° 171° 170° 169° 168° 167° 166° 165° 164° 163° 162° W
54° 53° 52° 51° 50° 49° 48° 47° 46° 45°
ADAK FRACTURE ZONE
AMLIA FRACTURE ZONE
GREAT MAGNETIC BIGHT
25
26
27
28
29
30
31
32A
32B
anomaly
ship track
Aleutian Trench depths >6400 m

ERICKSON AND GRIM, PLATE 1
Geological Society of America Bulletin, v. 80, no. 7

Reprinted from Journal of Geophysical Research
Vol. 74, No. 15, 3933-3934.

JOURNAL OF GEOPHYSICAL RESEARCH VOL. 74, NO. 15, JULY 15, 1969

Brief Reports

Heat Flow Measurements in the Tasman Sea

PAUL J. GRIM[1]

Pacific Oceanographic Research Laboratory, ESSA
Seattle, Washington 98102

In September 1967, 14 ocean bottom heat flow measurements were attempted in the Tasman Sea from the ESSA Coast and Geodetic Survey ship *Oceanographer*. Seven of these are considered successful and are presented in Table 1 and Figure 1.

The thermal gradient measurements were made with a Ewing thermograd [*Gerard et al.*, 1962]. Three thermistor probes were spaced approximately 2 meters apart on a 6-meter core barrel, with the separations measured to the closest centimeter. The recorder was located in the fin assembly of the corer and measured temperature differences between the probes to ±0.01°C. A mercury switch indicated when the core barrel made an angle of over 15° with the vertical. The relationship given by *Bullard and Day* [1961] was used to estimate thermal conductivities of the sediments from the water content of the sediments collected by the corer.

Heat flow values presented in Table 1 are the product of the thermal gradient and conductivity values. No tilt was indicated for any of the seven stations. At four locations (1, 3, 4, and 5), the gradient is based on a series of

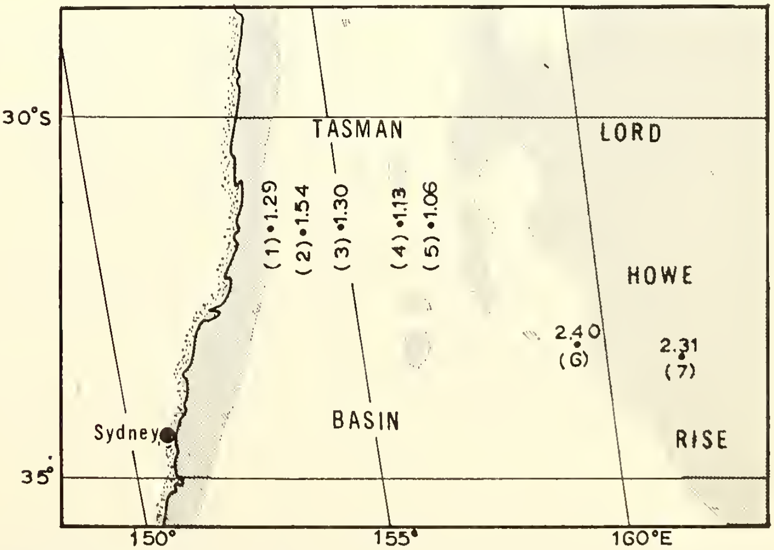

Fig. 1. Heat flow values in the Tasman Sea. Units are 10^{-6} cal/cm^2/sec. Station numbers are in parentheses. Depths less than 3000 meters are shaded (based on map by *Udintsev* [1964]).

---

[1] Now at Atlantic Oceanographic Laboratories, ESSA, Miami, Florida 33130.

Copyright © 1969 by the American Geophysical Union.

TABLE 1. Heat Flow Measurements from the Tasman Sea

Sta.	Latitude,* South	Longitude,* East	Depth, m	Probes in Mud	No. Conductivity Samples	Conductivity, × 10³ cal/cm/sec/°C	Gradient, × 10³ °C/cm	Heat Flow, × 10⁶ cal/cm²/sec	Estimated Error, %
1	31°33.9′	153°33.3′	3862	3	6	1.96	0.657	1.29	10
2	31°37.2′	154°14.0′	4565	2	4	2.25	0.685	1.54	15
3	31°30.5′	155°01.0′	4785	3	6	1.89	0.688	1.30	10
4	31°28.3′	156°12.5′	4689	3	4	1.99	0.567	1.13	10
5	31°30.5′	156°54.3′	4283	3	6	1.94	0.544	1.06	10
6	33°09.4′	159°27.0′	3609	2	5	2.02	1.19	2.40	15
7	33°22.6′	161°36.8′	1529	3	5	2.18	1.06	2.31	25

* Obtained with satellite navigation.

constant readings from the three thermistor probes that entered the sediment and showed, within the accuracy of the recorder, a linear temperature-depth relationship. These heat flow values are considered accurate to within 10%.

The heat flow values for the remaining stations are considered less accurate because of variations of conductivity along the core (station 2), curvature of the temperature-depth profile (station 7), and the quality of the film record (station 6).

Measurements 1–5 were closely spaced and show relatively little variation in heat flow. Station 1 is on the continental rise east of Australia, and stations 2 and 3 are of the Tasman abyssal plain. Stations 4 and 5 indicate that the heat flow just east of the Tasman abyssal plain is lower than on the plain, but this result should be considered with caution since the differences are so small. The relative uniformity of these five measurements suggests that much of the remainder of the Tasman basin may also have uniform heat flow. If this is so, it seems that this basin may be similar in this regard to other large areas of uniform heat flow, such as the one reported by *Reitzel* [1963] in the western Atlantic.

Stations 6 and 7 show two relatively high values of heat flow on the western part of Lord Howe rise; however, because of the poorer accuracy of these measurements, additional, more closely spaced, measurements are needed to determine if they are truly representative of the rise.

REFERENCES

Bullard, E. C., and A. Day, The flow of heat through the floor of the Atlantic Ocean, *Geophys. J.*, *4*, 282–292, 1961.

Gerard, R., M. G. Langseth, Jr., and M. Ewing, Thermal gradient measurements in the water and bottom sediment of the western Atlantic, *J. Geophys. Res.*, *67*, 785–803, 1962.

Reitzel, J., A region of uniform heat flow in the North Atlantic, *J. Geophys. Res.*, *68*, 5191–5196, 1963.

Udintsev, G. V. (Ed.), *Pacific Bathymetric Map of the Ocean: Pacific Ocean*, Department of Geodesy and Cartography, Geological Commission, Moscow, 1964.

(Received March 7, 1969.)

18

U. S. DEPARTMENT OF COMMERCE
Maurice H. Stans, Secretary
ENVIRONMENTAL SCIENCE SERVICES ADMINISTRATION
Robert M. White, Administrator
RESEARCH LABORATORIES
George S. Benton, Director

ESSA TECHNICAL REPORT ERL 93-POL 2

SEAMAP Deep-Sea Channel

PAUL J. GRIM

PACIFIC OCEANOGRAPHIC LABORATORY
SEATTLE, WASHINGTON
January 1969

For sale by the Superintendent of Documents, U.S. Government Printing Office, Washington, D.C. 20402
Price 35 cents.

TABLE OF CONTENTS

Page

ABSTRACT 1

1. INTRODUCTION 1

2. CHANNEL DESCRIPTION 5

3. DIRECTION OF FLOW 12

4. THE AXIAL PROFILE 12

5. LEVEE HEIGHT DIFFERENCES 14

6. ELEVATION 17

7. ORIGIN 19

8. AGE OF ALEUTIAN TRENCH 21

9. THE SEAMAP CHANNEL AND SEA-FLOOR SPREADING 21

10. ACKNOWLEDGMENTS 24

11. REFERENCES 25

SEAMAP DEEP-SEA CHANNEL

Paul J. Grim[1]

The SEAMAP deep-sea channel is a relic feature on the Aleutian abyssal plain south of the Aleutian trench. Along most of its 370-km length it has well-developed levees that are generally asymmetrical and differ in height. Typically the channel is about 50 m in depth and 6 km in width. From its northern end on the south wall of the Aleutian trench the channel floor rises towards the southwest from a depth of 4800 m to a minimum depth of 4590 m near its midpoint. Continuing in the same direction it deepens again to 4750 m. This gradient reversal precludes turbidity currents from flowing through the channel and supports the thesis that the Aleutian abyssal plain is a relic feature that has been cut off from its supply of turbidite material by the downbowing of the Aleutian trench. The channel apparently has been destroyed by slumping on the south wall of the trench north of the 4800-m contour. For much of its length, it is subparallel to the trench and from a topographic standpoint occupies the crest of the outer ridge south of the trench.

I. INTRODUCTION

As a result of ESSA's SEAMAP project in the central north Pacific, the SEAMAP deep-sea channel (Grim and Naugler, 1969) has been found on the Aleutian abyssal plain south of the Aleutian trench. Figure 1 shows its location in relation to the channels and abyssal plains in the northeast Pacific.

[1] Now at Marine Geology and Geophysics Laboratory, Miami, Florida.

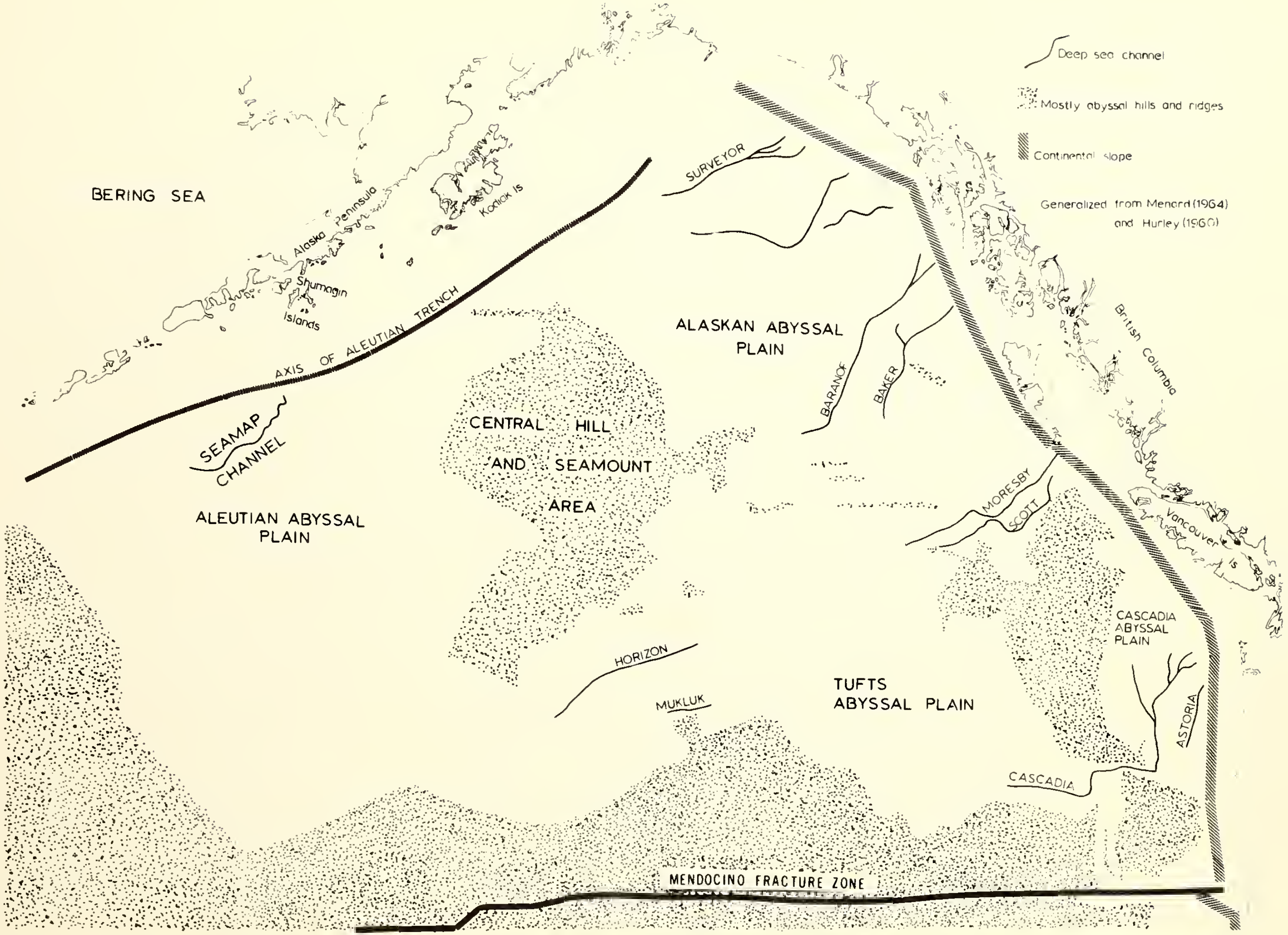

Figure 1. Generalized map of the northeast Pacific showing the SEAMAP channel, other deep sea channels and abyssal plains.

The most unusual aspect of the SEAMAP channel is the reversal of its axial gradient which precludes turbidity currents from flowing through it. It is the only known deep-sea channel that cannot be traced to a potential supply of turbidite material on the continental slope. This gives striking support to the thesis suggested by Hurley (1960) from bathymetric observations that the Aleutian abyssal plain is a "fossil" or relic plain that was cut off from its supply of turbidite material by the downbowing of the Aleutian trench and that the only present supply of sediment is pelagic material settling from the overlying water column.

Hamilton (1967) has given additional evidence of the fossil nature of this plain from seismic reflection results. He points out that, in addition to the plain sloping downward to the south and being blocked from turbidity currents on the north, east, and west, (1) the thickness of turbidite layers decreases towards the south and (2) the Aleutian abyssal plain (where he crossed it in an east-west direction between 47° and 48°N) is covered by an acoustically transparent 50- to 100-m layer of sediment that appears to be pelagic (this is supported by the fact that no turbidites have been cored on this plain).

The SEAMAP channel was first revealed by fathograms taken with a Precision Depth Recorder (PDR), a continuous echo sounding recorder that can be read to about ± 2 m. These were obtained by the U. S. Coast and Geodetic Survey ship PIONEER during the period 1961-1963. In April 1968, a 3-day study was conducted from the USC&GS ship OCEANOGRAPHER, and six crossings of the western part of the channel were made by the USC&GS ship

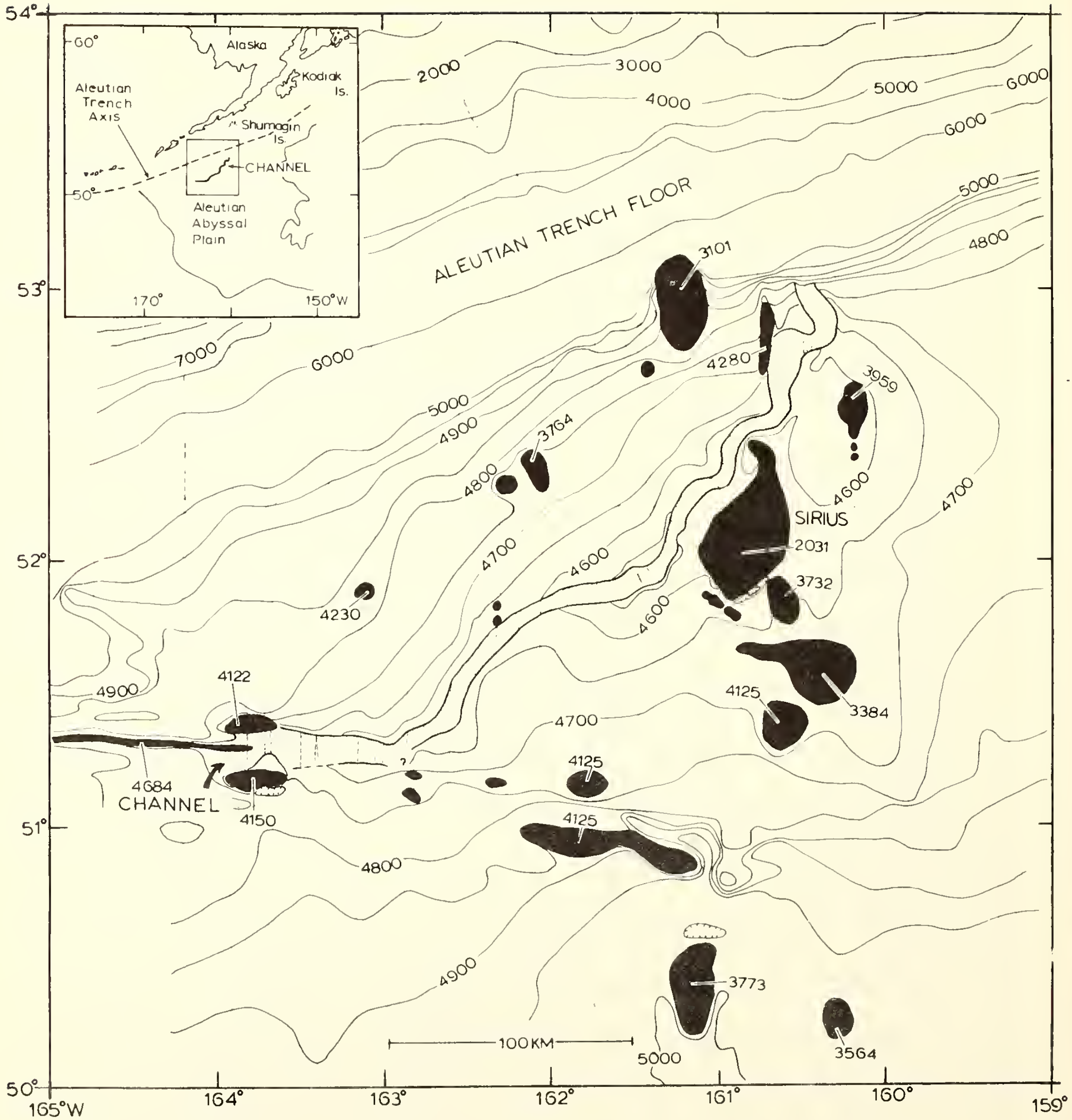

Figure 2. Bathymetric map of the SEAMAP channel area. Depths are in corrected meters. The contour interval varies as indicated. Ridges, seamounts, and abyssal hills are shown in black. Tracklines are indicated by dashed lines.

SURVEYOR in June 1968. Navigational control for the OCEANOGRAPHER was by satellite, which has an average error of about 300 m or less (Paulsen, 1966; Talwani et al., 1966), and for the PIONEER and SURVEYOR by Loran C, which has an accuracy of about 1/2 km in this region. All soundings were converted to corrected meters according to the method described by Ryan and Grim (1968).

In this report, "upstream" (towards the northeast) is the direction from which turbidity currents flowed when the channel was active. For easier correlation with location maps, all bathymetric profiles are presented with the channel viewed upstream.

2. CHANNEL DESCRIPTION

Figure 2 shows a bathymetric map of the channel; survey tracklines crossing the channel (arbitrarily serialized) are presented in figure 3. The channel has a general northeast-southwest trend, forming a slight angle with the Aleutian trench. Typically it is about 6 km wide and 50 m deep (measured from the tops of the levees to the channel bottom). The contours clearly show that the channel occupies the crest of a "ridge" (to be discussed below) along most of its course.

The northeast end of the channel is located on the south wall of the Aleutian trench at about the 4800-m contour. Farther north it has apparently been obliterated by slumping. North and west of Sirius seamount, there are meanders with an average "wavelength" of about 35 km. The channel floor rises irregularly along this segment (crossings 1 to 24) to a depth of about 4590 m and then deepens again towards the

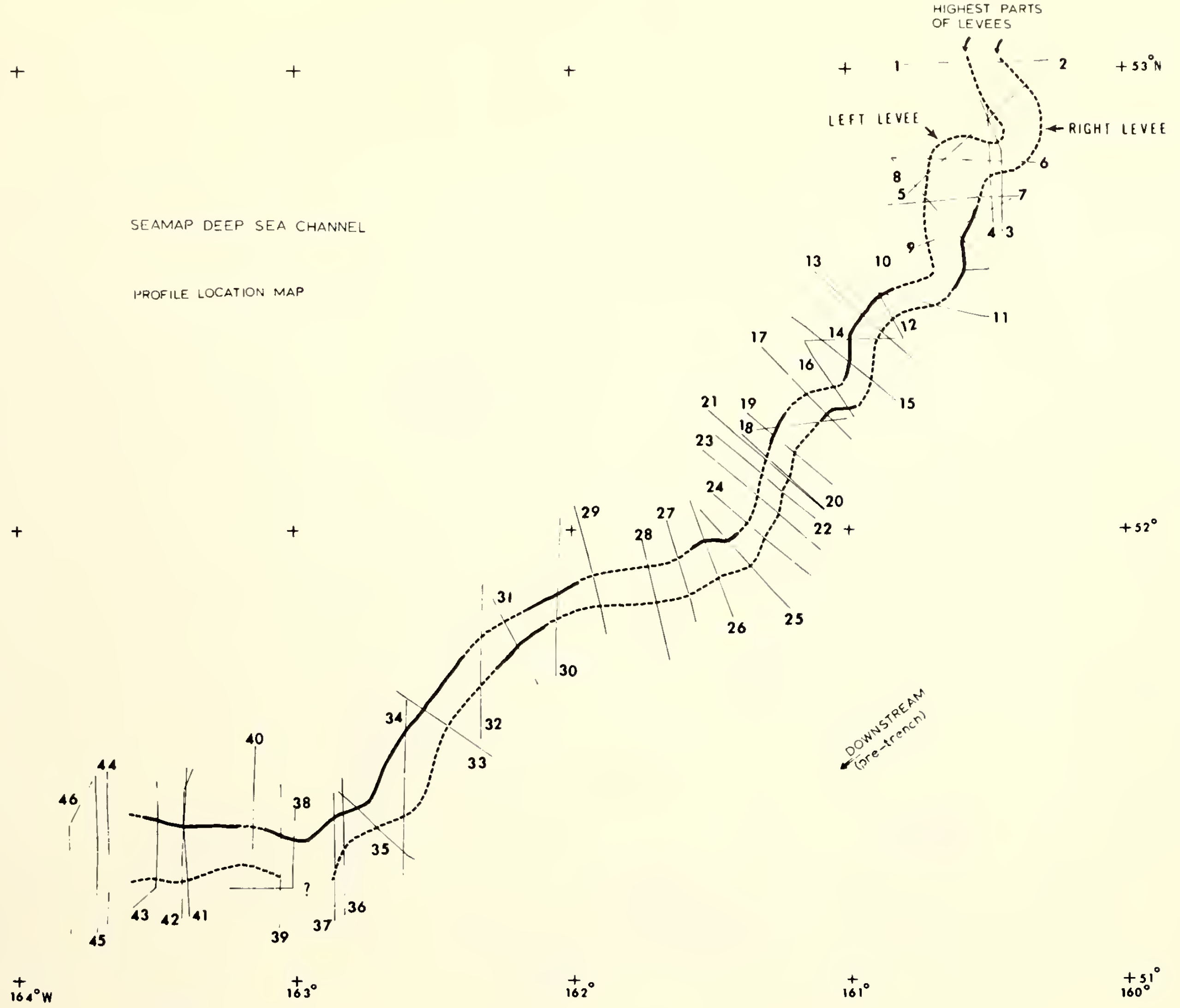

Figure 3. Profile location map for Precision Depth Recorder (PDR) tracings shown in figures 4, 5, 6, and 7. Where significant height differences seem to exist, the highest parts of the levees are indicated by solid lines.

southwest. At crossings 36 to 38 it bends sharply towards the west, widens, and at a depth of about 4750 m passes between two ridges (see fig. 2). West of the ridges it cannot be traced as a single feature.

Tracings of PDR records are presented in figures 4 through 7, where the horizontal scale is based on a ship speed of 15 kt. The error in this scale for individual profiles is judged to be less than 10 percent.

Profiles 1 to 8 (fig. 4) were made where the channel makes a very pronounced meander. The regional tilting caused by the Aleutian trench is clearly indicated in several of the crossings. Crossings 5, 6, 7, and 8 show that the channel is bordered on the west by a north-south trending ridge.

The PDR profiles in figure 5 were taken over the central part of the channel. The reversal of the axial gradient is clearly seen in this figure, i.e., the channel deepens both upstream and downstream from crossing 24. At crossings 20 and 21 the sharpness of the top of the right levee suggests that this may be a structural feature rather than a true levee.

In figure 6 the channel can be followed easily from profiles 30 to 37. Downstream from crossing 37, it bends abruptly to the west, probably as a result of structural control from underlying east-west trending ridges. At the bend itself there is a suggestion that the turbidity currents may have overridden the right levee and flowed to the south. However, fathograms are not available to substantiate this. At crossing 38 the channel is difficult to identify because of the very

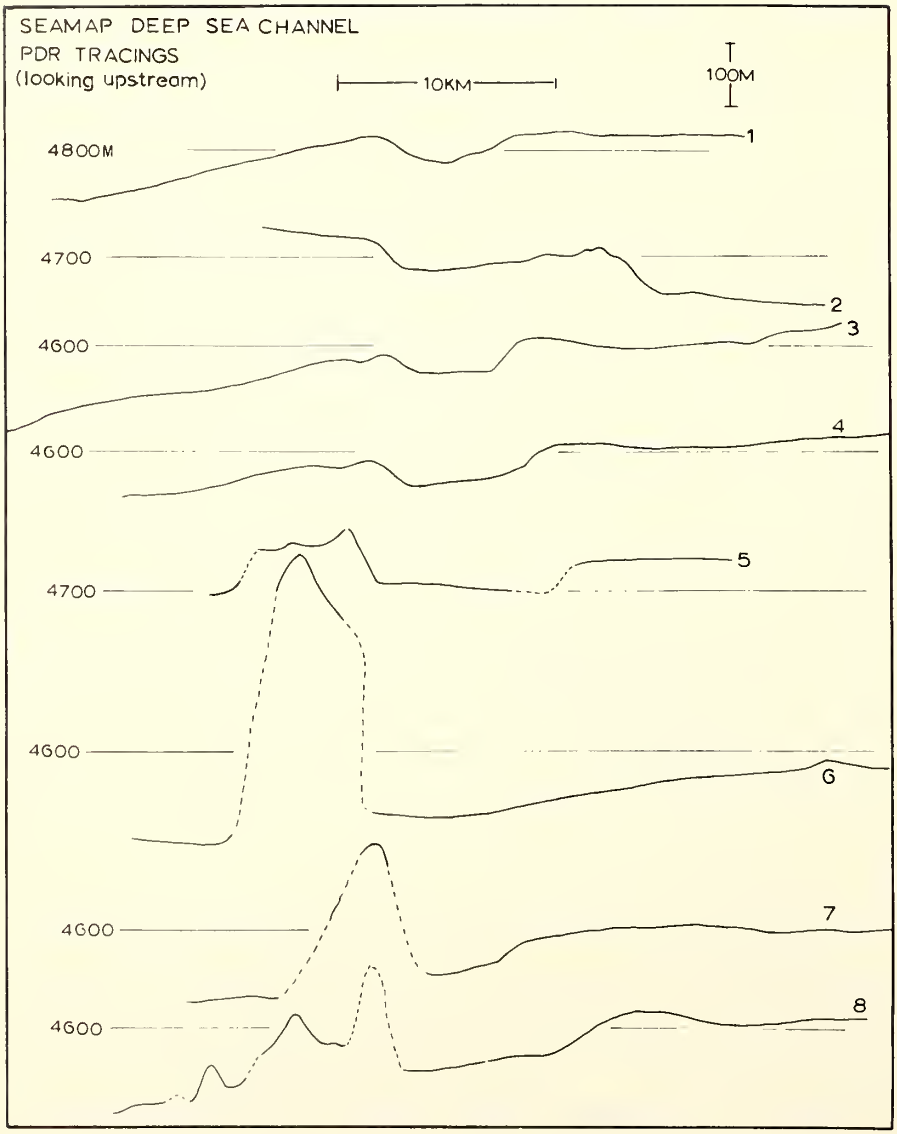

Figure 4. PDR tracings 1 through 8. See figure 3 for locations. Vertical exaggeration is about 30.

small right levee. This abrupt bend in the channel is further complicated by the secondary channel-type features seen in profiles 36 and 37. Farther to the west (crossings 41, 42, and 43) the channel widens and loses its distinctive shape.

To the west the channel passes between two ridges (fig. 7). Crossings 44 and 45 show a distinct single channel-like feature between the ridges but crossing 46 suggests that the turbidity currents probably flowed on either side of the small ridge between the large ridges. West of the ridges, i.e., west of profile 46, the flow was apparently more as sheet flow rather than channelized flow, since it is impossible to identify a single feature as the channel. Several channel-type features, such as relatively abrupt topographic changes similar to levees, occur, but these generally cannot be correlated across the tracklines run in this area (see fig. 2).

The channel profiles presented in figures 4 through 7 vary greatly. Much of this variation is caused by obvious structural control, e.g., profiles 5, 6, 7, and 8; some variations are the result of probable structural control, e.g., the right "levees" of profiles 20 and 21. Most of the profiles that appear to be unaffected by structure also show that the channel varies considerably in shape and cross-sectional area (with the angle of the crossing taken into consideration). For example: The shapes and relative heights of levees change appreciably over very short distances (crossings 13 to 17); some crossings (17 and 18) show a flat channel floor; others have a rounded floor or one that changes its slope very abruptly (crossings 31 and 33); and there is considerable variation

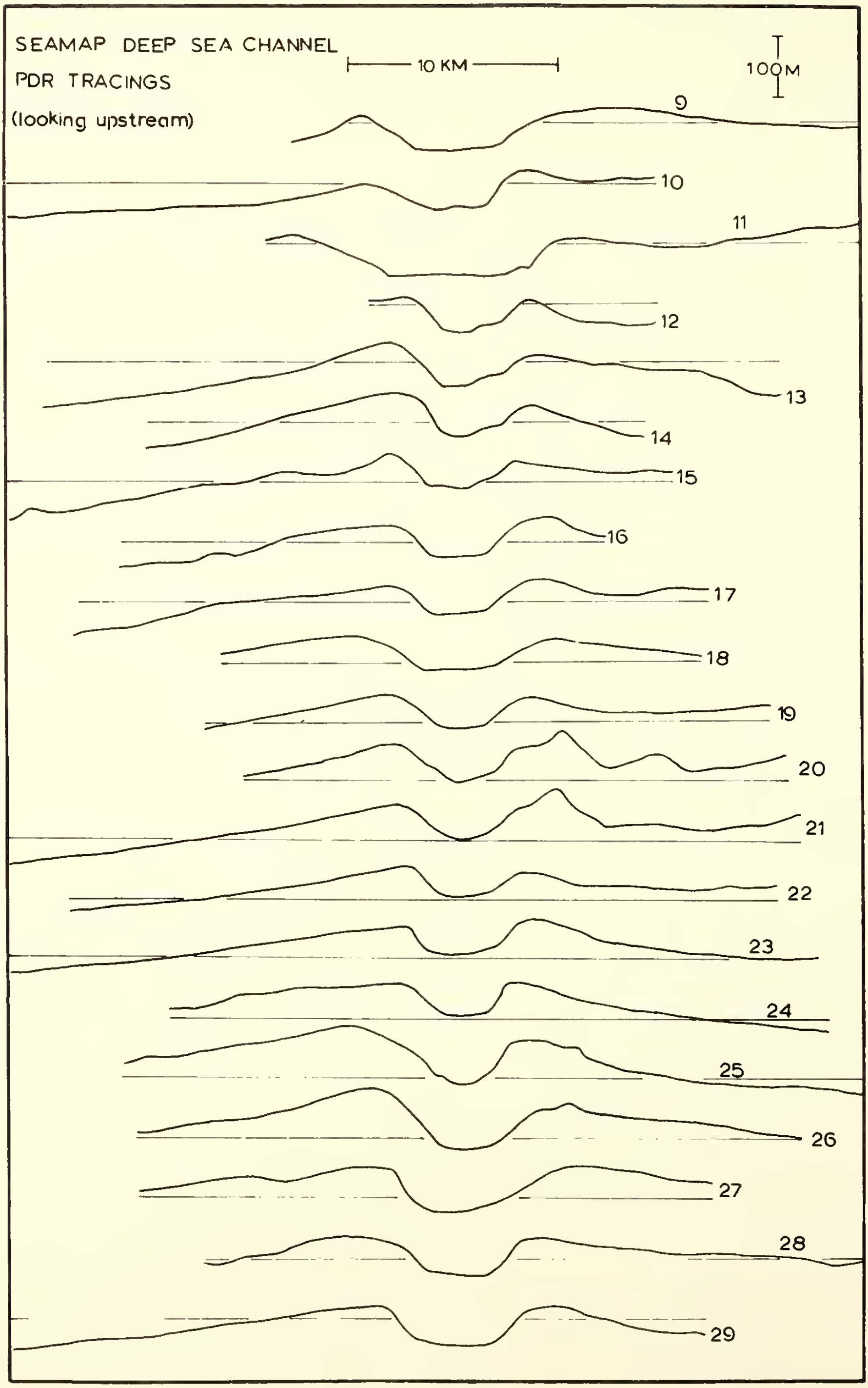

Figure 5. PDR tracings 9 through 29. A depth of 4600 m is indicated for each tracing. See figure 3 for locations. Vertical exaggeration is about 30.

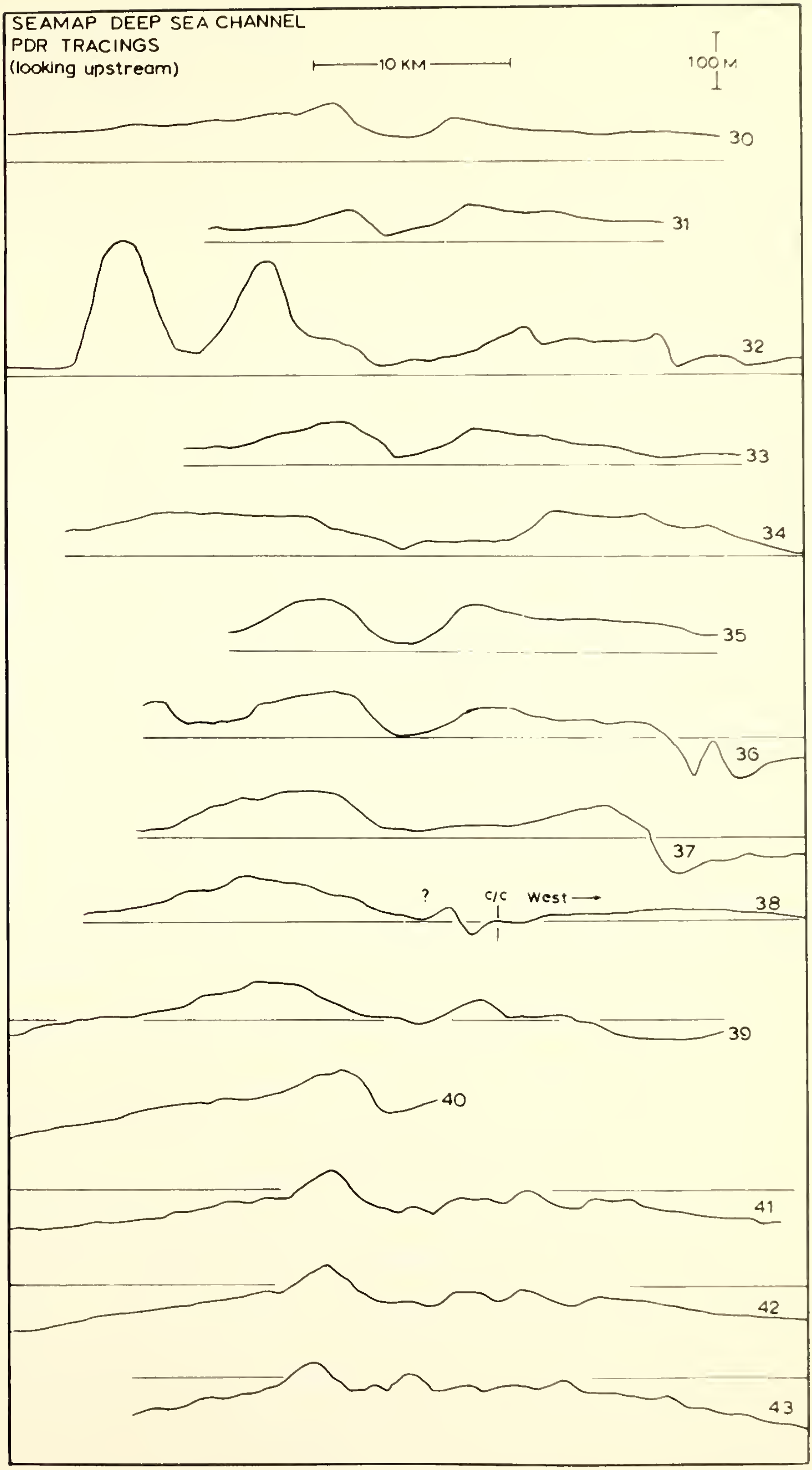

Figure 6. PDR tracings 30 to 43. A depth of 4700 m is indicated for each tracing. See figure 3 for locations. Vertical exaggeration is about 30.

in the cross-sectional area over short distances (crossings 25 to 31). Profiles 41, 42, and 43 are remarkably different in that they all display a rather indistinct right levee and a very irregular channel bottom.

3. DIRECTION OF FLOW

Turbidity currents must have flowed to the southwest when the channel was active because (1) the only plentiful supply of material for turbidites is continental North America,which is north and east of the channel, (2) in general the Aleutian abyssal plain deepens towards the south, and (3) the right levee (looking downstream) is consistently higher than the left levee between crossings 32 and 44 (where the relative heights of the channel levees have apparently been little affected by the formation of the trench, and where the channel does not meander). This is consistent with observations that in the northern hemisphere, looking downstream, the levee on the right side is higher because of the Coriolis effect. In addition, the SEAMAP channel is roughly parallel to the other active or potentially active channels in the northeast Pacific, all of which have a downstream direction towards the southwest (fig. 1).

4. THE AXIAL PROFILE

Figure 8 shows levee heights and the channel bottom plotted as a function of distance along the channel. From crossing 1 (the deepest part of the channel) the floor rises very irregularly with an average gradient of about 1.0 m/km to its highest point at crossing 24. Three prominent secondary "peaks" occur at crossings 3, 10, and 15. Downstream

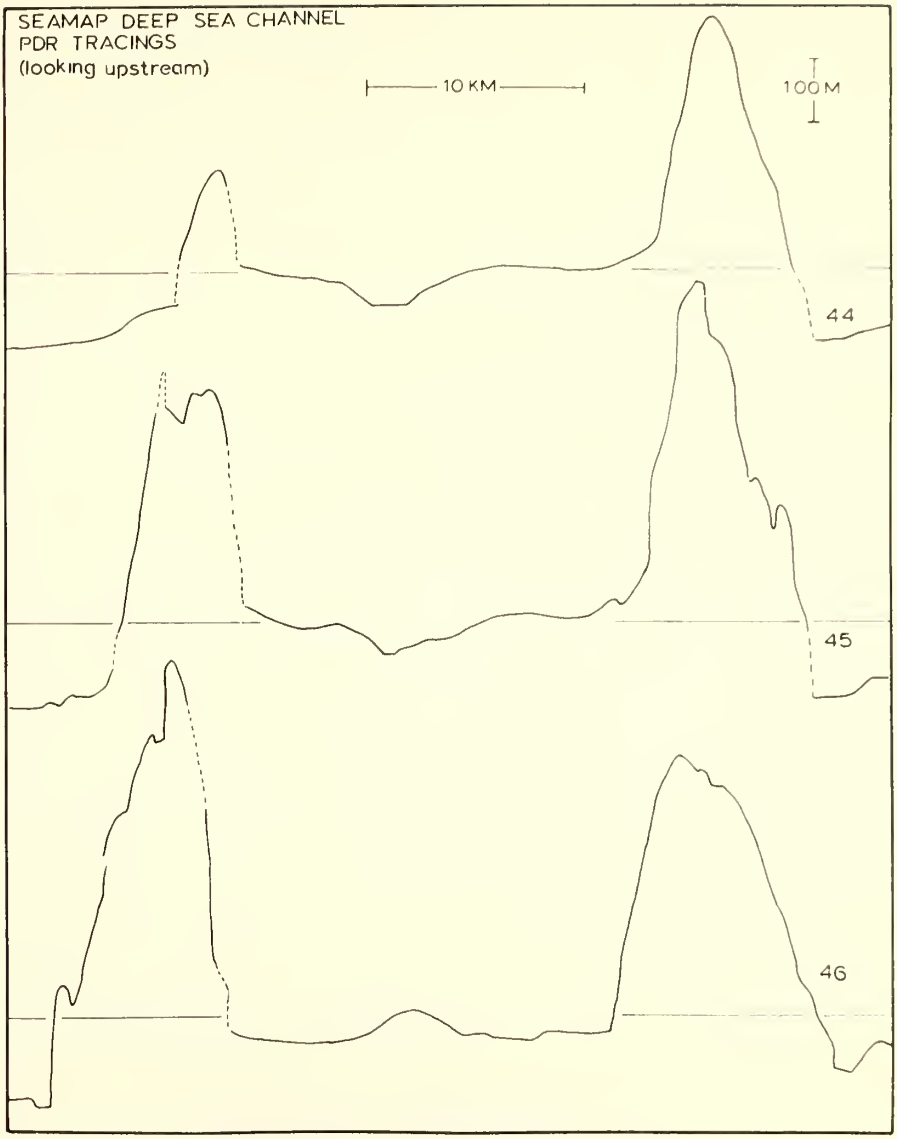

Figure 7. PDR tracings 44, 45, and 46. A depth of 4700 m is indicated for each tracing. See figure 3 for locations. Vertical exaggeration is about 30.

from crossing 24 the channel deepens with a relatively constant gradient of 1.4 m/km to crossing 31. Between crossings 31 and 37 the channel's gradient is essentially zero, and downstream from crossing 37 the channel deepens with a gradient of about 0.8 m/km to crossing 46.

The three secondary peaks upstream from crossing 24 may be, for the most part, the result of an irregular pre-trench axial gradient that was not uniformly downbowed by the trench. (The meanders cause the channel to "approach" the trench in an irregular manner, which would result in this uneven downbowing).

Because the channel consistently deepens from crossings 24 to 46 (with the exception of several minor gradient reversals) with gradients similar to known active or potentially active deep sea channels, the axial profile in this segment of the channel is probably similar to that which existed when the channel was active. The minor gradient reversals suggest that some minor changes, perhaps caused by the formation of the trench or post-trench processes, have occurred to alter the relative depths of different parts of this segment of the channel.

5. LEVEE HEIGHT DIFFERENCES

As shown in figure 8, the comparative heights of the right and left levees differ. Between crossings 11 and 19, where the channel meanders, the higher levee corresponds to that part of the channel where a turbidity current, flowing towards the southwest, would tend to overflow the channel because of the current's inertia (fig. 3). This agrees with the suggestion made by Buffington (1952) and Dietz (1958) that

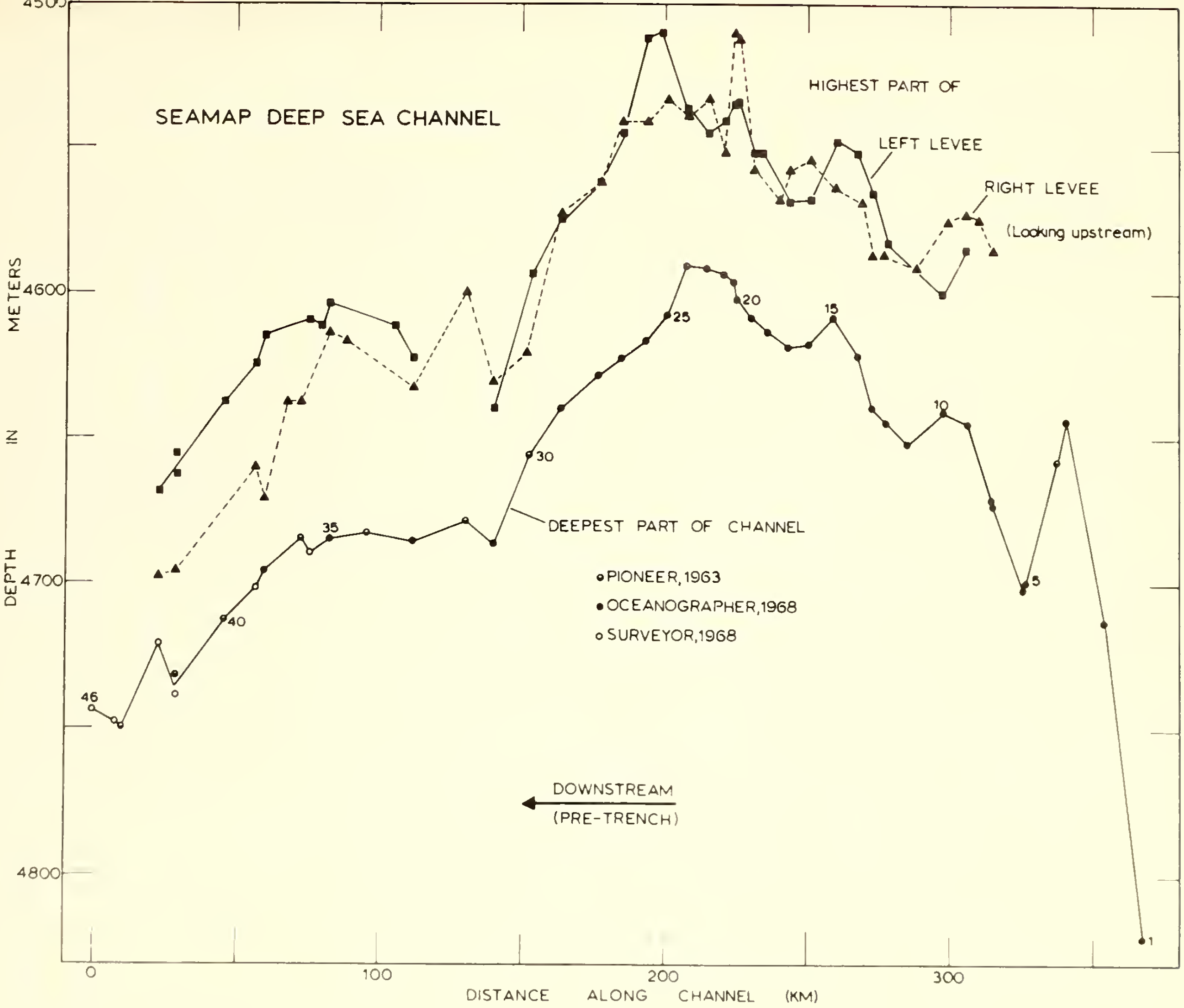

Figure 8. Depths of highest parts of levees and deepest part of channel as a function of distance along the channel. No levee depths are given where the channel is obviously flanked by a ridge or abyssal hill and in the northern section where it is judged that the tilting of the Aleutian trench has been strong enough to significantly alter the original differences in levee heights.

turbidity currents would tend to deposit more sediment on the levee of the outside bend of a channel, making this levee higher and resulting in an asymmetrical channel cross section.

Downstream from crossing 32, where the channel is straighter (except for the sharp bend near crossing 37), the left levee is consistently higher than the right levee. This is in accord with the proposal that, in the northern hemisphere, the Coriolis force causes the surface of turbidity currents to be tilted, so that when looking downstream the right side of the surface is higher than the left, resulting in a higher right levee being built (Menard, 1955; Menard et al., 1965; Hamilton, 1967). (Note that figures 4 through 7 are drawn as one would view the channel looking upstream).

Thus, between crossings 11 and 19 and downstream from crossing 32, the geometry of the levees supports both ideas advanced to explain levee height differences. For other parts of the channel, however, these explanations do not seem to be valid and in considering the causes of such differences the following complicating factors must be taken into account: (1) It is difficult to assess the relative contributions expected from the inertia and Coriolis effects; (2) apparently structural control influences levee heights to a considerable degree; for example, the shape of the right "levee" at crossings 20 and 21 suggests this may be a structural feature (fig. 5); and (3) the original relative heights may have been significantly changed by the effects of trench-forming or post-trench processes.

At crossings 25 and 26, the sharpness of the bends in the channel would suggest a higher right levee from the inertia effect, rather than the higher left levee shown. This is possibly due to structural control but, if so, it is not indicated by the profiles in figure 5. Similarly, a higher right levee would be predicted from considerations of the inertia effect at crossings 36, 37, and 38. There, however, the channel appears to be complicated by structural control and the right levee may have been partially destroyed in this section of the channel, possibly in a late stage of channel development.

6. ELEVATION

Along most of its length the channel lies on the crest of a "ridge" south of the Aleutian trench (figs. 2 and 9). Hamilton (1967) has observed similar, but less pronounced, channel elevations in other areas of the northeast Pacific. His seismic reflection results clearly show that deep-sea channels are depositional features. This suggests that the SEAMAP channel is located on an unusually thick accumulation of sediments.

The near-parallelism of much of the channel (and ridge) with the trench appears to be coincidental. It seems very likely that this ridge is a sedimentary feature unrelated to the structural outer ridge of the Aleutian trench because (1) the channel occupies the exact crest of the ridge and its distance from the trench is not constant and (2) as shown in figure 9, for tens of kilometers on either side of the channel, bathymetric profiles tend to be concave upwards and roughly symmetrical, except for seamounts, abyssal hills, and ridges.

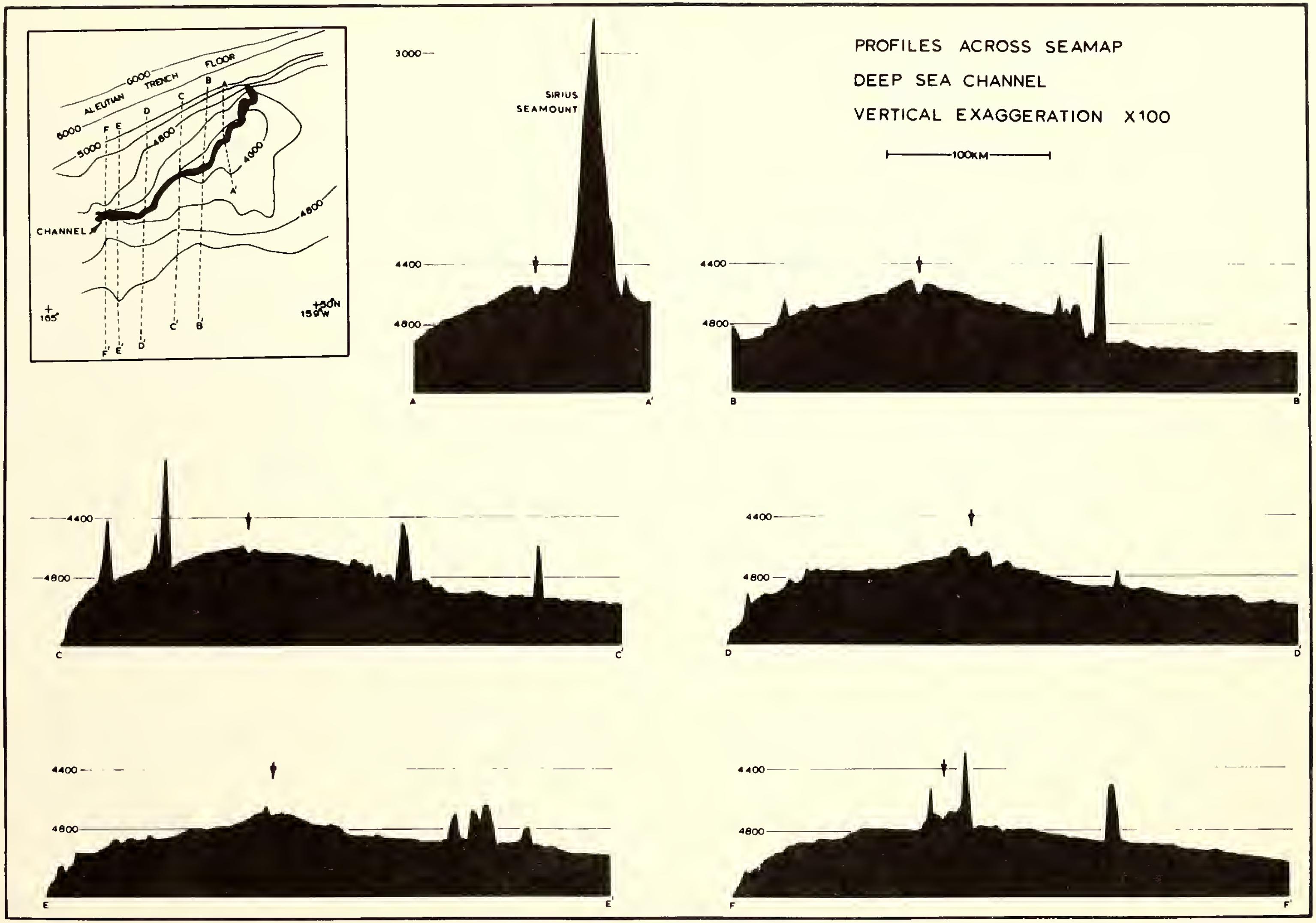

Figure 9. Profiles across channel with vertical exaggeration of 100. The channel is viewed looking upstream with arrows indicating the axis. Bathymetry of inset map is generalized and does not show seamounts, ridges, or abyssal hills.

The SEAMAP channel and its ridge of sediments pose many questions that may be answered when seismic reflection results become available. Some of these questions pertain to (1) the location of the outer ridge south of the trench as defined by basement; (2) the effects of buried ridges and abyssal hills on the course of the channel, especially near 163°W where it bends abruptly to the west; (3) the thickness of the pelagic sediment cover that overlies the turbidites; (4) the depositional development of the channel and the ridge and the possible lateral migration of the channel as shown for other deep-sea channels in the northeast Pacific by Hamilton (1967); and (5) the relation of the channel to the two ridges it passes between (profile FF' in fig. 9 and crossings 44, 45, and 46 in fig. 7) before losing its identity as a single feature west of the ridges.

7. ORIGIN

Assuming that the pre-trench gradient is approximated by that portion of the channel southwest of crossing 24, we can compare it with that of other active channels. The mean gradient from crossings 24 to 46 is about 0.75 m/km, but as pointed out above the gradient varies greatly from almost zero between 31 and 37 to 1.4 m/km between 24 and 31. Cascadia channel (fig. 1), whose axial profile is similar to that of other channels in the northeast Pacific, has gradients of 1.83, 1.67, and 1.17 m/km at respective distances of about 165, 275, and 435 km from the base of the continental slope (Hurley, 1960). Shepard (1966) shows that the gradient of the Monterey fan valley (upstream and continuous with the Monterey deep-sea channel) increases from 11 m/km on the inner fan close to Monterey canyon to 3.8 m/km at a meander about 75 km southwest of Monterey peninsula in California, and Heezen et al., (1959) have found that in the northwest Atlantic the midocean "canyon", where it is thousands of kilometers from its source, has a gradient generally ranging from about 0.25 to 0.5 m/km.

Although there are many difficulties in using such comparisons to obtain an approximate distance between the channel section from crossings 24 to 46 and the ancient source of turbidites, the comparisons suggest that this section was at least several hundred kilometers from the sediment source. On the other hand, as pointed out above, the location of the channel on top of a ridge implies an unusually thick accumulation of sediment, suggesting that the source area of the channel may have been relatively close, perhaps in the region between the Shumagin Islands and Kodiak Island (fig. 1). Our echo soundings, taken mainly along north-south lines, have not revealed the presence of the channel north of the trench. It seems likely that north of the segment discussed in this paper the channel has been obliterated.

An alternate explanation for its origin (suggested by R. Nayudu, personal communication) is that the channel may have been the downstream part of one of the channels in the northern part of the Gulf of Alaska, such as the Surveyor channel (fig. 1). This would mean that the part of the channel that looped over the area about to be downbowed was destroyed when the trench formed.

8. AGE OF ALEUTIAN TRENCH

Since turbidity currents cannot flow through the SEAMAP channel at present and cannot reach any part of the central and northern Aleutian abyssal plain because of the intervening Aleutian trench, dating of the top of the turbidite sequence should give the age of the trench, although, as will be shown, this is not necessarily true if the sea floor south of the trench is being thrust into the trench by the mechanism of sea-floor spreading. This age has been estimated by Hamilton (1967) at about 50 million years, based on a thickness of about 100 m of acoustically transparent sediment (the covering of pelagic material) and a sedimentation rate of 0.2 cm/1000 years. Using other combinations of thickness and sedimentation rates, he gives a range from about 20 to 100 million years. The sedimentation rate of 0.2 cm/1000 years is based on Scripps Chinook core 11 (Goldberg and Koide, 1958) located about 650 km west of the Aleutian abyssal plain. However, more recent rates derived from paleomagnetic studies of cores in the same area are much higher, suggesting a more probable average rate between 0.75 to 1 cm/1000 years (Ninkovitch et al., 1966). According to these rates, the pelagic cover would be 10 to 15 million years old.

9. THE SEAMAP CHANNEL AND SEA-FLOOR SPREADING

Because of its unique nature and its location south of the Aleutian trench, it is of interest to examine the SEAMAP channel in the light of the hypothesis of sea-floor spreading (Hess, 1962; Dietz, 1961), whereby oceanic crust, and the sediment accumulated on it, is carried to the trenches and thrust downward along active seismic zones. (For a current, well-documented discussion of this hypothesis, see Isacks et al., 1968). The SEAMAP channel, next to the active Aleutian trench (fig. 1), should, therefore, be carried into the trench where it will be destroyed within several million years. The hypothesis also predicts that much of the upstream part of the channel has already been so destroyed.

Recent studies show that sea-floor spreading is probably episodic, with the latest period beginning about 10 million years ago (e.g., Ewing and Ewing, 1967; Le Pichon, 1968; Isacks et al., 1968). The direction of spreading south of the trench for this period has been postulated as being from southeast to northwest (see, for example, McKenzie and Parker, 1967; Le Pichon, 1968; and Isacks et al., 1968). The amount of spreading can be estimated at about 500 km if we combine 10 million years with a spreading rate of about 5 cm/year, as deduced by Le Pichon (1968), for this part of the Aleutian trench. This agrees fairly well with the amount obtained independently by Isacks et al., (1968) who assume that the length of the seismic zones beneath island arcs is a measure of the amount of spreading in the last 10 million years. They show that the length of the seismic zone, and, therefore, the amount of spreading in this period, is about 350 to 400 km for this part of the Aleutian trench. Thus the SEAMAP channel 10 million years ago would have been about 350 to 500 km southeast of its present location.

If all of this is true, the following history of the SEAMAP channel is suggested. Ten million years ago the sea floor in this region was static, the Aleutian trench did not exist, and turbidity currents flowed through the SEAMAP channel onto the Aleutian abyssal plain. The channel was much longer, and the segment we see today was 350 to 500 km southeast of its present location. Spreading then started (which is in fair agreement with the 10 to 15 million years suggested in sec. 8 by pelagic sediment thickness and accumulation rates) and the Aleutian trench formed, cutting off the supply of the turbidite material from the SEAMAP channel and the Aleutian abyssal plain. The channel was carried towards the trench in a northwesterly direction at a rate of about 5 cm/year, and the upstream part was continuously destroyed as the sea floor was thrust into the trench. Today only 350 to 400 km of the channel remain. Continued spreading in a direction of about 50° west of north (as suggested by Le Pichon, 1968) will cause this part of the channel to be destroyed in about 2 or 3 million years.

Two aspects of the channel suggest, however, that it may have been close to its present position when the trench cut it off from its turbidite supply. The first, as pointed out above, is the probable presence of an unusually thick accumulation of sediment, which would indicate that the channel was relatively near a supply of turbidite material on the continental slope. The second is the well-developed meanders that occur only upstream (trenchward) of the gradient reversal (figs. 3 and 8), which suggest that these meanders are related in some manner to the formation of the trench, perhaps on a sea floor that was becoming flatter in response to the incipient formation of the trench, although it is of course also possible that the meanders result from structural control that by coincidence is far more dominant upstream than downstream from the reversal.

Another relationship between the channel and trench, based on the hypothesis of sea-floor spreading, is possible. Since the SEAMAP channel may be the downstream part of one of the channels in the Gulf of Alaska (fig. 1) as suggested above, turbidity currents could have continued to flow through it after the trench formed, since the sea floor was hundreds of kilometers southeast of its present location, with the result that the channel did not become isolated until an upstream segment of it was carried into the trench. If we accept this explanation, the time required for the pelagic cover of sediments to accumulate would be less than the age of the trench.

10. ACKNOWLEDGMENTS

I wish to thank the officers and crews of the U. S. Environmental Science Services Administration's Coast and Geodetic Survey ships PIONEER, SURVEYOR, and OCEANOGRAPHER whose care and skill in conducting the SEAMAP surveys provided the basic data used in this study. This paper has benefited from the comments of B. H. Erickson, F. P. Naugler, and T. V. Ryan.

11. REFERENCES

Buffington, E. C. (1952), Submarine natural levees, J. Geol. 60, 473.

Dietz, R. S. (1958), The channels on the deep sea floor, The New Scientist 2, 946.

Dietz, R. S. (1961), Continent and ocean basin evolution by spreading of the sea floor, Nature 190, 854.

Ewing, J., and M. Ewing (1967), Sediment distribution on the mid-ocean ridges with respect to spreading of the sea floor, Science 156, 1590.

Goldberg, E. D., and M. Koide (1958), Ionium-thorium chronology in deep-sea sediments of the Pacific, Science 128, 1003.

Grim, P. J., and F. P. Naugler (1969), A fossil deep-sea channel on the Aleutian abyssal plain, Science (in press).

Hamilton, E. L. (1967), Marine geology of abyssal plains in the Gulf of Alaska, J. Geophys. Res. 72, 4189.

Heezen, B. C., M. Tharp, and M. Ewing (1959), The floors of the oceans, I., The North Atlantic, Geol. Soc. Am., Spec. paper 65, 122 pp.

Hess, H. H. (1962), History of the ocean basins, Petrological Studies: A Volume in Honor of A. F. Buddington, ed. A. E. J. Engel et al., 599 (Geological Society of America, New York).

Hurley, R. J. (1960), The geomorphology of abyssal plains in the northeast Pacific Ocean, Scripps Inst. Oceanog. Ref. 60-7.

Isacks, B., J. Oliver, and L. R. Sykes (1968), Seismology and the new global tectonics, J. Geophys. Res. 73, 5855.

Le Pichon, X. (1968), Sea-floor spreading and continental drift, J. Geophys. Res. 73, 3661.

McKenzie, D., and R. L. Parker (1967), The North Pacific: An example of tectonics on a sphere, Nature 216, 1276.

Menard, H. W. (1955), Deep-sea channels, topography and sedimentation, Bull. Am. Assoc. Petrol. Geol. 39, 236.

Menard, H. W. (1964), Marine Geology of the Pacific,271 pp. (McGraw-Hill, New York).

Menard, H. W., S. M. Smith, and R. M. Pratt (1965), The Rhône deep-sea fan, Submarine Geology and Geophysics, 17, Colston papers, ed. W. F. Whittard and R. Bradshaw, 271 (Butterworths, London).

Ninkovitch, D., N. Opdyke, B. C. Heezen, and J. H. Foster (1966), Paleomagnetic stratigraphy, rates of deposition and tephrachronology in north Pacific deep-sea sediments, Earth Planet. Sci. Letters 1, 476.

Paulsen, F. G. (1966), Navy satellite navigation system, NASA CR-612.

Ryan, T. V., and P. J. Grim (1968), A new technique for echo sounding corrections, Intern. Hydrograph. Rev. 45, 41.

Shepard, F. P. (1966), Meander in valley crossing a deep-ocean fan, Science 154, 385.

Talwani, M., J. Dorman, J. L. Worzel, and G. M. Bryan (1966), Navigation at sea by satellite, J. Geophys. Res. 71, 5891.

GPO 848-850

Reprinted from Journal of Geophysical Research, Vol. 74, No. 6, 1484-1487.

JOURNAL OF GEOPHYSICAL RESEARCH VOL. 74, NO. 6, MARCH 15, 1969

Fracture Zones and Magnetic Anomalies South of the Aleutian Trench

PAUL J. GRIM AND BARRETT H. ERICKSON

Pacific Oceanographic Research Laboratory, ESSA, Seattle, Washington 98102

Magnetic anomalies south of the Aleutian trench between 164° and 180°W trend east–west. The magnetic pattern is disrupted at 173°W and 177°30′W by north–south-trending fracture zones named Amlia and Adak fracture zones, respectively. Correlation of magnetic anomaly profiles shows apparent left-lateral offsets of 220 km across the Amlia fracture zone and 30 km across the Adak fracture zone. The amplitudes of the anomalies are sharply reduced where they intersect the trench, resulting in a magnetically 'quiet zone' over most of the Aleutian trench and terrace. Although there are suggestions that the fracture zones extend north of the trench, the evidence is inconclusive.

INTRODUCTION

This paper describes two recently discovered fracture zones and shows magnetic trends south of the Aleutian trench between 164°W and 180° (Figures 1 and 2). The names Amlia and Adak have been proposed to the Board on Geographic Names for these fracture zones.

Most of the data are from the 1961–1964 work of the ships *Pioneer* and *Surveyor*, engaged in ESSA's North Pacific Seamap survey. In addition, several tracklines were run in 1968 by the *Surveyor* and *Oceanographer* to verify the southward extension of the Amlia fracture zone and to provide additional detailed data. The north–south tracklines indicated in Figure 2 are generally spaced about 18 km and were controlled by Loran C, which has an accuracy of about ½ km in this area. Measurements include depth soundings from a precision depth recorder (converted to corrected meters) and the total magnetic field of the earth made with a proton precession magnetometer.

The regional magnetic field was removed from the observations by using values calculated by a spherical harmonic expansion [*Hendricks and Cain*, 1966]. No corrections were made for daily variations. The magnetic anomalies are numbered by the system used by Lamont workers [*Pitman et al.*, 1968]. Since anomaly 32 appears as two prominent peaks, we have numbered these 32A and 32B.

During the last decade an extensive pattern of linear north–south-trending magnetic anomalies has been revealed in the northeastern Pacific [*Mason*, 1958; *Mason and Raff*, 1961; *Raff and Mason*, 1961]. Where this pattern is crossed by the Murray, Pioneer, and Mendocino fracture zones, it was found that the offset of the magnetic pattern provided a measure of the apparent horizontal slip along each fracture zone [*Mason*, 1958; *Vacquier*, 1959; *Mason and Raff*, 1961; *Vacquier et al.*, 1961; *Raff*, 1962]. *Raff* [1966] *and Peter* [1966] have shown that just north of the Mendocino fracture zone the anomalies are found as far west as 165°W (see Figure 1). Reports based on Seamap data have delineated the northward continuation of the anomalies [*Peter and Stewart*, 1965], their offset by the Surveyor fracture zone [*Peter*, 1966], and the westward bend (the Great Magnetic Bight) between 47° and 52°N [*Elvers, Peter, and Moses*, 1967; *Elvers, Mathewson, Kohler, and Moses*, 1967]. Our results show the westward continuation of the anomalies between 164° and 180°W and their offset by the Amlia and Adak fracture zones [*Grim and Erickson*, 1967]. The existence of the Amlia fracture zone has been shown independently by *Hayes and Heirtzler* [1968].

The east–west continuity of the magnetic anomalies is clearly demonstrated by profiles M through U in Figures 2 and 3. The total sequence of anomalies 28 through 32B is shown on profile K (Figures 2 and 5). We have observed no interruption of the anomalies at 171°W as speculated by *Hayes and Heirtzler* [1968].

The amplitudes of the anomalies are sharply

Copyright © 1969 by the American Geophysical Union.

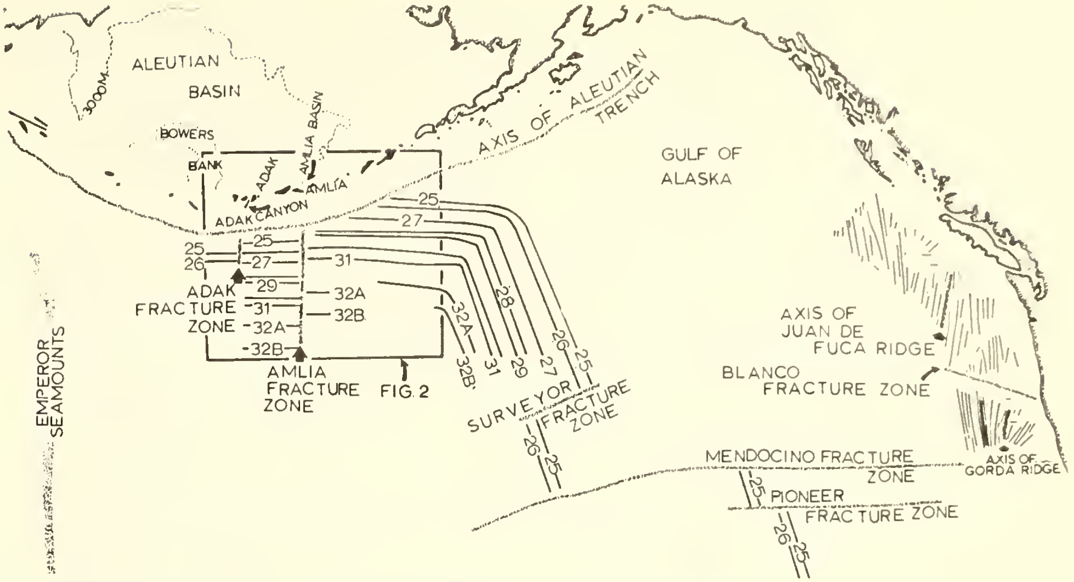

Fig. 1. Index map with some of the magnetic anomalies shown schematically. See Figure 2 for details within the outlined area. *Peter's* [1966] 'guide anomalies' (numbers 25 and 26) are shown to illustrate the offsets across fracture zones.

reduced where they intersect the trench. In Figure 3 profiles M, N, and P appear to show vestiges of anomaly 25 crossing the trench and continuing onto the Aleutian terrace with a greatly reduced amplitude. Profiles west of M (not shown) suggest that anomaly 26 likewise crosses the trench (see Figure 2 for these possible extensions). No indication of anomaly 27 is found beyond the trench, although the large negative anomaly south of anomaly 27 extends across the trench to the north wall (see profile K). Anomalies 28 and 29 are offset by the Amlia fracture zone south of the trench.

The magnetic field tends to be generally smooth over the trench. *Hayes and Heirtzler* [1968] have noted this and called it a 'quiet zone.' High-frequency anomalies are found in shallow water to the north [*Hayes and Heirtzler*, 1968; *Keller et al.*, 1954; *Skorpen*, 1967] where the tracklines cross the Aleutian ridge.

Amlia Fracture Zone

The Amlia fracture zone, named for Amlia Island, trends north–south at about 173°W (Figures 1 and 2). Its location is shown by changes in both the bathymetry and the magnetic pattern south of the trench (Figure 4). West of the Amlia fracture zone the topography is dominated by east–west-trending ridges and troughs with relief averaging about 500 meters; east of the fracture zone the topography is characterized by subdued east–west trends with a relief of about 200 meters. The location of the axis of the Amlia fracture zone (shown in Figure 4 by arrows) is based on the disruption of the magnetic pattern. The conspicuous topographic depression extending south from the Aleutian trench (outlined by the 5600-meter contour) is not reflected by the magnetic anomalies but is probably associated with the fracture zone. No obvious topographic expression of the fracture zone is found within the trench.

Figures 1 and 2 show a left-lateral displacement of the magnetic pattern across the Amlia fracture zone. Correlation across the fracture zone is based on a comparison of profiles H and J west of the Amlia fracture zone with profiles K, L, and S to the east (Figures 2 and 5). Anomalies 25 and 26 are not present on profiles K and L because they disappear at the trench farther east. The left half of Figure 5 has been shifted north by 2° of latitude to bring the pattern of magnetic anomalies into alignment. The correlation of the pattern with this shift,

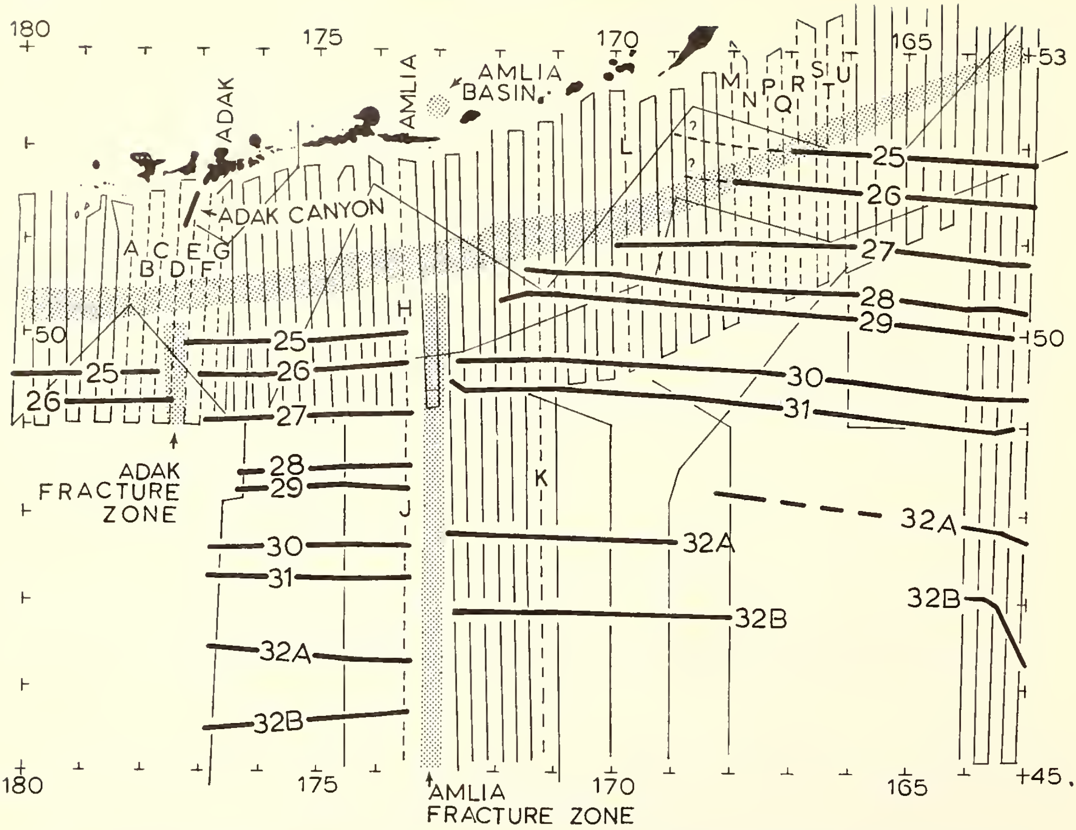

Fig. 2. Location of magnetic anomalies 25 through 32B. Heavy lines represent anomalies; lighter lines represent idealized tracklines. Shaded areas denote fracture zones, Aleutian trench depths greater than 3500 fathoms (6400 meters), and the Amlia basin. Magnetic anomaly profiles along the dashed tracklines A through U are shown in Figures 3, 5, and 6. The data east of 164°W have been previously described by *Elvers, Mathewson, Kohler, and Moses* [1967].

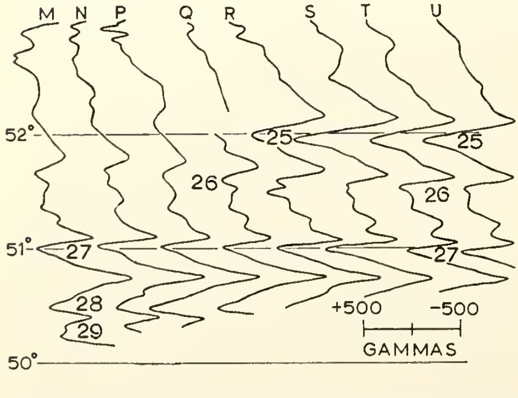

Fig. 3. Magnetic anomaly profiles showing the intersection of anomalies 25 and 26 with the Aleutian trench. See Figure 2 for profile locations.

therefore, indicates an apparent horizontal offset of 2° of latitude or 220 km for anomalies 25 through 31. This offset is approximately the same for each of these anomalies. The distances between anomalies 31, 32A, and 32B are not constant, however, which results in apparent offsets much less than 220 km.

Figure 2 shows that anomaly 32A has a relatively constant separation from anomaly 31 between 164° and 168°W. Between 168° and 169°W anomaly 32A appears to be offset left-laterally by about 60 km. Anomaly 32B may also have such an offset east of 168°W. This offset does not extend north of 49°N as shown by the continuity of anomaly 31. Between 169°W and the Amlia fracture zone, anomalies 32A and 32B trend east–west with a relatively constant separation of about 90 km. The apparent left-lateral offsets of 32A and 32B across the Amlia fracture zone are 160 and 120 km, respectively. West of the fracture zone anomaly 32B trends slightly south of west increasing its distance from 32A. Similar discrepancies of magnetic offset have been observed across the Murray fracture zone [*Raff*, 1962]. It seems likely that this varying separation of anomalies is responsible for what *Hayes and Heirtzler* [1968] identify as a repeated anomaly along one of their tracklines and tentatively interpret as indicating a fracture zone at 171°W.

South of the trench the amplitudes of anomalies 25 through 27 are uniformly high to the east of the fracture zone and uniformly low to the west. An examination of ocean floor depths shows that changes in bathymetry cannot account for this observation. The remaining anomalies (28 through 32B) generally have about the same amplitude on both sides of the fracture zone.

The Amlia fracture zone extends southward to at least 45°N, as shown by the offset of anomaly 32B. Further surveys of the Seamap type are likely to show the relationship of the north-south-trending Amlia fracture zone with the east-west-trending fracture zones to the south (see Figure 1).

ADAK FRACTURE ZONE

The anomalies continue westward from the Amlia fracture zone to approximately 177°30'W. Here the pattern is disturbed by the Adak fracture zone which has an apparent left-lateral offset of about 30 km. The offset of anomaly 25 is clearly shown by the sequence of profiles in Figure 6 and the magnetic anomaly map (Figure 7). This offset was not seen by *Hayes and Heirtzler* [1968] from their more widely spaced tracklines.

The topographic expression of the Adak fracture zone, which consists of several seamounts and depressions (Figure 7), is less striking than that of the Amlia fracture zone. As with the Amlia fracture zone, there is no obvious topographic expression of the Adak fracture zone within the trench. Both the magnetic and the bathymetric data indicate a general north-south trend.

DISCUSSION

Recent studies, based on the hypothesis of sea-floor spreading [*Hess*, 1962; *Dietz*, 1961] support the concept that the surface of the earth is made up of large mobile plates of lithosphere that interact along their common boundaries [see, for example, *Isacks et al.*, 1968]. The plates move apart along oceanic

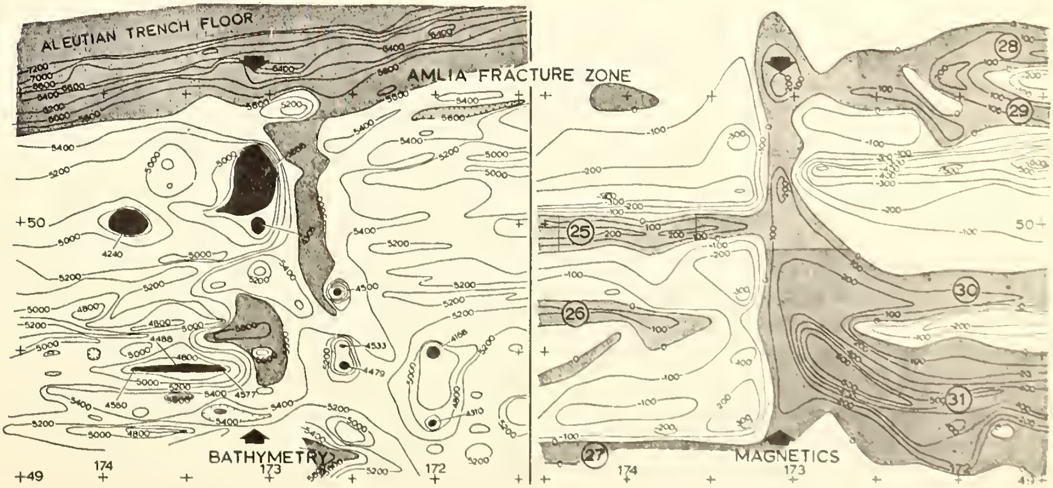

Fig. 4. Magnetic anomaly and bathymetric maps of the Amlia fracture zone. Depths are in corrected meters with a contour interval of 200 meters. Hills and seamounts with depths less than 4600 meters are in black with the minimum depth indicated. Depths greater than 5600 meters are shaded. Magnetic anomalies are contoured in hundreds of gammas; positive areas are shaded. The approximate axis of the fracture zone is indicated by the arrows.

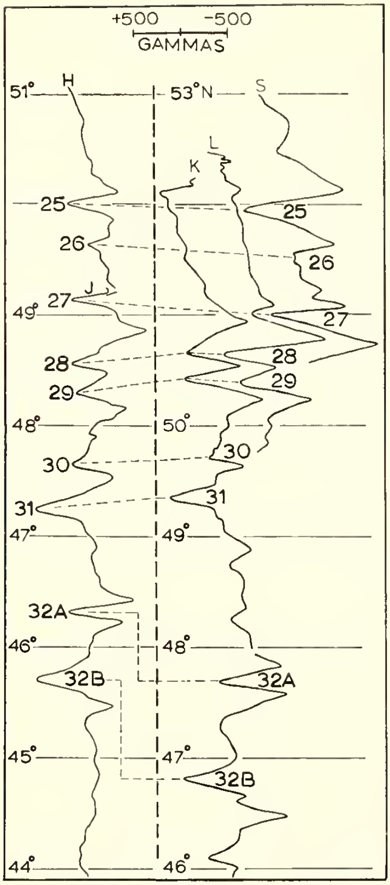

Fig. 5. Magnetic anomaly profiles showing the offset across the Amlia fracture zone. The vertical dashed line separates profiles that are east of the fracture zone from those to the west. See text for additional description and Figure 2 for profile locations.

ridges, where new crust is formed from ascending mantle materials, and they converge along island arcs, where one plate is overridden and thrust downward along the sloping seismic zone.

The mechanical and thermal processes associated with the downward thrusting of the oceanic plate would tend to destroy the remanent magnetism of the crustal rocks and the related magnetic anomalies (see, for example, the magnetic model presented by *Hayes and Heirtzler* [1968, p. 4644]). The distribution of the magnetic anomalies we have observed over a large part of the sea floor south of the Aleutian arc is in general agreement with this concept.

Recent studies indicate that in the last 10 m.y. the sea floor south of the Aleutian trench has moved about 500 km to the northwest relative to the Aleutian ridge [see, for example, *Le Pichon*, 1968]. Therefore, there should be no continuity of linear features on the sea floor across the trench onto the Aleutian ridge. However, prominent topographic features on the Aleutian ridge are approximately aligned with the fracture zones, which suggests that they may be related.

A hypothetical projection of the Amlia fracture zone northward along 173°W would pass through Amlia basin. The basin is a large elliptical submarine depression that lies in the area between the Andreanof Islands and the wider eastern segment of the Aleutian arc [*Perry and Nichols*, 1966]. Within this area the trends of the ridge, trench, and lines of volcanoes change markedly and the lines of volcanoes are noticeably offset (Figure 8). Most of these changes are, however, east of the northern projection of the Amlia fracture zone and perhaps lie along a northwest-trending zone between 51°N, 170°W, and 53°N, 174°W, indicating that Amlia basin and the offset of the volcanoes may be a result of factors other than the Amlia fracture zone.

A projection of the Adak fracture zone would be in general alignment with several discontinuities on the Aleutian ridge and terrace. Adak canyon separates regions of strikingly different topography [*Perry and Nichols*, 1965] (Figure 8). The sea floor east of the canyon is relatively smooth, whereas the sea floor to the west is chaotic and deeply incised by canyons

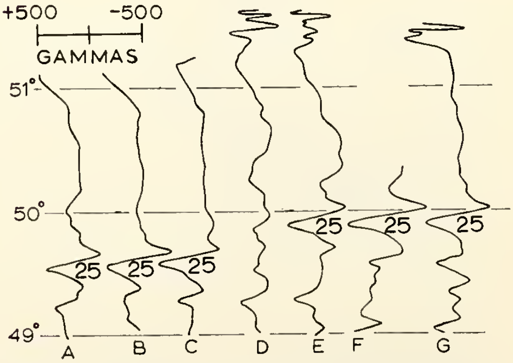

Fig. 6. Magnetic anomaly profiles showing the offset across Adak fracture zone. See Figure 2 for profile locations.

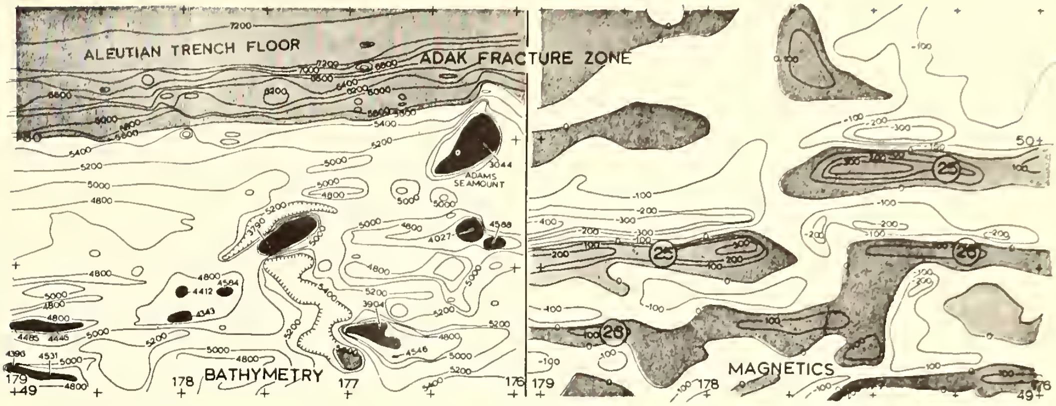

Fig. 7. Magnetic anomaly and bathymetric maps of the Adak fracture zone. See Figure 4 for description.

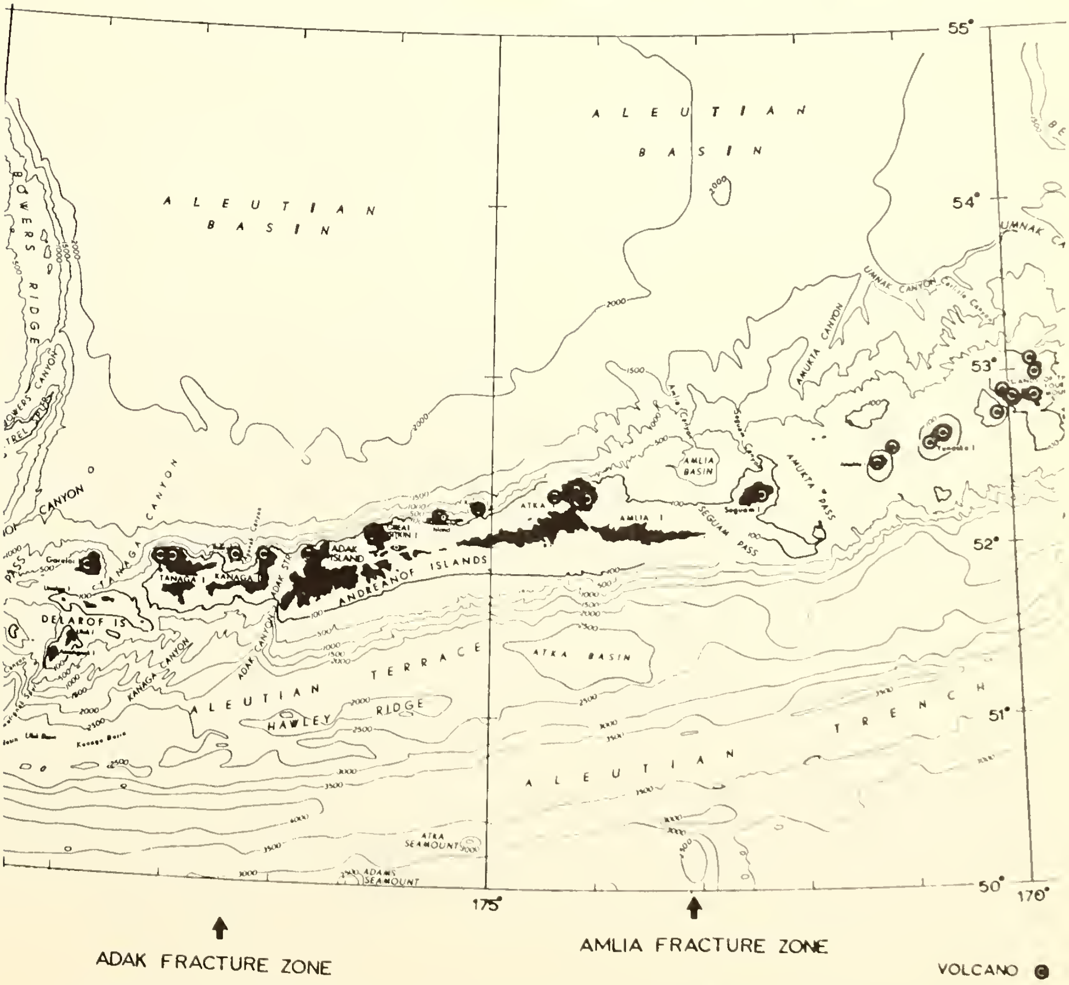

Fig. 8. Bathymetric map of part of the Aleutian arc showing its relationship to the Adak and Amlia fracture zones. Taken from the detailed maps of *Nichols and Perry* [1966]; contour interval is 500 fathoms (914 meters). Locations of the volcanoes are from *Coats* [1950].

[*Nichols and Perry*, 1966; *Perry and Nichols*, 1965], suggesting a structural difference between the two segments of slope. The Aleutian terrace is characterized in this area by discontinuities in ridges, basins, and the depth of the foot of the slope. Although these discontinuities occur near a northward projection of the Adak fracture zone, they also occur at the eastern boundary of the complex area at the intersection of Bowers ridge and the arc and therefore could also be associated with that major deformation rather than with the Adak fracture zone.

Although a genetic relation between the fracture zones and topographic features on the Aleutian ridge cannot now be established, the possibility warrants further consideration in view of the constraints that would be placed on the amount and direction of sea-floor spreading at Aleutian trench.

Acknowledgments. We thank T. V. Ryan, H. B. Stewart, G. Peter, F. P. Naugler, R. Perry, and D. E. Hayes for helpful discussions. J. R. Heirtzler kindly furnished the computer program for calculating the regional magnetic field. The skill and care taken by the officers and men of the USC&GS ships *Pioneer*, *Surveyor*, and *Oceanographer* have made this study possible.

REFERENCES

Coats, R. R., Volcanic activity in the Aleutian Arc, *U. S. Geol. Surv. Bull. 974-B*, 35, 1950.

Dietz, R. S., Continent and ocean basin evolution by spreading of the sea floor, *Nature, 190*, 854, 1961.

Elvers, D. J., C. C. Mathewson, R. E. Kohler, and R. L. Moses, Systematic ocean surveys by the USC&GSS *Pioneer* 1961-1963, *ESSA Operational Data Rept. C&GS DR-1*, 19 pp., 1967.

Elvers, D. J., G. Peter, and R. L. Moses. Analysis of magnetic lineations in the North Pacific (abstract), *Trans. Am. Geophys. Union, 48*, 89, 1967.

Grim, P. J., and B. H. Erickson, Marine magnetic anomalies and fracture zones south of the Aleutian trench, *Geol. Soc. Am. Program 1967 Ann. Meeting*, 84, 1967.

Hayes, D. E., and J. R. Heirtzler, Magnetic anomalies and their relation to the Aleutian island arc, *J. Geophys. Res., 73*, 4637, 1968.

Hendricks, S. J., and J. C. Cain, Magnetic field data for trapped-particle evaluations, *J. Geophys. Res., 71*, 346, 1966.

Hess, H. H., History of the ocean basins, in *Petrologic Studies*, pp. 599–620, Geological Society of America, New York, 1962.

Isacks, B., J. Oliver, and L. R. Sykes, Seismology and the new global tectonics, *J. Geophys. Res., 73*, 5855, 1968.

Keller, F., Jr., J. L. Mensche, and L. R. Alldredge, Aero-magnetic surveys in the Aleutian, Marshall, and Bermuda Islands, *Trans. Am. Geophys. Union, 35*, 558, 1954.

Le Pichon, X., Sea-floor spreading and continental drift, *J. Geophys. Res., 73*, 3661, 1968.

Mason, R. G., A magnetic survey off the west coast of the United States between latitudes 30° and 36°N and longitudes 121° and 128°W, *Geophys. J., 1*, 320, 1958.

Mason. R. G., and A. D. Raff, Magnetic survey off the west coast of North America, 32°N to 42°N, *Bull. Geol. Soc. Am., 72*, 1259, 1961.

Nichols, H., and R. B. Perry, *Bathymetry of the Aleutian Arc, Alaska*, 6 maps, U. S. Coast and Geodetic Survey, 1966.

Perry, R. B., and H. Nichols, Bathymetry of Adak canyon, Aleutian arc, Alaska, *Bull. Geol. Soc. Am., 76*, 365, 1965.

Perry, R. B., and H. Nichols, Geomorphology of Amlia basin, Aleutian arc, Alaska, *Geograph. Rev., 56*, 570, 1966.

Peter, G., Magnetic anomalies and fracture pattern in the northeast Pacific Ocean, *J. Geophys. Res., 71*, 5365, 1966.

Peter, G., and H. B. Stewart, Jr., Ocean surveys, the systematic approach, *Nature, 206*, 1017, 1965.

Pitman, W. C., III, E. M. Herron, and J. R. Heirtzler, Magnetic anomalies in the Pacific and sea-floor spreading, *J. Geophys. Res., 73*, 2069, 1968.

Raff, A. D., Further magnetic measurements along the Murray fault, *J. Geophys. Res., 67*, 417, 1962.

Raff, A. D., Boundaries of an area of very long magnetic anomalies in the northeast Pacific, *J. Geophys. Res., 71*, 2631, 1966.

Raff, A. D., and R. G. Mason, Magnetic survey off the west coast of North America 40°N latitude to 50°N latitude, *Bull. Geol. Soc. Am., 72*, 1267, 1961.

Skorpen, A. J., Magnetic profiles across the Aleutian trench and ridge, M.S. Thesis, Oregon State University, Corvallis, June 1967.

Vacquier, V., Measurement of horizontal displacement along faults in the ocean floor, *Nature, 183*, 452, 1959.

Vacquier, V., A. D. Raff, and R. E. Warren, Horizontal displacements in the floor of the northeastern Pacific Ocean, *Bull. Geol. Soc. Am., 72*, 1251, 1961.

(Received August 8, 1968;
revised November 18, 1968.)

Reprinted from Science, The American Association for the
Advancement of Science, Vol. 163, No. 3865

Fossil Deep-Sea Channel on the Aleutian Abyssal Plain

Abstract. *The discovery of a leveed deep-sea channel whose axial gradient reverses near the Aleutian trench supports the hypothesis that the downbowing of the trench interrupted the turbidity current processes that constructed the Aleutian abyssal plain.*

A study of fathograms (*1*) from Environmental Science Services Administration Seamap surveys has revealed a deep-sea channel which trends northeast to southwest for a distance of 370 km on the Aleutian abyssal plain south of the Aleutian trench (Fig. 1). The channel, here named Seamap channel, is unusual in that it slopes downward from a summit located about midway from either end (Fig. 2a), thus precluding the flow of turbidity currents from end to end. It is postulated that the section northeast of the present summit was once higher, but has been downwarped with the Aleutian trench, thus cutting the channel off from a northern source. This is in agreement with the thesis suggested by Hurley (*2*) from bathymetric considerations and supported by Hamilton's (*3*) seismic reflection results that the Aleutian plain has been cut off from its supply of turbidites by the Aleutian trench, leaving a fossil or relic abyssal plain whose only present-day supply of sediment is pelagic material settling from the water column.

The profiles across the channel shown in Fig. 2b are typical of the channel northeast of point *B* (Fig. 1). Its width, measured between the highest parts of the levees, averages about 6 km, and its depth (top of levees to channel bottom) averages about 50 m. West of *B*, the channel loses its distinctive shape as it turns into a region of east–west trending ridges. Farther west it widens and becomes indiscernible as a single feature. Upstream from point *E* (Fig. 1), the channel passes close to Sirius Seamount and has well-developed meanders averaging about 35 km in wavelength. It finally disappears at a depth of about 4800 m on the south wall of the Aleutian trench (Fig. 1, *I*); north of point *I* it has apparently been destroyed by slumping.

The direction that turbidity currents flowed when the channel was active must have been from northeast to southwest because (i) the only plentiful supply of material for turbidites is continental North America which is northeast of the channel; (ii) in general the Aleutian abyssal plain deepens toward the south; and (iii) to the southwest of point *E* (Fig. 1), where the relative heights of the channel levees have apparently been little affected by the formation of the trench (and where the channel does not meander), the right levee (as one looks southwest) is consistently higher than the left levee. This is consistent with observations that in the northern hemisphere, as one looks downstream, the levee on the right side is higher as a result of the Coriolis effect (*3, 4*).

It is difficult to tell how closely the axial profile (Fig. 2a) approximates the profile which existed immediately after the trench formed, and which parts of it, if any, represent the channel before the trench formed. The section of pro-

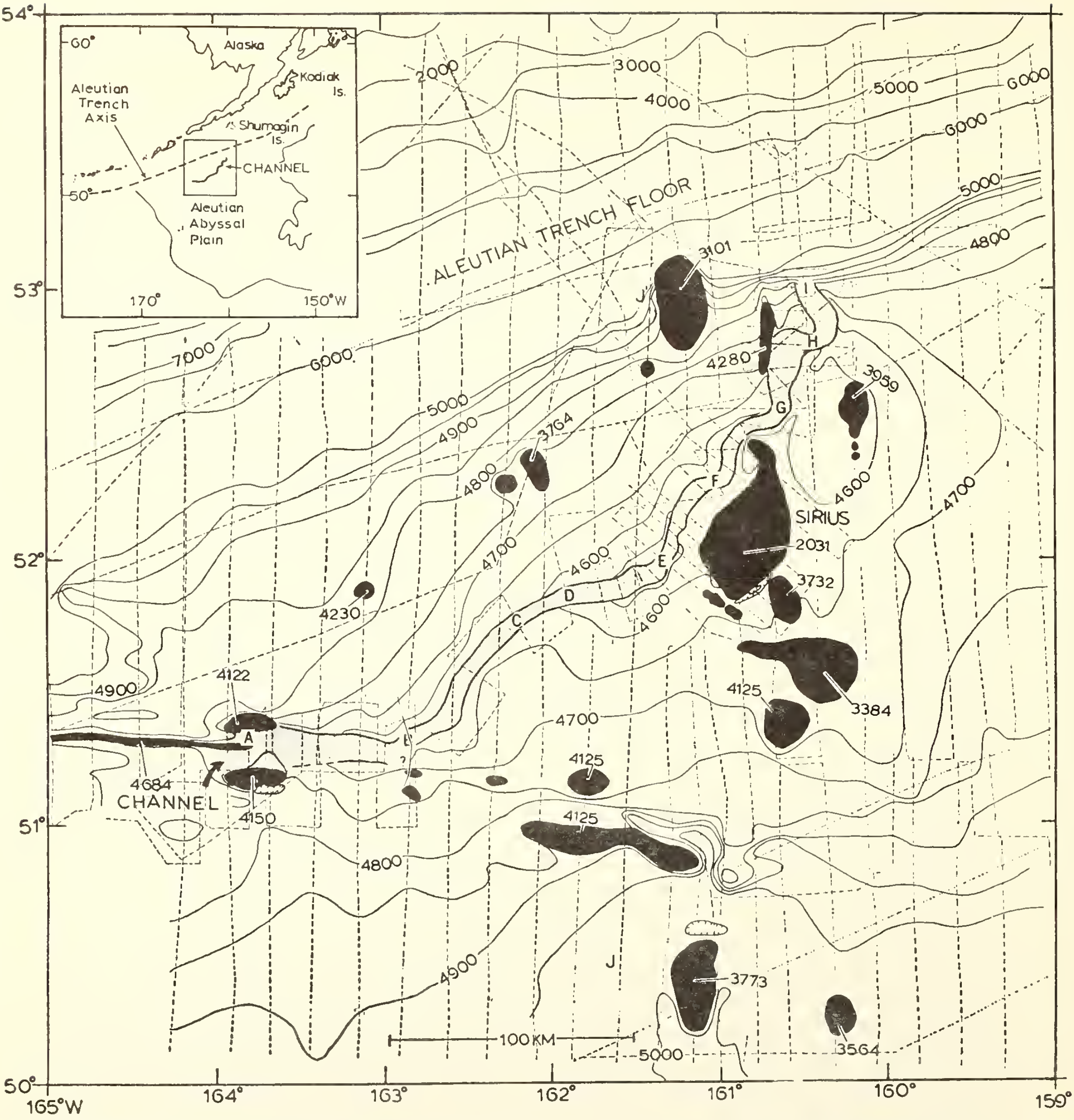

Fig. 1. Location of Seamap channel on the Aleutian abyssal plain. The channel is shaded between the highest parts of the levees. Depths are in corrected meters. Seamounts, ridges, and abyssal hills are shown in black. Tracklines are dashed. The contour interval changes north of the 5000-m contour on the south wall of the Aleutian trench. Letters *A* to *I* correspond to points along the axial profile shown in Fig. 2.

file from *A* to *E* may be close to that of the channel when it was active. The minor gradient reversals in this section of the channel could be the results of processes, operating during or after the trench formed, such as regional warping of the sea floor or nonuniform pelagic sedimentation rates.

The downbowed part of the profile (between *E* and *I*, Fig. 2a) shows three secondary peaks. These possibly are caused by the greater downbowing by the Aleutian trench of the north swings of the meanders impressed on an irregular original gradient.

The trend of Seamap channel is along the crest of a broad rise, with the floor of the channel elevated well above the general level of the adjacent area (Fig. 1 and Fig. 2c). Similar but less pronounced channel elevations have been observed elsewhere in the northeast Pacific (*3*). Hamilton's seismic reflection data for channels in the northeast Pacific clearly show that deep-sea channels are depositional features (*3*). This suggests that Seamap channel is located on an unusually thick wedge of sediment.

Assuming that the axial gradient which existed before the trench formed is approximated by that portion of the channel southwest of point *E*, we can

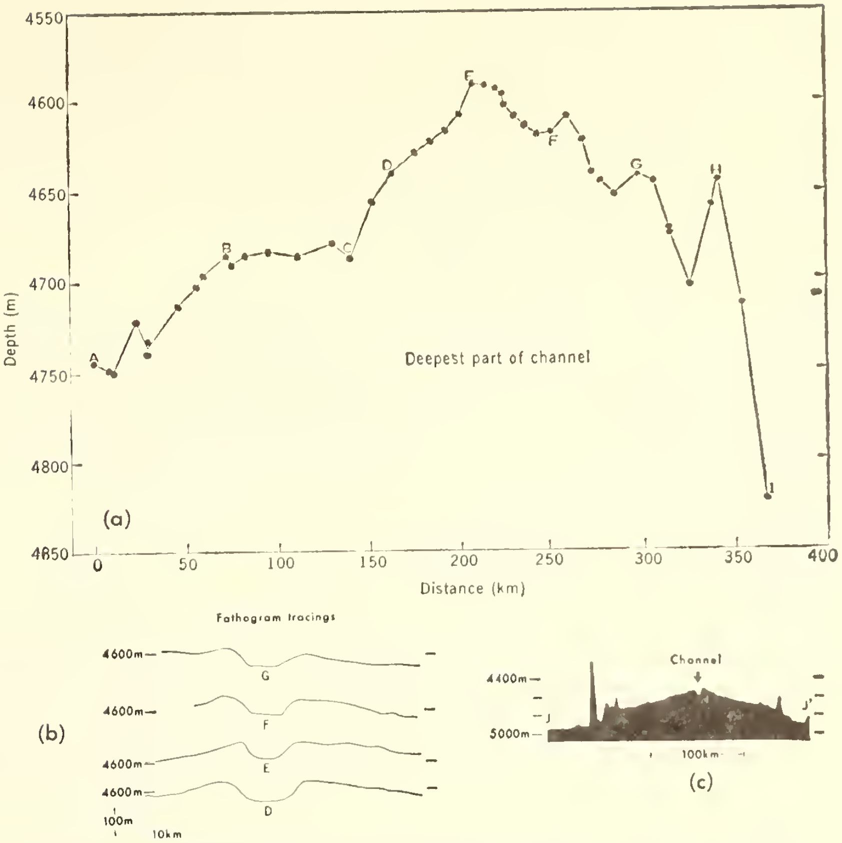

Fig. 2. (a) Longitudinal (axial) profile of Seamap channel. Vertical exaggeration is 1000. Letters *A* to *I* are points along the channel shown in Fig. 1. (b) Profiles across channel from echo soundings at points *D*, *E*, *F*, and *G* looking southwest. Vertical exaggeration about 30. (c) North–south profile across region along section *J–J′* of Fig. 1 (vertical exaggeration of 100).

compare its gradient with that of other active channels. The mean gradient from *A* to *E* is 0.75 m/km. However, it shows much variability (it is essentially zero between *B* and *C*, and 1.4 m/km between *C* and *E*). Cascadia channel, which has an axial profile similar to those of other channels, has gradients of 1.83, 1.67, and 1.17 m/km at respective distances of about 165, 275, and 435 km from the base of the continental slope (*2*). Although there are many difficulties in using such comparisons to obtain an approximate distance of section *A* to *E* from the ancient source of turbidites, it seems reasonable that this part of the channel was at least several hundred kilometers from the sediment source. An extrapolation of the channel north of the trench suggests that it may have originated somewhere in the area between the Shumagin Islands and Kodiak Island. However, our echo soundings (mainly along north–south lines) have not revealed the presence of the channel north of the trench.

PAUL J. GRIM
FREDERIC P. NAUGLER
Pacific Oceanographic Research Laboratory, Seattle, Washington 98102

References and Notes

1. The channel was first revealed by an examination of echo soundings taken by the U.S. Coast and Geodetic Survey ship *Pioneer* from 1961 to 1963. During April 1968, a 3-day study of the channel was conducted from the *Oceanographer* with the use of satellite-controlled navigation. Six additional crossings of the western part of the channel were made by the ship *Surveyor* in June 1968. All records were read to the closest fathom (1.83 m) and converted to corrected meters according to the method described by T. V. Ryan and P. J. Grim [*Int. Hydrograph. Rev.* 45, 41 (1968)].
2. R. J. Hurley, *Scripps Inst. Oceanogr. Ref. 60–7* (1960), p. 1.
3. E. L. Hamilton, *J. Geophys. Res.* 72, 4189 (1967).
4. H. W. Menard, Jr., *Bull. Amer. Ass. Petrol. Geol.* 39, 236 (1955); H. W. Menard, S. M. Smith, R. M. Pratt, in *Submarine Geology and Geophysics*, W. F. Whittard and R. Bradshaw, Eds. (Butterworths, London, 1965), p. 271. A more detailed description of the channel and a discussion of differences in levee heights and their causes is in preparation.
5. We thank C. A. Burk, B. H. Erickson, E. L. Hamilton, R. J. Hurley, T. V. Ryan, and H. B. Stewart, Jr., for discussions about the channel. The navigational skill of the officers and crew of the *Pioneer*, *Surveyor*, and *Oceanographer* made this study possible.

13 September 1968; revised 22 November 1968

Reprinted from Maritime Sediments Vol. 5, No. 1, 19-21.

Possible Morainal Deposits in the Gulf of Maine*

REGINALD N. HARBISON
Environmental Science Services Administration, Atlantic Oceanographic
Laboratories, Miami, Florida.

Introduction

A detailed hydrographic, seismic reflection and magnetic survey was conducted by the USC&GSS EXPLORER in the northeastern Gulf of Maine (Area A) along with an additional 1250 km of reconnaissance lines west of Area A (Fig. 1). Bathymetric, bedrock, isopachous and total magnetic field intensity maps have been prepared for Area A (Malloy and Harbison, 1966). A 160-joule sparker provided the sound energy for the seismic work, and reflected signals were recorded on a dual-channel recorder. Frequencies were recorded between 300 and 600 Hertz on one channel and 600 to 1200 on the other. Raydist was used for navigational control in Area A (Malloy et al., 1964).

Discussion

Throughout Area A a general northeast-southwest topographic trend prevails in the bedrock in the form of ridge and valley morphology. Seismic reflection profiles do not reveal any stratification within the bedrock which has been interpreted to be folded crystalline rock of Paleozoic age, overlain in part by Triassic formations (Malloy and Harbison, 1966). The bedrock is overlain by acoustically transparent sediments varying from 0 to 65 m in thickness. Bedrock valleys contain closed lows along their thalwegs, which suggest glacial erosion and there are many sediment blocked valleys which are probably caused by glacial outwash. Evidence for extensive glaciation in the Gulf of Maine has been presented by using seismic reflection data (Uchupi, 1966).

Unusual shadow zones on the seismic reflection profiles, apparently caused by areas of reverberated sound, occur in some places within the otherwise acoustically-transparent sediments. These zones of apparent reverberation have an appearance similar to the deep scattering layer on a fathogram, but are more intense and often mask out much of the bedrock surface below. The shadow zones are equally visible on both channels of the seismic reflection records with no obvious hyperbolic reflections. Many of these shadow zones are present within acoustically transparent sediments with their surface convex upward (Fig. 2).

Geographically, these shadow zones form predominantly sub-bottom ridges which are concentrated along a belt 14 km wide. This belt is centered on the 90 m isobath which is approximately parallel to the coast and is 30 to 40 km offshore (Fig. 3). These ridges average between 45 to 50 m in height above the bedrock and are located in water depths of 70 to 185 m. They often appear to be eroded level with the sea floor and are ponded by acoustically transparent sediment which is probably clay. The ridges are not continuous features throughout the area.

King (1969) reports an end moraine complex on the Scotian Shelf about 30 to 40 km off the coast. He describes this end moraine complex as a belt of low discontinuous ridges which are to a large degree sub-bottom features masked by ponded clay and silt deposits. He states that these ridges are on the average 50 m in height above the underlying bedrock and lie in water depths ranging from 70 to 200 m. He describes the dominant textural grade of the moraines as sand, but mentions that rock fragments in the gravel range are also present.

The Scotian Shelf end moraines are comparable to the ridges revealed by the shadow zones in the Gulf of Maine. The Gulf of Maine ridges are not found to extend above the sea floor as those on the Scotian Shelf sometimes do.

Conclusions

Shadow zones on the seismic reflection profiles are interpreted as graphic records of deposits of small-sized glacial debris surrounded by a matrix of acoustically transparent

---

*Manuscript received May 15, 1969.

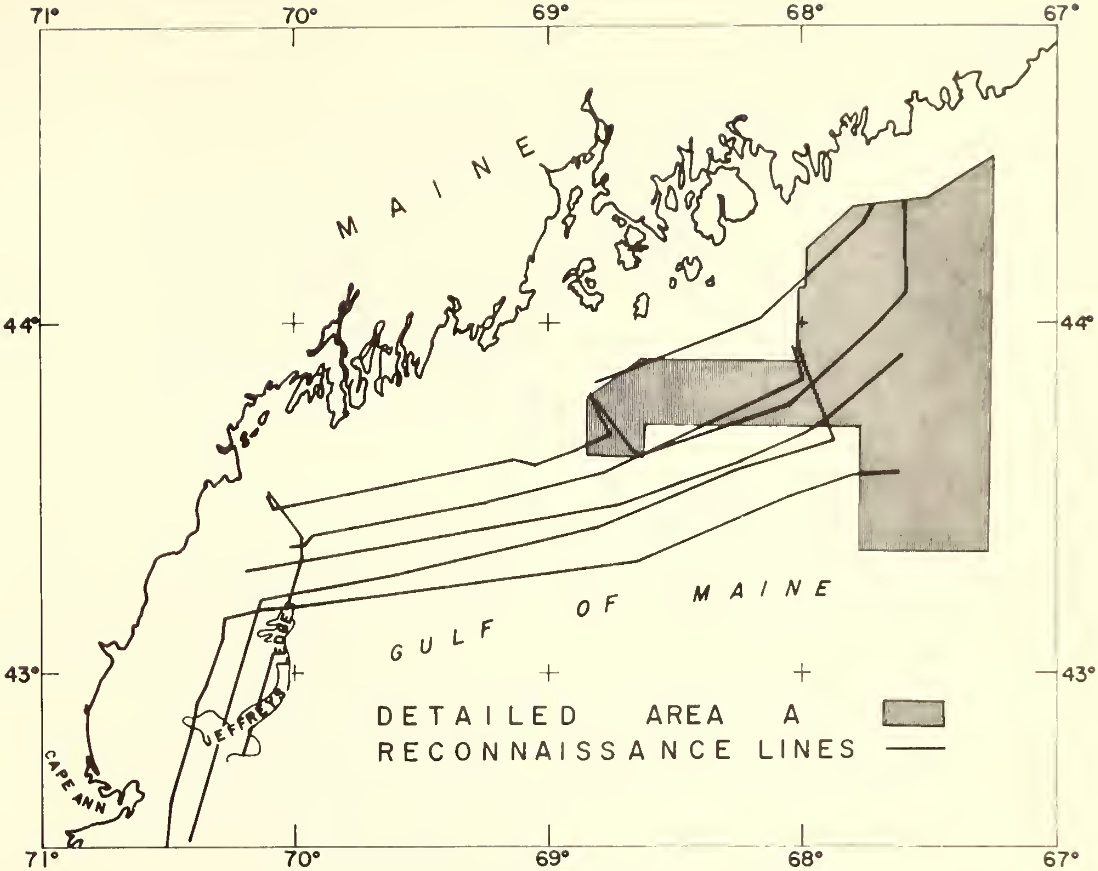

Fig. 1 Location of detailed survey area and reconnaissance lines in the Gulf of Maine.

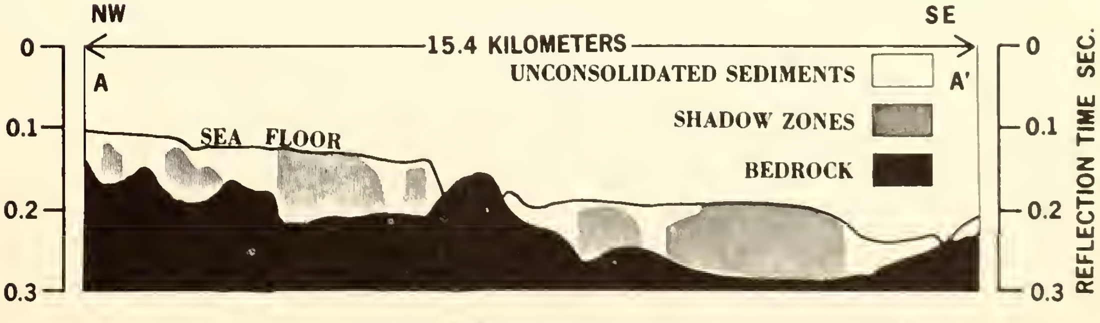

Fig. 2 A tracing of a seismic reflection profile across shadow zones. Profile AA' is located in Figure 3.

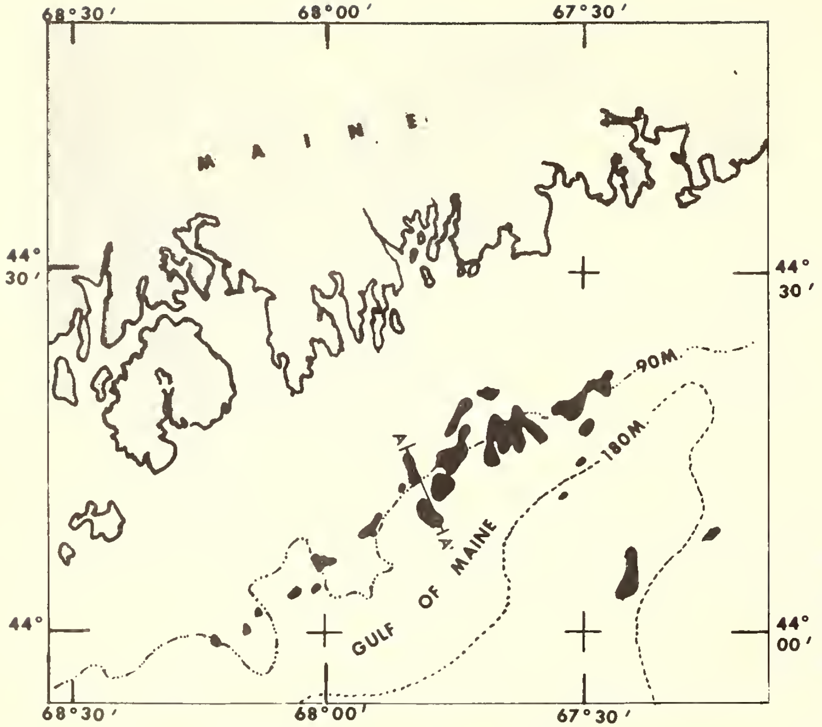

Fig. 3
Shadow zones, or zones of reverberated sound which are interpreted to be an end moraine complex are indicated in black.

sediment. The glacial material probably reverberates sound energy in the acoustically transparent sediments in the same manner that concentrations of small marine organisms reverberate sound in water as found in association with the deep scattering layer.

In areas where shadow zones are present, closed bedrock lows and maximum sediment thickness occur together. The closed bedrock lows are attributed to glacial erosion. Areas of maximum thickness are interpreted to be associated with an area of glacial stillstand. The absence of these shadow zones to the south and their concentration along a 14 km-wide belt in the vicinity of the 90 m isobath may indicate a former glacier-shoreline contact.

The Passadumkeag topographic sheet (USGS) for southeastern Maine shows sand and gravel morainal deposits extending to the present shoreline just north of Area A (Atwood, 1940). The shadow zones are in all probability a southern continuation of these morainal deposits.

The Gulf of Maine morainal deposits are interpreted to be gentle sub-bottom ridges of sand and gravel. These ridges are believed to be an end moraine complex similar to the one on the Scotian Shelf which they resemble in many ways.

References cited

ATWOOD, W. W, 1940, The physiographic provinces of North America, Ginn and Company, Boston, 536 pp.

KING, L. H., 1969, Submarine end moraines and associated deposits on the Scotian Shelf, Geol. Soc. of Amer. Bull., 80, 83-111.

MALLOY, R. J., HARBISON, R. N., and KEARSE, C. D., 1964, U. S. Coast and Geodetic Survey geological echo profiling program, International Hydrographic Rev., 41, 37-44.

______________________________, 1966, Marine geology of the northeastern Gulf of Maine, Tech. Bull. No. 28, U. S. Coast and Geodetic Survey, 11-15.

UCHUPI, E., 1966, Structural framework of the Gulf of Maine, J. Geophys. Res., 72 (13), 3013-3028.

Reprinted from Marine Geology Vol. 7, No. 2, 176-177. 22

the Irish Sea, in which he interprets the geophysical surveys that he has done so much to promote in this area. Gravity, magnetic and seismic surveys are all used to elucidate the structure of the Irish Sea in a very valuable contribution. J. L. Worzel covers a much wider area in his "Survey of continental margins". This final paper is presented largely in diagrammatic form. The continental margins of eastern U.S.A., parts of eastern South America, western Europe and western America are illustrated. These diagrams provide a very useful summary of present information on shelf structure. The book is very well produced, with many good diagrams and references lists are included. The lack of balance in its contents is a drawback to its general usefulness.

C. A. M. KING (Nottingham)

Marine Geotechnique. A. F. RICHARDS (Editor). University of Illinois Press, Urbana-London, 1967, 327 pp., 85 s.

Marine geotechnique is the study of the engineering and scientific aspects of submarine sediments and rocks. To date these investigations have been primarily concerned with Holocene deposits. This is a new and diversified field finding considerable interest among marine geologists and engineers who are concerned with the behavior of sea-floor deposits. The field of marine geotechnique is providing the marine geologist with a new approach to many of his problems. The highlights and diversity of this field have been drawn together admirably in this volume edited by A. F. Richards.

The book contains eighteen papers which have been organized under four major headings in such a way as to acquaint the reader not only with local studies made in various environments, but with specific problems such as slope stability, shock loading, sampling, in-place measurements, and laboratory analyses. The book is a collection of papers representing current research activities in marine geotechnique both in Europe and in the United States.

Part 1, "Laboratory Results and Areal Investigations", includes three papers on the Gulf of Mexico, two dealing with the Mississippi Delta by C. R. Kolb and R. I. Kaufman; and B. McClelland, and the third on the western portion of the Gulf by W. R. Bryant, P. Cernock, and J. Morelock. Papers pertaining to sediments from the Atlantic and Pacific basins are presented by S. Buchan, F. C. D. Dewes, D. M. McCann, and D. Taylor Smith; A. F. Richards and E. L. Hamilton; and E. C. Robertson. The section is rounded out with papers on the eastern Mediterranean (off the Israel coast) by G. Almagor; the Red Sea, Gulf of Aden and Nile Delta by G. Einsele; the Arabian Sea and Baltic Sea by F. C. Kögler; and the Gulf of Bothnia by A. Jerbo. These papers discuss and interpret the relationships of various mass properties of submarine sediments (shear strength, water content, bulk density, Atterberg limits, porosity, acoustical and consolidation characteristics, and sediment types), as well as the geochemical properties and sedimentary processes for a specific locale. The authors generally have included a discussion of the basic techniques and theory behind their observations, which is most helpful to the layman.

Part 2, "Submarine Slides, Slumps, and Slope Stability", deals with the mechanics and problems associated with movement of material down slope, both in mass and as a turbid flow. N. R. Morgenstern brings the reader up-to-date on the latest developments in the study of submarine slope failures and includes a discussion on the generation of turbidity currents. A. Andresen and L. Bjerrum (citing case histories) discuss the modes of slope failure in loose sand and silts.

Four papers comprise part 3, "Sampling and In-Place Measurements". The problem of collecting suitable samples, along with suggestions for improving samplers, is discussed by A. M. Rosfelder and N. F. Marshall. Papers by R. F. Scott and by W. Harrison and A. M. Richardson Jr., deal with in-place measurements of shear strength and bearing capacity. The paper "Effect of explosive loading on the strength of sea-floor sands", by R. F. Dill, concludes this section.

Part 4, "Nondestructive Testing and Literature Survey", consists of a paper by K. Preiss on the subject of measurement of water content and bulk density of sediments by nuclear techniques. The final paper, by A. F. Richards, is an excellent summary, directed specifically to the marine geologist and the engineer, of the basic literature pertinent to the field of marine geotechnique. This paper will be of particular interest to those who are not familiar with the available literature.

This book brings together a fine selection of papers introducing the layman to the young field of marine geotechnique. To those already in this field it provides the needed up-dating of the state of the art.

GEORGE H. KELLER (Miami, Fla.)

The Waters of the Sea. P. GROEN. Van Nostrand, London, 1967, 328 pp., 140 illus., 30 plates, 4 charts, 65 s.

Dr. Groen explains in the preface how he has endeavoured to present an authoritative introduction to physical oceanography for non-specialists and students of other marine disciplines. He, therefore, had to either assume a basic understanding of mathematics in his reader and incorporate this into the discussions or exclude all but the most elementary mathematics. The latter path was taken and as a consequence some of the more mechanical topics have had to be described at great length.

The Waters of the Sea begins with a moderately long introduction which consists of a historical note portraying the influence that the sea has had on different

Reprinted from Isotopes and Radiation Technology
Vol. 6, No. 4, 376-381.

Radioisotopes and Oceanography

By G. H. Keller*

Abstract: *A brief review of the literature indicates that, although radioisotope methodology in oceanography is not yet extensive, significant developments have been made. Radioisotope methods have been used for making observations directly in the environment and for tagging and dating both water masses and sediments. Only prototype nuclear instruments have been, in general, used thus far, but results obtained with them indicate the feasibility of using such instruments for measuring current velocity, oxygen content, deposited-sediment density, suspended-sediment concentration, and the elemental compositions of bottom sediments.*

Although oceans cover approximately 70% of the earth's surface, we understand very little about the processes taking place in this dynamic environment. Relatively little is known about the physical and chemical characteristics of the oceans or the processes responsible for shaping the ocean basins. Numerous investigations have been conducted in this environment, but its vastness plus the great expense per unit of data have left us far from adequately describing it. Technical advances in recent years, particularly computers and electronic sensors, have enabled the oceanographer to collect and process large amounts of information. Of particular significance are breakthroughs in the area of in-place measurements, which have provided the investigator with data of far greater accuracy and significance than have been obtained in the past.

Radioisotopes have recently become important in oceanographic and coastal engineering research. Both natural and artificial radioisotopes are used not only to trace and date water masses and to study their chemical characteristics but also to provide an entirely new field of instrumentation ideally suited to the in-place measurements of various properties of the ocean and the underlying sea floor. Some of these applications are summarized below.

Radioisotope Tracers

Radioisotope tracers used in oceanographic measurements may be those of natural origin — radioisotopes and their daughters present since the earth's formation or those produced by the interaction of cosmic rays with elements in the earth's atmosphere — or those produced artificially as by-products of nuclear explosions or atomic waste.

Naturally Occurring Radioisotopes

Radioisotopes, with their unique parent–daughter relationships, have provided the scientist with an excellent tracer as well as an age-dating method. For example, studies of the disequilibrium of ^{234}Th in the ocean have shown that in some areas of the sea the isotope has been removed from the surface waters and concentrated at the thermocline, i.e., the zone where the temperature gradient is greatest. Similar studies using ^{32}Si have enabled the oceanographer to date and trace the movement of specific water masses. Results of studies of the depth distribution of ^{234}Th show promise of providing an insight into the mechanism by which trace elements are removed from certain portions of the water column; this, in turn, could lead to a better understanding of the settling rate of variously sized particles through the water.[1]

The short residence time of thorium in seawater (35 ± 35 years) and the assumption that the isotopes ^{232}Th and ^{230}Th are precipitated in the same ratio permit determination of the accumulation rates of such elements as Mn, Ni, Co, and Cu in deep-sea deposits.[2] By measuring the activity of ^{26}Al, which is present in submarine sediments, the geological oceanographer has developed a suitable technique for calculating the rate at which the sea floor is receiving sediment particles.[3] Such observations are vital to an understanding of the depositional history of sea-floor deposits.

The disequilibrium technique of age dating has developed rapidly in recent years, and several isotopes (^{32}Si, ^{234}U, ^{231}Pa, and ^{14}C) are now used to provide absolute age determinations of rocks and shells found in the ocean basins.[4-6] These data have made it possible for scientists to define, with increasing accuracy, the time and mode of formation of the ocean basin as well as to determine the various stands of the sea through geologic time.[7]

Artificially Produced Radioisotopes

Radioisotopes added to the oceanic environment as a result of fallout from nuclear weapons, nuclear power plants, and disposal of atomic wastes in ocean basins have provided a new approach to the tracing of water-mass and sediment movements. A good example is the monitoring of the cooling waters from the Hanford reactors in Richland, Wash. Following ^{65}Zn and ^{51}Cr down the Columbia River, scientists are able to observe the dispersion of the river water and its sediment once it enters the Pacific Ocean.[8] It has been possible over the years to determine the distribution and movement of sediments off the Washington coast by measurement of the ^{65}Zn activities associated with these deposits.[9]

---

*Environmental Science Services Administration, Atlantic Oceanographic Laboratories, 901 South Miami Ave., Miami, Fla. 33130.

Studies of beach erosion and migration of coastal sands have benefited significantly by the use of radionuclides. Sand particles have been tagged with ^{133}Xe and ^{140}Ba–^{140}La, for example, and their movements traced by scintillation detectors used either directly in the field or on samples taken to the laboratory.[10] Although more caution is required in handling radioactive tags, they prove more effective than stains because lower concentrations can be monitored and buried grains can be detected. However, caution and public opinion have restricted the use of this technique in many areas.

Nuclear Instrumentation

A goal of scientists is to monitor or measure the parameters of interest under natural environmental conditions. For the oceanographer this has become a reality in a few areas, as some of his sampling techniques have advanced from those of rather simple, crude devices to the more sophisticated electronic in-place measuring packages. The adaptation of nuclear techniques to problems in the marine environment is a recent development, which is still in its early stages but appears promising.

Current Measurements

Instruments based on the detection of radiation emitted by a radionuclide and determination of the amount present have been developed using both sealed and unsealed (tracers) sources for the in-place measurement of various parameters in both the water column and the sea floor. One approach, the injection of a tracer amount of radioisotope and determination of the rate and direction of its movement, is the basis of an instrument that has been used to measure current flow rates in the range 0.17 to 1.67 ft/sec (0.1 to 1.0 knot), with a theoretical lower limit of 0.002 ft/sec. This instrument consists of a wagon-wheel configuration with a series of detectors mounted on the wheel rim and an isotopic source located at the hub (Fig. 1). The radioisotope (^{131}I) is injected into the water, and the rate and direction of flow are determined by the time of arrival of the radioactivity at a particular detector.[11] Three slightly different models have been built and taken through various phases of testing. The instrument is known as the Deep-Water Isotopic Current Analyzer (DWICA).

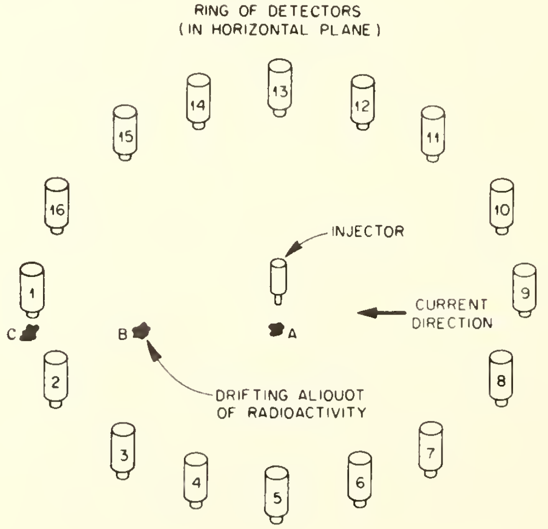

Fig. 1 Schematic diagram of DWICA operation.

Oxygen Determination

The oxygen content of seawater is of prime interest to the marine biologist. Its presence and amount noticeably control types and quantity of life sustained by the sea and thus are of major importance for assessing marine productivity. With a nuclear instrument the oxygen content in seawater can be measured in place. The instrument operates on a radioisotope-release principle[12] wherein the oxygen dissolved in the water reacts with radioactive thallium metal to release stoichiometric quantities of radioactive thallous ions. A Geiger tube capable of detecting ^{204}Tl beta rays serves as the brain center of the sensor. To ensure a uniform flow of water through the sensor, a pump is included in the instrument package.

Geological Measurements

The geological oceanographer has also been a beneficiary of recent advances in nuclear instrumentation, primarily in areas dealing with the mass physical and chemical characteristics of submarine sediments but also in investigations on suspended sediment in the water column.

Bottom-Sediment Density. Nuclear technology now makes it possible to conduct in-place measurements of sediment bulk density on the sea floor, with improvement in both the rate and accuracy of measurement. Since sediment cores do not have to be collected, many hours of laboratory testing are obviated.

The two types of instruments being used for these studies incorporate slightly different principles. In one,[13] a back-scatter system, a gamma-ray emitter (^{137}Cs) and a detector (G-M tubes) are housed in a single-barrel probe, which penetrates the sea floor in much the same way as a free-falling dart would enter the floor (Fig. 2). An internal driving mechanism moves the source-detector unit up and down inside the barrel, which is embedded in the sea floor. The density profile is obtained to a depth of 12 ft.

The other approach used to measure in-place density is based on attenuation of direct gamma-ray transmission.[14] Using a dual-barrel probe with a ^{137}Cs source in one barrel and a scintillation counter in the other, the density of the sediment between the barrels is readily determined by recording the gamma-ray attenuation. This particular probe is mounted on a tower, which is lowered slowly to the sea floor (Fig. 3). Once the tower is on the bottom, the probe is jacked into the sediment and the sensor output transmitted through a cable to the ship on the surface. This instrument is capable of providing a much more detailed density profile than the back-scatter device since measurements can be made in 0.5-in. increments to a depth of 10 ft. The back-scatter probe averages density over a 12-in. interval.

Using the same basic principle of measuring the attenuation of transmitted gamma rays as a measure of density, geological oceanographers can now measure sediment-density variation in cored samples that are still in the core barrel.[15] A ^{137}Cs source and a scintillation detector are mounted on a small cart in such a way that, as the cart is drawn along the length of the core barrel, the barrel with its sediment passes between the source and the detector. This instrument is capable of operating aboard ship as well as in the laboratory.

Suspended-Sediment Concentration. The sediment load carried by rivers and near-shore waters is of major importance to both marine geologists and coastal engineers, particularly in light of the cutting and filling that take place in such environments. The measurement of this load is difficult because instruments placed in the water interfere with the natural flow and thus distort the significance of the sediment-load measurement. A nuclear suspended-sediment concentration gage has now been developed which can detect

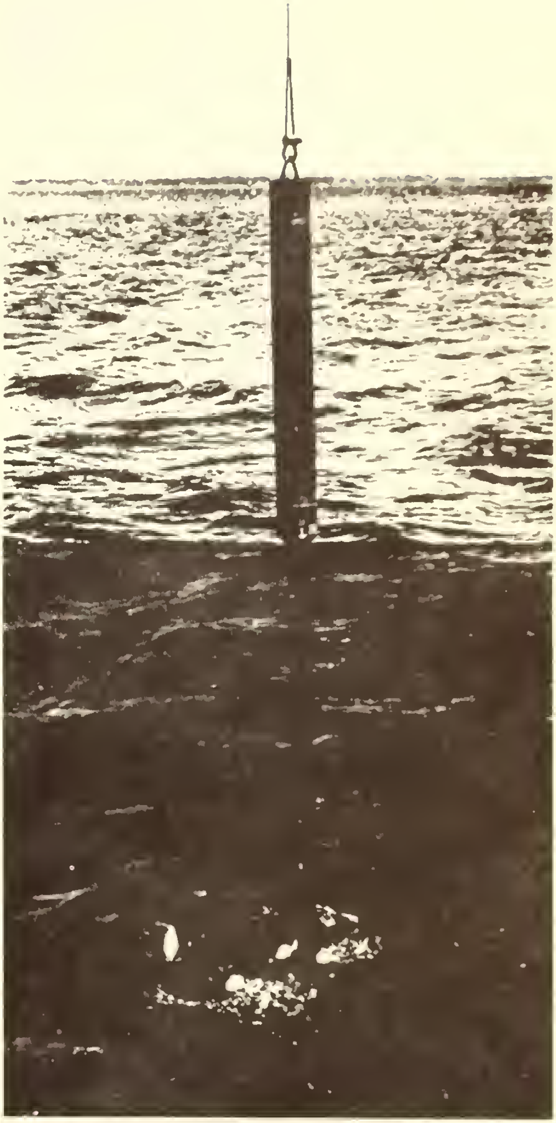

Fig. 2 Bottom-sediment density single-barrel probe.

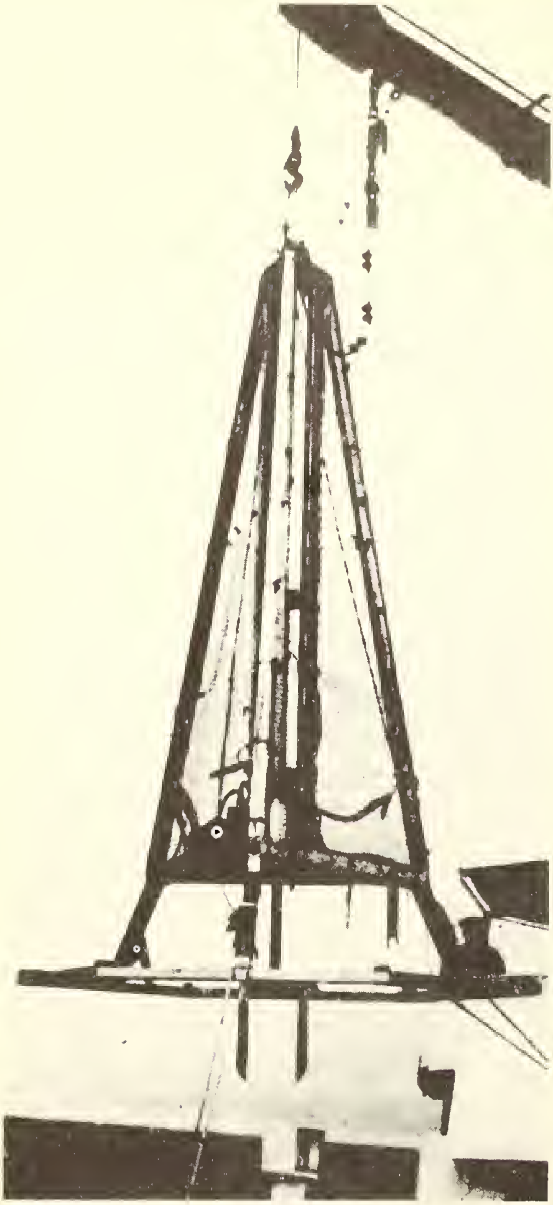

Fig. 3 Bottom-sediment density dual-barrel probe.

concentrations as low as 500 ppm. The instrument consists of a ^{241}Am source and detector arranged so that the water passes between them, utilizing the attenuation of gamma rays as a measure of sediment concentration.[16] With slight modification it is ex-pected that this instrument can be set in place and left unattended for several days at a time.

Sediment Analysis. With the increasing interest in sea-floor deposits, primarily for their economic values, the analyst requires a rapid technique for rough determination of the elemental compositions of these deposits. For the most part, the scientist is limited to collecting samples by remote techniques from a surface or submersible vessel and returning the samples to the laboratory for analysis. Efforts by the U. S. Atomic Energy Commission have shown that it may be feasible to adapt existing neutron activation systems to make in-place quantitative analyses on the sea floor.[17] Although several problems have yet to be solved, this approach holds much hope for a rapid assay technique in marine mining.

Nuclear Power Systems

Such unique characteristics of nuclear power systems as long life without refueling, no moving parts, and easy packaging for use in the oceans make them a very desirable power supply for certain oceanographic instruments. The oceanographer is tending more and more toward long-term observations, primarily by using large buoys, but a drawback to this arrangement is the power supply. The relatively short-lived batteries that are used today require either short observation periods or frequent battery replacement.

A few isotopic power systems have been put into operation, mainly to power remote weather stations or acoustic beacons on the sea floor.[18,19] There are, however, several isotopic power supplies under development for use with such instrument packages as navigational buoys, floating weather stations, and acoustic bench marks to be placed on the sea floor. The heat-producing characteristics of nuclear decay are also finding uses. Recently a miniature radioisotope-powered heat exchanger was built to heat and circulate warm water through a new type of suit used by scuba divers.[20,21]

Future Outlook and Uses

Undoubtedly, numerous applications of nuclear technology are yet to be conceived which could benefit the scientist in his studies of the sea. The problem to date has been primarily one of getting the nuclear scientist or engineer together with the oceanographer so that an exchange of ideas can take place. The instruments and techniques discussed above are examples of what can be done with proper communication between the concerned disciplines. With regard to future developments in nuclear technology as related to oceanography, there appears to be a high probability for significant progress in several areas.

Recent studies indicate the feasibility of designing a probe that would utilize a fast-neutron source and suitable detector and be capable of penetrating the sea floor to measure the water content and porosity of submarine deposits.[22] Water content and porosity along with density are key parameters when considering the engineering properties (load-bearing capacity, slope stability, settlement) as well as the acoustical characteristics of the sea floor. Such a probe used in conjunction with the existing instrumentation would be of great importance as more structures are placed on the sea floor and as the capabilities for mining the sea bottom are more fully developed.

Another potential instrument is one that would be towed along the sea floor on a sledlike frame while measuring the bulk density of the underlying sediment. By using a large gamma-emitting source and the back-scatter technique already in use for density measurements, it may be possible to develop a technique for measuring variations in sediment density over large areas in a relatively short time.

In order to make sea-floor mining profitable, the exploration and exploitation costs must be decreased considerably, and one way to do this is to obtain rapid analysis and assay of bottom deposits. Activation analysis may provide the means of achieving this. It may become feasible to include a neutron activation-analysis system as part of the sledlike frame mentioned.

Another possible use for radioisotopes would be the tagging of the sludge solids that are being dumped into the ocean off most major coastal cities. Such tagging would provide a means of determining whether or not some of this material is returned to the local beaches and harbors.

As a by-product of nuclear technology, it may become feasible in some areas to use the warm water leaving a nuclear power plant to aid the fishing industry. If the plant should be sufficiently close to deep water, the warm water could possibly be piped out along the sea floor, debouching some distance offshore. The rising warm water would then lift the nutrient-rich bottom water to the surface. This water would provide the food supply needed to support a greater number of fish.

To promote and increase the number of users of nuclear techniques in oceanography, oceanographers and nuclear scientists and engineers must develop a greater understanding of each other's capabilities. From such efforts, radioisotopes and associated techniques undoubtedly will make significant contributions to the future of oceanography. (MG)

References

References marked with an asterisk were not verified by the Isotopes Information Center (see the foreword).

1. S. Bhat, S. Krishnaswamy, Rama, and W. S. Moore, Thorium-234 Disequilibrium in the Ocean (Abstract), *Trans. Amer. Geophys. Union*, 49: 366 (1968).
2. E. D. Goldberg and M. Koide, Ionium Thorium Chronology in Deep-Sea Sediments of the Pacific, *Science*, 128. 1003 (1958).
3. A. T. Landis, Jr., Radioactive Aluminum in Ocean Sediments, *Undersea Technol.*, 8(3): 39 (1967).
4. J. N. Rosholt, C. Emiliani, J. Geiss, F. F. Koczy, and P. J. Wangersky, Absolute Dating of Deep-Sea Cores by the ^{231}Pa/^{230}Th Method, *J. Geol.*, 69: 162-185 (1961).
5. W. S. Broecker and D. L. Thurber, Uranium-Series Dating of Corals and Oolites from Bahaman and Florida Key Limestones, *Science*, 149: 58-60 (1965).
6. K. K. Turekian, Some Aspects of the Geochemistry of Marine Sediments, in *Chemical Oceanography*, Vol. 2, pp. 81-126, J. P. Riley and G. Skirrow (Eds.), Academic Press Inc., New York, 1965.
7. H. H. Veeh, ^{230}Th/^{238}U and ^{234}U/^{238}U Ages of Pleistocene High Sea Level Stand, *J. Geophys. Res.*, 71: 3379-3386 (1966).
8. C. A. Barnes and M. G. Gross, Distribution at Sea of Columbia River Water and Its Load of Radionuclides, in *Disposal of Radioactive Wastes into Seas, Oceans, and Surface Waters*, Symposium Proceedings, Vienna, 1966, pp. 291-302, International Atomic Energy Agency, Vienna, 1966 (STI/PUB/126).
9. M. G. Gross, Distribution and Movement of Radioactive Continental Shelf Sediment, Northwestern United States, in Proceedings of 7th International Sedimentological Congress, USAEC Report RLO-1725-73 (CONF-670803-2), January 1967.
10. N. Taney and D. B. Duane, Radioisotopic Tracer Investigation of Littoral Transport Around Point Conception, California, in Proceedings of 8th Annual Contractors Meeting, Washington, D. C., 1966, AEC Division of Isotopes Development, p. 26 (CONF-661203).
11. Wm. H. Johnston, A Family of New Isotopic Water Current Meters (the DWICA's), USAEC Report JLI-2748-86 Wm. H. Johnston Laboratories, Inc., January 1966 summarized in M. Gerrard, Deep-Water Isotopic Current Analyzer, *Isotop. Radiat. Technol.*, 5(3): 208-212 (Spring 1968).
12. J. F. Carden, Radio-Release in Review, *Isotop. Radiat. Technol.*, 5(2): 104-112, esp. pp. 106-107 (Winter 1967-1968).
13. G. H. Keller, Deep-Sea Nuclear Sediment Density Probe, *Deep-Sea Res.*, 12: 373-376 (1965).
14. A. F. Richards and G. H. Keller, In-Place Measurement of Shear Strength and Bulk Density in Gulf of Maine Clays (Abstract), *Trans. Amer. Geophys. Union* 49: 221-222 (1968).

15 *a*.K. Preiss, Non-Destructive Laboratory Measurement of Marine Sediment Density in a Core Barrel Using Gamma Radiation, *Deep-Sea Res.*, 15: 401-407 (1968).

b.K. Preiss, In-Situ Measurement of Marine Sediment Density by Gamma Radiation, *Deep-Sea Res.*, 15: 637-641 (1968).

16. J. R. McHenry, N. L. Coleman, J. C. Willis, C. E. Murphree, G. C. Bolton, O. W. Sansom, and A. C. Gill, Performance of Nuclear-Sediment Concentration Gauge, in *Isotopes in Hydrology*, Symposium Proceedings, Vienna, 1966, pp. 207-225, International Atomic Energy Agency, Vienna, 1967 (STI/PUB/141); M. Gerrard, Radioisotope Gage for Determining Suspended-Sediment Concentration in Streams, *Isotop. Radiat. Technol.*, 4(4): 358-362 (Summer 1967).

17. F. E. Senftle, Mineral Exploration by In Situ Neutron Activation, in Proceedings of 8th Annual Contractors Meeting, Washington, D. C., AEC Division of Isotopes Development, pp. 23-24 (CONF-661203).

18.*W. S. Stringham, Radioisotope Power Supplies for Moored Buoys, in *Trans. 1964 Buoy Tech. Symp.*, Marine Tech. Soc., 160-172 (1964).

19.*P. D. Cohn, N-Power and Oceanography, *Ocean Industry*, 2: 43-47 (1967).

20. G. T. Seaborg, Mass Production and Practical Applications of Actinide Elements, *Isotop. Radiat. Technol.*, 6(1): 1-18, esp. Fig. 5 (Fall 1968).

21. *Undersea Technol.*, November 1967, page 53 (news item).

22. A. H. Youmans, A Sediment Porosity Meter: A Feasibility Study, in Proceedings of 8th Annual Contractors Meeting, Washington, D. C., AEC Division of Isotopes Development, pp. 27-28 (CONF-661203).

Vertical Crustal Movement of the Sea Floor Associated with the Prince William Sound, Alaska, Earthquake

Richard J. Malloy and George F. Merrill

Atlantic Oceanographic Laboratories
Research Laboratories
Environmental Science Services Administration

CONTENTS

PAGE
Abstract 327
Introduction 327
Geological Setting 329
Previous Work 331
Equipment and Procedures 331
  Depth Sounding 331
  Side-Scanning Sonar 334
  Bottom Photography 335
Discussion 335
Acknowledgments 338
References 338

ABSTRACT

In 1965, the USC&GS ship *Surveyor* conducted hydrographic and ocean-bottom-scanning sonar surveys southwest of Montague Island, Alaska, to identify vertical crustal movement of the sea floor associated with the March 27, 1964, Prince William Sound Earthquake. The 1965 survey was controlled by precision navigation and covered portions of the *Surveyor*'s 1964 geophysical reconnaissance investigations during which sea-floor uplift in excess of 15 meters was discovered. A 21-kHz, conical-beam echo sounder was used for the depth soundings and a side-scanning sonar—with two laterally directed sonar beams of 150 and 160 kHz—to detect sea-floor features to a range of 366 meters to the right and left of the ship's trackline. Fresh fault scarps were traced seaward a distance of 19 kilometers. Data from the 1965 survey were used to prepare a bathymetric map of the uplifted area and, by comparison with preearthquake surveys, to construct profiles and a map showing the amount of sea-floor uplift. Lineaments detected by side-scanning sonar included scarps, strata ridges, and joint patterns. Areas of rock bottom yielded stronger reflections and more meaningful data than did areas of sediment.

INTRODUCTION

On March 28, 1964 (local time), the day after the Prince William Sound Earthquake, the U. S. Coast and Geodetic Survey began mobilizing equipment and personnel to assist in the emergency and to conduct scientific and technical investigations of the earthquake and its effects. Hydrographic annd oceanographic operations included the inspection and repair of tide-gage stations, reconstruction of portions of the geodetic control network, and geophysical investigations of the continental shelf and slope in the vicinity of the earthquake's epicenter. Marine reconnaissance studies included depth soundings, gravity and magnetic measurements, seismic-reflection profiling, core sampling of sea-floor sediments, and bottom photography. To assist in these postearthquake operations and investigations, four Coast and Geodetic Survey ships—the *Hodgson, Lester Jones, Pathfinder,* and *Surveyor*—were diverted to Alaska.

Soon after work began in the offshore epicentral region it became apparent that a major task would be the reconstruction of portions of the U. S. Coast and Geodetic Survey's geodetic network to provide accurate vertical and horizontal control. Vertical measurements could not be made on shore until the datum of reference (mean lower low water) was re-established. Offshore, vertical measurements of changes in depth could be made immediately because the datum of sea level had not changed—that is, the eustatic sea level remained fixed. Postearthquake geodetic operations are described in Volume I of *The Prince William Sound, Alaska, Earthquake of 1964 and Aftershocks,* Coast and Geodetic Survey Publication 10–3, 1966.

The USC&GS ship *Hodgson,* after completing her primary mission of installing portable tide gages, reoccupying portions of triangulation schemes, and conducting reconnaissance surveys in Prince William Sound, was directed to the area just off the southwest tip of Montague Island to investigate suspected extension of the faulting and crustal uplift observed on the island by geologists of the U. S. Geological Survey [described by A. Grantz and others, 1964]. On June 5, 1964, the *Hodgson* ran traverses across the projected strike of suspected faults and obtained three bottom profiles. Later, seven additional bottom profiles and seven subbottom profiles were obtained by the USC&GS ship *Surveyor* during geophysical survey work southwest of Montague Island completed July 3, 1964.

Depth soundings by the *Hodgson* and *Surveyor* were compared with those of preearthquake surveys made in 1927–1928. This comparison showed that a large area of the sea floor was uplifted in excess of 9 meters and that several areas of maximum uplift exceeded 15 meters [Malloy, 1964, 1965]. Because significant changes of the sea floor were detected, and because the Loran A and radar navigational control of the 1964 surveys provided less precise horizontal control than that of the 1927–1928 surveys, plans were initiated for a more detailed investigation of the area southwest of Montague Island.

In July 1965, the USC&GS ship *Surveyor* undertook a 1-week study of the sea floor off Montague Island (fig. 1). Raydist stations were erected to provide precise horizontal control for the work. As in 1964, depth soundings were made with a Raytheon DE 723 shallow-water Fathometer. A side-scanning sonar (Westinghouse Ocean Bottom Scanning Sonar, or WOBSS) was used to provide additional detail in the area shown in figure 2. Southeast of Montague Island visual control—using sextants to measure horizontal angles between prominent points—was used to reoccupy positions of the 1928 survey (lines 1–12 of figure 3). The side-scanning sonar was not used along these sextant-controlled lines. Corrections were made for sound propagation velocity in the area of the investigation and for the phases of the tide during the field work. The ship's speed was reduced to 3 knots when towing the large sonar transducers of the WOBSS system.

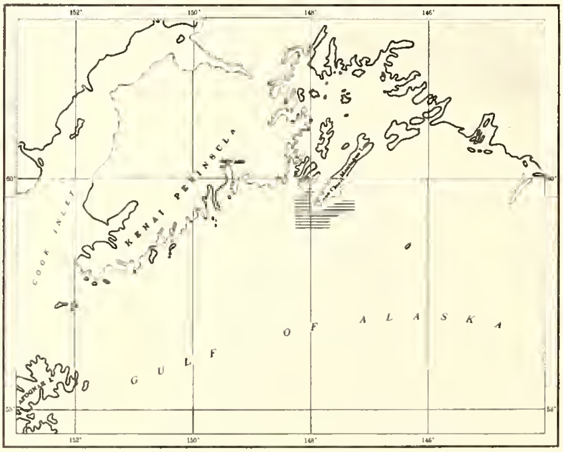

FIGURE 1.—Area of 1965 marine geophysical survey by USC&GS ship *Surveyor* southwest of Montague Island, Alaska.

This report is concerned primarily with the vertical uplift of the sea floor caused by the earthquake, as determined by depth soundings and side-scanning sonar. Supporting evidence, obtained by seismic-reflection profiling and bottom photography, was previously reported [Malloy, 1964, 1965].

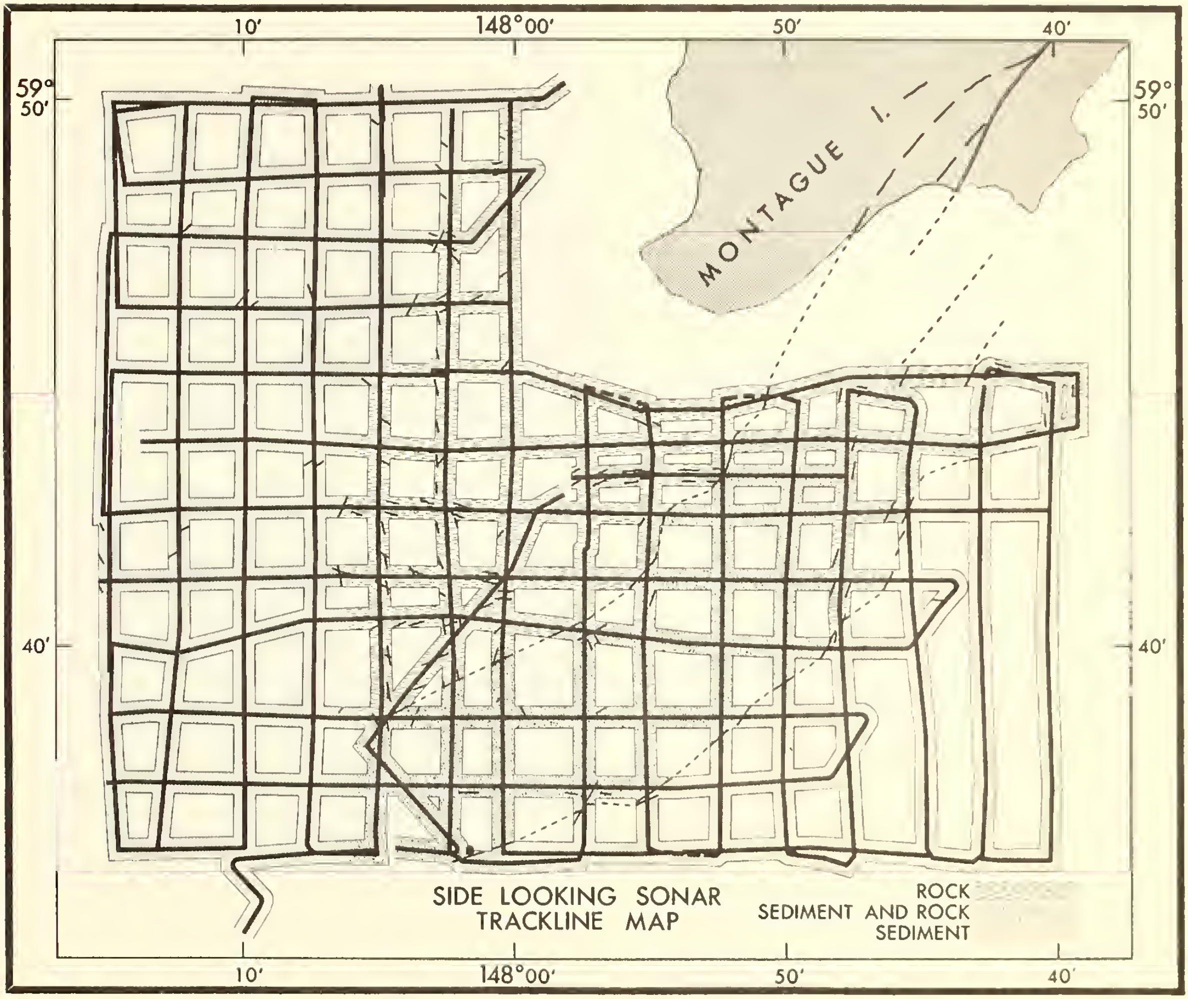

FIGURE 2.—Trackline map of side-scanning sonar survey, showing sonar-detected features of the sea floor.

GEOLOGICAL SETTING

The rocks comprising Montague Island have been mapped in some detail on the northwestern side of the island, but the southeastern side of the island has not received this attention because of the inaccessibility of its coastline. The northwest side of the island is composed of beds of graywacke, banded argillites, and some arkosic sandstone which probably belong to the Orca Group of the Upper Cretaceous [Moffit 1954]. Since the Prince William Sound Earthquake in 1964, a number of geological investigations have been made along the exposed southeastern side of Montague Island, but reports to date suggest that the southeastern side differs little from the better mapped northwestern side of the Island.

In general, Montague Island is composed of Cretaceous metasedimentary rocks. For the most part, these rocks are dark gray to black, and highly folded. Vertical dips are common. From what can be learned from the offshore seismic reflections, the rocks are acoustically opaque. Offshore bottom photography shows a well-defined joint pattern developed in the outcropping bedrock, with two sets of lineaments striking NE.-SW. and NW.-SE. (fig. 4).

The pattern of crustal uplift on the sea floor, as contoured from the reconnaissance data [Malloy, 1964, 1965], is similar to that mapped on land, that is, a northwesterly tilted block lies northwest of the northeasterly striking refaulted scarp known on land as the

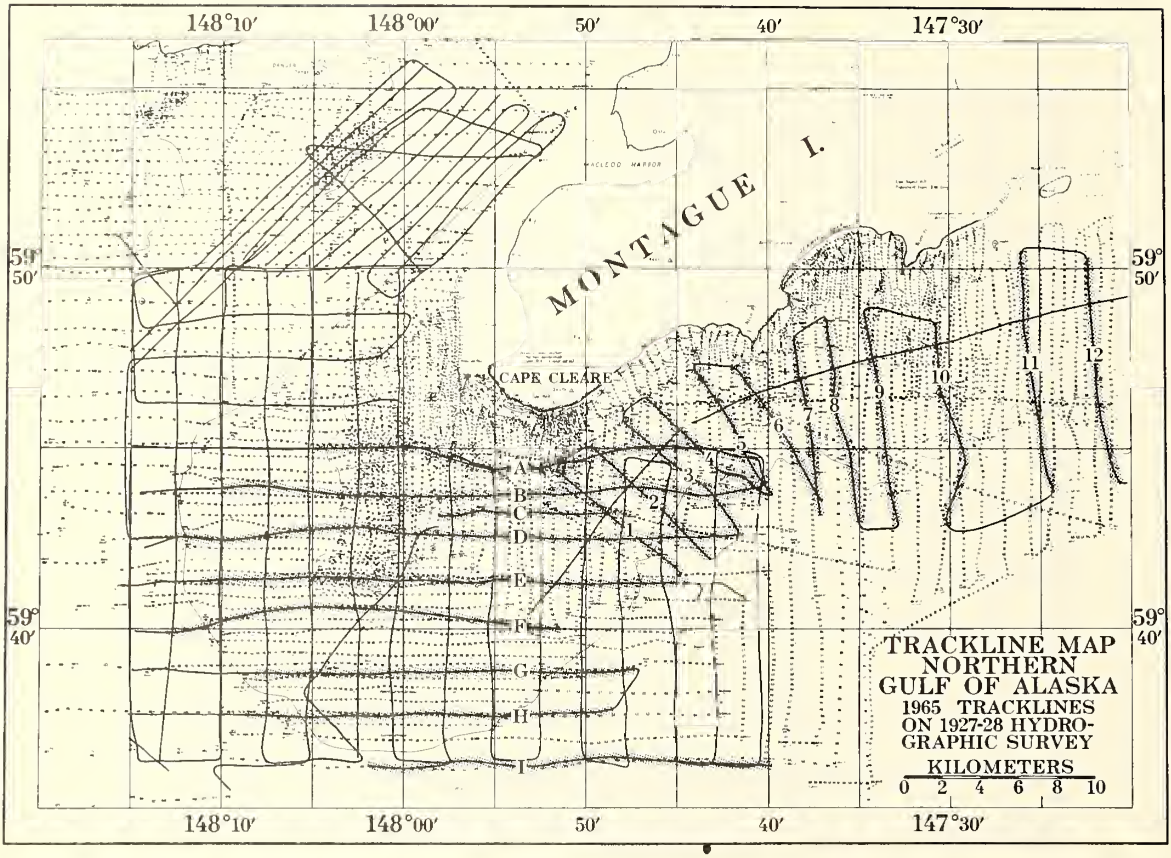

Figure 3.—Map showing 1965 hydrographic survey tracklines superimposed on 1927–1928 soundings. Hydrography of 1927–1928 and lines 1–12 of the 1965 hydrography were sextant controlled. All other lines (1965) were Raydist controlled.

Patton Bay Fault [Plafker, 1965]. The two major faults associated with the earthquake were identified at the southwestern end of Montague Island by a combination of aerial reconnaissance and observed vertical displacements of the barnacle line. Both faults strike more or less parallel to the long axis of Montague Island. The one on the southeast has been referred to as the Patton Bay Fault by Plafker [1965]. The fault on the northwestern side of the island has been informally designated as the Hanning Bay Fault. The Patton Bay Fault, according to Plafker, has been traced northeastward from the shore a distance of 16 kilometers and has a vertical displacement of 5.2 meters (northwestern side up) where it intersects the coastline. Presumably, all of the displacement is attributed to dip-slip movement. The Hanning Bay Fault has been traced by U. S. Geological Survey geologists a distance of about 5 kilometers, and like the Patton Bay Fault has its northwestern side upthrown relative to the southeastern side. The maximum displacement along the fault of 5 meters occurs on the beach at Hanning Bay [Plafker, 1965]. Neither fault exhibits much in the way of strike-slip movement, but Plafker did report 15 centimeters of left-lateral movement along the Hanning Bay Fault. The attitude of the fault which cuts through Patton Bay seems to be vertical, and the attitude of the Hanning Bay Fault plane is 70°, dipping toward the upthrown side, suggesting compression as the causative force.

Both faults on the southwestern tip of Montague appear to be rejuvenated faults [Plafker, 1965], that is, both faults occur along scarps that can be traced on pre-earthquake aerial photographs. The reconnaissance data of Malloy [1964, 1965] show that the Patton Bay Fault strikes into a preearthquake scarp at sea. This is

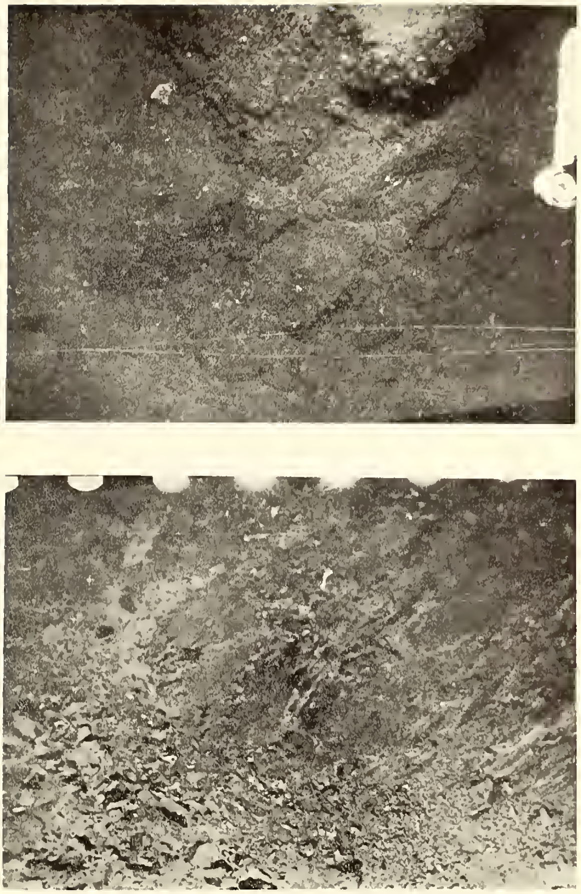

Figure 4.—Postearthquake photographs of sea floor southwest of Montague Island. Top photograph shows joint pattern (?) in encrusted bedrock. Bottom photograph shows angular nonencrusted features of fresh fault surface (?).

shown by the Coast Survey's depth sounding data of 1927 and 1928. The Hanning Bay Fault apparently follows no preearthquake scarp to sea and may not cut the sea floor to any extent southwest of Montague Island.

PREVIOUS WORK

Prior to the hydrographic and geophysical reconnaissance investigations immediately after the Prince William Sound Earthquake, the only significant submarine investigations in the epicentral area were the hydrographic surveys of the U. S. Coast and Geodetic Survey in the late 1920's. In 1927, a detailed hydrographic (bottom-sounding) survey was conducted off the southwest tip of Montague Island by an earlier ship also named *Surveyor,* using a then-new method of sounding, the sonic Fathometer. The designation of the instrument was the Submarine Signal Corporation Model 312 Sonic Fathometer. Several vertical casts, with lead-line and paraffin inserts to obtain sediment samples, were made to check the relatively new sonic device. Navigational control was obtained by using sextants to measure horizontal angles between prominent features on land. This horizontal control was exceptionally good because of the proximity of the shore with its many clearly visible and prominent peaks, crags, and promontories on which to sight. Figure 3 shows the 1927–1928 soundings and 1965 tracklines off the southwestern end of Montague Island.

Other early hydrographic work over the continental shelf and slope in the north-central Gulf of Alaska—where the concentration of aftershocks of strain release occurred—was controlled by visual bearings, celestial navigation, and dead reckoning and accomplished with the early model nonrecording echo sounders, hence preearthquake fathograms over critical portions of the epicentral and aftershock areas are not available for comparison with postearthquake hydrography made with recording echo sounders. Although many deep-sea tracklines were later made across the Gulf of Alaska, as Coast and Geodetic Survey ships steamed between work areas in Alaska and their home port of Seattle, the tracklines were discontinued when waters of the continental shelf were reached. The few tracklines for which fathograms of the shelf are available are considerably west of Montague Island and remote from the center of maximum uplift and sea-floor faulting.

Trackline data collected by the ships of the Coast and Geodetic Survey have been worked into bathymetric maps by Menard and Dietz [1951], and later by Gibson [1960] using additional data. These publications mainly treat the location, delineation, and distribution patterns of submarine volcanoes, the morphology of the Aleutian Trench, and the continental slope to the 100-fathom isobath.

EQUIPMENT AND PROCEDURES

Depth Soundings

Figure 3 shows three different sets of depth sounding data:

(1) 1927–1928, individual soundings—navigation control by sextant-measured horizontal angles;

(2) 1965, depth-sounding traverses numbered 1 to 12 and intersecting tie line—navigation control by sextant-measured horizontal angles; and

(3) 1965, depth-sounding traverses A to I and other tracklines between 147°40′ W., 148°15′ W. and 59°35′ N., 59°55′ N.—navigation control by Raydist.

The 1965 Raydist-controlled sounding data were used to prepare a bathymetric map showing the submarine

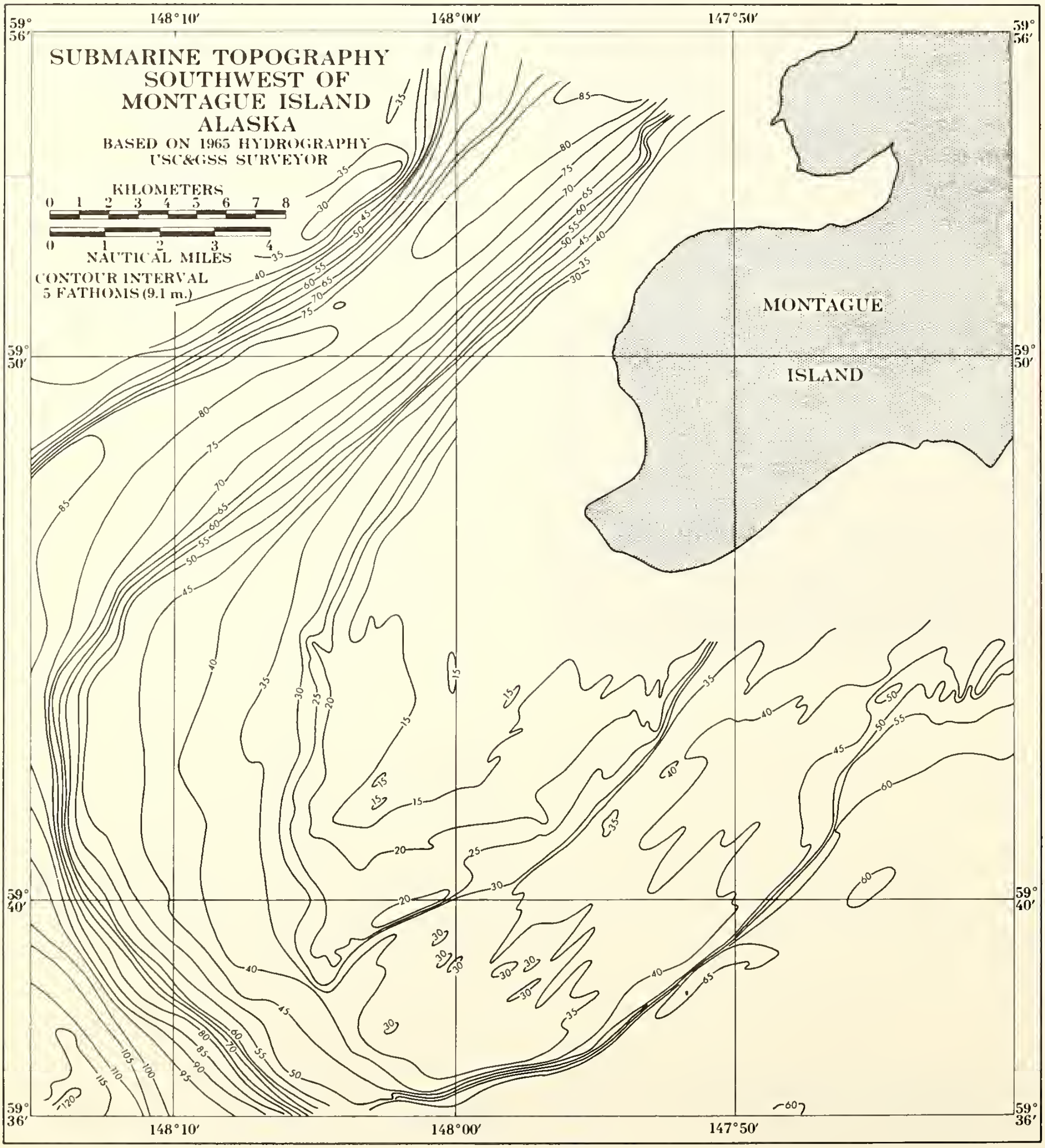

Figure 5.—Bathymetric map showing submarine topography southwest of Montague Island based on 1965 hydrographic survey by USC&GS ship *Surveyor.*

topography off the southwestern tip of Montague Island (fig. 5). To show the extent and patterns of sea-floor uplift, bottom profiles of preearthquake and postearthquake submarine topography were prepared for traverses A to I (fig. 6) and 1 to 12 (fig. 7). The postearthquake or upper profiles of the cross sections shown in figures 6 and 7 were prepared from the 1965 fathograms. To provide continuous profiles of preearthquake submarine topography from the individual soundings of the 1927–1928 surveys, the 1965 profiles were fitted to the 1927–1928 sounding data. In the process, all indications of recent faulting and tilting were removed or adjusted to achieve the best fit with the 1927–1928 sounding data. It was assumed in using this procedure that the only changes in sea-floor topography between the surveys of 1927–1928 and surveys of 1965 were brought about by the Prince William Sound, Alaska, Earthquake of 1964. The validity of this assumption has been reviewed by Malloy [1964, 1965].

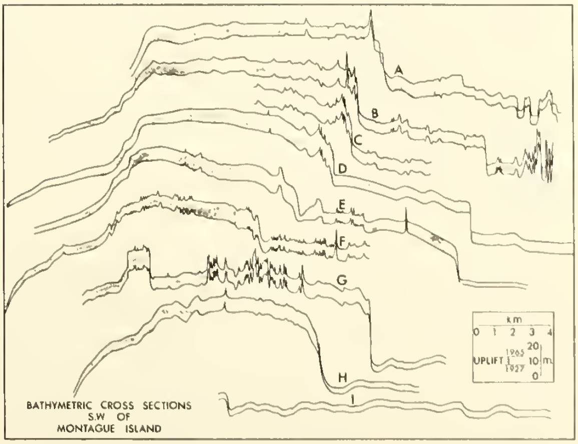

Figure 6.—Comparison of 1965 and 1927–28 sea-floor profiles southwest of Montague Island showing amount of uplift along lines A to I of figure 3.

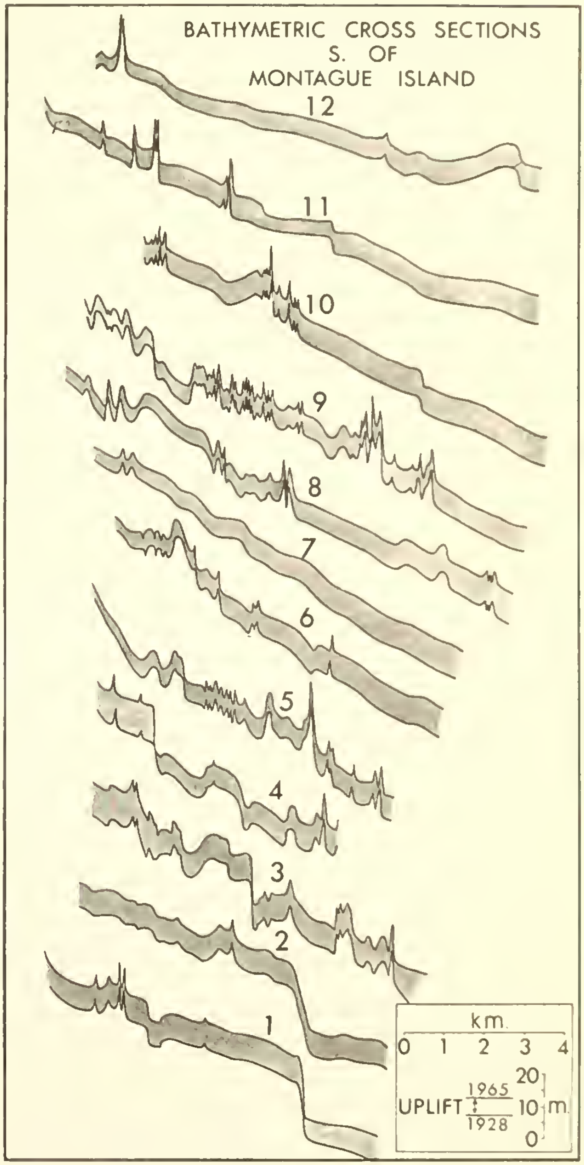

Figure 7.—Comparison of 1965 and 1927–28 sea-floor profiles southwest of Montague Island showing amount of uplift along lines 1 to 12 of figure 3.

Vertical uplift is evident on all the cross sections of figures 6 and 7. The accuracy of the comparison, however, is believed to be better in the shoaler areas where the 1927–1928 sounding surveys had numerous crosslines to disclose any discrepancies in depths, whereas some of the 1927–1928 offshore survey areas had no crosslines. The 1965 soundings southwest of Montague Island are along tracklines that form an evenly spaced pattern of squares and are considered to be uniformly reliable. However, in that part of the area where the Raydist-controlled tracklines cross the sextant-controlled tracklines, the Raydist-controlled soundings are consistently 3 meters deeper, although both surveys were made within a 2-week period by the USC&GS ship *Surveyor*. It is believed that these discrepancies in depths result from discrepancies in position of the Raydist-controlled tracklines, which may have been in the radio-wave shadow of Cape Cleare. One of the Raydist stations was located at 59°56.5′ N., 148°3′ W., north of Cape Cleare. Signals from this station had to pass over the surface features of the southwest tip of Montague Island before reaching the survey ship. The sextant-controlled soundings were not subject to this type of position error and are preferred wherever the two sets of survey tracklines overlap.

Emphasis in this paper is placed on the pattern of sea-floor uplift rather than on the exact amount of uplift, the details of which require additional hydrographic work. In general, the Raydist-controlled soundings corroborate the findings of the postearthquake reconnaissance surveys of 1964. Figure 8 shows contours of equal uplift and the faults along which movement occurred during the Prince William Sound, Alaska, Earthquake.

Side-Scanning Sonar

To obtain greater detail of the sea floor, a Westinghouse Ocean Bottom Scanning Sonar was towed along the Raydist-controlled tracklines southwest of Montague Island (fig. 2). The system consisted of two laterally directed scanning beams, and the instrument was towed above the ocean bottom by an electric-cable towing line, with the recording equipment and power source aboard the ship. The echo sounders were housed in an instrument case (fish) 3.96 m. long, 91 cm. high, 91 cm. wide, and weighing about 682 kg. in air. High-frequency transceivers were mounted on the starboard and port sides of the fish to scan the ocean floor both to the right and to the left of the path over which the fish was towed. To identify signals returning from each side-scanning beam, the starboard transceiver was operated at 150 kHz, and the port transceiver at 160 kHz.

The side scanner was towed from the ship by means of a combination strain and electric-cable tow line attached to the fish through a metal sleeve fitting and to the ship through an oceanographic winch equipped with heavy-duty slip rings. Extensive shipboard preparation was necessary before the side-scanning sonar equipment could be towed from the *Surveyor,* including installation of the winch on the afterdeck and A-frames on the starboard and port sides adjacent to the winch. To decrease the towing strain on the slightly underpowered winch, the fish was towed at a speed of 3 knots.

The shipboard equipment included a dual-channel amplifier and an Alden dual-channel wet-paper recorder which provided simultaneous graphic display of the port and starboard transducer return signals.

The swath of ocean floor covered by the side-scanning sonar sweeps was 732 meters wide (366 meters to each side of the fish) when the fish was towed 68.5 meters above the bottom. Side lobes of the main sound pulse were directed vertically, thus allowing the distance of the fish off the bottom to be displayed on both the recorder and the monitoring oscilloscope. The transducers, which were fired simultaneously twice a second, were arranged with their long axes fore and aft to produce a fan-shaped beam of sound with less than a degree of fore and aft width. Each laterally directed beam illuminated the sea floor in a somewhat trapezoidal pattern that was approximately 1.1 meters wide almost directly beneath the ship and 2 meters wide at the maximum range of 366 meters. In this manner, a new strip of ocean floor was illuminated each time the sonar was pulsed as the towed fish moved forward.

Reflected sound signals were fed from the unfocused receiving transducers into the amplifying and recording system. Variations in signal strength related to transmission geometry were compensated by the receiver circuitry. Distortions that normally would be caused by using a slant-range technique were compensated by equipping the recorder with helices that did not spiral linearly but coiled in such a manner that the distortions were removed. Speed of the recording paper also was adjusted so that the scale along the width of the paper equaled the scale along the length. The record, therefore, was of equal scale from edge to edge. However, small distortions resulting from changes in the ship's speed remained on the record. These changes in speed were caused by currents and wind, neither of which could be monitored constantly.

The graphic record produced by the side-scanning sonar consists of closely spaced lines that correspond to each scan of the sonar beam. Each line varies in intensity with the strength of the reflected signal. Signals reflected from sea-floor surfaces that are almost perpendicular to the fan-shaped sound beam have strong echoes and appear dark on the record. Areas of no echo remain white on the record and are presumed to be in the shadow zone behind some sea-floor prominence. Successive scans of the sea floor produce an image of consecutive lines having a three-dimensional quality of light and shadow as shown in figure 9. The principle of the side-scanning sonar technique is described in greater detail by Clay and others [1964].

BOTTOM PHOTOGRAPHY

Two camera lowerings were made from the USC&GS Ship *Surveyor* during the 1964 survey while searching for the seaward extension of faults observed on Montague Island after the Prince William Sound Earthquake. A line of bottom photographs was obtained during each lowering. One line extended from 59°46′ N., 147°56′ W. to 59°40′ N., 147°59′ W.,; the other from 59°41′ N., 147°56′ W. to 59°40′ N., 147°59′ W. An Edgerton, Germeshausen, & Grier, Inc. (EG&G), deep-sea stereocamera system was used. The camera apparently drifted across a fresh fault scarp, as a number of photographs showed rock debris and surfaces indicative of a fresh break in the sea floor (fig. 4, bottom). Bottom photographs taken northwest of the rejuvenated scarp showed a joint pattern oriented NE.-SW. and NW.-SE. (fig. 4, top). Color photography was used, but the black-and-white prints reproduced as figure 4 show sea-floor features in greater detail than do the color photographs.

DISCUSSION

The salient points concerning the patterns of uplift, as ascertained by the depth-sounding study, are: (1) Four NE.-SW. trending scarps off the southwestern tip of Montague Island appear to have been rejuvenated during the earthquake, (2) the sea floor northwest of each of the four rejuvenated scarps appears to have been tilted toward the northwest, (3) a moatlike band of lesser uplift surrounds the southwestern end of Montague Island, (4) the Hanning Bay Fault on the northwestern side of Montague Island does not appear to extend into the study area, and (5) the area covered by the study appears to have been uplifted at least 2 meters.

The two prominent northeasterly striking scarps off southwest Montague Island (fig. 8) both appear to be connected to the Patton Bay Fault complex, as the larger and more southeasterly scarp of the two cannot be traced on strike southeast of Cape Cleare. Also there is evidence of en échelon offset between the southeasterly scarp and its assumed continuation as the Patton Bay Fault on Montague Island.

Most of the uplift profiles in figures 6 and 7 show northwesterly tilting of the fault block between the more prominent scarps and of the adjacent fault block to the northwest. This northwesterly tilting follows the trend of the regional tilting and the observed local tilting on Montague Island [Plafker, 1965].

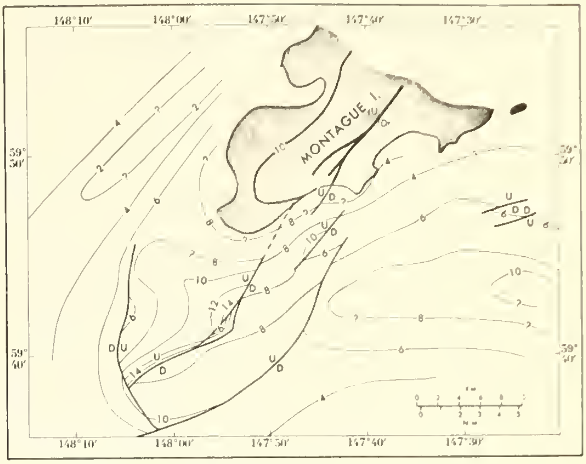

FIGURE 8.—Map showing faults and isopleths of equal crustal uplift (in meters).

The fault shown at the western edge of the uplift contour map (fig. 8) with a down-to-the-west relative movement is anomalous to the other faults on the sea floor and on Montague Island. The evidence for faulting here, however, is not as clear as for the other faults. Local flexing, which could explain the uplift discrepancies on either side of this gentle scarp, may have occurred. In either case, this zone of differential disturbance might explain why northeasterly striking faults are not found southwest of this zone.

The moatlike band of lesser uplift extending around Cape Cleare can be explained by the fault-and-tilt pattern southeast of the Cape. The apparent continuation of the moat southwest of Cape Cleare, however, requires a different explanation. It may be attributed to: (1) An artifact of the data, (2) the isostatic effect of the island mass, or (3) a secondary center of uplift.

The pattern of uplift on Montague Island [Plafker, 1965] shows a center of maximum uplift—uplift which decreases toward the shoreline. The presence of this slope and of the well-established maximum uplift offshore shows rather conclusively that an area of lesser uplift lies between the two maxima.

The cause of the uplift moat cannot easily be explained by isostasy. If the vertical forces of uplift as focused on Montague Island were restrained to any extent by the island's mass, the uplift maxima would not exist on or near the island's concentration of mass. Rather, it appears as though the forces which formed the land mass of Montague Island are still active.

The cause of the uplift moat is probably the result of the juxtaposition of two features of uplift minima defined by common contours. The major portion of the uplift moat, which lies southeast of Cape Cleare, can be explained by northeast faulting and northwest tilting. The portion of the uplift moat southwest of the Cape is probably best explained by its location between centers of uplift maxima along the Patton Bay Fault and its submarine extension.

Practically all of the depth-sounding comparisons made in the study area (as outlined in figure 1) show shoaler depths after the earthquake. Exceptions totaled less than 1 percent and suggest that the limit of accuracy of the upilft contour map is probably as good as the contour interval of 2 meters.

The complicated contour pattern immediately southeast of the northwesternmost scarp may be caused by a narrow zone of depression that is parallel to the scarp. This can be observed on the profiles of uplift (fig. 6). It is clearly brought out on the reconnaissance survey profiles of uplift described by Malloy [1964, 1965]. The depression probably is fault controlled, that is, caused by a small down-to-the-northwest fault running parallel to and southeast of the larger fault plane.

Rock strata along the major fault scarps were not displaced sufficiently to show any offset of magnetic anomaly lineaments on maps of magnetic field intensity prepared by the authors.

Results of the side-scanning (side-looking) sonar survey are summarized in figure 2, which shows the trackline pattern over which the side-scanning sonar fish was towed, the swath of sea floor covered by the laterally directed sonar beams, and the sea-floor features within the swath that could be interpreted from the sonar record—areas of rock bottom and sediment, and trends of certain topographic features. Features of fine detail, such as lineaments, were best detected in areas of rock bottom—the strength of the reflected signals being greater from rock bottom than from sediment-covered sea floor. Thus it was possible to record most of the scarps and associated lineaments on the tabularlike submarine extension of Montague Island where the sea floor was predominantly bedrock with only local lenses of sediment present.

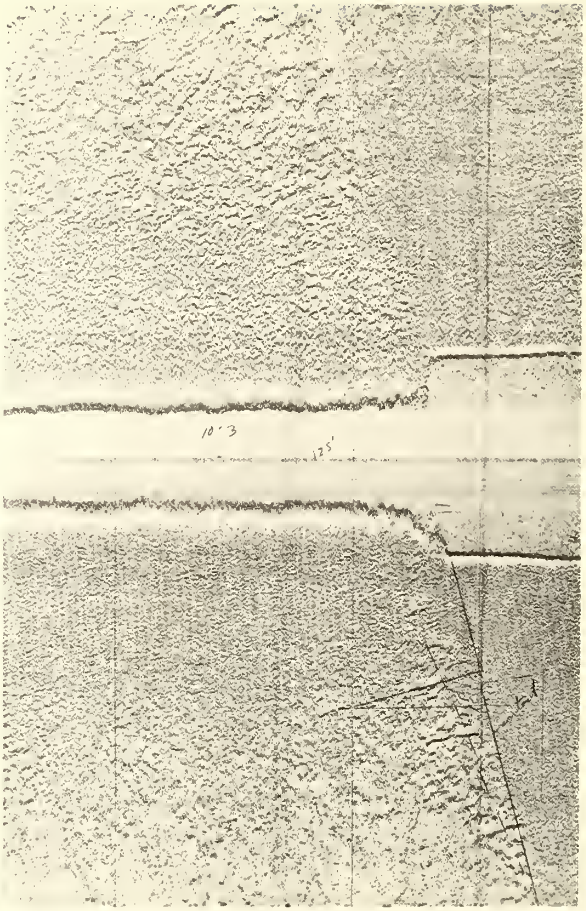

Figure 9.—Photograph of ocean-bottom-scanning sonar record showing fault scarp. The traverse runs NW.–SE. and the fault scarp strikes NE.

Figure 9, a portion of the side-scanning sonar record, shows the trend and magnitude of a scarp over which the sonar fish was towed. The center line represents the path of the towed sonar fish. The dark reflections immediately to the right and left of the path give the depth directly beneath the ship, as detected by the nearly vertical side-lobe of the sonar beam. The variously shaded reflections extending farther to the right and left on the record depict sea-floor conditions to the maximum range of the side-scanning sonar beams. Both the vertical- and side-scanning portions of this section of the record show a difference in the lithologic character of the sea floor above and below the scarp.

The sea-floor materials shown in figure 2 are of three types: Bare rock over almost the entire sea floor northwest of the northwesternmost fault scarp—in the area of shoaler water over the tabularlike extension of Montague Island; rock and lenses of sediment in the area between the two prominent fault scarps; and unconsolidated sediment southeast of the southeasternmost scarp (fig. 10). Many of the lineaments shown in figure 2 are presumed to be joints, scarps, and lines of outcropping strata. An interpretation of these lineaments, other than those which appear to be fault scarps, is not attempted

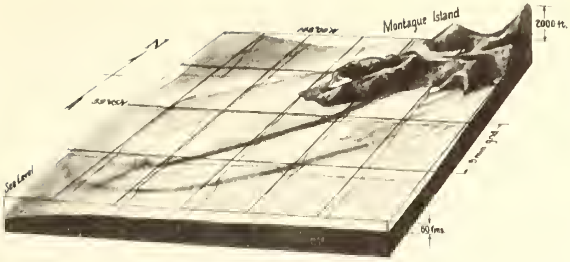

Figure 10.—Diagram of sea floor southwest of Montague Island showing two major submarine scarps. Southeasternmost scarp is connected to the island by en échelon scarps.

because the area of investigation belongs, geologically, to the complex structural features of southwestern Montague Island. On the other hand, the geology of the sea floor between islands, where fewer forces have interacted during regional uplift, can be relatively simple compared to that on land. For this reason, joint patterns—which provide clues to regional tectonic processes—might be studied to better advantage in the sediment-free offshore areas. In the 1965 side-scanning sonar survey, however, the detected lineaments did not produce the consistent patterns one might expect from studying the orientation of joint patterns on the bottom photographs. Perhaps outcropping strata deflected the echo returns and confused the joint-pattern picture.

Very little is known about the details of failure in the earth's crust and the forces of earthquake dimensions that cause crustal deformation, faulting, and vertical crustal changes. Most earthquakes for which epicenter data are available occur around the edge of the Pacific Basin and along the ocean rises and associated fracture zones of the world ocean. Thus a large number of earthquakes are submarine earthquakes, sometimes called seaquakes. Earthquakes whose hypocenters occur under land areas produce tectonic changes in the earth's surface, but these changes are rarely known in detail because the reference datum, by which land movements are determined, exists only as a series of scattered points or bench marks. Patterns of crustal deformation can be defined only to the extent the displacements of bench marks, and intervening surface features relative to the bench marks, can be measured. It is conceivable that an earthquake-deformed land surface, which was mapped by photogrammetrically controlled surveys before the earthquake, could be remapped by a similar survey following an earthquake after the disturbed reference points or bench marks were redetermined. This type of study would provide a method whereby an area of land surface could be examined in detail for patterns of uplift. To the writers' knowledge, this type of survey has not been reported.

The problem of determining patterns of crustal uplift on the sea floor differs from that on land in that there are no bench marks. The reference datum is not a series of isolated points; it is the continuous plane of the sea surface. Thus, it is only in areas where detailed depth soundings were made prior to crustal deformations that one can determine the patterns of crustal deformation on the sea floor. Plafker [1965] has pointed out that the Prince William Sound, Alaska, Earthquake was unique in that it not only produced a vast area of subsidence and uplift, but in that so many parts of the area could be measured and contoured because of the irregularity of the Alaska coastline and the numerous islands, all of which served as bench marks in determining the amount of deformation of the sea floor. Modern surveys and techniques will make it possible to extend investigations of submarine crustal deformations over more and more of the circumpacific zone of earthquake activity. Such studies will contribute to a better understanding of the generation of tsunami—one of many problems involving the interaction of land and sea in seismically active marine and coastal regions.

The importance of hydrographic work in Alaskan waters has two significant aspects. First, each year more ships with deeper drafts use Alaska's vast and complex waterways. This requires many long seasons of bottom-sounding investigations. The task is further complicated by Alaska's geology as the rugged mountains and many glaciers contribute enough sediment to the rivers, fiords, bays, and estuaries to change bottom-sounding charts radically within a 1-year period [Jordan, 1962]. Another cause of frustration to the hydrographic engineer is the continuing tectonic unrest in southern Alaska. During the March 27, 1964, Prince Willian Sound Earthquake as much as 90,000 square kilometers of sea floor and islands may have been uplifted [Plafker, 1965], causing dangerous shoaling of the sea floor in many areas.

Second, another aspect of relevancy is the need for continuing detailed hydrographic surveys in areas of crustal deformation. Each time crustal deformation resulting from earthquake forces is measured, more is learned about the strength and competency of the earth's crust. Among the major authenticated crustal deformations of large magnitude are those resulting from the

Yakutat Bay (Alaska) earthquake of 1899 and the Prince William Sound Earthquake of 1964, about 420 kilometers apart. The Yakutat Bay earthquake was investigated 6 years after the disturbance. Portions of the earth's crust were calculated to have been uplifted in excess of 14 meters, on the basis of new and old barnacle and other sessile organism lines on rocks along the shore [Tarr and Martin, 1912]. The 1964 Prince William Sound Earthquake was accompanied by uplift in excess of 10 meters on southwestern Montague Island and, according to detailed bathymetric studies, uplift in excess of 14 meters in offshore areas southwest of Montague Island. It may be coincidental that these two maxima of recorded uplift are about equal. It also is possible that these maxima are quantitatively related to local tectonic forces and to the strength of the earth's crust as deformed by a single seismic event.

ACKNOWLEDGMENTS

The writers are grateful for the assistance rendered during the field investigations by Capt. Don A. Jones, Commanding Officer of the USC&GS ship *Surveyor*. Cdr. A. R. Benton, Jr., Navigation and Field Operations Officer, L. A. Weeks, Chief Scientist, and other members of the ship's complement; and for the helpful suggestions and critical reading of the manuscript by H. B. Stewart, Jr., R. S. Dietz, G. H. Keller, L. A. Weeks, and R. N. Harbison, all of the Atlantic Oceanographic Laboratories, Research Laboratories, ESSA.

REFERENCES

Clay, C. S., Ess, John, and Weisman, Irving, "Lateral Echo Sounding of the Ocean Bottom on the Continental Rise," *Journal of Geophysical Research,* vol. 69, no. 18, pp. 3823–3835, 1964.

Gibson, William M., "Submarine Topography in the Gulf of Alaska," *Bulletin of the Geological Society of America,* vol. 71, no. 7, pp. 1087–1108, 1960.

Grantz, A., Plafker, G., and Kachadoorian, R., "Alaska's Good Friday Earthquake, March 27, 1964—A Preliminary Geologic Evaluation," *U. S. Geological Survey Circular 491,* 35 pp., 1964.

Jordan, G. F., "Redistribution of Sediments in Alaskan Bays and Inlets," *Geographical Review,* vol. 52, no. 4, pp. 548–558, 1962.

Malloy, R. J., "Crustal Uplift Southwest of Montague Island, Alaska," *Science,* vol. 146, no. 3647, pp. 1048–1049, 1964.

———, "Seafloor Upheaval," *Geo-Marine Technology,* vol. 1, no. 6, pp. 22–26, 1965.

Menard, H. W. and Dietz, R. S., "Submarine Geology of the Gulf of Alaska," *Bulletin of the Geological Society of America,* vol. 62, no. 10, pp. 1263–1285, 1951.

Moffit, F. H., "Geology of the Prince William Sound Region, Alaska," *U. S. Geological Survey Bulletin, 989–E,* 310 pp., 1954.

Plafker, George, "Tectonic Deformation Associated With the 1964 Alaska Earthquake," *Science,* vol. 148, no. 3678, pp. 1675–1687, 1965.

Tarr, R. S. and Martin, L., "The Earthquakes at Yakutat Bay, Alaska, in September 1899," *U. S. Geological Survey Professional Paper 69,* 135 pp., 1912.

Reprinted from EOS, Transactions of American Geophysical Union Vol. 50, No. 10, 552-555.

REFERENCES

Barnes, D. F., and R. V. Allen, Reconnaissance marine and shoreline geophysical data from the area south and west of Kodiak Island, Alaska (abstract), *Proc. 15th Alaskan Science Conf.*, 168, 1964.

Barnes, D. F., W. H. Lucas, and R. V. Allen, Gravity measurements over the southern Alaskan Continental Shelf (abstract), *Trans. Amer. Geophys. Union, 46*(1), 106, 1965.

Barnes, D. F., The U.S. Geological Survey's program of Alaskan gravity observations, *Trans. Amer. Geophys. Union, 46*(1), 231–233, 1965.

Barnes, D. F., Gravity changes during the Alaska earthquake, *J. Geophys. Res., 71*(2), 451–456, 1966*a*.

Barnes, D. F., Seismic, gravity and magnetic measurements, Chap. 11, in *Environment of the Cape Thompson Region, Alaska*, U.S. At. Energy Comm. Rept. PNE-481, 165–174, 1966*b*.

Barnes, D. F., W. H. Lucas, E. V. Mace, and R. J. Malloy, Reconnaissance gravity and other geophysical data from continental end of Aleutian arc (abstract), *Bull. Amer. Ass. Petrol. Geol., 50*(3), 644, 1966.

Barnes, D. F., Four preliminary gravity maps of parts of Alaska (open-file report), U.S. Geological Survey, 1967.

Barnes, D. F., Alaskan gravity base station network (open-file report), U.S. Geological Survey, 1968.

Berg, Eduard, and Jurgen Kienle, Gravity measurements in the Katmai Volcano area, Alaska, *Alaska Univ. Geophys. Inst. [Rept. ser.] UAGR-176*, 5 pp., 1966.

Case, J. E., D. F. Barnes, George Plafker, and S. L. Robbins, Gravity survey and regional geology of the Prince William Sound epicentral region, Alaska, *U.S. Geol. Survey Profess. Paper 543-C*, C1–C12, 1966.

Dehlinger, Peter, Michael Gemperle, R. W. Couch, and D. W. Hood, Free-air gravity anomalies along the inside passage of British Columbia and Alaska, *J. Geophys. Res., 71*(24), 6011–6015, 1966.

Ostenso, N. A., Geomagnetism and gravity of the Arctic Basin, *Proc. Arctic Basin Sympos., Oct. 1962*, Hershey, Pa., Arctic Inst. North America, 9–45, 1963.

Ostenso, N. A., A gravity survey of the Chukchi sea region, and its bearing on westward extension of structures in Northern Alaska, *Bull. Geol. Soc. Amer., 79*(2), 241–254, 1968.

Peter, G. A., D. J. Elvers, and M. J. Yellin, Geological structure of the Aleutian trench southwest of Kodiak Island, *J. Geophys. Res., 70*(2), 353–366, 1965.

Wood, F. J., ed.-in-chief, 1966, The Prince William Sound, Alaska, earthquake of 1964 and aftershocks, V. I, *U.S. Coast and Geod. Surv. Pub. 10-3*, 263 pp., 1966.

Woollard, G. P., chm., and H. R. Joesting, coordinator, Bouguer gravity anomaly map of the United States (exclusive of Alaska and Hawaii), *Amer. Geophys. Union and U.S. Geol. Survey*, 1964.

Woollard, G. P., and J. C. Rose, *International Gravity measurements*, 518 pp., Society of Exploration Geophysicists, Tulsa, Okla., 1963.

Worzel, J. L., *Pendulum gravity measurements at sea, 1936–1959*, 422 pp., Wiley & Sons, New York, 1965.

Gravity Anomalies over the Aleutian Trench

Alexander Malahoff

Hawaii Institute of Geophysics, Honolulu

Barrett H. Erickson

Pacific Oceanographic Research Laboratory, ESSA, Seattle, Washington

In 1964 the USC&GS *Surveyor* crossed the Aleutian trench 48 times between 165° and 180°W longitude. The data provide a basis for a free-air gravity map, a Bouguer gravity map (density 2.87 gm/cm^3), and three possible crustal models that fit the results and available seismic data. The area covered lies west of an earlier gravity survey described by *Peter, et al.* [1965], of the Aleutian trench between 155°W and 165° longitude and 53° and 55°N latitude. As on the earlier gravity survey, which was also carried out by the U.S. Coast and Geodetic Survey, the observations were made along north-south lines spaced 20 km apart and extending about 200 km south of the island arc. A LaCoste-Romberg sea gravimeter S-12 was used, and the measurements were part of the ESSA SEAMAP project [*Peter and Stewart*, 1965]. Gravimeter connections were made to 8 port bases, most of which were tied to stations of the world gravity network established by *Woollard and Rose*, [1963]. These ties suggest possible discrepancies as large as 3 mgal over parts of a six-month period, and were attributed to meter drift, although other factors may have contributed. Most of the gravity profiles observed across the Aleutian trench are smooth and the observed data are estimated to be accurate to within ±3.0 mgal. During rough seas the meter's performance was erratic, but by applying vertical acceleration corrections, as described by *Dehlinger et al.* [1966], it was possible to smooth out some of the erratic results.

The data reported by *Peter, et al.* [1965] were taken along 15 north-south profiles and one cross profile; and show a minimum free-air gravity anomaly of −70 to −80 mgal paralleling the axis of the trench but located about 10 to 20 km north of the trench axis. The axis of the trench lies in water depths ranging from 5700 meters at the eastern end to 6800 meters at the western end. At about 158°40'W and 53°50'N there is a sharp increase in the depth of the trench (down to 6400 meters from 5400 meters to the east); it is accompanied by a decrease in the free-air gravity anomaly to −80 mgal. South of the trench axis and at ocean depths of about 4500 to 5000 meters, the free-air anomaly over the smooth ocean floor averages +50 mgal.

By using the Nafe-Drake curve relating rock densities to rock velocities [*Talwani, et al.*, 1959] and seismic refraction profiles and interpretative sections obtained by *Shor* [1962] in the area of gravity survey, Peter et al. prepared a crustal section for which the computed and observed free-air gravity anomaly profiles generally matched within a few milligals. Two-dimensional computer techniques and crustal densities transposed from the data of Shor were used to construct the crustal density sections, using a mantle density of 3.3 gm/cm^3. The interpretation of the gravity anomalies for the eastern section of the Aleutian trench shows a 10.5 km depth to the mantle 100 km south of the trench axis (free-air gravity anomaly +50 mgal); a depth of 12 km to the mantle 50 km south of the trench axis (free-air anomaly +30 mgal); and a depth of 10 km to the mantle over the axis of the trench (free-air anomaly −65 mgal). Peter et al. did not achieve a good fit between the observed and calculated free-air anomaly profiles over the landward portion of the trench.

The most distinct difference in the gravity anomalies between the area of the trench east of 160°W (studied by Peter et al.) and the area between 165° and 180°W is the progressive westward decrease in the free-air anomaly values, which reach −160 mgal over the axis of the trench at about 168°W. This change in the free-air anomaly values corresponds to an increase in the depth of the trench down to 7250 meters. Between 165° and 180°W the depth and configuration of the trench are remarkably constant (see Figure 1). The free-air anomalies along the north-south sections also stay remark-

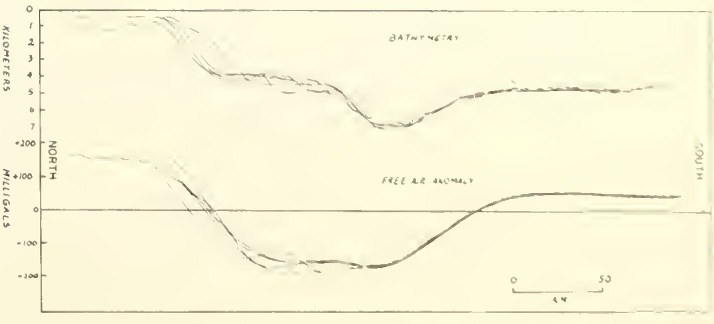

Fig. 1. Five evenly spaced bathymetric and associated free-air gravity anomaly profiles across the Aleutian trench between 165° and 180°W longitude

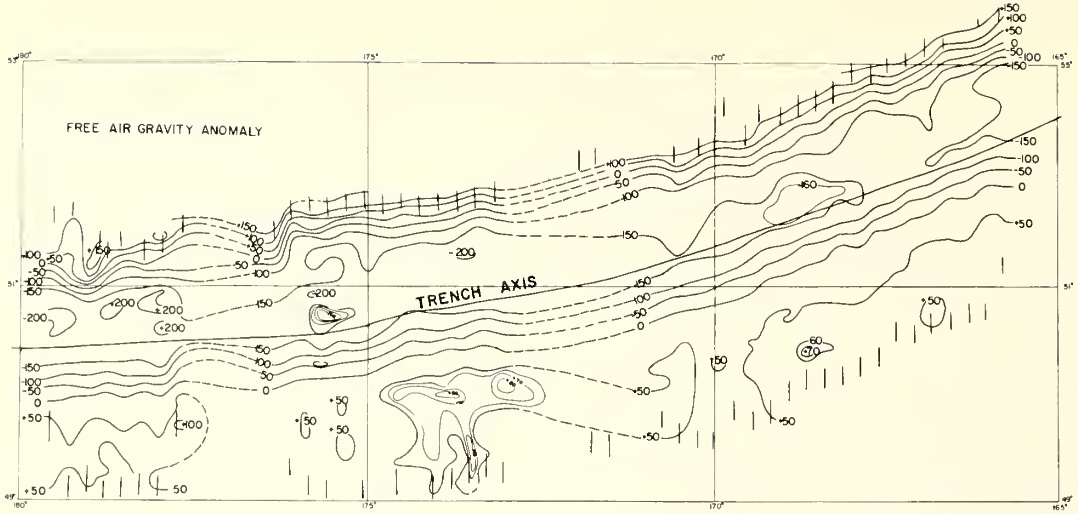

Fig. 2. Free-air gravity anomalies over the Aleutian trench between 165° and 180°W longitude. Contour interval 50 milligals.

ably constant between these longitudes (see Figure 2). Bathymetric profiles across the trench show that depth of 7000 to 7250 meters are present at the axis of the trench and that a 50-km wide bench occurs north of the axis at a depth of 4000 to 4500 meters with the continental shelf beginning at 150 km north of the axis. Two prominent aspects of the bathymetric and free-air gravity anomaly profiles are: (1) high (+50 mgal) anomalies over the 'undisturbed' 5000-meter deep oceanic crust south of the trench axis; and (2) the persistence of the −150 to −200 mgal free-air anomaly over the bench north of the trench despite a decrease of about 2000 meters in water depth.

A density of 2.87 g/cm^3 was used for the crust in constructing the Bouguer gravity anomaly map given in Figure 3. If the +450-mgal average Bouguer anomaly over the undisturbed oceanic crust south of the trench axis is plotted on *Woollard's* [1962] curve of Bouguer anomaly versus elevation of mantle for an oceanic crust, a depth to mantle of 11 km is found. By using the formula of *Rose et al.* [1968], $DMZ = 32 - 400DW - FAA/19.25$, where DMZ is the depth to the mantle from sea level; DW is the depth of water, $DW = 4.8$; FAA is the free-air anomaly, $FAA = +50$ mgal; a depth of 10.2 km to the mantle is obtained for the undisturbed portion of the oceanic crust south of the trench. The occurrence of a relative Bouguer gravity low of +200 mgal over the bench of the Aleutian trench north of the trench axis (see Figure

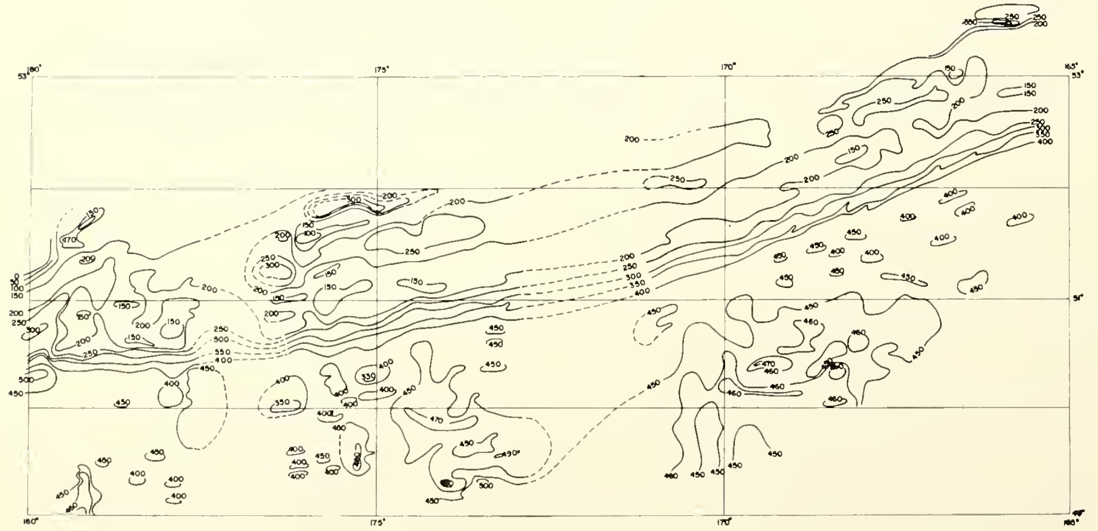

Fig. 3. Bouguer gravity anomaly over the Aleutian trench between 165° and 180°W longitude based on a rock density of 2.87 gm/cc. Contour interval 50 milligals.

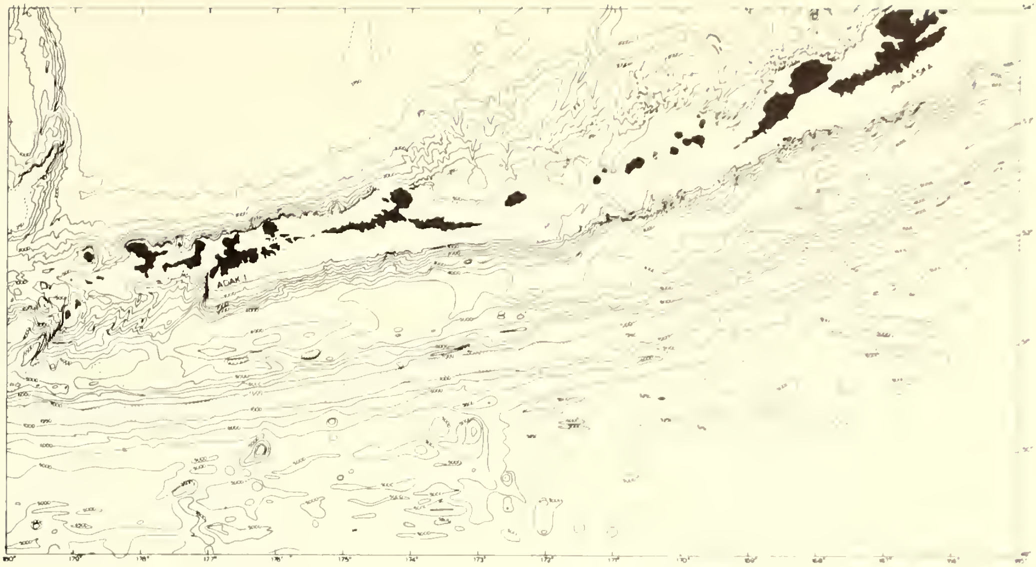

Fig. 4. Bathymetric map of the Aleutian trench. Contour interval 500 meters.

4) suggests a low density crust, or low density upper mantle. The general +250 mgal Bouguer high north of the +200 mgal low suggests a local thinning of the crust or a general increase in the density of the crust or upper mantle. The +200 mgal low coincides with the −200 to −250 mgal free-air low over the bench located north of the northern wall of the Aleutian trench.

Interpretation of the gravity anomalies in terms of crustal structure for the area of the Aleutian trench studied in this paper was based on the rock density-seismic velocity curve of *Woollard* [1968] and the few seismic refraction profiles obtained by *Shor* [1964] over the axis of the trench.

A computer program was used to compute several theoretical free-air gravity anomaly profiles over two-dimensional geological sections constructed by using the data of Shor as control. One such geological section constructed was based on a north-south bathymetric and free-air gravity anomaly profile across the trench located at 166°W longitude. The structural aspects of the section and the accompanying free-air anomalies are given in Table 1. The computations suggest a mantle depth of 10.6 km below sea level at 75 km south of the trench, intermediate between the 11.0- and 10.2-km depths suggested by *Woollard's* [1968] formula and the *Rose et al.* [1968] formula, respectively. Seismic data of *Shor* [1962] over the trench east of the area studied suggests a mantle depth of 14.6 km in a water depth of 6800 meters. Data in Table 1 suggest a mantle depth of 14.6 km beneath the trench in a water depth of 7.1 km. The crust-mantle interface configuration along 166°W longitude across the Aleutian

TABLE 1. Suggested Rock Density Layer Model for Crustal Section along 166°W Longitude across the Aleutian Trench

A	95N		75N		55N		35N		15N	
B	+165		+145		+ 20		−170		−160	
	(1)	(2)	(1)	(2)	(1)	(2)	(1)	(2)	(1)	(2)
	W	0	*W*	0	*W*	0	*W*	0	*W*	0
	2.3	0.8	2.3	1.0	2.0	1.7	1.9	3.8	1.9	4.9
	2.4	1.7	2.4	1.8	2.2	2.5	2.2	5.2	2.2	6.4
	2.7	3.8	2.7	3.8	2.3	3.4	2.3	5.9	2.4	7.4
	3.0	6.8	3.0	7.3	2.4	4.9	2.4	7.2	3.0	9.7
	3.4	19.6	3.4	20.5	2.7	7.0	2.7	8.9	3.4	14.5
					3.0	13.3	3.0	13.8		
					3.4	24.4	3.4	24.0		
A	0		15S		35S		55S		75S	
B	−145		− 50		+ 40		+ 50		+ 50	
	(1)	(2)	(1)	(2)	(1)	(2)	(1)	(2)	(1)	(2)
	W	0	*W*	0	*W*	0	*W*	0	*W*	0
	1.9	7.1	1.9	5.8	2.1	4.3	2.1	4.8	2.1	4.8
	2.2	8.1	2.2	6.4	2.7	5.3	2.7	5.2	2.7	5.1
	2.7	9.0	2.7	6.9	3.0	7.0	3.0	6.6	3.0	6.4
	3.0	10.4	3.0	8.3	3.4	11.2	3.4	10.9	3.4	10.6
	3.4	14.5	3.4	12.4						

A Distance in minutes of latitude north (N) or south (S) of trench axis.
B Free-air anomaly in milligals.
(1) Densities of implied layers (*W* is the water layer) in g/cm^3.
(2) Depth to top of layer from sea level in kilometers.

trench therefore appears to be adequately represented by the data contained in Table 1.

A density of 3.4 g/cm^3 was assumed for the upper mantle in calculating the crustal section and also assumed to be constant for the section. The apparent depression of the mantle to 24 km at 45 km north of the trench axis beneath the bench of the northern wall of the trench may also be intepreted in terms of the general decrease in the density of the upper mantle as a result of admixture of crustal rocks during episodes of island arc overthrusting over the downward moving oceanic crust, as postulated by *Isacks et al.* [1968]. The admixture of crustal rocks into the mantle would lead to the disappearance of 'sea floor spreading' magnetic anomaly patterns imprinted upon the rocks of the oceanic crust. The line of admixture of the crustal rocks into the mantle beneath the bench would then logically coincide with the line of disappearance of the 'sea floor spreading' magnetic anomaly patterns; the east-west aligned magnetic anomaly patterns located south of the trench do in fact lose their identity over the northern wall of the trench (Figure 5) and not over the trench axis. The magnetic anomaly patterns in Figure 5 do therefore substantiate that the zone of admixture of crustal rocks into the mantle does indeed appear to be located beneath the northern wall of the trench, as suggested above by the gravity and seismic data.

Conclusions

1. The smooth oceanic crust 150 km north of the Aleutian trench axis has an average depth of 4500 meters and an associated free-air anomaly of +50 mgal.

2. Free-air gravity anomalies and the bathymetric features of the Aleutian trench parallel one another. However, the −150 to −200-mgal free-air anomaly low extends from the axis of the trench onto the northern wall of the bench located at a depth of 4500 meters north of the trench axis.

3. A +150 to +200 mgal relative Bouguer gravity anomaly low is also located over the bench.

4. Interpretation of the free-air and Bouguer gravity anomalies suggests an oceanic crustal thickness of 10.6 km at 75 km south of the trench axis; a 14.5-km thick crust beneath the trench axis; and, probably, a low-density upper mantle at 45 km north of the trench axis.

REFERENCES

Dehlinger, P., R. W. Couch, and M. Gemperle, Surface ship gravity meter measurement corrected for vertical accelerations, *J. Geophys. Res., 71*(24), 6017–6023, 1966.

Isacks, B., J. Oliver, and L. R. Sykes, Seismology and the new global tectonics, *J. Geophys. Res., 73,* 18, 5855, 1968.

Peter, G., and H. B. Stewart, Jr., Ocean surveys, the systematic approach, *Nature, 206,* 1017–1018, 1965.

Peter, G., D. Elvers, and M. Yellin, Geological structure of the Aleutian trench southwest of Kodiak Island, *J. Geophys. Res., 70,* 353–366, 1965.

Rose, J. C., G. P. Woollard, and A. Malahoff, Marine gravity and magnetic studies of the Solomon Islands, *Geophys. Monograph 12, Amer. Geophys. Union,* 379–410, 1968.

Shor, G. G., Seismic refraction studies off the coast of Alaska, *Bull. Seismol. Soc. Amer., 52*(1), 37–55, 1962.

Shor, G. G., Structure of the Bering Sea and the Aleutian Ridge, *Marine Geol., 1,* 213–219, 1964.

Talwani, M., G. H. Sutton, and J. L. Worzel, A crustal section across the Puerto Rico trench, *J. Geophys. Res., 64,* 1545–1555, 1959.

Woollard, G. P., The relation of gravity anomalies to surface elevation, crustal structure, and geology, Univ. Wisc., Geophys., *Polar Res. Center, Res. Rep. 62–9,* 329 pp., 1962.

Woollard, G. P., The interrelationship of the crust, the upper mantle, and isostatic gravity anomalies in the United States, *Geophys. Monograph 12, Amer. Geophys. Union,* 312–341, 1968.

Woollard, G. P., and J. C. Rose, *International gravity measurements,* Society of Exploration Geophysicists, 518 pp., 1963.

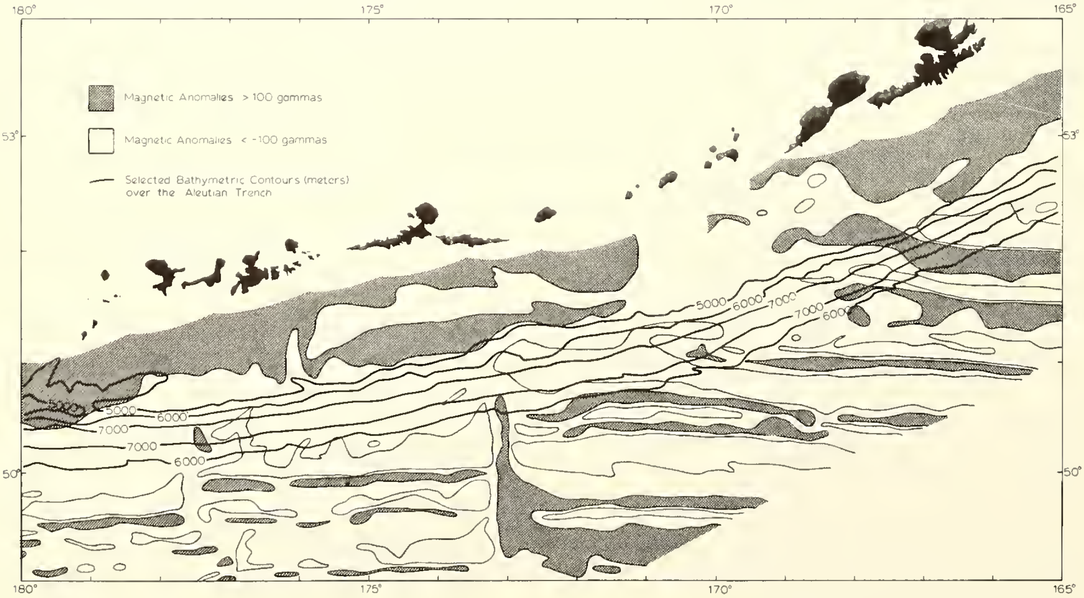

180°
175°
170°
165°
53°
50°
▨ Magnetic Anomalies > 100 gammas
☐ Magnetic Anomalies < -100 gammas
Selected Bathymetric Contours (meters) over the Aleutian Trench
5000
6000
7000

Fig. 5. Residual total force magnetic anomaly patterns over the Aleutian trench.

HIG-69-21 26

Data Report No. 14

BATHYMETRY OF THE NORTH INSULAR SHELF OF MOLOKAI ISLAND, HAWAII FROM SURVEYS BY THE USC&GSS MC ARTHUR

By

Christopher C. Mathewson

September 1969

Environmental Science Services Administration
Pacific Oceanographic Laboratories
Joint Tsunami Research Effort
with the
Hawaii Institute of Geophysics

Approved by Director
George P. Woollard

Date: September 29, 1969

ABSTRACT

Bathymetric surveys carried out by the U. S. Coast and Geodetic Survey Ship MC ARTHUR show that the north insular shelf of Molokai is a smooth plain, gently dipping seaward, with three slight steps, one occurring between the 30- and 60-foot isobaths, one between the 150- and 180-foot isobaths and one near the 300-foot isobath. The shelf break occurs near the 500-foot isobath. Off East Molokai Volcano the shelf is cut by eleven submarine canyons; along West Molokai the shelf is unbroken except for one canyon. About half of the canyons have bowl-shaped heads; the remainder have V-shaped heads. Generally speaking, the canyons originate about one mile offshore.

TABLE OF CONTENTS

Page

ABSTRACT iii

TABLE OF CONTENTS v

LIST OF FIGURES, MAP vi

INTRODUCTION 1

SURVEY OPERATION 2

CHARACTERISTICS OF THE SHELF 4

ACKNOWLEDGMENTS 7

REFERENCES 8

LIST OF FIGURES

Figure

1 Survey area and line density along the North Coast of Molokai. USC&GSS MC ARTHUR area shaded, R/V MAHI seismic reflection lines by Mathewson (1969).

2 North-south bathymetric profiles spaced 5 nautical miles apart showing the ancient shorelines that are apparent in the area.

3 Detailed bathymetric map of the North Molokai Volcanic Pipe Zone. Contour interval 30 feet corrected.

4 East-West profiles across the Pelekunu Canyon System. Profile spacing: 0.5 nautical miles.

5 Long profile of Pelekunu Canyon System. (Vertical Exaggeration 11:1.)

MAP

Topographic and Bathymetric Map of the Island of Molokai, State of Hawaii, May 1969 (scale ≈ 1:40,000). . . . . *(in pocket)*.

INTRODUCTION

The 1968 survey carried out by the U. S. Coast and Geodetic Survey Ship MC ARTHUR along the north coast of Molokai Island has made possible the construction of a bathymetric map for that area with a 60-foot contour interval. This map can now be matched to the existing topographic map of the island of Molokai so that the relationship between the geomorphology of the insular shelf and that of the island can be studied.

Previous studies of the Molokai area include that of Stearns and Macdonald (1947) on the geology and geomorphology of the island and that of Shepard and Dill (1966) on the submarine canyons. In addition, magnetic studies of the area have been reported by Malahoff and Woollard (1966), and gravity observations by Strange et al. (1965). Seismic reflection studies have been reported by Kroenke (1965) and Mathewson (1969).

SURVEY OPERATION

A total of 1,340.7 nautical miles of ship and launch hydrographic survey lines were run in a 120 square nautical mile survey area along the north coast of Molokai (Fig. 1). The spacing of the survey lines were set in the project instructions as follows:

Line Spacing:

50 meters - Maximum spacing on 1:5,000 scale sheets and in channels, anchorages, bays, boat harbors, Harbor of Refuge

50 - 100 meters - Less than 20 fathoms off rocky points and spits

100 meters - Less than 20 fathoms along general coastline

200 meters - 20 to 30 fathoms, maximum spacing on 1:10,000 scale sheets

400 meters - 30 to 110 fathoms

800 meters - over 110 fathoms

Figure 1 shows the line spacings obtained during the survey as measured on the survey boat sheets. About 10 per cent of the survey lines were run as crosslines to check the accuracy of the primary survey.

The entire survey was controlled by visual 3-point sextant fixes spaced from 1 to 5 minutes apart. A total of 5,765 position fixes were made. The launch sounding instruments were calibrated to a depth of six fathoms using a bar check. Physical oceanographic parameters obtained from Nansen bottle stations were used to determine sound velocity corrections from 0 to 100 fathoms. Corrections for deeper depths were obtained from Hawaii Institute of Geophysics Report HIG-67-18 (Belshé, 1967). Corrections for tide were based on a bubbler tide gage mounted on Kalaupapa Wharf, Molokai, 21°12'22" North latitude, 156°59'29" West longitude. The standard tide gage at Kahului, Maui was used as a back-up for the Kalaupapa gage.

CHARACTERISTICS OF THE SHELF

The north insular shelf of Molokai Island is a smooth plain, dipping about 1° toward the sea. Three slight steps occur along the shelf; one between the 30- and 60-foot isobaths, one between the 150- and 180-foot isobaths, and one near the 300-foot isobath (see Map, in pocket). The shelf dips about 2° between the shoreline and the 30- 60-foot isobath step, then at about a 1° dip to the 150- 180-foot isobath step, which dips at about 2°. Beyond this step the shelf again dips at about 1° until the 300-foot isobath where the dip of the shelf decreases slightly to about 0.75°, continuing at this dip to the shelf break which occurs at about the 500-foot isobath.

Six ancient shore lines around the Hawaiian Islands are now submerged: they are the Koko at 15 feet; the Waipio at 60 feet; the Penguin Bank at 180 feet; the Mamala-Kahipa at 300 feet; the Lualualei from 1200 to 1800 feet; and the Waho at 3600 feet below sea level (Easton, 1965; Ruhe et al., 1965; Stearns, 1966, 1967). The first four named ancient shorelines are apparent in bathymetric profiles across the north Molokai shelf (Fig. 2). The deeper ancient shorelines occur beyond the limits of the survey.

An anomalous bathymetric area off East Molokai, about 1-1/2 miles north of Pelekunu Bay and about 6 miles east of Kalaupapa Peninsula, is characterized by numerous small, steep-sided pinnacles (Fig. 3). These small features have a relief of about 75 feet and correspond to the

+270 mgal Bouguer gravity anomaly maximum (Strange et al., 1965), and to the inflection point in the magnetic anomaly (Malahoff and Woollard, 1966) related to the North Molokai Volcanic Pipe Zone. From these geophysical data it is suggested that the pinnacles are submerged stacks or other erosional features that mark the center of volcanism of the East Molokai Volcano.

The MC ARTHUR survey shows that the East Molokai submarine canyons except for two off Kalaupapa originate about one mile off shore, and that the West Molokai submarine canyon originates about three miles off shore. The shelf between the canyon heads and the shoreline is generally smooth with no distinct continuation between each submarine canyon and its corresponding land canyon (see Map, in pocket). However, east-west profiles across the Pelekunu submarine-subaerial canyon system (Fig. 4) show a direct relationship between the submarine and subaerial portions of the canyon system. The long profile of the Pelekunu canyon system which shows no distinct nick points can be divided into three basic sections (Fig. 5): (1) the inland canyon section, (2) the waterline section, and (3) the submarine canyon section. The average gradient of the inland canyon section is about 1/3 (slope 18°); the waterline section, about 1/30 (slope 2°); and the submarine canyon section, about 1/8 (slope 7°).

About half of the canyons have typical bowl-shaped heads, the remainder have V-shaped heads. In some cases, the canyons with bowl-shaped heads actually have two or more small, less than 0.1-mile long, V-shaped or U-shaped canyons as tributaries. These small canyons acting together form the generally bowl-shaped head of the major canyon.

REFERENCES

(1) Belshé, John, 1967, Tables of the Velocity of Sound and of Depth Corrections for Echo-Sounding in Hawaiian Waters, Applied Oceanography Series No. 5, Hawaii Institute of Geophysics report HIG-67-18, 10pp., 6 figures, 10 tables.

(2) Easton, W. H., 1965, New Pleistocene Shore Lines in Hawaii, Geol. Soc. Am. Cordilleran Sec., 61st Ann. Mtg., Program, p. 21.

(3) Kroenke, L. W., 1965, Seismic Reflection Studies of Sediment Thicknesses Around the Hawaiian Ridge, Pacific Science XIX, no. 3, pp. 335-338.

(4) Malahoff, A. and G. P. Woollard, 1966, Magnetic Surveys over the Hawaiian Islands and Their Geologic Implications, Pacific Science XX, no. 3, pp. 265-311.

(5) Mathewson, Christopher C., 1969, Origin of Submarine Canyons along the North Shore of Molokai Island, Hawaii, Abstract 1969 Annual Mtg. Geol. Soc. Am., Atlantic City, N. J.

(6) Ruhe, R. V., J. M. Williams, and E. L. Hill, 1965, Shorelines and Submarine Shelves, Oahu, Hawaii, Jour Geology, Vol. 73, pp. 485-497.

(7) Shepard, F. P. and R. F. Dill, 1966, Submarine Canyons and Other Sea Valleys, Rand McNally and Co., Chicago, pp. 211-214.

(8) Stearns, H. T., 1966, Geology of the State of Hawaii, Pacific Books, Palo Alto, Calif.

(9) Stearns, H. T., 1967, Geology of the Hawaiian Islands, Bull. No. 8, Dept. of Land and Natural Resources, State of Hawaii, Supplement by G. A. Macdonald.

(10) Stearns, H. T. and G. A. Macdonald, 1947, Geology and Groundwater Resources of the Island of Molokai, Hawaii, Bull. 11 Hawaii Div. Hydrography, 113 pp. (geologic map enclosed)

(11) Strange, W. E., G. P. Woollard, and J. C. Rose, 1965, An Analysis of the Gravity Field Over the Hawaiian Islands in Terms of Crustal Structure, Pacific Science XIX, no. 3, pp. 381-389.

ACKNOWLEDGMENTS

These data were collected by the officers and men of the U. S. Coast and Geodetic Survey Ship MC ARTHUR. Commander R. L. Newsom, C. O. MC ARTHUR, made the boat sheets available to the author.

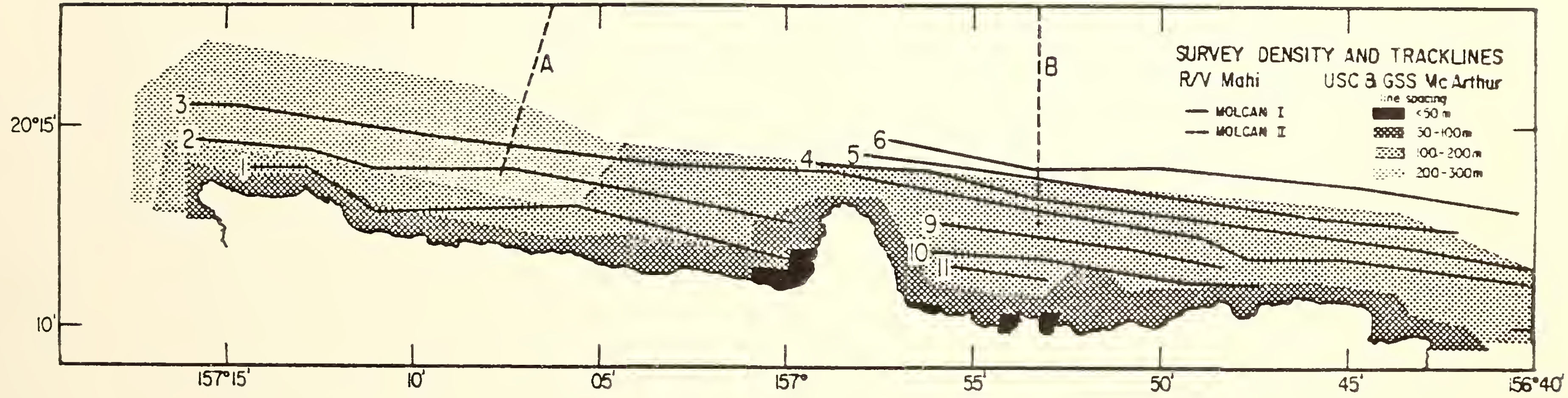

Fig. 1. Survey area and line density along the North Coast of Molokai. USC&GSS MC ARTHUR area shaded, R/V MAHI seismic reflection lines by Mathewson (1969).

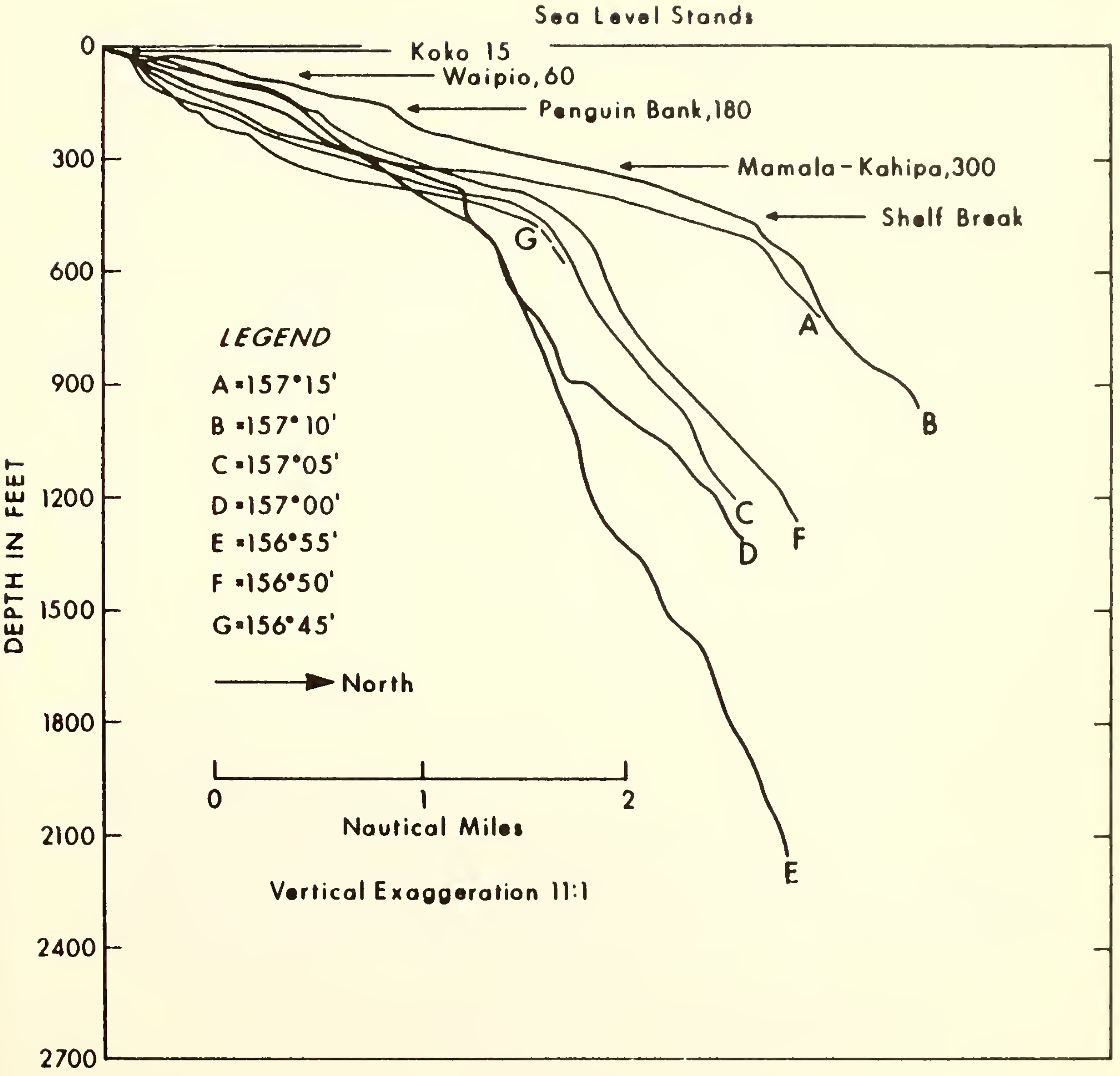

Fig. 2. North-south bathymetric profiles spaced 5 nautical miles apart showing the ancient shorelines that are apparent in the area.

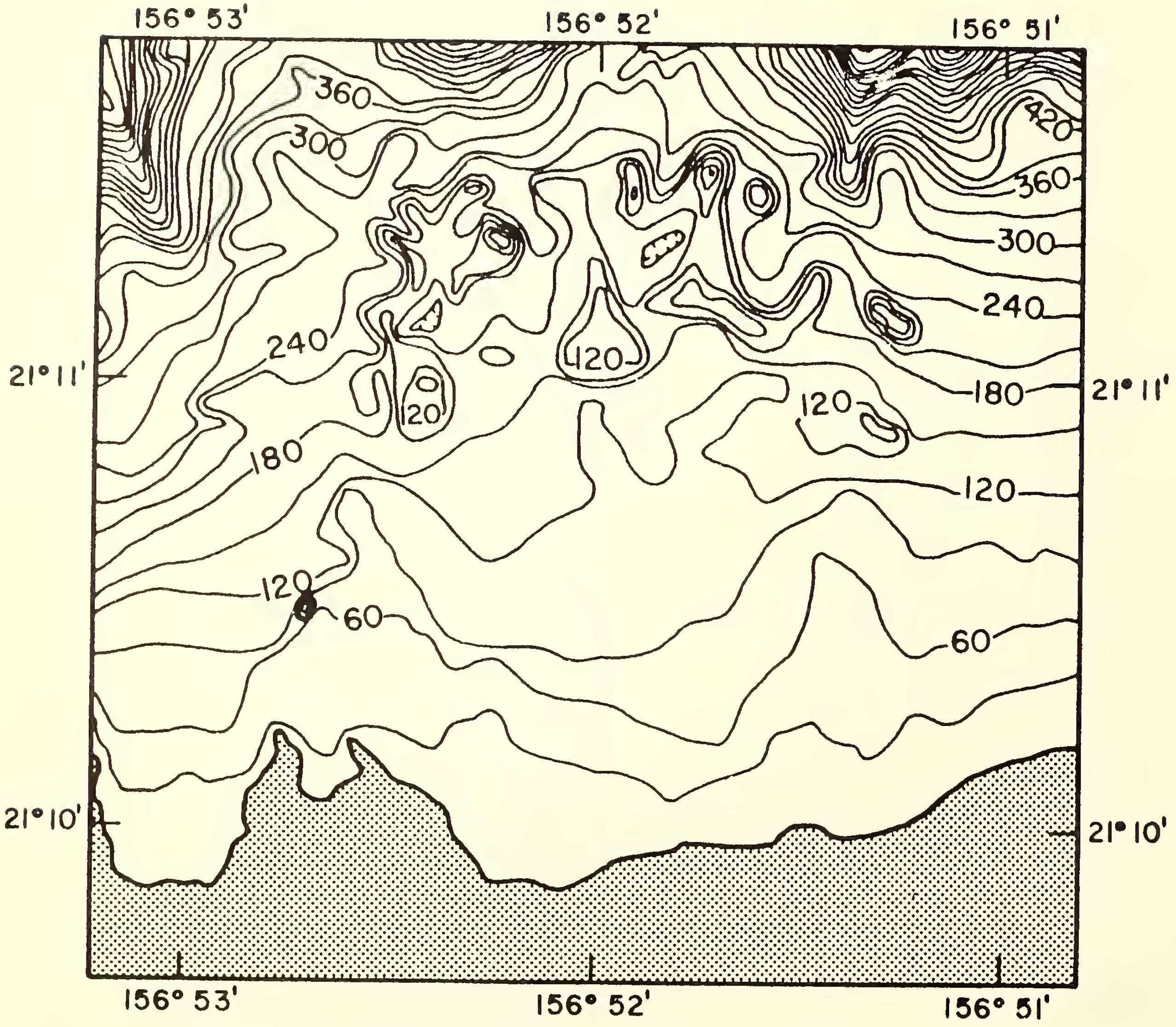

Fig. 3. Detailed bathymetric map of the North Molokai Volcanic Pipe Zone. Contour interval 30 feet corrected.

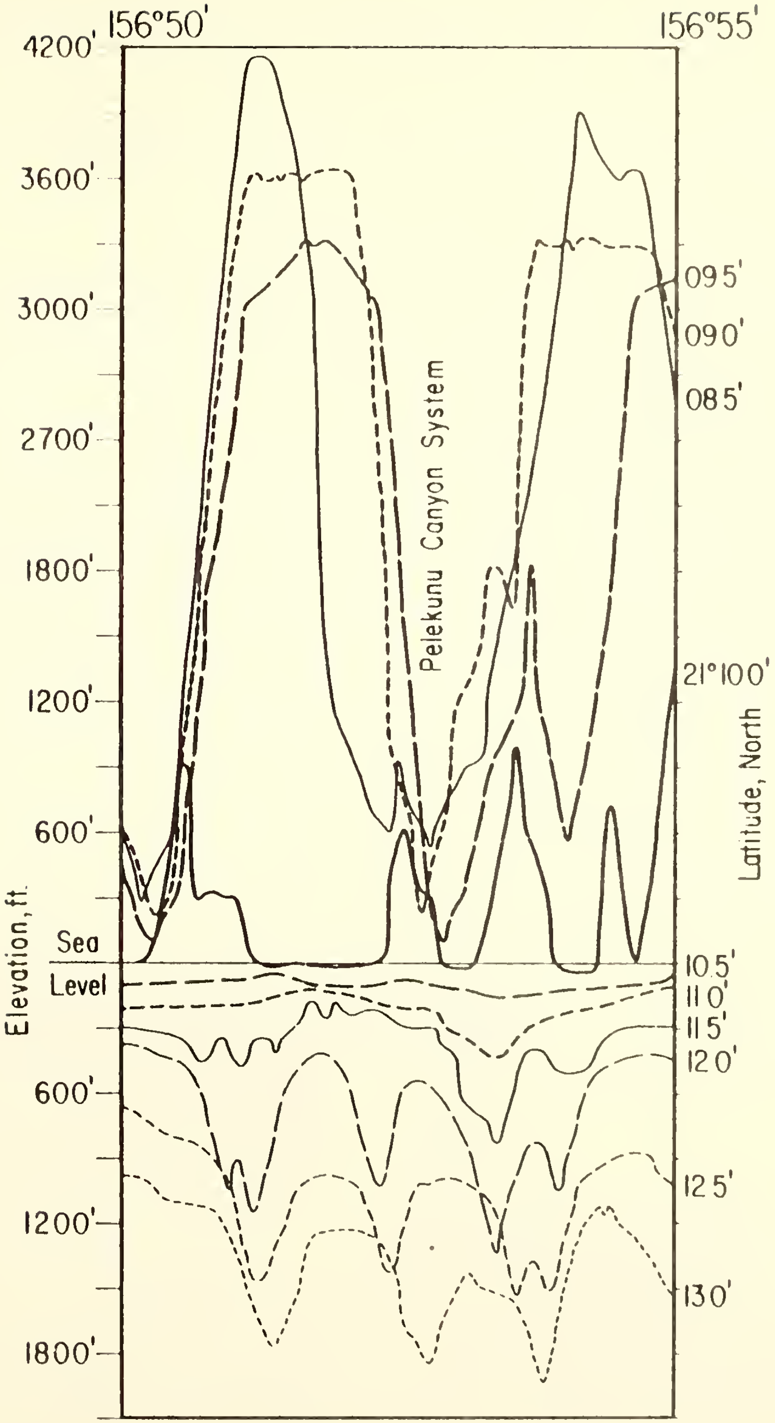

Fig. 4. East-West profiles across the Pelekunu Canyon System. Profile spacing: 0.5 nautical miles.

Maps not reprinted:
In Pocket

Topographic and Bathymetric Map of the Island of Molokai, State of Hawaii, May 1969 (scale : ≃1:40,000) (2 sheets)

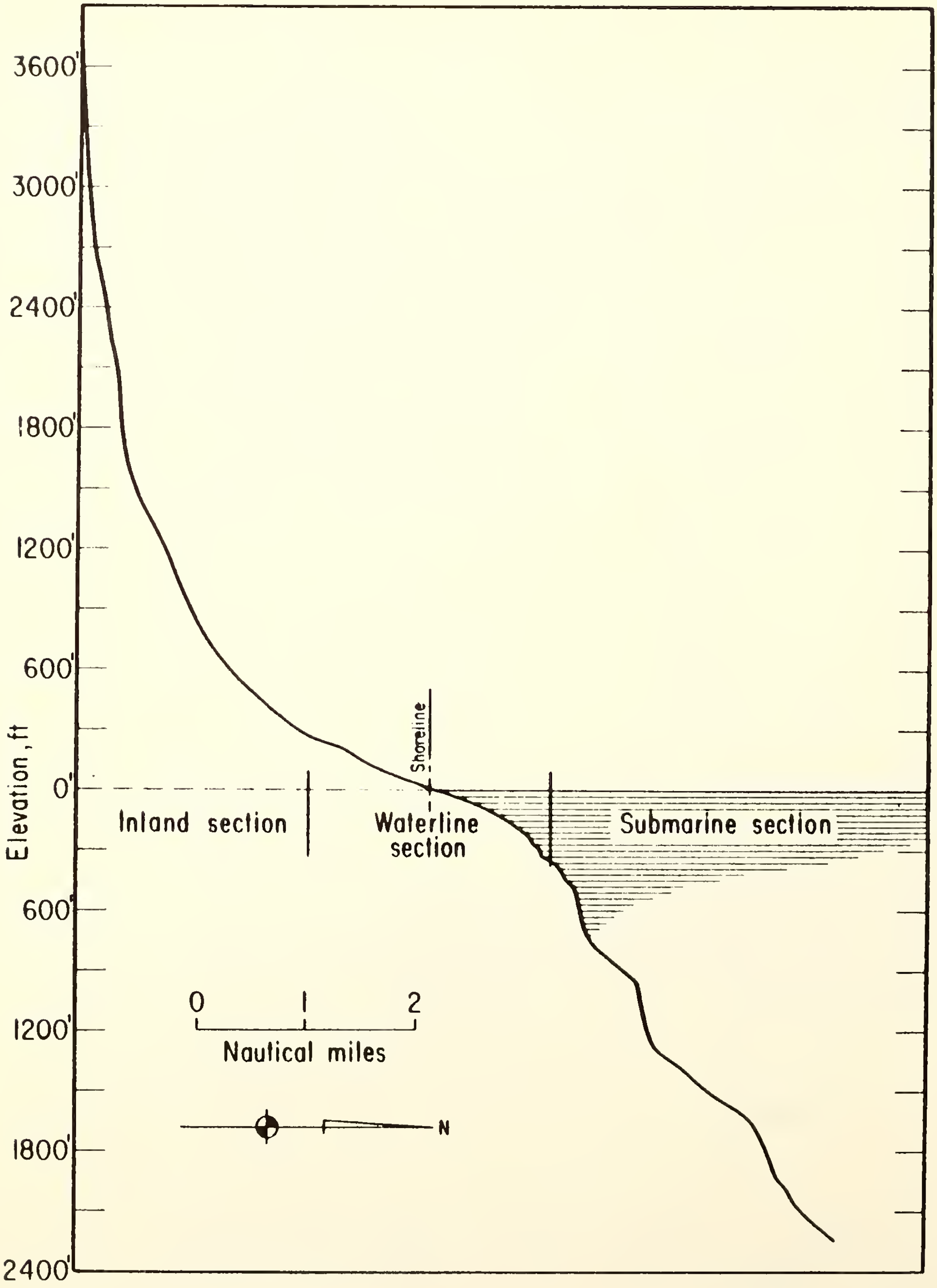

Fig. 5. Long profile of Pelekunu Canyon System. (Vertical Exaggeration 11:1.)

Reprinted from Geological Society of America
Bulletin Vol. 80, No. 2313-2316.

GEORGE PETER
OMAR E. DeWALD
Environmental Science Services Administration, Atlantic Oceanographic Laboratories, Miami, Florida 33130

Geophysical Reconnaissance in the Gulf of Tadjura

ABSTRACT

Bathymetric and magnetic surveys together with a seismic reflection line confirm the extension of the rift system from the Gulf of Aden westward into the Gulf of Tadjura. West of 43°18′ E., however, the identification of the rift is tenuous, subject to individual interpretation.

INTRODUCTION

The Gulf of Tadjura, a narrow westward projection of the Gulf of Aden, has long been suspected to link the East African Rifts with the mid-oceanic ridge of the Gulf of Aden (Heezen, 1959). A narrow seismic belt that follows the median valley of the mid-oceanic ridge runs into the African continent through the Gulf of Tadjura (Sykes and Landisman, 1964). Magnetic and bathymetric surveys in the Gulf of Aden (Laughton, 1966) have further supported the possibility of such a connection.

The U.S. Coast and Geodetic Survey Ship *Oceanographer* conducted a geophysical study of the Gulf of Tadjura in 1967 in order to investigate this proposed connection in detail. This note discusses a seismic reflection line and the bathymetric and magnetic total-intensity maps produced as a result of this study. During the preparation of these maps, data from the *RRS Discovery* (Roberts and Whitmarsh, 1969) and the *RV Vema* (Girdler and Peter, 1960) were also consulted. Bathymetric data were further supplemented by values from U.S. Naval Oceanographic Office Chart No. 3635.

ACKNOWLEDGMENTS

We are grateful to R. Harbison for supervising the field measurements and to H. B. Stewart, Jr., P. J. Grim, and R. K. Lattimore for reviewing the manuscript. We are further indebted to D. G. Roberts and R. B. Whitmarsh for providing us with their results prior to publication.

DATA COLLECTION

Depth and magnetic total field intensity measurements were recorded by a Raytheon PFR and a Varian Proton Precession Magnetometer, respectively. The seismic system utilized a Bolt 10-cubic inch airgun and an Alpine recording system and hydrophone array. The tracklines were run during daylight hours and used visual and radar fixes on shore for navigational control. Based on trackline crossings, the over-all positioning accuracy is better than 1 km.

The large amplitude of the local magnetic anomalies and the contour interval chosen permitted the daily variation of the magnetic field to be neglected. Because of the small area of the gulf, the removal of the regional field was unnecessary.

The western half of the magnetic map of Girdler and Peter (1960) has been incorporated to illustrate the continuation of the magnetic trends from the Gulf of Aden into the Gulf of Tadjura. As the 37,000-gamma contour of the recent survey is coincident with the 36,250-gamma contour of the earlier survey, an adjustment of +750 gammas was added to the contour values of the earlier work to bring the two into agreement.

DISCUSSION

Within the Gulf of Aden the mid-oceanic ridge system is an essentially east-west–striking feature offset by northeast-southwest–trending fault zones. In many cases these faults extend from the Somali shelf on the south to the Arabian shelf on the north. The faults are indicated by conspicuous northeast-southwest–trending scarps along the edge of these shelves (Laughton, 1966).

The relief of the mid-oceanic ridge system in the Gulf of Aden diminishes from east to west, and by 45° E. it is reduced to a single deep valley, trending west-southwest toward the northern coastline of the Gulf of Tadjura. At the entrance of the Gulf of Tadjura, the

---

Geological Society of America Bulletin, v. 80, p. 2313–2316, 3 figs., 1 pl., November 1969

average depth of the central valley is more than 700 fathoms (1300 m) (Fig. 1). At 43°18′ E. the valley shoals to less than 400 fathoms (700 m) and is offset toward the southwest by 9 km. Another shoaling and an offset to the southwest of approximately the same magnitude occurs at 43°07′ E. The offsets are along northeast-southwest trends in the bathymetry that are in close alignment with similar trends in the northern coastline and in the southern shelf break (100-fathom or 200-m isobath). This development, therefore, is in close agreement with the structural framework of the Gulf of Aden (Laughton, 1966).

The magnetic anomalies (Fig. 2) generally confirm the extension of the central valley into the Gulf of Tadjura, and its proposed offsets. The gulf is so narrow that the central valley and the associated negative anomaly appear to fill the gulf from shelf break to shelf break. The negative magnetic anomaly is not due to the topographic effect of the valley, but, as Girdler and Peter (1960) have proposed in their study of the mid-oceanic ridge system immediately east of this area, the intrusives below the central valley of the mid-oceanic ridge are responsible for the anomaly. If these intrusives were formed under the present direction of the earth's magnetic field, a case demonstrated for all mid-oceanic ridge segments studied by Vine (1966) and others, their magnetic effect could provide the observed negative anomaly at this magnetic latitude.

The valley actually ends as a major feature of the Gulf of Aden at the first offset (43°18′ E.). No clear-cut correlation can be established between the negative magnetic anomaly and the central valley from this point westward. Lack of correlation between the two offsets could be the result of fracturing of the narrow block in question; west of the second offset

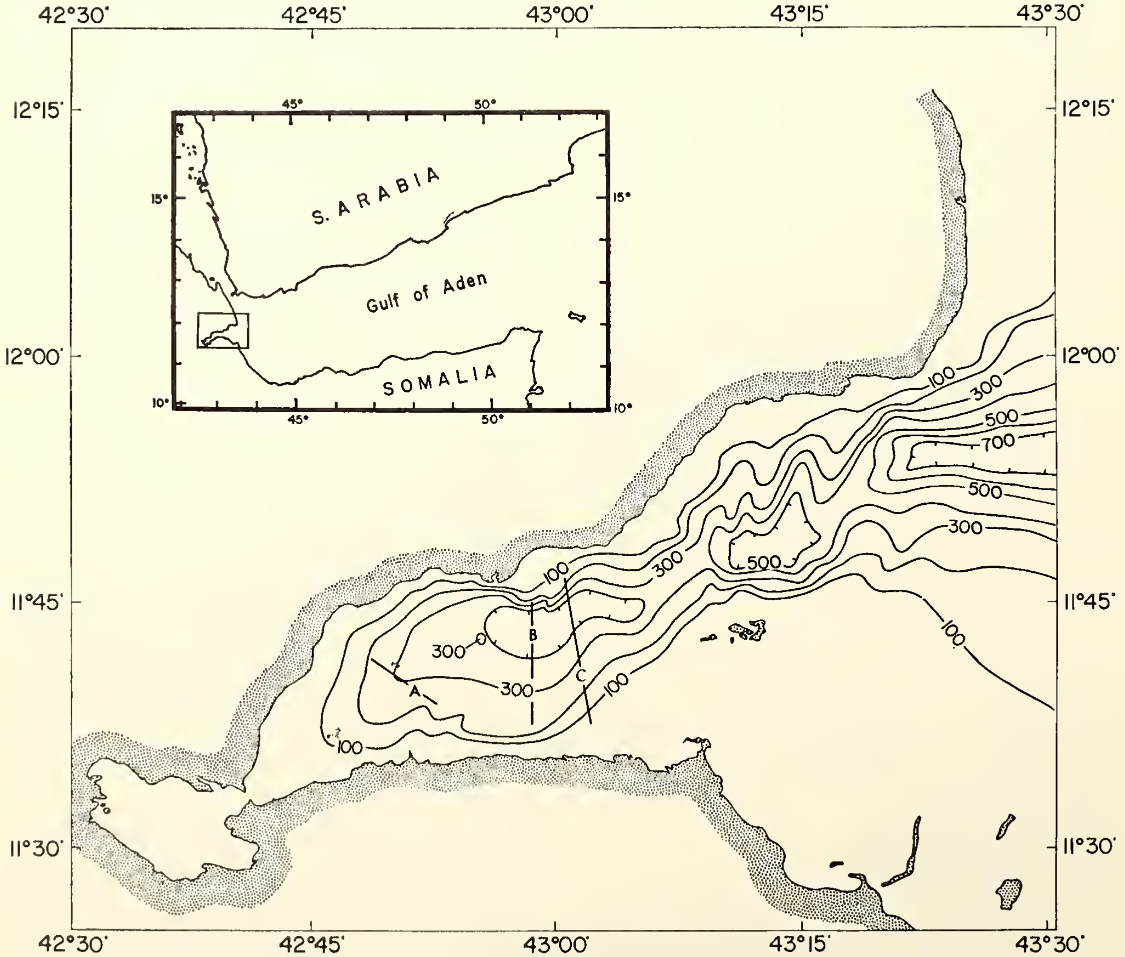

Figure 1. Generalized bathymetric map of the Gulf of Tadjura. Lines: A, seismic profile; B and C, bathymetric and magnetic cross sections (Fig. 3). Contour interval 100 fathoms (1 fathom = 1.83 m).

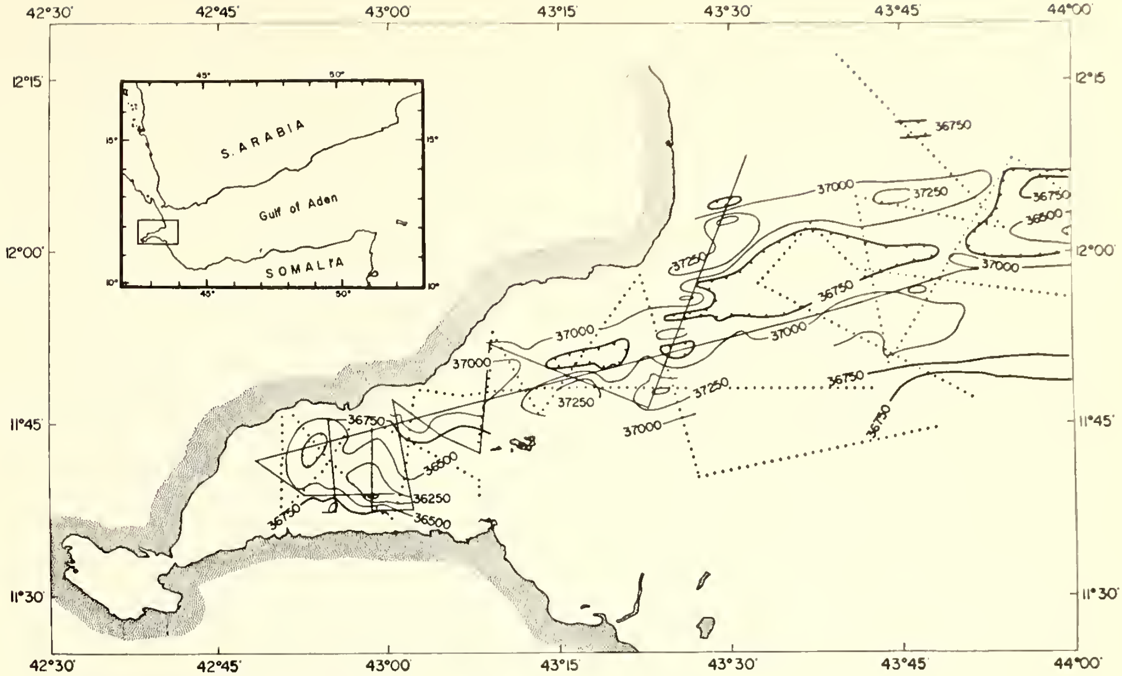

Figure 2. Magnetic total intensity anomaly contour lines in the Gulf of Tadjura and western Gulf of Aden. Contour interval 250 gammas. Solid lines for *Oceanographer* tracks; dotted lines for *Discovery* and *Vema* tracks.

(43°07′ E.) sediments and volcanics seem to have filled the valley from the south and shifted its axis northward. The magnetic low in this area is clearly to the south of the topographic deep (Fig. 3). Farther west of these sections, the single magnetic low splits into two, probably as a result of some local geologic influence.

In addition to magnetic and bathymetric data, seismic reflection measurements were made along the westernmost reconnaissance line (Fig. 1; Pl. 1*). The northern slope of the Gulf of Tadjura along this section displays approximately 100-m-thick (0.1-second two-way reflection time) steeply southward-dipping sedimentary strata that conformably overlie harder, possibly volcanic, rocks. Sediments exposed on the southern slope dip more gently below younger sediments and, after crossing the gulf, terminate against the sedimentary strata of the northern slope. The younger sediments form a wedge that fills the center of the gulf. Most of the strata within this wedge dip and thicken northward and, like the underlying sediments, terminate against the northern slope. The lower 100 m of the wedge are conformable to the underlying reflector, and there are weak indications that

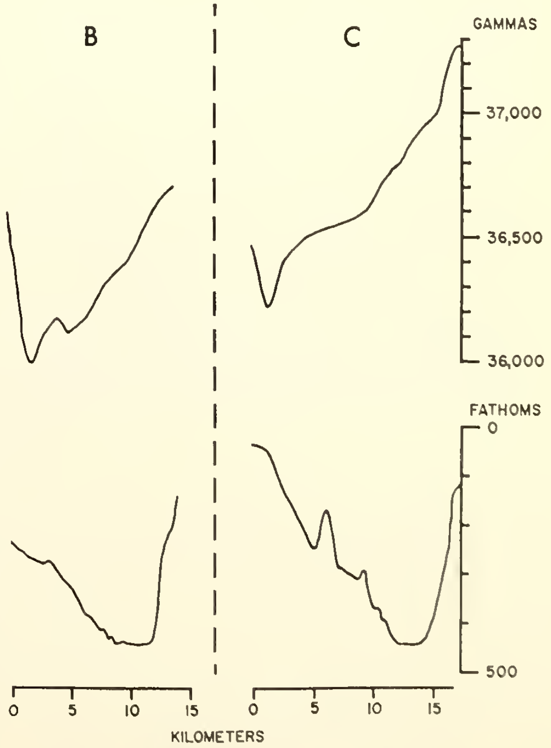

Figure 3. Bathymetric and magnetic sections across the Gulf of Tadjura along profiles B and C (Fig. 1). Bathymetric scale is in fathoms (1 fathom = 1.83 m). North is on the right-hand side of the profiles.

---

* See Plate Section for plate.

strata within this layer at one time outcropped on the sea floor. These former outcrops now seem to be covered with a thin veneer of recent sediments. Another interpretation would be a suggestion of a flexure of these sediments at Point B (Pl. 1). Below the recent sediments, next to the northern slope, there is a small pond of horizontally layered sediments overlying the dipping wedge. The deepest reflectors under the southern slope are again possibly volcanics, but their characteristics indicate that they are not identical with those under the northern slope.

As has been indicated earlier, the bathymetric and magnetic lows cannot be correlated west of 43°18′ E. Due to the shortness of the north-south reconnaissance lines, it is impossible to judge how severely the magnetic pattern of the ridge crest has been distorted in the Gulf of Tadjura. These facts must be considered in the interpretation of the seismic section and magnetic data. If we accept evidence of earthquake epicenter distribution suggesting that the rift of the mid-oceanic ridge extends this far west, then the broad magnetic low in the gulf could be interpreted to represent the deep-seated intrusions associated with the rift valley. The local short-wavelength anomalies are probably related to lava flows and effusives that are known to be abundant in the Afar region west of the Gulf of Tadjura (Laughton, 1966; Mohr, 1967). A deep-seated crustal extension, accompanying the intrusives, is probably responsible for the tilted southern block evidenced on the seismic profile. The contact of the northern- and southern-slope sediments, a fault scarp, is apparently along the northern slope of the gulf, against which the southern block appears to be sinking, with a hinge line located farther south. The steeply dipping sediments on the northern slope probably reflect an earlier deformation and subsidence of the area.

These data generally confirm the expected extension of the geological-geophysical trends from the east into the Gulf of Tadjura. There is insufficient evidence, however, to support or further elucidate the complex movement of the area proposed by Laughton (1966) and others.

REFERENCES CITED

Girdler, R. W., and Peter, G., 1960, An example of the importance of natural remanent magnetization in the interpretation of magnetic anomalies: Geophys. Prosp., v. 8, p. 474–483.

Heezen, B. C., 1959, Paleomagnetism, continental displacements, and the origin of submarine topography (abs.), p. 26–32 *in* Sears, M., *Editor*, International Oceanographic Congress—Preprints: Washington, American Association for the Advancement of Science.

Laughton, A. S., 1966, The Gulf of Aden, in relation to the Red Sea and the Afar depression of Ethiopia, p. 78–97 *in* Irvine, T. N., *Editor*, The world rift system: Canada Geol. Survey Paper 66-14.

Mohr, P. A., 1967, Major volcano-tectonic lineament in the Ethiopian rift system: Nature, v. 208, p. 664–665.

Roberts, D. G., and Whitmarsh, R. B., 1969, A bathymetric and magnetic survey of the Gulf of Tadjura, western Gulf of Aden: Earth and Planetary Sci. Letters, v. 5, p. 253–258.

Sykes, L. R., and Landisman, M., 1964, The seismicity of East Africa, the Gulf of Aden and the Arabian and Red seas: Seismol. Soc. America Bull., v. 54, p. 1927–1940.

Vine, F. J., 1966, Spreading of the ocean floor: new evidence: Science, v. 154, p. 1405–1415.

MANUSCRIPT RECEIVED BY THE SOCIETY APRIL 17, 1969

Reprinted from Journal of Geophysical Research, Vol. 74, No. 10, 586-593.

JOURNAL OF GEOPHYSICAL RESEARCH VOL. 74, NO. 2, JANUARY 15, 1969

Magnetic Structure of the Juan de Fuca-Gorda Ridge Area

GEORGE PETER AND ROBERT LATTIMORE

Atlantic Oceanographic Laboratories, ESSA, Miami, Florida 33130

By using the fracture pattern deduced by N. Pavoni (1966) with a different interpretation of the magnetic anomaly lineations, a reconstruction can be made in which the Juan de Fuca and Gorda ridges form a single, continuous, north-south trending feature. From this reconstruction, the present magnetic structural pattern can be derived by (1) development of northwest-southeast oriented zones of weakness, (2) left-lateral motion along a system of northwest-southeast faults in the area of the Blanco fracture zone, (3) clockwise rotation and left-lateral motion of blocks north of the Blanco fracture zone, and (4) continued left-lateral offset along the northwest-southeast faults, in the course of which 250 km of the original ridge crest was destroyed and the individual faults were compressed into the present Blanco fracture zone. This interpretation explains the present magnetic structural configuration and elucidates some of the problems involved in the application of the transform-fault concept to this area. The anomalous structural fabric (which may be related to the coastal geology) and the agreement of the postulated motion of the Gorda block along the Mendocino fracture zone with known motion on the San Andreas fault zone suggest that the Blanco fracture zone may have formed and the Juan de Fuca and Gorda ridges may have separated during the Late Tertiary coastal orogeny.

INTRODUCTION

Within recent years the most controversial hypothesis offered to explain the geologic structure of the ocean basins has been the concept of sea-floor spreading [*Dietz*, 1961; *Hess*, 1962; *Vine and Matthews*, 1963; *Vine*, 1966]. Increased impetus was given to this hypothesis by the discovery of the symmetry of magnetic anomaly lineations associated with many oceanic ridges and by the correlation of lineations in the area of the ridge crest with dated magnetic polarity reversals and with the magnetic stratigraphy of sea-floor sediments [*Pitman and Heirtzler*, 1966; *Vine*, 1966; *Ninkovich et al.*, 1966; *Opdyke et al.*, 1966; *Dickson and Forster*, 1966; *Pitman et al.*, 1968].

As a corollary of the sea-floor spreading hypothesis, *Wilson* [1965*a*, *b*] suggested that apparent lateral offsets of the mid-oceanic ridges do not represent displacements. Instead, the opening of the crust (along which the ridges subsequently formed) may have been offset originally. Movements along the planes joining the offset portions of the ridge crests are actually opposite in direction to that indicated by the apparent offset; Wilson named this mechanism 'transform faulting.' The required motions along transform-fault planes joining the ridge crests have been corroborated by the earthquake mechanism studies of *Sykes* [1967].

Copyright © 1969 by the American Geophysical Union.

Raff and Mason [1961] published the results of a closely spaced, well-controlled, marine magnetic survey over a large part of the Juan de Fuca and Gorda ridges, which, according to *Menard* [1964], are parts of the mid-ocean ridge system. A detailed tectonic interpretation of these anomalies has been presented by *Pavoni* [1966]. It is the aim of this paper to offer an alternative interpretation (Figure 1) of Pavoni's magnetic structural map, which takes into account a symmetrical relationship among certain lineations discovered after the publication of his work. The major structural features are located on the index map (Figure 2).

DISCUSSION

The reinterpreted magnetic lineation map (Figure 1) shows the positive magnetic anomaly bands and their postulated displacements. Correlation of the anomalies was performed by constructing profiles across the major crustal blocks. This procedure is illustrated in Figure 3; the locations of the profiles are shown in Figure 1. The numbering of the anomalies follows the system of *Pitman et al.* [1968].

The reinterpretation of the identity of the

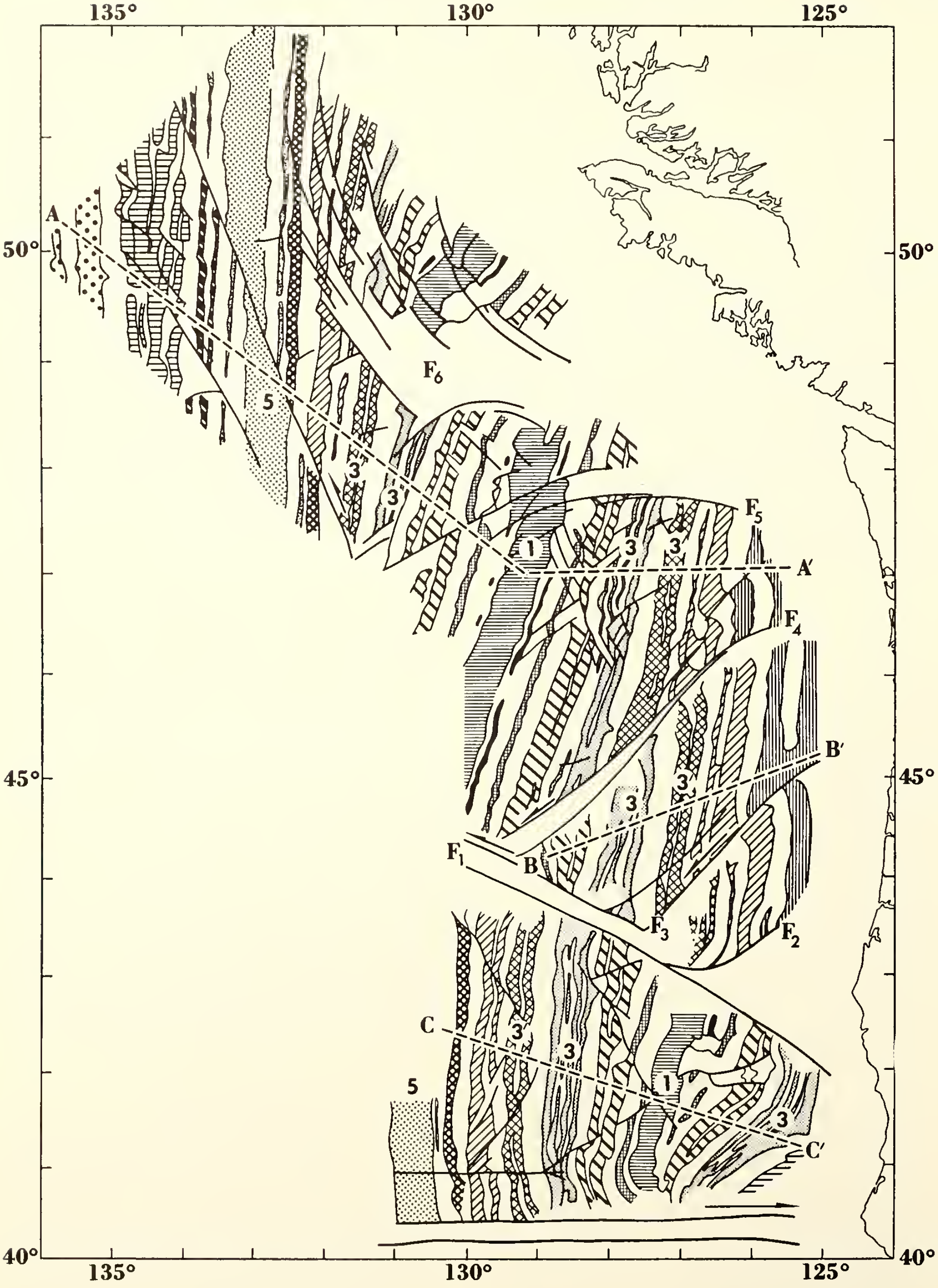

Fig. 1. Correlation of magnetic anomaly lineations associated with the Juan de Fuca and Gorda ridges. Dashed lines (A–A′, etc.) are the locations of profiles shown in Figure 3. Redrawn from *Pavoni* [1966].

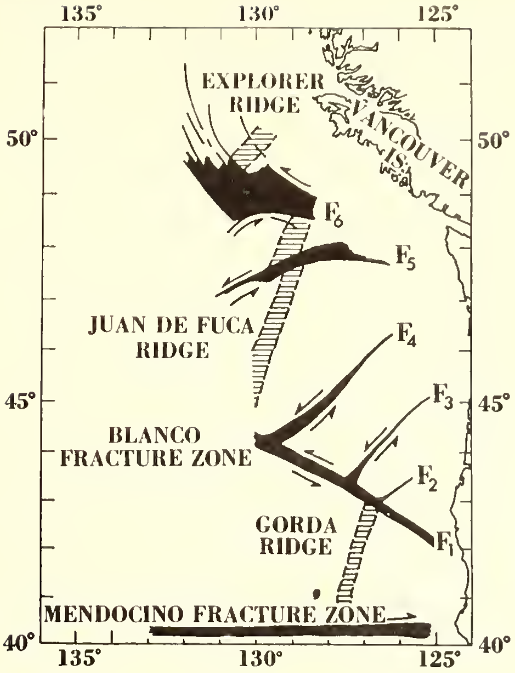

Fig. 2. Index map.

magnetic anomaly lineations does not alter *Pavoni*'s [1966] delineation of the crustal blocks and major fault zones. Although this interpretation requires an offset of the anomalies across the Blanco fracture zone (F_1) in a sense opposite to that proposed by *Pavoni* [1966], it actually lends strength to his argument that the Blanco fracture zone is not a transform fault. The principal strength for Pavoni's argument is in the offset pattern of anomalies 3 and 3′, east of the Juan de Fuca ridge. Explanation of the structural pattern of the area only in terms of sea-floor spreading from the crests of the Juan de Fuca and Gorda ridges leads to the conclusion that the anomaly bands east of F_4 originated from a 'point' source; there is no known segment of ridge crest from which they could have spread. It was assumed that this conclusion is untenable, and a reconstruction was made in which the offsets are explained by simple strike-slip motion.

In investigating the possible motions of the crustal blocks, the correlated magnetic anomaly lineations east of the Juan de Fuca ridge were aligned (Figure 4). As the crustal segments were shifted along faults F_2, F_3, and F_4 to bring the anomalies into line, it was necessary to shift the Gorda block about 400 km to the west, where it fitted the space between the other crustal blocks on the north and the Mendocino fracture zone on the south. With this reconstruction, the Juan de Fuca and Gorda ridges and the associated anomaly bands are in perfect alignment.

Given a number of northwest–southeast oriented zones of weakness along F_1 (Figure 4) and a force that would move the wedge-shaped Gorda block eastward along the Mendocino fracture zone, the formation of northeast–southwest fracture zones (F_2, F_3, and F_4) would be expected and the crustal blocks would shift laterally along these fracture zones to produce the present configuration, shown in Figure 1. The relative offset of these blocks would be left-lateral along a system of faults that is now compressed into the Blanco fracture zone.

Relative motion of the Gorda block along the Mendocino fracture zone would be right-lateral, opposite the over-all pattern of offset of the magnetic anomalies in the area but in agreement with motion along the San Andreas fault system and other minor faults along the coast. Realignment of the magnetic anomaly lineations along faults F_2, F_3, and F_4 implies that the relative left-lateral motion along F_1 caused the destruction of approximately 250 km of ridge crest. This interpretation assumes that

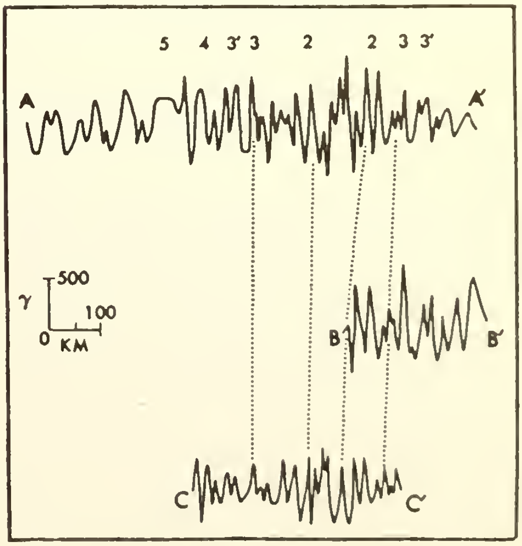

Fig. 3. Correlation of magnetic anomaly lineations. Locations of profiles are shown in Figure 1.

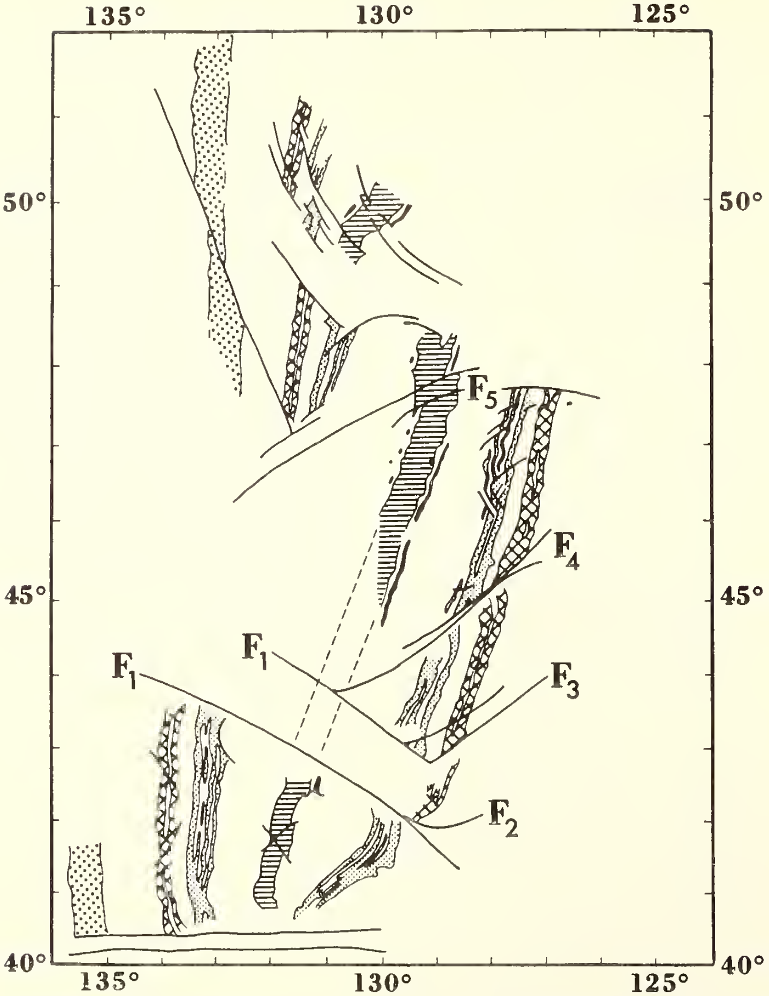

Fig. 4. Reconstruction of magnetic anomaly lineations shown in Figure 1. involving only lateral displacements.

the Mendocino fracture zone existed as a major structural and tectonic discontinuity prior to this activity, or, in other words, that the Mendocino fracture zone has not been displaced as a result of younger movements.

A more realistic reconstruction of Figure 1 can be made by assuming that the anomaly lineations originally were aligned north–south in conformance with the over-all magnetic trend of the area [*Raff and Mason,* 1961, Pl. 1], as shown in Figure 5. The present structural pattern (Figure 1) is derived by left-lateral displacement along fault F_1 and clockwise rotation of the block between F_1 and F_5 about a 'pivot' near its northern margin. Rotation and left-lateral displacement of this block are followed by relative eastward movement of the Gorda block; a total displacement of 200 km (measured on anomaly 5) is required. As a result of the clockwise rotation of the block to the north and its own relative eastward motion, an internal fracture pattern and distorted magnetic anomaly lineations suggestive of north-south as well as east–west compression were formed within the Gorda block.

At 41°N anomaly 7 occurs at 138°W, or over 600 km west of anomaly 5 [*Vacquier et al.*, 1961]. At this latitude, also, a number of low-amplitude, short-wavelength anomalies have been found on either side of anomaly 6 [*Vac-*

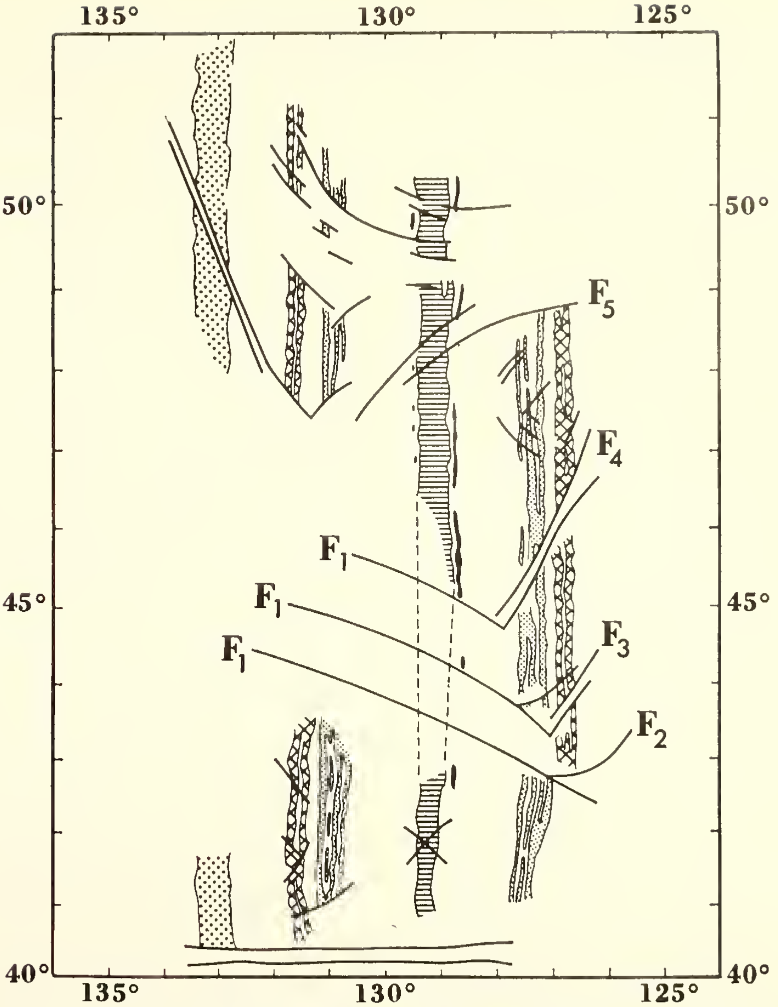

Fig. 5. Reconstruction of magnetic anomaly lineations shown in Figure 1, involving rotation of crustal blocks and lateral displacements.

quier et al., 1961]; these anomalies appear to be peculiar to this area of the Pacific [*Pitman et al.*, 1968, Fig. 5]. R. F. Obrochta (U. S. Naval Oceanographic Office, unpublished) has mapped anomaly 7 at 48°30′N, 138°W; the distance between this anomaly and anomaly 5 of Figure 1, measured along 48°30′N, is 360 km. Anomaly 6 appears to be missing west of the Juan de Fuca ridge [*Pitman and Hays*, 1968]. It is suggested that the 240-km increase in the distance between anomaly 5 and anomaly 7, at 41°N, may in part be due to relative eastward motion of the Gorda fault block, and that the low-amplitude, short-wavelength anomalies associated with anomaly 6 may represent new crust created as the block moved eastward. Similarly, the absence or destruction of anomaly 6 west of the Juan de Fuca ridge may be the result of the clockwise rotation and relative westward motion of the Juan de Fuca block.

In the reconstruction of the original relationship of the anomaly bands across the Blanco fracture zone, it is postulated that the eastward motion of the Gorda block was dominant over westward displacement of crustal blocks north of the fracture zone. Actual motion cannot be determined on the basis of relative offset of the magnetic anomalies alone; other factors must be considered. For example, if the anomaly bands of Figure 1 are realigned with respect to anomalies 1 and 5 of the Gorda block, a number of lineations east of the Juan de Fuca ridge would fall under the Washington-Oregon coast and the northern part of the ridge crest and central anomalies would fall under Vancouver Island. With westward motion of the crustal segments north of the Blanco fracture zone, these anomalies would have had to emerge from under the continent. If, to avoid this dilemma, it is postulated that the continent was farther to the east at that time, an additional assumption must be made, namely, that the continent drifted westward at a rate of 100 km/m.y.

Pitman and Heirtzler [1966] and *Vine* [1966] have 'dated' anomaly 2 (in B–B′ of Figures 1 and 2) as 2 m.y. old. If this age is accepted, the 100-km displacement of anomaly 2 across fault F_4 implies an average motion of 5 cm/yr along this fault. Seismic-reflection profiles across this area, reported by *Hamilton and Menard* [1968], indicate that there has been no disturbance of the sediments, although it would be expected to accompany such motion.

A possible explanation for the absence of near-surface evidence of fault motion is that the source of the magnetic anomaly lineations is in the deeper part of the crust or in the upper mantle; small offsets could then possibly be compensated within the upper part of the crust and not manifested on the sea floor. Objections to this proposal could be based on deep-towed magnetometer data [*Mudie and Harrison*, 1967]. The large-amplitude, short-wavelength anomalies observed near the sea floor could, however, be caused by small intrusives whose parent bodies are more deeply buried. Another possible explanation is that the faults are in fact much older than a few million years and that the magnetic chronology is not valid.

Although all available data seem to substantiate the magnetic chronology, examination of the offset pattern of the anomaly lineations associated with the Juan de Fuca and Explorer ridges casts further doubt on its validity. The two ridge crests are displaced about 150 km along a system of faults, F_6, which *Pavoni* [1966] named the 'Sovanco fault zone.' The relation of the two sets of central anomalies to anomaly 5, at 133°W (Figure 1), as well as the small-scale fracture pattern deduced from the anomalies, militate against the idea that the Sovanco fault zone is a simple transform fault: The offsets along F_6 are greatest in the area of the central anomalies and negligible at anomaly 5. West of the Explorer ridge some of the anomaly lineations are missing and others are closely spaced, suggesting that the horizontal motion may have been dissipated, in part, through crustal compression.

If the magnetic chronology is accepted and a transform-fault relationship does not hold for the Explorer and Juan de Fuca ridges, separation of the two would have had to have taken place during the past 0.7 m.y. represented by anomaly 1 [*Pitman and Heirtzler*, 1966; *Vine*, 1966]. From this it could be concluded that displacement along the Sovanco fault zone is taking place at an average rate of at least 20 cm/yr, a value that may be higher than generally expected for motion along strike-slip faults.

McManus [1965] recognized the structural anomaly intrinsic in the northwest–southeast trend of the Blanco fracture zone and suggested that it may be related to Miocene features in Washington and Oregon that have a similar orientation. In the area between the Pioneer and Murray fracture zones systems of northwest–southeast and northeast–southwest trending faults, similar to those associated with the Blanco fracture zone, may be interpreted from the anomaly map of *Mason and Raff* [1961, Pl. 1]. From more recent work in the same area [*Lattimore et al.*, 1968] it can be shown that, near the continental shelf, 'faults' in the northeast–southwest trending anomaly bands are reflected in the sea-floor topography; the topographic evidence can, in turn, be related to faults known in the continental geology. Consideration must be given to the possibility that the structure of these oceanic areas has been influenced by tectonic activity on the continent and that the present configuration may be related to the Pliocene-Pleistocene coastal orogeny [*Taliaferro*, 1951; *Oakeshott*, 1966]. This orogeny, in turn, may have been triggered by the late Tertiary reactivation of the East Pacific rise.

CONCLUSIONS

By using the fracture pattern deduced by *Pavoni* [1966], with a different interpretation of the magnetic anomalies, the existence of the Juan de Fuca and Gorda ridges, the Blanco fracture zone, and associated faults revealed by offsets of magnetic anomaly lineations may be explained by transcurrent faulting. By careful correlation of the anomaly bands across the major fractures shown by *Pavoni* [1966], a reconstruction can be drawn in which the Juan de Fuca and Gorda ridges form a single, continuous north–south axis, with magnetic anomaly bands disposed symmetrically on either side of it.

Transform faulting along the Blanco fracture zone and spreading of the sea floor away from the Juan de Fuca and Gorda ridges do not satisfactorily account for the northeast–southwest oriented pattern of left-lateral faults east of the Juan de Fuca ridge. The present structural configuration of the area can, however, be explained by the following sequence:

1. Originally, the Juan de Fuca and Gorda ridges form a continuous north–south trending structure.
2. A pattern of northwest–southeast oriented zones of weakness develops.
3. Clockwise rotation of crustal blocks to the north of F_1 produces (or is accompanied by) left-lateral movement along F_1 and development of the northeast–southwest oriented fault pattern east of the Juan de Fuca ridge (F_2, F_3, and F_4).
4. Continuing left-lateral movement along F_1 induces left-lateral displacement along fault F_2, subsequently along F_3, and finally along F_4.

During the relative eastward movement of the Gorda block, a 250-km section of the original ridge crest was progressively destroyed. The F_1 fault system was compressed into the present Blanco fracture zone, and the leading edge of the Gorda block was compressed in the north–south direction, producing distortions of the anomaly lineations.

On the basis of the anomalous structural pattern of the area and its similarities to structural trends observed in the adjacent continental areas, it is reasonable to suggest that the present configuration is related to the late Tertiary coastal orogeny, which in turn may be associated with renewed tectonic activity of the East Pacific rise. In particular, the inferred right-lateral motion of the Gorda block along the Mendocino fracture zone agrees with motion along the San Andreas fault system.

This interpretation, offered as an alternative explanation for the existence of the Juan de Fuca and Gorda ridges and the associated fault pattern, is independent of transform faulting. Once initial displacement has taken place, however, active growth of the individual ridges would produce relative motion that is in accord with the transform-fault relationship. Present-day transform-fault motion along the Blanco fracture zone, as confirmed by the recent work of *Tobin and Sykes* [1968], cannot be taken as proof that the offsets were not originally produced by transcurrent faults.

Acknowledgments. We thank R. S. Dietz, L. W. Butler, and G. H. Keller for their helpful suggestions and for critically reviewing the manuscript.

REFERENCES

Dickson, G. O., and J. H. Foster, Magnetic stratigraphy of a deep sea core from the North Pacific Ocean, *Earth Planetary Sci. Letters, 1,* 458, 1966.

Dietz, R. S., Continent and ocean basin evolution by spreading of the sea floor, *Nature, 190,* 854, 1961.

Hamilton, E. L., and H. W. Menard, Undistorted turbidites on the Juan de Fuca ridge (abstract), *Trans. Am. Geophys. Union, 49,* 208, 1968.

Hess, H. H., History of ocean basins, in *Petrologic Studies: A Volume in Honor of A. F. Buddington,* pp. 559–620, Geological Society of America, New York, 1962.

Lattimore, R. K., B. G. Bassinger, and O. E. DeWald, Magnetic map from the coast of California to 133° W longitude, *Misc. Geol. Invest. Map I-531A,* U. S. Geological Survey, Washington, D. C., 1968.

McManus, D. A., Blanco fracture zone, northeast Pacific Ocean, *Marine Geol., 3,* 429, 1965.

Mason, R. G., and A. D. Raff, Magnetic survey off the west coast of North America, 32°N latitude to 42°N latitude, *Bull. Geol. Soc. Am., 72,* 1259, 1961.

Menard, H. W., *Marine Geology of the Pacific,* McGraw-Hill, New York, 1964.

Mudie, J. D., and C. G. A. Harrison, Deep tow profiles across Mason-Raff lineations (abstract), *Trans. Am. Geophys. Union, 48,* 133, 1967.

Ninkovich, D., N. Opdyke, B. C. Heezen, and J. H. Foster, Paleomagnetic stratigraphy, rates of deposition and tephrachronology in North Pacific deep-set sediments, *Earth Planetary Sci. Letters, 1,* 476, 1966.

Oakeshott, G. B., San Francisco Bay area: Its geologic setting, *Geotimes, 11,* 11, 1966.

Opdyke, N. D., B. Glass, J. D. Hays, and J. Foster, Paleomagnetic study of antarctic deep-sea cores, *Science, 154,* 349, 1966.

Pavoni, N., Tectonic interpretation of the magnetic anomalies southwest of Vancouver Island, *Pure Appl. Geophys., 63,* 172, 1966.

Pitman, W. C., III, and D. E. Hayes, Sea-floor spreading in the Gulf of Alaska, *J. Geophys. Res., 73,* 6571, 1968.

Pitman, W. C., III, and J. R. Heirtzler, Magnetic anomalies over the Pacific-Antarctic ridge, *Science, 154,* 1164, 1966.

Pitman, W. C., III, E. M. Herron, and J. R. Heirtzler, Magnetic anomalies in the Pacific and sea-floor spreading, *J. Geophys. Res., 73,* 2069, 1968.

Raff, A. D., and R. G. Mason, Magnetic survey off the west coast of North America, 40°N latitude to 52°N latitude, *Bull. Geol. Soc. Am., 72,* 1267, 1961.

Sykes, L. R., Mechanism of earthquakes and nature of faulting on the mid-oceanic ridges, *J. Geophys. Res., 72,* 2131, 1967.

Taliaferro, N. L., Geology of the San Francisco Bay counties, in *Geologic Guidebook of the San Francisco Bay Counties, Bull. 154,* pp. 117–150, California Division of Mines, San Francisco, 1951.

Tobin, D. G., and L. R. Sykes, Seismicity and tectonics of the northeast Pacific Ocean, *J. Geophys. Res., 73,* 3821, 1968.

Vacquier, V., A. D. Raff, and R. E. Warren, Horizontal displacements in the floor of the northeastern Pacific Ocean, *Bull. Geol. Soc. Am., 72,* 1251, 1961.

Vine, F. J., Spreading of the ocean floor: New evidence, *Science, 154,* 1405, 1966.

Vine, F. J., and D. H. Matthews, Magnetic anomalies over oceanic ridges, *Nature, 199,* 947, 1963.

Wilson, J. T., A new class of faults and their bearing on continental drift, *Nature, 207,* 343, 1965*a*.

Wilson, J. T., Transform faults, oceanic ridges, and magnetic anomalies southwest of Vancouver Island, *Science, 150,* 482, 1965*b*.

(Received June 20, 1968;
revised September 13, 1968.)

Reprinted from Jour. of Sedimentary Petrology, Soc. of Economic Paleontologists and Minerologists, Vol. 39, No. 3, 1132-1141.

JOURNAL OF SEDIMENTARY PETROLOGY, VOL. 39, NO. 3, P. 1132–1141
FIGS. 1–7, SEPTEMBER, 1969

LINEAR "LOWER CONTINENTAL RISE HILLS" OFF CAPE HATTERAS[1]

PETER A. RONA
Hudson Laboratories of Columbia University, Dobbs Ferry, New York 10522[2]

ABSTRACT

A field of "lower continental rise hills" situated on the seaward flank of the Hatteras Outer Ridge was investigated with a grid of bathymetric profiles, a continuous seismic reflection profile, and short (1.2 m) gravity cores.

Throughout the field investigated the lower continental rise hills are not isolated "hills" but rather are linear waveforms with fairly regular distribution and orientation. The waveform parameters are as follows: trough-to-trough wavelength between 3 and 12 km, trough-to-peak amplitude between 10 and 100 m, crestal lengths of tens of kilometers trending NW-SE, asymmetric with steeper limb facing SW. Core samples recovered from the hills contain lutite and clay. The NW-SE crestal orientation and morphological similarity of these linear lower continental rise hills to megaripples or dunes are evidence that their development is related to deposition controlled by the deep Western Boundary Undercurrent, which flows southwest over the continental rise.

The waveforms may extend down to reflection horizon A (Late Cretaceous-Eocene). The similarity of the waveforms to megaripples that extend continuously from horizon A to the present ocean bottom in the Argentine Basin implies that the North and South Atlantic have been open and intercommunicating at least since the initiation of the waveforms.

INTRODUCTION

The "lower continental rise hills" constitute a physiographic province that occupies the lowermost continental rise from the mouth of the Hatteras Canyon System northeastward to the Bermuda Rise—Hatteras Abyssal Plain boundary (Heezen and others, 1959). A relatively detailed investigation was carried out of the lower continental rise hills at the southern end of the physiographic province (figs. 1 and 2). The investigation, based on a fine-grained grid of bathymetric profiles (figs. 2 and 3), a continuous seismic reflection profile (fig. 4), and sediment cores (table 1), attempts to delineate the morphology, orientation, spacing, and composition of the hills within a limited area. A three-dimensional reconstruction from these data would help to elucidate processes in the development of the hills.

On the basis of their orientations, Rona, Schneider, and Heezen (1967) differentiated primary morphologic features of the continental rise off Cape Hatteras into two sets (fig. 1). The first set is comprised of features oriented nearly perpendicular to regional isobaths and includes Hatteras and Pamlico canyons. The second set consists of features that are oriented nearly parallel to regional isobaths and includes Hatteras Transverse Canyon and Hatteras Outer Ridge. Features of the second set are nearly perpendicular (transverse) to the first set. On the basis of orientation, the authors inferred that the development of the first set of features was related to the downslope flow of turbidity currents, and that the development of the second set was related to deposition controlled by the flow of the Western Boundary Undercurrent parallel to the continental margin.

LOWER CONTINENTAL RISE HILLS OFF CAPE HATTERAS

The lower continental rise hills investigated constitute a field of secondary morphological features located on the seaward flank of the Hatteras Outer Ridge between the 4700 m and 5300 m isobaths (fig. 1). The detailed bathymetric chart (fig. 2) reveals that within the area investigated the lower continental rise hills are not circular in plan view but are elongate. The hills extend NW-SE as downslope-pointing fingers nearly perpendicular to the axis of the Hatteras Outer Ridge. The fingers delineating the hills gradually broaden and disappear to the SE on the margin of the Hatteras Abyssal Plain. The fingers abruptly end to the SW about 25 km from the channel where the Hatteras Canyon System joins the Hatteras Abyssal Plain.

The hills with intervening depressions resemble asymmetrical waveforms in individual bathymetric profiles; the hills correspond to peaks and the intervening depressions to troughs (fig.

---

[1] Manuscript received October 22, 1968; revised February 19, 1969.

[2] Present address: ESSA Atlantic Oceanographic Laboratories, 901 South Miami Ave., Miami, Florida.

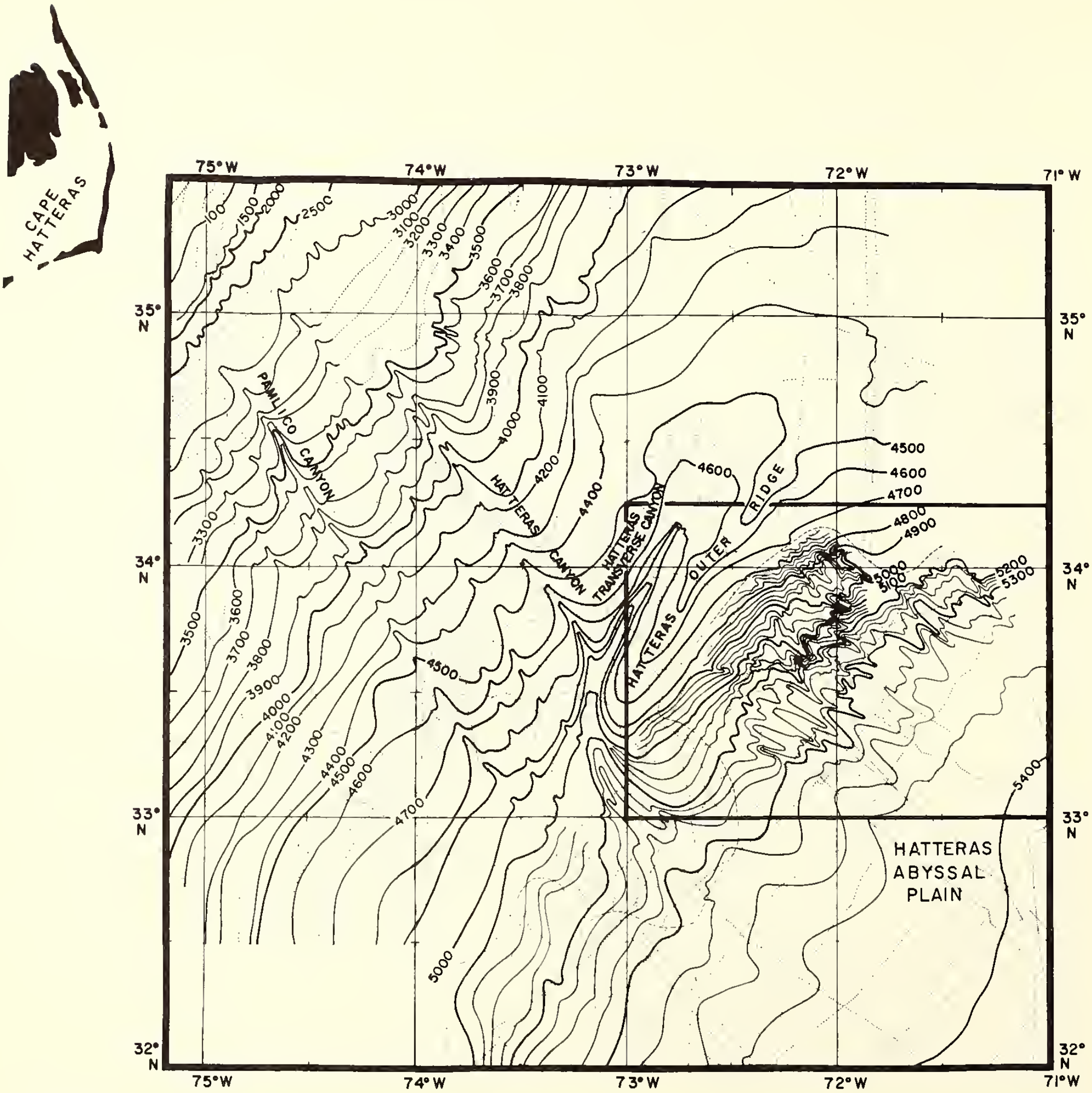

Fig. 1.—Bathymetric chart of the continental rise off Cape Hatteras revised from Rona, Schneider, and Heezen (1967). The area outlined on the lower continental rise is revised on the basis of the present detailed investigation. Sounding tracks are indicated by stippled lines. Basic isobath interval is 100 m. Soundings are corrected for velocity (Matthews, 1939, area 14), and ship's draft (3 m).

5). In order to facilitate visualizing the relation between these waveforms, the bathymetric profiles were assembled along sounding tracks (fig. 3). It is apparent that the wavelength and amplitude of the waveforms vary along individual tracks and between adjacent tracks. To characterize this variation, the wave index of each distinct waveform was measured (ratio of trough-to-trough wavelength to peak-to-trough amplitude). The wave indices are presented next to the position of corresponding peaks in figure 6.

The following observations on the distribution, magnitude, morphology, and orientation of the waveforms in the field investigated are derived from figures 3 and 6:

1. Waveforms are not evenly distributed throughout the field. The spacing of distinct waveforms is closest in the northern half of the field, in particular the north-central section, and widens toward the mouth of the Hatteras Canyon System and the Hatteras Abyssal Plain.

2. The wave indices vary least in the north-central section of the field; that is, the waveforms are most regularly developed.

3. The wavelength of distinct waveforms

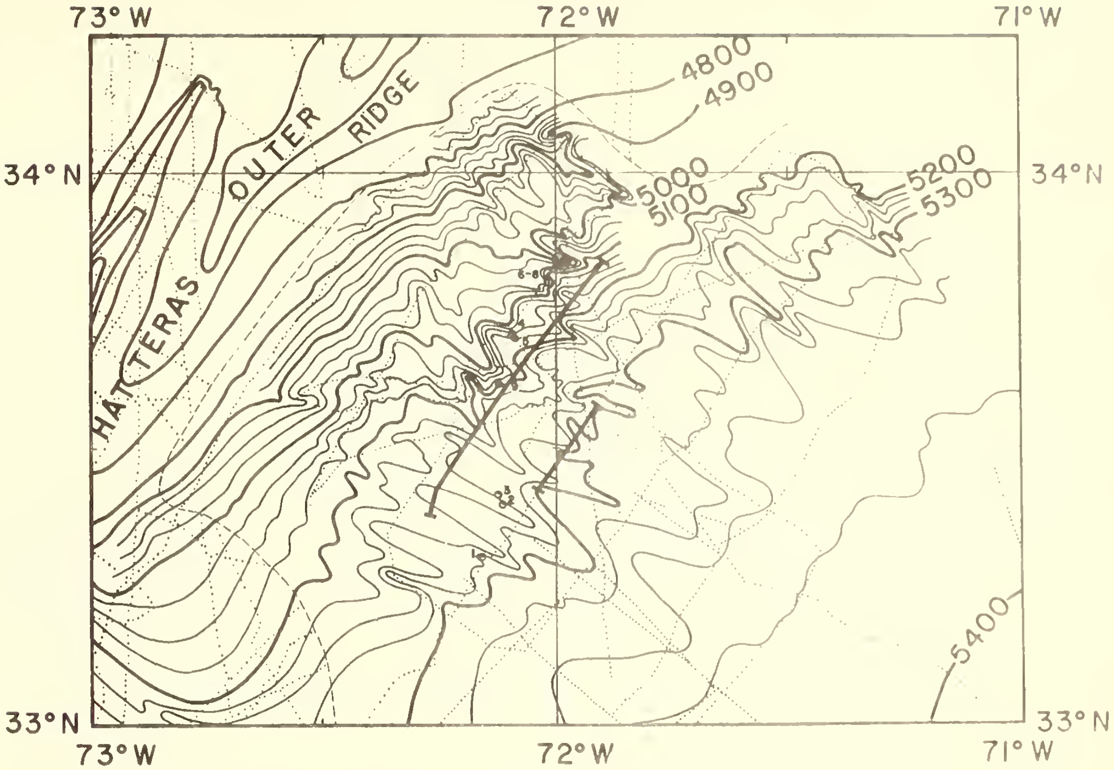

Fig. 2.—Enlargement of area of detailed investigation from fig. 1. Thick isobaths at 100 m intervals. Thin isobaths at 25 m intervals. Sediment cores 1–9 are circled.

ranges between 3 and 12 km with a mean of 5.6 km.

4. The amplitude of distinct waveforms ranges between 10 and 110 m with a mean of 43 m.

5. The waveforms are asymmetrical. The southwest-facing limbs with inclinations of several degrees are nearly twice as steep as the northeast-facing limbs. The troughs tend to be flat rather than concave upward.

6. The waveforms are more distinct along sounding tracks with N-S than E-W components. It is inferred that the former tracks are more nearly perpendicular to the axes of the waveforms than the latter tracks.

To determine the axial continuity of waveforms the bathymetric profiles (fig. 3) were traced on transparent mylar, and adjacent profiles were superimposed. The degree of cross correlation between sequences of waveforms on adjacent profiles was evaluated visually. Tentative correlations between peaks are shown with dashed lines on figure 3. Sequences of waveforms were observed to vary within several kilometers of separation. The greatest distance over which sequences of waveforms could be tentatively correlated is about 20 km in the case of the distinct waveforms of the north-central and northwest sections of the field. Correlations through distances greater than 20 km are considered unreliable. This indicates that the linear lower continental rise hills vary in shape and spacing through several kilometers, although the crestal lengths of certain hills may be as long as or longer than 20 km.

If the correlations between peaks are accurate, then the axial azimuth of the peaks curves continuously between 100° and 170°. The most reliable segment between transverses about 20 km apart trends 120° ± 5°.[3] The axial azimuths derived from cross correlation of sequences of waveforms on adjacent bathymetric profiles are consistent with the more general trends derived from bottom isobaths (fig. 2) and the shape of the waveforms. Investigation of the waveforms with a deep-towed lateral echo-sounder would provide more precise information on their axial lengths, sinuosity, and orientation.

A continuous seismic reflection profile was

---

[3] An azimuth error of ±5° between peaks on two parallel traverses 20 km apart results from a navigation inaccuracy of ±2 km. A considerably greater azimuth error between points on two intersecting traverses results from the same navigational inaccuracy; however, this latter error was minimized by adjusting intersections for agreement in depth.

TABLE 1.—*Sediment cores**

Core number	Latitude	Longitude	Length cm	Predominant particle size	Color†	Comment
249-1	33°19.0′N	72°09.5′W	79.2	Lutite‡	dark yellowish brown 10YR4/2	
249-2	33°24.0′N	72°06.5′W	96.8	Lutite	as above	
249-3	33°25.0′N	72°07.5′W	87.0	Lutite	mottled 10YR4/2 and 10YR5/4	
249-4	33°42.5′N	72°05.5′W	23.5	Lutite	moderate yellowish brown 10YR5/4	
249-5	33°42.0′N	72°05.0′W	93.8	Lutite	mottled 10YR4/2 and 10YR5/4	
249-6	33°50.5′N	71°58.5′W	80.6	Lutite	10YR5/4	Terminates in about 10 cm of clay, light olive gray (5Y5/2) relatively compact, plastic, sticky, dense (1.6 g cm^{-3} wet bulk density)
249-7	33°50.5′N	71°58.5′W	75.0	Lutite	mottled 10YR4/2 and 10YR5/4	Same as above
249-8	33°50.5′N	71°58.5′W	62.5	Lutite	10YR4/2	Terminates in about 5 cm of clay, light olive gray (5T5/2) relatively compact, plastic, sticky, dense (1.6 g cm^{-3} wet bulk density)
249-9	33°37.0′N	72°07.0′W	101.5	Lutite	mottled 10YR4/2 and 10YR5/4	

* Benthos cable-free core: core liner 1.2 m long, 6.3 cm inner diameter (Bowen and Sachs, 1964).
† Color designations were made on wet sediment according to Rock Color Chart, 1953, Geol. Soc. Amer.
‡ Silt and clay sized particles.

run along azimuth 215° for 65 km across the field of lower continental rise hills nearly perpendicular to the hill axes (figs. 2 and 4). The low frequency (50–150 Hz), narrow bandwidth (100 Hz), long duration (0.01 sec), and bubble pulse of the pneumatic sound source were unsuitable to resolve adequately the interior of the waveforms. The profile reveals the following:

1. The waveforms are underlain to at least 0.1 sec ($\sim$100 m) subbottom by reflection interfaces (sedimentary strata) which generally parallel the sediment-water interface. Certain strata appear to truncate against the SW limb of the waveforms.

2. The troughs between peaks are filled with horizontally stratified sediment to at least 0.5 sec ($\sim$50 m) subbottom, which accounts for the flat floor of the troughs. The amplitude of the waveforms thus are diminished by an amount equal to the sedimentary fill in the troughs.

3. An interval of transaural sediment is present between about 0.1 sec ($\sim$100 m) and 0.65 sec ($\sim$650 m) subbottom.

4. A series of reflection interfaces between about 0.65 sec (650 m) and 0.90 sec (900 m) subbottom probably corresponds to sedimentary strata at or just above reflection horizon A, which has been dated as Late Cretaceous or Early Cenozoic (Ewing and others, 1966). The subbottom series of strata exhibits nearly parallel waveforms with wavelengths of about 10 km and amplitudes of about 20 m (0.02 sec). The crests and troughs of the subbottom waveforms are in phase with those of the overlying waveforms on the surface of the continental rise (fig. 7).

The field of lower continental rise hills was

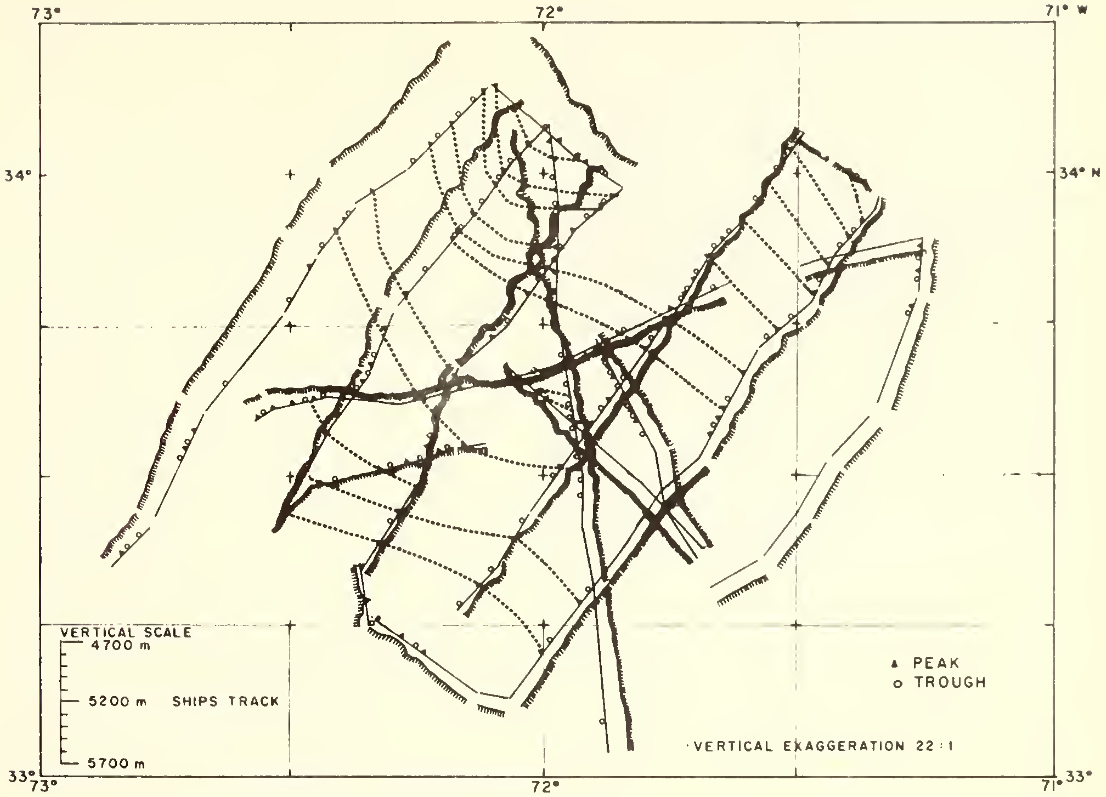

FIG. 3.—Bathymetric profiles constructed relative to ship's sounding tracks which represent a depth of 5200 m below sea level on the vertical scale shown. Peaks on the bathmetric profiles are tentatively correlated with dashed lines.

sampled with nine cable-free gravity cores 1.2 m long. Core locations are spotted on figure 2 and the information summarized in table 1. All of the sediment sampled was lutite (silt and clay sized particles) and clay.

PROCESS OF FORMATION

Ballard (1967) has interpreted the lower continental rise hills as gravitational glide blocks. As an example he shows a bathymetric chart of a portion of the lower continental rise hills, with elongate axes trending generally E-W adjacent to the abyssal gap between the Hatteras and Sohm abyssal plains. Regional isobaths of the lower continental rise on which the hills are situated trend NE-SW. The discrepancy in direction between the regional isobaths and the axes of hills appears to be inconsistent with the interpretation of the hills as gravitational glide blocks, for as glide blocks their axes would be expected to trend more nearly parallel to regional isobaths.

The process of formation of the field of lower continental rise hills investigated may be partly inferred from the configuration of the hills and associated features. The field is superimposed on the Hatteras Outer Ridge; Rona and Clay (1967) inferred from continuous seismic reflection profiles that this feature was initiated as a gentle fold by massive gravitational gliding of previously deposited continental rise strata. Subsequently, the Hatteras Outer Ridge has been shaped by deposition controlled by the Western Boundary Undercurrent (Rona and others, 1967). According to Heezen and others (1966) the deposition of the entire continental rise may have been controlled by the Western Boundary Undercurrent which flows southwest over the continental rise. Near bottom current velocities up to about 20 cm sec^{-1} have been measured east and southeast of Cape Hatteras and east of Cape Cod (Swallow and Worthington, 1961; Barrett, 1964; Volkman, 1962). The measured velocities are competent to transport sediment sizes generally found on the continental rise (Heezen and Hollister, 1964). The effects of a swift southwesterly current in the area of the lower continental rise hills were observed on compass-oriented sea-floor photographs, echograms, and sediment cores by Schneider and others (1967).

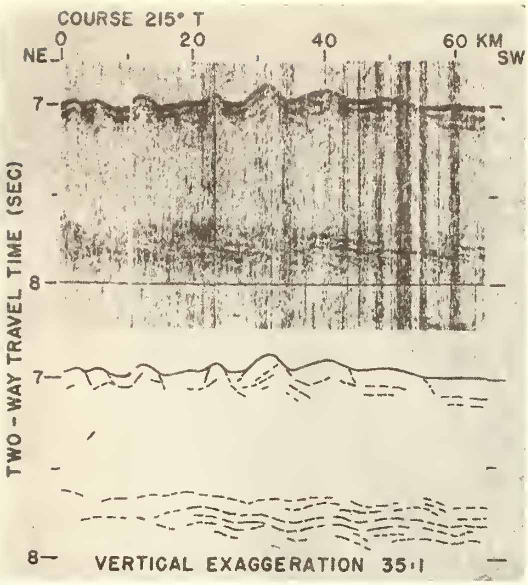

FIG. 4.—Continuous seismic reflection profile of waveforms on the lower continental rise and a line drawing from the profile. The location of the profile is shown on fig. 2 (longer of two parallel lines). The relatively low frequency range of the pneumatic sound source (50-150 Hz) provides acoustic penetration at the expense of high resolution.

The NW-SE axial trend of the field of lower continental rise hills is nearly perpendicular to the axis of the Hatteras Outer Ridge. The axial trend of the hills is inconsistent with development as folds or blocks formed by gravitational gliding or by slumping movements of continental rise strata. The orientation of the hills, their asymmetric waveform, and their fairly regular distribution over the field are best explained as the product of deep currents. Was the orientation of such currents parallel or perpendicular to the axes of the waveforms? The finger-like distribution of the waveforms pointing downslope may suggest some type of downslope flow parallel to their axes. Turbidity currents which flow downslope are not known to produce such waveforms and, in any case, would have been blocked by the crest of the Hatteras Outer Ridge. It is considered more likely that the development of the waveforms is related to an oceanic current flowing perpendicular to their axes. Is the water motion oscillatory or unidirectional? Equal oscillatory water motions such as generated by the passage of a gravity wave train would produce symmetrical waveforms in bottom sediments. The asymmetry of the waveforms indicates that they were produced by a unidirectional current flowing nearly perpendicular to their axes. By analogy with ripple marks and dunes, the steeper limb faces downcurrent (Bucher, 1919). Therefore, the current must have had a southwesterly flow direction. The only known present current in the area which fits these specifications is the Western Boundary Undercurrent.

A difference in scale exists between the linear lower continental rise hills and other sedimentary waveforms observed in nature. The wavelengths of the linear hills are greater than, and the amplitudes are comparable to certain terrestrial dunes (Bagnold, 1941) and large submarine sand waves (Jordan, 1962; Clay and Rona, 1964). The linear hills are larger than current ripple marks (Bucher, 1919) by several orders of magnitude.

The formation and development of ripple marks in cohesionless sediment (sand) have been observed in flumes (Gilbert, 1914). A unidirectional current flow over a sandy bottom will cause rearrangement of the particles in definite phases as a function of increasing rate of fluid discharge as follows:

1. Threshold of grain movement.
2. Formation of sand ripples and migration of ripple forms downcurrent, by grain movement up the gentle upstream face of the ripple and deposition on the steeper lee face.
3. Disappearance of ripples and shear flow over a smooth bottom.
4. Formation of nearly sinusoidal sand waves

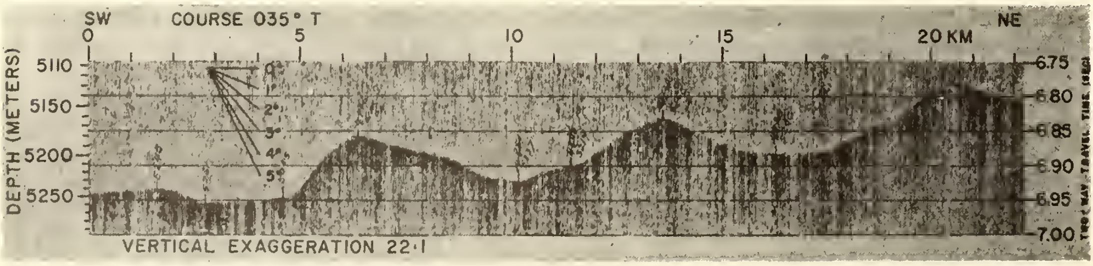

FIG. 5.—Bathymetric profile of waveforms on the lower continental rise. The location of the profile is shown on fig. 2 (shorter of two parallel lines).

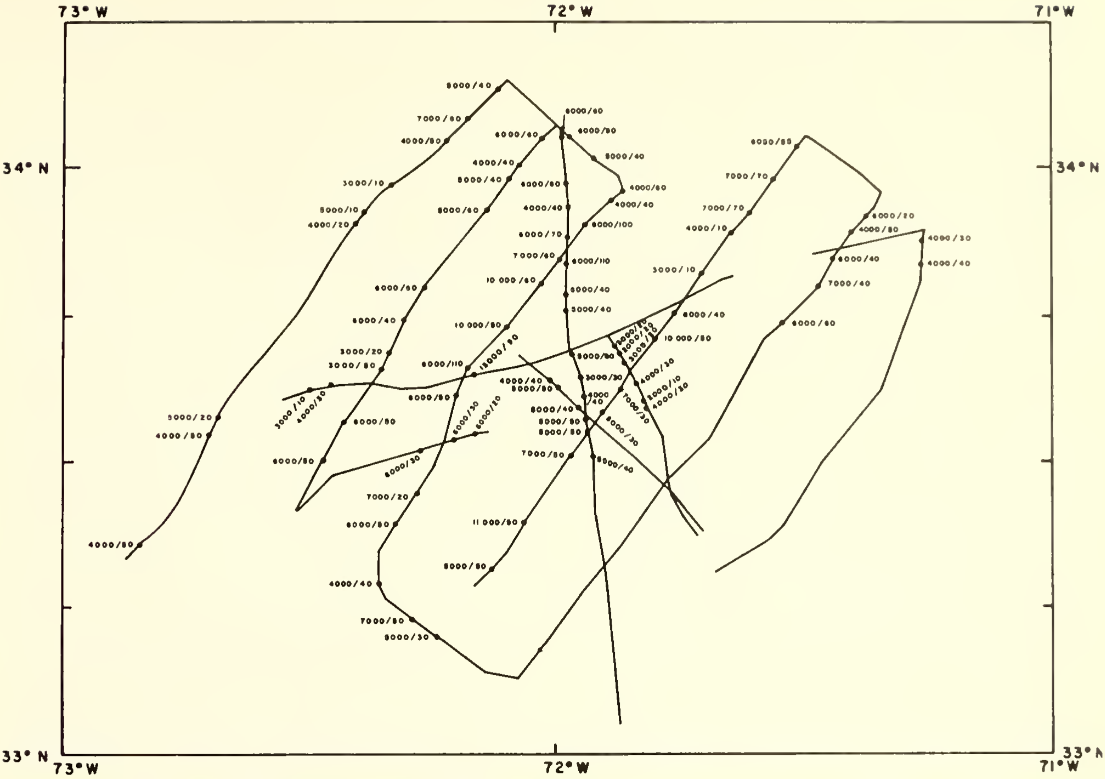

FIG. 6.—Wave indices (ratios of trough-to-trough wavelengths to peak-to-trough amplitudes in meters) at prominent peaks along the sounding tracks shown in fig. 3.

and movement upcurrent, by erosion of sand on the lee face and deposition on the upstream face of each succeeding wave crest.

The development of ripples in cohesive sediment has been less adequately observed, and the processes may be different from those affecting cohesionless sediment (van Straaten, 1951). The development of the linear continental rise hills composed of cohesive sediment (lutite and clay) may be related to sediment fallout from volume suspension, rather than to the rearrangement of sediment which has already been deposited. Nephelometer measurements by Ewing and Thorndike (1965) revealed that a layer of suspended matter a few hundred meters thick exists adjacent to the bottom along the continental slope of the United States. Suspended sediment has been obtained in a near-bottom water sample collected over the continental rise (Groot and Ewing, 1963). A single bottom photograph taken in the southwestern end of the field investigated revealed slightly muddy water (Schneider and others, 1967, fig. 1, 33° 08′ N, 71° 30′ W).

It is not known how the linear hills were initiated. The process by which suspended sediment may be deposited or redeposited on the linear hills is problematic. On the scale of ripple marks Sanders (1965, p. 203) observes that where fine-grained sediment fallout occurs, "layers of finer-grained sediment tend to be thicker on anticlines of convoluted laminae and to be thinner or absent in the adjoining synclines. This arrangement of the fine-grained

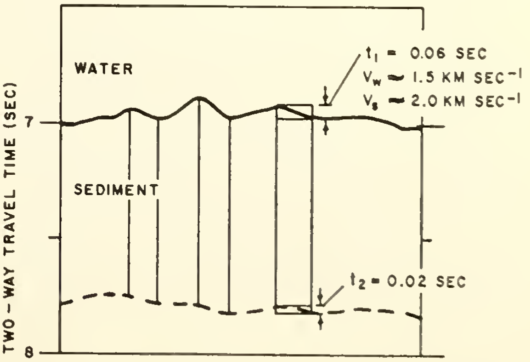
WATER
SEDIMENT
TWO-WAY TRAVEL TIME (SEC)
7
8
t_1 = 0.06 SEC
V_w ~ 1.5 KM SEC^{-1}
V_s ~ 2.0 KM SEC^{-1}
t_2 = 0.02 SEC

FIG. 7.—The undulations in the subbottom reflection interface at about 7.75 sec two-way travel time (dashed line) may be attributed to a seismic velocity effect produced by the overlying topographic hills as discussed in the text (traced from fig. 4).

sediment suggests that some kind of plastering-on mechanism has operated during sedimentation and that no subsequent reworking has occurred." A more rapid rate of sediment accumulation on the upcurrent limb of the waveforms would result in a migration of the entire field of waveforms in an upcurrent direction, in opposition to the generally downcurrent migration observed in ripples and dunes constructed of cohesionless materials. Equal rates of sediment accumulation on the upcurrent and downcurrent limbs of the waveforms would result in upbuilding. A more rapid rate of sedimentation on the downcurrent limb would result in migration of the entire field of waveforms in a downcurrent direction. Ichiye (1968) has suggested that stationary internal waves in a near bottom nepheloid layer superposed on a slow bottom current may augment sedimentary waveforms migrating in the direction of the current. The internal structure of the waveforms is not resolved well enough on the seismic profile to determine whether the stratification thickens on the upcurrent or the downcurrent limb. Such internal stratification could probably be resolved by drifting a ship operating a 3.5 kHz echo sounder over the field of waveforms. Fox and others (1968; fig. 3) show a N-S sparker reflection profile across two lower continental rise hills about 200 km northeast of the field investigated; each hill is underlain to about 400 m (0.4 sec) subbottom by a sequence of hill-shaped reflection interfaces in which the crests of the hills appear to progressively shift from south to north from bottom to top of the sequence. These reflection interfaces appear to terminate at the southern flank of each hill. Fox and others interpret the configuration of reflection interfaces to indicate a continuous northerly and upslope migration of the hill crests through time, produced by deposition controlled by the deep Western Boundary Undercurrent flowing southwest oblique to the crestal orientation of the hills. Lowrie and Heezen (1967) observed a thickening of sedimentary layers on the upcurrent side of a knoll on the continental rise near Hudson Canyon. They attributed this thickening to deposition resulting from deceleration of the Western Boundary Undercurrent upcurrent of the obstructing knoll. Fox et al. (1968) apply the term "abyssal antidunes" to the lower continental rise hills because of the inferred mode of development.

The field of lower continental rise hills investigated may be representative of lower continental rise hills throughout large areas. Large abyssal waveforms have been observed in the western north Atlantic in the Blake-Bahama Basin (Clay and Rona, 1964), on the Blake-Bahama Outer Ridge (Zarudzski, 1966), the Bermuda Rise-Sohm Abyssal Plain boundary, and the Bermuda Rise-Hatteras Abyssal Plain boundary (Fox and others, 1968). Fox and others report that continental rise hills corresponding to the description in the present investigation extend from the Hatteras Canyon northeastward to the Bermuda Rise-Sohm Abyssal Plain boundary, covering an area of about 32,000 km^2 (520 km long and 64-128 km wide) and ranging in depth between about 4500 m (NW boundary) and 5300 m (SE boundary).

The development in time of the lower continental rise hills may be partly inferred from the seismic profile (fig. 4). At present the rate of sediment accumulation in the troughs appears to be greater than on the peaks, so that the peaks are gradually being buried. Sedimentation rates measured on adjacent portions of the continental rise may be applied to the continental rise hills with the realization that special hydrodynamic conditions exist over the hills which could significantly alter the rates. The sediment fill about 50-m thick observed in the troughs would require at most about 3.5×10^6 years to accumulate, based on the lowest adjacent continental rise sedimentation rates (Ericson and others, 1961; Turekian, 1964). The hills are visible as waveforms to at least 0.1 sec (100 m) subbottom, which represents at most about 7×10^6 years of accumulation. Assuming that the hills began to develop after deposition of horizon A as an abyssal plain about 70×10^6 years ago, then the mean rate of sediment accumulation at the site of figure 4 would be about 1 cm per 10^3 years.

The rate of development of the lower continental rise hills is probably not uniform. The hills may be relict, having been formed under a previous sedimentary regime. The most rapid development of the hills might be expected during episodes of accelerated deep oceanic thermohaline circulation and large input of suspended sediment, such as at times of maximum global climatic contrast and lowered sea levels during the Pleistocene Epoch. The dense cold waters which drive the Western Boundary Undercurrent originate in the Arctic seas. Therefore, the existence of the Western Boundary Undercurrent requires open seas between North America, Greenland, and northern Europe. The initiation of the lower continental rise hills may be related to the initiation of conditions favorable to thermohaline circulation about $60–70 \times 10^6$ years ago when Norway and Baffin Island are inferred to have started to move from Greenland (Avery and others, 1968) and wide opening of the northern North Atlantic is supposed to have begun.

The sequence of undulatory reflection interfaces between about 650 m (0.65 sec) and 900 m (0.90 sec) subbottom at or just above horizon A (fig. 4) at first appears to be buried waveforms analogous to the present lower continental rise hills. However, the subbottom undulatory reflection interfaces may be attributed simply to a seismic velocity effect. From figure 7 it is apparent that the reflection times of signals from the subbottom undulations are less under topographic peaks and greater under topographic troughs. The decrease in travel time is due to the increased length of sediment travel time through the topographic peaks, relative to the travel time through the adjacent water filled troughs.

The variations in travel time that produced the subbottom undulations may be related to the topographic waveforms as follows:

$$t_2 = \frac{V_s - V_w}{V_s} t_1,$$

where t_1 = peak-to-trough amplitude of topographic waveform in two-way travel time; t_2 = peak-to-trough amplitude of underlying subbottom waveform in two-way travel time; V_w = mean vertical seismic velocity through water within the interval t_1; V_s = mean vertical seismic velocity through sediment within the interval t_1.

If V_w is taken as 1.5 km sec^{-1} and V_s as 2.0 km sec^{-1} from calculated values nearby (Rona and Clay, 1967), then the undulating subbottom interface may be corrected to a nearly planar interface.

The configuration and scale of the lower continental rise hills are strikingly similar to that of megaripples discovered by Ewing and others (1968) in the Argentine Basin. The megaripples extend continuously from reflection horizon A about 1 km (1 sec) below the bottom up to the present sea floor. Ewing and others inferred that the megaripples indicate control of sedimentation in the South Atlantic by the same deep circulation system dominated by the strong Antarctic Bottom Current since deposition of horizon A. The observation of similar waveforms on and beneath the continental rise off Cape Hatteras implies that conditions of strong deep circulation prevailed in the North Atlantic simultaneously with the South Atlantic, and that the entire Atlantic has been open at least since the co-development of the waveforms. Because the significance of the interval of transaural sediment between horizon A and the lower continental rise hills off Cape Hatteras is unknown, it cannot be ascertained from the seismic data (fig. 4) whether the strong deep circulation was continuous from the deposition of horizon A to Recent in the North Atlantic. The linear lower continental rise hills composed of lutite which is transaural at the low frequencies of the seismic source used probably extend downward to Horizon A as waveforms, within the transaural interval.

CONCLUSIONS

The lower continental rise hills investigated are large sedimentary transverse waveforms. The hills investigated appear to be representative of hills described from the entire lower continental rise hills physiographic province of the western north Atlantic. Based on their crestal orientation, configuration, and sediment size the hills are inferred to have been produced by deposition controlled by a deep southwest flowing ocean current, presently the Western Boundary Undercurrent. The downward extent and configuration of the hills in the interval of transaural sediment above reflection horizon A provides an index to the magnitude and direction of Cenozoic deep thermohaline circulation.

ACKNOWLEDGEMENTS

Mr. Chester Brier was electronic engineer in charge of preparation and operation of the seismic and bathymetric systems. Mr. Joseph Smith assisted in all electronic work. Mr. Hugo Mellace prepared the mechanical equipment and was in charge of shipboard handling of seismic and coring equipment. Mr. Curt Conner acted as navigator and assisted with data acquisition. Mr. William Osborn contributed to the reduction and graphic representation of the data.

Conversations with Dr. John E. Sanders and Dr. Chester E. Grosch of Hudson Laboratories regarding the dynamics of sedimentary deposition were valuable.

This work was supported by the Office of Naval Research under Contract Nonr-266(84). Reproduction in whole or in part is permitted for any purpose of the United States Government. It is Hudson Laboratories of Columbia University Contribution No. 348.

REFERENCES

Avery, Otis E., Burton, Gordon D., and Heirtzler, James R., 1968, An aeromagnetic survey of the Norwegian sea: Jour. Geophys. Res., v. 73, p. 4583–4600.

Bagnold, R. A., 1941, (reprinted 1954) The physics of blown sand and desert dunes. Methuen and Co., London, 165 p.

BALLARD, JAMES A., 1966, Structure of the Lower Continental Rise Hills of the Western North Atlantic: Geophysics, v. 31, p. 506–523.

BARRETT, JOSEPH R., JR., 1965, Subsurface currents off Cape Hatteras: Deep-Sea Res., v. 12, p. 173–184.

BUCHER, W. H., 1919, On ripples and related sedimentary surface forms and their paleogeographic interpretation: Amer. Jour. Science, ser. 4, v. 47, p. 149–210, 241–269.

BOWEN, V. T., AND SACHS, P. L., 1964, The free corer: Woods Hole Oceanographic Institution, Oceanus, v. 11, p. 2–6.

CLAY, C. S., AND RONA, PETER A., 1964, On the existence of bottom corrugations in the Blake-Bahama Basin: Jour. Geophys. Res., v. 69, p. 231–234.

ERICSON, D. B., EWING, MAURICE, WOLLEN, GOESTA, AND HEEZEN, B. C., 1961, Atlantic deep-sea sediment cores: Geol. Soc. of Amer. Bull., v. 72, p. 193–286.

EWING, MAURICE, AND THORNDIKE, E. M., 1965, Suspended matter in deep ocean water: Science, v. 147, p. 1291–1294.

EWING, JOHN I., WORZEL, J. L., AND EWING, MAURICE, 1966, Ages of horizon A and the oldest Atlantic sediments: Science, v. 154, p. 1125–1132.

EWING, MAURICE, EITTREIM, S. L., EWING, J. I., AND LE PICHON, X., 1968, Sediment transport and distribution in the Argentine Basin: Part 3, Nepheloid layer and processes of sedimentation. Progress in Physics and Chemistry of the Earth, v. 8, London, Pergamon Press.

FOX, P. J., HEEZEN, B. C., AND HARIAN, A. M., 1968, Abyssal anti-dunes: Nature, v. 220, p. 470–472.

GILBERT, G. K., 1914, The transportation of debris by running water: U.S. Geol. Survey Prof. Paper 86, 263 p.

GROOT, JOHAN J., AND EWING, MAURICE, 1963, Suspended clay in a water sample from the deep ocean: Science, v. 142, p. 579–580.

HEEZEN, BRUCE C., AND HOLLISTER, CHARLES D., 1964, Deep-sea current evidence from abyssal sediments: Marine Geology, v. 1, p. 141.

HEEZEN, BRUCE C., HOLLISTER, CHARLES D., AND RUDDIMAN, WILLIAM F., 1966, Shaping of the continental rise by deep geostrophic contour currents: Science, v. 152, p. 502–508.

HEEZEN, BRUCE C., THARP, MARIE, AND EWING, MAURICE, 1959, The floors of the ocean. I. The North Atlantic: Geol. Soc. Amer. Spec. Paper 65, 122 p.

ICHIYE, TAKASHI, 1968, A theory on generation of giant bottom undulations in the Argentine Basin: Progress Report to NSF for Grant GA-258.

JORDON, G. F., 1962, Large submarine sand waves: Science, v. 136, p. 839.

LOWRIE, ALLEN, JR., AND HEEZEN, BRUCE C., 1967, Knoll and sediment drift near Hudson Canyon: Science, v. 157, p. 1552–1553.

MATTHEWS, D. J., 1939, Tables of the velocity of sound in pure water and sea water for use in echo-sounding and sound-ranging. 2nd ed., Hydrographic Department, Admiralty, London, 52 p.

RONA, PETER A., AND CLAY, C. S., 1967, Stratigraphy and structure along a continuous seismic reflection profile from Cape Hatteras, North Carolina, to the Bermuda Rise: Jour. Geophys. Res., v. 72, p. 2107–2130.

RONA, PETER A., SCHNEIDER, ERIC D., AND HEEZEN, BRUCE C., 1967, Bathymetry of the continental rise off Cape Hatteras: Deep-Sea Res., v. 14, p. 625–633.

SANDERS, JOHN E., 1965, Primary sedimentary structures formed by turbidity currents and related resedimentation mechanisms, p. 192–219 *in* Middleton, G. V., ed., Primary sedimentary structures and their hydrodynamic interpretation. Amer. Assoc. Petrol. Geol., Spec. Pub. no. 12, 265 p.

SCHNEIDER, ERIC D., FOX, PAUL J., HOLLISTER, CHARLES D., NEEDHAM, H. DAVID, AND HEEZEN, BRUCE C., 1967, Further evidence of contour currents in the Western North Atlantic: Earth and Planetary Science Letters, v. 2, p. 351–359.

SWALLOW, J. C., AND WORTHINGTON, L. V., 1961, An observation of deep countercurrent in the Western North Atlantic: Deep-Sea Res., v. 8, p. 1–19.

TUREKIAN, KARL K., 1964, The geochemistry of the Atlantic Ocean Basin: N. Y. Acad. Science Trans., Ser II, v. 26, p. 312–330.

VAN STRAATEN, L. M. J. U., 1951, Longitudinal ripple marks in mud and sand: Jour. Sedimentary Petrology, v. 21, p. 47–54.

VOLKMAN, G. H., 1962, Deep current observations in the Western North Atlantic: Deep-Sea Res., v. 9, p. 493–500.

ZARUDZSKI, EDWARD F. K., 1966, Geophysical investigations of some areas of the Blake Plateau and the Blake-Bahama Basin: Amer. Geophys. Union Trans., v. 47, p. 121.

Reprinted from American Association of Petroleum
Geologists Bulletin, Vol. 54, No. 1, 129-157.

30

The American Association of Petroleum Geologists Bulletin
V. 54, No. 1 (January, 1970), P. 129-157, 10 Figs., 3 Tables

Comparison of Continental Margins of Eastern North America at Cape Hatteras and Northwestern Africa at Cap Blanc[1]

PETER A. RONA[2]
Miami, Florida 33130

Abstract The opposing continental margins of Cape Hatteras and Cap Blanc appear broadly symmetric with respect to (1) distribution of physiographic provinces, with the exception of the lower continental rise hills which have not been observed off Cap Blanc, (2) early and middle Paleozoic, Mesozoic, and Cenozoic stratigraphic frameworks, (3) late Precambrian, Paleozoic, and Mesozoic tectonic frameworks, with certain qualifications, and (4) certain offshore residual magnetic anomalies, including a positive anomaly associated with the continental shelf edge and the boundary between smooth and rough magnetic fields. The third point must be qualified because (a) the absence of late Paleozoic (post-Devonian) strata in the Mauritanides fold belt of northwest Africa, as opposed to their involvement in the Appalachian fold belt of eastern North America, limits resolution of the respective orogenic movements and (b) the existence of a system of Triassic fault-block basins parallel with the northwest African continental margin, corresponding to the system in eastern North America, has not been well documented.

The opposing continental margins appear broadly asymmetric with respect to Cenozoic tectonic frameworks. Sedimentary strata underlying the coastal plain, continental terrace, and continental rise near Cape Hatteras are predominantly undeformed, except by superficial gravitational displacement processes acting above Horizon A (Late Cretaceous-Eocene). Sedimentary strata underlying the corresponding physiographic provinces off Cap Blanc are deformed by deep structural processes including (1) compressional folding related to Alpine diastrophism, (2) tensional faulting along west-northwest fracture trends, coincident with eastward projections of fracture zones which cross the Mid-Atlantic Ridge, and along inferred north-northeast fracture trends which regionally parallel the continental margin, (3) volcanism, at least of Oligocene to Holocene age, concentrated along the fracture zones, and (4) diapirism, probably produced by rock salt deposits beneath the continental terrace and continental rise correlative with Late Triassic and Jurassic evaporites in the northwest African coastal basins.

Mesozoic and Cenozoic mean rates of subsidence and sequences of gross lithology generally correlate between the opposing continental margins. Similarities in the stratigraphic records of the opposing continental margins and the adjacent ocean basin indicate that the continental margins have behaved as if vertically, as well as horizontally, coupled to the ocean basin.

Mesozoic and Cenozoic mean subsidence rates of the opposing continental margins (1–9 cm/1,000 year) are about 10^{-3} of inferred mean spreading rates of the intervening sea floor (1–4 cm/year). The mean subsidence rates vary in unison with the independently inferred mean spreading rates, to a first approximation. The limited data suggest that the epeirogenic subsidence of the opposing continental margins and the inferred spreading of the intervening sea floor are related genetically.

The apparent symmetry in space and time of tensional rifting, orogenic compression, and epeirogenic subsidence on the opposing continental margins is consistent with a hypothesis of sea-floor spreading. These findings imply that geologic conditions relevant to the occurrence of petroleum can be predicted between the opposing continental margins.

INTRODUCTION[3]

Sections of the continental margins of eastern North America and northwestern Africa were chosen for comparison because these two continental margins are associated in pre–continental-drift reconstructions (Wegener,

---

[1] Manuscript received, June 18, 1969; accepted, October 13, 1969. Read before the Association at Dallas, Texas, April 16, 1969. Hudson Laboratories of Columbia University Contribution No. 358.

[2] ESSA Atlantic Oceanographic and Meteorological Laboratories.

[3] This paper keynotes the planned ESSA Trans-Atlantic Geophysical Traverse which aims to establish a standard crustal section across the Atlantic between Cape Hatteras and Cap Blanc in conjunction with the proposed Trans-Atlantic Extension of the U.S. Transcontinental Geophysical Survey of the International Upper Mantle Project.

This work was supported by the Office of Naval Research under Contract Nonr-266(84). Reproduction in whole or in part is permitted for any purpose of the United States Government.

C. Brier contributed to the design of the seismic reflection profiling system and was responsible for engineering-at-sea; J. Smith contributed to the fabrication, preparation, and operation of the electronic instrumentation; T. Farrell and H. Mellace designed an effective vehicle for the pneumatic sound source and were responsible for the mechanical engineering-at-sea; and J. Brakl processed the magnetic data.

Conversations with A. A. Meyerhoff of The American Association of Petroleum Geologists, G. E. Abbey and M. Lizotte of American International Oil Company, R. O. Mitchell of Planet Oil and Mineral Corporation, and R. E. King of the Woods Hole Oceanographic Institution regarding the geology of the northwest African continental margin, and with G. M. Friedman of Rensselaer Polytechnic Institute regarding evaporite deposition, were particularly helpful. W. A. Oliver, Jr., of the U.S. Geological Survey advised on the Devonian paleontology.

The good will and cooperation of Capt. R. E. Salman and the officers and crew of the USNS *J. W. Gibbs* (T-AGOR-1) made the time at sea profitable and pleasant.

© 1970. The American Association of Petroleum Geologists. All rights reserved.

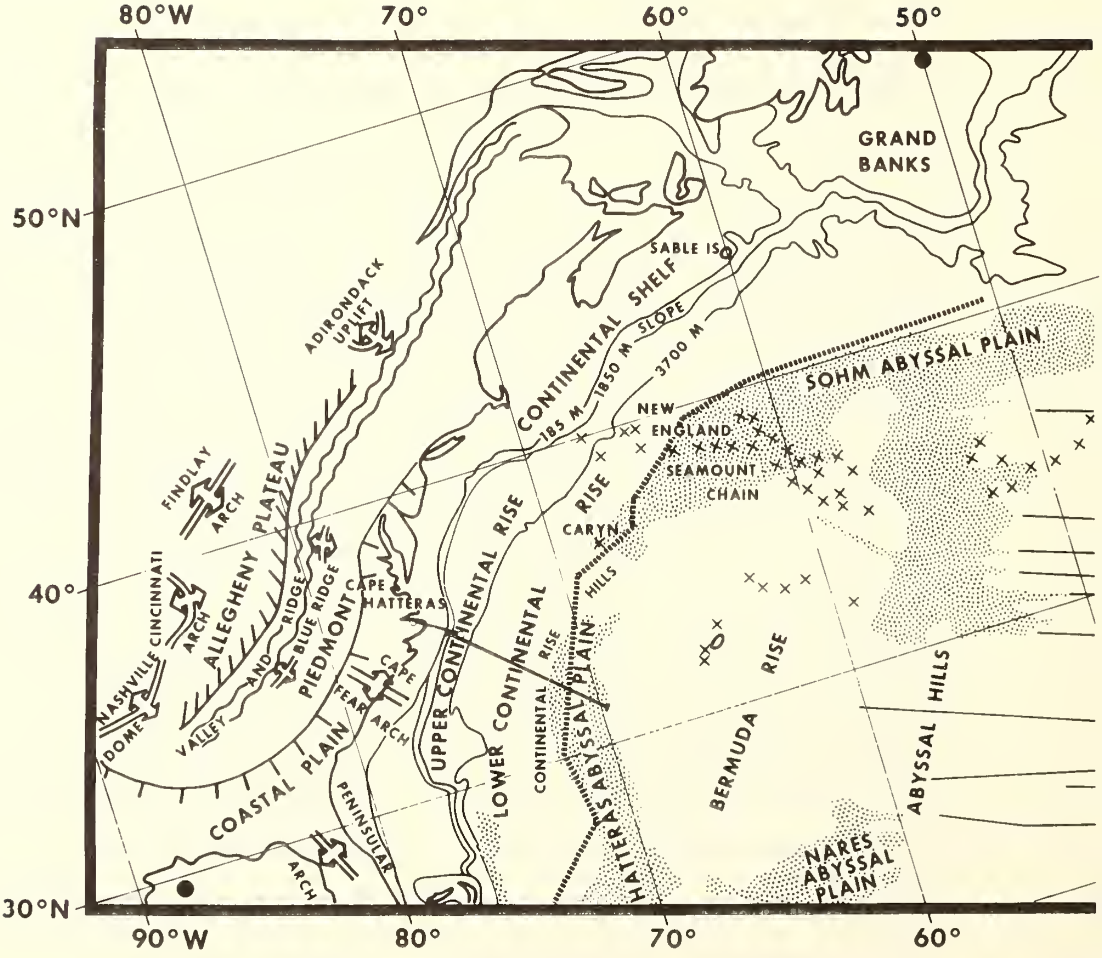

1929). A "fit" at the two continental slopes (900 m isobath) places Cape Hatteras, North Carolina, opposite Cap Blanc, Mauritania (Bullard *et al.*, 1965).

The literature on the Atlantic continental margin of North America, including the Appalachian mountain system, is extensive (Drake, 1965; Drake *et al.*, 1959, 1968; Heezen *et al.*, 1959; King, 1959; Murray, 1961; Uchupi and Emery, 1967). The northwest African continental margin, including the Mauritanides mountain system (Fig. 1), has been investigated less extensively (Heezen *et al.*, 1959; Reyre, 1966a; Sougy, 1962).

Findings from seismic reflection and magnetic profiles of the northwest African continental margin between the Canary and Cape Verde Islands made on a 1968 cruise of the USNS *J. W. Gibbs* (Rona, 1968, 1969a, b; Rona *et al.*, 1969) combined with published work support a preliminary comparison of the structure and development of the two continental margins in the vicinities of Cape Hatteras and Cap Blanc. Geologic symmetries and asymmetries should help to elucidate the nature of the forces which have acted on the opposing continental margins and should aid in the prediction of conditions favorable to the occurrence of petroleum.

This comparison is limited in two respects. First, it is limited geographically to the opposing continental margins in the vicinities of Cape Hatteras and Cap Blanc. Second, it is limited geologically to my offshore seismic reflection and magnetic data on the configuration of the sedimentary layer and to consideration of the regional geology.

The purpose of the comparison is to distin-

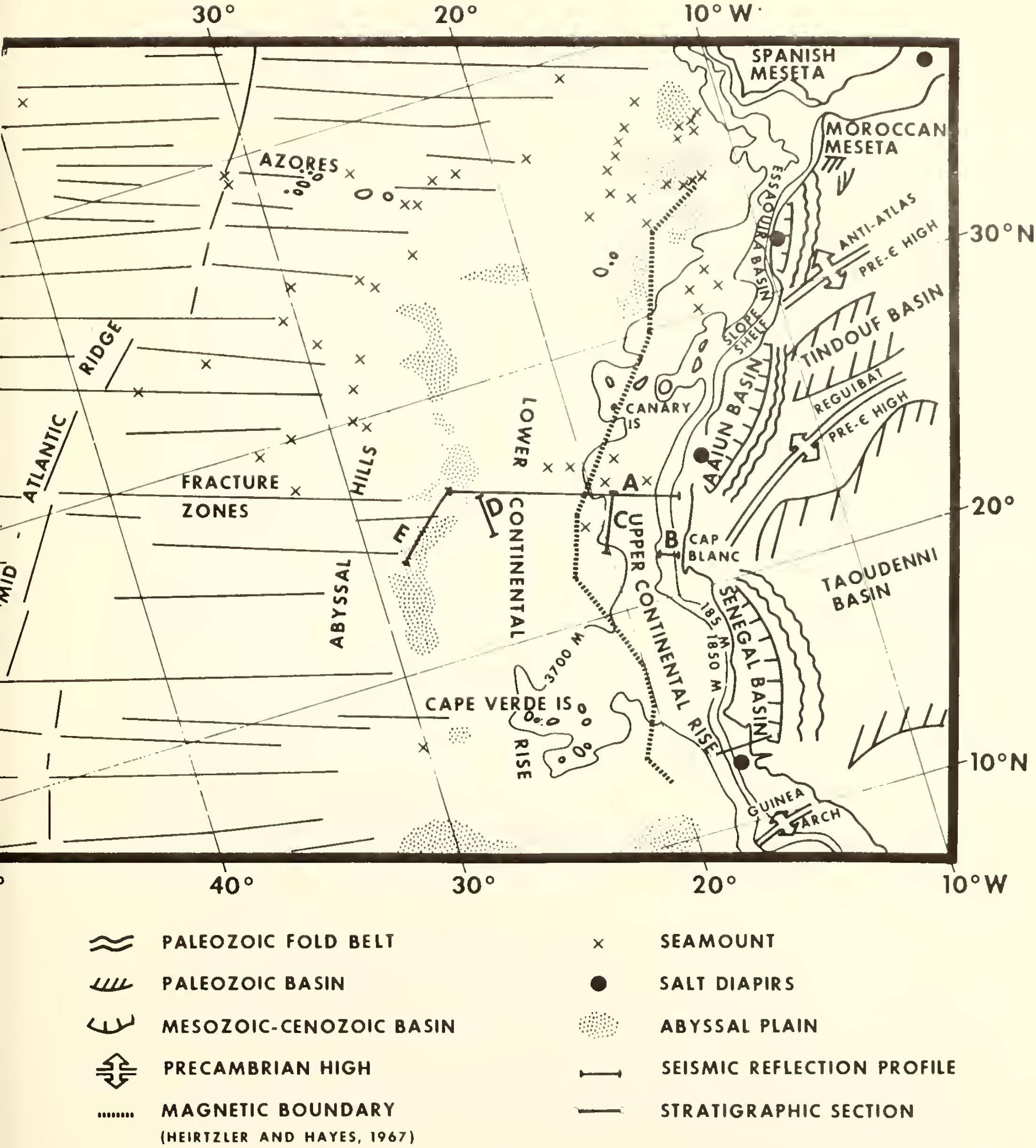

FIG. 1.—Major physiographic and structural features of onshore (Cohee, 1962; King, 1959, 1964; Querol, 1966, Fig. 5) and offshore (Heezen and Tharp, 1968) parts of continental margins of eastern North America and northwestern Africa. Locations of stratigraphic sections (Figs. 2, 5) and seismic reflection and magnetic profiles (Figs. 3, 4, 6–9) are shown.

guish broad symmetries and asymmetries in physiographic provinces, stratigraphic frameworks, tectonic frameworks, offshore residual magnetic anomalies, and deformation of the offshore sedimentary layer.

METHODS

The seismic profiles were made with a pneumatic sound source (J. Ewing and Zaunere, 1964) which released 360 cm^3 of air at pressures of 100–140 bars into the water. Pulse duration was about 0.01 sec and center frequency was about 70 Hz with a band width of about 100 Hz. The source repeated at about 20-sec intervals, giving one data point for every 72 m of lateral translation at ship's speed of 7 knots (3.6 m/sec). Two-way travel time of the acoustic pulse from source to bottom and sub-bottom reflection interfaces is presented. A mean vertical compressional velocity of 2.0 km sec^{-1} is assumed to convert travel time through sediment to sediment thickness; 1.5 km sec^{-1} is assumed to convert travel time through water to water depth. The magnetic profiles were made with a proton precession magnetometer.

Loran A and C were used to navigate off Cape Hatteras. Omega in conjunction with celestial navigation was used off Cap Blanc. Fixes were plotted at least twice per hour with good tracking consistency. Absolute positional inaccuracies up to about ± 5 n. mi (9.3 km) were indicated by comparison of Omega fixes with fixes obtained by other navigational methods (Zuccaro and Rona, 1968).

PHYSIOGRAPHIC PROVINCES

The distribution of physiographic provinces of the Cape Hatteras and Cap Blanc continental margins is symmetric, with minor exceptions (Fig. 1, Table 1). The lower continental rise hills province appears to be absent off Cap Blanc. The position of the Bermuda Rise off Cape Hatteras corresponds to the position of the abyssal hills province off Cap Blanc.

The widths of the individual provinces differ between the two continental margins (Fig. 1, Table 1). The continental slope off Cape Hatteras is relatively narrow and has a mean inclination of about 9°. The wider Cape Blanc continental slope has a mean inclination of about 2°. The continental rise off Cape Hatteras is about one third the width of the Cap Blanc continental rise, which would extend across the Hatteras abyssal plain and 300 km across the Bermuda Rise. The Hatteras abyssal plain is relatively wide and continuous; the Cape Verde abyssal plain off Cap Blanc is narrow and discontinuous.

Volcanic seamounts are unknown from the continental rise directly off Cape Hatteras (Rona *et al.*, 1967). The closest known seamount, Caryn, is a conical volcanic peak at the base of the continental rise about 650 km northeast of Cape Hatteras (Miller and Ewing, 1956). Late Cretaceous limestone (reworked) has been cored from Caryn (Ericson *et al.*, 1961, cores A158–2, A158–4, A164–10). The New England Seamount Chain, a group of seamounts aligned along westward projections of fracture zones from the Mid-Atlantic Ridge, crosses the continental rise about 1,200 km northeast of Cape Hatteras (Northrop *et al.*, 1962). The island of Bermuda is on a volcanic pedestal about 1,300 km east of Cape Hatteras (Foreman, 1951; Pirsson, 1914). Upper Cretaceous shallow-water limestone is the oldest sedimentary rock that has been sampled from Bermuda (Ericson and Wollin, 1963). Volcanic seamounts on the continental rise directly off Cap Blanc are aligned along the eastward projections of fracture zones which cross the Mid-Atlantic Ridge (Heezen and Tharp, 1968). Sediment of Maestrichtian age has been cored from one of these seamounts (Weiss, 1969). The chiefly volcanic Canary and Cape Verde Islands are, respectively, about 900 km north and southwest of Cap Blanc.

STRATIGRAPHIC FRAMEWORK

Paleozoic Basins

Basins interior to Paleozoic mountain belts along both continental margins contain gently

Table 1. Distribution and Width of Physiographic Provinces (km) of Continental Margins at Cape Hatteras and Cap Blanc

	Interior Lowlands	*Interior Mountains*	*Coastal Plain*	*Continental Shelf*	*Continental Slope*	*Continental Rise*		*Lower Continental Rise Hills*	*Abyssal Plain*	*Abyssal Hills*
						Upper	*Lower*			
Cape Hatteras (widths measured in km along azimuth 130°)	>200 (Allegheny Plateau)	325 (Valley and Ridge, Blue Ridge, and Piedmont)	200	35	10	135	170	60	220	Bermuda Rise
Cap Blanc (widths measured in km along azimuth 300°)	>200	150	125	40	75	250	600	not observed	30	450

From Geological Map of Africa, 1963; Geological Map of North America, 1946; Heezen and Tharp (1968); King (1964, Fig. 1); Rona and Clay (1967, Fig. 2); Sougy (1962, Fig. 1).

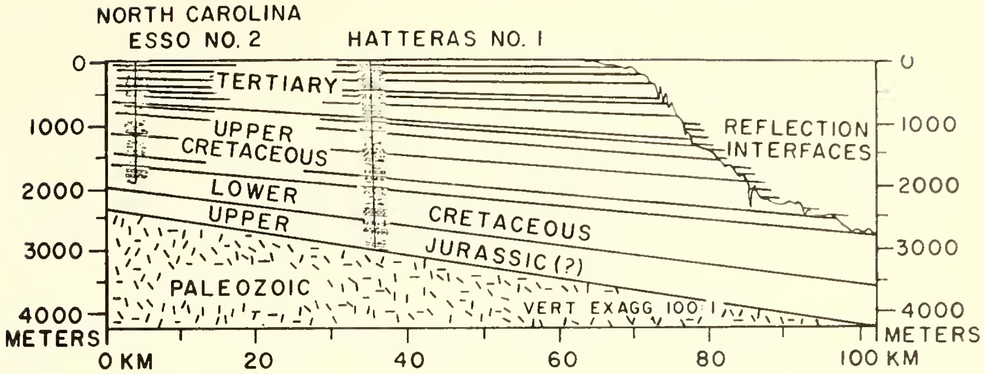

FIG. 2.—NW-SE stratigraphic section through Cape Hatteras; strata found in wells on coastal plain are projected beneath continental shelf to terminations at continental slope (after Heezen *et al.*, 1959, Fig. 22; Rona and Clay, 1967, Fig. 9; Spangler, 1950, Fig. 10).

deformed Paleozoic strata (Fig. 1). The Paleozoic strata overlap Precambrian highs on the landward margins of the basins. The strata have been studied paleontologically, but few systematic comparisons have been made. Within the Ordovician, similar Llandeilo trilobite faunas are identified on the generic level from Florida and northwest Africa (Whittington, 1966, Fig. 2). Several Eifelian tetracorals from Morocco have been assigned to North American species (Le Maitre, 1947; *Eridophyllum seriale* and *Prismatophyllum articulum* are known only from Morocco and North America; *Heliophyllum halli, Cystiphyllum vesiculosum,* and *Siphonophrentis gigantea* are also known from both North America and northwest Africa).

Coastal Plain and Continental Terrace

The coastal plains and continental terraces (continental shelf and slope) in the vicinities of Cape Hatteras and Cap Blanc are underlain by seaward-thickening wedges of lower Mesozoic through Cenozoic sedimentary strata (Aymé, 1965, Fig. 3; de Spengler *et al.*, 1966; Furon, 1963; Haughton, 1963; Querol, 1966; Spangler, 1950; Swain, 1947, 1952). The Cenozoic and upper Mesozoic strata appear to terminate at the continental slope (Figs. 2–6; Heezen *et al.*, 1959, Fig. 22; Rona and Clay, 1967, Fig. 9). The sedimentary strata form homoclines dipping seaward regionally at less than 5°, and are underlain by Paleozoic rocks. Grabens containing Triassic continental sediment intercalated with lava flows may be downfaulted into the Paleozoic. The sedimentary wedges reach thicknesses of about 3.0–5.0 km beneath the coasts and 3.5–6.0 km beneath the shelf breaks of both continental margins. The thicknesses of Jurassic(?) through Tertiary strata are comparable on the two continental margins, with the exception of the Lower Cretaceous which is about one fifth as thick at Cape Hatteras as near Cap Blanc (Figs. 2, 5; Table 2). Jurassic(?) through Tertiary mean rates of subsidence derived from the thicknesses of sedimentary strata are comparable for the two continental margins, with the exception of the Lower Cretaceous (Table 2). The Mesozoic through Cenozoic strata underlying the two continental margins are composed of similar lithologic sequences of sandstone, shale, and limestone of shallow marine or nearshore origin which interfinger with sandstone, siltstone, and claystone of continental origin in the Upper Jurassic(?) and lower Upper Cretaceous (Table 2).

Continental Rise

The continental rises of both margins are formed of seaward-thinning wedges of sedimentary strata. The Cape Hatteras continental rise is of Cenozoic age because the sediments which form the rise extend over reflection Horizon A, a relict abyssal plain of Late Cretaceous or Eocene age (Fig. 3; J. Ewing *et al.*, 1966). Horizon A has not been identified off northwest Africa (J. Ewing, personal commun.).

TECTONIC FRAMEWORK

Southern Appalachian Geosyncline

The major structural units of the southern Appalachians trend parallel with the continental margin (NE-SW). Seaward these units are

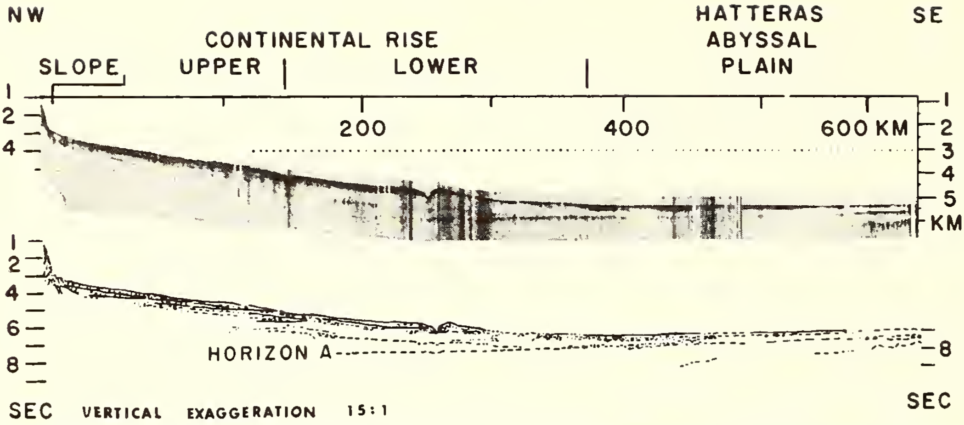

Fig. 3.—Photograph of continuous seismic reflection profile from continental slope off Cape Hatteras to Bermuda Rise (upper trace) and corresponding line drawing (lower trace). After Rona and Clay (1967, Fig. 2).

as follows (Fig. 1; Cohee, 1962; Hadley, 1964; King, 1959, 1964; Rodgers, 1967; Sanders, 1963; Stose, 1946).

1. A synclinorium (Allegheny Plateau province) contains gently deformed Paleozoic strata and constitutes a foreland area adjacent to the craton.

2. A belt of unaltered folded and faulted Pa-

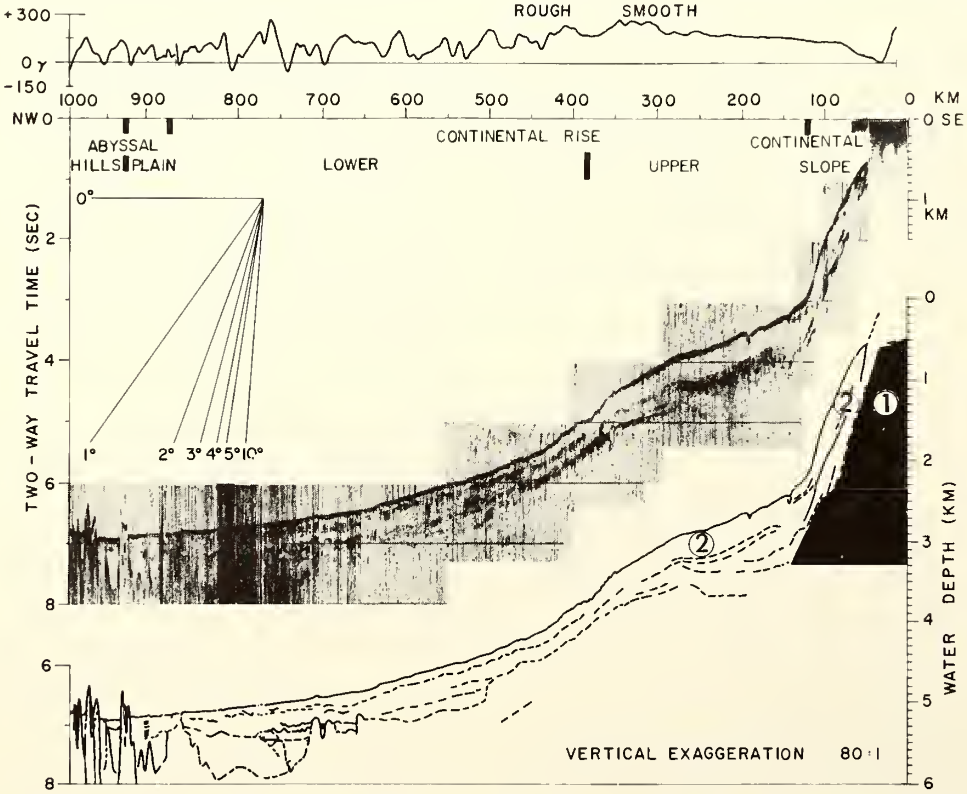

Fig. 4.—Profile A extends from middle of continental shelf off Punta Durnford, Spanish Sahara, to abyssal hills. Residual magnetic profile (upper trace), photograph of seismic reflection profile (middle trace), and corresponding line drawing (lower trace) are shown. Figures 6 and 9 follow the same format.

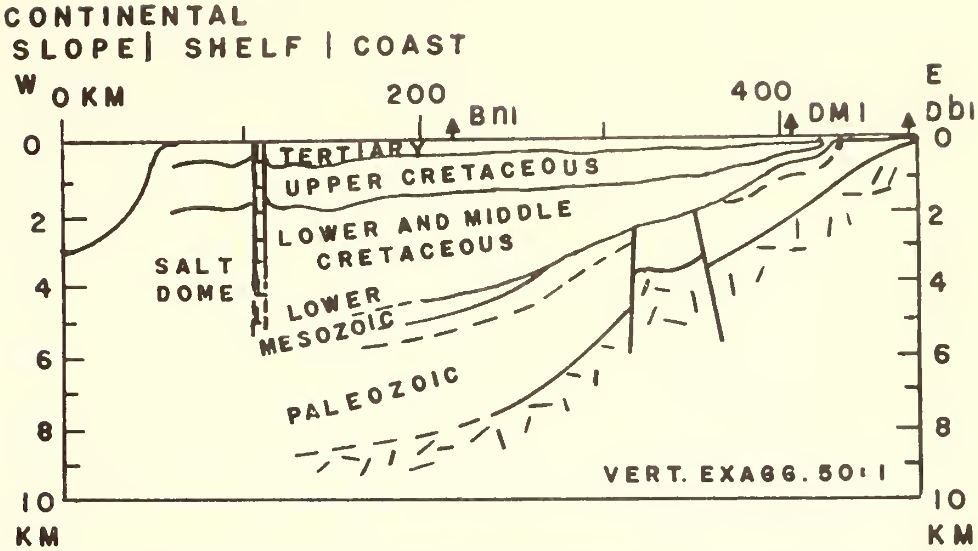

FIG. 5.—Schematic stratigraphic section across coastal plain and continental terrace of Senegal basin about 975 km south of Cap Blanc (after Aymé, 1965, Fig. 3).

leozoic strata (Cambrian through Early Permian, depending on the locality; Valley and Ridge province) was deformed principally in the Pennsylvanian and Permian Alleghany orogeny (Westphalian and younger; 260–230 m.y.). The sedimentary facies is considered miogeosynclinal.

3. An anticlinorium (Blue Ridge province) comprises metamorphic and plutonic basal Paleozoic and Precambrian rocks overfolded in a landward direction. Cambrian and Ordovician strata are preserved in marginal downfolds. Thermal events are dated in the basement complex at 1,150 and 850 m.y.

4. A belt of metamorphosed Paleozoic strata and plutonic rocks (Piedmont province) is differentiated into landward high-grade and seaward low-grade metamorphic zones. A thermal event is dated at about 440 m.y. (Middle and Late Ordovician [Caradoc] Taconian orogeny); ages in this range may represent crustal heating between 550 and 450 m.y. ago (Kulp and Eckelman, 1961, p. 413). Other thermal events are dated at about 350 m.y. (probably Middle-Late Devonian [Emsian-Eifelian] Acadian orogeny), and at about 260 m.y. (late Paleozoic Alleghany orogeny). The sedimentary facies of the Piedmont province is considered eugeosynclinal.

5. Igneous and metamorphic Paleozoic rocks of the Piedmont incline seaward beneath the Mesozoic through Cenozoic seaward-thickening sedimentary wedge that underlies the coastal plain and continental shelf at Cape Hatteras (Denison *et al.*, 1967). Practically unmetamorphosed Paleozoic strata are present at certain other localities both north and south of Cape Hatteras as, for example, beneath Sable Island off Nova Scotia and beneath northern Florida (Applin, 1951). The Mesozoic through Cenozoic strata are in basins delineated by structural highs in the crystalline basement (Drake *et al.*, 1959). Thermal events ranging between 585±40 and 250±5 m.y. are dated from the basement complex near Cape Hatteras (Denison *et al.*, 1967).

6. Grabens with their axes regionally parallel with the continental margin are downfaulted into the rocks of the Piedmont province and contain Late Triassic and Jurassic basaltic lava flows intercalated with continental redbeds. A thermal event is dated from the basalt flows at about 200–190 m.y. (Late Triassic [Carnian-Norian] Palisades disturbance).

Northwest African Geosyncline

Major structural units of the northwest African continental margin (seaward) are as follows (Fig. 1; Choubert and Faure-Muret, 1968; Furon, 1963; Querol, 1966; Sougy, 1962; UNESCO, 1963).

1. Interior basins (Tindouf, Taoudenni) trending ENE-WSW contain nearly flat-lying chiefly clastic Paleozoic strata which overlap the Precambrian African shield and constitute a foreland area.

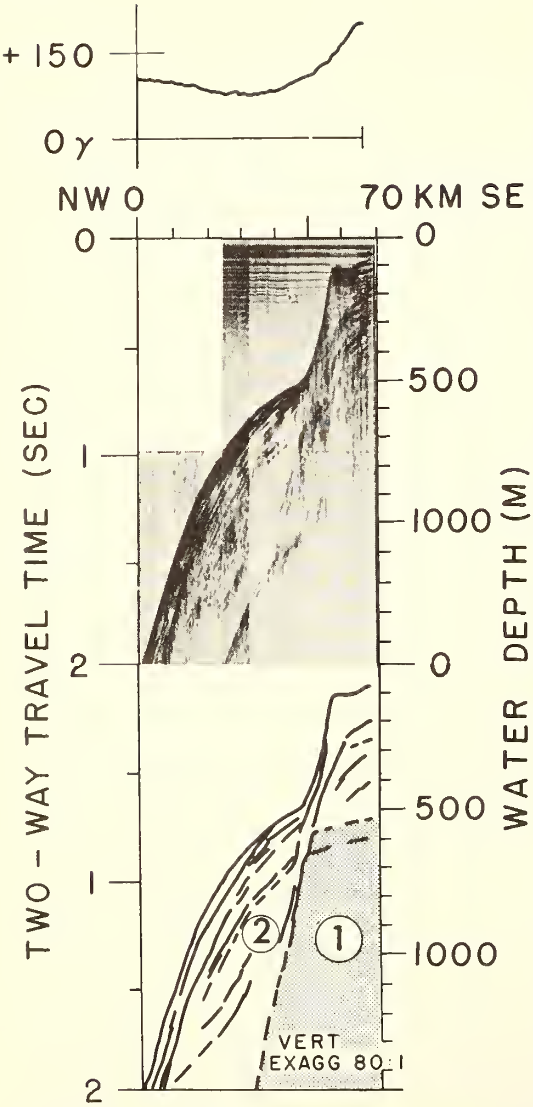

FIG. 6.—Profile B extends from continental shelf off Cap Blanc, Mauritania, to upper continental slope.

2. A Precambrian structural high (Anti-Atlas) trending ENE-WSW plunges seaward toward the Canary Islands.

3. A Precambrian structural high (Reguibat or Yetti Eglab) trending ENE-WSW plunges seaward toward the Cape Verde Rise. Rocks with ages of nearly 2,000 m.y. correlative with the African shield crop out along both the Anti-Atlas and Reguibat highs.

4. A belt of folded and faulted early and middle Paleozoic rocks (Cambrian through Devonian), designated the "Mauritanides" (Sougy, 1962), extends along the continental margin from Morocco at least as far south as Senegal. The belt comprises a folded zone (landward side) and a zone exhibiting strong deformation, dynamic metamorphism, and possibly igneous intrusion (seaward side). The folded zone in the Spanish Sahara and adjacent Mauritania comprises a thick sequence of Infracambrian (earliest Paleozoic) dolomites and clastic rocks overlain by quartzitic sandstones of Cambrian to Ordovician age; the sedimentary facies may be considered miogeosynclinal. Deformed and slightly metamorphosed Infracambrian and Cambrian sandstone, graywacke, volcanic rock, and shale exposed in the Moroccan Meseta may be considered eugeosynclinal. Landward overthrusting of the metamorphic zone is observed in Morocco, the Spanish Sahara, and Mauritania (Sougy, 1962, Fig. 1). Dates of 600 ± 200 m.y. have been measured in rocks from the metamorphic zone in the southern Spanish Sahara, northwestern Mauritania (Akjoujt district), and Senegal (Hurley *et al.*, 1967, Fig. 1). Precambrian rocks are also probably present in the metamorphic zone (Sougy, 1969).

An erosional hiatus in the Paleozoic strata of the fold belt indicates mild Caledonian (Ordovician-Silurian) deformation. The main fold movements were post-Devonian within the Paleozoic (Hercynian).

5. Igneous and metamorphic Paleozoic rocks of the Mauritanides metamorphic zone incline seaward and are buried unconformably beneath a seaward-thickening wedge of Mesozoic through Cenozoic strata that underlies the coastal plain and continental shelf near Cap Blanc. Practically unmetamorphosed Paleozoic strata are present beneath the coastal plain both north and south of Cap Blanc as, for example, beneath parts of the Aaiun basin (Hedberg, 1961, p. 1181) and beneath the Senegal basin (Aymé, 1965; Moody, 1962, p. 1232). The Mesozoic and Cenozoic strata are in basins (Essaouira, Aaiun, Senegal) delineated by the Precambrian structural highs. A thermal event dated at 650 m.y. in crystalline rocks underlying the Aaiun basin represents a Precambrian orogeny (Querol, 1966, p. 29–32). The entire African continent underwent a major pan-African thermal event about 500 m.y. ago in which the Mauritanides and other regions of mobility, tectonism, and granitization were differentiated from stable cratonic nuclei (Cahen, 1961; Kennedy, 1965). A thermal event dated at 304 m.y. from a dolomite (Infracambrian?) under-

Table 2. Stratigraphy at Cape Hatteras and Near Cap Blanc

	Cape Hatteras: *Esso Hatteras Light Well No. 1* (*Fig. 2; Swain, 1952*)	*Cap Blanc:* *Senegal Basin* (*Fig. 3; Aymé, 1965, Fig. 3*)
Sediment thickness (m) near present coastline		
Tertiary	925	600
Upper Cretaceous	805	1,200
Lower Cretaceous	860	2,900
Upper Jurassic(?)	420	500
Lithology		
Tertiary	Sand in upper part with increasing amounts of limestone, clay, calcareous marl, and shale in lower part	Sand in upper part with increasing amounts of limestone, clay, calcareous marl, and shale in lower part
Upper Cretaceous	Interbedded sandstone, gray and green shale, and calcareous marl	Interbedded sandstone, gray and green shale, and calcareous marl
Lower Cretaceous	Interbedded sandstone, limestone, and gray shale	Interbedded sandstone, limestone, and gray shale
Upper Jurassic(?)	Interbedded limestone, dolomite, sandstone, gray shale, and anhydrite in upper part; red arkosic sandstone and red shale in lower part	Present but not described from Senegal basin; in Essaouira basin (Société Chérifienne des Pétroles, 1966, Pl. 2) interbedded limestone, dolomite, sandstone, gray shale, and anhydrite in upper part; red sandstone and red shale in lower part.
Environment of deposition inferred from lithology and paleontology		
Tertiary	Shallow-water marine	Shallow-water marine and continental
Upper Cretaceous	Shallow-water nearshore marine including beach deposits; interfingering continental deposits in lower part	Shallow-water nearshore marine including beach deposits; interfingering continental deposits in lower part
Lower Cretaceous	Shallow-water marine	Shallow-water marine
Upper Jurassic(?)	Shallow-water marine with interfingering continental deposits	Shallow-water marine with interfingering continental deposits
Mean rate of subsidence (cm/1,000 year) near present coastline derived from sediment thickness		
Tertiary (1–70 m. y.)	1.3	0.9
Upper Cretaceous (70–102 m. y.)	2.5	3.8
Lower Cretaceous (102–135 m. y.)	2.6	8.8
Upper Jurassic(?)(135–157 m. y.)	1.9	2.3
Upper Jurassic(?)-Tertiary (1–157 m. y.)	1.9	3.3
Tectonic phase		
Tertiary	Epeirogeny (relatively slow or discontinuous subsidence)	Early Cenozoic Alpine orogeny followed by epeirogeny (relatively slow or discontinuous subsidence)
Late Cretaceous	Epeirogeny (relatively fast subsidence)	Epeirogeny (relatively fast subsidence)
Early Cretaceous	Epeirogeny (relatively fast or discontinuous subsidence)	Epeirogeny (relatively fast subsidence)
Late Jurassic(?)	Epeirogeny (moderately fast subsidence)	Epeirogeny (moderately fast subsidence)
Late Triassic	Tensional rifting and volcanism	Tensional rifting and volcanism
Post-Devonian	Orogeny	Orogeny
Rates of sea floor spreading (cm/year) from Mid-Atlantic Ridge between lats. 10° and 46°N interpreted from magnetic anomalies according to Vine and Matthews (1963) hypothesis		
0–6 m. y.	1.3 (Phillips, 1967)	
6–10 m. y.	1.7 (Phillips, 1967)	
10–40 m. y.	Lapse (Ewing and Ewing, 1967; Langseth *et al.*, 1966; Schneider and Vogt, 1968)	
70–120 m. y.	3.3–3.8 (LePichon, 1968)	

lying Mesozoic strata of the Aaiun basin is associated with the Hercynian orogeny (Querol, 1966).

6. A Precambrian structural high (Guinea arch or Liberia-Upper Volta uplift) trends ENE-WSW nearly parallel with a WSW seaward deflection of the Mauritanides fold belt south of Senegal (Lavrov and Syrskiy, 1967; Sheridan *et al.*, 1969, Fig. 6; Sougy, 1962, Fig. 1).

7. Late Triassic continental redbeds and evaporites, including rock salt interbedded with basaltic lavas, are distributed in linear trends nearly parallel with the continental margin beneath the Essaouira and Aaiun basins (Martinis and Visintin, 1966, Fig. 11; Querol, 1966; Reyre, 1966b, Fig. 3; Société Chérifienne des Pétroles, 1966, Figs. 1, 2). The distribution of these deposits suggests that they may be contained within grabens faulted into underlying Paleozoic rocks. Grabens filled with Triassic(?) coarse clastic beds were found by seismic methods and drilling near the hingeline of the Aaiun basin (Querol, 1966). Basic dikes intrude Ordovician to Upper Devonian strata in the western part of the Tindouf basin. Late Triassic basalt sills and dikes cut the Paleozoic rocks, including the Westphalian of the Taoudenni basin (Furon, 1963).

Asymmetries

Asymmetries in the Paleozoic frameworks of the opposing continental margins include the following.

1. The Appalachian fold belt appears to curve more regularly than the Mauritanides fold belt. The north-south trend of the Mauritanides fold belt is deflected at intersections with the east-northeast trending Anti-Atlas, Reguibat, and Guinea Precambrian highs (Fig. 1). Precambrian highs on the corresponding landward side of the Appalachian fold belt—the Nashville dome, Cincinnati and Findlay arches, and Adirondack uplift—do not trend transverse to the fold belt and are not associated with marked deflections.

2. Precambrian through Early Permian rocks are involved in the southern Appalachian fold belt and adjacent plateau province. Precambrian through Devonian strata are involved in the Mauritanides fold belt and the upper Paleozoic is apparently absent and is represented by a surface of unconformity beneath the Mesozoic (Fig. 5; Haughton, 1963; Sougy, 1962). Clastic Carboniferous deposits in the Tindouf basin thicken eastward and presumably were derived from the west during an incipient phase of the Hercynian orogeny (Querol, 1966).

Symmetries

In several respects, the southern Appalachian and Mauritanide mountain systems appear to be nearly mirror images in space and time within the limitations of geologic resolution.

1. Miogeosynclinal and eugeosynclinal deposits can be recognized in the Appalachian and northwest African geosynclines.

2. Gently deformed Paleozoic strata are present as forelands interior to the folded mountain belts.

3. The fold belts are both two sided. A zone of folded Paleozoic strata trends nearly parallel with each continental margin and was folded mainly after the Devonian within the Paleozoic. A metamorphic zone parallels the seaward margins of both fold belts and appears to be overfolded or thrust primarily in a landward direction.

4. Metamorphosed and unmetamorphosed Paleozoic strata and igneous rocks, depending on locality, incline seaward under a seaward-thickening wedge of Mesozoic through Cenozoic shallow-water marine and continental strata deposited in basins beneath the coastal plain and continental shelf.

5. The orientation of the Anti-Atlas and Reguibat Precambrian highs nearly transverse to the regional trend of the Mauritanides fold belt is similar to that of the Cape Fear arch which extends beneath the coastal plain and continental shelf as a transverse structural salient from the anticlinorium of the Blue Ridge province (Fig. 1; Hersey *et al.*, 1959; Woollard *et al.*, 1957). The Guinea arch and the Peninsular arch are both near apparent southern terminations of the respective fold belts (Fig. 1). Further investigation should evaluate the possibility of predrift "matches" between these structures.

6. The lithologic sequences and thicknesses of Jurassic(?) through Tertiary sedimentary strata generally correspond beneath the opposing continental margins.

7. Late Triassic continental redbeds intercalated with basaltic lava flows along the northwest African continental margin suggest that a fault-block basin system may be present corresponding to the Late Triassic system of eastern North America.

OFFSHORE RESIDUAL MAGNETIC ANOMALIES

Major features of the residual magnetic fields measured over the offshore parts of the two continental margins appear broadly symmetric.

1. Positive magnetic anomalies are associated with the edges of the continental shelves off both continental margins. A positive magnetic anomaly is associated with the shelf edge off eastern North America at least as far south as Cape Hatteras (Drake *et al.*, 1963; Taylor *et al.*, 1968). Positive magnetic anomalies are associated with the shelf edge in profiles A and B off Punta Durnford and Cap Blanc (Figs. 1, 4, 6).
2. A magnetic boundary between relatively rough (seaward) and smooth (landward) magnetic fields is found nearly parallel with each of the continental margins (Fig. 1; Heirtzler and Hayes, 1967, Fig. 3). The magnetic boundary strikes NNE-SSW about 500 km seaward of Cape Hatteras near the western margin of the Bermuda Rise. The magnetic boundary strikes north-south about 550 km seaward of Cap Blanc coincident with the middle of the continental rise (Fig. 4; Rona *et al.*, 1969). South of the Guinea arch the magnetic boundary appears to turn east and run along the base of the continental slope (Krause, 1964; Dickson, *in* Sheridan *et al.*, 1969).
3. Successive magnetic anomalies seaward from the magnetic boundary can be correlated in a N-S-striking linear band about 300 km wide parallel with the magnetic boundary from about the latitude of the Cape Verde Islands to just south of the Canary Islands (Rona *et al.*, 1969). Certain magnetic anomalies within this band show mirror-image correlations with a similar NNE-SSW-striking band of linear magnetic anomalies seaward of the magnetic boundary off Cape Hatteras (Schneider *et al.*, 1969).
4. Magnetic anomalies over the Mid-Atlantic Ridge near 27°N are parallel with the ridge axis and fairly symmetric about the ridge axis out to a distance of at least 100 km (Phillips, 1967).

The symmetry of the magnetic boundary and associated parallel anomalies off Cape Hatteras and Cap Blanc is consistent with the interpretation of the magnetic anomalies as remanent according to the Vine and Matthews (1963) hypothesis. The magnetic anomalies may have been generated by polarity reversals and recorded in magnetic rocks symmetrically spreading away from the Mid-Atlantic Ridge (Holmes, 1931; Hess, 1962; Dietz, 1961).

The significance of the magnetic boundary is problematic. Interpretation of the magnetic boundary as a remanent magnetic anomaly according to the hypothesis of sea-floor spreading implies that at the time of generation of the magnetic boundary the opposing continental margins at Cape Hatteras and Cap Blanc were about 1,050 km apart on the basis of the present distances of the magnetic boundaries from the two capes. The magnetic boundary is interpreted as an isochron in the age range of 250–200 m.y. (Middle Permian to Middle Triassic; Heirtzler and Hayes, 1967) or 190 m.y. (Late Triassic; Schneider *et al.*, 1969).

OFFSHORE STRUCTURAL DEFORMATION

Continental Margin Off Cape Hatteras

A seismic reflection profile recorded along azimuth 130° reveals the configuration of sedimentary strata beneath the continental slope, continental rise, and abyssal plain off Cape Hatteras (Fig. 3). The continental terrace off Cape Hatteras consists of a constructional continental shelf underlain by sedimentary strata with low ($<1°$) seaward inclinations which are truncated at an erosional continental slope (Rona and Clay, 1967). North of Cape Hatteras the stratal terminations are buried progressively by a sedimentary cover that mantles the continental slope (Rona, 1969c).

Horizon A is the deepest reflection interface visible on the profile (Fig. 3) and can be traced seaward under the lower continental rise and Hatteras abyssal plain (180–590 km), and beneath the margin of the Bermuda Rise (590–645 km). As a relict abyssal plain of Late Cretaceous or Eocene age (J. Ewing *et al.*, 1966) Horizon A is both a structural and a time datum. It is a nearly horizontal interface under the lower continental rise and Hatteras abyssal plain; thus sediments comprising the continental rise and Hatteras abyssal plain were deposited during the Cenozoic and any deformation in strata above Horizon A must be limited to shallow gravitational displacement processes. Such processes acting above Horizon A are inferred to include massive rotational slumping of strata from the outer continental terrace onto the upper continental rise and gravitational gliding of strata beneath the continental rise along bedding planes inclined nearly parallel with the sediment-water interface (Rona and Clay, 1967). Beneath the western margin of the Bermuda Rise, Horizon A and overlying strata are deformed into undulations produced either by differential compaction of sediment over basement topography or, more likely, by Cenozoic structural deformation involving differential vertical components of movement of basement blocks (Rona and Clay, 1967, Fig. 6).

Regional Geology of Northwest African Offshore Continental Margin

From the Strait of Gibraltar at least as far south as the Canary Islands, sedimentary strata beneath the continental terrace are strongly folded and faulted (McMaster and Lachance, 1968). The structural deformation probably is related to Alpine tectonic activity of the Mediterranean region.

North of Cap Blanc, strata underlying the coastal plain and continental terrace of the Essaouira and Aaiun basins are involved in down-to-basin normal faulting related to seaward subsidence (Martinis and Visintin, 1966; Querol, 1966). South of Cap Blanc, the continental terrace of the Senegal basin is underlain by Jurassic(?) through Upper Cretaceous (Maestrichtian) strata which are faulted, weakly folded, and intruded chiefly by Miocene and Quaternary igneous rock (de Spengler *et al.*, 1966, Fig. 3). The structures of the Senegal basin are controlled primarily by block faulting of the crystalline basement. An inferred direction of block faulting is along subsidence flexures regionally parallel with the coast. Strata underlying the coastal plain and continental terrace at Cap Blanc also may be involved in block faulting of the crystalline basement.

On the partly volcanic island of Fuerteventura (eastern Canary Islands) about 100 km from the African coast (Fig. 1), a stratigraphic section more than 1,000 m thick consists of Jurassic(?) marine limestone, sandstone, siltstone, and shale, through shallow-water Eocene marls. The Fuerteventura section is lithologically similar to known Lower Jurassic through Eocene strata in the Aaiun basin (Rothe, 1968). The sedimentary strata on Fuerteventura are folded with NW-SE axial strikes and are partly overturned (Fuster *et al.*, 1968); the difference between the strike of the fold axes and the NNE strike of associated basaltic and trachytic dikes and flows emplaced from Oligocene to Holocene time suggests independent structural origins (Abdel-Monem *et al.*, 1967; Fuster Casas and Aguilar Tomas, 1965; Hausen, 1958; Rothe, 1968; Rothe and Schmincke, 1968). Seismic refraction profiles of the 1967 *Meteor* expedition indicate that the crust is continental between Africa and Fuerteventura (Kegel, 1968) and is oceanic west of Fuerteventura (Dash and Bosshard, 1968). Abrupt thinning of unconsolidated sediment from more than 6 km to less than 1 km between Fuerteventura and Gran Canaria, the next island west, indicates the presence of a major fault (Dash and Bosshard, 1968). The NE-SW elongation and linearity of the eastern Canary Islands suggest that the fault system trends parallel with the long coasts of these islands and the adjacent African continental margin.

Sedimentary sections also are exposed on the chiefly volcanic Cape Verde Islands. Late Jurassic (Tithonian) to Early Cretaceous (Aptian) deep-water siliceous limestone containing *Aptychus (Lamellaptychus) rectecostatus* is exposed on the island of Maio in the eastern Cape Verde Islands (Colom, 1955; Pires Soares, 1948, 1953; Sousa Torres and Pires Soares, 1946; Stahlecker, 1934). The post-Aptian in the Cape Verde Islands is predominantly of shallower water origin and includes Cretaceous limestone and clay, intercalated with basalt, and Eocene (Lutetian?) marl. The Late Jurassic though Eocene (Lutetian?) sedimentary strata are intensely folded.

Continental Margin Near Cap Blanc

Profile A (Figs. 1, 4) was recorded along azimuth 290° from the middle of the continental shelf off Punta Durnford, the Spanish Sahara, across the continental slope and continental rise, to the abyssal hills. The seismic reflection profile reveals several major features of the sedimentary layer which are seen in greater detail on profiles B-E (Figs. 6–9). The magnetic profile shows a transition between rough and smooth magnetic fields at the magnetic boundary over the middle of the continental rise (Fig. 4).

Outer Continental Terrace Off Cap Blanc

Profile B extends from the middle of the continental shelf off Cap Blanc to the upper continental slope (Figs. 1, 6). The features observed on profile B are similar to those observed in the corresponding section of profile A 400 km north (Figs. 1, 4).

Profile B shows that the margin of the continental terrace is compounded of at least four components, which are described hereafter in stratigraphic succession.

1. A buried margin of the continental terrace is represented by the shaded areas labeled *1* beneath the present margin of the continental terrace in profiles A and B. The buried margin consists of an outer continental shelf constructed of strata with low ($<1°$) seaward in-

Table 3. Locations of Profiles in Figures 3–4 and 6–9

Profile	*From*		*To*		*Physiographic Province*
	Lat. N	*Long. W*	*Lat. N*	*Long. W*	
Cape Hatteras	35°12′	74°59′	31°28′	69°44′	Continental slope to Bermuda Rise
A	23°34′	16°35′	26°33′	25°48′	Continental shelf to abyssal hills
B	21°27′	17°18′	21°38′	18°02′	Continental shelf to upper continental slope
C	24°20′	19°12′	22°13′	20°02′	Upper continental rise
D	25°52′	24°33′	24°20′	24°27′	Lower continental rise
E	26°33′	25°48′	24°12′	28°23′	Abyssal hills

clinations and an erosional continental slope which truncates strata underlying the associated shelf. The buried shelf break is at about 600 m (0.6 sec) subbottom or 700 m below sea level. In profile A (Fig. 5) the erosional continental slope can be traced downward at a constant inclination of about 5° beneath the base of the present continental slope to the limit of seismic penetration at about 1 km (1 sec) subbottom.

The buried erosional continental slope apparently controls the seaward limit of sedimentary progradation across the present continental shelf by demarcating a line between regions of erosion and deposition in the overlying sediments. The updip projection of the buried erosional continental slope aligns with the present upper continental slope and shelf break in profile B (Fig. 6). Semiconsolidated sediment of the buried continental margin supports the weight of overlying unconsolidated sediment. The overlying unconsolidated sediment that progrades beyond the buried shelf break has sheared under its own weight along the updip projection of the buried erosional continental slope. As a result of gravitational shearing, the present shelf break is about 5 km landward of the buried shelf break. Gravitational shearing limits either seaward progradation or landward retreat of the continental terrace. As a consequence of the geometry, successively younger shelf breaks migrate landward in small increments, so that the present shelf break should be about 100 km landward of an original shelf break (Jurassic?), presumably buried beneath the toe of the continental slope.

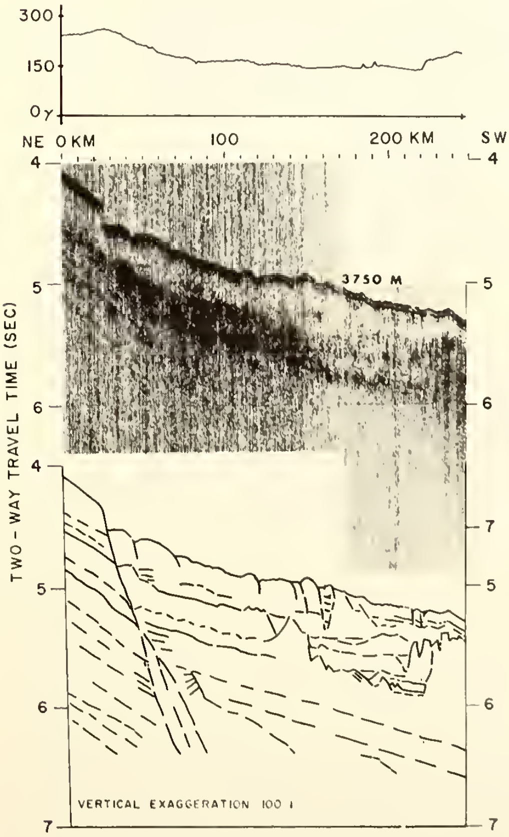

Fig. 7.—Profile C traverses section of upper continental rise.

2. A buried shelf break at about 200 m (0.2 sec) subbottom or 300 m below sea level overlying the buried continental terrace margin is constructed of foreset bedding. The foreset beds may have been deposited by a fluviatile delta during a former pluvial climatic regime when a higher precipitation/evaporation ratio prevailed.

3. The present shelf break is 100 m below sea level. The present continental shelf is constructional and the upper continental slope is erosional with an inclination of about 5° down to 500 m below sea level.

4. A cover of acoustically transparent sediment labeled *2* in profiles A and B conformably mantles the continental slope. The upper margin of the sedimentary cover begins sharply at 500 m below sea level, coincident with a decrease in the mean inclination of the continental slope from 5 to 2° and forms a convex-up-

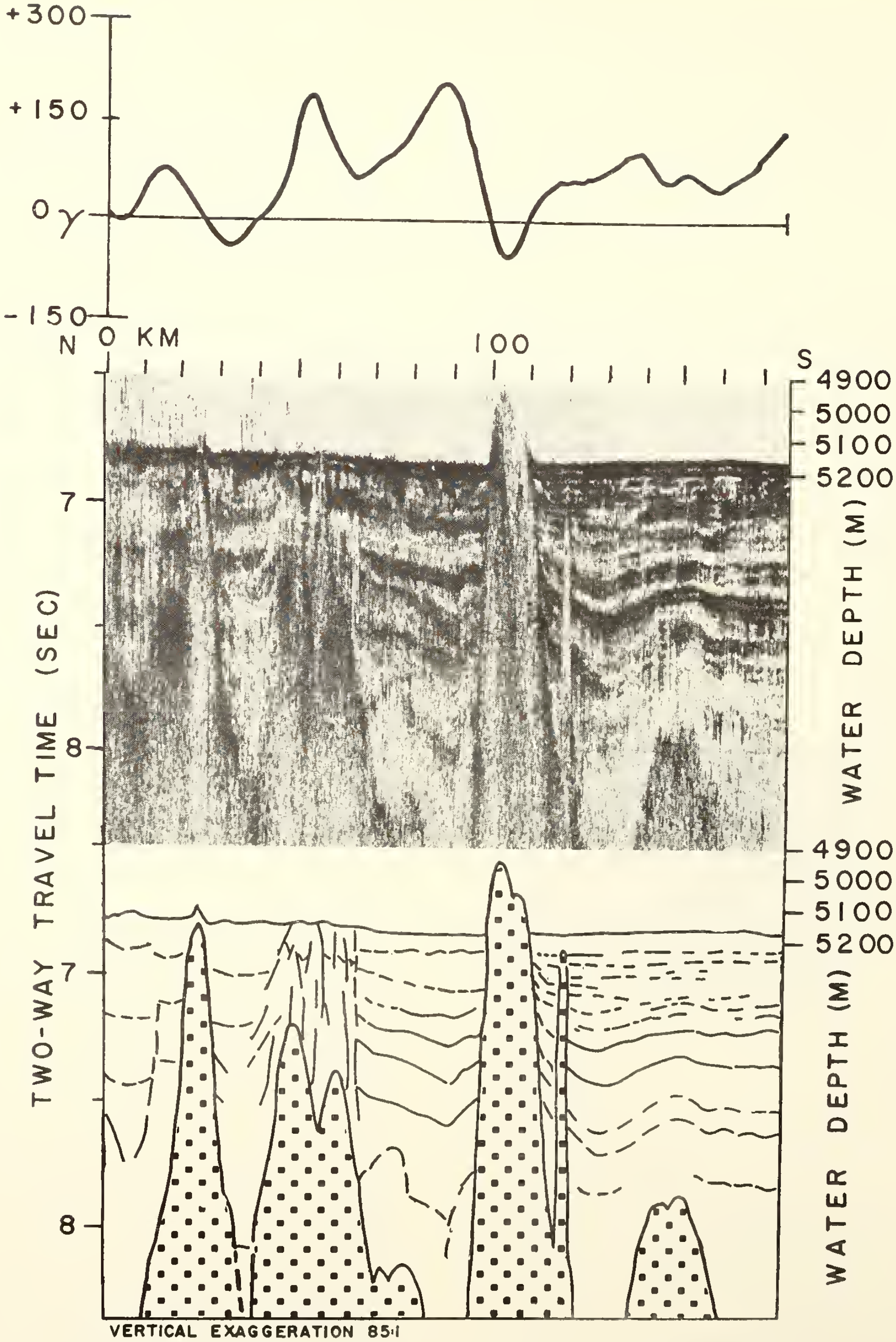

Fig. 8.—Profile D traverses section of lower continental rise (after Rona, 1969e).

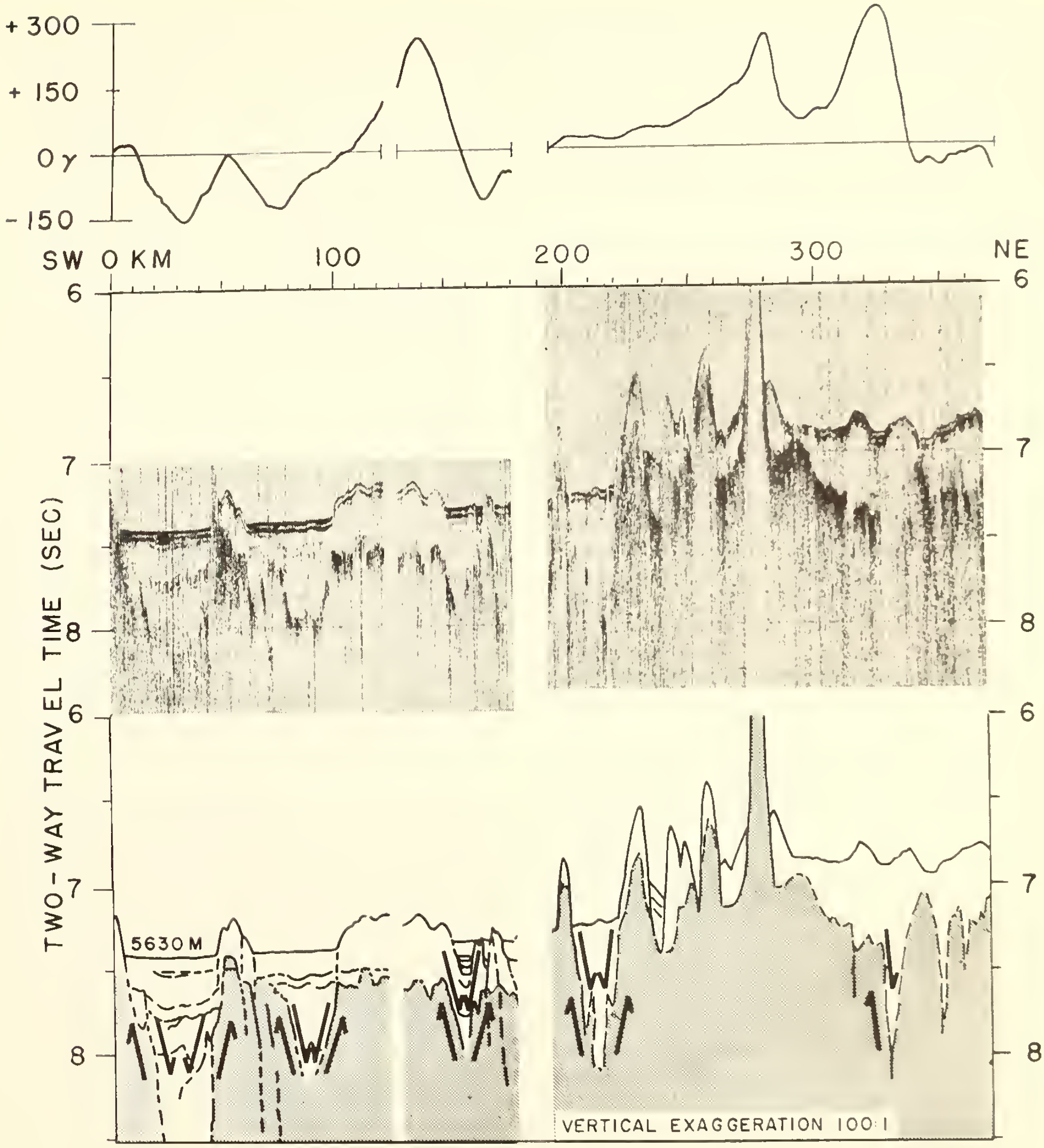

FIG. 9.—Profile E traverses section of abyssal hills.

ward bulge. The sedimentary cover can be traced continuously as a transparent interval about 500 m (0.5 sec) thick on profile A (Fig. 4) down the continental slope, over the upper continental rise, beneath irregular topography at the transition between the upper and lower continental rise where the cover thins to about 200 m (0.2 sec), and over the lower continental rise where the cover lenses out. The cover probably is composed of lutite on the basis of analogy with other transparent sediment. Deposition of the cover has built out (prograded) the continental slope and built up the continental rise.

The two major components described from the northwest African continental terrace, labeled *1* and *2* on profiles A and B (Figs. 4, 6), are identified in the middle Atlantic continental terrace of eastern North America (Rona, 1969c). The continental terrace off Cape Hatteras consists of a constructional continental shelf and an erosional continental slope corresponding to component *1* which forms the basic stratigraphic framework of the two continental margins (Figs. 2, 3). North of Cape Hatteras the erosional continental slope is progressively prograded by a sedimentary cover, shaped by ocean currents, corresponding to component *2*. The identification of corresponding components in the opposing continental margins indicates that the major change in sedimentary regimen from component *1* to component *2* may have affected both sides of the North Atlantic simultaneously.

By control of deposition and erosion, ocean currents that flow adjacent to the ocean bottom have been important agents in shaping the continental slope and rise off Cape Hatteras during the Cenozoic (Heezen *et al.*, 1966; Rona, 1969c; Rona *et al.*, 1967). The North Atlantic deep water originates in sub-Arctic regions of the North Atlantic. As its southward flow is influenced by the Coriolis force, it branches into a strong concentrated western current (Western Boundary Undercurrent), which flows over the continental slope and rise of eastern North America, and a weak diffuse eastern current, which apparently flows over the continental slope and rise off northwest Africa (Defant, 1961; Wüst, 1957). Deposition of the sediments that compose the continental rise off Cape Hatteras is controlled primarily by the Western Boundary Undercurrent, so deposition of the much wider continental rise off Cap Blanc may be related to the wider area presumably covered by the diffuse eastern current. The transparent sedimentary cover which mantles the continental slope and rise off Cap Blanc is thicker than that off Cape Hatteras, possibly because of greater sediment accumulation under the weaker bottom-current regime off Cap Blanc.

A sharp topographic change occurs about 400 m below sea level on the upper continental slope off Cape Hatteras coincident with the boundary between the Western Boundary Undercurrent flowing southwest and the overlying Florida Current of the Gulf Stream flowing northeast (Rona, 1970). The sharp upper margin of the sedimentary cover at 500 m below sea level off Cap Blanc also may coincide with a boundary between ocean currents. The irregular topography and thinning of the sedimentary cover at the transition between the upper and lower continental rise off Cap Blanc have counterparts off Cape Hatteras where these features are attributed to erosion in a zone of accelerated ocean-current flow (Schneider *et al.*, 1967). The apparent absence off Cap Blanc of lower continental rise hills, the presence of which off Cape Hatteras is related to deposition controlled by the Western Boundary Undercurrent (Fox *et al.*, 1968; Rona, 1969d), may be attributed to the generally weaker bottom-current regime that has prevailed off Cap Blanc.

Upper Continental Rise Off Cap Blanc

Sedimentary strata beneath the upper continental rise between 100 and 300 km along profile A (Fig. 4) have a broad concave-upward configuration extending to the limit of seismic penetration at about 1 km (1 sec) subbottom. Profile C (Figs. 1, 7) intersects this section of profile A.

Profile C crosses a scarp with about 150 m of topographic relief on the upper continental rise. The scarp can be traced downdip as a fault plane which extends at least 2 km through the underlying sedimentary strata. The relative vertical component of displacement along the fault has been down to the southwest as deduced from the topographic scarp. The association of the fault with a broad 100-γ step in the residual magnetic profile indicates that magnetic basement is involved in the faulting. An azimuth of 109° ± 5° is established for the fault by three transverse crossings about 50 km apart (24°01′N, 18°54′W; 24°07′N, 19°19′W; 24°10′N, 19°24′W). The position and azimuth of the fault coincide with the eastward projection of a fracture zone which crosses the axis of the Mid-Atlantic Ridge near 30°05′N, 42°30′W (Fig. 1), where the ridge axis appears to have right-lateral offset of about 100 km (Heezen and Tharp, 1968); the projection of the fracture zone westward from the Mid-Atlantic Ridge intersects the New England Seamount Chain. A right-lateral offset of about 100 km is observed in the position of the magnetic boundary and the N-S-trending band of linear residual magnetic anomalies north and south of the fault (Rona *et al.*, 1969). The broad concave-upward configuration of strata observed beneath the upper continental rise in profile A may be folding produced by motion along this fault.

The fault may be one of a class of faults designated "'transform" (Wilson, 1965). Where crossed in profile C (Fig. 7) it is about 500 km south and parallel with the eastward projection of an inferred mid-Paleozoic right-lateral fault which may extend from the Appalachian fold belt through the New England Seamount Chain

(Drake and Woodward, 1963) and which may have joined the South Atlas fault before continental drift (Drake *et al.*, 1968, Fig. 15). A similar fracture zone is inferred to have extended across the Atlantic in the Mesozoic on the basis of geometric considerations of continental rotation during continental drift (LePichon, 1968, Fig. 9). With the possible exception of the South Atlas fault, the dominant NW-SE and NE-SW directions of the fracture system of the African continent as shown by Furon (1963, Fig. 3) do not correspond to the WNW-ESE directions of the present fracture zones which cross the Mid-Atlantic Ridge (Fig. 1).

Lower Continental Rise Off Cap Blanc

The lower continental rise on profile A (Fig. 4) is underlain to at least 1.5 km (1.5 sec) seismic penetration by sedimentary strata with the configuration of undulations. The undulations have wavelengths of about 20 km and are repeated in phase through the overlying sedimentary column up to the sediment-water interface, where some of the crests underlie topographic highs.

Profile D crosses the lower continental rise near where the undulations are seen on profile A (Figs. 1, 8). Bodies with nearly conical cross sections are buried to varied depths by sedimentary strata which reach a thickness of at least 1.5 km (1.5 sec). The bases of the bodies continue to diverge downward at the limit of seismic penetration beneath the bottom. Some of the bodies have pierced overlying sedimentary strata and form topographic highs with relief up to about 225 m as seen at 100 km; other bodies are buried and lack topographic expression. The fact that individual bodies cannot be correlated between adjacent seismic profiles indicates that they are more circular than elongate in map view (Rona, 1969b). Sedimentary strata have a convex-upward configuration above the crests of the buried bodies and a concave-upward configuration between them. The concave configuration between bodies generally decreases upward toward the sediment-water interface. The sedimentary strata maintain a nearly constant thickness over and between the buried bodies, and turn upward at their margins. Fault systems, apparently of tensional origin, have formed above certain buried bodies, *e.g.*, 40 and 70 km along the profile shown (Fig. 8). The bodies generally are associated with low values of magnetic intensity. Profile D was recorded along a north-south track nearly parallel with the strike of magnetic anomalies interpreted as remanent in this region (Rona *et al.*, 1969), so the low values of magnetic intensity associated with the bodies may be structurally induced. Bodies with similar characteristics are observed on all my seismic profiles which cross the lower continental rise within the area investigated between lats. 21°N and 27°N, and are identified tentatively on a profile which crosses the adjacent abyssal plain (Rona, 1969c, Fig. 1). The depth range of such bodies is from approximately 4,685 to 5,670 m below sea level at distances between about 650 and 1,300 km from the African coast. No similar bodies are visible to about 1.5 sec (1.5 km) penetration beneath the upper continental rise.

Two alternative interpretations of the bodies and the configuration of surrounding sedimentary strata are possible. One is that the bodies are buried topographic features and the configuration of the surrounding sedimentary strata was produced by differential compaction of sediment over the buried topography. Specifically, the bodies may be buried volcanic seamounts rising from layer 2, the layer defined by intermediate values of seismic velocity in the ocean basins.

This interpretation is considered unlikely for several reasons. First, the height of the bodies appears to be related to the thickness of sediment. They are not observed more than 1 km beneath the sediment-water interface or 300 m above the sediment-water interface. But no regular relation between height of body and sedimentary thickness would be expected for topography on layer 2 which ranges in height from several meters to several kilometers. Moreover, the shapes of the bodies are symmetric and smooth, contrary to expectations for buried topography; the bodies are not associated with positive magnetic anomalies as may be induced by topography involving magnetic rocks; and sedimentary strata do not thin over bodies and thicken between them as would be expected in differential compaction, but are of nearly constant thickness.

The second possible interpretation is that the bodies intrude the sedimentary strata. The deformation of the sedimentary strata associated with the bodies (Rona, 1968) and particularly the nearly constant thickness of strata over and between bodies, the abrupt upturn of strata on the flanks, and the presence of faults above certain bodies support this interpretation.

The intrusive bodies could be either igneous intrusive masses or diapirs containing salt or clay.

The low values of magnetic intensity associated with the bodies can be interpreted to indicate either low induced magnetization of salt-clay diapirs or reversed remanent magnetization in an igneous mass. The igneous interpretation is considered unlikely because it necessitates emplacement of all the bodies during a single period of magnetic reversal in order for them to record low values of remanent magnetic intensity. Gravity data are required for an unequivocal geophysical distinction between the two types of intrusive bodies cited.

The seismic reflection profiles resemble those of unsampled diapirs in the Mediterranean basin (Glangeaud, 1966; Glangeaud *et al.*, 1967; Hersey, 1965; Menard *et al.*, 1965; Watson and Johnson, 1968) where Triassic evaporites are found (Gill, 1965), and also profiles of diapirs in the Gulf of Mexico (Moore and Curray, 1963; Uchupi and Emery, 1968) of probably Late Triassic and known Middle Jurassic rock salt (Murray, 1961). The possible salt diapirs in profile D are similar in cross-sectional dimensions to those which form the Sigsbee Knolls at about 3,800 m below sea level near the middle of the Gulf of Mexico (Ewing *et al.*, 1958; Worzel *et al.*, 1968). JOIDES drilling has shown the latter to be salt diapirs and samples of caprock contain a probably Middle to Late Jurassic pollen-spore assemblage (Burk *et al.*, 1969). Diapirs containing Late Triassic (Keuper) and Jurassic rock salt are reported from the Essaouira and Aaiun basins (Fig. 1; Querol, 1966; Societé Chérifienne des Pétroles, 1966). In the Essaouira basin Upper Triassic saliferous red shales (les argilles d'Argana) reach a thickness of 1,200 m; in the western Essaouira basin near the Moroccan coast the Upper Triassic terminates upward with rock salt interbedded with numerous layers of basalt. Offshore seismic work has revealed subcircular uplifts with the characteristics of salt diapirs on the continental shelf off the Aaiun basin (R. E. King, *in* Querol, 1966, p. 39). Salt diapirs present in the offshore Senegal basin (Figs. 1, 5; Aymé, 1965) are of pre-Aptian age, "probably Early Jurassic or Triassic like the Louann Salt of Texas-Louisiana" (J. M. Aymé, personal commun.). Bodies with physical characteristics similar to those described from profile D have been observed on the Cape Verde Rise where they are interpreted to be salt diapirs (Schneider *et al.*, 1969).

Therefore, geophysical data and regional geology are consistent with the view that the observed bodies (Fig. 8) are salt domes (Rona, 1969e). If this interpretation is correct the salt source beds must be deep within the sedimentary layer or interstratified with basalt layers beneath the overlying sedimentary layer. The minimum rate of ascent of those diapirs that have reached the sediment-water interface must exceed the minimum rate of sediment accumulation, which is 0.5 cm/1,000 year measured in a core containing Pleistocene lutite from the upper continental rise southwest of the Canary Islands (Ericson *et al.*, 1961). At this rate, a maximum time of ascent of 200–600 m.y. would be required for the salt to rise through the sedimentary layer, which is 1–3 km thick in the vicinity of the Canary Islands (Dash and Bosshard, 1968). Diapirism may be suppressed beneath the upper continental rise by the thick sedimentary overburden (Parker and McDowell, 1955). The observed structures are situated to about 700 km seaward of the magnetic boundary (Fig. 1) which is interpreted as an isochron in the age range of 250–190 m.y. (Heirtzler and Hayes, 1967; Schneider *et al.*, 1969) according to the hypotheses of sea-floor spreading. If a spreading rate of 2 cm/year is assumed, the magnetic sea floor underlying the most seaward of these structures would be about 35 m.y. younger than that at the magnetic boundary, or of Middle Jurassic age.

Abyssal Hills Off Cap Blanc

The abyssal plain off Cap Blanc is restricted to a width of about 50 km where crossed by profile A (Fig. 4). The stacked reflections from nearly horizontally stratified interfaces characteristic of turbidite sequences of the Hatteras abyssal plain are practically absent here. The abyssal hills begin abruptly at 925 km along profile A as block-shaped topographic forms with steep sides that can be traced at least 1.5 km (1.5 sec) beneath the bottom at constant inclination.

Profile E crosses the abyssal hills transverse to the seaward end of profile A (Figs. 1, 9). Topographic blocks and troughs seen between 0 and 200 km along profile E range in width from 10 to 50 km. They are underlain by corresponding blocks and troughs in the acoustic basement, which is shaded in Figure 9. The topographic blocks, with relief of about 125 m, are mantled with acoustically transparent sediment. The intervening troughs are filled with sediment. The depositional slopes at the sides of the blocks incline several degrees. The sides of the underlying blocks in the buried acoustic basement are characterized by diffraction returns which indicate that their inclinations may exceed 45°. Residual magnetic highs coincide with blocks and lows coincide with troughs. The track of profile E is nearly parallel with the strike of regional magnetic lineations interpreted as remanent (Rona *et al.*, 1969); therefore, the magnetic anomalies associated with profile E may be attributed to structurally induced magnetization.

The blocks and troughs are interpreted as horsts and grabens. Inferred relative vertical components of motion are indicated with arrows in Figure 9. Recent movement is evidenced by deformation of sedimentary layers within the grabens. Horsts and grabens have been identified on the Mid-Atlantic Ridge at 22°N lat. (Melson *et al.*, 1968) and on the East Pacific and Gorda rises (Atwater and Mudie, 1968; Menard, 1960). Their presence suggests that the structures may originate under tension on a spreading oceanic ridge, as inferred on the East Pacific Rise (Menard and Mammerickx, 1967).

The regular structures interpreted as horsts and grabens between 0 and 200 km along profile E are complicated by additional features between 200 and 370 km. A volcanic seamount associated with a short-wavelength magnetic high is present between 270 and 280 km along profile E. Another magnetic high is centered at 325 km along the profile. A magnetic low intervenes between two magnetic highs. The volcanic seamount and the adjacent magnetic low are where profile E crosses the seaward projection of the fault identified on the upper continental rise in profile C (Fig. 7).

Inferred Mesozoic and Cenozoic History of Continental Margins Off Cape Hatteras and Cap Blanc

Atlantic Ocean Basin

Atlantic oceanic circulation in the Triassic and Early Jurassic was restricted by the inferred former positions of the continents. A fit between west Africa and South America is fixed in space by the matching of lithologic age provinces and geologic structures (Allard and Hurst, 1969; Hurley *et al.*, 1967) and comparative stratigraphy indicates that the two continents were nearly contiguous until the Cretaceous (Martin, 1961, 1968). A Paleozoic fit between Newfoundland and the British Isles is supported by the alignment of principal tectonic and stratigraphic belts (Kay, 1968), whereas the contiguity of Northern Europe, Greenland, and Laborador until about 70 m.y. ago follows from remanent magnetic anomalies (Avery *et al.*, 1968; Mayhew *et al.*, 1968).

During the Late Triassic and Jurassic, the Atlantic between the east coast of North America and the northwest coast of Africa may have been a restricted sea analogous to the Dead Sea during the Plio-Pleistocene, when 1–4 km of rock salt was deposited (Neev and Emery, 1967). The paleolatitudes of northwest Africa during the Late Triassic and Early Jurassic nearly coincide with the present latitudes, and the present latitudes of northwest Africa bracket the predominant climatic zone for evaporite deposition (Irving, 1964, Fig. 9.47).

The northwest African coastal basins apparently lack distinct seaward structural terminations. During the Late Triassic and Jurassic, when evaporites were being deposited in the coastal basins, suitable conditions for evaporite deposition may have extended at least 1,300 km seaward of the present northwest African coast, which is the distance of the farthest seaward possible salt diapir observed (Rona, 1969e). From considerations of symmetry about the magnetic boundary, the restricted Atlantic sea may have been twice this width or at least 2,600 km wide measured between Cape Hatteras and Cap Blanc (Fig. 10). The evidence for a proto-Atlantic about 1,000 km wide at the magnetic boundaries off Cape Hatteras and Cap Blanc (Drake *et al.*, 1968, Fig. 15) is consistent with a restricted Atlantic sea, and may represent an earlier stage of development. According to Arkell (1956, p. 605), "'The evidence from Jurassic stratigraphy requires the existence in Jurassic times of the North Pacific, North Atlantic, Scandic and Arctic oceans; it has nothing to contribute to the existence or non-existence of the South Atlantic."

This restricted Atlantic sea may have included or been temporarily connected with the evaporite basins which produced rock salt in the Gulf of Mexico and the Mediterranean. Like the salt in the Dead Sea, which is the first sediment restricted to the Dead Sea graben (Neev and Emery, 1967), the salt in the Atlantic sea may have been deposited initially within the tectonic setting provided by the Late Triassic rifting, evidence of which is provided by block faulting of that age parallel with the margin of eastern North America and, possibly, the margin of northwestern Africa. The inferred rock salt beds in the Atlantic may be partially interbedded with Late Triassic and Jurassic

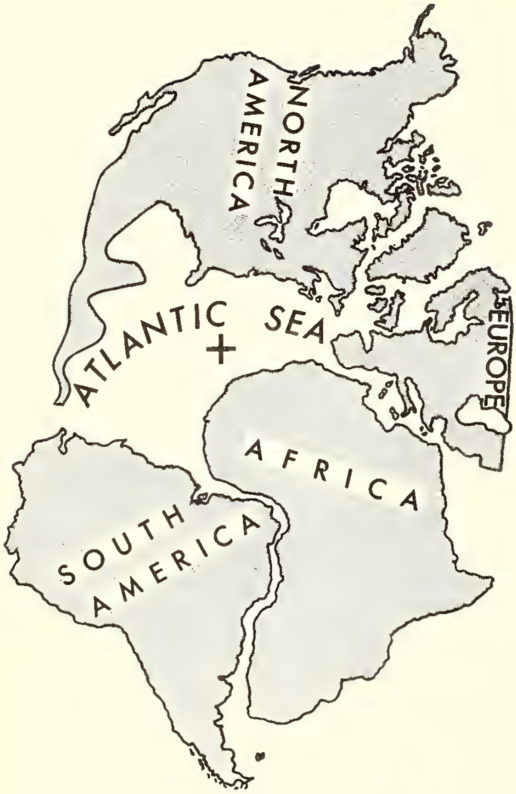

FIG. 10.—Interpretive sketch of Atlantic sea restricted by inferred positions of continents during Jurassic time. Cross marks region of possible salt diapirs.

basalt as observed in the western Essaouira basin and may be of comparable thickness.

The deposition of thick salt in the restricted Atlantic sea, as in the Dead Sea, would have required a saline source and would imply a limited connection between the restricted Atlantic sea and an exterior ocean. The presence in the Late Jurassic (Tithonian) of deep-water limestones on the Cape Verde Islands (Colom, 1955; Pires Soares, 1948, 1953; Sousa Torres and Pires Soares, 1946; Stahlecker, 1934), possibly on the eastern Canary Islands (Rothe, 1968), and east of the Bahamas (Ewing, 1969), together with the deposition of marine limestones in the northwest African coastal basins (Querol, 1966), indicate that the restriction on the Atlantic must have opened by that time. The opening of the barrier may have resulted from acceleration in the subsidence of the opposing continental margins and adjacent ocean basin in the Late Jurassic.

Rock salt deposits should be present beneath and seaward of the continental margin of eastern North America, corresponding in space and time to the rock salt deposits of northwestern Africa. In particular, Jurassic rock salt deposits should be present seaward of Cape Hatteras. Although salt diapirs had not been reported from the continental margin or adjacent ocean basin off eastern North America, the presence of such structures had been anticipated by the writer. Recently, McKelvey and Wang (1969) have shown salt diapirs on the Grand Banks south of Newfoundland. The Louann Salt of Jurassic(?) age may extend from the Gulf of Mexico coastal plain into northwestern Florida (Marsh, 1967) and minor rock salt deposits are reported in the Lower Cretaceous of southwestern Florida. The Upper Triassic redbeds of Connecticut were originally evaporitic in character, as evidenced by molds of salt and gypsum crystals in cavities (Cushman, 1964). Anhydrite beds are found in the Upper Jurassic (?) of the ESSO Hatteras Light Well No. 1 and the Lower Cretaceous of the North Carolina ESSO Well No. 2 (Swain, 1952). Thickening of evaporite deposits seaward of the coastal plain is indicated by two lines of evidence. First, the Jurassic(?) and Lower Cretaceous anhydrite beds interfinger increasingly with redbeds in a seaward direction in the Cape Hatteras region (P. M. Brown, *in* Manheim and Horn, 1968, p. 230) The second line of evidence concerns salinity and dissolved solids of interstitial waters from coastal-plain wells (Manheim and Horn, 1968). Salt concentrations greater than 100,000 ppm are found in pre-Late Cretaceous strata in the Salisbury embayment (Maryland and Delaware), Hatteras embayment, southernmost Georgia, and beneath the coast of Florida. The very saline interstitial waters generally are observed within, or near, sequences of evaporitic sediments and redbeds (varicolored shales, sandstones, and oölitic limestones). Relatively high concentrations of Na and Cl were measured in the interstitial waters from the ESSO Hatteras Light Well No. 1. The very saline interstitial waters may have moved updip from better developed evaporitic facies (Jurassic?) seaward of the coastal plain.

Continental Margins

The sequences of depositional environments on the opposing continental terraces, as inferred from lithology and paleontology, are similar from Jurassic(?) through Tertiary

(Table 2). The environment of deposition is influenced by the relative rates of sediment supply and subsidence, as well as by eustatic changes in sea level. A high rate of seaward subsidence of the continental terrace relative to sediment supply or a eustatic rise in sea level would result in an increase in water depth (marine transgression) and vice versa (marine regression). The effect of a change in rate of subsidence presumably would be limited geographically and that of a eustatic change in sea level would be worldwide.

The two continental terraces simultaneously underwent moderately fast mean rates of subsidence (1.9–2.3 cm/1,000 year) during Late Jurassic marine transgression, changing from the predominantly evaporitic and continental environments of the Triassic and Early Jurassic to a predominantly marine environment. A discrepancy in thicknesses of Lower Cretaceous strata indicates a relatively fast mean rate of subsidence at Cape Hatteras (2.6 cm/1,000 year) and an anomalously fast mean rate near Cap Blanc (8.8 cm/1,000 year) accompanied by marine transgression that produced shallow-water marine environments. Interfingering continental and marine beds in the lower Upper Cretaceous indicate alternating conditions of marine regression with transgression. The mean rates derived for the Upper Cretaceous (2.5–3.8 cm/1,000 year) indicate relatively fast subsidence accompanied simultaneously by marine transgression and shallow-water nearshore environments. The slowest mean subsidence rates for both continental terraces are derived for the Tertiary (1.3–0.9 cm/1,000 year), when a shallow-water marine environment prevailed through the late Eocene (Lutetian?), followed by marine regression and continental deposition (Continental Terminal) on large areas of west Africa until the Quaternary (Haughton, 1963). Unconformable surfaces on upper Eocene, upper Oligocene, and upper Miocene strata of the two continental margins (de Spengler *et al.*, 1966; Querol, 1966; Société Chérifienne des Pétroles, 1966; Swain, 1952) represent intervals of nondeposition and erosion.

Relation Between Atlantic Ocean Basin and Opposing Continental Margins

The Mesozoic and Cenozoic stratigraphic history of the continental margins in the vicinities of Cape Hatteras and Cap Blanc appears to correlate with what is known of the stratigraphic history of the adjacent ocean basin. As discussed, conditions for evaporite deposition may have extended from coastal basins into the adjacent ocean basin during the Late Triassic and Jurassic. The establishment of a normal marine environment on the opposing continental margins in the Late Jurassic occurred when deep-water sediments were deposited initially in the adjacent ocean basin, as inferred from sediments sampled in the Cape Verde and Canary Islands and east of the Bahamas.

Lower Cretaceous (Neocomian) algal calcarenites dredged from 5 km water depth near the base of the Blake escarpment have subsided from a shallow-water environment; Aptian-Albian calcilutites obtained from water depths of less than 3 km mark the establishment of a deeper water environment (Heezen and Sheridan, 1966). A shallow-water Lower Cretaceous fauna (Hauterivian-Barremian), possibly allogenic, and a deep-water Upper Cretaceous fauna (Cenomanian) were sampled in sediment cores east of the Bahamas from a water depth of about 5 km (Habib, 1968; Windisch *et al.*, 1968).

Abundant chert and siliceous shale have been sampled in Paleocene-Eocene sediments beneath Cape Hatteras (Swain, 1952), beneath the ocean basin between Cape Hatteras and Cap Blanc (Peterson, 1969), on the Canary and Cape Verde Islands (Rothe, 1968), and beneath the coastal basins of the northwest African continental margins (Querol, 1966; Socété Chérifienne des Pétroles, 1966). The widespread occurrence of silica indicates that similar physicochemical conditions simultaneously prevailed at the opposing continental margins and the adjacent ocean basin during the Paleocene-Eocene. Worldwide volcanism may have provided a widespread source, and patterns of vigorous oceanic circulation, established in the early Cenozoic after the inferred opening of the northernmost Atlantic and the South Atlantic (Rona, 1969d), may have distributed the silica in the oceans.

The possible Late Triassic–Jurassic salt deposits in the deep ocean basin off northwest Africa, the Jurassic(?) through Eocene stratigraphic similarities, and structural relations between the eastern Canary and Cape Verde Islands and the coastal basins together support the following regional synthesis.

1. Upper Triassic through Eocene strata laterally equivalent to strata in the coastal basins may have subsided beneath the entire continental terrace and continental rise in an area at least 1,700 km long between the Canary and

Cape Verde Islands, at least 200 km wide between Fuerteventura and the Aaiun basin, and at least 900 km wide between Maio and the Senegal basin. The eastern Canary and Cape Verde Islands may be parts of fault blocks that have undergone vertical uplift resulting in exposure of the Jurassic through Eocene strata.

2. The folded strata on the Canary and Cape Verde Islands may have been deformed by movements of the fault blocks that are inferred to form the islands.

Alternatively, the folded strata may be segments of a fold belt continuous with the folded strata beneath the continental shelf between the Canary Islands and the Strait of Gibraltar. The Eocene (Lutetian?) age of the youngest involved strata indicates that the folding is related to Alpine diastrophism. Uplift of the strata in fault blocks may have occurred during tensional relaxation following crustal compression. Upper Eocene sandstones in the Essaouira and Aaiun basins may mark initial stages of uplift.

Barbados Island in the Venezuela-Trinidad-Tobago fold belt may provide an analog to the folded-uplifted strata of the Canary and Cape Verde Islands. A sedimentary section is exposed on Barbados similar to that underlying the adjacent deep ocean basin (Beckman, 1953; Peterson, 1969, JOIDES Site 27; Senn, 1940, 1947; Trenchmann, 1933).

The stratigraphic record available suggests that the opposing continental margins and adjacent parts of the intervening ocean basin subsided simultaneously during most of the Mesozoic and Cenozoic. The continental crust underlying the continental margins has behaved as if vertically coupled to the adjacent oceanic crust. The stratigraphic evidence for vertical coupling is supported by the aseismic character of the Atlantic continental margins (Barzangi and Dorman, 1968), which indicates that differential movement between continental and oceanic crust is now negligible.

EPEIROGENY AND SEA-FLOOR SPREADING

According to the hypothesis of sea-floor spreading, the deep sea floor is supposed to be *coupled horizontally* to the opposing Atlantic continental margins and is moving the Atlantic continents apart as new sea floor is generated symmetrically at the Mid-Atlantic Ridge (Holmes, 1931; Hess, 1962; Dietz, 1961). *Vertical coupling* between the continental margins and the spreading sea floor is open to question.

The mean subsidence rates derived from stratigraphic thicknesses on the opposing continental margins are about 10^{-3} of the rates of sea-floor spreading estimated from magnetic anomalies according to the Vine and Matthews (1963) hypothesis. Rates of crustal spreading of 1–5 cm/year away from the Mid-Atlantic Ridge have been estimated (Pitman and Heirtzler, 1966). If the magnetic boundary off Cape Hatteras and Cap Blanc is interpreted as a 200-m.y. isochron, the mean rate of spreading from the Late Triassic to Quaternary would be about 1.2 cm/year. Mean rates of subsidence of the opposing continental terraces during the same time interval are, respectively, 1.9 and 3.3 cm/1,000 year (Table 2).

Tectonic processes generally are episodic. If the deep sea floor is coupled vertically to the continental margin, discontinuities in the processes of continental-margin subsidence and sea-floor spreading should be symmetric in space and simultaneous within the time constants of the processes involved. Discontinuities inferred in the rate of sea-floor spreading during the Mesozoic and Tertiary in the North Atlantic compare with the subsidence history of the opposing continental margins, as follows.

1. An active phase of Atlantic sea-floor spreading is inferred to have begun in the Mesozoic (LePichon, 1968), when accelerated subsidence of the opposing continental margins commenced.

2. A mean spreading rate of 3.3–3.8 cm/year is estimated from 120 to 70 m.y. ago between lats. 20°N and 40°N (LePichon, 1968). Mean rates of subsidence of 2.5–3.8 cm/1,000 year are derived from 102 to 70 m.y. ago for the Cape Hatteras and Cap Blanc continental terraces (Table 2).

3. A major change in the pattern of Atlantic sea-floor spreading between the Mesozoic and Cenozoic is inferred from discrepancies in direction between theoretical lines of flow and present fracture systems (Morgan, 1968). A major change in mean continental-margin subsidence rates occurred between the Mesozoic and Cenozoic (Table 2).

4. A Tertiary lapse in the spreading of the Mid-Atlantic Ridge between about 40 and 10 m.y. ago (late Eocene and late Miocene) is deduced from systematic discontinuities in topography, sediment thickness, age of crust, magnetic symmetry, and heat flow with distance away from the axis of the ridge between lats. 10°N and 45°N (Ewing and Ewing, 1967; Langseth *et al.*, 1966; Schneider and Vogt, 1968). A lapse in spreading is defined as an in-

terval during which sea-floor spreading decelerates, stops, starts, and accelerates. A marked decrease in the mean subsidence rates and possible post-late Eocene lapses in subsidence are inferred from the Tertiary stratigraphy of the opposing continental margins (Table 2).

The comparisons suggest that, to a first approximation, the mean subsidence rates of the opposing continental margins and the inferred mean spreading rates of the intervening sea floor have varied in unison during much of the Mesozoic and Cenozoic. This apparent covariation is consistent with the stratigraphic and seismologic data cited which indicate that the opposing continental margins and adjacent basins have behaved as if vertically coupled.

If continental crust is coupled both horizontally and vertically to oceanic crust in the area investigated, it is obvious that convective transfer of material could not involve differential movement between the two. Any convection beneath the continental margin would be subcrustal. The apparent covariation of mean rates of marginal subsidence and inferred mean rates of sea-floor spreading would favor explanation by *in situ* material volume changes produced by thermal and phase changes. Steady-state thermal-expansion models, which attribute uplift of the Mid-Atlantic Ridge to heat supplied by igneous intrusions, indicate subsidence rates at the ridge flanks of the same order of magnitude as at the opposing continental margins (Langseth *et al.*, 1966; Schneider and Vogt, 1968). Symmetric subsidence of the opposing continental margins would then be controlled by subsidence of the adjacent ocean basin as the opposing continental blocks move down the flanks of the ridge in response to bilateral spreading of the intervening sea floor. If the Mid-Atlantic Ridge is considered a heat source and the opposing continental margins heat sinks, nonsteady-state thermal expansion at the ridge attributable to discontinuities in sea-floor spreading would be communicated as changes in subsidence (or uplift) rates at the continental margins within the time constants of the processes involved. A lapse in sea-floor spreading, thermal contraction at the ridge caused by a decrease in the rate of heat supplied, eustatic lowering of sea level resulting from subsidence of the ridge, and symmetric decrease in subsidence rate of the opposing continental margins all should be related. Deciphering the precise relations will require detailed measurements and statistical studies of the sedimentary and magnetic stratigraphy.

Orogeny and Sea-Floor Spreading

The logic of plate tectonics may be applied to the southern Appalachian and Mauritanides mountain systems. The conditions that must be satisfied are (1) broadly symmetric development in space and time of the two mountain systems and (2) almost mirror-image compressional folding of the two mountain systems after the Devonian within the Paleozoic.

According to the principles of plate tectonics, the loci of compressional systems are the leading boundaries of moving blocks where these boundaries impinge against other blocks (Morgan, 1968). The compression may be expressed as a trench or as a folded mountain range (Isacks *et al.*, 1968, Fig. 2). The apparently simultaneous compression that produced the folding in the Appalachian and Mauritanide mountain systems implies that the motion of the North American and African blocks was convergent during the late Paleozoic. An Atlantic at least large enough to accommodate the marine deposits of the Appalachian and northwest African geosynclines must have existed in early and middle Paleozoic times.

The tension rifting that occurred during the Triassic is evidence of change to divergent motion between the North American and African blocks. The change from predominantly continental and evaporitic conditions on the opposing continental margins and intervening restricted Atlantic sea during the Triassic and Early Jurassic to a normal marine environment in the Late Jurassic apparently was produced by accelerated subsidence related to accelerated divergent motion. Magnetic and seismologic interpretations according to the hypothesis of sea-floor spreading suggest that motion between the North American and African blocks has been divergent throughout the Mesozoic and Cenozoic (Heirtzler *et al.*, 1968) and is now divergent (Sykes, 1968).

The estimated time of initiation of the inferred Tertiary lapse in crustal spreading from the Mid-Atlantic Ridge about 40 m.y. ago coincides with the initiation of Alpine orogenic movements on the northwest African continental margin. The northern margin of the African block moving generally eastward may have impinged against the southern margin of the Eurasian block moving southeastward to produce the compressional stress field required for the observed folding on the northwest African continental margin. A compressive period culminated in the Oligocene and Miocene in the Mediterranean (Glangeaud, 1962). Strata underlying the narrow southern California continental terrace appear to be folded in a manner similar to that of strata underlying the northwest African continental margin north of the Canary Islands (McMaster and Lachance, 1968; Moore, 1960). A compressional stress field may have been produced on the California continental margin by resistance to westward motion when the western border of North America overrode the adjacent Pacific trench system (Hamilton and Myers, 1966) and the East Pacific Rise (Menard, 1964; Vine, 1966; Wilson, 1965). The resistance offered by either the northwestern continental margin of Africa or the western continental margin of North America, or both, during the Eocene may have contributed to the slowing and temporary stopping of the sea-floor spreading from the Mid-Atlantic Ridge. Consideration of thermal inertia and crustal geometry suggests that the duration of a spreading lapse may have been about 30 m.y. (Oliver and Isacks, 1967). The active spreading is inferred to have resumed in the Atlantic about 10 m.y. ago (Ewing and Ewing, 1967; Langseth *et al.*, 1966; Schneider and Vogt, 1968) and the direction of spreading in the northeast Pacific changed within the last 10 m.y. (Vine, 1966). The next orogenic episode to compress the Mesozoic and Cenozoic sedimentary strata of the opposing continental margins will occur when the motion of the North American and African blocks again becomes convergent.

Conclusions

1. The opposing continental margins of Cape Hatteras and of Cap Blanc (Fig. 1) appear asymmetric with respect to Cenozoic tectonic frameworks. Sedimentary strata underlying the coastal plain, continental terrace, and continental rise in the vicinity of Cape Hatteras are predominantly undeformed, except by superficial gravitational processes acting above Horizon A (Late Cretaceous-Eocene; Figs. 2, 3). Sedimentary strata underlying the corresponding physiographic provinces in the vicinity of Cap Blanc are deformed by the following deep structural processes (Figs. 1, 4).

a. Compressional structures. Intense folding involves Jurassic through upper Eocene sedimentary strata on the chiefly volcanic Cape Verde Islands, Jurassic (?) through upper Eocene sedimentary strata on the eastern Canary Islands, and strata beneath the continental terrace between the Canary Islands and the Strait of Gibraltar.

b. Tensional structures. An active WNW-ESE-trending fault, coincident with the eastward projection of a fracture zone from the Mid-Atlantic Ridge, exhibits a normal component of displacement associated with folding and volcanism where the fault crosses the abyssal hills and the continental rise off Cap Blanc (Figs. 4, 7, 9). Down-to-basin block faulting related to seaward subsidence occurs along fracture zones inferred to trend regionally parallel with the continental margin. The abyssal hills are interpreted to be active horsts and grabens (Fig. 9).

c. Volcanism. Considered extinct off Cape Hatteras since the early Cenozoic, volcanism has been active on the continental rise off Cap Blanc, including the Cape Verde and Canary Islands, at least from Oligocene through Holocene times. Volcanic islands and seamounts are aligned along eastward projections of fracture zones from the Mid-Atlantic Ridge (Fig. 1). The active volcanism on the northwest African continental rise may exemplify the concept of a eugeosyncline as a surface that has subsided deeply in a belt having active volcanism (Kay, 1951, p. 4; Stille, 1940, p. 15).

d. Diapirism. Intrusive bodies have deformed strata beneath the lower continental rise and are interpreted as diapirs containing rock salt correlative with Late Triassic–Jurassic evaporites which form salt diapirs in the northwest African coastal basins (Fig. 8). An Atlantic sea about 2,600 km wide restricted by the Jurassic positions of the continents is postulated to account for the evaporite deposition (Fig. 10).

Crystalline basement behaves coherently beneath the coastal plain, continental terrace, and the continental rise in the vicinity of Cape Hatteras. Crystalline basement behaves incoherently beneath the corresponding provinces in the vicinity of Cap Blanc where basement fracturing and displacement occur. Major fracture directions off northwest Africa are inferred to be WNW-ESE, coincident with trends of fracture zones which cross the Mid-Atlantic Ridge, and NNE-SSW nearly parallel with the continental margin (Fig. 1).

The Cenozoic structural deformation of the northwest African continental margin is related to Alpine tectonic activity which did not affect the continental margin off Cape Hatteras.

2. The opposing continental margins in the vicinities of Cape Hatteras and Cap Blanc appear broadly symmetric with respect to (a) distribution of physiographic provinces, with the exception of the lower continental rise hills which have not been observed off Cap Blanc; (b) early and middle Paleozoic, Mesozoic, and Cenozoic stratigraphic frameworks; (c) late Precambrian, Paleozoic, and Mesozoic tectonic frameworks, with certain qualifications; and (d) certain offshore residual magnetic anomalies, including a positive anomaly associated with the shelf edge and the boundary between smooth and rough magnetic fields (Figs. 1, 4, 6). Point (c) must be qualified because the absence of late Paleozoic (post-Devonian) strata in the Mauritanides fold belt of northwest Africa, as opposed to their involvement in

the Appalachian fold belt of eastern North America, limits resolution of the respective orogenic movements, and because the presence of a system of Triassic fault-block basins parallel with the northwest African continental margin, corresponding to the system in eastern North America, has not been well documented.

3. The elements of symmetry in space and time imply the activity of symmetric forces on the opposing continental margins.

4. Mesozoic and Cenozoic mean rates of subsidence and gross lithologic sequences generally correlate between the opposing continental terraces (Figs. 2, 5; Table 2).

5. Similarities in the Mesozoic and early Cenozoic stratigraphic records of the opposing continental terraces and the adjacent ocean basin indicate that the continental crust beneath the continental margins investigated has behaved as if vertically coupled to the oceanic crust beneath the adjacent ocean basin. In particular, an Upper Triassic through upper Eocene stratigraphic section laterally equivalent to the section beneath the northwest African coastal basins is inferred to have subsided beneath the continental rise between the Canary and Cape Verde Islands; a corresponding section may be present off Cape Hatteras.

6. A comparison of mean subsidence rates of the opposing continental margins with independently inferred mean spreading rates of the intervening sea floor during the Mesozoic and Cenozoic indicates (Table 2) that (a) mean subsidence rates (1–9 cm/1,000 year) are about 10^{-3} the values of inferred mean rates of sea-floor spreading (1–4 cm/year) and (b) mean subsidence rates appear to vary in unison with independently inferred mean spreading rates. For example, relatively fast subsidence and an active phase of sea-floor spreading are inferred to have been initiated in the early Mesozoic. Mean subsidence rates during the Late Cretaceous (2.5–3.8 cm/1,000 year) are inferred to have been relatively fast. Mean subsidence rates during the Tertiary were relatively slow (0.9–1.3 cm/1,000 year) at a time when a lapse in sea-floor spreading is inferred.

7. These limited data suggest that epeirogenic subsidence of the opposing continental margins and inferred spreading of the intervening sea floor are related genetically. Coupled variation in rates of epeirogenic subsidence and inferred spreading of the sea floor, as well as variation in sediment supply, have controlled synchronous marine transgressions and regressions on the opposing continental margins and resulted in the formation of similar stratigraphic sequences.

8. The apparent symmetry in space and time of tensional rifting, orogenic compression, and epeirogenic subsidence on the opposing continental margins is consistent with an hypothesis of sea-floor spreading.

9. These findings imply that geologic characteristics relevant to the occurrence of petroleum, such as the distribution of salt deposits, can be predicted between the opposing continental margins.

REFERENCES CITED

Abdel-Monem, A., N. D. Watkins, and P. W. Gast, 1967, Volcanic history of the Canary Islands (abs.): Am. Geophys. Union Trans., v. 48, p. 226.

Allard, O., and V. J. Hurst, 1969, Brazil-Gabon geologic link supports continental drift: Science, v. 163, p. 528–532.

Applin, P. C., 1951, Preliminary report on buried pre-Mesozoic rocks in Florida and adjacent states: U.S. Geol. Survey Circ. 91, 28 p.

Arkell, W. J., 1956, Jurassic geology of the world: New York, Hafner Publishing Co., 806 p.

Atwater, T. M., and J. D. Mudie, 1968, Block faulting on the Gorda Rise: Science, v. 159, p. 729–732.

Avery, O. E., G. D. Burton, and J. R. Heirtzler, 1968, An aeromagnetic survey of the Norwegian Sea: Jour. Geophys. Research, v. 73, p. 4583–4600.

Aymé, J. M., 1965, The Senegal salt basin, p. 83–90 *in* Salt basins around Africa: London, Inst. Petroleum, 112 p.

Barzangi, M., and J. Dorman, 1969, World seismicity map of ESSA Coast and Geodetic Survey epicenter data for 1961–1967: Seismol. Soc. America Bull., v. 59, p. 369–380.

Beckmann, J. P., 1953, Die Foraminiferen der Oceanic Formation (Eocaen-Oligocaen) von Barbados, Kleinen Antillen: Eclogae Geol. Helvetiae, v. 46, no. 2, p. 301–412.

Bullard, E. C., J. E. Everett, and A. G. Smith, 1965, The fit of the continents around the Atlantic: Royal Soc. London Philos. Trans., Ser. A, v. 258, p. 41.

Burk, C. A., M. Ewing, J. L. Worzel, A. O. Beall, Jr., W. A. Berggren, D. Bukry, A. G. Fisher, and E. A. Pessagno, Jr., 1969, Deep-sea drilling into the Challenger Knoll, central Gulf of Mexico: Am. Assoc. Petroleum Geologists Bull., v. 53, p. 1338–1347.

Cahen, L., 1961, Review of geochronological knowledge in middle and northern Africa: New York Acad. Sci. Annals, v. 91, p. 535–567.

Choubert, G., and A. Faure-Muret, 1968, Tectonic map of Africa: UNESCO, Nat. Resources, v. 4, no. 2, p. 18–19.

Cohee, G. V., chm., 1962, Tectonic map of the United States: U.S. Geol. Survey and Am. Assoc. Petroleum Geologists.

Colom, G., 1955, Jurassic-Cretaceous pelagic sediments of the western Mediterranean and the Atlantic area: Micropaleontology, v. 1, p. 109.

Cushman, R. V., 1964, Ground-water resources of north-central Connecticut: U.S. Geol. Survey Water Supply Paper 1752, 96 p.

Dash, B. P., and E. Bosshard, 1968, Crustal studies around the Canary Islands: 23d Internat. Geol. Cong., v. 1, p. 249–260.

Defant, A., 1961, Physical oceanography, v. 1: New York, Macmillan, 729 p.

Denison, R. E., H. P. Raveling, and J. T. Rouse, 1967, Age and descriptions of subsurface basement rocks, Pamlico and Albemarle Sound areas, North Carolina: Am. Assoc. Petroleum Geologists Bull., v. 51, p. 268–272.

Dietz, R. S., 1961, Continent and ocean basin evolution by spreading of the sea floor: Nature, v. 190, p. 854–857.

Drake, C. L., 1965, Recent investigations on the continental margin of eastern United States, p. 33–47 *in* W. H. Poole, Continental margins and island arcs: Canada Geol. Survey Paper 66–15, 486 p.

——— J. I. Ewing, and H. Stockard, 1968, The continental margin of the eastern United States: Canadian Jour. Earth Sci., v. 5, p. 993–1010.

——— M. Ewing, and G. H. Sutton, 1959, Continental margins and geosynclines: the east coast of North America north of Cape Hatteras, *in* Physics and chemistry of the earth: London, Pergamon Press, v. 3, p. 110–198.

——— J. Heirtzler, and J. Hirshman, 1963, Magnetic anomalies off eastern North America: Jour. Geophys. Research, v. 68, p. 5259–5275.

——— and H. P. Woodward, 1963, Appalachian curvature, wrench faulting, and offshore structures: New York Acad. Sci. Trans. 26, p. 38–63.

Ericson, D. B., M. Ewing, G. Wollin, and B. C. Heezen, 1961, Atlantic deep-sea sediment cores: Geol. Soc. America Bull., v. 72, p. 193–286.

——— and G. Wollin, 1963, Time traces in sediment: Nat. History, v. 72, no. 2, p. 53–61.

Ewing, J., and M. Ewing, 1967, Sediment distribution on the mid-ocean ridges with respect to spreading of the sea floor: Science, v. 156, p. 1590–1592.

——— J. L. Worzel, and M. Ewing, 1966, Ages of Horizon A and the oldest Atlantic sediments: Science, v. 154, p. 1125–1132.

——— and R. Zaunere, 1964, Seismic profiling with a pneumatic sound source: Jour. Geophys. Research, v. 69, p. 4913–4915.

Ewing, M., 1969, Deep-water drilling: Atlantic basin (abs.): Am. Assoc. Petroleum Geologists Bull., v. 53, p. 717.

——— D. B. Ericson, and B. C. Heezen, 1958, Sediments and topography of the Gulf of Mexico, p. 995–1053 *in* L. G. Weeks, ed., Habitat of oil, a symposium: Am. Assoc. Petroleum Geologists, 1384 p.

Foreman, F., 1951, Study of some Bermuda rocks: Geol. Soc. America Bull., v. 62, p. 1297–1330.

Fox, P. J., B. C. Heezen, and A. M. Harian, 1968, Abyssal anti-dunes: Nature, v. 220, p. 470–472.

Furon, R., 1963, Geology of Africa: Edinburgh and London, Oliver and Boyd, 377 p.

Fúster Casas, J. M., and M. J. Aguilar Tomás, 1965, Nota previa sobre la geología del macizo de Betancuria, Fuerteventura (Islas Canarias): Madrid, Estudios Geol. 21, p. 181–197.

——— A. Cendrero, P. Gastesi, E. Ibarrola, and J. L. Ruis, 1968, Fuerteventura: Madrid, Inst. "Lucas Mallada," Consejo Superior de Investigaciones Científicas, 239 p.

Gill, W. D., 1965, The Mediterranean basin, *in* Salt basins around Africa: London, Inst. Petroleum, p. 101–111.

Glangeaud, L., 1962, Paléogeographie dynamique de la Méditerranée et de ses bordures. Le rôle des phases Ponto-Plio-Quaternaries, p. 125–165 *in* Oceanographie géologique et géophysique de la Méditerranée occidentale: Paris, Centre Nationale de La Recherche Scientifique.

——— 1966, Les grands ensembles structuraux de la Méditerranée occidentale d'après les données de Géomède: Paris, Sci. Comptes Rendus, t. 262, p. 2405–2408.

——— J. Alinat, J. Polvèche, A. Guillaume, and O. Leenhardt, 1967, Grandes structures de la mer Ligure, leur évolution et leurs rélations avec les chaînes continentals: Soc. Géol. France Bull., sér 7, v. 8 (1966), p. 921–937.

Habib, D., 1968, Spores, pollen, and microplankton, from the Horizon Beta outcrop: Science, v. 162, p. 1480–1481.

Hadley, J. B., 1964, Correlation of isotopic ages, crustal heating and sedimentation in the Appalachian region, p. 33–44 *in* W. D. Lowry, ed., Tectonics of the southern Appalachians: Virginia Polytech. Inst. Dept. Geol. Sci. Mem. 1, 114 p.

Hamilton, W., and W. B. Myers, 1966, Cenozoic tectonics of the western United States: Rev. Geophysics, v. 4, p. 509.

Haughton, S. H., 1963, The stratigraphic history of Africa south of the Sahara: New York, Hafner Publishing Co., 365 p.

Hausen, H., 1958, On the geology of Fuerteventura (Canary Islands): Soc. Sci. Fennica, Comm. Phys.-Mat. 22, no. 1, 211 p.

Hedberg, H. D., 1961, Petroleum developments in Africa in 1960: Am. Assoc. Petroleum Geologists Bull., v. 45, p. 1143–1185.

Heezen, B. C., C. D. Hollister, and W. F. Ruddiman, 1966, Shaping of the continental rise by deep geostrophic contour currents: Science, v. 152, p. 502–508.

——— and R. E. Sheridan, 1966, Lower Cretaceous rocks (Neocomian-Albian) dredged from Blake escarpment: Science, v. 154, p. 1644–1647.

——— and M. Tharp, 1968 (rev.), Physiographic diagram of the North Atlantic Ocean: Geol. Soc. America Spec. Paper 65.

——— ——— and M. Ewing, 1959, The floors of the oceans. I. The North Atlantic: Geol. Soc. America Spec. Paper 65, 122 p.

Heirtzler, J. R., G. O. Dickson, E. M. Herron, W. C. Pitman, III, and X. LePichon, 1968, Marine magnetic anomalies, geomagnetic field reversals and motions of the ocean floor and continents: Jour. Geophys. Research, v. 73, p. 2119–2136.

——— and D. R. Hayes, 1967, Magnetic boundaries in the North Atlantic Ocean: Science, v. 157, p. 185–187.

Hersey, J. B., 1965, Sedimentary basins of the Mediterranean Sea, p. 75–89 *in* W. F. Whittard and R. Bradshaw, eds., Submarine geology and geophysics: London, Butterworth, 503 p.

——— E. T. Bunce, R. F. Wyrick, and F. T. Dietz, 1959, Geophysical investigation of the continental margin between Cape Henry, Virginia, and Jacksonville, Florida: Geol. Soc. America Bull., v. 70, p. 437–466.

Hess, H. H., 1962, History of ocean basins, p. 599–620 *in* A. E. J. Engel, ed., Geol. Soc. America Petrologic Studies.

Holmes, A., 1931, Radioactivity and earth movements: Geol. Soc. Glasgow Trans., v. 18 (pt. 3), p. 559–606. (Paper delivered at fourth meeting of 70th session, Geol. Soc. Glasgow, Glasgow, January 12, 1928.)

——— Principles of physical geology: New York, Ronald Press, 1288 p.

Hurley, P. M., F. F. M. de Almeida, G. C. Melcher, V. G. Cordani, J. R. Rand, K. Kawashita, P. Vandoros, W. H. Pinson, and H. W. Fairburn, 1967, Test of continental drift by comparison of radiometric ages: Science, v. 157, p. 495–500.

Irving, E., 1964, Paleomagnetism and its application to geological and geophysical problems: New York, Wiley, 399 p.

Isacks, B., J. Oliver, and L. R. Sykes, 1968, Seismology and the new global tectonics: Jour. Geophys. Research, v. 73, p. 5855–5899.

Joint Oceanographic Institutions Deep Earth Sampling Program (JOIDES), 1965, Ocean drilling on the continental margin: Science, v. 150, p. 709–716.

Kay, G. M., 1951, North American geosynclines: Geol. Soc. America Mem. 48, 143 p.

——— 1968, North Atlantic continental drift, p. 321–323 *in* Gondwanaland revisited: new evidence for continental drift: Am. Philos. Soc. Proc., v. 112, 353 p.

Kegel, W., 1968, Sobre a deriva continental Africa-America: Acad. Brasileira Ciênc. Anais, supp. v. 40, p. 321–323.

Kennedy, W. Q., 1965, The influence of basement structure on the evolution of the coastal (Mesozoic and Tertiary) basins of Africa, p. 7–16 *in* Salt basins around Africa: London, Inst. Petroleum, 122 p.

King, P. B., 1959, The evolution of North America: Princeton Univ. Press, 190 p.

——— 1964, Further thoughts on tectonic framework of southeastern United States, p. 5–31 *in* W. D. Lowry, ed., Tectonics of the southern Appalachians: Virginia Polytech. Inst. Dept. Geol. Sci. Mem. 1, 114 p.

Krause, D. C., 1964, Guinea fracture zone in the Equatorial Atlantic: Science, v. 146, p. 57–59.

Kulp, J. L., and F. D. Eckelman, 1961, Potassium-argon isotopic ages on micas from the southern Appalachians: New York Acad. Sci. Annals, v. 69, p. 408–419.

Langseth, M. G., X. LePichon, and M. Ewing, 1966, Crustal structure of the mid-ocean ridges. 5. Heat flow through the Atlantic Ocean floor and convection currents: Jour. Geophys. Research, v. 71, p. 5321–5355.

Lavrov, V. M., and V. N. Syrskiy, 1967, Extensions of the west African structural elements into the oceanic floor: Akad. Nauk SSSR, Doklady, v. 177, p. 92–94.

LeMaitre, D., 1947, Contribution a l'étude du Dévonien du Tafilalet. II. Le récif coralligene de Anihalane: Service Géol. Maroc Nôtes et Méms. no. 67, 115 p.

LePichon, X., 1968, Sea floor spreading and continental drift: Jour. Geophys. Research, v. 73, p. 3661–3697.

Manheim, F. T., and M. K. Horn, 1968, Composition of deeper subsurface waters along the Atlantic continental margin: Southeastern Geology, v. 9, p. 215–236.

Marsh, O. T., 1967, Evidence for deep salt deposits in western Florida Panhandle: Am. Assoc. Petroleum Geologists Bull., v. 51, p. 212–222.

Martin, H., 1961, The hypothesis of continental drift in the light of recent advances in geological knowledge on Brazil and southwest Africa: Geol. Soc. South Africa Trans., annex to v. 64, 47 p.

——— 1968, A critical review of the evidence for a former direct connection of South America with Africa, *in* E. J. Fittkau, J. Illies, H. Klinge, G. H. Schwabe, and H. Sioli, eds., Biogeography and ecology in South America: The Hague, Dr. W. Junk N.V., 53 p.

Martinis, B., and V. Visintin, 1966, Données géologiques sur le bassin sedimentaire côtier de Tarfaya, p. 13–26 *in* D. Reyre, ed., Sedimentary basins of the African coasts. Pt. 1. Atlantic Coast: Paris, Assoc. African Geol. Surveys, 304 p.

Mayhew, M., C. L. Drake, and J. E. Nafe, 1968, Marine geophysical evidence of sea-floor spreading in the Labrador Sea: Am. Geophys. Union Trans., v. 49, p. 202.

McKelvey, V. E., and F. F. H. Wang, 1969, World subsea mineral resources, preliminary maps: U.S. Geol. Survey Misc. Geol. Inv. Map I-632.

McMaster, R. L., and T. P. Lachance, 1968, Seismic reflectivity studies on northwestern African continental shelf: Strait of Gibraltar to Mauritania: Am. Assoc. Petroleum Geologists Bull., v. 52, p. 2387–2395.

Melson, W. G., G. Thompson, and T. H. van Andel, 1968, Volcanism and metamorphism in the Mid-Atlantic Ridge, 22° N latitude: Jour. Geophys. Research, v. 73, p. 5925–5941.

Menard, H. W., 1960, The East Pacific Rise: Science, v. 132, p. 1737–1746.

——— 1964, Marine geology of the Pacific: New York, McGraw-Hill, 271 p.

——— and J. Mammerickx, 1967, Abyssal hills, magnetic anomalies and the East Pacific: Earth and Planetary Sci. Letters, v. 2, p. 465–472.

——— S. M. Smith, and R. M. Pratt, 1965, The Rhône deep-sea fan, p. 271–284 *in* W. F. Whittard and R. Bradshaw, eds., Submarine geology and geophysics: London, Butterworth, 503 p.

Miller, E. T., and M. Ewing, 1956, Geomagnetic measurements in the Gulf of Mexico and in the vicinity of Caryn Peak: Geophysics, v. 21, p. 406–432.

Moody, J. D., 1962, Petroleum developments in Africa in 1961: Am. Assoc. Petroleum Geologists Bull., v. 46, p. 1193–1240.

Moore, D. G., 1960, Acoustic-reflection studies of the continental shelf and slope off southern California: Geol. Soc. America Bull., v. 71, p. 1121–1136.

——— and J. R. Curray, 1963, Structural framework of the continental terrace, northwest Gulf of Mexico: Jour. Geophys. Research, v. 68, p. 1725–1747.

Morgan, W. J., 1968, Rises, trenches, great faults and crustal blocks: Jour. Geophys. Research, v. 73, p. 1959–1982.

Murray, G. E., 1961, Geology of the Atlantic and Gulf coastal province of North America: New York, Harper, 692 p.

Neev, D., and K. O. Emery, 1967, The Dead Sea: depositional processes and environments of evaporites: Israel Geol. Survey Bull. 41, 147 p.

Northrop, J., R. A. Frosch, and R. Frasseto, 1962, Bermuda-New England Sea Mount Arc: Geol. Soc. America Bull., v. 73, p. 587–594.

Oliver, J., and B. Isacks, 1967, Deep earthquake zones, anomalous structures in the upper mantle, and the lithosphere: Jour. Geophys. Research, v. 72, p. 4259–4275.

Parker, T. J., and A. N. McDowell, 1955, Model studies of salt-dome tectonics: Am. Assoc. Petroleum

Geologists Bull., v. 39, p. 2384–2470.

Peterson, M. N. A., 1969, Scientific goals and achievements (JOIDES): Ocean Industry, v. 4, no. 5, p. 62–67.

Phillips, J. D., 1967, Magnetic anomalies over the Mid-Atlantic Ridge near 27°N: Science, v. 157, p. 920–923.

Pires Soares, J. M., 1948, Observations géologiques sur les îles du Cape Vert: Soc. Géol. France Bull., v. 18, p. 303–390.

——— 1953, A propósito dos Aptychi da Ilha de Maio (Arquipélago de Cabo Verde): Lisbon, Ministerio de Ultramar.

Pirsson, L. V., 1914, Geology of Bermuda Island: the igneous platform and petrology of the lavas: Am. Jour. Sci., v. 36, p. 70–71.

Pitman, W. C., III, and J. R. Heirtzler, 1966, Magnetic anomalies over the Pacific-Antarctic ridge: Science, v. 154, p. 1164.

Querol, R., 1966, Regional geology of the Spanish Sahara, p. 27–38 *in* D. Reyre, ed., Sedimentary basins of the African coasts. Pt. 1. Atlantic Coast: Paris, Assoc. African Geol. Surveys, 304 p.

Reyre, D., ed., 1966a, Sedimentary basins of the African coasts. Pt. 1. Atlantic Coast: Paris, Assoc. African Geol. Surveys, 304 p.

——— 1966b, Particularités géologiques des bassins côtiers de l'ouest Africain (essai de récapitulation), p. 253–301 *in* D. Reyre, ed., Sedimentary basins of the African coasts. Pt. 1, Atlantic Coast: Paris, Assoc. African Geol. Surveys, 304 p.

Rodgers, J., 1967, Chronology of tectonic movements in the Appalachian region of eastern North America: Am. Jour. Sci., v. 265, p. 408–427.

Rona, P. A., 1968, Northwest African continental margin between Canary and Cape Verde Islands (abs.): Geol. Soc. America 1968 Ann. Mtg. Prog., p. 253–254.

——— 1969a, Comparison of continental margins off Cape Hatteras and northwest Africa (abs.): Am. Assoc. Petroleum Geologists Bull., v. 53, p. 738–739.

——— 1969b, Seismic reflection profiles from northwest African continental margin between Canary and Cape Verde Islands (abs.): Am. Geophys. Union Trans., v. 50, p. 211.

——— 1969c, Middle Atlantic continental margin of the United States: deposition and erosion: Am. Assoc. Petroleum Geologists Bull., v. 53, p. 1453–1465.

——— 1969d, Linear "lower continental rise hills" off Cape Hatteras: Jour. Sed. Petrology, v. 39, p. 1132–1141.

——— 1969e, Possible salt domes in the deep Atlantic off northwest Africa: Nature, v. 224, p. 141–143.

——— 1970, Canyon origin on upper continental slope off Cape Hatteras: Jour. Geology, in press.

——— J. Brakl, and J. R. Heirtzler, 1969, Magnetic anomalies between the Canary and Cape Verde Islands (abs.): Am. Geophys. Union Trans., v. 50, p. 189.

——— and C. S. Clay, 1967, Stratigraphy and structure along a continuous seismic reflection profile from Cape Hatteras, North Carolina, to the Bermuda Rise: Jour. Geophys. Research, v. 72, p. 2107–2130.

——— E. D. Schneider, and B. C. Heezen, 1967, Bathymetry of the continental rise off Cape Hatteras: Deep-Sea Research, v. 4, p. 625–633.

Rothe, P., 1968, Mesozoiche Flysch-Ablagerungen auf der Kanareninsel Fuerteventura: Geol. Rundschau, Bd. 58, Heft 1, p. 314–332.

——— and H.-U. Schmincke, 1968, Contrasting origins of the eastern and western islands of the Canarian Archipelago: Nature, v. 218, p. 1152–1154.

Sanders, J. E., 1963, Late Triassic tectonic history of northeastern United States: Am. Jour. Sci., v. 261, p. 501–524.

Schneider, E. D., P. J. Fox, C. D. Hollister, H. D. Needham, and B. C. Heezen, 1967, Further evidence of contour currents in the western North Atlantic: Earth and Planetary Sci. Letters, v. 2, p. 351–359.

——— and P. R. Vogt, 1968, Discontinuities in the history of sea-floor spreading: Nature, v. 217, p. 1212–1222.

——— ——— and A. Lowrie, 1969, Diapiric structures and magnetic anomalies of the pre-Cenozoic Atlantic Ocean (abs.): Am. Geophys. Union Trans., v. 50, p. 212.

Senn, A., 1940, Paleogene of Barbados and its bearing on history and structure of Antillean-Caribbean region: Am. Assoc. Petroleum Geologists Bull., v. 24, p. 1548–1583.

——— 1947, Die geologie der Insel Barbados (Kleine Antillen) und die morphogenese der umliegende marine grossformen: Eclogae Geol. Helvetiae, v. 40, no. 2, p. 199–222.

Sheridan, R. E., R. E. Houtz, C. L. Drake, and M. Ewing, 1969, Structure of continental margin off Sierra Leone, West Africa: Jour. Geophys. Research, v. 74, p. 2512–2530.

Société Chérifienne des Pétroles, 1966, Le bassin du sud-ouest Marocain, p. 5–12 *in* D. Reyre, ed., Sedimentary basins of the African coasts. Pt. 1. Atlantic Coast: Paris, Assoc. African Geol. Surveys, 304 p.

Sougy, J., 1962, West African fold belt: Geol. Soc. America Bull., v. 73, p. 871–876.

——— organizer, 1969, Meeting on the Mauritanides and their foreland (abs.): Soc. Géol. France Compte Rendu, Fasc. 3, p. 84–92.

Sousa Torres, A., and J. M. Pires Soares, 1946, Formaçoes sedimentares do arquipélago de Cabo Verde: Portugal, Junta Mis. Geog. e Inves. Colonias Mem. Sér. Geol. 3, 397 p.

Spangler, W. B., 1950, Subsurface geology of Atlantic coastal plain of North Carolina: Am. Assoc. Petroleum Geologists Bull., v. 34, p. 100–132.

Spengler, A. de, J. Castelain, J. Cauvin, and M. Leroy, 1966, Le bassin secondaire-tertiare du Senegal, p. 80–94 *in* D. Reyre, ed., 1966, Sedimentary basins of the African coasts. Pt. 1. Atlantic coast: Paris, Assoc. African Geol. Surveys, 304 p.

Stahlecker, R., 1934, Neokom auf der Kapverden-Insel Maio: Neues Jahrb. Mineralogie Beil.-Bd. 73, Abt. B., Heft 2, p. 265–301.

Stille, H., 1940, Einführung in den Bau Amerikas: Berlin, Gebrüder Borntraeger, 717 p.

Stose, G. W., compiler, 1946, Geological map of North America: Geol. Soc. America.

Swain, F. M., 1947, Two recent wells in coastal plain of North Carolina: Am. Assoc. Petroleum Geologists Bull., v. 31, p. 2054–2060.

——— 1952a, Ostracoda from wells in North Carolina. 1. Cenozoic Ostracoda: U.S. Geol. Survey Prof. Paper 234-A, p. 1–58.

——— 1952b, Ostracoda from wells in North Carolina. 2. Mesozoic Ostracoda: U.S. Geol. Survey Prof. Paper 234-B, p. 59–152.

Sykes, L. R., 1968, Seismological evidence for transform faults, sea floor spreading, and continental drift, p. 120–150 *in* R. A. Phinney, ed., The history of the earth's crust: Princeton Univ. Press.

Taylor, P. T., I. Zietz, and L. S. Dennis, 1968, Geologic implications of aeromagnetic data for the eastern continental margin of the United States: Geophysics, v. 33, p. 755–780.

Trechmann, C. T., 1933, The uplift of Barbados: Geol. Mag., p. 19–47.

Uchupi, E., and K. O. Emery, 1967, Structure of continental margin off Atlantic Coast of United States: Am. Assoc. Petroleum Geologists Bull., v. 51, p. 223–234.

——— and ——— 1968, Structure of continental margin off Gulf Coast of United States: Am. Assoc. Petroleum Geologists Bull., v. 52, p. 1162–1193.

United Nations Educational, Scientific and Cultural Organization (UNESCO), 1963, Geological map of Africa: Paris, Assoc. African Geol. Surveys, sheet 1, scale 1:5,000,000.

Vine, F. J., 1966, Spreading of the ocean floor—new evidence: Science, v. 154, p. 1405–1415.

——— and D. H. Matthews, 1963, Magnetic anomalies over oceanic ridges: Nature, v. 199, p. 947–949.

Watson, J. A., and G. L. Johnson, 1968, Mediterranean diapiric structures: Am. Assoc. Petroleum Geologists Bull., v. 52, p. 2247–2249.

Wegener, A., 1929, The origin of continents and oceans (Dover ed. of 4th rev. ed., 1966): Brauschweig, Friedr. Vieweg and Sohn, 246 p.

Weiss, M., 1969, Mesozoic sediments from the eastern North Atlantic (abs.): Am. Geophys. Union Trans., v. 50, p. 196.

Whittington, H. B., 1966, Phylogeny and distribution of Ordovician trilobites: Jour. Paleontology, v. 40, p. 696–737.

Wilson, J. T., 1965, A new class of faults and their bearing on continental drift: Nature, v. 207, p. 343–347.

Windisch, C. C., R. J. Leyden, J. L. Worzel, T. Saito, and J. Ewing, 1968, Investigation of Horizon Beta: Science, v. 162, p. 1473–1479.

Woollard, G. P., W. E. Bonini, and R. P. Meyer, 1957, A seismic refraction study of the sub-surface geology of the Atlantic coastal plain and continental shelf between Virginia and Florida: Wisconsin Univ. Dept. Geology, Geophysics Sec. Tech. Rept., Contract no. N7onr-28512, 128 p.

Worzel, J. L., R. Leyden, and M. Ewing, 1968, Newly discovered diapirs in Gulf of Mexico: Am. Assoc. Petrol. Geologists Bull., v. 52, p. 1194–1203.

Wüst, G., 1957, Stromgeschwindigkeiten und Strominengen in den Tiefen des Atlantischen Ozeans: Berlin, Wiss. Erg. Deutsch Atl. Exp. "Meteor" 1925–1927, 6, pt. 2, p. 261–420.

Zuccaro, A., and P. A. Rona, 1968, Omega navigation performance off northwest Africa during Operation No. 267, April 23-May 28, 1968: Columbia Univ. Hudson Lab. Tech. Rept. No. 153, 36 p., D.D.C. No. AD-678 443.

Reprinted from American Association of Petroleum Geologists Bulletin, Vol. 53, No. 7, 1453-1465.

The American Association of Petroleum Geologists Bulletin
V. 53, No. 7 (July, 1969), P. 1453-1465, 11 Figs.

Middle Atlantic Continental Slope of United States: Deposition and Erosion[1]

PETER A. RONA[2]
Dobbs Ferry, New York 10522

Abstract Continuous seismic reflection profiles across outer continental terrace (outer continental shelf and slope) show that directly off Cape Hatteras reflection interfaces (sedimentary strata) with low seaward inclination ($\leq 1°$) underlie the continental shelf and terminate at the continental slope, which inclines about 9°. On traverses about 200 km north of Cape Hatteras, reflection interfaces (sedimentary strata) do not terminate but incline about 3°, nearly parallel with the continental slope. On the continental slope about 100 km north of Cape Hatteras both relationships are present.

The stratal terminations were produced primarily by erosional processes, on scales ranging from erosion of individual strata ($<$ 100 m thick) at the shelf break to rotational slumping of the entire stratigraphic section beneath the continental slope (1.5 km thick). The thickening mantle of sedimentary strata on the continental slope north of Cape Hatteras may have been derived from adjacent fluviatile sources as a result of former discharge regimens. Deposition of the sedimentary mantle on the continental slope may be controlled by the Western Boundary Undercurrent, which flows over the continental slope and the adjacent continental rise.

The association of erosional and depositional features is consistent with a model of continental terrace development in which strata accumulate on the continental shelf by upbuilding and on the continental slope by outbuilding while basement subsides during seaward tilting. At the continental slope, strata are terminated primarily by erosional processes. Periodically, rotational slumping of the continental slope occurs, causing strata from the slope and outer shelf to shift to the continental rise and exposing shelf strata at the edge of the continental terrace.

Introduction

On the physiographic diagram of the North Atlantic (Heezen and Tharp, 1959), the middle Atlantic continental slope of the United States is depicted as an escarpment between the continental shelf and the deep ocean basin. Although the general configuration is known, the actual shape of the middle Atlantic continental slope is not known in detail. Other features of interest are the attitudes and lateral variations of the strata underlying that section of the continental slope. Information on the strata should clarify the processes of development of the continental shelf and slope. Such information is shown in representative continuous seismic reflection profiles of the outer continental shelf and continental slope between the latitudes of Cape Hatteras, North Carolina, and Norfolk, Virginia. The lines traversed by the seismic profiles are shown on Figure 1.

Several authors have discussed the processes in the development of the middle Atlantic continental slope of the United States. On the basis of a continuous seismic reflection profile off Norfolk, Moore and Curray (1963; 1964) showed that the continental shelf has been building up depositionally at the same time that the continental slope has been building outward (prograding). Taking as an example the continental terrace (continental shelf plus slope) off Cape Hatteras, Dietz (1964a) stressed upbuilding of the continental shelf primarily by paralic sedimentation with depositional terminations of strata at the continental slope and erosion of the continental slope by gravitational processes dominated by turbidity currents. Although evidence of both deposition and erosion appears in continuous seismic reflection profiles made at intervals across the entire Atlantic continental margin of the United States by Uchupi and Emery (1967), effects of deposition are predominant. The configuration of the continental terrace as a seaward-thickening sedimentary wedge must be primarily of depositional origin.

In the writer's investigation, a seismic reflection profiling system with a 400-Hz piezoelectric source (Clay and Liang, 1962) was used. The source projected a ping of 0.020-second

---

[1] Manuscript received, April 18, 1968; accepted, May 15, 1968.

Read before the Geological Society of America Northeastern Section Meeting, Washington, D.C., February 16, 1968.

[2] Hudson Laboratories of Columbia University.

C. S. Clay and W. L. Liang advised on the operation of the seismic reflection profiling system. John Smith, assisted by Joseph Smith, prepared and operated the system. Thomas Gilliard performed the navigation and aided data acquisition. J. R. Heirtzler, T. E. Pochapsky, and J. E. Sanders of Hudson Laboratories, and K. O. Emery of Woods Hole Oceanographic Institution reviewed the manuscript, which has benefited from their pertinent comment. K. O. Emery suggested several references on artesian pressure in continental-margin strata.

This work was supported by the Office of Naval Research under Contract Nonr-266(84). Reproduction in whole or in part is permitted for any purpose of the United States Government. The report is Hudson Laboratories of Columbia University Contribution No. 361.

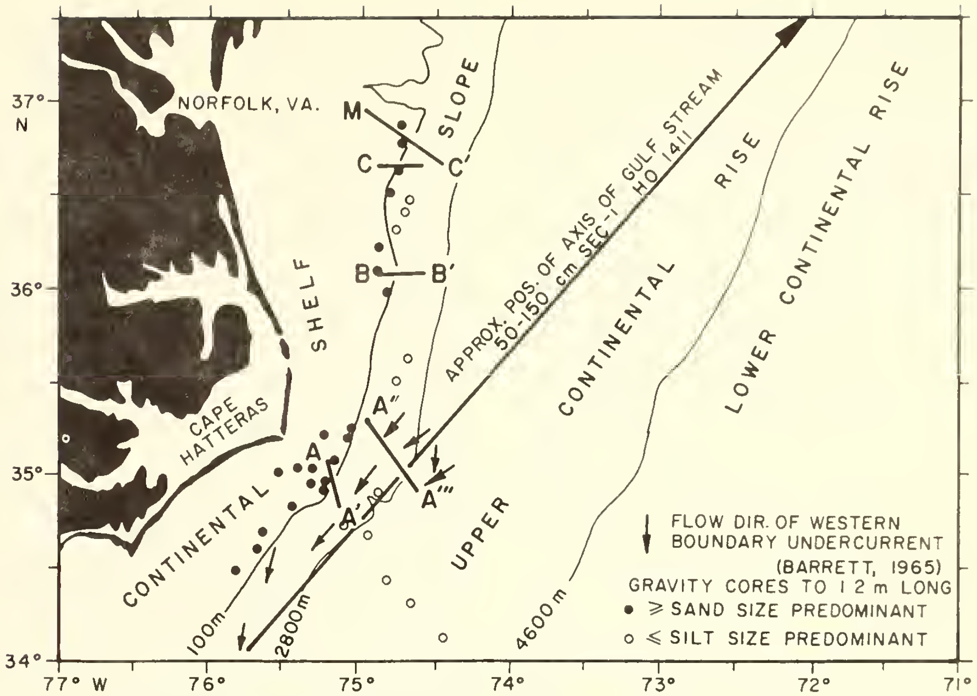
37° N
36°
35°
34°
77° W
76°
75°
74°
73°
72°
71°
NORFOLK, VA.
CAPE HATTERAS
CONTINENTAL SHELF
SLOPE
UPPER CONTINENTAL RISE
LOWER CONTINENTAL RISE
APPROX. POS. OF AXIS OF GULF STREAM 50-150 cm SEC-1 HO 1411
M
C
C'
B
B'
A'
A''
A'''
100m
2800m
4600m
FLOW DIR. OF WESTERN BOUNDARY UNDERCURRENT (BARRETT, 1965)
GRAVITY CORES TO 1.2 m LONG
● ≥ SAND SIZE PREDOMINANT
○ ≤ SILT SIZE PREDOMINANT

Fig. 1.—Middle Atlantic continental margin of United States with lines of traverse of continuous seismic reflection profiles (A-A′, A″-A‴, B-B′, C-C′, M-C′), current directions (arrows), and sediment cores (circles). Profiles are Figures 2, 3, 5, 6, and 7.

duration with about a 100-Hz bandwidth at a repetition rate of 2 per second. The system resolved reflecting interfaces spaced as closely as about 20 m. Estimated radiated source power was 250 watts. The source and a 10-m-long array consisting of 32 acceleration-balanced barium titanate hydrophones mounted in an oil-filled hose were towed at ship's speed of about 5 knots (9 km hr^{-1}). Navigation was by loran A with estimated accuracy of ± 2 km. In the interpretation of the profiles the reflecting interfaces are assumed to correspond to interfaces between sedimentary strata.

The continuous seismic reflection profiles display two-way travel time of the acoustic pulse in seconds from source to bottom or subbottom reflector at normal incidence and back to the surface-towed receiver. To convert water travel time to water depth, a mean velocity of 1.5 km sec^{-1} was assumed. To convert subbottom travel time to sediment thickness, an increase in seismic velocity with depth beneath the bottom was assumed (Rona and Clay, 1967, p. 2108).

Hatteras Profiles A-A′, A″-A‴

Continuous seismic reflection profile A-A′ extends 28 km along azimuth 170° from the outer continental shelf to the upper continental slope off Cape Hatteras (Figs. 1, 2). Between 3.5 and 7 km on the outermost continental shelf are four ridges with relief up to about 10 m and intervening sediment-filled troughs. Calcareous algae with a radiometric date of 19,000 b.p. have been sampled from the seaward ridge (Menzies *et al.*, 1966). The ridges may be algal reefs (Menzies *et al.*, 1966), barrier beaches with an overgrowth of algae (and intervening lagoonal deposits), or a combination of barrier beaches behind a shelf-edge organic reef. The upper continental slope inclines seaward at about 4° between the shelf break at the seaward ridge near 7 km and a bench at 23 km. The upper continental slope is underlain by sedimentary strata which nearly parallel the water-sediment interface to about 280 m (0.3 second) subbottom acoustic penetration. A bench about 1,000 m below sea level extends between 23 and 25 km. The profile crosses obliquely a canyon situated on the bench. The bench is underlain by a sequence of parallel strata, inclined seaward at about 1°. The strata terminate at the continental slope, where the inclination of the slope increases to about 9°.

Continuous seismic reflection profile A″-A‴ extends from the bench at about 1,000 m below sea level to the upper continental rise (Fig. 3). The profile shows that the sequence of parallel strata with low seaward inclination that terminates at the continental slope is present under the entire continental slope between the bench at about 1,000 m and the base about 3,000 m below sea level. Terminations are mantled by a veneer of sediment several tens of meters thick. The nature of the stratal terminations can be inferred from the configuration of strata on the continental slope and upper continental rise, as seen in Figure 3. Strata on the uppermost continental rise have landward inclination that can be explained by a model of rotational slump as shown in Figure 4. A coherent block of strata from the continental slope moved down a surface of displacement. The displaced strata rotated into landward inclination during emplacement on the upper continental rise (Rona and Clay, 1967). The thickness of strata with landward inclination on the upper continental rise is about 1,500 m, which closely corresponds to the thickness of the section of strata that terminates at the continental slope. The block containing the displaced strata is about 5 km wide.

The strata with low seaward inclination that terminate at the continental slope probably correspond to projections of strata found in wells on the coastal plain adjacent to Cape Hatteras (Heezen *et al.*, 1959, Fig. 22; Rona and Clay, 1967, Fig. 9; Spangler, 1950; Swain, 1947). If the projections are correct, these strata should range in age from Late Cretaceous through Cenozoic.

INTERMEDIATE PROFILE B-B′ BETWEEN CAPE HATTERAS AND NORFOLK, VIRGINIA

Continuous seismic reflection profile B-B′, about 110 km north of the Hatteras profile, extends 30 km along azimuth 090° across the outer continental shelf and upper continental slope (Figs. 1, 5). Strata with low seaward inclination ($< 1°$), slightly greater than the inclination of the water-sediment interface, underlie the outer continental shelf to about 135 m (0.15 second) acoustic penetration. The strata underlying the outer continental shelf between 7 km and the shelf break near 12 km increase successively in seaward inclination and thickness with depth below the bottom.

On the outermost continental shelf and uppermost continental slope, from 10 to 16 km (100–500 m below sea level), the water-sediment interface is smooth and convex upward. The strata underlying the outermost shelf do not curve continuously beneath this region but terminate at a subbottom surface of unconformity having the configuration of a chord whose seaward inclination intersects the smooth convex-upward transitional zone. Every stratum visible beneath the outermost continental shelf appears to terminate against the surface of unconformity, which suggests that erosional processes are almost continuously active near the shelf break.

The water-sediment interface of the continental slope becomes irregular at depths below 500 m. As in the Hatteras profiles, stratal terminations are visible under the continental slope between 17 and 23 km along profile B-B′. The inclination of the terminating strata (about 2° seaward) is about twice that of corresponding strata in the Hatteras profiles. To at least 280 m (0.3 second) acoustic penetration, most of the continental slope is mantled by strata inclined nearly parallel with the water-sediment interface. The mean inclination of the continental slope is about 4°, which is less than half its mean inclination off Cape Hatteras. The increase in seaward inclination of successive strata beneath the outer continental shelf and of strata terminating at the continental slope may indicate that the outer continental terrace between Cape Hatteras and Norfolk has subsided relative to the outer continental terrace off Cape Hatteras.

NORFOLK PROFILES M-C′, C-C′

The line of traverse of a continuous seismic reflection profile made by Moore and Curray (1963, Fig. 2) is labeled M-C′ on Figure 1, and the profile is reproduced in Figure 6. The profile shows that the continental shelf and slope are underlain to an acoustic penetration of at least 1,000 m (1.0 second) by sequences of strata nearly parallel with the water-sediment interface. The mean inclination of the continental slope is about 3°. From their profile, Moore and Curray infer that the continental terrace has developed by simultaneous depositional upbuilding of the continental shelf and outbuilding of the continental slope.

A seismic reflection profile made near that of Moore and Curray (1963) investigated in detail the transition between the continental shelf and slope (Figs. 1, 7). Acoustic penetration increases from about 40 m (0.055 second) beneath the shelf to about 280 m (0.3 second) beneath the slope. Sedimentary strata that mantle the continental slope cannot be traced landward under the continental shelf, but appear to terminate beneath the shelf break. A distinct terrace is present seaward of the shelf break between 18 and 19.5 km, approximately 175 m below sea level. The terrace is similar to one at 165 m below sea level about 300 km north off the Hudson apron, described by Ewing *et al.* (1963), which is interpreted to have been cut by surf into the sedimentary strata that mantle the continental slope. The Norfolk and Hudson apron terraces must be related to a eustatic lowering of sea level that occurred after most of the sediment mantling the continental slope had been deposited.

Stratigraphic Framework of Middle Atlantic Continental Margin

The continuous seismic reflection profiles clearly show that between Cape Hatteras and Norfolk, a distance of 200 km, the configuration of strata underlying the continental slope changes progressively and suggests certain developmental processes. Erosion, predominantly by massive rotational slumping that caused the continental terrace to retreat, may explain the stratal terminations of the continental slope off Cape Hatteras. As proposed by Moore and Curray (1963), progradation of the continental terrace explains the sedimentary mantling of the continental slope off Norfolk. In the intermediate profile, the stratal terminations seen at the continental slope off Cape Hatteras are partially mantled by sediment, and the outer continental terrace apparently has subsided in relation to the outer terrace off Cape Hatteras.

A cross section summarizes observations on the overall stratigraphic framework of the continental terrace and upper continental rise off Cape Hatteras (Fig. 8). Strata of shallow-water marine deposition of Late Cretaceous through Cenozoic ages, with low seaward inclination ($< 1°$), probably extend from the coastal plain under the continental shelf and terminate at the continental slope. The boundary region between the continental rise and Lower Cretaceous strata underlying the continental terrace is indistinct on seismic profiles. It is not clear whether the Lower Cretaceous strata terminate under the continental slope or continue under the continental rise. However, as Rona and Clay (1967, p. 2125) have pointed out, it is possible that Lower Cretaceous strata have retreated landward by erosional processes as much as 150 km from an original position under the transitional region between the present upper and lower continental rise. The upper continental rise is underlain by several hundred meters of landward-dipping strata which unconformably overlie strata dipping seaward. The thickness of sedimentary strata above the crystalline basement (5.6–6.1 km sec^{-1}) is about the same under both the outer continental shelf and the upper continental rise. The mean seaward inclination of the pre-Cretaceous basement off Cape Hatteras is approximately 0.5° (Woollard *et al.*, 1957). If a peneplain cut on the basement has been tilted seaward since the end of the Jurassic Period, the mean angular velocity of tilting would be about 13 minutes per 10^6 years; the actual tilting rate probably would have been variable. The inferred stratigraphic framework of the continental margin off Cape Hatteras is consistent with JOIDES (1965) drilling, which found strata on the outer continental shelf about 500 km south. A gradually deepening sedimentary environment during most of the Tertiary period was indicated.

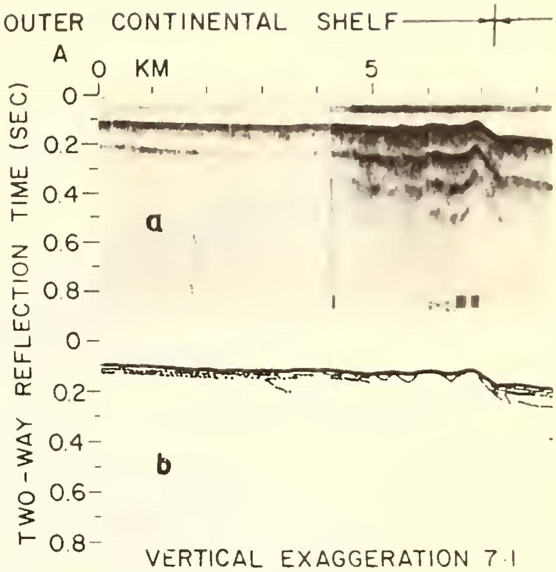

Fig. 2.—Continuous seismic reflection profile A-A′ off Cape Hatteras. a. Photograph of seismic reflection profile. b. Line drawing of seismic reflection profile. Location of profile shown on Figure 1.

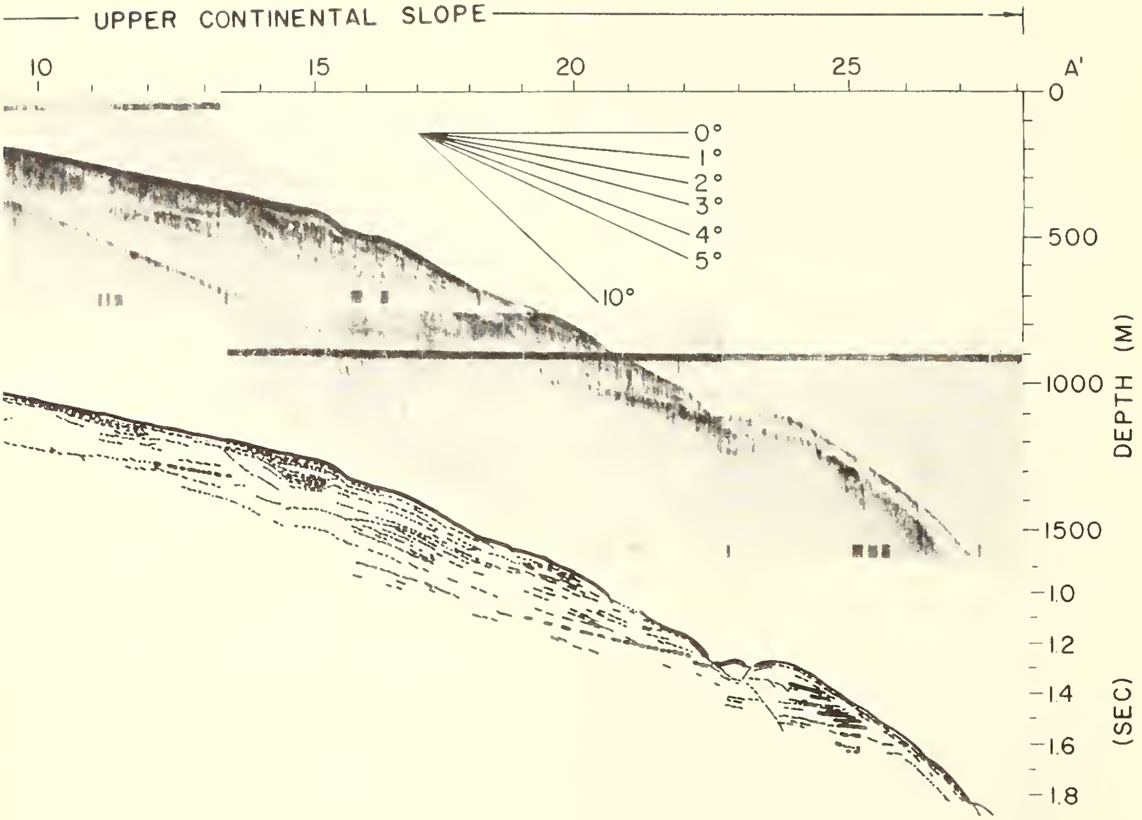

Depositional Processes on Continental Slope

The progressive increase in thickness of sediment mantling the continental slope between the Hatteras and Norfolk profiles can be attributed to local variations of sediment supply, as well as to depositional patterns controlled by variations in structure of oceanic currents and in sea-floor topography. Dietz (1964a) pointed out that the Norfolk profile may be at the ancestral seaward limit of the Susquehanna-Chesapeake and James River systems. The lack of sedimentary outbuilding of the continental slope off Cape Hatteras is a point of evidence against the suggestion that Cape Hatteras may have been the locus of a major Pleistocene continental drainage system (Rona and Clay, 1964; Sanders and Oaks, 1963; White, 1966).

The continental shelf and the continental slope are distinct depositional realms. This is evident in seismic reflection profiles from abrupt changes in the configuration of sedimentary strata under the shelf break, the lack in visible continuity of sedimentary strata underlying the continental shelf and slope, and an increase in acoustic penetration on the continental slope. That the increase in acoustic penetration is probably related to a decrease in grain size is suggested by the fact that lutite has been cored where strata mantle the continental slope; sand and coarser particles have been cored from the outer continental shelf in the region of the profiles (Fig. 1). The lutite is similar to that cored from the adjacent continental rise. Certain continuous seismic reflection profiles from adjacent sections of the continental margin indicate that strata which mantle the continental slope are continuous with strata of the upper continental rise to an acoustic penetration of several hundred meters (Uchupi and Emery, 1967, Figs. 4, 5). The similarity of surficial sediment and the continu-

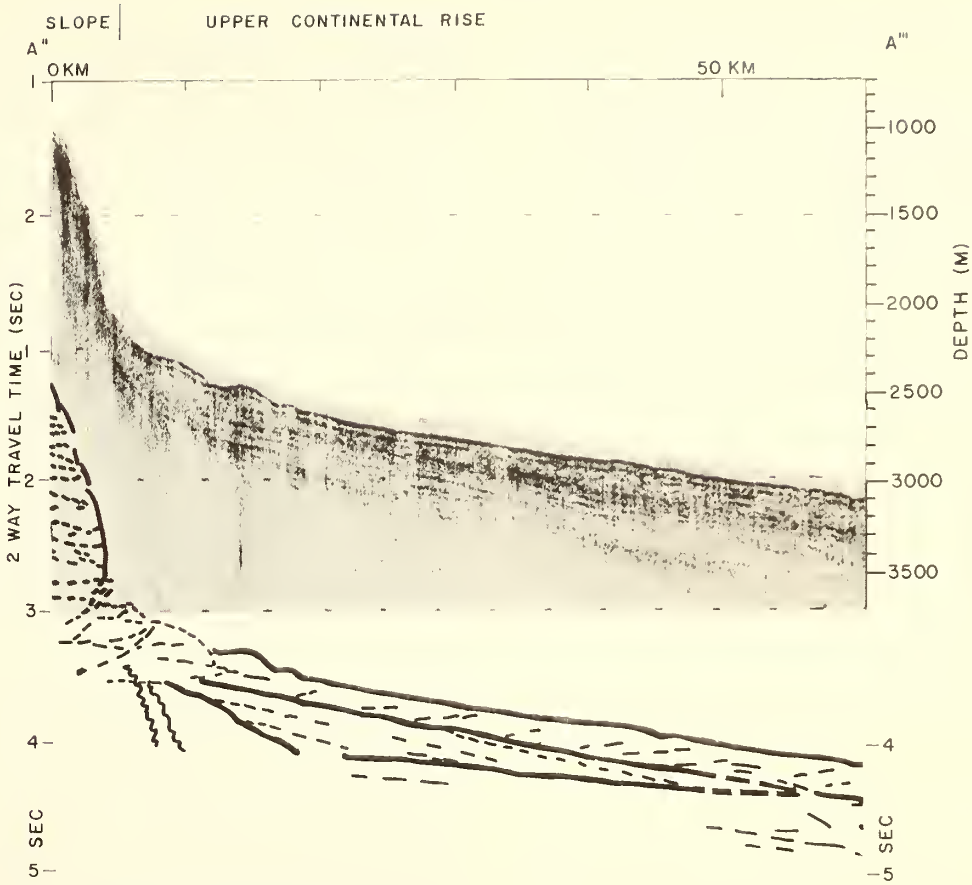

FIG. 3.—Continuous seismic reflection profile A″-A‴ off Cape Hatteras (Rona and Clay, 1967). a. Photograph of seismic reflection profile. b. Line drawing of seismic reflection profile. Location of profile shown on Figure 1.

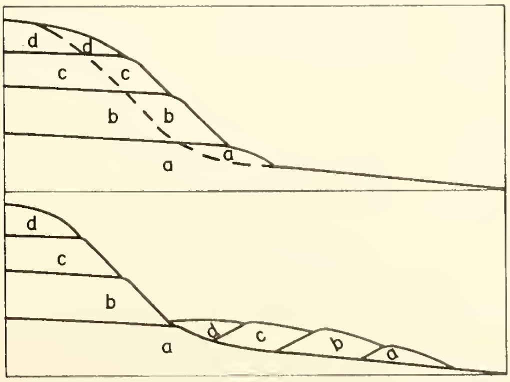

FIG. 4.—Model of rotational slump to explain configuration of strata in profile A″-A‴. As slump block moves down surface of displacement (dashed line), strata within block rotate about an axis perpendicular to plane of drawing (Rona and Clay, 1967).

ity of strata support the inference that the continental slope and rise may have been subject to the same depositional conditions for at least the time required to deposit the continuous strata.

The apparent continuity of deposition between the continental slope and continental rise of the middle Atlantic continental margin may be controlled by oceanic current pattern. The oceanic current pattern off Cape Hatteras has been delineated by Barrett (1965), who tracked neutrally buoyant floats at several depths to measure the direction and velocity of water movements. The Florida Current of the Gulf Stream flows northeast at a maximum of 150 cm sec^{-1} over the outer continental shelf and upper continental slope to a depth of approximately 400 m below sea level. Barrett (1965) measured a countercurrent flowing southwest beneath the Florida Current off Cape Hatteras at velocities up to 20 cm sec^{-1}. He considered the countercurrent to be part of the Western Boundary Undercurrent, supposed on theoretical grounds to flow adjacent to the entire Atlantic continental margin of North America (Stommel, 1957; Wüst, 1936). Heezen *et al.* (1966) have inferred from sedimentary evidence that the entire Atlantic continental rise has been shaped by deposition controlled by the Western Boundary Undercurrent; further evidence off the middle Atlantic sector has been contributed by Schneider *et al.* (1967, Fig. 1). Investigation of topographic features on the continental rise (Rona *et al.*, 1967) and continental slope (Rona, in press) off Cape Hatteras indicates that, in both those physiographic provinces, the Western Boundary Undercurrent influences sedimentation. Deposition of the sedimentary strata that thinly mantle the continental slope off Cape Hatteras and increase in thickness to the continental slope off Norfolk, is inferred to be controlled by the Western Boundary Undercurrent. Deposition of the sedimentary mantle on the continental slope may be continuous with deposition of strata on the adjacent continental rise.

EROSIONAL PROCESSES ON CONTINENTAL SLOPE

Termination of strata at the continental slope may occur on a wide range of scales and can result from a variety of erosional processes. The rotational slumping inferred on the slope off Cape Hatteras involves a stratigraphic section estimated to be about 1,500 m thick by 5 km wide. The upper 100 m of strata on the outermost continental shelf in the intermediate profile B-B′ (Fig. 5) terminates against a surface of unconformity beneath the shelf break. The unconformity could have been eroded by acceleration of impinging oceanic currents. Alternatively, the characteristic form of an unconfined *depositional* termination would be a lensing-out, no evidence of which was observed in the profiles. Therefore, the observed terminations of strata at the continental slope can be ascribed to erosional processes acting on a scale ranging from that of an individual stratum, as suggested by Heezen *et al.* (1959, p. 50), to that of the entire stratigraphic succession.

The stratigraphic framework of the continental terrace is important in determining the stability of strata which mantle the continental slope. For example, if seaward projections of coastal-plain strata are correct, the strata with low seaward inclination that terminate at the continental slope should be continuous with the system of aquifers underlying the coastal plain. Under proper conditions, fluid pressures related to the piezometric surface would be highest at lowest elevations in the aquifer system where water-bearing strata terminate at the continental slope. Manheim (1967) has compiled evidence for submarine discharge of water on the Atlantic continental slope of the southern United States. The JOIDES drillings found fresh and brackish waters in sedimentary strata as far as 120 km seaward of the Florida coast (JOIDES, 1965). JOIDES drill hole J-1 on the inner continental shelf off Jacksonville, Florida, found a minimum hydrostatic head 9 m above sea level that flowed through the drill pipe from an Eocene aquifer at a depth of about 130 m below the sea floor (155 m below sea level). Pratt (1966) attributed depressions which he found in Tertiary limestone at the base of the continental slope above the Blake Plateau to erosion by the Gulf Stream, possibly aided by groundwater solution during the Pleistocene Epoch.

Confinement of fluid pressures in aquifers by fine-grained sediments that mantle the continental slope could have many effects. Discharge from an aquifer that intersects the continental slope may undermine parts of the slope. If the sediments mantling the slope act as an impermeable layer over the aquifers at points of discharge on the continental slope, then a fluid pressure $p_{aquifer}$ from the aquifers would be exerted at the base of the sedimentary mantle (Fig. 9). If a closed pressure system were present, a fluid pressure $p_{overburden}$ derived from the weight of the overlying column of water plus rock also would act at the base of the sedimentary mantle (Hubbert and Rubey, 1959). The sedimentary mantle thus would be subjected to a total buoyant force p equal to the higher of the two pressures $p_{aquifer}$ and $p_{overburden}$ acting normal to its base. The buoyant force p would reduce the effective normal stress σ as follows:

$\sigma = S - p$

$S =$ normal component of stress resulting from total weight of column of water plus sediment from sea level to the base of the strata mantling the continental slope.

Reduction of the effective normal stress σ would correspondingly diminish the critical value of the shear stress τ required to produce gravitational gliding of the sedimentary mantle (Hubbert and Rubey, 1959).

Fluctuations in the piezometric surface in the coastal-plain aquifer system resulting from fluctuations in precipitation or sea level, or from engineering projects, may change fluid pressures at the continental slope. If the piezometric surface is high and thick impermeable strata mantle the continental slope, conditions should favor massive gravitational displacements.

Development of Middle Atlantic Continental Margin

Certain processes of deposition and erosion are inferred to have been important in determining the present stratigraphic framework of the middle Atlantic continental slope of the United States. The processes can be extrapolated back in time to infer general models for the development of the continental margin.

To limit the models to the observed stratigraphic framework, several assumptions are required. First, thicknesses of sediment which accumulated on the outer continental shelf and upper continental rise are assumed to have been roughly equal. This assumption is consistent with seismic refraction data (Katz and Ewing, 1956). Second, the basement is assumed to subside along a hinge line landward of the continental shelf, as suggested by measured seaward thickening of sedimentary strata underlying the coastal plain and continental terrace. Third, the continental shelf and continental slope are considered to be distinct depositional regimes. The continental slope regime is related to that of the continental rise. Seismic and sedimentary data support this assumption. Fourth, deposition and erosion are assumed to be periodic. Because the number of periods is unknown, the number of stages represented in the models is suggestive of processes but not of actual events. The balance between deposition

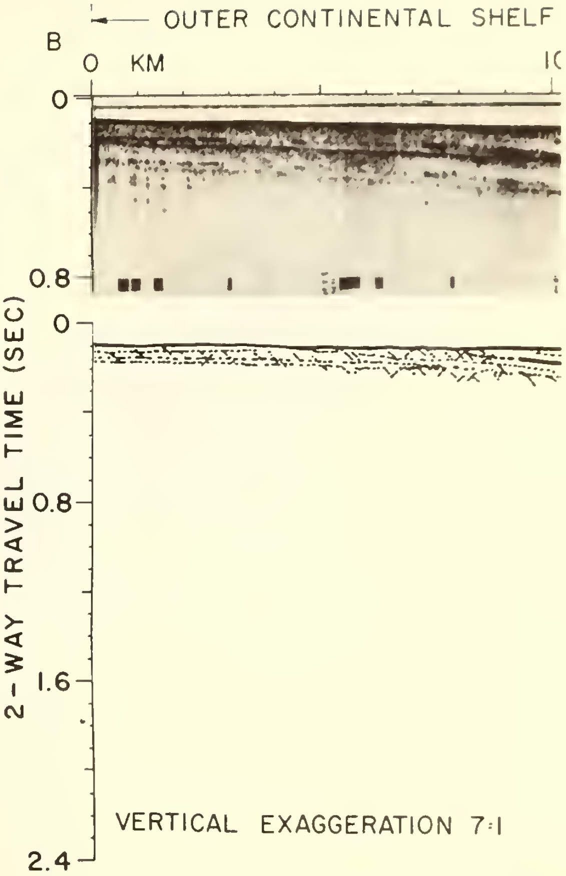

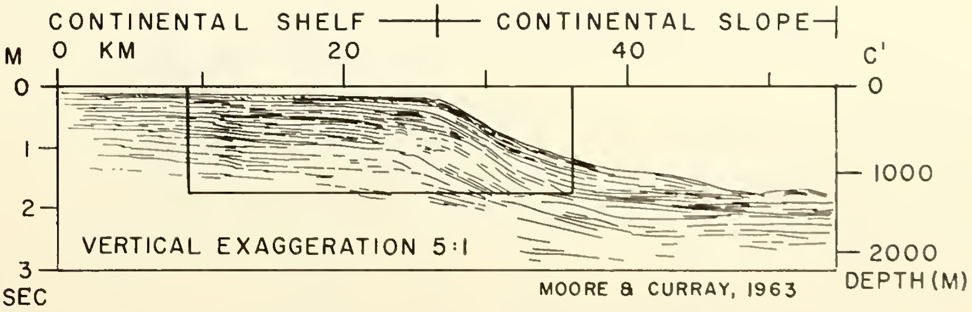

Fig. 6.—Line drawing of continuous seismic profile M-C′ reproduced from Moore and Curray (1963). Area outlined corresponds to profile C-C′ in Figure 7. Location shown on Figure 1.

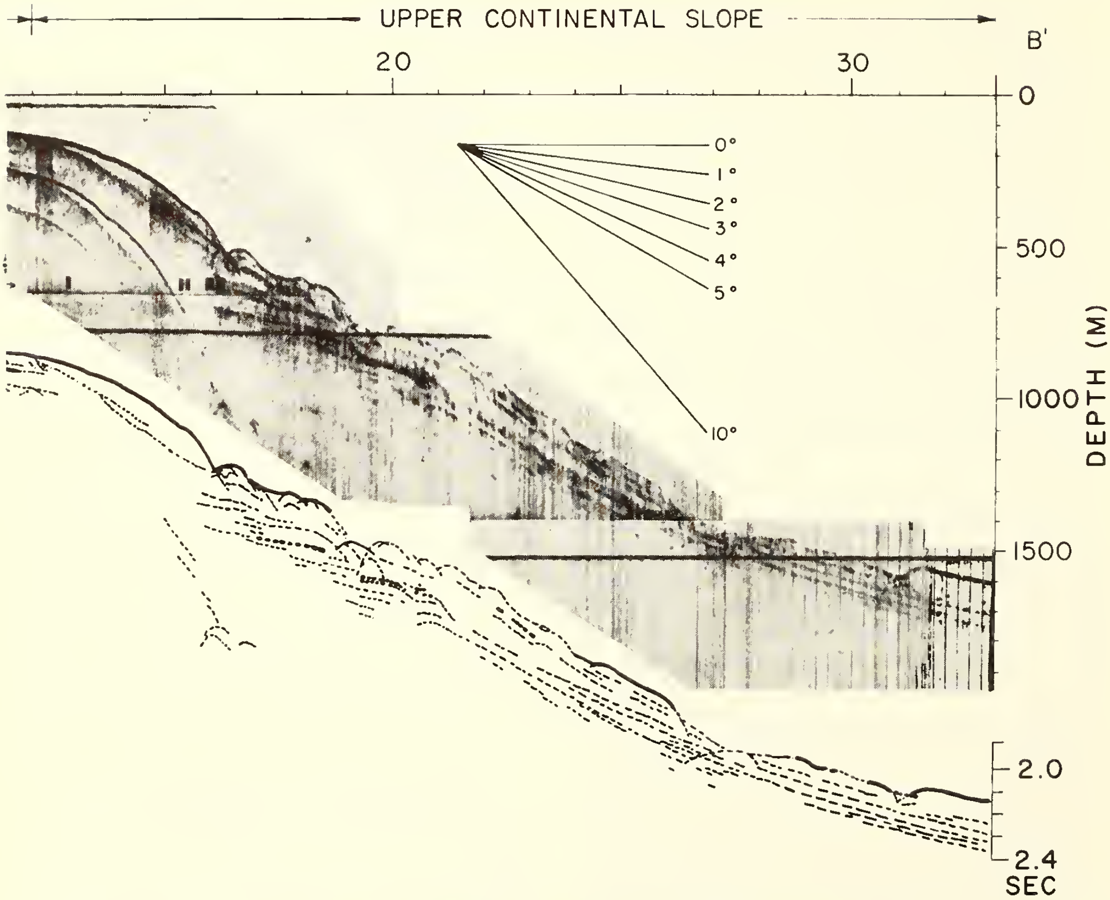

FIG. 5.—Continuous seismic reflection profile B-B′ between Cape Hatteras and Norfolk, Virginia. **a.** Photograph of seismic reflection profile. **b.** Line drawing of seismic reflection profile. Location shown on Figure 1.

and erosion may vary at adjacent sections of the continental margin, thereby producing variations in the stratigraphic framework.

In addition to these general postulates, an assumption must be made as to whether deposition on the continental shelf and on the continental slope and rise is simultaneous or alternating in time.

A sequential model of simultaneous deposition on the continental shelf and on the continental slope plus rise is shown in Figure 10. At stage 1 development begins with a topographic step which represents the initial difference in elevation between the continent and the ocean basin. The origin of this difference may be constructional or structural and has been considered by Dietz (1952, 1964b), Shepard (1963), and others. In stages 2, 4, and 6, deposition proceeds simultaneously on the continental shelf and on the continental slope plus upper continental rise, with a distinct change in sedimentary facies at the shelf break, while the basement subsides. In intervening stages 3, 5, and 7, strata underlying the continental shelf are terminated periodically by erosional processes, including rotational slumping of strata onto the upper continental rise. The continental terrace retreats, and the slumped strata are incorporated into the continental rise.

A sequential model of alternating deposition on the continental shelf and on the continental slope plus rise is shown in Figure 11. In this model, terminations near the shelf break of strata deposited on the continental shelf would be primarily depositional. Although rotational slumping could occur, its role in terminating

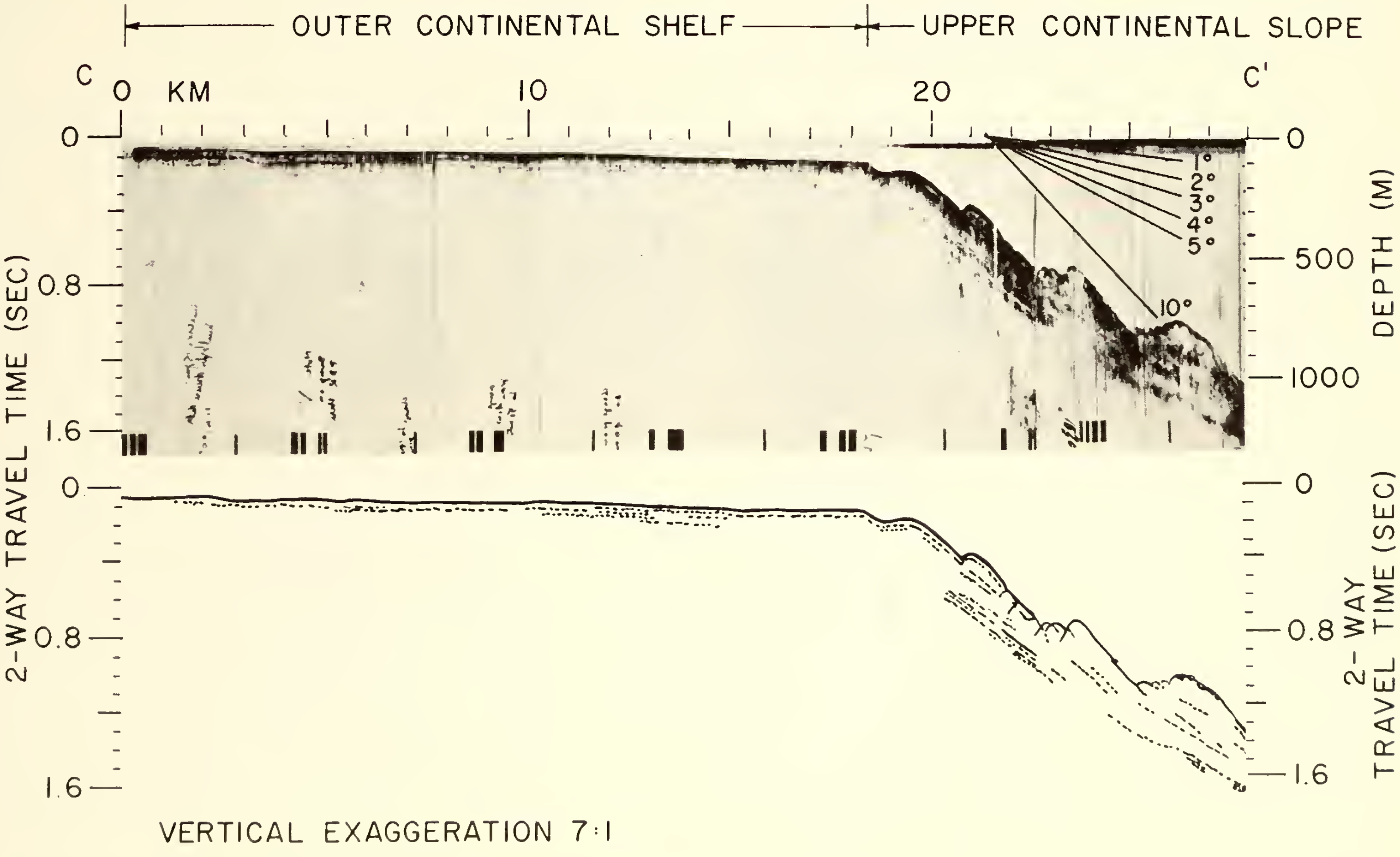

Fig. 7.—Continuous seismic profile C-C′ off Norfolk, Virginia. a. Photograph of seismic reflection profile. b. Line drawing of seismic reflection profile. Location of profile shown on Figure 1.

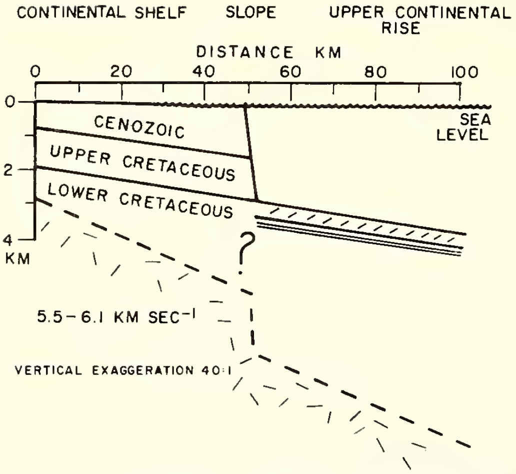

FIG. 8.—Stratigraphic framework of continental margin off Cape Hatteras. Sediment-crystalline basement (5.5-6.1 km sec^{-1}) boundary has been projected about 275 km south from seismic refraction profile (Katz and Ewing, 1956, profile b, p. 475 insert). Boundary region between continental rise and Lower Cretaceous strata underlying continental terrace which is indistinct on seismic profiles is indicated by question mark (?).

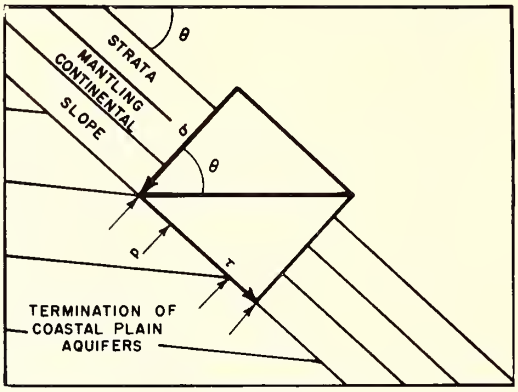
θ
STRATA MANTLING CONTINENTAL SLOPE
b
θ
p
τ
TERMINATION OF COASTAL PLAIN AQUIFERS

FIG. 9.—Hypothetical geometry of stresses between coastal-plain aquifers which terminate at continental slope and overlying strata which mantle continental slope.

θ = angle of inclination, τ = effective tangential stress, σ = effective normal stress, and p total fluid pressure related to weight of overlying column of water plus sediment and piezometric surface in aquifer. Reduction of σ by increase in p should reduce critical value of τ required to produce gravitational gliding of strata mantling continental slope.

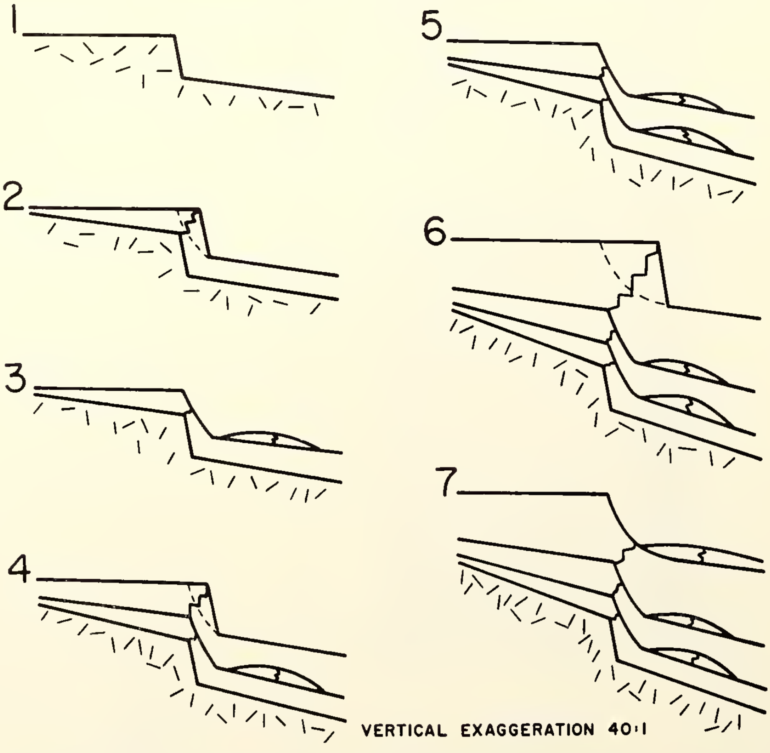

FIG. 10.—Sequential model for development of middle Atlantic continental terrace. Deposition on continental shelf and slope plus upper continental rise is simultaneous, with distinct sedimentary facies separated by wavy line at shelf break.

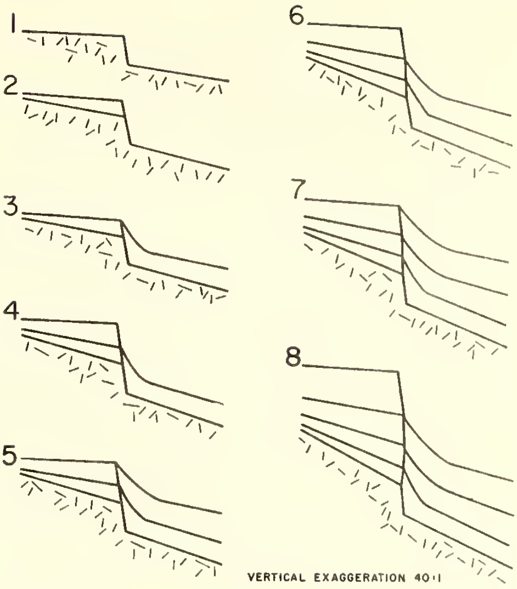

Fig. 11.—Sequential model for development of middle Atlantic continental terrace. Deposition on continental shelf and deposition on slope plus upper continental rise alternate in time.

strata at the continental slope would be minimized. The sequence begins with an initial difference in elevation between the continent and ocean basin (Fig. 11, stage 1). While the basement subsides, sediment is deposited alternately on the continental shelf (stages 2, 4, 6, 8) and on the continental slope plus rise (stages 3, 5, 7).

Conclusions

Sedimentary strata with low seaward inclination ($\leq 1°$) that terminate at the continental slope off Cape Hatteras are covered progressively by strata which conformably mantle the continental slope about 200 km north, off Norfolk, Virginia. The stratal terminations are inferred to have been produced primarily by erosional processes ranging in scale from erosion of individual strata to rotational slumping of the entire stratigraphic section underlying the continental slope. Massive gravitational displacement of continental-slope strata may be aided by fluid pressure in coastal-plain aquifers which extend under the continental shelf and terminate at the continental slope. Rotational slumping has caused strata from the slope and outer shelf to shift to the continental rise, exposing shelf strata at the edge of the continental terrace. Mantling of the continental terrace off Norfolk may have resulted from proximity to the Chesapeake-James River systems, which may have provided an increased sediment supply under a former regime of greater discharge. The Western Boundary Undercurrent flowing southwest along the middle Atlantic continental slope of the United States (Barrett, 1965) apparently controls deposition of sediments which mantle the continental slope, as Heezen *et al.* (1966) have inferred for deposition on the adjacent continental rise.

As the continental slope develops by periodic deposition and erosion, it interacts with the development of the continental rise. Displaced strata from the continental terrace are intercalated periodically with sediment being deposited on the continental rise. The emplacement of terrace strata would increase the effective overburden and consequently increase the interstitial pore water pressure in continental-rise strata. This mechanism may contribute to the triggering of massive gravitational gliding of continental-rise strata (Ballard, 1966; Rona and Clay, 1967; Uchupi, 1967).

References Cited

Ballard, J. A., 1966, Structure of the lower continental rise hills of the western North Atlantic: Geophysics, v. 31, no. 3, p. 506–523.

Barrett, J. R., Jr., 1965, Subsurface currents off Cape Hatteras: Deep-Sea Research, v. 12, p. 173–184.

Clay, C. S., and W. L. Liang, 1962, Continuous seismic profiling with matched filter detector: Geophysics, v. 27, no. 6, p. 786–795.

Dietz, R. S., 1952, Geomorphic evolution of continental terrace (continental shelf and slope): Am. Assoc. Petroleum Geologists Bull., v. 36, p. 1802–1819.

——— 1964a, Wave-base, marine profile of equilibrium, and wave-built terraces: Reply: Geol. Soc. America Bull., v. 75, p. 1275–1282.

——— 1964b, Origin of continental slopes: Am. Scientist, v. 52, p. 50–69.

Ewing, J., X. Le Pichon, and M. Ewing, 1963, Upper stratification of Hudson apron region: Jour. Geophys. Research, v. 68, no. 23, p. 6303–6316.

Heezen, B. C., C. D Hollister, and W F. Ruddiman, 1966, Shaping of the continental rise by deep geostrophic contour currents: Science, v. 152, p. 502–508.

——— and Marie Tharp, 1959, Physiographic diagram, Atlantic Ocean (Sheet 1): Geol. Soc. America Spec. Paper 65.

——— ——— and Maurice Ewing, 1959, The North Atlantic, pt. 1 *of* The floors of the oceans: Geol. Soc. America Spec. Paper 65, 122 p.

Hubbert, M. K., and W. W. Rubey, 1959, Role of fluid pressure in mechanics of overthrust faulting: Geol. Soc. America Bull., v. 70, p. 115–166.

Joint Oceanographic Institutions' Deep Earth Sampling Program (JOIDES), 1965, Ocean drilling on the continental margin: Science, v. 150, no. 3697, p. 709–716.

Katz, Samuel, and Maurice Ewing, 1956, Seismic-refraction measurements in the Atlantic Ocean, pt. VII, Atlantic Ocean basin, west of Bermuda: Geol. Soc. America Bull., v. 67, p. 475–510.

Manheim, F. T., 1967, Evidence for submarine discharge of water on the Atlantic continental slope of the southern United States, and suggestions for further research: New York Acad. Sci. Trans., ser. 2, v. 29, no. 7, p. 839–853.

Menzies, R. J., O. H. Pilkey, B. W. Blackwelder, D. Dexter, P. Huling, and L. McCloskey, 1966, A submerged reef off North Carolina: Internat. Rev. der Gesamten Hydrobiol., v. 51, 3, p. 393–431.

Moore, D. G., and J. R. Curray, 1963, Sedimentary framework of the continental terrace off Norfolk, Virginia, and Newport, Rhode Island: Am. Assoc. Petroleum Geologists Bull., v. 47, p. 2051–2054.

——— and ——— 1964, Wave-base, marine profile of equilibrium, and wave-built terraces: Discussion: Geol. Soc. America Bull., v. 75 p. 1267–1274.

Pratt, R. M., 1966, The Gulf Stream as a graded river: Limnology and Oceanography, v. 11, no. 1, p. 60–67.

Rona, P. A., 1968, Submarine canyon origin on upper continental slope off Cape Hatteras: Jour. Geology, in press.

——— and C. S. Clay, 1964, Continuous seismic profiles and cores from the shelf and slope off Cape Hatteras (abs.): Am. Geophys. Union Trans., v. 45, no. 1, p. 72.

——— and ——— 1967, Stratigraphy and structure along a continuous seismic reflection profile from Cape Hatteras, North Carolina, to the Bermuda Rise: Jour. Geophys. Research, v. 72, no. 8, p. 2107–2130.

——— E. D. Schneider, and B. C. Heezen, 1967, Bathymetry of the continental rise off Cape Hatteras: Deep-Sea Research, v. 14, p. 625–633.

Sanders, J. E., and R. Q. Oaks, Jr., 1963, Origin and significance of sand-ridge and mud-flat complex, Back Bay area, southeastern Virginia (abs.): Geol. Soc. America Spec. Paper 73, p. 309.

Schneider, E. D., P. J. Fox, C. D Hollister, H. D. Needham, and B. C. Heezen, 1967, Further evidence of contour currents in the western North Atlantic: Earth and Planetary Sci. Letters, 2, p. 351–359.

Shepard, F. P., 1963, Submarine geology, 2d ed.: New York, Harper and Row, 557 p.

Spangler, W. B., 1950, Subsurface geology of Atlantic coastal plain of North Carolina: Am. Assoc. Pettoleum Geologists Bull., v. 34, p. 100–132.

Stommel, H. M., 1957, A survey of ocean current theory: Deep-Sea Research, v. 4, p. 184–194.

Swain, F. M., 1947, Two recent wells in coastal plain of North Carolina: Am. Assoc. Petroleum Geologists Bull., v. 31, p. 2054–2060.

Uchupi, Elazar, 1967, Slumping on the continental margin southeast of Long Island, New York: Deep-Sea Research, v. 14, p. 635–639.

——— and K. O. Emery, 1967, Structure of continental margin off Atlantic Coast of United States: Am. Assoc. Petroleum Geologists Bull., v. 51, p. 223–234.

White, W. A., 1966, Drainage asymmetry and the Carolina Capes: Geol. Soc. America Bull., v. 77, p. 223–240.

Woollard, G. P., W. E. Bonini, and R. P. Meyer, 1957, A seismic refraction study of the sub-surface geology of the Atlantic coastal plain and continental shelf between Virginia and Florida: Wisconsin Univ., Dept. Geology and Geophysics Sec. Tech. Rept., Contract no. N7 Onr-28512, 128 p.

Wüst, G., 1936, Schichtung und Zirkulation des Atlantischen Ozeans. Die Stratosphäre: Deutsche Atlantische Exped. Meteor, VI, 1, Berlin.

(Reprinted from Nature, Vol. 224, No. 5215, pp. 141–143, October 11, 1969)

Possible Salt Domes in the Deep Atlantic off North-west Africa

by
P. A. RONA
Hudson Laboratories of Columbia University, Dobbs Ferry, New York

The presence of diapirs under the lower continental rise and abyssal plain off north-west Africa indicates that the salt basins of the continental margin may have extended seaward during the Late Triassic and Early Jurassic periods.

THE precise association of the east coast of North America and the north-west coast of Africa[1,2] before continental drift began is difficult because the two continental margins lack distinctive configurations or marked transverse structures. It is, however, reasonable to expect that some record of the association may be preserved in the sedimentary layer of the intervening ocean basin, for the environment of deposition must have changed progressively with changes in the configuration of the ocean basin.

The sedimentary layer of the continental margin off north-west Africa, between the Canary and Cape Verde islands, has been investigated using seismic reflexion (air gun) and magnetic profiles (Fig. 1). The seismic reflexion profiles show that the sedimentary strata underlying the lower continental rise are deformed by intrusive bodies (Figs. 2 and 3*b*) into an upward-convex configuration above the crests of the buried intrusive bodies and an upward-concave configuration between them. The degree of deformation between buried bodies seems to decrease upwards, indicating syndepositional deformation rather than abrupt emplacement of the intrusive bodies. Faults, apparently caused by tension, have formed above certain buried intrusive bodies as, for example, between 40 and 60 km along the profiler record shown (Fig. 3*b*). Some of the intrusive bodies have pierced through overlying sedimentary strata and form topographic highs with relief up to about 225 m as seen at 100 km along the profiler record.

The intrusive bodies are 20–40 km wide at their bases, which continue to diverge downward at about 1·5 s (1·5 km) seismic penetration beneath the bottom (Fig. 3*b*). They are reasonably symmetrical, converge evenly toward their crests and have smooth outlines. Individual intrusive bodies cannot be correlated between adjacent seismic reflexion profiler records, indicating that the bodies are more circular than elongate in plan view. The bodies tend to be associated with low values of residual magnetic intensity (Fig. 3*a*). Intrusive bodies with similar characteristics are also seen on our other seismic profiles which cross the lower continental rise and are tentatively identified on a profile which crosses the adjacent abyssal plain (Fig. 1). The intrusive bodies are observed on profiles at distances between about 650 and 1,300 km from the African coast in water depths ranging from about 4,685 to 5,670 m. No intrusive bodies are visible to about 1·5 s (1·5 km) seismic penetration beneath the upper continental rise, where the sedimentary layer is considerably thicker than on the lower continental rise.

The deformation of sedimentary strata adjacent to the intrusive bodies (Figs. 2 and 3*b*) indicates that they are diapirs and the low magnetic intensity indicates that they may contain rock salt or clay (Fig. 3*a*). The seismic reflexion profiles resemble those of unsampled diapirs in the Mediterranean basin[3], where Triassic evaporites are found[4], and also the profiles of diapirs in the Gulf of Mexico[5], of probable Late Triassic and known Middle Jurassic rock salt[6]. The diapirs beneath the lower continental rise and abyssal plain off north-west Africa have similar cross-sectional dimensions to those which form the Sigsbee knolls at about 3,800 m below sea level near the middle of the Gulf of Mexico[7], and JOIDES drilling has shown the latter to be salt domes[8]. Diapirs of Triassic (Keuper) and Lower Jurassic rock salt have been reported from the Essaouira and Aaiun basins of north-west Africa[9,10] and older than Aptian salt domes are reported from the Senegal basin[11]. Offshore seismic work has revealed sub-circular uplifts with the characteristics of salt domes on the continental shelf off the Aaiun basin[12] (Fig. 1).

The geophysical data and the regional geology are consistent with the view that the observed diapirs (Figs. 1, 2 and 3*a*, *b*) are salt domes, and their origin deep within the sedimentary layer suggests a pre-Tertiary age. The minimum rate of ascent of the diapirs which have reached the sediment–water interface must exceed the minimum rate of sediment accumulation, which is 0·5 cm per 1,000 years measured in a core containing Pleistocene lutite from the upper continental rise south-west of the Canary Islands[13]. At this rate, a maximum time of ascent of 200–600 million years would be required to rise through the sedimentary layer, which is 1–3 km thick in the

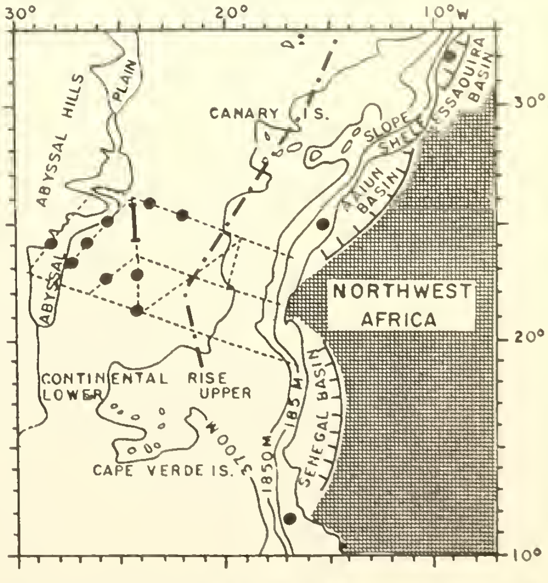

Fig. 1. Locations of concurrent seismic reflexion and magnetic profiles used in this study (dashed lines); the seismic reflexion and residual magnetic profiles in Figs. 2 and 3*a*, *b* are indicated by a solid line. Locations of diapirs (solid circles) and the magnetic boundary[14] (dashed and dotted line) are shown.

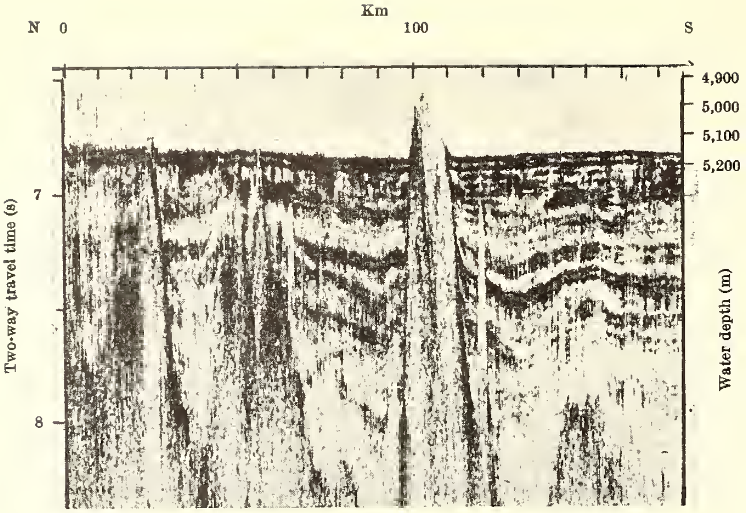

Fig. 2. Photograph of seismic reflexion profiler record (air gun) reveals intrusive bodies beneath the lower continental rise.

vicinity of the Canary Islands[14]. The observed structures are situated up to about 700 km seaward of a magnetic boundary (Fig. 1) which has been interpreted as an isochron in the age range of 250–200 million years[15], according to the hypothesis of sea floor spreading[16–19]. Assuming a sea floor spreading rate of 2 cm per year, then the sea floor underlying the most seaward of these structures would be about 35 million years younger than at the magnetic boundary, or still Middle Jurassic in age.

The north-west African coastal basins have no distinct seaward structural terminations[12]. During the Late Triassic and Early Jurassic, suitable conditions for evaporite deposition in the coastal basins may have extended at least 1,300 km seaward of the present north-west African coast. The palaeolatitudes of north-west Africa during the Late Triassic and Early Jurassic nearly coincide with the present latitudes and the present latitudes of north-west Africa bracket the predominant climatic zone for evaporite deposition[20]. Atlantic oceanic circulation in the Late Triassic and Early Jurassic would have been restricted by the then positions of the continents. The fit between west Africa and South America is fixed in space by the matching of lithological age provinces and geological structures[21,22], and comparative stratigraphy indicates that the two continents were contiguous until the Cretaceous[23]. A Palaeozoic fit between Newfoundland and the British Isles is suggested by the alignment of principal tectonic and stratigraphic belts[24], while the contiguity of Northern Europe, Greenland and Labrador until about 70 million years ago follows from remanent magnetic anomalies[25,26].

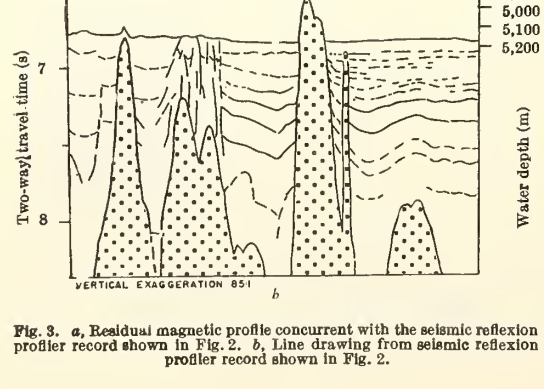

Fig. 3. *a*, Residual magnetic profile concurrent with the seismic reflexion profiler record shown in Fig. 2. *b*, Line drawing from seismic reflexion profiler record shown in Fig. 2.

The Atlantic between the east coast of North America and the north-west coast of Africa in the Late Triassic and Early Jurassic periods may have been a restricted sea analogous to the Dead Sea during the Plio-Pleistocene, when 1–4 km of rock salt was deposited[27]. From considerations of symmetry about the magnetic boundary, the restricted Atlantic sea may have been twice the width of the farthest seaward possible rock salt deposits or at least 2,600 km wide. This restricted Atlantic sea may have included or been temporarily connected with the evaporite basins which produced the rock salt in the Gulf of Mexico and the Mediterranean. Like the rock salt in the Dead Sea, which is the first sediment restricted to the Dead Sea graben[27], the deposition of rock salt in the Atlantic sea may have been initiated within the tectonic setting provided by the Late Triassic rifting, evidence of which is provided by block faulting of that age parallel to the margins of eastern North America and north-western Africa[12,28,29].

The deposition of thick rock salt in the restricted Atlantic sea, as in the Dead Sea, would have required a saline source and would imply a limited connexion between the restricted Atlantic sea and an exterior ocean. The appearance in the Late Jurassic of deep water limestones on the Cape Verde Islands[30–32] and possibly on the eastern Canary Islands[33], together with the deposition of good marine limestones in the north-west African coastal basins[10], indicate that the restriction on the Atlantic must have opened by that time.

I thank J. A. Ballard and E. D. Schneider for discussion of the seismic data and the US Office of Naval Research for financial support.

Received April 14, 1969.

[1] Wegener, A., *The Origin of Continents and Oceans*, 246 (Dover Press, 1966).

[3] Bullard, E. C., Everett, J. E., and Smith, A. G., in *Phil. Trans. Roy. Soc.*, A, **41** (1965).

[4] Watson, J. A., and Johnson, G. L., *Bull. Amer. Assoc. Petrol. Geol.*, **52**, 2247 (1968).

[5] Gill, W. D., in *Salt Basins Around Africa*, 101 (Inst. Petroleum, London, 1966).

[6] Uchupi, E., and Emery, K. O., *Bull. Amer. Assoc. Petrol. Geol.*, **52**, 1162 (1968).

[6] Murray, G. E., *Geology of the Atlantic and Gulf Coastal Province of North America*, 692 (Harper and Brothers, New York, 1961).

[7] Ewing, M., Ericson, D. B., and Heezen, B. C., in *Habitat of Oil, a Symposium*, 995 (Amer. Assoc. Petrol. Geol., Tulsa, Okla., 1958).

[8] Burke, C. A., *Bull. Amer. Assoc. Petrol. Geol.*, **53**, 710 (1969).

[9] Société Chérifienne des Petroles, in *Sedimentary Basins of the African Coasts*, **1**, 5 (Assoc. African Geol. Surveys, Paris, 1966).

[10] Quérol, R., in *Sedimentary Basins of the African Coasts*, **1**, 27 (Assoc. African Geol. Surveys, Paris, 1966).

[11] Aymé, J. M., in *Salt Basins Around Africa*, 83 (Inst. Petroleum, London, 1965).

[12] Reyre, D., *Sedimentary Basins of the African Coasts*, **1**, 39 (Assoc. African Geol. Surveys, Paris, 1966).

[13] Ericson, D. B., Ewing, M., Wollin, G., and Heezen, B. C., *Bull. Geol. Soc. Amer.*, **72**, 193 (1961).

[14] Dash, B. P., and Bosshard, E., in *Twenty-third Intern. Geol. Cong.*, **1**, 249 (Prague, 1968).

[15] Hertzler, J. R., and Hayes, D. E., *Science*, **157**, 185 (1967).

[16] Holmes, A., *Trans. Geol. Soc. Glasgow*, **18-3**, 559 (1931).

[17] Hess, H. H., *Petrologic Studies: A Volume in Honor of A. F. Buddington*. 599 (Geol. Soc. Amer., 1962).

[18] Dietz, R. S., *Nature*, **190**, 854 (1961).

[19] Vine, F. J., and Matthews, D. H., *Nature*, **199**, 947 (1963).

[20] Irving, E., *Paleomagnetism and Its Application to Geological and Geophysical Problems*, 399 (Wiley, New York, 1964).

[21] Hurley, P. M., de Almeida, F. F. M., Melcher, G. C., Cordani, U. G., Rand, J. R., Kawashita, K., Vandoros, P., Pinson, W. H., and Fairburn, H. W., *Science*, **157**, 495 (1967).

[22] Allard, G. O., and Hurst, V. J., *Science*, **163**, 528 (1969).

[23] Martin, H., *Trans. Geol. Soc. South Africa*, **64** annex, 47 (1961).

[24] Kay, M., *Proc. Amer. Phil. Soc.*, **112**, 321 (1968).

[25] Avery, O. E., Burton, G. D., and Heirtzler, J. R., *J. Geophys. Res.*, **73**, 4583 (1968).

[26] Mayhew, M., Drake, C. L., and Nafe, J. E., *Trans. Amer. Geophys. Union*, **49**, 202 (1968)

[27] Neev, D., and Emery, K. O., *Bull. Geol. Surv. Israel*, **41**, 147 (1967).

[28] King, P. B., *The Evolution of North America*, 190 (Princeton Univ. Press, Princeton, 1959).

[29] Furon, R., *Geology of Africa*, 377 (Oliver and Boyd, Edinburgh and London, 1963).

[30] Sousa Torres, A., and Pires Soares, J. M., *Minist. Colonias, Mem. ser. Geol.*, **3**, 397 (Lisboa, 1946).

[31] Pires Soares, J. M., *Bull. Soc. Géol. France*, **18**, 383 (1948).

[32] Colom, G., *Micropaleo.*, **1**, 109 (1955).

[33] Rothe, P., *Geologische Rundschau*, **58**, 314 (1968).

Printed in Great Britain by Fisher, Knight & Co., Ltd., St. Albans.

(*Reprinted from Nature, Vol.* 222, *No.* 5191, *pp.* 345–348, *April* 26, 1969)

Morphological Continental Drift Fit of Australia and Antarctica

by

WALTER P. SPROLL
ROBERT S. DIETZ

ESSA,
Atlantic Oceanographic Laboratories,
901 South Miami Avenue,
Miami, Florida 33130

A quantitative morphological fit of Australia and Antarctica which is also geologically permissible.

The jigsaw or morphological fit between South America and Africa was an important stimulus of early theories of continental drift[1–4], but it is only recently that the excellence of the fit has been demonstrated numerically[5–7]. The problem of fitting together the southern continents around the Indian Ocean to form the Gondwana supercontinent is more difficult and remains unsolved. All fits so far proposed have a large central gap, although it is possible that submerged missing sialic pieces ("microcontinents") may be an answer to the problem. We here attempt to discover the best morphological fit between Australia and Antarctica by a precise and objective method.

The numerous fits of Australia to Antarctica[2,4,6,8,16] are mostly of the sketch-map variety. No one has attempted to fit the south-western terminus of Australia farther west around Antarctica than latitude 70° E (ref. 10), presumably because such an oblique translation is intuitively unreasonable. On the other hand, palaeomagnetic considerations[15] place south Australia adjacent to western Antarctica east of the Ross Sea. An even more extreme possibility is the placing of the Great Bight of Australia against Chile[8].

To illustrate the need for a more precise solution, Fig. 1 shows three previous fits for Antarctica and Australia—those of Du Toit[4], Carey[6] and Wilson[12]. Even in this generally preferred region of fit there is considerable variation.

We accept the 1,000 fathom isobath as the proper contour to be tested for congruency. Although somewhat too shallow, this isobath represents approximately one half of the continental relief above the ocean floor, or one half of the so-called isostatic freeboard of the continents. The supposedly vertical faces of the rifted sialic plate would tend to adjust their shape by slumping of the continental slope and by flow within the roots of the continent so that an overall continental extension would occur. The position of the top of the continental slope would, however, actually retreat, so that the 1,000 fathom isobath might be a better marker of the original position of the primary rift than the bottom of the continental slope, its top or especially the shoreline. Between Africa and South America, the 500 fathom line was found to fit slightly better than the 1,000 fathom isobath[7], but we suspect that this resulted from poor knowledge as to the exact position of the 1,000 fathom isobath and because deeper topography is more subject to post-rift alterations. We prefer to use the logically correct 1,000 fathom isobath, but where its position is vague or unreasonably complex, we have drawn a synthetic 1,000 fathom isobath by extrapolating down from the 500 fathom line.

For a meaningful fit, the two continental outlines to be matched should have roughly equivalent lengths. Matching a short segment against a long one could lead to many good fits but would be meaningless unless second and third order curvatures were also conformable. The technique we have used is a corollary of that used by Bullard *et al.*[7]. Centres are determined for each of the two continental outlines so that they are approximately equidistant from most points along the given isobaths. A quantitative determination of the quality of fit is obtained by minimizing the amount of overlap plus underlap between the two critical isobaths when they are juxtaposed by a superposition of their centres. Test positioning of the two curves is accomplished by considering the isobath and centre of one continent as being fixed, while the other continent's isobath is adjusted in increments with respect to its superimposed centre in three ways: radially, along one of the radii, causing separation to vary; circumferentially, so that the movable isobath slides approximately along the fixed one; and by endpoint rotation, so as to change the basic orientation between the two isobaths (Fig. 2). Overlap and underlap are then measured by separation of the two isobaths along regularly spaced radii from the superimposed centres. The smallest mean absolute separation defines the best fit. The solution is made on a theoretical sphere with the aid of a computer and then mapped stereographically with a Calcomp plotter about the superimposed centres of curvature. In this way, projection distortions between the two isobaths are made uniform.

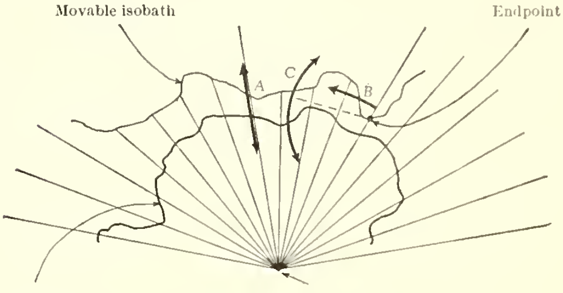

Fig. 2. The test positioning of a movable isobath relative to a fixed isobath by (*A*) radial translation, (*B*) circumferential rotation, and (*C*) endpoint rotation.

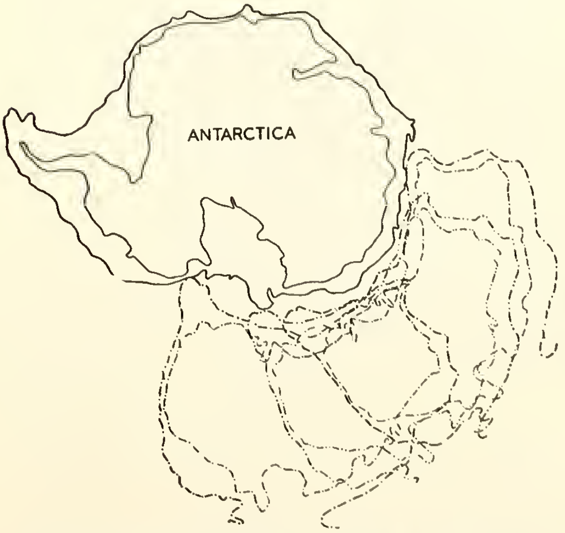

Fig. 1. Three previous fits of Australia into Antarctica which cover the sector approximately examined for a computerized best fit. The continents are represented by double lines, the inner line showing the shoreline and the outer one the undersea isobath which the pertinent authors regarded as the true continental margin. —·—·—, Carey[6]; —··—··—, Du Toit[4]; – – · – –, Wilson[12].

The source material for the two continents was obtained from collection sheets and contour charts of the US Naval Oceanographic Office (the "BC" series), the GEBCO (General Bathymetric Chart of the Oceans) prepared under the auspices of the International Hydrographic Bureau by the Royal Australian Navy, various special survey charts and, especially, new surveys made by the USC or GSS *Oceanographer* on her 1967 Global Expedition. During that cruise, the southern margin of Australia between Perth and Sydney was surveyed while one of us (R. S. D.) was the chief scientist aboard. A lazy-Z pattern was laid out especially for the purpose of delineating the 1,000 fathom isobath, and satellite navigation was used to give fixes to within 0·2 nautical miles. Thus the position and morphology of the southern continental slope of Australia are now well known. Unfortunately, the outline of the continental slope of Antarctica remains poorly defined. Sea ice, poor position control and few sounding lines all contribute to this deficiency, which is a major defect of this study.

Position of Best Fit

We have attempted computerized fits for southern Australia against several different sectors of Antarctica and upon somewhat different basic assumptions. The best fit is shown in Fig. 3, which juxtaposes southern Australia against the Wilkesland sector of east Antarctica. In this fit, Tasmania hooks slightly into the Ross Sea and off Victorialand. The south-western end of Australia then fits against Antarctica off the Knox Coast.

The position of best fit was obtained by a superposition of the Australian centre of curvature at 51·2° S, 122·7° E, over the Antarctic centre located at 81·0° S, 106·0° E, followed by a 47·5° clockwise rotation of the western end of the Australia isobath relative to the western end of the Antarctica isobath about the combined centre. Overlap area amounts to 95,248 km², while the underlap area equals 55,399 km². The total area of misfit is equal to 150,647 km², or a little more than the area of the state of Illinois.

We regard this fit as excellent and as the probable position of the two continents before their rifting in the late Mesozoic. The mean absolute misfit is 40·3 km, and the root mean square misfit is 51·9 km. In contrast, our Africa–South America fit has a mean absolute misfit of 68·5 km and a root mean square misfit of 101·6 km. Thus the fit achieved by closing this portion of the Antarctic Ocean seems better than that obtained by closing the South Atlantic Ocean.

Some comments are in order. Excluded from the test fittings were the Bruce Plateau and the Iselen Plateau (our name), the region in the vicinity of Iselen Seamount. These are rather anomalous protuberances of Antarctica's margin, the form of which might be considerably modified on a modern survey. Omitting them from consideration seemed to introduce less bias to our result. The Antarctica isobath actually used for fitting in the vicinity of these projections is shown by the dashed line in Fig. 3.

A satisfying aspect of our fit is that both the Iselen and Bruce plateaus are nicely accommodated when replaced after the best fit determination. Both salients provide constraining "toe ends" for Tasmania to the east and for the south-western tip of Australia to the west. This suggests that both of these projections are an integral part of the old predrift craton of eastern Gondwana and are not young accretionary volcanic or tectonic additions to Antarctica. Thus we have a fit of Australia which seems to be keyed into the Antarctic margin.

We also find that the Naturaliste Plateau fits rather snugly against the Bruce Plateau, although as the inner portion of this deep terrace is deeper than 1,000 fathoms it, too, was not considered in our computer program. Oceanographer's survey, however, indicated that the Naturaliste Plateau does have abrupt margins like continental slopes and its magnetic signature is consistent with sialic rock, so that it is probably a true continental projection. Intuitively, it seems reasonable that such triple-point junctions in the breakup of Gondwana would result in more complex topography than the simple separation along a suture.

Our quantitative best fit, of course, can only approximate reality. The margins of continents must undergo some tectonic and sedimentary modification resulting in extensions or retractions of the original continental outline. Sizable underlaps may be due to the presence of microcontinents such as exist in the Indian Ocean—Seychelle Islands, for example—but apparently not in the South Atlantic. There do not seem to be any microcontinents which would affect the Australia–Antarctica fit.

The greatest mismatch is an overlap which superimposes the isobath off Antarctica's George V Coast over the Australian margin extending from the region near Kangaroo Island and eastward across the offshore Otway Basin. The overlap has a width of as much as 74 nautical miles (137 km) and extends horizontally for 1,089 nautical miles (2,017 km). Why this overlap exists we can only surmise.

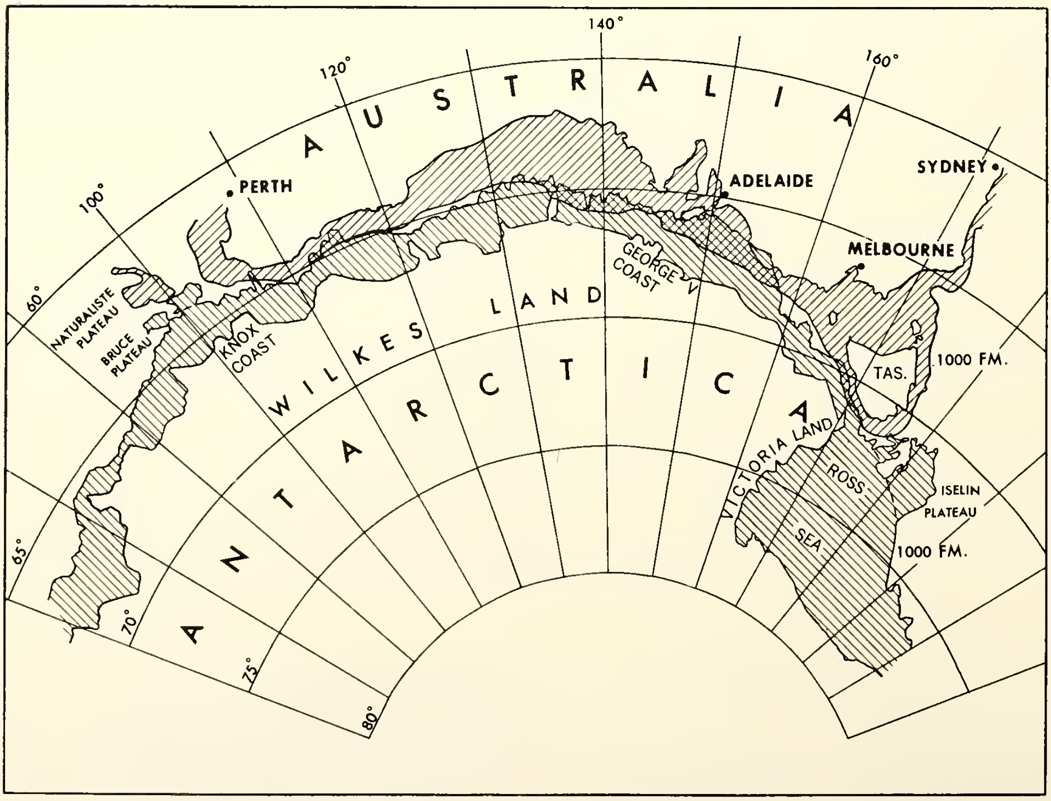

Fig. 3. The best fit of Australia with respect to Antarctica by computerized matching of the 1,000 fathom isobaths. Ruled line pattern indicates continental shelf and slope from shoreline (inner contour) to the 1,000 fathom isobath (outer contour). Overlap areas are cross-ruled and underlap areas are blank.

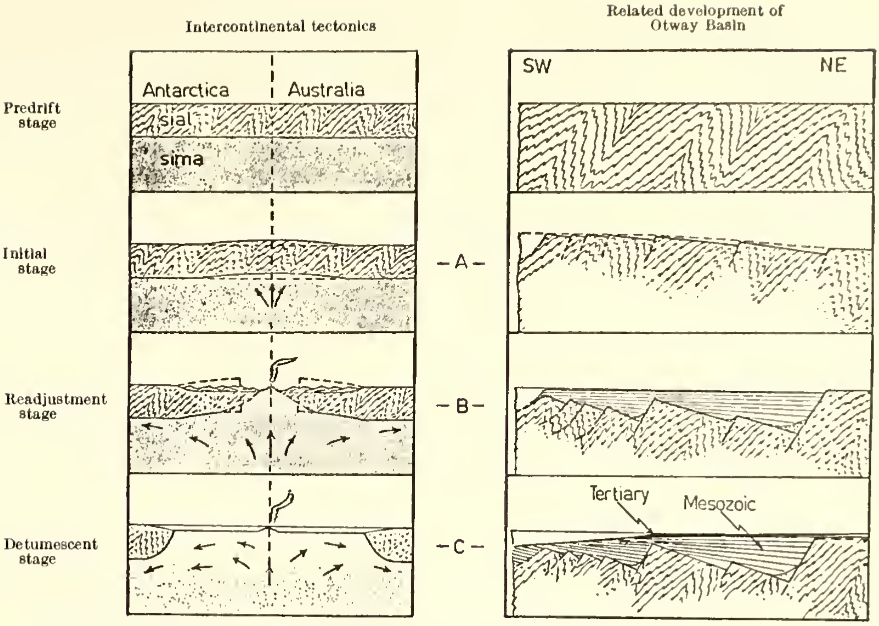

Fig. 4. Time-sequence diagram to show the presumed rifting and drifting apart of Australia and Antarctica with some resultant extension of the Australian margin.

Possibly the true outline of Antarctica along this sector is considerably in error. Another possibility is that there is a post-rift volcanic accretion, perhaps related to the Balleny Island volcanics[17], or that sedimentary material has been draped over the continental slope.

The thin and depressed crustal region of the Antarctic craton landward of the George V Coast between the Trans-Antarctic Range and the central craton of East Antarctica[18,19] may have controlled the position of a major drainage basin. This, in turn, would cause extensive offshore sedimentation and continental slope progradation by funnelling sedimentary detritus from the Antarctic craton to the continental margin.

On the Australian side of this sector, results from the Global Expedition of the USC and GSS Oceanographer and oil company offshore data also provide support for marginal extension of southern Australia (unpublished work). There is a thick section of sediments on the continental shelf and slope off the Otway Basin in which the beds dip landward and the section is downdropped in a steplike fashion presumably by normal faulting. We suggest that this represents taphrogenic relaxation associated with rifting and continental drift, as shown in Fig. 4. A parallel may be drawn with the downdropped blocks marginal to the Red Sea[20] and between Tasmania and the mainland of Australia[21]. The overall effect of this tensional faulting and extensive sedimentation must be to extend somewhat the continental margin beyond its pre-rift position. This may not account for all the overlap in this sector of our fit, but it may at least be a partial explanation.

Geological Considerations

The fit is, of course, purely morphological, but it is also geologically permissible and roughly agrees with that commonly obtained by geological reasoning[22,23].

In our fit, the Adelaide Pre-Cambrian–Cambrian miogeosyncline is correlated with a similar foldbelt of similar age extending across Antarctica from the George V Coast to the Weddell Sea. The Cambrian pleospongе, Archeocyatha, characterizes both of these foldbelts. From radiometric data, in both Australia and Antarctica an old Pre-Cambrian foldbelt lies to the west of this foldbelt, while a lower Palaeozoic basement of eugeosynclinal character lies to the east. Sutherland[24] has pointed out the similarity of age (Jurassic, roughly 160 m.y.) and orientation of dolerite dikes in Tasmania with those of Victorialand in Antarctica just west of the Ross Sea. The reconstruction we propose places them in close juxtaposition.

There remains an urgent need for a detailed bathymetric and geophysical survey along the margin of East Antarctica to define further the true outline of this continent and, especially, to reveal the exact nature of the Bruce and Iselen plateaus, which seem to provide constraining toe ends for our proposed fit.

Received October 28, 1968; revised February 7, 1969.

[1] Snider, A., *La Création et ses Mystères Dévoilés* (Paris, 1858).
[2] Wegener, A., *The Origin of Continents and Oceans* (London, 1924).
[3] Du Toit, A. L., *Carnegie Inst. of Washington, DC*, 38 (1927).
[4] Du Toit, A. L., *Our Wandering Continents* (Oliver and Boyd, London, 1937).
[5] Carey, S. W., *Geol. Mag.*, **92**, 196 (1955).
[6] Carey, S. W., *Continental Drift—A Symposium*, 177 (Univ. Tasmania, 1958).
[7] Bullard, E. C., Everett, J. E., and Smith, A. G., *Phil. Trans. Roy. Soc. London*, **1088**A, 41 (1965).
[8] Chevallier, J. M., and Cailleur, A., *Z. Geomorphol.*, **3**, 257 (1959).
[9] Maack, R., *Twenty-first Intern. Geol. Cong., Copenhagen, Part 12*, 35 (1960).
[10] Ma, T. Y. H., *J. Geomag. Geoelec.*, **13**, 133 (1962).
[11] King, L. C., *Morphology of the Earth* (Hafner Pub. Co., New York, 1962).
[12] Wilson, J. T., *Nature*, **198**, 925 (1963).
[13] Gough, D. I., Opdyke, N. D., and McElhinny, M. W., *J. Geophys. Res.*, **69**, 2509 (1964).
[14] Irving, E., *Palaeomagnetism and Its Application to Geological and Geophysical Problems*, chap. 10, 256, Special Topics, Sect. B (Wiley, New York, 1964).
[15] Van Hilten, D., *Tectonophysics*, **1**, 3 (1964).
[16] Creer, K. M., *Discovery*, **26**, 34 (1965).
[17] Lisitzin, A. P., *Deep-Sea Res.*, **7**, 89 (1960).
[18] Woollard, G. P., *Amer. Geophys. Union Geophys. Monog.* 7, 53 (1962).
[19] Thiel, E. C., *Amer. Geophys. Union Geophys. Monog.*, 7, 172 (1962).
[20] Drake, C. L., and Girdler, R. W., *Geophys. J.*, 8, 473 (1964).
[21] Weeks, L., and Hopkins, *Amer. Assoc. Petrol. Geol. Bull.*, **51**, 742 (1967).
[22] Hamilton, W., *Polar Wandering and Continental Drift*, Spec. Pub. 10, 74 (Soc. Econ. Geologists and Paleontologists, 1963).
[23] Hurley, P., *Sci. Amer.*, **218**, 4, 52 (1968).
[24] Sutherland, F. L., *Papers and Proc. Roy. Soc. Tasmania*, **100**, 133 (1966).

Printed in Great Britain by Fisher, Knight & Co., Ltd., St. Albans.

ENVIRONMENTAL SCIENCE SERVICES ADMINISTRATION

RESEARCH LABORATORIES

NATIONAL HURRICANE RESEARCH LABORATORY TECHNICAL MEMORANDA

Reports by units of the ESSA Research Laboratories, contractors, and cooperators working on the hurricane problem are preprinted in this series to facilitate immediate distribution of the information among the workers and other interested units. As the limited reproduction and distribution in this form do not constitute formal scientific publication, reference to a paper in the series should identify it as a preprinted report.

Other reports in this series have been prepared by the National Hurricane Research Project of the U. S. Weather Bureau, by the National Hurricane Research Laboratory, as a part of the Weather Bureau Technical Note Series, and as NHRL Technical Memoranda, a subseries of the Institute of Environmental Research Technical Memoranda series.

Beginning with No. 81, they are identified as NHRL Technical Memoranda, a subseries of the ESSA Research Laboratories (ERL).

The reports are available, at a cost of $3.00 per hard copy (microfische, 65 cents), from the Clearinghouse for Federal Scientific and Technical Information, U. S. Department of Commerce, Sills Building, Port Royal Road, Springfield, Virginia 22151.

U.S. DEPARTMENT OF COMMERCE
Environmental Science Services Administration
Research Laboratories

ESSA Technical Memorandum ERLTM-NHRL 86

NUMERICAL EXPERIMENTS ON RING CONVECTION AND EFFECT OF VARIABLE RESOLUTION ON CELLULAR CONVECTION

Richard A. Anthes

National Hurricane Research Laboratory
Miami, Florida
June 1969

TABLE OF CONTENTS

Page

ABSTRACT iv

LIST OF SYMBOLS v

1. INTRODUCTION 1

2. BASIC EQUATIONS AND COMPUTATIONAL PROCEDURE 2

3. CELLULAR CONVECTION 4

4. EFFECT OF GEOMETRY ON CONVECTION RINGS AND CELLS 5

5. RATE OF DEVELOPMENT AND GEOMETRY ASSOCIATED WITH RING 7

6. EFFECT OF SCALE (SIZE OF DOMAIN) ON CELLULAR CONVECTION 9

7. EFFECT OF SCALE ON RING CONVECTION 10

8. INCREASED HORIZONTAL RESOLUTION 12

9. LARGE-SCALE CONVECTION WITH VARIABLE RESOLUTION 13

10. SMALL-SCALE CONVECTION WITH VARIABLE RESOLUTION 15

11. SUMMARY 16

12. ACKNOWLEDGMENTS 17

13. REFERENCES 18

ABSTRACT

Ring convection is studied with Ogura's shallow moist convection model. Small-scale rings, 3 km in diameter, grow at slower rates than single cells. Thirty-three percent of the updraft recirculates nearly uniformly inside the ring, with 67 percent descending outside the ring. Downdrafts associated with large-scale rings, 30 km in diameter, however, approach line symmetry, with 43 percent of the mass recirculating inside and 57 percent outside the updraft.

The effect of variable radial resolution on cellular convection is also examined. Large-scale cellular convection described by a constant coarse resolution develops slowly because of artificial damping of the faster growing shorter waves. Introducing a variable resolution through the transformation $r = x^2 + Cx$ allows the development of these shorter waves in the fine-mesh region. Growth rates from the variable resolution experiments are in closer agreement than those from the constant resolution experiments with rates predicted from linear theory.

LIST OF SYMBOLS

u = radial component of velocity

w = vertical component of velocity

θ = temperature

p = pressure

P = constant reference pressure (1000 mb)

$\textcircled{H}$ = reference potential temperature (300°K)

T_{oo} = reference temperature (300°K)

q_v = mixing ratio of water vapor to dry air

q_l = mixing ratio of liquid water to dry air

$q = q_v + q_l$

$\pi = (p/P)^{R/C_p}$

T_o = temperature in dry adiabatic atmosphere

$'$ = prime symbol denoting deviation from reference atmosphere

ϕ = specific entropy

ν = coefficient of eddy viscosity

θ_e = equivalent potential temperature

The other symbols used have their standard meteorological meaning.

NUMERICAL EXPERIMENTS ON RING CONVECTION AND EFFECT OF VARIABLE RESOLUTION ON CELLULAR CONVECTION

Richard A. Anthes[1]

1. INTRODUCTION

Buoyant convection has been studied as an initial value problem in recent years through numerical experiments that time-integrate a complete set of hydro-dynamical equations. Malkus and Witt (1959) examined the results of introducing a temperature perturbation in a neutral or stratified environment initially at rest. Lilly (1962) investigated the two-dimensional vortex generated by the release of a buoyant fluid in a stable environment and later (Lilly, 1964) transformed the Boussinesq equations so that shape-preserving buoyant elements were steady-state solutions in the transformed variables.

Ogura (1962) studied axially symmetric dry convection and in a later paper (Ogura, 1963) modelled moist convection in a conditionally unstable atmosphere by including the effect of latent heat of condensation. He presents results for cylindrical and rectilinear axially symmetric convection over a computational domain 3 km deep. The effects of latent heat of condensation and downward drag of liquid water are included. The condensed water is carried along with the cloud and is available for evaporation at a later time (reversible pseudo-adiabatic process). Turbulent mixing processes are implicit in the differencing scheme and, in some experiments, included explicitly in terms of constant eddy coefficients.

The clouds resulting from Ogura's experiments are characterized by a head in which the vertical velocity, temperature excess, and liquid water are a maximum and by a columnar trunk extending from the head to cloud base. After an initial "organizational phase" of a few minutes, the growth rates (Q) of W_{max} (maximum upward velocity) and θ_{max} (maximum temperature excess) are nearly exponential, although smaller by a factor of two than those predicted by linear theory. Because Ogura's (1963) moist convection model was reasonably successful in simulating many features of shallow convection, because it includes the release of latent heat, and because of its relative simplicity, additional numerical experiments with this model were performed and are discussed in this paper.

---

[1] Part of this research was done while the author was with the Department of Meteorology, University of Wisconsin, Madison, Wisconsin.

2. BASIC EQUATIONS AND COMPUTATIONAL PROCEDURE

Ogura's (1963) dynamic equations for moist convection are summarized for convenience. (The notation is the same as Ogura's and is given in the List of Symbols.) The equations of motion, continuity, the first law of thermodynamics, and the continuity equation for water vapor are written in cylindrical coordinates as

$$\frac{\partial u}{\partial t} = -u\frac{\partial u}{\partial r} - w\frac{\partial u}{\partial z} - C_p\Theta\frac{\partial \pi'}{\partial r} + F_r\,, \tag{1}$$

$$\frac{\partial w}{\partial t} = -u\frac{\partial w}{\partial r} - w\frac{\partial w}{\partial z} - C_p\Theta\frac{\partial \pi'}{\partial z} + g\frac{\theta'}{\Theta} + g q_l + F_z\,, \tag{2}$$

$$\frac{\partial (ru)}{\partial r} + \frac{\partial (rw)}{\partial z} = 0\,, \tag{3}$$

$$\frac{\partial \phi'}{\partial t} = -u\frac{\partial \phi'}{\partial r} - w\frac{\partial \phi'}{\partial z} + D_\phi\,, \tag{4}$$

$$\frac{\partial q}{\partial t} = -u\frac{\partial q}{\partial r} - w\frac{\partial q}{\partial z} + D_q\,, \tag{5}$$

where

$$\phi' = \frac{\theta'}{\Theta} + \frac{L}{C_p T_\infty}q \tag{6}$$

Ogura calculates the saturation specific humidity from the approximate formula

$$q_s = \frac{Re_s}{p} \exp\left(\frac{L\theta'}{R_v \Theta} \right) \qquad (7)$$

and the saturation vapor pressure from

$$e_s\,(T_o) = 6.11 \times 10^{a\,(T_o - 273)/(T_o - b)}\,, \qquad (8)$$

with $a = 7.5$ and $b = 36.0$.

Where friction is calculated explicitly, the following equations are used:

$$F_r = \nu \left(\nabla^2 u - \frac{u}{r^2} \right), \qquad (9)$$

$$F_z = \nu \nabla^2 w \;, \qquad (10)$$

$$D_\phi = \nu \nabla^2 \phi' \,, \qquad (11)$$

$$D_q = \nu \nabla^2 q \;, \qquad (12)$$

where $$\nabla^2 = \frac{\partial^2}{\partial r^2} + \frac{1}{r}\,\frac{\partial}{\partial r} + \frac{\partial^2}{\partial z^2}\,.$$

The stream function, ψ , is defined by

$$u = -\frac{1}{r}\frac{\partial \psi}{\partial z}\;, \qquad w = \frac{1}{r}\frac{\partial \psi}{\partial r}\;, \qquad (13)$$

and a vorticity equation is obtained by eliminating π' from (1) and (2):

$$\frac{\partial \eta/r}{\partial t} = -u\frac{\partial \eta/r}{\partial r} - w\frac{\partial \eta/r}{\partial z} + \frac{g}{\textcircled{H} r}\frac{\partial \theta'}{\partial r} - \frac{g}{r}\frac{\partial q_l}{\partial r}$$

$$+\nu\left[\frac{1}{r}\frac{\partial\left(r\,\partial/\partial r\right)}{\partial r} + \frac{2}{r}\frac{\partial}{\partial r} + \frac{\partial^2}{\partial z^2}\right]\frac{\eta}{r}\;, \tag{14}$$

with

$$\eta = \frac{\partial w}{\partial r} - \frac{\partial u}{\partial z} = \frac{1}{r}\left(\frac{\partial^2\psi}{\partial r^2} - \frac{1}{r}\frac{\partial\psi}{\partial r} + \frac{\partial^2\psi}{\partial z^2}\right). \tag{15}$$

After u, w, η, and ϕ' have been calculated from initial distributions of ψ, θ', q_v, and q_l (from (13), (15), and (6)), ϕ', q, and η are extrapolated in time from (4), (5), and (14) based on forward time differences and uncentered space differences taken along the direction of the flow. The ψ-field is then determined from the η-field by solving (15) as an elliptic partial differential equation, with $\psi = 0$ on the boundaries.

3. CELLULAR CONVECTION

Our first calculation was an attempt to duplicate Ogura's Run 2 (1963) in which initial lapse rate $(\partial T/\partial z)$ is -7.2°C/km, temperature excess (θ_0) is 1°C, initial relative humidity is 100 percent, and coefficient of eddy viscosity is 4.0 x 10^4 cm^2 sec^{-1}. The stream function and vertical velocities after 7 min are shown in figure 1, and the variation with time of w_{max} is shown in figure 2.

Although the basic features (e.g., shape of circulation, growth rates) of the experiments agree so that the models appear quite similar, it was impossible to duplicate Ogura's results exactly. The differences probably result from different choices of T_∞ and $\textcircled{H}$, since the static stability, $S = \frac{1}{\textcircled{H}}\frac{\partial\theta}{\partial z}$ is dependent on these reference parameters.

Ogura calculated the saturation specific humidity from (7) using the constant reference pressure (P). However, the pressure varies by about 300 mb over the 3-km depth, and this

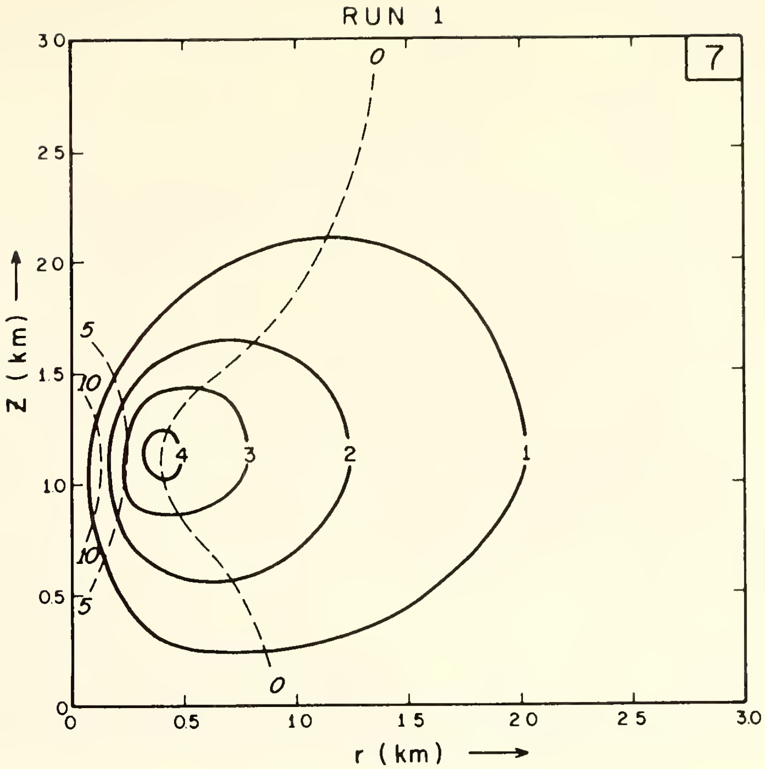

Figure 1. Stream function (solid lines, $10^5\ m^3\ sec^{-1}$) and vertical velocity fields (dashed lines, $m\ sec^{-1}$) for Run 1.

affects the distribution of q_s and, hence S. For example, the stability (approximated by $\frac{\theta e_{sec} - \theta e_{3km}}{\textcircled{H}\ 3000\ m}$) based on (7) is $7.7 \times 10^{-5}\ m^{-1}$. If the pressure variation is considered, this value is reduced to $3.8 \times 10^{-5}\ m^{-1}$. In all experiments discussed here, the height dependence of pressure based on the initial temperature distribution was included in computing q_s.

4. EFFECT OF GEOMETRY ON CONVECTION RINGS AND CELLS

Recent ATS-1 satellite photographs over the tropical oceans indicate the presence of ring- or doughnut-shaped convection consisting of an annular ring of clouds surrounding a clear center. The diameters of typical well-developed rings vary between 30 and 90 km and the ratio of inside to outside diameters is about .7 (Vonder Haar et al., 1968). For example, figures 3 and 4 show an ATS-1 photograph of a group of such rings over the Pacific and an enlargement of a region in the tropical Pacific containing an isolated ring.

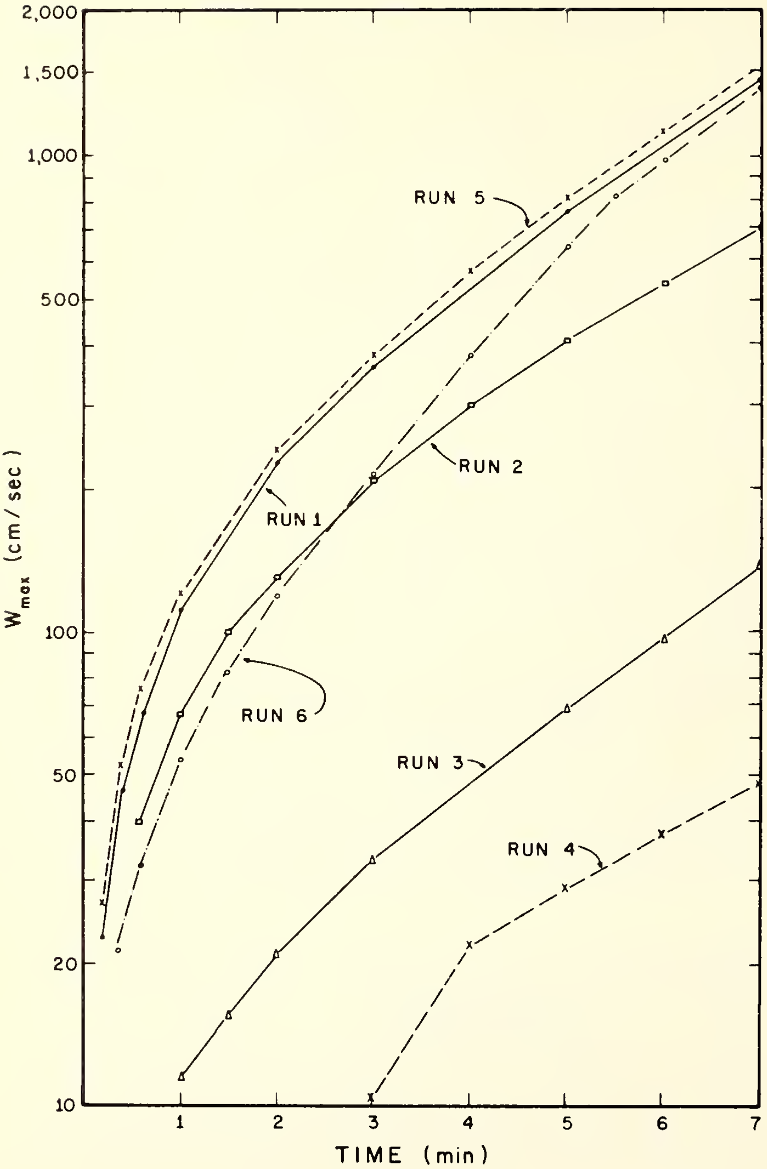

Figure 2. Variation with time of maximum upward velocity (log scale).

To apply Ogura's cloud model in describing convective rings, several experiments were performed, beginning with the initial temperature perturbation at various distances from the axis of symmetry, instead of on the axis as in the case of a single cell. This initial condition corresponds physically to a ring of hot air. Although it is difficult to imagine a physical mechanism responsible for such a ring, these conditions lead to development of ring convection by the model, and in this way the physical properties of such rings may be studied.

In using this model we assume, of course, that the ring-shaped cloud patterns consist of a single circularly symmetric cloud annulus, but the distinct possibility exists that the ring-shaped patterns consist of many cylindrical cells organized in a circular pattern. If this is indeed the case, we neglect, by using this model, the interactions between adjacent cells and the azimuthal variations of the dependent variables. Solution to this problem would require further observational studies and, possibly, development of a three-dimensional convection model.

Experiments 1, 2, and 5 deal with small-scale (dimensions of "box" 3 km x 3 km, as in Ogura's experiments) cellular and

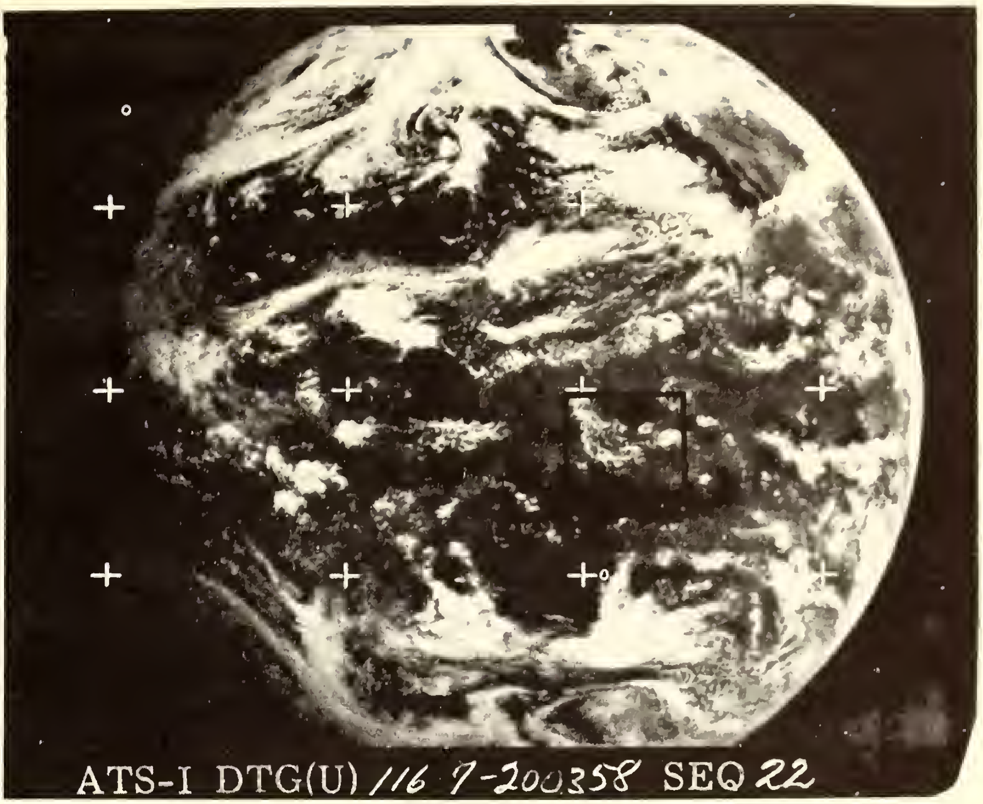

Figure 3. ATS-1 satellite photograph over the Pacific.

ring convection. In experiments 3, 4, and 6, we examine the cell and ring on a larger horizontal scale (30 km x 3 km).

5. RATE OF DEVELOPMENT AND GEOMETRY ASSOCIATED WITH RING

In Runs 1 and 2, all conditions were identical except that the radial (r) dependence of initial temperature excess in Run 2 was given by $T_0 \exp(-2.3\,|1.5-r|\,/0.32)$, instead of by $T_0 \exp(-2.3\,(r/0.32))$.

The maximum initial temperature excess is, therefore, at 1.5 km instead of at the origin.

In Run 2, convection develops in a ring at the center of the domain; the descending motion occurs on both sides of the ring. Figures 1 and 5 show the stream functions and vertical velocities after 7 min for Runs 1 and 2, respectively. The circulation associated with ring convection develops more slowly than that of the single cell (see the plot of w_{max} vs. time, fig. 2). The exponential growth rate of w_{max}, as determined by the slope of the straight line after 4 min in Run 1,

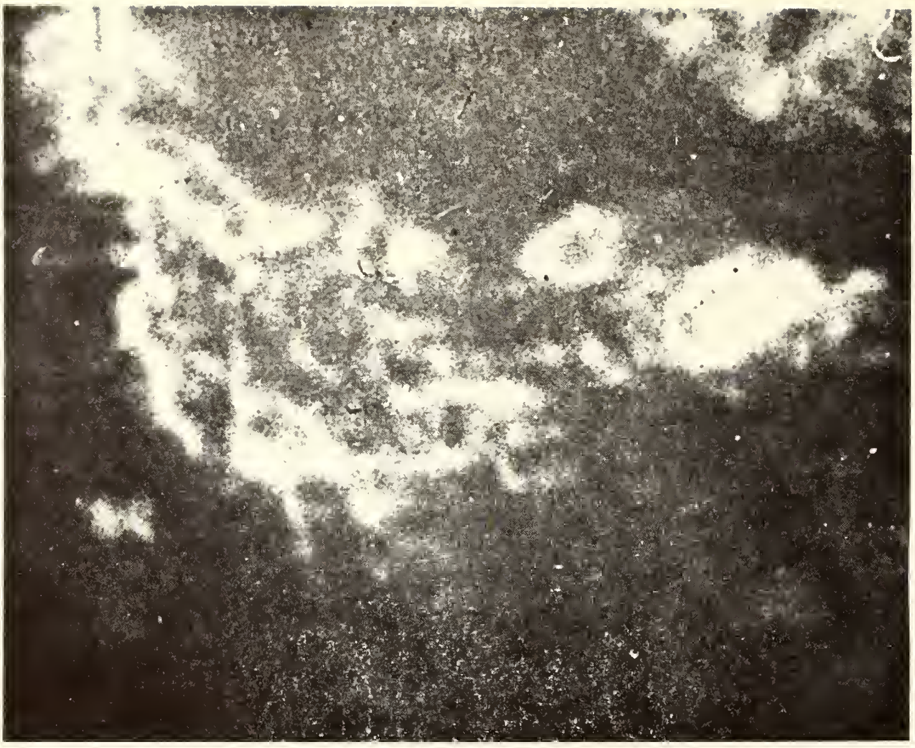

Figure 4. Enlargement of region in fig. 3 containing single convection ring.

is 5.15×10^{-3} sec^{-1}, which is about 1.2 times the growth rate of 4.75×10^{-3} sec^{-1} observed in Run 2.

Another difference between these two types of convection is the relative size and distribution of the downdraft. In the cellular convection, the downdraft is confined to a rather narrow ring surrounding the updraft, and the maximum downward velocity is only 4 percent of the maximum upward velocity. In contrast, the downdraft outside the ring convection (Run 2) is concentrated near the updraft and is 20 percent of the updraft in magnitude. Inside the ring subsidence occurs more uniformly over the region and is 35 percent of the updraft in magnitude. These differences are illustrated in figures 6a and 6b by the radial profile of normalized vertical velocity w/W_{max} at the level of W_{max} for Runs 1 and 2.

The differences in the downdraft may be explained by the mass dependence on radius in the cylindrical coordinate system. If the downdraft occurs at radii less than that of the updraft, greater velocities are required for mass balance than if it occurs at radii greater than the updraft's. In Run 1 the radius of the cell is about 400 m, while in Run 2 the thickness of the ring is about 500 m. Since the mass involved in the ring updraft is nine times the mass in the updraft of the cell, the ring's rate of mass (and consequently heat) transpo is 4.5 times that of th cell, even though the mean upward velocity in the cell is twice that of the ring.

Because of the mass dependence on radius, the downward mass transport outside the ring is about twice that inside, although the velocities outside are smaller. Thus, approximately 2/3 of the updraft recirculate outside the convective ring, while 1/3 returns inside it.

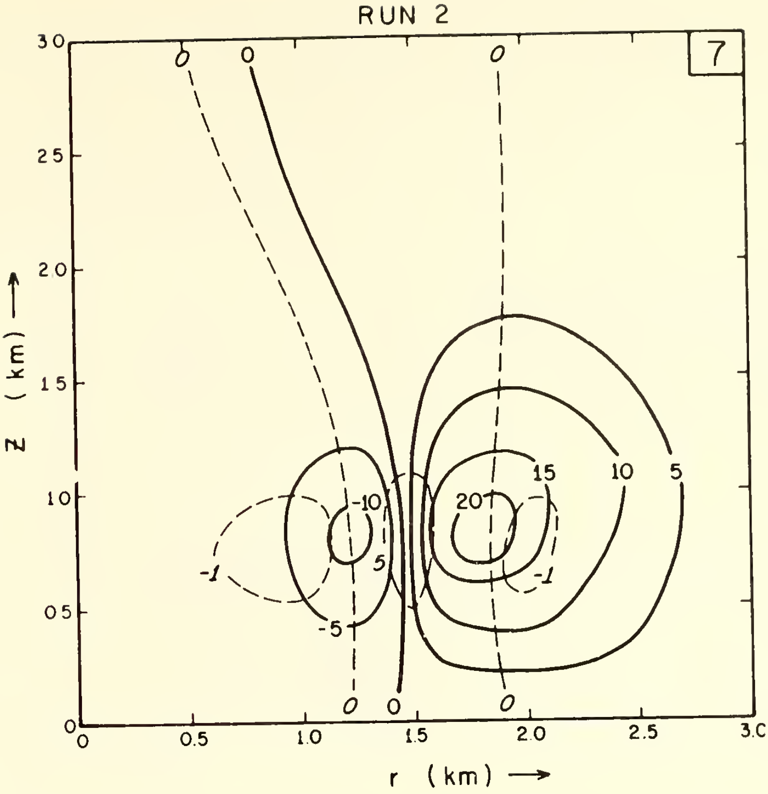

Figure 5. Stream function and vertical velocity fields for Run 2. Key same as in fig. 1.

6. EFFECT OF SCALE (SIZE OF DOMAIN) ON CELLULAR CONVECTION

Runs 3 and 1 contrast small-scale with large-scale cellular convection. In Run 3, all horizontal dimensions from Run 1 (3 km x 3 km) were scaled by 10, giving a horizontal distance of 30 km and a grid size Δr of 1 km. The temperature perturbation was given by $T' = T_0 \exp(-2.3\, r/3200)$, with $T_0 = 1^{\circ}$C so that the initial temperature gradients were 1/10 of those in Run 1.

As expected, the large-scale convection developed at a muc slower rate than the small-scale. Figure 7 shows the stream function and vertical velocities from Run 3 after 7 min, which may be compared with those from Run 1 (fig. 1). Figure 6 shows the radial profile of normalized vertical velocity. The width of the updraft is about 1.5 km in Run 3 compared with 400 m in Run 1. For the large scale, W_{max} is 1.4 m/sec or about 10 times smaller than W_{max} for the smaller scale. The growth rate of W_{max} after 4 min in Run 3 is 4.15×10^{-3} sec^{-1} or 73 percent that of Run 1 (fig. 2).

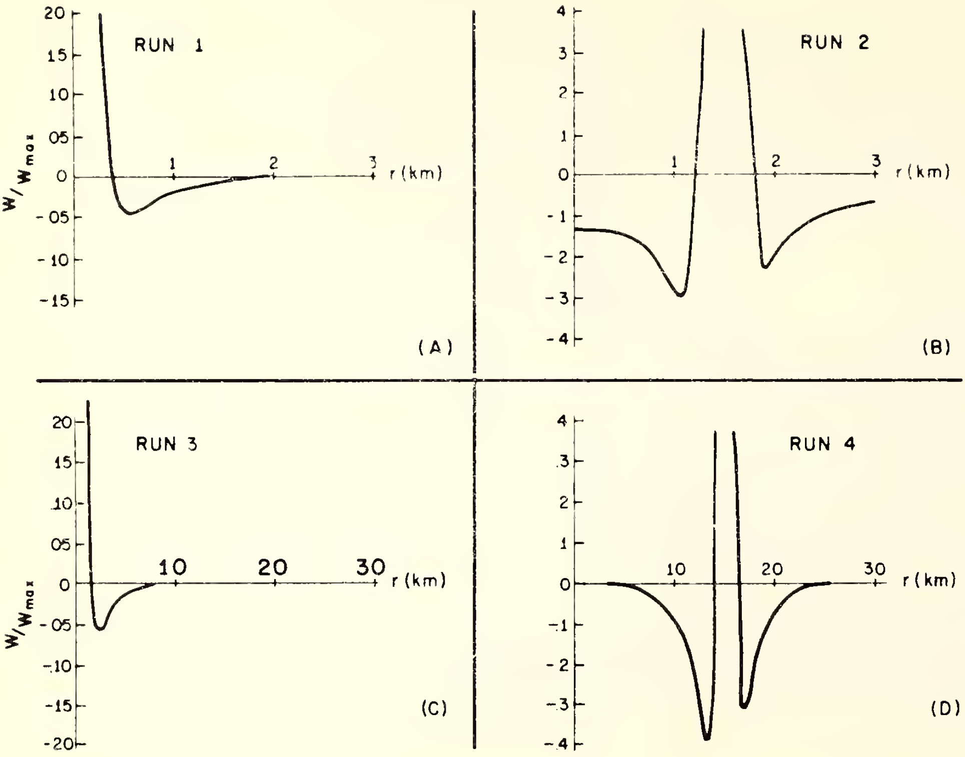

Figure 6. Radial profile of normalized vertical velocity.

An interesting feature in Run 3 is the development of small amplitude waves at large distances from the cell. These waves appear after 5 min at the upper levels and build downward. Since computational instability is usually indicated by oscillations of the wavelength 2Δr (2 km in this case), the waves observed here may be internal gravity waves generated by the rising disturbance in the center. These waves do not appear in the 3 km x 3 km experiments where there is sufficient instability to allow continued growth of the cloud, since the smaller dimensions restrict development of such secondary waves. However, in some of Ogura's experiments in which the initial buoyancy of the thermal was insufficient for the conditional instability to be realized, the primary cell oscillates and generates similar gravity waves.

7. EFFECT OF SCALE ON RING CONVECTION

Experiments 2 and 4 contrast small- and large-scale ring convection. Figure 8 shows the stream function and vertical velocity distribution after 7 min for Run 4. The large-scale

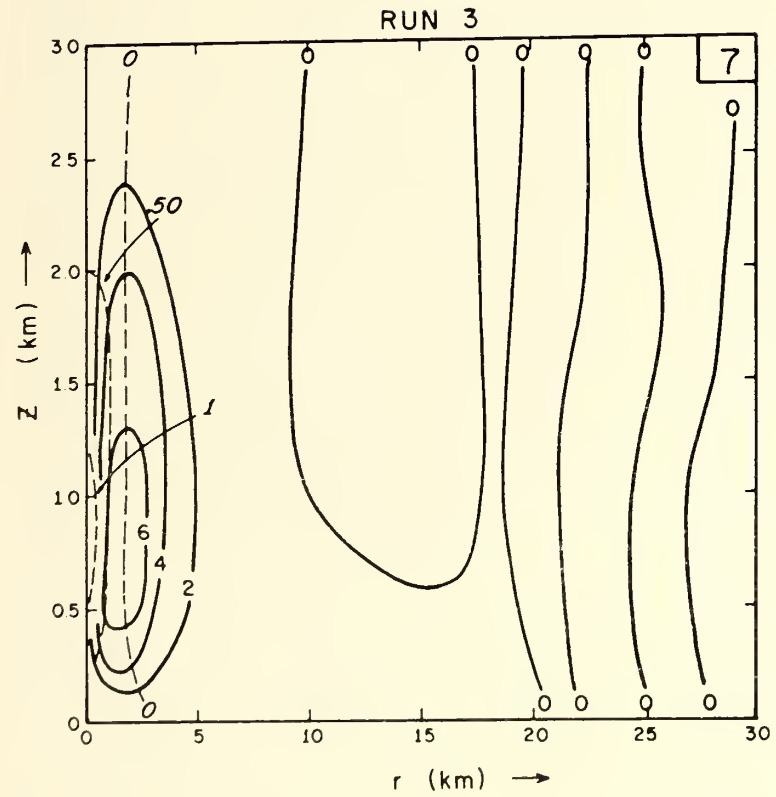

Figure 7. Stream function and vertical velocity fields for Run 3. Key same as in fig. 1.

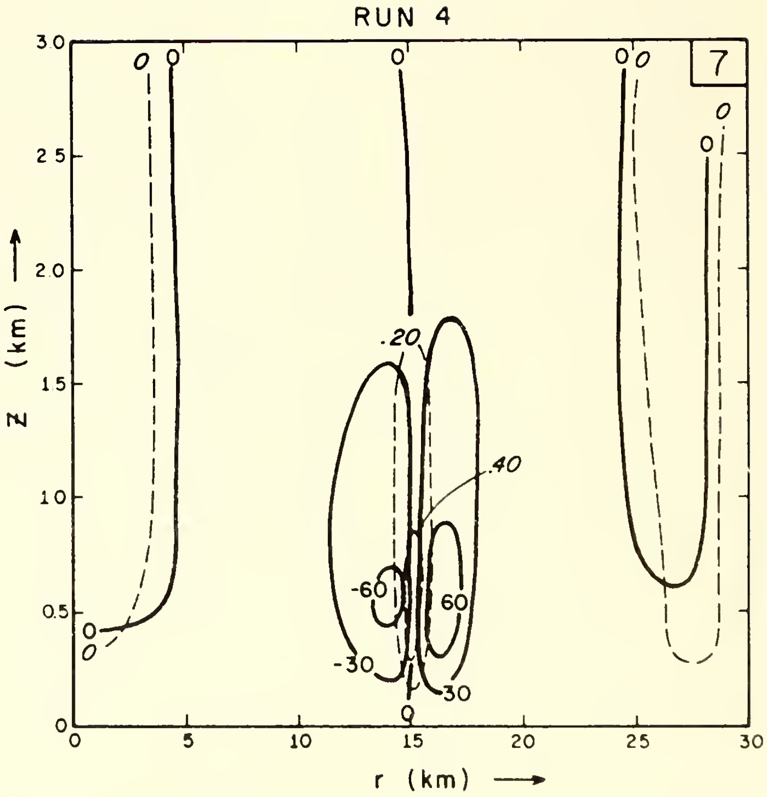

Figure 8. Stream function and vertical velocity fields for Run 4. Key same as in fig. 1.

ring convection develops more slowly than the small-scale and is 5 times wider (2.5 km).

As shown by the normalized vertical velocity profile (fig. 6d), the downdrafts are more symmetric with the updraft in the large-scale ring than they are with the small-scale ring (Run 2). The percentage of mass recirculating inside the ring rose from 33 percent in Run 2 to 43 percent in Run 4, which is expected as the radius of curvature increases and the behavior of the ring approaches that of a cloudline.

8. INCREASED HORIZONTAL RESOLUTION

In numerical models of atmospheric convective phenomena, such as cumulus clouds, squall lines, or hurricanes, it is frequently desirable to have a greater resolution in one part of the domain than in another. In numerical models of hurricanes, for example, a fine mesh is desirable near the eyewall where horizontal gradients are large; on the outskirts of the storm, gradients are weak and a fairly coarse grid is adequate. In models of cumulus convection, higher resolution in the vicinity of the cloud is more desirable than in the regions farther away from the cloud. In the transformation $r = x^2 + Cx$, where r is the radial distance and x is the new transformed distance, the physical grid distance Δr is proportional to the transformed distance x for a fixed $\Delta x (\Delta r = (2x + C)\Delta x)$. The finite difference approximations of the equations of motion may be written in terms of x and Δx, to obtain a continuously varying resolution.

Estoque (1962), Syōno (1962), and Kuo (1965) have made similar transformations in their numerical models of hurricanes. However, little has been written on the effect of these transformations on the behavior of the models. To better understand the advantages and disadvantages (if any) of such transformations and to gain further insight into Ogura's model, several experiments were run based on the transformation $r = x^2 + Cx$. The conclusion is that such a transformation is useful and that the convection described by the increased resolution differs significantly from the convection with less resolution. In particular, growth rates from the highly resolved convection are in closer agreement with the growth rates predicted by linear theory.

For the transformation $r = x^2 + Cx$, all equations were written in terms of the new coordinate system x, z, and the finite difference equations were written in terms of constant Δx. The transformed versions of (4), (14), and (15) are as follows:

$$\frac{\partial \phi'}{\partial t} = -\frac{u}{(2x+c)}\frac{\partial \phi'}{\partial x} - w\frac{\partial \phi'}{\partial z} + \nu \nabla^2 \phi' , \qquad (4')$$

$$\frac{\partial \eta}{\partial t} = u\eta(x^2+cx)^{-1} - u(2x+c)^{-1}\frac{\partial \eta}{\partial x} - w\frac{\partial \eta}{\partial z} + \frac{g}{\textcircled{H}}(2x+c)^{-1}\frac{\partial \theta'}{\partial x} \qquad (14')$$

$$-g(2x+c)^{-1}\frac{\partial q_l}{\partial x} + \nu\left[\nabla^2\eta - \eta(x^2+cx)^{-2}\right],$$

$$\eta = (2x+c)^{-1}\frac{\partial w}{\partial x} - \frac{\partial u}{\partial z} . \qquad (15')$$

The ∇^2 operator in the transformed coordinate is

$$\nabla^2 = (2x+c)^{-2}\frac{\partial^2}{\partial x^2} - 2(2x+c)^{-3}\frac{\partial}{\partial x} + (x^2+cx)^{-1}(2x+c)^{-1}\frac{\partial}{\partial x} + \frac{\partial^2}{\partial z^2} .$$

The constant c was chosen to give 10 times the untransformed (constant) resolution at the origin and to keep the total number of grid points the same 31. Thus, for the 3 km x 30 km domain, $c = 12.4\ m^{1/2}$, $x = 5.56\ m^{1/2}$, so that Δr varies from 100 m at the origin to 1923 m at r = 30 km, as indicated schematically below.

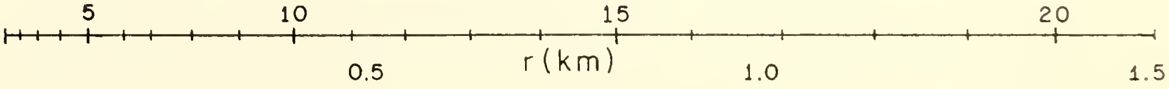

Note that a gain of 10 times the resolution near the center is accompanied by a loss of only 2 times at the edge of the domain. The time increment Δt was chosen to satisfy the computational stability requirement for the minimum Δr.

9. LARGE-SCALE CONVECTION WITH VARIABLE RESOLUTION

Runs 3 and 6 compare the large-scale cumulus cell as described by the normal coordinate system (Run 3) and the transformed system (Run 6). Figures 7 and 9 show the stream functions and vertical velocities from the two runs after 7 min. In the variable resolution case (Run 6), the vertical velocities at the origin are about 10 times larger than those

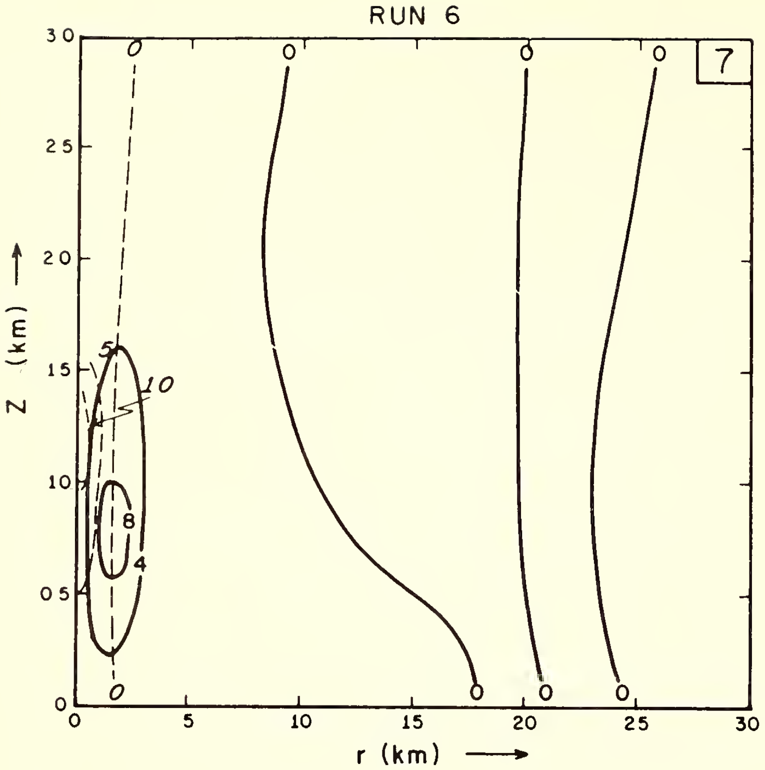

Figure 9. Stream function and vertical velocity fields for Run 6. Key same as in fig. 1.

in Run 3. In the constant resolution case, 2 km is only two grid points from the boundary, while in the transformed case 2 km is seven gridpoints from the boundary. The fine mesh in Run 6 apparently resolves the greater velocities in the core, while the coarser grid averages the velocities. The growth rate of W_{max} in Run 6 after 4 min is about 7.0 x 10^{-3} sec^{-1} compared with 4.15 x 10^{-3} sec^{-1} in Run 3 (fig. 2). If the theortical growth rate is computed from Kuo's (1961) formula

$$Q = \left(\frac{g\alpha S - f^2}{1+\alpha^2}\right)^{1/2} - \frac{(3.14)^2}{h^2}\left(\nu_z - \alpha^2 \nu_h\right) ,$$

with the Coriolis parameter f = 0; the depth of the fluid h = 3 km; α (the ratio of h to updraft diameter x) = 1.0; S = 3 x 10^{-5} m^{-1}; and $\nu_z = \nu_h = \nu$ = 4.0 m^2 sec^{-1}, we obtain Q = 12 x 10^{-3} sec^{-1}. Hence, the growth rate observed in Run 6 is much closer to the theoretical rate than that observed in Run 3. It should be noted, however, that the theoretical growth rate of 12 x 10^{-3} does not include the implicit diffusion in the upstream differencing scheme. Ogura also notes that the growth rates observed in his calculations appear too small.

Another important difference between the two convection experiments is the horizontal width of the updraft. The updraft in the high resolution experiment is 1.2 km wide, which is somewhat lower than that in the constant resolution experiment. This difference is probably related to the theoretical result that, in a conditionally unstable atmosphere, disturbances with the shortest wavelengths grow most rapidly when viscous effects are neglected. Figure 10 shows the growth rates as a function of updraft diameter X for ν = 4.0×10^4 cm^2 sec^{-1} and several values of stability. For this choice of ν, the fastest growin waves have updrafts about 600 m in diameter. In the lower resolution case (Run 3), where Δr = 1 km, the wavelength is restricted by the grid size and artificial damping of the shorter waves occurs; in Run 6 the higher resolution (100 m at r = 0) can describe the faster growing wavelengths.

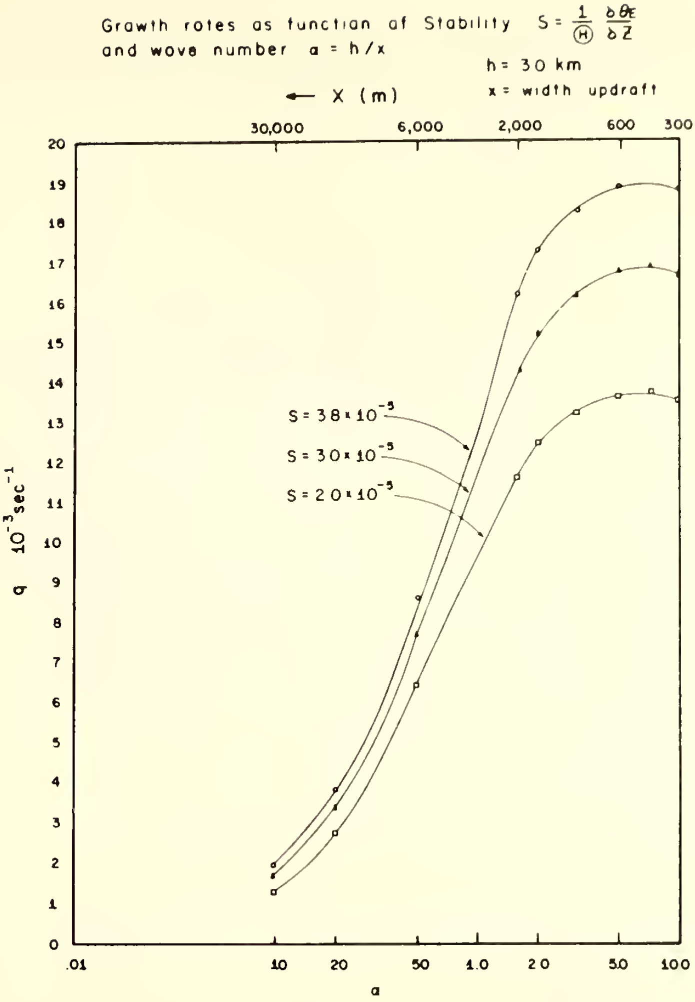

Figure 10. Growth rates as a function of updraft diameter and stability.

10. SMALL-SCALE CONVECTION WITH VARIABLE RESOLUTION

To determine the effects of the transformation $r = x^2 + Cx$ on convection in the 3-km x 3-km domain, C was taken to be 4.0 and Δx = 1.76 m$^{\frac{1}{2}}$, which again gives a resolution 10 times higher in the center (10 m) and 2 times smaller (194 m) at r = 3 km. Figures 1 and 11 show the stream functions and vertical velocities after 7 min for normal resolution (Run 1) and variable resolution (Run 5).

The differences between the variable and constant resolution experiments are small. The development in both experiments occurs at nearly the same rate: the growth rate in Run 5 is

5.8×10^{-3} $\sec^{-1}$ compared with 5.65×10^{-3} $\sec^{-1}$ in Run 1.

The wavelength of the disturbance, as measured by the width of the updraft, does not differ appreciably in the two runs. The close similarity between the two experiments is probably because in both cases the resolution is sufficiently fine to adequately describe the disturbance of preferred wavelength, which is close to 600 m.

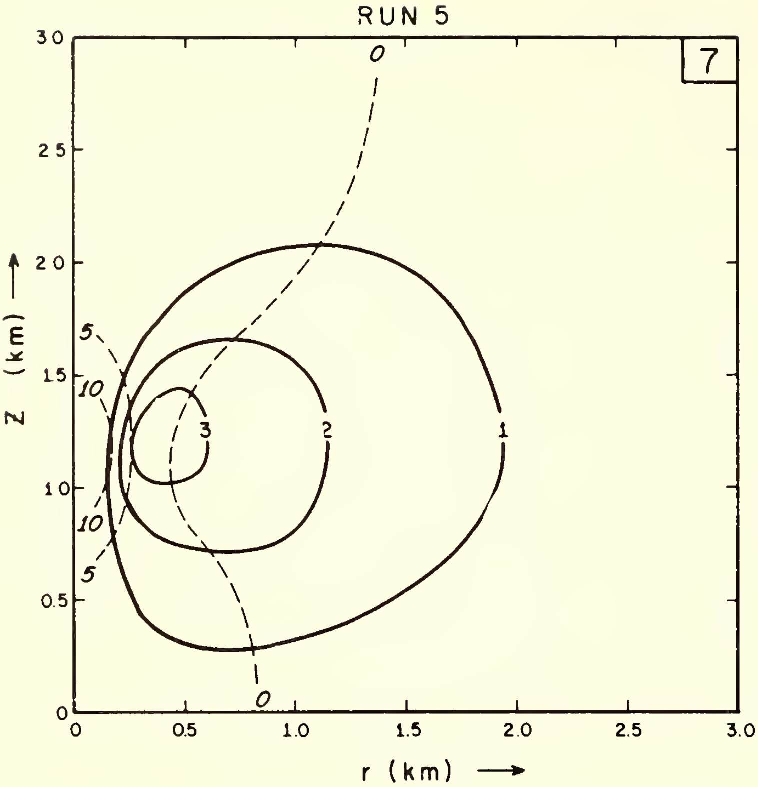

Figure 11. Stream function and vertical velocity fields for Run 5. Key same as in fig. 1.

11. SUMMARY

We have investigated some effects of stability, geometry, scale, and resolution on a numerical model of shallow moist convection. The results may be summarized as follows:

(a). Circulation features of ring convection were studied in several experiments. With the initial conditions of a ring of hot air, the resulting circulation is a uniform cloud ring. However, the observed rings in nature may well not be unique circulations but organized systems of individual cumulus cells. Such azimuthal variation, of course, cannot be studied in the two-dimensional model used here.

(b). Increasing the horizontal scale from 3 km to 30 km results in a slower development of convection caused by the larger initial disturbance and by the artificial damping of the faster growing short waves. The second effect is partly counteracted by introducing a variable resolution through the transformation $r = x^2 + Cx$. The growth rates of convection resulting from this transformation are closer to theoretical growth rates than those from the untransformed coordinates; thus the use of such a transformation to economically gain higher resolution in particular regions of interest appears useful.

12. ACKNOWLEDGMENTS

This research was sponsored by the National Science Foundation through a graduate fellowship and the National Hurricane Research Laboratory. The author expresses his sincere appreciation to Drs. John A. Young and Donald R. Johnson and Mr. Robert W. Reeves for their stimulating discussions and to Dr. Stanley L. Rosenthal for carefully reading the manuscript and making many helpful suggestions. Thanks are also due Mr. Tom Vonder Haar for supplying the satellite photographs.

13. REFERENCES

Estoque, M. A. (1962), "Vertical and radial motions in a tropical cyclone," Tellus 14, 394-402.

Kuo, H. L. (1961), "Convection in a conditionally unstable atmosphere," Tellus 13, 441-459.

Kuo, H. L. (1965), "On formation and intensification of tropical cyclones through latent heat release by cumulus convection," J. Atmospheric Sci. 22, 40-63.

Lilly, D. K. (1962), "On the numerical simulation of buoyant convection," Tellus 14, 148-172.

Lilly, D. K. (1964), "Numerical solutions for the shape-preserving two-dimensional thermal convection element," J. Atmospheric Sci. 21, 83-102.

Malkus, J. S., and G. Witt (1959), "The evolution of a convective element: a numerical calculation," The Atmosphere and the Sea in Motion (Rockefeller Institute Press, New York), 509 pp.

Ogura, Y. (1962), "Convection of isolated masses of buoyant fluid: a numerical calculation," J. Atmospheric Sci. 19, 492-502.

Ogura, Y. (1963), "The evolution of a moist convective element in a shallow, conditionally unstable atmosphere: a numerical calculation," J. Atmospheric Sci. 20, 407-424.

Syōno, S. (1962), "A numerical experiment on the formation of tropical cyclones," Proc. Intern. Symp. Numerical Weather Prediction, Tokyo, Meteorological Society of Japan, 405-418.

Vonder Haar, T., K. Hanson, V. Suomi, and U. Shafrir (1968), "Phenomenology of convective ring clouds in the tropics derived from geosynchronous satellite observations," Proc. Intern. Conf. Cloud Physics., Toronto, Canada, University of Toronto.

MARINERS WEATHER Log 35
Vol. 13, No. 5, 197-202.

HURRICANE GENESIS FROM DISTURBANCES FORMED OVER AFRICA

Toby N. Carlson
National Hurricane Research Laboratory , ESSA
Coral Gables, Fla.

During the early phases of the Atlantic hurricane season (June and July) and in the autumn (late September to early November), the main spawning ground for hurricanes and tropical storms in the North Atlantic region is over the Gulf of Mexico and the western Caribbean Sea. An initial seedling disturbance in the Tropics, from which a hurricane can grow, is often triggered in this area by the proximity of relatively cold air masses that penetrate southward over the continents from higher latitudes. These cold and drier air masses favor the lifting and condensation of moist and unstable air over the warmed tropical oceans. The air rises violently in giant cumulonimbi, releasing heat of condensation in the rising cloud towers, which eventually can lead to a gradual pressure fall at the surface in the disturbed area. The result may be the birth of a weak tropical disturbance characterized by increased cloudiness and showers in association with a shallow low-pressure area.

Provided that other conditions are favorable for continued growth, this initial disturbance can intensify further and become a tropical storm (minimum winds of 34 kt) and eventually a hurricane (minimum winds of 64 kt). Whether or not such development takes place, the disturbance, drifting along with the steering winds, remains an entity for a time.

From August through late September, the primary spawning ground shifts eastward to a corridor lying between Africa and the eastern Caribbean (fig. 1).* The Gulf of Mexico and the western Caribbean are very warm throughout the entire hurricane season and therefore might be expected to remain highly favorable for tropical storm formation in terms of sea-surface temperature considerations alone. Numerous studies of the hurricane problems have indicated that the sea-surface temperature is possibly the single most important external factor affecting the growth and intensity of tropical storms and hurricanes. These studies generally point toward a value of about 80°F, above which the ocean surface is sufficiently warm to provide the necessary heat energy to fuel the storm. Figure 1 illustrates the sensitivity of tropical storm formation to the disposition of the 80°F isotherm. Few storms are shown to form at temperatures colder than about 79° to 80°F. Of course, once a tropical storm or hurricane comes into being, it can sustain itself for a time by its own internal workings, even over water appreciably colder than 80°F.

Despite the presence of rather warm water in the Gulf of Mexico and the western Caribbean, the majority of storms form elsewhere during August and September, and it is rare for a really important storm to generate there at that time of year. From mid-July until late September, the overwhelming majority of tropical storms and hurricanes in the North Atlantic area originate from disturbances that can be traced back to the continent of Africa. The approach of summer brings on a monsoonal flow of moist and unstable air onto the sub-Saharan portion of the African Continent. This flow of air is sufficiently deep in July to sustain vigorous thunderstorm activity between latitudes 10° and 20° N. At about this time, a succession of disturbances moves across this area from some un-

---

*Some of the data for this figure have been presented in the U.S. Weather Bureau publication Tropical Cyclones of the North Atlantic Ocean, Technical Paper No. 55, 1965.

MEAN SEA SURFACE ISOTHERMS JUNE AND JULY AND INITIAL POSITIONS OF TROPICAL STORMS, 1901 – 1967

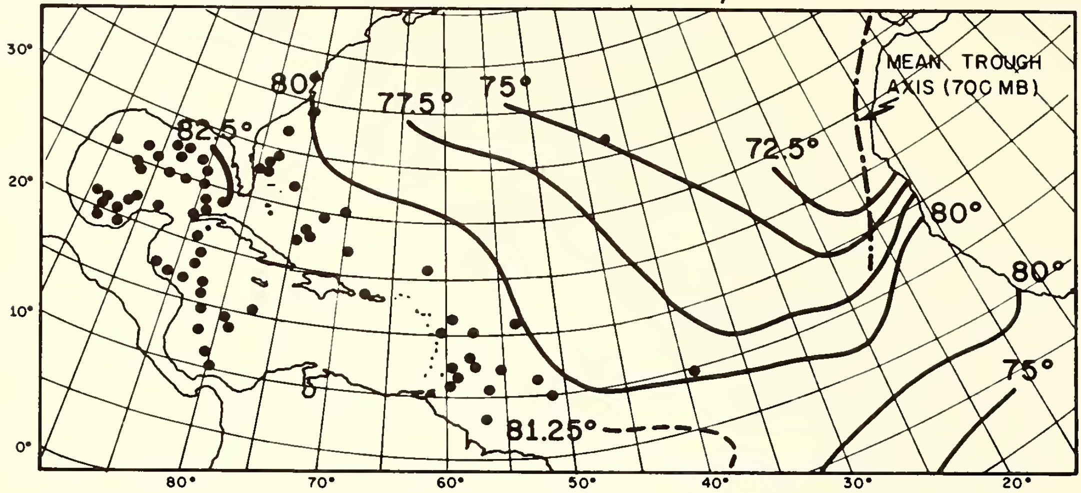

MEAN SEA SURFACE ISOTHERMS, AUGUST, AND INITIAL POSITIONS OF TROPICAL STORMS, 1901 – 1967

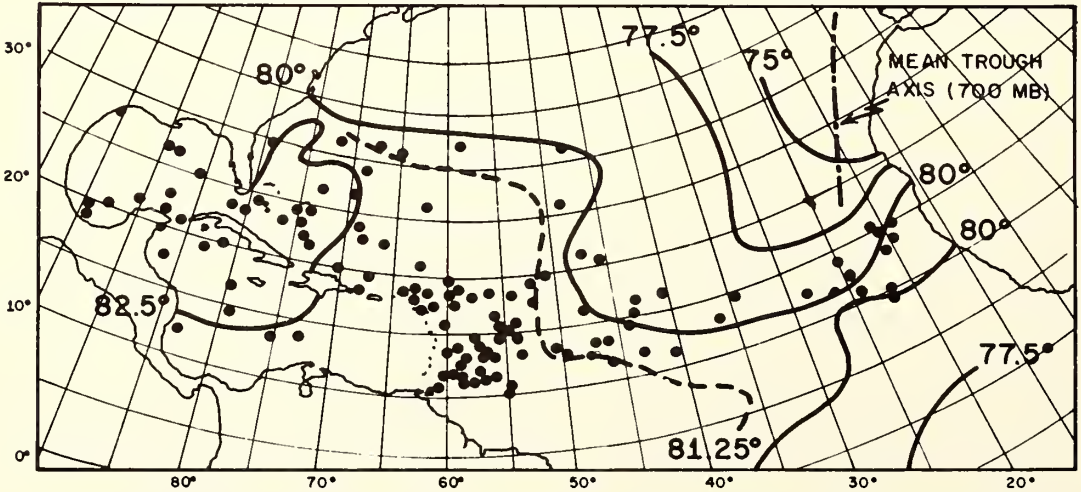

MEAN SEA SURFACE ISOTHERMS, SEPTEMBER, AND INITIAL POSITIONS OF TROPICAL STORMS, 1901 – 1967

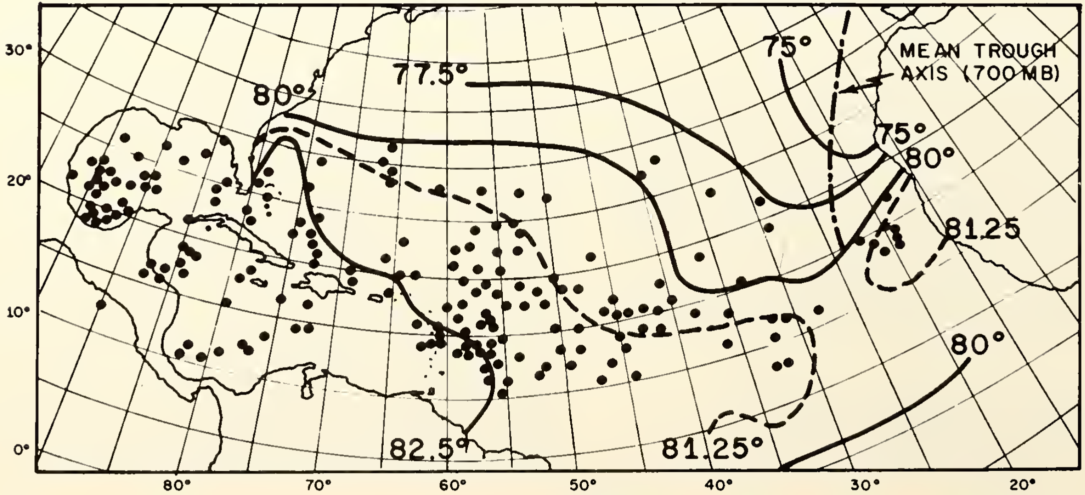

Figure 1. Mean sea-surface isotherms (°F) and the distribution of initial tropical cyclone fixes (1901-1967).

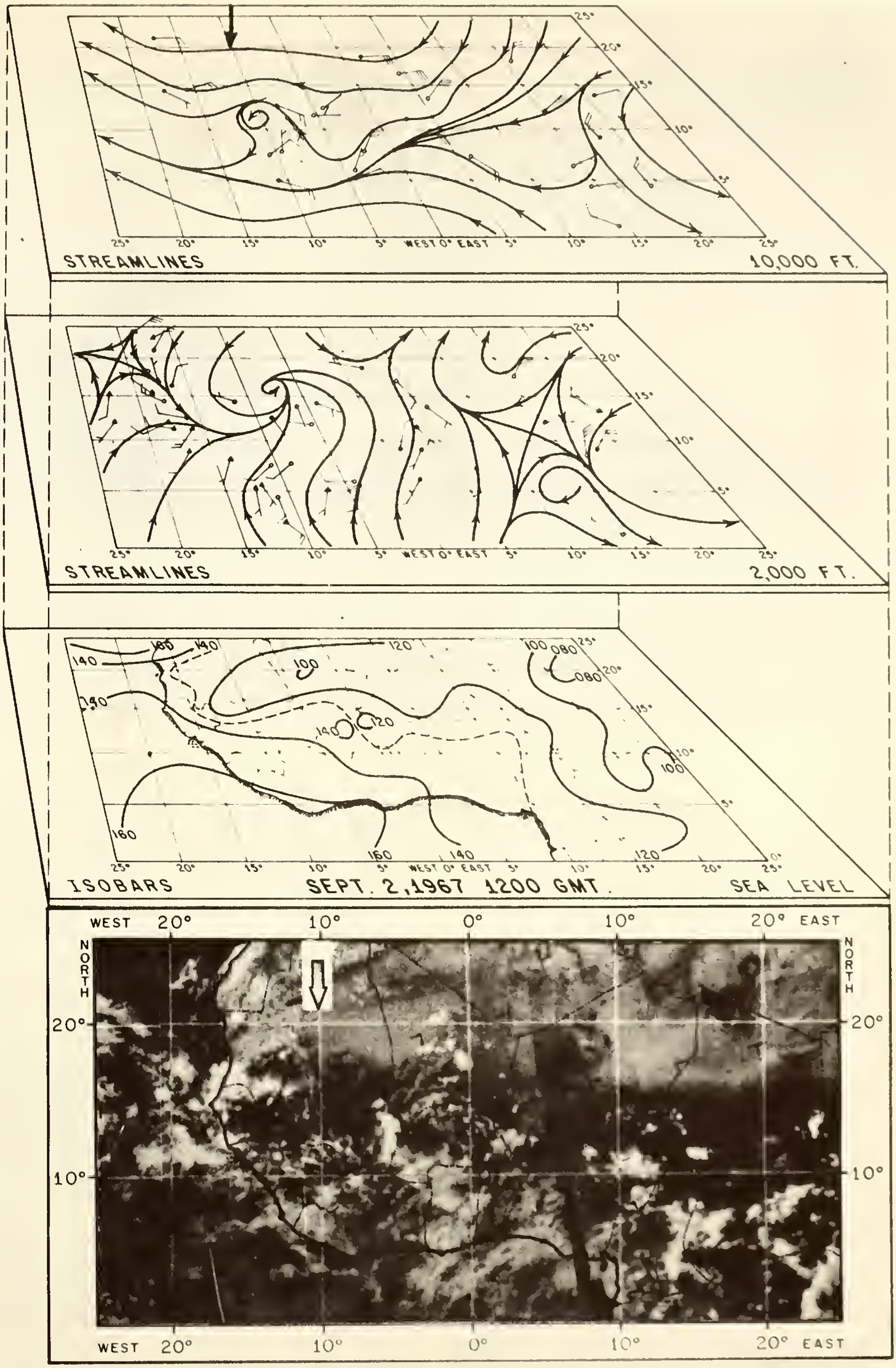

Figure 2. Streamlines at 10,000 and 2,000 ft, contours of sea-level pressure in tenths of millibars (labeled every 2 mb with tens and thousands digits omitted), and an ESSA 5 satellite photograph. The position of the disturbance is indicated by the arrow.

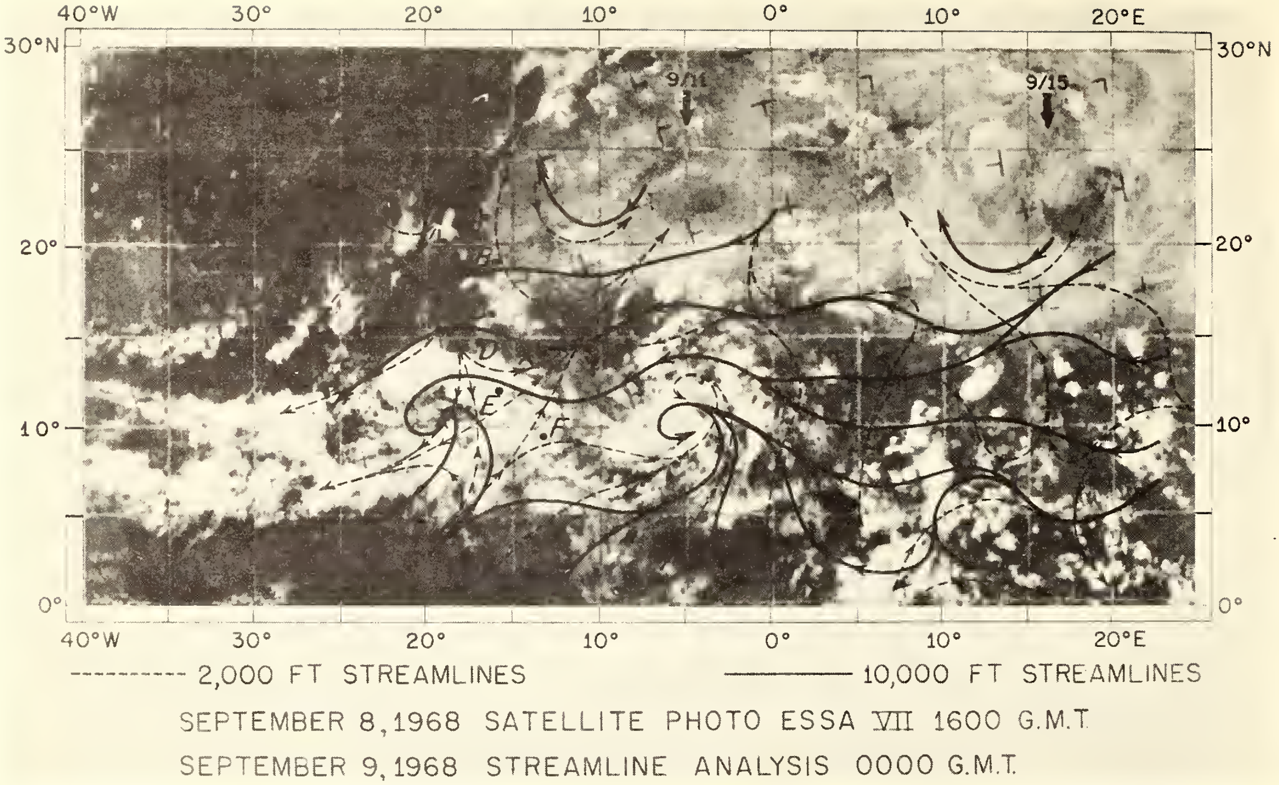
40°W
30°
20°
10°
0°
10°
20°E
30°N
20°
10°
0°
9/11
9/15
B
D
E
F
2,000 FT STREAMLINES
10,000 FT STREAMLINES
SEPTEMBER 8,1968 SATELLITE PHOTO ESSA VII 1600 G.M.T
SEPTEMBER 9,1968 STREAMLINE ANALYSIS 0000 G.M.T.

Figure 3. Streamlines at 10,000 and 2,000 ft superimposed on ESSA 5 satellite photograph. Positions of the disturbances are indicated by an arrow and labeled according to the date the wave passed the coast. Letters refer to the locations of pressure records shown in figure 5.

known source region deep in the interior of the African Continent. When the disturbances are active, as they often are between July and October, they can be seen crossing the western coast of Africa at intervals of about one every 3 or 4 days.

The existence of African disturbances and the possibility of their growth into Atlantic hurricanes has been known for several years, but because of the lack of meteorological data over the eastern Atlantic it was thought that the midseason hurricanes more often formed from initiating disturbances whose origins were in the Intertropical Convergence Zone south of the Cape Verde Islands. Recently a different conclusion has been reached as a result of reliable satellite observations and the availability of large quantities of useful meteorological information over continental Africa, that has made it possible to determine a more reliable continuity of weather patterns between Africa and the Caribbean. It now appears that most of the disturbances that form over Africa survive to reach the Caribbean and that most tropical disturbances (including tropical storms and hurricanes) that pass near or over the eastern Caribbean in August and September have had their origin over Africa.

The progress of these disturbances and their continuity on crossing the Atlantic has been documented in some detail during the past 2 yr. In 1967 three hurricanes and two tropical storms, out of a total for the Atlantic season of five hurricanes and three tropical storms grew from these weak incipient disturbances, whose origin had been over Africa. Hurricanes Arlene, Beulah, and Chloe of that year all crossed the African coast in incipient stages during a single 10-day interval in August and early September. Figure 2 shows incipient hurricane Chloe as a weak but intensifying disturbance at about 10° W. Later, Chloe was to reach tropical storm strength at 38° W.

The 1968 hurricane season was one of the least formidable on record in terms of the number and intensity of hurricanes and tropical storms. During August and September, one hurricane and two tropical storms were observed over the tropical Atlantic; of these, the hurricane and one of the tropical storms could be traced back to the interior of Africa. Figures 3 and 4 show the progress of a typical train of wavelike disturbances over Africa. The longitudinal axes of the waves are labeled by an arrow and a number represents the date (month/day) on which the wave crossed the African coast. The one labeled 9/11 at longitude 5° W is the most impressive-looking of the four shown and actually did become a tropical storm (Edna) at 35° W.

At 10,000 ft the disturbances are evident on the conventional weather map and resemble wavelike perturbations in the basic easterly current. Near the surface (2,000 ft) they are much more poorly resolved, although disturbance number 9/11 exhibits a distinct cyclonic eddy that coincides with a dense blob of cloudiness. Like their counterparts in the Caribbean, these disturbances are usually most intense between 5,000 and 15,000 ft and are often poorly defined at the surface and in the attendant cloud pattern. In most

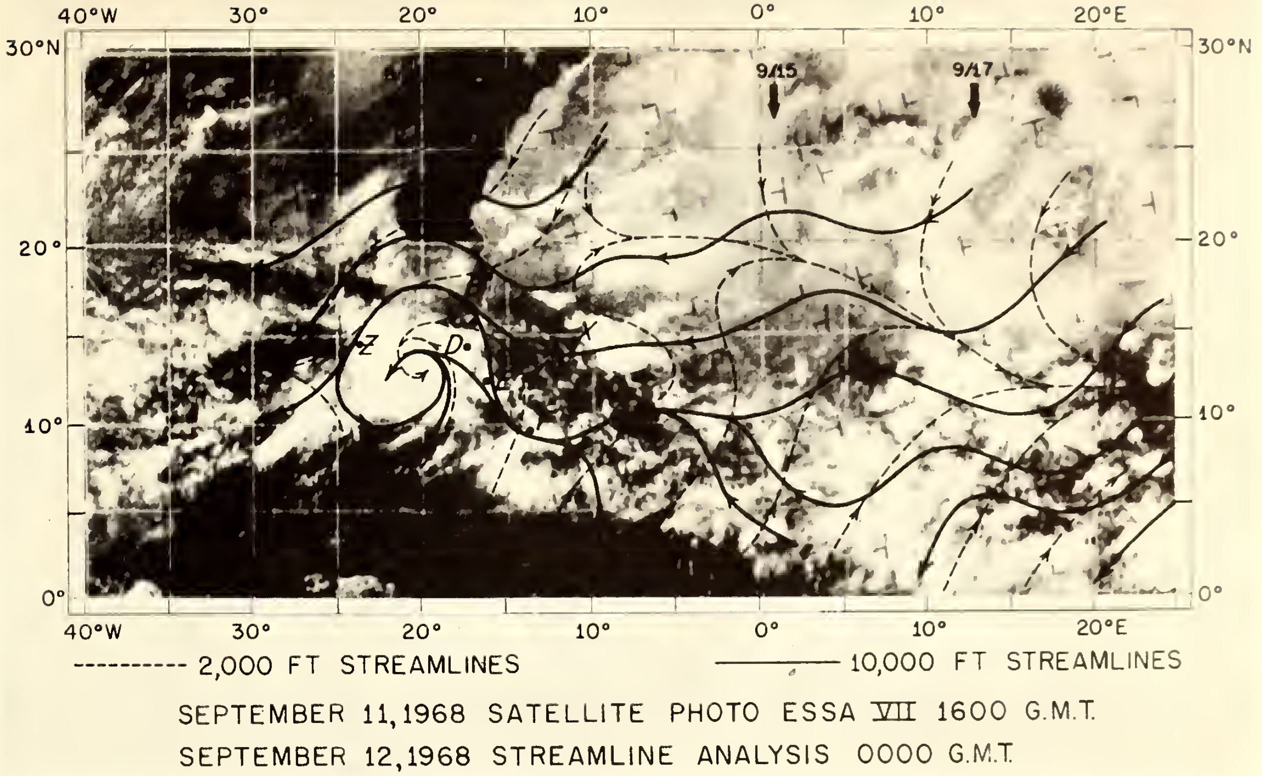
40°W
30°
20°
10°
0°
10°
20°E
30°N
20°
10°
0°
9/15
9/17
Z
D
2,000 FT STREAMLINES
10,000 FT STREAMLINES
SEPTEMBER 11, 1968 SATELLITE PHOTO ESSA VII 1600 G.M.T.
SEPTEMBER 12, 1968 STREAMLINE ANALYSIS 0000 G.M.T.

Figure 4. Same as figure 3, but 3 days later. Note that the disturbances have moved about 900 mi westward in this interval.

instances it is exceedingly difficult to track these systems over the ocean using conventional surface (ship) data alone. Satellite observations and continuity of motion are most helpful in this effort. In general, the tracking of these disturbances out over the ocean is somewhat speculative by any of the present methods, not only because of the lack of data but because the majority of African disturbances begin to disintegrate upon arriving west of the Cape Verde Islands. Only a few achieve tropical storm status--the remainder arrive in the Caribbean in a highly weakened state or disappear altogether.

Even when surface analysis fails to reveal any definite cyclonic vortex, a strong sea-level pressure oscillation (and at higher levels a wind shift from northeast to southeast) accompanies the passage of the disturbance past observing stations on the coast. Variations of 2 to 3 mb accompanying the three disturbances in figure 3 are evident in the pressure traces of figure 5. These pressure variations are seen to propagate westward with the disturbance and are about as large near the Cape Verde Islands as they were over Africa. The mean westward speed of the disturbances during 1968 was about 15 kt, with a gradual slowing down of their movement during the course of the summer (fig. 6). The mean speed was slightly greater than 15 kt over the Atlantic Ocean.

The majority of African disturbances appear to reach maximum intensity near the west coast of Africa. Moving through this coastal region, they find themselves in an area meteorologically favorable for intensification, being immediately east of the large-scale upper (700 mb) trough shown in figure 1. At the same time they are being fed at low levels by an ample supply of moist air over the western part of the continent and by the adjacent warm ocean. As the disturbances pass west of this upper trough, they enter a region meteorologically unfavorable for growth and at the same time encounter a rather cold part of the ocean, revealed as a southward thrust of sea-temperature isotherms in figure 1. An irreversible dissipation then starts in most cases, although some disturbances are able to revive themselves later as they encounter warmer water.

African disturbances are most intense during the period from mid-August until mid-September. Indications are that slight variations in sea-surface temperature from year to year may influence the total annual number of developing cases that always represent a small percentage of all tropical disturbances. We still do not know what makes a given disturbance develop and a succeeding one dissipate, but a combination of warm ocean temperatures plus a prolific source region for tropical disturbances, such as Africa, is a statistically favorable set of circumstances for hurricane growth.

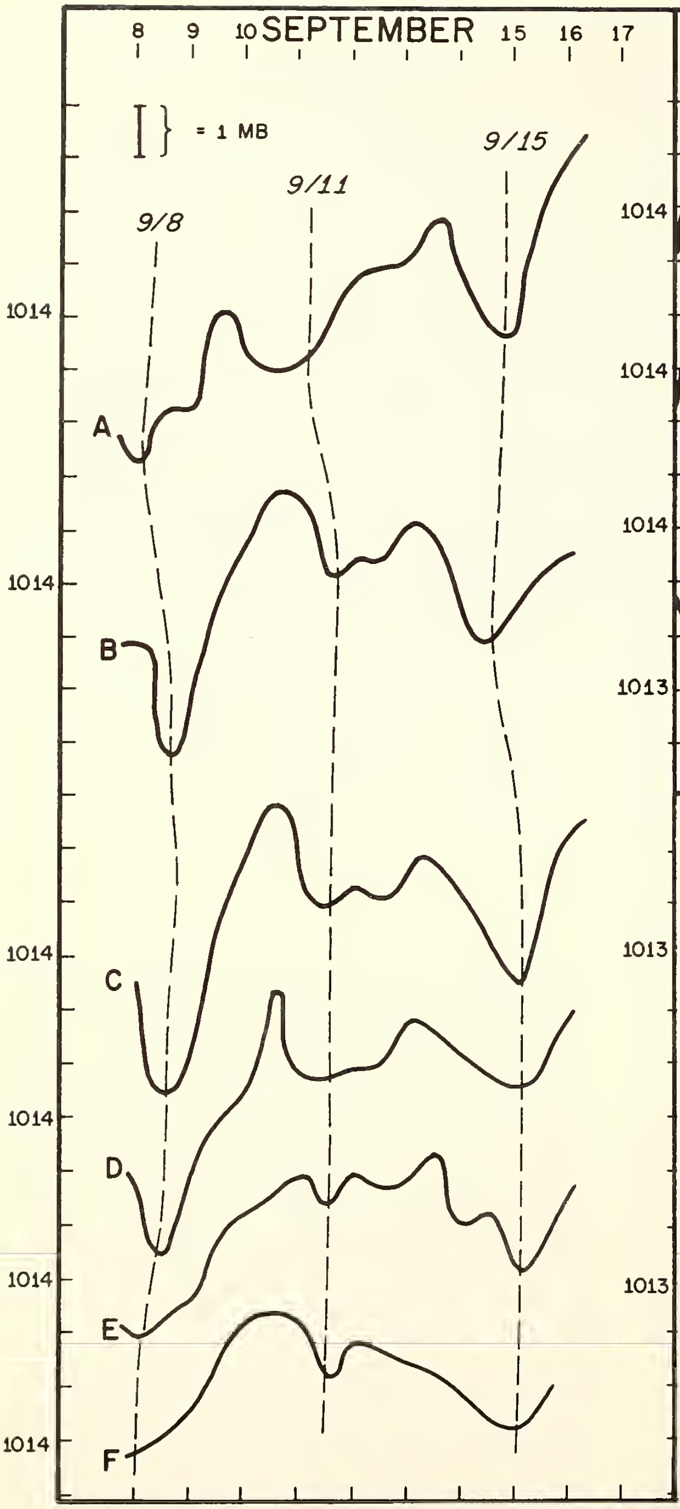

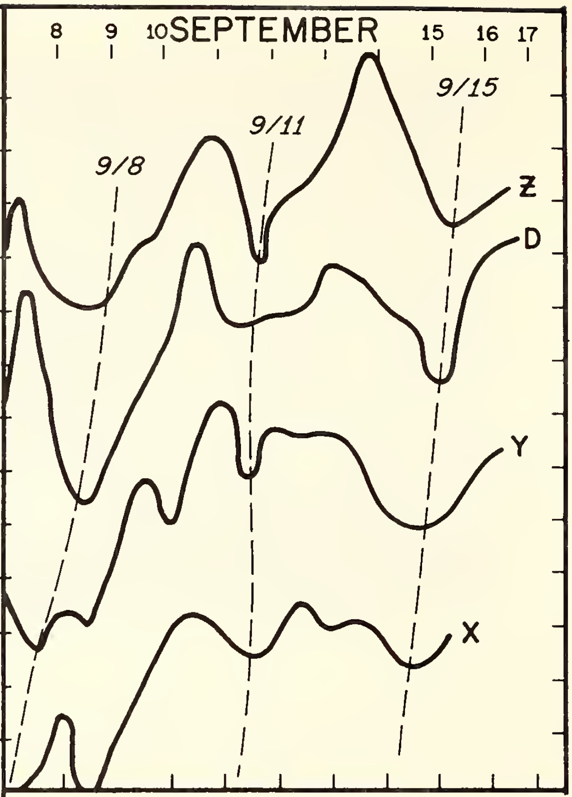

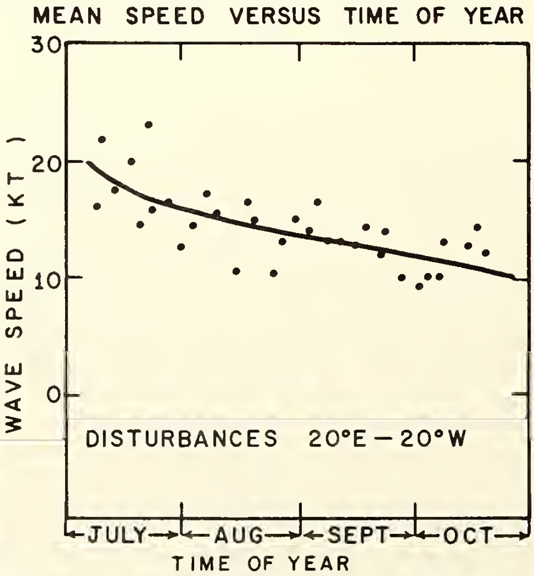

Figure 6. Mean speed (westward) of disturbances over Africa for the summer of 1968. Most of these disturbances could be traced back to east of longitude 10° E.

Figure 5. Sea-level pressure traces for stations labeled in figures 3 and 4. This figure shows pressure perturbations accompanying the passage of the three disturbances shown in figure 3. The locations of the various lettered stations are shown in figure 3.

Reprinted from Monthly Weather Review
Vol. 97, No. 10, 716-726.

UDC 551.515.5:551.5[illegible].1:551.507.362.2 551.576(264.1)(66)"19[illegible] 323"

SOME REMARKS ON AFRICAN DISTURBANCES AND THEIR PROGRESS OVER THE TROPICAL ATLANTIC

TOBY N. CARLSON

National Hurricane Research Laboratory, ESSA, Miami, Fla

ABSTRACT

A daily analysis of the 2,000- and 10,000-ft streamlines over West Africa was made for a 3½-mo period beginning in July 1968. With the aid of satellite photographs and auxiliary sea-level pressure data, a total of 33 synoptic scale wave perturbations were observed to move across West Africa and the tropical Atlantic Ocean during this period. Some general features of these disturbances are summarized, including facts on their origin, speed, intensity, distribution of sea-level pressure, appearance on the satellite photographs, and movement over the Atlantic Ocean. The effects of the large-scale circulation and the influence of sea-surface temperatures on the movement and intensity of disturbances are also discussed.

1. INTRODUCTION

During the past 2 yr, investigations by Simpson and others (1968, 1969), Frank (1969), and Carlson (1969) (the latter henceforth will be referred to as paper I) have probed into the origin and complete life cycle of Atlantic tropical disturbances. Their results underscore the fact that the majority of disturbances that cross the Antilles from the east during the summer months originate over Africa, while comparatively few form within the maritime portion of the intertropical convergence zone (ITC). A large number of disturbances are found to cross the African coast during the summer, and most of these can be tracked as far as the Caribbean. Initial investigations into the continuity of African disturbances and their development into Atlantic hurricanes have been made by Erickson (1963) and Arnold (1966). Although only a very few of these disturbances develop into Atlantic tropical storms and hurricanes, African disturbances apparently account for a significant percentage of mid-season (August and September) storms.

It is therefore important to investigate the disturbances in their earlier stages over Africa where a data network makes it possible to readily identify synoptic scale features of the flow pattern. Following the method described in paper I, in which wave disturbances and their attendant cloud distributions were tracked across West Africa, a set of daily analyses for this region were constructed for an extended period during the summer of 1968 (July 5 to October 18). These analyses consist of 2,000- and 10,000-ft streamline charts and selected sea-level pressure traces for the portion of tropical West Africa between longitudes 25° W. and 20° E. With the further aid of satellite photographs, the movement of synoptic scale wave perturbations across West Africa was readily discernible. It is our intention in this paper to outline some general features of African disturbances and to relate their movement and development to external influences in the environment.

2. SYNOPTIC DESCRIPTION OF THE DISTURBANCES OVER AFRICA

Selected examples of the 2,000- and 10,000-ft streamline analyses have been superimposed on their respective satellite photographs for display in figures 1A–C and 2A–C. The disturbances are labeled in the figures by an arrow, which signifies the mean longitude of the wave axis at 10,000 ft (the level at which the disturbances were most easily recognizable). The arrows are labeled according to the date on which the wave axis crossed the longitude of Dakar, 17° W.; disturbance 9/11 therefore is that perturbation whose 10,000-ft axis reached 17° W. on September 11. Table 1 is a catalog of the African disturbances; listed in the first column are the date and time of wave passage at longitude 17° W. The date and longitude at which the disturbance first became recognizable are listed in column 2.

Altogether, 33 such disturbances were observed during the 3½-mo period, a frequency of one wave every 3.2 days. A series of traveling waves are clearly evident in the sequence of analyses in figure 1, the disturbances broadly corresponding to areas of cloud enhancement. A few disturbances presented difficulties in analysis and in construction of a smooth track, either because they weakened to the point of unrecognizability or because minor side lobes present in a number of waves became temporarily large enough to confuse the analysis. Usually it was possible to track the main wave pocket and with the aid of hindsight smoothing to remove sudden jumps in speed.

The mean wavelength of the disturbances was about 1,300 mi over West Africa; it is apparent from the analyses that there was a considerable meridional extent to the waves as well. This is further illustrated in figure 3, which shows that systematic variations in sea-level pressure accompanying the series of the waves analyzed in figure 1 occurred almost simultaneously over the 700-mi-long chain of coastal stations, A–F. As was the usual situation, the largest pressure variations occurred in the northern part of the network. A striking illustration of this fact is displayed in figure 3C in which the upper wave axis is shown to be preceded by 3- to 4-mb pressure falls at station A, 2-mb pressure falls at C, and about 1-mb falls at F. The figures listed in column four of table 1 represent the magnitude of the pressure oscillation (at about 16° N.) which accompanied the passage of the wave across the

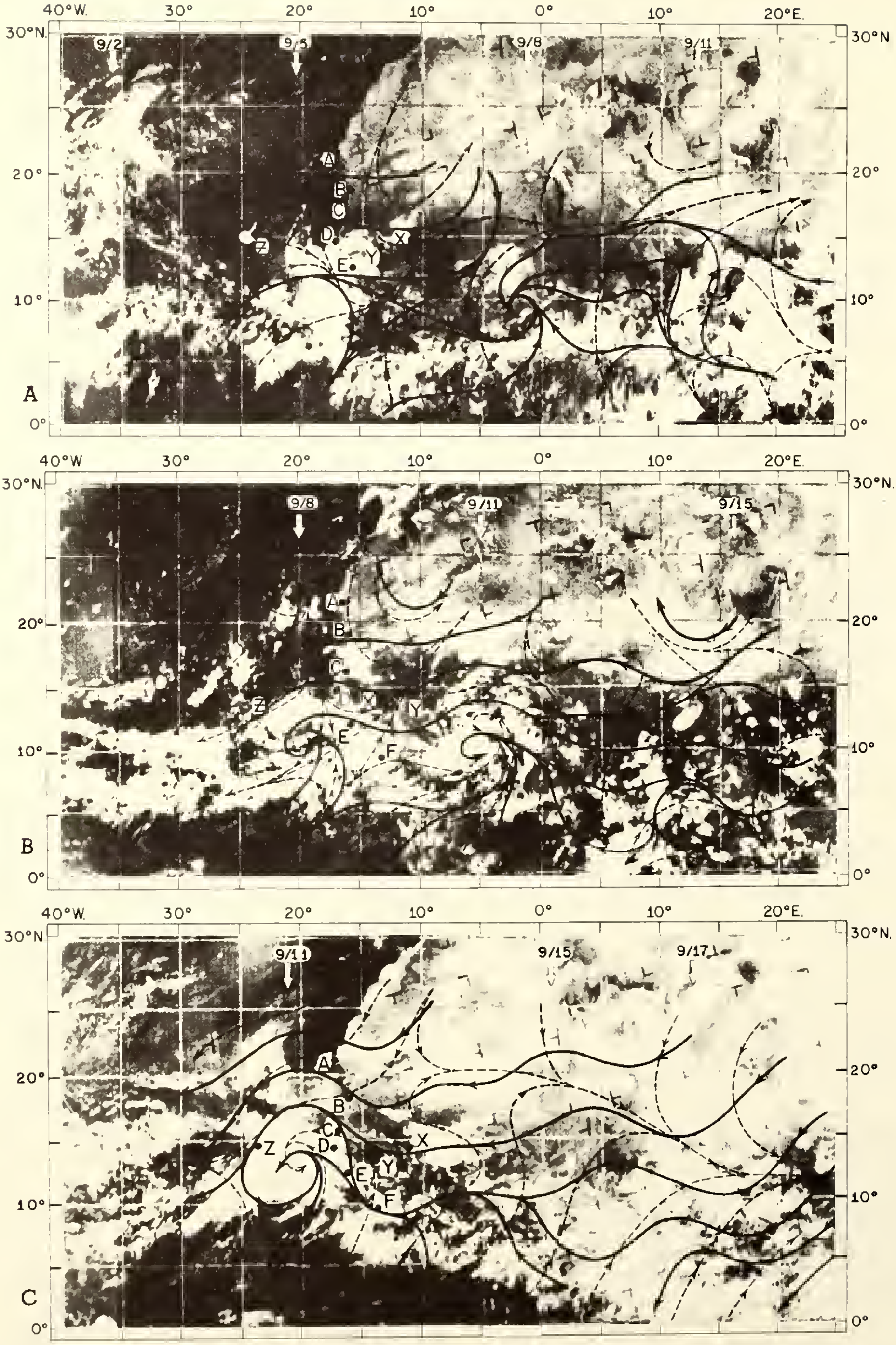

FIGURE 1.—A series of digitalized ESSA 7 satellite mosaics, upon which are superimposed the 10,000-ft (solid lines) and 2,000-ft (dashed lines) streamline analyses; (A) view at 1600 GMT on Sept. 5, 1968, and streamline analysis at 0000 GMT on Sept. 6, 1968; (B) view at 1600 GMT on Sept. 8, 1968, and streamline analysis at 0000 GMT on Sept. 9, 1968; (C) view at 1600 GMT on Sept. 11, 1968, and streamline analysis at 0000 GMT on Sept. 12, 1968. The capital letters shown in the vicinity of the West African coast refer to the location of the sea-level pressure barographs whose traces appear in figure 3. The longitudinal positions of the wave axis are indicated by an arrow and labeled according to the date the wave passed longitude 17° W.

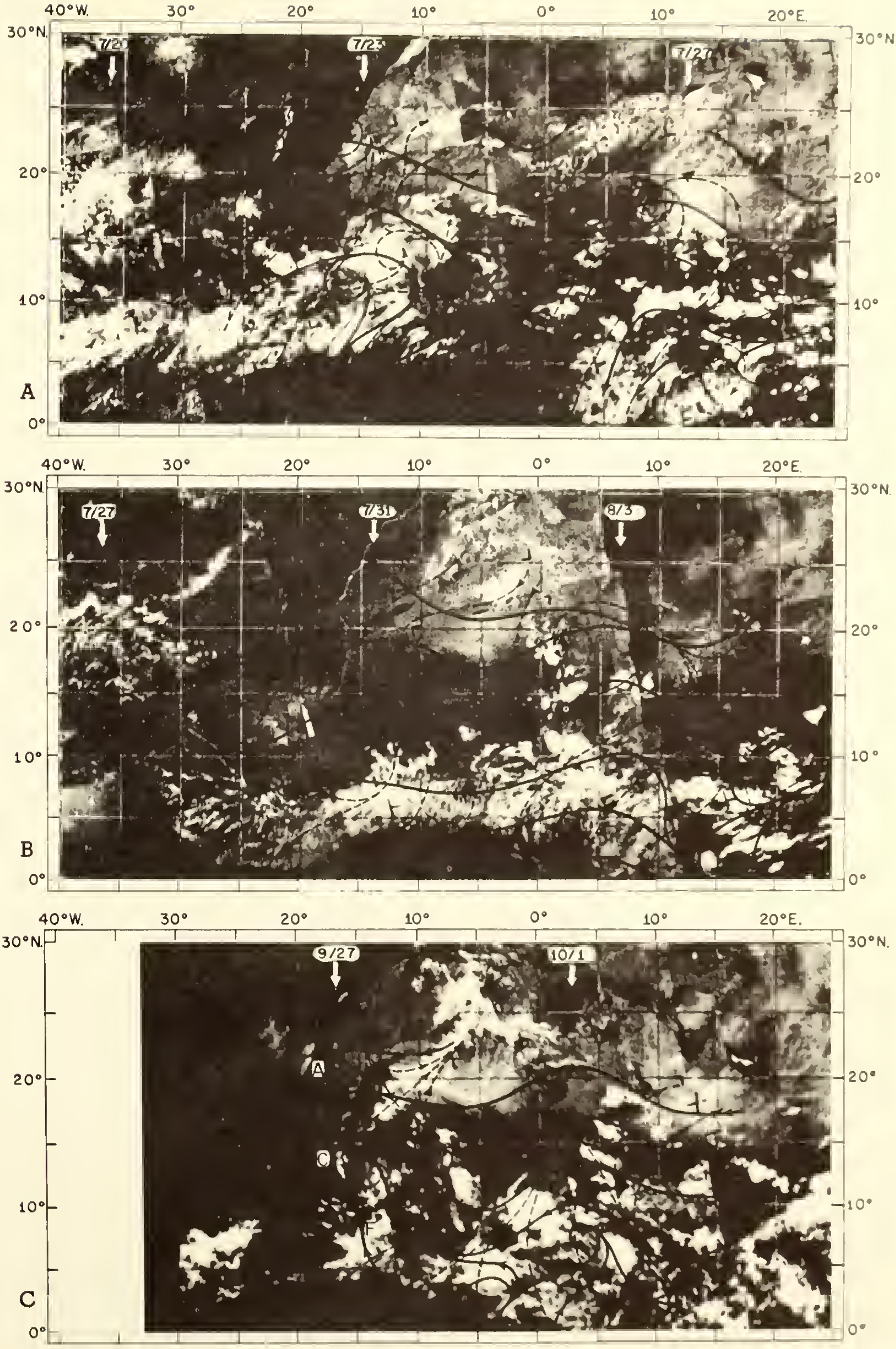

Figure 2.—Same as figure 1, but for selected examples of African disturbances, (A) view at 1600 GMT on July 22, 1968, and streamline analysis at 0000 GMT on July 23, 1968; (B) view at 1600 GMT on July 30, 1968, and streamline analysis at 0000 GMT on July 31, 1968; (C) view at 1600 GMT on Sept. 27, 1968, and streamline analysis at 0000 GMT on Sept. 28, 1968.

TABLE 1.—*African disturbances in 1968*

Wave Rchd. 17°W Mo/Day/Time (GMT)	Wave First Obsvd. Mo/Day/Long.	Speed Crossing W. Africa (kt)	Press. Fluc. 16°N, 17°W (mb)	Init. Location Surface Vortex, Other Details	Satellite Obs.: Init. Location Circular Cloud Pattern	Arrival 60°W Mo/Day	Speed Crossing At. Ocean (kt)	Last Obsvd. Mo/Day/Long.	Comments on Devel. West of Africa
07/07/0000		16.0	3.1		10°W, 12°N	07/13	18.0	07/16/82°W	
07/09/1800	7/08/07°W	22.0	2.5	Low Lat.		07/15	18.5	07/18/81°W	Wknd. 35°W
07/12/1200	07/08/15°E	17.5	4.1			07/18	19.5	07/24/94°W	
07/16/2100	07/11/23°E	20.0	3.0			07/22	17.5	07/27/93°W	
07/20/0600	07/15/11°E	14.5	2.4	05°W, 14°N	03°W, 14°N	07/26	19.0	07/28/68°W	
07/23/0900	07/18/19°E	16.0	2.7	07°W, 12°N	07°W, 12°N	07/29	16.0	08/04/86°W	
07/27/0600	07/22/19°E	16.5	2.7	18°W, 11°N	10°W, 12°N	08/03	16.0	08/07/78°W	
07/31/1200	07/25/10°E	12.5	5.0	05°W, 13°N	15°W, 12°N	08/07	17.0	08/11/80°W	Hurricane Dolly Florida Straits
08/03/1200	07/30/08°E	14.5	1.8	Low Lat. Weak 19°W, 11°N	13°W, 12°N	08/08	20.0	08/16/106°W	Tropical Storm in Pac. Ocean
08/06/1800	08/01/21°E	17.0	1.9	Notably Weak	14°W, 16°N	08/13	17.0	08/14/66°W	
08/09/0300	08/06/02°E	15.5	2.0	Notably Weak Low Lat.		08/15	17.5	08/20/91°W	
08/14/0000	08/05/21°E	10.5	2.7	16°W, 15°N	17°W, 12°N	08/20	18.5	08/23/79°W	
08/17/1200	08/13/12°E	16.5	4.8	21°W, 16°N	01°W, 11°N	08/23	18.5	08/26/82°W	Trop. Depression Gulf of Mexico Wknd. 50°W
08/20/1800	08/15/17°E	15.0	4.4	00°W, 11°N		08/28	14.0	09/02/82°W	Wknd. 34°W
08/24/1800	08/19/06°E	10.5	<1.0	Notably Weak Small Wave Length		09/01	13.0	09/07/92°W	Tropical Storm in Pac. Ocean
08/26/0600	08/21/10°E	13.0	1.8	Dominated by 08/28				08/30/38°W	
08/28/1800	08/21/20°E	15.0	4.5	13°W, 13°N	04°E, 14°N	09/05	15.0	09/06/64°W	Wknd. 32°W
09/02/1800	08/28/14°E	14.0	4.9	17°W, 13°N	02°W, 13°N	09/09	15.5	09/12/73°W	Wknd. 56°W
09/05/1200	08/31/20°E	16.5	2.8	Low Lat.	18°W, 12°N	09/12	16.0	09/17/87°W	
09/08/0600	09/04/06°E	13.0	3.5					09/15/58°W	Wknd. 35°W
09/11/0000	09/04/20°E	13.0	2.0	05°W, 13°N	05°W, 12°N	09/20	11.0	09/21/60°W	Hurricane Edna 37°W, 09/15 Wknd. 43°W
09/15/0000	09/08/18°E	13.0	2.9	12°W, 12°N		09/22	14.5	09/22/57°W	Wknd. 33°W
09/17/0900	09/11/19°E	14.5	3.3	17°W, 12°N Low Lat.		09/24	16.5	09/25/65°W	Wknd. 46°W
09/21/0000	09/16/12°E	12.0	3.5	13°W, 12°N		09/26	18.0	10/01/86°W	
09/22/2000	09/17/15°E	14.0	1.5	Low Lat. Weak		09/29	16.0	10/04/86°W	
09/27/1200	09/18/22°E	10.0	3.4	13°W, 12°N		10/05	14.5	10/07/70°W	Wknd. 33°W
10/01/0300	09/21/20°E	7.5	3.0	17°W, 14°N		10/09	11.5	10/10/65°W	Wknd. 37°W
10/03/1200	10/02/11°W	10.0	3.0	16°W, 13°N Part of 10/05?		10/12	13.5	10/13/65°W	Wknd. 41°W
10/06/0000	09/20/12°E	10.0	<1.0			10/14	13.0	10/16/67°W	
10/08/2100	10/05/03°E	13.0	3.9	03°W, 06°N Low Lat.		10/21	9.5	10/21/60°W	
10/13/0600	10/05/26°E	13.0	1.7	Low Lat. Weak				10/17/41°W	
10/14/0900	10/08/21°E	14.5	<1.0	Low Lat. Weak				10/17/26°W	
10/18/0000	10/11/19°E	12.5	3.3	12°W, 13°N		10/25	14.0	10/28/77°W	Wknd. 38°W

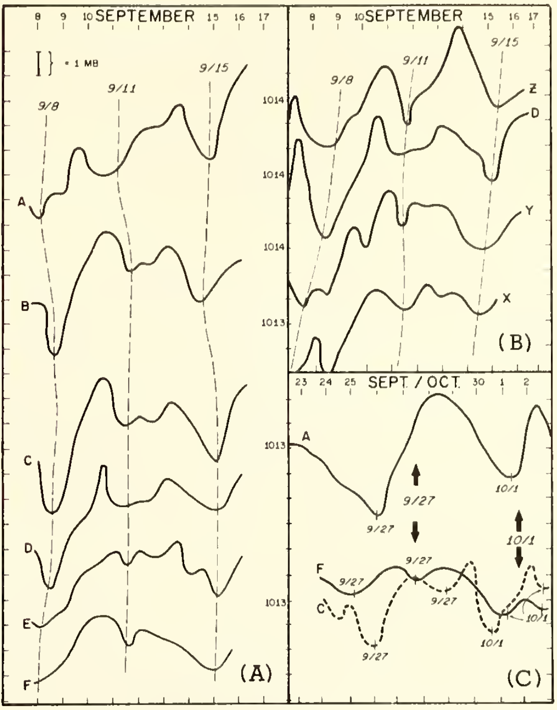

Figure 3.—(A) sea-level barograph traces (adjusted for diurnal trends) at the longitudinal sequence of stations A–F and (B) the latitudinal sequence of stations X–Z for the series of waves shown in figure 1; (C) the barograph traces for stations A, C, and F for a period beginning in late September.

Table 2.—*Frequency distribution of sea-level pressure fluctuations accompanying wave passage at 17° W.*

Pressure interval (mb)	<1.0	1.0-1.9	2.0-2.9	3.0-3.9	4.0-4.9	≥5.0
Number of cases	3	5	9	10	5	1

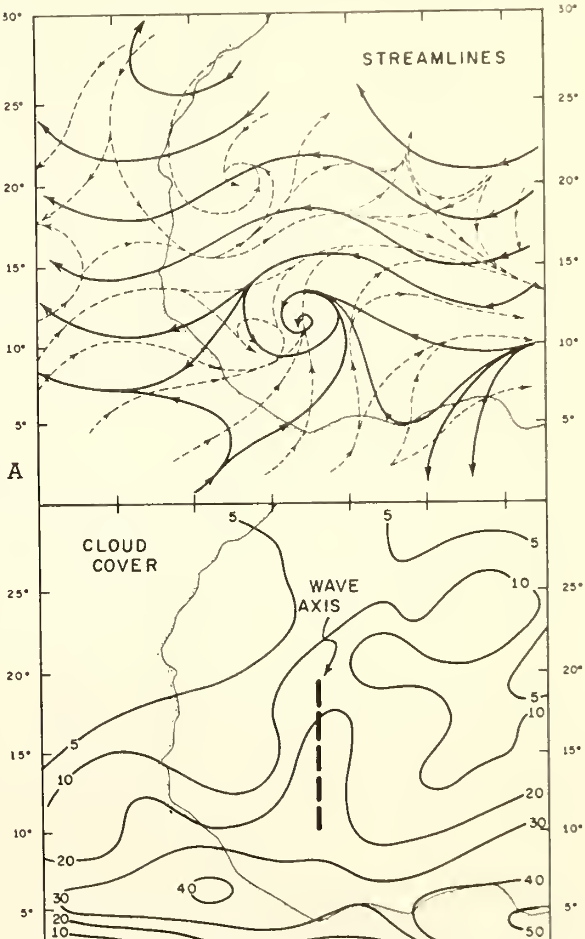

Figure 4.—(A) schematic flow pattern at 10,000 ft (solid lines) and 2,000 ft (dashed lines) for the typical African disturbance; (B) contours show a mean percentage cover of cloud with respect to the schematic flow pattern shown in (A). The field represents an average cover for 23 disturbances as measured near 10° W.

network of coastal stations. Table 2 shows that the median value of this pressure fluctuation was close to 3.0 mb.

These large sea-level pressure fluctuations appear to be centered near 20° N. in the vicinity of a major cyclonic eddy which was often observed to move with the disturbances along the southern fringe of the desert in the confluence between moist air arriving from the south and dry Saharan air. An idealized representation of this vortex is shown in the schematic flow pattern of figure 4. The analyses in figures 2A–C contain examples of disturbances having attendant vortices located near latitude 20° N. which closely resemble the idealized analysis in figure 4. The lack of moisture associated with this vortex is apparent in the analyses which show that the latitude at which it is located is largely free of cloud, the main zone of cloudiness being centered far to the south. (The large fluctuations in sea-level pressure occurring at station A during the period September 23 to October 20 (fig. 3C) were unaccompanied by any rainfall or significant cumulus buildups.) According to figure 4 the mean areal cloud cover (an average of individual observations of cloud cover made from satellite photographs and determined with respect to the longitude of the wave axis for 23 disturbances in the vicinity of 10° W.) at 20° N. is generally less than 10 percent, although there is a slight increase noticeable in the amount of cover near the wave axis. It seems probable that the vortex located at this latitude is produced indirectly by the wave's circulation in which its formation is the result of a southward ad-

Table 3.—*Distance surface-pressure trough lies ahead (to the west) of upper wave axis for disturbances passing 17° W.*

Distance ahead (n.mi.)	−240 to −120	−120 to 0	0 to +120	120 to 240	240 to 360	360 to 480	480 to 600
Number of cases	4	3	5	9	7	2	1

vection of relatively warm air (high thickness) from the vicinity of the Saharan heat low which would necessarily occur in the northeasterly flow ahead of the wave axis. Indeed, a comparison of two soundings made at station B, one on September 28 at a time of relatively low sea-level pressure and the other on October 1 when the pressure was high, shows that most of the pressure deficit could be accounted for by the presence of substantially warmer air between 700 mb and the surface on the day of lower pressure. The air was also much less humid in this layer and the flow was northeasterly, as compared to southeasterly on October 1. The axis of the sea-level pressure trough was found ahead of the upper wave axis in most cases, according to table 3.

In contrast to the soundings made in the relatively dry part of the system near 20° N., the data consistently show that in the vicinity of 15° N. the wave disturbances are relatively warm in the high troposphere and cold near the ground, with the strongest geopotential variations across the wave axis occurring near 600 mb. This is in agreement with the findings of paper I and the results of Simpson and others (1969). To this extent, and to the extent that the wave axis tends to slope eastward with height in the lower troposphere, the disturbances resemble the classical easterly wave of Riehl (1954). On the other hand, the symmetrical distribution of cloudiness in figure 4 is in contrast to the findings of paper I which showed a maximum of disturbed weather just ahead of the trough axis.

Another noteworthy aspect of figure 4 is a weak vortex located in the vicinity of the disturbance axis near 12° N. Examples of this type of vortex feature are found in figures 1 and 2. Figure 4 also illustrates that the greatest longitudinal variation in cloud cover across the wave axis (a change from 10 percent in the environment to 25 percent in the wave axis) is found between the latitudes of about 11° and 15° N. where, according to the results of paper I, the greatest instability and most intense convection are located. (Farther south, the clouds are mainly a dense and highly persistent stratocumulus.) The moist cloud-associated nature of this weak vortex is self evident in the analyses and suggests an origin and energy source related to the convective processes. In figure 2C, the weak vortex centered at 13° N. on the eastern side of disturbance 9/27 may have produced the minor fluctuation of the sea-level pressure (shown in fig. 3C) which followed the primary pressure oscillations at stations C and F. The same situation occurred with the subsequent disturbances 10/1. Interestingly, these minor wriggles in the pressure field were not observed at station A, which experienced a single strong pressure oscillation prior to the passage of the disturbance.

As can be seen in figure 1, the weak southern vortex associated with disturbance 9/11 is readily tracked over the ocean, while the northern center appears to vanish at the coastline or remain over land. Although this was characteristic for most disturbances, figure 3B shows that the pressure variations at Sal in the Cape Verde Islands (station Z) were as large as at Dakar (station D), suggesting that the low-level vorticity field associated with the disturbances continues to propagate over the ocean. It may be that the two vortexes merged together, although this could not be determined. Most probably, the southern vortex is identically that type of feature followed by Aspliden, Dean, and Landers (1966), who have tracked trains of surface vortices across the ocean from an apparent origin at the African coast between 10° and 15° N. The coordinates listed in column five of table 1 are the longitudes at which these vortexes first became recognizable in the analyses, and the latitudes of the centers.

In many instances, the aforementioned vortex was associated with a circular cloud area with noticeable spiral bands. Examples appear in disturbances 9/11 (fig. 1B) and 7/23 (fig. 2A). The appearance of such a cloud pattern is listed in column six of table 1 according to the longitude where it first became recognizable and the latitude of its apparent center. Merritt (1964) and Frank and Johnson (1969) both discuss the significance of vortical cloud patterns associated with weak tropical disturbances. Although many disturbances were very often associated with scanty amounts of cloud cover or poorly defined cloud systems well inland, the majority of waves developed a recognizable and coherent cloud structure (though not necessarily a circular one) and a vortex at 2,000 ft south of 15° N. prior to reaching the coast. Listed in column six of table 1 is the initially observed position (and latitude) of the circular cloud system.

According to paper I, the amount and degree of convective instability generally increases westward from the central portion of the West African bulge, creating an increasingly favorable environment for intensification after the disturbance reaches about 5° W. Although the disturbances appeared to achieve their greatest intensity in the area between 10° and 20° W. and sometime thereafter suffered a disintegration and disorganization of the cloud pattern, it was not difficult to follow prominent features of the cloud pattern over the ocean (see Frank, 1969). Accordingly, the date at which the disturbance reached the Antilles (60° W.), the speed in crossing the Atlantic Ocean and the date and longitude at which the wave was last observed were determined from satellite and wind data; and the information is listed in columns 7, 8, and 9, respectively, of table 1. Additional comments are made in column 10. These include the longitude at which the cloud pattern appeared to weaken over the ocean, another highly subjective evaluation but one which was derived from notes made concurrently with the events themselves.

TABLE 4.—*Frequency distribution of initial wave positions versus longitude*

Longitude interval	West of 4° E.	4° E. to 6° E.	7° E. to 9° E.	10° E. to 12° E.	13° E. to 15° E.	16° E. to 18° E.	East of data network
Number of fixes	4	2	1	6	3	2	14

Some of the disturbances appeared to be centered distinctly farther south than usual. These were labeled as "low latitude" disturbances in column five of table 1, although they are merely a variant of the type of system portrayed in the schematic diagram of figure 4A.

Table 4 contains a summary of the information contained in column 2 of table 1 according to the frequency of initial sightings versus intervals of longitude. According to the table, almost one-half of the disturbances appeared to originate east of the data network (18° E.), while only a few were first observed west of longitude 4° E. A minor peak exists in the interval between 10° and 12° E., suggesting a possible site favorable for wave initiation over the Cameroon Mountains. The generating mechanism over Africa may be, therefore, associated with an interaction of the convective processes with the terrain. If so, other mountainous sources would exist to the east of the data network over the Sudan and Ethiopia.

3. THE STATE OF AFRICAN DISTURBANCES OVER THE CARIBBEAN

The vast majority of the African disturbances in 1968 began to weaken west of the Cape Verde Islands, while only two hurricanes of marginal intensity developed from African disturbances. Visible on the satellite photographs was an increasing disintegration and disorganization of the cloud pattern followed by a collapse of the apparent cloud structure of the disturbance (Simpson and others, 1969); the weakening over the mid-Atlantic proved to be irreversible in almost all cases during 1968. As indicated in column 10 of table 1, the most rapid disintegration may have begun near 35° W.

Despite the visible weakening of the disturbances, the rainfall data (fig. 5) for St. Thomas (Virgin Islands) and Barbados (Windward Islands), two islands in the Antilles where a representative areal coverage of rain gages exists (seven for the former island and four on Barbados, the latter being available for only 2 mo in 1968), shows that there were a number of instances of wave passage over the particular island which corresponded closely to isolated peaks in the daily rainfall there. In order to present this observation in a statistical framework, a set of 5-day means centered on the day of wave passage by the island, as indicated by the arrows in figure 5, were determined for each disturbance to reach the island. The ratios of daily-to-mean rainfall for each of 5 days were composited for all cases where the data are available to form a normalized rainfall distribution. These results are shown in table 5.

Both stations display a mutually similar and systematic variation in rainfall during the period, in which the precipitation amount rises to a value substantially greater than normal on the day prior to wave passage and then falls to about one-half of the average daily rainfall on the day after wave passage. The table clearly implies that the disturbances retain a sufficient vertical-motion field over the Antilles to contribute significantly to the precipitation of these islands, although the contribution was occasionally little more than the heightening of the local island convection.

Also shown in figure 5 are the pressure fluctuations at longitudes 17° W. and 60° W., as indicated by the pair of digits listed above the box appropriate to that disturbance. The first figure corresponds to the pressure fluctuation at 17° W., as shown in column 4 of table 1 (rounded to the nearest whole millibar). The second figure, separated from the first by a dash, represents the corresponding sea-level fluctuation over the Antilles for that disturbance, as measured in a similar network of stations there. Comparison shows that the rises and falls in sea-level pressure over the Antilles were generally very much less than those over Africa, irrespective of the wave's initial intensity and organization. There is very little apparent relationship between either the magnitude of the sea-level pressure fluctuation or the degree of organization of the disturbance over Africa and the effects of the disturbance on the rainfall of the Antilles.

4. THE LARGE-SCALE WIND FIELD AND WAVE SPEED

The large-scale wind field over Africa in the belt of disturbances is characterized by southwesterly winds at low levels and strong easterlies aloft which are a consequence of the strong meridional temperature gradient between desert and ocean. In July, the northernmost penetration of the moist air is near 20° N., but as the systems shift southward in August and September (mirroring their northward advance during the spring), so does the confluence between the moist and dry regimes and the zone of convection. At the same time the desert air mass cools while the waters of the cross-equatorial flow in the Gulf of Guinea *warm*. The result is a weakening in the strength of the upper easterlies which is followed by a radical equatorward shift of the convective activity beginning in September or October.

The decrease in the mean easterly component of the atmosphere in the disturbance belt and the equatorward shift in the easterlies, which is especially pronounced over the African Continent, is illustrated by the graph of vertically integrated easterly flow in figure 6A.[1] According to figure 6B, there was a steady decrease in the phase speed of the waves from about 19 to 11 kt between July and

---

[1] The mean vertically averaged zonal wind refers to the 950- to 150-mb layer. The data comes from the U.S. Weather Bureau (Crutcher, 1961).

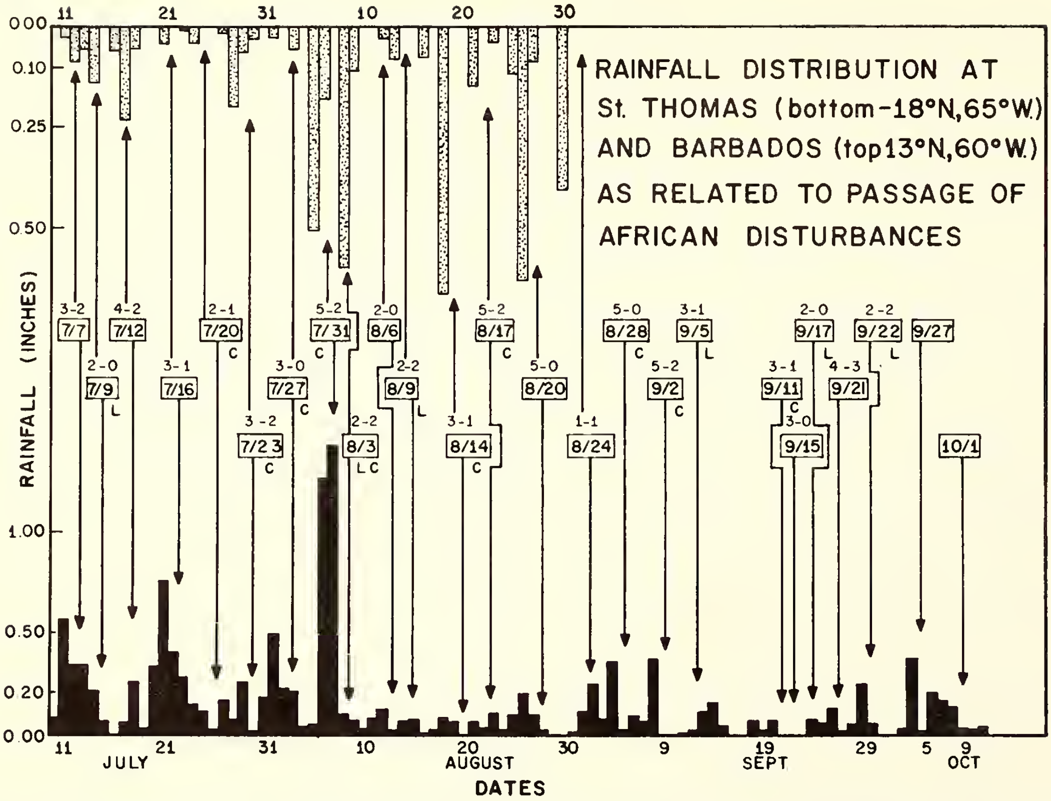

Figure 5.—Distribution of average daily rainfall at St. Thomas (bottom: average of seven stations) and Barbados (top: average of four stations), as related to the passage of African disturbances over the island (arrows labeled in boxes). The two digits at the top of the box (separated by a dash) are the sea-level pressure fluctuations (in millibars) for the disturbance when it was at the coast of Africa at 17° W. (left figure) and over the Antilles (right figure). The letter C, located just below the box, refers to systems that displayed a circular cloud pattern with attendant low-level vortex over Africa; the letter L refers to those systems that were observed to be at a lower latitude than usual (see table 1).

Table 5.—*Five-day normalized rainfall totals for African disturbances with respect to the day of passage by station (presented as fraction of average daily rainfall)*

Station	Number of cases	2 days earlier	1 day earlier	Day of passage	1 day later	2 days later	Average daily rainfall (inches)
(7 stations) St. Thomas	21	1.02	1.69	0.89	0.41	1.00	0.19
(4 stations) Barbados	14	0.81	1.19	1.02	0.60	1.38	0.10

October, which undoubtedly reflects the slowing of the large-scale easterly flow, shown in figure 6A.

Figure 6C is a plot of the average wave speed versus longitude. Although variations in speeds of less than a knot are considered statistically insignificant, the figure does show that the disturbances moved somewhat less rapidly over the continent than over the ocean (a fact which is readily apparent upon comparison of the values of the overall wave speed in column three with those in column nine of table 1). The point at which the disturbances began to accelerate (22° W.) corresponds to the axis of a large-scale upper trough (see fig. 7) which exists as a semipermanent feature along the entire coastline of the Euro-African landmass (U.S. Weather Bureau, 1952). Its presence is related to the geography and is necessitated by the removal and poleward transport of warm air from the continent. The corresponding ridge is found to coincide with the speed maximum at 45° W. By implication, the speed of disturbances is affected by the presence of large-scale trough and ridge patterns; in the mean they decelerate in the difluent (southeasterly) flow east of a trough and accelerate in the confluent (northeasterly) flow to the west of a trough, as is indicated by the segmented arrows in figure 6C. This is to be expected in a quasi-barotropic

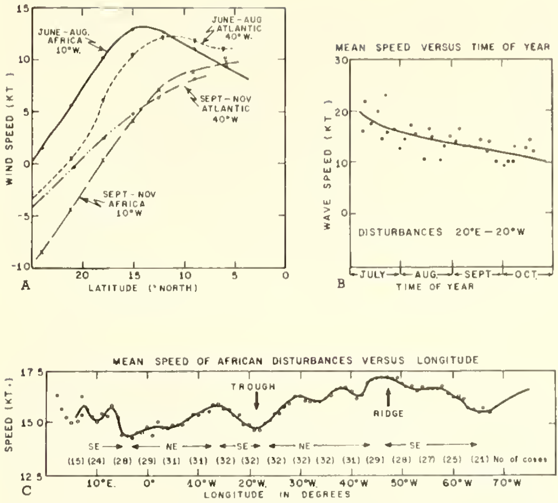

FIGURE 6.—(A) mean vertically averaged easterly wind profile between 150 and 950 mb versus latitude over Africa (10° W.) and over the mid-Atlantic (40° W.) for two periods of 3-mo averages centered on July and October; (B) seasonal distribution of wave speed over Africa for 1968; (C) composite distribution of wave speed versus longitude, averaged over the total number of cases indicated in parentheses. The arrow segments suggest intervals of southeasterly (SE) and northeasterly (NE) winds. The mean positions of major upper trough and ridge areas are also indicated.

current provided that the disturbances move with the mean (vertically integrated) speed of the flow. Interestingly, the areas favorable for large-scale ascent, the southeasterly regimes, are also those areas favorable for disturbance intensification, and vice versa with respect to northeasterly winds and disturbance dissipation. Certainly the strong northeasterly trades which exist from the longitude of the Cape Verde Islands westward are associated with cloud suppression.

5. THE INFLUENCE OF SEA-SURFACE TEMPERATURE

In addition to the dynamical factors in the suppression and enhancement of disturbances are the effects of sea-surface temperature. Closely linked to the geography and to the large-scale flow pattern, the strong northeasterly ocean current conveys cold water equatorward along the west coast of Africa to form a pronounced trough of cold water, shown in figures 7A–C,[2] which is located approximately between longitudes 25° and 45° W. Figures 7A–C illustrate the effects on tropical storm *formation* of the cold trough in the sea-surface temperature fields; in particular, the sensitivity of formation to the location of the 80°F (26.7°C) isotherm can be noted. The range of temperatures from 78°–82°F (26°–27°C) is generally accepted as being adequate for deepening of tropical disturbances from the depression stage through coupling of its convective processes and circulation with the oceanic energy source.

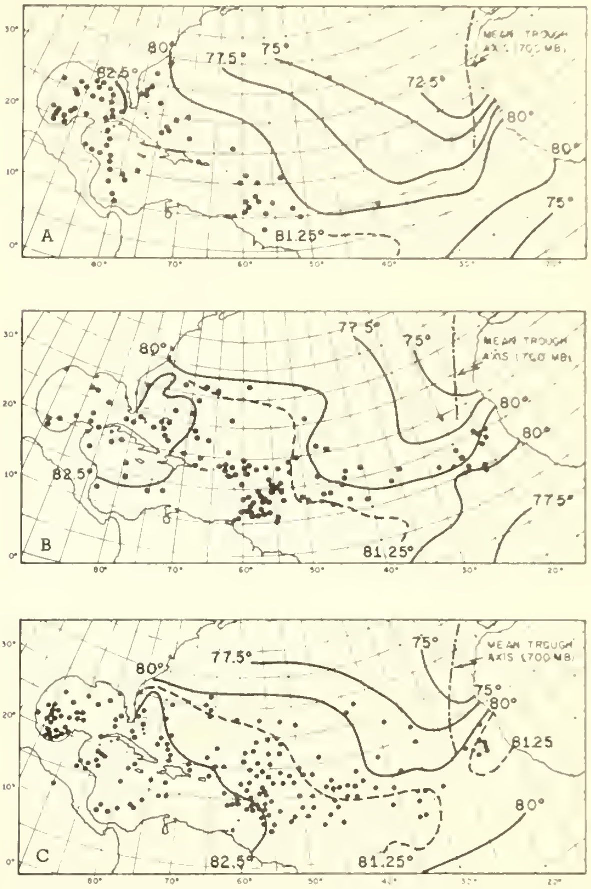

FIGURE 7.—Mean sea surface isotherms (°F), the distribution of initial tropical storm fixes, 1901–1967 (filled circles), and the mean position of the 700-mb wave axis for (A) June and July, (B) August, and (C) September.

According to paper I, the distribution of convective instability over West Africa, as measured by the wet-bulb potential temperature at cloud base, θ_{w_b}, is strongly influenced by the temperature of the ocean surface over which the trajectories of the low-level flow are originating. Figure 8 attempts to illustrate a relationship between sea-surface temperature and convective instability as it exists over the eastern tropical Atlantic during the summer months. It contains a plot of θ_{w_b} (as computed for the 950-mb level but derived entirely from deck-level observations made onboard several research vessels in the tropical eastern Atlantic during the summer of 1963 and based on

---

[2] The sea temperatures in figures 7A–C are based upon values by Mazeika (1968) and upon those by the U.S. Hydrographic Office (1944). The tropical storm positions are updated to 1967 by the U.S. Weather Bureau (1965).

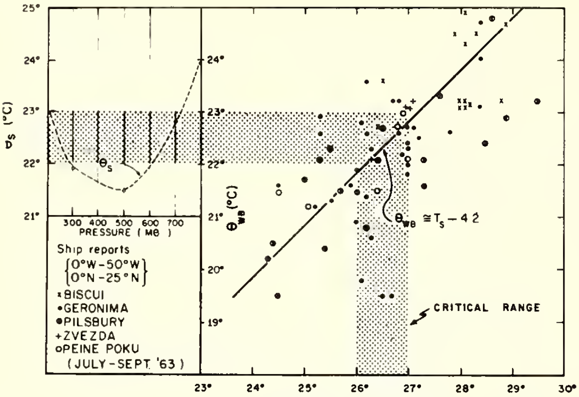

Figure 8.—Distribution of wet-bulb potential temperature at cloud base (θ_{wb}) and the sea-surface temperature (T_s) for the eastern tropical Atlantic during summertime. (Surface data were obtained from the five research ships identified at the lower left.) The straight line represents a visual fit to the scatter of points. At the upper left is the mean summertime saturation wet-bulb potential temperature (θ_s) versus pressure (in millibars) over the eastern tropical Atlantic. The shaded region signifies that sea-surface temperatures of 26° to 27°C are comparable to a θ_{wb} of 22° to 23°C which is barely sufficient to exceed θ_s in the middle and upper troposphere and thereby permit deep cumulonimbus convection.

lapse rates of potential temperature, adiabatic, and dew point, 0.5°C/10 mb, near the surface) versus sea-surface temperature, T_s. The cigar-shaped scatter of points suggests a straight line through its major axis having the analytical relationship $\theta_{wb} \approx T_s - 4.2$.

Since a variation in θ_{wb} of 1°C is equivalent to a change of 2.5°C in the temperature of a parcel ascending moist adiabatically into the high troposphere, it seems reasonable to assume that the convective instability (and hence the existence of the cumulonimbi) is closely controlled by the sea-surface temperature and its modification of the subcloud layer. Furthermore, when the value of θ_{wb}, as given by a particular sea-surface temperature in figure 8, is read against the scale of saturation wet-bulb potential temperature, θ_s (the temperature at a given pressure as measured on the scale of the moist adiabats), at the left of the diagram the former begins to exceed the mean value of θ_s in the middle and upper troposphere[3] (22°–23°C) where the temperature of the sea surface begins to exceed 26°–27°C (shaded region). At these latitudes deep convection, in which air parcels can reach the high troposphere, will therefore tend to be suppressed over water much cooler than about 80°F (26.7°C), even in the presence of large-scale ascending motion. Conversely, the growth of cumulonimbi is favored over water warmer than 80°F, provided that large-scale convergence is present in the lower layers.

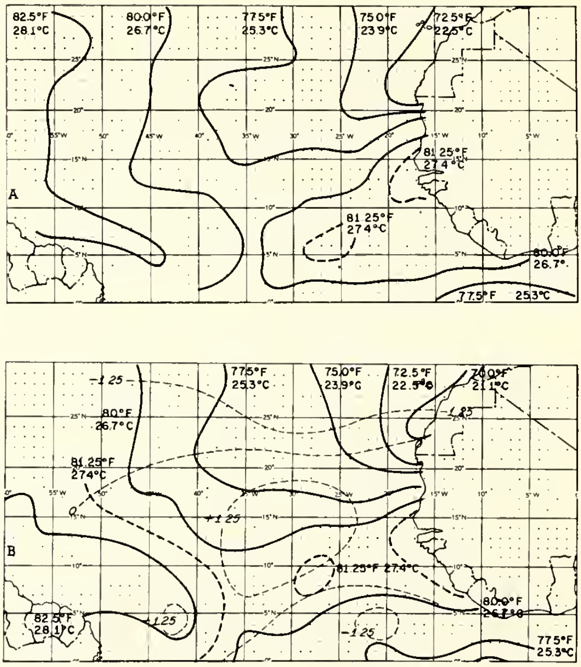

Figure 9.—Mean sea surface temperature field (in °C and °F) for (A) August 1968 and (B) August 1966. Also included in (B) is the departure isotherm field (dashed lines labeled in °F) of August 1966 from August 1968.

Figures 7A–C show that the 80°F isotherm extends south of 10° N. in early July but advances to a position a little north of 15° N. in September. Disturbances reaching 25° W. experience large-scale descent and an influx of stable air at low levels for a period of 3 to 5 days as they move westward. This normally hostile environment for disturbances mitigates as the season progresses. While only a very few disturbances are allowed to intensify in any year, the difference in tropical storm activity over the tropical Atlantic between seasons with abnormally cold and warm sea-surface temperatures may be highly significant as far as the total number of developing systems is concerned. This is particularly likely if the intrusion of cold sea temperatures and the strength of the upper trough are correlated positively.

Figure 9 shows the mean sea surface isotherms for August of 1968 and 1966. These fields were composited by the U.S. Fleet Numercial Weather Facility, Monterey, Calif., from an average of about 60 twice-daily computerized temperature fields drawn from their automated analysis program. August of 1968 is demonstrably cooler than that of 1966, a situation that is significant in view of the fact that 1968 was a notably weak hurricane season while 1966 was the most recent year with an above-average hurricane activity in the tropical Atlantic. The greatest differences in sea-surface temperature between the 2 mo occurred in the latitudes of the disturbance belt between 25° and 45° W. and near the mean position of the 80°F isotherm in that area (maximum difference of 2°F at 15° N., 35° W.). On the other hand, the waters immediately to the south and west of the southern coast of West Africa were warmer in August of 1968 than in August of any of the preceding years, a situation which would favor a higher degree of convective activity over Africa in 1968.

---

[3] The mean sounding is a 3-yr average for three stations in the tropical Atlantic, Sal, Dakar, and Teneriffe, for the months of July through September during 1965–1967.

6. CONCLUSION

This paper represents an attempt to illustrate some important aspects of African disturbances, based on a wide sample of analyses for 1968. It is evident that the disturbances are large-scale (synoptic) wave pertubations with considerable latitudinal extent that exist apart from the ITC region, although they extend into that area. They are apparently not formed near the African coast nor (for the most part) over West Africa; rather, the disturbances originate primarily east of the African bulge, possibly over mountainous terrain. African disturbances are not a singular occurrence but move in continuous wave trains off the African coast. Most of them survive to reach the Antilles, their numbers constituting a possible majority of the population of disturbances in the eastern Caribbean. African disturbances achieve their greatest intensity near the African coast where they encounter an abundant supply of moist, convectively unstable air in the presence of a favorable large-scale wind regime. Thereafter they customarily suffer a disintegration which causes most of the disturbances to become very weak by the time they reach the Antilles. The disintegration seems to be related to the long-wave pattern of cold sea-surface temperatures west of the Cape Verde Islands and to the stabilizing effects of large-scale descent west of an offshore trough.

ACKNOWLEDGMENTS

The author is indebted to various members of the National Hurricane Center in Miami, Fla., for their cooperation in making available the synoptic and satellite data. In addition, we would like to thank the U.S. Naval Fleet Numerical Weather Facility in Monterey, Calif., for furnishing us upon request the computerized mean sea temperature fields. Critical suggestions and comments were offered by Mr. Harry F. Hawkins and Dr. R. Cecil Gentry of the National Hurricane Research Laboratory. Mr. Robert L. Carrodus was very helpful in drafting the figures. This author would also like to thank his assistant for the summer, Mr. Brian Jarvinen, for his help in analyzing the data. Additional rainfall data for Barbados was provided by Mr. Russ De Souza of the Florida State University. Mrs. Judy Greene typed the manuscript.

REFERENCES

Arnold, J. E., "Easterly Wave Activity Over Africa and in the Atlantic With a Note on the Intertropical Convergence Zone During Early July 1961," *Satellite and Mesometeorology Research Project Research Paper* No. 65, Department of the Geophysical Sciences, University of Chicago, Dec. **1966**, 23 pp.

Aspliden, C. I., Dean, G. A., and Landers, H., "Satellite Study, Tropical North Atlantic, 1963: Part 1. Surface Wind Analyses, September 1–September 30," *Research Report* No. 66–2, Department of Meteorology, Florida State University, Tallahassee, Mar. **1966**, 13 pp. plus numerous charts.

Crutcher, H. L., "Meridional Cross-Sections, Upper Winds over the Northern Hemisphere," *Technical Paper* No. 41, U.S. Weather Bureau, Washington, D.C., **1961**, 307 pp.

Carlson, T. N., "Synoptic Histories of Three African Disturbances That Developed Into Atlantic Hurricanes," *Monthly Weather Review*, Vol. 97, No. 3, Mar. **1969**, pp. 256–276.

Erickson, C. O., "An Incipient Hurricane Near the West African Coast," *Monthly Weather Review*, Vol. 91, No. 2, Feb. **1963**, pp. 61–68.

Frank, N. L., "The 'Inverted V' Cloud Pattern—An Easterly Wave?," *Monthly Weather Review*, Vol. 97, No. 2, Feb. **1969**, pp. 130–140.

Frank, N. L., and Johnson, H. M., "Vortical Cloud Systems Over the Tropical Atlantic During the 1967 Hurricane Season," *Monthly Weather Review*, Vol. 97, No. 2, Feb. **1969**, pp. 124–129.

Mazeika, P., "Mean Monthly Sea Surface Temperatures and Zonal Anomalies of the Tropical Atlantic," *The Serial Atlas of the Marine Environment*, American Geographical Society of New York, **1968**, (see Folio 16).

Merritt, E. S., "Easterly Waves and Perturbations, a Reappraisal," *Journal of Applied Meteorology*, Vol. 3, No. 4, Aug. **1964**, pp. 367–382.

Riehl, H., *Tropical Meteorology*, McGraw-Hill Book Co., Inc., New York, **1954**, 392 pp.

Simpson, R. H., Frank, N., Shideler, D., and Johnson, H. M., "Atlantic Tropical Disturbances, 1967," *Monthly Weather Review*, Vol. 96, No. 4, Apr. **1968**, pp. 251–259.

Simpson, R. H., Frank, N., Shideler, D., and Johnson, H. M., "Atlantic Tropical Disturbances of 1968," *Monthly Weather Review*, Vol. 97, No. 3, Mar. **1969**, pp. 240–255.

U.S. Hydrographic Office, *World Atlas of Sea Surface Temperatures*, 2d Edition, H.O. No. 225, Washington, D.C., **1944**.

U.S. Weather Bureau, "Normal Weather Maps for the Northern Hemisphere," *Technical Paper* No. 21, Washington, D.C., **1952**, 74 pp.

U.S. Weather Bureau, "Tropical Cyclones of the North Atlantic Ocean," *Technical Paper* No. 55, Washington, D.C., **1965**, 148 pp.

[*Received March 18, 1969; revised April 21, 1969*]

37

Reprinted from Monthly Weather Review
Vol. 97, No. 3, 256-276.

UDC 551.515.23:551.509.327(6) 551.507.362.2(084.12)

SYNOPTIC HISTORIES OF THREE AFRICAN DISTURBANCES THAT DEVELOPED INTO ATLANTIC HURRICANES

TOBY N. CARLSON

National Hurricane Research Laboratory, ESSA, Miami, Fla.

ABSTRACT

Surface and upper air (700 mb) analyses along with high-quality satellite photographs are presented for a 2-week period during August and September 1967. These show, in particular, the structure and motion over the continent of Africa of four major wave disturbances, three of which later became Atlantic hurricanes. The evolution of cloudiness and convection and the intensification of the disturbance at low levels over West Africa are examined in detail and related to certain climatological features of the area. Some general characteristics of the disturbances are discussed.

1. INTRODUCTION

In a recent article by Simpson et al. (1968) summarizing the origin and movement of Atlantic tropical disturbances during the 1967 hurricane season, it was pointed out that about one-half of the 61 disturbances tracked by satellite photographs and ship reports across the tropical Atlantic were first observed close to the African Continent. About one-half of these were classed as tropical depressions, almost all of which formed during August and September. Of the 25 disturbances in the Caribbean that were not associated with a cold Low, 12 were traceable back to the African coast. Out of a seasonal total of six hurricanes and two tropical storms, three hurricanes and both tropical storms developed from African disturbances.

Similar statistics probably apply to other seasons as well as that of 1967, but there have been only a few well-documented cases of hurricanes forming from African disturbances. Such documentary evidence (e.g., the formation of hurricanes Debbie, 1961 (Erickson, 1963), and Anna of that same year (Arnold, 1966)) has shown that the hurricane formed from an African system that had been a particularly well-developed wave perturbation in the upper easterly flow over the continent prior to its arrival at the coast of Africa. Less explicit examples of such development are to be found in annual summaries of hurricane activity (Dunn, 1961; Dunn and Staff, 1962, 1963, 1965; Sugg, 1966, 1967) that describe the destructive hurricane Donna of 1960, hurricane Becky of 1962, hurricanes Florence and Gladys of 1964, hurricanes Betsy and Carol of 1965, and hurricanes Faith and Inez of 1966 as having originated near the African coast. Undoubtedly, had better satellite data been available for those years and more effort expended, other hurricanes and tropical storms would have been tracked back to this region.

An excellent opportunity for studying the nature and possible origin of disturbances over Africa prior to their intensification into the hurricane stage presented itself during the 1967 hurricane season when, following the advent of the high quality satellite pictures from ESSA 5, hurricanes Arlene, Beulah, and Chloe originated from disturbances that crossed the West African coast in the incipient stage during a 10-day period from August 24 to September 3. It is the purpose of this paper to present in some detail a synoptic account of these disturbances as they moved across the Continent of Africa. Satellite, surface, and upper air data are combined to serve as a guide for early recognition of incipient hurricanes over West Africa.

2. ANALYSIS

In order to describe the important features of the weather associated with traveling disturbances, the 1200 GMT streamlines at 2,000 and 10,000 ft (700 mb) and the surface pressures were analyzed for each of 15 successive days from August 21 to September 5. The area of analysis over land was prescribed by the data network, which is interrupted at the Sudanese border in the east and at the desert in the north. The western edge of the analysis is terminated at the Cape Verde Islands. Although figure 1 suggests that the coverage of surface and upper air data in the area is abundant, the actual transmission of reports from stations was erratic. Many stations, in fact, transmitted at different times on different days and sometimes not at all. Other stations reported occasionally or transmitted at 0600 or 1800 GMT. Since the diurnal fluctuations were often larger than those produced by weather systems and since many stations contained an appreciable bias in the surface pressure as the result of a barometric inconsistency, a procedure was followed for all stations to maximize the quality and density of data. This procedure was to examine in linear display the 15-day records and recover the missing pressure data, where possible, from the 24-hr pressure change values that are transmitted for all sub-Sahara stations. Next, the average pressures were computed at 1200 GMT, and a mean isobaric map (fig. 1) constructed. The magnitude of adjustment necessary to make the station pressure fit the analysis was considered as a constant bias to be added to the individual values. A similar procedure was used to obtain the diurnal corrections, from which further estimates of 1200 GMT pressure were made, using an interpolation of off-time reports and their 24-hr pressure tendencies.

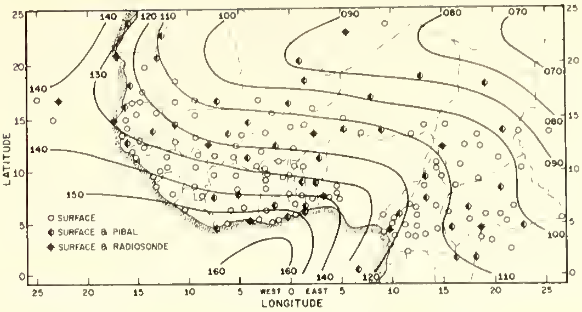

FIGURE 1.—Mean sea-level isobars at 1200 GMT for the period Aug. 21–Sept. 4, 1967. Contours are labeled in millibars and tenths above 1000. The distribution and type of reporting stations are indicated by the circles.

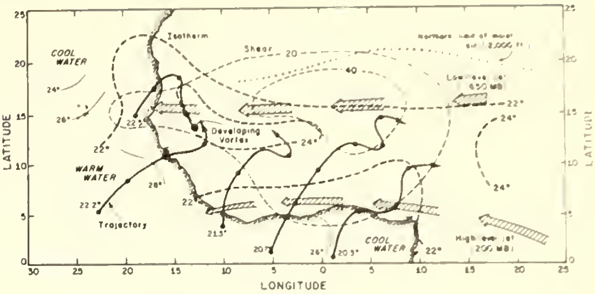

FIGURE 2.—Lower tropospheric zonal vertical shear (light dashed lines labeled in knots), wet-bulb potential temperature at 950 mb (heavy dashed lines labeled in °C), and air trajectories at 2,000 ft for 1200 GMT, Sept. 3, 1967. The 950-mb wet-bulb potential temperature at the origin of the trajectory is indicated by a single figure. Duration of travel in days is equal to the number of segmented intervals along the trajectory. Sea-surface temperatures (thin lines labeled in °C) were taken from values obtained by the research vessel *Geronima* during early August 1963. Representative positions of the low- and high-level easterly jet streams are indicated. The center of a developing surface depression is shown by a filled circle.

Wind reports were also erratic during this period. In some instances interpolation between off-time soundings was used to construct the 1200 GMT streamline maps, but in general the data were plotted at the station location as if they applied to 1200 GMT. When it became apparent that the weather systems were translatory, the first analyses were used to construct a second set of maps in which off-time data were displaced longitudinally from the station circle by a distance equal to the appropriate wave speed times the time differential from 1200 GMT (6 or 12 hr). In addition, surface wind and ship reports were used in places to supplement the 2,000-ft winds.

Besides the surface and upper air analyses, satellite pictures, such as those shown by Simpson et al. (1968), furnished a highly visual aid in identifying and following the weather systems. Because the satellite scans coincide with local noon, the photographs, digitally rectified to map coordinates, were highly relevant to the 1200 GMT analyses and are presented next to them.

3. CLIMATOLOGICAL BACKGROUND

It has been known for some time that wavelike disturbances in the easterly flow, associated with squally weather at the surface, move westward across the bulge of West Africa during the monsoon season of June–October (see Arnold, 1966, for example). During the early part of the season their occurrence is sporadic and they tend to be rather weak, but by August, when the depth and northward penetration of the moist southwesterly monsoon air are the greatest, the disturbances are rather more intense and are observed to pass Dakar at intervals of 3 or 4 days. Even in these months there may be periods of relative inactivity lasting from several days to a week or two. Both Erickson and Arnold found that the perturbations originated somewhere east of longitude 10°–20°E and moved westward at a fairly regular speed of about 15 kt. The accompanying cloudiness and bands of thunderstorms are undoubtedly related to Eldridge's (1957) traveling disturbance lines, which consist of more-or-less north-south-oriented line squalls. These are known to produce quite violent weather over the interior, but are somewhat less intense as they reach the western coastline.

The flow pattern over West Africa is strongly dominated by the effect of the Sahara Desert, a vast area of uniformly high potential temperature ($\theta \sim 45°C$) and low relative humidity throughout much of a very deep layer of dry convection. In contrast, the Atlantic Ocean and Gulf of Guinea comprise a relatively cold area ($\theta \sim 25°C$) over which a shallow southwesterly current of moist air flows inland, cutting across the isobars from a subequatorial high-pressure cell (see figs. 1 and 2). Interestingly, both the extremes of cold sea-surface temperatures in the Gulf of Guinea and warmth over the Sahara Desert are reached in August. Between the relatively cold waters of the Gulf of Guinea and the cold North Equatorial Current flowing southward along the African coast exists a narrow tongue of warmer water, associated with an equatorial countercurrent, which is warmest in late August.

The thermal wind produced by this striking temperature gradient results in a very rapid increase in easterly wind with height over the land and the existence of a strong easterly current aloft (see Reiter, 1963). During the late summer months the transition level between the easterly and westerly flow slopes upward from its intersection with the surface at about 20° lat. to a height of about 1 or 2 km at 5°–10°N, south of which the transition ceases to become well defined and the winds themselves are light. At middle levels the temperature gradient reverses from that at low levels, and the thermal wind reversal leads to a very narrow easterly jet, centered between 600 and 700 mb and at 15°–17°N. The strength of this jet is variable in time and space and is often as high as 30 or 40 kt (a shear of 40 or 50 kt from 2,000 ft). Outside the region of the African bulge the meridional temperature contrast is less pronounced, and the strong middle-level easterlies are therefore confined to the area between long. 15°E and 20°W (see fig. 2).

The velocity of the disturbances is about equal to that of the mean tropospheric wind and is contrary in direction to the low-level flow. The basic easterly current overlying the moist monsoon current enables the convective disturbances to possess the characteristic, unique for Africa, of long-term propagation. The strong wind shear and lid of drier air aloft somewhat resemble conditions found over the Middle West of the United States and may be responsible for producing a similarly violent convection.

West of longitude 15°E and south of about lat. 8°–10°N, the uncommon occurrence of intense thunderstorms during the months of August and September, traveling or otherwise, is due not so much to the absence of any strong basic current but to a notable lack of convective instability at low levels in air whose recent origin had been over the cold Gulf of Guinea. According to figure 2, the wet-bulb potential temperature, θ_w, at 950 mb (the cloud base), as estimated from surface conditions using appropriate lapse rates of temperature and dewpoint, is closely related to the sea-surface temperature in the region where the 2,000-ft trajectories show the air to be originating. Temperature soundings for West Africa show that a parcel of air lifted from 950 mb is convectively unstable throughout most of the troposphere when its θ_w exceeds about 22.5°C. Air originating over the Gulf of Guinea is therefore stable as it crosses the southern coast of West Africa but it later achieves a marginal instability north of about 10° lat. Air originating over the warm current of water south of the Cape Verde Islands is initially somewhat unstable, having a θ_w at cloud base of about 22.5°, and later achieves a rather large instability over a wide portion of the interior. Disturbances that pass through this region of high instability can be expected to intensify, although the convection itself will once more become weaker along the immediate coast and out over the ocean. Of course, other factors, such as large-scale descent in this area, can cause the disturbances to dampen once they reach the coast.

Before proceeding to the individual wave disturbances, some remarks concerning the interpretation of the satellite photographs may be useful.

From an analysis of the cloud data, available from the standard synoptic reports, it was found that five or six characteristic weather types could be readily identified by their brightness and texture on the satellite pictures. The following descriptions are pertinent only to the vicinity of sub-Sahara West Africa during August and September:

A) *Intense convection:* thunderstorms associated with cumulonimbus clouds and accompanied by heavy precipitation. Appears on digitalized satellite photographs as a white, bright area. An example of this type is shown for August 22 (fig. 5d).

B) *Weak convection:* heavy, dense middle and high cloud with some showers. Low clouds either suppressed or with some swelling cumulus. Appears on satellite pictures as a smooth, light gray area surrounding convective regime (fig. 5d).

C) *Stratiform:* much of the cloud seen over tropical West Africa, south of 10°N, falls into this category. Low cloud is broken-to-overcast stratocumulus or stratus having little or no precipitation. Middle and high cloud cover, when visible at the surface, is broken to overcast. It appears on satellite pictures as a mottled and lusterless gray (fig. 5d).

D) *Rain, not associated with thunderstorms:* light or moderate precipitation; intermittent and showery and usually associated with stratiform variety of cloud cover. This type appears smoother and thicker than stratiform (fig. 5d).

E) *Broken stratiform:* similar to stratiform type but lower clouds are broken and may consist of cumuliform as well as stratiform cloud. Middle and high cloud cover tends to be highly broken. It appears on satellite pictures as a mottled gray with numerous open spaces (fig. 5d).

F) *Fair weather:* few or scattered low clouds, usually cumulus. Middle and high cloud cover is thin and up to broken cover. It appears on satellite pictures as a mostly open area with faint gray streaks (fig. 5d).

4. THE WAVE DISTURBANCES

During the 15-day period a total of six wave disturbances reached the west coast of Africa; a seventh already existed over the ocean on the 21st. Two of the six waves were weak and short lived, leaving four waves of similar intensity and character, each of which accompanied the formation of a major depression at surface near the coast of West Africa (fig. 3). For discussion purposes the *mean* longitude of wave axis (wind shift line) at 700 mb, which was adjusted for continuity of motion to remove sudden jumps in speed, is designated by an arrow and labeled according to a system followed by Arnold (1966). This discussion is concerned primarily with the four major disturbances, W–1, W–3, W–4, and W–6. It should be pointed out that because of the rather large (for low latitudes) pressure gradient across the lower portion of West Africa the existence of a vortex center may not be significant in itself insofar as a greater amount of vorticity may be concentrated in the high-speed portion of the wave. Similarly, an apparently closed isobar at sea level may not be present, despite obvious pressure falls there.

Wave W–1 (later to become hurricane Arlene) appears on the 21st with its axis near long. 5°E (see the sequence of figs. 4–9). During the next 2 days it increased its forward speed slightly; the area of cloudiness and intense convection increased and became quite striking on the satellite picture for the 23d. Subsequently, the wave slowed its forward speed, and the thunderstorm activity diminished. At the same time both the weak confluence and cyclonic curvature, previously noted in the 2,000-ft streamlines, and the surface pressure trough intensified beneath the upper wave (see also fig. 3). A closed vortex formed near 14.5°N prior to 1200 GMT on the 25th, producing 4-mb pressure falls at Dakar and over the Cape Verde Islands. On the 30th, after reaching long. 45°E, it became a tropical storm.

Wave W–3 (later to become hurricane Beulah) appears first on the 22d near the eastern edge of the analysis network (figs. 5–13). A widspread area of enhanced rainfall and convection east of the Cameroon Mountains

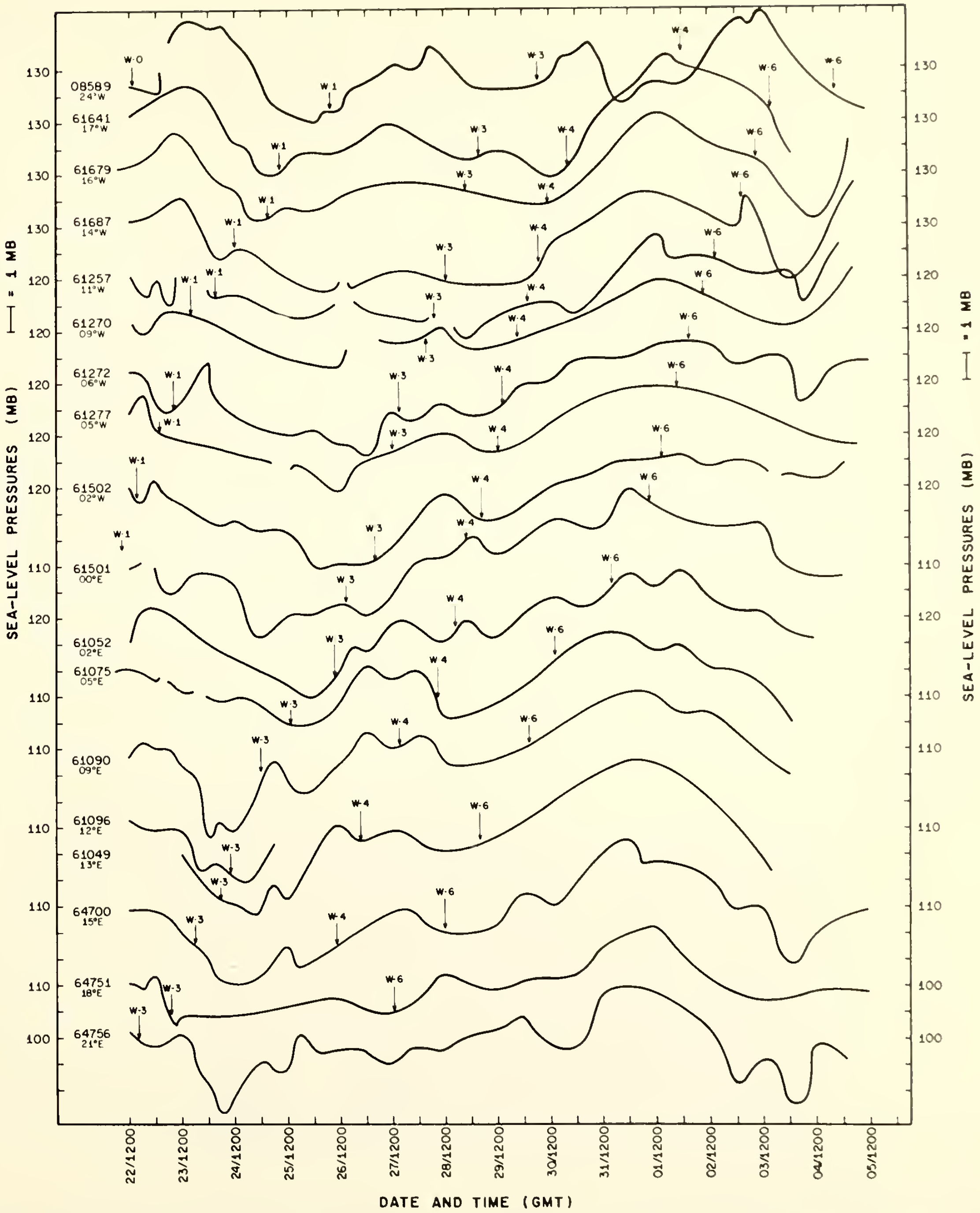

Figure 3.—Time variation of diurnally corrected sea-level pressure in millibars for stations situated approximately along lat. 14°N and at the longitude indicated below the station identification number. The approximate mean pressure for each station during the period (in millibars and tenths above 1000) is shown in the margins.

(15°E long.) accompanied the wave's passage westward across these mountains. After its arrival over their west slopes on August 24 the rainfall area became more coherent, while the convection itself was confined to a relatively narrow zone between 10° and 18°N lat. Cyclonic circulation and confluence in the 2,000-ft streamlines became more noticeable after the 27th, and a closed vortex formed beneath the wave axis at 12°N on the 29th. Pressure falls associated with the depression amounted to 2 mb at Dakar and the Cape Verde Islands. It remained quiescent, however, for some time, and it was not until September 8 at long. 60°W that the depression became a tropical storm.

Wave W–4 may have formed within the data network and appears first as a weak perturbation near long. 15°E on August 26 (figs. 9–14). It intensified during the following day and subsequently arrived near the coast on August 30, where it closely resembled the preceding two waves. The satellite photograph for the 30th shows a widespread cloud system with cyclonic bands whose center of circulation coincides with a newly formed depression just offshore at lat. 14.5°N. Pressure falls associated with this vortex were about 2 mb (fig. 3) at Dakar and the Cape Verde Islands. The disturbance maintained its circular cloud pattern for a few days, but despite its likely appearance it failed to develop.

Wave W–6 (later to become hurricane Chloe) was first noticed near long. 15°E on the 27th (figs. 10–18) along with some increase in convective activity east of the Cameroon Mountains. It moved westward unaccompanied by any appreciable cloudiness or convection until September 3, when numerous thunderstorms appeared some distance behind the wave axis. During the next 2 days the increase in low-level circulation and precipitation was rather dramatic, and on September 3 a vortex began to form overland southeast of Dakar. The circulation, whose circular banding and definite center are strikingly apparent on the satellite picture for September 4, coincided with a depression located at 14.5°N. Pressure falls of 4 mb were observed along the African coast and over the Cape Verde Islands (fig. 3) as the system passed westward. On September 8 at long. 38°W it achieved the status of a tropical storm.

5. DISCUSSION

Figures 4–18 (a–c) illustrate some of the details associated with the passage of traveling wave disturbances across West Africa and the extreme eastern tropical Atlantic Ocean. The waves moved in a coherent fashion across much of West Africa, and their eastward speed varied from 12 to 20 kt. Far inland, the disturbances were rather difficult to track in the surface pressure field or the 2,000-ft streamlines, even with the aid of satellite pictures. At this stage the magnitude of the surface pressure falls accompanying the disturbances usually did not exceed more than 1 or 2 mb, although the flow pattern often showed weak cyclonic curvature beneath the upper wave. The most positive means for tracking the disturbances over the continent proved to be the 700-mb wind field, although a combination of surface isobars, satellite pictures, and 2,000-ft winds was most helpful in augmenting and supporting the upper air data.

When the waves reached the coast, intensification in the low-level circulation resulted in the development of a depression near or just inland from the coast. At this point the cloud pattern in its vicinity became noticeably circular or banded and was accompanied by a 2- to 4-mb anomaly in central pressure of the vortex. The incipient depression was recognizable during its intensification into a closed vortex by a pronounced shift in the surface winds from northwest to southwest with the passage of the upper wave.

These cloud and rainfall patterns, recognizably associated with the traveling disturbances, were at first widely scattered east of the Cameroon Mountains; once on the other side there was often little convection accompanying the wave, as a consequence of its passage through a region of less convectional instability. Later, as the wave began to encounter more unstable air whose origin was over the warmer water southwest of Dakar, cloudiness increased, and an intensification of the system took place. Figure 2 shows that the rapid development of the surface depression on September 3 occurred as the wave passed through the region of maximum instability. According to Gray (1967), the removal of the strong shear and the subsequent passage of the tropical depression across the warm water south of 15°N would have favored its continuance or intensification, even though the instability was somewhat smaller over the ocean.

The mean distribution of rainfall and thunderstorm activity with respect to the 700-mb position of the wave axis (fig. 19) shows that (at lat. 14°N) the maximum occurred some distance *ahead* of the trough and a minimum immediately *behind*. A minor maximum is also found behind the trough. Such a distribution may be related to the peculiar wind profile, which, unlike that found with the classical Easterly Wave, requires a low-level convergence ahead of the wave and also at lower middle levels behind it. Somewhat contrary to the findings of Arnold (1966), the mean soundings for this 15-day period show that the wave is cold core only up to 500–600 mb and is warm core above, suggesting that the waves are therefore most intense at that level (fig. 20). The combination of upper level warmth and relatively moist conditions in the wave axis at all levels further suggests that the wave structure is closely controlled by the convection, wherein heat of condensation is released predominantly at high levels while the low-level air is cooled by downdraft evaporation in thunderstorms. On the sounding for Sal a pronounced inversion at low levels is recognizable, which suggests the presence of air aloft whose recent origin had been over the desert and whose effect would be to suppress the convection in this area.

A final consideration is the possible origin of the traveling disturbances. Thompson (1965) has stated that easterly waves and traveling disturbance lines have not been detected over the East African synoptic network, but he concedes that such phenomena do exist over West Africa. This study indicates that the wave disturbances formed somewhere east of 10°–15°E and points toward a favorable source region over the high ground that stretches east-

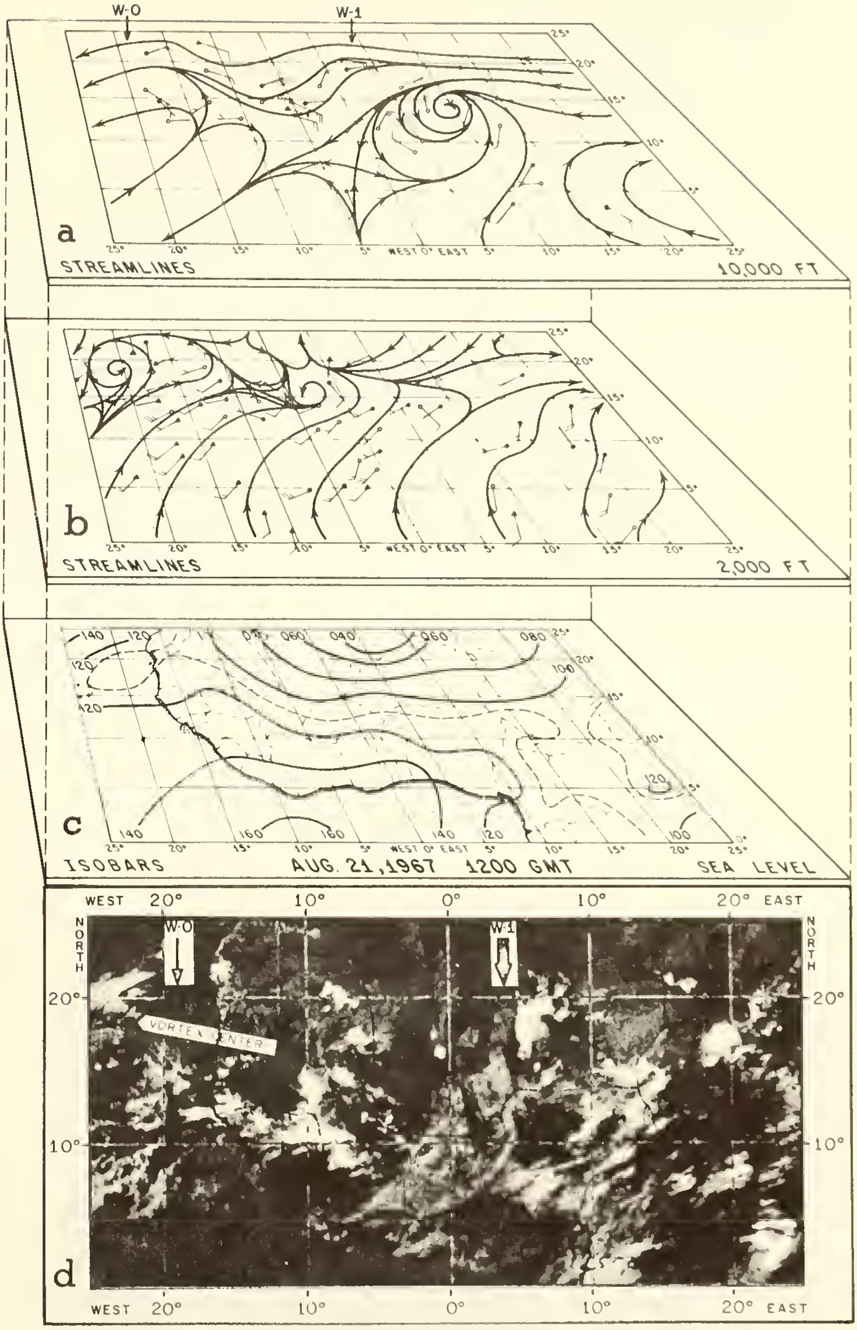

Figure 4.—(a) streamlines in perspective at 700 mb for Aug. 21, 1967. The wind vectors at 1200 gmt are plotted at the station location (filled circles). Off-time observations are displaced from their station location according to the wave speed (open circles). Off-level winds, pertaining to the 7,000- or 13,000-ft levels, are signified by a triangle. The longitudinal positions of the upper wave axis are designated by an arrow at the top. (b) same as figure 4a but for 2,000 ft. Off-level wind sectors refer to surface (coastal) or ship reports. (c) surface isobars at 1200 gmt, Aug. 21, 1967. Contour intervals (solid and dashed lines) are labeled in millibars and tenths above 1000. (d) digitalized mosaic of ESSA–5 satellite photograph (Orbits 1560–1561) at approximately 1500 gmt, Aug. 21, 1967. Wave axes are indicated as in figure 4a.

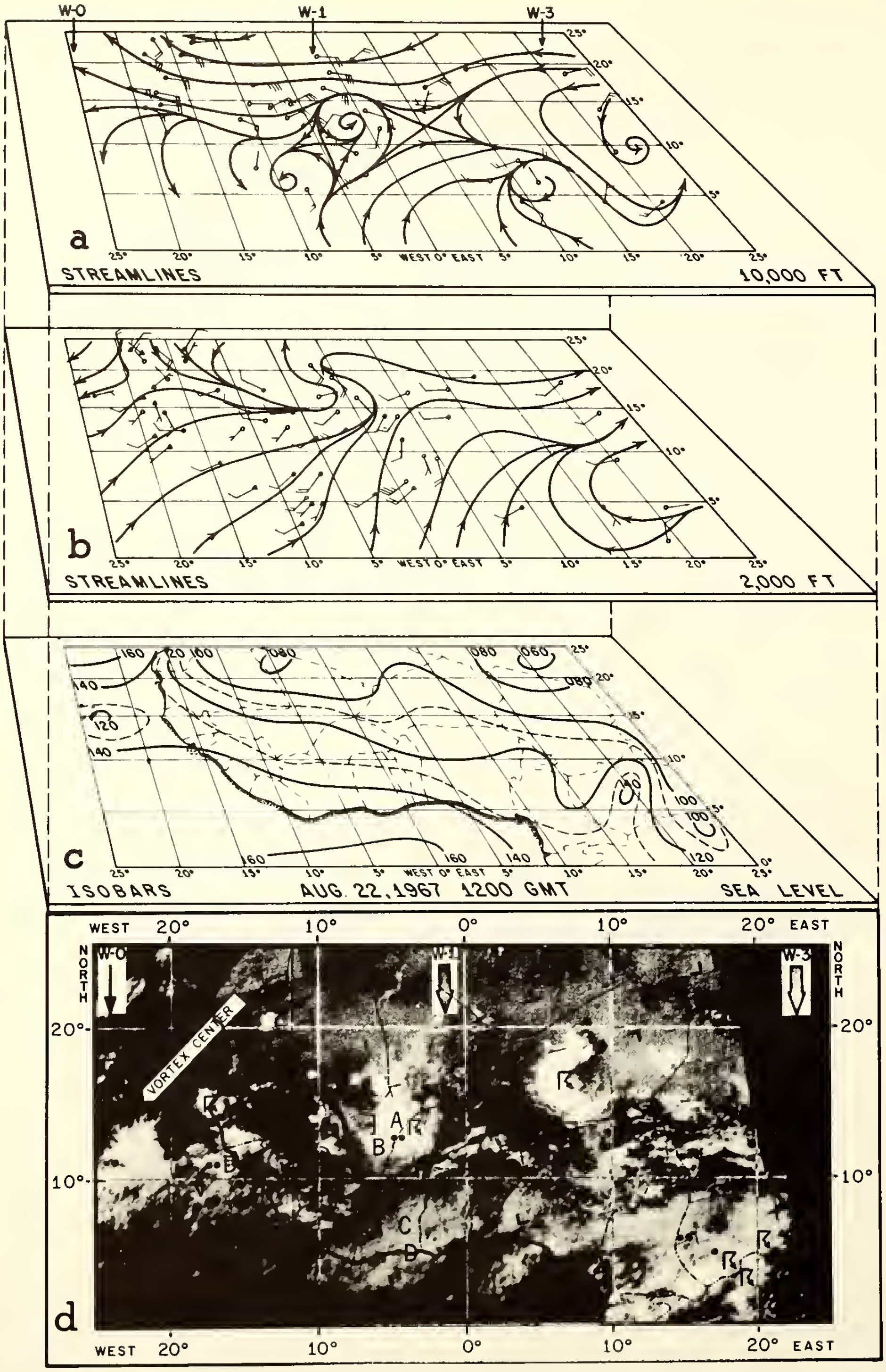

FIGURE 5.—Same as figures 4 (a–d) except for Aug. 22, 1967. On the satellite photograph (Orbits 1573–1574, 1425–1619 GMT), the letters A (intense convection), B (weak convection), C (stratiform), D (rain without thunderstorms), E (broken), and F (fair weather) pertain to the descriptions given in the text. Various weather symbols are also shown.

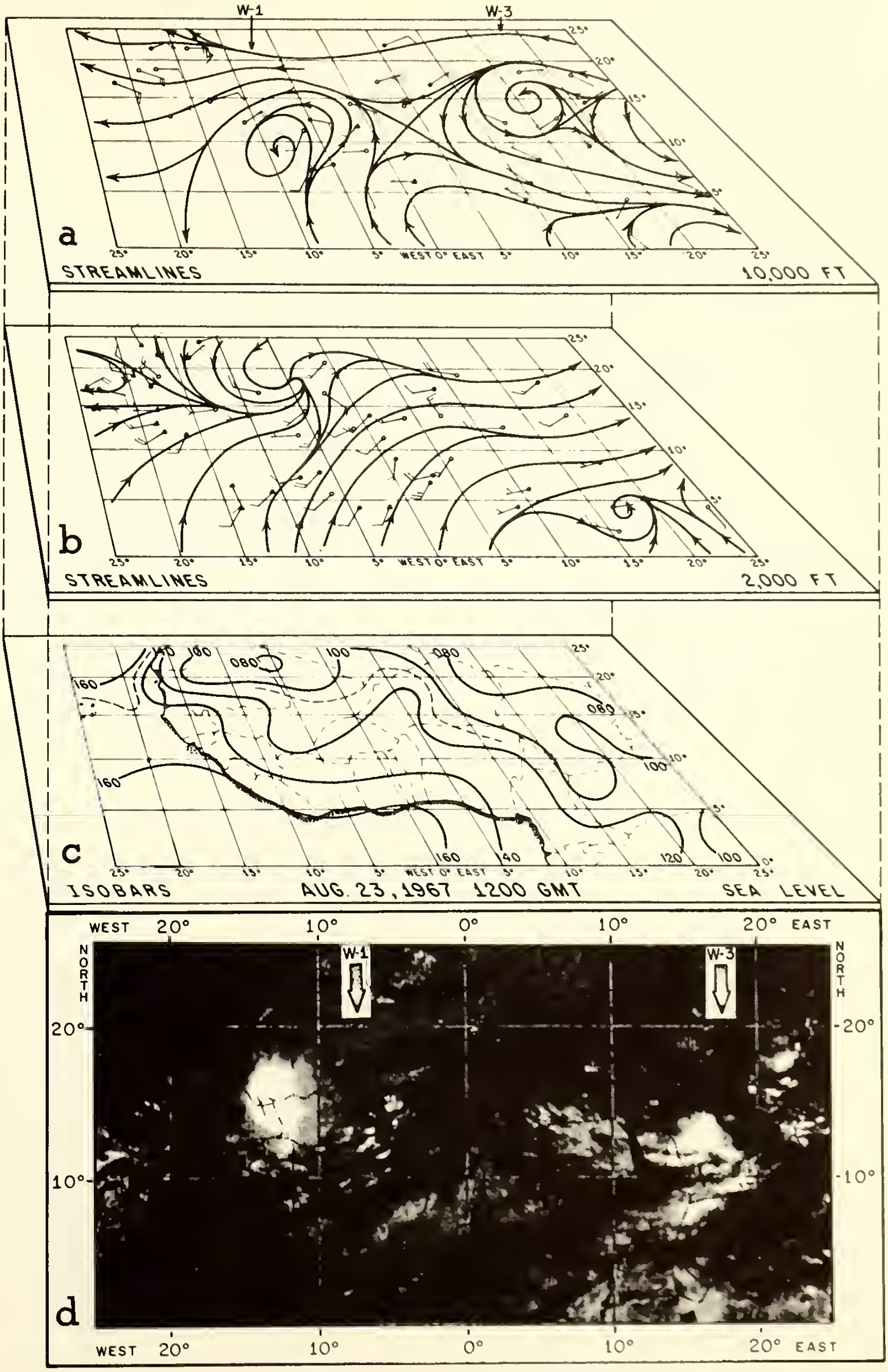

Figure 6.—Same as figures 4 (a–d) except for Aug. 23, 1967, Orbits 1585–1587, 1308–1655 gmt.

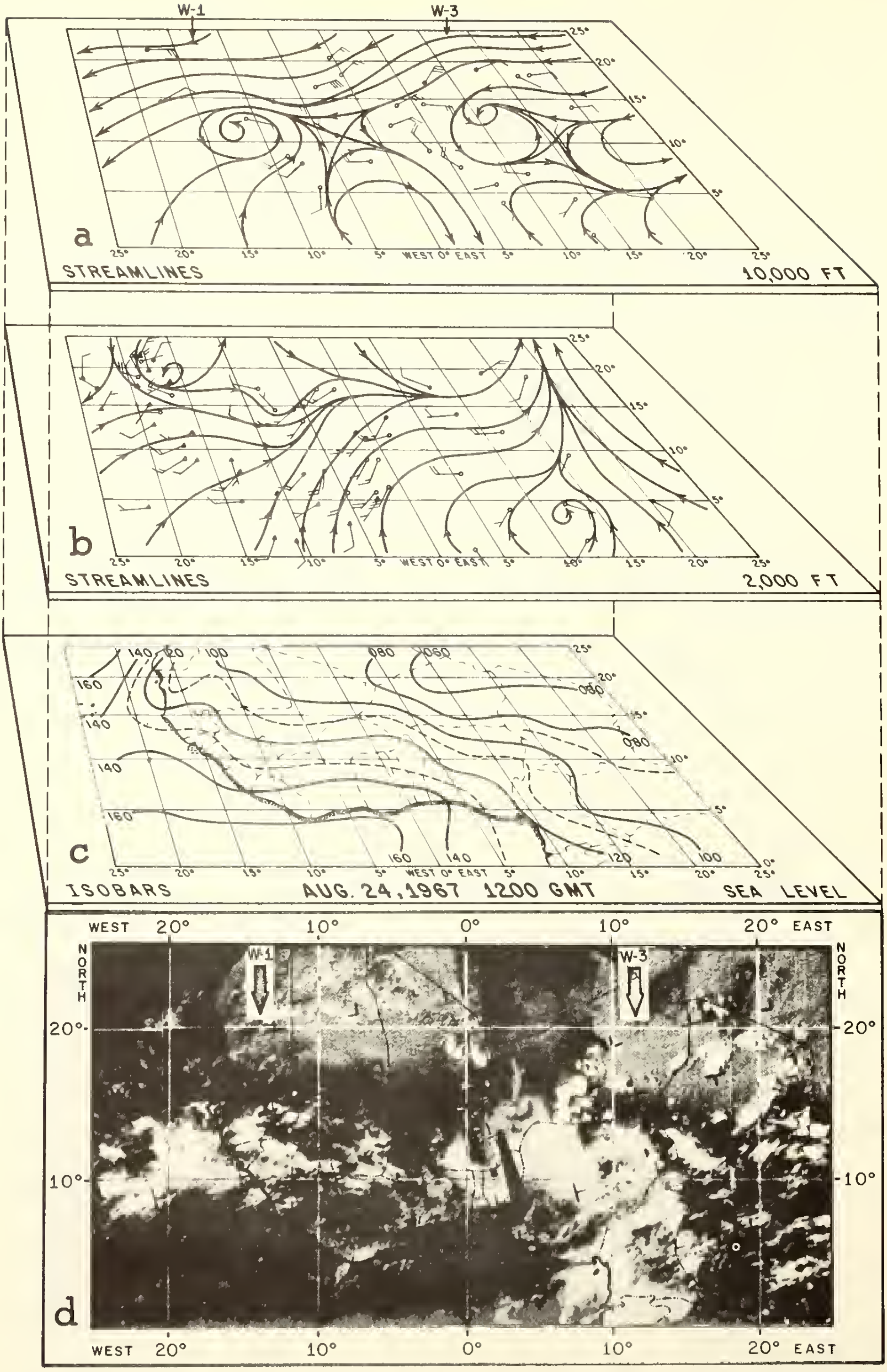

Figure 7.—Same as figures 4 (a–d) except for Aug. 24, 1967, Orbits 1598–1599, 1345–1538 GMT.

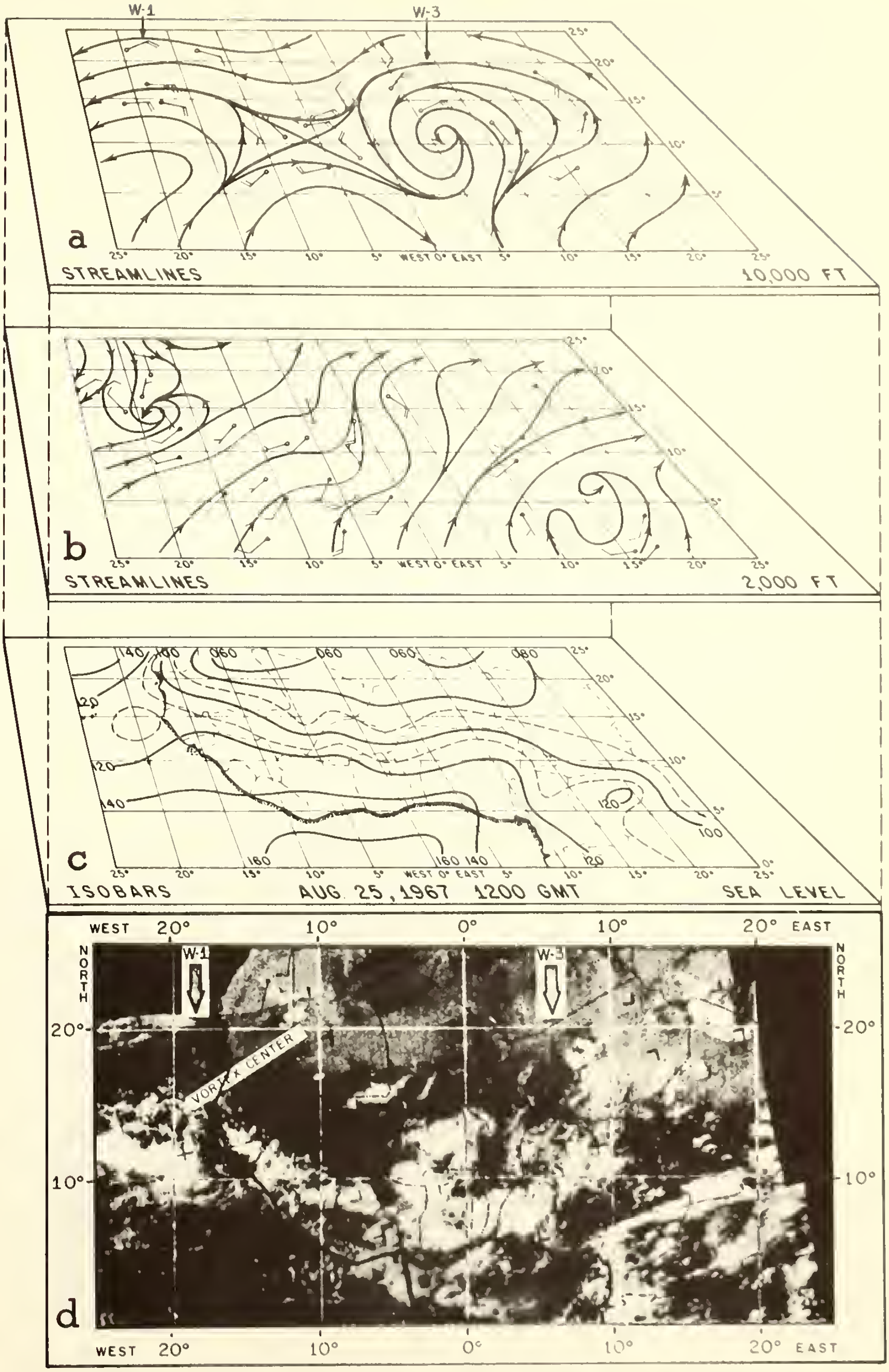

FIGURE 8.—Same as figures 4 (a–d) except for Aug. 25, 1967, Orbits 1611–1612, 1422–1615 GMT.

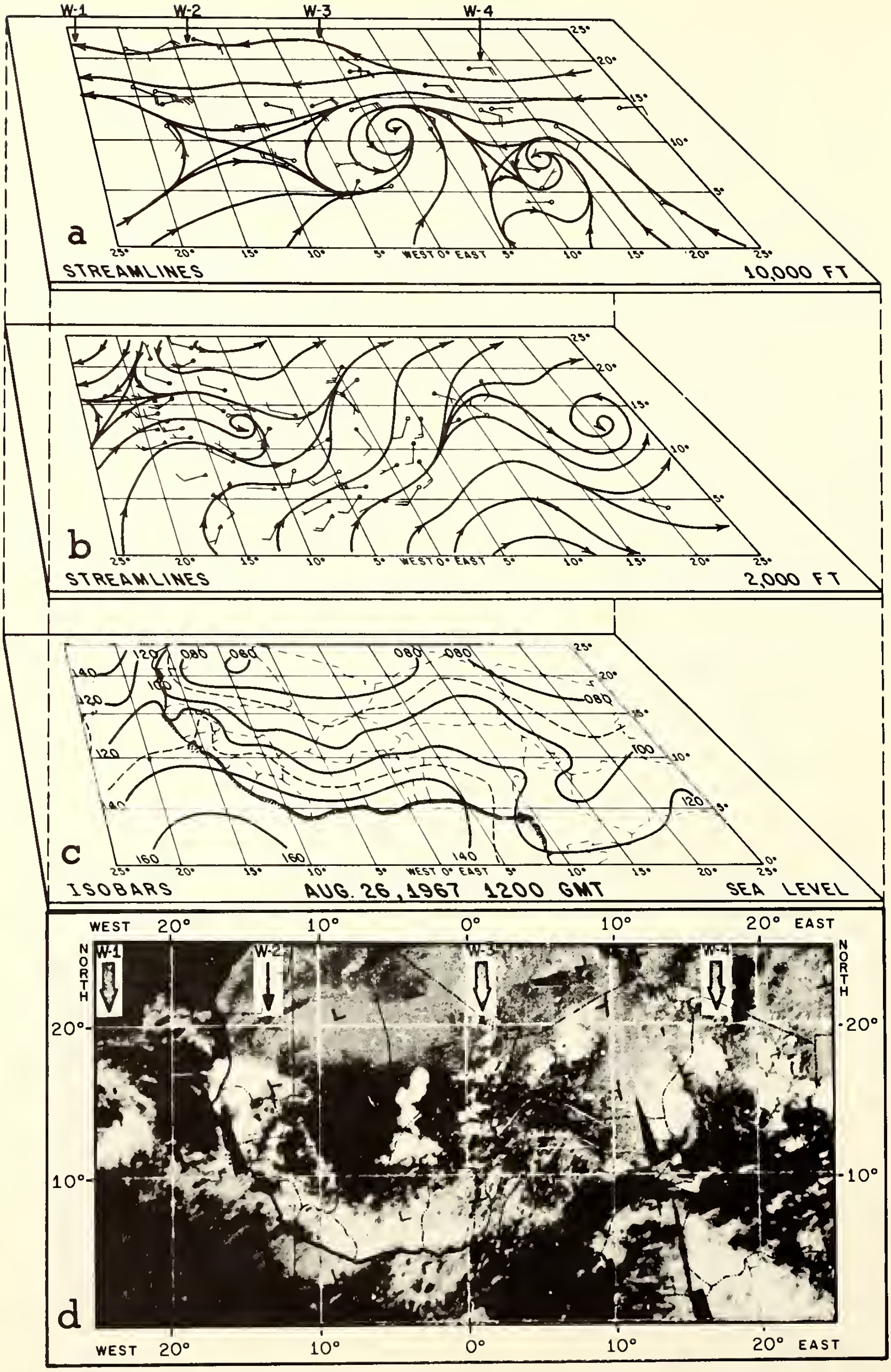

Figure 9.—Same as figures 4 (a–d) except for Aug. 26, 1967, Orbits 1623–1625, 1305–1652 gmt.

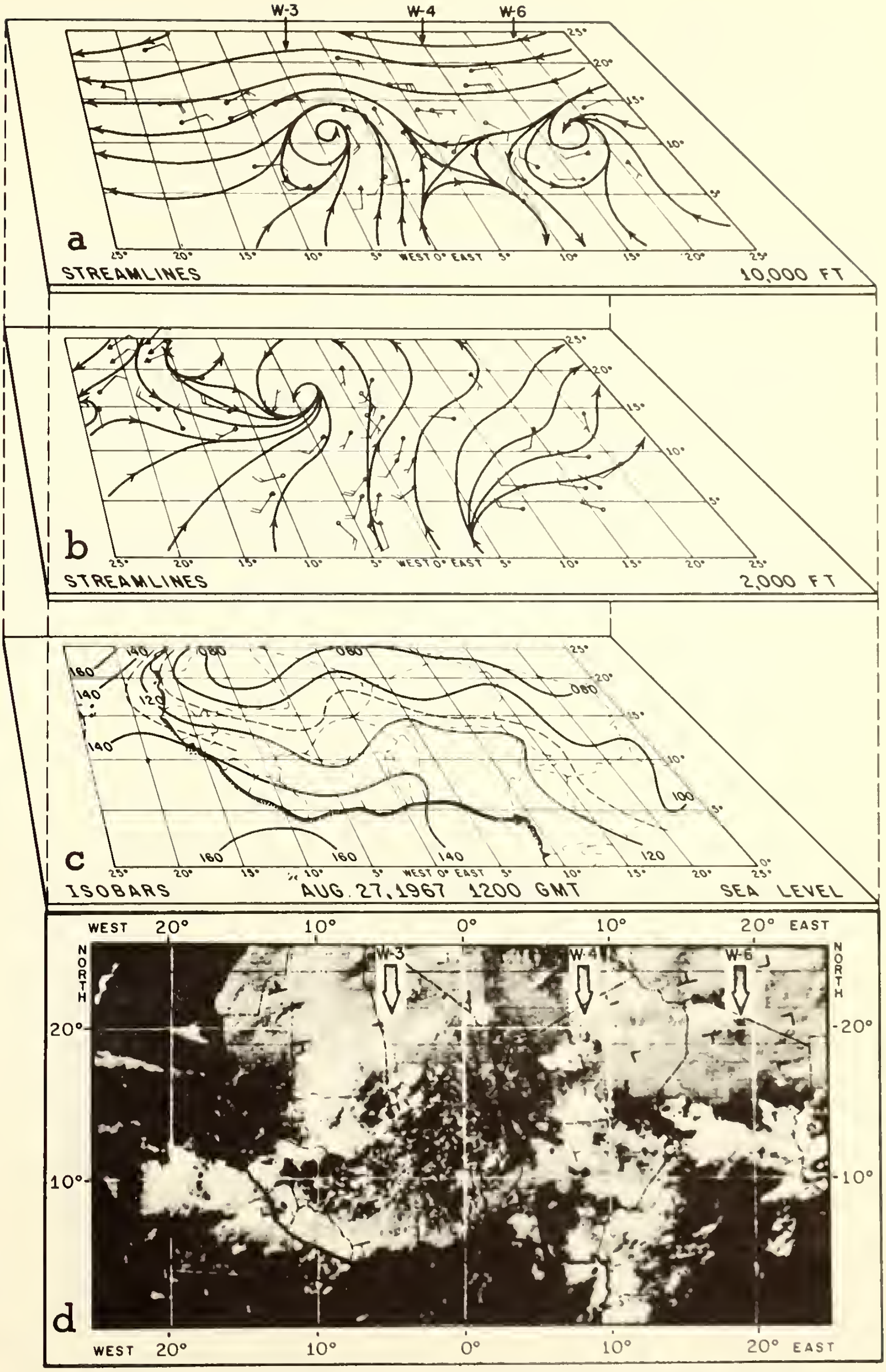

Figure 10.—Same as figures 4 (a–d) except for Aug. 27, 1967, Orbits 1636–1637, 1400–1600 GMT.

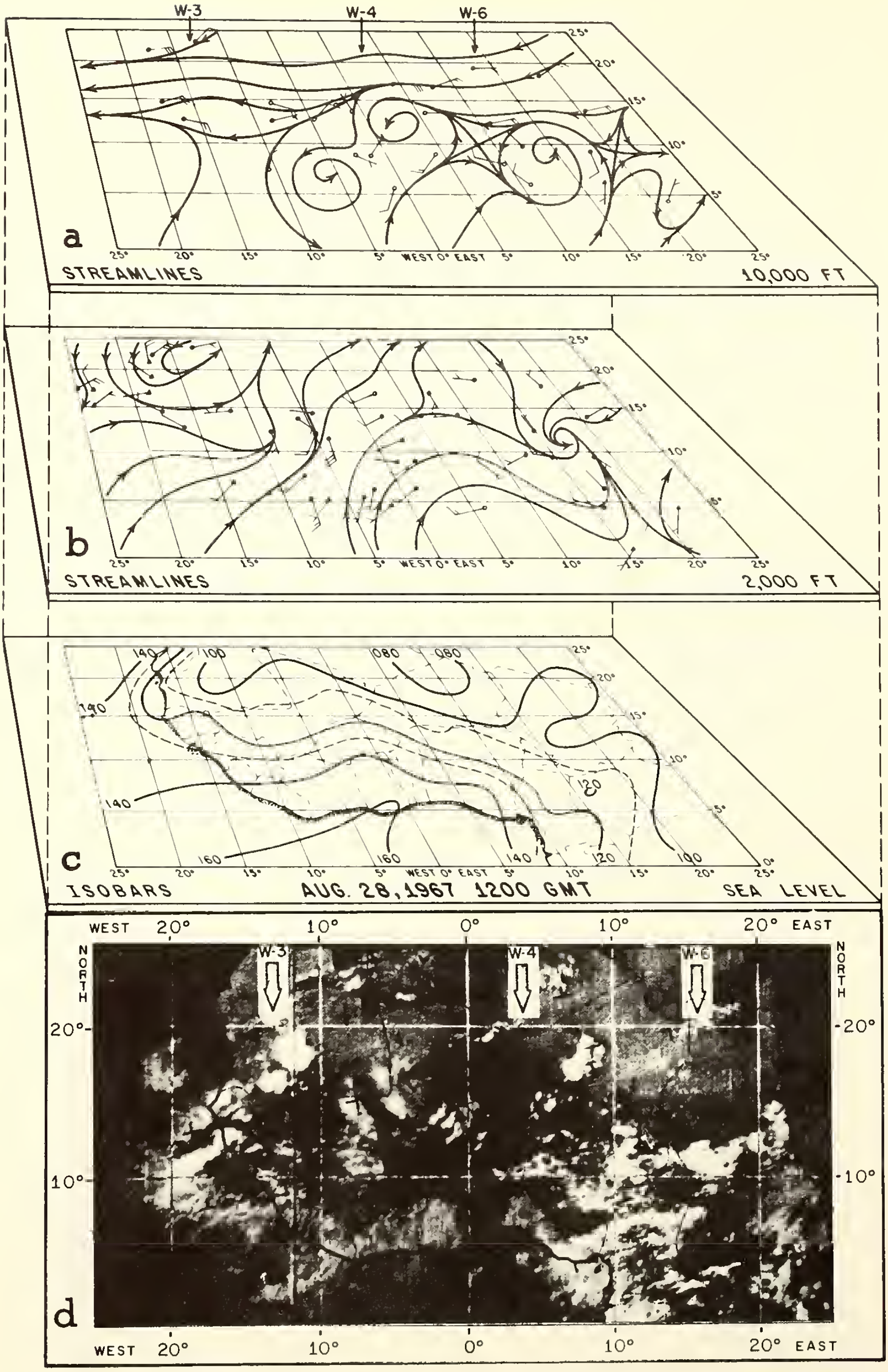

Figure 11.—Same as figures 4 (a–d) except for Aug. 28, 1967, Orbits 1649–1650, 1419–1612 GMT.

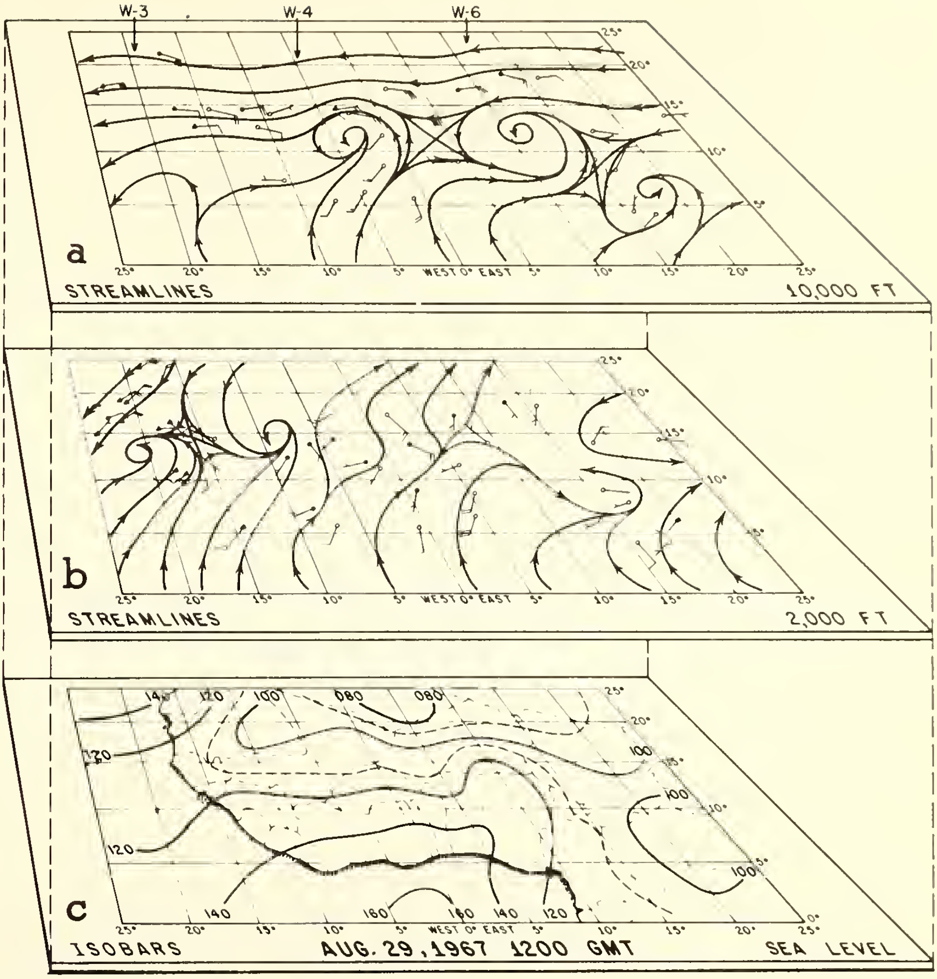

Figure 12.—Same as figures 4 (a–c) except for Aug. 29, 1967. (The satellite photograph was voided by transmission difficulty.)

ward from the Cameroon Mountains (Eldridge, 1957, p. 306).

6. CONCLUSION

Hurricanes Arlene, Beulah, and Chloe of the 1967 season developed from traveling wave disturbances that were tracked back to the interior of the African Continent. Typically, the disturbances moved westward with little development aloft or reflection at the surface until they approached the western part of the African bulge. There they encountered a supply of highly unstable air at low levels that accommodated a development of the wave into a more intense disturbance and was accompanied by enhanced convection and a formation of a weak depression at the surface. Upon reaching the coast, the convection diminished and became somewhat suppressed, although the area cloudiness and rainfall remained large. While recent evidence suggests that hurricanes and tropical storms not uncommonly originate from African disturbances, the vast majority of such disturbances, including many that are highly similar to or even stronger than these three disturbances, fail to continue their intensification out over the ocean. An example of this is also shown in the analyses.

ACKNOWLEDGMENTS

I would like to thank Mr. Neil Frank for making available the satellite photographs and for his helpful suggestions along the way. Special credit should go to Mr. Robert Carrodus who was responsible for the imaginative use of perspective in drafting the figures. Additional helpful criticism and comments concerning the manuscript itself were made by Messrs. Neil Frank, Harry Hawkins, and Dr. Banner I. Miller. Mr. Leslie Thomas did the typing.

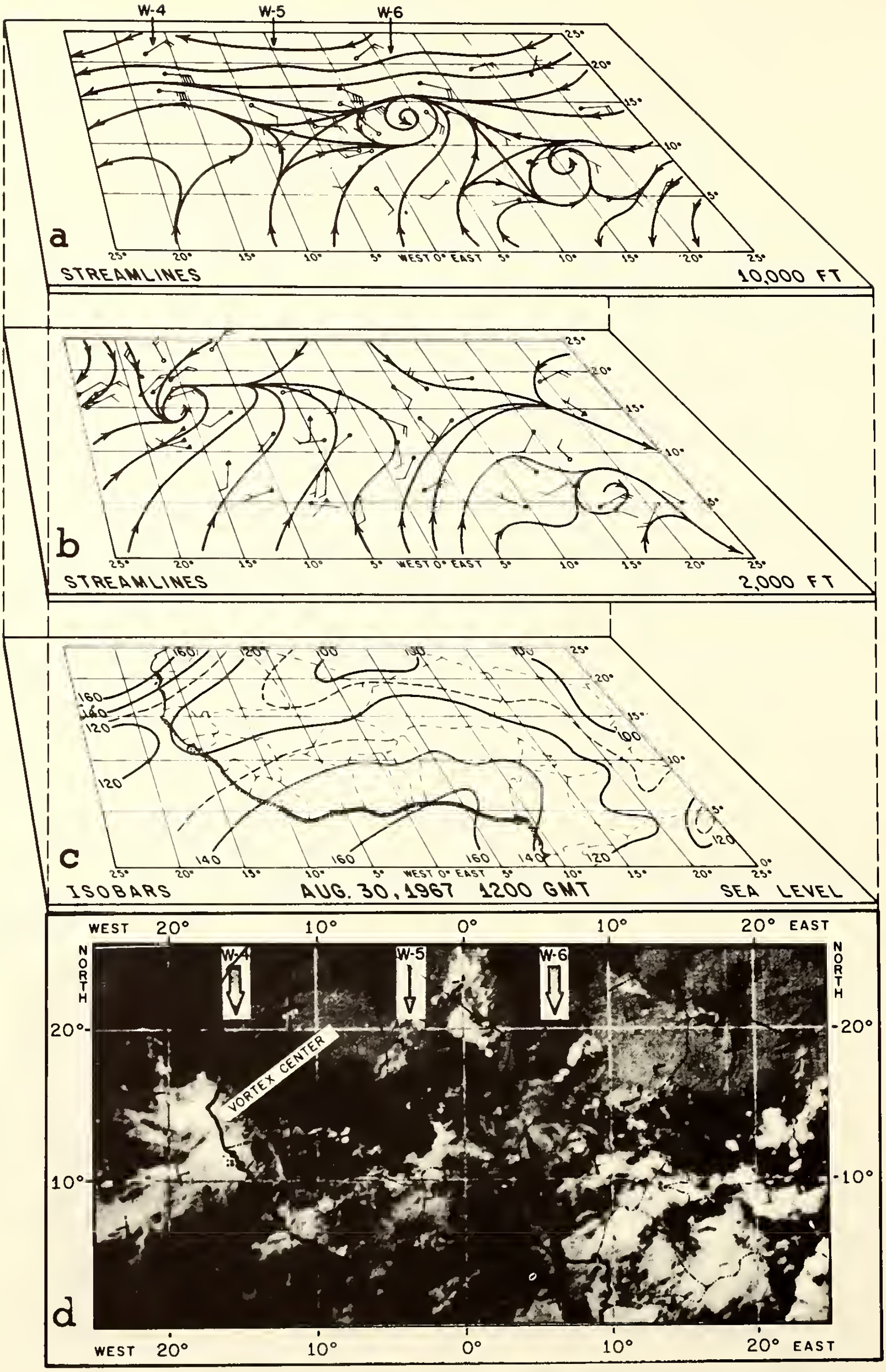

Figure 13.—Same as figures 4 (a–d) except for Aug. 30, 1967, Orbits 1674–1676, 1339–1726 gmt.

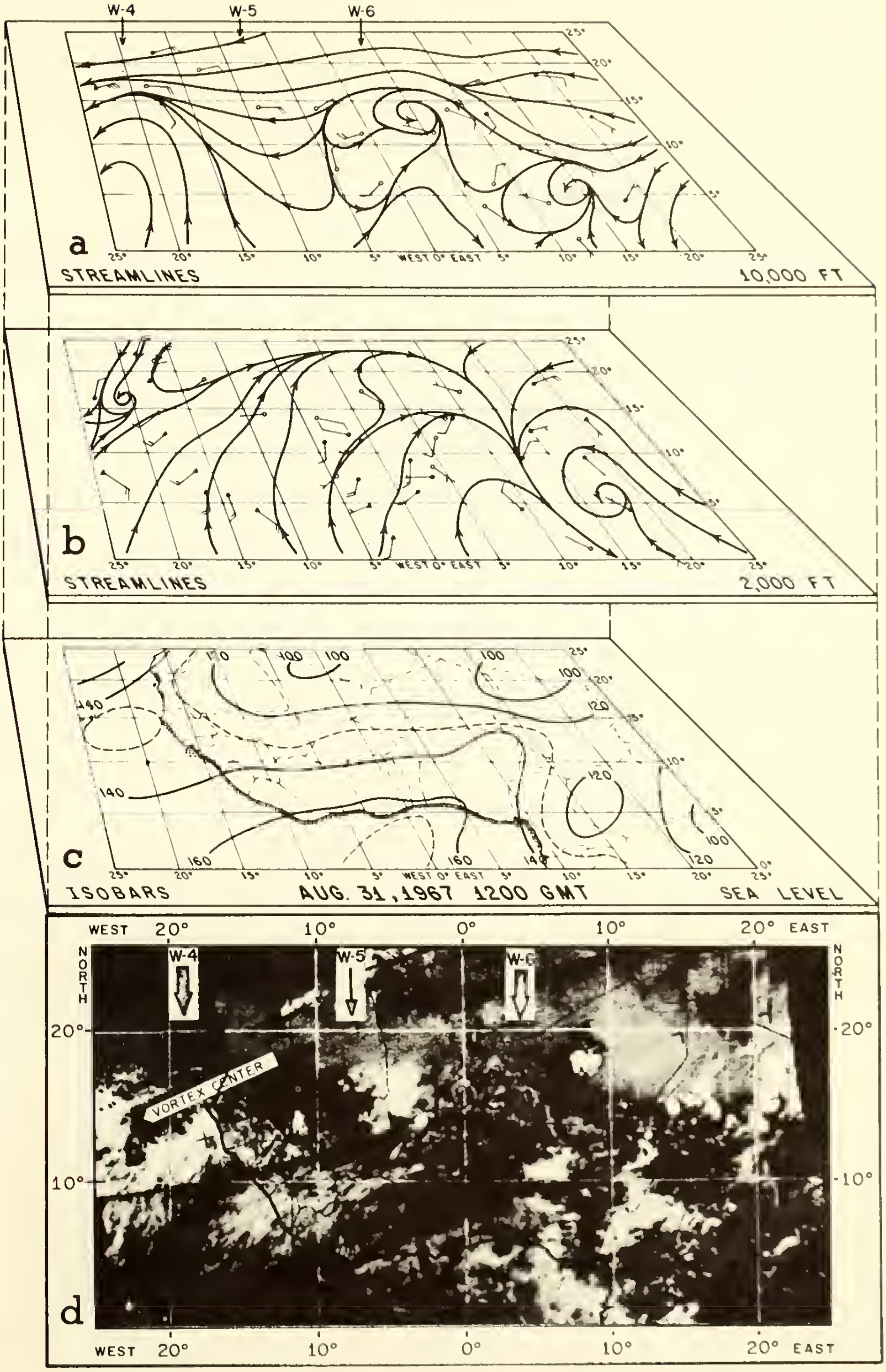

FIGURE 14.—Same as figures 4 (a–d) except Aug. 31, 1967, Orbits 1687–1688, 1415–1609 GMT.

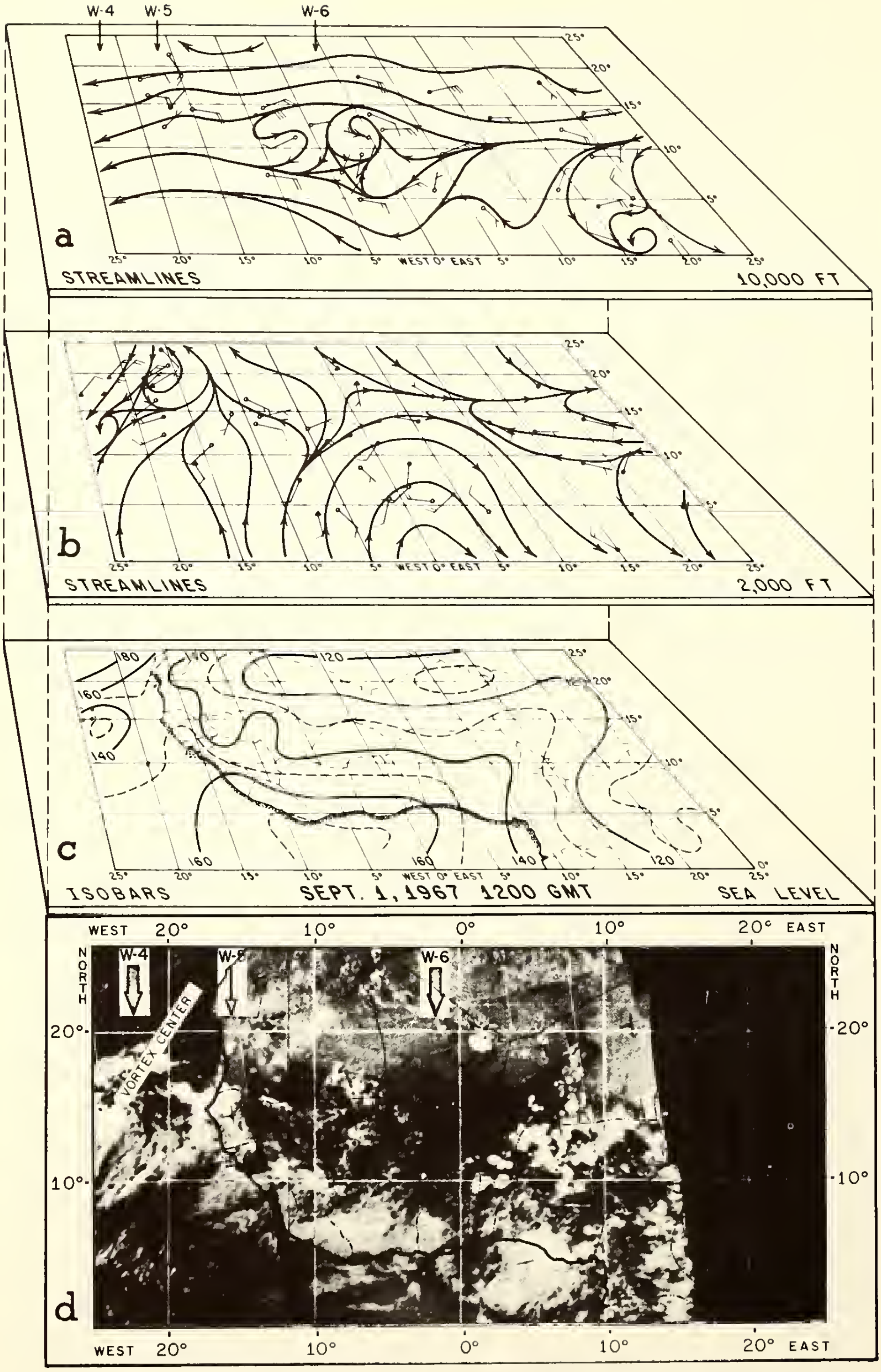

Figure 15.—Same as figures 4 (a–d) except for Sept. 1, 1967, Orbits 1700–1701, 1452–1645 GMT.

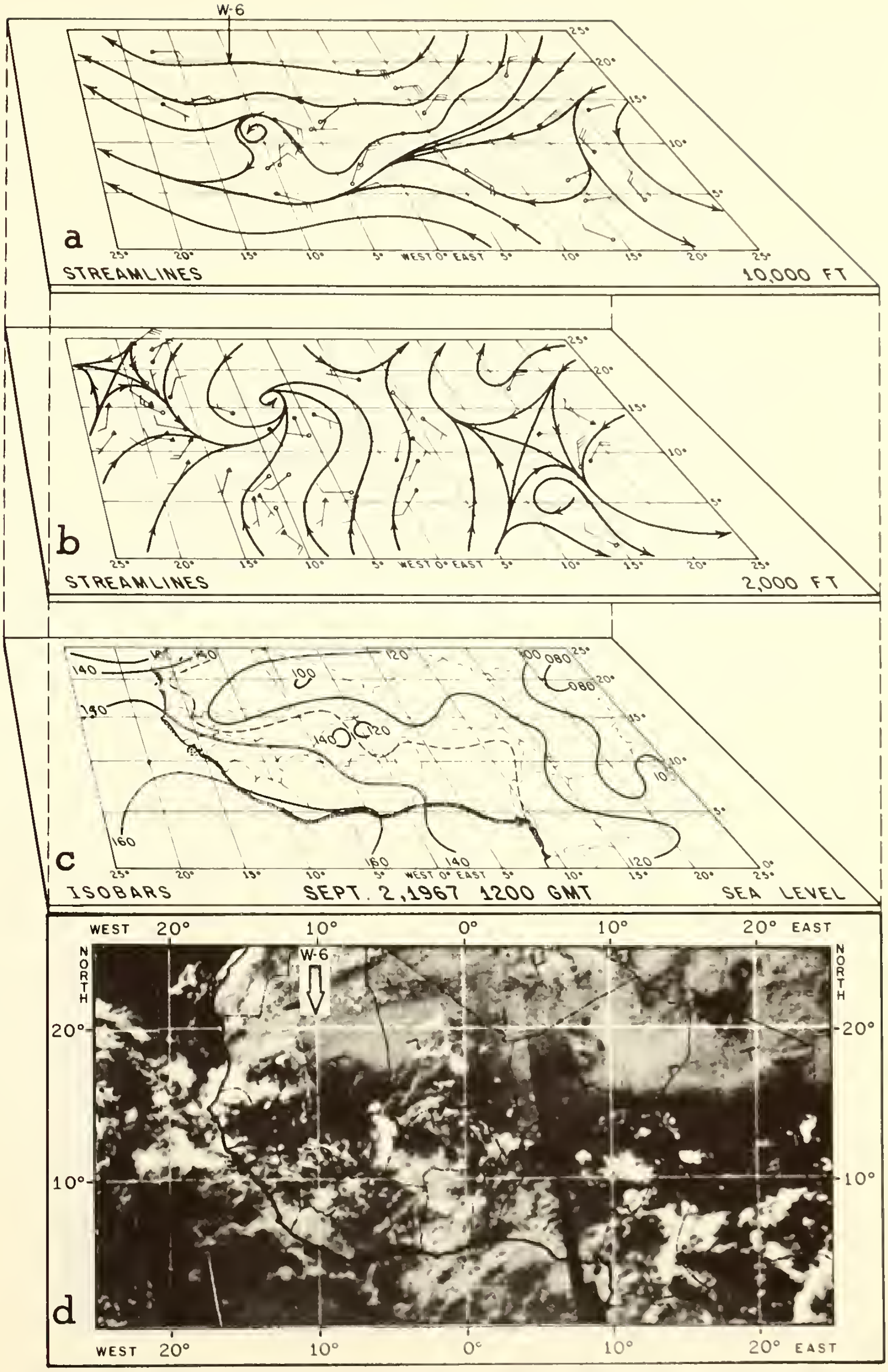

Figure 16.—Same as figures 4 (a–d) except for Sept. 2, 1967, Orbits 1712–1714, 1335–1722 GMT.

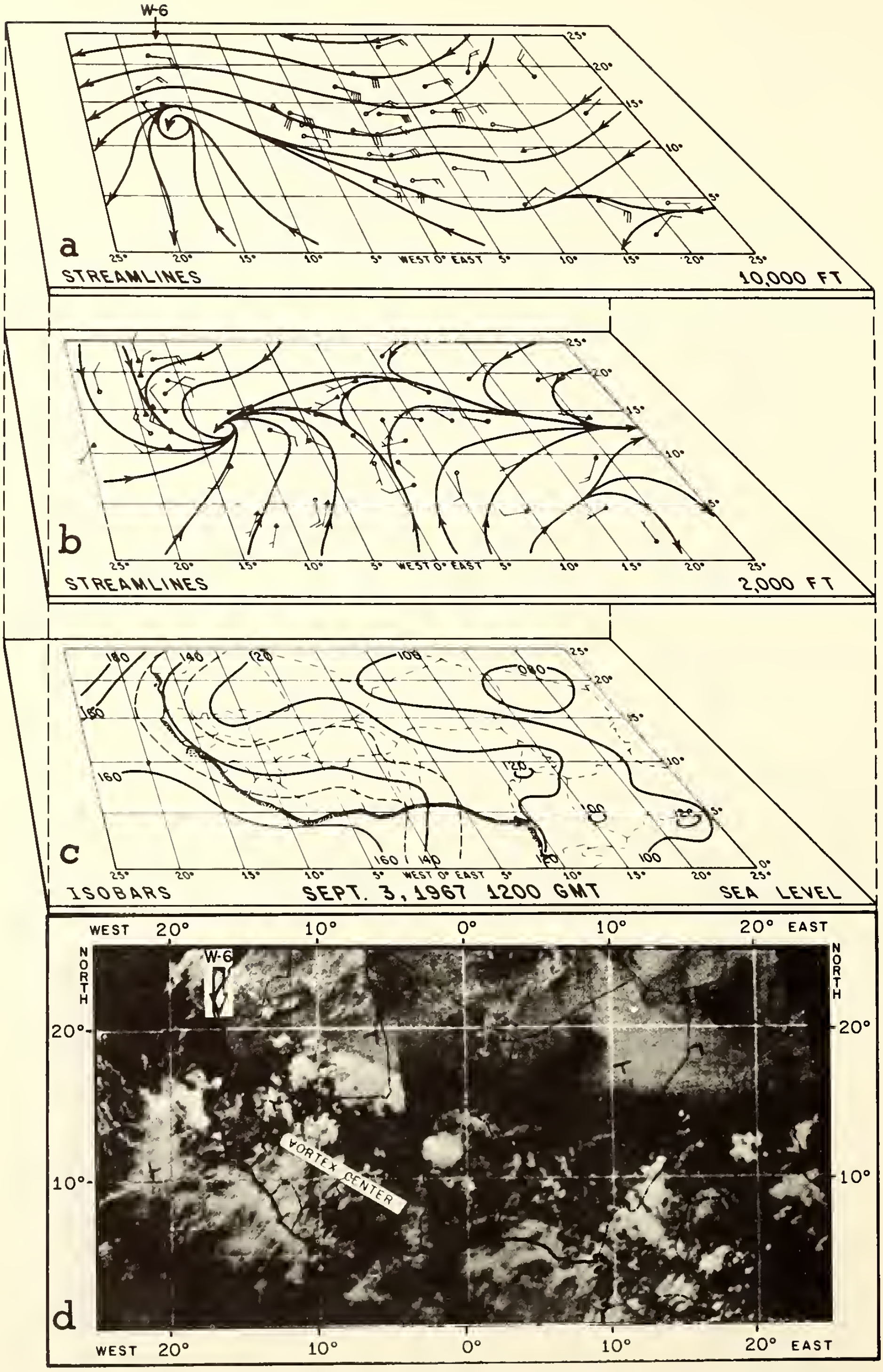

Figure 17.—Same as figures 4 (a–d) except for Sept. 3, 1967, Orbits 1725–1726, 1412–1605 gmt.

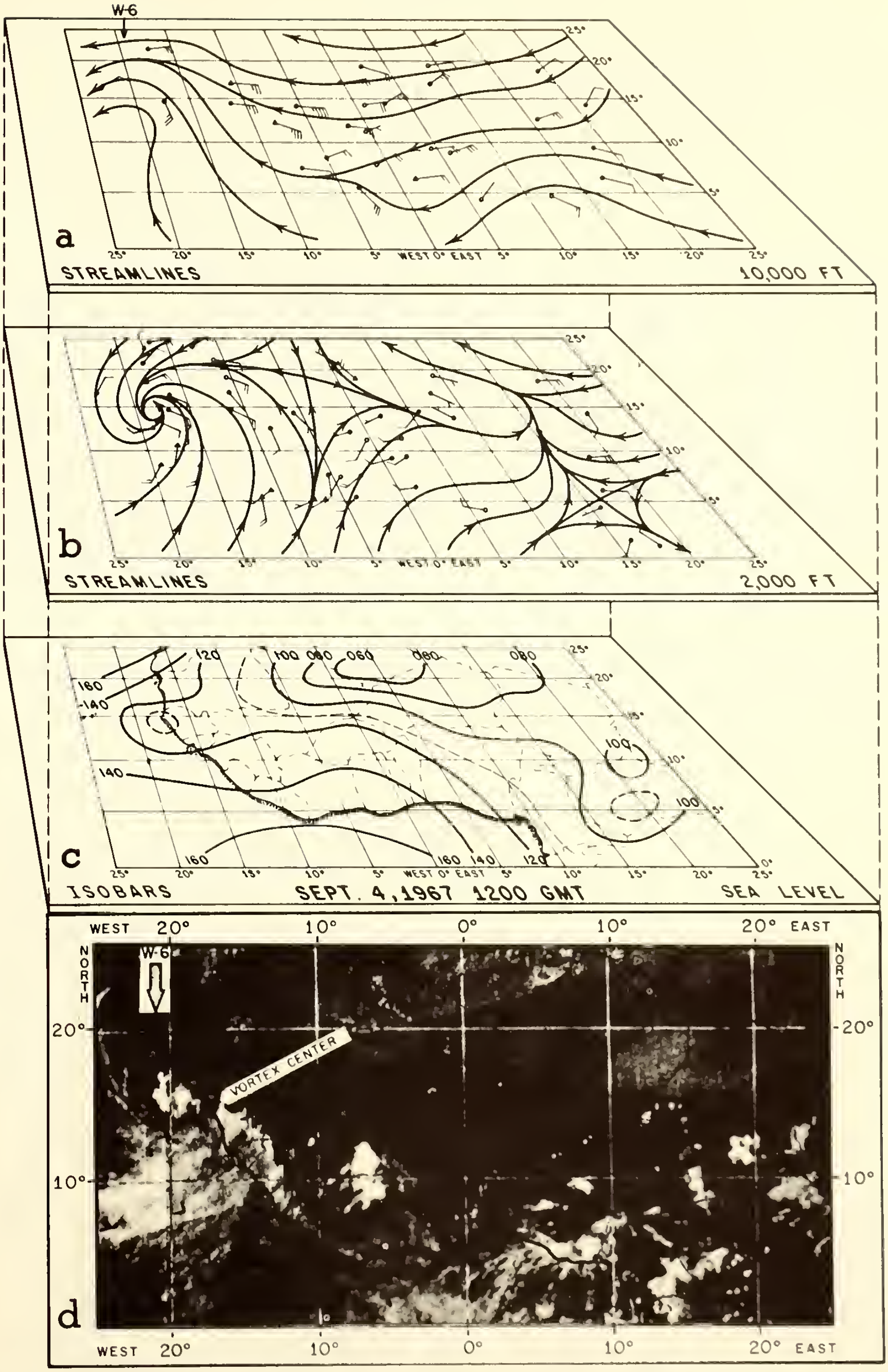

Figure 18.—Same as figures 4 (a–d) except for Sept. 4, 1967, Orbits 1738–1739, 1335–1642 GMT.

REFERENCES

Arnold, J. E., "Easterly Wave Activity over Africa and in the Atlantic with a Note on the Intertropical Convergence Zone During Early July 1961," *Satellite and Mesometeorology Research Project Research Paper* No. 65, Department of Geophysical Sciences, University of Chicago, Dec. **1966,** 23 pp.

Dunn, G. E., "The Hurricane Season of 1960," *Monthly Weather Review,* Vol. 89, No. 3, Mar. **1961,** pp. 99–108.

Dunn, G. E., and Staff, "The Hurricane Season of 1961," *Monthly Weather Review,* Vol. 90. No. 3, Mar. **1962,** pp. 107–119.

Dunn, G. E., and Staff,"The Hurricane Season of 1962," *Monthly Weather Review,* Vol. 91, No. 4, Apr. **1963,** pp. 199–207.

Dunn, G. E., and Staff, "The Hurricane Season of 1964," *Monthly Weather Review,* Vol. 93, No. 3, Mar. **1965,** pp. 175–187.

Eldridge, R. H., "A Synoptic Study of West African Disturbance Lines," *Quarterly Journal of the Royal Meteorological Society,* Vol. 83, No. 357, July **1957,** pp. 303–314.

Erickson, C. O., "An Incipient Hurricane Near the West African Coast," *Monthly Weather Review,* Vol. 91, No. 2, Feb. **1963,** pp. 61–68.

Gray, W. M., "Global View of the Origin of Tropical Disturbances and Storms," *Atmospheric Science Paper* No. 114, Colorado State University, Fort Collins, Oct. **1967,** 105 pp.

Reiter, E. R., *Jet-Stream Meteorology,* University of Chicago Press, **1963,** 515 pp.

Simpson, R. H., Frank, N., Shideler, D., and Johnson, H. M., "Atlantic Tropical Disturbances, 1967," *Monthly Weather Review,* Vol. 96, No. 4, Apr. **1968,** pp. 251–259.

Sugg, A. L., "The Hurricane Season of 1965," *Monthly Weather Review,* Vol. 94, No. 3, Mar. **1966,** pp. 183–191.

Sugg, A. L., "The Hurricane Season of 1966," *Monthly Weather Review,* Vol. 95, No. 3, Mar. **1967,** 131–142.

Thompson, B. W., *The Climate of Africa,* Oxford Press, New York, **1965,** 132 pp.

[Received July 22, 1968; revised September 9, 1968]

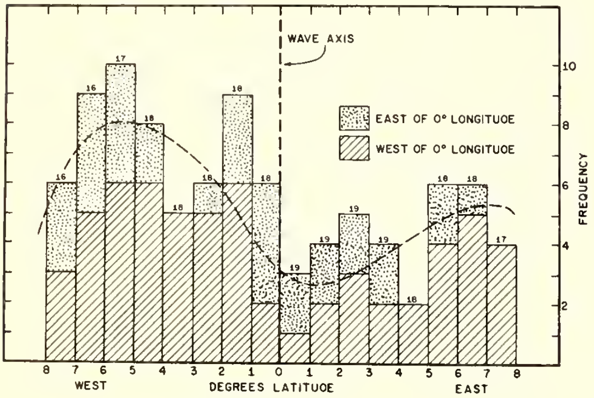

FIGURE 19.—Frequency distribution of disturbed weather (weather categories A, B, or D—see text) per degree of longitude versus distance from the wave axis for waves W-1, W-3, W-4, and W-6. Shaded and open bars refer to waves situated west and east of long. 0°, respectively. The figure at the top of the bar refers to the number of observations for that interval.

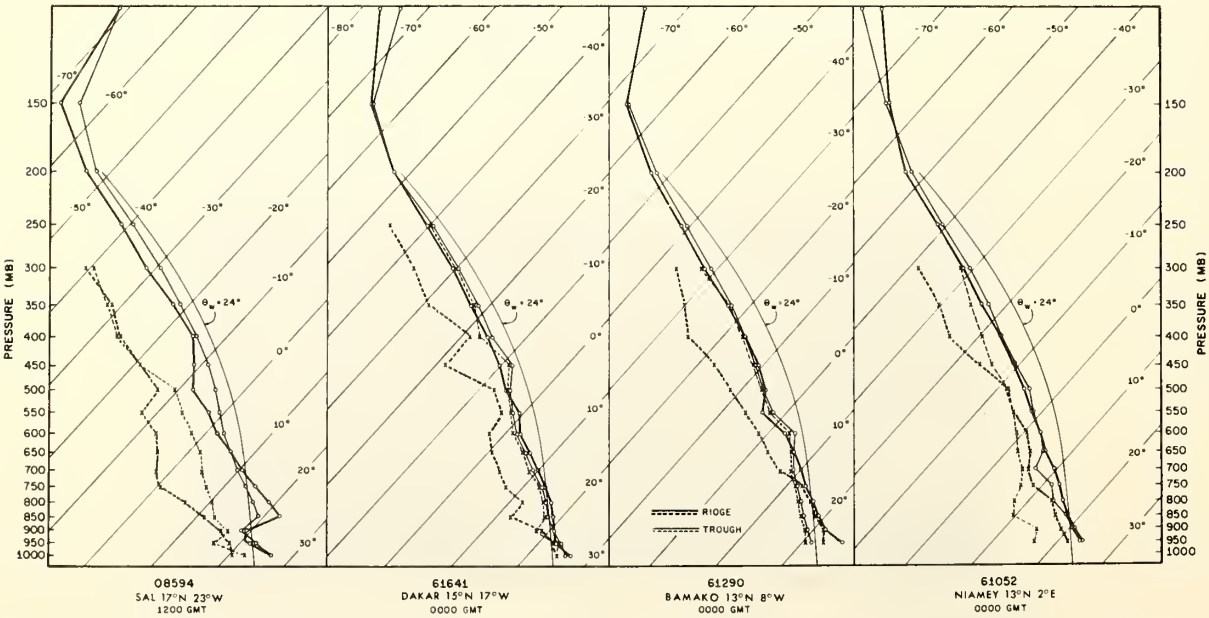

FIGURE 20.—Skew-T diagram for four West African radiosonde stations. Each sounding represents an average of about three individual ones that were made when the station was either close to the axis of one of the four major waves (light solid and dashed curves for temperature and dewpoint respectively) or near the ridge lines on either side of the trough (heavy solid and dashed curves). Temperature and pressure coordinates are labeled in °C and millibars. The wet-bulb potential temperature curve, $\theta_w = 24°C$, is also drawn.

Reprinted from Monthly Weather Review
Vol. 97, No. 8, 602-603.

UDC 551.515.2:551.509.314:551.509.57

A NOTE ON DRAWING PROBABILITY SECTORS

PETER P. CHASE

National Hurricane Research Laboratory, ESSA, Miami, Fla.

ABSTRACT

The problem of finding the probability that a tropical storm will be in a given area at forecast time is considered graphically.

With given bivariate data that have a joint normal distribution, a method is presented for plotting ellipses and rays which partition the data area into annuli and sectors having equal values of integrated probability.

Refer to Hoel (1954), page 150. With given data points (x,y) as deviations from the mean, if values in each component are normally distributed with standard deviations σ_x and σ_y and if the components are correlated with coefficient ρ, the probability density function is defined to be:

$$f(x,y)=\frac{\exp\left\{\frac{-1}{2(1-\rho^2)}\left[\frac{x^2}{\sigma_x^2}-2\rho\frac{x}{\sigma_x}\frac{y}{\sigma_y}+\frac{y^2}{\sigma_y^2}\right]\right\}}{2\pi\sigma_x\sigma_y(1-\rho^2)^{1/2}}. \tag{1}$$

If f is held fixed, the above equation determines an ellipse. Rapp and Isnardi (1951) showed that the inclination angle θ_0 of this ellipse is given by:

$$\theta_0=\frac{1}{2}\arctan\frac{2\rho\sigma_x\sigma_y}{\sigma_x^2-\sigma_y^2}. \tag{2}$$

They integrated equation (1) over the area of such ellipses, obtaining the probability distribution function P:

$$P=\iint f(x,y)dxdy$$

$$=1-\exp\left\{\frac{-1}{2(1-\rho^2)}\left[\frac{x^2}{\sigma_x^2}-2\rho\frac{x}{\sigma_x}\frac{y}{\sigma_y}+\frac{y^2}{\sigma_y^2}\right]\right\} \tag{3}$$

where x and y are constrained by $f(x,y)\equiv$constant. The ellipses (1) are more usefully characterized by P:

$$\frac{x^2}{\sigma_x^2}-2\rho\frac{x}{\sigma_x}\frac{y}{\sigma_y}+\frac{y^2}{\sigma_y^2}=-2(1-\rho^2)\ln(1-P). \tag{4}$$

This integration was accomplished by the transformation:

$$\xi=\left(\frac{x}{\sigma_x}-\frac{\rho y}{\sigma_y}\right)(1-\rho^2)^{-1/2};\quad \eta=\frac{y}{\sigma_y} \tag{5}$$

which has the property that the ellipses (4) become circles in the ξ,η plane, while rays in the x,y plane remain rays in the ξ,η plane. For polar coordinates r, θ in the x,y plane and s,ϕ in the ξ,η plane, we have:

$$\tan\phi=\frac{\sigma_x(1-\rho^2)^{1/2}\tan\theta}{\sigma_y-\rho\sigma_x\tan\theta}. \tag{6}$$

and

$$\exp(-s^2/2)=1-P. \tag{7}$$

Integration of (1) over the elliptical sector A of figure 1 is thus equivalent to integration of the transform of (1) divided by the Jacobian of the transformation over the circular sector B of figure 2 in the ξ, η plane.

$$\iint_A f=(\phi_2-\phi_1)(P_2-P_1)/2\pi \tag{8}$$

where ϕ_1 and ϕ_2 are the transforms of θ_1 and θ_2. This result shows that given an area divided into annuli having equal probability by ellipses (4), the sectors formed by two fixed rays will have equal probability from one annulus to another.

On a mechanical plotter, the ellipses can be drawn using:

$$r=\pm\left[\frac{-2(1-\rho^2)\ln(1-P)}{\frac{\cos^2\theta}{\sigma_x^2}-2\rho\frac{\cos\theta}{\sigma_x}\frac{\sin\theta}{\sigma_y}+\frac{\sin^2\theta}{\sigma_y^2}}\right]^{1/2} \tag{9}$$

The area can be divided into N sectors, each having equal probability, by rays θ_j, $j=0, 1, \ldots N-1$, where θ_0 is given by (2) and:

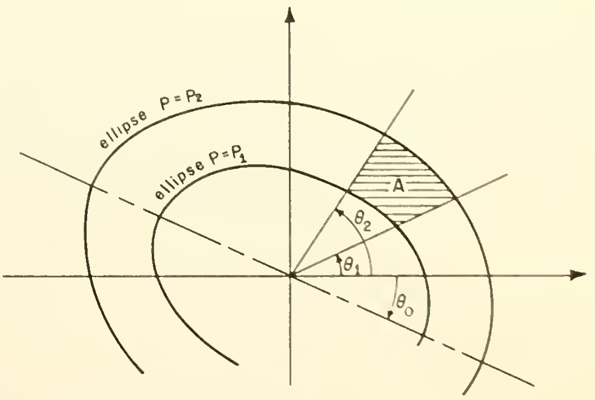

FIGURE 1.—An elliptical sector in the data area.

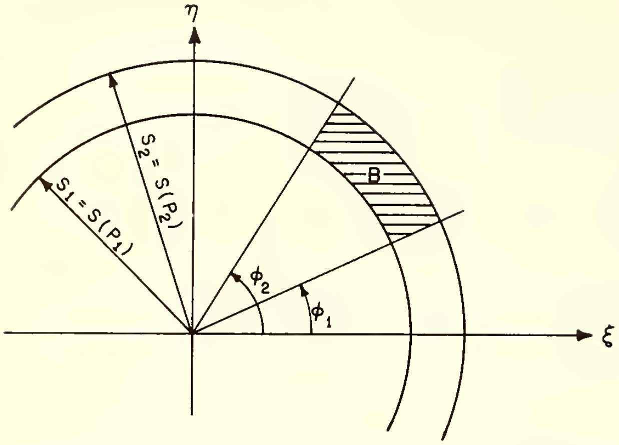

Figure 2.—The elliptical sector transformed to ξ, η coordinates.

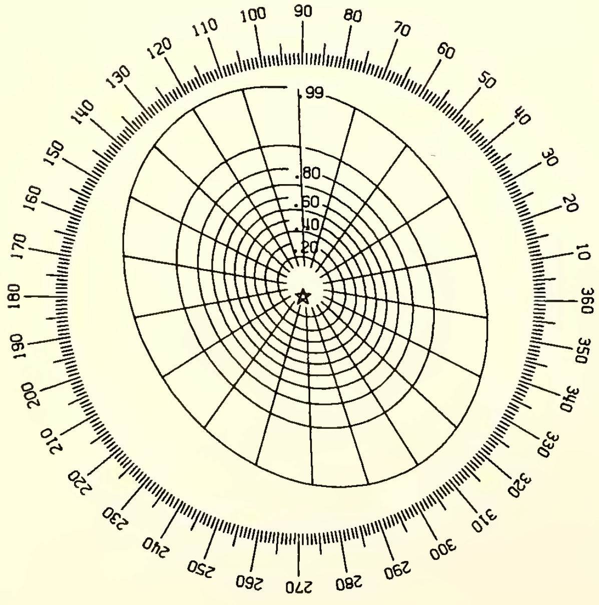

NHC-64 24-HOUR FORECASTS - INDEPENDENT SAMPLE 1962-67
OVERLAY DRAWN FOR 30.0 DEG LAT.
LAMBERT CONFORMAL PROJECTION. 1 TO 10000000
⊢——⊣ = 1 DEG OF LAT.
PUT STAR ON FCST PSN. TURN DIRECTION OF MOTION TO TOP

Figure 3.—Probability sectors and legend drawn by a mechanical plotter.

Table 1.—*Statistical parameters generating figure 3*

(y is along forecast track, x is to the right)
$\mu_x = -0.1°$ lat.
$\mu_y = -0.261°$ lat.
$\sigma_x = 1.296°$ lat.
$\sigma_y = 1.416°$ lat.
$\rho = -0.1959$
Latitude = 30° N.
Scale = 1:10,000,000

Ellipse	P	s (in.)
1	0.1	0.459
2	0.2	0.668
3	0.3	0.845
4	0.4	1.011
5	0.5	1.177
6	0.6	1.354
7	0.7	1.552
8	0.8	1.794
9	0.9	2.146
10	0.99	3.035

Ray	ϕ (deg)	θ (deg)
1	297	303
2	315	317
3	333	333
4	351	351
5	9	11
6	27	33
7	45	55
8	63	75
9	81	93
10	99	108
11	117	123
12	135	137
13	153	153
14	171	171
15	189	191
16	207	213
17	225	235
18	243	255
19	261	273
20	279	288

$$\phi_0 = \arctan \frac{\sigma_x (1-\rho^2)^{1/2} \sin \theta_0}{\sigma_y \cos \theta_0 - \rho \sigma_x \sin \theta_0}, \tag{10}$$

and

$$\phi_j = \phi_0 + 2\pi j / N, \tag{11}$$

$$\theta_j = \arctan \frac{\sigma_y \sin \phi_j}{\sigma_x (1-\rho^2) \cos \phi_j + \rho \sigma_x \sin \phi_j}, \tag{12}$$

for $j = 1, 2, \ldots, N-1$.

Figure 3 was generated on an incremental plotter for 24-hr forecast errors in the NHC–64 hurricane forecast system. (See Miller and Chase, 1966; also Miller, Hill, and Chase, 1968.) Each sector contains 0.5 percent of the total probability. Error components were taken with respect to the forecast direction of motion of a sample of hurricanes between 1962 and 1967; means, standard deviations, and correlation were computed by Mr. Billy M. Lewis of this laboratory. These are given in table 1. The azimuth scale of figure 3 is forecast direction of motion, read at the top. As a transparent overlay, the diagram can be used to estimate the probability of the storm center being within a given area in 24 hr.

REFERENCES

Hoel, P. G., *Introduction to Mathematical Statistics*, John Wiley and Sons, Inc., New York, **1954**, 331 pp.

Miller, B. I., and Chase, P. P., "Prediction of Hurricane Motion by Statistical Methods," *Monthly Weather Review*, Vol. 94, No. 6, June **1966**, pp. 399–406.

Miller, B. I., Hill, E. C., and Chase, P. P., "A Revised Technique for Forecasting Hurricane Movement by Statistical Methods," *Monthly Weather Review*, Vol. 96, No. 8, Aug. **1968**, pp. 540–548.

Rapp, R. R., and Isnardi, A. H., "Variability of Upper Winds," *Progress Report* 138–03, U.S. Army Signal Corps Contract No. DA 36–039 sc–72, Research Division, College of Engineering, New York University, Mar. **1951**, 23 pp.

[*Received February 14, 1969; revised April 9, 1969*]

Reprinted from WMO Bulletin Vol. XVIII, No. 3, 146-154.

PROJECT STORMFURY

By R. Cecil Gentry

Project Stormfury is a co-operative venture of the Departments of Commerce and Defense of the United States, with the Environmental Science Services Administration (ESSA) and the Navy, respectively, as the principal participants. Its objective is to determine to what extent man can beneficially alter tropical cyclones (Gentry and Edelstein, 1968). * The project was formally organized in 1962 after the same groups had attempted modification of hurricane *Esther* in 1961 with encouraging if inconclusive results. They later conducted modification experiments on hurricane *Beulah* in 1963 with similar results. Since then, researchers have greatly expanded our knowledge of the structure and energy processes of hurricanes and of the convective processes in tropical clouds. Better instrumentation and techniques for counting freezing nuclei and measuring liquid and solid water content of clouds and other parameters have become available. Theoretical models of the synoptic scale features of tropical cyclones and of the microscale cumulus convective elements found in them have been greatly improved. As a result of these developments the emphasis and experimental design have gradually evolved for *Project Stormfury*. It seems pertinent, therefore, to summarize the programme and the current status of the project.

In this paper we will list the reasons for having such a project, explain its goals, describe approaches being considered, and outline the research programme proposed for the next two to five years.

Two general considerations justify *Project Stormfury*: (1) recent improvements in our understanding of the physical processes fundamental to the maintenance of hurricanes suggest promising avenues of experimentation; and (2) enormous rewards can be derived from even a slight degree of beneficial modification. The first will be elaborated in later sections; the second may be illustrated by the following rough *cost/benefit* analysis.

Tropical cyclones caused an average annual damage in the United States of 13 million dollars between 1915 and 1924. By the period 1959 to 1968, this figure had jumped to 295 million dollars. Even after considering the inflated cost of construction in more recent years, a 475 per cent increase in the average annual cost of hurricane damage has occurred in less than 50 years (Gentry, 1966). The current practice of constructing valuable buildings in vulnerable areas indicates that hurricane damage costs will continue to increase. Hurricane *Betsy* of 1965 alone caused more than 1.4 thousand million dollars in damage. If the United States continues to support hurricane modification research at the present rate for the next ten years and if by that time we modify just one severe hurricane, such as *Betsy*, sufficiently to reduce its damage by only 10 per cent, the nation will obtain more than 1,000 per cent return on its investment. Similarly, if within ten years we can reduce the damage caused by such a storm by only one per cent, the nation will have a 100 per cent return on its investment. The benefits in terms of prevention of human suffering throughout the world are, of course, incalculable.

NOTE: Dr. Gentry is director of *Project Stormfury* at the National Hurricane Research Laboratory, Miami, Florida, U.S.A.

* See references on p. 154.

At least two fundamentals established in recent years by studies of tropical cyclone structure and maintenance suggest possible avenues for beneficial modification: (1) an internal energy source is necessary if a hurricane is to reach or retain even moderate intensity — this source is the sensible and latent heat transferred from the sea surface to the air inside the storm; and (2) the energy for the entire synoptic-scale hurricane is released by moist convection in highly organized convective-scale circulations located primarily in the eye wall and major rain bands. In the first, we find an explanation of the observations that hurricanes form only over warm tropical waters and begin dissipating soon after moving over either cool water or land. Neither of these provides a flux of energy to the atmosphere sufficient to keep the storm at full intensity. In the second, we find a more rational explanation of the low percentage of tropical disturbances that become of hurricane intensity. If a warm sea with its large reservoir of energy were the only requirements, we would have five to ten times as many hurricanes as normally form. During the 1967 and 1968 hurricane seasons 130 tropical waves were tracked in the Atlantic and adjacent areas where sea surface temperatures were warm enough for hurricane genesis, but only 13 of the areas developed storms of full hurricane intensity (Simpson *et al.*, 1968 and 1969). If, however, there are only a limited number of ways in which the convective and synoptic scales can interact to achieve optimum utilization of the energy flowing upward from the ocean, then it is not surprising that few tropical disturbances intensify and become hurricanes.

Both of the above findings suggest possible field experiments which may beneficially modify a hurricane. On the basis of the first, we may attempt to reduce the flux of energy from the sea surface to the atmosphere, probably through attempts to inhibit evaporation. On the basis of the second, we may try to modify the release of latent heat in the small portion (one to five per cent) of the total storm occupied by the organized active convective-scale motions in a manner that redistributes heating to produce a weakening of the storm. The logistics and scientific feasibility of both types of field experiment will be discussed.

Can the scientific feasibility of such experiments be investigated by simulating them with the theoretical mathematical models developed within the last few years? Researchers in ESSA and at a number of universities have been developing numerical models to portray the life cycle of tropical cyclones (Ooyama, 1969; Rosenthal, 1968; Yamasaki, 1968; and Kuo, 1965). These models show that hurricanes are sensitive to the sea-surface temperature and the heat flux from the ocean to the air (Ooyama, 1969) as well as to the vertical distribution of the latent-heat release (Rosenthal and Koss, 1968; Yamasaki, 1968). Current models are capable, however, of simulating only an axially-symmetric cyclone with rather limited vertical resolution. They parameterize in a relatively simple fashion the effect of air-sea interaction and the transfer of energy by cumulus convection. They cannot predict the effects on storm motion of artificial intervention. More sophisticated models to eliminate many of these restrictions are being formulated.

Even though the developers do not consider that their current models simulate nature sufficiently to be used for evaluating proposed modification experiments, great progress has been made in this field in recent years. Two of the more advanced models have been used to run simple experiments, the results of which suggest modification attempts for the two approaches mentioned above, namely: (1) reducing the rate of heat transfer from the ocean to the atmosphere; or (2) altering physical processes in convective clouds to effect changes in the interaction between the convection and synoptic scales.

Modification of rate of heat transfer from ocean to atmosphere

The first dynamical-numerical model that simulated many of the features of a hurricane (Ooyama, 1969) indicated that the intensity of the hurricane varied directly with the rate of transfer of heat from the ocean to the air inside the hurricane. This indication is also given by earlier empirical budget calculations (Palmén and Riehl, 1957) and theoretical and experimental studies (Miller, 1964). They all suggest that hurricane intensity would be substantially reduced if the flux of sensible and/or latent heat from the ocean to the storm circulation could be significantly lowered. In particular, the intensity would be lessened if evaporation from the ocean could be inhibited.

Projects for reducing evaporation from a water surface have been conducted in many water-deficient regions of the world. Successful experimenters have used a monomolecular film that can be developed from fatty alcohol compounds. One of the better-documented experiments was at Lake Hefner, Oklahoma (Bean and Florey, 1968), where a 58 per cent reduction in evaporation was effected by the monolayer during a three-day test period. In all known experiments, however, the film has broken when the winds exceeded a critical level, for example, 25 knots or less. To be effective in modifying a hurricane, the film would need to be used where surface winds greatly exceed 30 knots; thus, development work may be needed to provide more durable films for the ocean surface and to study the effect the film may have on evaporation of droplets or spray.

Use of such monofilms to inhibit evaporation beneath a hurricane introduces large problems in logistics. To spread the film over an area the size of a typical moderately intense hurricane could require more than 50 cargo-type aircraft and chemicals worth about US $500,000. If, as is probable, the film blew away from the storm, additional chemicals should be spread for as long as the film was required. This is obviously too great an expense and effort to consider unless the film will be effective in reducing the intensity of the storm significantly. On the other hand, this would be a small price to pay for modifying an intense hurricane poised to devastate a densely populated coast. Results from theoretical models suggest that this approach offers great promise if evaporation from the ocean surface can be sufficiently decreased. We should therefore encourage investigations aimed at developing better means for diminishing the evaporation. In addition, we need to learn more about the properties of films that have already been used. We do not know, for example, to what extent the films retain their evaporation-inhibitory powers after being broken by high waves. We should conduct feasibility experiments to verify that they will work in salt water (they have been used primarily in fresh water), to determine at what rate their effectiveness decreases with increasing wind speed, and to confirm that they have no undesirable side effects. Much of this work can be done in a laboratory. In view of engineering technology, expense and forbidding logistics at this time, one cannot justify full-scale field experimentation that aims to reduce sea-air fluxes in a hurricane. Vigorous pursuit of these possibilities should be encouraged.

There is strong evidence that other factors act as regulators on the storm's intensity. The rate of heat transfer from the ocean to the atmosphere is a function of several items, including wind speed, air temperature, relative humidity and sea temperature. If the air temperature and humidity are relatively high, heat transfer will be slow, but then the air flowing into the storm already contains the sensible and latent heat necessary to fuel an intense hurricane. Once the winds are strong, the sea temperature is the critical parameter related to sea-air heat transfer processes that controls the storm intensity. Figure 1 relates the maximum intensity of several tropical cyclones to the temperatures of the sea beneath them and shows that both severe and weak tropical cyclones occur when ocean temperatures are relatively high. This suggests that variations in parameters other than the transfer of heat from the ocean to the atmosphere also influence the storm's intensity, which leads us to consider our second approach suggested for hurricane modification.

Modification of the physical processes in convective clouds

Observations clearly reveal that the physical processes essential for maintaining the hurricane as a coherent weather system occur in concentrated regions of intense cumulus convection in the eye wall and the principal rain bands. Even within the wall cloud, major convective elements are not uniformly distributed and may often be restricted to a single quadrant. They usually occupy less than five per cent of the total storm volume and in some cases, less than one per cent. They are located in the wall clouds and principal rain bands, which can be identified easily by radar.

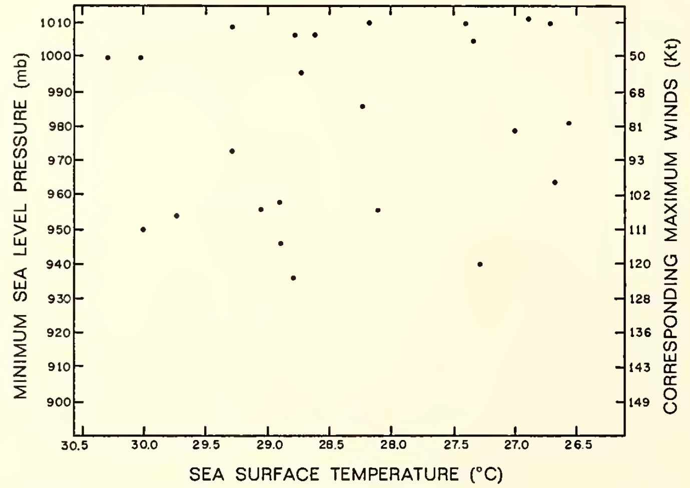

Figure 1. — Relation of minimum sea-level pressures in tropical cyclones to sea temperatures (each dot represents relation for an individual storm selected from 1955-67 seasons)

Convective-scale processes essential to the energy balance of the hurricane scale are the releases of latent energy associated with phase changes of water substance (from water vapour to droplets and to ice crystals). Such processes have been modified in individual tropical cumulus clouds by artificial nucleation (Simpson *et al.*, 1967). We need to learn more about the mechanisms by which energy releases on this small cumulus scale are systematically organized to maintain the larger-scale hurricane.

Full-scale experiments to modify natural convective processes in hurricanes by cloud seeding with artificial freezing nuclei are indeed logistically feasible. A limited number have already been performed by the *Stormfury* group in 1961 and 1963 (Simpson and Malkus, 1964), and recent developments in pyrotechnics make it even more feasible to carry out massive seeding of hurricane clouds. Furthermore, reasonable qualitative arguments indicate that modification of the convective-scale processes might result in some changes of the temperature field — and possibly of the macrostructure of the hurricane.

Since numerical models of hurricanes are now reproducing many features of the life cycle of tropical cyclones with considerable reliability, we might ask what is said about the chance of modifying a hurricane by altering the convective processes. The developers of these models do not believe they sufficiently simulate nature to give definite answers to such questions. We are, however, using the seven-level primitive equation model developed by Dr. S. Rosenthal (1969) at the National Hurricane Research Laboratory to get information for improving the design of the field experiments. In experimental seeding of the wall cloud of hurricanes in 1961 and 1963 in the *Project Stormfury* group, freezing nuclei were introduced along a line perpendicular to the eye wall from just inside the radius of maximum winds outward for several miles. Later research suggested that better results might be obtained by seeding outside the radius of maximum winds. Rosenthal's model was used to simulate the seeding experiment on two different circular bands by increasing the heating function at 500 mb and 300 mb by 2°C per 30 minutes for 30 minutes. When the maximum winds were 35 km from the centre, two bands, 30–50 km and 50–70 km, were selected for simulated seeding in experiments run on the computer with the model hurricane. One band spanned the radius of maximum winds, the other was outside that radius. The results of the two simulations are compared in Figure 2. The inference is that the greatest reduction in maximum intensity can be accomplished by seeding outside the radius of maximum winds.

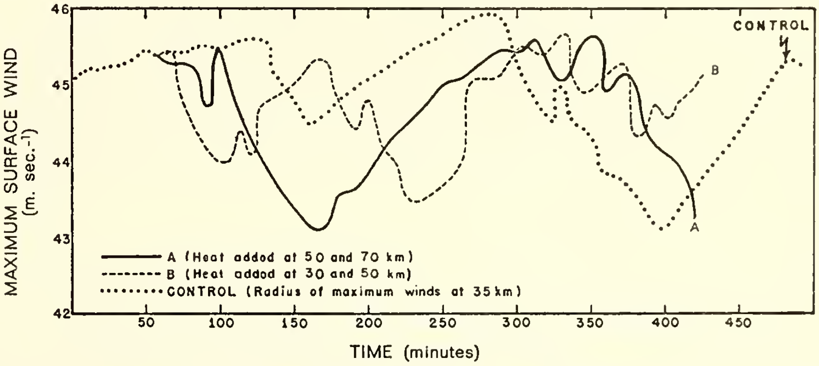

Figure 2. — Maximum surface wind versus time — one simulated seeding at $t_0 + 60$ minutes (plotted from data at 10-minute intervals; $t_0 = 177.9$ hours). The dotted line represents results from the unmodified model (Rosenthal, 1969); the dashed line gives results of the simulated seeding across the radius of maximum winds; and the solid line gives results of the simulated seeding outside the radius of maximum winds. (Dashed and solid lines based on unpublished work of Stanley L. Rosenthal)

The results from these experiments (Figure 2) can be interpreted to mean either that the seeding would cause a temporary reduction in intensity of the storm or that the seeding would cause a change in phase of the quasi-periodic variation of the maximum winds generated by the model. To the extent that the results indicate a change in the storm's intensity, they indicate that it would decrease. The potential benefit of hurricane modification to cost ratio is so great that even the small decrease in intensity suggested by the experimental results in Figure 2 would be worth while. These results can hardly be considered as the final answer. Since neither this model nor those of any of the other investigators are sufficiently advanced to simulate these cloud-seeding experiments adequately, a field programme is the only method currently available for determining whether modification of the convective processes will result in a quantitatively significant and beneficial change in the hurricane. Recent theoretical work in hurricane modelling has shown sufficient promise to warrant the hope of skilful computer simulation of these field experiments within the next few years. Now the best procedure is to use models for improving the design of field experiments and to use the results from the latter as a feed-back to support further improvement in the models.

Some individual tropical cumulus experiments have already been made, such as modification of cumulus clouds during periods of typical tropical conditions, by J. Simpson and her collaborators, who have also developed a numerical model that predicts how high individual cumulus clouds will grow under natural and seeded conditions (Simpson *et al.*, 1967). Using mean hurricane soundings (Sheets, 1969), we have made computations with the Simpson cumulus model to determine the seedability of hurricane clouds. With reasonable assumptions about cloud bases and diameters, the computations showed that hurricane clouds should grow after seeding just as many of the individual seeded tropical cumulus. The amount of growth in the hurricane clouds that could be attributed to seeding varied directly with the radius, that is, the closer to the centre of the hurricane, the less additional growth should be expected from the seeding.

Proposed programme for Stormfury

Earlier hurricane modification experiments (Simpson and Malkus, 1964) and the more recent research suggest that hurricanes may be modified by seeding the clouds with freezing nuclei. Some recent research suggests that more favourable results may be obtained by modifications of original experimental designs. Some people have proposed seeding in a different area of the storm, seeding the storm at a different stage of development, or seeding rain bands in areas where growth of the clouds might serve to divert some of the energy from the main centre.

The first urgent task of *Stormfury* and one of its goals is gathering of data from additional tropical cyclones about the structure of cumulus convection to determine how often, to what extent, and under what conditions a valid physical basis exists in tropical cyclones for cloud modification by introduction of freezing nuclei. This task requires more measurements of liquid-water content, cloud drop-size distributions, precipitation characteristics, composition (ice and liquid phases), temperature, and vertical motion in the eye wall, in the rain bands, and in the non-precipitating cloud bands associated with both young and mature disturbances.

In 1968, we recorded the first data collected in a hurricane at a level above the 0°C isotherm of the drop-size distribution and the phase of H_2O. In three passes along a rain band in hurricane *Gladys* at temperatures of —5°C to —8°C, the Formvar Replicator data showed that only water drops were present in most of the clouds. This is excellent support for the hurricane seeding modification hypotheses, but measurements are needed from more tropical cyclones. We have some measurements of liquid-water content but, again, data from more storms are needed to determine frequency and under what conditions sufficient raw material (supercooled water) is available for seeding. ESSA research aircraft are now equipped to measure many of the desired cloud physics parameters and efforts are continuing to improve instrumentation. In addition, we are seeking a cloud physicist to work in the project to assist in the collection and interpretation of these data.

Second, *Stormfury* must determine the physical effects of various kinds of seeding treatment on the clouds associated with tropical weather systems. This includes the complete spectrum of cloud systems; groupings of individual cumulus clouds; cloud bands; cloud structures associated with *disturbances,* such as easterly waves; inner and outer rain bands; and the eye-wall clouds.

To achieve these first two listed goals, *Stormfury* should use every opportunity to seed and observe convective cloud systems over tropical oceans. Disturbances in all stages of development are suitable targets for seeding provided that proper measurements of the cloud structure are made before and after seeding. Aircraft available to the project are equipped to make such measurements, and every effort is being made to improve instrumentation, observing techniques, and training of personnel to obtain more accurate and dependable measurements. Observations of the variations in non-seeded clouds near seeded ones are also of great interest.

Third, *Stormfury* must press on with general hurricane research. Efforts to develop improved theoretical models should be accelerated. Efforts to learn more about the structure and energy exchange processes in hurricanes should be continued by means of well-designed observational and analytical programmes. Conditions or locations in the storm, if any, where a modified hurricane rain band might cause a hurricane to weaken or to change course must be known.

A difficulty in interpreting results of a hurricane modification experiment is the lack of suitable controls. This problem is accentuated by the large natural variability of hurricanes and the few opportunities we have for experimenting with mature hurricanes. If the changes wrought in a hurricane by a seeding experiment were of the magnitude indicated in Figure 2, the project aircraft could measure those changes, but there would still be the question whether they were due to the action of the artificial freezing nuclei.

In research flights of recent years, we have developed measuring techniques and ways of grouping the data that help to filter the natural variations associated with the microscale features of the hurricane, making it easier to identify trends in hurricane intensity in a shorter time. The project aircraft are now equipped to measure changes in the structure and size of the clouds; to record changes in temperature, pressure and winds in and near the seeded clouds; and to record the changes in phase of the water substance and the amounts of liquid and total water content. Efforts to improve these latter measurements and to add recordings of the vertical wind components continue. By designing flight patterns to obtain measurements both before and after the seeding, it should be possible to determine whether changes in parameters occur in the right sequence and at approximately the right time intervals to have been caused by the seeding. In addition, measurements can be made of changes in the hurricane on synoptic and convective scales to determine whether these changes are in accordance with indications from the various theoretical models.

The field programme planned for the 1969 and successive hurricane seasons is based not only on the foregoing considerations but also on available resources. The plans call for: (1) seeding of the clouds around a hurricane eye wall five times during a period of eight hours; (2) seeding of hurricane rain bands; (3) seeding of cloud lines in the tropics not associated with hurricanes or tropical storms; (4) intensification of efforts to collect data discussed in earlier paragraphs; (5) feasibility of laboratory experiments on the use of monofilms to reduce evaporation from the sea surface; and (6) increased research on models to simulate hurricanes and to predict their behaviour.

Seeding of clouds in hurricanes will be restricted to those storms predicted to remain at sea at least for 24 hours after the seeding. This will simplify collecting data to evaluate the results and give time for any storm selected for experiment to return to its natural state before it strikes a populated land area.

It is hoped there will be opportunities to repeat each of the three seeding experiments more than once. The objectives of the first experiment are to determine whether: (1) cumuli in the major convective regions of hurricanes will react to seeding in as predictable a manner as individual cumuli; (2) the reaction of the macrostructure will be significant and along the lines suggested by qualitative reasoning and by simple experiments performed on the computer with the numerical models; (3) responses to single seedings are periodic and in phase with repetitive seedings; and (4) responses to repetitive seeding are accumulative. To obtain help in the evaluation of the experimental results, sufficient measurements will be made of conditions in the seeded clouds to determine if changes in phase of water substance, temperature, pressure and wind occur in the proper sequence to have been caused by the seeding.

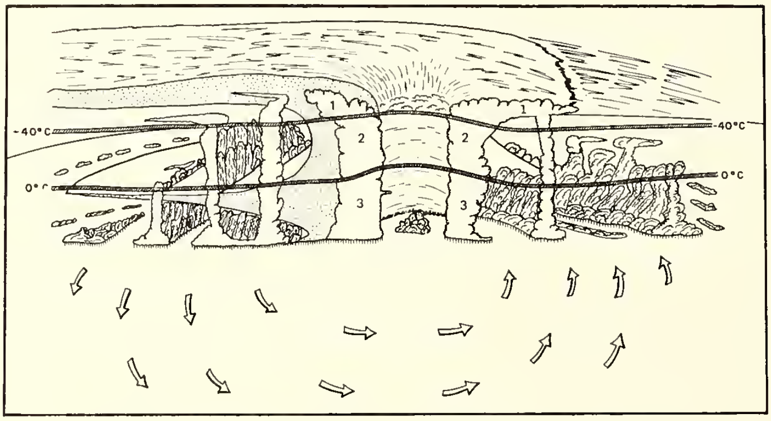

Figure 3. — A schematic cross-section of a hurricane showing the location of the eye-wall clouds and the rain bands. The pyrotechnics producing the freezing nuclei are dropped into the clouds at levels with temperatures between −15°C and −30°C. They fall as the material burns and continue to distribute the nuclei down to the 0°C to −4°C layer (1 = ice; 2 = ice + water; 3 = water)

The objectives of the second and third experiments are to determine: (1) under what conditions the life cycle of cumulus convection cloud systems can be altered by man; (2) whether the reaction to seeding of larger systems of cumuli is similar to that found in individual cumuli; (3) to what extent models of individual clouds can be used for predicting the reaction of a cloud system to seeding; and (4) what effect changes in modified clouds have on nearby clouds in the same line or band, and on clouds in adjacent lines or bands. When possible, controls (clouds, cloud lines or rain bands) will be observed simultaneously with the seeded clouds and statistical techniques will be used in evaluating results when appropriate and feasible.

It should be emphasized, however, that *Project Stormfury* is not a controlled experiment entirely amenable to statistical evaluation. The low frequency of occurrence of hurricanes as experimental targets precludes the accumulation of a large body of test data in a short time and application of statistical methods for testing of the complete hypothesis. The project is still exploratory, and is aimed at a better physical understanding of the dynamics of hurricanes, in addition to eventual modification of a storm. The theoretically possible potential benefits are so great compared to the experimental costs that the artificial modification of tropical cyclones is a justifiable scientific pursuit and could be of great importance for mankind.

Acknowledgments

This report has been reviewed and approved by the Advisory Committee to *Projet Stormfury:* Dr. Noel E. LaSeur (chairman), Dr. Edward N. Lorenz, Dr. James E. McDonald, Dr. Daniel F. Rex, and Dr. Jerome Spar. The members of the committee have also made many suggestions as to its format and context. In addition, the following contributed significantly to preparation of this report: Dr. Stanley L. Rosenthal, Harry F. Hawkins, William D. Mallinger, and Max Edelstein. Jack Tracy collected the data for Figure 1.

REFERENCES

BEAN, B. R. and FLOREY, Q. L. (1968): *A field study of the effectiveness of fatty alcohol mixtures as evaporation reducing monomolecular films.* Water Resources Research, **4**, 206–208.

GENTRY, R. Cecil (1966): *Nature and scope of hurricane damage.* Hurricane Symposium, 10–11 October 1966, American Society for Oceanography, Houston, Texas, 229–254.

GENTRY, R. C. and EDELSTEIN, M. W. (1968): *Project Stormfury, a hurricane modification experiment.* Proceedings of the First National Conference on Weather Modification, Am. Meteor. Soc., 296–305.

KUO, H. L. (1965): *On the formation and intensification of tropical cyclones through latent heat release by cumulus convection.* J. Atmos. Sci., **22**, 40–63.

MILLER, B. I. (1964): *A study of the filling of Hurricane Donna (1960) over land.* Mon. Wea. Rev., **92**, 389–406.

OOYAMA, K. (1969): *Numerical simulation of the life cycle of tropical cyclones.* J. Atmos. Sci., **26**, 3–40.

PALMÉN, E. and RIEHL, Herbert (1957): *Budget of angular momentum and energy in tropical cyclones.* J. of Meteor., **14**, 150–159.

ROSENTHAL, Stanley L. (1968): *Preliminary results from numerical experiments with a primitive equation model designed to simulate the development of tropical cyclones.* Proccedings of WMO/IUGG Conference on Numerical Weather Prediction, 26 November to 4 December 1968. To be published by Japan Meteorological Agency, Tokyo.

ROSENTHAL, Stanley L. (1969): *Numerical experiments with a multilevel primitive equation model designed to simulate the development of tropical cyclones, Experiment 1.* ESSA Technical Memorandum ERLTM-NHRL-82, Environmental Science Services Administration, 36 pp.

ROSENTHAL, S. L. and KOSS, W. J. (1968): *Linear analysis of a tropical cyclone model with increased vertical resolution.* To be published in Mon. Wea. Rev.

SHEETS, R. C. (1969): *Some mean hurricane soundings.* J. Appl. Meteor., **8**, 134–146.

SIMPSON, J., BRIER, G. W. and SIMPSON, R. H. (1967): *Stormfury cumulus seeding experiment 1965 : Statistical analysis and main results.* J. Atmos. Sci., **24**, 508–521.

SIMPSON, R. H. and MALKUS, J. S. (1964): *Experiments in hurricane modification.* Sci. Am., **211**, 27–37.

SIMPSON, R. H., FRANK, Neil, SHIDLER, David and JOHNSON, H. M. (1968): *Atlantic tropical disturbances, 1967.* Mon. Wea. Rev., **96**, 251–259.

SIMPSON, R. H., FRANK, Neil, SHIDLER, David and JOHNSON, H. M. (1969): *Atlantic tropical disturbances, 1968.* Mon. Wea. Rev., **97**, 240–255.

YAMASAKI, M. (1968): *A tropical cyclone model with parameterized vertical partition of released latent heat.* J. Meteor. Soc. Japan, **46**, 202–214.

Reprinted from Bulletin of American Meteorological Society Vol. 50, No. 6, 404-409.

[Reprinted from BULLETIN OF THE AMERICAN METEOROLOGICAL SOCIETY, Vol. 50, No. 6, June, 1969, pp. 404–409]
Printed in U. S. A.

Project STORMFURY

R. Cecil Gentry
Director, Project STORMFURY
National Hurricane Research Lab.
Miami, Fla.

Abstract

Project STORMFURY is a project of Commerce and Defense for experimenting at modification of hurricanes. Justification for the work is based on recent discoveries about hurricanes and the high potential benefit to cost ratio of the experiments. Evidence is presented that two approaches for modification should be considered: 1) seeding of clouds, and 2) inhibiting evaporation from the ocean. The scientific aspects and logistic problems of both approaches are reviewed. The Program and goals of Project STORMFURY are discussed.

1. Introduction

Project STORMFURY is a cooperative venture of the Department of Commerce, ESSA, and the Department of Defense, U. S. Navy. Its objective is to determine to what extent man can beneficially alter tropical cyclones including, of course, hurricanes (Gentry and Edelstein, 1968). The Project was formally organized in 1962 after the same groups had attempted modification of hurricane Esther in 1961 with encouraging if inconclusive results. They later conducted modification experiments on hurricane Beulah in 1963 with similar results. Since then, researchers have greatly expanded our knowledge of the structure and energy processes of hurricanes and of the convective processes in tropical clouds. Better instrumentation and techniques for counting freezing nuclei and measuring liquid and solid water content of clouds and other parameters have become available. Theoretical models of the synoptic scale features of a hurricane and of the microscale cumulus convective elements found in hurricanes have been greatly improved. As a result of these developments the emphasis and experimental design have gradually evolved for Project STORMFURY. It seems pertinent, therefore, to summarize the program and the current status of the Project.

In this paper we will list the reasons for having such a project, explain its goals, describe approaches being considered, and outline the research program proposed for the next 2 to 5 years.

Two general considerations justify Project STORMFURY: 1) recent improvements in our understanding of the physical processes fundamental to the maintenance of hurricanes suggest promising avenues of experimentation, and 2) enormous rewards can be derived from even a slight degree of beneficial modification. The first will be elaborated in later sections; the second may be illustrated by the following rough "cost-benefit" analysis.

Hurricanes caused an average annual damage in the United States of 13 million dollars between 1915 and 1924. By the period 1959 to 1968, this figure had jumped to 295 million dollars. Even after considering the inflated cost of construction in more recent years, a 475% increase in the average annual cost of hurricane damage has occurred in less than 50 years (Gentry, 1966). The current practice of constructing valuable buildings in vulnerable areas indicates that hurricane damage costs will continue to increase. Hurricane Betsy of 1965 alone caused more than 1.4 billion dollars in damage. If the United States continues supporting hurricane modification research at the present rate for the next 10 years and if by that time we modify just one severe hurricane, such as Betsy, sufficiently to reduce its damage by only 10%, the nation will obtain more than 1000% return on its investment. Similarly, if within 10 years we can reduce the damage caused by such a storm by only 1%, the nation will have a 100% return on its investment. The benefits in terms of prevention of human suffering are, of course, incalculable.

At least two fundamentals established in recent years by studies of hurricane structure and maintenance suggest possible avenues for beneficial modification; 1) an internal energy source is necessary if a hurricane is to reach or retain even moderate intensity; this source is the sensible and latent heat transferred from the sea surface to the air inside the storm, and 2) the energy for the entire synoptic-scale hurricane is released by moist convection in highly organized convective scale circulations located primarily in the eyewall and major rain bands. In the first, we find an explanation of the observations that hurricanes form only over warm tropical waters and begin dissipating soon after moving over either cool water or land. Neither of these provides a flux of energy to the atmosphere sufficient to keep the storm at full intensity. In the second, we find a more rational explanation of the low percentage of tropical disturbances that become hurricanes. If a warm sea with its large reservoir of energy were the only requirements, we would have 5 to 10 times as many hurricanes as normally form. During the 1967 and 1968 hurricane seasons 130 tropical waves were tracked in the Atlantic and adjacent areas where sea surface temperatures were warm enough for hurricane genesis, but only 13 of the areas developed storms of full hurricane intensity (Simpson *et al.,* 1968 and 1969). If, however, there are only a limited number of ways in which the convective and synoptic scales can interact to achieve optimum utilization of the energy flowing upward from the ocean, then it is not surprising that few tropical disturbances intensify and become hurricanes.

Both of the above findings suggest possible field experiments which may beneficially modify a hurricane. On the basis of the first, we may attempt to reduce the flux of energy from the sea surface to the atmosphere, probably through attempts to inhibit evaporation. On the basis of the second, we may try to modify the release of latent heat in the small portion (1 to 5%) of the total storm occupied by the organized active convective-scale motions in a manner that redistributes heating to produce a weakening of the storm. The logistics and scientific feasibility of both types of field experiments will be discussed.

Can the scientific feasibility of such experiments be investigated by simulating them with the theoretical mathematical models developed within the last few years? Researchers in ESSA and at a number of universities have been developing numerical models to portray the life cycle of tropical cyclones (Ooyama, 1969; Rosenthal, 1969; Yamasaki, 1968; and Kuo, 1965). These models show that hurricanes are sensitive to the sea surface temperature and the heat flux from the ocean to the air (Ooyama, 1969) as well as to the vertical distribution of the latent-heat release (Rosenthal and Koss, 1968; Yamasaki, 1968). Current models are capable, however, of simulating only an axially-symmetric cyclone with rather limited vertical resolution. They parameterize in a relatively simple fashion the effect of air-sea interaction and the transfer of energy by cumulus convection. They cannot predict the effects of storm motion of artificial intervention. More sophisticated models to eliminate many of these restrictions are being formulated.

Even though the developers do not consider that their current models simulate nature sufficiently to be used for evåluating proposed modification experiments, great progress has been made in this field in recent years. Two of the more advanced models have been used to run simple experiments whose results suggest modification attempts for the two approaches mentioned above, that is: 1) reducing the rate of heat transfer from the ocean to the atmosphere, or 2) altering physical processes in convective clouds to effect changes in the interaction between the convection and synoptic scales.

2. Modification of rate of heat transfer from ocean to the atmosphere

The first dynamical-numerical model that simulated many of the features of a hurricane (Ooyama, 1969) indicated that the intensity of the hurricane varied directly with the rate of transfer of heat from the ocean to the air inside the hurricane. This indication is also given by earlier empirical budget calculations (Palmén and Riehl, 1957) and theoretical and experimental studies (Miller, 1964). They all suggest that hurricane intensity would be substantially reduced if the flux of sensible and/or latent heat from the ocean to the storm circulation could be significantly lowered. In particular, the intensity would be lessened if evaporation from the ocean could be inhibited.

Projects for reducing evaporation from a water surface have been conducted in many water deficient regions of the world. Successful experimenters have used a monomolecular film that can be developed from fatty alcohol compounds. One of the better documented experiments was at Lake Hefner, Oklahoma (Bean and Florey, 1968), where a 58% reduction in evaporation was effected by the monolayer during a 3-day test period. In all known experiments, however, the film has broken when the winds exceeded a critical level, e.g., 25 knots or less. To be effective in modifying a hurricane, the film would need to be used where surface winds greatly exceed 30 knots; thus, development work may be needed to provide more durable films for the ocean surface and to study the effect the film may have on evaporation of droplets or spray.

Use of such monofilms to inhibit evaporation beneath a hurricane introduces large problems in logistics. To spread the film over an area the size of a typical moderately intense hurricane could require more than 50 cargo-type aircraft and chemicals worth about $500,000.00. If, as is probable, the film blew away from the storm, additional chemicals should be spread for as long as the film was required. This is obviously too great an expense and effort to consider unless the film will be effective in reducing the intensity of the storm significantly. On the other hand, this would be a small price to pay for modifying an intense hurricane poised to devastate a densely populated coast. Results from theoretical models suggest that this approach offers great promise if evaporation from the ocean surface can be sufficiently decreased. We should, therefore, encourage investigations aimed at developing better means for diminishing the evaporation. In addition, we need to learn more about the properties of films that have already been used. We do not know, for example, to what extent the films retain their evaporation inhibitory powers after being broken by high waves. We should conduct feasibility experiments to verify that they will work in salt water (they have been used primarily in fresh water), to determine what rate their effectiveness decreases with increasing wind speed, and to confirm that they have no undesirable side effects. Much of this work can be done in a laboratory. In view of engineering technology, expense and forbidding logistics at this time one cannot justify full scale field experimentation that aims to reduce sea-air fluxes in a hurricane. Vigorous pursuit of these possibilities should be encouraged.

There is strong evidence that other factors act as regulators on the storm's intensity. The rate of heat transfer from the ocean to the atmosphere is a function of several items, including wind speed, air temperature, relative humidity and sea temperature. If the air temperature and humidity are relatively high, heat transfer will be slow, but then the air flowing into the storm already contains the sensible and latent heat necessary to fuel an intense hurricane. Once the winds are strong, the sea temperature is the critical parameter related to sea-air heat transfer processes that controls the storm intensity. Fig. 1 relates the maximum intensity of several tropical cyclones to the temperatures of the sea beneath them and shows that both severe and weak tropical cyclones occur when ocean temperatures are relatively high. This suggests that variations in parameters other than the transfer of heat from the ocean to the atmosphere also influence the storm's intensity which leads us to consider our second approach suggested for hurricane modification.

3. Modification of the physical processes in convective clouds

Observations clearly reveal that the physical processes essential for maintaining the hurricane as a coherent weather system occur in concentrated regions of intense cumulus convection in the eyewall and the principal rainbands. Even within the wall cloud, major convective elements are not uniformly distributed and may often be restricted to a single quadrant. They usually occupy less than 5% of the total storm volume and, in some cases, less than 1%. They are located in the wall clouds and principal rainbands, which can be identified easily by radar.

Convective scale processes essential to the energy balance of the hurricane scale are the releases of latent energy associated with phase changes of water substance (i.e., from water vapor to droplets and to ice crystals). Such processes have been modified in individual tropical cumulus clouds by artificial nucleation (Simpson *et al.*, 1967). We need to learn more about the mechanisms by which energy releases on this small cumulus scale are systematically organized to maintain the larger scale hurricane.

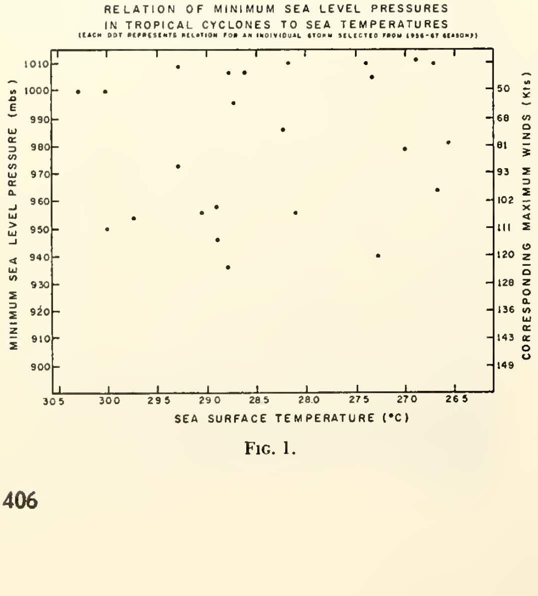

Fig. 1.

Full scale experiments to modify natural convective processes in hurricanes by cloud seeding with artificial freezing nuclei are indeed logistically feasible. A limited number have already been performed by the STORMFURY group in 1961 and 1963 (Simpson and Malkus, 1964), and recent developments in pyrotechnics makes it even more feasible to do massive seeding of hurricane clouds. Furthermore, reasonable qualitative arguments indicate that modification of the convective scale processes might result in some changes of the temperature field—and possibly of the macrostructure of the hurricane.

Since numerical models of hurricanes are now reproducing many features of the life cycle of tropical cyclones with considerable reliability, we might ask what they say about the chance of modifying a hurricane by altering the convective processes. The developers of these models do not believe they sufficiently simulate nature to give definitive answers to such questions. We are, however, using the 7-level primitive equation model developed by Rosenthal (1969) at the National Hurricane Research Laboratory to get information for improving the design of the field experiments. In experimental seeding of the wall clouds of hurricanes in 1961 and 1963 in the Project STORMFURY group, freezing nuclei were introduced along a line perpendicular to the eye wall from just inside the radius of maximum winds outward for several miles. Later research suggested that better results might be obtained by seeding outside of the radius of maximum winds. Rosenthal's model was used to simulate the seeding experiment on two different circular bands by increasing the heating function at 500 mb and 300 mb by 2C per 30 minutes for 30 minutes. When the maximum winds were 35 km from the center, two bands, 30–50 km and 50–70 km were selected for simulated seeding in experiments run on the computer with

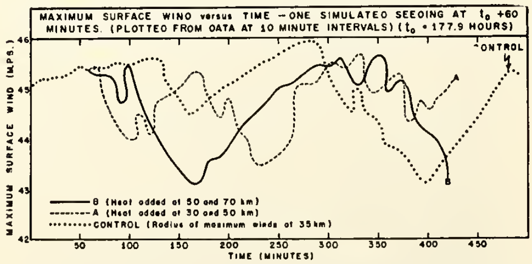

Fig. 2. The dotted line represents results from the unmodified model (Rosenthal, 1969); the dashed line gives results of the simulated seeding across the radius of maximum winds; and the solid line gives results of the simulated seeding outside the radius of maximum winds. (Dashed and solid lines based on unpublished work of Stanley L. Rosenthal.)

the model hurricane. One band spanned the radius of maximum winds, the other was outside that radius. The results of the two simulations are compared in Fig. 2. The inference is that the greatest reduction in maximum intensity can be accomplished by seeding outside the radius of maximum winds.

The results from these experiments (Fig. 2) can be interpreted to mean either that the seeding would cause a temporary reduction in intensity of the storm or that the seeding would cause a change in phase of the quasi-periodic variation of the maximum winds generated by the model. To the extent that the results indicate a change in the storm's intensity, they indicate that it would decrease. The potential benefit of hurricane modification to cost ratio is so great that even the small decrease in intensity suggested by the experimental results in Fig. 2 would be worthwhile. These results can hardly be considered as the final answer. Since neither this model nor those of any of the other investigators are sufficiently advanced to adequately simulate these cloud seeding experiments, a field program is the only method currently available for determining whether modification of the convective processes will result in a quantitatively significant and beneficial change in the hurricane. Recent theoretical work in hurricane modeling has shown sufficient promise to warrant the hope of skillful computer simulation of these field experiments within the next few years. Now the best procedure is to use models for improving the design of field experiments and to use the results from the latter as a feed-back to support further improvement in the models.

Some individual tropical cumulus experiments have already been made, such as modification of cumulus clouds during periods of typical tropical conditions, by J. Simpson and her collaborators, who have also developed a numerical model that predicts how high individual cumulus clouds will grow under natural and seeded conditions (Simpson *et al.,* 1967). Using mean hurricane soundings (Sheets, 1969), we have made computations with the Simpson cumulus model to determine the seedability of hurricane clouds. With reasonable assumptions about cloud bases and diameters, the computations showed that hurricane clouds should grow after seeding just as many of the individual seeded tropical cumulus. The amount of growth in the hurricane clouds that could be attributed to seeding varied directly with the radius, that is, the closer to the center of the hurricane, the less additional growth that should be expected from the seeding.

4. Proposed program for STORMFURY

Earlier hurricane modification experiments (Simpson and Malkus, 1964), and the more recent research suggest that hurricanes may be modified by seeding the clouds with freezing nuclei. Some recent research suggests that more favorable results may be obtained by modifications of original experimental designs. Some people have proposed seeding in a different area of the storm, seeding the storm at a different stage of development, or seeding rainbands in areas where growth of the clouds might serve to divert some of the energy from the main center.

The first urgent task of STORMFURY and one of its goals is gathering of data from additional tropical cyclones about the structure of cumulus convection to determine how often, to what extent, and under what conditions a valid physical basis exists in tropical cyclones for cloud modification by introduction of freezing nuclei. This task requires more measurements of liquid-water content, cloud drop size distributions, precipitation characteristics, composition (ice and liquid phases), temperature, and vertical motion in the eye wall, in the rainbands, and in the nonprecipitating cloud bands associated with both young and mature disturbances.

In 1968, we recorded the first data collected in a hurricane at a level above 0C isotherm of the drop size distribution and the phase of H_2O. In three passes along a rainband in hurricane Gladys at temperatures of −5C to −8C, the Formvar Replicator data showed that only water drops were present in most of the clouds. This is excellent support for the hurricane seeding modification hypotheses, but measurements are needed from more tropical cyclones. We have some measurements of liquid-water content, but, again, data from more storms are needed to determine frequency and under what conditions that sufficient raw material (supercooled water) is available for seeding. ESSA research aircraft are now equipped to measure many of the desired cloud physics parameters and efforts are continuing to improve instrumentation. In addition we are seeking a cloud physicist to work in the Project to assist in the collection and interpretation of these data.

Second, STORMFURY must determine the physical effects of various kinds of seeding treatments on the clouds associated with tropical weather systems. This includes the complete spectrum of cloud systems; groupings of individual cumulus clouds; cloud bands; cloud structures associated with "disturbances," such as easterly waves; inner and outer rainbands; and the eye wall clouds.

To achieve these first two listed goals, STORMFURY should use every opportunity to seed and observe convective cloud systems over tropical oceans. Disturbances in all stages of development are suitable targets for seeding provided that proper measurements of the cloud structure are made before and after seeding. Aircraft available to the STORMFURY Project are equipped to make such measurements, and every effort is being made to improve instrumentation, observing techniques, and training of personnel to obtain measurements more accurately and dependable. Observations of the variations in nonseeded clouds near those seeded are also of great interest.

Third, STORMFURY must press on with general hurricane research. Efforts to develop improved theoretical models should be accelerated. Efforts to learn more about the structure and energy exchange processes in hurricanes should be continued by means of well designed observational and analytical programs. Conditions or locations in the storm, if any, where a modified hurricane rainband might cause a hurricane to weaken or to change course must be known.

A difficulty in interpreting results of a hurricane modification experiment is the lack of suitable controls. This problem is accentuated by the large natural variability of hurricanes and the few opportunities we have for experimenting with mature hurricanes. If the changes wrought in a hurricane by a seeding experiment were of the magnitude indicated in Fig. 2, the Project aircraft could measure those changes, but there would still be the question whether they were due to the action of the artificial freezing nuclei?

In research flights of recent years, we have developed measuring techniques and ways of grouping the data that help to filter the natural variations associated with the microscale features of the hurricane, making it easier to identify trends in hurricane intensity in a shorter time. The Project aircraft are now equipped to measure changes in the structure and size of the clouds; to record changes in temperature, pressure and winds in and near the seeded clouds; and to record the changes in phase of the water substance and the amounts of liquid and total water content. Efforts to improve these latter measurements and to add recordings of the vertical wind components continue. By designing flight patterns to obtain measurements both before and after the seeding, it should be possible to determine if changes in parameters occur in the right sequence and at approximately the right time intervals to have been caused by the seeding. In addition, measurements can be made of changes in the hurricane on synoptic and convective scales to determine if these changes are in accordance with indications from the various theoretical models.

The field program planned for the 1969 and successive hurricane seasons is based not only on the foregoing considerations but also on available resources. The plans call for: 1) seeding of the clouds around a hurricane eye wall five times during a period of 8 hours, 2) seeding of hurricane rainbands, 3) seeding of cloud lines in the tropics not associated with hurricanes or tropical storms, 4) intensification of efforts to collect data discussed in earlier paragraphs, 5) feasibility or laboratory experiments on the use of monofilms to reduce evaporation from the sea surface, and 6) increased research on models to simulate hurricanes and to predict their behavior.

It is hoped there will be opportunities to repeat each of the three seeding experiments more than once. The objectives of the first experiment are to determine whether: 1) cumuli in the major convective regions of hurricanes will react to seeding in as predictable a manner as individual cumuli, 2) the reaction of the macrostructure will be significant and along the lines suggested by qualitative reasoning and by simple experiments performed on the computer with the numerical models, 3) responses to single seedings are periodic and in phase with repetitive seedings, and 4) responses to repetitive seeding are accumulative. To get help in the evaluation of the experimental results, sufficient measurements will be made of conditions in the seeded clouds to determine if changes in phase of water substance, temperature, pressure and wind occur in the proper sequence to have been caused by the seeding.

The objectives of the second and third experiments are to determine: 1) under what conditions the life cycle of cumulus convection cloud systems can be altered by man, 2) whether the reaction to seeding of larger systems of cumuli is similar to that found in individual cumuli, 3) to what extent models of individual clouds can be used for predicting the reaction of a cloud system to seeding, and 4) what effect changes in modified clouds have on nearby clouds in the same line or band, and on clouds in adjacent lines or bands. When possible, controls (clouds, cloud lines or rainbands) will be observed simultaneously with the seeded clouds and statistical techniques will be used in evaluating results when appropriate and feasible.

It should be emphasized, however, that Project STORMFURY is not a controlled experiment entirely amenable to statistical evaluation. The low frequency of occurrence of hurricanes as experimental targets precludes the accumulation of a large body of test data in a short time and application of statistical methods for testing of the complete hypothesis. The Project is still exploratory, and is aimed at a better physical understanding of the dynamics of hurricanes, in addition to eventual modification of a storm. The theoretically possible potential benefits are so great compared to the experimental costs that the artificial modification of tropical cyclones is a justifiable scientific pursuit and could be of great importance for mankind.

Acknowledgments. This report has been reviewed and approved by the Advisory Committee to Project STORMFURY: Dr. Noel E. LaSeur (Chairman), Dr. Edward N. Lorenz, Dr. James E. McDonald, Dr. Daniel F. Rex, and Dr. Jerome Spar. The members of the Committee have also made many suggestions as to its format and context. In addition, the following contributed significantly to preparation of this report: Dr. Stanley L. Rosenthal, Harry F. Hawkins, William D. Mallinger, and Max Edelstein. Jack Tracy collected the data for Fig. 1.

References

Bean, B. R., and Q. L. Florey, 1968: A field study of the effectiveness of fatty alcohol mixtures as evaporation reducing monomolecular films. *Water Resources Research*, **4**, 206–208.

Gentry, R. Cecil, 1966: Nature and scope of hurricane damage. Hurricane Symposium. October 10–11, American Society for Oceanography, Houston, Tex., 229–254.

——, and M. W. Edelstein, 1968: Project STORMFURY, a hurricane modification experiment. *Proc. First Nat. Conf. Wea. Modif.*, Amer. Meteor. Soc., 296–305.

Kuo, H. L., 1965: On the formation and intensification of tropical cyclones through latent heat release by cumulus convection. *J. Atmos. Sci.*, **22**, 40–63.

Miller, B. I., 1964: A study of the filling of hurricane Donna (1960) over land. *Mon. Wea. Rev.*, **92**, 389–406.

Ooyama, K., 1969: Numerical simulation of the life cycle of tropical cyclones. *J. Atmos. Sci.*, **26**, 3–40.

Palmén, E., and Herbert Riehl, 1957: Budget of angular momentum and energy in tropical cyclones. *J. Meteor.*, **14**, 150–159.

Rosenthal, Stanley L., 1969: Preliminary results from numerical experiments with a primitive equation model designed to simulate the development of tropical cyclones. *Proc. WMO/IUGG Conf. Num. Wea. Prediction, November 26 through December 4, 1968.* To be published by Japan Meteorological Agency, Tokyo.

——, 1969: Numerical experiments with a multilevel primitive equation model designed to simulate the development of tropical cyclones, Experiment I. ESSA Technical Memorandum ERLTM-NHRL-82, Environmental Science Services Administration, 36 pp.

——, and W. J. Koss, 1968: Linear analysis of a tropical cyclone model with increased vertical resolution. *Mon. Wea. Rev.*, **96**, 858–866.

Sheets, R. C., 1969: Some mean hurricane soundings. *J. Appl. Meteor.*, **8**, 134–146.

Simpson, J., G. W. Brier and R. H. Simpson, 1967: STORMFURY cumulus seeding experiment 1965: Statistical analysis and main results. *J. Atmos. Sci.*, **24**, 508–521.

Simpson, R. H., and J. S. Malkus, 1964: Experiments in hurricane modification. *Sci. Amer.*, **211**, 27–37.

——, Neil Frank, David Shideler and H. M. Johnson, 1968: Atlantic tropical disturbances, 1967. *Mon. Wea. Rev.*, **96**, 251–259.

——, ——, ——, and ——, 1969: Atlantic tropical disturbances, 1968. *Mon. Wea. Rev.*, **97**, 240–255.

Yamasaki, M., 1968: A tropical cyclone model with parameterized vertical partition of released latent heat. *J. Meteor. Soc. Japan*, **46**, 202–214.

41 Reprinted from Monthly Weather Review
Vol. 97, No. 12, 896-901.

UDC 551.509.313 : 519.28

NOTE ON THE ACCUMULATED ERROR IN THE NUMERICAL INTEGRATION OF A SIMPLE FORECAST MODEL

WALTER JAMES KOSS

National Hurricane Research Laboratory, ESSA, Miami, Fla.

ABSTRACT

A linearized, two-level forecast model with known analytic solution is numerically integrated to examine the behavior of the accumulated error (truncation and machine word "round-off" error). The results indicate that for linear models numerically integrated with centered differences: 1) the ratio of space increment to disturbance wavelength that yields sufficient accuracy in a reasonable amount of computation real time is on the order of 10^{-1} to 10^{-2}; 2) the largest time increment consistent with the stability criterion should be used for computation expediency.

Computations performed on computers having different word lengths did not yield significant differences in the results for this model integrated out to 7 days.

1. INTRODUCTION

The stability and accuracy of various finite-difference approximations to differential equations encountered in fluid dynamics problems have been investigated by various authors. The reader is directed to the work of Richtmyer (1962, 1957), Fischer (1965), Lilly (1965), Kurihara (1965), Phillips (1960), Molenkamp (1968), Crowley (1968), Kasahara (1965), Holton (1967), and Young (1968) for a detailed overview of the difference forms encountered in meteorological problems. Forsythe and Wasow (1960) present an excellent introduction to the general mathematical problem.

In this paper, we examine the accumulated error incurred during the time integration of a linearized, two-level forecast model that has a known analytic solution. The accumulated error at a given time is defined as the difference between the analytic and the numerical solutions and is produced by both truncation and round-off (machine word-size truncation). Integrations were performed with various values of the space and time increments and with different machine word lengths in order to determine 1) the importance of varying Δt with fixed Δs (providing the stability criterion is met) in terms of reducing the accumulated error and 2) the relative effects of truncation error versus round-off error in the accumulated error.

2. THE FORECAST MODEL

The numerical model forecasts the perturbation wind shear and geopotential thickness for the 750- to 250-mb layer over a 2000-km square bounded on the south by the Equator. The analytic equations govern linear, nonviscous, adiabatic, quasi-hydrostatic β-plane flow on a stagnant base state. For a detailed description of the model, the equations, and their solutions, see Rosenthal (1965) and Koss (1967). The vertical structure of the model is given in figure 1. The model equations are

$$\frac{\partial \hat{u}}{\partial t}-\beta y\hat{v}+\frac{\partial \hat{\phi}}{\partial x}=0, \tag{1a}$$

$$\frac{\partial \hat{v}}{\partial t}+\beta y\hat{u}+\frac{\partial \hat{\phi}}{\partial y}=0, \tag{1b}$$

and

$$\frac{\partial \hat{\phi}}{\partial t}+\frac{p_2^2\bar{\sigma}_2}{2}\left(\frac{\partial \hat{u}}{\partial x}+\frac{\partial \hat{v}}{\partial y}\right)=0 \tag{1c}$$

where

$$\hat{u}=u_1-u_3,$$
$$\hat{v}=v_1-v_3,$$

and

$$\hat{\phi}=\phi_1-\phi_3; \tag{2}$$

u_k, v_k are the wind velocity components at level k. ϕ_k is the geopotential of the kth pressure level, $p_2=50$ cb. $\bar{\sigma}_2$ = 3 mts units (section 3) is the mean static stability, $\beta=\partial f/\partial y$, where f is the Coriolis parameter, y is distance north from the Equator, and x is east-west distance measured positive eastward. Equation (1c) was obtained by discretizing the continuity and thermodynamic equations in the vertical and combining the two resulting equations. Here, $\omega_0=\omega_4=0$ was used as a boundary condition. A solution (see Koss, 1967, for details) is given by

$$\hat{u}=\hat{v}_{max}\frac{[\gamma^2-(c+\gamma)\beta y^2]}{k(c^2-\gamma^2)}\left(\frac{\beta}{\gamma}\right)^{1/2}e^Y\sin k(x-ct), \tag{3a}$$

$$\hat{v}=\hat{v}_{max}y\left(\frac{\beta}{\gamma}\right)^{1/2}e^Y\cos k(x-ct), \tag{3b}$$

and

$$\hat{\phi}=\hat{v}_{max}\frac{[c\gamma-(c+\gamma)\beta y^2]}{k(c^2-\gamma^2)}(\beta\gamma)^{1/2}e^Y\sin k(x-ct) \tag{3c}$$

where

$\gamma^2=\frac{p_2^2\bar{\sigma}_2}{2}$, $k=\frac{2\pi}{L}$, $Y=\frac{1}{2}\left(1-\frac{\beta y^2}{\gamma}\right)$, and L is the wavelength.

The c is the phase speed of the meteorologically significant solution which is obtained by solving the frequency equation

$$c^3-\frac{1}{k^2}[k^2\gamma^2+\gamma\beta+2\alpha\beta\gamma]c-\frac{\gamma^2\beta}{k^2}=0$$

with $\alpha=1$. This particular solution gives a meridional

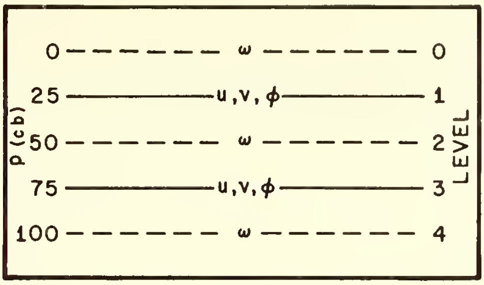

FIGURE 1.—Vertical structure of the model; u, v, and ϕ are defined at levels 1 and 3; $\omega = dp/dt$ is defined at levels 0, 2, and 4.

TABLE 1.—*Comparison of the floating-point format of the 32- and 36-bit word used in the numerical integrations. S refers to a single precision word, D refers to a double precision word.*

	36-bit word	32-bit word
Characteristic	7-bit S	7-bit S 7-bit D
Mantissa	28-bit S	24-bit - 6 hexadecimal digit S 56-bit - 14 hexadecimal digit D
Significance (decimal)	~9-digit S	~7.2-digit S ~16.8-digit D

perturbation velocity component which is asymmetric about the Equator and tends to zero with increasing distance from the Equator.

The finite-difference scheme used in the integrations was the familiar centered difference (leapfrog) scheme which has the following well-known properties:

(I) conditional computational stability,

(II) no changes in wave amplitude result from the integration,

(III) fictitious changes in phase speed occur during the integration,

(IV) splitting of solutions at alternate time steps due to the presence of the "computational" mode introduced by the use of a second-order approximation to a first-order derivative (Kurihara, 1965, and page 73 of Phillips, 1960), and

(V) the uncoupling of solutions of a linear system of equations at alternate time steps due to the use of centered difference approximations to both the space and time derivatives (Platzman, 1958).

Property (V) does not manifest itself in this study since the equations are coupled at alternate time steps through the Coriolis terms.

The "leapfrog" difference analog of equations (1a, b, and c) is

$$\hat{u}^{n+1}_{i,j} = \hat{u}^{n-1}_{i,j} + 2\Delta t\left[\beta y_i \hat{v}^n_{i,j} - \frac{(\hat{\phi}^n_{i,j+1} - \hat{\phi}^n_{i,j-1})}{2\Delta s}\right], \tag{4a}$$

$$\hat{v}^{n+1}_{i,j} = \hat{v}^{n-1}_{i,j} - 2\Delta t\left[\beta y_i \hat{u}^n_{i,j} + \frac{(\hat{\phi}^n_{i+1,j} - \hat{\phi}^n_{i-1,j})}{2\Delta s}\right], \tag{4b}$$

and

$$\hat{\phi}^{n+1}_{i,j} = \hat{\phi}^{n-1}_{i,j} - \frac{\Delta t}{\Delta s}\gamma^2[\hat{u}^n_{i,j+1} - \hat{u}^n_{i,j-1} + \hat{v}^n_{i+1,j} - \hat{v}^n_{i-1,j}] \tag{4c}$$

where Δs is the space increment in both the x (j) and y (i) directions and Δt is the time increment. A forward time difference set of equations is used to initiate the integrations.

3. RESULTS

The following values of parameters were used in all of the integrations:

$$L = 2000 \text{ km},$$

$$c = -2.0827 \text{ m sec}^{-1},$$

$$\beta = 2.2865 \times 10^{-11} \text{ (m sec)}^{-1},$$

$$\hat{v}_{max} = 5 \text{ m sec}^{-1}, \text{ and}$$

$$\bar{\sigma} = 3 \text{ mts units}.$$

The initial fields of $\hat{u}$, $\hat{v}$, and $\hat{\phi}$ were computed using equations (3a, b, and c) with $t=0$. During the integrations 1) cyclic continuity was used in computing the tendencies at the east-west boundaries (which is reasonable since the solutions are neutral waves) and 2) the tendencies at the north-south boundaries were computed from the analytic expressions to avoid using one-sided space differences.

The integrations are divided into two sets: the first set was obtained on a computer having a 36-bit binary word and the second from a 32-bit (hexadecimal) word. All integrations were performed in normalized floating-point arithmetic. Table 1 gives the accuracy characteristic of these word sizes.

The measure of the accumulated error used here is the root-mean-square error (RMSE) given by

$$\left\{\frac{1}{I^*J}\left[\sum_{i=1}^{I}\sum_{j=1}^{J}(F_{i,j} - F^*_{i,j})^2\right]\right\}^{1/2}$$

where $F_{i,j}$ is the value of the analytic solution at the (i,j)th grid point, $F^*_{i,j}$ is the result of the time integration at the same point, and I^*J is the total number of grid points.

THE INTEGRATIONS IN SET 1

Table 2 lists the RMSE of the $\hat{\phi}$ field (in meters) at the end of 12-hr forecast periods up to 72 hr and percentage errors at the 12- and 72-hr elapsed times. Δs was varied from 40 km to 250 km[1] and Δt was varied from 225 sec to an appropriate upper limit which satisfied the approximate computational stability criterion

$$\left|U\frac{\Delta t}{\Delta s}\right| < 1.$$

---

[1] Forty kilometers was the smallest allowable value of Δs because of computer memory restrictions on a 32K-36-bit word computer without peripherals, that is, tapes, discs, etc. Approximately 28K words were available for the program and variable storage.

TABLE 2.—*RMSE of the $\hat{\phi}$ field (in meters) at the end of 12-hr forecast periods and percentage error of the $\hat{\phi}$ field at the end of 12 hr and 72 hr. The percentage error is defined as the ratio of the RMSE to the average value of the amplitude of $\hat{\phi}$ with a value of 3.4 m and is listed following the RMSE. The bracketed quantity in the Δt column is the number of time steps needed for a 72-hr forecast using that value of Δt. The bracketed quantity with Δs is the total number of grid points in the 2000-km square region using that value of Δs.*

Δt (sec)	Elapsed time (hr)					
	12	24	36	48	60	72
			Δs=250 km [81]			
3600 [72]	.91977 27.	13.9 (409%)	259.	5. × 10^4	9. × 10^7	2. × 10^{11}
2400 [108]	.45351 13.3	.51657	.41766	.66503	.48026	.69119 20.3
1800 [144]	.43677 12.8	.54985	.38438	.59349	.49279	.60916 17.9
900 [288]	.41891 12.3	.56610	.35459	.53203	.59469	.55990 16.5
450 [576]	.41424 12.2	.56791	.35223	.52029	.61878	.54152 15.9
			Δs=125 km [289]			
1200 [216]	.11706 3.4	.10450	.11163	.15693	.15435	.18309 5.4
900 [288]	.11638 3.4	.10709	.10975	.16184	.15038	.19021 5.6
450 [576]	.11570 3.4	.10961	.10832	.16558	.14593	.19485 5.7
225 [1152]	.11552 3.4	.11023	.10797	.16641	.14475	.19540 5.7
			Δs=62.5 km [1089]			
600 [432]	.029845 0.87	.025132	.030313	.038035	.041705	.043266 1.27
450 [576]	.029804 0.87	.025325	.030071	.038379	.041527	.043791 1.28
225 [1152]	.029768 0.87	.025516	.029850	.038715	.041340	.044279 1.30
			Δs=40 km [2601]			
400 [648]	.012327 0.36	.010226	.012694	.015496	.017408	.017627 0.51
225 [1152]	.012316 0.36	.010281	.012628	.015596	.017355	.017755 0.52

Since the system will support inertia-gravity waves having a phase speed of approximately ±65 m $\sec^{-1}$ (L=2000 km), the largest value of Δt used satisfied the criteria with U=75 m $\sec^{-1}$. One integration was performed where the stability criterion was violated (Δs=250 km, Δt=3600 sec). In this case, the RMSE is about twice the maximum value of $\hat{\phi}$ after only 24 time steps.

For each integration, we note an oscillation in the values of the RMSE with time; but in general, the error is increasing with time. The error increase with time can be attributed to the cumulative error. The possible causes of the oscillation will be discussed in a following paragraph.

With Δs fixed, the RMSE both increases and decreases with Δt, depending on which elapsed time column one examines. Since amplitudes are invariant with time (property (II) of the differencing scheme), the data in table 2 suggest that one is probably better off by choosing the largest possible Δt which satisfies the stability criterion, since there may not be a reduction of the accumulated error associated with a reduction of the time-scale truncation error. Gates (1959) has shown for the centered difference form of the linearized barotropic vorticity equation that after the initial time steps the average phase speed of the computed solution can be expressed as a function of Δt and Δs. For values of the parameters used here, the change in phase speed (as computed from equation (76) by Gates (1959)) with respect to Δt is extremely small. Under the assumption that the computed solution phase speed for the system (4a, b, and c) behaves in a similar manner, we conclude that the phenomenon described in the first sentence of this paragraph is not related to property (III). The reason for this behavior will become apparent in the discussion of the 7-day integrations.

Since the differencing scheme is second order, the truncation error is on the order of the square of the normalized space increment. Therefore, halving Δs reduces the truncation error by one-fourth. From the values in the 72-hr column, we see that the percentage error behaves in a similar way as Δs is reduced.

The RMSE for the $\hat{u}$ and $\hat{v}$ fields exhibit the same overall behavior as that of the $\hat{\phi}$ field; hence, those results are not shown here.

Several 7-day integrations were performed with fixed $\lambda=\Delta t/\Delta s$=.0096 for Δs=40, 62.5, 125, and 250 km. The results are shown in figure 2 where the RMSE has been plotted at every time step for the Δs=250-km and 125-km

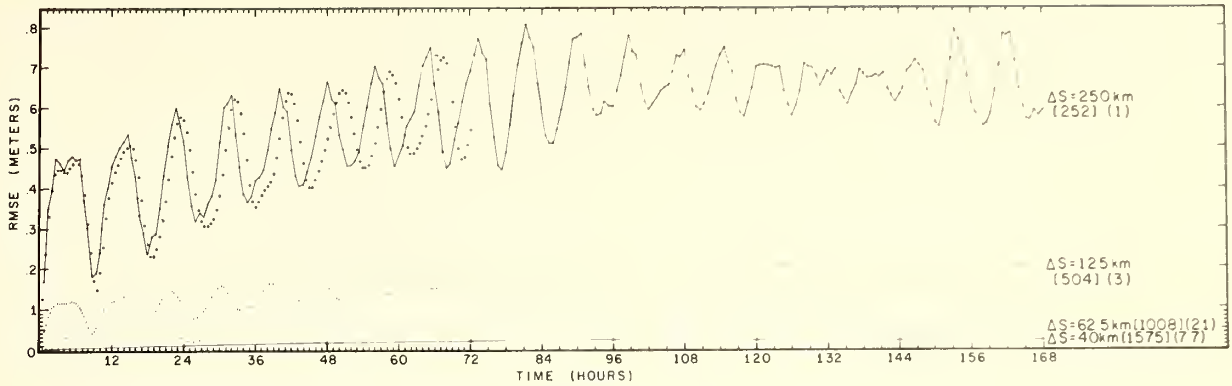

FIGURE 2.—RMSE (in meters) for 7-day integrations, with $\lambda=\Delta t/\Delta s=$constant for various values of Δs, and for a 3-day integration with $\Delta s=250$ km, $\Delta t=450$ sec (the data points are given by circles). Every time step has been plotted for the 7-day $\Delta s=250$-km and 125-km cases. Alternate time steps are plotted for the $\Delta s=62.5$-km case. The results for the 24-hr forecast periods are given for the $\Delta s=$ 40-km case. For the 3-day forecast, the data are plotted at half-hourly intervals. The boxed quantity is the number of time steps needed to complete the 7-day forecast. The bracketed quantity is the relative real time of the integration with the $\Delta s=250$-km case assigned the base value of 1. (The lines joining the data points have no physical significance.)

cases, at alternate time steps for the $\Delta s=62.5$-km case, and at 24-hr intervals for the $\Delta s=40$-km case. Also shown in the figure are the number of time steps and the relative time needed to complete the integration with the 250-km case assigned the base value of 1. For this forecast period, the reduction of space truncation error is still the important factor in reducing the accumulated error. Here the space/time increments are large enough so that truncation can be considered the major contributor to the error, that is, the round-off error incurred in the many space/time arithmetic operations is not yet dominant. The graphs for the 250-, 125-, and 62.5-km cases exhibit the time oscillation which was suggested by the data in table 2. At first thought, one is tempted to attribute the oscillation to the effect of property (III) of the leapfrog scheme, but there is another explanation for this behavior. Although the initial conditions were given in terms of the meteorologically important wave ($c=-2.0827$ m sec^{-1}), the computational system will support inertia-gravity waves as does the analytic system. The phase speed of these waves (for $L\leq 5000$ km) is on the order of ± 70 m sec^{-1}, which gives a period of about 8 hr. The oscillations in the RMSE graphs have a period of approximately 8 hr which is independent of both Δs and Δt. The independence from Δt is shown by the plot of the $\Delta s=250$ km and $\Delta t=450$ sec 72-hr forecast data, which has the same period as the $\Delta s=250$ km and $\Delta t=2400$ sec forecast data. This suggests that the errors generated in the initial time steps excite the inertia-gravity waves which then propagate through the system. The use of a small Δt only delays the excitation (here there is a lag of about 1 hr for the two compared cases), since it takes longer for the smaller truncation error to accumulate.

There is the possibility that the error caused by the computational change of phase speed is not revealed by the RMSE, which would be the case if the phase speed error is very small. But, if the analytic wave and computational wave become more out-of-phase as the forecast progresses, this error would manifest itself as a monotonic increase in the RMSE. Also, there is no indication throughout the forecast period that property (IV) of the leapfrog scheme (the solution splitting at alternate time steps) has occurred. This phenomenon could also be hidden by the RMSE, through the squaring of the error in the formation of the RMSE.

THE INTEGRATIONS IN SET 2

Three 7-day integrations were performed on a computer having a 32-bit word. Of these, one intergration was computed using double precision-type arithmetic (64-bit word). In all three integrations the analytic data were computed in double precision. This allows a comparison of these results with those computed with the 36-bit word. Table 3 shows the RMSE for the ϕ fields (in these computations $\lambda=.0096$). Here, the last digit in the 36-bit word result was obtained by rounding off the stored number for output display. All digits of the 32- and 64-bit words are certain (table 1); to compare the results with those of the 36-bit word, use the usual rounding convention when rounding to six (or five) digits. The differences in the results are insignificant. We must keep in mind that these results apply for a linear model; a similar experiment with a complex nonlinear system could possibly yield the opposite conclusion.

4. REMARKS

During the course of the computations reported on in this paper, we were not concerned primarily with the question of the stability and accuracy of the finite-differ-

TABLE 3.—*RMSE of the $\hat{\phi}$ field (in meters) computed on a 32-bit word computer in single and in double precision arithmetic and on a 36-bit word computer. Time is the elapsed forecast time in hours. For these computations,* $\lambda=\Delta t/\Delta s=$*constant.*

Time (hr)	$\Delta s=40$ km		$\Delta s=125$ km		
	32-bit word	36-bit word	32-bit word	64-bit word	36-bit word
12			.11705 89	.11705 88	.11706
24	.010225 60	.010225	.10449 92	.10449 91	.10450
36			.11163 30	.11163 29	.11163
48	.015507 72	.015507	.15692 59	.15692 56	.15693
60			.15435 56	.15435 53	.15435
72	.017635 46	.017634	.18309 31	.18309 27	.18309
84			.17208 68	.17208 69	.17209
96	.020381 05	.020379	.20326 68	.20326 62	.20327
108			.18195 96	.18195 91	.18196
120	.020659 76	.020659	.19120 75	.19120 72	.19121
132			.20379 57	.20379 54	.20380
144	.019077 01	.019074	.19149 46	.19149 30	.19149
156			.20765 61	.20765 59	.20765
168	.019412 13	.019411	.17597 78	.17597 70	.17598

ence scheme used in integrating the system of differential equations. Instead, we considered the practical aspect of the problem, that is, the interrelation of truncation error and round-off error in the error accumulated during the integration. The model, being linear and free of diabatic and viscous effects, allows verification of the integrations to within the machine accuracy of the computed values of the analytic solutions. Therefore, one is able to associate the overall behavior of the error with changes in the space/time parameters. The error incurred by evaluating the analytic expressions for the tendencies on the north and south boundary is a maximum when Δt is large, and this is when the truncation error is at a maximum over the entire grid. The effects of this error are, therefore, secondary in the overall evaluation.

The rate of error accumulation is strongly dependent upon the complexity of the physical system being examined. Here, although the model is linear and basically simple, it is determined by a system of three equations, one of which is strongly space-increment dependent: the $\hat{\phi}$ tendency is given by the horizontal divergence of the perturbation wind shear. This computation is an excellent source of truncation error.

Several conclusions concerning the computer application of the leapfrog scheme can be made based on these integrations:

1) For a given value of the space increment, one should choose the largest value of the time increment consistent with the stability criterion. The use of a smaller value of Δt does not always guarantee a reduction of the accumulated error even though the theoretical truncation error in the time scale is reduced. The additional computations needed with a smaller Δt will usually introduce compensating round-off errors. More important is the effect of the excited gravity waves which may be supported by the system. The lag in the oscillation of the error curves caused by changes in Δt can give results as those given in table 2: the "goodness" of the smaller Δt depends on the forecast period examined. Hence, the space truncation is the important factor in the error accumulation.

2) Once the characteristic scale (L) of the motions being studied has been determined, there is an optimal range of values of the space increment (Δs) in terms of both "acceptable" error accumulation and computer time. Reduction of the magnitude of Δs will reduce the accumulated error because of the reduction in both the space- and time-scale truncation error. But extremely small values of Δs yield rapid accumulation of round-off error which will dominate the truncation error.[2] This phenomenon is a function of the computer word size and the total number of arithmetic operations in the computation. Inspection of table 3 shows that this was not the case here for either word size. Figure 2 shows that the slight gain in accuracy made in going from $\Delta s=62.5$ km to $\Delta s=40$ km was at the expense of a three-fold increase in computer running time. If $h=\Delta s/L$, then $h=0.03$, for this experiment yields less than a 2 percent average error in the $\hat{\phi}$ field in a reasonable amount of computing time. As mentioned above, that the round-off error was not dominant in the examined cases is shown by comparing the results of the single precision and double precision computations. Round-off error would become evident in the accumulated error for values of Δs much smaller than 40 km, that is, for $h <\!\!< 0.02$, through an increase in the percentage error of the $\hat{\phi}$ fields as Δs decreases. The small percentage errors for $h \sim 0.03$ and the large amounts of computation needed for integrations with smaller values of h are justification for not performing the computations with $\Delta s < 40$ km.

Modifying the governing equations by the addition of nonlinear advection, viscous effects, and diabatic effects would not alter the magnitude of the truncation error if the same finite-difference approximations are used, but the round-off error possibly could be greatly increased. (We are assuming that the system remains computationally stable with the addition of terms.)

In general, one could use the same technique employed here in other problems to determine feasible choices of integration parameters, regardless of the existence or nonexistence of comparison analytic solutions to the problem at hand. The choice of space increment can be established by noting the relative change in the computed field variable for a short forecast period as the grid is modified from a coarse to a fine one. (The stability criterion determines the time increments, therefore the number of time steps required.) As table 2 demonstrates for the problem considered here, the magnitude of the error is roughly determined in relatively few time steps. Hence, knowledge of the absolute error is not absolutely necessary.

From a few preliminary "dry" runs (in which viscous and diabatic effects can be suppressed) the "optimal" space increment can be chosen on the basis of 1) computer economics (running times and memory requirements), and more importantly, 2) the physical reality of the results. The addition of forcing functions to the equations could possibly alter the stability properties of the system and require a change in the value of the space increment. The dry run equations define a physical system whose behavior can be qualitatively diagnosed from the equations. The numerical results of the dry run should concur with the qualitative reasoning when suitable values of the parameters are used in the integration.

---

[2] This can be amply demonstrated by numerically integrating the ordinary differential equation $dy/dx=y$, $y(x=0)=1$, over the interval [0, 1], allowing $h=\Delta x$ to vary from 10^{-1} to 10^{-6} and graphing the error at $x=1$ against the step size h.

REFERENCES

Crowley, W. P., "Numerical Advection Experiments," *Monthly Weather Review*, Vol. 96, No. 1, Jan. **1968**, pp. 1–11.

Fischer, G., "A Survey of Finite-Difference Approximations to the Primitive Equations," *Monthly Weather Review*, Vol. 93, No. 1, Jan. **1965**, pp. 1–10.

Forsythe, G. E., and Wasow, W. R., *Finite Difference Methods for Partial Differential Equations*, John Wiley and Sons, Inc., New York, **1960**, 444 pp.

Gates, W. L., "On the Truncation Error, Stability, and Convergence of Difference Solutions of the Barotropic Vorticity Equation," *Journal of Meteorology*, Vol. 16, No. 5, Oct. **1959**, pp. 556–568.

Holton, J. R., "A Stable Finite Difference Scheme for the Linearized Vorticity and Divergence Equation System," *Journal of Applied Meteorology*, Vol. 6, No. 3, June **1967**, pp. 519–522.

Kasahara, A., "On Certain Finite-Difference Methods for Fluid Dynamics," *Monthly Weather Review*, Vol. 93, No. 1, Jan. **1965**, pp. 27–31.

Koss, W. J., "Further Theoretical Considerations of Tropospheric Wave Motions in Equatorial Latitudes," *Monthly Weather Review*, Vol. 95, No. 5, May **1967**, pp. 283–297.

Kurihara, Y., "On the Use of Implicit and Iterative Methods for the Time Integration of the Wave Equation," *Monthly Weather Review*, Vol. 93, No. 1, Jan. **1965**, pp. 33–46.

Lilly, D. K., "On the Computational Stability of Numerical Solutions of Time-Dependent Non-linear Geophysical Fluid Dynamics Problems," *Monthly Weather Review*, Vol. 93, No. 1, Jan. **1965**, pp. 11–26.

Molenkamp, C. R., "Accuracy of Finite-Difference Methods Applied to the Advection Equation," *Journal of Applied Meteorology*, Vol. 7, No. 2, Apr. **1968**, pp. 160–167.

Phillips, N. A., "Numerical Weather Prediction," *Advances in Computers*, Vol. 1, Academic Press, New York, **1960**, pp. 43–90.

Platzman, G. W., "A Numerical Computation of the Surge of June 26, 1954 on Lake Michigan," *Geophysica*, Vol. 6, No. 3/4, **1958**, pp. 407–438.

Richtmyer, R. D., *Difference Methods for Initial Value Problems*, Interscience Publishers, New York, **1957**, 238 pp.

Richtmyer, R. D., "A Survey of Difference Methods for Nonsteady Fluid Dynamics," *NCAR Technical Note* 63–2, National Center for Atmospheric Research, Boulder, Colo., **1962**, 25 pp.

Rosenthal, S. L., "Some Preliminary Theoretical Considerations of Tropospheric Wave Motions in Equatorial Latitudes," *Monthly Weather Review*, Vol. 93, No. 10, Oct. **1965**, pp. 605–612.

Young, J. A., "Comparative Properties of Some Time Differencing Schemes for Linear and Nonlinear Oscillations," *Monthly Weather Review*, Vol. 96, No. 6, June **1968**, pp. 357–364.

[*Received May 2, 1969; revised August 13, 1969*]

Reprinted from McGraw-Hill Yearbook of Science and Technology
McGraw-Hill, New York, 193-196.

Hurricane

Since the establishment of the National Hurricane Research Laboratory in 1956, hurricanes have been under intensive observation by aircraft, radar, Earth satellites, and conventional meteorological networks surrounding the Atlantic hurricane regions. At the end of the 1967 hurricane season, the Research Flight Facility, an agency of the Environmental Science Services Administration (ESSA), had flown approximately 3500 hr into hurricanes and tropical storms. Flying at altitudes ranging from a few hundred feet above the sea to more than 40,000 ft, these specially instrumented research aircraft have collected enough data to permit a fairly complete description of the winds, temperatures, and pressures associated with these destructive storms.

Wind velocity. In the outer portion of the hurricanes, winds increase gradually as the center of the cyclone is approached. In large storms this region may extend over several hundred kilometers. At low levels the wind profile for the outer portion has been found to follow approximately the relationship $VR^x = K$, where V is the wind speed, R the radial distance from the center of the hurricane, and K a constant. For typical hurricanes, x has a characteristic value of 0.50–0.65.

The region of maximum winds surrounds the eye. This region is easily the most spectacular part of the storm. In this area, averaging 5–10 mi in width, the winds are almost constant and may attain speeds of 150–200 mph. In Hurricane Inez (1966) research aircraft recorded an instantaneous wind speed of 199 mph at an elevation of about 8000 ft on Sept. 28 while Inez was passing through the Caribbean just south of Puerto Rico. This observation was the highest ever recorded by aircraft in any hurricane since the inauguration of research flights. The ring of maximum winds coincides with the wall cloud, so called because it is also an area of violent convection and heavy rains.

Inside the region of maximum winds lies the eye, or innermost portion, of the storm. Winds diminish with amazing rapidity in the eye, but seldom approach absolute calm.

Air circulation. In major hurricanes the circulation extends from sea level to elevations in excess of 40,000 ft, and some may even reach the stratosphere. Hurricane circulations may be divided into three vertical layers—inflow, middle, and outflow.

Inflow layer. The lower 10,000 ft is called the inflow layer, and in this region there is a pronounced component of the wind inward toward the center. The inflow is partly controlled by frictional forces caused by tangential shearing stresses exerted by the hurricane winds on the sea surface. Without this frictional force, hurricanes could not form. The inflow layer is important because the air flowing inward is moving down the pressure gradient, that is, going from high to low pressure and thereby converting potential energy to kinetic energy. The inflow layer is, therefore, the dynamo which runs the storm. Moisture and sensible heat are also brought into the storm via the inflow layer, either by lateral advection or by turbulent transfer from the ocean surface.

Middle layer. At the middle layers the motion is predominately cyclonic, with little or no radial component of the wind. There may, however, be asymmetries in the wind field, as shown by Fig. 1, which is based on aircraft measurements made in Hurricane Daisy in 1958. Note the 100-knot isotach maxi-

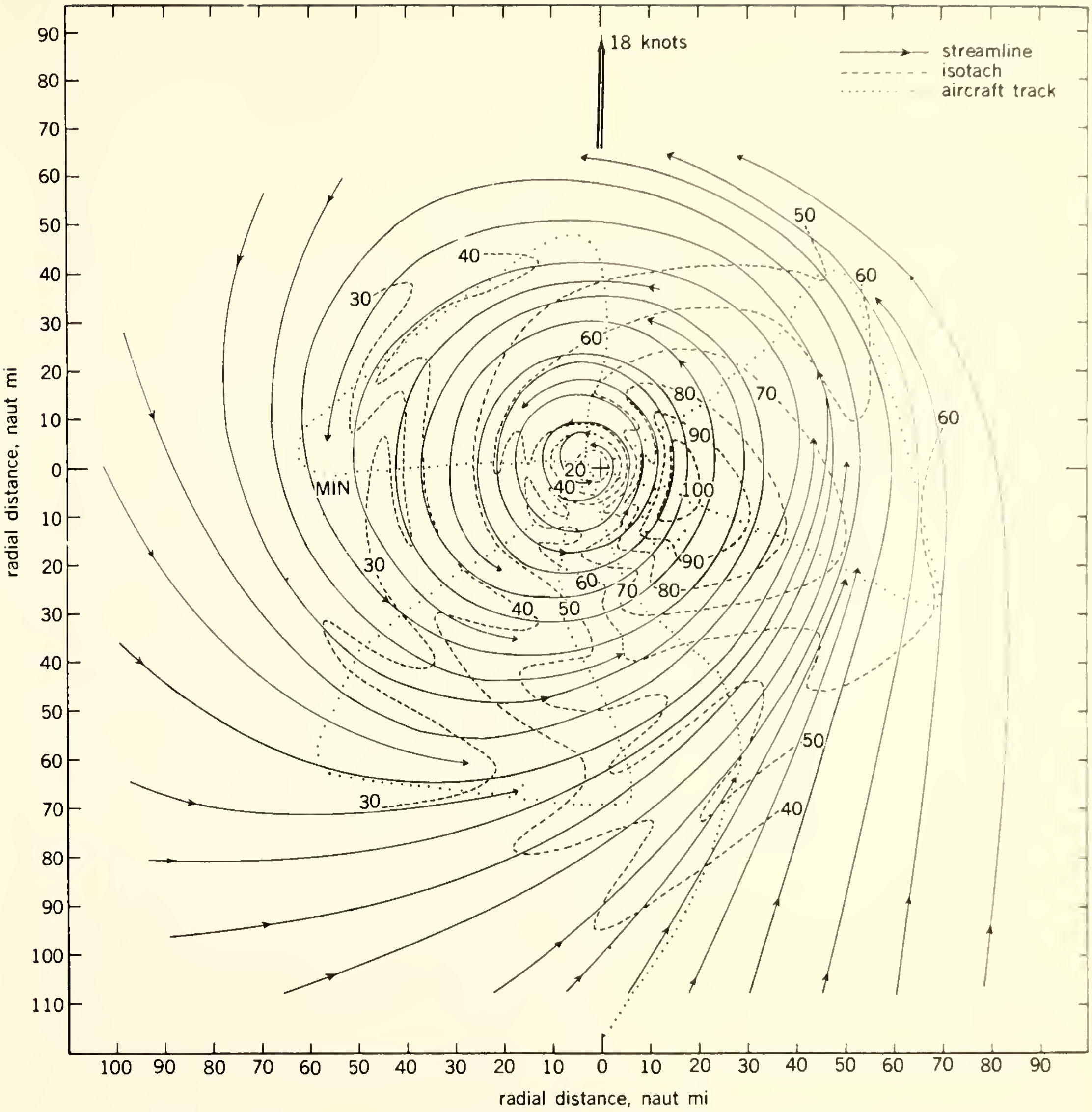

Fig. 1. Wind circulation in Hurricane Daisy at 13,000 ft, Aug. 28, 1958. Numbers represent wind speed in knots.

mum to the right of the center and the considerably lesser speeds to the left. The streamlines show some convergence to the rear of the center, but closer in the motion is mainly cyclonic in nature.

Outflow layer. The outflow layer occupies the upper third of the storm. Air which has entered via the inflow layer and then ascended to the upper levels in the region of the wall cloud then flows outward and away from the storm. Through much of the outflow layer, winds decrease, change direction, and frequently become anticyclonic, in sharp contrast to the violent cyclonic flow existing at sea level. This occurs because the hurricane is a warm-core system and because the absolute angular momentum tends to be conserved in the outflow layer. The outflowing air may sink back to the lower levels at some great distance from the hurricane.

Energy exchange. The hurricane is a warm-core, direct atmospheric circulation; that is, warm air rises and cold air sinks, thereby converting heat energy to potential energy and potential energy to kinetic energy. Calculations have shown that in an average hurricane from 2.0×10^{26} to 6.0×10^{26} ergs/day are liberated in the form of latent heat. Only about 3% of this energy is converted to kinetic energy, much of the remainder being converted to potential energy and exported through the outflow layer.

Temperature levels. At a given pressure, warm air is lighter than cold air. The formation of a hurricane, the extreme low pressures observed near the center, the intense radial pressure gradients, and

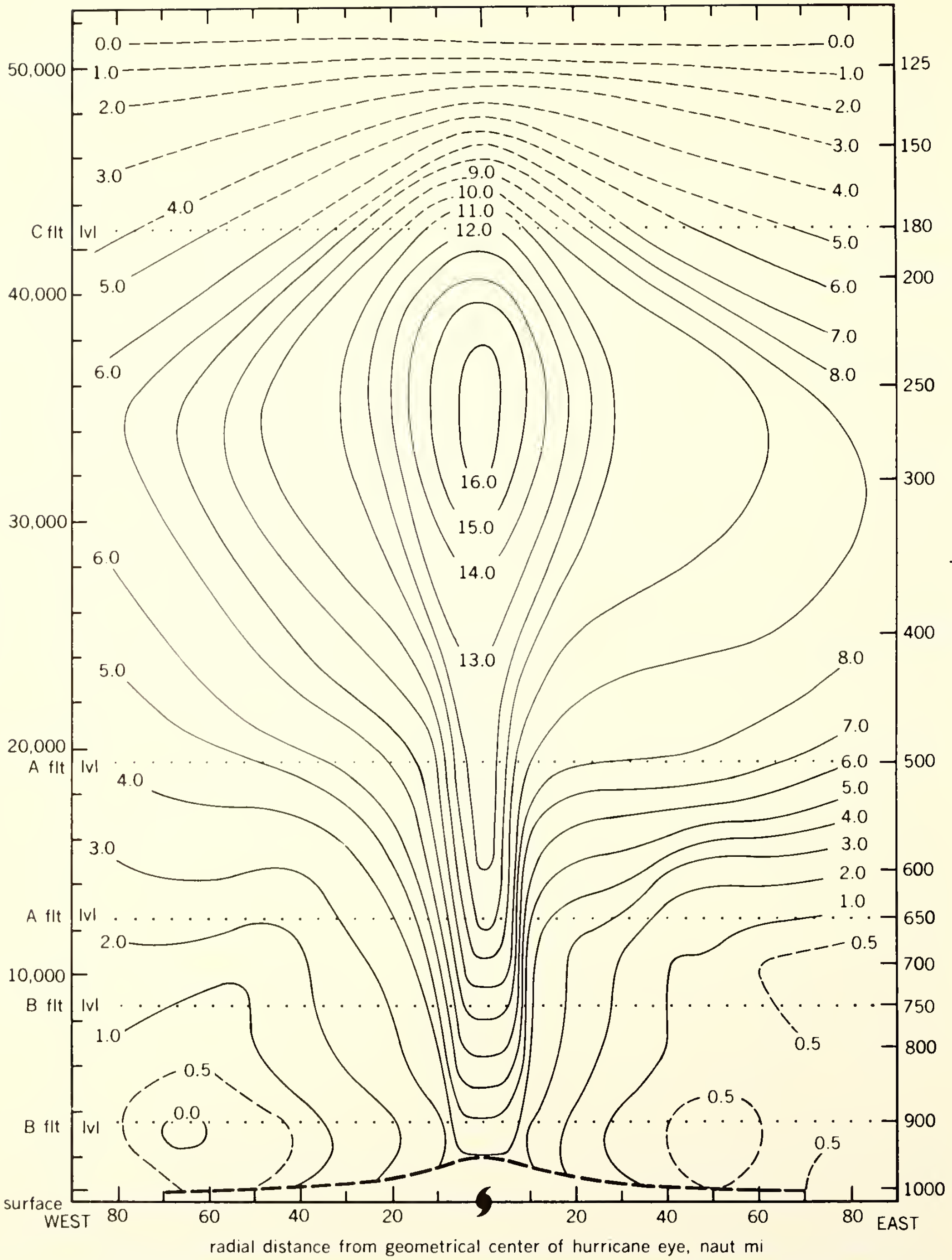

Fig. 2. Temperature anomalies (departures from mean tropical atmosphere) in degrees Celsius, Oct. 1, 1964, based on aircraft measurements at five levels. The maximum warming usually is found around 40,000 ft.

the violent cyclonic circulations depend upon the development and concentration of very warm air near the core of the storm.

Figure 2 shows the temperature anomalies found in Hurricane Hilda in the Gulf of Mexico in 1964. This analysis was based on aircraft data collected at five levels, as indicated in Fig. 2. This pattern is characteristic of the temperature fields found in other similar storms. The maximum warming is almost always found at the upper levels, usually around 40,000 ft. In Hilda the air within the 30,000–40,000 ft layer was 16°C above that normally found in the tropics at that level. The strong lateral gradients at the intermediate levels observed at radii of 10–15 naut mi coincide with the ring of maximum winds and the wall cloud. This feature is also typical. Little or no anomalies are found below 5000 ft except near the wall cloud. In some cases temperatures in this region have been found to be slightly below normal.

The warming of the upper levels shown in Fig. 2 is the result of the oceanic heat source. Air flowing into a hurricane is moving toward lower pressure, and hence it must expand during the process. In the absence of a heat source the air would cool, but no significant cooling is observed. The cooling is prevented by the addition of sensible heat by contact with, and turbulent exchange from, the warm waters of the ocean surface. Moisture is also added through evaporation. These two processes cause the equivalent potential temperature of the surface air to rise, and it is the ascent of air with greatly enhanced equivalent potential temperatures which causes the upper-level warming indicated in Fig. 2. When a hurricane moves inland or over cold water, the storm usually decays rapidly since it has moved away from its primary heat source.

Meteorological satellites. The advent of meteorological satellites during the past few years has provided the research scientist with a powerful new observational tool which is particularly valuable in studying tropical weather systems, including hurricanes, many of which form and die in geographical locations devoid of conventional meteorological data. Already the satellites have led to greatly increased capability in detecting the birth of hurricanes and in tracking them in remote areas. Satellites have also contributed to knowledge about hurricane cloud patterns and the thermodynamics of these storms; satellite photographs have been used to estimate circulation patterns around hurricanes and to estimate their intensity.

The possibility of eventual hurricane control is an intriguing one. Project STORMFURY, a joint undertaking of ESSA and the U.S. Navy, is designed to explore ways of modifying hurricanes. No fully satisfactory hypothesis for the control of hurricanes is yet in existence, and its formulation may have to await a better understanding of the manner in which hurricanes form.

For background information *see* HURRICANE; METEOROLOGICAL SATELLITES in the McGraw-Hill Encyclopedia of Science and Technology.

[BANNER I. MILLER]

Bibliography: J. A. Colon, *Natl. Hurricane Res. Lab. Rept.*, no. 48, 1961; H. F. Hawkins and D. T. Rubsam, *Mariners Weather Log*, 11(5):157–160, 1967; H. F. Hawkins and T. Rubsam, *Monthly Weather Rev.*, 1968; B. I. Miller, *Science*, 157(3795): 1389–1399, 1967.

43

U.S. DEPARTMENT OF COMMERCE
Environmental Science Services Administration
Research Laboratories

ESSA Technical Memorandum ERLTM-NHRL 85

EXPERIMENT IN FORECASTING HURRICANE DEVELOPMENT WITH REAL DATA

Banner I. Miller

National Hurricane Research Laboratory
Miami, Florida
April 1969

TABLE OF CONTENTS

Page

LIST OF SYMBOLS iv

ABSTRACT 1

1. INTRODUCTION 1

2. FORECAST MODEL 1

3. INITIALIZATION OF DATA 6

4. NUMERICAL PROCEDURES 9

5. DEVELOPMENT OF HURRICANE ALMA (1962) 14

    5.1 Evolution of wind and Pressure Systems 16
    5.2 Thermal Structure 22

6. SOME OTHER RESULTS 24

7. SUMMARY AND CONCLUSIONS 25

8. ACKNOWLEDGMENTS 25

9. REFERENCES 26

LIST OF SYMBOLS

c_d	drag coefficient
c_p	specific heat of air at constant pressure
D	divergence
f	Coriolis parameter
f_0	mean value of Coriolis parameter
F_q	flux of water vapor
F_s	flux of sensible heat
g	acceleration of gravity
H	total heating function
H_s	sensible heat (cal gm^{-1} sec^{-1})
H_l	latent heat (cal gm^{-1} sec^{-1})
I	net moisture convergence
J	Jacobian operator
K_h	a coefficient for lateral mixing
K_m	a coefficient for vertical mixing
L	latent heat of condensation
m	map scale factor
p	pressure
q	mixing ratio
q_s	saturated mixing ratio
Q	total moisture required to saturate and warm a column
σ	static stability $-\frac{\alpha}{\theta}\frac{\partial\theta}{\partial p}$
τ_x, τ_y	horizontal shearing stresses
χ	velocity potential

R	gas constant
s	distance
t	time
T	temperature
T^*	virtual temperature
u	zonal component of the wind
v	meridional component of the wind
V_0	wind speed at the surface
V_r	radial wind speed
$\mathbb{V}$	horizontal velocity vector
x	distance in east-west direction
y	distance in north-south direction
α	specific volume
β	$= df/dy$
ζ	relative vorticity
η	absolute vorticity
θ	potential temperature
π	$\equiv \frac{RT}{P\theta}$
ρ	density
ϕ	geopotential
ψ	stream function
ω	dp/dt vertical p velocity
∇^2	horizontal Laplacian operator

EXPERIMENT IN FORECASTING HURRICANE DEVELOPMENT WITH REAL DATA

Banner I. Miller

A multi-level primitive equation model incorporating diabatic and frictional influences has been developed for numerical weather prediction in the tropics. When tested on a limited geographical area in the Western Atlantic, the model appeared capable of predicting the development of a vortex similar to a hurricane. Real data were used and a tropical cyclone did occur. Many typical features of hurricanes, such as the formation of an intense low level vortex, the warming of the upper troposphere, the development of an upper level anticyclone, low level inflow, and high level outflow, were forecast.

1. INTRODUCTION

One of the most challenging and elusive tasks in tropical meteorology is forecasting the development of tropical cyclones, but researchers have succeeded in identifying many conditions favorable for tropical cyclogenesis (Miller, 1958; 1967; Hawkins and Rubsam, 1968). Symmetrical dynamical models, particularly those of Ooyama (1967) and Rosenthal (1969), have simulated realistically many of the features of the life cycle of tropical cyclones, and general circulation experiments (Manabe and Smagorinsky, 1967) have shown development of weak disturbances that resemble those observed at low latitudes. To the writer's knowledge, however, no numerical experiments have successfully predicted the development of a mature hurricane from real initial data. This paper describes an experiment with real data that resulted in the prediction of the formation of Hurricane Alma in 1962.

2. FORECAST MODEL

A prediction model was designed specifically for use in tropical and subtropical regions, with forecasting the movement of tropical cyclones one of the primary objectives. The importance of latent heat, sensible heat, and friction in the development and maintenance of tropical cyclones is well known, and it was obvious that a tropical forecast model would have to include these effects to be successful. Therefore a primitive equation, diabatic, viscous model was selected for the experimental forecasts. The variables to be forecast were the horizontal wind, the potential temperature, and the mixing ratio. The forecast equations are

$$\frac{\partial u}{\partial t} = -u\frac{\partial u}{\partial x} - v\frac{\partial u}{\partial y} - \omega\frac{\partial u}{\partial p} + fv - \frac{\partial \phi}{\partial x} + K_H \nabla^2 u + g\frac{\partial \tau_x}{\partial p} \tag{1}$$

$$\frac{\partial v}{\partial t} = -u\frac{\partial v}{\partial x} - v\frac{\partial v}{\partial y} - \omega\frac{\partial v}{\partial p} - fu - \frac{\partial \phi}{\partial y} + K_H \nabla^2 v + g\frac{\partial \tau_y}{\partial p} \tag{2}$$

$$\frac{\partial \theta}{\partial t} = -u\frac{\partial \theta}{\partial x} - v\frac{\partial \theta}{\partial y} - \omega\frac{\partial \theta}{\partial p} + \frac{\theta}{T}\frac{g}{C_p}\frac{\partial F_s}{\partial p} + \frac{\theta}{T}K_H \nabla^2 \theta + \frac{\theta}{C_p T}(H_L) \tag{3}$$

$$\frac{\partial q}{\partial t} = -u\frac{\partial q}{\partial x} - v\frac{\partial q}{\partial y} - \omega\frac{\partial q}{\partial p} + g\frac{\partial F_q}{\partial p} + K_H \nabla^2 q \tag{4}$$

The tangential shearing stresses, $\tau_{x,y}$, are defined at 1000 mb in terms of the total wind speed, V_0 , and a drag coefficient,

$$\tau_{x,0} = -\rho C_D V_0 U \tag{5}$$

$$\tau_{y,0} = -\rho C_D V_0 V \tag{5a}$$

At the upper levels, these quantities are defined by use of an eddy viscosity for vertical mixing, K_m ,

$$\tau_x = -\rho^2 g K_m \frac{\partial u}{\partial p} \tag{6}$$

$$\tau_y = -\rho^2 g K_m \frac{\partial v}{\partial p} \tag{6a}$$

The fluxes of water vapor and sensible heat at the surface are proportional to the surface wind, the surface drag coefficient, the air-sea differences in mixing ratio and temperatures,

$$F_s = \rho_0 C_D C_p (T_w - T_a) V_0 \tag{7}$$

$$F_q = \rho_0 C_D (q_w - q_a) V_0 \tag{7a}$$

These quantities are assumed to decrease linearly with pressure and were allowed to go to zero at 700 mb, in the manner suggested by Petterssen et al. (1962), i.e., $H_s = g \dfrac{\partial F_s}{\partial p}$. This technique is consistent with maintaining a quasi-moist adiabatic lapse rate in the lower layers and permits the upward transport of sensible heat against a potential temperature gradient. The surface drag coefficient over water is an empirical function of the surface wind speed (Miller, 1962; 1964; 1967; Hawkins and Rubsam, 1968).

$$C_D = (1.0 + 0.07\, V_0) \times 10^{-3} \tag{8}$$

with V_0 being measured in meters per second. Empirical values of K_m and K_h which were designed to produce realistic values of vertical motion, depth of the inflow layer, and the radial motions in hurricanes (Miller, 1965; Barrientos, 1964) are also used. It is assumed that K_h, a lateral mixing coefficient, is the same for heat, momentum, and water vapor. Evaporation and the sensible heat over land are set equal to zero and a constant value of 0.005 for the drag coefficient is assumed; this is the same as the value used by Palmen and Holopainen (1963) in their investigation of an extratropical disturbance over the central United States.

The latent heat added to the system is composed of two parts. The first part is a parameterization of the heat released by cumulus convection, originally proposed by Kuo (1965), who defined a quantity, Q, as the moisture required to saturate the atmosphere and (following condensation of a portion of the water vapor) to raise its temperature to that of the moist adiabat passing through the base of the cloud:

$$Q = \int_{P_B}^{P_t} (q_s - q) \frac{\delta p}{g} + \int_{P_B}^{P_t} \frac{C_p}{L} (T_s - T) \frac{\delta p}{g} \tag{9}$$

The net moisture convergence within a column may be obtained by integrating (4) in the vertical

$$I = -\int_{P_B}^{P_t} \frac{\partial q}{\partial t} \frac{\delta p}{g} - \frac{\omega_0 q_0}{g} \qquad (10)$$

where q_0 is the mixing ratio, ω_0 is the vertical motion at 1000 mb, P_B and P_t are the pressures at the base and the tops of the clouds, q_s refers to the saturation mixing ratio, T_s is the temperature along the moist adiabat determined by the lifting condensation level of the sub-cloud air, and q and T refer to the environmental conditions. The heating function may now be expressed by

$$HL_1 = \frac{I}{Q} C_p \, (Ts - T) \qquad (11)$$

and HL_1 is set equal to zero at 1000 mb and at 100 mb, if I is zero or negative or if T is equal to or greater than T_s. Note that the Kuo heating function is self-limiting, since it tends to approach zero as the lapse rate within the cloud becomes moist adiabatic and the cloud becomes saturated.

The second part of the latent heat release is due to the ascent of moist air with the broad-scale vertical motion and is defined as

$$HL_2 = - C_p \left[\frac{L}{C_p} \frac{\partial q_s}{\partial p} \right] \omega \qquad (12)$$

An examination of the variation of the saturation mixing ratio with pressure reveals that it is almost linear for the tropical atmosphere within the range from 700 to 200 mb. Accordingly, the quantity in the brackets is set equal to a constant, to speed up calculations, and has the value of about 0.06.

The evaluation of (12) can lead to instabilities in the calculations, particularly if strong upward motion occurs at only a few adjacent points within the network. To alleviate this fluctuation, the following procedure was devised:

1. The vertical motion was smoothed over nine points with a "smoothing operator" (Shuman, 1957b).

2. If the smoothed vertical motion was negative and relative humidity was 95% or greater H_{L_2} was evaluated from (12); otherwise it was set to zero.

3. The heating was then distributed over nine points, resulting in uniform heating over a region of uniformly ascending saturated air (see fig. 1). This procedure is obviously experimental and completely arbitrary, but no difficulties have occurred in its use in forecasts for periods up to 24 hours.

The total heat source, H, may now be expressed as the sum of the sensible and latent heat,

$$H = H_s + H_{L_1} + H_{L_2} \tag{13}$$

and H is applied in forecasting potential temperature (3), and in the omega equation described in a later section.

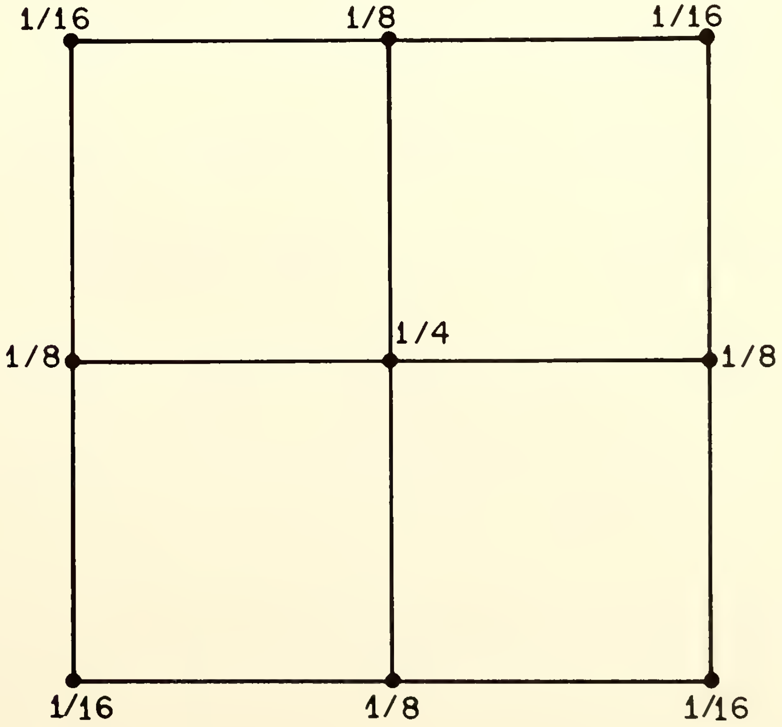

Figure 1. Diagram showing how latent heating function is distributed to adjacent points.

3. INITIALIZATION OF DATA

Large scale motions of the atmosphere are in a quasi-balanced state; a completely balanced state does not and cannot exist - particularly when one attempts to evaluate diabatic and viscous forces. Since observational data contain a sufficient number of inaccuracies to cause spurious amplification of the natural atmospheric gravitational and inertial oscillations with time (particularly when the primitive equations are used as a forecast model), we must modify initial data so that the forecast period begins with as near a balanced state as possible. It may also be necessary to repeat the initialization process periodically throughout the forecast period, especially if intense vorticity maxima of relatively small scale develop inside the forecast domain.

Numerous authors have discussed the initialization problem and proposed methods of obtaining an initially balanced state (Phillips, 1960; Charney, 1962; Krishnamurti and Baumhefner, 1966; Nitta and Hovermale, 1967; Miyakoda and Moyer, 1968; Shuman and Hovermale, 1968). The methods chosen for this experiment follow closely those described by Charney (1962) and Krishnamurti and Baumhefner (1966). The basic equations in our initialization process are the divergence,[1] balance, omega, continuity, and hydrostatic equations, which will follow in the same order.[2]

$$\frac{\partial D}{\partial t} + \mathrm{I}V\cdot\nabla D + \omega\frac{\partial D}{\partial p} + D^2 - 2J(u,v) - f\xi + \beta u + \frac{\partial w}{\partial x}\frac{\partial u}{\partial p} + \frac{\partial w}{\partial x}\frac{\partial u}{\partial p} + \frac{\partial w}{\partial y}\frac{\partial v}{\partial p} - K_H\nabla^2 D - g\frac{\partial}{\partial p}\left(\frac{\partial \tau_x}{\partial x} + \frac{\partial \tau_y}{\partial y}\right) + \nabla\phi = 0\,, \tag{14}$$

$$f\nabla^2\psi - \beta u + 2\left(\psi_{xx}\psi_{yy} - \psi_{xy}^2\right) = \nabla^2\phi\,, \tag{15}$$

---

[1] In principle the time-dependent terms in the divergence and omega equations can be evaluated from the forecast, but these were omitted in the forecasts of Hurricane Alma. Attempts will be made to include them in subsequent experiments.

[2] Symbols are defined on page iv.

$$
\begin{aligned}
\nabla^2 \sigma \omega + f_0 \eta \frac{\partial^2 \omega}{\partial p^2} - f_0 \omega \frac{\partial^2 \eta}{\partial p^2} - f_0 \frac{\partial}{\partial p} \left(\frac{\partial \omega}{\partial x} \frac{\partial v}{\partial p} - \frac{\partial \omega}{\partial y} \frac{\partial u}{\partial p} \right) \\
= f_0 \frac{\partial}{\partial p} (\mathbb{V} \cdot \nabla \eta) - f_0 K_H \nabla^2 \frac{\partial \eta}{\partial p} - f_0 g \frac{\partial^2}{\partial p^2} \left(\frac{\partial \tau_y}{\partial x} - \frac{\partial \tau_x}{\partial y} \right) \\
+ \pi \nabla^2 (\mathbb{V} \cdot \nabla \theta) - \nabla^2 \left[\frac{R}{P} \frac{\partial}{\partial p} \left(\rho^2 g^2 K_m \frac{\partial \theta}{\partial p} \right) \right] \\
- \nabla^2 \frac{R}{P} (K_H \nabla^2 \theta) - \nabla^2 \frac{R}{P} \frac{H}{C_p} + \pi \nabla^2 \frac{\partial \theta}{\partial t} \\
+ f \frac{\partial}{\partial t} \left(\frac{\partial \eta}{\partial p} \right) ,
\end{aligned}
\qquad (16)
$$

$$
\nabla^2 \chi = - \frac{\partial \omega}{\partial p} , \qquad (17)
$$

$$
\frac{\partial \phi}{\partial p} = - \frac{RT}{P} \qquad (18)
$$

The initialization procedure consisted of the following steps:

1. If wind data were available, the u - and v -components were smoothed once in the horizontal by using a 9-point smoothing operator and a coefficient of 0.50, and once in the vertical, over three points, with the top and bottom levels being omitted from the vertical smoothing. Winds on the boundary were not smoothed, but the normal component was set equal to the geostrophic.

2. The divergence equation (14) was solved for the height field, with the analyzed heights being retained on the boundary. At this stage the time-dependent terms and the vertical motion were assumed to be zero.

3. The temperatures were obtained by solving (18) subject to the condition that the temperature at 1000 mb should differ

from the mean virtual temperature for the 1000- to 850-mb layer by a constant value, based on climatology (Jordan, 1958) and the relationship

$$T_* = (1.0 + 0.6\,q)\,T. \qquad (19)$$

4. The balance equation, (15), was solved for the stream function using the method described by Shuman (1957a), with the boundary values for ψ being determined by setting the normal velocity at the boundary equal to the geostrophic wind and requiring that

$$CS + \oint \frac{1}{f}\frac{\partial \phi}{\partial s}\,ds = 0\ , \qquad (20)$$

with C being a small correction applied to insure that both ψ and ϕ return to their original value following the line integral (Bolin, 1956). For all interior points, the original winds were replaced by the rotational winds derived from the stream function.

5. The original winds were retained on the boundary up to this point. To avoid any spurious gradients in the wind field near the boundary, the boundary winds were now smoothed five times, with the normal component being returned to the geostrophic following each smoothing. The smoothing on the boundary resulted in a spurious gradient in the vorticity near the boundary. This was eliminated by adjusting the tangential wind on the boundary in such a way that

$$\oint V_T\,\partial s = \oint V_{gT}\,\partial s_1\ , \qquad (21)$$

where V_{gT} is the tangential geostrophic wind on the inner boundary, s_1 , and V_T is the tangential wind on the outer boundary, s . This adjustment was made to preserve the areal integral of the relative vorticity.

6. Steps 2 through 5 were repeated.

7. Forecasts of u , v , θ , and q were prepared with zero vertical motion. The vertical motion was obtained by

solving (15), subject to the restrictions (Cressman, 1963) that the vertical motion at 1000 mb was determined by

$$\omega_g = \mathbb{V}_g \cdot \nabla p_g + \frac{\rho g}{f} \left[\frac{\partial}{\partial y} C_D u V_o - \frac{\partial}{\partial x} C_D v V_o \right] \qquad (22)$$

and that ω at 100 mb was zero.

8. Steps 2 through 4 were repeated.

9. Equation (17) was solved for the velocity potential, with χ set equal to zero on the boundary. The total wind was obtained by adding the divergent and the rotational components

$$u = -\frac{\partial \psi}{\partial y} + \frac{\partial \chi}{\partial x} \qquad (23)$$

and

$$v = \frac{\partial \psi}{\partial x} + \frac{\partial \chi}{\partial y} \ . \qquad (24)$$

This completes the initialization process. Steps 7 through 9 were repeated at the end of 2 hours and then every 4 hours thereafter. Whether this repetition is too frequent or infrequent has not yet been determined; further experience with the model will tell.

4. NUMERICAL PROCEDURES

The finite difference methods developed by Shuman (1962) and now used at the National Meteorological Center (NMC) in the operational primitive equation forecast model developed by Shuman and Hovermale (1968) were modified slightly and used in our experiment. The variables u , v , w , q , θ , and ϕ were defined at grid points, with averages and first differences being defined between grid points, e.g.,

$$\overline{f}^{x} = \frac{f_{i+1/2} + f_{i-1/2}}{2} \ , \qquad (25)$$

$$f_x = \frac{f_{i+1/2} - f_{i-1/2}}{\Delta X} , \qquad (26)$$

$$\overline{f}^{xx} = \frac{f_{i+1} + 2f_i + f_{i-1}}{4} \qquad (27)$$

In this system, (1) may be written as

$$\overline{u}^t_t = -\overline{m^y\left[\overline{u}^{xy}\overline{u}^y + \overline{V}^{xy}\overline{u}^x_y + \overline{\phi}^x_y\right] - \overline{\omega}^{pp}\overline{u}^{xy} + \overline{f}^y\overline{V}^{xy}}^{xy}$$

$$+ m^2 K_H \nabla^2 u + g \frac{\partial \tau_x}{\partial p} \qquad (28)$$

Equations (2) through (4) are transformed in a similar fashion. In the operational NMC difference system, certain quantities are also averaged with respect to the vertical coordinate. We experimented with vertical averaging and concluded that it was probably undesirable for the tropical atmosphere, although further trials with the model are necessary before a definite decision can be reached. Vertical derivatives for u , v , and q were evaluated by centered differences over two pressure increments. The vertical derivative of θ was determined by noncentered upstream differences, because the use of centered differences nearly always resulted in cooling at the 250-mb level, even when saturated air was rising. This spurious cooling was caused by the strong vertical gradient of potential temperature between 400 and 100 mb, and the use of noncentered upstream differences resulted in a more realistic balance between cooling from adiabatic expansion and warming by the release of latent heat.

The grid length was 140 km at 22.5°N on a Mercator projection. A 21x21 horizontal array and seven vertical levels were used. The geographical region covered by the calculations varied slightly but was essentially that shown in figure 2, extending from 90°W to just east of Bermuda. The north-south extent of the grid ranged from about 11°N to 36°N, or from about 18°N to 42°N. The vertical levels were 1000 mb to 100 mb, with a pressure increment of 150 mb.

The divergence equation for the height field and the equation of continuity for the velocity potential were solved by standard over-relaxation techniques. In both cases, a nine-point approximation to the Laplacian and a relaxation coefficient of 0.087 were used. This scheme has been found more accurate and converges nearly twice as fast as methods based on the more conventional five-point Laplacian (Wurtele and Clark, 1965). The omega equation is generally elliptic, but becomes hyperbolic if the static stability, σ , or the absolute vorticity, η , is negative, although this rarely happens at more than a few points within the network. At grid points where the equation was hyperbolic, the value of a at that point was replaced by the average of the four surrounding horizontal points. A relaxation coefficient of 0.25 was used in the solution of the omega equation. During the forecast period, the omega equation was solved once every 4 hours. At intermediate time steps the divergence was computed from the wind field, and the vertical motion obtained by integrating

$$\frac{\partial^2 \omega}{\partial p^2} = -\frac{\partial D}{\partial p} \quad , \qquad (29)$$

with ω at 1000 mb determined by (23), and $w_{100} = 0$.

Fifteen-minute time steps were used in preparing the forecasts. Because of the length of time required to run the forecast program, it was necessary to stop and restart the forecasts several times during a 24-hour period. Forward time differences were used for the first step each time a forecast was restarted. Otherwise, centered time differences were used for u , v , and θ . Forward time differences were always used in forecasting mixing ratio to conserve computer space, but apparently these caused no difficulties, since mixing ratio was never allowed to exceed the saturated value.

To obtain the geopotential field after each time step, the divergence equation was first summed in the vertical (the numerical equivalent to vertical integration), and the mean geopotential for the seven levels was obtained by relaxation. The geopotential for the seven levels was

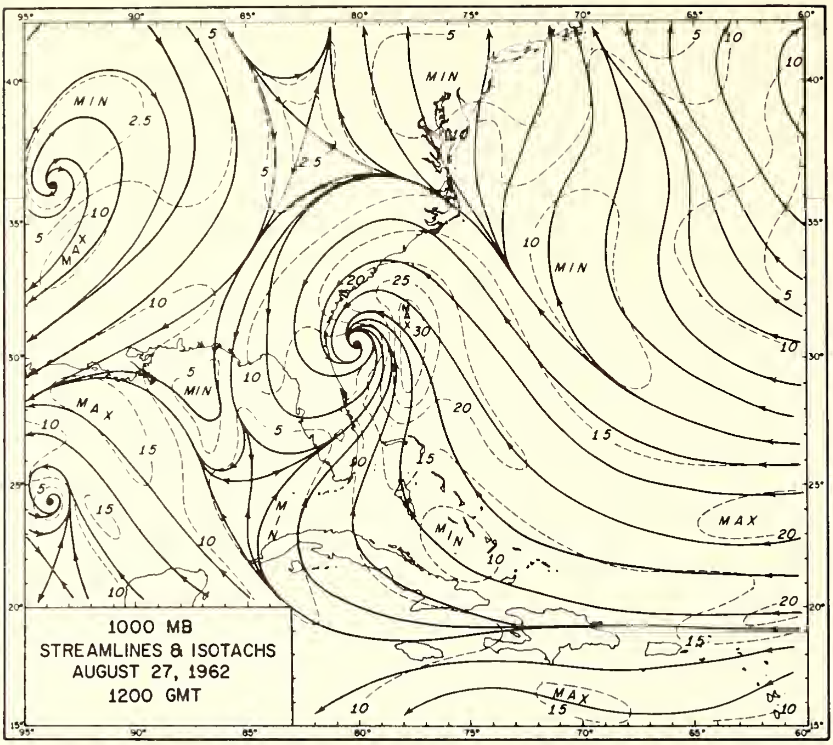

Figure 2a. Initial data for 1200 GMT; August 27, 1962; 1000-mb streamlines.

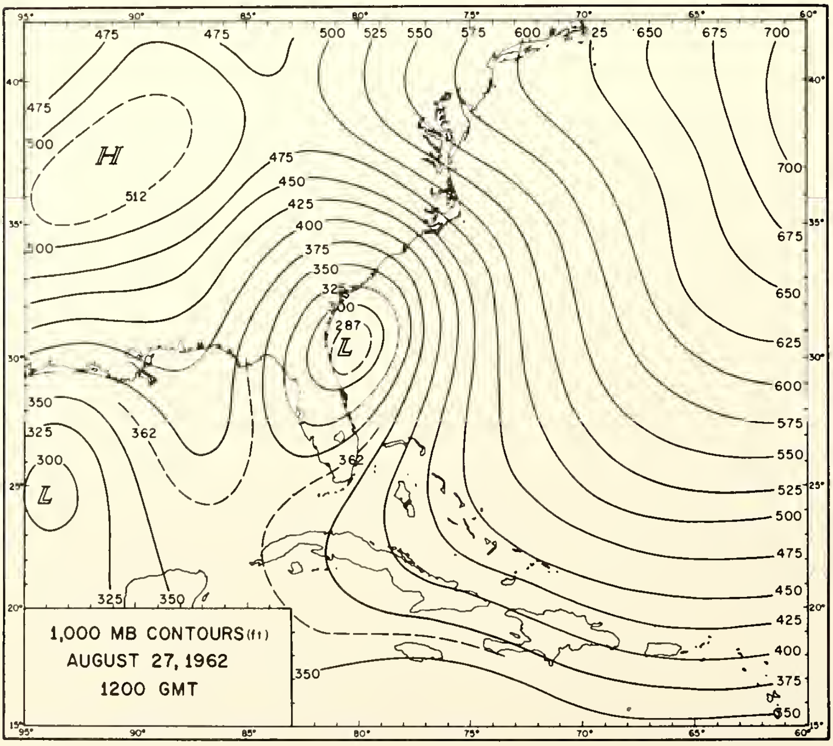

Figure 2b. Initial data for 1200 GMT; August 27, 1962; 1000-mb heights.

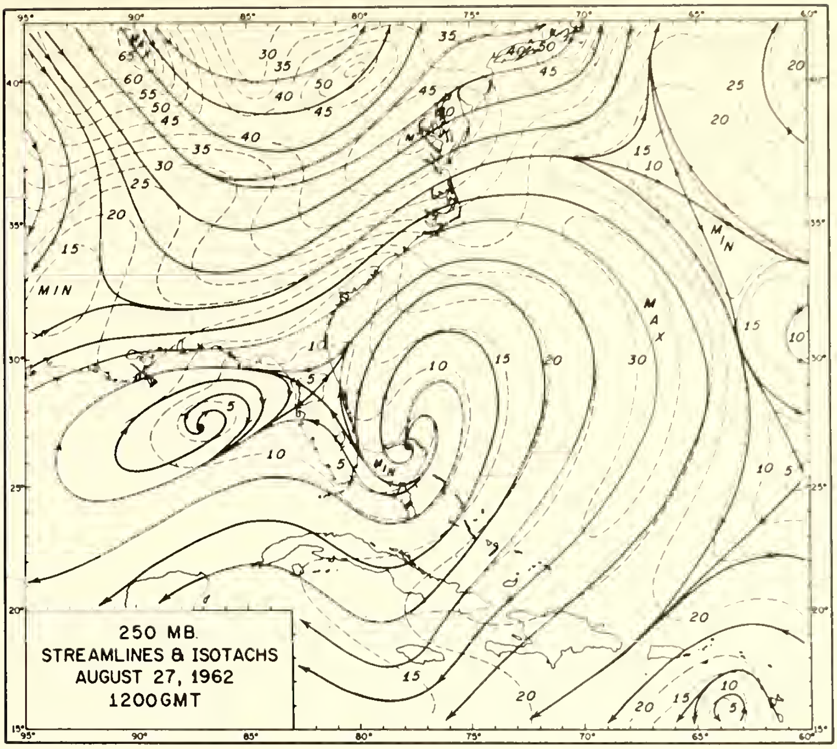

Figure 2c. Initial data for 1200 GMT; August 27, 1962; 250-mb streamlines.

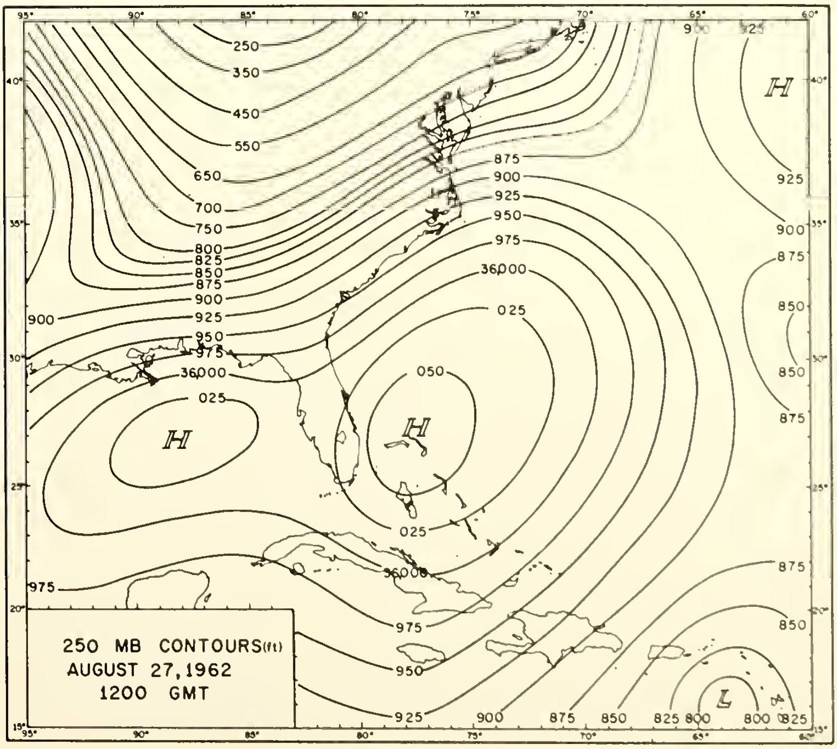

Figure 2d. Initial data for 1200 GMT; August 27, 1962; 250-mb heights.

calculated from the mean virtual temperatures between levels and the mean heights. This procedure avoids the problem of too rapid deepening of the surface vortex that results if the hydrostatic equation is integrated downward to obtain the height field, while the heights of some upper level, say 100 mb are held fixed (Rosenthal, 1964). Conversely, if one integrates upward, after having determined the heights of the 1000-mb surface in some way (e.g., by relaxation of the divergence equation after forecasting the winds at that level), warming of the tropical atmosphere at some upper level will result in an unrealistically large rise in the height of the 100-mb surface. The methods used here seem to eliminate both difficulties, and warming of the atmosphere results in moderate deepening at the surface and a small rise in the height of the 100-mb surface.

Our prediction model has been tested on a relatively small geographical area because of the relatively small computer available to NHRL. Influences outside the boundary can and usually do affect forecasts inside an area of this size within 24 hours. For this reason the model needed a time-dependent lateral boundary, with values on the boundary being supplied by the forecast of the broad scale motion; however, the problem of meshing a forecast from a small area and grid with that from a larger area and grid has not been satisfactorily resolved.

In testing the model, forecasts could be made in two ways, i.e., with boundaries held fixed or specified from known values obtained from successive analyses. The boundaries in the following two experiments were kept constant during the forecast period.

5. DEVELOPMENT OF HURRICANE ALMA (1962)

The disturbance that grew into Hurricane Alma was first sighted by TIROS V in the eastern Atlantic on August 14, 1962 (Dunn and staff, 1963). Four days later a weak center was located by aircraft near 12.5°N, 51°W, and by August 21 it had reached the Lesser Antilles (fig. 3). Little or no development occurred until the morning of August 26, when deepening began off the east coast of Florida. The center progressed north-northeastward, reached tropical storm intensity on the 27th, and became a hurricane north of the Virginia Capes for about 12 hours, with the maximum sustained winds of 80 kt being reported by reconnaissance aircraft (Dunn and staff, 1963). The lowest reported sea level pressure in the center of the hurricane was about 988 mb.

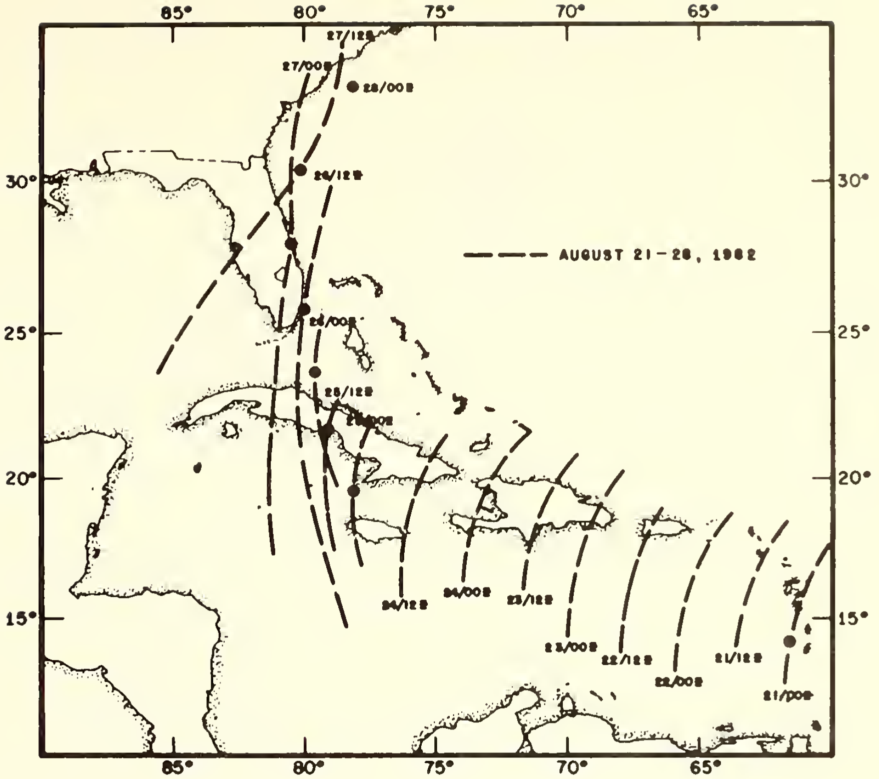

Figure 3. Positions of the wave axis at the 1000-mb surface, August 21-27, 1962. Crossed circles indicate positions of the vortex center (Lateef and Smith, 1967).

The initial data used in this experiment covered the 3-day period August 25-27. The data were analyzed for another purpose (Lateef and Smith, 1967) and were not specifically prepared for this model. Streamline, isotach, and height analyses were performed for the seven levels, and mixing ratio for five levels up to 400 mb. At 250 and 100 mb, mixing ratios were computed on the basis of an assumed relative humidity of 60 percent. The air-sea temperature difference was assumed to be a constant 2°C, and the differences between the air-sea dew point temperatures were assumed to be 3°C, since no water temperatures were available. Temperatures were computed from the geopotential field, with all other initial data being taken from the analyses.

The first portion of the experiment began with data for 1200 GMT, August 27, when the center of the disturbance was located just off the northeast Florida coast. Maximum winds were about 30 kt east of the center, and the minimum sea level pressure was about 1006 mb. The first advisory, issued at 1830 GMT, stated that maximum winds were 30 to 40 mph east of the center, with a few squalls of 45 mph. The initial streamline and height analyses for the 1000-mb and 250-mb levels are shown in figure 2.

5.1 Evolution of Wind and Pressure Systems

During the initialization process, the low level vortex was weakened slightly. At the end of 30 min the central pressure had risen a little less than 2 mb. No significant changes in intensity were observed for the next several hours, but deepening began during the 6-to 12- hour portion of the forecast, and at the end of 12 hours the central pressure was about 1004 mb, and the maximum winds were again about 30 kt. Slow intensification continued for several hours, with rapid deepening taking place during the last 3 or 4 hours of the 24-hour forecast. The forecast winds at 1000, 850, and 240 mb are shown in figure 4. The forecast heights for 1000 and 250 mb are shown in figure 5, and the forecast height changes for these two levels are shown in figure 6.

At the end of 24 hours (fig. 7) the low level vortex had deepened to about 993 mb and moved north-northeastward to the northeastern North Carolina coast. Maximum winds at 1000 mb were about 50 kt, but at 850 mb a maximum of 60 kt was present to the east of the center. The vertical shear was apparently due to frictional influences, since the intensity of the vortex at 1000 mb was slightly more than it was at 850 mb, i.e., the system was warm core. At 250 mb the flow was anticyclonic over and to the east, south of the surface center. The characteristic low level inflow and high level outflow are evident from the streamline

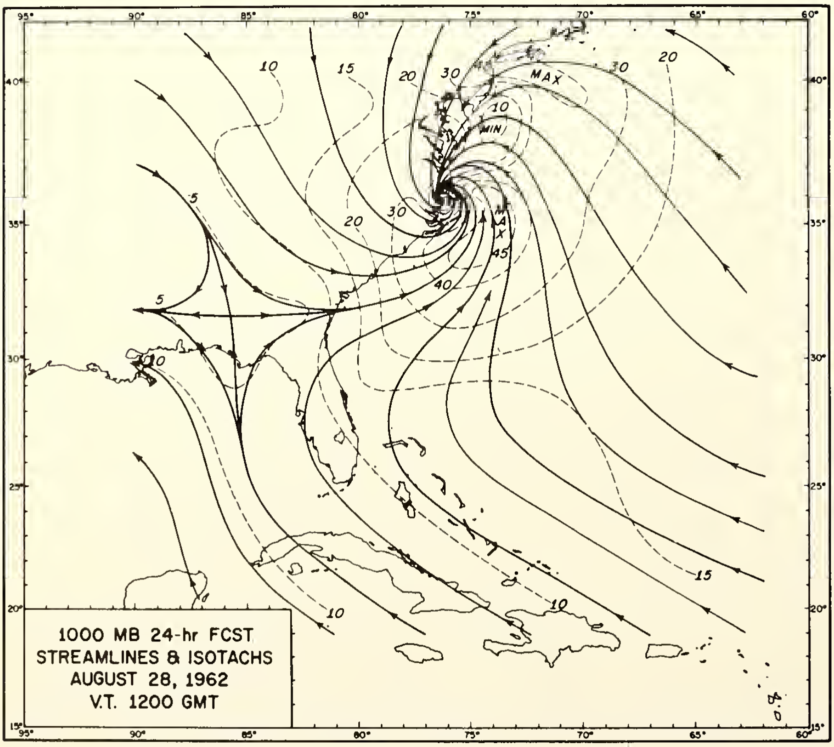

Figure 4a. A 24-hour forecast of the winds at 1000 mb.

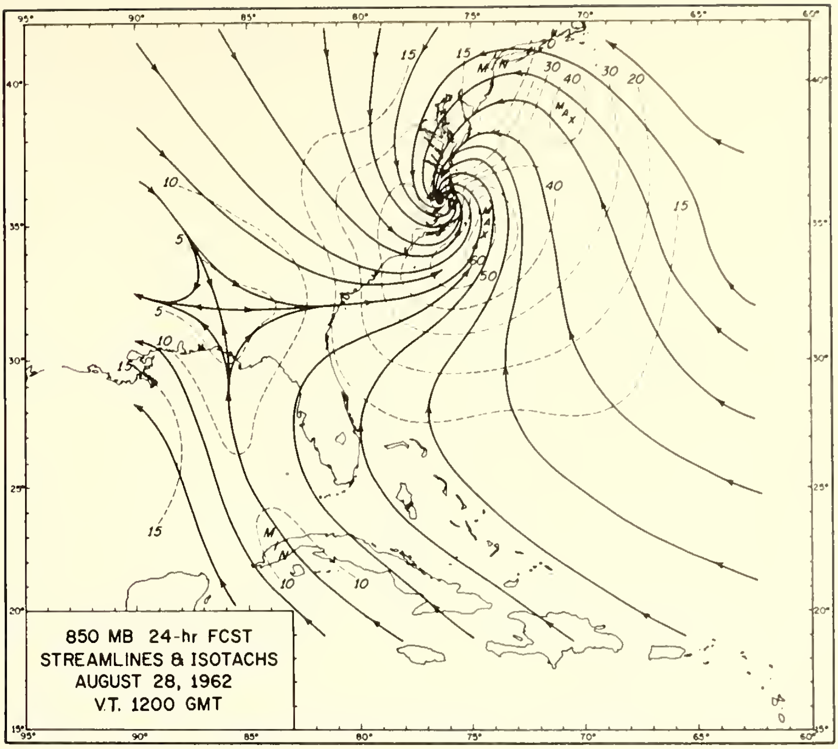

Figure 4b. A 24-hour forecast of the winds at 850 mb.

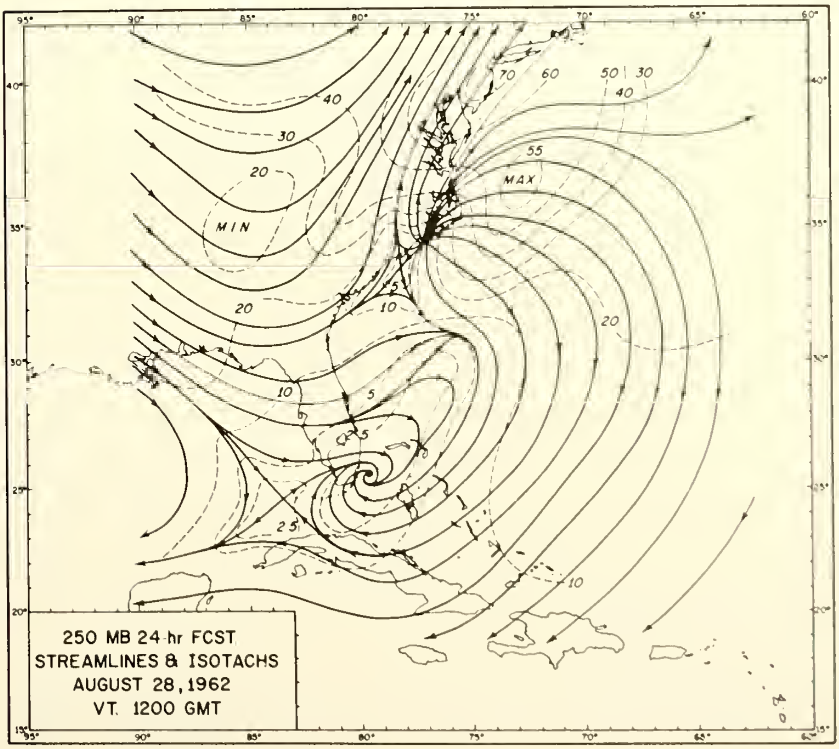

Figure 4c. A 24-hour forecast of the winds at 250 mb.

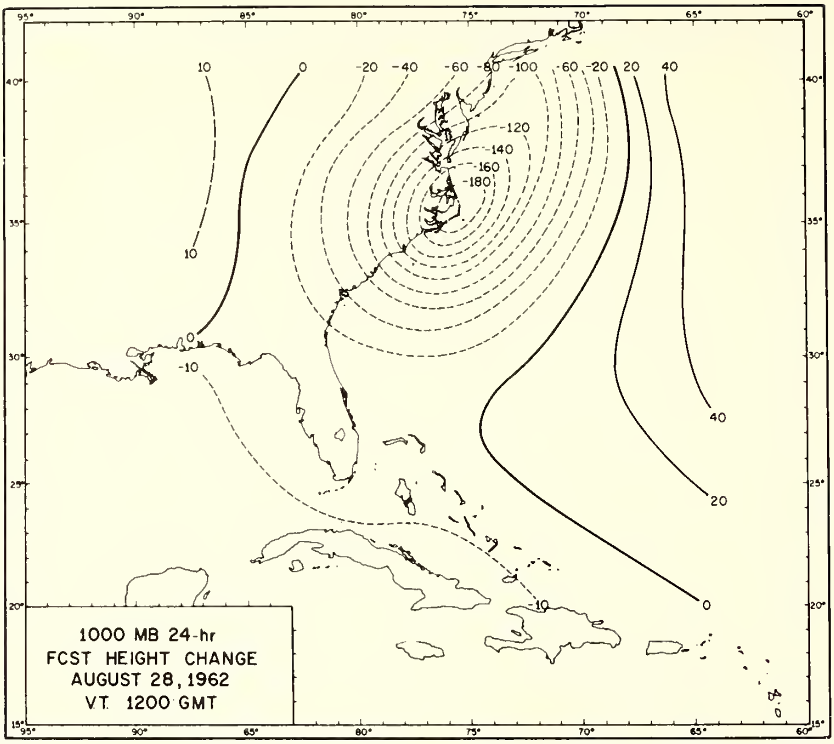

Figure 5a. Twenty-four-hour forecast heights (meters, departure from mean tropical atmosphere) at 1000 mb.

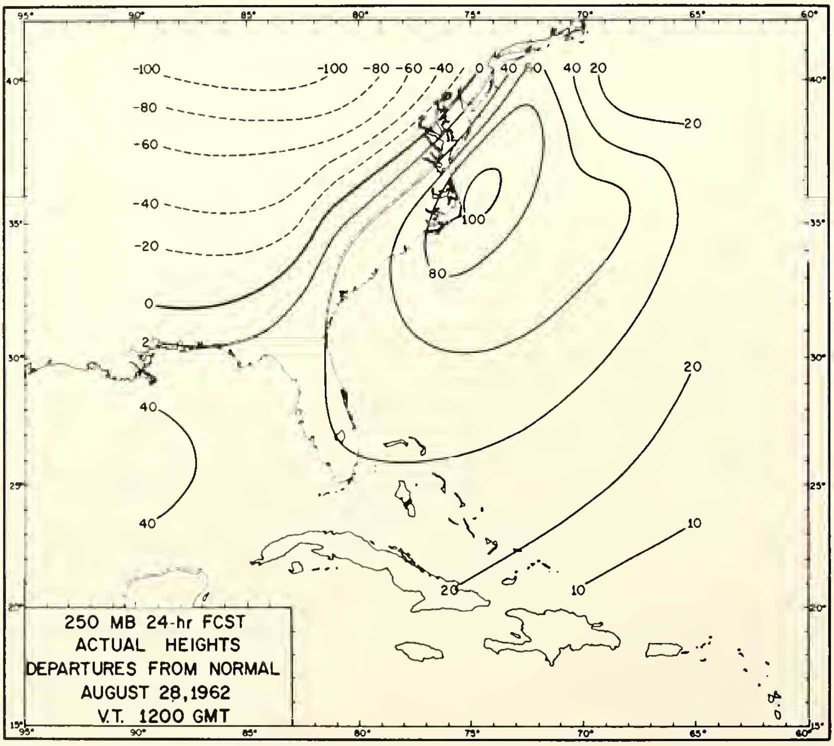

Figure 5b. Twenty-four-hour forecast heights (meters, departure from mean tropical atmosphere) at 250 mb.

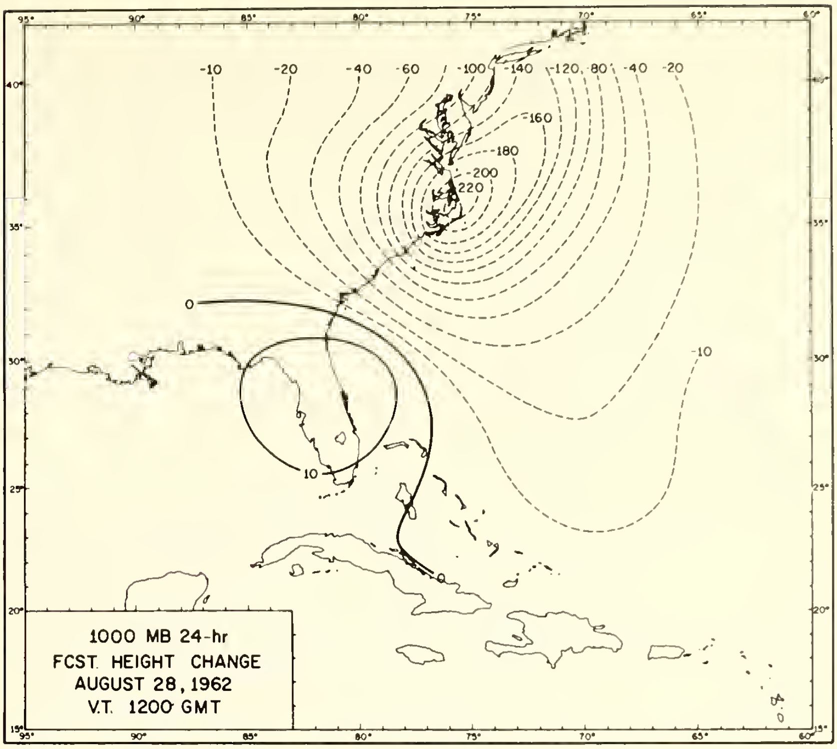

Figure 6a. Twenty-four-hour height changes (meters) at 1000 mb.

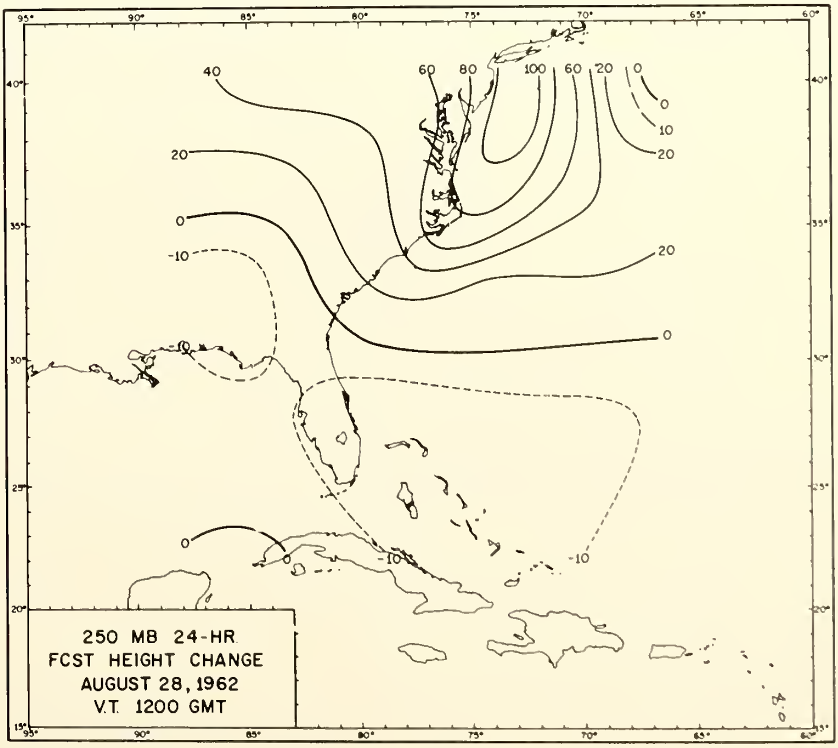

Figure 6b. Twenty-four-hour height changes (meters) at 250 mb.

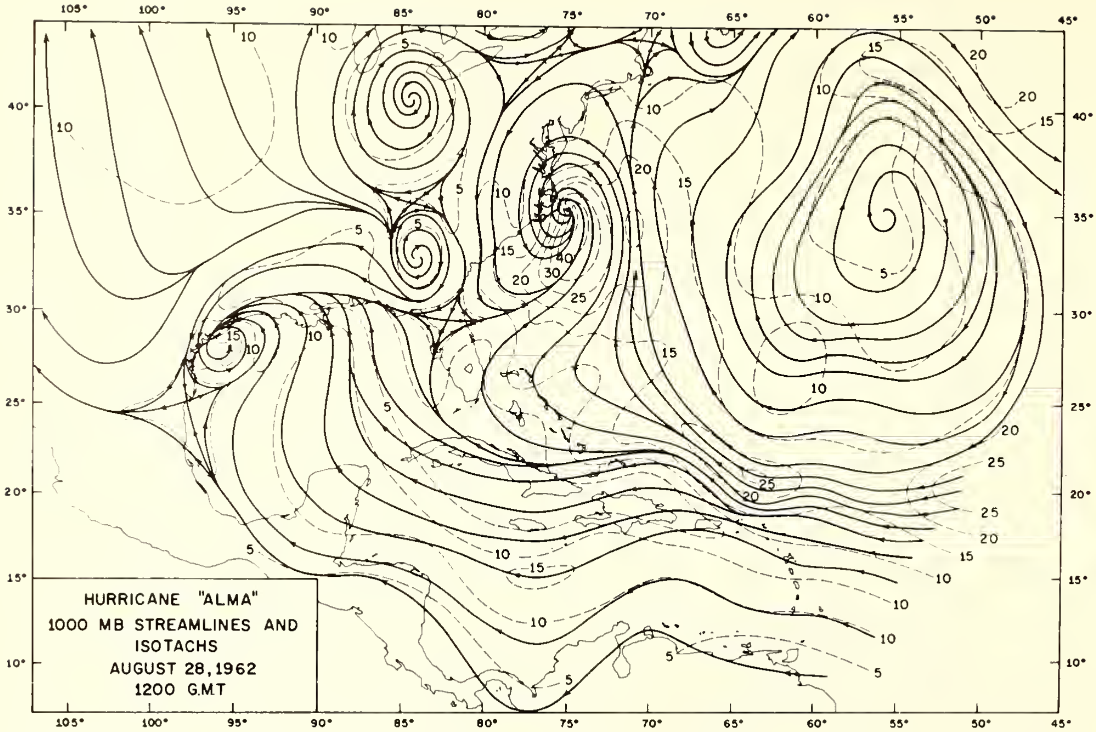

Figure 7a. One-thousand-mb streamlines and isotachs for 1200 GMT; August 28, 1962.

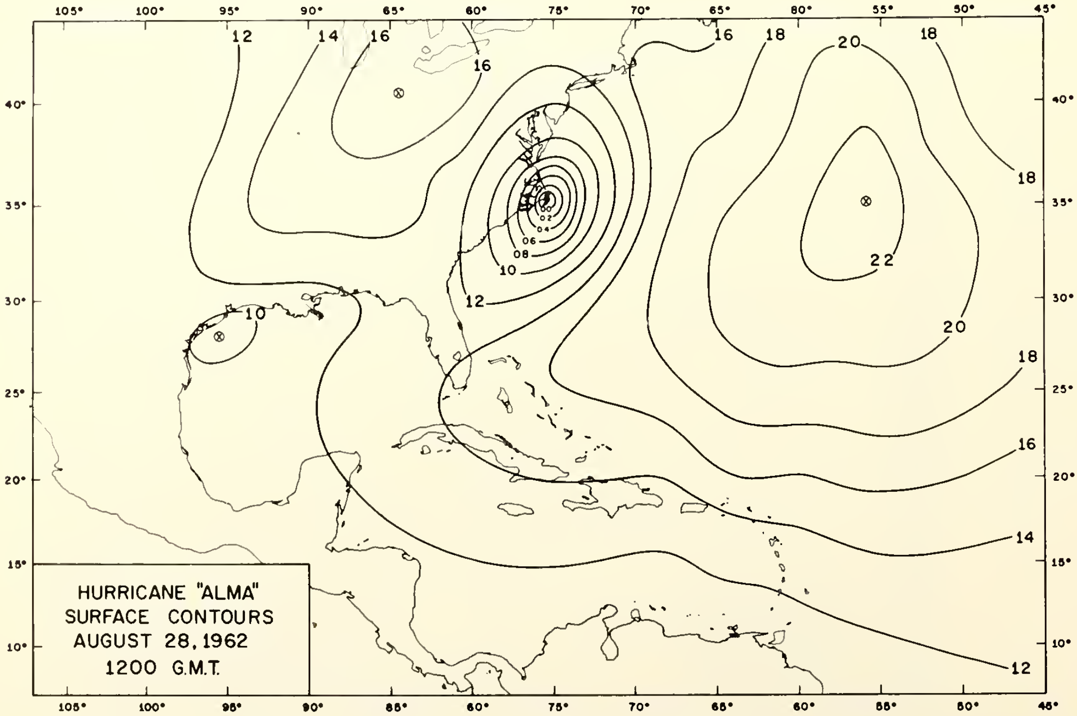

Figure 7b. Sea level pressure for 1200 GMT; August 28, 1962.

analyses (fig. 4). The average inflow at 1000 mb at a radius of three grid lengths was about 14 kt, while the average outflow at 250 mb was nearly 21 kt. These values are typical (see Miller, 1962; 1964; 1965; Colon, 1961). The advisory issued at 1600 GMT, August 28, stated that maximum winds were about 60 mph (52 kt), but later in the afternoon reconnaissance aircraft reported winds of 80 kt, and Alma had reached hurricane status. The low level center at the end of 24 hours was near 36.0°N, 76.0°W, while the best track position at 1200 GMT, August 28, was 35.2°N, 75.3°W. This is slightly to the left of the observed track, which is probably to be expected, since the boundaries were held constant during the forecast.

Initially there was an anticyclone at 250 mb to the southeast of the surface vortex (see fig. 2). At the end of the forecast period, the maximum heights at 250 mb were near - slightly to the east and northeast of - the surface center (fig. 5). This does not appear to be the same anticyclone, but a new development created by the release of latent heat. It is interesting to compare our results with the hypothesis expressed by Dunn and staff (1963).

> "At 200 mb, a possible contributing cause of the eventual intensification was noted. On August 22-23 an anticyclone at 200 mb was moving through the Lesser Antilles some 600 mi. to the east of the surface disturbance. Both systems moved at about 10 kt through August 24, maintaining about the same distance between them (fig. 8). During the period August 24-26 the anticyclone accelerated to about 17.5 kt with the surface Low continuing at 10 kt. Development began when the upper High reached a position within 200 mi of the surface system. Apparently surface deepening began to influence the upper anticyclone as well, since there was considerable intensification of it on the 26th. On August 27-28 Alma began to develop its own upper anticyclone. A well developed upper High noted on the 28th just east of the tropical cyclone definitely was not the one which had been previously tracked. It is not maintained that this is the complete explanation of the development of the tropical cyclone but it may have been an important contributing factor."

The results of our prediction model seem to support Dunn's explanation. Height rises of around 100 m in 24 hours were forecast at 250 mb northeast of the surface vortex (fig. 6).

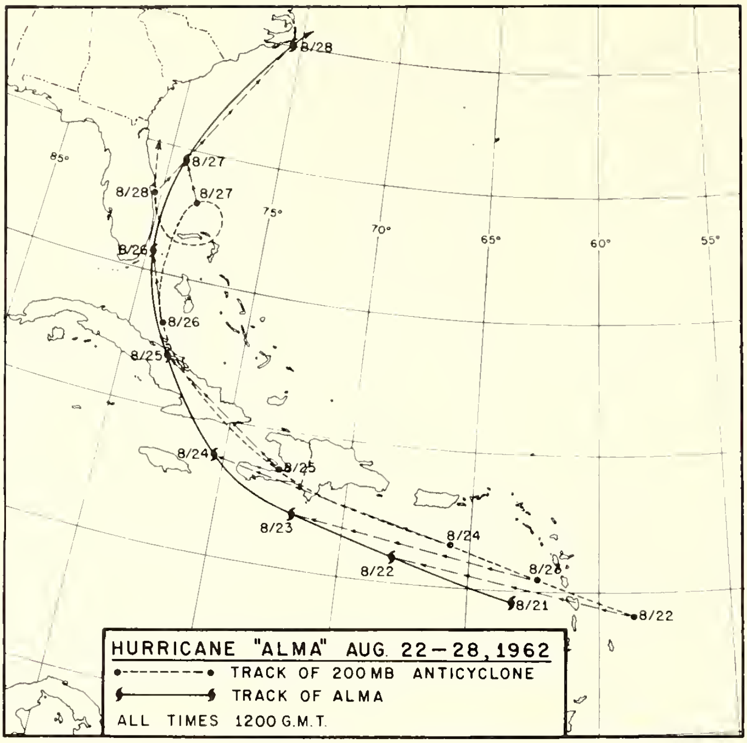

Figure 8. Tracks of surface vortex and 200-mb anticyclone, August 22-28, 1962 (Dunn and staff, 1963).

At the 1000-mb level, falls of about 225 m (equivalent to a pressure drop of about 25 mb) were forecast just off the North Carolina coast. Actual 24-hour pressure falls of this magnitude were observed in that area.

5.2 Thermal Structure

Numerous case studies of tropical cyclones, based on aircraft data collected during the past 12 years, have confirmed that the development of tropical cyclones is accompanied by intense warming of the upper troposphere (Colón and staff, 1961; Yanai, 1961; LaSeur and Hawkins, 1963; Hawkins and Rubsam, 1968). Our model successfully predicted the upper level warming (figs. 9 and 10).

Figure 9 shows the 24-hour temperature changes that were forecast at 250 mb. Maximum warming was of the order of 10° to 12°C, which is realistic for a minimal hurricane, but the geographical area covered by the warming is too large because the grid size (140 km) is too large to permit good resolution of the hurricane scale motion. The low level vortex (fig. 5) is also too large in diameter. As the vortex

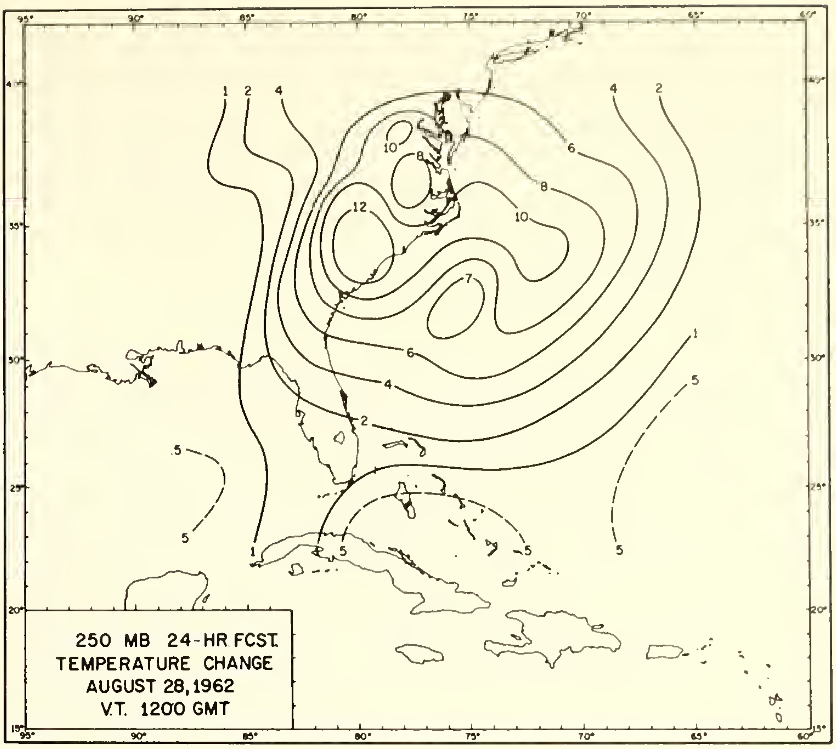

Figure 9. Twenty-four-hour temperature forecast (°C) at 250 mb.

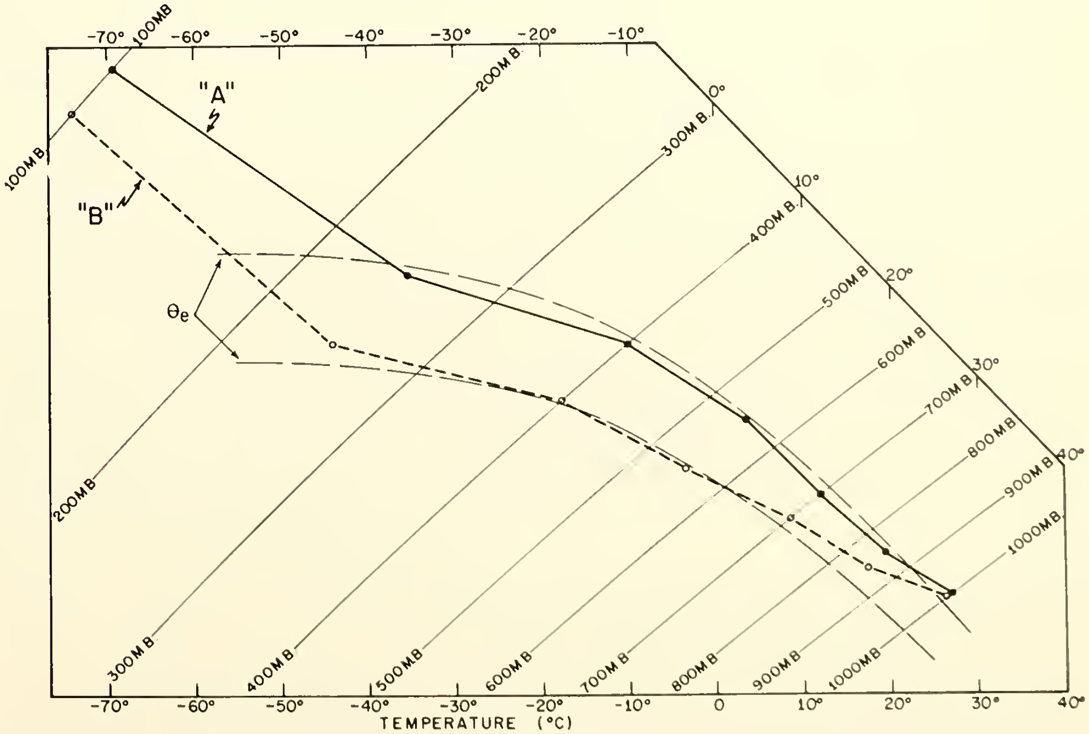

Figure 10. Forecast temperatures at point of lowest pressure, Curve A, compared with mean tropical sounding, Curve B.

progressed northward, a region of strong downward motion developed to the rear of the center. This is a realistic phenomenon, and part of the warming to the south of the surface center can be attributed to warming by subsidence. Another interesting feature is the relative minimum in the amount of warming over land just west of the surface center, which probably can be attributed to the absence of the oceanic heat source (Miller, 1964).

Two soundings have been plotted in figure 10: "A", taken from the 24-hour forecast at the point of lowest pressure, and "B" taken from Jordan's (1958) mean sounding for the hurricane season. Curve "A" is realistic as to amount of warming and lapse rate up to 250 mb. Above 250 mb, it is much too stable because the 100-mb temperature is too warm. This reflects a defect in the model - no provision has been made to allow strong cooling at 100 mb as the hurricane develops (e.g., Gentry, 1967; Koteswaram, 1967), which causes an unrealistic rise in the height of the 100-mb surface. This rise can probably be corrected by including radiational cooling and revising the model to allow vertical motion at the 100-mb level.

6. SOME OTHER RESULTS

Three additional forecasts have been made. One was based on the Alma data with initial time 48 hours earlier than the forecast described in preceding sections. At that time (1200 GMT, August 25) a weak vortex was located near the north coast of Cuba (fig. 8). There was little or no development for the first 15 hours, but at the end of 17 hours the forecast "blew up", apparently because the omega equation failed to converge during the balancing procedure after 16 hours. The forecast was terminated after 17 hours.

Both forecasts were rerun after the following changes had been made in the input parameters:

1. The air-sea temperature difference was reduced from 2.0°C to 1.5°C.

2. The value for the eddy viscosity for vertical mixing was reduced by one-third.

3. Heating due to the large scale vertical motion (12) was not permitted unless the relative humidity was 100 percent. In addition, the maximum value for this heating was set equal to $-L/C_p \, \partial q_s/\partial t$, which greatly reduced the influence of the heating from the large scale vertical motion.

Forecasts for both days (1200 GMT, August 25 and 1200 GMT, August 27) were rerun out to 24 hours. In both cases, the initial vortex moved in an approximately steady state with little or no changes in intensity during the forecast period. Movement in both cases, however, was forecast quite well.

7. SUMMARY AND CONCLUSIONS

Only limited conclusions can be drawn from these results, since the forecast domain was rather small. However, it is perhaps safe to say that the features forecast in the developing case were too realistic to be purely accidental. These features included good forecasts of low level inflow, high level outflow, upper level warming, and the development of an upper level anticyclone, intensification of the surface vortex, and a movement that resulted in an error somewhat less than one-half that which is considered acceptable in 24-hour forecasts (Dunn et al., 1968).

Future experiments include testing the model on additional cases and use of a bigger forecast domain. Attempts should be made to evaluate the time-dependent terms in the divergence and omega equations, and the effects of the air-sea temperature differences on both development and movement should be investigated on the basis of real sea surface temperature data, where available. Effects of the large scale vertical motion on development or nondevelopment should also be assessed.

8. ACKNOWLEDGMENTS

I am indebted to Mr. Clark L. Smith, who prepared the analyses used as initial data, and to Messrs. Peter P. Chase, Billy M. Lewis, and Eugene M. Page who offered numerous suggestions on mathematical and programming problems. Dr. Stanley L. Rosenthal suggested the method of obtaining the forecast height field by simultaneous solution of the divergence and hydrostatic equations.

9. REFERENCES

Barrientos, C. S. (1964), "Computations of transverse circulations in a steady state symmetric hurricane," J. Applied Meteorol. 3, 685-692.

Bolin, B. (1956), "An improved barotropic model and some aspects of using the balance equation," Tellus 8, 61-75.

Charney, J. (1962), "Integration of the primitive and balance equations," Proc. Inter. Symp. Numerical Weather Prediction, Tokyo, November 7-13, 1960, Japan Meteorological Agency, Tokyo, 131-151.

Colon, J. A. and staff (1961), "On the structure of Hurricane Daisy," National Hurricane Research Project Rept. No. 48, 102 pp.

Cressman, G. P. (1963), "A three-level model suitable for daily numerical forecasting," Tech. Memo. NMC-22, 43 pp.

Dunn, G. E. and staff (1963), "The hurricane season of 1962," Monthly Weather Rev. 91, 199-207.

Dunn, G. E., R. C. Gentry and B. M. Lewis (1968), "An eight-year experiment in improving forecasts of hurricane motion," Monthly Weather Rev. 96, 708-713.

Gentry, R. C. (1967), "Structure of the upper troposphere and lower stratosphere in the vicinity of Hurricane Isbell, 1964," Papers Meteorol. Geophys. 18, No. 4. 293-310.

Hawkins, H. F. and D. T. Rubsam (1968), "Hurricane Hilda, 1964: Part I. Genesis as revealed by satellite photographs, conventional and aircraft data," Monthly Weather Rev. 96, 428-452.

Jordan, C. L. (1958), "Mean soundings for the West Indies area,' J. Meteorol. 15, 91-97.

Koteswaram, P. (1967), "On the structure of hurricanes in the upper troposphere and lower stratosphere," Monthly Weather Rev. 95, 541-564.

Krishnamurti, T. N. and D. Baumhefner (1966), "Structure of a tropical disturbance based on solutions of a multi-level baroclinic model," J. Applied. Meteorol. 5, 396-406.

Kuo, H. L. (1965), "On formation and intensification of tropical cyclones through latent heat release by cumulus convection," J. Atmospheric Sci. 22, 40-63.

LaSeur, N. E. and H. F. Hawkins (1963), "An analysis of Hurricane Cleo (1958) based on data from research reconnaissance aircraft," Monthly Weather Rev. 91, 694-709.

Lateef, M. A. and C. L. Smith (1967), "A synoptic study of two tropical disturbances in the Caribbean," ESSA Tech. Memo. IERTM-NHRL 78, 33 pp.

Manabe, S. and J. Smagorinsky (1967), "Simulated climatology of a general circulation model with a hydrologic cycle: II. Analysis of the tropical atmosphere," Monthly Weather Rev. 95, 155-169.

Miller, B. I. (1958), "On the maximum intensity of hurricanes," J. Meteorol. 15, 184-195.

Miller, B. I. (1962), "On the momentum and energy balance of Hurricane Helene (1958)," NHRL Rept. No. 53, 19 pp.

Miller, B. I. (1964), "A study of the filling of Hurricane Donna (1960) over land," Monthly Weather Rev. 92, 389-406.

Miller, B. I. (1965), "A simple model of the hurricane inflow layer," NHRL Rept. No. 75, 16 pp.

Miller, B. I. (1967), "Characteristics of hurricanes," Science 157, 1389-1399.

Miyakoda, K. and R. W. Moyer (1968), "A method of initialization for dynamical forecasting," Tellus 20, 113-128.

Nitta, T. and J. B. Hovermale (1967), "On analysis and initialization for the primitive equation forecasts," Weather Bureau Tech. Memo. NMC-42, 24 pp.

Ooyama, K. (1967), "Numerical simulation of the life cycle of tropical cyclones," Dept. of Meteorol. and Oceanography. New York Univ., 133 pp.

Palmen, E. and E. O. Holopainen (1963), "Divergence, vertical velocity and conversion between potential and kinetic energy in an extratropical disturbance," Geophysica 8, No. 2, 89-112.

Petterssen, S., D. L. Bradbury, and K. Pedersen (1962), "The Norwegian cyclone model in relation to heat and cold sources," Geophysica Norveqica 24, 243-280.

Phillips, N. (1960), "On the problem of initial data for the primitive equations," Tellus 12, 121-126.

Rosenthal, S. L. (1964), "Some attempts to simulate the development of tropical cyclones by numerical methods," Monthly Weather Rev. 92, 1-21.

Rosenthal, S. L. (1969), "Numerical experiments with a multilevel primitive equation model designed to simulate the development of tropical cyclones, Experiment I. (in press)

Shuman, F. G. (1957a), "Numerical methods in weather prediction: I. The balance equation," Monthly Weather Rev. 85, 329-332.

Shuman, F. G. (1957b), "Numerical methods in weather prediction: II. Smoothing and filtering," Monthly Weather Rev. 85, 357-361.

Shuman, F. G. (1962), "Numerical experiments with the primitive equations," Proc. Inter. Symp. Numerical Weather Prediction, Tokyo, November 7-13, 1960, Japan Meteorological Agency, Tokyo, 85-107.

Shuman, F. G. and J. B. Hovermale (1968), "An operational six-layer primitive equation model," J. Appl. Meteorol. 7, 525-547.

Wurtele, M. G. and C. Clark (1965), "The relative efficiency of certain schema in the solution of a Poisson equation," J. Atmospheric Sci. 22, 436-439.

Yanai, M. (1961), "A detailed analysis of typhoon formation," J. Meteorol. Soc. Japan 39, 187-214.

44

U.S. DEPARTMENT OF COMMERCE
Environmental Science Services Administration
Research Laboratories

ESSA Technical Memorandum ERLTM-NHRL 87

EXPERIMENTS WITH A NUMERICAL MODEL OF TROPICAL CYCLONE DEVELOPMENT. SOME EFFECTS OF RADIAL RESOLUTION

Stanley L. Rosenthal

National Hurricane Research Laboratory
Miami, Florida
August 1969

TABLE OF CONTENTS

Page

ABSTRACT 1

1. INTRODUCTION 1

2. REVIEW OF MODEL 1

3. DESIGN OF EXPERIMENTS D10 AND D20 4

4. LIFE CYCLE AND STRUCTURE AT SEA LEVEL 4

5. VERTICAL CROSS SECTIONS 12

6. PRECIPITATION AND EFFICIENCY 12

7. GENERATION OF AVAILABLE POTENTIAL ENERGY 19

8. KINETIC ENERGY BUDGETS 19

9. LATERAL MIXING AND PSEUDO-VISCOSITY 23

10. SUMMARY AND DISCUSSION 32

11. ACKNOWLEDGMENTS 36

12. REFERENCES 37

APPENDIX 39

EXPERIMENTS WITH A NUMERICAL MODEL OF TROPICAL CYCLONE DEVELOPMENT. SOME EFFECTS OF RADIAL RESOLUTION

Stanley L. Rosenthal

Experiments with 10-km and 20-km radial resolution are compared. The 10-km calculation yields a storm with more realistic structure. The 20-km case does not contain a well-defined eye, whereas the 10-km experiment does. Rainfall, kinetic energy production, and efficiency are all larger with 20-km resolution. In both experiments, computational damping is an important component of the kinetic energy budget; however, the total dissipation of kinetic energy (computational plus explicit) is fairly reasonable in comparison to that found in empirical studies. This result provides an estimate of the eddy viscosity coefficients, which would be needed to obtain realistic results with a nondissipative numerical model.

1. INTRODUCTION

A recent report (Rosenthal, 1969) described our tropical cyclone model and showed the results of a preliminary calculation (Experiment I). We concluded that the model could simulate the life cycle of tropical cyclones with some degree of reality despite obvious deficiencies. Prominent among these was the rather coarse radial resolution (20 km between grid points) that had been adopted for computational economy.

For purposes of comparison, the results of an experiment with 10-km resolution are presented in section 2. Because economic considerations dictate that we continue to use 20-km resolution for test calculations, the material presented here is an important benchmark for assessing the effects of resolution errors.

2. REVIEW OF THE MODEL

For details concerning the model, the reader is referred to our earlier report (Rosenthal, 1969).[1] We assume the storm to be circularly symmetric. The vertical coordinate is geometric height; table 1 lists the information levels.

Table 1. Heights and Mean Pressures of the Information Levels.

Level	Height (m)	Mean Pressure (mb)*
1	0	1,015
2	1,054	900
3	3,187	700
4	5,898	500
5	9,697	300
6	12,423	200
7	16,621	100

*The mean pressures are approximate and are based on a mean hurricane season sounding (Hebert and Jordan, 1959).

Dependent variables are defined at all levels. At the radial limit of the computational domain (440 km), the system is open, and the boundary conditions are zeros for relative vorticity, horizontal divergence, and radial gradient of potential temperature. At level 1, the vertical motion is zero. The vertical integral of the mass divergence from level 1 to level 7 is also required to be zero. This, with a simplified form of the continuity equation (see app.), forces the vertical motion to vanish also at level 7.

Air-sea exchanges of sensible and latent heat are treated implicitly through steady-state assumptions for relative humidity and temperature at the two lowest levels.

Cyclone-scale heating, attributable to the presence of organized systems of cumulonimbi, is simulated by a convective adjustment of the lapse rate toward a pseudoadiabat representative of parcel ascent from the surface boundary layer. The rate at which this adjustment is allowed to take place is determined by the constraint that all water vapor converging in the boundary layer rises in convective clouds, condenses, and falls out as rain (see app.). For activation of the convective heating function, the required conditions are boundary layer convergence and conditional instability for parcels rising from the boundary layer.

---

[1] The appendix to this report summarizes the basic equations and the computational cycle.

After convection has been operative for some time, lapse rates become coincident with the reference pseudoadiabat (see Rosenthal, 1969, fig. 8). In Experiment I, the release of latent heat was terminated when this occurred. The so-called "large-scale" precipitation to be expected with macroscale ascent of statically stable, or neutral, saturated air was, therefore, neglected. The new experiments attempt to include this second source of latent heat by use of a technique employed in previous hurricane models (Yamasaki, 1968).[2]

"Large-scale" precipitation is activated only after convection has neutralized the conditional instability along a vertical. When the macroscale vertical motion is upward along such a vertical, the macroscale relative humidity is assumed to be 100 percent. Except for the effects of eddy diffusivity (which are ignored for this purpose) the macroscale motion must then be along a pseudoadiabat which coincides with the actual thermal stratification of the atmosphere, and, therefore, adiabatic cooling is exactly balanced by "large-scale" condensation; the temperature at a given point in space is, therefore, unaffected.

The numerics of the model are extremely simple: advection terms are calculated by upstream differences, and time derivatives are estimated by forward differences; nonadvective space derivatives are calculated as centered differences. This scheme contains substantial computational damping. As partial compensation for the numerical damping, dissipative effects associated with vertical mixing of momentum by small-scale eddies are neglected (except at the air-sea interface where they are treated as drag). Further discussion on this point is found in section 9.

---

[2] While a series of experiments to be reported on at a future date includes an explicit prediction of the specific humidity, neither Experiment I nor the new experiments described here include specific humidity as a dependent variable. The assumptions which allow us to proceed without an explicit forecast of water vapor have already been listed: the time invariance of the boundary layer relative humidity, and the requirement that all water vapor that converges in the boundary layer rises in convective clouds, condenses, and falls out as rain. It is further assumed that the boundary layer relative humidity is 100 percent.

Grid points in the radial direction are staggered. Horizontal velocity is defined at the radii

$$r_j = (j-1)\Delta r, \quad j = 1, 2 \text{---}. \tag{1}$$

where Δr is the grid increment. Temperature, pressure and vertical motion are defined at

$$r_j = (j-\tfrac{1}{2})\Delta r, \quad j = 1, 2 \text{---}. \tag{2}$$

3. DESIGN OF EXPERIMENTS D10 AND D20

The two new experiments are designated D10 and D20. Except for the release of latent heat by large-scale precipitation (see sec. 2), the physics of D10 and D20 are identical to Experiment I; D10 and D20 differ from each other only in the radial and temporal increments. Basic parameters for the three experiments are summarized in table 2. Initial conditions are identical and consist of a weak, nondivergent vortex in gradient balance. The method by which this state of balance is achieved has already been described (Rosenthal, 1969). Strongest winds at the initial instant are about 7 m-sec^{-1} and are located at a radius of 250 km; the central pressure at this time is 1013 mb.

4. LIFE CYCLE AND STRUCTURE AT SEA LEVEL

The evolution of central pressure[3] and maximum surface wind for Experiments I and D20 are shown in figure 1. We find differences only after 168 hours, when D20 is somewhat more intense. This difference is entirely due to the large-scale precipitation included in D20 but not in Experiment I. Before 144 hours, precipitation in both experiments is entirely convective. Thereafter, D20 is supplied latent heat by both types of precipitation, whereas Experiment I receives energy only through the convective release of latent heat. The latter process supplies energy in continually decreasing amounts as more

---

[3] Pressure is not defined at zero radius because of the grid staggering (eqs. (1) and (2). For experiments I and D20. central pressure is pressure at z =0, r =10 km. For Experiment D10, central pressure is that at z =0, r =5 km.

Table 2. Some Experimental Parameters.

Parameter	Experiment I	Experiment D20	Experiment D10
Kinematic coefficient of eddy viscosity and/ or eddy conductivity for lateral mixing	$10^4 m^2$-sec^{-1}	same	same
Kinematic coefficient of eddy viscosity for vertical mixing	$10 m^2$-sec^{-1} at level 1; zero elsewhere	same	same
Drag coefficient	3×10^{-3}	same	same
Coriolis parameter	$5 \times 10^{-5} sec^{-1}$	same	same
Time increment	120 sec	120 sec	60 sec
Radial increment	20 km	20 km	10 km
Radial extent of computational domain	440 km	same	same
Latent heat by large-scale precipitation	no	yes	yes

more of the storm is neutralized with respect to pseudoadiabatic ascent (Rosenthal, 1969, fig. 6)

The analogous data for Experiment D10 are shown in figure 2. Differences between D10 and D20 are relatively minor. Peak intensity for D10 is reached about 24 hours earlier than for D20. Also, D10 decays somewhat more rapidly than D20. At

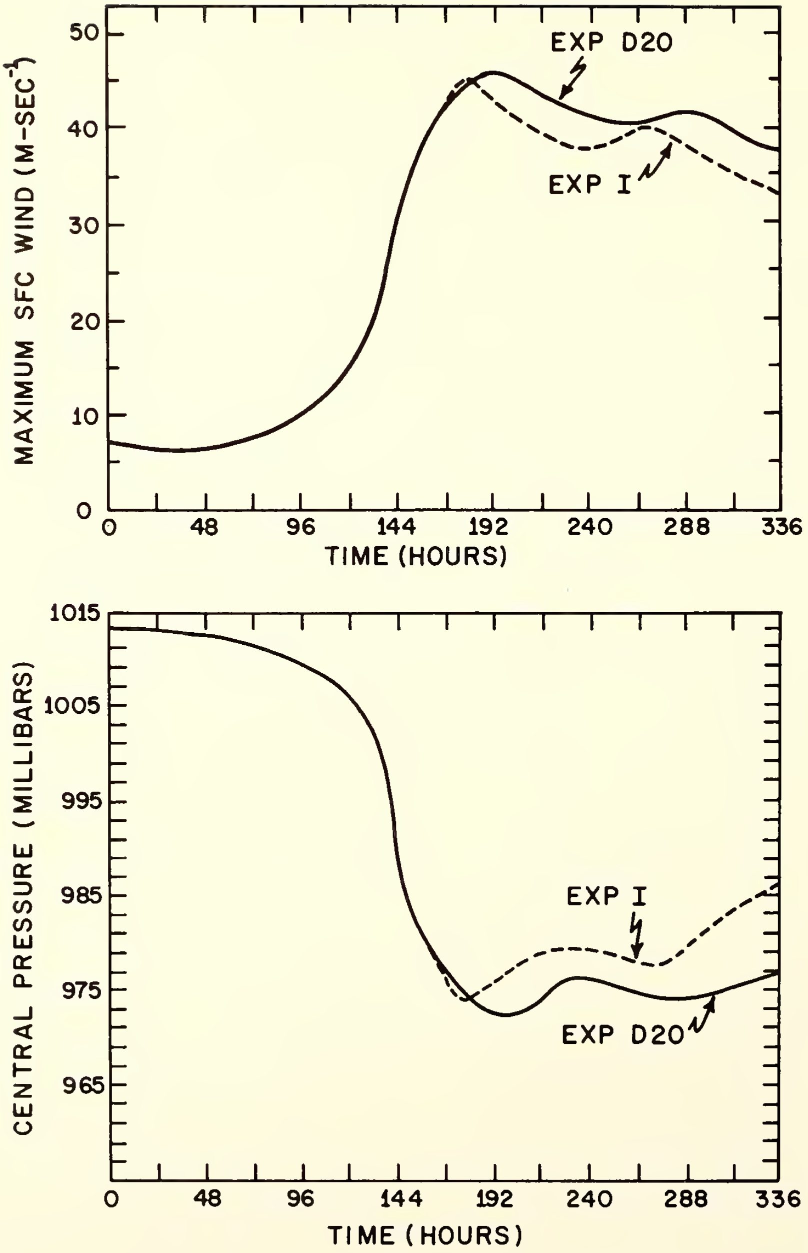

Figure 1. Top: Maximum surface wind as a function of time, Experiment I and D20. Bottom: Central pressure as a function of time, Experiment I and D20.

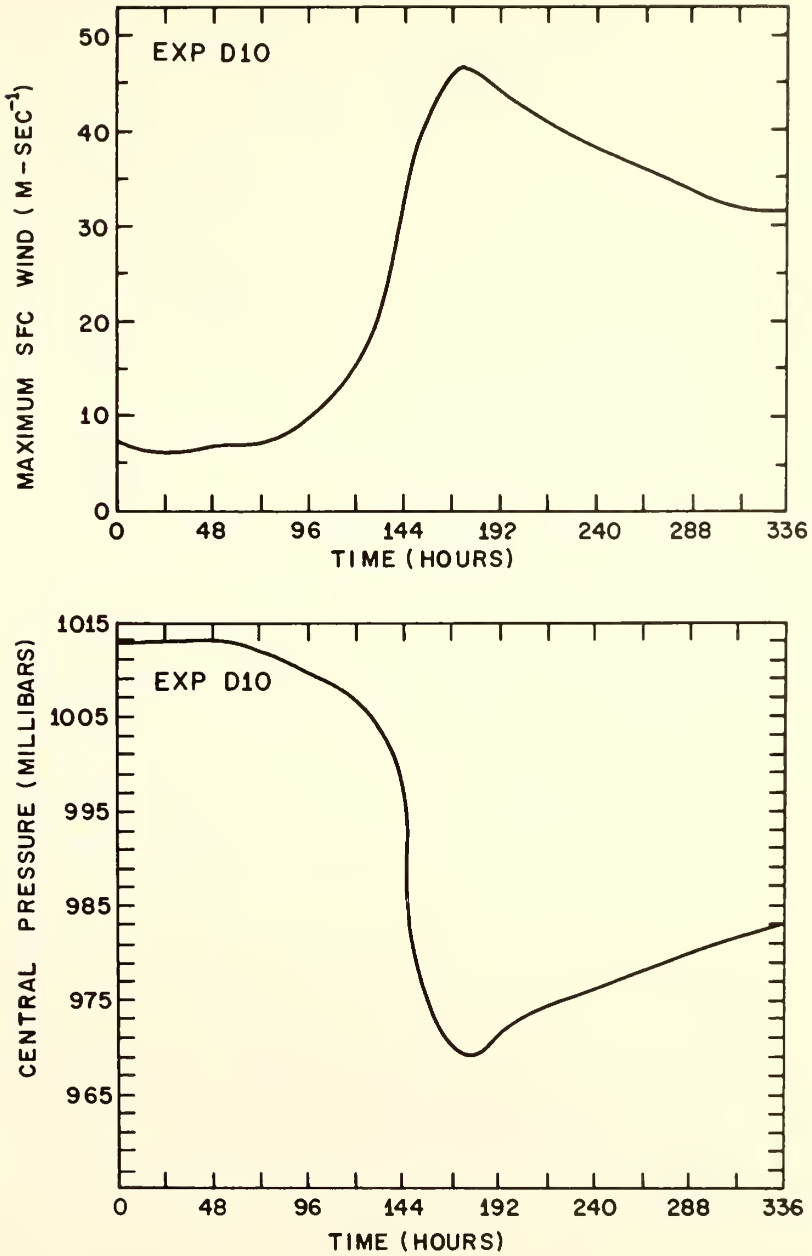

Figure 2. Top: Maximum surface wind as a function of time, Experiment D10. Bottom: Central pressure as a function of time, Experiment D10.

peak intensity, however, the maximum surface wind for D10 is only about 1 m-sec^{-1} greater than that for D20. Minimum central pressure for D10 is only 3.5 mb less than for D20.

On the basis of a recent calculation by Ooyama (1968), greater differences between D10 and D20 had been expected. Ooyama (1968) compared results of his model (Ooyama, 1967) for different grid sizes with the numerical integration scheme used here. He found computational damping to decrease markedly as the radial resolution was refined. Significantly stronger winds and deeper central pressure were found with the smaller grid increments. Such a result is generally to be expected with upstream differencing (see e.g., Molenkamp, 1968a). The rather minor differences between D10 and D20 were, therefore, surprising.

Figure 3 shows that D20 gives a larger storm with a substantially longer period of hurricane force winds. In Experiment D10, the strongest winds and vertical motions occur closer to the storm center than is the case for D20. In general, such a result might be anticipated with more closely spaced grid points. However, part of the explanation is fairly subtle. Ooyama's (1967) study as well as a series of experiments with our model (sec. 9) indicate maximum winds and vertical motions occur closer to the storm center when smaller lateral mixing coefficients are used. Although the explicit coefficient of lateral mixing is identical for D10 and D20, these calculations contain a computational lateral mixing which is produced by upstream differencing of advection terms (sec. 9). The implicit or computational lateral mixing is proportional to the grid increment and, hence, is smaller in Experiment D10.

From figure 3 we also find that the region covered by winds in excess of gales continually expands in Experiment D20, whereas in Experiment D10 gale force winds are constrained to lie within 200 km of the storm center. One might first attempt to explain this difference on the basis of the larger computational lateral viscosity appropriate to D20. However, other experiments with 20-km resolution in which the explicit lateral viscosity was reduced showed the region covered by gales to expand even more rapidly than it does in D20. After examination of the thermal structures yielded by these experiments (not reproduced here), as well as the results from D10 and D20, we arrived at the explanation given below.

Just prior to the time at which lapse rates become coincident with the reference pseudoadiabats, condensation heating and adiabatic cooling very nearly cancel each other. The major effects at this time on the local potential temperature tendency seem to be horizontal advection and lateral diffusity (both computational and explicit).

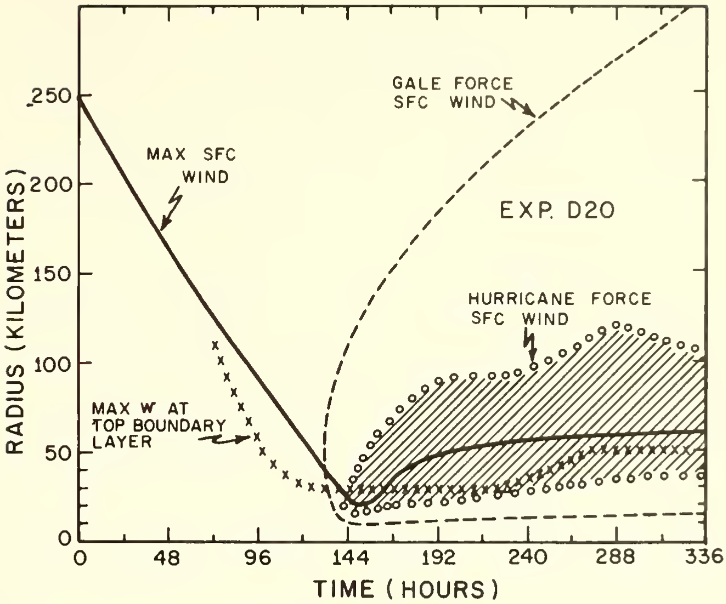

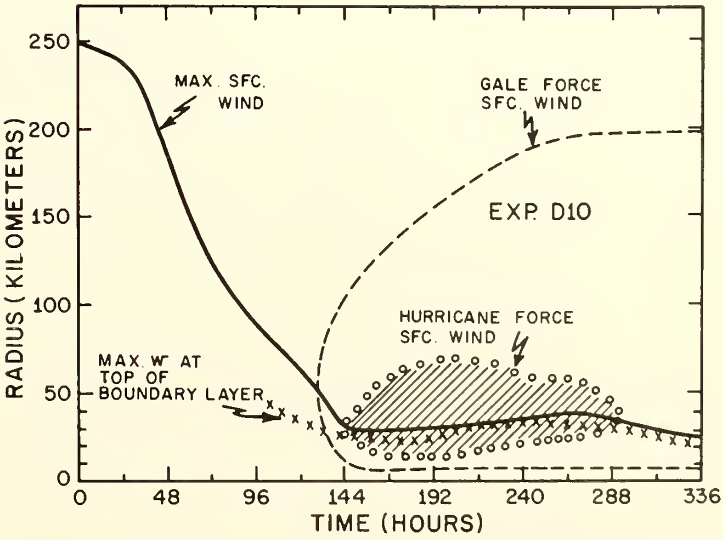

Figure 3. Radii of maximum surface wind and maximum vertical motion at 1054-m level. Outer and inner limits of gale and hurricane force winds at the surface. Top: Experiment D20. Bottom: Experiment D10.

Now, consider the upper troposphere where the strongest temperature gradients are found and further consider the case where the total diffusivity becomes vanishingly small. In such a situation, there will be a tendency for the temperature pattern to be advected away from the storm center. As time passes, the strongest temperature gradients will be found at larger and larger radii. On the other hand, in situations where the diffusivity is more important, there will be a tendency for the thermal pattern to decay in situ, which could counteract the advective effect.

This appears to explain the increased rate of expansion of the storm as the explicit lateral viscosity is decreased with fixed radial resolution. It is also supported by results obtained with a more advanced version of the model (footnote 2). In a series of experiments (both 10-and 20-km resolution), the explicit lateral mixing coefficients for momentum and water vapor were fixed at $10^3 m^2\text{-sec}^{-1}$ and $10^4 m^2\text{-sec}^{-1}$, respectively; the coefficient for heat was varied between 10^4 and $10^3 m^2\text{-sec}^{-1}$. With the larger value, the region covered by gales reached a maximum size and did not increase thereafter. With the smaller value, the results were similar to that obtained in D20.

On the basis of the last few paragraphs, one might have expected the area covered by gale force winds to expand even more rapidly in D10 than was the case for D20. The fact that this did not occur is related to the method used to compute the condensation heating due to large-scale precipitation. As described in section 2, when upward motion was associated with a pseudoadiabatic thermal structure, it was assumed that there was sufficient large-scale condensation to hold the potential temperature in a steady state. Under these circumstances, the effects of lateral diffusion and horizontal advection were no longer operative and the mechanisms discussed in the previous paragraphs were no longer present.

The differences between D10 and D20 are explained by the fact that in the former case the finer resolution allows the model to concentrate temperature gradients in the inner 50 to 60 km of the storm. In this region, at the mature stage, large-scale precipitation was present. Hence, the temperature gradients could not be advected outward. On the other hand, Experiment D20, because of the coarser resolution, built a broader region of significant temperature gradient which extended beyond the region of large-scale precipitation and, therefore, was subjected to the outward advection discussed above.

One final aspect of figure 3 should be noted. In both experiments, the largest boundary-layer vertical motion occurs inside the maximum-surface wind. This is in contrast to

Ooyama's (1967) results and is explicable (Ooyama, 1968) by his use of the gradient-wind assumption in the boundary layer.

Radial profiles of surface wind and surface pressure at the time of deepest central pressure are shown in figure 4. The profiles for both experiments are quite realistic; however,

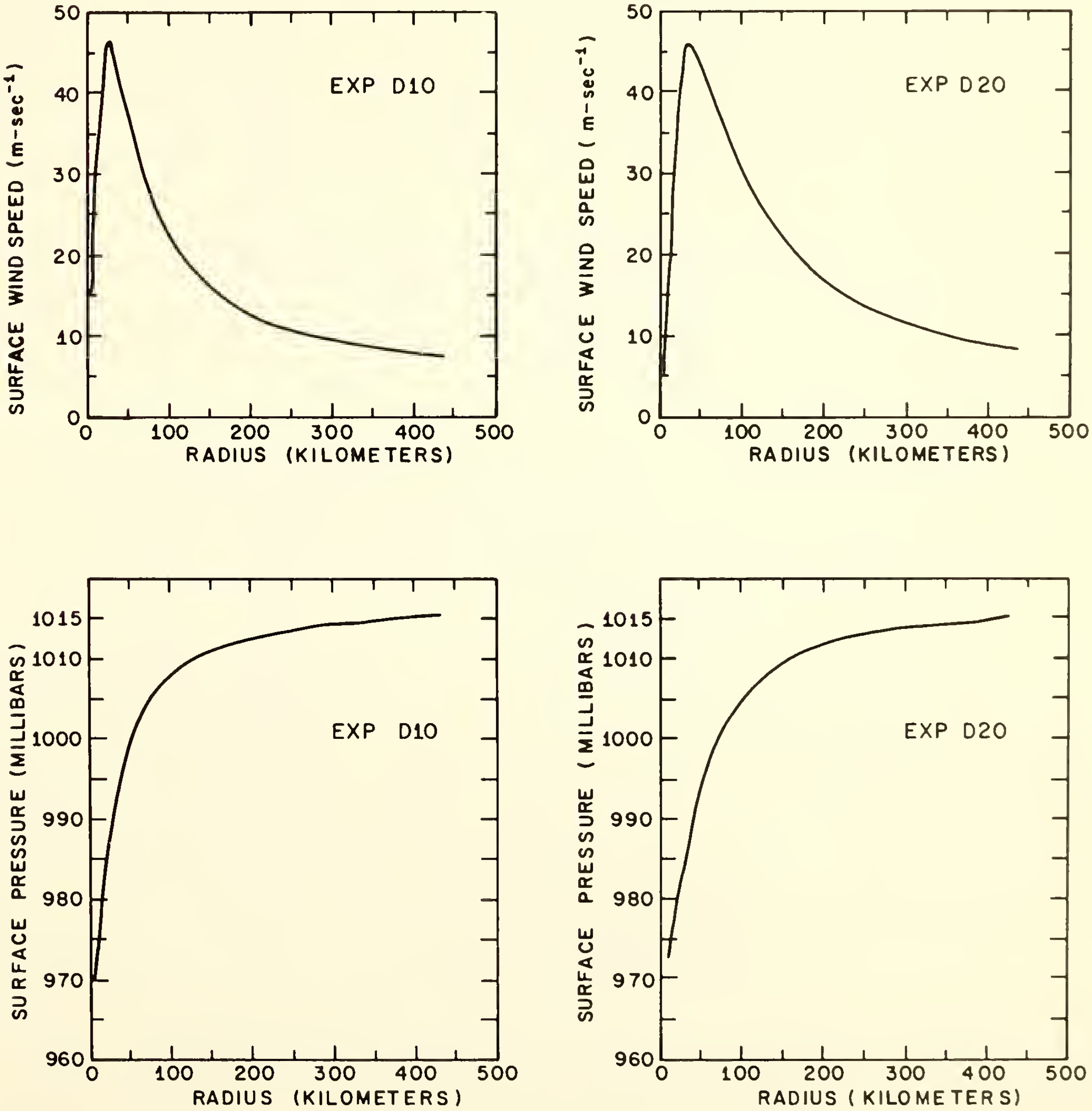

Figure 4. Radial profiles of surface wind speed and surface pressure. Left: Experiment D10 at 168 hours. Right: Experiment D20 at 192 hours.

as already indicated by figure 3, D10 yields a much more compact storm with greater concentration of wind speed and pressure deficit in the inner core.

5. VERTICAL CROSS SECTIONS

Figures 5 through 8 compare vertical cross sections of tangential wind, temperature anomaly, radial wind, and vertical motion for experiments D10 and D20. As before, the data are appropriate to the time of deepest central pressure. Both experiments provide quite realistic storm structure (compare with empirical results of, for example, Hawkins and Rubsam, 1968).

A number of important, if subtle, improvements in structure are, however, found in D10. In figure 6, we note that between radii of 50 and 150 km, D20 yields greatest temperature anomoly at 500 mb. This somewhat unrealistic feature was also found in Experiment I (Rosenthal, 1969) and is substantially improved in D10.

The results of Experiment I (Rosenthal, 1969) showed maximum outflow at the 100-mb level, and, from figure 7, we see that this is also the case with D20. On the other hand, D10 shows an outflow pattern more consistent with ideas of previous writers (see, for example, Hawkins and Rubsam, 1968).

Experiment I showed 20-km resolution to be insufficient for resolving the eye dynamics. As a result, subsidence at the storm center was not a permanent feature of the mature stage but rather a feature that appeared, dissappeared, and reappeared (Rosenthal, 1969). A similar result is found for Experiment D20, as is verified by inspecting figure 8. Experiment D10, on the other hand, shows a distinct region of subsidence at the storm center, and this persists throughout the mature stage.

6. PRECIPITATION AND EFFICIENCY

Rainfall rates, averaged over the inner 100 km, are shown in figure 9. Experiments D10 and D20 both give fairly reasonable, if somewhat large[4], precipitation. Rainfall is

---

[4] The tendency for the rainfall to be on the heavy side was also found in Experiment I. This appears to be directly attributable to the absence of a mechanism for atmospheric storage of water vapor. Newer experiments (see footnote 2) remedy this situation.

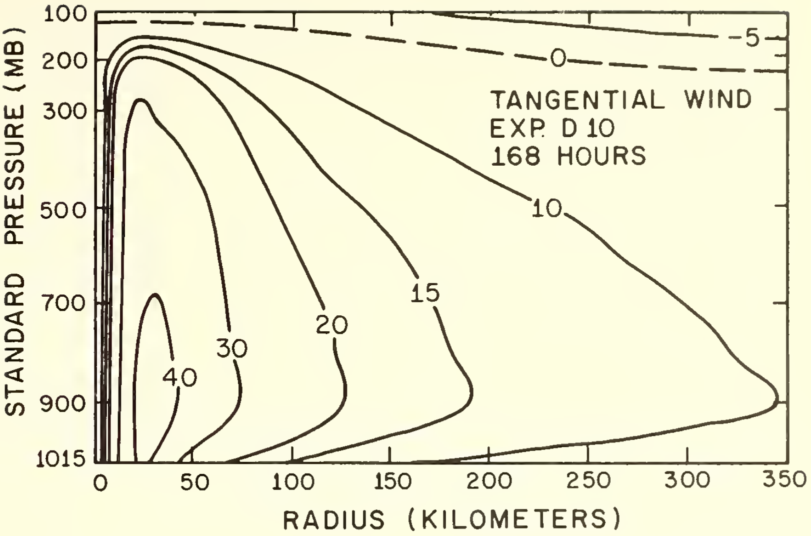

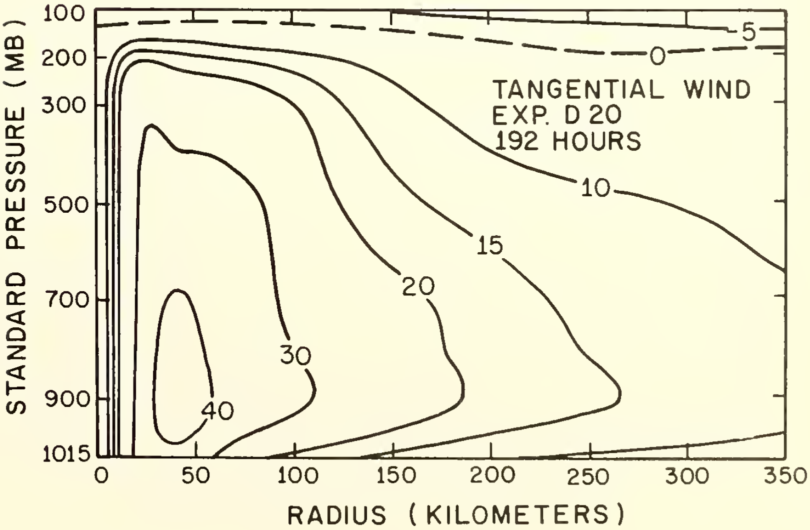

Figure 5. Vertical cross sections of tangential wind. Top: Experiment D10 at 168 hours. Bottom: Experiment D20 at 192 hours. Isopleths are labeled in m-sec^{-1}. Positive values are cyclonic winds.

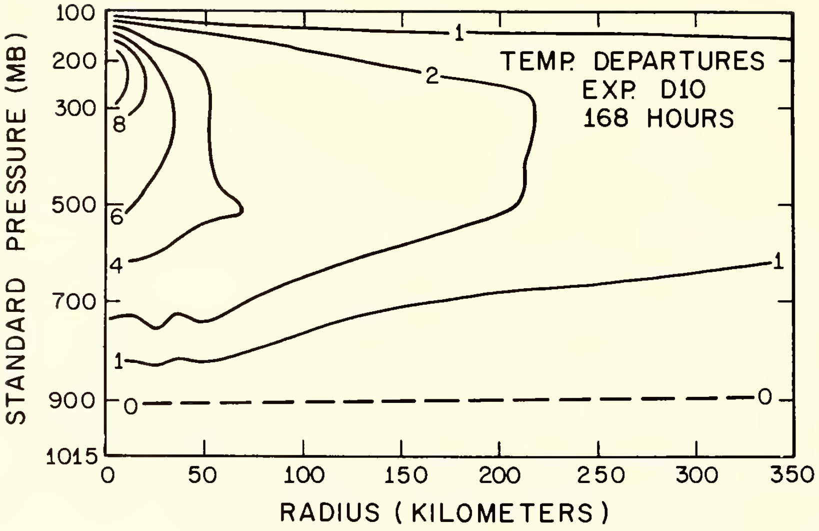

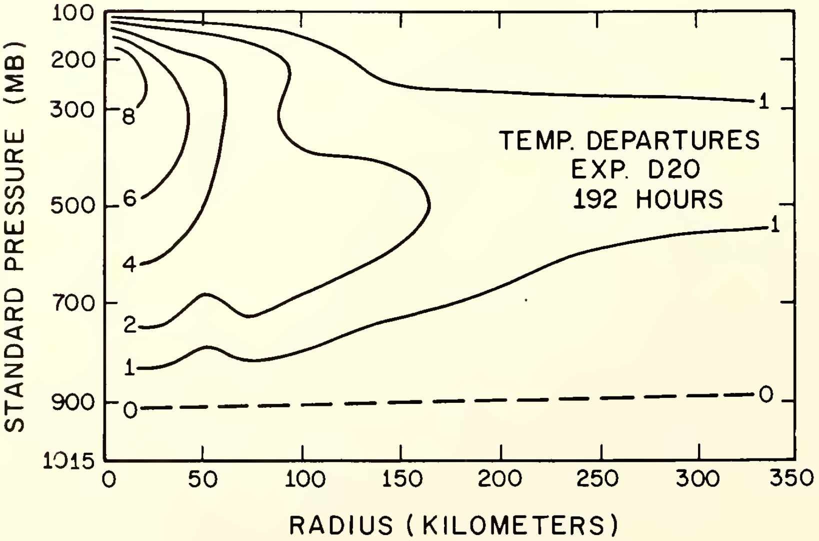

Figure 6. Vertical cross sections of temperature excess over the mean tropical atmosphere. Top: Experiment D10 at 168 hours. Bottom: Experiment D20 at 192 hours. Isopleths are labeled with °K.

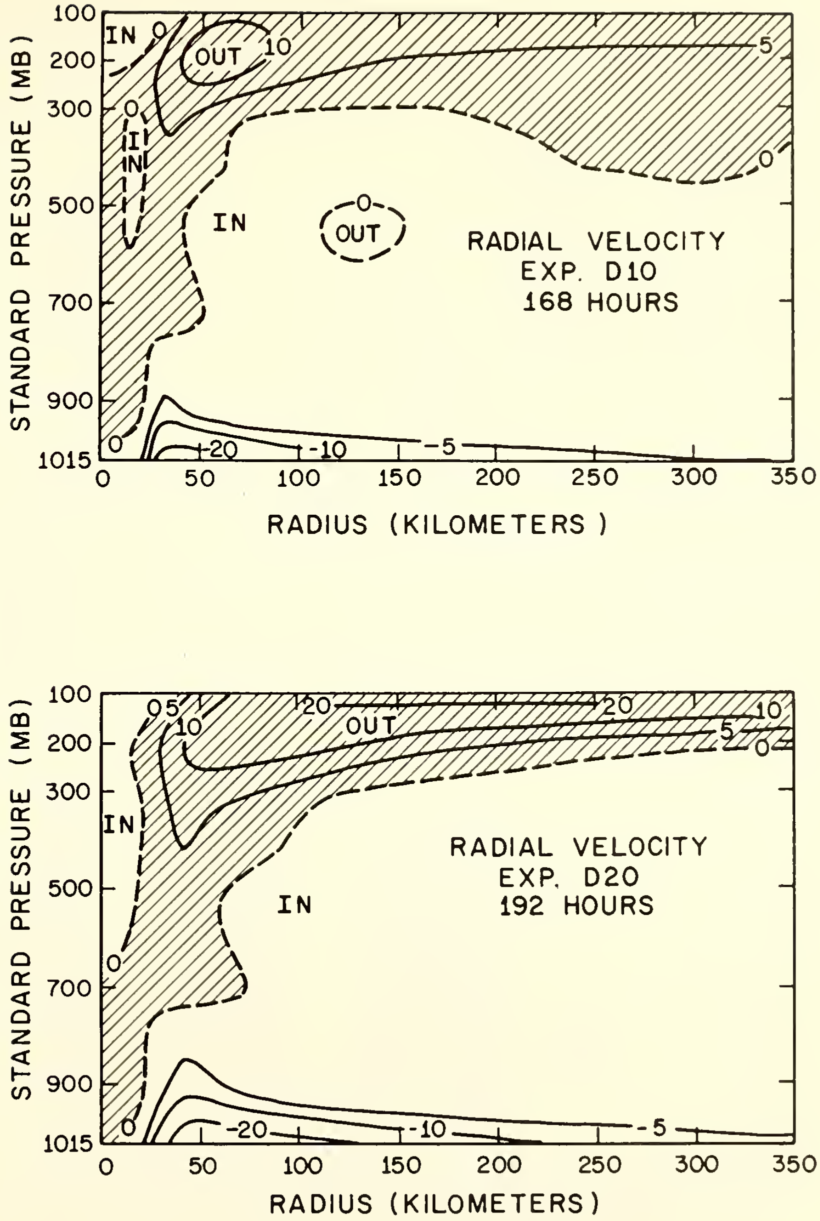

Figure 7. Vertical cross sections of radial wind. Top: Experiment D10 at 168 hours. Bottom: Experiment D20 at 192 hours. Isopleths are labeled with m-sec^{-1}.

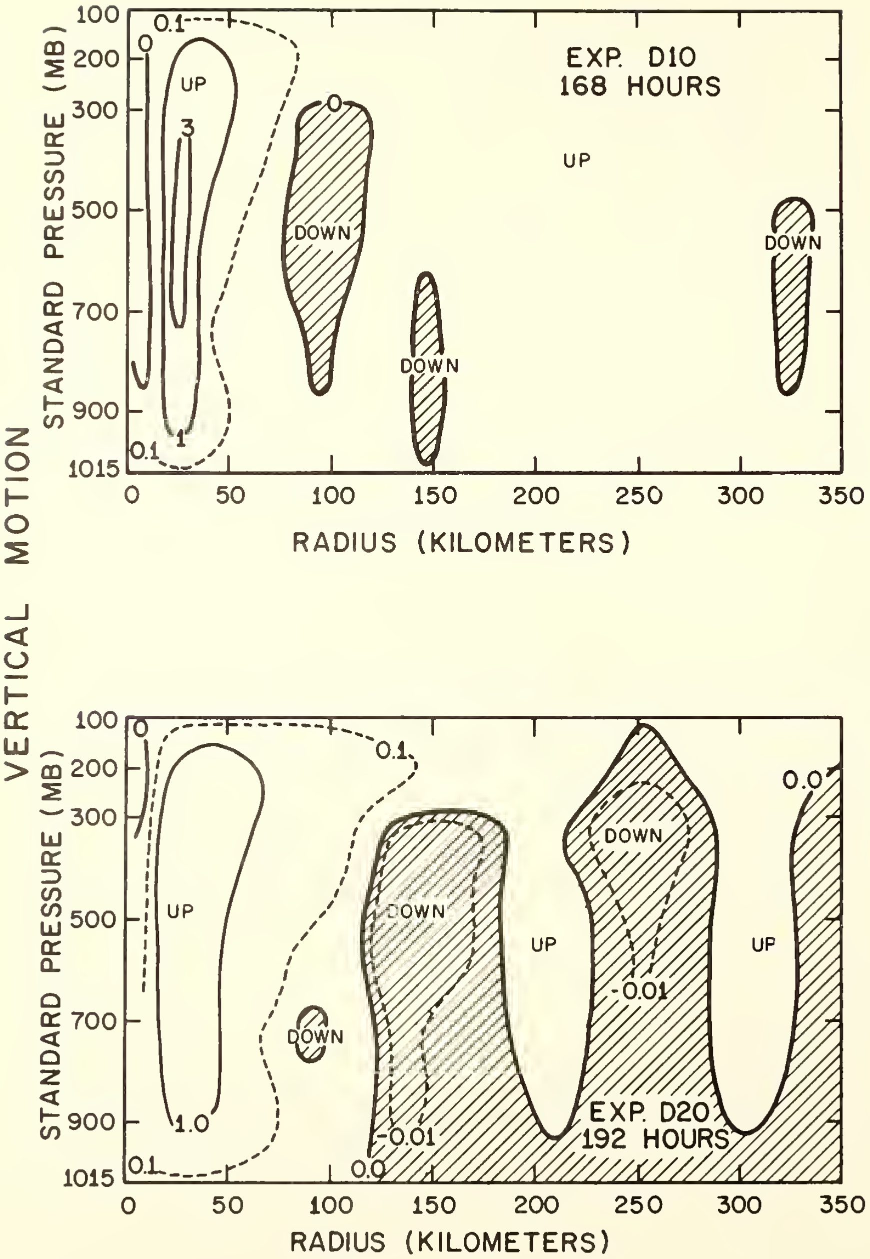

Figure 8. Vertical cross sections of vertical velocity. Top: Experiment D10 at 168 hours. Isopleths are drawn at variable intervals and labeled with m-sec^{-1}. Bottom: Experiment D20 at 192 hours.

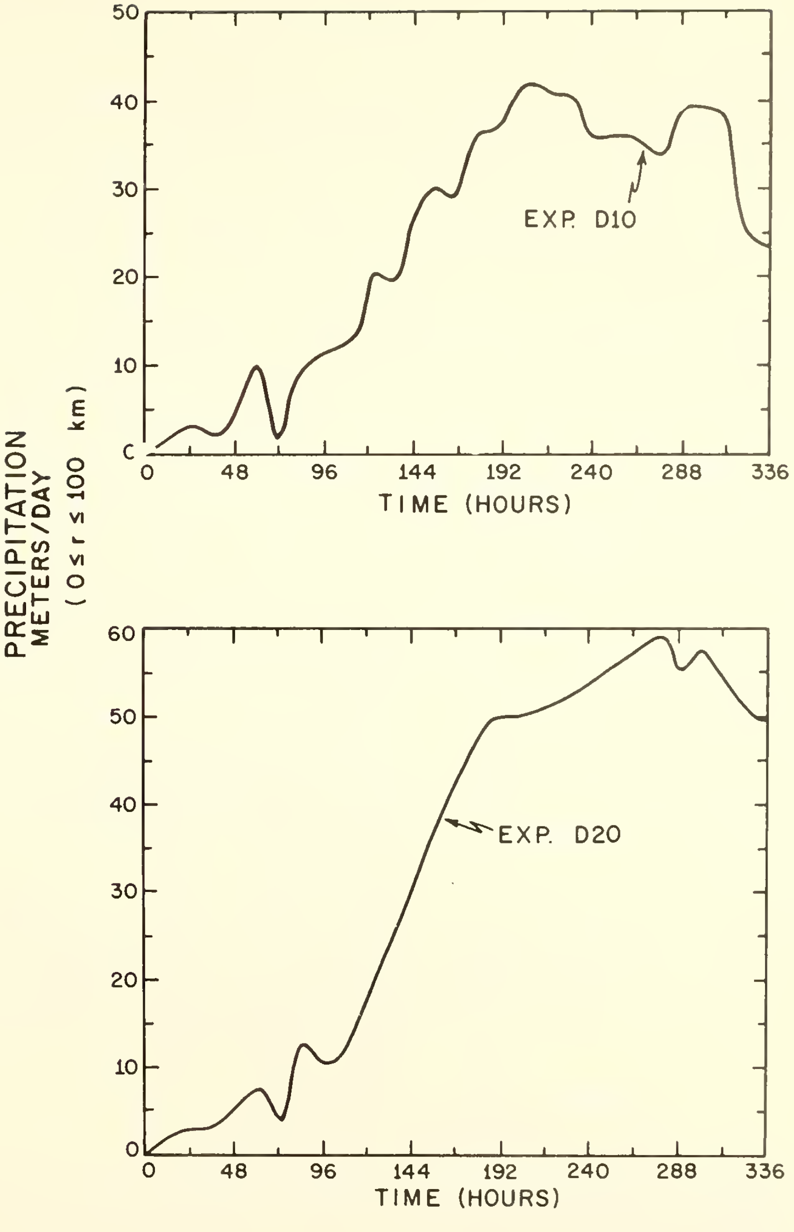

Figure 9. Average precipitation (label should be centimeters per day) over the radial interval zero to 100 km. Precipitation values are sums of the convective and large-scale rainfall rates. Top: Experiment D10. Bottom: Experiment D20.

somewhat less in D10. In neither experiment does large-scale precipitation appear before the 144th hour. Comparison of the convective and large-scale rainfall rates (figure not shown), shows that by the end of the calculation the rainfall in the inner 100 km of D10 is entirely large scale; the thermal structure there has been neutralized and pseudoadiabatic lapse rates prevail. For experiment D20, on the other hand, large-scale precipitation is never found beyond the inner 60 km.

The main controlling factor for the convective rainfall is the vertical motion at level 2 (see app., for $\dot{Q}$). Figure 10 shows radial profiles of this quantity at the times of deepest central pressure. The maximum vertical motion for D10 is about 40 percent greater than for D20. Because of the difference in resolution, D20 builds a broader "eye wall" and the

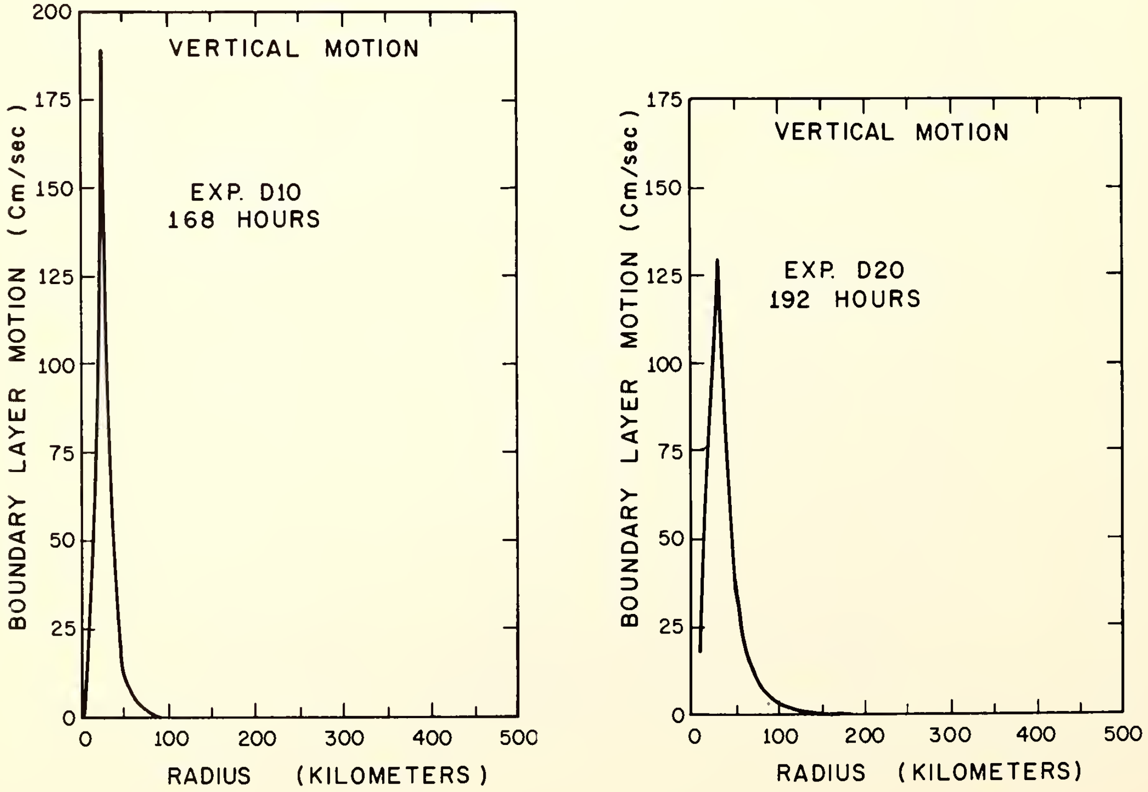

Figure 10. Radial profiles of the vertical velocity at level 2. Left: Experiment D10 at 168 hours. Right: Experiment D20 at 192 hours.

average-vertical motion over the inner 100 km is larger for D20. This explains the larger average rainfall rate (fig. 9) for D20.

The "efficiency" of a tropical cyclone is usually defined as the ratio of kinetic energy production to latent heat release. Figure 11 shows average values of these efficiencies for the inner 200 km of the two experiments. Both experiments give reasonable values (Ooyama, 1968; Palmen and Riehl, 1957), but those for D20 are somewhat larger.

7. GENERATION OF AVAILABLE POTENTIAL ENERGY

The generation of available potential energy[5] by the total release of latent heat (convective plus large scale) is shown in figure 12. During the earlier phases of the experiments, the generation rates for D10 are significantly greater than those for D20. This is in contrast to the total release of latent heat which, as we have already seen, is larger for D20.

In both experiments, generation during the first 200 hours or so is largely limited to the inner 100 km. Only late in the life cycle do the remaining portions of the circulation become active as generators of available potential energy. Even then, however, generation beyond the inner 100 km is quite small in D10. Experiment D20, on the other hand, generates substantial available potential energy in the 100- to 400-km ring.

Compared with empirical data (Anthes and Johnson, 1968), the generation rates for both experiments are of the correct order of magnitude but somewhat too large. This is probably related to the excessive rainfall rates discussed in section 6.

8. KINETIC ENERGY BUDGETS

Figures 13 and 14 show that reasonable agreement between the kinetic energies of the two experiments is achieved only in the inner 100 km. In the outer rings, the kinetic energy content of D20 is two to three times greater than that of D10. In the 200- to 300-km and 300- to 400-km rings, kinetic energy increases throughout the history of D20. In D10, on the other hand, maxima of kinetic energy are reached near the end of the calculation. In D10 the storm as a whole (0 to 400 km) has

---

[5] The computational method is described in the appendix.

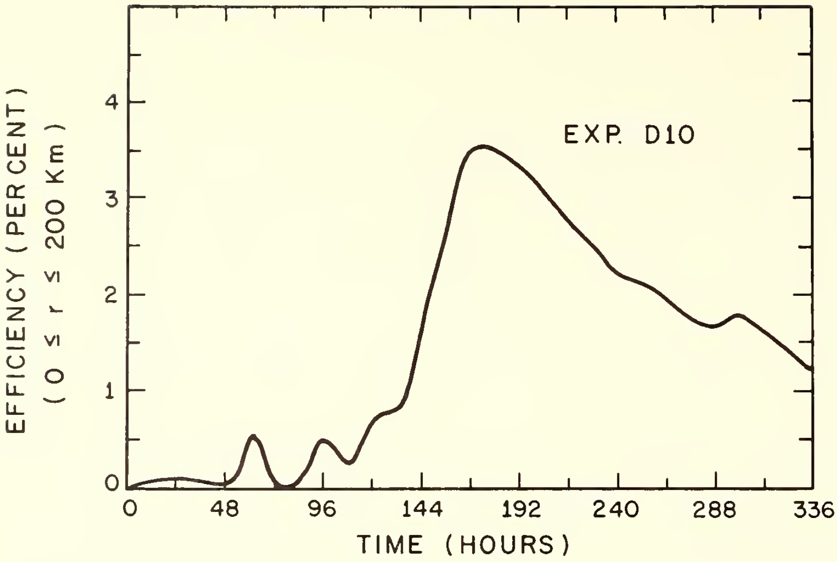

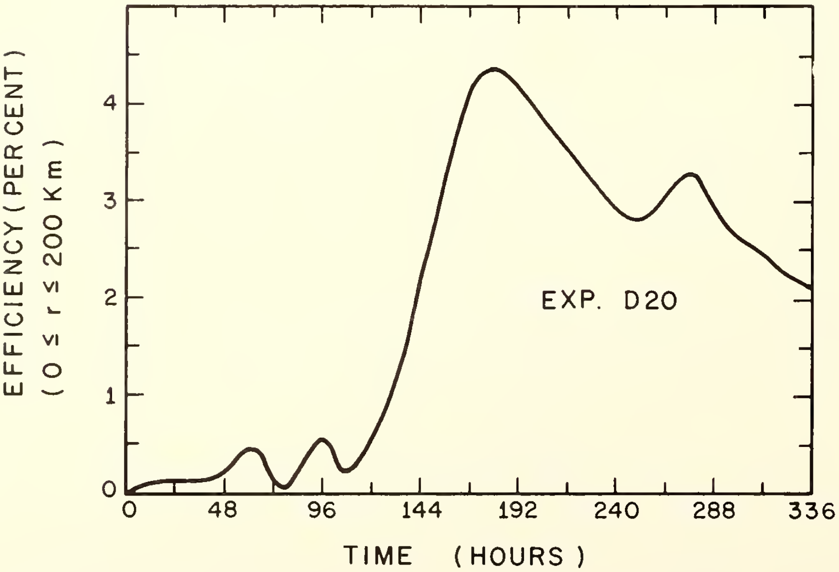

Figure 11. Efficiency of the tropical cyclone. Efficiency is defined as the ratio of the rate of kinetic energy production to the rate of condensation heating. Condensation heating includes both the convective and the large-scale contributions. Values plotted are averages over the radial interval zero to 200 km. Top: Experiment D10. Bottom: Experiment D20.

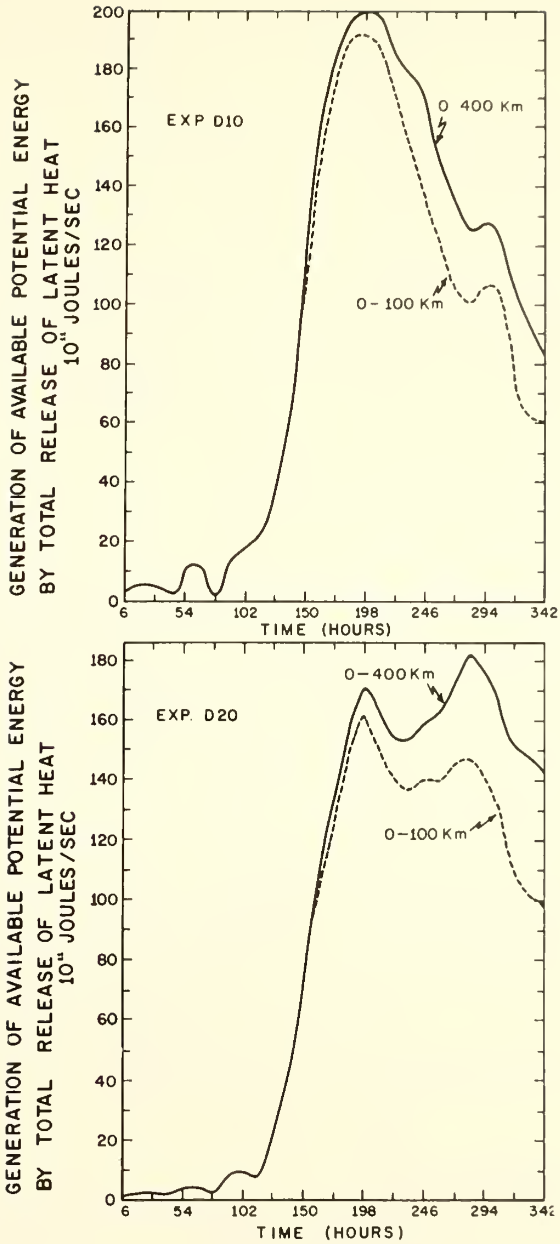

Figure 12. Generation of available potential energy by condensation heating (total of convective and large-scale releases of latent heat). Solid lines represent totals for the radial interval zero to 400 km. Dashed lines give contributions for the radial interval zero to 100 km.

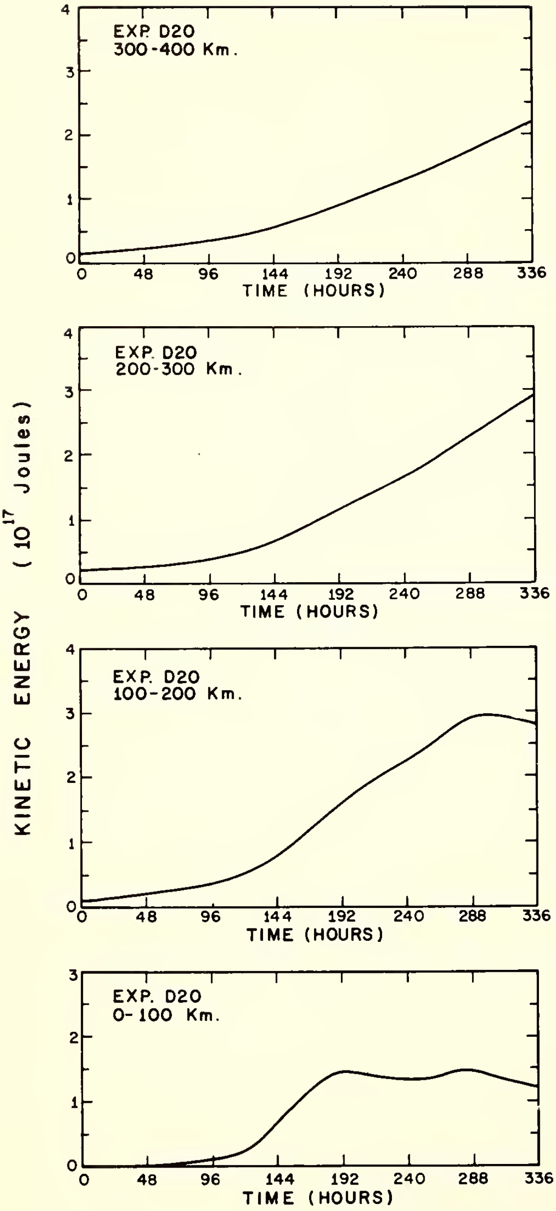

Figure 13. Variation with time of the kinetic energy content of various rings of the storm, Experiment D20.

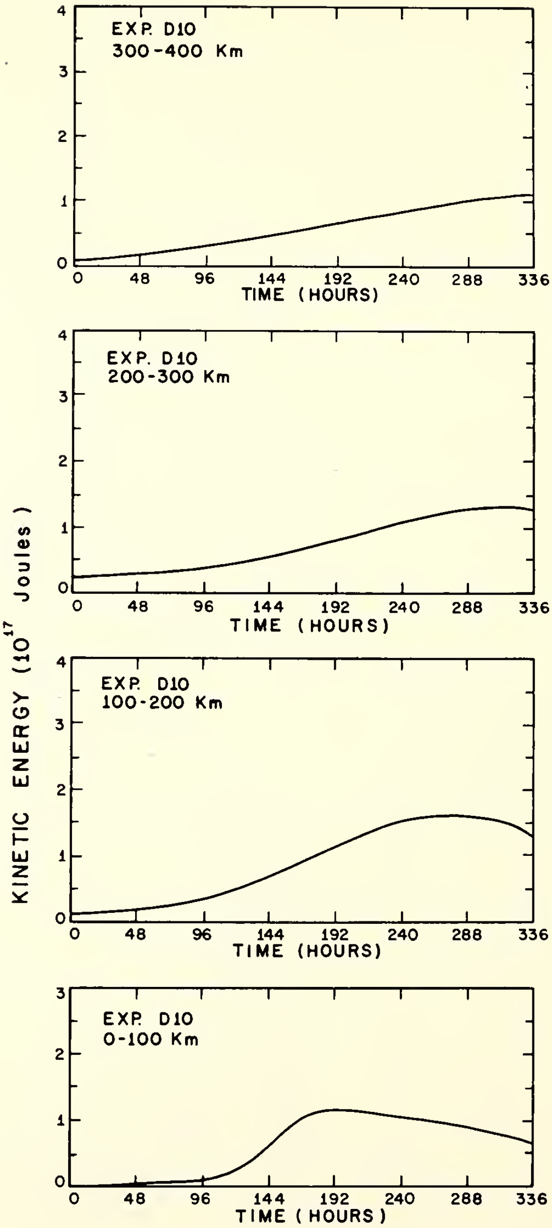

Figure 14. Variation with time of the kinetic energy content of various rings of the storm, Experiment D10.

clearly passed its maximum of kinetic energy by the end of the computation, but in D20 the kinetic energy is increasing even at this time (figs. 15 and 16).

Components of the kinetic energy budgets are shown by figures 17 and 18. Except for the lateral mixing term, the components of the D20 budget are each substantially greater than their counterparts in D10. During most of both experiments, the only positive contribution to the kinetic energy tendency is the generation term. The only possible explanation for the higher kinetic energy content of D20 is that, in comparison to D10, it overestimates the generation term. This, in turn, can only occur if D20 overestimates the pressure gradient force (see app.).

9. LATERAL MIXING AND PSEUDO-VISCOSITY

Figure 19 compares the results of a series of experiments (20-km resolution) in which the lateral mixing coefficient was varied. These experiments have already been mentioned (sec. 4). In view of the rather minor contribution to the kinetic energy budget (fig. 17) made by lateral mixing, the differences between the results with $K_H = 10^4\ m^2\ sec^{-1}$ and $10^3\ m^2\ sec^{-1}$ (fig. 19) are at first surprising. By comparison of figures 17 and 20, however, it becomes clear that the dissipation by lateral mixing is of the same order of magnitude as the time rate of change of kinetic energy. The differences in the experimental results when K_H is reduced from 10^4 to $10^3\ m^2\ sec^{-1}$ are, therefore, understandable. On the other hand, figure 19 also shows that further reduction of K_H from $10^3\ m^2\ sec^{-1}$ to zero has rather little effect. This can be explained on the basis of the computational damping.

Consider the simple advection equation,

$$\frac{\partial A}{\partial t} = -U\frac{\partial A}{\partial s}\ , \qquad (3)$$

and the finite-difference analogue attained with upstream space and forward time differences,

$$A_j^{\tau+1} - A_j^{\tau} = -\frac{U(A_j^{\tau} - A_{j-1}^{\tau})\Delta t}{\Delta s}\ , \qquad (4)$$

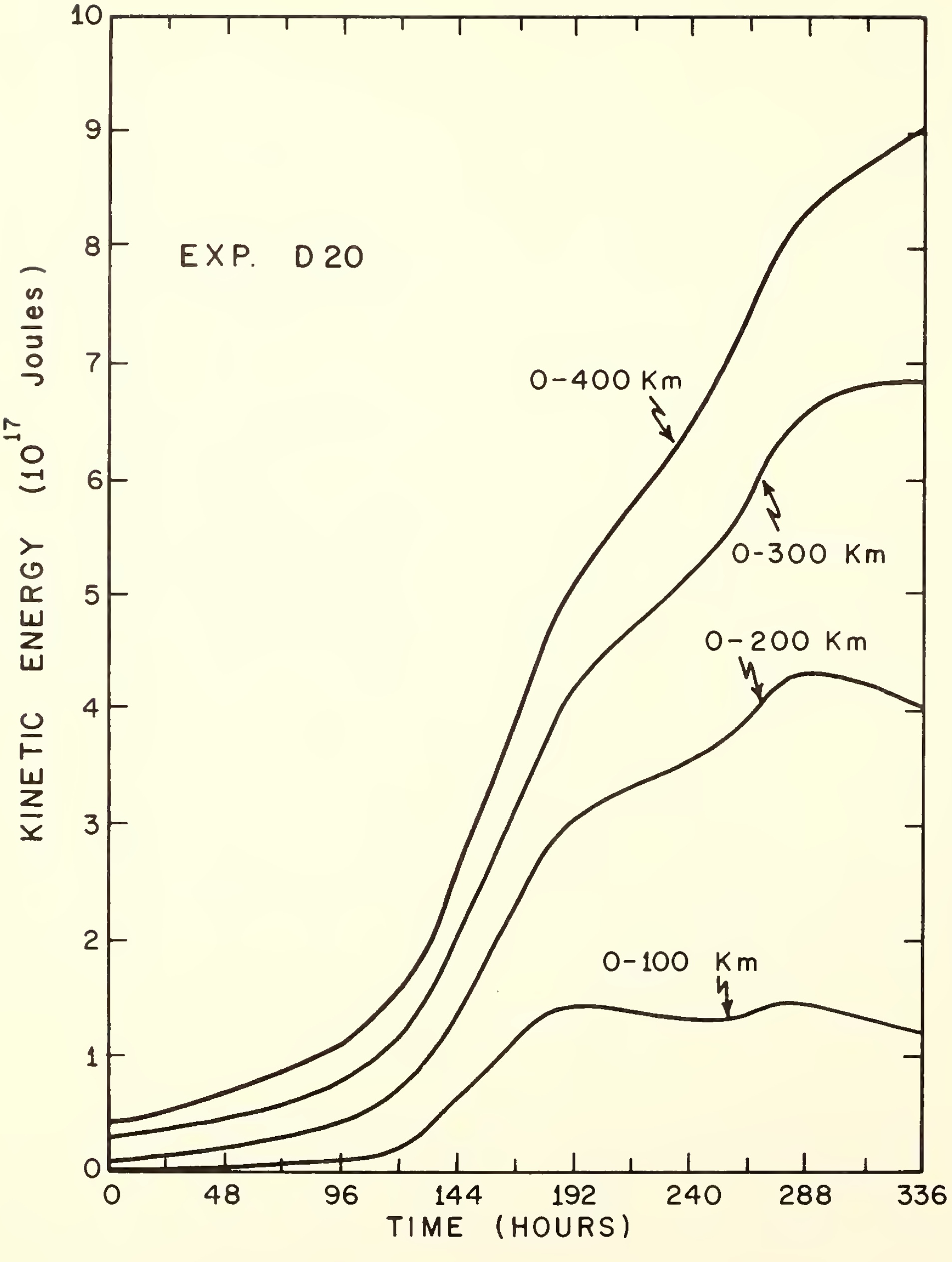

Figure 15. Variation with time of the kinetic energy content of various radial intervals, Experiment D20.

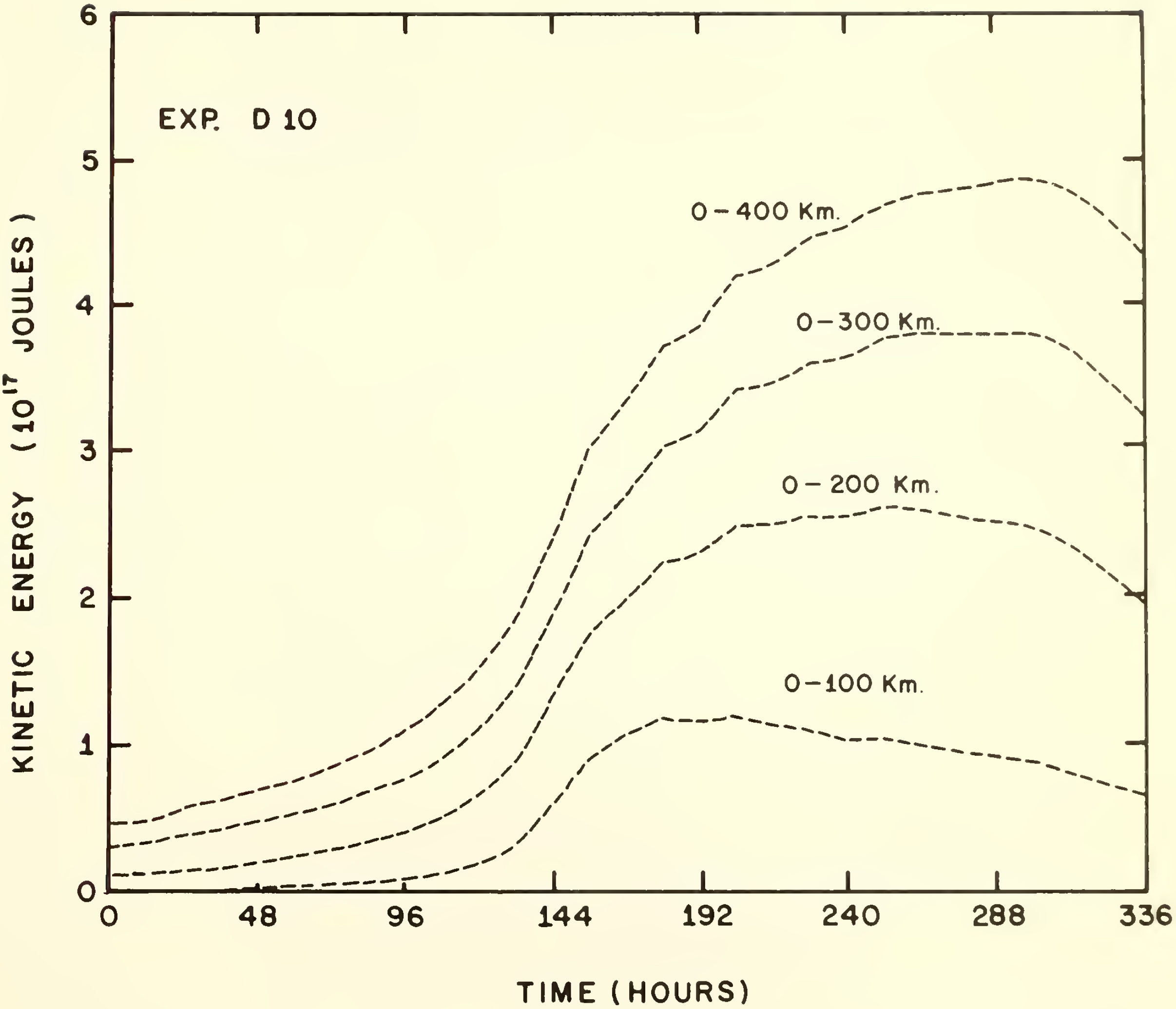

Figure 16. Variation with time of the kinetic energy content of various radial intervals, Experiment D10.

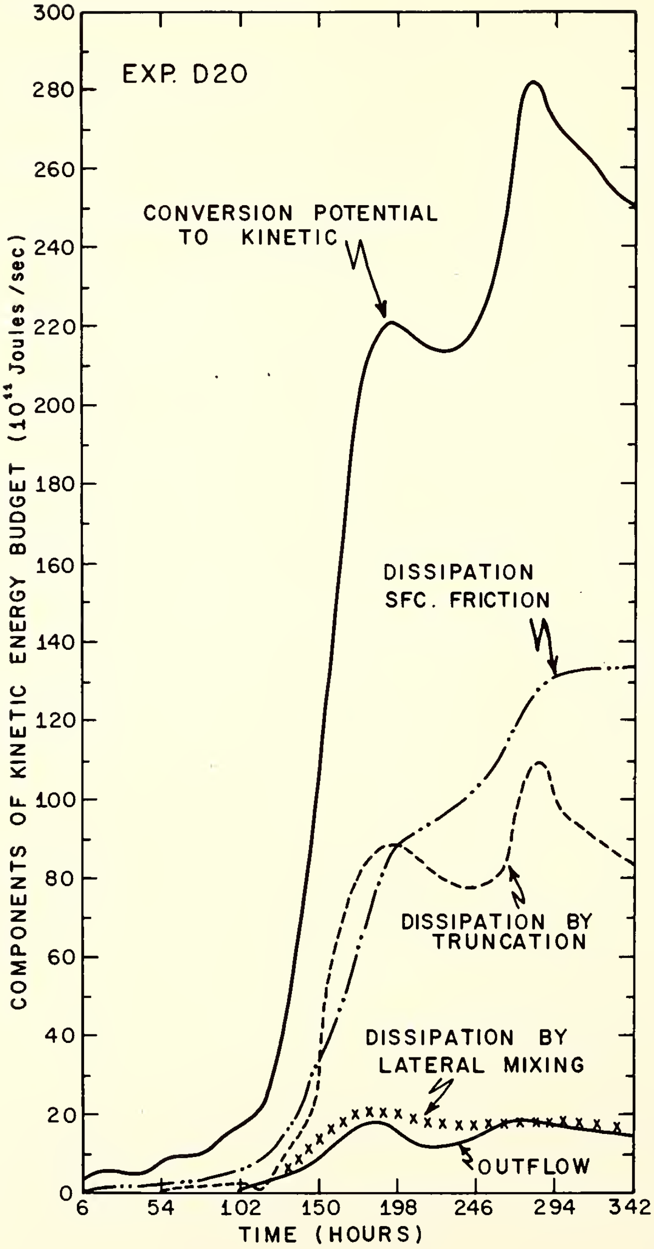

Figure 17. Experiment D20: Components of the kinetic energy budget as a function of time. Values are appropriate to the radial interval from zero to 400 km and are 12-hour averages.

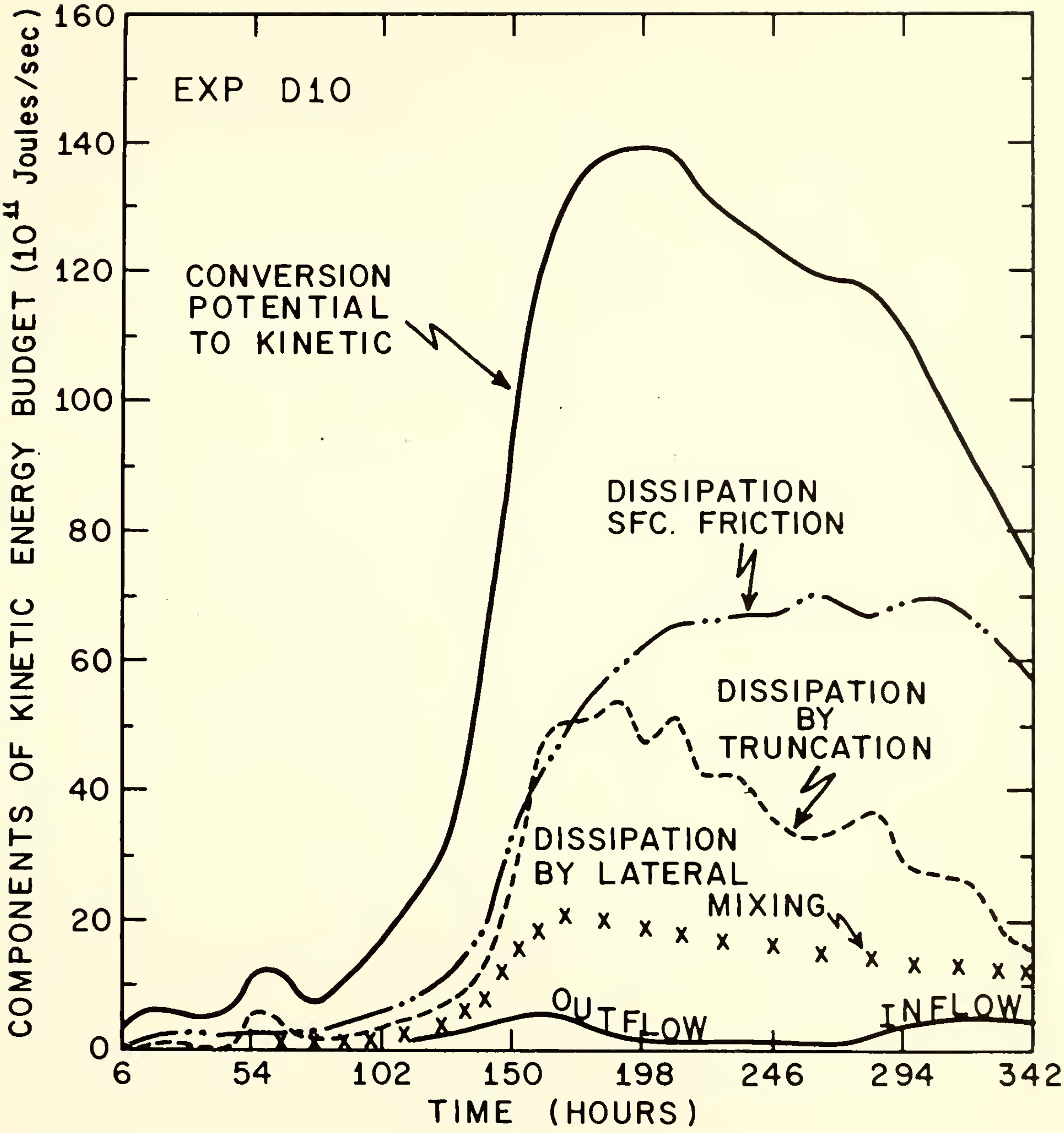

Figure 18. Same as fig. 17 but for Experiment D10.

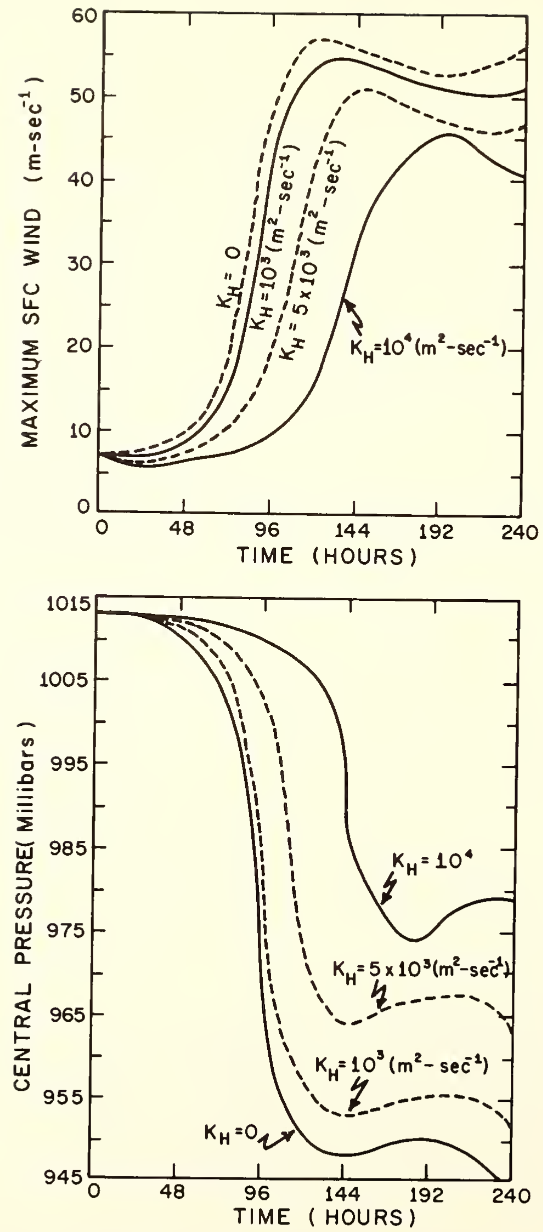

Figure 19. Top: Maximum surface wind as a function of time for a series of experiments in which the lateral mixing coefficient is varied. Radial resolution is 20 km. Bottom: Central pressure as a function of time for the same series of experiments.

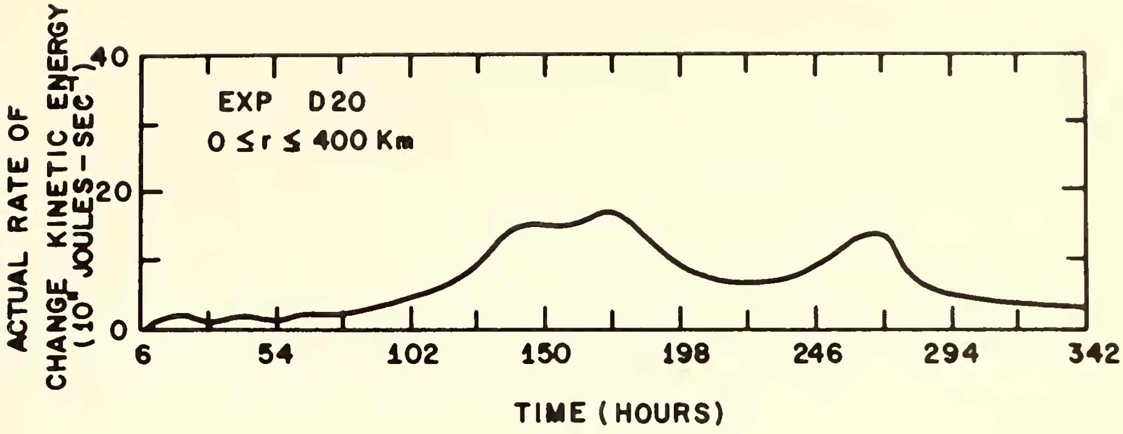

Figure 20. Actual time rate of change of kinetic energy in the radial interval zero to 400 km for Experiment D20. Differences are taken over 12 hours and calculations were made every 12 hours.

where U is presumed to be positive and constant. It may be shown (Molenkamp, 1968a)[6] that the solutions of (4) approximate those of

$$\frac{\partial A}{\partial t} = -U\frac{\partial A}{\partial s} + \nu\frac{\partial^2 A}{\partial s^2}, \tag{5}$$

where the pseudo-viscosity coefficient (ν) is given by

$$\nu = \frac{1}{2}|U|\left\{1 - \frac{|U|\Delta t}{\Delta s}\right\}\Delta s. \tag{6}$$

---

[6] He obtains (5) and (6) by replacing the finite differences in (4) with differential expressions obtained from second order power series expansions of A in time and space and by use of (3). A more exact expression for ν may be found by equating the exact solution of (4) to the solution of $\partial A/\partial t = -U^{*}\partial A/\partial s + \nu\partial^2 A/\partial s^2$. This yields two equations that can be solved for U^{*} and ν . It may further be shown that (6) is an approximation to the ν calculated by the method described in this footnote.

By use of equation (6), the pseudo-viscosity coefficients for both lateral and vertical mixing were computed for experiments D10 and D20. Those for lateral mixing, mass-averaged over the entire storm, are given in figure 21, which shows the pseudo-viscosity for lateral mixing to be on the order of 10^4 m^2-sec^{-1}. Since this is also the order of the explicit lateral mixing coefficient, reduction of K_H from 10^4 to 10^3 m^2-sec^{-1} produces a substantial reduction in the total effective lateral dissipation. On the other hand, when the explicit lateral viscosity is 10^3 m^2-sec^{-1}, the total effective lateral dissipation is already dominated by the pseudo-viscosity; further reduction of K_H therefore has a negligible effect on the total effective lateral mixing. A similar effect in Ogura's (1963) convection experiments is discussed by Molenkamp (1968a).

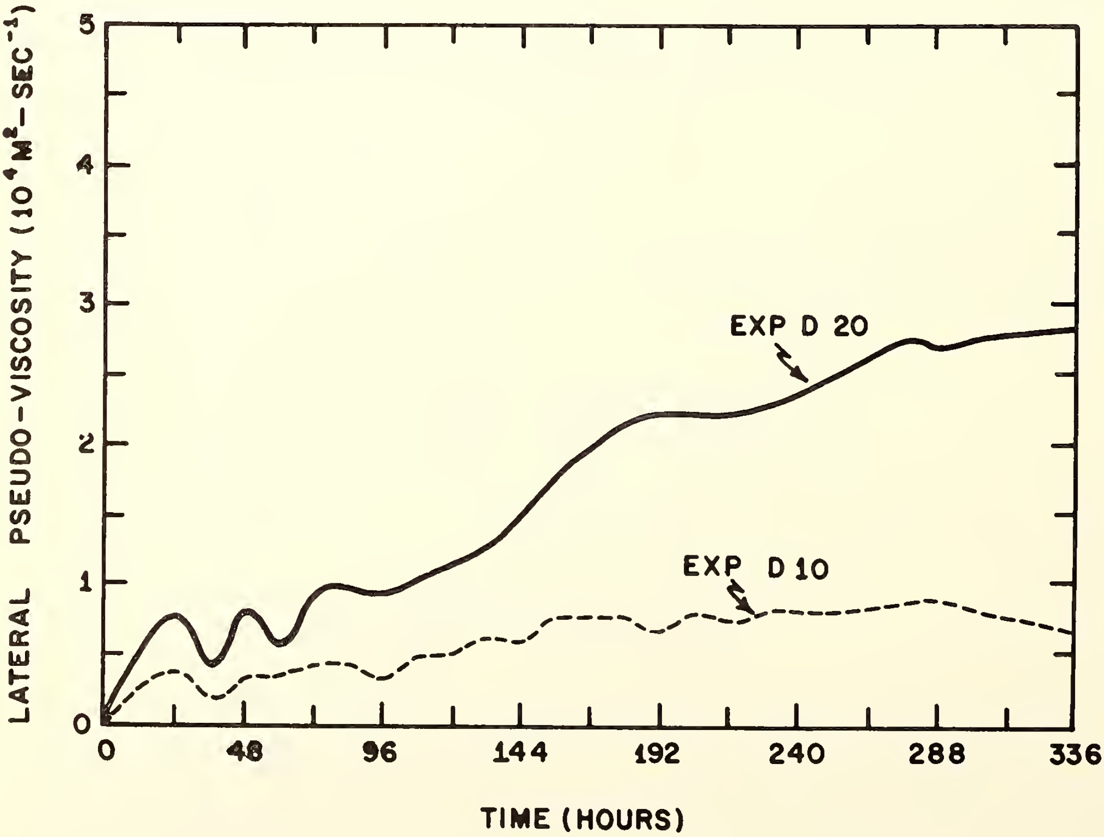

Figure 21. Variation with time of the mass averaged lateral pseudo-viscosity for Experiments D10 and D20. Averages are taken over the radial interval zero to 400 km and from level 1 to level 7.

As noted in section 2, explicit internal vertical mixing was not included because the numerical damping was believed to provide sufficient internal dissipation. In Experiment I (Rosenthal, 1969), it was found that the sum of the computational damping and explicit lateral mixing gave a total effective internal dissipation comparable to that produced by drag friction. This rough one-to-one relationship between internal and surface dissipation is about that found for some real storms (Miller, 1962; Riehl and Malkus, 1961) and therefore provides some justification for omission of the explicit vertical viscosity.

Additional information on this matter is given in figure 22, which shows the pseudo-viscosity coefficients for vertical

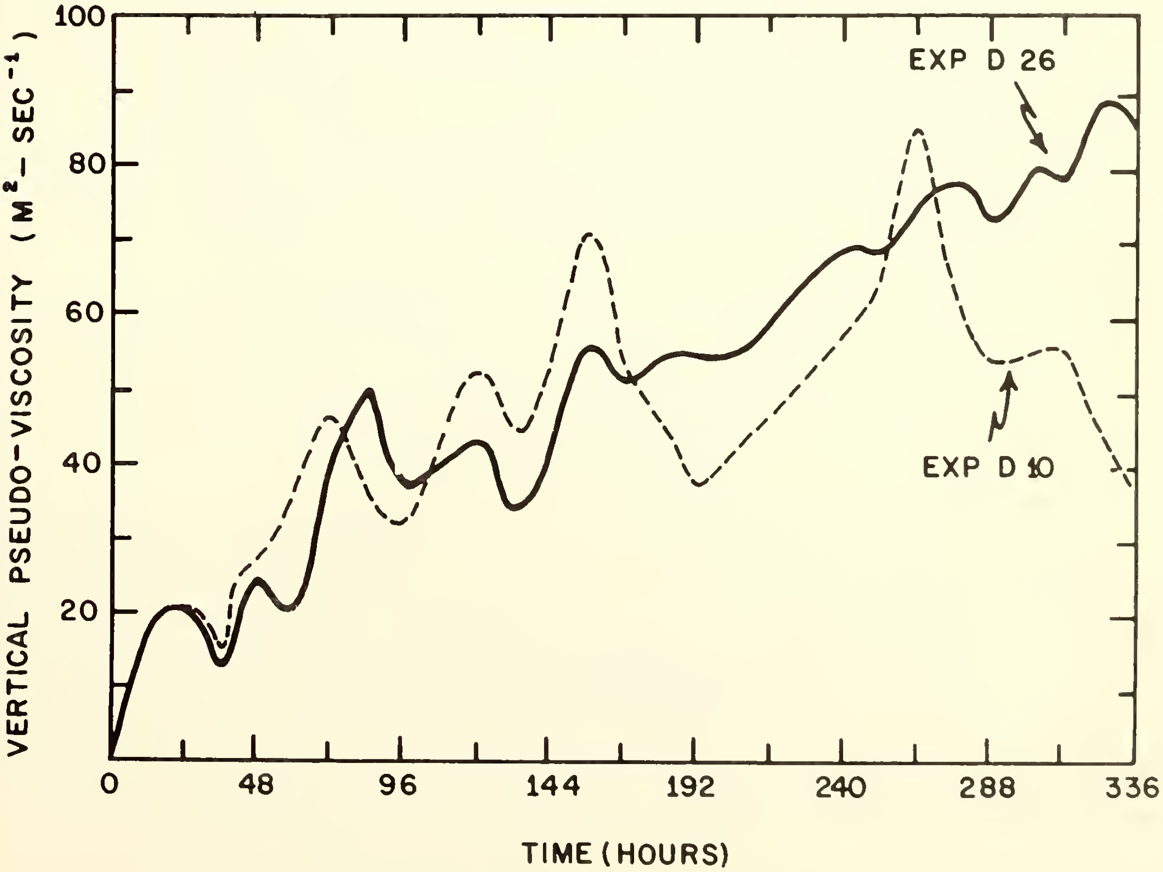

Figure 22. Same as fig. 21 but for the vertical pseudo-viscosity.

mixing averaged over the entire storm. Compared with explicit eddy viscosities suggested by previous hurricane investigators (e.g. Ooyama, 1967; Kasahara, 1961), the pseudo-viscosities are quite large. Vertical averages for individual 100-km rings are shown in figures 23 and 24. The magnitudes are startling especially in the inner 100 km, where the coefficients approach 10^3 m^2-sec^{-1}.

Since the results of Experiments I, D20, and D10 are all fairly realistic, it seems reasonable to conclude that a model written in a nondissipative finite difference scheme would require explicit dissipation roughly comparable in magnitude to the pseudo-viscosity.

10. SUMMARY AND DISCUSSION

Reduction of the radial increment from 20 to 10 km improves some aspects of the storm structure. Most noteworthy is the appearance of a distinct region of subsidence at the center, which is analagous to the eye of a real hurricane. With 20-km resolution, the size of the storm (measured by the area covered by winds exceeding gale force) continually increases with time. In the 10-km case, this region is contained within a radius of 200 km of the storm center.

The distribution of outflow in the upper troposphere is also improved with 10-km resolution. With the coarser resolution, outflow is largest at 100 mb. Such a structure has no empirical support. With 10-km resolution, the outflow pattern is more acceptable. The temperature anomaly pattern is also improved somewhat with 10-km resolution.

In comparison to 10-km resolution, 20-km resolution tends to overestimate rainfall, efficiency and kinetic energy production; generation of available potential energy is underestimated. While computational damping due to upstream differencing of the advection terms is substantially greater with 20-km resolution, the deepest central pressure and the strongest surface winds are almost the same for the two experiments. The kinetic energy budgets for the two experiments show the 20-km experiment to have substantially greater kinetic energy and kinetic energy generation.

The rainfall rates in both experiments are reasonable but somewhat heavy. This is attributable to the lack of a water-vapor storage mechanism, which, in turn, is related to the absence of an explicit forecast of specific humidity. This deficiency has already been corrected, and the results of a new series of experiments will be reported in the near future.

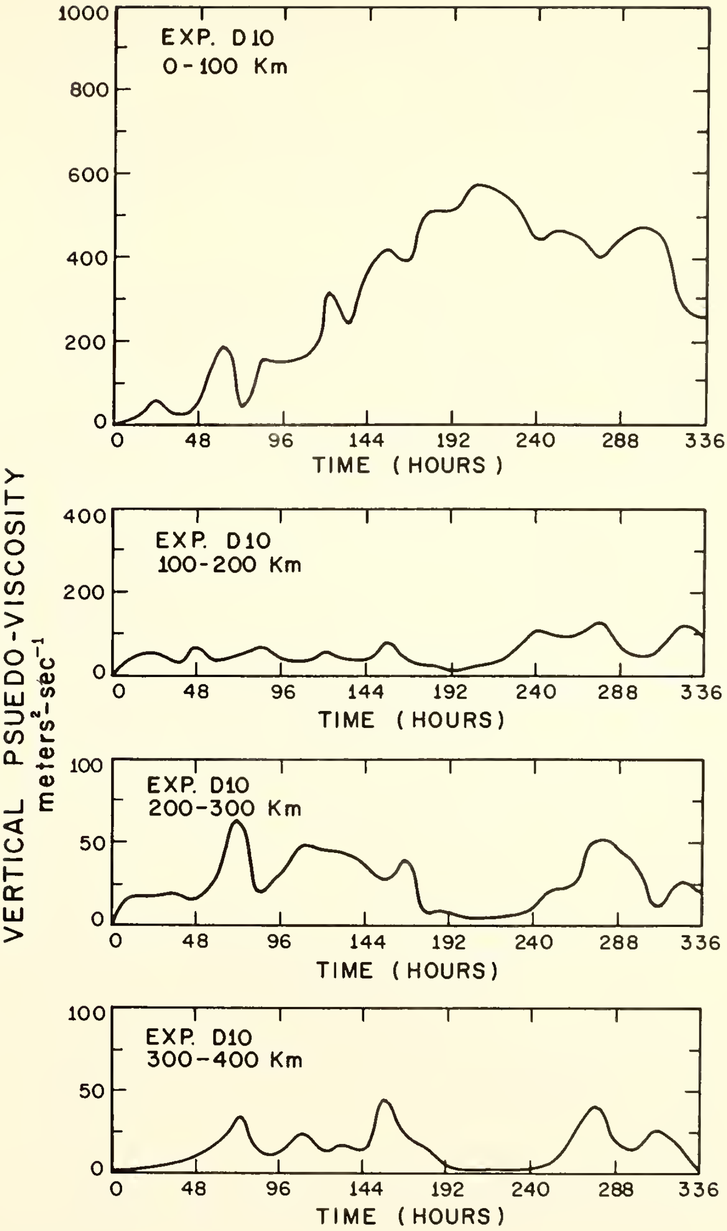

Figure 23. Experiment D10: Variation with time of mass averaged vertical pseudo-viscosity for various rings of the storm.

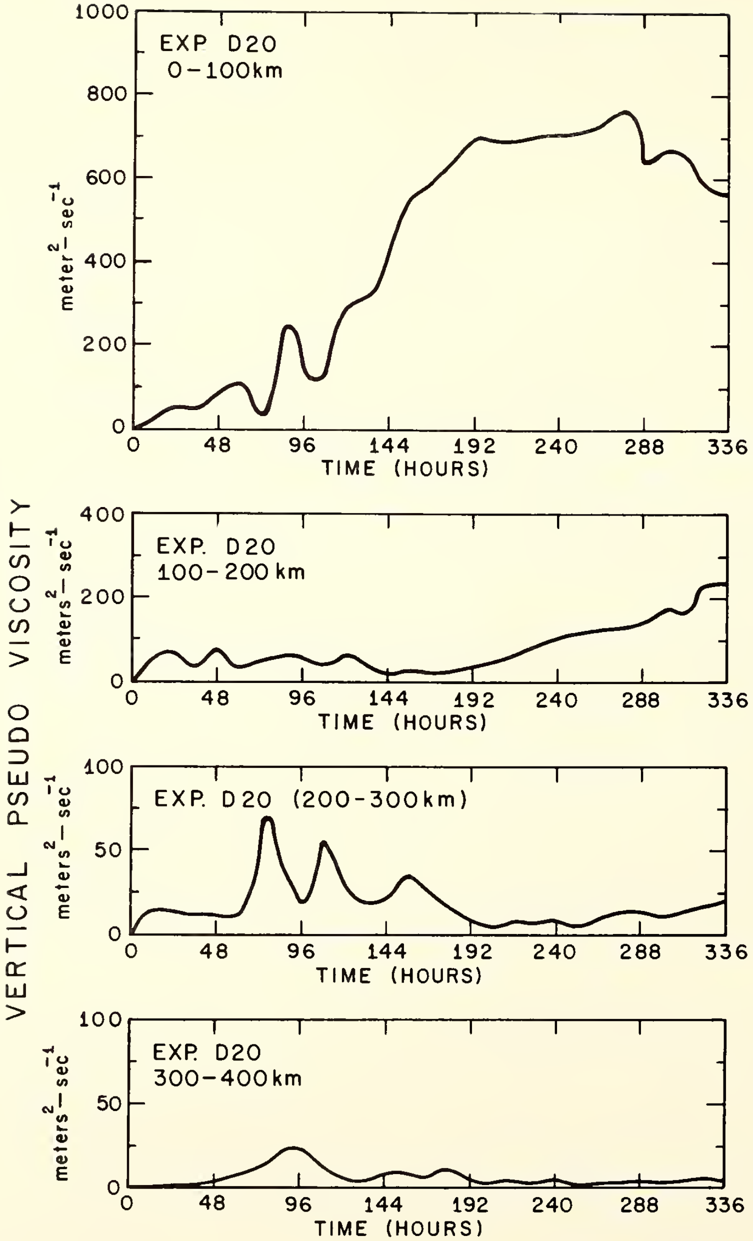

Figure 24. Same as fig. 23 but for experiment D20.

As a measure of the computational damping produced by upstream differencing, the pseudo-viscosity coefficients derived by Molenkamp (1968a) were presented. Averaged over the entire storm, the values for lateral mixing in both experiments were on the order of 10^4 m^2-sec^{-1}. The values with 20-km resolution were two to three times larger than those found with 10-km resolution. In both experiments the lateral pseudo-viscosity was of the same order of magnitude as the explicit lateral mixing.

For vertical mixing, the pseudo-viscosity coefficients were quite large compared with eddy viscosities generally accepted to be valid for hurricanes. Averaged over the storm as a whole, these pseudo-viscosities were 40 to 80 m^2 sec^{-1}. When averaged only over the inner 100 km, values on the order of 200 to 800 m^2 sec^{-1} were obtained. This is over an order of magnitude greater than explicit eddy viscosities suggested earlier by hurricane modelers.

In both experiments, the total internal dissipation (sum of the explicit lateral viscosity, the vertical pseudo-viscosity, and the lateral pseudo-viscosity) of kinetic energy is roughly comparable to the dissipation at the lower boundary by drag friction. A rough equivalence between internal and external dissipation is also found in empirical studies. This, together with the fact that the major part of the internal dissipation is computational rather than explicit, leads to the conclusion that if the model were to be expressed in a nondissipative numerical system, explicit lateral and vertical viscosities as large as these pseudo-viscosities would be required to obtain reasonable results.

As pointed out before (Rosenthal, 1969), upstream differencing for this model is dictated by economic considerations. Despite the undesirable aspects of this numerical system, it has yielded important results for a number of meteorological problems (examples are, Ogura, 1963; Orville, 1964). For this, and other reasons given below, the rather strong condemnations of this method that have appeared in recent literature (Molenkamp, 1968a, 1968b) cannot be entirely accepted. The major criticism appears to be the computational damping discussed above, but severe computational damping is also a feature of a number of schemes which enjoy fairly respectable reputations. Most noteworthy of these is the Lax-Wendroff (Lilly, 1965; Richtmyer, 1962). Indeed, Richtmyer finds this computational damping to be desirable since it is an effective control on nonlinear computational instability. It has been pointed out (Lilly, 1961) that the damping provided by upstream differencing also is effective in the suppression of nonlinear computational instability and that its general behavior is similar to that of the explicit nonlinear eddy viscosity used through the years by Smagorinsky and his group (Smagorinsky, 1963).

11. ACKNOWLEDGMENTS

We are indebted to Mr. James W. Trout, who provided substantial assistance with many of the calculations discussed above.

12. REFERENCES

Anthes, R. A., and D. R. Johnson (1968), Generation of available potential energy in Hurricane Hilda (1964), Monthly Weather Rev. 96, No. 5, 291-302.

Hawkins, H. F., and D. T. Rubsam (1968), Hurricane Hilda, 1964; II. Structure and budgets of the hurricane on October 1, 1964, Monthly Weather Rev. 96, No. 9, 617-636.

Hebert, Paul J. and C.L. Jordan (1959), Mean soundings for Gulf of Mexico area, Rept. 30, National Hurricane Research Project, U.S. Weather Bureau, 10 pp.

Kasahara, A. (1961), A numerical experiment on the development of a tropical cyclone, J. Meteorol. 18, No. 3, 259-282.

Lilly, D. K. (1961), A proposed staggered grid system for numerical integration of dynamic equations, Monthly Weather Rev. 89, No. 3, 59-65.

Lilly, D. K. (1965), On the computational stability of numerical solutions of time-dependent non-linear geophysical fluid dynamics problems, Monthly Weather Rev. 93, No. 1, 11-26.

Miller, B. I. (1962), On the momentum and energy balance of Hurricane Helene (1958), NHRP Report 53, 19 pp.

Molenkamp, C. R. (1968a), Accuracy of finite difference methods applied to the advection equation, J. Appl. Meteorol. 7, No. 2, 160-167.

Molenkamp, C. R. (1968b), Reply to a letter by Harold D. Orville, J. Appl. Meteorol. 7, No. 5, 938-939.

Ogura, Y. (1963), The evolution of a moist convective element in a shallow, conditionally unstable atmosphere: a numerical calculation, J. Atmospheric Sci. 20, No. 5, 407-424.

Ooyama, K. (1967), Numerical simulation of the life-cycle of tropical cyclones, NSF Grant No. GA-623, Dept. Meteorol. and Oceanography, New York Univ., New York, 133 pp.

Ooyama, K. (1968), Numerical simulation of tropical cyclones with an axi-symmetric model, Paper presented at Intern. Symp. Numerical Weather Prediction, Tokyo, December 1968.

Orville, H. D. (1964), On mountain upslope winds, J. Atmospheric Sci. 21, No. 6, 622-633.

Palmén, E., and H. Riehl (1957), Budget of angular momentum and energy in tropical cyclones, J. Meteorol. 14, No. 2, 150-159.

Richtmyer, R. D. (1962), A survey of difference methods for non-steady fluid dynamics, NCAR Tech. Notes 63-2, National Center for Atmospheric Research, Boulder, Colorado, 25 pp.

Riehl, H., and J. S. Malkus (1961), Some aspects of Hurricane Daisy, 1958, Tellus 13, No. 2, 181-213.

Rosenthal, S. L. (1969), Numerical experiments with a multi-level primitive equation model designed to simulate the development of tropical cyclones. Experiment I, ESSA Tech. Memo. ERLTM-NHRL 82, 36 pp.

Smagorinsky, J. (1963), General circulation experiments with the primitive equations: I. The basic experiment, Monthly Weather Rev. 91, No. 3, 99-165.

Yamasaki, M. (1968), A tropical cyclone model with parameterized vertical partition of released latent heat, J. Meteorol. Soc. Japan 46, No. 3, 202-214.

13. APPENDIX

The basic system of equations, when circular symmetry is assumed, is

$$\frac{\partial M}{\partial t} = -u\frac{\partial M}{\partial r} - w\frac{\partial M}{\partial z} - fru + \frac{1}{\bar{\rho}}\frac{\partial}{\partial z}\left(\bar{\rho}K_z\frac{\partial M}{\partial z}\right) + \frac{K_H}{r}\frac{\partial}{\partial r}\left\{r^3\frac{\partial}{\partial r}\left(\frac{v}{r}\right)\right\}, \tag{A-1}$$

$$\frac{\partial u}{\partial t} = -u\frac{\partial u}{\partial r} - w\frac{\partial u}{\partial z} + \frac{M}{r}\left(f + \frac{M}{r^2}\right) - \theta\frac{\partial \phi}{\partial r} + \frac{1}{\rho}\frac{\partial}{\partial z}\left(\rho K_z\frac{\partial u}{\partial z}\right) + \frac{K_H}{r^2}\frac{\partial}{\partial r}\left\{r^3\frac{\partial}{\partial r}\left(\frac{u}{r}\right)\right\}, \tag{A-2}$$

$$\frac{\partial \theta}{\partial t} = -u\frac{\partial \theta}{\partial r} - w\frac{\partial \theta}{\partial z} + \frac{c_p K_H}{r\phi}\frac{\partial}{\partial r}\left(r\frac{\partial \theta}{\partial r}\right) + \frac{\dot{Q}}{\phi}, \tag{A-3}$$

$$\frac{\partial \phi}{\partial z} = -\frac{g}{\theta}, \tag{A-4}$$

$$\frac{\partial \bar{\rho}w}{\partial z} = -\frac{1}{r}\frac{\partial \bar{\rho}ru}{\partial r}, \tag{A-5}$$

$$\phi = c_p\left(\frac{p}{p_0}\right)^{R/c_p}, \tag{A-6}$$

$$\theta\phi = c_p T, \tag{A-7}$$

and

$$M = rv. \tag{A-8}$$

The symbols are defined as follows:

r	radius,
z	height,
t	time,
M	relative angular momentum,
u	radial velocity,
v	tangential velocity,
w	vertical velocity,
f	Coriolis parameter,
$\bar{\rho} = \bar{\rho}(z)$	density of a reference tropical atmosphere,
K_z	kinematic coefficient of eddy viscosity for vertical mixing,
K_H	kinematic coefficient of eddy viscosity and conductivity for lateral mixing,
θ	potential temperature,
c_p	specific heat capacity at constant pressure for dry air,

$\dot{Q}$	condensation heating per unit time and mass appropriate to the cyclone-scale flow,
g	acceleration of gravity,
P_0	1000 mb,
p	pressure,
T	air temperature, and
ρ	density.

Equations (A-1) and (A-2) are forms of the tangential and radial equations of motion, respectively. Equation (A-3) is the first law of thermodynamics. Equation (A-5) is a simplified form of the continuity equation that filters acoustic waves (Ogura and Charney, 1962; Ogura and Phillips, 1962) and can easily be justified on the basis of an order of magnitude analysis. Equation (A-4) is the hydrostatic equation.

Boundary conditions on the vertical motion at the top and bottom levels are

$$w_1 = w_7 = 0. \tag{A-9}$$

At each time step, the field of ϕ is calculated by vertical integration of the hydrostatic equation (A-4). To begin this calculation, a lower boundary condition is needed. This is obtained as follows. From (A-5) and (A-9),

$$\int_{z_1}^{z_7} \bar{\rho} u \, dz = 0. \tag{A-10}$$

From (A-2) and (A-10),

$$\int_{z_1}^{z_7} \bar{\rho} \theta \frac{\partial \phi}{\partial r} dz = \int_{z_1}^{z_7} \bar{\rho} \left\{ \frac{M}{r}\left(f + \frac{M}{r^2}\right) - u \frac{\partial u}{\partial r} - w \frac{\partial u}{\partial z} \right\} dz$$
$$+ \int_{z_1}^{z_7} \bar{\rho} \left\{ \frac{K_H}{r^2} \frac{\partial}{\partial r}\left[r^3 \frac{\partial}{\partial r}\left(\frac{u}{r}\right)\right] + \frac{1}{\bar{\rho}} \frac{\partial}{\partial z}\left(\bar{\rho} K_z \frac{\partial u}{\partial z}\right) \right\} dz \equiv B. \tag{A-11}$$

By use of the hydrostatic equation (A-4), we obtain

$$\int_{z_1}^{z_T} \bar{\rho}\theta \frac{\partial \phi}{\partial r} dz = \frac{\partial \phi_1}{\partial r} \int_{z_1}^{z_T} \bar{\rho}\theta dz - \int_{z_1}^{z_T} \bar{\rho}\theta \frac{\partial H}{\partial r} dz, \qquad \text{(A-12)}$$

where

$$H = \int_{z_1}^{z} \frac{g}{\theta} dz', \qquad \text{(A-13)}$$

and z' is a dummy variable.

From (A-11), (A-12), and (A-13),

$$\frac{\partial \phi_1}{\partial r} = \frac{B + \int_{z_1}^{z_T} \bar{\rho}\theta \frac{\partial H}{\partial r} dz}{\int_{z_1}^{z_T} \bar{\rho}\theta dz}. \qquad \text{(A-14)}$$

Given the potential temperature and velocity fields, ϕ_1 may be calculated from (A-14), provided that a boundary condition is given at the outer limit of the computational domain.

The condensation heating per unit time and mass produced by the net effect of the organized cumulus convection is written

$$\dot{Q} = \frac{\bar{\rho}_2 L w_2 \tilde{q} (T_c - T)}{\int_{z_a}^{z_b} \bar{\rho} (T_c - T) dz}, \qquad \text{(A-15)}$$

provided that

$$w_2 > 0, \quad T_c > T.$$

Otherwise,

$$\dot{Q} = 0.$$

(A-16)

In these expressions, L is the latent heat of evaporation; $\bar{\rho}_2$ is a standard density at level 2; w_2 is the cyclone-scale vertical motion at that level; $\tilde{q}$ is the average specific humidity for the layer between levels 1 and 2; T_c is the temperature of a surface air parcel rising with constant equivalent potential temperature, T is the actual air temperature; z_a is the lifting condensation level of the surface air; and z_b (the cloud top) is the level at which the pseudoadiabat, through the lifting condensation level, becomes cooler than the environment (Kuo, 1965).

According to (A-15):

(1) Convection occurs only in the presence of low-level convergence ($w_2 > 0$) and conditional instability for surface air parcels ($T_c > T$).

(2) All the water vapor that converges in the boundary layer rises in convective clouds, condenses, and falls out as precipitation.

(3) All the latent heat thus released is made available to the large-scale flow.

(4) The vertical distribution of this heating is such that the large-scale lapse rate is adjusted towards the pseudoadiabat appropriate to ascent from the surface.

The prognostic cycle proceeds as follows:

(1) Calculate $\dot{Q}$ by the method described above.

(2) Forecast M with (A-1).

(3) Calculate ϕ from (A-4) and (A-14).

(4) Forecast u with (A-2).

(5) Calculate w from (A-5).

(6) Forecast θ with (A-3)

(7) Return to (1) above.

Dependent variables are replaced with their new values as soon as they become available. The scheme is, therefore, semi-implicit, and the results depend on the order in which the calculations are carried out. Indeed, computational stability is dependent on the order of the calculations. The sequence given above has proven to be highly stable.

By use of (A-1), (A-2), (A-5), (A-8), and (A-9), we may derive the following expression for the kinetic energy tendency of the storm:

$$\frac{\partial K}{\partial t} = T_E + I - D_V - D_H, \tag{A-17}$$

where

$$K = 2\pi \int_0^{r_G} \int_{z_1}^{z_7} \bar{\rho} r \left(\frac{u^2+v^2}{2}\right) dz\,dr, \tag{A-18}$$

$$T_E = -2\pi \int_0^{r_G} \int_{z_1}^{z_7} \bar{\rho} r u \theta \frac{\partial \phi}{\partial r} dz\,dr, \tag{A-19}$$

$$I = -2\pi \int_{z_1}^{z_7} \bar{\rho} r_G u_G \left(\frac{u_G^2+v_G^2}{2}\right) dz, \tag{A-20}$$

$$D_V = -2\pi \int_0^{r_\theta} \int_{z_1}^{z_7} r \left\{ u \frac{\partial}{\partial z} \left(\bar{\rho} K_z \frac{\partial u}{\partial z} \right) + v \frac{\partial}{\partial z} \left(\bar{\rho} K_z \frac{\partial v}{\partial z} \right) \right] dz\,dr, \tag{A-21}$$

$$D_H = -2\pi K_H \int_0^{r_\theta} \int_{z_1}^{z_7} \frac{\bar{\rho}}{r} \left\{ u \frac{\partial}{\partial r} \left[r^3 \frac{\partial}{\partial r} \left(\frac{u}{r} \right) \right] + v \frac{\partial}{\partial r} \left[r^3 \frac{\partial}{\partial r} \left(\frac{v}{r} \right) \right] \right\} dz\,dr. \tag{A-22}$$

To evaluate the vertical mixing terms, we invoke the boundary conditions

$$\left(\bar{\rho} K_z \frac{\partial M}{\partial z} \right)_{z=z_1} = C_D \left(\bar{\rho}_1 |V_1| M_1 \right), \tag{A-23}$$

and

$$\left(\bar{\rho} K_z \frac{\partial u}{\partial z} \right)_{z=z_1} = C_D \left(\bar{\rho}_1 |V_1| u_1 \right), \tag{A-24}$$

where C_D is the (constant) drag coefficient, and $|V_1|$ is an approximation to $(u_1^2 + v_1^2)^{1/2}$ made for computational economy. With the distribution of K_z used for these experiments (see table 2) and from (A-23) and (A-24), we have

$$D_V \approx 2\pi \int_0^{r_\theta} r \bar{\rho}_1 C_D |V_1| (u_1^2 + v_1^2)\,dr. \tag{A-25}$$

For the sake of brevity, the dissipation produced by lateral eddy viscosity is written in the form (A-22), rather than in a form that separates internal dissipation from dissipation at the lateral boundary.

If we average (A-17) over a time interval τ , we obtain

$$\frac{\partial \tilde{K}}{\partial t} = \frac{K^{(t+\tau)} - K^{(t)}}{\tau} = \tilde{T}_E + \tilde{I} - \tilde{D}_V - \tilde{D}_H , \tag{A-26}$$

where

$$\widetilde{(\ )} = \frac{1}{\tau}\int_t^{t+\tau} (\ )\, dt' . \tag{A-27}$$

All terms of (A-26) may be evaluated directly from the output of the model. In general, there will be a significant imbalance because of truncation error. Since the finite difference system is one that dampens, the truncation error will usually act as a pseudo dissipation. The kinetic energy budgets shown in figures 17 and 18 of the text are based on 12-hour averages with computations at 12-hour intervals.

The generation of available potential energy was calculated from the approximate relationship

$$G = \frac{2\pi g}{c_p}\int_0^{r_L}\int_{z_1}^{z_7} \frac{T'S'}{\bar{T}^2\bar{N}^2}\bar{\rho}\, r\, dr\, dz , \tag{A-28}$$

where

$$\overline{(\ )} = \frac{2\pi \int_0^{r^*} (\ )\, r\, dr}{\pi r^{*2}}, \tag{A-29}$$

$$r^* = 400\ \text{Km}, \tag{A-30}$$

$$(\ )' = (\ ) - \overline{(\ )}, \tag{A-31}$$

$$N = \frac{g}{\theta} \frac{\partial \theta}{\partial z}, \tag{A-32}$$

and S is the total (convective plus large-scale) condensation heating per unit time and mass.

REFERENCES

Kuo, H. L. (1965), On formation and intensification of tropical cyclones through latent heat release by cumulus convection, J. Atmospheric Sci. 22, No. 1, 40-63.

Ogura, Y., and J. G. Charney (1962), A numerical model of thermal convection in the atmosphere, Proc. Intern. Symp. Numerical Weather Prediction, Meteorol. Soc. Japan, Tokyo, 431-452.

Ogura, Y., and N. A. Phillips (1962), Scale analysis of deep and shallow convection in the atmosphere, J. Atmospheric Sci. 19, No. 2, 173-179.

GPO 853-446

45

U.S. DEPARTMENT OF COMMERCE
ENVIRONMENTAL SCIENCE SERVICES ADMINISTRATION
RESEARCH LABORATORIES

ESSA Technical Memorandum ERLTM-NHRL 82

NUMERICAL EXPERIMENTS WITH A MULTILEVEL PRIMITIVE EQUATION MODEL DESIGNED TO SIMULATE THE DEVELOPMENT OF TROPICAL CYCLONES

EXPERIMENT I

Stanley L. Rosenthal

NATIONAL HURRICANE RESEARCH LABORATORY
MIAMI FLORIDA
JANUARY 1969

TABLE OF CONTENTS

	Page
Abstract	1
1. Introduction	1
2. Design of Experiment I	3
3. Results	12
4. Conclusions	33
5. Acknowledgements	33
6. References	34

NUMERICAL EXPERIMENTS WITH A MULTILEVEL PRIMITIVE EQUATION MODEL DESIGNED TO SIMULATE THE DEVELOPMENT OF TROPICAL CYCLONES

EXPERIMENT I

Stanley L. Rosenthal

The model assumes the storm to be circularly symmetric and is expressed in z-coordinates. The information levels correspond to pressures in the mean tropical atmosphere of 1015, 900, 700, 500, 300, 200, and 100 mb. The heating function for the cyclone-scale motion is simulated by a convective adjustment of the lapse rate towards a pseudoadiabat representative of ascent from the surface boundary layer. The rate of this adjustment is calibrated so that the vertically integrated heating function is related to the upward flux of water vapor through the surface boundary layer.

Initial conditions are given by a weak, near-barotropic vortex in gradient balance. The initial balance is then destroyed by friction, and the meridional circulation and heating function establish themselves. Hurricane force winds are generated in 5 to 6 days and continue for several days thereafter. By the end of the 18th day (at which time the integration is terminated), winds have reduced to about 20 m/sec and the system is clearly in a state of decay. The entire evolution, from start to finish, is slow, and for most of the time conditions are nearly balanced (except for the boundary and outflow layers).

Although the transfer of sensible and latent heat from the ocean to the atmosphere is treated rather pragmatically, these preliminary calculations clearly show the sensible heat exchange to be of crucial importance to the development process.

1. INTRODUCTION

Nonlinear dynamical models have been shown (Ooyama, 1967) to be valuable in extending our knowledge of the genesis and maintenance of tropical cyclones. In principle, these models also have potential use in the design of hurricane modification experiments. The model proposed below differs from Ooyama's (1967) in that it employs primitive rather than balanced equations and has substantially greater vertical resolution. In contrast to Yamasaki's primitive equation model (Yamasaki, 1968a and b), our model uses "z" rather than "p" coordinates and has greater vertical resolution. Also, our system is open at the lateral boundary, whereas Yamasaki's is closed. The information levels are listed in table 1; all dependent variables are defined at all levels.

Table 1. Heights and mean pressures of the information levels. The mean pressures are approximate and are based on a mean hurricane season sounding (Hebert and Jordan, 1959)

Level	Height (meters)	Mean Pressure (mb)
1	0	1,015
2	1,054	900
3	3,187	700
4	5,898	500
5	9,697	300
6	12,423	200
7	16,621	100

The primary source of energy for the development of tropical cyclones is the release of latent heat in organized systems of cumulonimbi; a successful model must contain a reasonable parametric representation of this heating function. Our formulation contains ingredients suggested by previous investigators - in particular, Charney and Eliassen (1964); Kuo (1965); Ogura (1964); Ooyama (1967); Syono and Yamasaki (1966); Yamasaki (1968a and b) - and is justified in the next paragraph.

The lower 400 to 500 mb of the undisturbed, marine tropical atmosphere is almost always conditionally unstable (Gray, 1967; Hebert and Jordan, 1959; Garstang et al., 1967; Malkus, 1960). Empirical evidence (Gray, 1967; Garstang et al., 1967; Malkus, 1960) suggests that the organized systems of deep cumulonimbi associated with synoptic disturbances tend to neutralize this conditional instability by adjusting the lapse rate towards a pseudoadiabat representative of parcel ascent from near sea level. Furthermore, these organized systems of deep cumulonimbi seem to occur only in the presence of low-level mass convergence (Malkus, 1960) and the compensation for this mass convergence appears to take the form of ascent in the convective clouds (Riehl and Malkus, 1961).

Finally, there seems to be a close relationship between water vapor convergence in the lowest layers and the rate of precipitation (Ogura, 1964; Syono, 1950, 1951; Syono et al., 1951).

A heating function that is reasonably consistent with these observations may be written

$$\dot{Q} = \frac{\bar{\rho}_2 L w_2 \tilde{q}(T_c - T)}{\int_{z_a}^{z_b} \bar{\rho}(T_c - T)\,dz}, \qquad (1)$$

provided that $w_2 > 0,\ T_c > T$.

Otherwise, $\dot{Q} = 0$. (1a)

In these expressions, L is the latent heat of evaporation, $\bar{\rho}_2$ is a standard density at level 2, w_2 is the cyclone-scale vertical motion at that level, $\tilde{q}$ is the average specific humidity for the layer between levels 1 and 2, T_c is the temperature of a surface air parcel rising with constant equivalent potential temperature, T is the actual air temperature, z_a is the lifting condensation level of the surface air, and z_b (the cloud top) is the level at which the pseudoadiabat, through the lifting condensation level, becomes cooler than the environment (see Kuo, 1965).

According to (1):

1. Convection occurs only in the presence of low-level convergence ($w_2 > 0$) and conditional instability for surface air parcels ($T_c > T$).
2. All the water vapor that converges in the boundary layer rises in convective clouds, condenses, and falls out as precipitation.
3. All the latent heat thus released is made available to the large-scale flow.
4. The vertical distribution of this heating is such that the large-scale lapse rate is adjusted towards the pseudoadiabat appropriate to ascent from the surface.

2. DESIGN OF EXPERIMENT I

Experiment I was based on a highly simplified version of a rather general model under development at NHRL. While carried out primarily to test certain features of the model, it yielded results that are reasonable enough to present at this time. The major simplifications are as follows:

1. The lifting condensation level of the surface air is assumed to be fixed for all time halfway between levels 1 and 2 (527 m).

2. The average specific humidity over the lowest 1054 m is assumed to be the average saturation value for this layer.

3. The vertical transport of momentum by small-scale eddies is neglected, except at the air-sea interface where it is treated as a drag effect.

4. The air-sea exchange of sensible heat is pragmatically simulated by the requirement that air temperature in the lowest 1054 m be steady state.

5. Vertical redistribution of momentum by transport in cumuli is neglected.

6. The computational domain extends over a radial distance of only 440 km, with a grid increment of 20 km.

These assumptions and simplifications are made primarily for reasons of computational economy. However, some of them also eliminate the need for explicit formulations for relatively obscure physical processes. Items 1 and 2 eliminate the need for a water vapor conveyance equation. A lifting condensation level of 527 m is probably about 30 percent too high for the core of a developing or mature tropical cyclone and helps explain why the experiment develops only a minimal hurricane. On the other hand, assumption 2 overestimates the boundary layer humidity and tends to compensate for the high lifting condensation level. The lack of internal dissipation by vertical mixing -- assumption 3 -- is partly compensated for by the use of one-sided space and time differences which provide an implicit internal dissipation. Assumption 4, although not satisfying from a theoretical point of view, is justifiable on empirical grounds and also used by Yamasaki (1968b). It eliminates the need for a temperature forecast at levels 1 and 2 and for an explicit formulation of the air-sea exchange of sensible heat.

The basic system of equations, assuming circular symmetry, is

$$\frac{\partial M}{\partial t} = -u\frac{\partial M}{\partial r} - w\frac{\partial M}{\partial z} - f r u + \frac{1}{\bar{\rho}}\frac{\partial}{\partial z}\left(\bar{\rho} K_z \frac{\partial M}{\partial z}\right) + \frac{K_H}{r}\frac{\partial}{\partial r}\left\{r^3 \frac{\partial}{\partial r}\left(\frac{v}{r}\right)\right\} \quad (2)$$

$$\frac{\partial u}{\partial t} = -u\frac{\partial u}{\partial r} - w\frac{\partial u}{\partial z} + \frac{M}{r}\left(f + \frac{M}{r^2}\right) - \theta\frac{\partial \phi}{\partial r} + \frac{1}{\bar{\rho}}\frac{\partial}{\partial z}\left(\bar{\rho} K_z \frac{\partial u}{\partial z}\right) + \frac{K_H}{r^2}\frac{\partial}{\partial r}\left\{r^3 \frac{\partial}{\partial r}\left(\frac{u}{r}\right)\right\} \quad (3)$$

$$\frac{\partial \theta}{\partial t} = -u\frac{\partial \theta}{\partial r} - w\frac{\partial \theta}{\partial z} + \frac{c_p K_H}{r\phi}\frac{\partial}{\partial r}\left(r\frac{\partial \theta}{\partial r}\right) + \frac{\dot{Q}}{\phi} \quad (4)$$

$$\frac{\partial \phi}{\partial z} = -g/\theta \quad (5)$$

$$\frac{\partial \bar{\rho} w}{\partial z} = -\frac{1}{r}\frac{\partial \bar{\rho} r u}{\partial r} \quad (6)$$

$$\phi = c_p \left(p/p_0\right)^{R/c_p} \quad (7)$$

$$\theta\phi = c_p T \quad (8)$$

$$M = rv. \quad (9)$$

The symbols are defined as follows:

r	Radius
z	Height
t	Time
M	Relative angular momentum
u	Radial velocity
v	Tangential velocity
w	Vertical velocity
f	Coriolis parameter

$\bar{\rho} = \bar{\rho}(z)$	Density of a reference tropical atmosphere
K_z	Kinematic coefficient of eddy viscosity for vertical mixing
K_H	Kinematic coefficient of eddy viscosity and conductivity for lateral mixing
θ	Potential temperature
c_p	Specific heat capacity at constant pressure for dry air
$\dot{Q}$	Condensation heating per unit time and mass appropriate to the cyclone scale flow
g	Acceleration of gravity
p_0	1000 mb
p	Pressure
T	Air temperature
ρ	Density

Equations (2) and (3) are forms of the tangential and radial equations of motion, respectively. Equation (4) is the first law of thermodynamics. Equation (6) is a simplified form of the continuity equation that filters acoustic waves (Ogura and Charney, 1962; Ogura and Phillips, 1962) and can easily be justified on the basis of an order of magnitude analysis. Equation (5) is the hydrostatic equation.

Boundary conditions on the vertical motion at the top and bottom levels are

$$w_1 = w_7 = 0, \qquad (10)$$

where the subscript denotes level. Discarding viscous and diabatic effects, this sytem of equations with the boundary conditions (10) gives the energy integral

$$\frac{\partial}{\partial t}\int_0^{z_7}\int_0^{r^*}\bar{\rho}\left\{\frac{u^2+v^2}{2}+c_pT+gz\right\}r\,dr\,dz=-\int_0^{z_7}\int_0^{r^*}r\,\frac{\bar{\rho}}{\rho}\,\frac{\partial p}{\partial t}\,r\,dr\,dz, \qquad (11)$$

provided that the domain is mechanically closed at $r=r^*$. If the complete form of the continuity equation,

$$\frac{\partial\rho}{\partial t}=-\frac{\partial\rho w}{\partial z}-\frac{1}{r}\,\frac{\partial(\rho r u)}{\partial r},$$

is used in place of (6), the energy integral analogous to (11) is

$$\frac{\partial}{\partial t}\int_0^{z_7}\int_0^{r^*}\rho(\frac{u^2+v^2}{2})+c_pT+gz)r\,dr\,dz=-\int_0^{z_7}\int_0^{r^*}r\,\frac{\partial p}{\partial t}\,dr\,dz, \qquad (12)$$

which can be written in the more familiar form

$$\frac{\partial}{\partial t}\int_0^{z_7}\int_0^{r^*}\rho\left(\frac{u^2+v^2}{2}+c_vT+gz\right)r\,dr\,dz=0\,. \qquad (13)$$

At each time step, the field of ϕ is calculated by vertical integration of the hydrostatic equation (5). To begin this calculation, a lower boundary condition is needed. This is obtained as follows. From (6) and (10),

$$\int_{z_1}^{z_7}\bar{\rho}\,u\,dz=0\,. \qquad (14)$$

From (3) and (14),

$$\begin{aligned}\int_{z_1}^{z_7}\bar{\rho}\,\theta\,\frac{\partial\phi}{\partial r}\,dz&=\int_{z_1}^{z_7}\bar{\rho}\left\{\frac{M}{r}\left(f+\frac{M}{r^2}\right)-u\frac{\partial u}{\partial r}-w\frac{\partial u}{\partial z}\right\}dz\\&\quad+\int_{z_1}^{z_7}\bar{\rho}\left\{\frac{K_H}{r^2}\frac{\partial}{\partial r}\left[r^3\frac{\partial}{\partial r}\left(\frac{u}{r}\right)\right]+\frac{1}{\bar{\rho}}\frac{\partial}{\partial z}\left(\bar{\rho}K_z\frac{\partial u}{\partial z}\right)\right\}dz \qquad (15)\\&\equiv B\,.\end{aligned}$$

By use of the hydrostatic equation (5)

$$\int_{z_1}^{z_7} \bar{\rho}\Theta \frac{\partial\phi}{\partial r} dz = \frac{\partial\phi_1}{\partial r}\int_{z_1}^{z_7} \bar{\rho}\Theta dz - \int_{z_1}^{z_7} \bar{\rho}\Theta \frac{\partial H}{\partial r} dz, \tag{16}$$

where

$$H = \int_{z_1}^{z_7} \frac{g}{\Theta} dz' \quad , \tag{17}$$

and z' is a dummy variable.

From (15), (16), and (17),

$$\frac{\partial\phi_1}{\partial r} = \frac{B + \int_{z_1}^{z_7} \bar{\rho}\Theta \frac{\partial H}{\partial r} dz}{\int_{z_1}^{z_7} \bar{\rho}\Theta dz} . \tag{18}$$

Given the potential temperature and velocity fields, ϕ_1 may be calculated from (18), provided that a boundary condition is given at the outer limit of the computational domain.

The advection terms in (2), (3), (4), and (15) are calculated by the upstream, noncentered method and the time derivatives are calculated as forward differences. In the vertical, all variables are defined at all levels. Along the radius, a staggered grid is employed. M and u are defined at the grid points

$$r_j = (j-1)\Delta r, \quad j=1,2,...,23, \tag{19}$$

while Θ, ϕ, w and $\dot{Q}$ are given at

$$r_j = (j-\tfrac{1}{2})\Delta r, \quad j=1,2,...,23. \tag{20}$$

The lateral mixing terms in (2), (3), (4), and (15) are evaluated by expressions similar to those used by the author (1964). The vertical mixing terms in (2) and (3) are evaluated by expressions similar to equation (37) given by the author (1964), with due allowance being made for the variable vertical increment. To evaluate these vertical mixing terms at levels 1 and 2, we invoke the boundary conditions

$$\left(\bar{\rho} K_z \frac{\partial M}{\partial z}\right)_{z=z_1} = C_D\left(\bar{\rho}_1 |v_1| M_1\right) \tag{21}$$

$$\left(\bar{\rho} K_z \frac{\partial u}{\partial z}\right)_{z=z_1} = C_D\left(\bar{\rho}_1 |v_1| u_1\right), \tag{22}$$

where C_D is the (constant) drag coefficient, and $|v_1|$ is an approximation to $\sqrt{u_1^2 + v_1^2}$ made for computational economy.

The integrals required to calculate w from (6) and ϕ from (5) are evaluated by the trapezoidal rule. The prognostic equations (2) and (3) are applied at the radial grid given by (19) for $j = 2,3\ldots,22$ and at vertical grid points for $i = 1,2,\ldots,7$. At $j = 1$ ($r = 0$),

$$M = 0, \quad u = 0. \tag{23}$$

At $j = 23$ ($r = 440$ km),

$$(ru)_{j=23} = (ru)_{j=22}, \tag{24}$$

$$M_{j=23} = M_{j=22}, \tag{25}$$

which are the conditions, respectively, that the horizontal divergence and relative vorticity vanish at

$$r = 21.5\,\Delta r = 430 \text{ km}.$$

The potential temperature tendencies are evaluated on the radial grid defined by (20) for $j = 1,2,\ldots,22$ and at vertical grid points for $i = 3,4,\ldots,7$. The boundary condition at $j = 23$ in the potential temperature forecast is

$$\Theta_{j=23} = \Theta_{j=22}\,. \tag{26}$$

The initial conditions consist of a weak vortex in gradient balance with no meridional circulation. This state of balance is achieved as follows. A field of standard potential temperature ($\bar{\Theta} = \bar{\Theta}(z)$) is specified. These values are very nearly those of the mean hurricane season sounding (Hebert and Jordan, 1959) and are listed in table 2. The lower boundary condition

$$\phi_1 = c_p \left(\frac{1015}{1000} \right)^{R/c_p}$$

is adopted, and a set of standard $\bar{\Phi} = \bar{\Phi}(z)$ are calculated from the hydrostatic equation (5). A set of standard temperatures ($\bar{T} = \bar{T}(z)$) are calculated from (8). Equation (7) is then used to calculate standard pressures ($\bar{p} = \bar{p}(z)$). Finally, the standard densities ($\bar{\rho} = \bar{\rho}(z)$) are obtained from

$$\bar{\rho} = \frac{\bar{p}}{R\bar{T}} \; .$$

Table 2. Standard values of thermodynamic variables (See text for method of calculation)

Level	Height (m)	$\bar{\Theta}$(°K)	$\bar{T}$(°K)	$\bar{p}$(mb)	$\bar{\rho}$(ton/m^3)
1	0	300	301.3	1015.0	1.174×10^{-3}
2	1,054	303	294.1	900.4	1.067×10^{-3}
3	3,187	313	282.6	699.4	0.862×10^{-3}
4	5,898	325	266.5	499.2	0.653×10^{-3}
5	9,697	340	240.8	299.2	0.433×10^{-3}
6	12,423	347	218.9	199.5	0.318×10^{-3}
7	16,621	391	203.1	101.1	0.173×10^{-3}

The initial temperature field is given by

$$T_{i,j} = \bar{T}_i + \epsilon \left\{ \cos \frac{\pi}{\hat{r}} r_j + 1 \right\} \sin \frac{\pi}{z_7} z_i \, , \qquad (27)$$

where ϵ = 0.16°K and $\hat{r}$ = 430 km. With the boundary condition $\phi_{7,j} = \bar{\Phi}_7$, the hydrostatic equation, in the form

$$\frac{\partial \phi}{\partial z} = -g\phi / c_p T \, , \qquad (28)$$

is integrated by the trapezoidal rule to obtain $\phi_{i,j}$ for $i = 6,5,\ldots,1$. With T and ϕ initialized, initial values of Θ are calculated from (8), the gradient wind equation is solved for the initial distribution of v, and M is then calculated from (9).

The prognostic cycle proceeds as follows:

1. Calculate $\dot{Q}$ by the method described in section 1.
2. Forecast M with (2).
3. Calculate ϕ from (5) and (18).
4. Forecast u with (3).
5. Calculate w from (6).
6. Forecast Θ with (4).
7. Return to 1 above.

Dependent variables are replaced with their new values as soon as they become available. The scheme is, therefore, semi-implicit, and the results depend on the order in which the calculations are carried out. Indeed, computational stability is dependent on the order of the calculations. The sequence given above has proven to be highly stable. Table 3 lists certain parameters of interest for Experiment I.

Table 3. Parameters used for Experiment I.

Term	Symbol	Value
Kinematic coefficient of eddy viscosity and/or eddy conductivity for lateral mixing	K_H	$10^4 m^2/sec$
Drag coefficient	C_D	3×10^{-3}
Time step	Δt	120 sec
Radial increment	Δr	20 km
Coriolis parameter	f	5×10^{-5} sec^{-1}
Kinematic coefficient of eddy viscosity for vertical mixing	K_z	$10 m^2/sec$ at level 1; zero elsewhere

3. RESULTS

The cyclone's history is summarized in figure 1. The central pressure and maximum surface wind change little during the first 3 days. This period probably can be related to the development of the well-known "preexisting" disturbances from which hurricanes evolve. A similar organizational period is found in Ooyama's (1967) experiments, as well as in those of Yamasaki (1968 a and b). The intensity, as measured by central pressure and maximum surface wind, reaches a peak at about 180 hr, when the central pressure is 974 mb and the strongest surface wind is 45 m $\sec^{-1}$.

Hurricane force winds are present at the surface from about 144 to 336 hr. By the end of the integration (432 hr), the strongest surface winds have dropped to about half of their peak values. The temporal variations of the positions of the maximum surface wind, surface gale force winds, surface hurricane force winds, and maximum $w^*(=w_2)$, shown by the top section in figure 1, are all fairly similar to those of Ooyama's experiment. During the organizational period, the radius of the maximum surface wind (initially 250 km) decreases rapidly. A distinct maximum in the $w*$ profile (to be identified with the eye wall) does not appear until 96 hr, and thereafter the storm begins to deepen rapidly.

The dashed curve in the bottom section of figure 1 represents a calculation in which the air-sea exchange of sensible heat was neglected and temperatures in the boundary layer were forecast from an adiabatic form of the thermodynamic equation. This calculation clearly illustrates the crucial role played by the sensible heat source.

Figure 2 illustrates temporal variations of the radial profiles of surface wind, surface pressure, and $w*$. The initial surface wind is shown by the dashed curve in the upper left section. The concentration of kinetic energy, pressure deficit, and ascent in a fairly narrow ring close to the storm center, so typical of mature hurricanes, is remarkably well reproduced by the model at peak intensity (180 hr). Figure 3 shows that the storm structure, in general, is also fairly realistic (see, for example, Colon, 1961; Hawkins and Rubsam, 1968; Miller, 1964).

Inflow and outflow, respectively, are concentrated in the boundary layer and in the upper troposphere in much the same way as has been found in numerous empirical studies based on

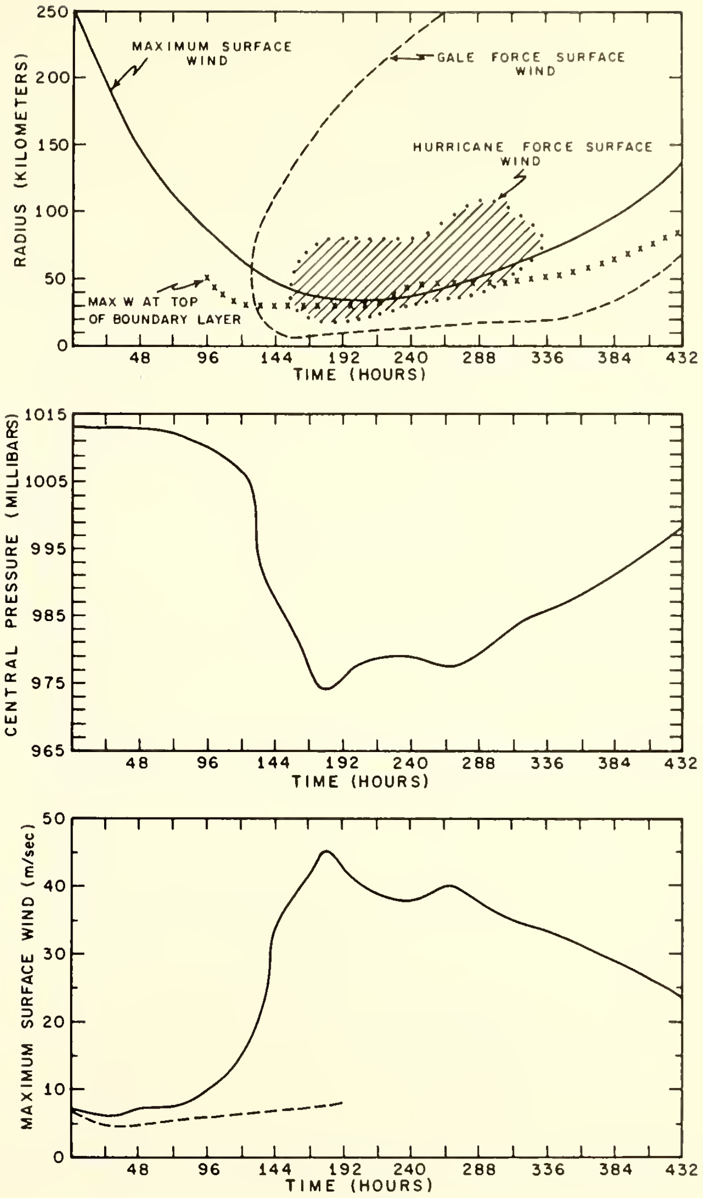

Figure 1. - Top: Radii of maximum surface wind and maximum vertical motion at the 1054-m level. Outer and inner limits of gale and hurricane force winds at the surface. Middle: Central pressure as a function of time. Bottom: Maximum surface wind as a function of time.

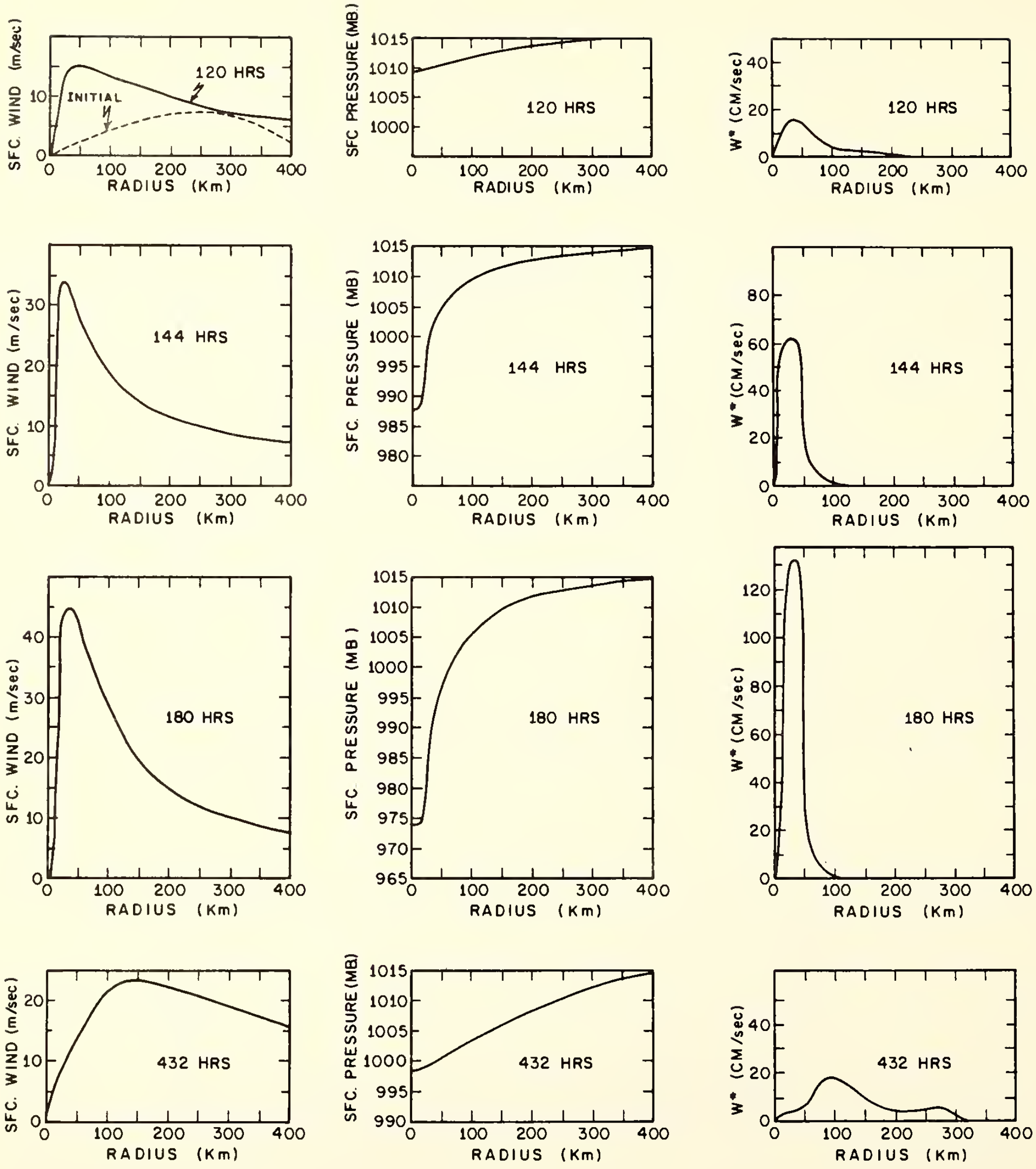

Figure 2. - Radial distribution of certain variables at selected times. Left: Surface wind speed. Center: Surface pressure. Right: Vertical motion at the 1054-m level.

data gathered by reconnaissance aircraft. This characteristic distribution is even more vividly portrayed by figure 4. On the other hand, the surface inflow (fig. 3), especially between radii of 50 to 100 km, is much stronger than has been deduced from observation (Hawkins and Rubsam, 1968; Miller, 1964; Riehl and Malkus, 1961). Indeed, the inflow angle near 100 km is somewhat greater than 45°. It is difficult to determine to what extent this discrepancy is physically real. Aircraft flight data are taken well above the main boundary layer and cannot, by themselves, be used to determine the strength of inflow close to the surface. This is dramatically illustrated if we attempt to deduce the surface radial wind shown in figure 4 from data at, say, 700 or 900 mb. Some studies have supplemented aircraft data with ship observations. These data are, however, usually well out from the core of the storm and would be of little help in estimating inflow in the region of maximum radial wind shown in figure 3. Some theoretical studies (Malkus and Riehl, 1960; Miller, 1965; Ooyama, 1967) have found inflow fairly close in magnitude to those obtained here.

The outflow maximum at 100 mb is also in conflict with the empirically deduced distributions (see, for example, Hawkins and Rubsam, 1968; Miller, 1964; Riehl and Malkus, 1961), which characteristically show greatest outflow at 200 mb and assume zero outflow at 100 mb. However, there is little in the way of observational data in the core of hurricanes above 200 mb. If, as suggested above, the empirical studies underestimate low-level inflow, then there is a great deal of latitude for adjusting the empirical distributions of outflow above 200 mb to compensate for the increased inflow. The distributions of radial wind shown in figures 3 and 4 may then be more reasonable than they first appear. The outflow magnitudes shown in figures 3 and 4 are substantially greater than those given by Yamasaki (1968a and b). The reason may well be differences in vertical resolution between the two models. His upper tropospheric radial velocity should be considered an average over a pressure depth of 300 mb. If we take this into account, the mass outflows of the two experiments are comparable.

Figure 3 shows no well-defined region of subsidence at the storm center that would be analogous to the eye wall of a real hurricane. Yamasaki (1968a and b) also had difficulty in producing an eye and attributed this to the shape of the initial wind profile. It seems more attractive, however, to attribute eye formation to the dynamics of cyclone development rather than to fortuitous initial conditions. Our Experiment I does attempt to develop descent at the storm center, but this is a transitory feature, which appears, disappears, and reappears. Figure 5 shows conditions 12 hr after those in figure 3. A distinct region of descent at the storm center is present at this time. The lack of a "permanent" eye may well be due to the coarse radial resolution used for these calculations.

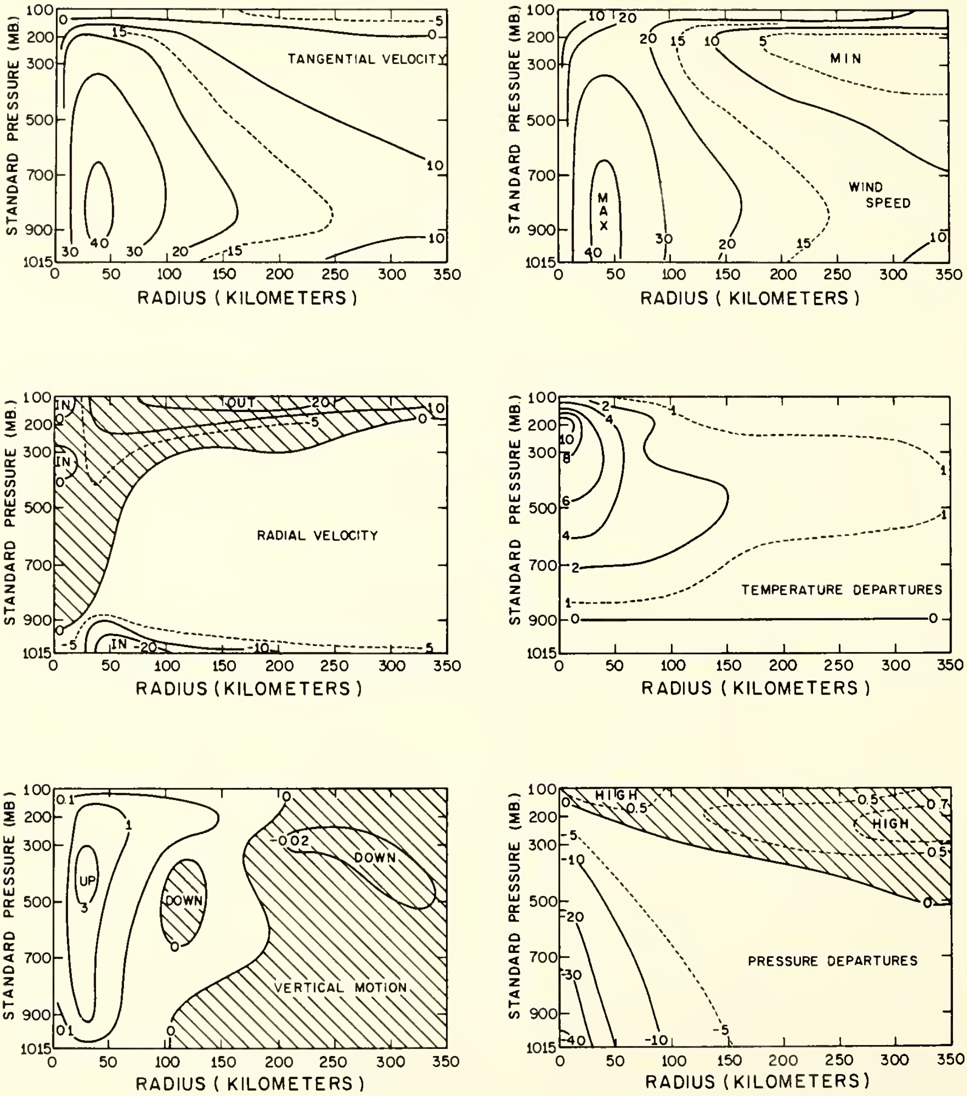

Figure 3. - Vertical cross sections of various dependent variables at 180 hr. Upper Left: Tangential velocity in m sec^{-1}. Upper Right: Total wind speed in m sec^{-1}. Center Left: Radial velocity in m sec^{-1}. Center Right: Temperature excess over the mean tropical atmosphere in °K. Lower Left: Vertical velocity in m sec^{-1}. Isopleths are drawn at variable intervals. Lower Right: Pressure departures from mean tropical atmosphere in mb. Isopleths are drawn at variable intervals.

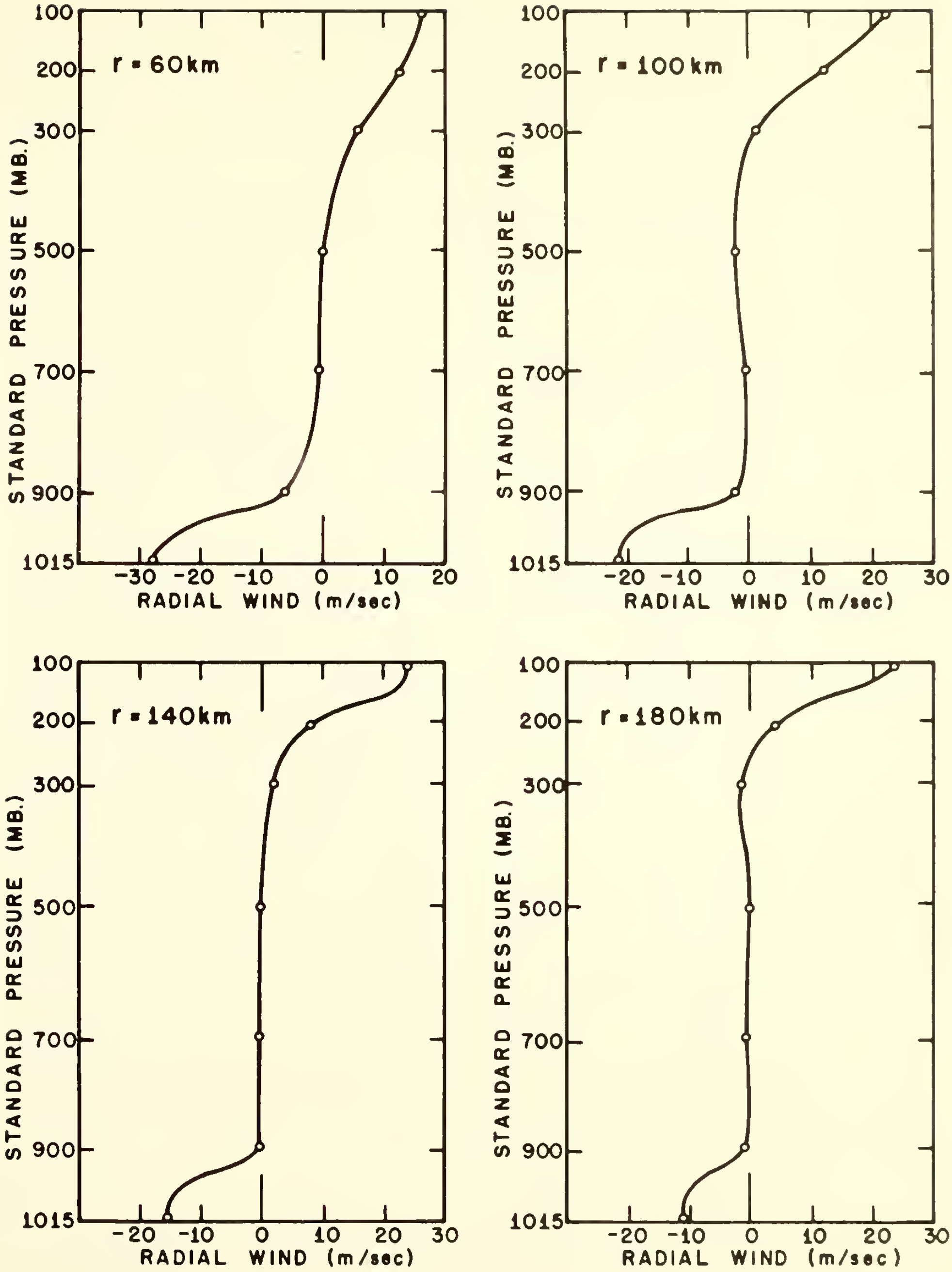

Figure 4. - Vertical profiles of radial velocity at 180 hr for selected radii.

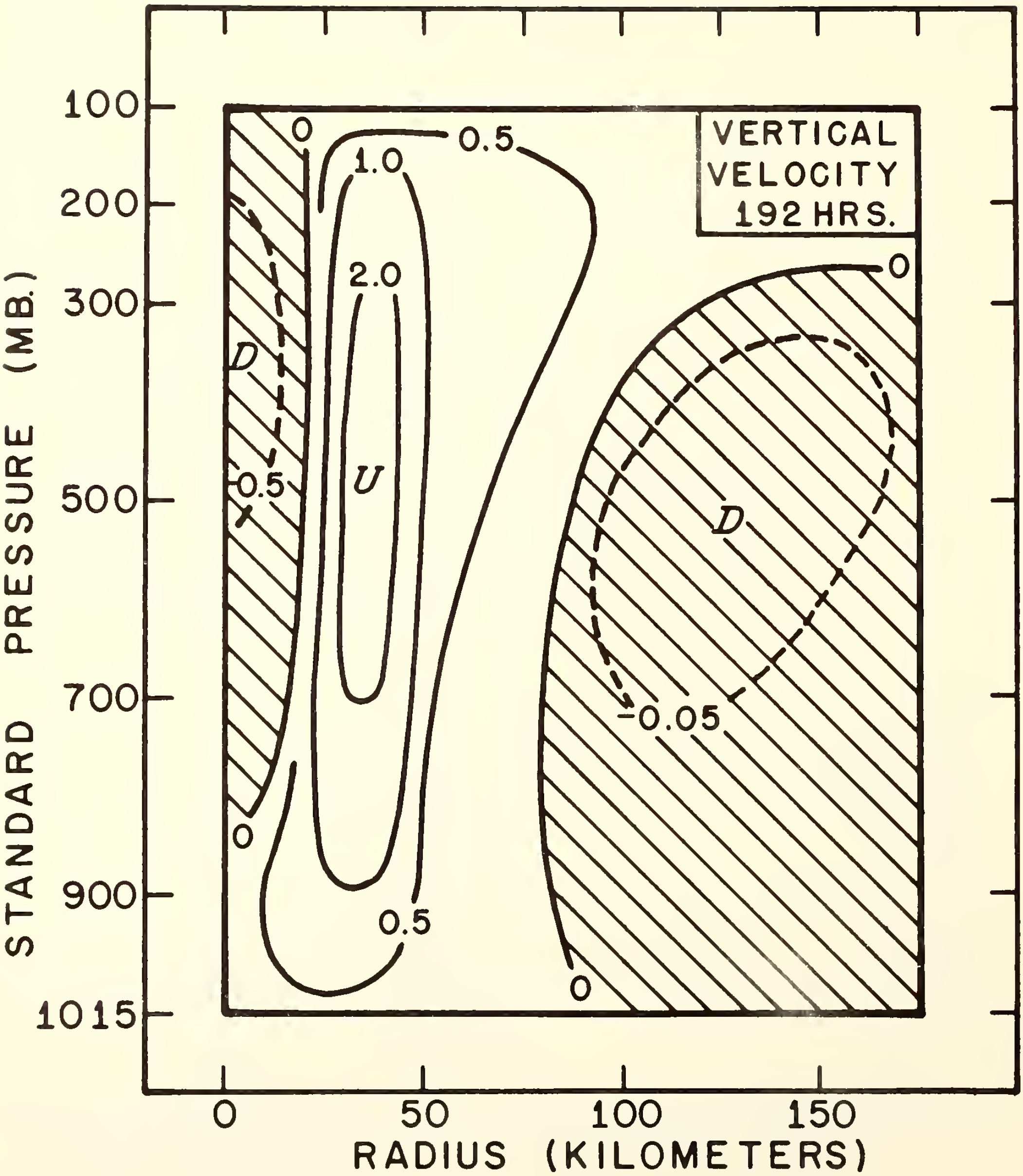

Figure 5. - Cross section of vertical motion at 192 hr. Isopleths are drawn at variable intervals and labeled in m sec^{-1}.

Figure 6 gives further information concerning the storm's history. The kinetic energy curves (center section) clearly show that peak intensity (at 180 hr) as indicated by the central pressure and maximum surface wind is really only indicative of conditions in the innermost 100 km; the kinetic energy of the storm as a whole (0-400 km) does not reach its maximum until about 360 hr. With regard to the kinetic energy content of individual rings (fig. 7), peak intensity is reached at about 280 hr for the 100-200-km ring, at about 380 hr for the 200-300-km ring, and kinetic energy increases throughout the period of integration in the 300-400-ring.

The top section of figure 6 shows the average precipitation in the innermost 100 km of the system (based on the assumptions given in sec. 1). The values shown during the mature stage, say from 180 to 290 hr, compare reasonably well with those of real tropical cyclones (Miller, 1964; Riehl and Malkus, 1961).

The bottom section of figure 6 shows the efficiency of the storm's innermost 200 km. This quantity is defined in the usual manner as the ratio of the rate of kinetic energy production to the rate of latent heat release. The peak value of 4.7 percent (at about 180 hr) is a little higher than that found in other models (Ooyama, 1967; Yamasaki, 1968a) and empirically (Palmen and Riehl, 1957). The average over the period from 180 to 288 hr falls fairly close to the usual 3 to 4 percent found by the authors cited above.

At this point it is appropriate to attempt explanations for the transitions from one phase of the storm's life cycle to next. The initial 96 hr are clearly an organizational period during which the meridional circulation is taking form. During this time, there is no distinct maximum of w^* (and, hence, no eye wall) and, as can be seen from figure 6, there is little release of latent heat. The relatively rapid intensification between 120 and 168 hr may possibly be explained by recent perturbation analyses (Rosenthal and Koss, 1968; Syono, 1966). These studies show that tropical cyclone development tends to be slower when the upper tropospheric heating function is large compared to that of the lower troposphere and that development becomes more rapid as the vertical distribution of the heating function becomes more uniform.

Figure 8 shows vertical profiles of the differences T_c-T which, by (1), are proportional to the heating function. At the 10-km radius, in particular, the tendency for T_c-T to take on a more nearly uniform vertical distribution during the period of rapid deepening is clear. Yamasaki (1968a and b) offered the same explanation for the period of rapid intensification given by his model. However, a similar period of

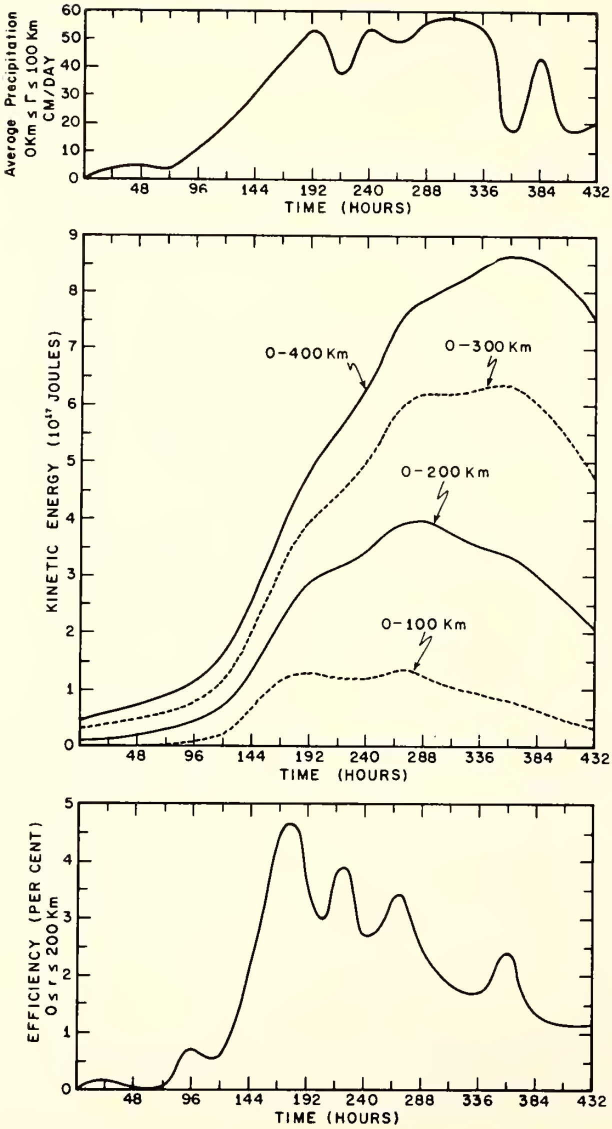

Figure 6. - Variations with time of various quantities. Top: Average precipitation over the radial interval zero to 100 km. Middle: Total kinetic energy contained in various radial intervals. Bottom: Efficiency of the storm defined as the ratio of the rate of kinetic energy production to the rate of condensation heating in the radial interval 0 to 200 km.

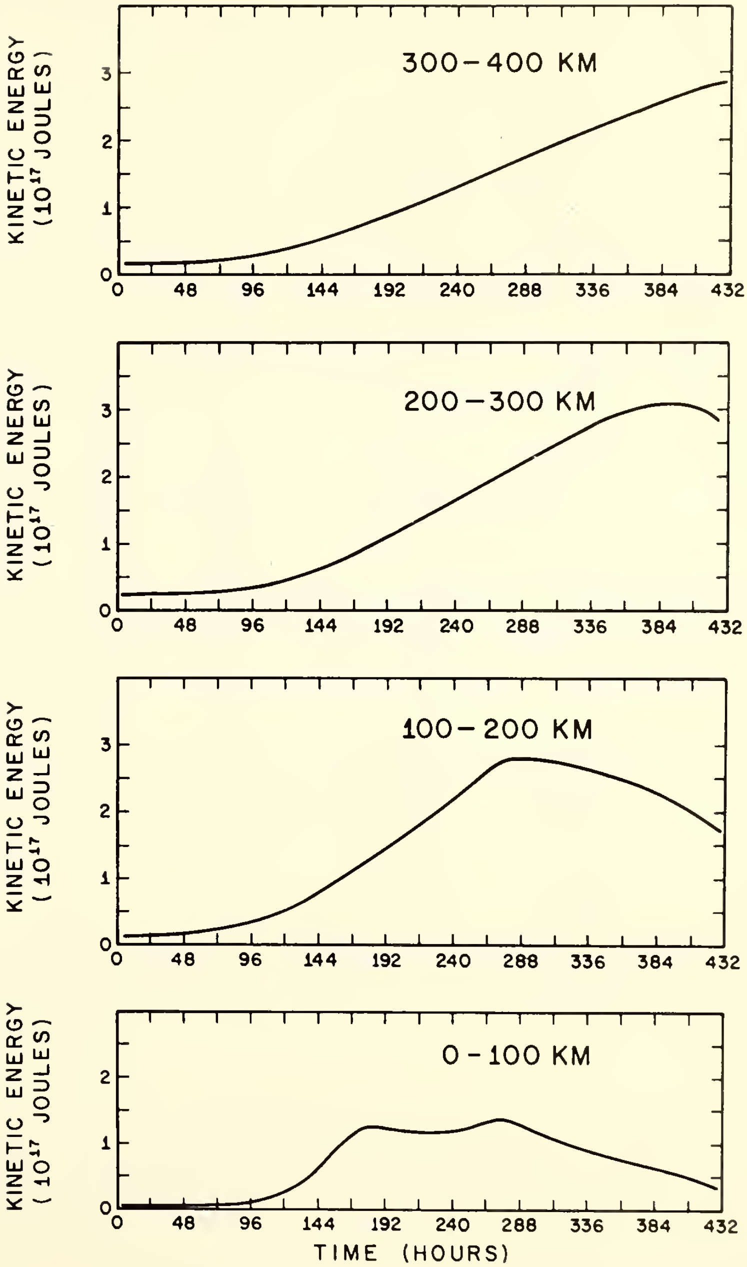

Figure 7. - Variations with time of the kinetic energy content of various rings of the storm.

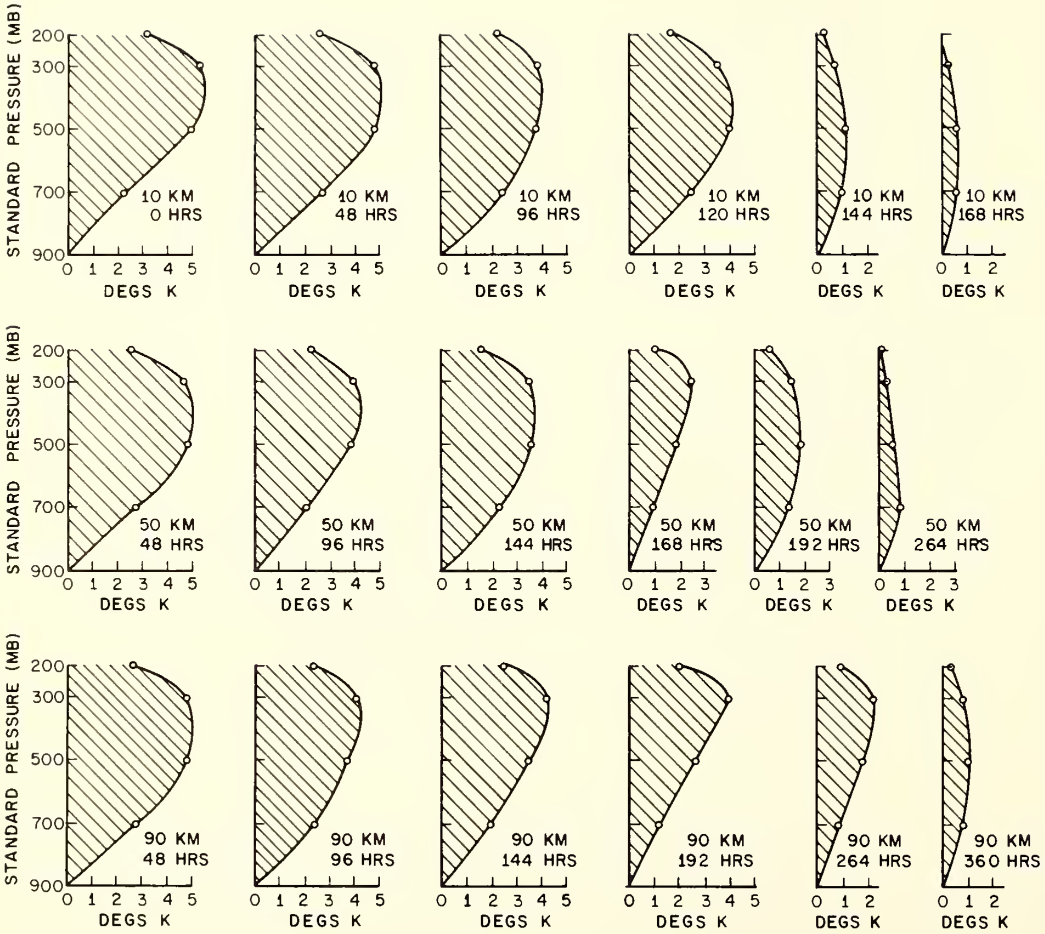

Figure 8. - Vertical profiles of "cloud" temperature minus air temperature (^{o}K) at selected radii and times. Top: Radius of 10 km. Center: Radius of 50 km. Bottom: Radius of 90 km.

rapid deepening is found in Ooyama's results. Since his model does not contain a vertical variation of heating, the mechanism discussed above cannot explain Ooyama's results and may, therefore, not be of primary importance.

At 168 hr, the temperature profile at 10 km is very nearly coincident with the "cloud" pseudoadiabat, and by 180 hr (at which time the central pressure and maximum surface wind reach their extreme values) the temperature profile at the 10-km radius is indeed coincident with the cloud pseudoadiabat, and heating at this radius is cut off. The approach of the temperature profile to the "cloud" pseudoadiabat at the 50- and 90-km radii occurs more slowly but is clearly indicated by figure 8. Note that the equivalent potential temperatures of the "clouds" are not constant with time but vary inversely with the boundary layer pressures (as illustrated by figure 9).

By use of (2), (3), (6), (9), and (10), we may derive the following expression for the kinetic energy tendency of the storm:

$$\frac{\partial K}{\partial t} = T_E + I - D_v - D_H , \tag{29}$$

where

$$K = 2\pi \int_0^{r_b} \int_{z_1}^{z_7} \bar{\rho} r \left(\frac{u^2 + v^2}{2} \right) dz\, dr \tag{30}$$

$$T_E = -2\pi \int_0^{r_b} \int_{z_1}^{z_7} \bar{\rho} r u \theta \frac{\partial \phi}{\partial r} dz\, dr \tag{31}$$

$$I = -2\pi \int_{z_1}^{z_7} \bar{\rho} r_b (uK)_{r_b} dz \tag{32}$$

$$D_v = -2\pi \int_0^{r_b} \int_{z_1}^{z_7} r \left\{ u \frac{\partial}{\partial z} \left(\bar{\rho} K_z \frac{\partial u}{\partial z} \right) + v \frac{\partial}{\partial z} \left(\bar{\rho} K_z \frac{\partial v}{\partial z} \right) \right\} dz\, dr \tag{33}$$

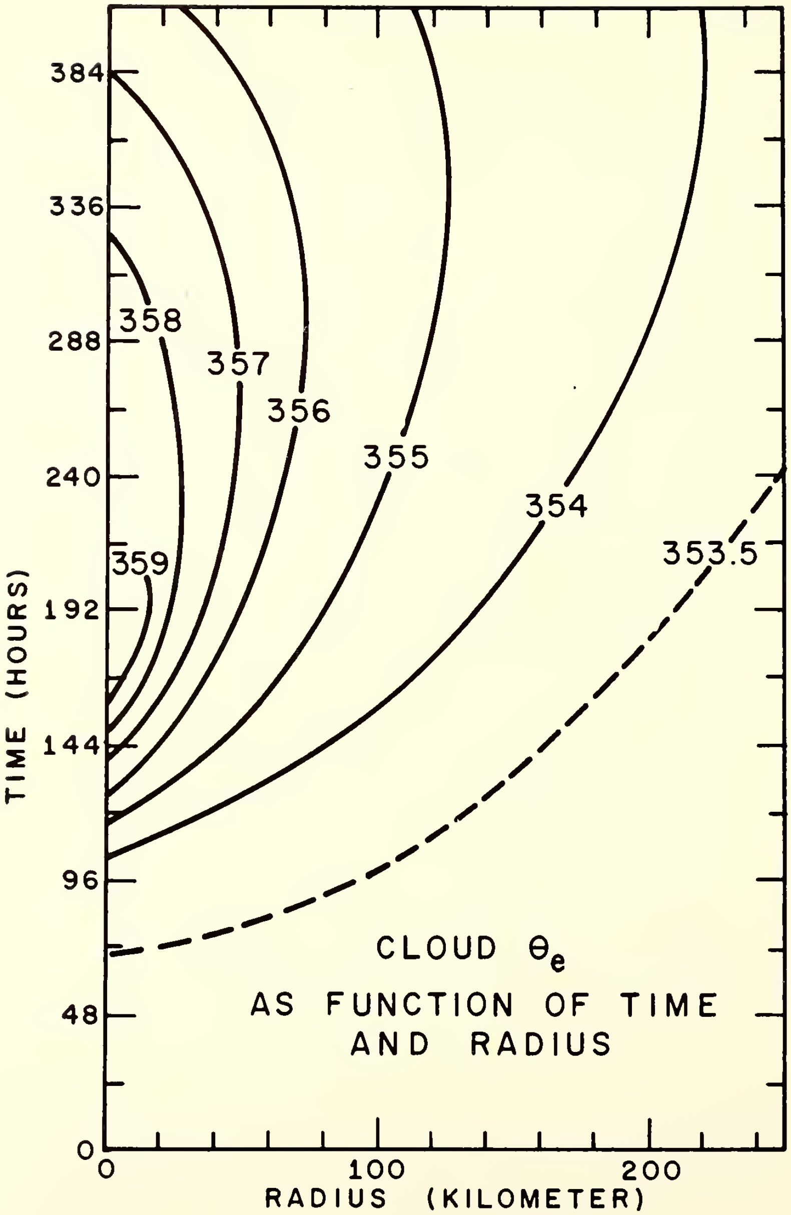

Figure 9. - Equivalent potential temperature of the "clouds" as a function of radius and time. Isopleths are labeled in °K.

$$D_H = -2\pi K_H \int_0^{r_b} \int_{z_1}^{z_7} \frac{\bar{\rho}}{r} \left\{ u \frac{\partial}{\partial r}\left[r^3 \frac{\partial}{\partial r}\left(\frac{u}{r}\right)\right] + v \frac{\partial}{\partial r}\left[r^3 \frac{\partial}{\partial r}\left(\frac{v}{r}\right)\right] \right\} dz\, dr. \tag{34}$$

The physical interpretation of these terms is well known and will not be elaborated upon here. With the distribution of K_z used for Experiment I (see table 3) and from (21) and (22), we have

$$D_V \approx 2\pi \int_0^{r_b} r \bar{\rho} C_D |v_1| (u_1^2 + v_1^2)\, dr. \tag{35}$$

For the sake of brevity, the dissipation due to lateral eddy viscosity is written in the form (34) rather than in a form that separates internal dissipation from dissipation at the lateral boundary.

If we average (29) over a time interval τ, we obtain

$$\frac{\partial \bar{K}}{\partial t} = \frac{K^{(t+\tau)} - K^{(t)}}{\tau} = \bar{T}_E + \bar{I} - \bar{D}_V - \bar{D}_H , \tag{36}$$

where

$$\overline{(\ )} = \frac{1}{\tau} \int_t^{t+\tau} (\ )\, dt' . \tag{37}$$

All terms of (36) may be evaluated directly from the output of the model. In general, there will be a significant imbalance due to truncation error. Since the finite difference system is one that dampens, the truncation error will usually act as a pseudo dissipation.

The history of the storm's kinetic energy budget is shown in figure 10. The averages are over 2 hr and calculations were made at intervals of 24 hr. The storm exports kinetic energy to its environment throughout the period of integration. Both the outflow of kinetic energy and the dissipation by lateral eddy viscosity are relatively small components of the budget. The dissipation by truncation error is substantial

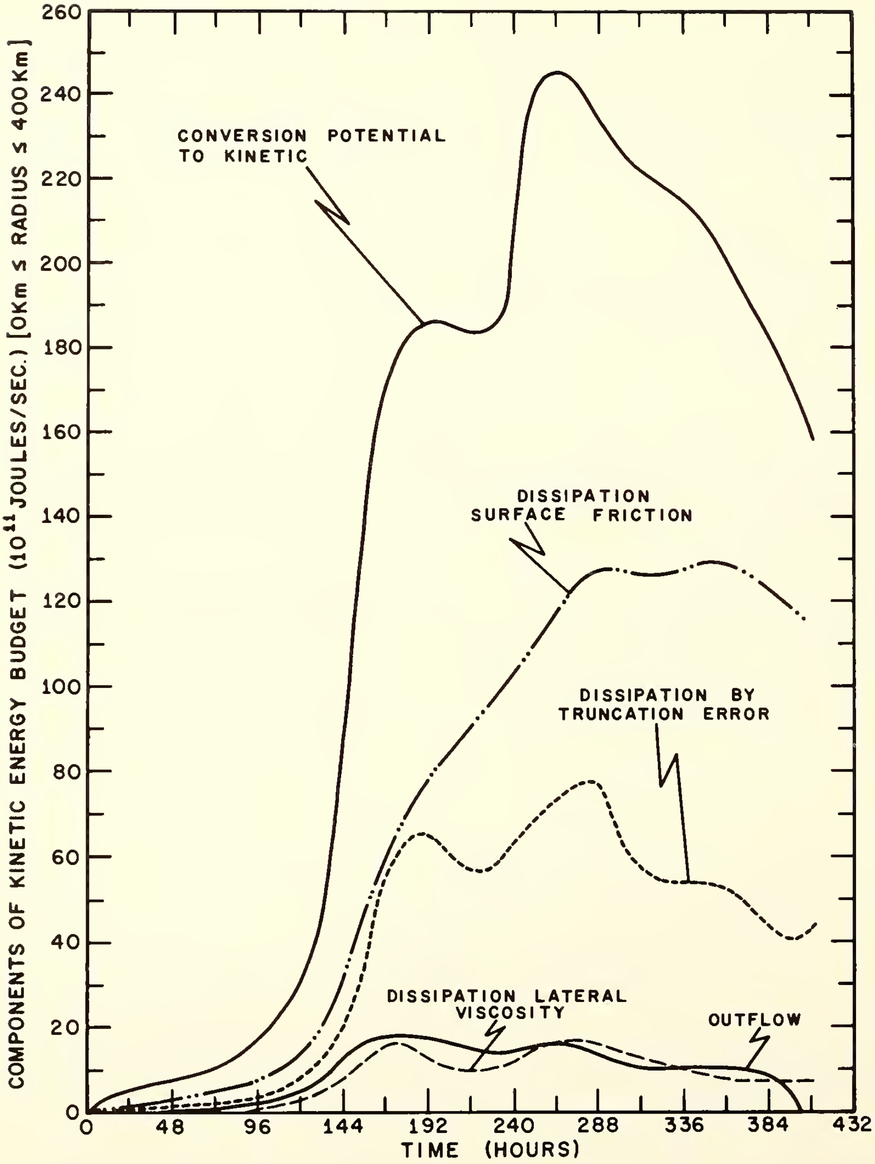

Figure 10. - Components of the kinetic energy budget as a function of time. The values are appropriate to the radial interval from zero to 400 km and are 2-hr averages. Only the conversion term gives a positive contribution to the kinetic energy tendency.

and justifies the neglect of explicit internal dissipation by vertical eddy viscosity. The total internal dissipation (truncation error plus lateral eddy viscosity) is of the same order of magnitude as the dissipation by surface drag friction, which is consistent with empirical energy budgets (Hawkins and Rubsam, 1968; Miller, 1964; Riehl and Malkus, 1961).

Figures 11, 12, 13, and 14 show more detailed kinetic energy budgets at 148 hr (developing stage), 184 hr (near peak intensity in the innermost 100 km), 244 hr (mature stage) and 316 hr (decaying stage). The averaging period for these budgets is 10 hr. The vertically integrated budgets (bottom sections of figs. 11, 12, 13, and 14) show the innermost 100 km of the storm to be crucially dependent on the import of kinetic energy generated at larger radii, since total dissipation in this inner region is substantially greater than generation, (except during the developing stage — 148 hr — when these two effects are nearly of equal magnitude). Similar results have been found in observational studies (Hawkins and Rubsam, 1968; Riehl and Malkus, 1961) and in models (Ooyama, 1967). The kinetic energy tendency in the inner areas of the storm is a small balance between large contributing terms, which is similar to Ooyama's result.

In the innermost 100 km, the upper troposphere converts kinetic energy to potential energy and also exports kinetic energy laterally to the center areas of the storm. The sole source of the kinetic energy required to maintain the motion in this region is the vertical import of kinetic energy generated in the lower troposphere. The same is true of the middle troposphere of the innermost 100 km at 244 and 316 hr.

At 148 and 184 hr, kinetic energy production is greatest in the innermost 100 km. On the other hand, at 244 and 316 hr, after the storm has started to spread radially, production is greatest in the 100- to 200-km ring. At all four times, virtually all of the kinetic energy production is in the lower troposphere. The truncation error, while energy consuming for the storm as a whole (figure 10) and strongly energy consuming in the innermost 100 km of the lower troposphere (figs. 11, 12, 13, and 14), is energy producing in some individual rings and layers. In these cases, the largest error contributions are in the upper troposphere.

Table 4 shows the extent of gradient wind balance at selected times. At 200 and 100 mb, the tangential wind is highly non-gradient and even antibaric at several grid points. At 900, 700, and 500 mb, fairly close gradient balance prevails,

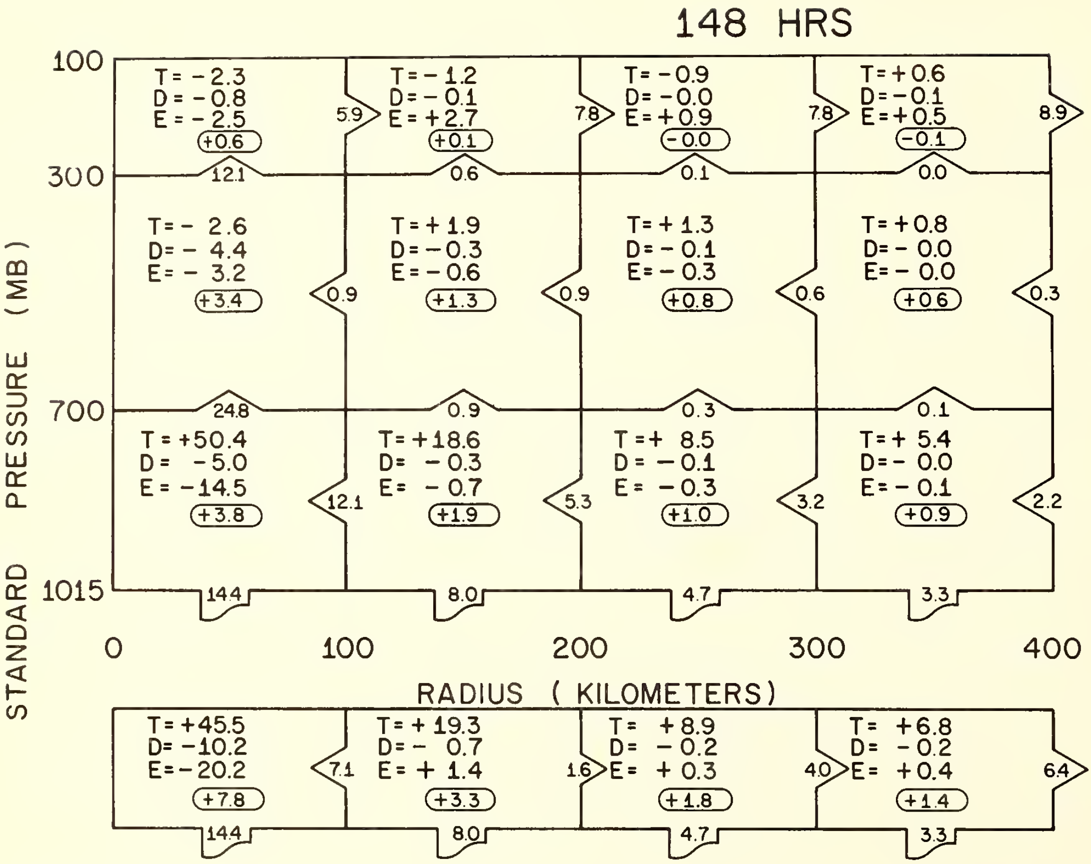

Figure 11. - Detailed kinetic energy budget at 148 hr. Bottom section is the vertically integrated budget. Top section shows the interaction between atmospheric layers. All numerical values are in units of 10^{11} joules sec^{-1}. Symbols are: T = rate of conversion of potential to kinetic energy; D = rate of internal dissipation by lateral mixing; E = rate of energy addition by truncation errors. Values in ovals are the kinetic energy tendencies. Values at the lower boundary in irregular shaped outlines are surface friction dissipation rates. Kinetic energy transports by the meridional circulation are found in the large arrows on the appropriate boundaries that point in the direction of the transport.

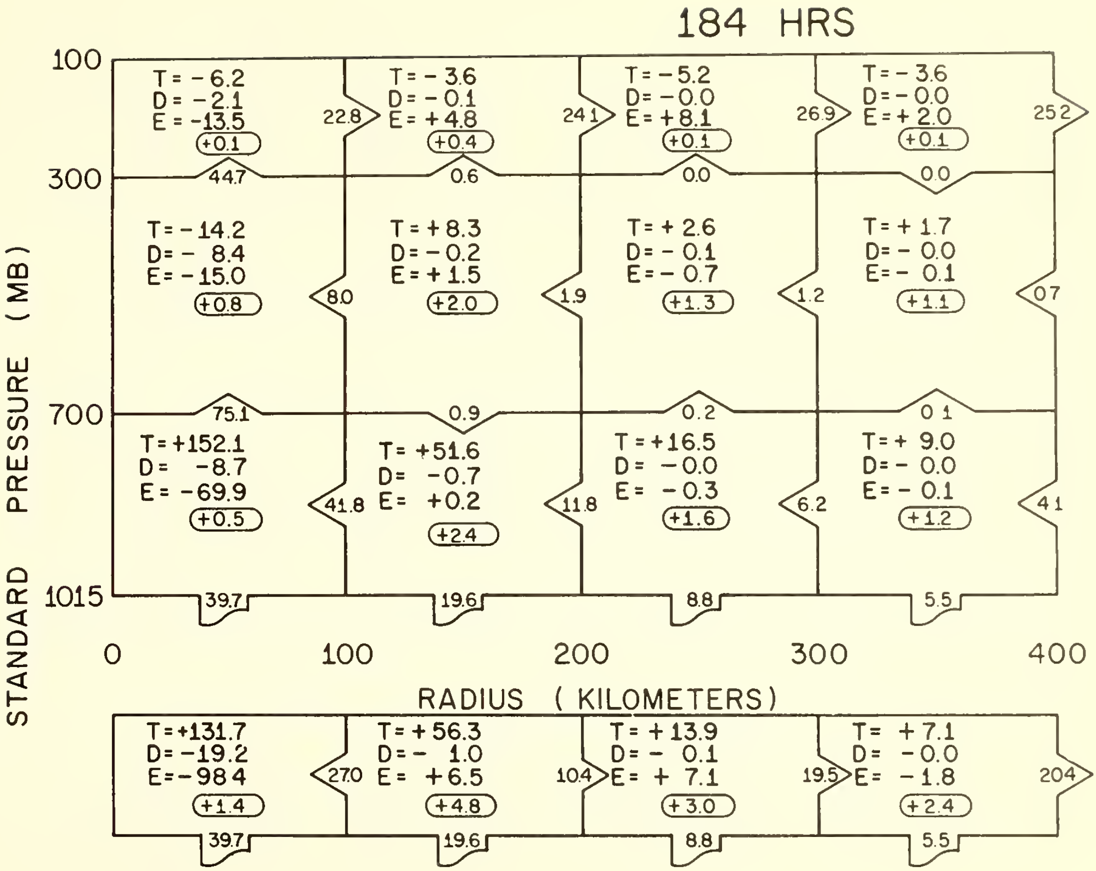

Figure 12. - Same as fig. 11 but for 184 hr.

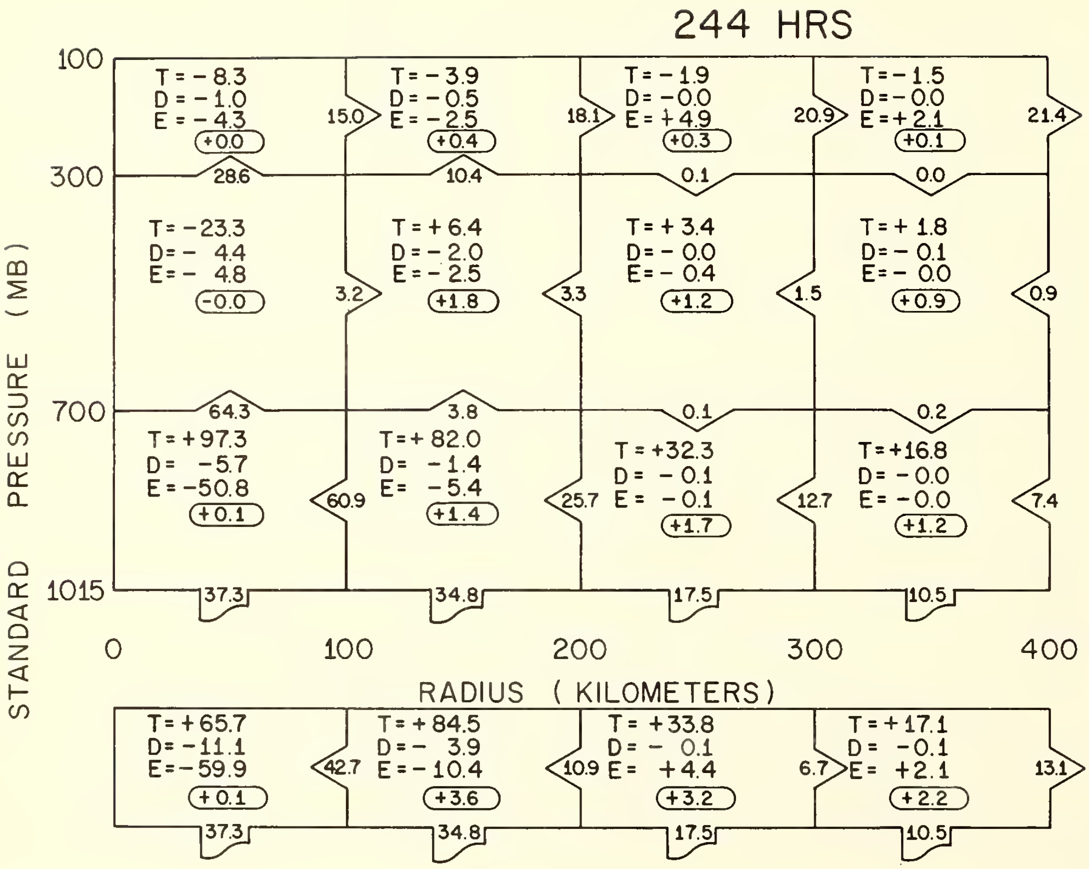

Figure 13. - Same as fig. 11 but for 244 hr.

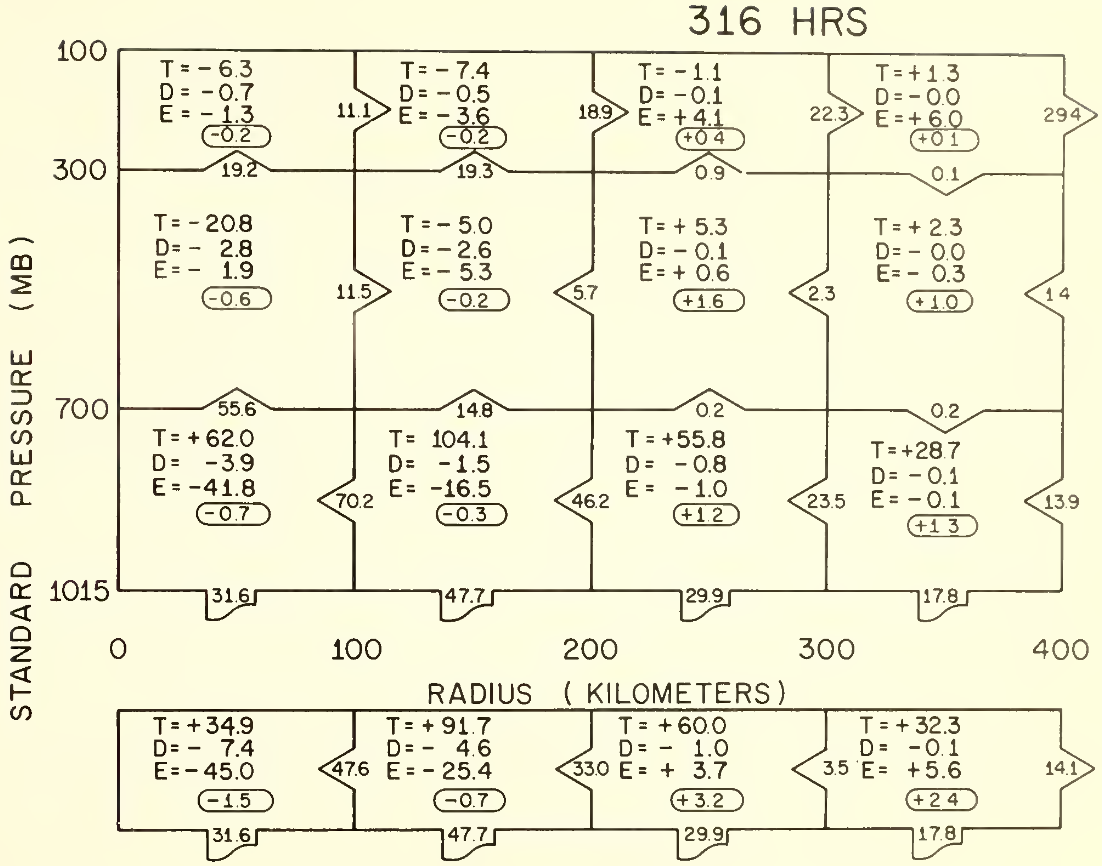

Figure 14. - Same as fig. 11 but for 316 hr.

while at 300 mb near-gradient conditions are present only during the second half of the period of integration. At the surface, gradient balance is prevented by the drag friction effect.

Table 4. Horizontal Averages of $\frac{\left|\frac{1}{\rho}\frac{\partial p}{\partial r}\right|}{\left|fv + v^2/r\right|}$, ratio of pressure gradient force to the sum of the Coriolis and centrifugal forces per unit mass (Asterisks denote averages that include one or more antibaric points)

Time	Standard Pressure (mb)						
(hr)	1015	900	700	500	300	200	100
0	1.00	1.00	1.00	1.00	1.00	1.00	1.00
72	1.11	0.86	0.90	0.92	4.47*	4.90*	3.95*
144	1.50	0.92	0.95	0.95	1.74*	2.87*	4.07*
192	1.75	0.91	0.95	0.97	0.93	1.62*	50.36*
240	1.82	0.91	0.94	0.95	0.95	1.09*	12.85*
360	1.81	0.88	0.94	0.95	0.94	0.88*	6.16*

The solutions were examined for the presence of inertial instability as measured by

$$\left(f + \frac{2v}{r}\right)\left(\frac{\partial v}{\partial r} + \frac{v}{r} + f\right) < 0 .$$

Inertial instability first appeared at 100 mb at a radius of 40 km at 162 hr. This was well after rapid intensification of the system had started and must be viewed as a result rather than a cause of the storm's development. This region of instability persisted until 186 hr and then disappeared. From 246 hr until the end of the integration, it was possible to find one or two 100-mb grid points with inertial instability between radii of 60 and 140 km. After 186 hr, points of inertial instability were almost always present at 300 and/or 200 mb. These first appeared at a radius of 120 km and slowly drifted outward. By the end of the integration they were present only at 300 mb between radii of 320 and 360 km. At no time were there more than three such grid points. In most instances, there were only one or two. The presence of this small region of instabilty seemed to have no significant effect on the evolution of the system.

4. CONCLUSIONS

The results obtained indicate that the model is capable of simulating the life cycle of a tropical cyclone with a fair degree of reality. These results, together with those of Yamasaki (1968a and b), show that the primitive equations can be successfully integrated for the tropical cyclone problem. The results also indicate that a supply of sensible heat from the ocean surface is a crucial ingredient without which development would not occur.

The tangential winds were found to be in near-gradient balance at 900, 700, and 500 mb at all times and at 300 mb during the later phases of the integration. At the surface, where drag friction is present, the winds are subgradient. The main outflow at 200 and 100 mb is highly unbalanced. Inertial instability, while present in small regions after the storm's organizational period, appears to be an effect of the development rather than a cause.

The model has several distinct deficiences, which were cited in section 2. Future work will be aimed at (1) an explicit calculation of the air-sea exchange of sensible heat, with a boundary layer temperature forecast made by use of the first law of thermodynamics, (2) introduction of a water vapor conveyance equation for prediction of the specific humidity, (3) inclusion of the vertical transport of momentum by the cumulus scale circulations, and (4) reworking the model in a more accurate finite difference system, with an explicit formulation of internal dissipation.

5. ACKNOWLEDGEMENTS

We are indebted to Mr. Robert W. Reeves, who wrote the machine program for the kinetic energy budget, and to Mr. James W. Trout, who programmed the inertial instability analysis.

6. REFERENCES

Charney, J. G., and A. Eliassen (1964), "On the growth of the hurricane depression," J. Atmospheric Sci. 21, No. 1, 68-74.

Colon, J. A. (1961), "On the structure of Hurricane Daisy (1958)," National Hurricane Res. Proj. Rept. 48, U.S. Weather Bureau, 102 pp.

Gray, W. M. (1967), "Global view of the origin of tropical disturbances and storms," Atmospheric Sci. Paper 114, Dept. of Atmospheric Sci., Colorado State Univ., Fort Collins, Colo., 105 pp.

Hawkins, H. F., and D. T. Rubsam (1968) "Hurricane Hilda, 1964; II. Structure and budgets of the hurricane on October 1, 1964," Monthly Weather Rev. 96, No. 9, 617-636.

Hebert, P. J., and C. L. Jordan (1959), "Mean soundings for the Gulf of Mexico area," National Hurricane Res. Proj. Rept. 30, U.S. Weather Bureau, 10 pp.

Kuo, H. L. (1965), "On formation and intensification of tropical cyclones through latent heat release by cumulus convection," J. Atmospheric Sci. 22, No. 1, 40-63.

Garstang, M., N. E. LaSeur and C. Aspliden (1967), "Equivalent potential temperature as a measure of the structure of the tropical atmosphere," Grant No. BA-AMC-28-043-66-G25, Final Rept. to U.S. Army Electronics Res. and Develop. Lab., Dept. of Meteorology, Florida State Univ., Tallahassee, Fla., 44 pp.

Malkus, J. S. (1960), "Recent developments in studies of penetrative convection and an application to hurricane cumulonimbus towers," Cumulus Dynamics, 65-84 (Pergamon Press, New York).

Malkus, J. S., and H. Riehl (1960), "On the dynamics and energy transformations in steady-state hurricanes," Tellus 12, No. 1, 1-20.

Miller, B. I. (1964), "A study of the filling of Hurricane Donna (1960) over land," Monthly Weather Rev. 92, No. 9, 389-406.

Miller, B. I. (1965), "A simple model of the hurricane inflow layer," National Hurricane Res. Lab. Rept. 75, U. S. Weather Bureau, 16 pp.

Ogura, Y., and J. G. Charney (1962), "A numerical model of thermal convection in the atmosphere," Proc. Intern. Symp. Numerical Weather Prediction, Meteorol. Soc. Japan, Tokyo, 431-452.

Ogura, Y., and N. A. Phillips (1962), "Scale analysis of deep and shallow convection in the atmosphere," J. Atmospheric Sci., 19, No. 2, 173-179.

Ogura, Y. (1964), "Frictionally controlled, thermally driven circulations in a circular vortex with application to tropical cyclones," J. Atmospheric Sci., 21, No. 6, 610-621.

Ooyama, K. (1967), "Numerical simulation of the life cycle of tropical cyclones," NSF Grant No. GA-623, Dept. of Meteorology and Oceanography, New York Univ., New York, 133 pp.

Palmen, E., and H. Riehl (1957), "Budget of angular momentum and energy in tropical cyclones," J. Meteorol., 14, No. 2, 150-159.

Riehl, H., and J. S. Malkus (1961), "Some aspects of Hurricane Daisy, 1958," Tellus, 13, No. 2, 181-213.

Rosenthal, S. L. (1964), "Some attempts to simulate the development of tropical cyclones by numerical methods," Monthly Weather Rev., 92, No. 1, 1-21.

Rosenthal, S. L., and W. J. Koss (1968), "Linear analysis of a tropical cyclone model with increased vertical resolution," Monthly Weather Rev., 96, No. 12.

Syono, S. (1950), "On the vortical rain," Geophys. Notes, 3, No. 25, Tokyo Univ., Tokyo, Japan, 3 pp.

Syono, S. (1951), "On the structure of atmospheric vortices," J. Meteorol., 8, No. 2, 103-110.

Syono, S., Y. Ogura, K. Gambo and A. Kasahara (1951), "On the negative vorticity in a typhoon," J. Meteorol. Soc. Japan, 29, 397-415.

Syono, S., and M. Yamasaki (1966), "Stability of symmetrical motions driven by latent heat released by cumulus convection under the existence of surface friction," J. Meteorol. Soc. Japan, 44, No. 6, 353-375.

Yamasaki, M. (1968a), "Numerical simulation of tropical cyclone development with the use of primitive equations," J. Meteorol. Soc. Japan, 46, No. 3, 178-201.

Yamasaki, M. (1968b), "A tropical cyclone model with parameterized vertical partition of released latent heat," J. Meteorol. Soc. Japan, 46, No. 3, 202-214.

U.S. DEPARTMENT OF THE NAVY
J.H. CHAFEE, Secretary

Naval Weather Service Command
E.T. HARDING, Captain, USN, Commander

U.S. DEPARTMENT OF COMMERCE
M.H. STANS, Secretary

Environmental Science Services Administration
R.M. WHITE, Administrator

DEPARTMENT OF DEFENSE
UNITED STATES OF AMERICA

PROJECT STORMFURY

ANNUAL REPORT 1968

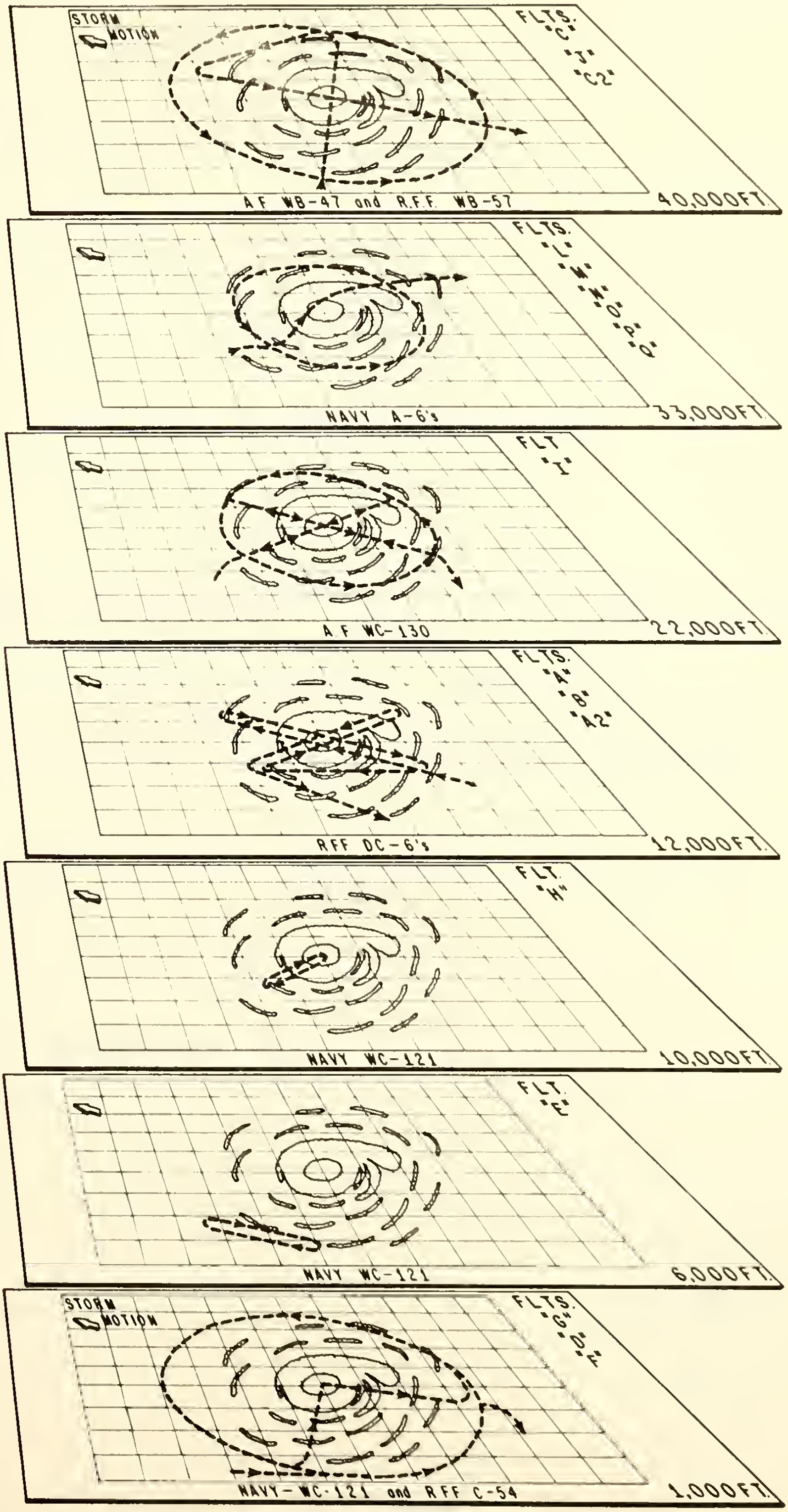

MIAMI, FLORIDA
MAY 1969

DEPARTMENT OF DEFENSE
UNITED STATES OF AMERICA

U.S. DEPARTMENT OF THE NAVY
J.H. CHAFEE, Secretary

Naval Weather Service Command
E.T. HARDING, Captain, USN, Commander

U.S. DEPARTMENT OF COMMERCE
M.H. STANS, Secretary

Environmental Science Services Administration
R.M. WHITE, Administrator

PROJECT STORMFURY ANNUAL REPORT 1968

MIAMI, FLORIDA
MAY 1969

TABLE OF CONTENTS

Page

INTRODUCTION 1

HISTORY OF ORGANIZATION 3

PROJECT STORMFURY ADVISORY PANEL 5

PUBLIC AFFAIRS 5

PYROTECHNIC DEVICES - SILVER IODIDE 6

AREAS OF OPERATIONS 6

PLANS FOR FIELD OPERATIONS - 1968 8

FIELD OPERATIONS - DRY RUNS 9

FIELD OPERATIONS 10

RESEARCH ACTIVITIES 10

OPERATIONAL AND RESEARCH DATA PROBLEM AREAS 12

OUTLOOK FOR 1969 14

SUMMARY 15

REFERENCES AND SPECIAL REPORTS BY STORMFURY GROUP . 16

APPENDIX A. Recommendations of the Advisory Panel to Project STORMFURY With Respect to Overall Project and 1969 Operations A-1

APPENDIX B. "STORMFURY Pyrotechnics," by S. D. Elliott, Jr., R. Steele, and W. D. Mallinger B-1

APPENDIX C. "Navy Weather Research Facility STORMFURY Activity and Research" . . C-1

APPENDIX D. Preliminary Analysis of Cloud Physics Data Collected in Hurricane Gladys (1968)," by R. C. Sheets D-1

APPENDIX E. "Computations of the Seedability of Clouds in the Environment of a Hurricane," by R. C. Sheets E-1

APPENDIX F. "Feasibility of Project STORMFURY Operations in the Pacific Ocean," by W. D. Mallinger F-1

Project STORMFURY was established by an interdepartmental agreement between the Department of Commerce and the Department of the Navy, signed July 30, 1962. Additional support has been provided by the National Science Foundation under Grant NSF-G-17993.

This report is the seventh of a series of annual reports to be prepared by the Office of the Director in accordance with the Project STORMFURY interdepartmental agreement.

Additional copies of this report may be obtained from:

U. S. Naval Weather Service Command
Department of the Navy
Washington Navy Yard
Washington, D. C. 20390

or

National Hurricane Research Laboratory
P. O. Box 8265, University of Miami Branch
Coral Gables, Florida 33124

PROJECT STORMFURY ANNUAL REPORT - 1968

INTRODUCTION

The 1968 hurricane season offered both opportunities and frustrations for Project STORMFURY, an interdepartmental program of the Department of Defense (Navy) and the Department of Commerce, Environmental Science Services Administration (ESSA). As in the two previous seasons, nature failed to provide a storm suitable for large field experiments. Yet, overall, 1968 was a very successful year. More progress was made than before in the collection of data needed to confirm that the hurricane clouds could be modified by seeding with freezing nuclei, and significant achievements were made in basic research on hurricane models. The latter has reached the stage where calculations can be made with the models to assist in designing field modification experiments.

No modification attempts were made during the 1968 hurricane season because no hurricane was available at the right place at the right time. The aircraft units assigned to STORMFURY became available August 5, and some of them were released to other activities on October 15. In a normal year 80 percent of the hurricanes occur between August 5 and October 15. Unfortunately for the Project, during this period in the areas south of about 35^{o}N latitude, 1968 was the least active hurricane season since 1925. Only one other year, 1914, had less activity since before 1866, the first year for which there are reasonably complete track charts.

Figure 1 shows the tropical cyclone tracks for 1968 near the STORMFURY areas. Of the seven storms, six were near the areas, but they all formed either early in the season, intensified to hurricane force after moving to more northerly latitudes beyond the operational range of the Project, or reached hurricane intensity after October 15. Hurricane Gladys, through which research flights were made on October 16, 17, and 19, was the only hurricane available for the researchers. This storm remained so close to land that there would have been no modification experiments even if all the Project forces had remained available after October 15.

Valuable data were collected in the research flight on October 16. The seeding hypothesis for hurricane modification assumes that there is an abundance of liquid water in these layers of subzero temperatures and that introduction of freezing nuclei would cause the water to freeze and give up

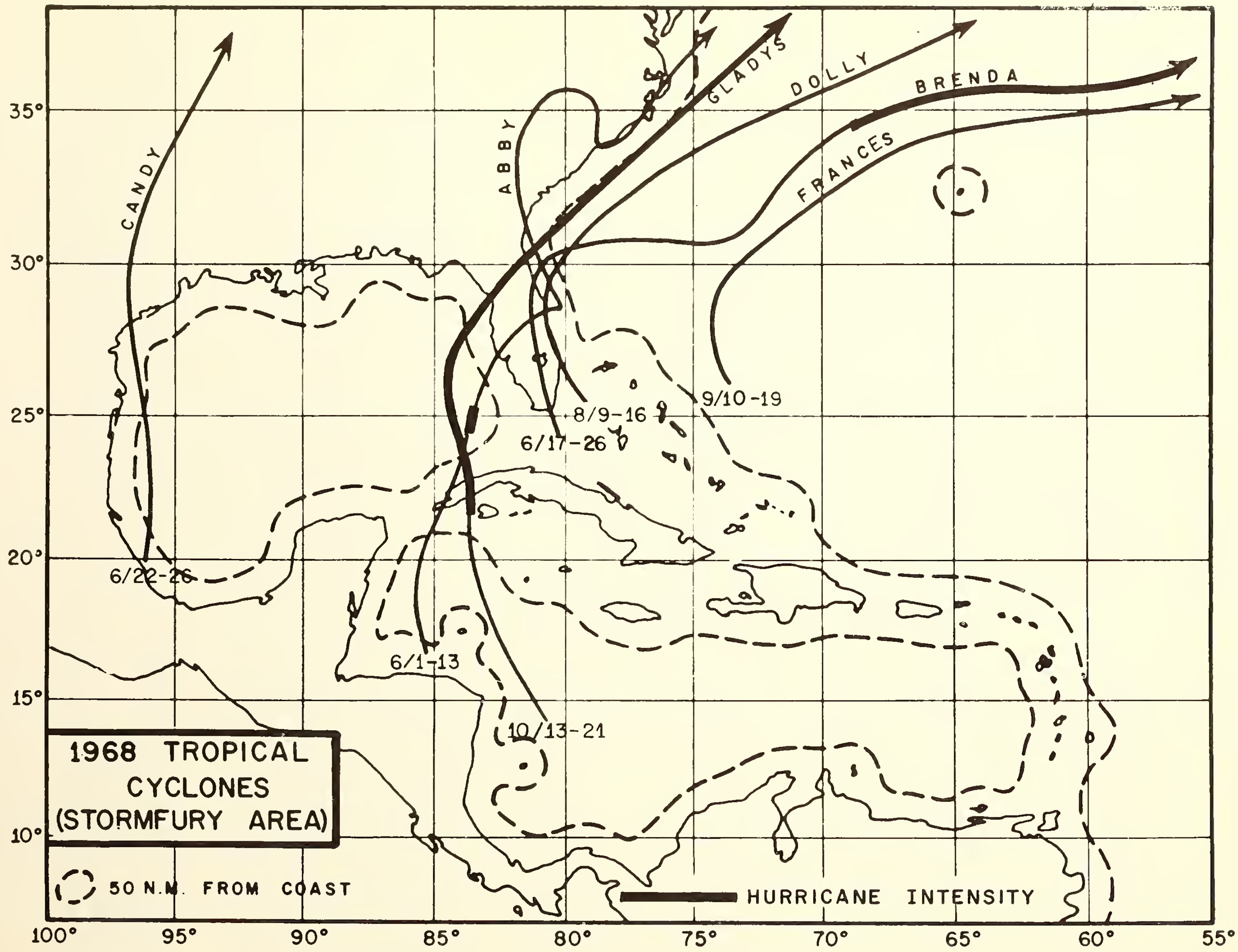
1968 TROPICAL CYCLONES (STORMFURY AREA)
50 N.M. FROM COAST
HURRICANE INTENSITY
CANDY
ABBY
GLADYS
DOLLY
BRENDA
FRANCES
6/22-26
6/1-13
6/17-26
8/9-16
9/10-19
10/13-21
35°
30°
25°
20°
15°
10°
100°
95°
90°
85°
80°
75°
70°
65°
60°
55°

Figure 1.

latent heat while changing phase. Although much indirect evidence had been collected in the past, lack of proper instrumentation had prevented direct measurements of the water substance. This year a DC-6 of ESSA's Research Flight Facility (RFF) was equipped with various water content measuring devices and with a Formvar replicator to get images of the water drops and ice crystals. In two passes through a rainband in Hurricane Gladys at temperatures between -5°C and -9°C over a distance of more than 20 mi, most of the water substance was in the liquid state. On another rainband penetration more ice was found, but still much less than various investigators have been finding in tropical cumuli outside hurricanes. These data are discussed more fully in Appendix D.

Later on the same flight, the aircraft encountered severe turbulence while traversing developing wall clouds at 10,000 ft. This caused the aircraft to be grounded for several days for thorough inspection. There was no further opportunity for additional measurements in a hurricane in 1968. In the portions sampled of these developing wall clouds the water content was over 6 g/m^3.

Remarkable progress has been made in recent years in the development of numerical-dynamical models of hurricanes (Ooyama, 1969; Rosenthal, 1969; Rosenthal and Koss, 1968: Yamasaki, 1968; Kuo, 1965). Within the last 12 months, both Ooyama and Rosenthal have simulated simple hurricane modification experiments with their models. These promising model experiments are discussed more fully in the "Research Activities" section of this report.

With the progress made in data collection and hurricane modeling during the 1968 STORMFURY season, we believe that we are much closer to the point where we can redesign our field experiments to lead to new and better approaches for modifying hurricanes.

In the later sections of this report, the 1968 organization, activities, and operations of the Project are more completely described.

HISTORY AND ORGANIZATION

Project STORMFURY is a joint ESSA-Navy program of scientific experiments designed to explore the structure and dynamics of tropical storms and hurricanes and their potential for modification. It was established in 1962 with the principal objective of testing a physical model of the hurricane's energy exchange by strategic seeding with silver iodide crystals.

These crystals have been dispensed by Navy aircraft using Navy-developed special pyrotechnic devices. The hypothesis would call for a measurably modified storm or hurricane. Navy and ESSA scientists and aircraft, supplemented by those of the U.S. Air Force, have cooperated in STORMFURY experimental operations since 1962 when the Project began. To date, one mature hurricane (Beulah, 1963) and two series of tropical cumulus clouds (August 1963 and July-August 1965) have been experimentally seeded in the Western Atlantic and Caribbean Sea.*

The initial 1962 Project STORMFURY agreement between the Department of Commerce and the Department of the Navy covered three years, and it has been renewed annually since then. The 1968 agreement covered a larger area of operations and was based on the criteria for eligibility for seeding and experimentation adopted in 1967.

Dr. Robert M. White, ESSA Administrator, and Captain E. T. Harding, U.S. Navy, Commander of the Naval Weather Service Command, have over-all responsibility for this cooperatively administered Project.

The Project Director in 1968 was Dr. R. Cecil Gentry, Director of the National Hurricane Research Laboratory (NHRL), Miami, Florida. The Alternate Director was Mr. Harry F. Hawkins, also of NHRL. The Assistant Project Director and Navy Project Coordinator was Captain Robert J. Brazzell, U.S. Navy, Commanding Officer of the Fleet Weather Facility, Jacksonville, Florida (FLEWEAFAC JAX). The alternate to the Assistant Project Director was Commander James D. McGill, U.S. Navy, also of FLEWEAFAC JAX. Mr. Clement J. Todd of the Navy Weather Research Facility, Norfolk, Virginia (WEARSCHFAC) was Technical Advisor to the Navy for STORMFURY, and Mr. Jerome W. Nickerson, also of WEARSCHFAC acted as Navy Liaison for Instrument Matters. Mr. Max W. Edelstein of the Naval Weather Service Command Headquarters, Washington, D.C. was assigned liaison duties representing the Navy,and Mr. William D. Mallinger of the National Hurricane Research Laboratory was assigned liaison duties for the Project Director and acted as Data Quality Control Coordinator.

---

*See Project STORMFURY Annual Reports for 1963, 1964, 1965, 1966, and 1967.

PROJECT STORMFURY ADVISORY PANEL

The Advisory Panel is representative of the scientific establishment and provides guidance to the Project through its consideration of various scientific and technical problems. Its recommendations have proved of great value, particularly in planning.

The Panel reviews proposed experiments and makes recommendations concerning priorities and adequacy of design. It continues to be extremely interested in the cloud-nucleating capabilities of the silver iodide pyrotechnic devices used in cloud seeding and has emphasized the necessity for an objective testing system to delineate accurately the nucleation efficiency under various conditions.

During 1968 the Advisory Panel consisted of the following prominent scientists:

Dr. Noel E. LaSeur, Panel Chairman, Florida State University
Dr. Daniel F. Rex, National Center for Atmospheric Research
Dr. Jerome Spar, New York University
Dr. Edward N. Lorenz, Massachusetts Institute of Technology
Dr. James E. McDonald, University of Arizona.

Meetings of the Advisory Panel and representatives of the cooperating agencies were held in San Francisco, California, on February 1 and 2, 1968, and in Miami, Florida, December 18-20, 1968. The recommendations of the Miami Advisory Panel Meeting are included in this report as Appendix A.

PUBLIC AFFAIRS

The public affairs team plan, implemented in 1967, was continued in 1968. The teams, composed of ESSA and Navy public affairs personnel at the staging base and at Miami and Washington, handled much of the public information on Project STORMFURY. A coordinated press release and fact sheet on plans for STORMFURY were distributed in advance of the hurricane season. Although no forces were deployed for tropical storm or hurricane seeding during 1968, they were assembled during the dry runs in August and again during cloudline experiments in October.

Particularly during these periods, and throughout the season, the press and other news media were very interested in the Project. Two aircraft seats were to be made available on a pool basis to their representatives during each day's operation, one for the printed news media and the other for a cameraman representing TV networks. This team concept appeared to best fit STORMFURY's public affairs requirements.

PYROTECHNIC DEVICES - SILVER IODIDE

The "Alecto" pyrotechnic device for generating silver iodide crystals was no longer used in 1968. It was replaced because of chemical deterioration after long periods of storage under sometimes less than ideal conditions.

In the 1968 season, the pyrotechnic used was the Naval Weapons Center, China Lake, STORMFURY I unit , containing a composition called LW-83, developed under the leadership of Dr. Pierre St. Amand. Testing and evaluation of the nucleation effectiveness of the LW-83 unit is continuing and closer agreement between various testing facilities is being achieved by improved testing facilities and refined techniques. This and other STORMFURY pyrotechnics are discussed in Appendix B of this report.

AREAS OF OPERATIONS

Eligible areas for experimentation were increased in 1968 by the addition of the Gulf of Mexico and the Caribbean Sea to the previously authorized southwestern North Atlantic region.

These areas are defined by the following guidelines: a tropical cyclone in the southwestern North Atlantic Ocean, Gulf of Mexico, or Caribbean Sea is considered eligible for seeding as long as there is only a small probability (10 percent or less) of the hurricane center coming within 50 mi of a populated land area within 24 hours after seeding (see fig. 2).

There are two primary reasons for not seeding a storm near land. First, a storm seeded further out at sea will have reverted to "nature's own" before affecting a land mass. Second, marked changes in the structure of a hurricane occur when it passes over land. These land-induced modifications would obscure the short-range effects produced by the seeding experiments and greatly complicate the scientific evaluation of the results.

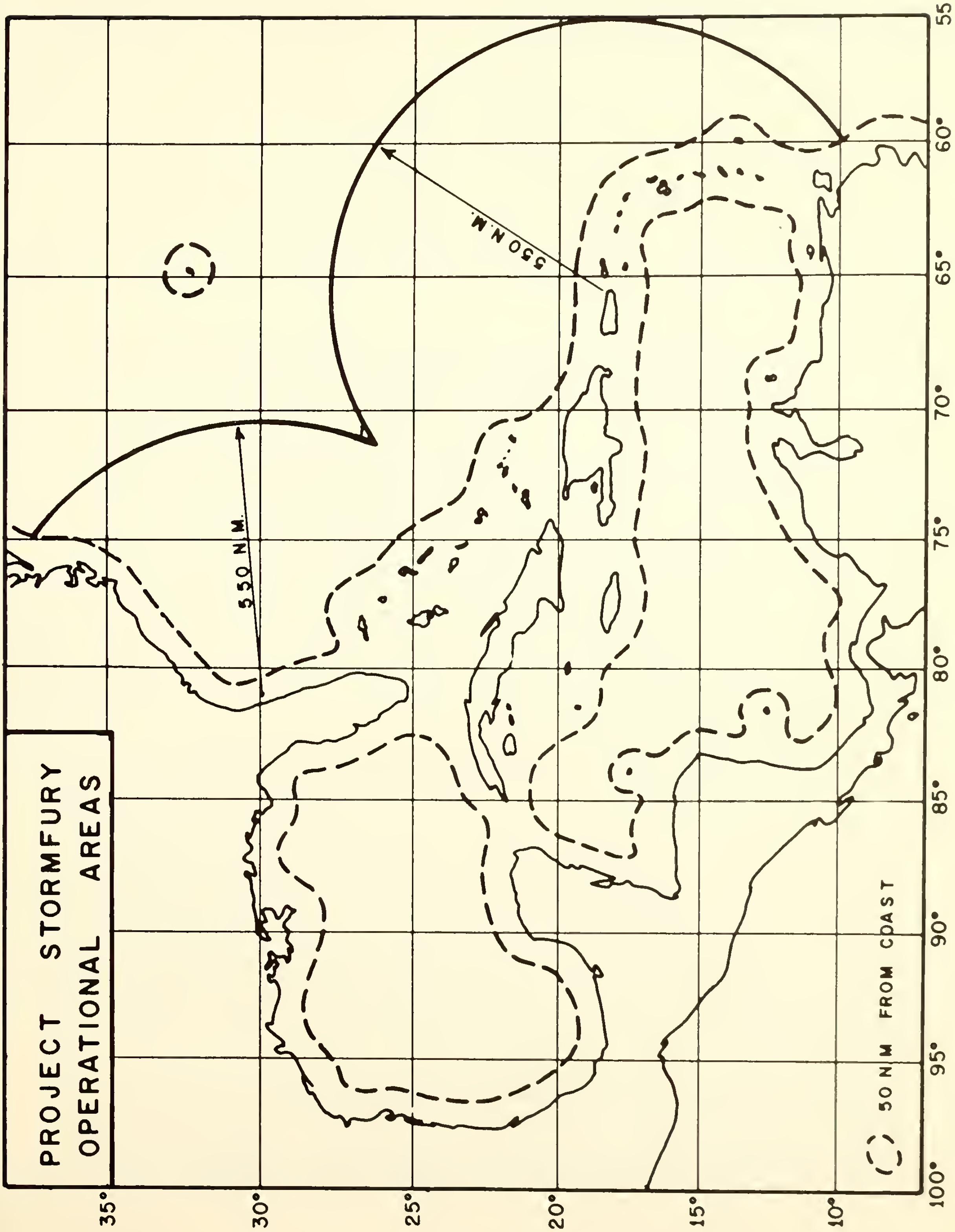
PROJECT STORMFURY
OPERATIONAL AREAS
550 N.M.
550 N.M.
50 NM FROM COAST
35°
30°
25°
20°
15°
10°
100°
95°
90°
85°
80°
75°
70°
65°
60°
55°

Figure 2.

PLANS FOR FIELD OPERATIONS - 1968

The period August 5 to October 15 was established for STORMFURY operations in 1968. The following aircraft units were maintained in readiness:

1. Navy Weather Reconnaissance Squadron FOUR - five WC-121N'

2. Navy Attack Squadron SEVENTY FIVE - five A-6 Intruders.

3. ESSA Research Flight Facility - two DC-6's, one WB-57, and one C-54.

4. Air Force, 53rd Weather Reconnaissance Squadron - one WC-130A and one WB-47.

The basic operational plan for 1967 was revised and updated based on the aircraft and instrumentation available and scientific information desired.

Project STORMFURY Operational Plan No. 1-68 was the result of the combined efforts of many persons representing ESSA; Headquarters, Naval Weather Service Command; Fleet Weather Facility, Jacksonville; Navy Weather Research Facility, Norfolk; Naval Weapons Center, China Lake; Air Force Air Weather Service; the Federal Aviation Agency; and the aviation squadrons and units participating in the Project. The plan specified in detail the flight operations, communications, instrument calibration and use, data collection, distribution and archiving, logistic and administrative procedures, air space reservations agreement, and public affairs.

As recommended by the STORMFURY Advisory Panel, Project officials gave first priority to the multiple seeding of the hurricane eyewall experiment. Almost equal priority went to the hurricane rainband experiment. A cloudline experiment was also planned in the event that after deployment of the aircraft, opportunities for neither of the first two experiments presented themselves. Plans also provided for a series of fall-back research missions, if no eligible hurricane or cloud system was available after deployment of Project forces. These would be data-gathering and storm-monitoring operations in unseeded storms.

The multiple seeding eyewall experiment calls for five seedings at 2-hour intervals, each consisting of dropping 208 pyrotechnic units along a radial flight path across the eyewall, starting just outside the region of maximum winds. The hypothesis was that these 1040 pyrotechnic units, if properly placed in the clouds in and around the eyewall should cause variations in the pressures and reductions in the maximum winds that could be distinguishable from the variations that occur naturally in hurricanes. A great deal of experimental data must be obtained, however, before definite conclusions can be reached, because the magnitude of natural variations in hurricanes is very often nearly the same as that of the hypothesized artificially-induced changes.

The rainband is an important link in the hurricane's circulation system and may prove to be the best region in which to attempt hurricane modification. Several research findings suggest that a redistribution of energy in the rainbands could lead to modification of the storm itself.

The cloudline experiment may provide vital data to help understand the dynamics of clouds organized into systems, such as in rainbands. It is important to know whether and to what extent modification of groups of clouds will affect other clouds in the same or nearby lines. These experiments can be conducted when there are no hurricanes and should provide opportunities for improving knowledge of seeding effects and for testing seeding procedures.

Project STORMFURY field experiments are very complex operations requiring extensive planning. At times during the eyewall experiment, as many as 10 aircraft could be operating in the hurricane's circulation. Safety of the aircraft and personnel is paramount in the successful conduct of the experiments. Considering the high winds, torrential rains, mountainous seas, and turbulent conditions under which these operations are carried out, it is obvious that training, professionalism, and dedication are vital to safe and successful operations.

Radars and communication equipment must be completely reliable. The seeder aircraft must be carefully vectored to their pyrotechnic release points by both radar and voice communications. Radar is vital to data collection and determination of experimental results. For these reasons it becomes almost mandatory that flight crews undergo dry-run rehearsals before actual hurricane experiments to test equipment and procedures and to provide proper training for the crews.

FIELD OPERATIONS - DRY RUNS

Dry runs were conducted at the Naval Station, Roosevelt Roads, Puerto Rico, on August 6 and 7, 1968, with briefing on the afternoon of the 5th. Simulated hurricane eyewall, rainband, and cloudline experiments were conducted in the operations area north of Roosevelt Roads. Participating in the dry runs were personnel and aircraft of the Navy Weather Reconnaissance Squadron FOUR (VW-4), Jacksonville, Florida; Navy Attack Squadron SEVENTY FIVE (VA-75), Oceana, Virginia; ESSA Research Flight Facility, Miami, Florida; and the Air Force 53rd Weather Reconnaissance Squadron, Ramey AFB, Puerto Rico. Also taking part were scientists from the Naval Weather Service Command Headquarters, Washington, D.C.; Naval Weapons Center, China Lake, California; Navy Weather Research Facility, Norfolk, Virginia; and ESSA's National Hurricane Research Laboratory.

The dry runs were considered a success. They provided an opportunity not only for practicing coordination and flight patterns, but for finding better methods of obtaining information from data sensors and recording equipment and for training operators in their optimum use. Some pyrotechnics were actually dropped to test the releasing racks and the exercises were made as realistic as possible. All groups performed in an outstanding manner.

FIELD OPERATIONS

No tropical storm or hurricane became eligible for seeding under the prescribed seeding rules in 1968, but a portion of the forces did combine for a cloudline experiment off of the coast of Florida on October 1-4. The units participating were: two WC-121N's, two DC-6's, a WB-57, and a WC-130. No seeding was performed, however, because the weather systems did not produce suitable cloudlines. Valuable cloud physics data were collected, and experience was gained in conducting an experiment of this type. As a result, aircraft flight tracks were redesigned to make them more practical and to permit optimum data collection.

RESEARCH ACTIVITIES

Research programs on the hurricane problem and tropical meteorology have continued throughout the year at the National Hurricane Research Laboratory and at the Naval Weather Research Facility. The latter continued its broad program of research in tropical meteorology, especially on tropical cyclones. It is also extensively involved in weather modification studies, with emphasis placed on experiment design and evaluation, including computer exploration of the relevant atmospheric processes with mathematical simulation models. Substantial progress has been made in obtaining a clearer understanding of the possibilities of, and procedures for, modifying severe tropical storms, in initiating collection of the basic cloud physics data, and in upgrading radarscope photography capabilities. See Appendix C for a report by the WEARSCHFAC.

The NHRL has made significant progress in several areas directly related to hurricane modification. New cloud physics instruments were used effectively in the cloudline experiment and on research flights into Hurricane Gladys in measuring liquid and solid water content of the cumuloform clouds. Additional studies have also been made based on radiosonde data collected near hurricane centers. Appendices D and E contain reports on these studies.

Hurricane structure and energetics are also being studied in efforts to develop new or modified STORMFURY hypotheses and experiments. In addition, research is being conducted on the feasibility of sea-air evaporation suppression in tropical cyclones.

During 1968 and 1969, development of hurricane modeling continued to advance. In the past 12 months, both Drs. Ooyama and Rosenthal have simulated simple hurricane modification experiments with their models. At NHRL's request, Dr. Ooyama has used his model of a hurricane to calculate the effect of reducing the transfer of energy from the ocean to the atmosphere within 100 km of the center of the storm. This would simulate the effect of putting a film on the ocean to inhibit evaporation. As indicated by earlier theoretical and experimental investigations (Miller, 1964; Palmen and Riehl, 1957) the calculations showed that such action would indeed reduce the intensity of the model hurricane.

Dr. Rosenthal's model has more resolution and degrees of freedom in the vertical than Dr. Ooyama's and uses the primitive equations. It has been used to obtain information for designing the seeding experiments. Rosenthal (1969) has made numerous integrations, with results that closely resemble the life cycle of real tropical cyclones. Initial conditions consist of a vortex that is only weakly baroclinic and in gradient balance. This initial balance is destroyed by friction, and the meridional circulation and heating function establish themselves. Although the model is still being improved, it already simulates many features of a hurricane quite well.

In one of the seeding experiments planned for STORMFURY, silver iodide crystals are deposited in the clouds near the eye of the storm (Gentry and Edelstein, 1968). Dr. Rosenthal asked his model whether to seed across the belt of maximum winds or just beyond them. He simulated the seeding experiment by increasing the heating function at the rate of 2°C per one-half hour for one-half hour. For guidance on where to seed, the model was used to simulate the seeding experiment on two different concentric bands. One band spanned the radius of maximum winds at 30 to 50 km from the center; the other was outside that radius at 50 to 70 km. The results of the two simulations are compared in figure 3. The dotted line represents results from the unmodified model, the broken line gives the results of simulated seeding across the radius of maximum winds, and the solid line gives results of simulated seeding outside the radius of maximum winds. The inference is that the greatest reduction in maximum intensity can be accomplished by seeding outside the radius of maximum winds.

The important point here is that models have become sufficiently developed that their output can be used in designing field experiments. The results could be interpreted to mean either that seeding would cause a temporary reduction in intensity of the storm or cause a change in phase of the quasi-periodic variation of the maximum wind generated by the model. Either interpretation must be tempered by the fact that none of the hurricane models is sufficiently perfected for complete reliance on its results. They are encouraging, however, in that these calculations can be made and that the results appear reasonable.

OPERATIONAL AND RESEARCH DATA PROBLEM AREAS

Continued emphasis was placed on the perennial problem of improving the data collected to increase their research potential. One central commercial developer was used by the Project for radar photography. The Data Quality Control Coordinator was designated to ensure expeditious processing, copying, and handling of all STORMFURY film. Reports of radar photography discrepancies were quickly transmitted to the parent squadron so that corrections to the radars or cameras could be made. Cameras were thoroughly pre-checked and adjusted to provide better focusing and more dependable operations. These actions, and diligence on the part of the radar operators and photographers, notably improved the quality of the radar photographs during the 1968 season.

A continued deficiency was the lack of a properly instrumented aircraft that could measure the liquid- and solid-water content for particle size and distribution at altitudes

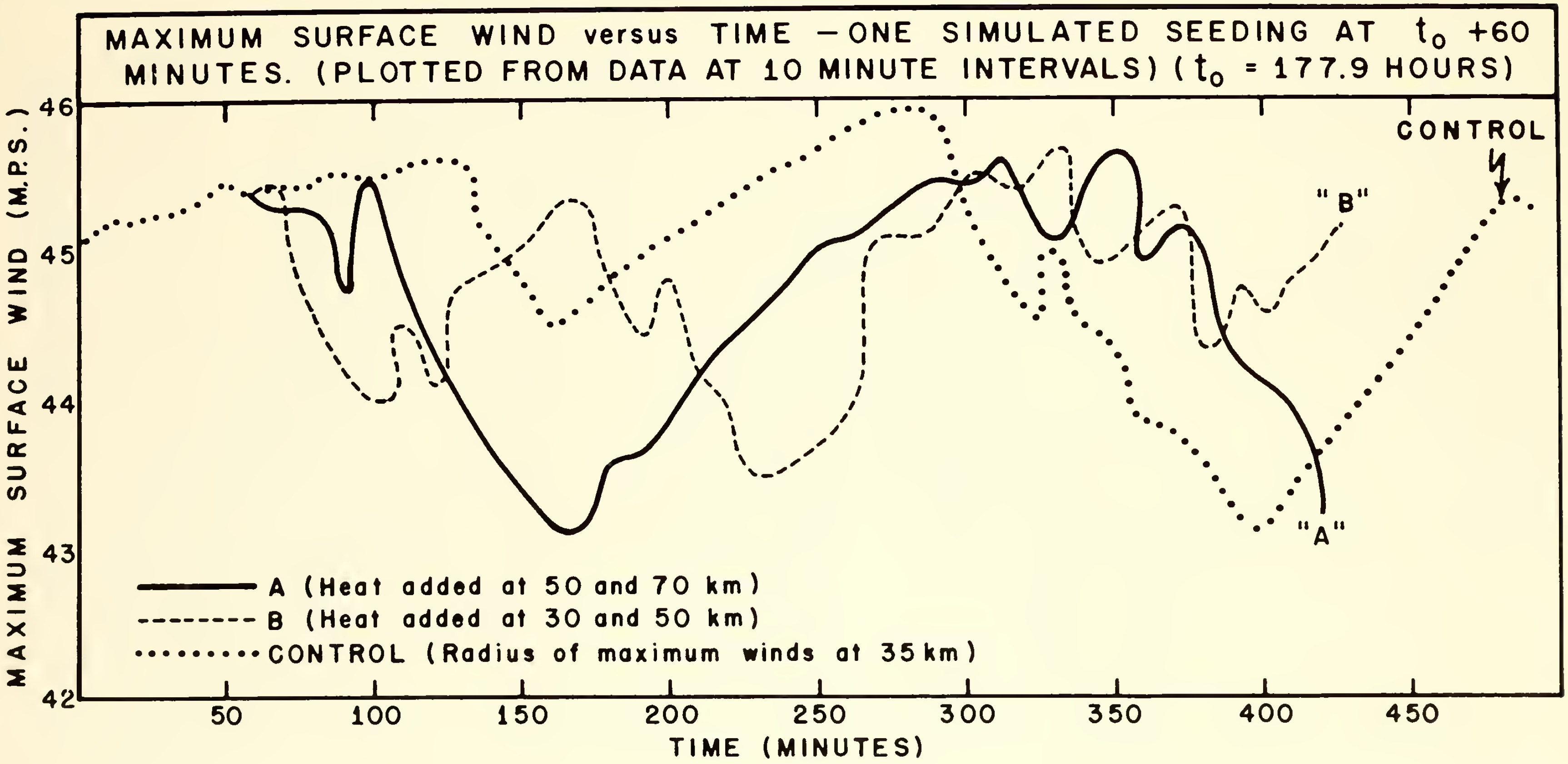
MAXIMUM SURFACE WIND versus TIME —ONE SIMULATED SEEDING AT t_0 +60 MINUTES. (PLOTTED FROM DATA AT 10 MINUTE INTERVALS) (t_0 = 177.9 HOURS)
MAXIMUM SURFACE WIND (M.P.S.)
46
45
44
43
42
50
100
150
200
250
300
350
400
450
TIME (MINUTES)
CONTROL
"B"
"A"
A (Heat added at 50 and 70 km)
B (Heat added at 30 and 50 km)
CONTROL (Radius of maximum winds at 35 km)

Figure 3.

from 22,000 to 26,000 ft. Some measurements were made at levels up to 22,000 ft by ESSA's DC-6 aircraft, which, however, cannot make sustained flights at this altitude or at the higher altitudes required.

Although the area for eligible seeding was enlarged, no opportunities for conducting experiments in tropical cyclones appeared. This was the second year in a row that such a dearth of storms during this period occurred and the only two years out of the past fifteen when no storms were eligible under current seeding eligibility rules. (See 1967 STORMFURY Annual Report, Appendix B.)

OUTLOOK FOR 1969

Current plans are for continued Project STORMFURY operations in 1969. No changes in the authorized areas for seeding or in the eligibility rules are envisioned. Priorities will be changed slightly to reflect the Advisory Panel's recommendations. (See fig. 1.)

The Assistant Project Director, Captain Robert J. Brazzell, U.S. Navy, is scheduled for transfer prior to the 1969 operational season. His relief will be Commander Leland J. Underwood, U.S. Navy. The alternate to the Assistant Project Director, Commander James D. McGill, U.S. Navy, has been transferred, and will be replaced by Commander James O. Heft, U.S. Navy, for 1969. No other changes in top management are foreseen at this time. Membership of the Project STORMFURY Advisory Panel for 1969 changed in February 1969, with Dr. Daniel F. Rex of the National Center for Atmospheric Research, Boulder, Colorado, requesting replacement because he had accepted a visiting professorship in the Department of Geosciences at the University of Hawaii.

Forces in 1969 will be approximately the same as in 1968, with the possible addition of high-level aircraft support from the Air Force during some of the operations. The pyrotechnic units will also be the same as in 1968, with the possible addition of some units with less nucleating material to be used in cloudline or rainband experiments.

There is a good likelihood that new cloud physics instruments will be available to the Project. If practicable, they will be mounted on the Air Force WC-130 aircraft so that data can be gathered from the 22,000- to 30,000-ft layer.

Chances for sea-air evaporation field experiments in

1969 are slim at this time. Work on finding improved chemicals and possible techniques for this type of hurricane modification will continue.

Operations in the Pacific during 1969 are not planned. A report on potential tropical cyclones in the Pacific for experimentation is attached as Appendix F.

SUMMARY

Project STORMFURY experimental operations planned by ESSA and the Navy for 1968 specified the hurricane eyewall experiment at first priority, due to the infrequency of a suitable hurricane for this purpose. Of almost equal priority was the hurricane rainband experiment. The cloudline experiments were to be performed whenever forces were assembled and suitable cloudlines could be found, or near the end of the STORMFURY season if enough other experiments had not been conducted before that time.

Full forces were assembled only for the dry-run exercises at Naval Station Roosevelt Roads, Puerto Rico. Partial forces flew in cloudline experiments off the east coast of southern Florida near the end of the STORMFURY season.

Research on hurricane modeling and future modification experiments continued throughout the year, and plans for the 1969 season provide for improved opportunities for experimentation and increased capabilities for collecting the quality research data needed.

Judging by the tropical cyclone tracks of the last 14 years, the 1969 season should bring seeding opportunities. The new areas of operation will increase the probability of conducting seeding experiments, as will exploratory experiments on lines of cumulus that can be carried out in tropical weather systems other than cyclones.

REFERENCES AND SPECIAL REPORTS

Edelstein, M. W. (1968): Project STORMFURY operations 1968. Presented at Tenth Interagency Conference on Weather Modification, Skyland, Virginia, October 17, 1968.

Gentry, R. C. (1968): Tropical cyclone modification. Presented at Tenth Interagency Conference on Weather Modification, Skyland, Virginia, October 17, 1968.

Gentry, R. C. and M. W. Edelstein (1968): Project STORMFURY, a hurricane modification experiment. Proc. First Natl. Conf. on Weather Modification, Am. Meteor. Soc., 296-305.

Gentry, R. C. (1968): Hurricane modification experiments - a progress report. Presented at 48th Annual Meeting of the Am. Meteor. Soc., January 29-February 1, 1968, San Francisco, California.

Kuo, H. L. (1965): On the formation and intensification of tropical cyclones through latent heat release by cumulus convection. J. Atmospheric Sci., 22, 40-60.

Mallinger, W. D. (1968): A view for mariners of Project STORMFURY. Mariners Weather Log, 12, No. 4, 111-113.

Miller, B. I. (1964): A study of the filling of Hurricane Donna (1960) over land. Monthly Weather Rev., 92, 389-406.

Ooyama, K. (1969): Numerical simulation of the life cycle of tropical cyclones. J. Atmospheric Sci., 26, 3-40.

Palmen, E. and H. Riehl (1957): Budget of angular momentum and energy in tropical cyclones. J. Meteorol., 14, 150-159.

Rosenthal, S. L. (1969): Numerical experiments with a multi-level primitive equation model designed to simulate the development of tropical cyclones, experiment I. ESSA Tech. Memo. ERLTM-NHRL-82, 36 pp.

Rosenthal, S. L. and W. J. Koss (1968): Linear analysis of a tropical cyclone model with increased vertical resolution. Monthly Weather Rev., 96, No. 12, 858-866.

Sheets, R. C. (1969): Some mean hurricane soundings. J. Appl. Meteorol., 8, No. 1, 134-146.

Yamasaki, M. (1968): A tropical cyclone model with parameterized vertical partition of released latent heat. J. Meteorol. Soc. Japan, 46, 202-214.

APPENDIX A

RECOMMENDATIONS OF THE ADVISORY PANEL TO PROJECT STORMFURY

January 1969

INTRODUCTION

Two years ago, when Project STORMFURY became associated with the National Hurricane Research Laboratory (NHRL), the Advisory Panel, after considerable deliberation, recommended long-term continuation of the Project with expanded support and broadened scope. It was the unanimous opinion of the panel members that previous Project efforts provided a foundation for an expanded effort within the logical framework of NHRL. More specifically the Panel recommended at that time the adoption of new criteria governing permissibility of experiments in hurricanes in order that opportunities for such experiments would be increased in number; reconsideration and redesign of cloud-seeding experiments to include convective systems of varying degrees of intensity and organization in the range from the hurricane eyewall to simple cloud lines; the investigation of other possible avenues of hurricane modification; the improvement of instrumentation for monitoring both treated and control systems, especially in the area of cloud-physics data; the continued pursuit of mathematical modelling of hurricanes with the simulation of various possible field experiments as one objective; and continued testing of the pyrotechnic seeding devices to resolve the uncertainties as to absolute and relative nucleating efficiency.

In spite of the adoption of the revised permissibility criteria, no opportunity for a hurricane seeding experiment has occurred during the 1967 and 1968 seasons. To offset disappointment from these (uncontrollable) circumstances, the Panel is pleased to recognize progress in implementing several other of the above recommendations. A wider range of seeding experiments has been designed and several executed in the field on a "dry-run" basis, although no actual seeding was carried out. New instruments for measuring liquid and solid water contents and particle size have been installed in aircraft of the Research Flight Facility (RFF) and successful measurements have been obtained. Other improvements in instrumentation have also been effected. A new mathematical model of the hurricane has been developed within NHRL, which has been utilized in a preliminary way to simulate eyewall seeding experiments and other aspects of hurricane behavior. This model is a useful supplement to previously existing models which continue to be used. None of the models as yet gives conclusive answers to the pertinent questions, but further improvements should yield more realistic results. Finally, there are indications that new testing facilities and techniques are now producing more stable and reproducible results as to the nucleating efficiency of the pyrotechnic seeding devices employed by the Project.

RECOMMENDATION ONE

The Panel recommends continuation of Project STORMFURY for at least 5 years together with appropriate increases in funds and facilities.

Reasons: The objectives of Project STORMFURY are such as to require a long-term approach along many avenues of research. The Panel believes past performance and results to be sufficiently encouraging and the benefit/cost ratio to be so potentially high as to warrant continuation and expansion of the effort. A recent survey of the activities and objectives of Project STORMFURY, prepared by the Project Director and others, has been endorsed by the Advisory Panel with the recommendation that it be disseminated to the scientific community and the general public.

RECOMMENDATION TWO

With regard to field experiments in seeding convective clouds in hurricanes and other tropical weather systems, the Panel recommends that significantly greater emphasis and priority be placed on the seeding of organized cloud lines, within or without the hurricane circulation. However, when and if the opportunity for multiple seeding of the eyewall arises, that experiment should be given the top priority.

Reasons: Limitations imposed previously by available pyrotechnic seeding devices are no longer so severe. The potential value of comparing the behavior of seeded and control-portions of organized convective cloud lines fully justifies the expenditure of available pyrotechnics. In the absence of suitable opportunity for multiple eyewall seeding, advantage should be taken of the earliest opportunity for cloud line seeding experiments.

RECOMMENDATION THREE

It is recommended that each period of authorized field experiments begin with a "dry-run" exercise and that this include practice cloud line experiments.

Reasons: In this way all personnel involved acquire familiarity with the complex operational plans, such as to increase the probability of successful execution of the various experiments when opportunities arise.

RECOMMENDATION FOUR

It is recommended that all types of data and analysis techniques previously employed, plus any new possibilities not used in the past, be investigated and reviewed with the objective of improving the detectability of possible effects from seeding experiments. Additional monitoring of natural variability in tropical storms and cloud lines is desirable.

Reasons: There is increasing evidence that effects induced by seeding are comparable in magnitude to natural variability. In itself, this is not necessarily discouraging, since induced changes comparable to natural changes could be valuable in many instances. However, it is essential that means for better discrimination between natural and induced variations be developed.

RECOMMENDATION FIVE

The Panel recommends increased effort in the improvement of mathematical models of hurricanes, the initiation of effort to develop models of cloud lines, and the utilization of these models to simulate various modification experiments. In order to study the possible effects of cloud seeding on hurricane paths, a fully three-dimensional model capable of dealing with asymmetry is needed.

Reasons: Although present models reproduce several essential features of hurricane structure and behavior to an encouraging degree, improvements can be made. Certain physical processes can be included in a more realistic manner and computations can be made with better space-time resolution, both of which should increase the probability of realistic simulation of experimental influences. Similar techniques can be developed for cloud lines. Extension of the studies to include fully three-dimensional models, which will permit investigation of asymmetrical effects, is a logical evolution of the program.

RECOMMENDATION SIX

The Panel recommends that increased effort be devoted to the exploration of other possible means of modifying hurricanes, such as influencing sea-air energy exchange. These investigations may include preliminary field or laboratory tests on a limited scale.

Reasons: There can be no reasonable doubt that significant interference with normal sea-air energy exchange in the hurricane would greatly influence the storm. The basic question is one of the required magnitude of the needed influence and the logistic feasibility of applying it. Preliminary calculations and limited field or laboratory results are necessary before the design of any extensive field experiments.

RECOMMENDATION SEVEN

The Panel recommends further improvement in the capability for aircraft measurements of cloud physical parameters including ice nuclei concentration.

Reasons: The distribution of water vapor, liquid and ice and the associated changes of phase are of critical importance. Further it is the distribution of various natural and artificial nuclei and their nucleating efficiency in the *actual* atmospheric environment which must be studied. Significant beginnings have been made along these lines during the past 2 years, but much more is needed for proper assessment of the many related questions.

RECOMMENDATION EIGHT

Efforts should be continued to determine the absolute and relative nucleating efficiencies of the pyrotechnics under laboratory conditions, and these should be disseminated to the scientific community by means of publications in appropriate periodicals without delay.

Reasons: Although there is now better evidence that these pyrotechnics can effect "massive seeding" in reproducib laboratory experiments, residual questions as to absolute and relative efficiency and mechanisms should be answered and the knowledge disseminated.

Noel E. LaSeur, Chairman
Edward N. Lorenz
James E. McDonald
Jerome Spar

APPENDIX B

STORMFURY PYROTECHNICS

Shelden D. Elliott, Jr.
Naval Weapons Center
China Lake, California

Roger Steele
Mechanical Engineering Department
Colorado State University
Fort Collins, Colorado

William D. Mallinger
National Hurricane Research Laboratory
Environmental Science Services Administration
Miami, Florida

The pyrotechnics employed since the inception of Project STORMFURY in 1962 have all been developed by the Naval Weapons Center, China Lake, California, under the direction of Dr. Pierre St.-Amand. This report summarizes basic information on the formulation and performance of these pyrotechnics. It also describes the evolution of the procedures employed in measuring their effectiveness in the Colorado State University testing facility and presents some of the data thus obtained.

The pyrotechnic formulation,developed in 1962 and employed in the 1963 experiment on Hurricane Beulah and in cumulus seeding experiments in 1963 and 1965,was designated CY 21 (table 1). Two types of units, CYCLOPS II and ALECTO, containing respectively 60 and 3.0 lbs of CY 21 were employed on Beulah. Only the smaller ALECTO unit was used in the subsequent experiments. A second formulation, CY 35, producing smaller nuclei with greater effectiveness at -5°C, but somewhat less effective than CY 21 at lower temperatures, was also developed for the 1965 experiments. For the 1966 and 1967 seasons, Alectos loaded with both Cy 35 and a modification, CY 21M, of the original formulation were prepared. These formulations are also given in table B-1.

The ALECTOs consisted of a steel motor canister 2.5 in. in diameter and 7 in. long, weighing 4.8 lbs ejected from an M-123 photoflash cartridge case; the round had a total weight of 6.8 lbs and produced 2.3 lbs of AgI (CY 21M). Eighty units were carried aboard the seeder aircraft in standard photoflash

Table B-1. ALECTO Chemical Compositions.

Formulation (by wt)	CY 21 (%)	CY 35 (%)	CY 21M (%)
$AgIO_3$	89.0	80.0	86.0
Al	1.5	5.0	1.5
TMETN*	2.5	3.5	5.5
Binder	7.0	11.5	7.0
	100.0	100.0	100.0

*Trimethylolethane Trinitrate

AgI output (calculated)	73.9%	66.5%	71.4%

ejector racks. Burning time varied considerably, between approximately 40 and 75 sec, as changes in composition, construction, and exit nozzle size were specified. Vertical fall velocity averaged approximately 300 ft/sec, with a downrange travel of about 5,000 ft over 12,000 to 22,000 ft of fall.

Based upon experience acquired in other programs during the intervening period, NWC recommended the use of a larger quantity of smaller units for the 1968 and subsequent seasons. Ambient-pressure burning pyrotechnic formulations which avoided the need for massive pressure-resistant motor housings were also recommended.

The LW 83 formulation (table B-2), in the form of a grain 1.375 in. in diameter and 4.0 in. long, weighing 290 g, and loaded into an M-112 photoflash cartridge case, was selected for the primary seeding round, designated STORMFURY I. In tests at NWC, units dropped from 35,000 ft (pressure altitude) at 250 kt burned for an average period of 110 sec, falling 22,000 ft vertically and travelling 4,000 to 5,000 ft downrange. Due to the decreasing vertical fall velocity as the grain is consumed, at least half of the burn occurs between 20,000 and 13,000 ft, concentrating the AgI nuclei produced in the desired altitude region. Each seeder aircraft carries 208 STORMFURY I units in four ejector racks of fifty-two rounds each.

A second unit, STORMFURY II, similar in configuration but using a 5.2-in. grain containing 275 g of EW 20 formulation (table B-3) was also developed for 1968, but production was terminated when it became evident that the scarcity of suitable storms would preclude their use.

Table B-2. LW 83 Formulation (Stormfury I).

Component	% by Wt
$AgIO_3$	78
Al	12
Mg	4
Binder	6
	100
AgI output (calculated)	65% (190 grams/unit)

Table B-3. EW 20 Formulation (Stormfury II).

Component	% by Wt
$AgIO_3$	28
Al	15
Mg	7
KNO_3	44
Binder	6
	100
AgI output (calculated)	23.2% (49 grams/unit)

Although the EW 20 formulation yields a considerably lower AgI output, the nuclei produced are of relatively high efficiency and have the added advantage of becoming inactive upon prolonged exposure to a humid environment, thereby reducing "carryover" effects.

For 1969, the STORMFURY I round will be retained and additional quantities will be procured for eyewall experiments. Units similar to STORMFURY II, using EW 20 or related mixtures, will be developed for deployment from lower altitudes in cloud line and rainband experiments.

The above formulations and units have been subjected to continuous field and laboratory tests at NWC as part of the over-all Navy weather modification program.

Independent laboratory testing on a more extensive scale has been conducted at Colorado State University.[1]

Until about mid-1968, all pyrotechnic sources as well as steady-state sources were tested in a small dilution tunnel that had a test section about 18 in. in diameter and about 12 ft long, with the flow limited to about 5000 cfm. The small diameter of the test section constrained the plume produced by field-type pyrotechnic devices, and the results were poor because of excessive wall and coagulation losses. Also, because air velocities were well below those encountered in the field, the plume from the pyrotechnic was not ventilated in the same way as it would be in free fall, and the concentrations within the plume therefore were much higher than those encountered in the field.

The reported effectiveness in production of freezing nuclei was low, probably because of extreme coagulation in the plume caused by the very high particle density resulting from inadequate ventilation during testing. The results obtained in these earlier nucleation effectiveness tests for CY 21, CY 35, and LW 83 are shown, for reference only by the curves in figure B-1.

For these reasons, meaningful measurements for field use could not be made. Only comparative data could be obtained, i.e., one formulation could be compared with another under the same conditions. It was then assumed that the pyrotechnic producing the highest effectiveness was the best, a procedure that is open to criticism since the coagulation characteristics of different formulations may produce artifacts that would not be present in a free falling pyrotechnic. The comparative

---

[1] Steele, R. L. and C. I. Davis, Performance Characteristics of Various Artificial Ice Nuclei Sources. Journal of Applied Meteorology, Vol. 7, No. 4, August 1968.

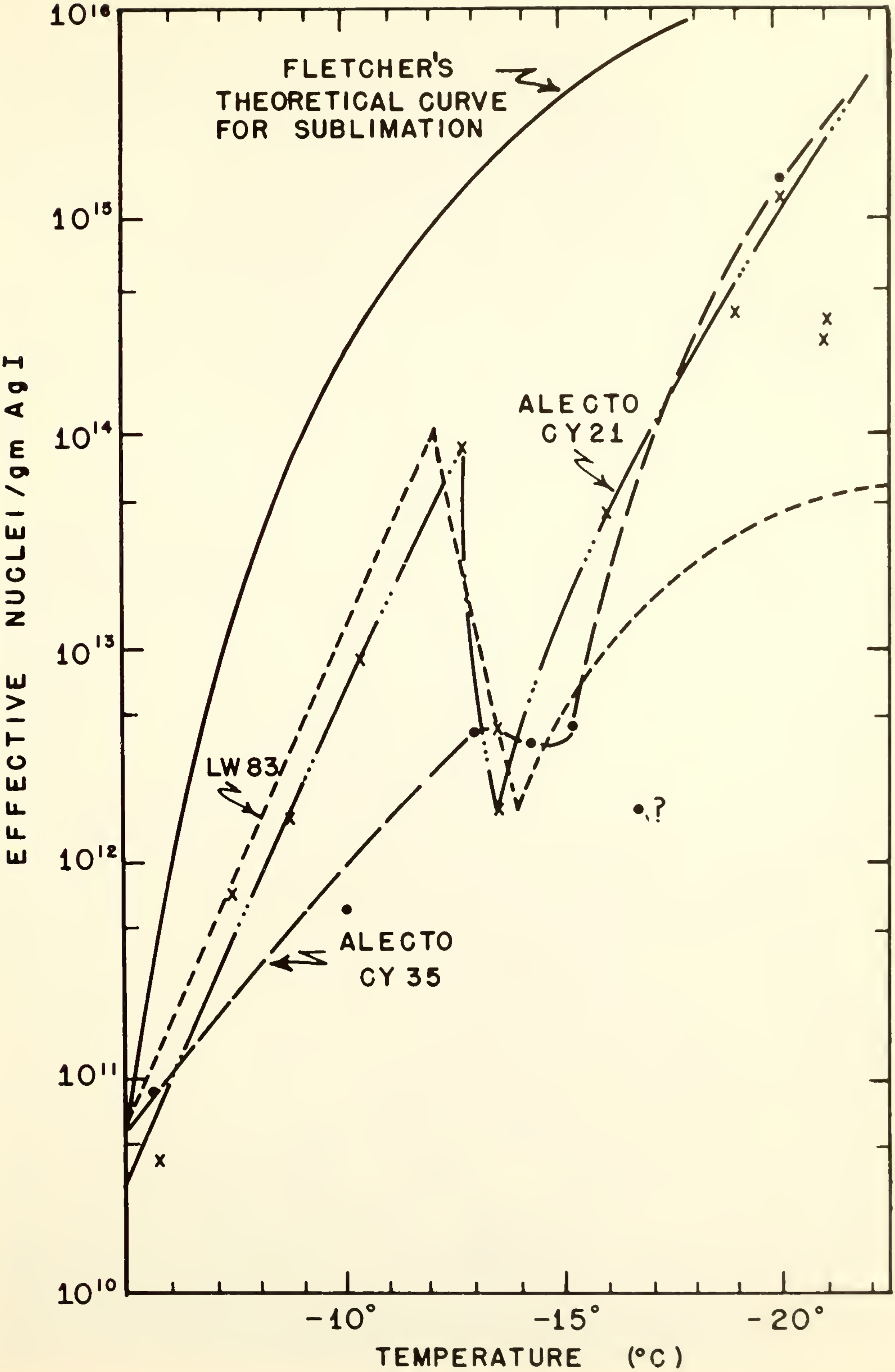
FLETCHER'S THEORETICAL CURVE FOR SUBLIMATION
ALECTO CY21
LW83
ALECTO CY 35
?
EFFECTIVE NUCLEI/gm AgI
TEMPERATURE (°C)
10^{16}
10^{15}
10^{14}
10^{13}
10^{12}
10^{11}
10^{10}
-10°
-15°
-20°

Figure B-1.

data were also of little value to the field investigator for estimating the amount of treatment material to be applied to a given cloud system.

The limitations of the old dilution facility clearly identified the needs for realistic evaluation of STORMFURY and other pyrotechnic devices as well as for conventional steady-state generations. As a result, the vertical wind tunnel, shown in figure B-2, was designed late in 1967. Funds were requested from the National Science Foundation to build the facility. A substantial portion of these funds were granted, and the remainder was obtained from ESSA and the U.S. Bureau of Reclamation.

Specifications of this wind tunnel are as follows: test section, 45 in. in diameter and about 60 ft long; over-all height of the tunnel, including the fan, about 80 ft; maximum air flow, 130,000 cfm at a corresponding velocity of 205 ft/sec; and minimum controlled flow, 400 cfm under natural draft conditions. This rather wide range of test section velocities permits evaluation of all types of ice-nuclei-producing devices under natural simulated conditions.

After a normal shakedown period and after necessary initial tests with steady-state generators, evaluation of pyrotechnics began. To date, preliminary results are available for two formulations of interest to STORMFURY, namely, the LW 83 and EW 20. These units were tested under simulated free fall conditions in the vertical wind tunnel, and the results, shown in figures B-3 and B-4, were reported at the STORMFURY Panel Meeting in Miami in December 1968. Effectiveness is plotted against tunnel flow. Performance is shown at three temperatures, -20°C, -15°C, and -10°C, respectively. Also shown are the dilution ratios used in sampling from the tunnel.

These results strongly indicate that the performance of the pyrotechnic in the testing chambers rises rapidly as the free fall velocity is approached. The effectiveness is therefore about an order of magnitude higher at free fall velocity than that reported under the initial test conditions.

The results shown in figure B-5 are included to demonstrate that coagulation is still a dominant variable in the effectiveness of the pyrotechnic. The increase in effectiveness with increase in the dilution factor (parameter in parentheses at right of curves) indicates that coagulation is still present in significant amounts, even at the free fall velocity. The effectiveness value reported, therefore, may still not be representative of the actual field effectiveness, and for this reason the results remain preliminary.

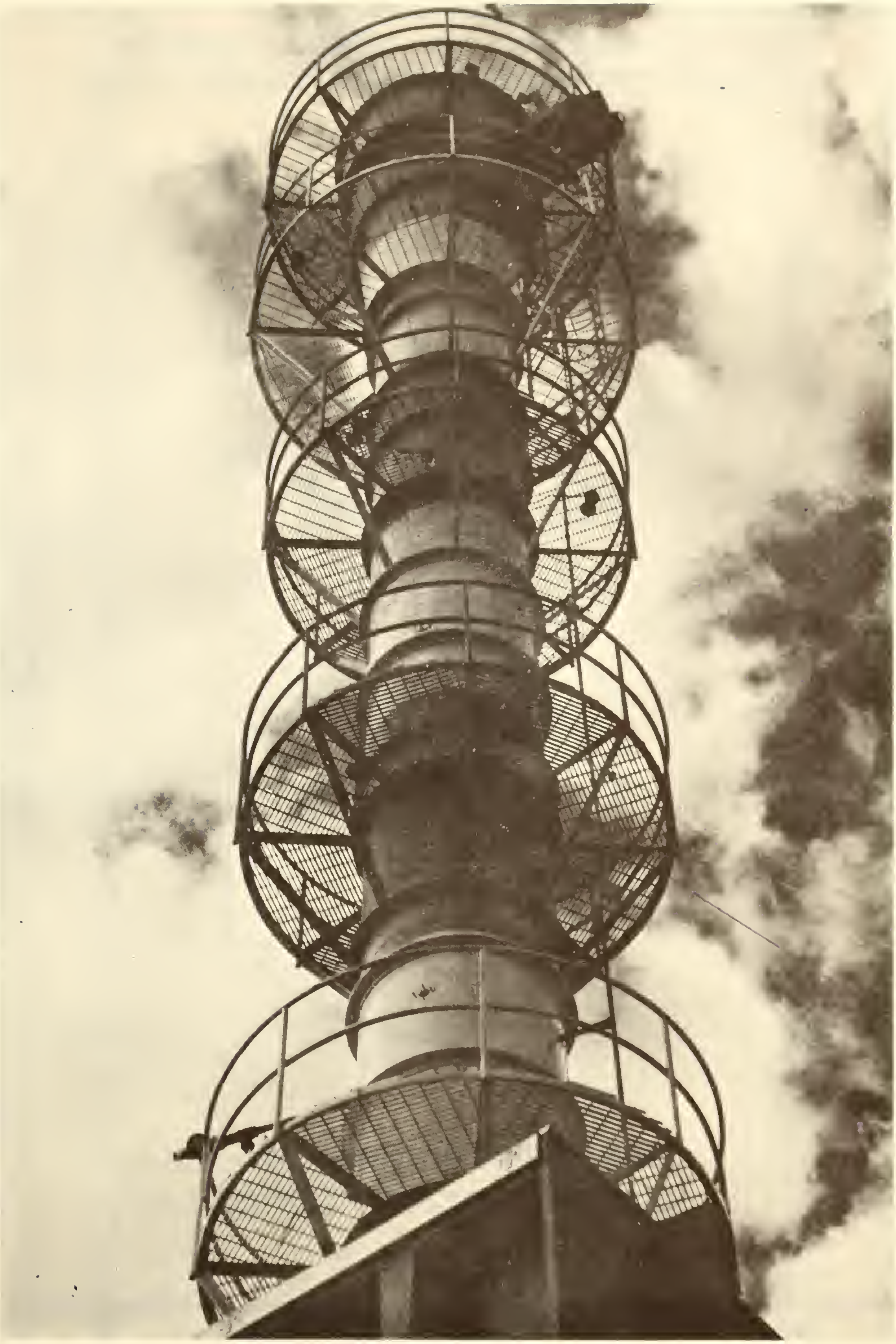

Figure B-2.

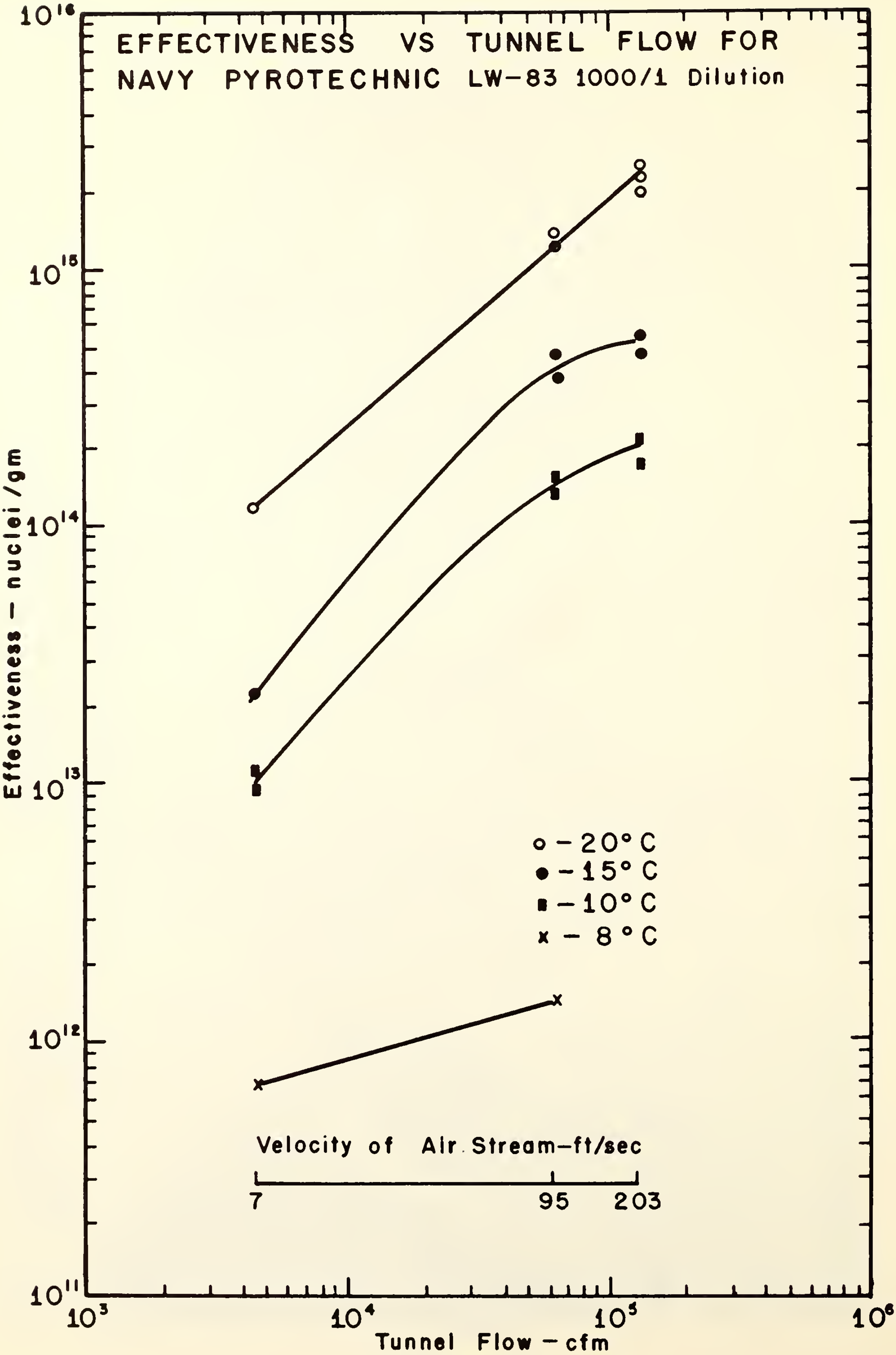
EFFECTIVENESS VS TUNNEL FLOW FOR
NAVY PYROTECHNIC LW-83 1000/1 Dilution
Effectiveness – nuclei /gm
10^{16}
10^{15}
10^{14}
10^{13}
10^{12}
10^{11}
○ – 20° C
● – 15° C
▪ – 10° C
x – 8° C
Velocity of Air Stream–ft/sec
7
95
203
10^3
10^4
10^5
10^6
Tunnel Flow – cfm

Figure B-3.

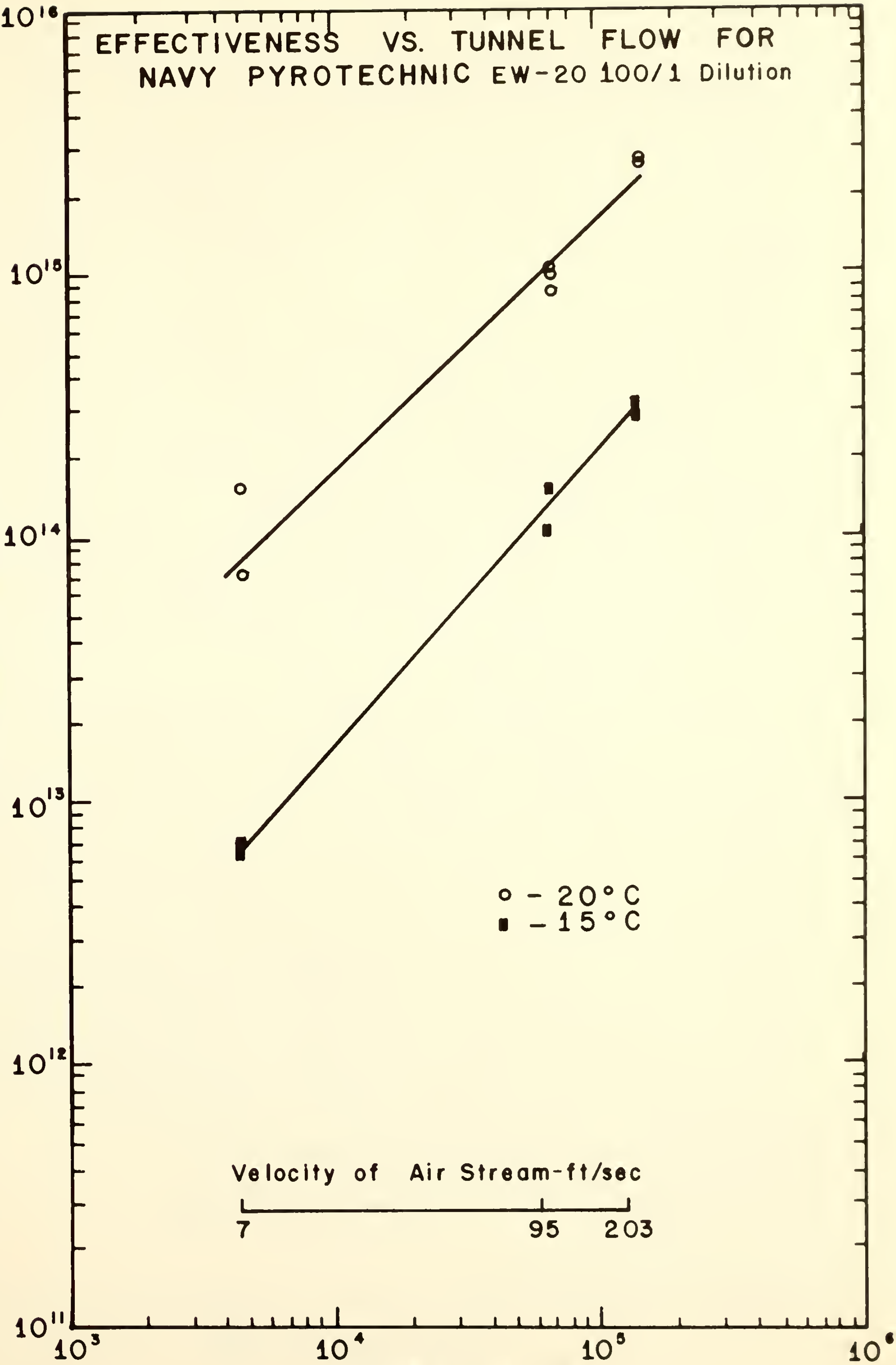
EFFECTIVENESS VS. TUNNEL FLOW FOR
NAVY PYROTECHNIC EW-20 100/1 Dilution
Effectiveness - nuclei/gm
Tunnel Flow - cfm
10^{16}
10^{15}
10^{14}
10^{13}
10^{12}
10^{11}
10^{3}
10^{4}
10^{5}
10^{6}
○ - 20°C
■ - 15°C
Velocity of Air Stream - ft/sec
7
95
203

Figure B-4.

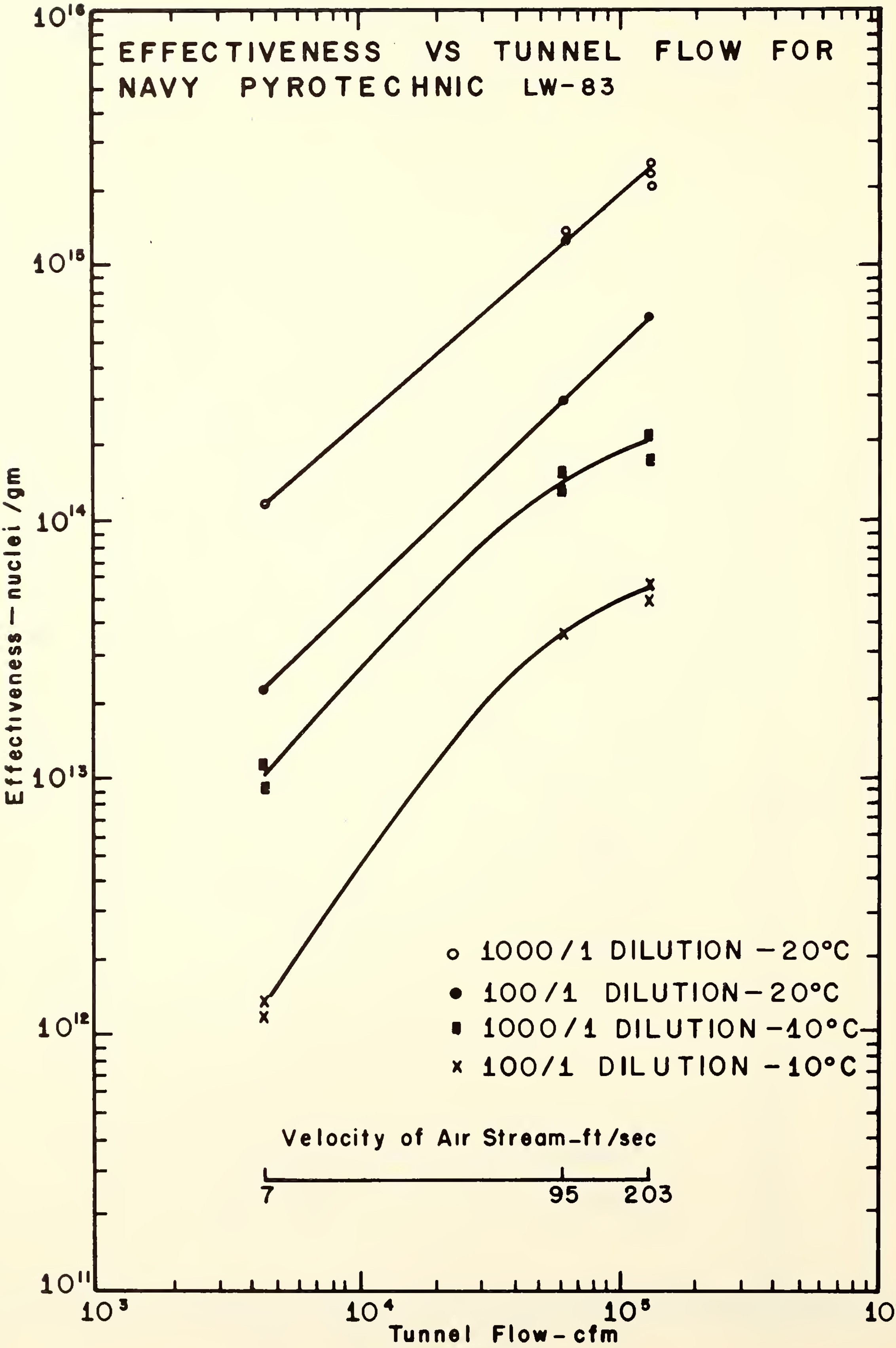
EFFECTIVENESS VS TUNNEL FLOW FOR NAVY PYROTECHNIC LW-83
Effectiveness — nuclei /gm
10^{16}
10^{15}
10^{14}
10^{13}
10^{12}
10^{11}
10^{3}
10^{4}
10^{5}
10^{6}
Tunnel Flow – cfm
○ 1000/1 DILUTION –20°C
● 100/1 DILUTION –20°C
▪ 1000/1 DILUTION –10°C
× 100/1 DILUTION –10°C
Velocity of Air Stream–ft/sec
7
95
203

Figure B-5.

Other work under ESSA and Navy sponsorship should permit final resolution of this question. Current evaluation of the effectiveness of a given pyrotechnic at various distances from it, by study of samples taken in the tunnel at various operating platforms, will make it possible to determine effectiveness versus distance from the pyrotechnic and, in turn, to evaluate plume coagulation loss. The latter quantity can then be employed to predict in situ effectiveness of the pyrotechnic.

Studies under this same sponsorship will permit the variation of nuclei concentration within the plume by a factor of 100, which will make it possible to establish concentrations in which coagulation is not a dominant variable in the effectiveness function. Also included is research on the influence of the cloud-size water droplets on the pyrotechnic plume by introduction of liquid water at the inlet of the tunnel while the pyrotechnic is burning to note the change in effectiveness. Of importance is that the amount of aerosol collected by the droplets will thereby be evaluated; the ice nuclei collected by the droplets may in turn promote future freezing of these drops when they are lifted above the freezing level.

Progress has been made in evaluating the nucleation performance of pyrotechnics in free fall by use of the vertical wind tunnel described above. The effectiveness of these devices is about an order of magnitude higher as measured under free fall conditions than under the old test conditions. Coagulation in the plumes at free fall is still significant, however, and much work remains to be done before final effectiveness can be reported.

APPENDIX C

NAVY WEATHER RESEARCH FACILITY STORMFURY ACTIVITY AND RESEARCH

Staff, Navy Weather Research Facility

INTRODUCTION

The Navy Weather Research Facility (WEARSCHFAC) is engaged in a continuing broad program of research in tropical meteorology, especially on tropical cyclones and is also extensively involved in weather-modification studies, with emphasis on experiment design and evaluation incorporating computer exploration of the relevant atmospheric processes with mathematical simulation models. Project STORMFURY participation includes a number of coordinated and/or cooperative programs with the Environmental Science Services Administration's (ESSA) National Hurricane Research Laboratory (NHRL), Research Flight Facility (RFF), and Experimental Meteorology Branch (EMB) of the Atmospheric Physics & Chemistry Laboratory in planning, observing, and evaluating tropical cyclone modification and related experiments.

Although a lack of eligible mature hurricanes prevented the conduct of an eyewall seeding experiment during the 1968 season, WEARSCHFAC devoted considerable effort to supporting overall and long-term aspects of the Project STORMFURY concept. Substantial progress has been made in obtaining a clearer understanding of the possibilities of and procedures for modifying severe tropical storms, in initiating collection of the basic cloud-physics data, and in upgrading airborne radarscope photography capabilities.

PLANNING

During the annual meeting of the Project STORMFURY Advisory Panel at Miami in December 1968, the WEARSCHFAC representative reaffirmed the conviction of this activity that the rainband experiment should vigorously be prosecuted - not only because of its inherent soundness, but in view of the need for systematically acquiring improved understanding of convective and dynamic processes as well as modification potential at progressively larger and more complex scales of motion. Thus, whereas there is reason to advocate that the original hypothesis of seeding the eyewall should be tested when a favorable opportunity arises - despite the fact this phenomenon is poorly understood - no chance should be overlooked (indeed, suitable occasions should emphatically be sought) to test the rainband hypothesis. In this regard, there exist two apparent discrepancies which suggest a reexamination of currently proposed tropical cyclone models and therefore the STORMFURY concept:

1. Typhoon/hurricane reconnaissance crews advise that whereas convective turbulence is pronounced in feeder bands, it is only occasionally encountered in eyewall penetrations. It is recognized that reconnaissance aircraft endeavor generally to penetrate at points where radar indicates that severe weather is minimal; nevertheless, there is also a distinct possibility that the rising air in the eyewall is predominantly a convergence-induced upward spiraling about the center, and that the eyewall is largely composed of stratiform rather than cumuliform clouds. Perhaps the extreme horizontal and vertical wind shears which exist in and near the eyewall support this contention. If so, an eyewall modification hypothesis which is predicated upon ice-phase seeding of cumuli may bear reconsideration.

2. Typhoon/hurricane reconnaissance crews report the existence from time to time (in storms of less (thus far) than 100-kt, maximum-wind intensity) of hurricane-intensity tropical cyclones in which, except for overlying cirrus, all cloudiness occurred below the freezing level - and even below 700 mb. Occasions have also been reported in which there was no definable eyewall. Such occurrences are also grounds for reexamining not only existing tropical cyclone models, but the basic Project STORMFURY concept as well. WEARSCHFAC is attempting to determine the extent to which the existence of storms of this nature may infer that the STORMFURY hurricane modification experiment should be subjugated to a STORMFURY hurricane investigation effort.

During the interim, an aggressive program must be pursued in the laboratories and with simulation models to develop the quantitative guidelines needed for enhanced success in modification experiments. This should involve:

1. A study of the thermodynamic structure of tropical cyclones to seek indications as to the amount of potential energy that could be converted into kinetic energy by ice-phase seeding or other feasible modification techniques.

2. From investigations of a number of tropical cyclones, determine a more realistic estimate as to the frequency with

which significant energy releases could actually be achieved by ice-phase seeding. It seems likely that suitable conditions would most frequently be found toward the outer extremity of feeder bands at the point where sizable organized convection first penetrates the freezing level, and vertical as well as horizontal wind shears are not yet pronounced. If these cumuli can be triggered to grow to the tropopause, as has been observed in ice-phase seeding of other tropical cumuli, it would suggest an additional approach to the modification of tropical cyclone dynamics.

3. Simulated modification procedures should be explored with computer models to determine quantitative estimates as to the effect of the energy released by seeding upon tropical cyclone behavior. In the absence of suitable tropical cyclones for actual experiments, it is assumed the reasonably analogous clouds and cloud systems can be found in other tropical regions where the conduct of tests independent of Project STORMFURY operations would be permissible. Presumably, these could be used for practice and to develop the very necessary improved understanding of seeding effects, without the complexities inherent in a full-scale tropical cyclone experiment.

To date, Project STORMFURY has resorted to seeding from above with pyrotechnic devices that burn through long fall trajectories, and which are difficult to deliver accurately upon the target cloud(s). WEARSCHFAC has suggested the testing of low-level seeding into the inflow regions of organized convective systems (e.g., feeder bands and supposedly the eyewall). If this system is effective it would have many advantages in better targeting of the treatment, and in producing the sustained treatment that may be necessary to modify tropical cyclones. Low-level seeding has been used with success in precipitation-management programs, and should be evaluated both by simulation studies and actual experiments as a prospective STORMFURY technique.

OPERATIONAL SUPPORT

Five WEARSCHFAC personnel and a WEARSCHFAC consultant participated in the Project STORMFURY dry-run and cloudline operations, and were on standby for Project STORMFURY eyewall/feeder-band operations throughout the 1968 season.

WEARSCHFAC is sponsoring a sustained effort to upgrade the weather radar and radarscope photography capabilities of Navy hurricane/typhoon reconnaissance aircraft, and to achieve more comprehensive documentation during routine hurricane/typhoon reconnaissance as well as STORMFURY operations. Initially, this should enhance the acquisition of more detailed tropical cyclone data for research purposes. The ultimate objective is, of course, the development of improved operational observing and diagnostic techniques. ESSA/RFF assisted in this effort by making the services of a radar photography expert temporarily available to both AEWRON ONE and WEARECONRON FOUR.

WEARSCHFAC has provided assistance to ESSA/RFF and EMB/APCL in obtaining and analyzing cloud-replica samples in tropical storms, in connection with studies to determine the conditions during which there is supercooled water suitable for ice-phase modification.

A cloud model that uses upper-air soundings to predict the potential for modification of convection with ice-phase seeding has been developed and is now being used to explore hurricane soundings. One hundred soundings from within the circulation of hurricanes which were collected by NHRL are being analyzed to determine the frequency with which opportunities occur for making an appreciable modification in the dynamics of convection through ice-phase seeding.

WEARSCHFAC is continuing to study the feeder-band seeding hypothesis ("Proposed Rainband Seeding Experiment for 1965 STORMFURY Operations," NAVWEARSCHFAC Tech. Paper No. 6-65), and in this regard plans to exploit a two-dimensional computer model developed with Naval Research Laboratory (NRL) support for analyzing the effect of ice-phase seeding on line clouds. Exploration of the feeder-band hypothesis with this model should facilitate decisions as to prospective applications prior to the conduct of actual physical experiments.

A WEARSCHFAC investigation of tropical cyclones passing over the cold-water trail of an earlier typhoon (within 1 to 2 weeks) indicates that a definite decrease in the rate of change of storm intensity occurs. The possibility of movement over a "cold" underlying sea surface should be considered in any STORMFURY evaluations of hurricane-modification experiments.

APPENDIX D

PRELIMINARY ANALYSIS OF CLOUD PHYSICS DATA COLLECTED IN HURRICANE GLADYS (1968)

Robert C. Sheets
Environmental Science Services Administration
National Hurricane Research Laboratory
Miami, Florida

INTRODUCTION

The hurricane season of 1968 was somewhat disappointing from a research point of view, because comparatively few opportunities existed for investigating the internal structure of mature hurricanes. However, some enlightening and historic data were collected in Hurricane Gladys on October 16, 1968, when continuous cloud-particle samples were obtained in a hurricane for the first time. They were obtained with an airborne continuous particle sampler developed by Meteorology Research, Inc. (fig. D-1), which basically consists of a mechanism that continuously moves 16-mm Mylar film by an exposure slot mounted in an airfoil-shaped probe extending approximately 3 ft outside the aircraft into the nearly undisturbed air (Meteorology Research, Inc., 1968). The film is coated with a solution of Formvar and chloroform just before exposure. During this operation, the film was being transported past the 1/8-in. wide exposure slot at a speed of approximately 11 in./sec, resulting in an exposure time of 1/88 sec. The total volume of air sampled on 1 mm^2 of the coated film is then approximately 1.16 cm^3.

Three sets of data were obtained in a relatively strong rainband at temperatures of -5°C to -10°C. Figure D-2 shows a sample with nearly all water droplets, and figure D-3 is a photograph taken of a sample collected from a cloudline and shows considerable ice present. These data were the main reason for the research mission and will be discussed in detail later.

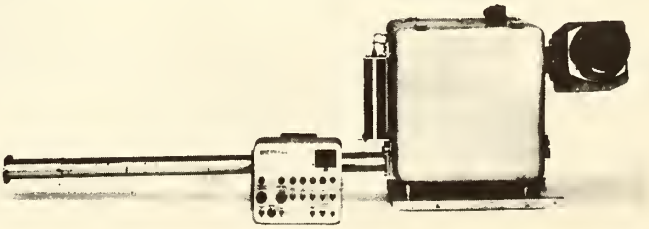

Figure D-1. Continuous cloud particle sampler system with viewer.

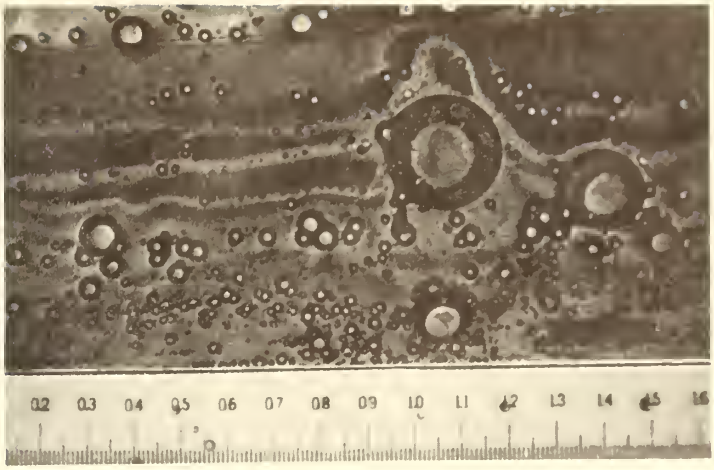

Figure D-2. Sample of cloud particles obtained in Hurricane Gladys, 1968. Scale in millimeters.

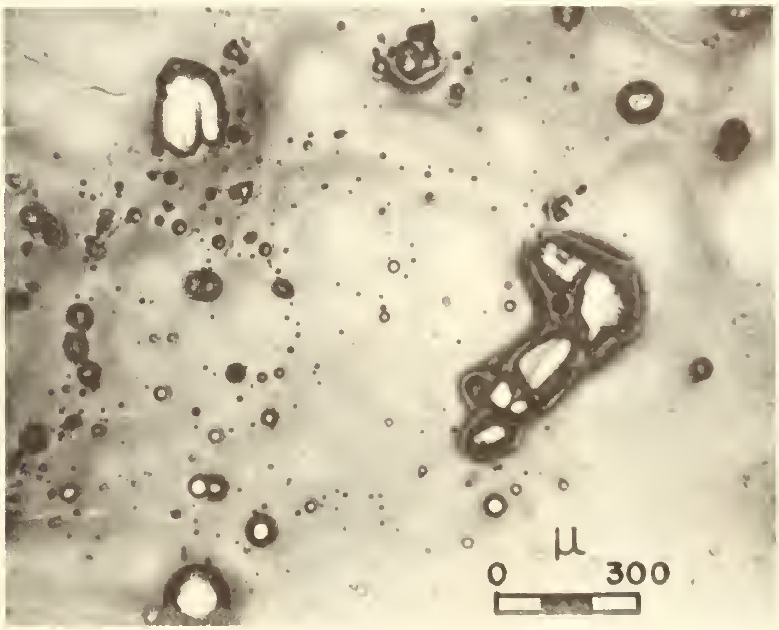

Figure D-3. Sample of cloud particles obtained in a cloud line, 1968.

STORM STRUCTURE

Hurricane Gladys had passed over Cuba during the morning and early afternoon of October 16, 1968. The central portion of the storm was in an unorganized and changing state during the sampling mission, but one major band located on the north side of the center of the circulation was quite prominent on the scopes of the APS-20, 10-cm, and WP-101, 5.2-cm, radar systems during the period of the investigation. Figure D-4 shows the track of Hurricane Gladys (bold line) and the track flown by the DC-6 Research Flight Facility aircraft. The large hatched area is the radar presentation recorded on the scope of the WSR-57, 10.3-cm, radar system located at Key West, Florida, at 2000 GMT on October 16, 1968. The stippled areas were obtained by compositing the echoes observed on the APS-20 and WP-101 radar systems onboard the DC-6 aircraft over the approximately 1½-hour time period when the central portion of the storm was being investigated. No distinct eye was observed. From a sequence of radar observations made at Key West, it appears that an eye was trying to form in the extreme southwestern portion of the displayed radar echoes at 2200 GMT on October 16, but it was completely open on the south and southwest sides (fig. D-5). No distinct closed eye was observed until 0100 GMT on October 17 (fig. D-6) 3 to 4 hours after the period of the airborne investigation, when the eye formed in the extreme southwestern portion of the radar echo.

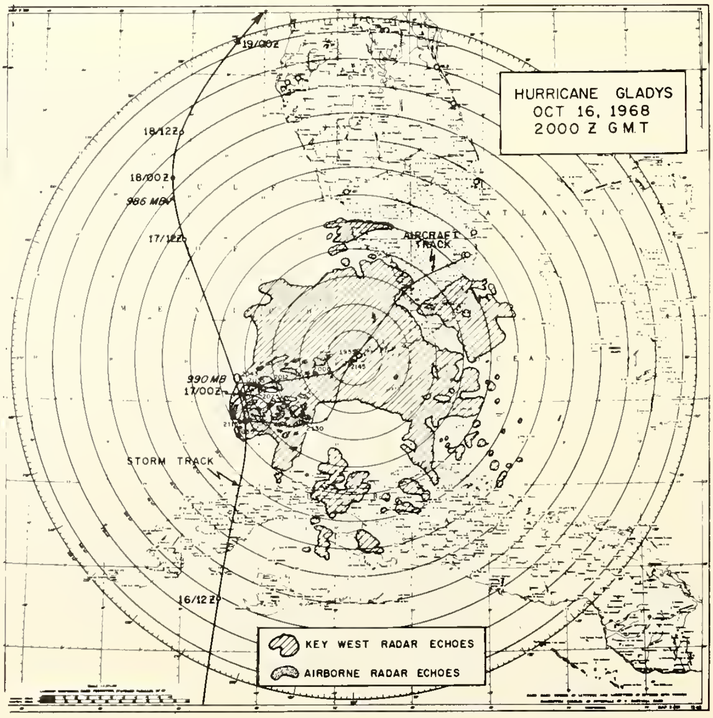

Figure D-4. Key West WSR-57 radar presentation of Hurricane Gladys at 2000 GMT October 16, 1968 (hatched areas), with superimposed radar composites (stippled areas) obtained from the scopes of the airborne APS-20 and WP-101 radar systems from 2000 to 2145 GMT. Also shown are the tracks of the storm (bold line) and the aircraft.

The wind speeds were generally of the order of 40 to 50 kt at flight level within 80

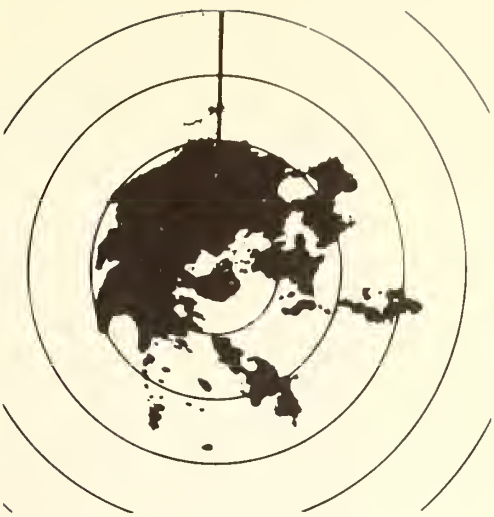

Figure D-5. Key West WSR-57 radar presentation of Hurricane Gladys at 2200 GMT, October 16, 1968.

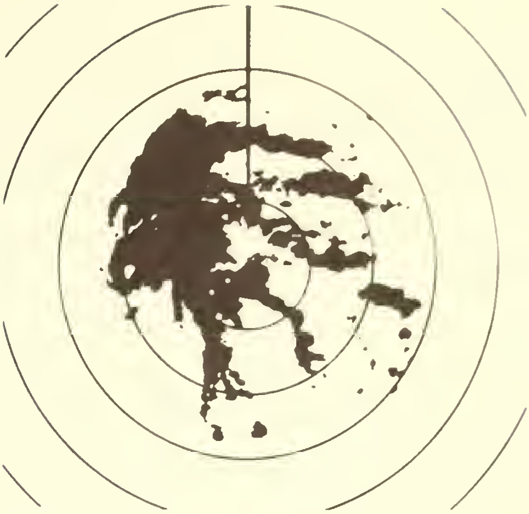

Figure D-6. Key West WSR-57 radar presentation of Hurricane Gladys at 0100 GMT, October 17, 1968.

to 100 n mi of the storm center. Surface winds were estimated to be 60 kt or greater near the center of the storm from observations of the state of the sea, and nearly continuous rain with complete overcast existed from Miami to the storm center. However, just 25 to 30 n mi west of the center the low-level clouds were broken to scattered, with very few high clouds present. This structure is depicted very well by the radar presentations from Key West and the ESSA-7 satellite picture, pass 768, which was obtained near 2000 GMT, October 16 (fig. D-7). Nearly all the high-level cloudiness associated with the outflow portion of the storm is located east of the low-level circulation center. A distinct outflow pattern is observed.

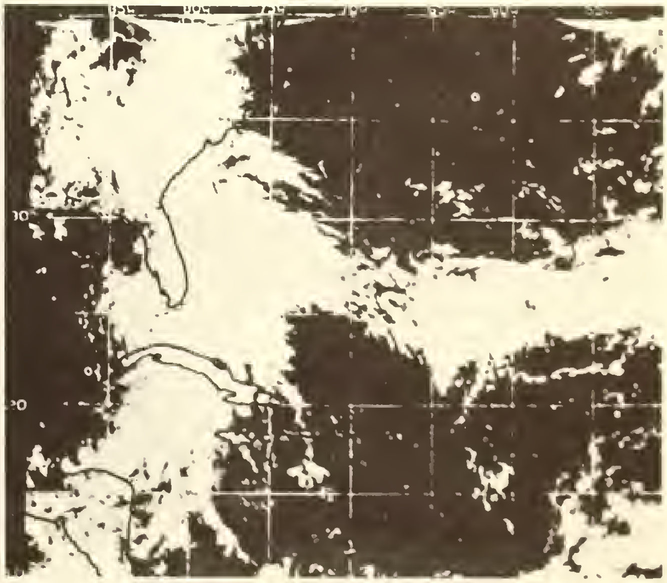

Figure D-7. ESSA-7 satellite picture, pass 768, obtained over Hurricane Gladys at 2000 GMT, October 16, 1968.

After the Formvar samples had been obtained, the aircraft descended close to an altitude of 10,000 ft in search of an operational fix on the location of the center of the storm circulation. As previously mentioned, no radar eye was present at this time. There appeared to be more than one center of circulation, but the main center seemed to be near the point indicated by the time 2055 GMT in figure D-8. At 211540 GMT severe turbulence was encountered, primarily in the form of one violent updraft in which the aircraft rose rapidly, hesitated, then rose some more. The aircraft dropped abruptly, and all loose objects including crew members were suspended against the top of the aircraft until the aircraft abruptly stopped falling. In some cases, the loose objects struck the top of the aircraft with such force as to dent it. Several objects were jarred loose from their installed positions and crashed to the floor of the aircraft at the abrupt end of the fall. Structural damage to the aircraft was feared, and one crew member was seriously injured. An attempt was therefore made to avoid all areas containing major radar echoes on the return to the base of operations in Miami. Only minor turbulence was encountered during the remainder of the flight.

A composite of the presentations obtained from the vertically oriented 3-cm radar shows echoes extending only to altitudes of 15,000 to 20,000 ft along the flight path in the region of the major 'bump (fig. D-9). However, from the RDR presentation (fig. D-10), the aircraft appears to be on the edge of a major echo at the time of this bump. The echo located 5 n mi to the left of the aircraft reached an altitude of 35,000 ft. A post-analysis showed that this echo was probably the reforming eyewall. The sequence of radar presentations collected by the WSR-57 radar system (located at Key West) does show that the eye did reform in this region.

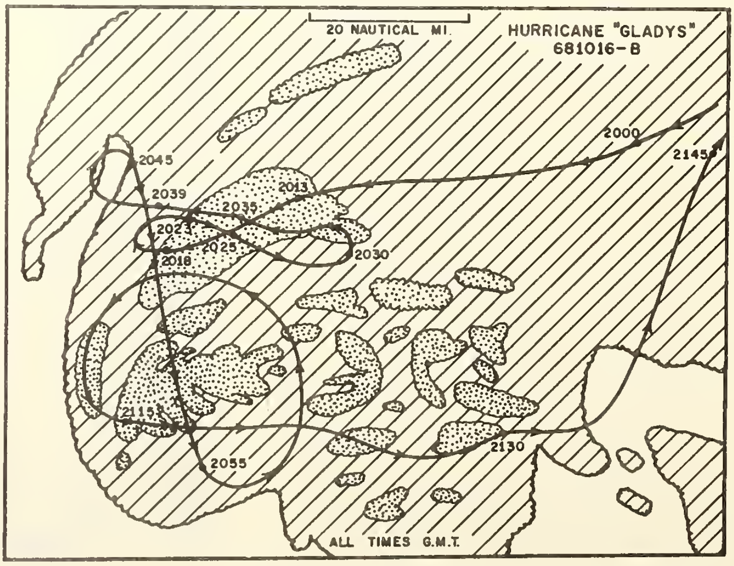

Figure D-8. Enlarged central portion of figure D-4, showing the Key West radar presentation (hatched area), the composited airborne radar presentations (stippled area) and the track flown by the research aircraft.

The traces of the total liquid water content for this region in figure D-11 show large fluctuations over short time

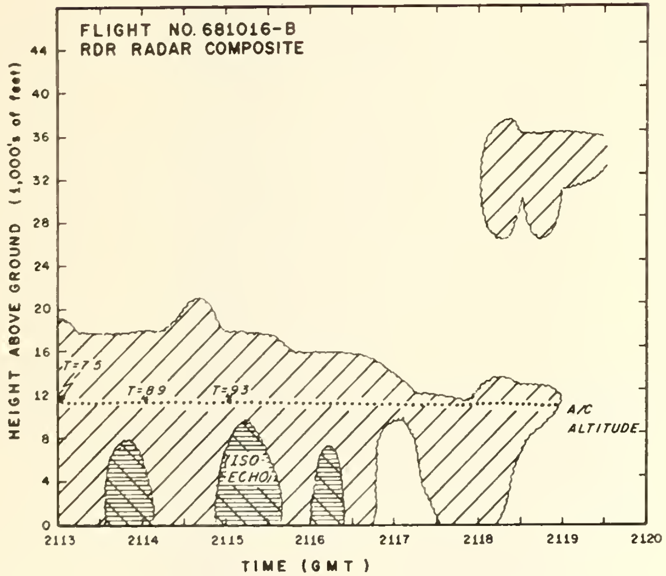

Figure D-9. Composite of vertically oriented RDR 3-cm radar presentations along the flight path from 2113 to 2120 GMT.

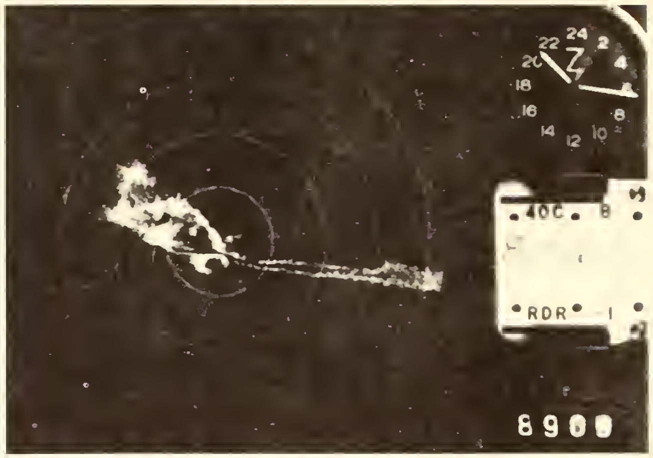

Figure D-10. RDR vertically oriented radar presentation for 201548 GMT, October 16, 1968. Range markers are 5 n mi apart.

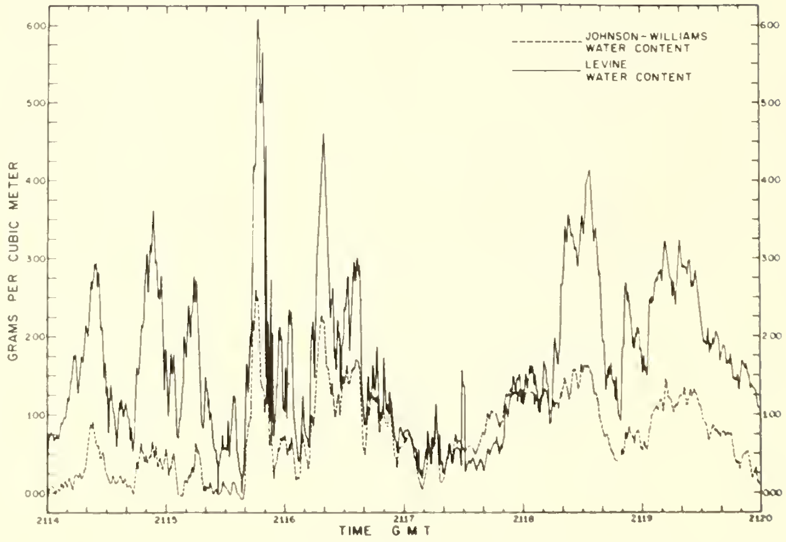

Figure D-11. Graphs of liquid water content for the region of severe turbulence (traces from the Johnson-Williams and Levine instruments).

intervals, with a maximum of greater than 6 g/m^3 being recorded by the Levine instruments at the time of the bump.

CLOUD PARTICLE SAMPLES

The first sampling pass was made down the rainband, as shown by the flight track in figure D-8, from 2012 to 2019 GMT. The total distance was approximately 25 n mi, and nearly 400 ft of continuous cloud particle samples were obtained. A composite of the vertically oriented RDR radar presentations (cf. fig. D-10) for this sampling pass is shown in figure D-12. The isoecho region is that portion of the cloud or echo giving the largest radar return, i.e., the strong portion of the echo. As shown in figure 12, the altitude of the aircraft was slightly above 20,000 ft upon entering the rainband and decreased slowly as the aircraft picked up ice during the traverse down the band. The temperature range was -7.6°C to -5.3°C. Maximum tops of the radar echoes were approximately 40,000 ft. A preliminary analysis of the Formvar samples obtained on this pass shows some ice at the beginning of the traverse, with the percentage of ice versus water decreasing and the sample becoming almost totally water midway through the pass. Large amounts of liquid water were present throughout the pass, which was also indicated by large amounts of ice picked up by the aircraft, causing some loss of altitude. The liquid water content measured independently of the Formvar sampler showed maximum values exceeding .75 g/m^3.

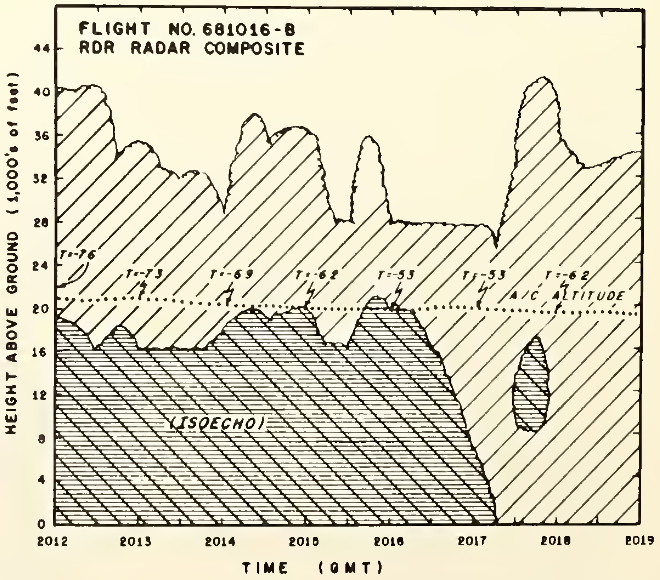

Figure D-12. Composite of vertically oriented RDR 3-cm radar presentations along the path for the sampling pass, 2012 to 2019 GMT.

The second sampling pass (2022 to 2028 GMT) was at a slight angle across the major rainband (fig. D-8) in a stronger portion of the rainband than the first pass. The radar echo tops extended to an altitude of nearly 48,000 ft, and the isoecho portion of the presentation extended to altitudes of more than 24,000 ft (fig. D-13). The aircraft altitude fluctuated between 19,000 and 20,000 ft, and temperatures ranged from -5°C to -6.3°C. A preliminary analysis of the Formvar samples showed ice to be almost nonexistent during this pass. Again, the aircraft picked up considerable ice, indicating the presence of large amounts of liquid water. The maximum liquid water content exceeded 1.75 g/m^3, or much more than during the first pass.

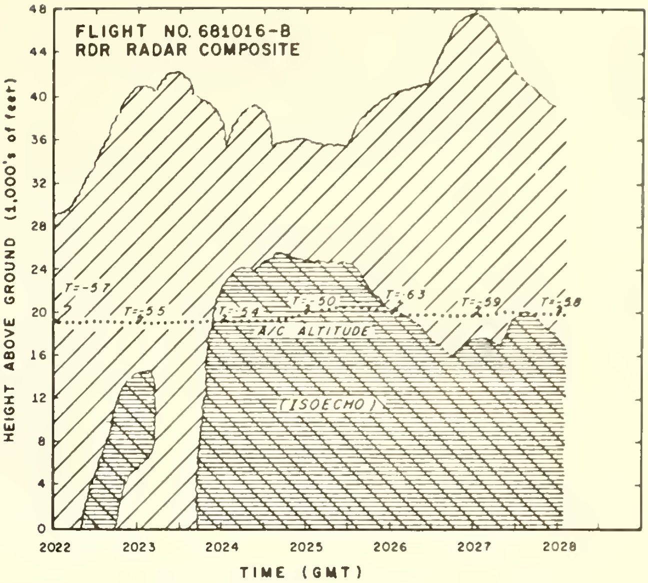

Figure D-13. Composite of the vertically oriented RDR 3-cm radar presentations along the path for the second sampling pass, 2022 to 2028 GMT.

The aircraft then climbed to its maximum altitude before making the third and final sampling pass on this flight. This pass was at an angle of approximately 45° across the rainband (fig. D-8). Figure D-14 shows the WP-101 radar presentation as the band was entered. The top of the scope is the heading of the aircraft, and the range markers are at 10-n mi intervals. The echo in the center of the scope is the rainband being sampled, and the disorganized, somewhat broken echoes 15 to 25 n mi left of the center are in the region where the severe turbulence was encountered, which apparently was the reforming north eyewall.

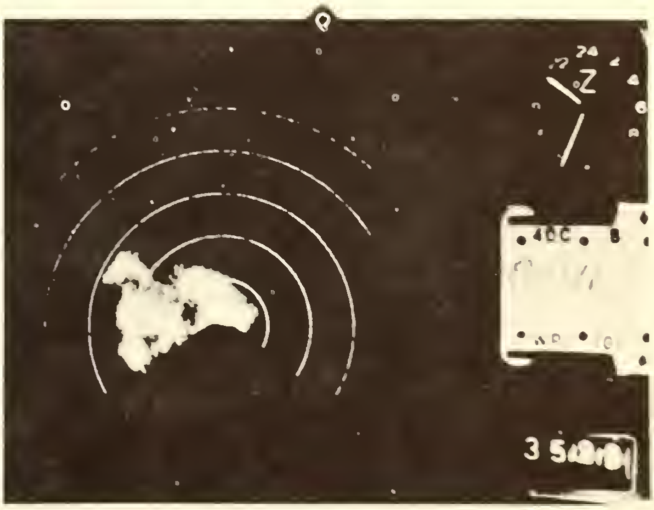

Figure D-14. WP-101 5.2-cm radar presentation at the time of the third sampling pass. Range markers are at intervals of 10 n mi, and the top of the scope is the heading of the aircraft.

The aircraft altitude was near 21,000 ft, and temperatures ranged from -7.4°C to -8.4°C. The radar echoes extended to a maximum altitude of 36,000 ft, while maximum height of the isoecho portion of the presentation was close to 20,000 ft (fig. D-15). Figure D-16 shows the RDR presentation for the center portion of this traverse through the rainband. The range markers are at 5-n mi intervals, with the aircraft located in the center of the scope. The narrow band almost free of echoes located 4 n mi below the aircraft, i.e., 21,000 ft, and extending horizontally left and right of the aircraft is the sea surface. The echo-free region from the sea surface to just below the aircraft (center of the scope) and 5 n mi right to 20 n mi left is the isoecho portion of the displayed return. The vertically oriented radar composites (figs. D-9, D-12, D-13, and D-15) were made from similar presentations obtained at 16-sec intervals. A preliminary analysis of the Formval samples again indicates that virtually all the cloud particle samples were water droplets; relatively little ice was observed. The liquid water content for this pass averaged between .75 to 1 g/m^3.

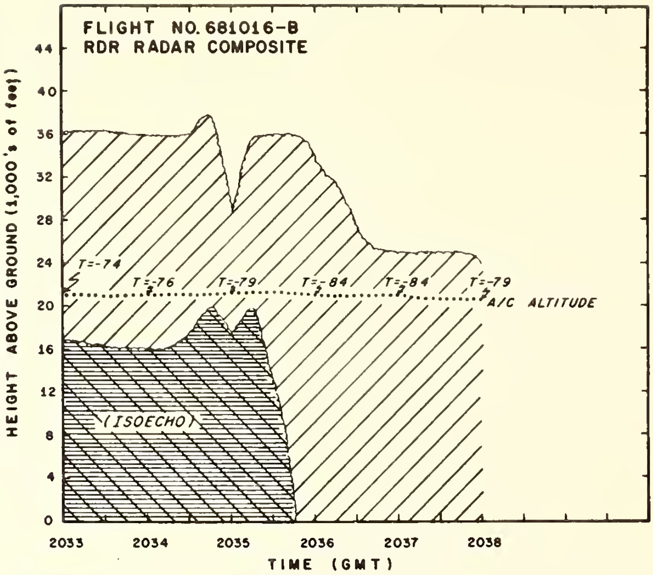

Figure D-15. Composite of the vertically oriented RDR 3-cm radar presentations along the flight path for the third sampling pass, 2033 to 2038 GMT.

SUMMARY AND CONCLUSIONS

The cloud particle samples collected during the flight into Hurricane Gladys, October 16, 1968, basically confirm what has been believed for some time: large amounts of liquid water are present above the freezing level in hurricane rainbands. This is not surprising, but the fact

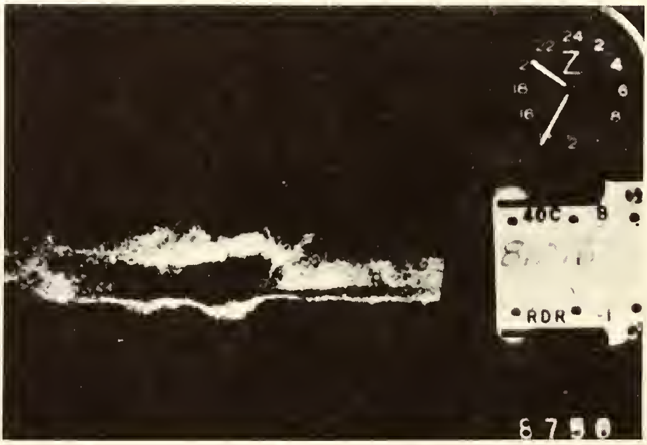

Figure D-16. RDR vertically oriented radar presentation for 203433 GMT, October 16, 1968. Range markers are 5 n mi apart.

that little ice was found on two of the passes and on a major portion of the third pass is quite interesting, especially since other investigators using similar instruments have found large amounts of ice present at these temperatures in tropical cumulus clouds (Ruskin, 1967).

It is believed that at least part of the reason for the dominance of ice over water in some of these cumuli is that sampling was done mostly in the quiescent portion of the cloud; in the more active portion of the cloud, more and larger liquid water droplets would probably have been present (Todd, 1965). However, so far as the author is aware, considerable ice was still present in all samples obtained at temperatures of -5°C or colder. If the Formvar samples had shown a few small areas in which nearly all the cloud particles sampled had been liquid, it would not have been surprising. However, since the area sampled was approximately 50 n mi long and nearly 3/4 of it showed ice to be almost nonexistent, it is surprising and has significant implications for considering modification of the storm through artificial seeding of the water droplets above the freezing level. These data are not sufficient, of course, to draw strong conclusions from, since they were obtained in a single hurricane and essentially in the same rainband over a period of 25 min, and are certainly not independent of each other. Therefore, considerable caution should be used in applying these findings to hurricanes in general. Because the foil sampler (for measuring the large cloud particles) malfunctioned, an exact measure of the total water content, percentage of ice versus water, and cloud droplet spectra cannot be obtained, but rough approximations of these quantities probably can and will be attempted.

The next logical step seems to be to obtain similar samples horizontally and vertically in other hurricanes to see if a great dominance of water over ice generally exists in hurricane rainbands or if it just exists at selected levels and locations within the storm. The value of the Formvar instrument is readily apparent in a modification experiment to sample a cloud, rainband, or eyewall before and after an artificial seeding agent is introduced.

REFERENCES

Meteorology Research Inc. (1968), Instruction manual, airborne continuous particle sampler.

Ruskin, R. E. (1967), Measurements of water-ice budget changes at -5°C in AgI-seeded tropical cumulus, J. Appl. Meteorol., 6, No. 1, 72-81.

Todd, C. J. (1965), Ice crystal development in a seeded cumulus cloud, J. Atmospheric Sci., 22, No. 1, 70-78.

APPENDIX E

COMPUTATIONS OF THE SEEDABILITY OF CLOUDS IN A HURRICANE ENVIRONMENT

Robert C. Sheets
Environmental Science Services Administration
National Hurricane Research Laboratory
Miami, Florida

INTRODUCTION

A study was recently completed by the author that attempted to determine some mean conditions present in hurricanes (Sheets, 1969). It was based on radiosonde data collected within 100 n mi of hurricane centers during the past few years. The data were stratified by the surface pressure of the observations, resulting in more than one mean sounding. The surface pressure categories used were less than 995 mb, 995 to 999 mb, 1000 to 1004 mb, 1005 to 1009 mb, and 1010 to 1015 mb. These soundings, which could be inferred to represent the mean conditions of different intensities of hurricanes or at various radial distances from the center of a hurricane, were used in a cumulus cloud model to determine the possible effects of seeding clouds contained in these environments.

CLOUD MODEL

The cloud model used was developed by Dr. Joanne Simpson et al. (1967), who describe the model basically as follows:

> The model calculations consist of integrating the vertical equation of motion for the rising cloud tower. The vertical acceleration of its center is expressed as the difference between buoyancy and drag forces. The formulation of the forces depends on two major physical postulates, namely 1) that the cloud tower behaves as a rising plume with a vortically circulating cap or like an entraining jet, and 2) it entrains environment air at a rate inversely proportional to its horizontal dimension.
>
> The heart of the seeding subroutine is the release of latent heat resulting from freezing of the cloud's liquid water content.

The seeding subroutine used in this study releases the latent heat linearly with height between the two levels at which the cloud has temperatures of -5°C and -15°C. It also releases in the same interval the latent heat added by the change from water saturation to ice saturation. At temperatures lower than -15°C, ice saturation is maintained in seeded clouds. The temperature range of -5°C to -15°C results in lower buoyancies, especially in the middle levels, than the -4°C to -8°C range used by Simpson et al. (1967) in their 1965 experiments. The inputs into the model are the temperature interval over which the latent heat, etc.,are to be released, the environmental sounding, the cloud base, and the cloud radius.

The model has been refined at various times, and the version used in this study is described in a paper by Simpson and Wiggert (1969). Details are also contained in other papers (Simpson et al., 1965, 1967).

COMPUTATIONAL RESULTS

Various cloud bases and radii were used with the mean hurricane soundings, because the exact values within the hurricane vary and are not precisely known; a summary of the results is given in table E-1. The range presented is believed to effectively span the probable cloud sizes present in the hurricane. The 1000-mb temperature of some of the soundings was increased by a small amount to make the soundings more realistic at the lowest levels. This correction was applied because the data used in the compilation of the mean soundings were obtained at land-based stations, with a significant number of these soundings obtained at night. The correction applied to each sounding and the final temperature used (in °C) are listed in column T_{1000} in table E-1. These values are certainly conservative when compared with the sea surface temperatures in the vicinity of a hurricane.

The cloud base was arbitrarily chosen to decrease inward toward the storm center (lower surface pressures) in order to simulate conditions that exist in hurricanes. Various combinations of cloud bases and cloud radii were used with each surface pressure category. Table E-1 lists results for the natural cloud, the cloud generated by the model from the sounding and the cloud base and radius without any seeding, and the seeded cloud, the change that results in the natural cloud by the release of latent heat as described earlier. The quantity T_B, which is the difference between the virtual temperatures of the cloud and the environment, essentially

Table E-1. Summary of Results of Computations Based on the Mean Hurricane Soundings and Simpson's Cloud Model.

				NATURAL CLOUD			SEEDED CLOUD		
Mean Hurricane Soundings	T_{1000}	Cloud Base (m)	Cloud Radius (m)	Cloud Top (m)	W_{max} (m/sec)	T_B (°C)	ΔH (m)	ΔW_{max} (m/sec)	ΔT_B (°C)
SP < 995 mb	25.3 (+0.2)	200	1500	9100	11.588	1.10	0	0	1.06
		200	3200	12750	14.949	2.24	5500	1.953	2.51
		200	5000	15500	16.358	2.70	6050	7.486	3.32
995 ≤ SP ≤ 999 mb	25.7 (+1.4)	200	3200	13600	11.005	1.72	4250	6.511	3.01
		300	3200	11750	13.520	1.90	5850	0.264	2.29
		200	5000	16000	12.008	2.53	5150	10.978	3.40
		300	5000	14200	14.756	2.32	6650	5.126	3.01
1000 ≤ SP ≤ 1004 mb	25.5 (+0.5)	300	3200	13950	14.110	2.53	4600	5.345	2.52
		500	3200	11950	11.195	1.87	5200	2.850	2.12
		300	5000	16900	15.610	3.02	4600	10.376	3.21
		500	5000	14350	12.200	2.29	6150	6.865	3.74
1005 ≤ SP ≤ 1009 mb	25.6 (0)	500	1500	10850	12.201	1.51	3100	0	1.79
		500	3200	16200	16.252	2.91	2550	8.168	3.08
		750	3200	14100	12.936	2.40	3650	5.761	2.36
		500	5000	19200	18.848	3.53	2300	12.726	3.71
1010 ≤ SP ≤ 1014 mb	25.7 (+0.5)	500	1500	12600	12.803	2.16	2400	2.305	2.09
		500	3200	17750	19.426	3.66	1750	9.898	3.40
		750	3200	16350	15.250	2.98	2500	8.758	2.93

T_B — Maximum value of the virtual temperature of the cloud minus the virtual temperature of the environment above the freezing level.

ΔH — The increase in the natural cloud height as a result of seeding.

ΔW_{max} — The increase in the maximum vertical velocity in the cloud as a result of seeding.

ΔT_B — The increase in T_B as a result of seeding.

gives a measure of the buoyancy. In all cases shown, the buoyancy increased with the introduction of the seeding material, and in all but one or two the maximum vertical velocity and the height of the cloud increased as a result of the seeding routine. In some cases, the final cloud top after seeding reaches considerably above the tropopause. The basic reason is that the final cloud top is listed in the cloud program as the height where the vertical velocity equals zero plus the sum of the cloud-base and cloud-radius values, but the increase in the cloud height due to seeding (ΔH) remains the same.

If we compare values of the measure of the buoyancy (T_B) for the various surface pressure categories for constant cloud radii and bases, we see that these values generally decrease as the surface pressure of the sounding decreases. That is, in general, the thermodynamics are such that, as the storm becomes weaker or the sounding is obtained at a greater distance from the storm center, the difference between the virtual temperature in the cloud and the virtual temperature in the environment (the sounding) becomes larger. This correlates very well with the calculations of the available instability energy made for these mean hurricane soundings, in which the amount of available instability energy generally decreased as the surface pressure became lower (Sheets, 1969). In other words, as the surface pressure of the sounding decreases, the vertical temperature distribution approaches a moist adiabatic lapse rate, a fact further illustrated in these calculations, since the values of the arbitrary cloud bases and radii were found to be not nearly as critical for the soundings with the high surface pressures as for those with low surface pressures.

These results have significant implications for the possible modification of a hurricane by artificial seeding of convective clouds. They indicate that, if the object of a seeding program is to make the cloud grow, good results can be obtained almost anywhere within the hurricane as long as the cloud bases are low enough and the cloud radii large enough. However, the soundings become more conditionally unstable as the surface pressures of the mean soundings increase. Therefore, seeding a convective area some distance from the storm center would appear to have a higher probability of making the cloud grow, which, of course, does not necessarily mean that the resulting modification of the storm would be the largest with this type of seeding. Other factors must also be considered.

REFERENCES

Sheets, R. C. (1969), Some mean hurricane soundings, J. Appl. Meteorol., 8, No. 1, 134-146.

Simpson, J., R. H. Simpson, D. A. Andrews, and M. A. Eaton (1965) Experimental cumulus dynamics, Rev. Geophys., 3, 387-431.

Simpson, J., G. W. Brier, and R. H. Simpson (1967), STORMFURY cumulus seeding experiment 1965: Statistical analysis and main results, J. Atmospheric Sci., 24, 508-521.

Simpson, J. and V. Wiggert (1969), Models of precipitating cumulus towers, Monthly Weather Rev. (to be published in June issue).

APPENDIX F

FEASIBILITY OF PROJECT STORMFURY OPERATIONS IN THE PACIFIC OCEAN

William D. Mallinger
Environmental Science Services Administration
National Hurricane Research Laboratory
Miami, Florida

INTRODUCTION

It has often been proposed that the hurricane modification project conduct its field experiments in the Pacific Ocean, where so many more tropical cyclones occur. In this study of the feasibility of such proposals, two separate areas are considered: the hurricane area of the Eastern Pacific and the typhoon area of the Western Pacific.

EASTERN PACIFIC

A sharp increase in the number of tropical cyclones and hurricanes in the Eastern Pacific has been reported in recent years. Since the observational network in this area is so sparse and the reported increase occurred since the utilization of weather satellites has become common, it is assumed that many storms were neither detected nor reported in earlier years.

Table F-1 lists the occurrence of tropical cyclones in the Eastern Pacific for the past 20 years. Although the annual average number of occurrences is 10.2 for this 20-year period, the real average, although unknown, is probably higher for the reasons stated previously.

The following assumptions were made in order to estimate the feasibility of operations in the Eastern Pacific area:

1. The STORMFURY aircraft would be those currently in use, or similar types.

2. The maximum effective range of operations from base would be near 550 mi.

3. Operations would have to be conducted from Acapulco, Mexico, because alternate suitable airfields are not available.

4. Rules for seeding eligibility would be similar to those used in the Atlantic STORMFURY experiments.

5. Forces (manpower and aircraft) would be available and permitted to operate from Mexico.

6. Logistics problems could be overcome.

Table F-1. Tropical Cyclones in the Eastern Pacific.

	Number Each Month								
Year	May	June	July	Aug.	Sept.	Oct.	Nov.	No/yr	Total Hurricanes
1968	0	2	6	8	3	5	0	24	6
1967	1	3	5	3	4	4	0	20	6
1966	0	1	0	4	6	2	0	13	6
1965	0	4	0	3	3	0	0	10	1
1964	0	0	3	2	1	0	0	6	1
1963	0	1	2	0	4	1	0	8	4
1962	0	1	1	2	3	1	0	8	2
1961	0	1	4	1	1	2	2	11	2
1960	0	2	1	2	1	2	0	8	6
1959	0	2	3	4	2	2	0	13	4
1958	0	2	3	3	3	2	0	13	5
1957	0	0	1	2	4	3	1	11	9
1956	2	2	2	1	3	1	0	11	5
1955	0	2	1	0	1	2	0	6	2
1954	0	1	3	0	4	2	0	10	4
1953	0	0	0	1	2	1	0	4	3
1952	1	1	2	0	2	1	0	7	3
1951	1	2	1	2	2	0	1	9	2
1950	0	1	2	2	0	1	0	6	5
1949	0	2	0	0	4	0	0	6	2
Total	5	30	40	40	53	32	4	204	79
Ave.	.25	1.5	2.0	2.0	2.65	1.6	0.2	10.2	3.95

Although, as pointed out above, rough data are available for the past 20 years, only the years 1965 through 1968 were examined in detail, because of the satellite coverage during this period.

In 1965, only one hurricane occurred. It was beyond the range of Project aircraft.

In 1966, with seven hurricanes, none was suitable for STORMFURY operations. Most were too far from the base when they became hurricanes; one was too close to Mexico.

In 1967, with six hurricanes, only one was within the range of the aircraft. This hurricane varied in intensity between 60 and 70 kt while in the area and would be considered marginal for experimentation.

In 1968, with six hurricanes, again only one was within range of the Project aircraft. This hurricane would have had to be seeded near maximum allowable distance from base. It was rapidly decreasing in intensity at the time, which made it an undesirable target.

Therefore, it appears that the Eastern Pacific offers relatively few desirable Project STORMFURY targets. A random check on data for earlier years confirms the lack of truly eligible storms for the type of experiment currently envisioned.

Even if these storms were closer to the ideal for experimentation, modification attempts would require military aircraft from the Atlantic reconnaissance squadrons. To use these limited resources would drastically reduce aircraft reconnaissance capability in the Atlantic during its hurricane season. Other problems are those of communications, international agreements required, and lack of forecasting experience in selecting storms that would be eligible for seeding under current rules.

Unless separate resources can be made available for these field experiments, they must be conducted in areas where some resources and capabilities already exist. This limits operations to the Atlantic Ocean, Gulf of Mexico, Caribbean Sea, or the Western Pacific Ocean.

WESTERN PACIFIC

In the Western Pacific, the typhoons appear to be much more desirable experimental modification targets. If and when the Vietnam war ends, the Navy Reconnaissance Squadron (VW-1) based at Guam, would perhaps be available for the Project. Although training and indoctrination of the crews would be required, the aircraft are very similar to those now used in the Atlantic (VW-4).

Whether seeder aircraft, such as the Navy A-6 Intruder, would be available in the Pacific for a project of this type is not known. For this reason, serious consideration should be given to the procurement of a different type of seeding aircraft. A C-130 or similar aircraft offers many advantages over smaller jet aircraft. With the larger plane, communications would be improved, and only one seeder (plus backup) would be required. In addition, range would be extended with added flexibility in drop altitudes, safety and control problems would be fewer, and selected scientists and Project officials could fly with the seeder to decide on drop times and locations.

The study of typhoons passing within range of Pacific bases was governed by the following guidelines:

1. The typhoon must be within 600 mi of the operating base.

2. Maximum winds should be at least 65 kt.

3. The typhoon must be within range for a minimum of 12 daylight hours.

4. The predicted movement of the typhoon must indicate that it will not be within 50 mi of a land mass within 24 hours after seeding.

A primary base at Guam, with Okinawa as a secondary base, quickly appeared to give the best combination (see table F-2). Most of the eligible storms that could be reached by staging from the Philippines would be more accessible staging from Okinawa.

Table F-2. Number of Typhoons Meeting Criteria-Staging Operations from Guam Okinawa

	Guam/Okinawa							
Year	June	July	Aug.	Sept.	Oct.	Nov.	Dec.	Total
1961	0/0	0/0	0/3	2/2	2/2	1/0	0/0	5/7
1962	0/0	0/0	1/2	1/1	1/2	1/0	0/0	4/5
1963	0/2	1/1	0/1	0/2	2/2	0/0	1/0	4/8
1964	0/0	2/1	0/0	2/0	0/1	0/0	1/0	5/2
1965	1/0	2/1	1/2	1/2	1/0	1/0	0/0	7/5
1966	0/1	0/0	0/0	3/2	0/0	0/0	0/0	3/3
1967	0/0	0/2	0/0	0/0	2/0	3/1	0/0	5/3

From 1961 through 1967, with August, September, and October being the key months, 19 typhoons would have been eligible for experiments conducted from Guam, and 24 from Okinawa. This gives an average of 2.7 per year for Guam-based operations and 3.4 per year for Okinawa.

Because the 43 eligible typhoons include six that passed within range of both bases, the average number of individual eligible typhoons per 3-month period is near five. The many tropical storms during these months would provide plentiful opportunities for additional rainband experiments and research missions.

With a change in seeder aircraft, the number of opportunities would increase slightly. The current maximum range of the Project aircraft is limited because of the endurance of the jet seeders and the B-57.

Table F-3 from the Project STORMFURY Annual Report lists the number of hurricanes eligible for seeding in the Atlantic, Gulf of Mexico, and Caribbean Sea during the past 15 years.

Table F-3. Annual Frequency of Hurricanes Eligible for Seeding Under Forecasting Techniques Criteria Approved for 1967 STORMFURY Operations (Listed by Area).

Year	Atlantic	Gulf of Mexico	Caribbean Sea	Total
1954	1	0	1	2
1955	4	0	1	5
1956	1	0	0	1
1957	1	0	0	1
1958	5	0	0	5
1959	2	0	0	2
1960	1	0	1	2
1961	2	1	0	3
1962	2	0	0	2
1963	3	0	0	3
1964	3	0	0	3
1965	2	0	0	2
1966	1	0	0	1
1967	0	0	0	0
1968	0	0	0	0
Total	28	1	3	32

During these 15 years, an average of about two hurricanes per year were eligible. The average of five per year in the Western Pacific being two-and-one-half times that of the opportunities in the Atlantic regions indicates that conducting modification experiments in the Western Pacific has definite merit. If the problems of funding, manpower, and national and international agreements can be solved, more than twice as many modification experiments could be accomplished per season. This could save years of waiting for sufficient opportunities to test, evaluate, redesign, and retest the effectiveness of these experiments.

GPO 851-504

Reprinted from Journal of Applied Meteorology, The American Meteorological Society, Vol. 8, No. 1, 134-146.

Some Mean Hurricane Soundings

Robert C. Sheets

National Hurricane Research Laboratory, ESSA, Miami, Fla.

(Manuscript received 3 September 1968)

ABSTRACT

Some "mean hurricane soundings" have been computed from 92 radiosonde observations collected within 100 n mi of the centers of hurricanes. High correlations between various parameters and the sea-level pressures of the observations are shown. The data have been stratified by sea-level pressure, giving more than one mean hurricane sounding. Diurnal variations were investigated and temperature differences that are statistically significant were found to exist in the middle and upper troposphere. In addition, potential buoyancies and available instability energies were computed for some of the mean soundings. Potential and equivalent potential temperatures were found to increase, while the net available instability energy decreased, and the tropopause became higher and colder as the sea-level pressures of the observations decreased. The mean soundings are shown to be conditionally unstable in the lower levels and very stable in the upper troposphere.

1. Introduction

Schacht (1946) used the limited number of soundings available in 1946 to obtain a mean hurricane sounding for the Caribbean area. His soundings were all from within 200 n mi of a hurricane center but only nine observations were located within 100 n mi of the center. Jordan (1958) states that Schacht must have had very few reports available that reached the 100-mb level since even in the years 1946–1948 less than 25% of the months had as many as five out of a possible 60 soundings reaching the 100-mb level under ordinary conditions.

Jordan and Jordan (1953) computed some mean hurricane soundings in 1954. Their data consisted of approximately 300 soundings obtained within 6° of latitude of the centers of mature hurricanes in the Atlantic-Caribbean-Gulf of Mexico area during the years 1946–1952. However, the total number located within 120 n mi of the centers of mature hurricanes was only 27, and of these only 10 reached the 100-mb level. In computing these mean soundings, they stratified the data by radial distance from the storm centers. This procedure was probably of little consequence, since their computations were generally confined to regions outside the high-energy portions of the storms. However, a similar stratification in the study presented here resulted in numerous problems, which will be discussed later.

Schacht's (1946) mean soundings show relatively large diurnal variations of the order of 2–3C in the levels from 400 mb to the upper limits of his soundings. He states that radiation errors in the noontime radiosondes were suspected, but, probably because of the small sample size, he concluded that the noon and midnight soundings were in good agreement. Since the diurnal variations in Schacht's mean soundings were rather large, they should be either verified or rejected through analysis of more plentiful and reliable data. The instrumentation used at the time of these two earlier studies was considerably less reliable than that used in the period of this study.

The above reasons prompted a more detailed study of the mean conditions present in hurricanes, based on radiosonde data obtained over the past few years. Approximately 100 soundings were obtained within 100 n mi of the centers of hurricanes for the period 1956–1967, inclusive. They were made in the regions of the Gulf of Mexico, the Caribbean Sea, and the North Atlantic Ocean at latitudes south of 35N. All cases that had extratropical characteristics were excluded from the sample. Also, no soundings that were in the eye or eyewall portions of the storm were included in the sample, since no eyewall soundings were available. One eye-sounding is presented for comparison purposes. Various quantities computed from the data are discussed below.

In processing the data for the mean hurricane sounding, it became obvious that the values obtained were generally a function of the sea level pressure (SLP) of the soundings. The question then arose of what is meant by a mean hurricane sounding. For the purposes of this paper, the mean hurricane sounding was computed from 92 soundings obtained within 100 n mi of a hurricane center. Other mean soundings computed from these data, stratified by the SLP of the observations, are also presented. Of course, this stratification reduces the sample size, and the usual problems which arise from small samples are present. These problems, however, do not appear to be significant enough to materially affect the results.

It is difficult to obtain an accurate vertical sounding of the atmosphere in the strong winds near or within a hurricane, and it is obviously easier to do so in the vicinity of weaker storms than near intense storms. Some bias, therefore, is probably present in the data, but enough soundings were obtained in the vicinity of storms of hurricane strength to warrant some meaningful and useful computations. These include the mean values of temperature, moisture, and heights of pressure surfaces, mean tropopause data, equivalent potential temperatures, potential temperatures, and correlations between the various parameters. Also, computations of stability and the amount of instability energy available for release by parcel ascent may be of interest, especially for possible application to storm modification hypotheses. Most of these computations were made and are included in this paper. Some caution must be exercised in interpreting results obtained from the surface temperatures, however, since these observations were taken at land-based stations. If they had been obtained over the warm waters (≥26C) generally associated with hurricanes, the surface temperatures could have been from 1–2C warmer than are shown for the mean soundings.

2. Processing of the data

Several techniques for stratifying the data were investigated: grouping the data by quadrants, distance from the storm center, surface pressure of the observation, and combinations of the above. The problems that arose as a result of stratification of the data by radial distance were numerous. These included the uncertainty of knowing exactly where the observation was made in relation to the storm center, and the size, intensity, and areal extent of the high energy portion of the storm. Because of these uncertainties, this method of stratification was rejected. The other methods mentioned above were tried and are discussed later.

Each individual sounding was plotted, and values of the various parameters were either computed or recorded for the standard reporting levels as well as for the 950-, 900- and 600-mb levels. The mean soundings were then computed from these data. The relative humidity values were obtained up through the 250-mb level and were computed in two different ways. When "motor-boating" occurred, threshold values were inserted for the first computation, and, in the second computation, the "motor-boating" values were replaced by an arbitrary value of 5%. Since most of the soundings included moisture values through the 250-mb level, the difference in the two mean values ranged from 2–5% at the upper levels. Considering the accuracy of the humidity measurements, these differences seem negligible. Therefore, the values presented in this paper were obtained by using threshold values for "motor-boating" conditions. Since the tropopause was usually well defined, and the discontinuity in the temperature curve was very sharp, the recorded tropopause data were used, rather than values read off, say, at every 10 mb in the vicinity of the tropopause. This resulted in emphasizing the sharpness of the "bend" in the temperature curve at the tropopause, but is probably more realistic than the rounded curve obtained by the other method. Also, this method helped in bringing out features of the tropopause to be discussed later.

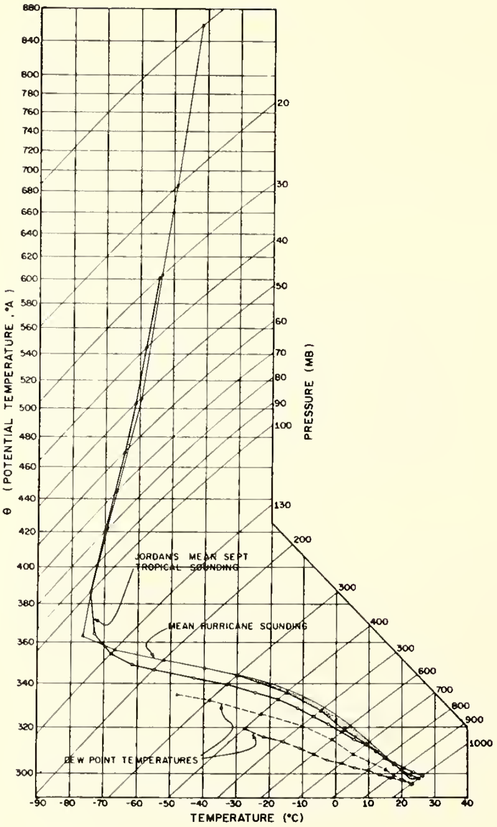

Fig. 1. A mean hurricane sounding computed from 92 radiosonde flights obtained with 100 n mi of hurricane centers. (Shaded area represents available instability energy.)

It was observed early in the study that many of the parameters were highly correlated with the SLP of the observation. For this reason, correlation coefficients were computed for most of the parameters with respect to the sea level pressure. Also included were computations of the means, variances and standard deviations of the various parameters at each level.

3. A mean hurricane sounding

All the data collected from the selected soundings were processed by the methods mentioned above and are listed and illustrated in Table 1 and Fig. 1, respec-

Table 1. - A Mean Hurricane Sounding

	Pressure Levels (mb)																		
	1000	950	900	850	700	600	500	400	300	250	200	150	Trop	100	70	50	30	20	10
Temp. (°C)	25.2	22.6	19.8	17.3	9.1	2.5	-4.7	-14.9	-29.7	-39.5	-51.8	-66.4	-76.2	-73.8	-66.3	-59.1	-53.1	-48.5	-41.5
Std. Dev.	1.9	1.4	1.2	1.1	1.4	1.5	2.0	2.2	2.4	2.4	2.4	2.4	3.9	4.0	2.9	2.5	2.0	2.4	3.8
*Cor. Coef.	.221	.119	-.100	-.214	-.453	-.465	-.611	-.730	-.662	-.682	-.646	-.453	.272	.301	.209	-.069	-.299	-.172	.271
No. Cases	92	92	92	92	91	91	88	84	80	79	76	70	61	60	39	35	26	17	8
Heights (m)	46			1465	3101	4368	5819	7545	9658	10932	12412	14215	15432	16591	18708	20786	24010	26332	31317
Std. Dev.	58			67	59	59	52	45	42	46	66	76	76	106	96	84	79	70	96
*Cor. Coef.	.946			.877	.833	.800	.857	.737	.402	.163	.002	-.212	-.393	-.216	-.190	-.111	-.051	-.066	.00
No. Cases	91			92	91	91	87	84	80	79	76	70	61	59	31	35	20	15	7
Rel. Hum.(%)	86	87	87	85	77	76	65	54	44	40									
Std. Dev.	8.8	8.0	8.3	10.1	16.7	18.2	28.2	27.1	18.0	17.0									
*Cor. Coef.	-.487	-.477	-.440	-.482	-.431	-.303	-.120	-.100	-.347	-.216									
No. Cases	92	92	92	90	88	87	84	80	76	76									
Theta E (°A)	349.8	346.7	343.7	341.7	338.5	338.6	339.9	342.3	346.5	349.0	351.7	356.9							
Std. Dev.	5.5	4.8	4.9	4.8	5.9	5.6	6.3	5.4	4.2	4.2	3.9	4.2							
*Cor. Coef.	-.118	-.252	-.436	-.571	-.685	-.617	-.506	-.555	-.669	-.683	-.643	-.461							
No. Cases	92	92	92	91	88	87	84	80	77	76	75	70							
Theta (°A)	298.2	299.9	301.7	304.1	312.7	318.9	327.5	335.9	344.1	347.9	351.6	356.9							
Std. Dev.	1.9	1.4	1.2	1.1	1.5	1.8	2.5	2.8	3.4	3.6	3.8	4.2							
*Cor. Coef.	.236	.113	-.129	-.250	-.446	-.514	-.605	-.722	-.665	-.682	-.648	-.460							
No. Cases	92	92	92	92	91	91	88	84	80	79	76	70							

Trop. Press. (mb)	118.6
Std. Dev.	12.3
Cor. Coef.	.292
No. Cases	61

*Cor. Coef. = Correlation coefficients of parameters with surface pressure.

tively. Fig. 1 shows a temperature lapse rate slightly greater than moist adiabatic from the surface to 600 mb. It then becomes slightly less than moist adiabatic through the 300-mb level, with stability increasing with height. The dewpoint curve shows a generally steady decrease with height. Fig. 1 also contains Jordan's (1958) mean September tropical sounding. From the surface through the 800-mb level, temperatures were warmer for Jordan's sounding than for the mean hurricane sounding. Above this level to near the tropopause, however, the mean hurricane sounding is up to 3C warmer than the mean tropical sounding. Between the 100-mb level and 80-mb level the soundings have about equal temperatures, while the mean hurricane sounding is colder at higher levels. The mean tropical sounding, of course, was considerably less moist than the hurricane sounding, especially in the middle and upper levels. Both soundings are convectively stable from approximately the 600-mb level to the 300-mb level and then become very stable in the upper troposphere. In both cases there is a net available instability energy, with the mean tropical sounding showing a much larger degree of convective instability than the hurricane sounding. The instability aspect will be discussed in greater detail later.

Some interesting observations can be made from the data listed in Table 1. For instance, the correlation coefficients of the various parameters with SLP for the respective observations are quite revealing. In the case of temperature, a positive correlation exists in the lowest levels, i.e., as SLP decreased so did the temperatures. Since most of the observations were taken from landbased stations, this is probably a result of the increased cloud cover and precipitation associated with hurricanes. The correlation becomes negative and increases in magnitude with increasing heights, being relatively large between the 500-mb and 200-mb levels, as a result of the release of latent heat from the increased convective activity associated with hurricanes. Another interesting correlation relates to the tropopause, which in general becomes higher and colder with decreasing SLP. The relative humidity is negatively correlated with SLP, the coefficient generally decreasing with height to the 400-mb level. The heights of the various pressure surfaces have a "built-in" positive correlation in the low levels that decreases with increasing heights. The correlation coefficient sign reverses near the 200-mb level and, as previously mentioned, is negatively correlated at the tropopause. The location of the level of zero correlation agrees well with that found in hurricane Isbell (Gentry, 1967).

The correlations of equivalent potential temperature θ_e and potential temperature θ with SLP show high negative coefficients centered in the middle and upper troposphere. Also of interest is the location of the minimum equivalent potential temperature value which occurrs near the 650-mb level. This level was basically determined by the temperature lapse rate since the relative humidity varies by only 10% from the surface to the 600-mb level.

4. Mean soundings stratified by sea level pressure

The radiosonde data were stratified by the SLP of the observations. A 5-mb interval was chosen, so that all the individual soundings with SLP of 995–999 mb were in one group, 1000–1004 mb in another group, etc. These data are listed and illustrated in Tables 2–6 and Figs. 2–6. Included in the figures is Jordan's mean September tropical sounding, which was chosen for comparison with the mean hurricane soundings as representing the general conditions present in the tropical atmosphere during the hurricane season.

Some general observations can be made concerning these data, certain conditions having already been indicated by the correlation coefficients previously computed for the mean hurricane sounding. For instance, as SLP decreased, the temperature, moisture, equivalent potential temperature and potential temperature increased, especially in the middle and upper troposphere. In general, as SLP decreased, the temperature approached a moist adiabatic lapse rate through the 300-mb level. Above the 300-mb level, the temperatures were much warmer than one would expect from moist adiabatic ascent. The tropopause was higher and colder when the SLP was lower. The cold and high tropopause condition was also reflected in the lower portion of the stratosphere where colder temperatures were recorded. In comparing the temperatures of the mean hurricane soundings with those obtained in a time-space composite of radiosonde data obtained in the vicinity of hurricane Dora of 1964 (Sheets, 1965), it was found that the temperatures in the middle-to-upper troposphere were generally lower for the mean soundings. This was basically a result of the structure of hurricane Dora, which was a massive storm covering a very large area. Dora would be classified as a "Helene-type" storm (Colón, 1964). A comparison with values obtained in small concentrated storms such as hurricane Inez on 28 September 1966 would show the mean hurricane values to be generally warmer in these levels except within the very intense warm core in the eye and eyewall regions. Hurricane Inez is classified as the "Daisy-type" (Colón *et al.*, 1961). These examples indicate some of the problems in using a single mean hurricane sounding.

5. Diurnal variations

The data were stratified by time with two time periods chosen that were centered near the time of the maximum and minimum of the diurnal temperature variation as normally observed in the tropics. The mean soundings for these time periods (0000–0700 and 1200–1700 LST) are illustrated in Fig. 7. For the 0000–0700 LST sounding, 33, 29 and 24 observations were available for the 1000-, 200- and 100-mb levels, respectively. For

Table 2. - Mean Sounding with Surface Pressure of 1010-1014 mb

	Pressure Levels (mb)																		
	1000	950	900	850	700	600	500	400	300	250	200	150	Trop	100	70	50	30	20	10
Temp (°C)	25.2	22.9	19.9	17.1	8.8	2.1	-5.6	16.5	-31.0	-41.4	-53.8	-68.1	-77.0	-74.2	-65.6	-59.6	-55.9	-50.8	-45.7
Std. Dev.	2.5	1.6	1.4	1.1	1.0	0.6	0.9	1.0	1.1	0.9	0.9	1.5	2.8	2.4	2.7	2.8	3.3	1.4	0.7
No. Cases	10	10	10	10	10	10	10	10	9	9	9	9	7	6	3	2	2	2	2
Heights (m)	100.7			1514	3150	4413	5867	7581	9689	10955	12429	14215	15190	16584	18677	20745	23985	26580	31210
Std. Dev.	10.4			10	13	15	13	14	9	12	17	22	569	15	21	1.5	45	60	10
No. Cases	10			10	10	10	10	10	9	9	9	9	7	6	3	2	2	2	2
Rel. Hum.(%)	81.2	80.4	80.3	81.8	72.8	76.1	65.1	53.0	35.7	35.1									
Std. Dev.	7.0	6.0	8.3	7.5	21.9	22.7	24.0	25.7	16.2	14.2									
No. Cases	10	10	10	10	10	10	10	10	9	9									
Theta E(°A)	346.9	344.2	341.0	339.0	335.7	337.0	338.3	338.7	343.7	345.7	348.4	353.9	361.0	386.0					
Std. Dev.	7.9	4.7	4.2	3.0	5.2	4.8	5.0	4.1	2.7	1.8	1.6	2.8							
No. Cases	10	10	10	10	10	10	10	10	9	9	9	9	7	6					
Theta (°A)	298.1	300.2	301.7	303.6	312.4	318.2	326.3	333.8	342.1	345.2	348.3	353.9	361.0	386.0					
Std. Dev.	2.5	1.5	1.6	1.4	0.9	0.8	1.1	1.2	1.6	1.5	1.4	2.8							
No. Cases	10	10	10	10	10	10	10	10	9	9	9	9	7	6					

Trop. Press. (mb)	119.0
Std. Dev.	8.0
No. Cases	7

Table 3. - Mean Sounding with Surface Pressure of 1005-1009 mb

	Pressure Levels (mb)																		
	1000	950	900	850	700	600	500	400	300	250	200	150	Trop	100	70	50	30	20	10
Temp (C)	25.6	22.6	19.6	17.0	8.5	2.0	-5.2	-15.8	-30.8	-40.8	-52.9	-67.3	-75.4	-72.3	-66.0	-58.0	-52.3	-46.5	-37.9
Std. Dev.	1.9	1.4	1.3	1.3	1.4	1.4	1.6	1.7	2.2	1.8	1.6	2.0	3.5	3.2	2.7	2.4	1.2	1.8	1.2
No. Cases	30	30	30	30	29	29	27	26	25	25	24	24	21	20	13	13	9	5	4
Heights (m)	74.4			1505	3123	4387	5841	7557	9664	10931	12409	14203	15355	16561	18741	20794	23988	26953	31445
Std. Dev.	23.1			50	24	26	35	34	45	54	63	.67	684	114	99	105	67	282	25
No. Cases	30			30	29	29	26	26	25	25	24	24	21	20	9	13	8	3	2
Rel. Hum.(%)	83.3	84.6	86.0	85.3	78.4	75.3	55.7	49.8	40.2	35.6									
Std. Dev.	10.3	8.9	8.5	9.7	12.4	12.7	30.3	25.2	18.0	15.5									
No. Cases	30	30	30	28	27	27	25	23	23	23									
Theta E (°A)	349.8	346.1	343.1	341.3	337.8	337.8	337.9	341.2	345.2	347.3	350.2	355.3	364.0	389.5					
Std. Dev.	4.6	4.4	4.4	3.8	3.6	4.2	6.4	4.9	3.4	3.4	2.8	3.4							
No. Cases	30	30	30	30	27	27	25	23	23	23	24	24	21	20					
Theta (°A)	298.5	299.9	301.6	303.8	312.1	318.2	326.9	334.8	342.6	346.0	349.9	355.3	364.0	389.5					
Std..Dev.	1.9	1.5	1.4	1.3	1.6	1.6	2.1	2.3	3.1	2.6	2.6	3.4							
No. Cases	30	30	30	30	29	29	27	26	25	25	24	24	21	20					

Trop. Press. (mb)	119.3
Std. Dev.	11.0
No. Cases	21

Table 4. - Mean Sounding with Surface Pressure of 1000-1004 mb

	Pressure Levels (mb)																		
	1000	950	900	850	700	600	500	400	300	250	200	150	Trop	100	70	50	30	20	10
Temp (°C)	25.0	22.5	20.0	17.6	9.4	3.0	-4.1	-13.9	-28.5	-38.5	-50.7	-65.8	-76.9	-74.0	-65.3	-60.1	-52.5	-49.3	
Std. Dev.	1.4	1.2	0.8	0.8	1.2	1.1	1.3	1.2	1.7	2.2	2.6	2.8	5.2	5.4	3.8	2.4	1.7	1.9	
No. Cases	24	24	24	24	24	24	23	21	20	19	17	14	12	12	7	6	3	2	
Heights (m)	21.1			1436	3080	4350	5802	7531	9656	10933	12409	14211	15377	16599	18663	20770	23967	26680	31370
Std. Dev.	15.1			15	27	29	19	23	31	41	88	118	746	155	136	99	113	10	
No. Cases	24			24	24	24	23	21	20	19	17	14	12	12	7	6	3	2	1
Rel. Hum.(%)	90.0	90.0	88.6	85.7	81.8	77.6	70.0	58.5	45.0	42.0									
Std. Dev.	6.0	4.8	6.2	9.5	11.2	20.5	26.0	28.6	17.6	16.2									
No. Cases	24	24	24	24	24	24	23	21	19	19									
Theta E (°A)	350.2	347.8	345.1	342.4	339.9	339.0	341.9	344.2	348.4	350.8	353.7	358.1	362.2	386.5					
Std. Dev.	4.1	3.9	4.2	4.6	4.1	4.6	4.5	4.0	3.6	4.0	4.1	4.4							
No. Cases	24	24	24	24	24	24	23	21	20	19	17	14	12	12					
Theta (°A)	297.8	299.9	302.0	304.4	313.0	319.5	328.2	337.1	345.6	349.4	353.5	358.1	362.2	386.5					
Std. Dev.	1.5	1.3	0.9	1.0	1.4	1.4	1.6	1.7	2.6	3.5	4.1	4.5							
No. Cases	24	24	24	24	24	24	23	21	20	19	17	14	12	12					

Trop. Press. (mb)	118.8
Std. Dev.	11.3
No. Cases	12

Table 5. - Mean Sounding with Surface Pressure of 995-999 mb

	Pressure Levels (mb)																		
	1000	950	900	850	700	600	500	400	300	250	200	150	Trop	100	70	50	30	20	10
Temp (°C)	24.3	21.9	19.7	17.5	10.2	3.3	-3.3	-13.8	-28.6	-38.2	-50.3	-65.1	-77.3	-75.4	-67.3	-59.5	-52.9	-47.0	-44.5
Std. Dev.	1.4	1.2	0.9	0.8	1.1	1.8	2.1	1.9	1.9	1.5	1.4	2.2	3.5	3.6	1.3	1.7	1.8	2.1	1.5
No. Cases	12	12	12	12	12	12	12	12	12	12	12	11	11	11	7	6	4	2	2
Heights (m)	-13.3			1398	3065	4337	5773	7509	9634	10916	12397	14230	15795	16615	18711	20767	24020	26670	31270
Std. Dev.	16.0			12	64	66	26	38	48	55	78	67	708	68	56	39	41	50	20
No. Cases	11			12	12	12	12	12	12	12	12	11	11	10	7	6	3	2	2
Rel. Hum.(%)	91.5	91.7	90.9	90.3	84.9	79.3	60.5	52.3	53.0	43.9									
Std. Dev.	4.8	3.8	5.0	6.2	8.7	13.3	31.3	30.3	14.6	12.4									
No. Cases	12	12	12	12	12	12	12	12	12	12									
Theta E(°A)	349.2	346.8	345.3	345.1	344.3	341.8	341.8	344.3	348.5	351.3	354.1	359.3	366.0	383.5					
Std. Dev.	5.6	5.1	4.3	3.7	3.0	5.9	7.1	6.4	3.5	2.7	2.3	3.9							
No. Cases	12	12	12	12	12	12	12	12	12	12	12	11	11	11					
Theta (°A)	297.3	299.2	301.8	304.5	314.0	320.0	329.1	337.5	345.6	350.0	354.0	359.3	366.0	383.5					
Std. Dev.	14.	1.3	0.8	0.8	1.2	2.2	2.7	22.6	2.7	2.5	2.1	3.9							
No. Cases	12	12	12	12	12	12	12	12	12	12	12	11	11	11					

Trop. Press. (mb)	115.1
Std. Dev.	13.1
No. Cases	11

Table 6. - Mean Sounding with Surface Pressure Less than 995 mb

	Pressure Levels (mb)																		
	1000	950	900	850	700	600	500	400	300	250	200	150	Trop	100	70	50	30	20	10
Temp (°C)	25.1	22.8	20.1	17.5	9.9	3.5	-3.0	-12.2	-26.8	-36.2	-49.3	-63.6	-78.1	-76.6	-68.1	-58.5	-52.2	-48.9	
Std. Dev.	1.8	1.3	0.9	0.6	1.0	1.1	1.4	1.7	1.0	1.4	1.2	1.0	3.6	3.8	3.5	2.6	1.7	2.1	
No. Cases	9	9	9	9	9	9	9	8	8	8	8	6	4	5	4	4	4	2	
Heights (m)	-53.4			1364	3006	4273	5741	7488	9628	10920	12425	14258	16203	16653	18750	20830	24093	26695	
Std. Dev.	28.2			42	41	44	40	33	31	33	33	41	817	47	27	25	29	35	
No. Cases	9			9	9	9	9	8	8	8	8	6	4	5	4	4	4	2	
Rel. Hum. (%)	90.8	89.9	92.0	93.2	81.3	87.1	82.3	60.1	53.7	47.6									
Std. Dev.	7.2	8.9	5.9	5.1	14.5	10.9	13.0	14.7	12.0	14.2									
No. Cases	9	9	9	9	8	7	7	7	7	7									
Theta E (°A)	351.8	349.2	346.8	345.7	342.5	345.1	346.6	347.9	351.1	354.4	356.0	361.3	368.5	381.5					
Std. Dev.	6.8	5.7	4.6	2.7	5.7	3.6	3.5	2.4	1.3	1.8	2.1	1.8							
No. Cases	9	9	9	9	8	7	7	7	7	7	7	6	4	5					
Theta (°A)	298.1	300.1	301.9	304.3	313.7	320.1	329.5	339.5	348.1	352.6	355.6	361.3	368.5	381.5					
Std. Dev.	1.7	1.3	0.7	0.7	1.3	1.3	1.9	2.0	1.4	1.7	2.0	1.8							
No. Cases	9	9	9	9	9	9	9	8	8	8	8	6	4	5					

Trop. Press. (mb)	109.5
Std. Dev.	16.0
No. Cases	4

the 1200–1700 LST sounding, 15, 14 and 11 observations were available for these same levels, respectively. The afternoon sounding is shown to be warmer than the night sounding throughout nearly the entire troposphere. The maximum difference in the free atmosphere of approximately 2C was centered near the 300-mb level. Since the mean SLP of the two soundings differed by only 0.3 mb, one can practically eliminate any effects caused by the high negative correlation of temperatures with SLP (if the distribution about the mean is assumed to be nearly the same in both cases). While the mean heights of the 100-mb surface differed by 45 m, the temperature and heights of the 70-mb surface were nearly the same. However, the number of observations available above the 100-mb surface decreased rapidly with increasing heights, and a complete comparison between the two soundings may not be valid.

To determine whether these temperature differences were real or not, certain questions had to be answered. The first question was whether the instrumentation may have been biased toward daytime or nighttime temperature readings. Before 1960, some rather large errors existed in daytime temperature readings because of radiation. Harris *et al.* (1962) found that these errors were of the order of 1C at the 200-mb level and increased upward. Since around 1960, the temperature element on the radiosonde instrument has been shielded, and the radiation factor is believed to be minimal. In this study, the radiation factor is believed to be only a minor problem below the tropopause for two reasons. First, less than 20% of the observations used were obtained before 1960. Second, the characteristic increase in cloud cover associated with the hurricane would tend to minimize radiation effects, especially below the 200-mb level.

The second question concerned the statistical significance of the observed temperature differences. The temperature differences were found to be statistically significant at the 0.05 level from 200–300 mb, and at the 0.10 level at 350 mb. The degree of confidence then decreased below and above these levels, except near the surface, where the temperature differences were significant at the 0.01 level. The large temperature differences at the surface were a result of the observations having been made at land-based stations. Similar observations over water show small diurnal variations.

The third question pertains to the actual distribution of the data about the mean SLP for the daytime and nighttime soundings. To check this distribution and its effects, the data were further stratified by SLP as well as time. It was found in each SLP category that the mean values of the daytime temperatures in the troposphere were warmer than the respective nighttime temperatures. However, since the multiple stratification resulted in much smaller samples, the temperature differences in some cases were not statistically significant, except at very low degrees of confidence. This

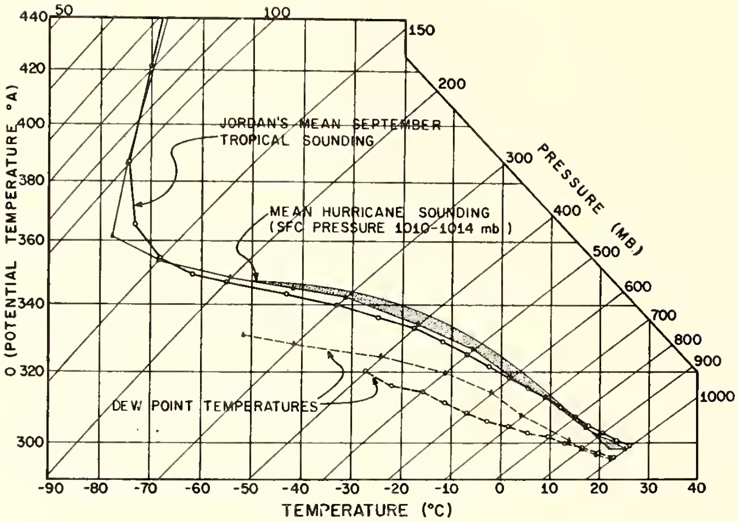

Fig. 2. A mean sounding computed from radiosonde flights with SLP's of 1010–1014 mb, obtained within 100 n mi of hurricane centers. (Shaded area represents available instability energy.)

stratification did show, however, that the distribution of the observations with respect to SLP was nearly the same for both the night and daytime data.

6. Mean soundings stratified by quadrants

The data were stratified by quadrants of the storms, and some differences in the computed mean soundings were noted. Because the mean SLP for the observations varied from quadrant to quadrant, the data were then further stratified by SLP and quadrant. The result was that only small differences were noted within each pressure category between the various quadrants, and these differences were not consistent from one pressure category to the next. From this information it seems that any variations that may have existed between quadrants were either too small to be detected by the radiosonde instrumentation, or the sample size for each category after the multiple stratification was too small.

7. Stability aspects of the mean sounding

The stability of the environment becomes of major interest when the question of weather modification

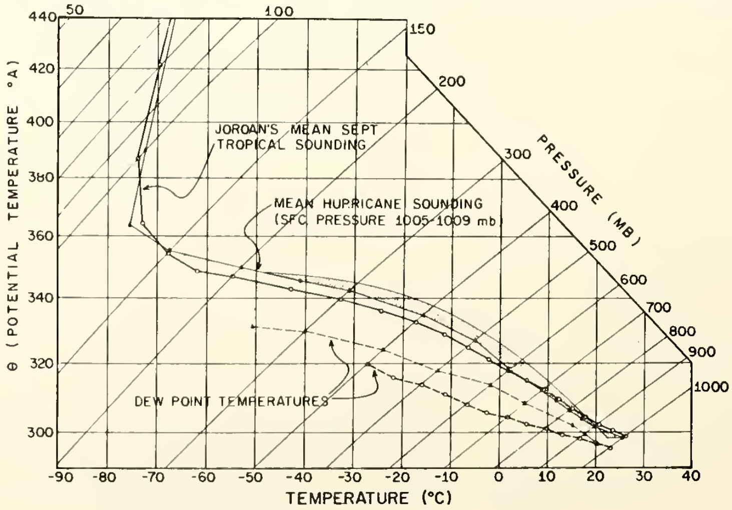

Fig. 3. Same as Fig. 2 except for SLP's of 1005–1009 mb.

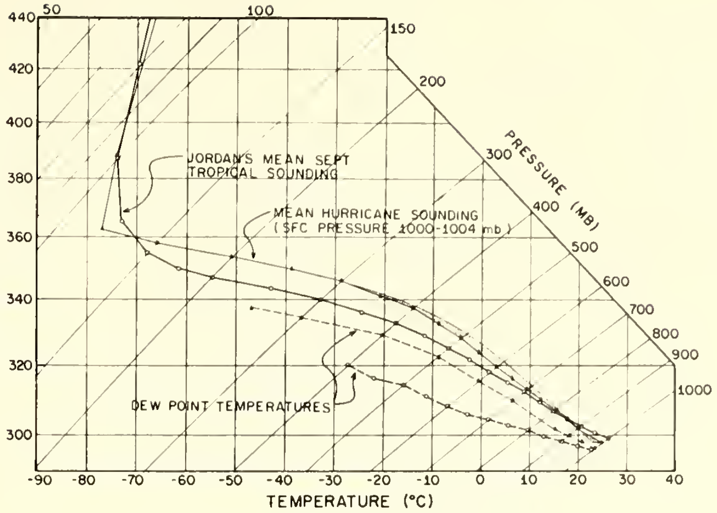

FIG. 4. Same as Fig. 2 except for SLP's of 1000–1004 mb.

arises. Some aspects of the stability have already been mentioned such as the stable conditions existing in the upper troposphere of the various soundings. These features are further illustrated in Fig. 8, which shows the vertical distributions of equivalent potential temperature and potential temperature for some of the mean soundings. Also included is a sounding made within eye of a hurricane as it passed over Tampa, Fla., in 1944. As readily observed, most of the soundings become increasingly stable above the 500-mb level, but all the soundings presented show that they were conditionally unstable in the lowest levels. Both figures show that at nearly all levels the values of both θ_e and θ steadily increase with decreasing SLP. The minimum values of θ_e for all the soundings except the eye sounding were recorded between the levels of 600 and 700 mb. The largest values of θ_e and θ shown at nearly all but the lowest levels were recorded in the eye sounding. The largest differences in equivalent potential temperature between the eye sounding and the mean hurricane soundings were found near the 700-mb level and just below the tropopause. The high values of θ_e in the eye sounding were a result of the sounding being quite moist in the lowest levels and very dry in the middle to upper

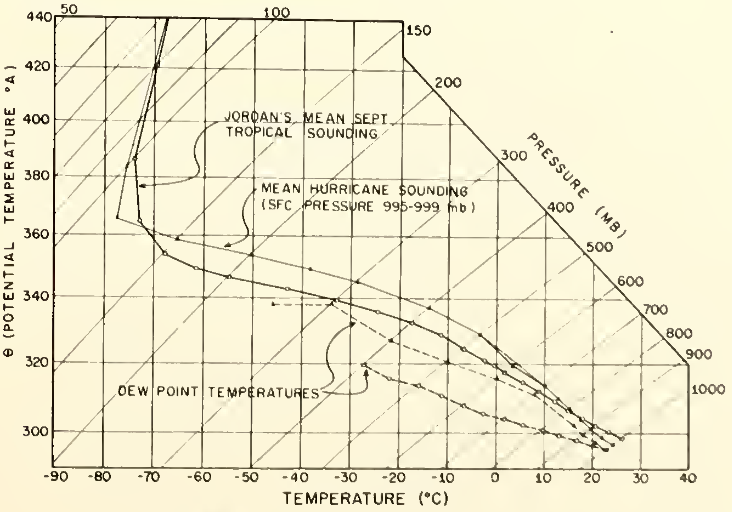

FIG. 5. Same as Fig. 2 except for SLP's of 995–999 mb.

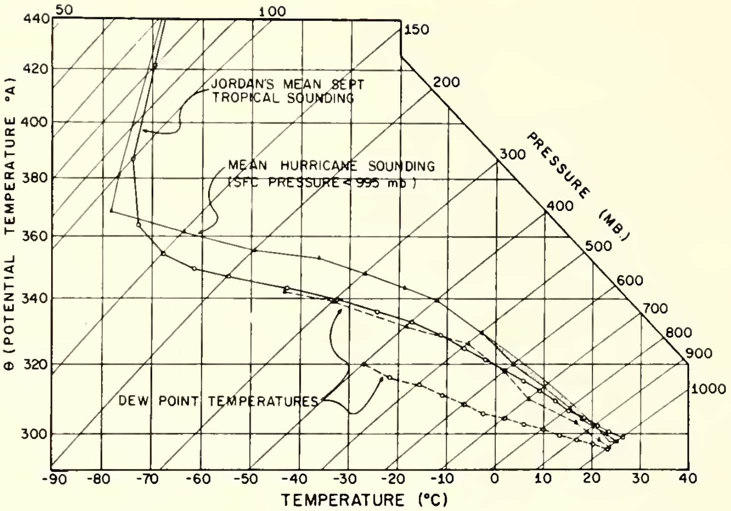

Fig. 6. Same as Fig. 2 except for SLP's of less than 995 mb.

troposphere, where temperatures were also quite high due largely to subsidence. The increased θ_e and θ values shown for decreased SLP's are a direct result of the larger amounts of latent heat released by the increased convective activity associated with the deeper (lower SLP) tropical cyclones.

Gray (1967) has defined a potential buoyancy for the lower half of the troposphere as the difference of the equivalent potential temperature from the surface to the 500-mb level. He obtained average values for the mean summertime tropical atmosphere and the mean tropical disturbance of 18–20C and 14–17C, respectively. The potential buoyancy values for a number of the presented soundings were computed and are listed in Table 7. The values Gray obtained are much larger than those obtained for the mean hurricane soundings presented in this paper. The values he computed decrease with the presence of a disturbance, which is in agreement with the general decreases shown for the mean hurricane soundings as SLP falls.

To get a more quantitative measure of the stability or instability of the atmospheric conditions depicted by

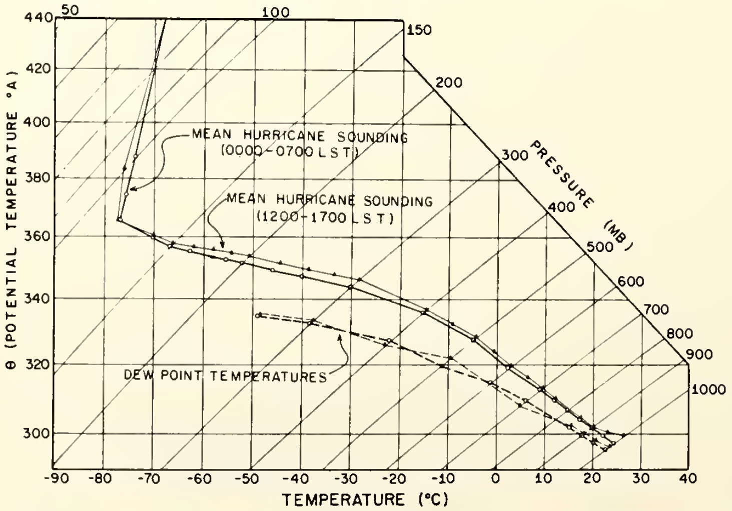

Fig. 7. Mean hurricane soundings computed from radiosonde flights with observation times of 0000–0700 and 1200–1700 LST obtained within 100 n mi of hurricane centers.

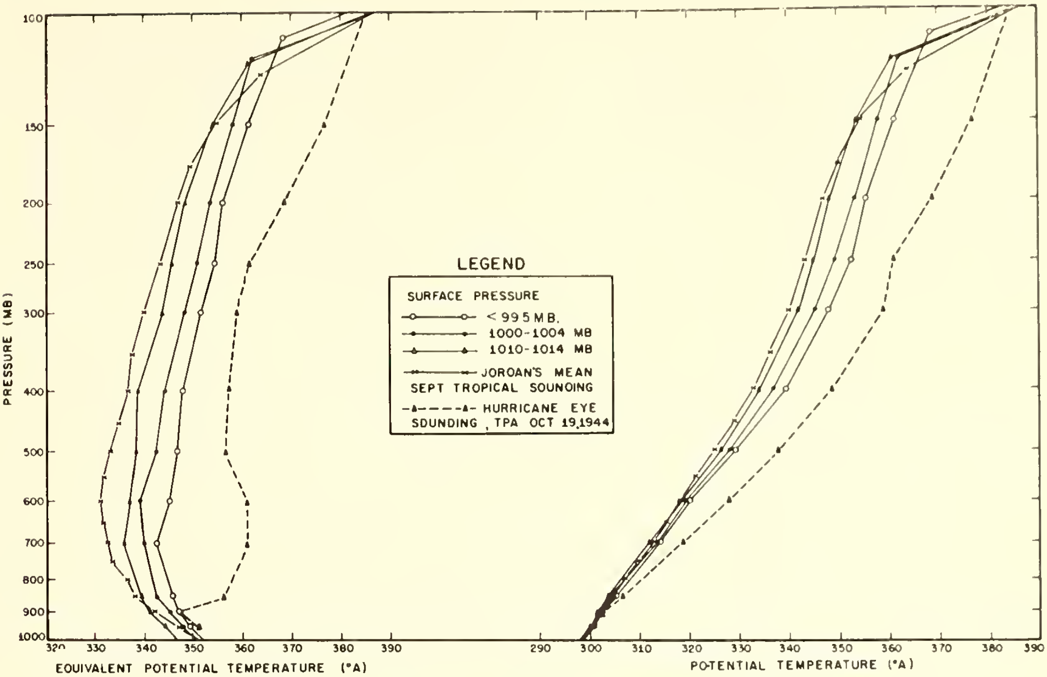

FIG. 8. The vertical distribution of equivalent potential temperature (left) and potential temperature (right) for selected soundings.

these soundings, the available instability energy I^* (Belinski, 1958; Haurwitz, 1941) was computed using the relation

$$I^* = I_{\theta_e} - I_{\text{env}} = \frac{Jc_v}{g} \int_{p_0}^{p_h} (T_{\theta_e} - T_{\text{env}}) dp,$$

where $J = 4.187 \times 10^7$ ergs cal^{-1}, $c_v = 0.172$ cal gm^{-1} (°K)$^{-1}$, $g = 980$ cm sec^{-2}, T_{θ_e} is the temperature of the parcel at the specified pressure and θ_e, and T_{env} the temperature of the environment at the specified pressure. The value specified for θ_e was the value of the moist adiabat passing through the lifting condensation level (LCL) of a parcel initially at the 1000-mb level. The net instability energy available through parcel ascent is represented by the shaded areas in Figs. 1–6. The limits of the integration were from the 1000-mb surface to the level of free convection (LFC), with this energy being defined as negative, and then from the LFC to the pressure level where the specified moist adiabat recrossed the actual temperature sounding, this latent energy being defined as positive. Positive values, therefore, indicate a net available instability energy, while negative values indicate that the work required is greater than the energy available for release through parcel ascent. Table 7 shows that the instability energy and potential buoyancy generally decreased with decreasing SLP's. The depth of the conditionally unstable layer, however, seemed to vary considerably. Figs. 2–6 show that the positive instability energy areas were centered near the 600-mb level and generally decreased as the SLP dropped. This, of course, indicates that within the storm circulation the effects of convection make the total sounding more stable by increasing the stability of the lower levels. Palmén (1948) indicated values of instability energy available for mean September conditions, which generally increased from east to west across the Atlantic Ocean and Caribbean Sea to the Gulf of Mexico. Again, as was the case for the potential buoyancies, the values were larger than those obtained for the mean hurricane soundings.

TABLE 7. Net available instability energy ($\times 10^6$ ergs) and potential buoyancy.

Surface pressure	Instability energy	Potential buoyancy
<995 mb	1.93606	5.2
995–999 mb	0.29954	7.4
1000–1004 mb	3.48491	8.3
1005–1009 mb	8.79630	11.9
1010–1014 mb	6.01275	8.6
all cases	4.61002	9.9

Those who have physically observed hurricanes on a regular or semi-regular basis have often expressed the opinion that a diurnal effect exists in the intensity or at least the "activity" of a hurricane. In particular, flight crews who participate in reconnaissance and research missions into hurricanes have often stated that nighttime "penetrations" seem to be "rougher" than similar daytime flights. To get some measure of any differences that might exist in the stability of the daytime vs nighttime hurricane conditions, the static stability of the two soundings presented in Fig. 7 was computed. A measure of the static stability for dry and moist adiabatic processes is given by the expressions (Eliassen and Klunschmidt, 1957)

$$\sigma_0 = -\frac{\alpha}{\theta}\frac{\partial\theta}{\partial P} \quad \text{and} \quad \sigma_M = -\frac{\alpha}{\theta_e}\frac{\partial\theta e}{\partial P},$$

respectively, where σ is a measure of the static stability, α the specific volume, θ potential temperature, and θ_e equivalent potential temperature. Values of σ were computed in cgs units with dimensions of cm^4 sec^2 gm^{-2} and are listed in Table 8.

Table 8. Static stability for dry and moist adiabatic processes (10^{-3} cm^4 sec^2 gm^{-2}).

	Dry adiabatic processes		Moist adiabatic processes	
Level	0000–0700 LST	1200–1700 LST	0000–0700 LST	1200–1700 LST
950 mb	3.834	2.176	−3.322	−5.160
850 mb	4.806	4.997	−3.426	−4.006
750 mb	5.856	6.265	−0.842	−2.630
650 mb	6.927	7.040	−1.907	+0.956
550 mb	10.988	10.849	+0.733	+2.674
450 mb	12.362	12.660	+4.731	+3.011
350 mb	13.909	16.177	+6.790	+9.730
250 mb	16.518	17.414	+11.360	+12.222

The computed values show, except for the lowest levels, that the mean daytime sounding was generally more stable than the mean nighttime sounding for dry adiabatic processes. For moist adiabatic processes, the daytime sounding was more stable in the upper levels but less stable than the nighttime sounding in the lower levels. These observations were taken at land-based stations and it is believed that if the soundings were taken over water, the mean soundings would be almost identical in the lowest levels because of the very low diurnal variation of the water temperature. If this is true, then the available instability energy is much greater at night than in the afternoon.

8. Summary and conclusions

The high correlation of the various parameters with radiosonde observed SLP requires exact specification of what is meant by a "mean hurricane sounding." For this reason more than one sounding has been presented with stratification of the observations by SLP. Even these soundings do not include that portion of the storm containing the very warm core that has been shown to exist in the eye and eyewall regions (LaSeur and Hawkins, 1959; Sheets, 1967a, b).

These mean soundings show, as the surface pressure decreased, that the temperature, moisture, potential temperature and equivalent potential temperature increased at most levels within the middle and upper troposphere. The tropopause rose and became colder, and the available instability energy decreased as the vertical temperature distribution approached a moist adiabatic lapse rate. The soundings were generally conditionally unstable in the low levels but became very stable in the upper troposphere.

Not much has been said about the conditions in the stratosphere because of the decreased sample sizes, but some of these data are presented as a point of interest.

The values of the potential buoyancy and the instability energy obtained in this study, when compared with those obtained by Gray (1967) and Palmen (1948), give further evidence that the net effect of the increased convective activity associated with tropical cyclones is to decrease the convective instability of the atmosphere as it approaches the centers of hurricanes.

Diurnal variations of temperatures have been shown to occur within the hurricane, especially in the middle to upper troposphere. While the static stability computations have shown that there may be some basis for the belief that hurricanes are more active at night, this certainly has not been conclusively demonstrated and should be an area for future studies as more data become available. No consistent variations were noted between quadrants, but with the multiple stratification the sample sizes were too small to be conclusive. Again, this could be an area for possible future studies.

Acknowledgments. The author expresses his appreciation to Dr. R. Cecil Gentry, Mr. Harry F. Hawkins, Dr. S. L. Rosenthal and Dr. Banner I. Miller for their guidance and critical reviews of the manuscript. Thanks are also due R. L. Carrodus, R. Dirks, C. H. True and Mrs. Judy Greene for preparation of the illustrations and manuscript and to those members of the radiosonde teams whose dedication to duty enabled them under very difficult conditions to obtain the data which made this study possible.

REFERENCES

Belinski, V. A., 1958: *Dynamic Meteorology*. Moscow-Leningrad, OGIZ, 591 pp.

Colón, J. A., and NHRP Staff, 1961: On the structure of hurricane Daisy (1958). National Hurricane Res. Proj. Rept. No. 48, U. S. Weather Bureau, 102 pp.

——, 1964: On the structure of hurricane Helene (1958). National Hurricane Res. Proj. Rept. No. 72, U. S. Weather Bureau, 56 pp.

Eliassen, A., and E. Klunschmidt, 1957: Dynamic meteorology. *Handbuch der Physik*, Vol. 48, Berlin, 1–54.

Gentry, R. Cecil, 1967: Structure of the upper troposphere and lower stratosphere in the vicinity of hurricane Isbell, 1964. *Papers Meteor. Geophys., Tokyo*, **18**, 293–310.

Gray, W. M., 1967: Global view of the origin of tropical disturbances and storms. Dept. Atmos. Sci., Paper No. 114, Colorado State Univ., 105 pp.

Harris, M. F., F. G. Finger and S. Teweles, 1962: Diurnal variation of wind, pressure, and temperature in the troposphere and stratosphere over the Azores. *J. Atmos. Sci.*, **19**, 136–149.

Haurwitz, B., 1941: *Dynamic Meteorology.* New York and London, McGraw–Hill, 365 pp.

Jordan, C. L., 1958: Mean soundings for the West Indies area. *J. Meteor.*, **15**, 91–97.

——, and E. S. Jordan, 1954: On the mean thermal structure of tropical cyclones. *J. Meteor.*, **11**, 440–448.

LaSeur, N. E., and Harry F. Hawkins, 1963: An analysis of hurricane Cleo (1958) based on data from research reconnaissance aircraft. *Mon. Wea. Rev.*, **91**, 694–709.

Palmén, E., 1948: On the formation and structure of tropical hurricanes. *Geophysics (Helsinki)*, 3, 28–38.

Schacht, E. J., 1946: A mean hurricane sounding for the Caribbean area. *Bull. Amer. Meteor. Soc.*, **27**, 324–327.

Sheets, R. C., 1965: The three-dimensional large scale structure of hurricane Dora (1964). Atmos. Res. Lab., Univ. of Oklahoma, Norman, 51 pp.

——, 1967a: On the structure of hurricane Janice (1958). National Hurricane Res. Lab. Tech. Memo. No. 76, 38 pp.

——, 1967b: On the structure of hurricane Ella (1962). National Hurricane Res. Lab. Tech. Memo. No. 77, 33 pp.

48

U. S. DEPARTMENT OF COMMERCE
Environmental Science Services Administration
Weather Bureau

ESSA Technical Memorandum WBTM SR-42

MEMORABLE HURRICANES OF THE UNITED STATES SINCE 1873

SOUTHERN REGION HEADQUARTERS
SCIENTIFIC SERVICES DIVISION
FORT WORTH, TEXAS
January 1969

MEMORABLE HURRICANES OF THE UNITED STATES SINCE 1873

Arnold L. Sugg, NHC, Miami
Robert L. Carrodus, NHRL, Miami

Whether or not a hurricane is notable and should be remembered depends upon many things. The selections in this publication are limited to those which have made landfall in the United States or have been near misses. Also, most of them were major, extreme, or great hurricanes; these adjectives usually refer to intensity as determined by the maximum wind or the sea level pressure within the eye. Some hurricanes were great while at sea but reached land with considerably diminished intensity. Connie 1955 is a good example. On the other hand, some which did not have particularly low pressures or high winds were devastating because of flooding. Most notable in this category was Diane 1955. For these reasons the criteria used to determine the memorable hurricanes of this century were not rigid and have been omitted here.

The data on each map should be considered extremes. Needless to say, some are subject to contradiction depending upon what source or reference one reviews. For the most part, the data were drawn from the Monthly Weather Review articles, Hurricanes and Tropical Storms In The Gulf of Mexico, WBO, New Orleans, Atlantic Hurricanes by Dunn and Miller and Hurricanes by Tannehill. Tracks are from the Weather Bureau Technical Paper No. 55 by Cry, but the varying intensities along the tracks have been omitted.

It is hoped that this paper will serve as a ready reference, and will be useful as a climatological aid in forecasting, for speeches, and for preparedness conferences.

Table I lists the greatest United States hurricanes of all time based upon death and damage figures. Dollar estimates have not been adjusted for inflation. It is also quite obvious that damage figures have increased and will continue to do so as population and industry increase, especially along the coastal areas.

We are grateful to Miss Esther Monserrat of the National Youth Corps for clerical help.

SELECTED MEMORABLE HURRICANES OF THE UNITED STATES

DAMAGES (Millions of Dollars)

BETSY	1965	1419.8
DIANE	1955	800.0
CAROL	1954	450.0
CARLA	1961	400.0
NEW ENGLAND	1938	387.1
DONNA	1960	386.5
HAZEL	1954	251.6
DORA	1964	250.0
BEULAH	1967	200.0
AUDREY	1957	150.0
CLEO	1964	128.5
MIAMI	1926	111.8

DEATHS

GALVESTON	1900	6000
LOUISIANA	1893	2000
SOUTH CAROLINA	1893	1000-2000
OKEECHOBEE	1928	1838
KEYS AND TEXAS	1919	600-900
GA. AND S.C.	1881	700
NEW ENGLAND	1938	600
AUDREY	1957	550
KEYS	1935	405
ATLANTIC COAST	1944	390
MISS. AND LA.	1909	350
GALVESTON	1915	275
MISS. AND LA.	1915	275

TABLE I

AREAS WHERE MEMORABLE HURRICANES MADE LANDFALL

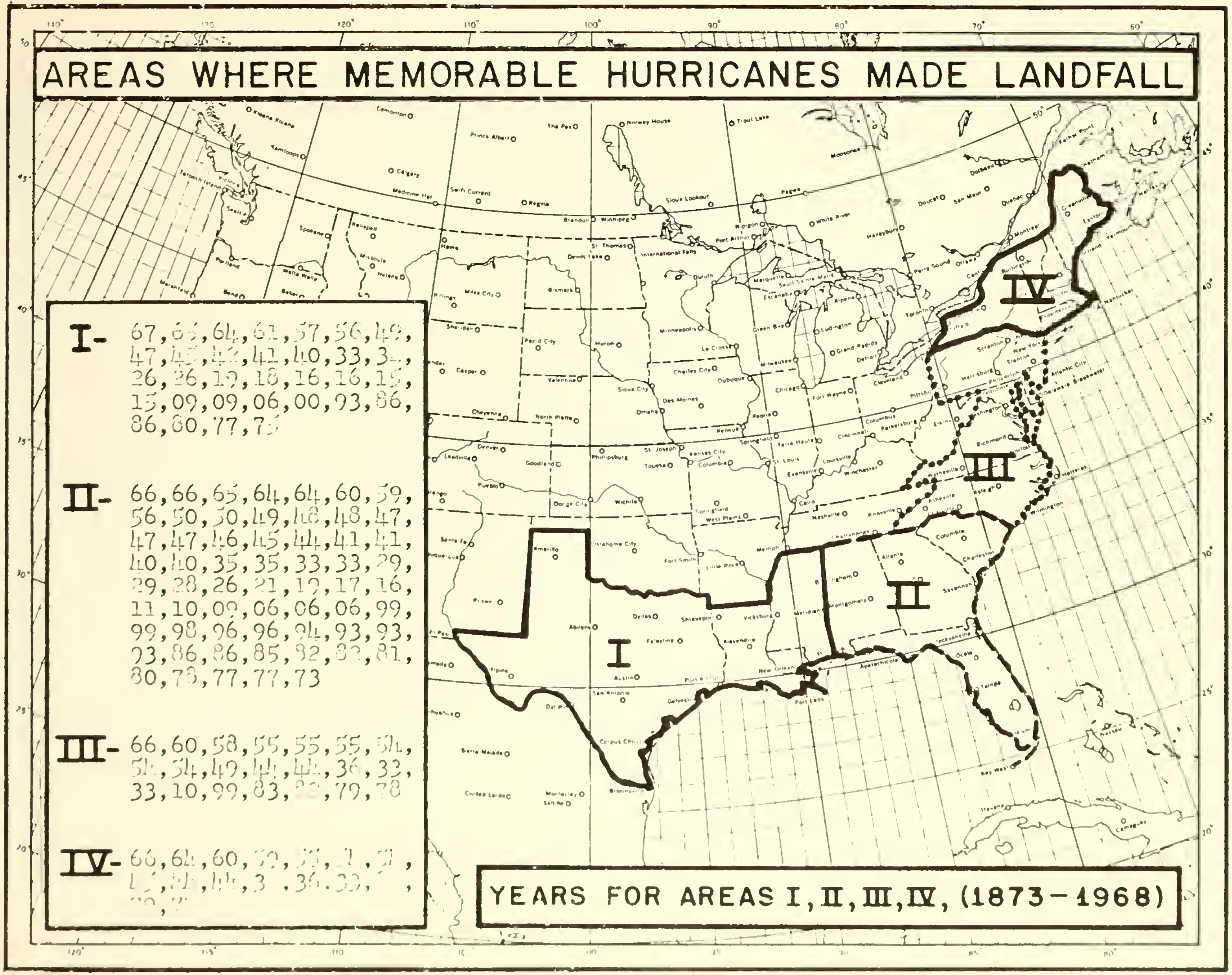

I- 67,65,64,61,57,56,49,
47,45,42,41,40,33,34,
26,26,19,18,16,16,15,
15,09,09,06,00,93,86,
86,80,77,75

II- 66,66,65,64,64,60,59,
56,50,50,49,48,48,47,
47,47,46,45,44,41,41,
40,40,35,35,33,33,29,
29,28,26,21,19,17,16,
11,10,09,06,06,06,99,
99,98,96,96,94,93,93,
93,86,86,85,82,82,81,
80,78,77,77,73

III- 66,60,58,55,55,55,54,
54,54,49,44,44,36,33,
33,10,99,83,[illegible],79,78

IV- 66,64,60,[illegible],[illegible],[illegible],[illegible],
[illegible],[illegible],44,3[illegible].36.33,[illegible],
[illegible],[illegible]

YEARS FOR AREAS I, II, III, IV, (1873-1968)

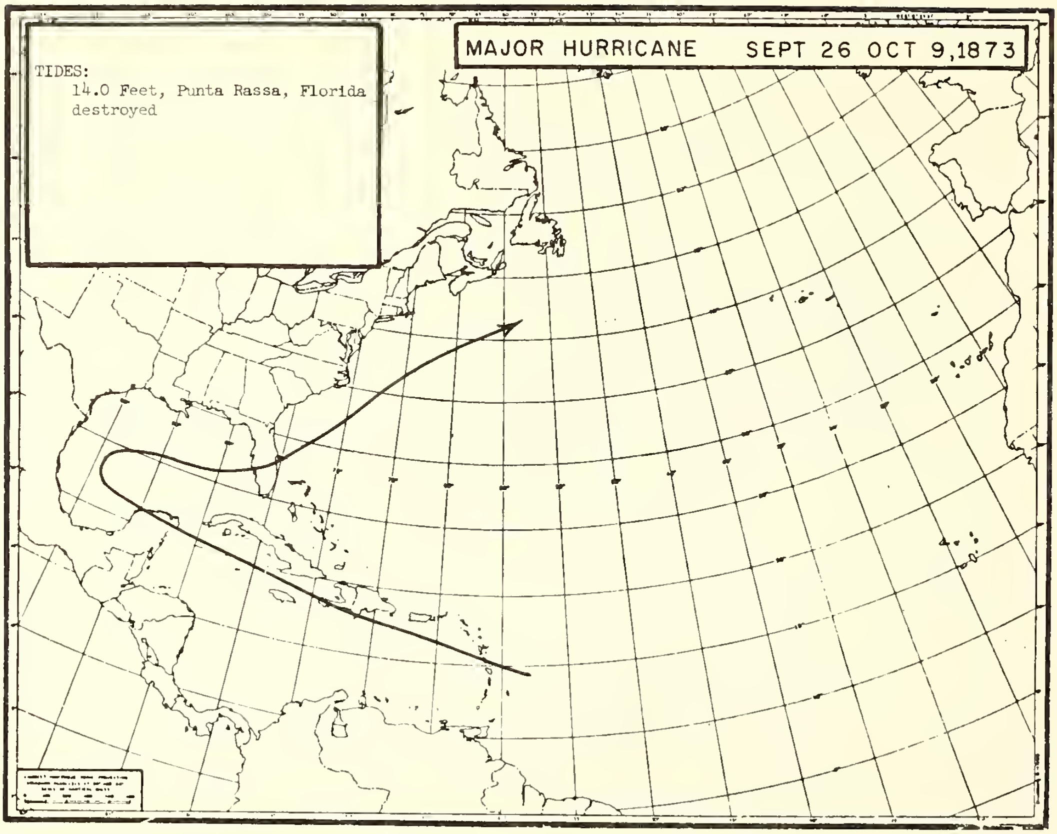

MAJOR HURRICANE SEPT 26 OCT 9,1873

TIDES:
14.0 Feet, Punta Rassa, Florida destroyed

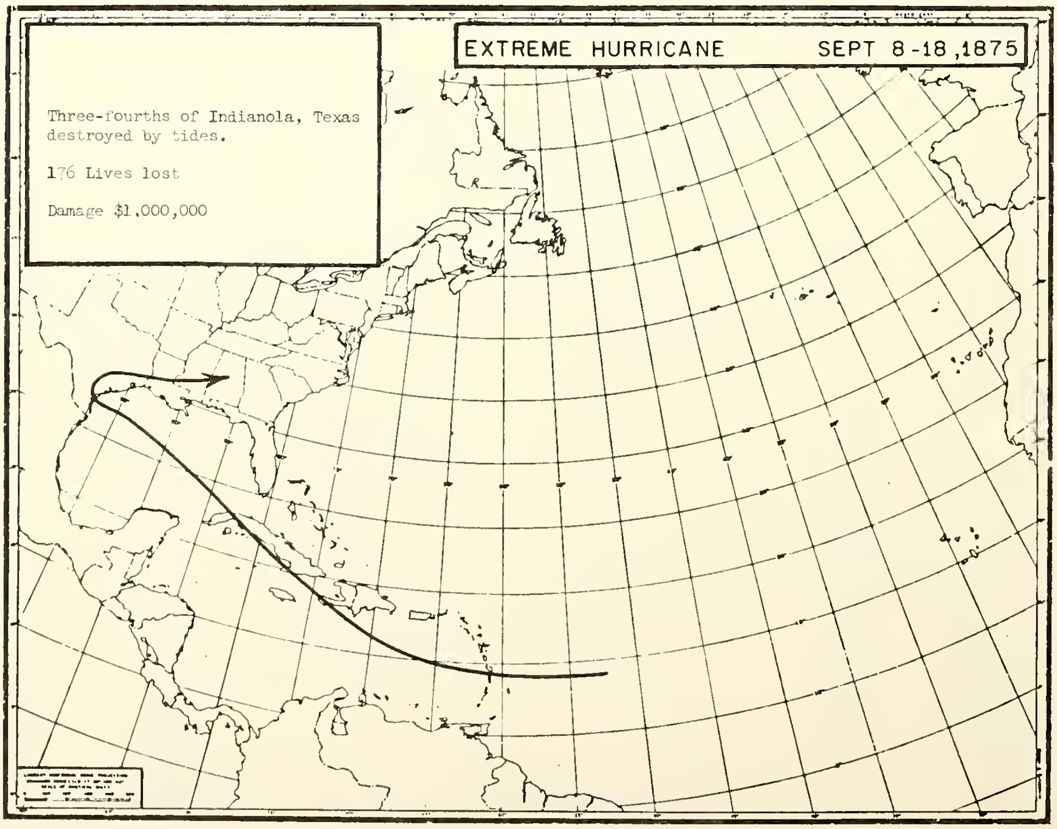

EXTREME HURRICANE SEPT 8-18,1875

Three-fourths of Indianola, Texas destroyed by tides.

176 Lives lost

Damage $1,000,000

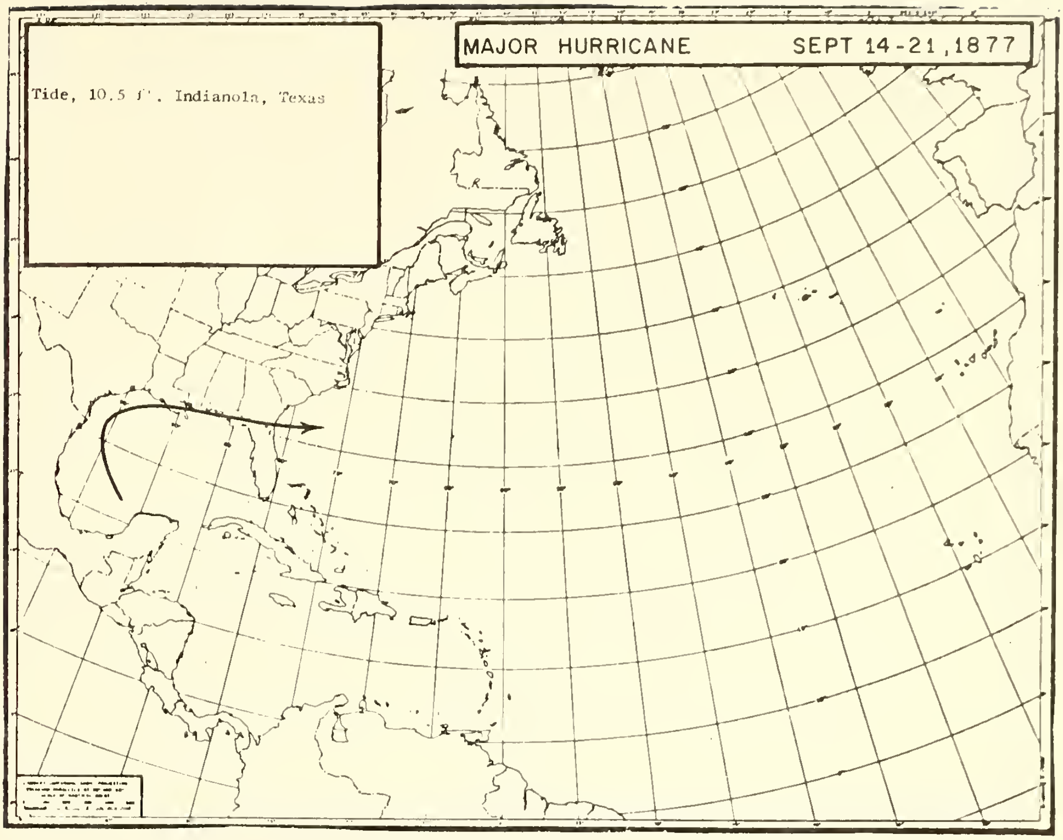
MAJOR HURRICANE SEPT 14-21, 1877

Tide, 10.5 ft. Indianola, Texas

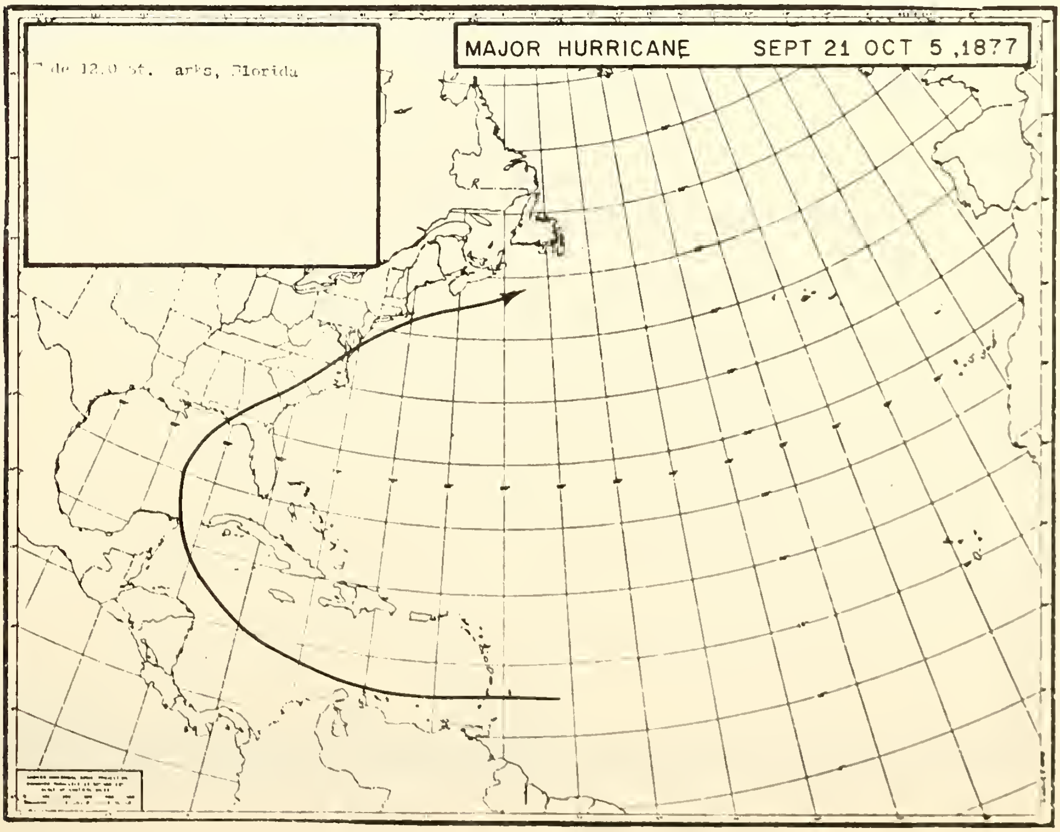
MAJOR HURRICANE SEPT 21 OCT 5, 1877

Tide 12.0 ft. St. Marks, Florida

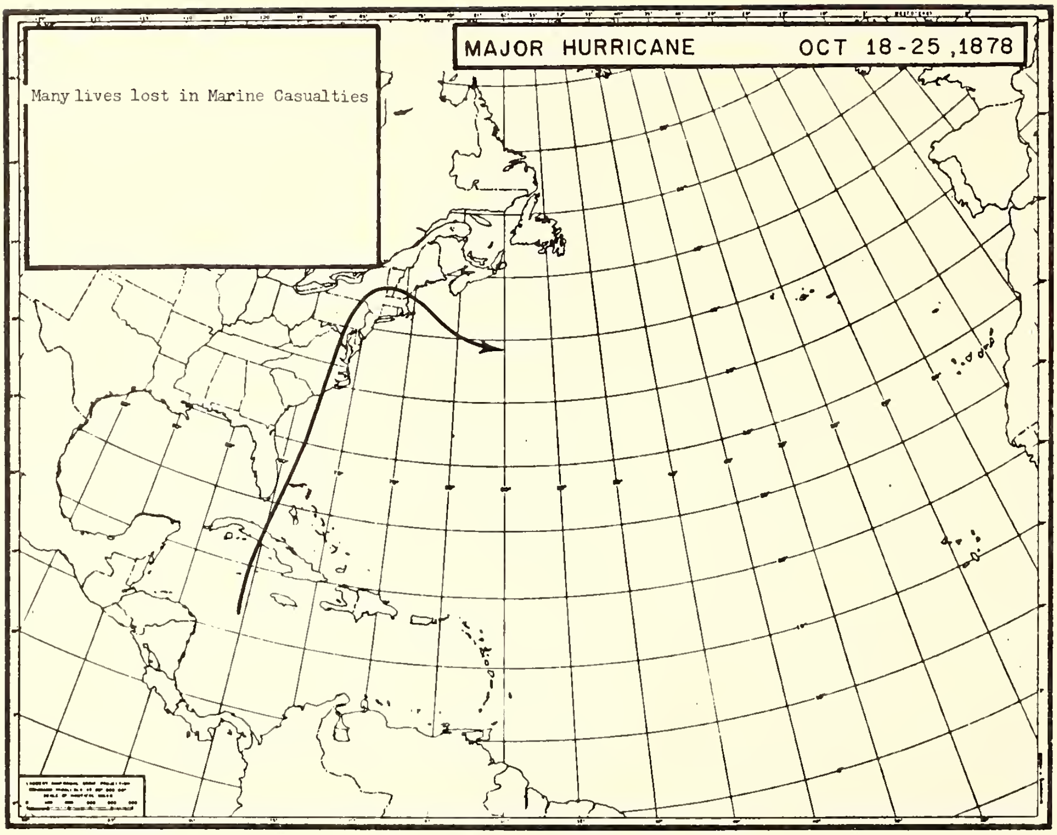

MAJOR HURRICANE OCT 18-25, 1878

Many lives lost in Marine Casualties

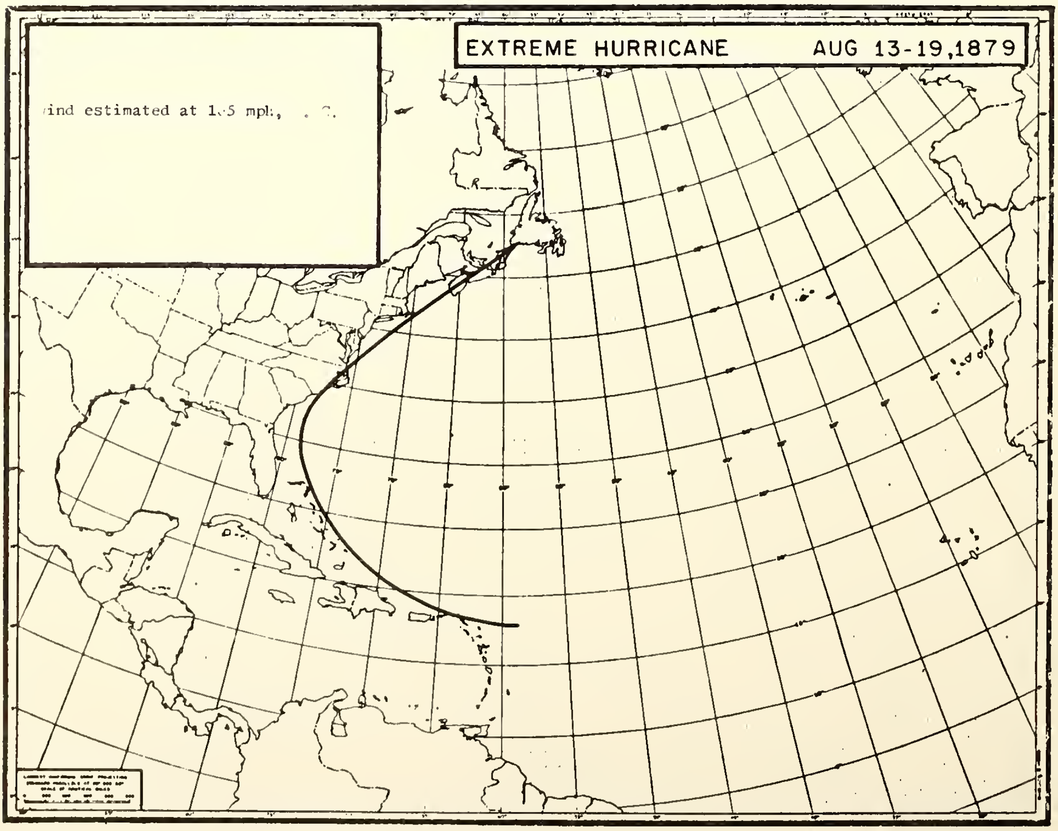

EXTREME HURRICANE AUG 13-19, 1879

Wind estimated at 1[illegible]5 mph, [illegible]

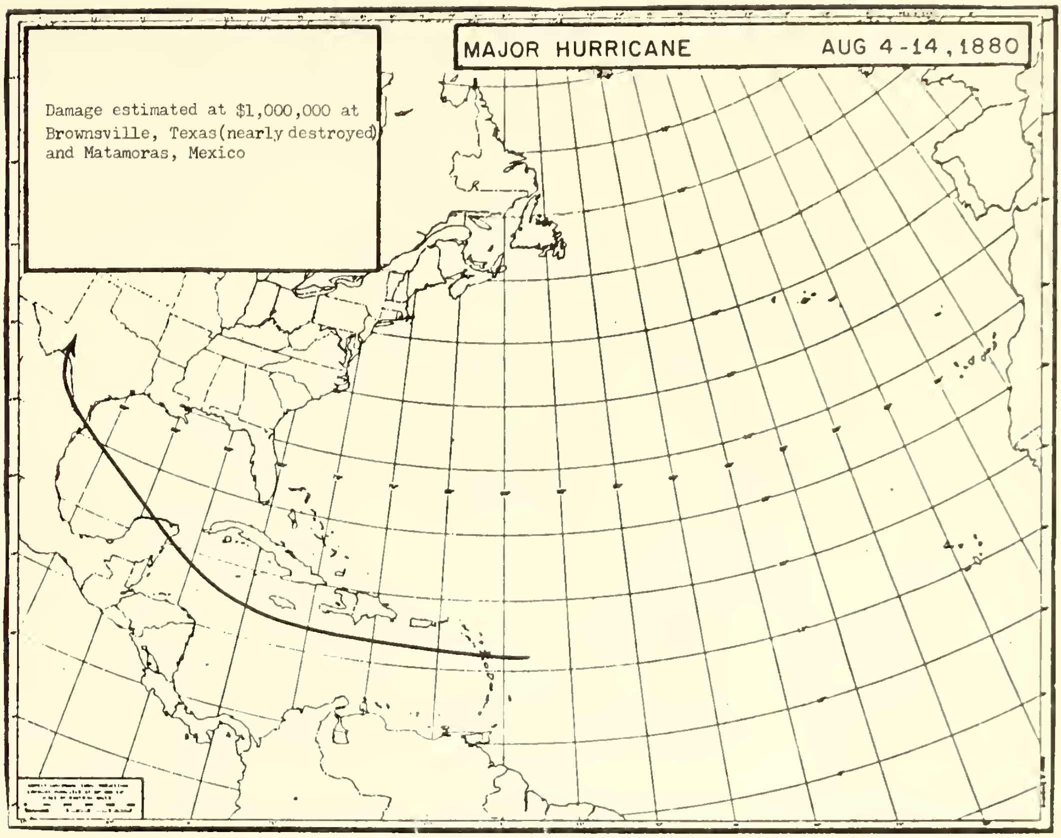

MAJOR HURRICANE AUG 4-14, 1880

Damage estimated at $1,000,000 at Brownsville, Texas (nearly destroyed) and Matamoras, Mexico

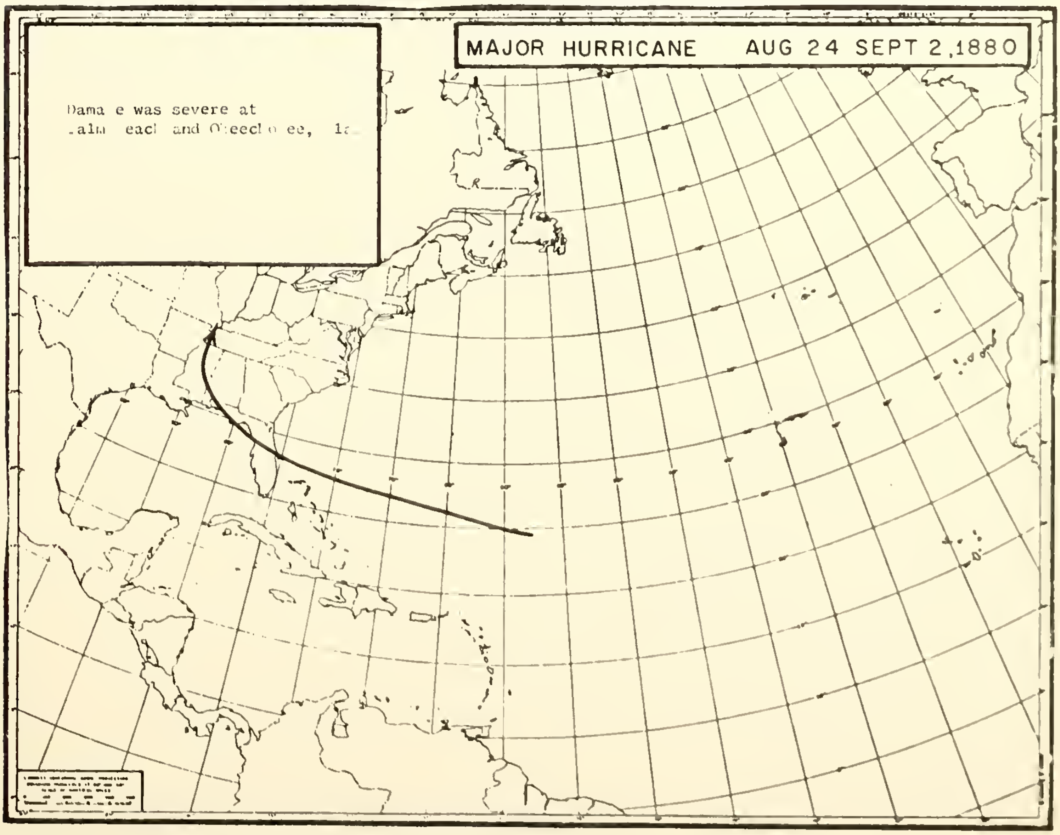

MAJOR HURRICANE AUG 24 SEPT 2, 1880

Damage was severe at Palm Beach and Okeechobee, Fla.

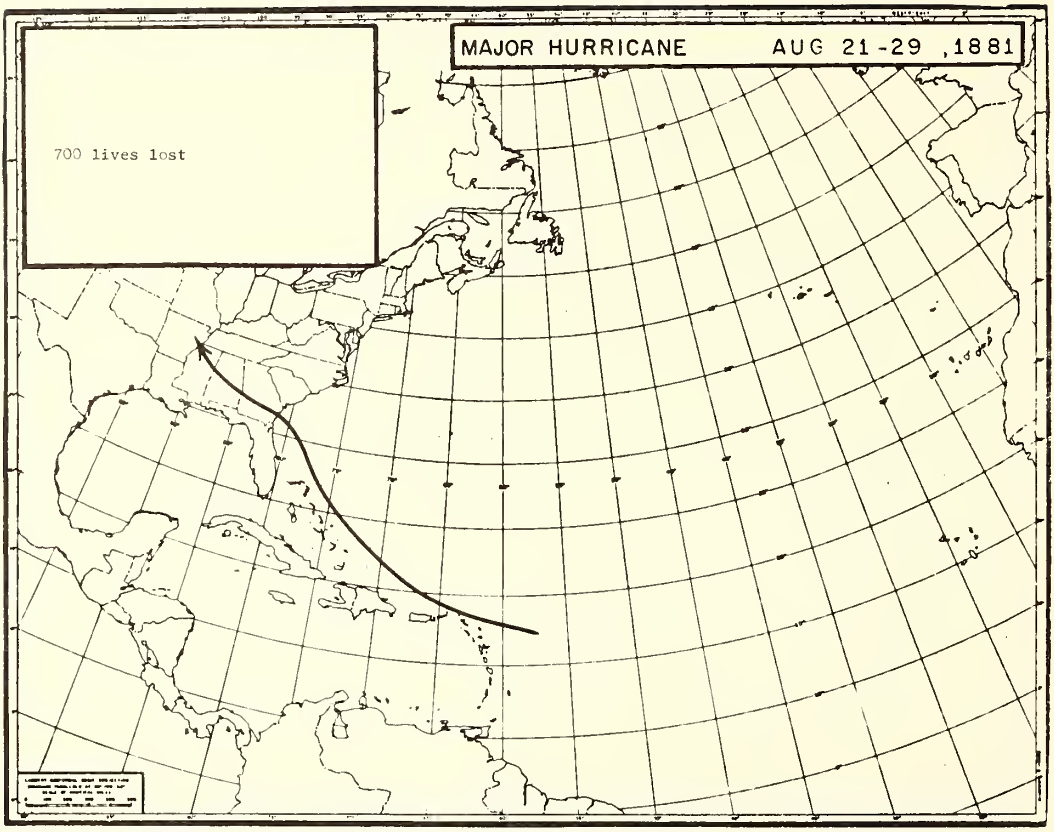

MAJOR HURRICANE AUG 21-29 ,1881

700 lives lost

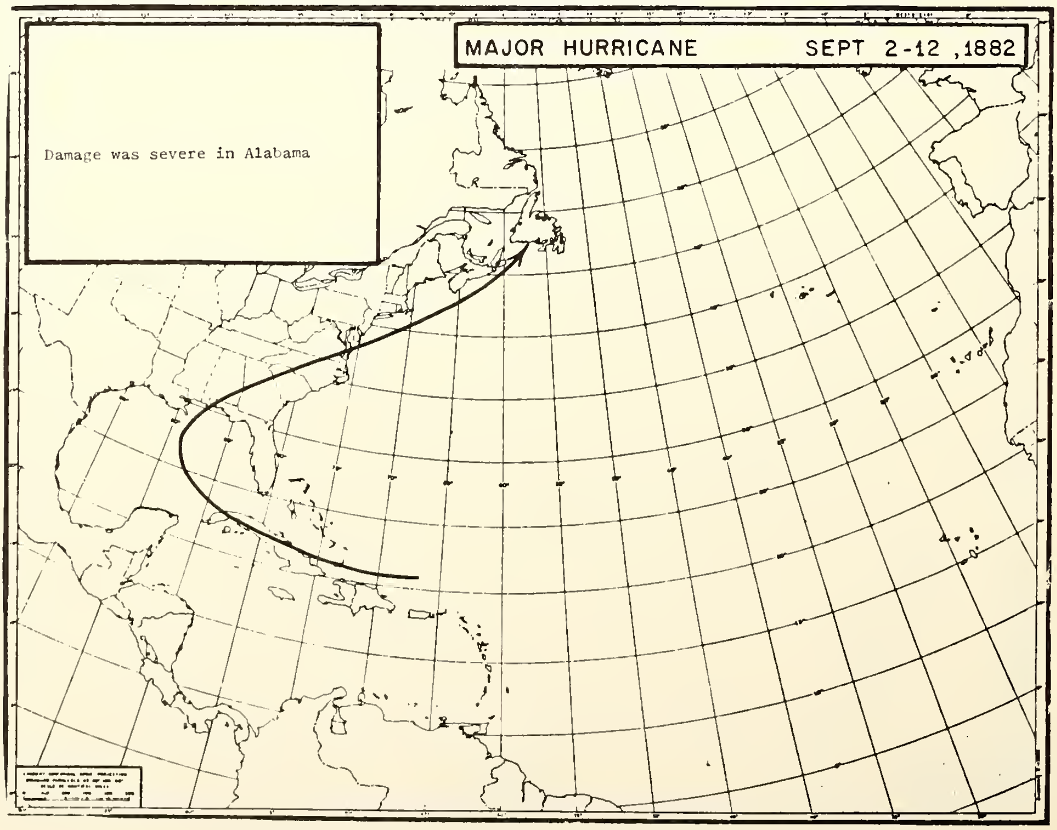

MAJOR HURRICANE SEPT 2-12 ,1882

Damage was severe in Alabama

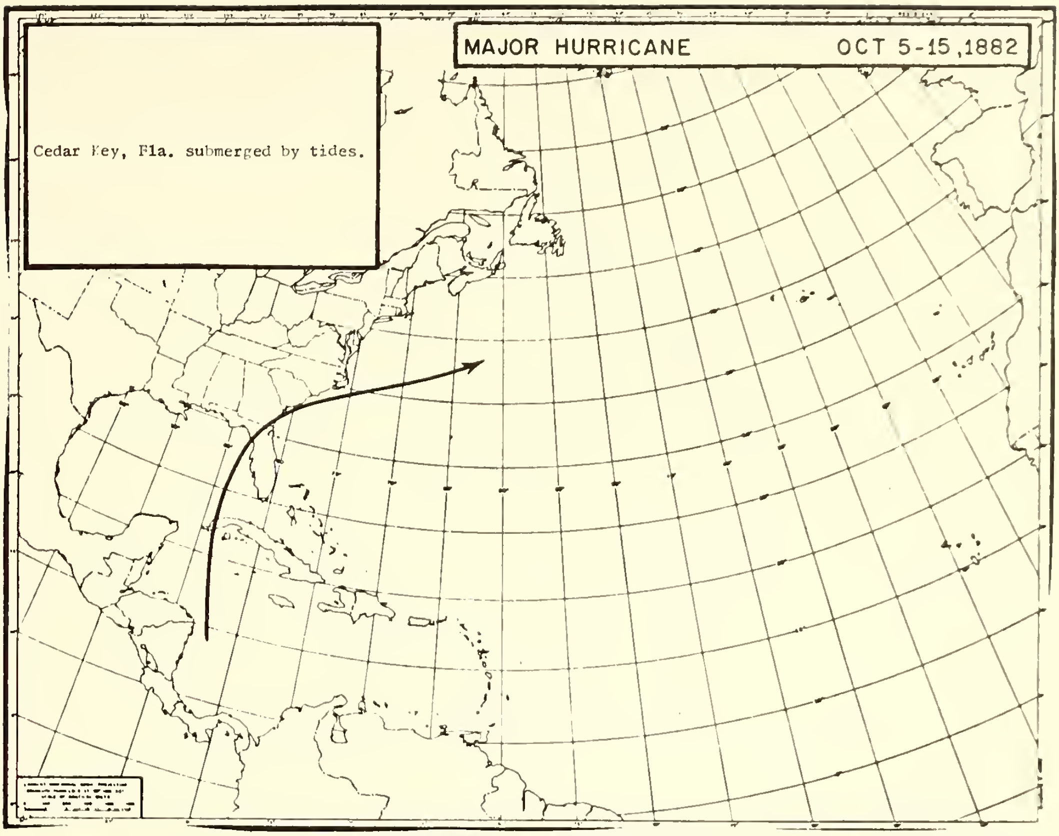
MAJOR HURRICANE OCT 5-15,1882

Cedar Key, Fla. submerged by tides.

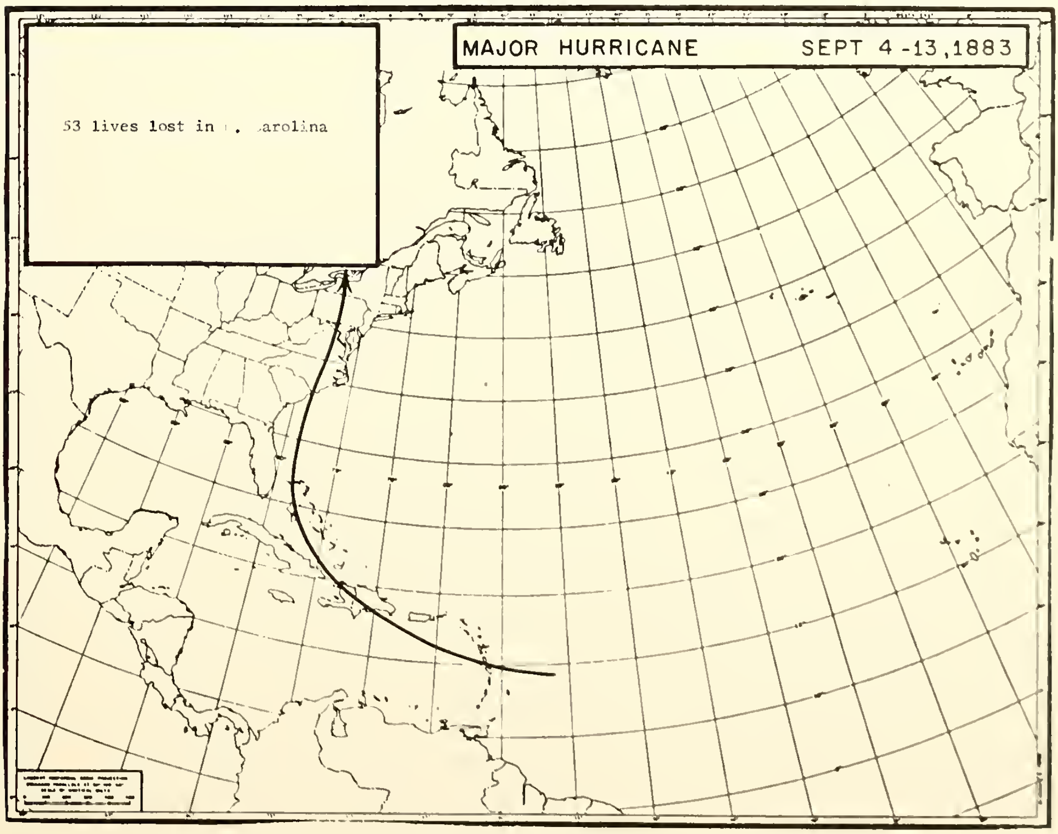
MAJOR HURRICANE SEPT 4-13,1883

53 lives lost in N. Carolina

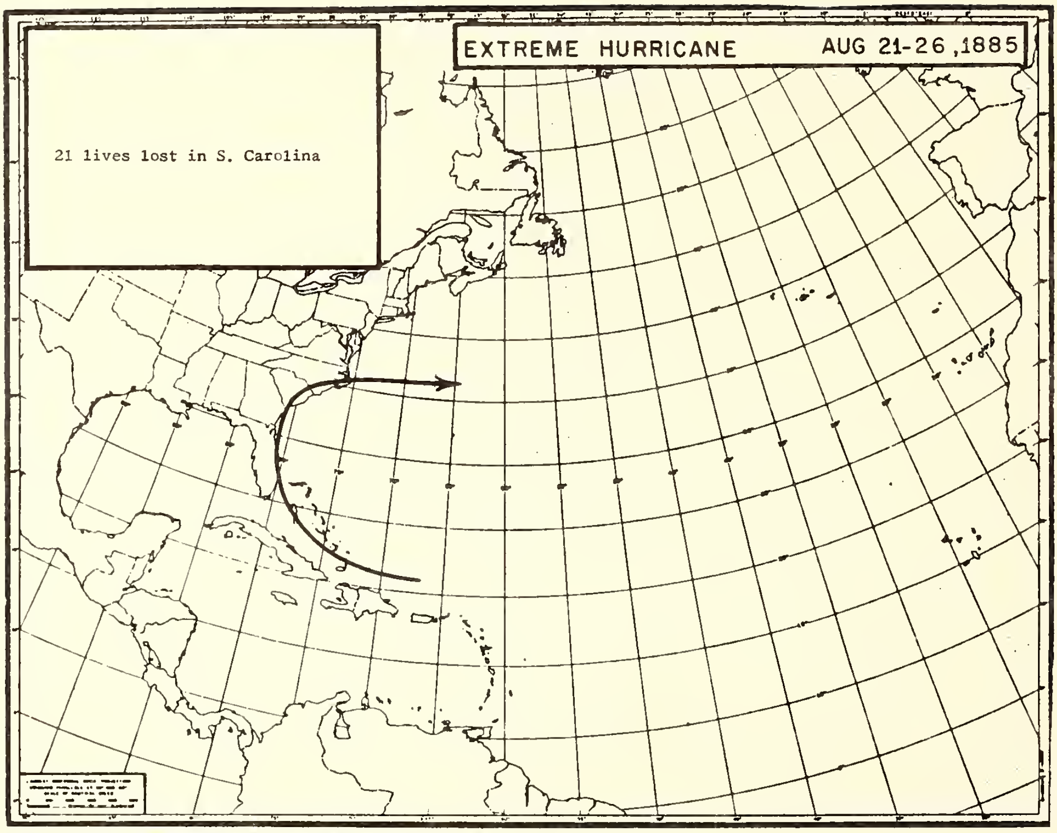

EXTREME HURRICANE AUG 21-26, 1885

21 lives lost in S. Carolina

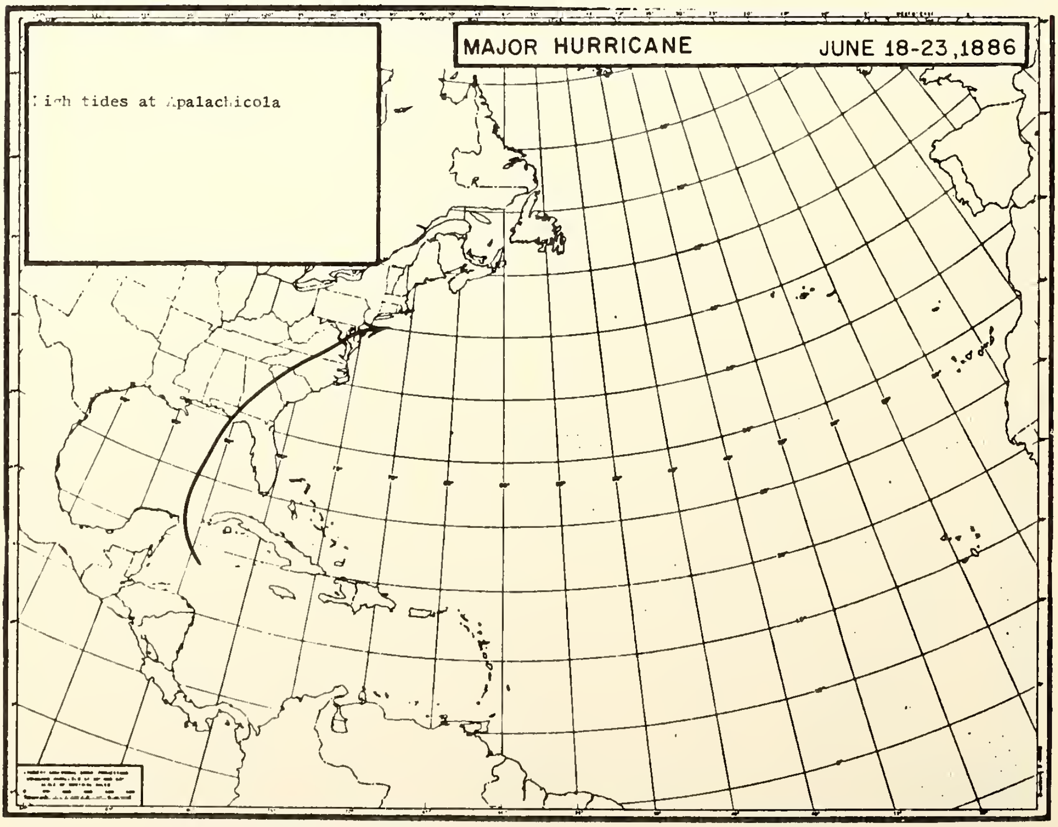

MAJOR HURRICANE JUNE 18-23, 1886

High tides at Apalachicola

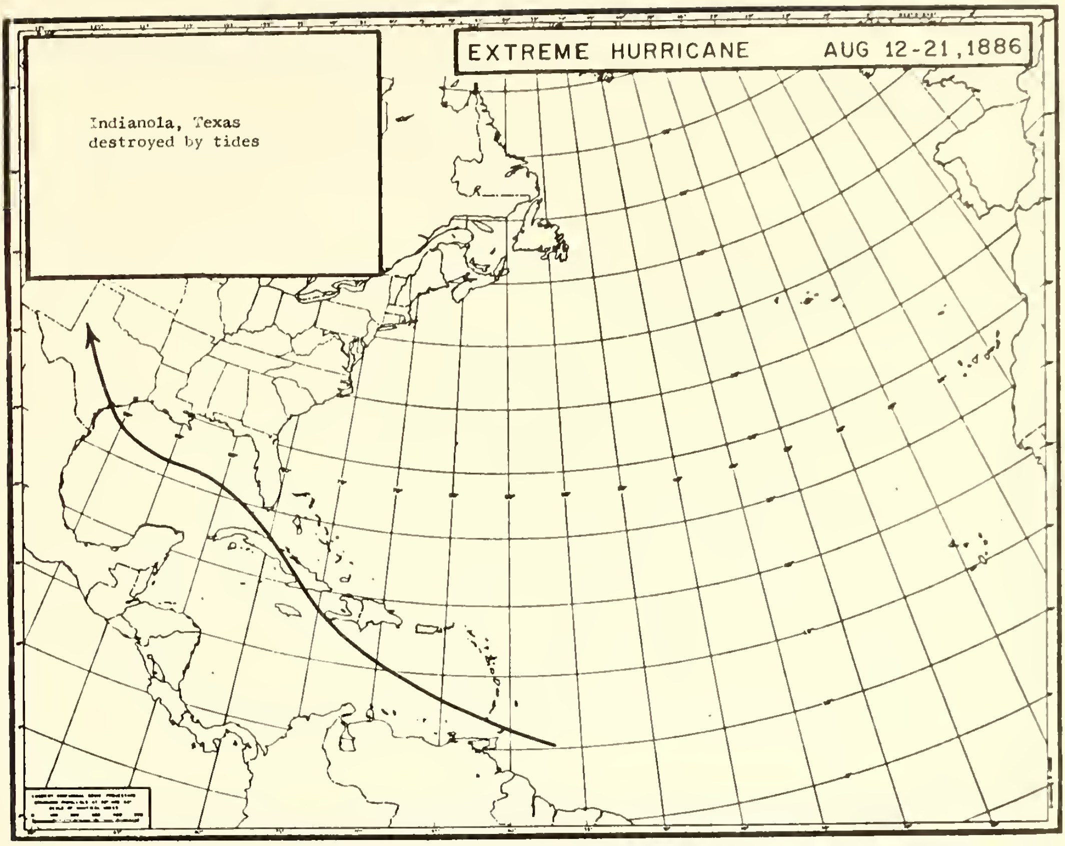

EXTREME HURRICANE AUG 12-21,1886

Indianola, Texas
destroyed by tides

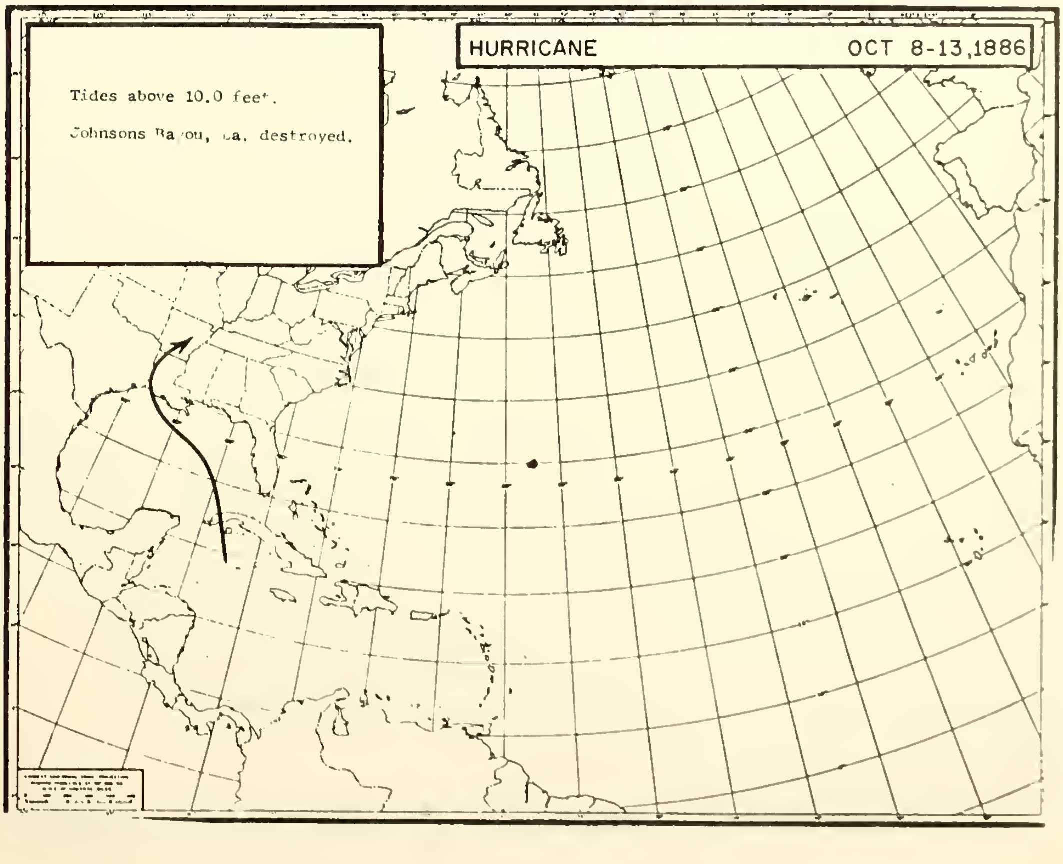

HURRICANE OCT 8-13,1886

Tides above 10.0 feet.

Johnsons Bayou, La. destroyed.

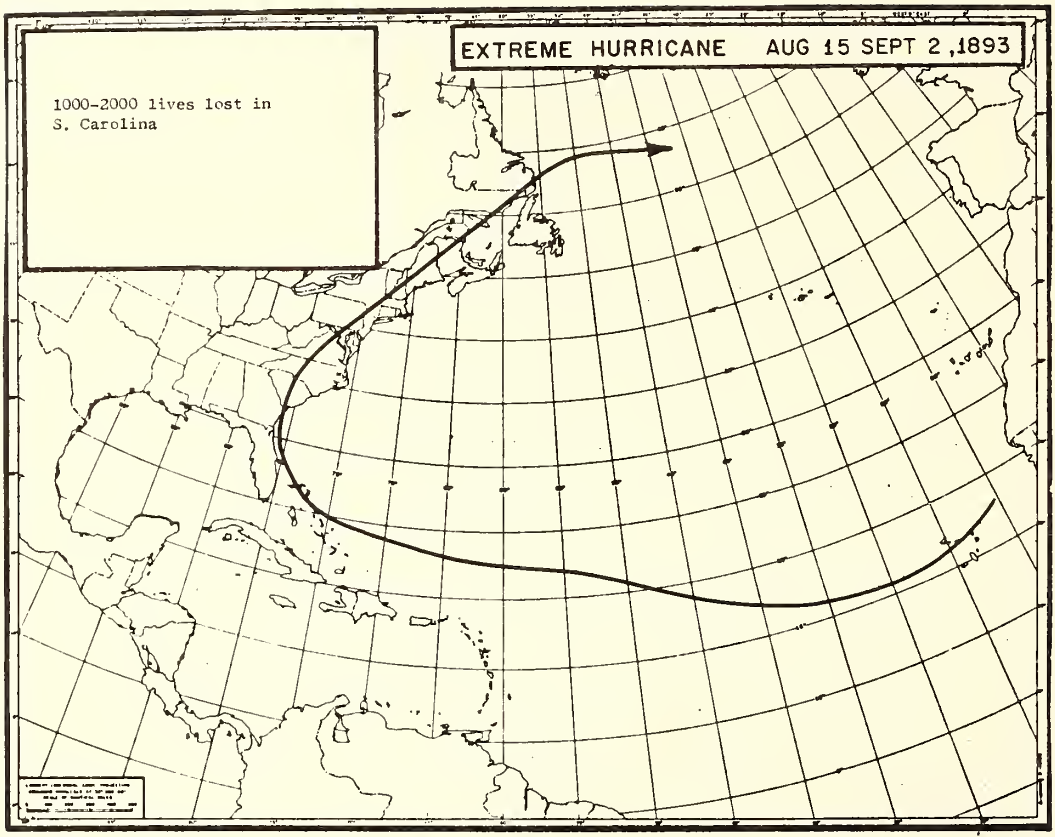

EXTREME HURRICANE AUG 15 SEPT 2, 1893

1000-2000 lives lost in
S. Carolina

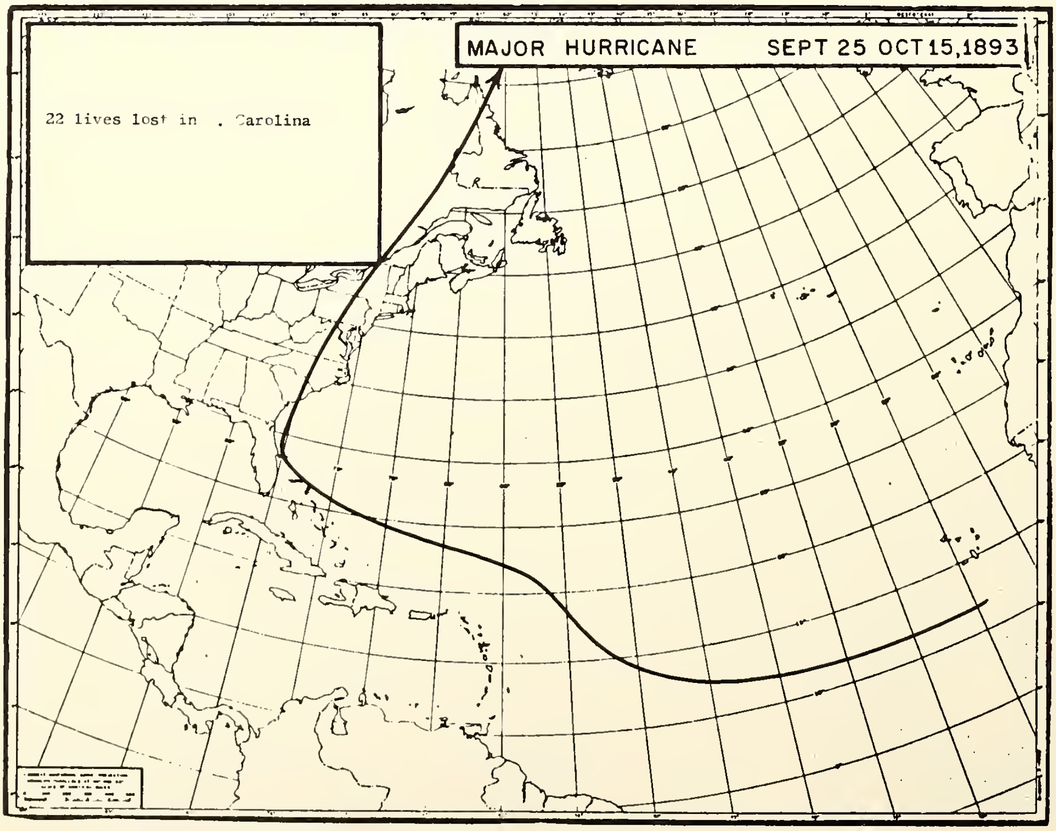

MAJOR HURRICANE SEPT 25 OCT 15, 1893

22 lives lost in . Carolina

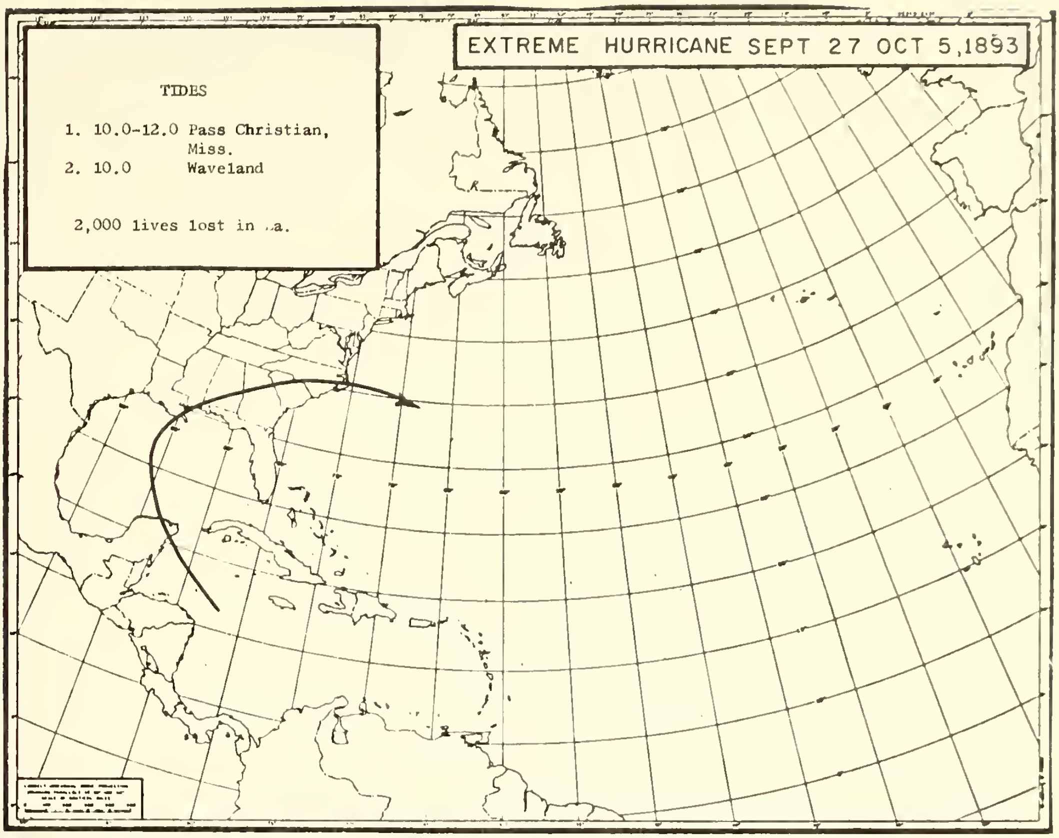

EXTREME HURRICANE SEPT 27 OCT 5,1893

TIDES

1. 10.0-12.0 Pass Christian, Miss.
2. 10.0 Waveland

2,000 lives lost in La.

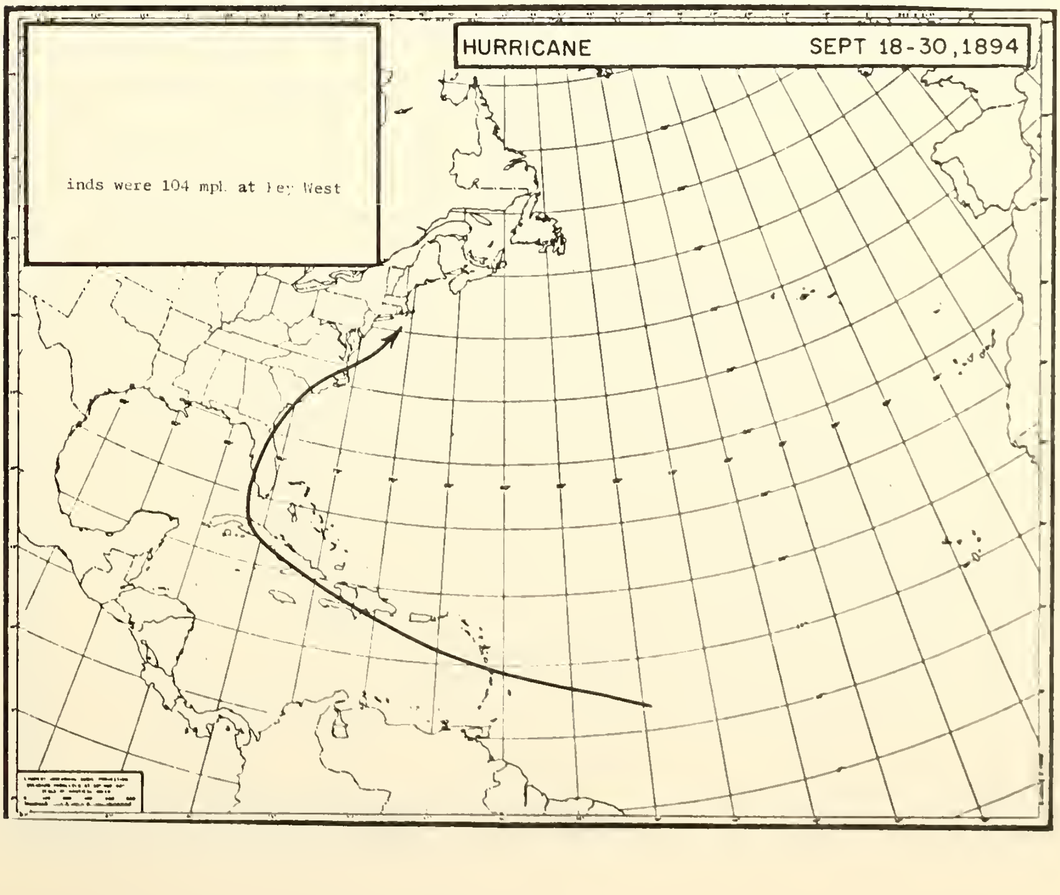

HURRICANE SEPT 18-30,1894

inds were 104 mph. at Key West

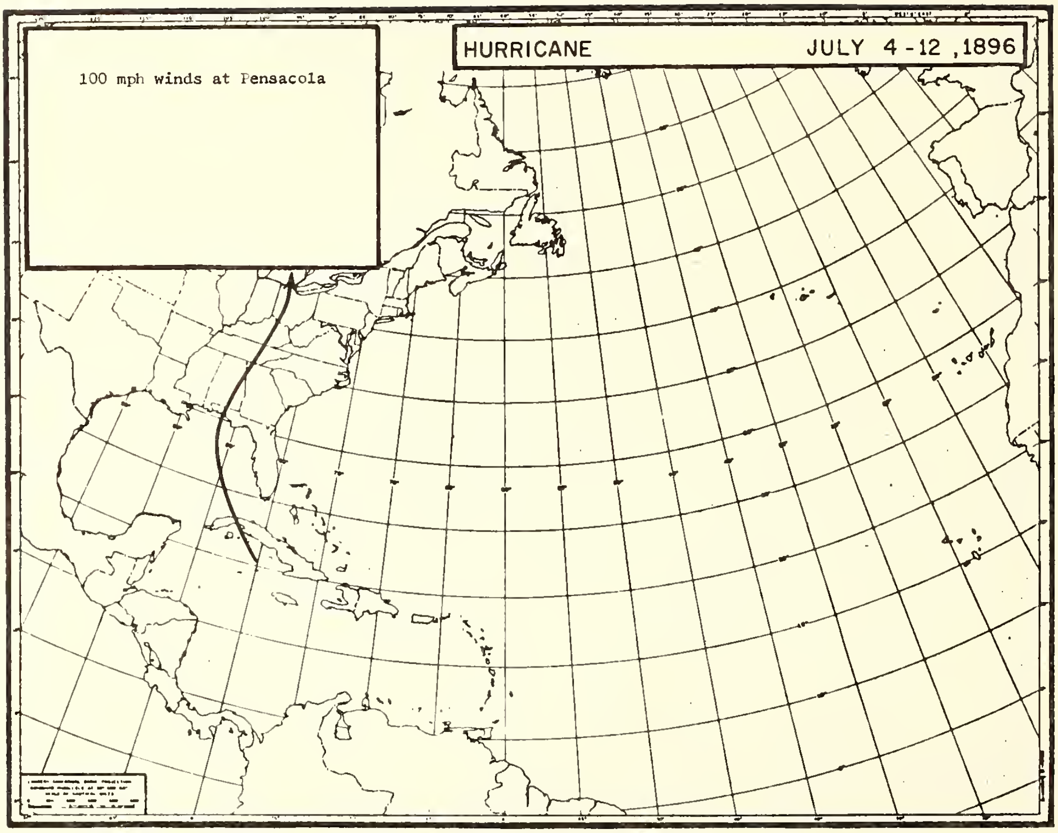

HURRICANE JULY 4-12, 1896

100 mph winds at Pensacola

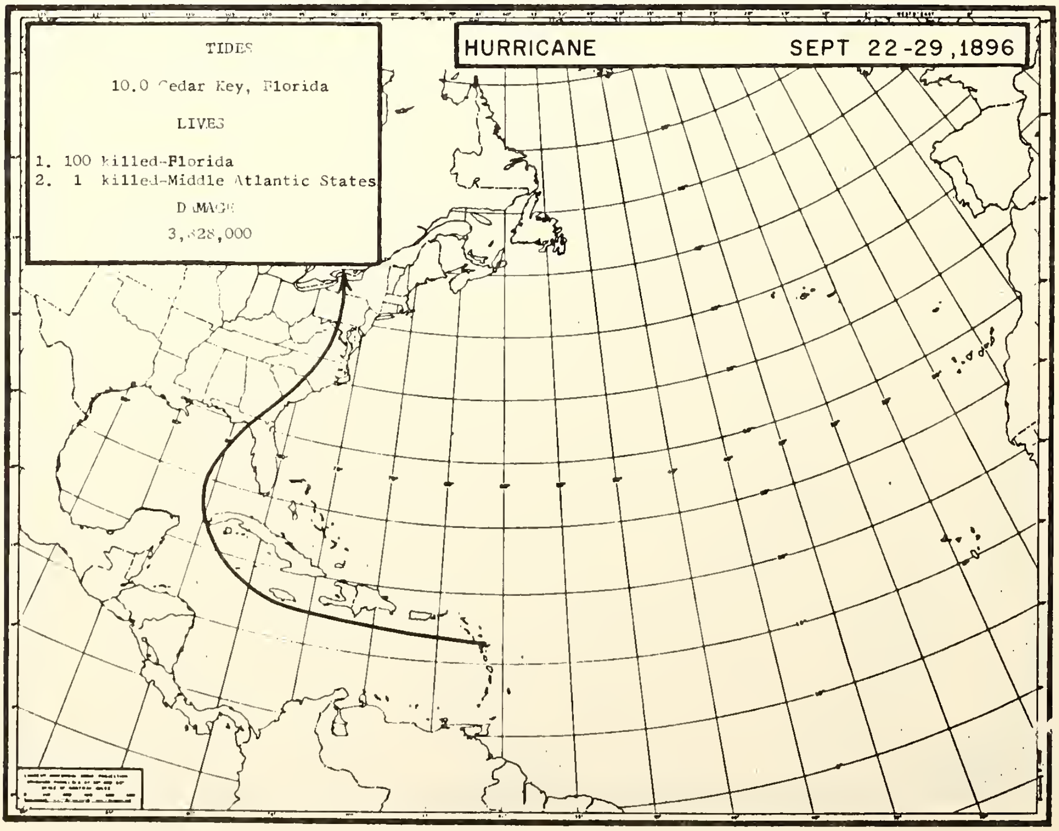

HURRICANE SEPT 22-29, 1896

TIDES

10.0 Cedar Key, Florida

LIVES

1. 100 killed-Florida
2. 1 killed-Middle Atlantic States

DAMAGE

3,828,000

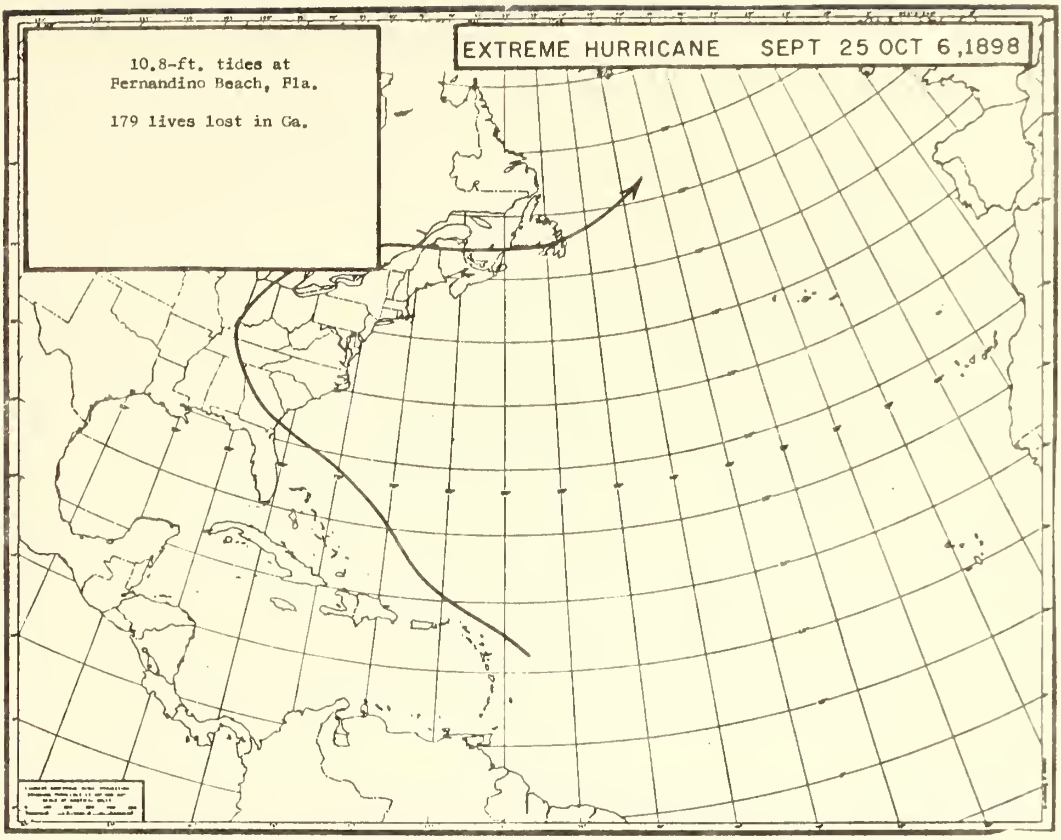

EXTREME HURRICANE SEPT 25 OCT 6,1898

10.8-ft. tides at
Fernandino Beach, Fla.

179 lives lost in Ga.

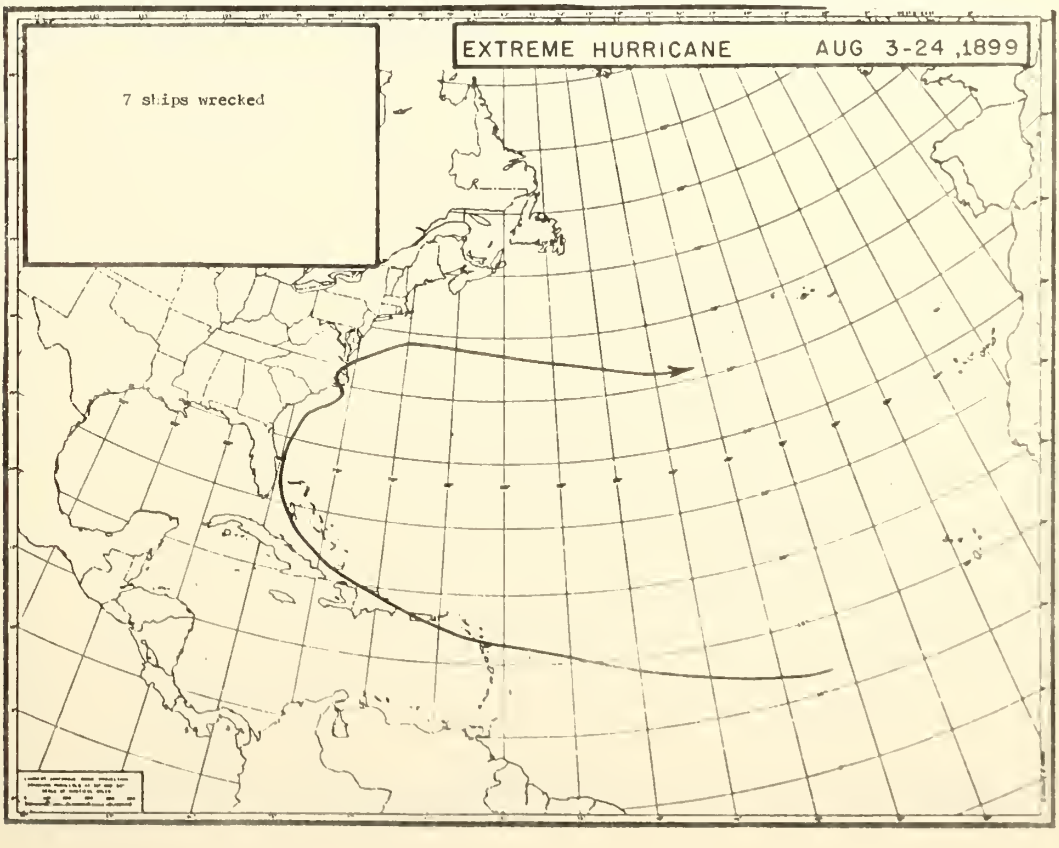

EXTREME HURRICANE AUG 3-24,1899

7 ships wrecked

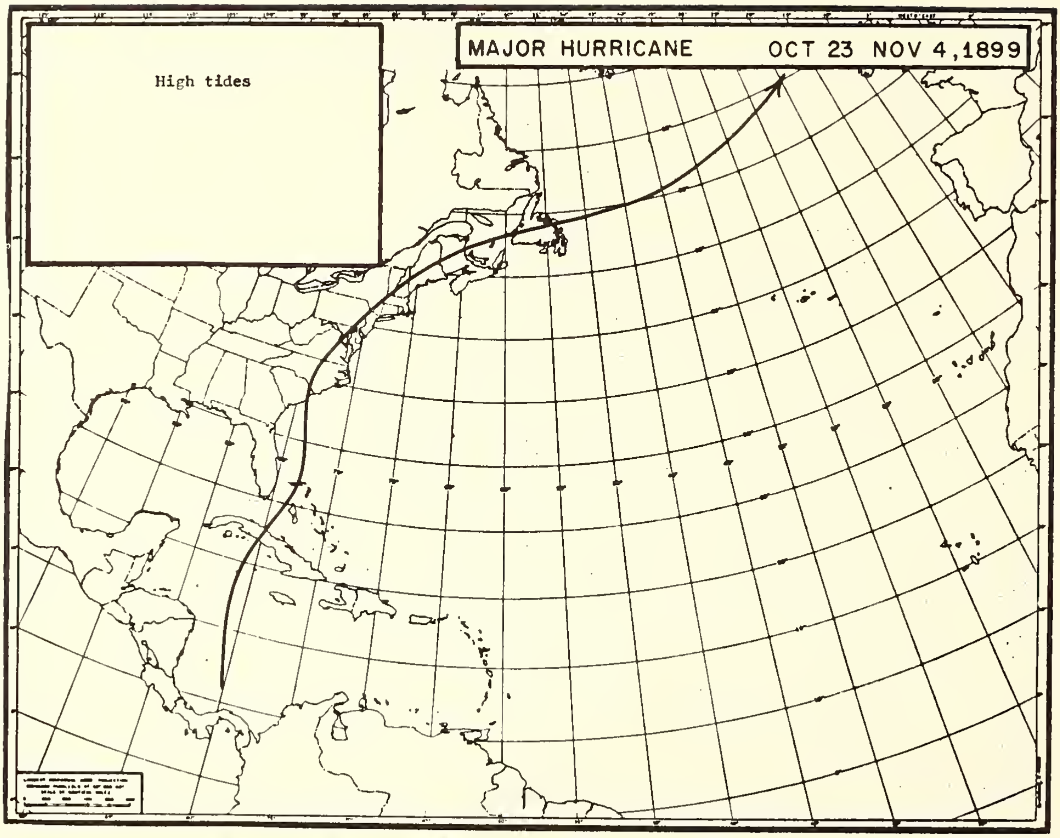

MAJOR HURRICANE OCT 23 NOV 4,1899

High tides

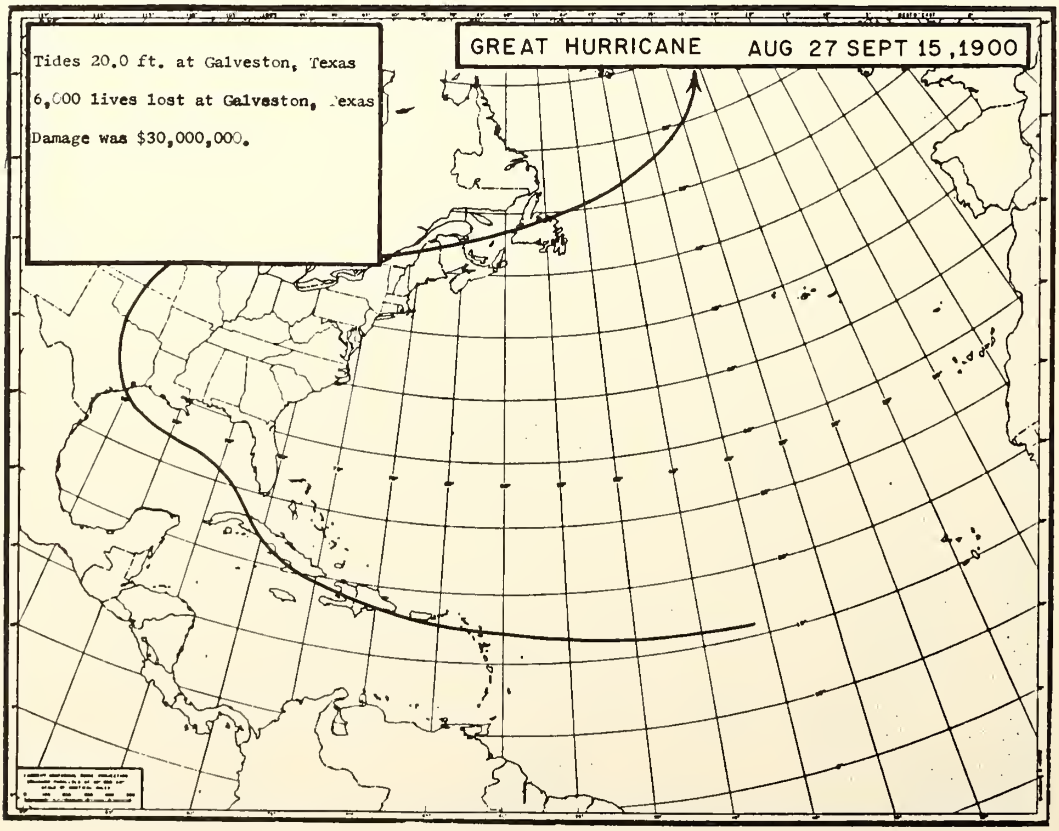

GREAT HURRICANE AUG 27 SEPT 15,1900

Tides 20.0 ft. at Galveston, Texas

6,000 lives lost at Galveston, Texas

Damage was $30,000,000.

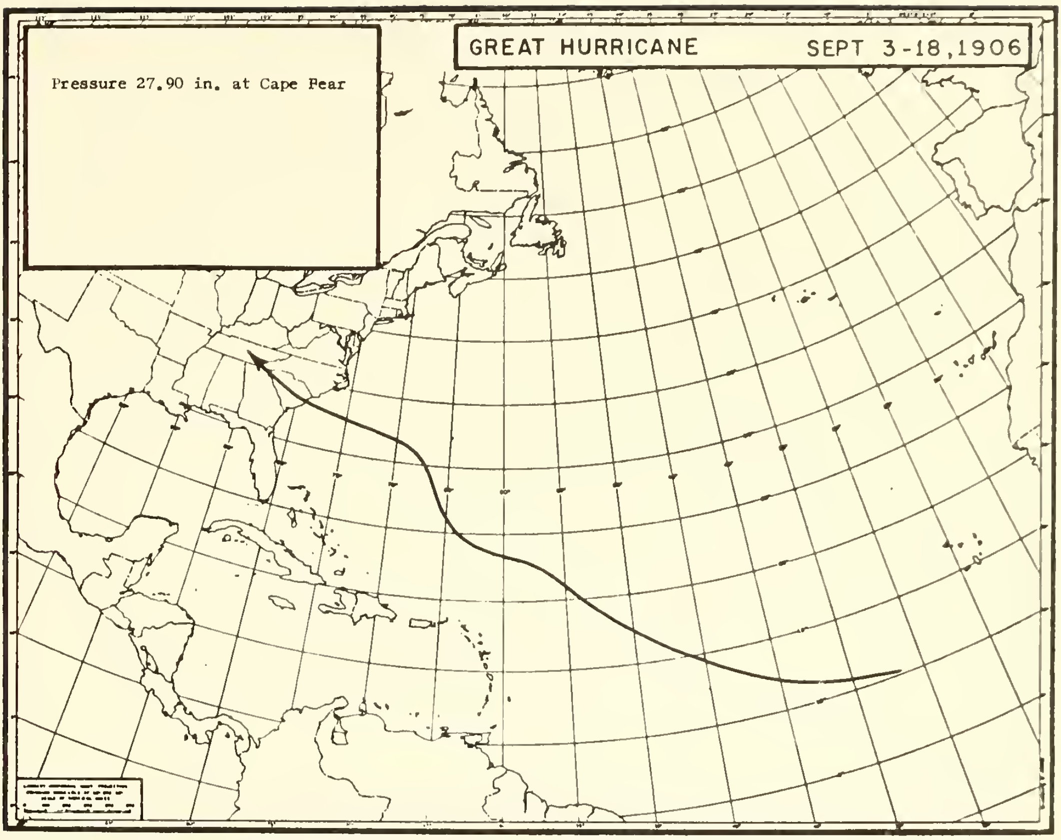

GREAT HURRICANE SEPT 3-18,1906

Pressure 27.90 in. at Cape Fear

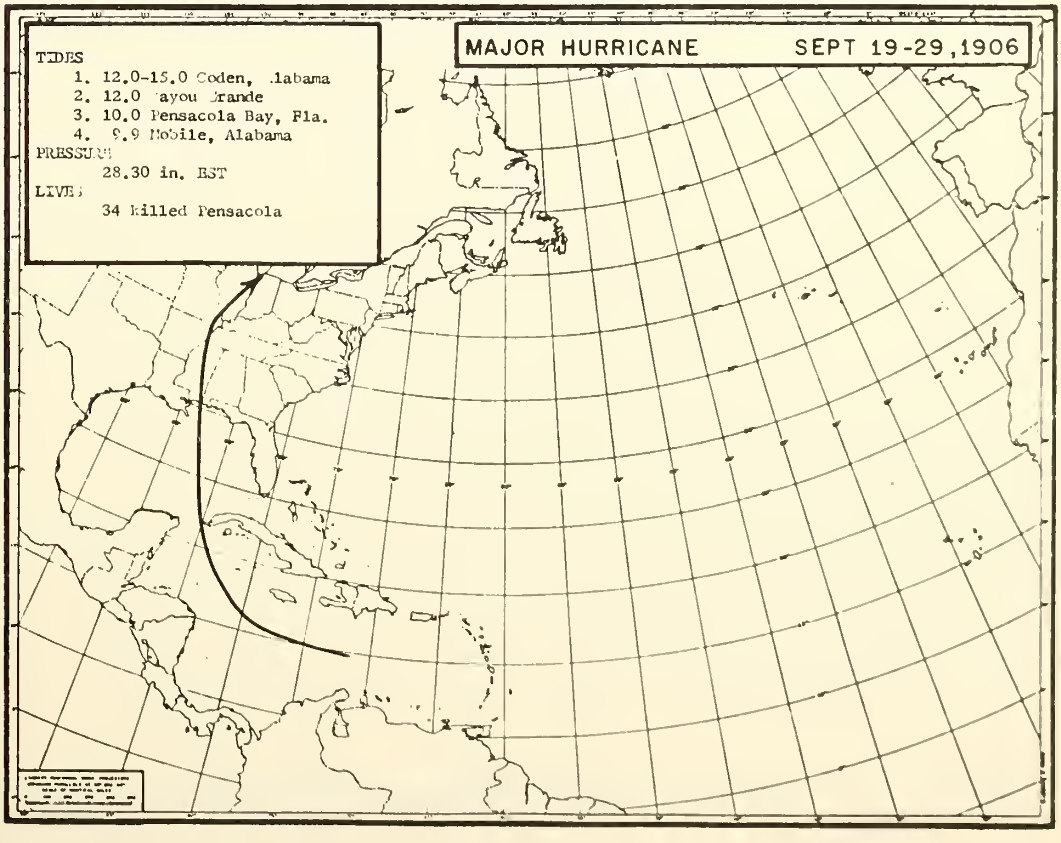

MAJOR HURRICANE SEPT 19-29,1906

TIDES
1. 12.0-15.0 Coden, Alabama
2. 12.0 Bayou Grande
3. 10.0 Pensacola Bay, Fla.
4. 9.9 Mobile, Alabama

PRESSURE
28.30 in. EST

LIVES
34 killed Pensacola

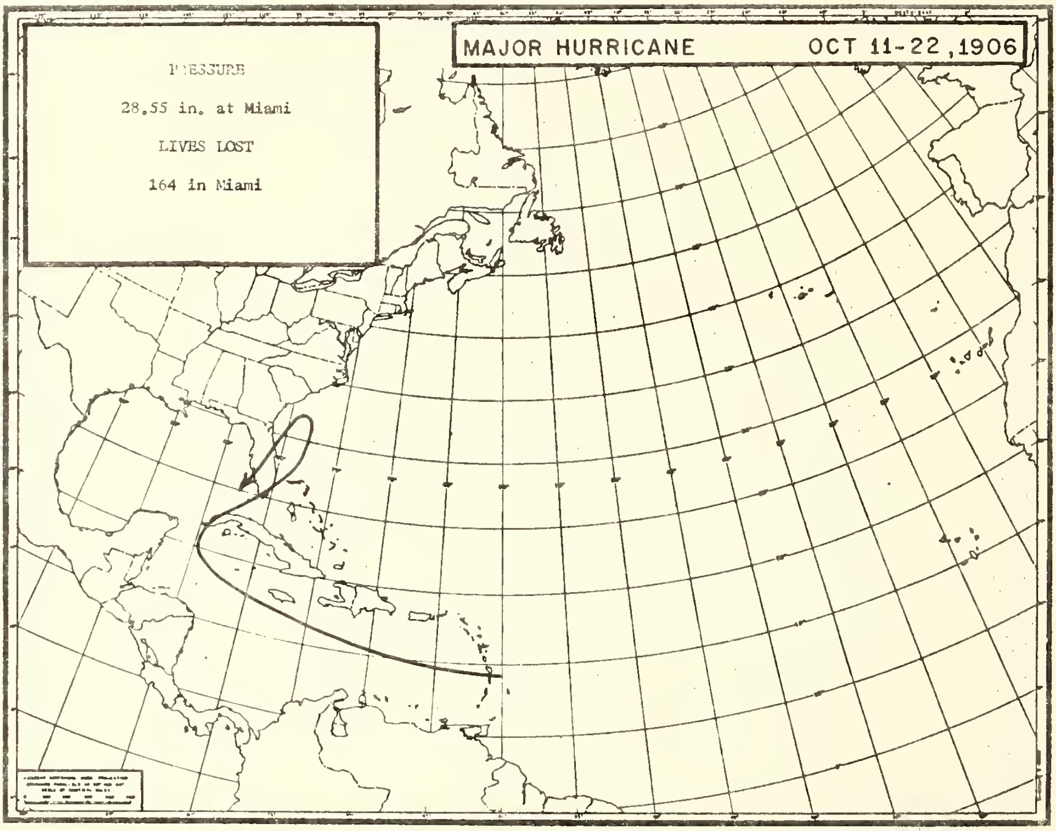

MAJOR HURRICANE OCT 11-22, 1906

PRESSURE

28.55 in. at Miami

LIVES LOST

164 in Miami

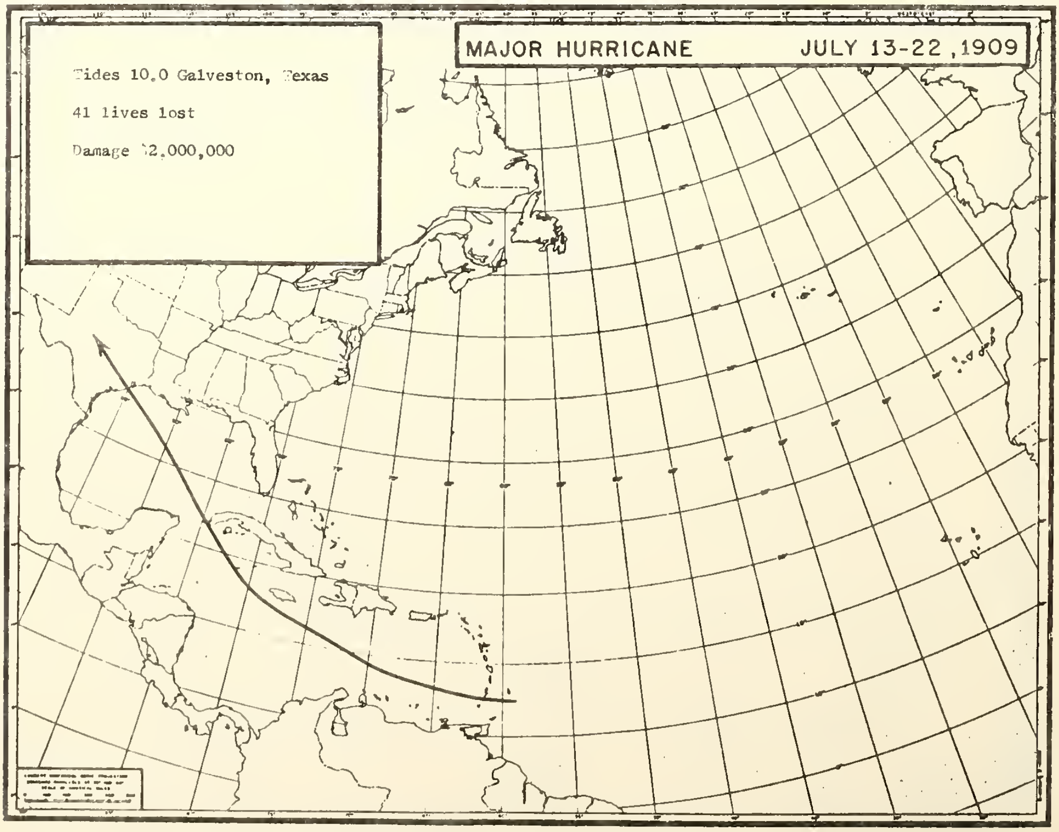

MAJOR HURRICANE JULY 13-22, 1909

Tides 10.0 Galveston, Texas

41 lives lost

Damage $2,000,000

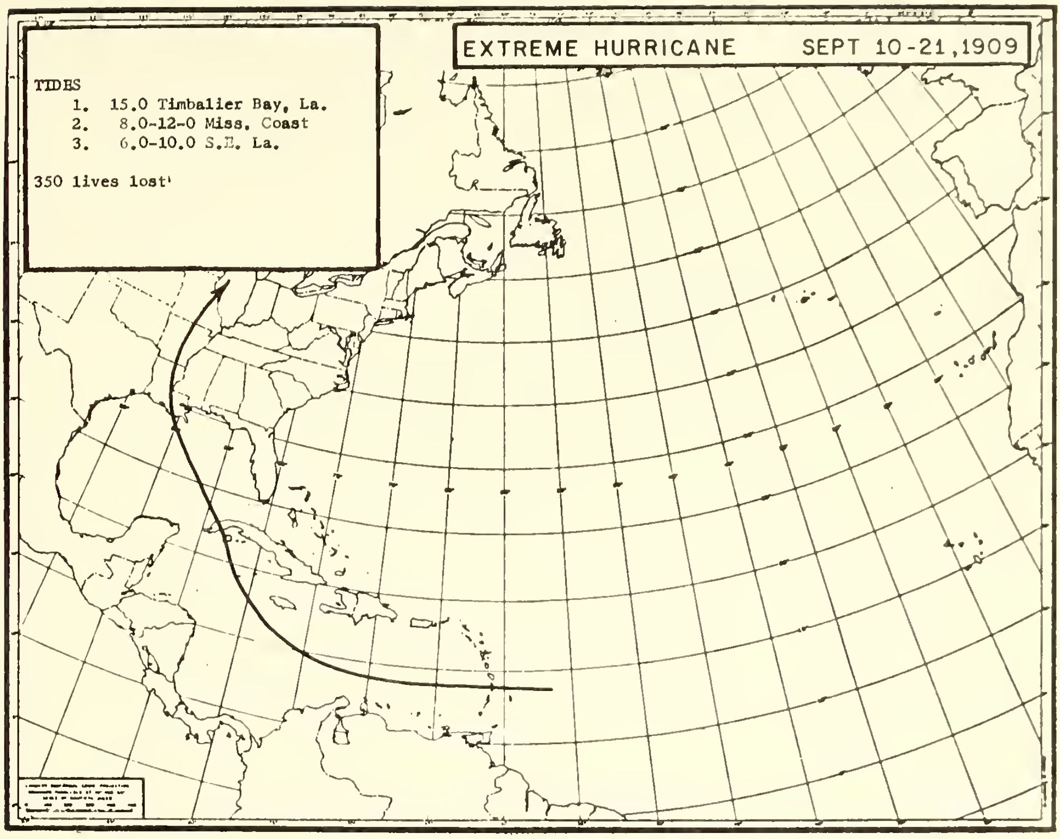

EXTREME HURRICANE SEPT 10-21,1909

TIDES
1. 15.0 Timbalier Bay, La.
2. 8.0-12-0 Miss. Coast
3. 6.0-10.0 S.E. La.

350 lives lost

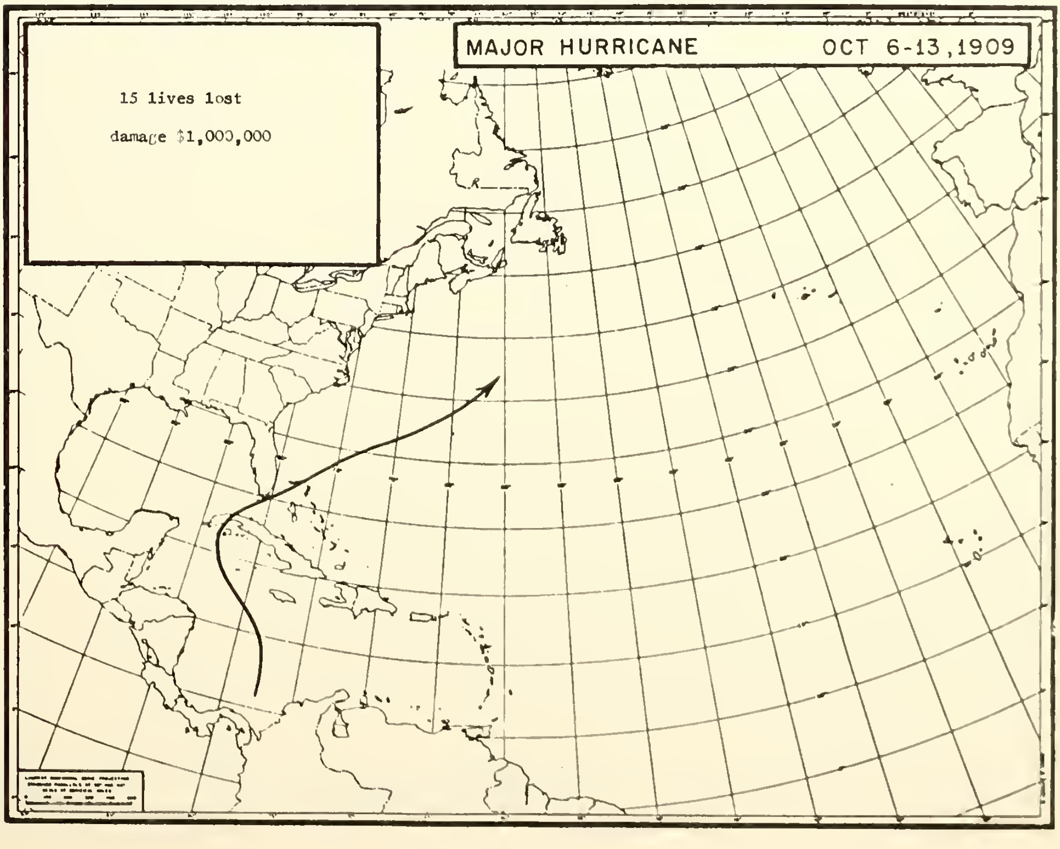

MAJOR HURRICANE OCT 6-13,1909

15 lives lost

damage $1,000,000

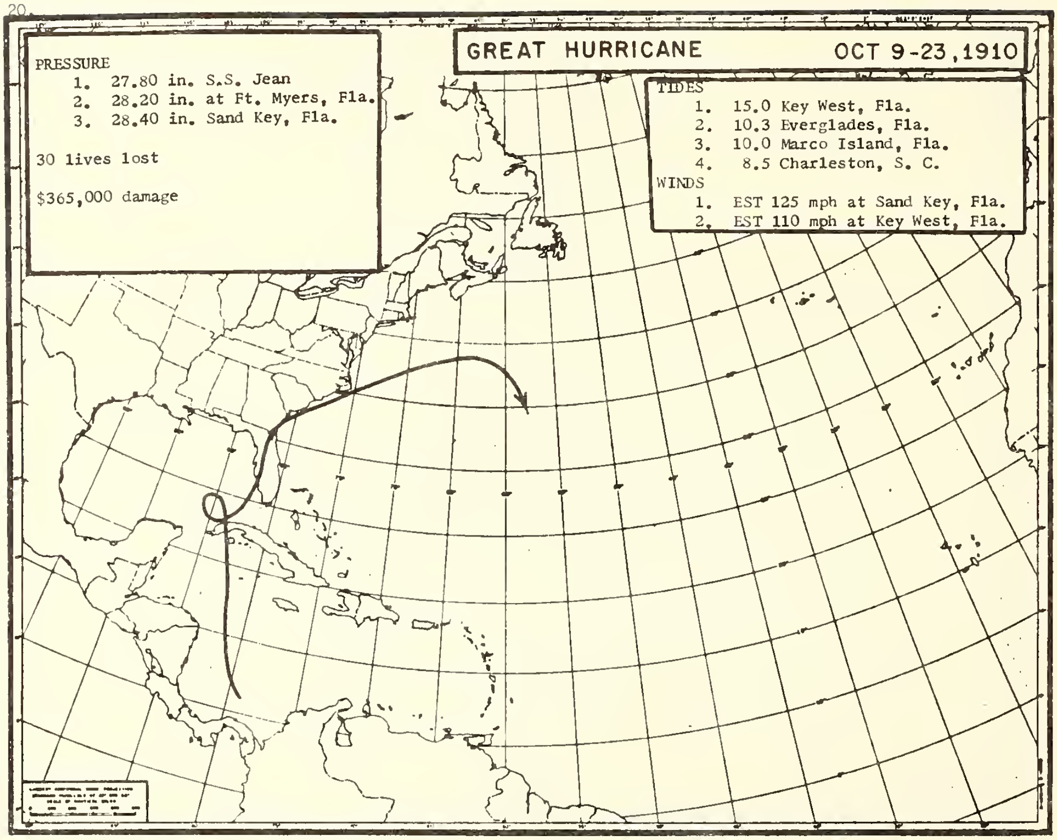

GREAT HURRICANE OCT 9-23,1910

PRESSURE
1. 27.80 in. S.S. Jean
2. 28.20 in. at Ft. Myers, Fla.
3. 28.40 in. Sand Key, Fla.

30 lives lost

$365,000 damage

TIDES
1. 15.0 Key West, Fla.
2. 10.3 Everglades, Fla.
3. 10.0 Marco Island, Fla.
4. 8.5 Charleston, S. C.

WINDS
1. EST 125 mph at Sand Key, Fla.
2. EST 110 mph at Key West, Fla.

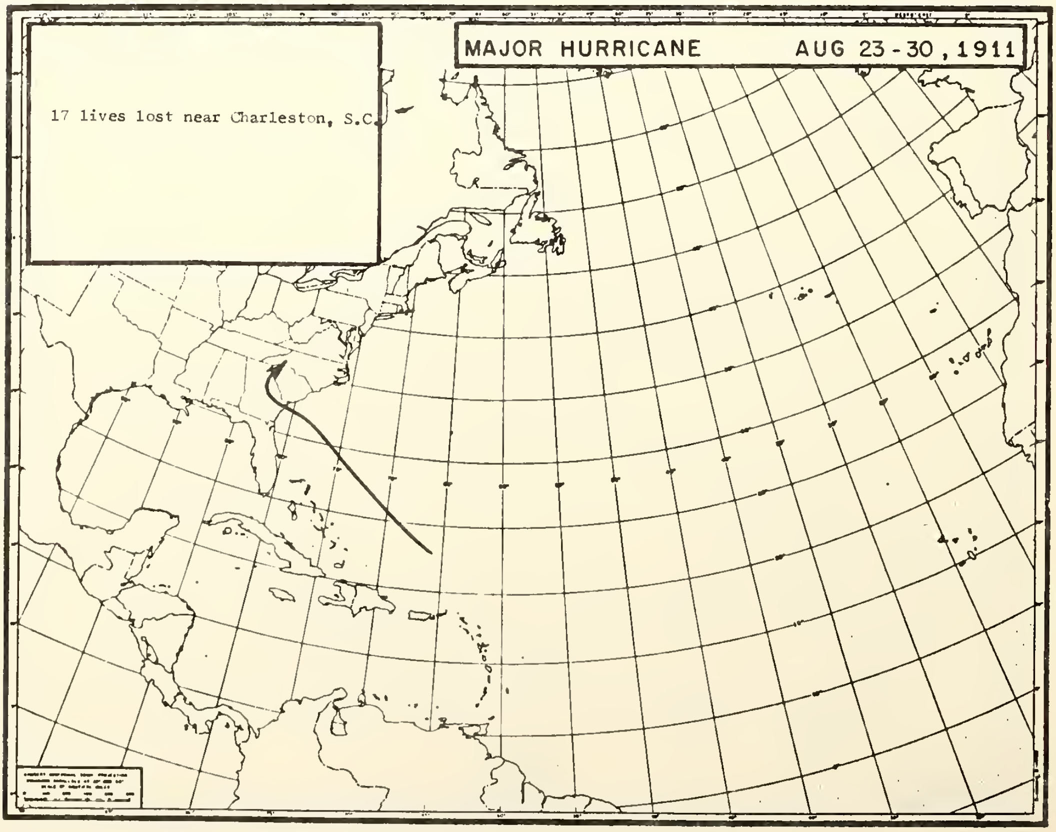

MAJOR HURRICANE AUG 23-30,1911

17 lives lost near Charleston, S.C.

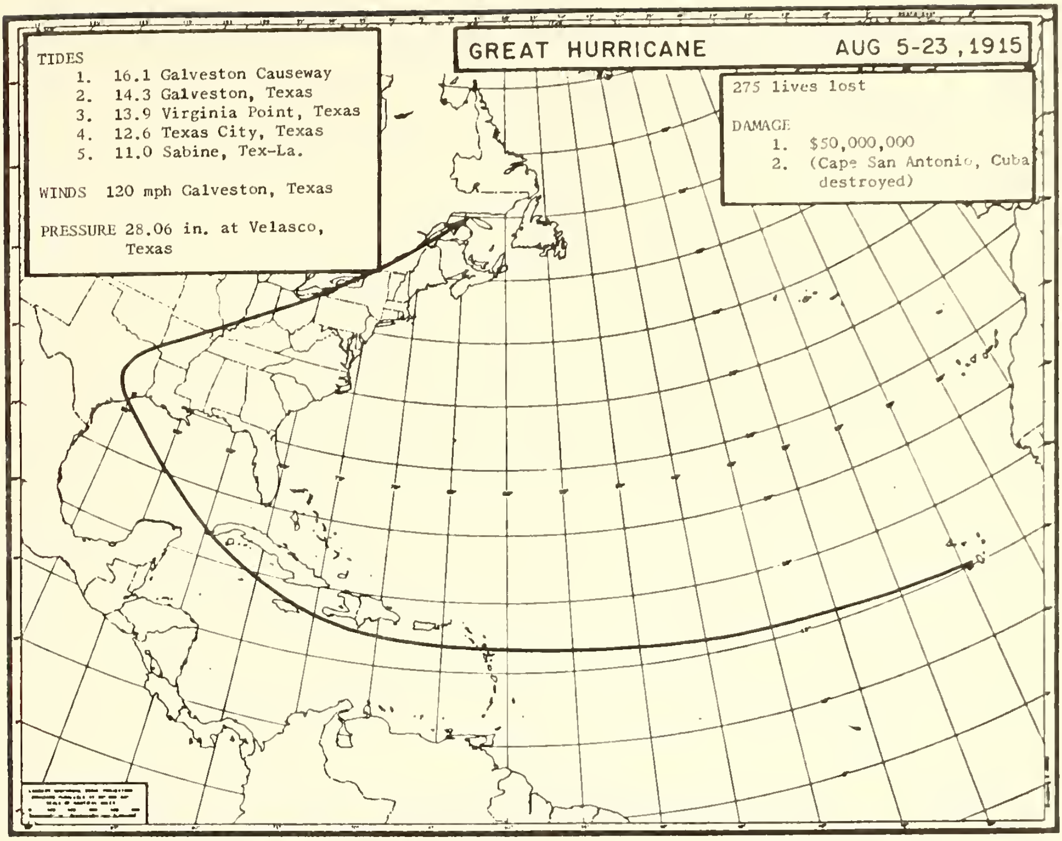

GREAT HURRICANE AUG 5-23 ,1915

TIDES
1. 16.1 Galveston Causeway
2. 14.3 Galveston, Texas
3. 13.9 Virginia Point, Texas
4. 12.6 Texas City, Texas
5. 11.0 Sabine, Tex-La.

WINDS 120 mph Galveston, Texas

PRESSURE 28.06 in. at Velasco, Texas

275 lives lost

DAMAGE
1. $50,000,000
2. (Cape San Antonio, Cuba destroyed)

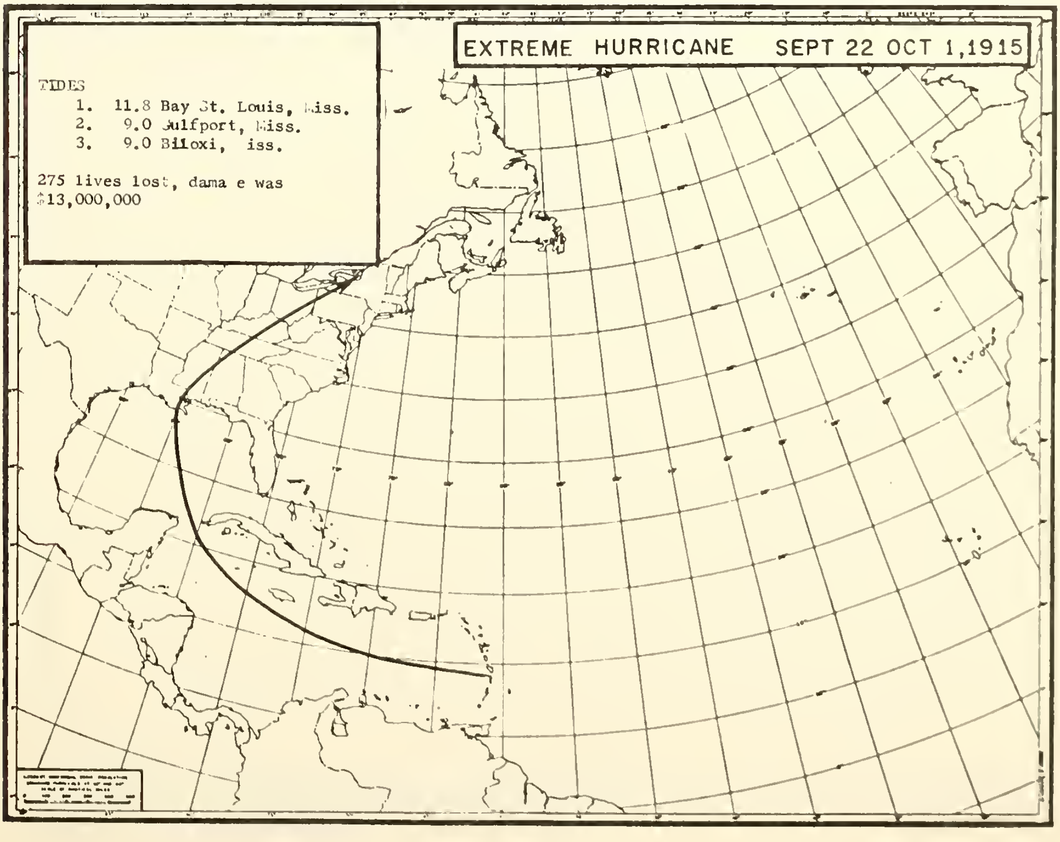

EXTREME HURRICANE SEPT 22 OCT 1,1915

TIDES
1. 11.8 Bay St. Louis, Miss.
2. 9.0 Gulfport, Miss.
3. 9.0 Biloxi, Miss.

275 lives lost, damage was $13,000,000

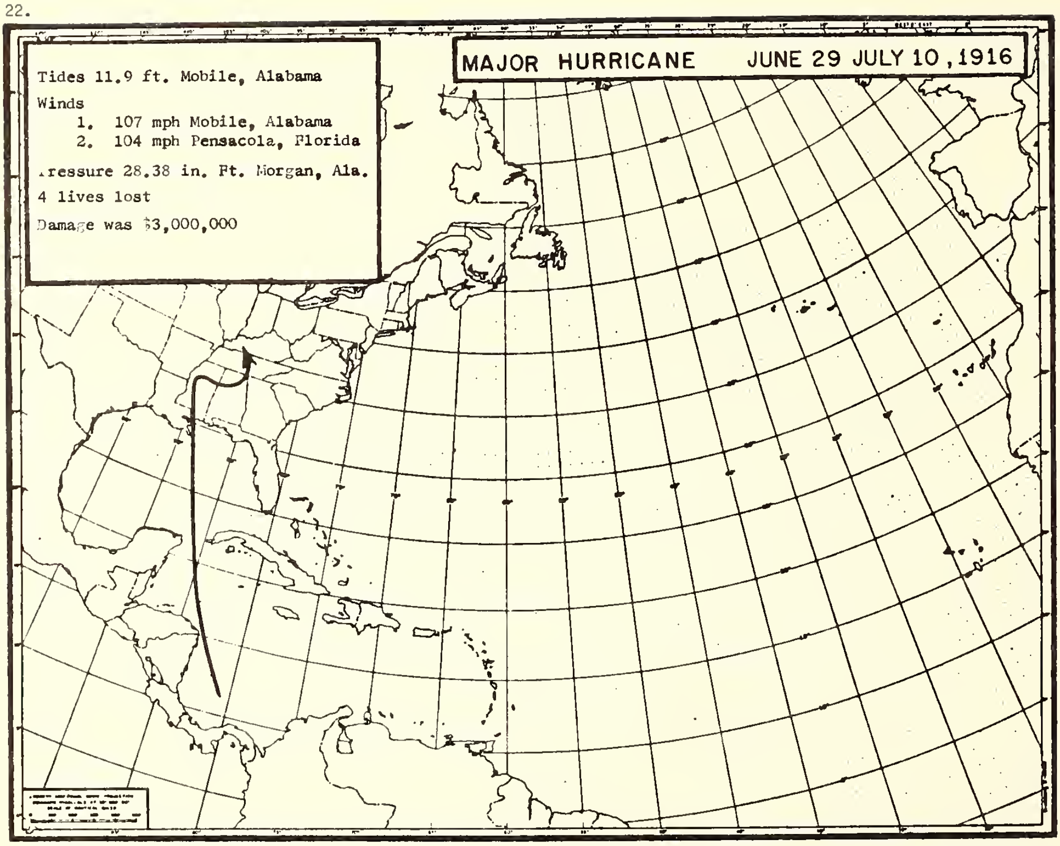

MAJOR HURRICANE JUNE 29 JULY 10,1916

Tides 11.9 ft. Mobile, Alabama

Winds
   1. 107 mph Mobile, Alabama
   2. 104 mph Pensacola, Florida

Pressure 28.38 in. Ft. Morgan, Ala.

4 lives lost

Damage was $3,000,000

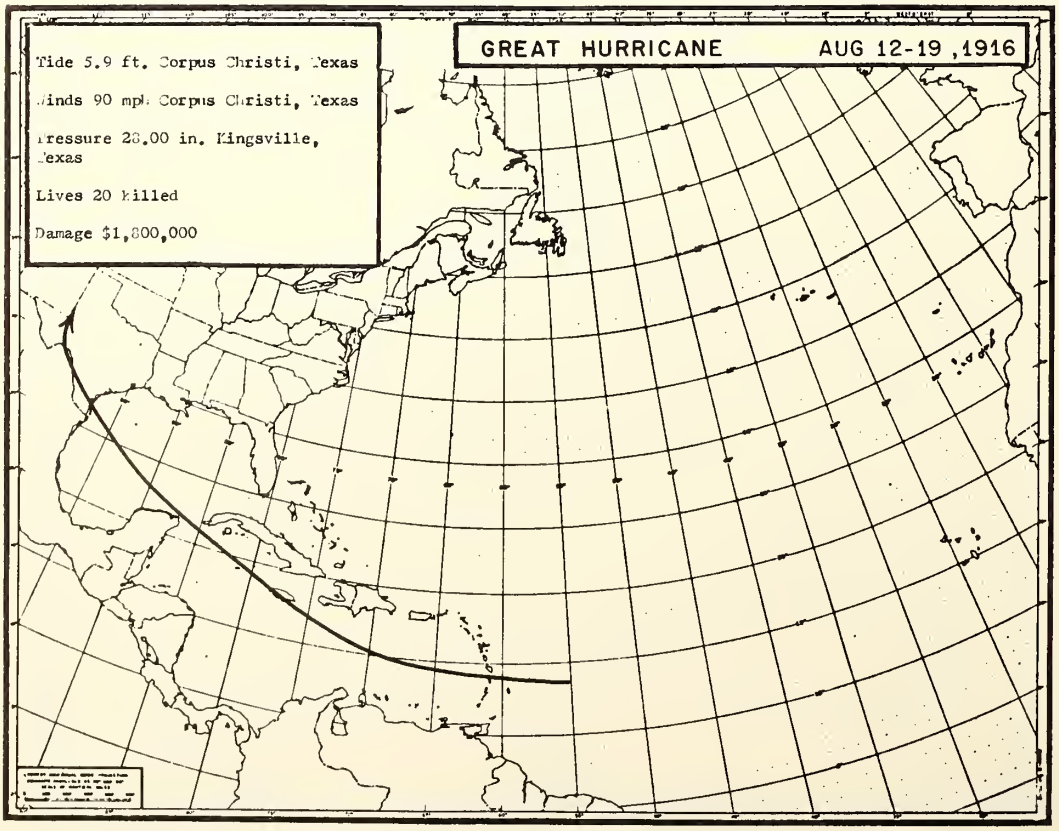

GREAT HURRICANE AUG 12-19,1916

Tide 5.9 ft. Corpus Christi, Texas

Winds 90 mph Corpus Christi, Texas

Pressure 28.00 in. Kingsville, Texas

Lives 20 killed

Damage $1,800,000

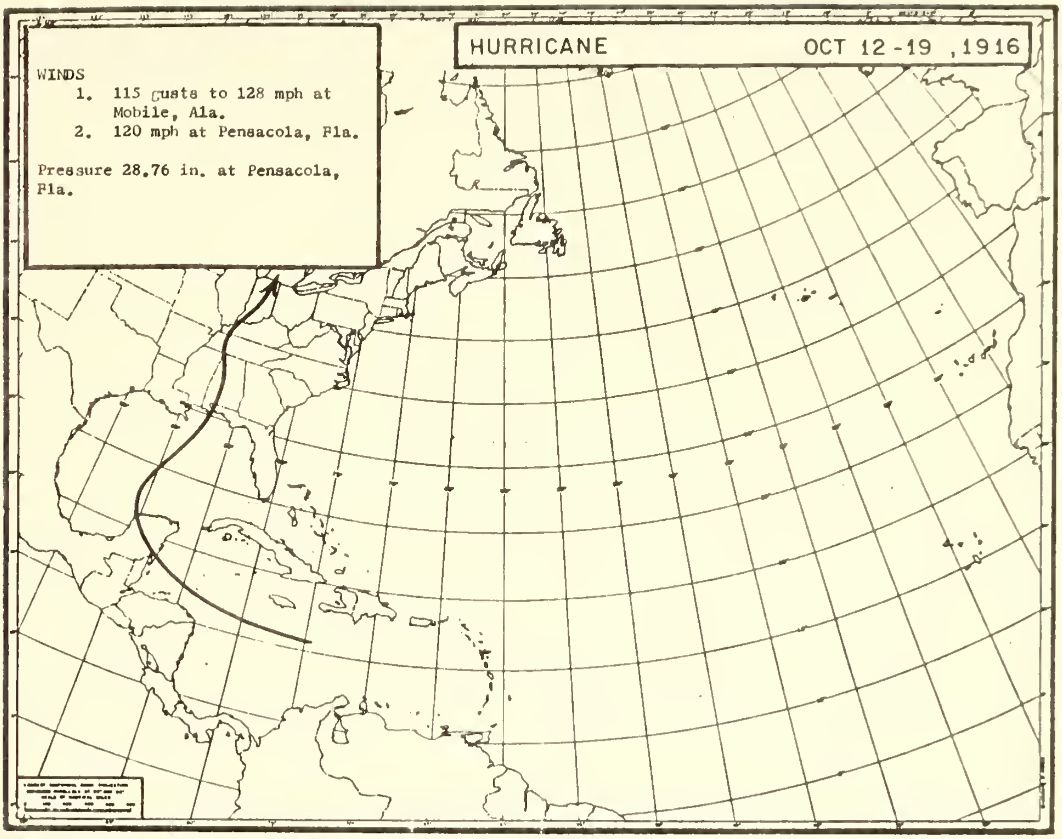

HURRICANE OCT 12-19 ,1916

WINDS
1. 115 gusts to 128 mph at Mobile, Ala.
2. 120 mph at Pensacola, Fla.

Pressure 28.76 in. at Pensacola, Fla.

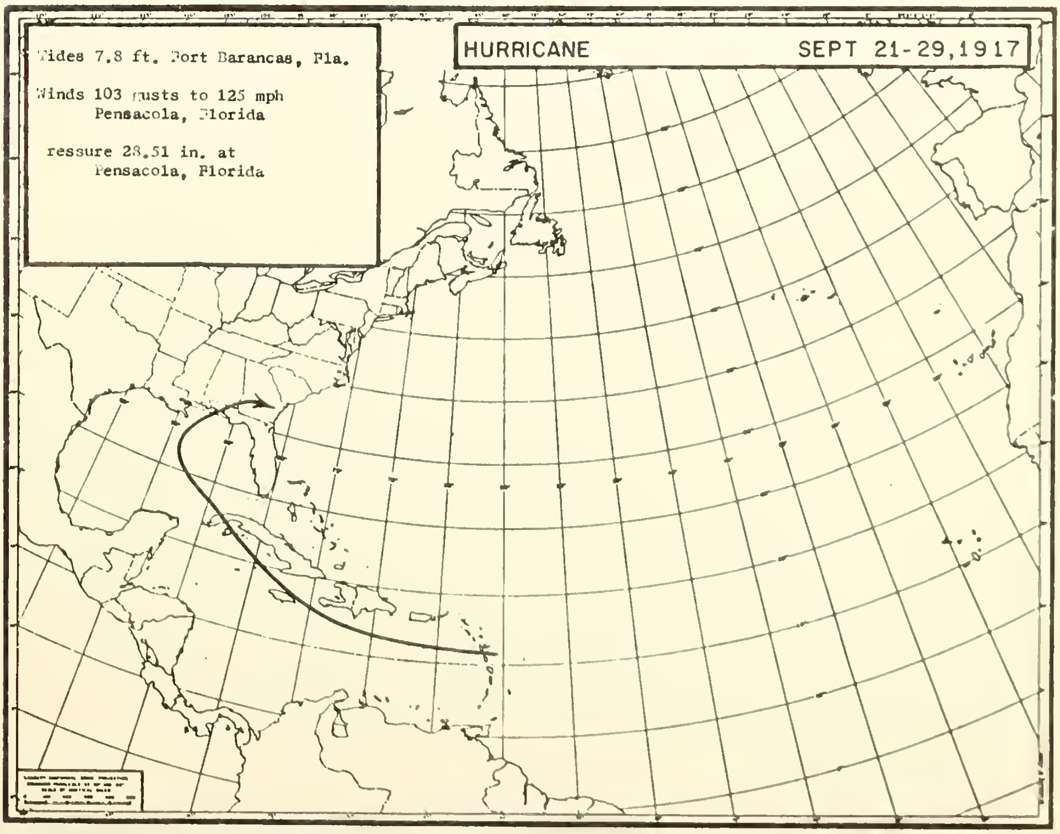

HURRICANE SEPT 21-29,1917

Tides 7.8 ft. Fort Barancas, Fla.

Winds 103 gusts to 125 mph Pensacola, Florida

ressure 28.51 in. at Pensacola, Florida

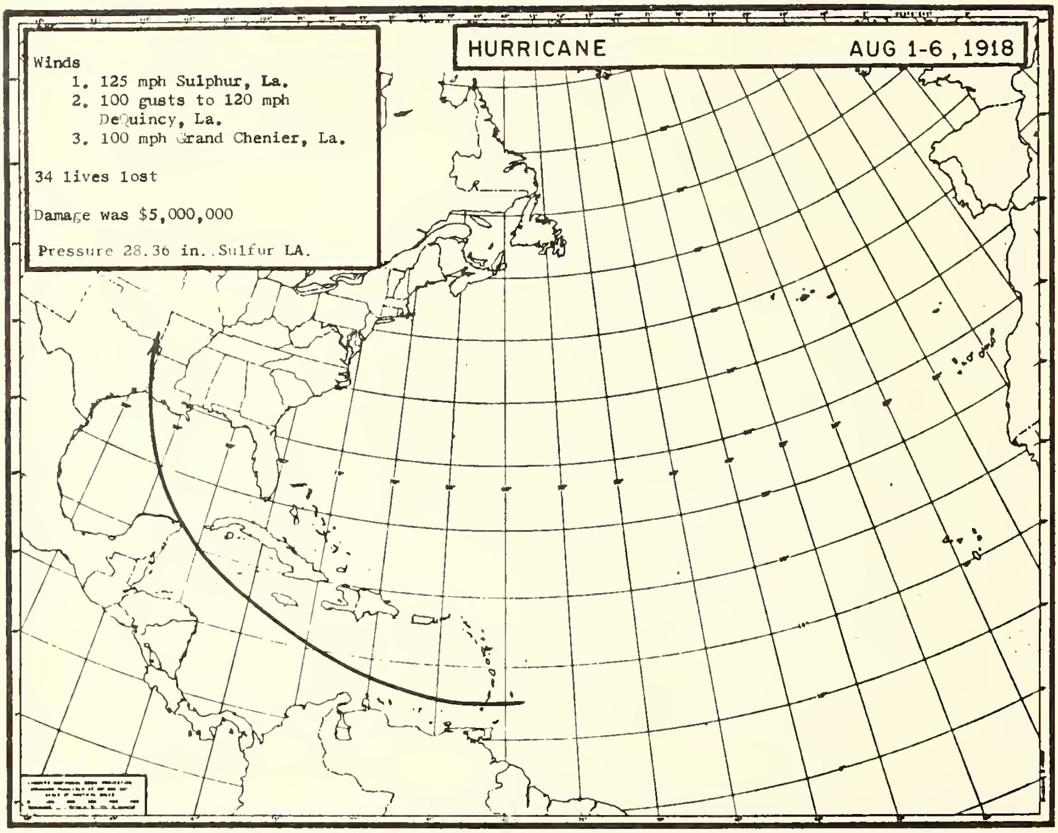

HURRICANE AUG 1-6, 1918

Winds
1. 125 mph Sulphur, La.
2. 100 gusts to 120 mph DeQuincy, La.
3. 100 mph Grand Chenier, La.

34 lives lost

Damage was $5,000,000

Pressure 28.36 in. Sulfur LA.

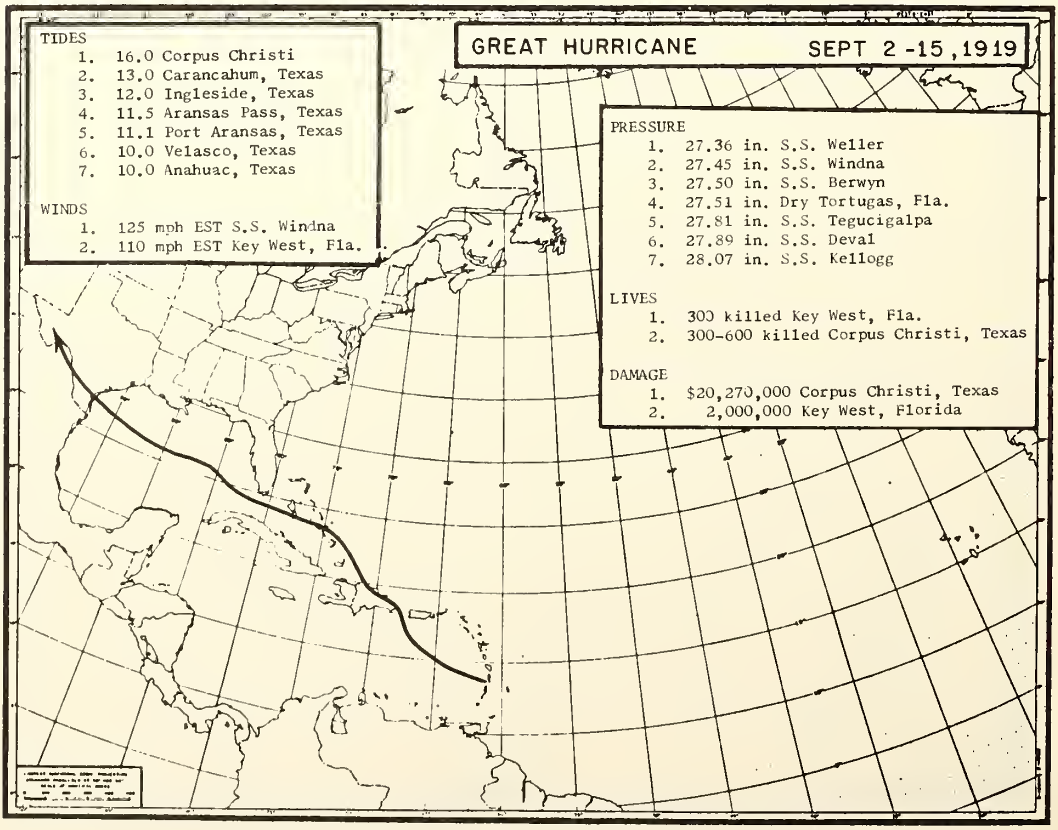

GREAT HURRICANE SEPT 2-15, 1919

TIDES
1. 16.0 Corpus Christi
2. 13.0 Carancahum, Texas
3. 12.0 Ingleside, Texas
4. 11.5 Aransas Pass, Texas
5. 11.1 Port Aransas, Texas
6. 10.0 Velasco, Texas
7. 10.0 Anahuac, Texas

WINDS
1. 125 mph EST S.S. Windna
2. 110 mph EST Key West, Fla.

PRESSURE
1. 27.36 in. S.S. Weller
2. 27.45 in. S.S. Windna
3. 27.50 in. S.S. Berwyn
4. 27.51 in. Dry Tortugas, Fla.
5. 27.81 in. S.S. Tegucigalpa
6. 27.89 in. S.S. Deval
7. 28.07 in. S.S. Kellogg

LIVES
1. 300 killed Key West, Fla.
2. 300-600 killed Corpus Christi, Texas

DAMAGE
1. $20,270,000 Corpus Christi, Texas
2. 2,000,000 Key West, Florida

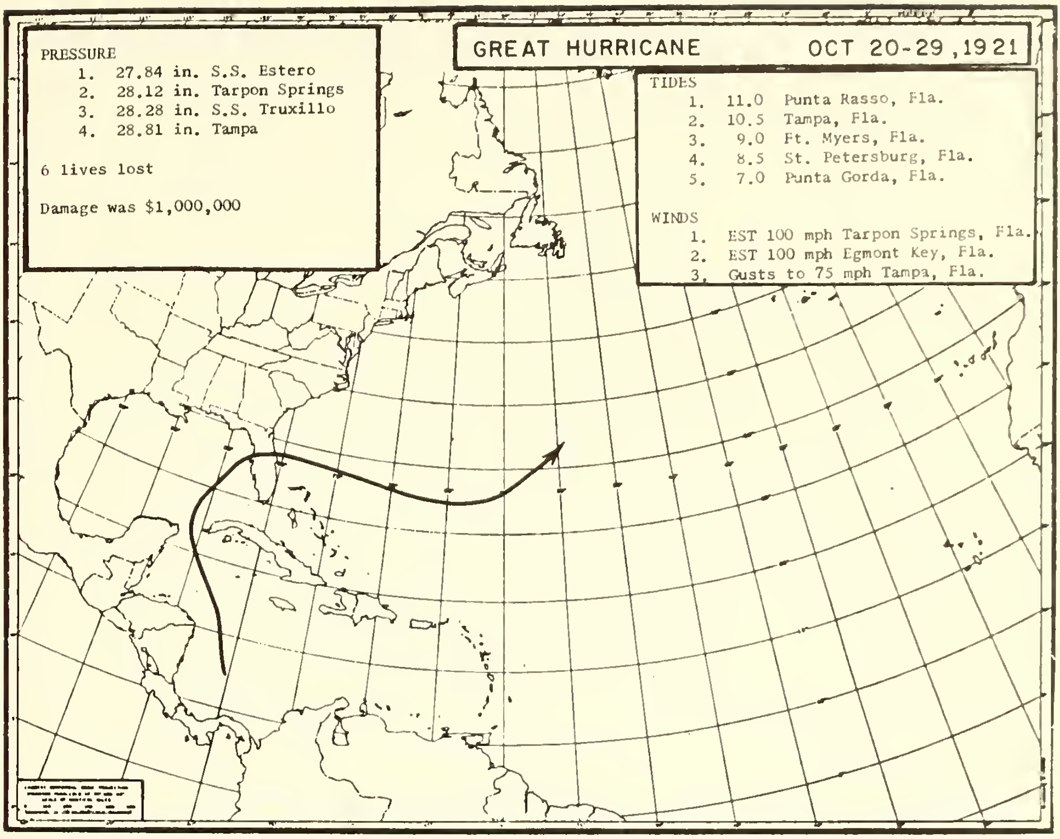

GREAT HURRICANE OCT 20-29, 1921

PRESSURE
1. 27.84 in. S.S. Estero
2. 28.12 in. Tarpon Springs
3. 28.28 in. S.S. Truxillo
4. 28.81 in. Tampa

6 lives lost

Damage was $1,000,000

TIDES
1. 11.0 Punta Rasso, Fla.
2. 10.5 Tampa, Fla.
3. 9.0 Ft. Myers, Fla.
4. 8.5 St. Petersburg, Fla.
5. 7.0 Punta Gorda, Fla.

WINDS
1. EST 100 mph Tarpon Springs, Fla.
2. EST 100 mph Egmont Key, Fla.
3. Gusts to 75 mph Tampa, Fla.

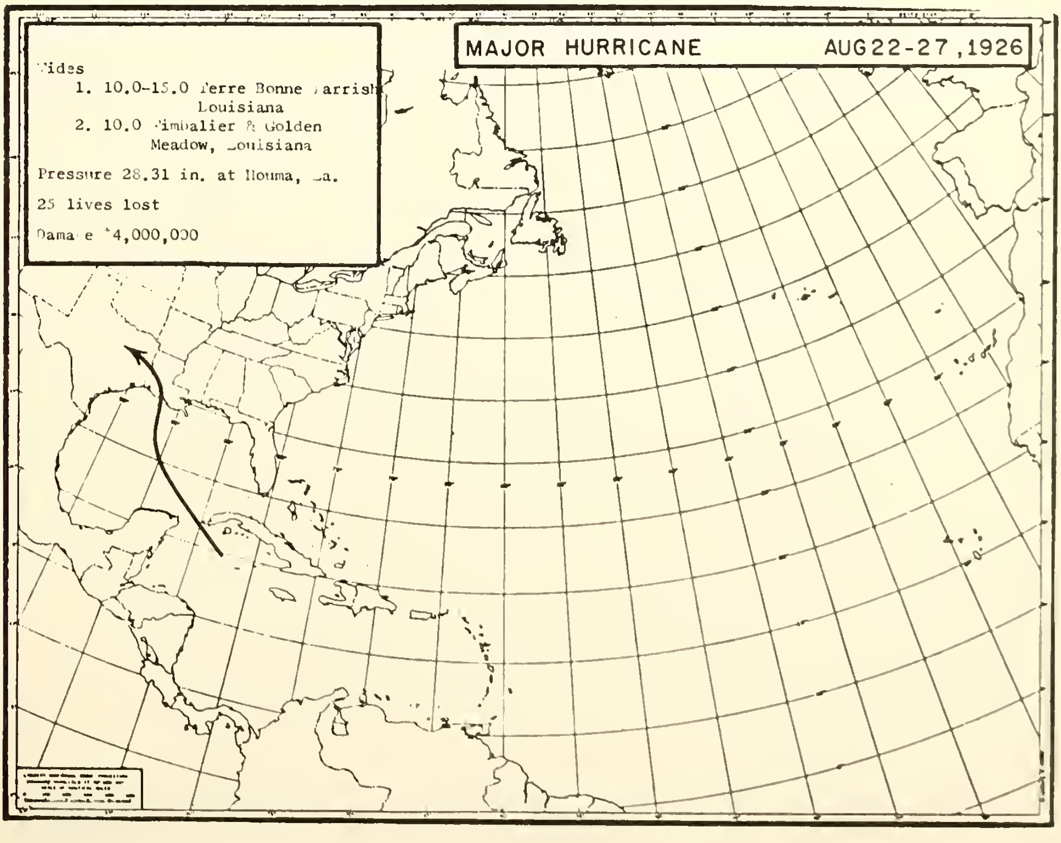

MAJOR HURRICANE AUG 22-27, 1926

Tides
1. 10.0-15.0 Terre Bonne Parrish Louisiana
2. 10.0 Timbalier & Golden Meadow, Louisiana

Pressure 28.31 in. at Houma, La.

25 lives lost

Damage $4,000,000

GREAT HURRICANE SEPT 11-22, 1926

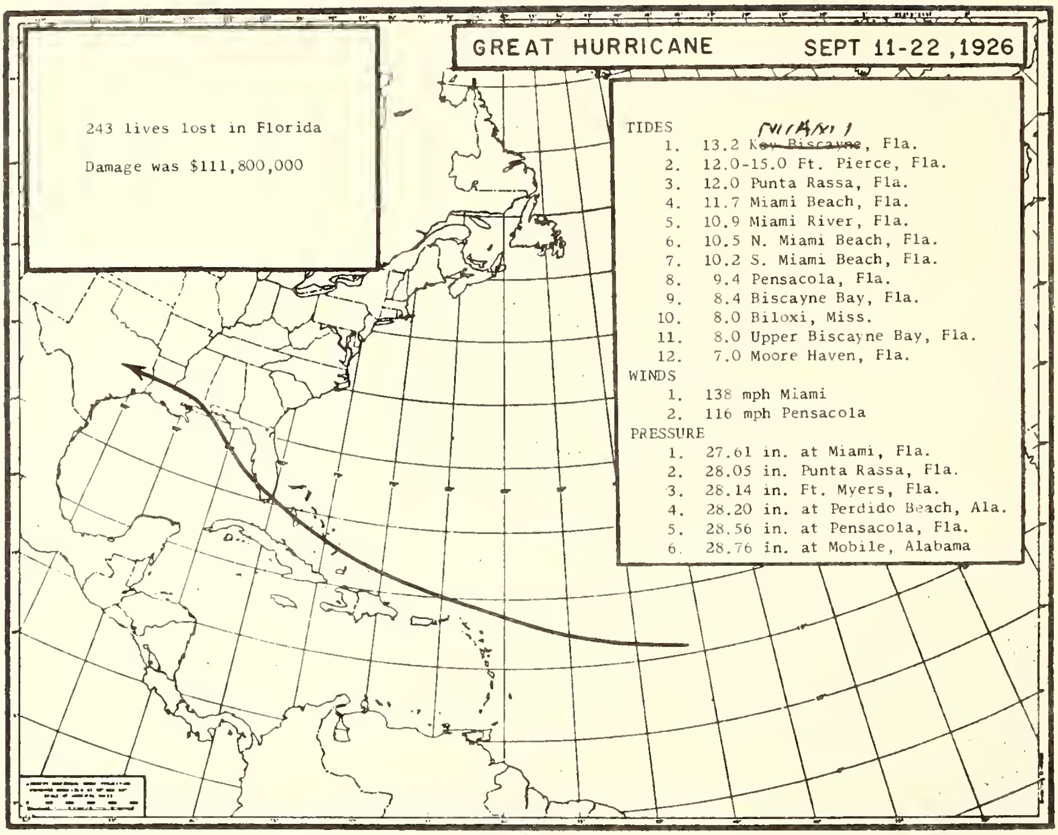

243 lives lost in Florida

Damage was $111,800,000

TIDES
1. 13.2 ~~Key Biscayne~~ MIAMI, Fla.
2. 12.0-15.0 Ft. Pierce, Fla.
3. 12.0 Punta Rassa, Fla.
4. 11.7 Miami Beach, Fla.
5. 10.9 Miami River, Fla.
6. 10.5 N. Miami Beach, Fla.
7. 10.2 S. Miami Beach, Fla.
8. 9.4 Pensacola, Fla.
9. 8.4 Biscayne Bay, Fla.
10. 8.0 Biloxi, Miss.
11. 8.0 Upper Biscayne Bay, Fla.
12. 7.0 Moore Haven, Fla.

WINDS
1. 138 mph Miami
2. 116 mph Pensacola

PRESSURE
1. 27.61 in. at Miami, Fla.
2. 28.05 in. Punta Rassa, Fla.
3. 28.14 in. Ft. Myers, Fla.
4. 28.20 in. at Perdido Beach, Ala.
5. 28.56 in. at Pensacola, Fla.
6. 28.76 in. at Mobile, Alabama

GREAT HURRICANE SEPT 6-20, 1928

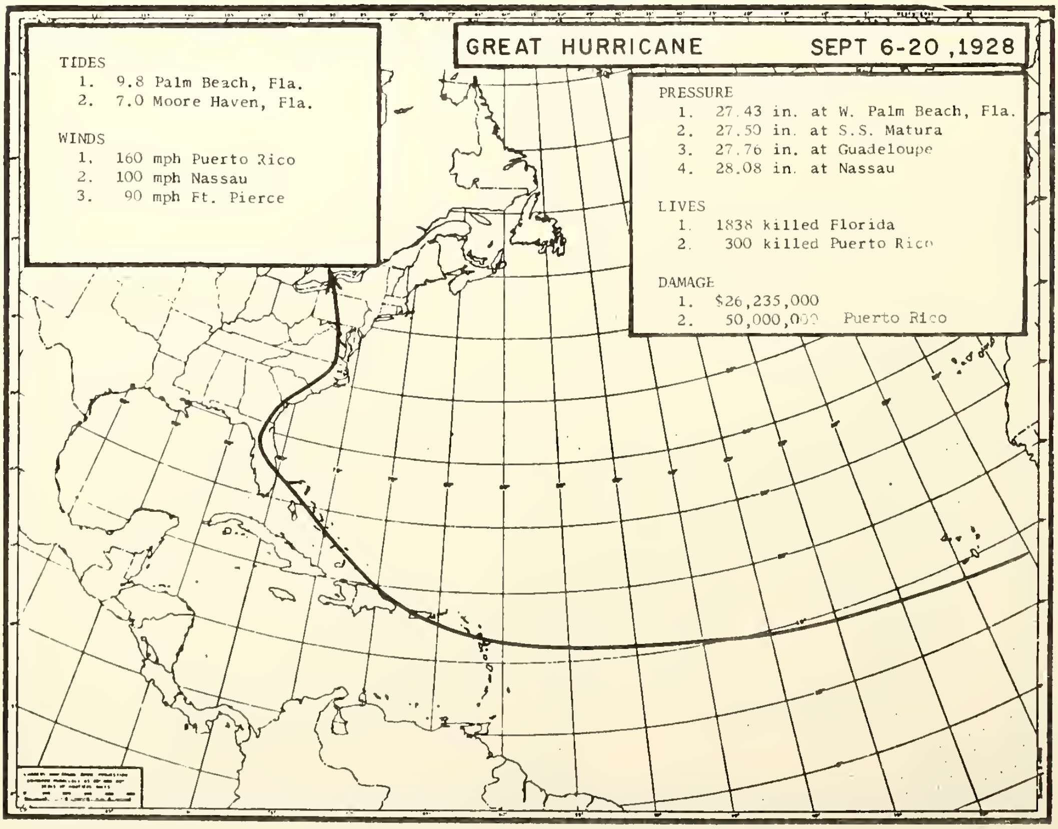

TIDES
1. 9.8 Palm Beach, Fla.
2. 7.0 Moore Haven, Fla.

WINDS
1. 160 mph Puerto Rico
2. 100 mph Nassau
3. 90 mph Ft. Pierce

PRESSURE
1. 27.43 in. at W. Palm Beach, Fla.
2. 27.50 in. at S.S. Matura
3. 27.76 in. at Guadeloupe
4. 28.08 in. at Nassau

LIVES
1. 1838 killed Florida
2. 300 killed Puerto Rico

DAMAGE
1. $26,235,000
2. 50,000,000 Puerto Rico

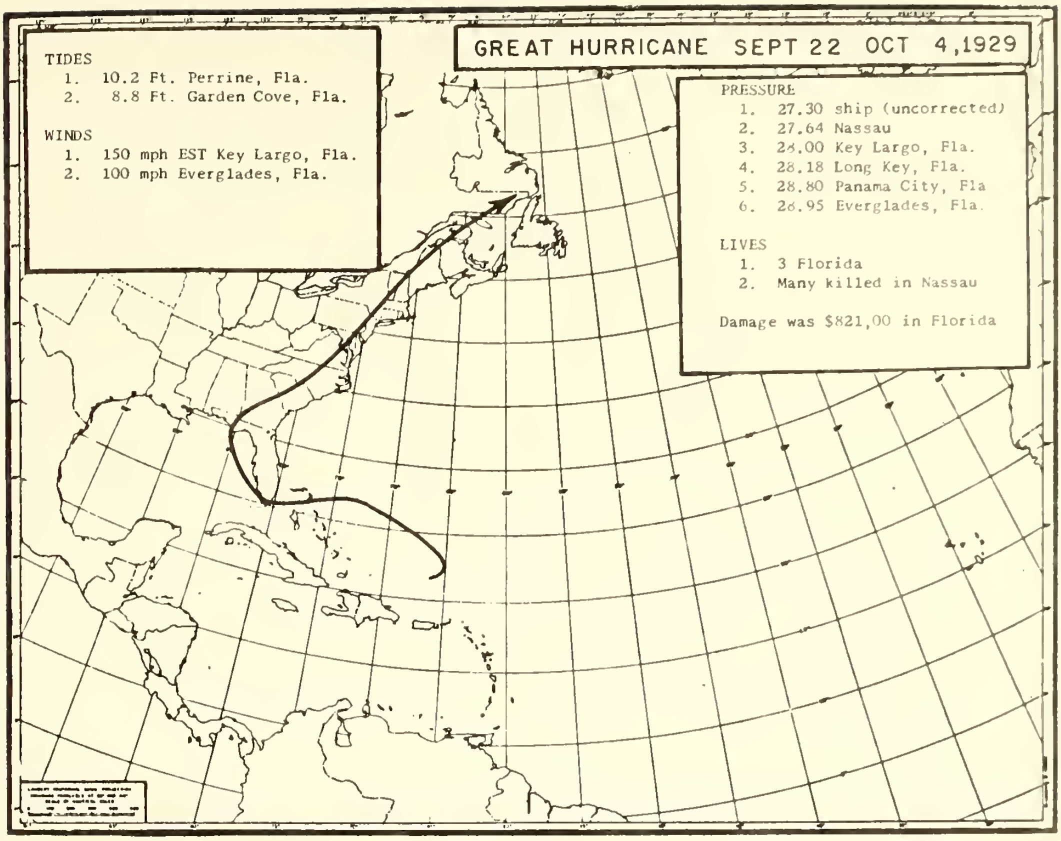

GREAT HURRICANE SEPT 22 OCT 4,1929

TIDES
1. 10.2 Ft. Perrine, Fla.
2. 8.8 Ft. Garden Cove, Fla.

WINDS
1. 150 mph EST Key Largo, Fla.
2. 100 mph Everglades, Fla.

PRESSURE
1. 27.30 ship (uncorrected)
2. 27.64 Nassau
3. 28.00 Key Largo, Fla.
4. 28.18 Long Key, Fla.
5. 28.80 Panama City, Fla
6. 28.95 Everglades, Fla.

LIVES
1. 3 Florida
2. Many killed in Nassau

Damage was $821,00 in Florida

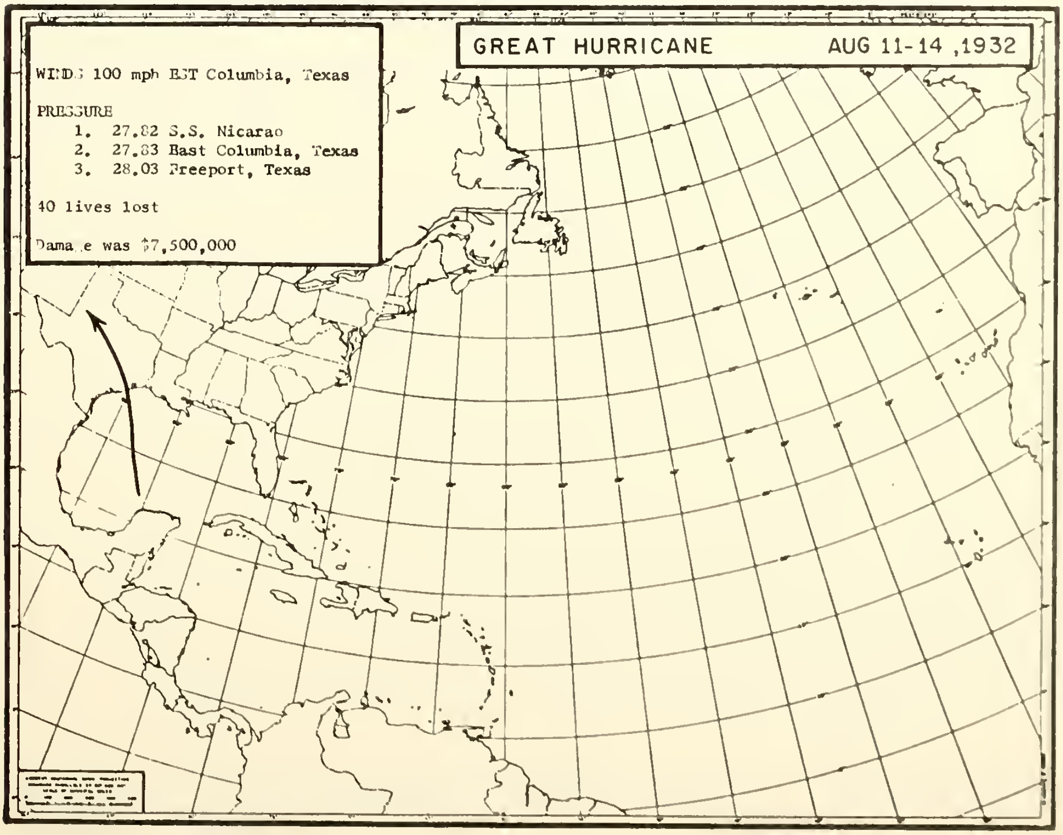

GREAT HURRICANE AUG 11-14 ,1932

WINDS 100 mph EST Columbia, Texas

PRESSURE
1. 27.82 S.S. Nicarao
2. 27.83 East Columbia, Texas
3. 28.03 Freeport, Texas

40 lives lost

Damage was $7,500,000

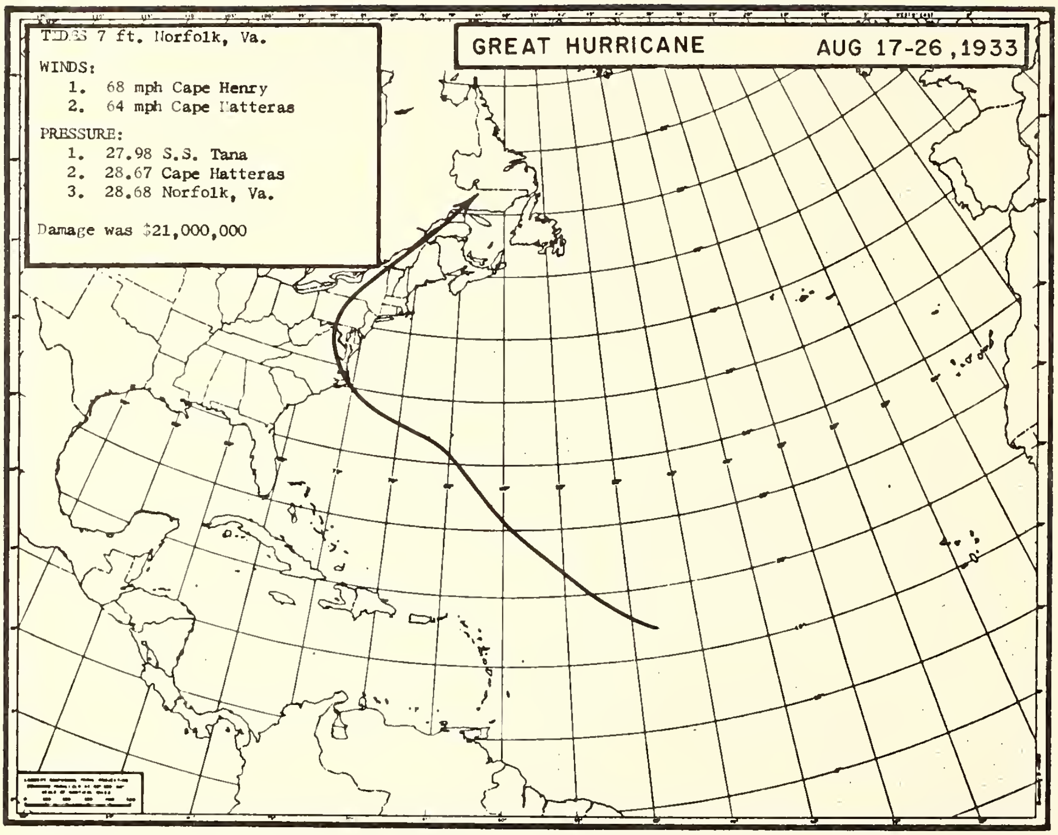

GREAT HURRICANE AUG 17-26, 1933

TIDES 7 ft. Norfolk, Va.

WINDS:
1. 68 mph Cape Henry
2. 64 mph Cape Hatteras

PRESSURE:
1. 27.98 S.S. Tana
2. 28.67 Cape Hatteras
3. 28.68 Norfolk, Va.

Damage was $21,000,000

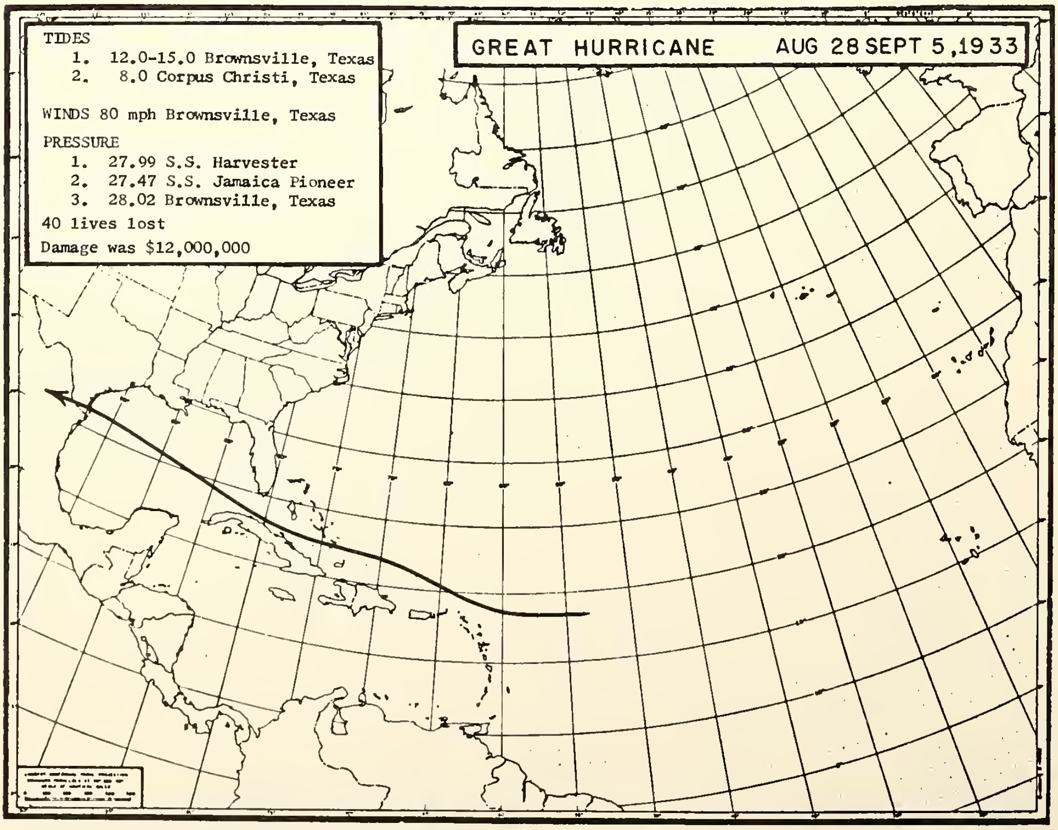

GREAT HURRICANE AUG 28 SEPT 5, 1933

TIDES
1. 12.0-15.0 Brownsville, Texas
2. 8.0 Corpus Christi, Texas

WINDS 80 mph Brownsville, Texas

PRESSURE
1. 27.99 S.S. Harvester
2. 27.47 S.S. Jamaica Pioneer
3. 28.02 Brownsville, Texas

40 lives lost

Damage was $12,000,000

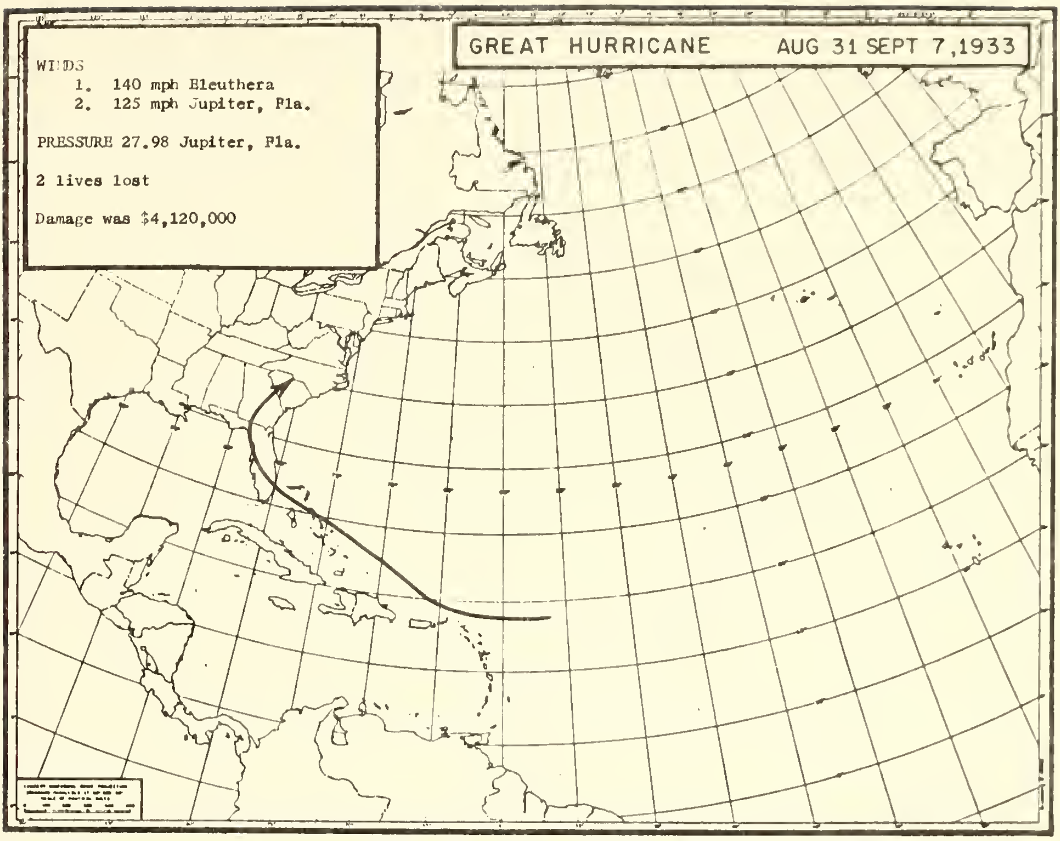

GREAT HURRICANE AUG 31 SEPT 7,1933

WINDS
1. 140 mph Eleuthera
2. 125 mph Jupiter, Fla.

PRESSURE 27.98 Jupiter, Fla.

2 lives lost

Damage was $4,120,000

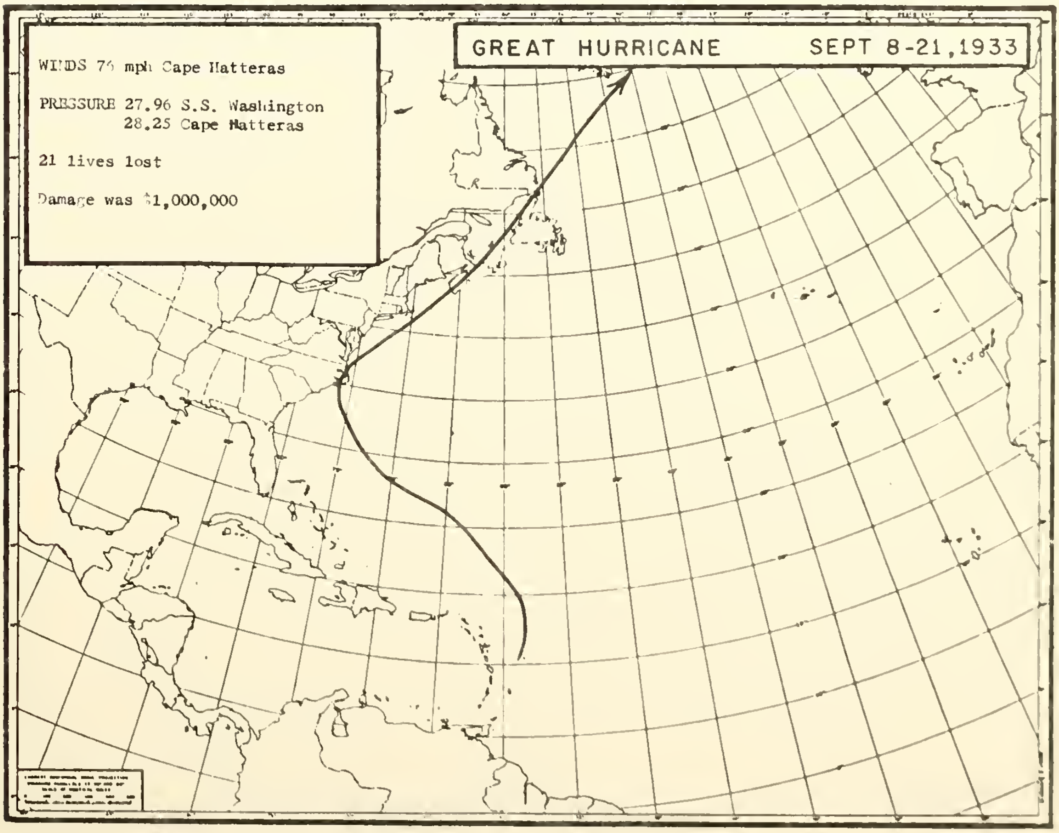

GREAT HURRICANE SEPT 8-21,1933

WINDS 76 mph Cape Hatteras

PRESSURE 27.96 S.S. Washington
28.25 Cape Hatteras

21 lives lost

Damage was $1,000,000

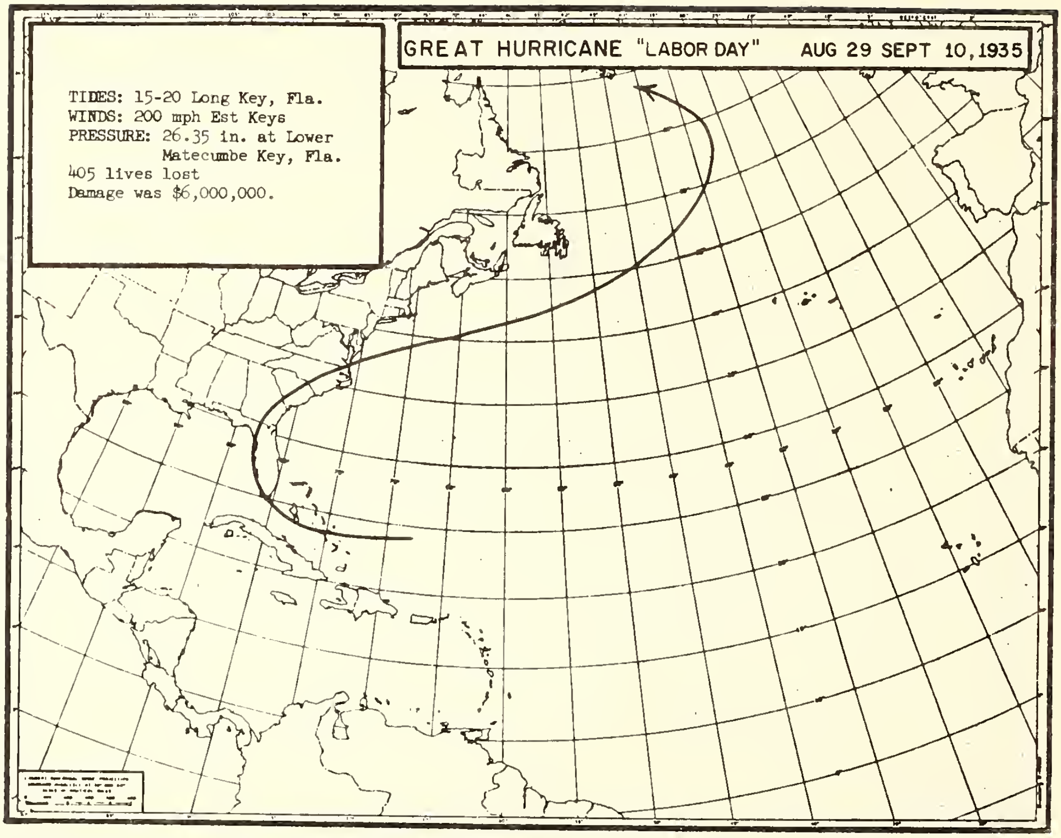

GREAT HURRICANE "LABOR DAY" AUG 29 SEPT 10,1935

TIDES: 15-20 Long Key, Fla.
WINDS: 200 mph Est Keys
PRESSURE: 26.35 in. at Lower
Matecumbe Key, Fla.
405 lives lost
Damage was $6,000,000.

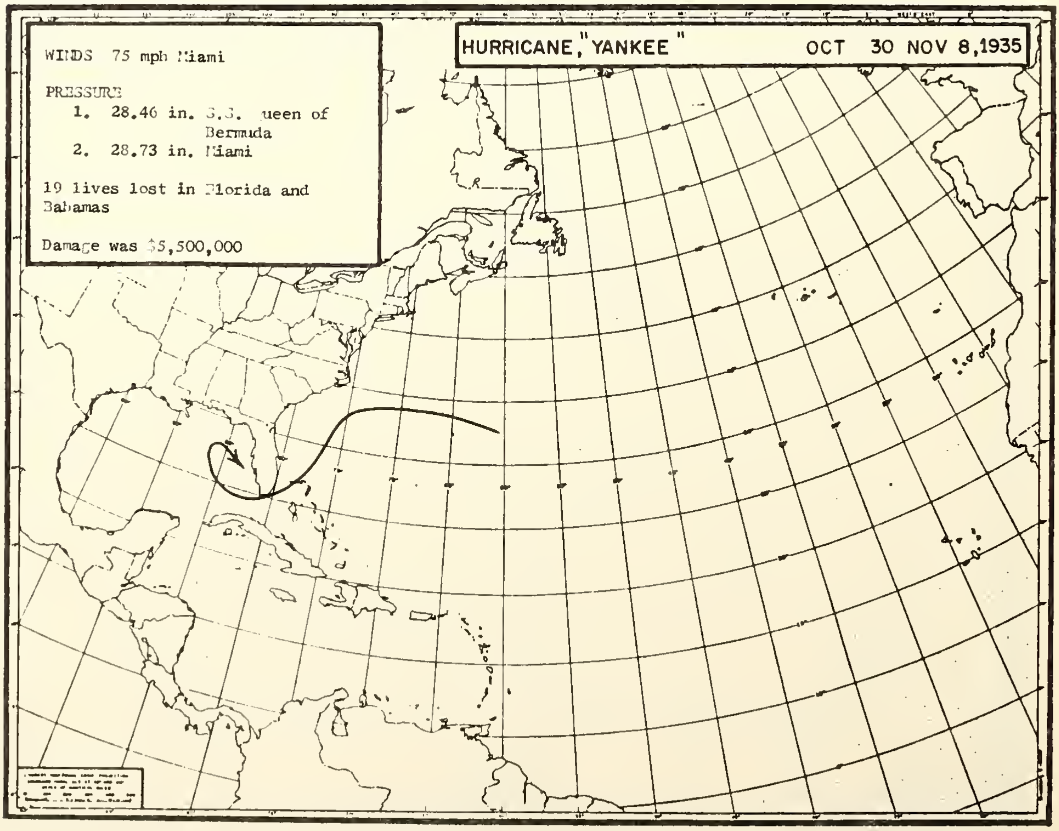

HURRICANE, "YANKEE" OCT 30 NOV 8,1935

WINDS 75 mph Miami

PRESSURE
1. 28.46 in. S.S. Queen of Bermuda
2. 28.73 in. Miami

19 lives lost in Florida and Bahamas

Damage was $5,500,000

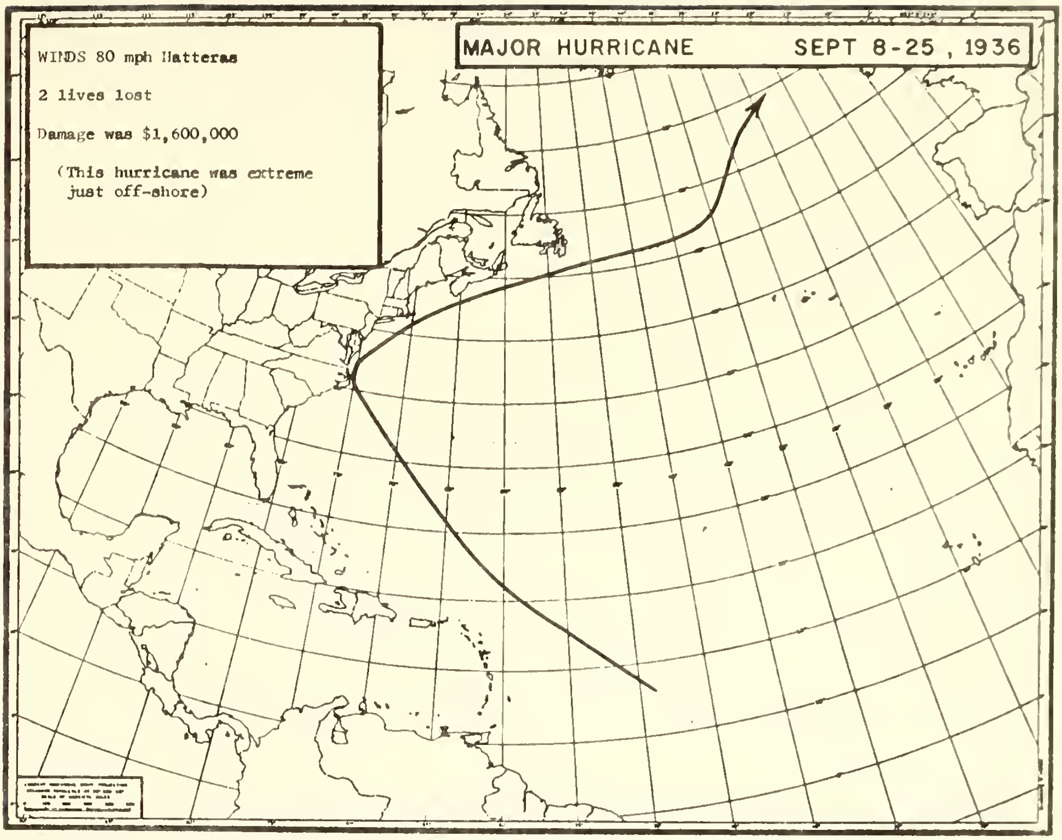

MAJOR HURRICANE SEPT 8-25, 1936

WINDS 80 mph Hatteras

2 lives lost

Damage was $1,600,000

(This hurricane was extreme just off-shore)

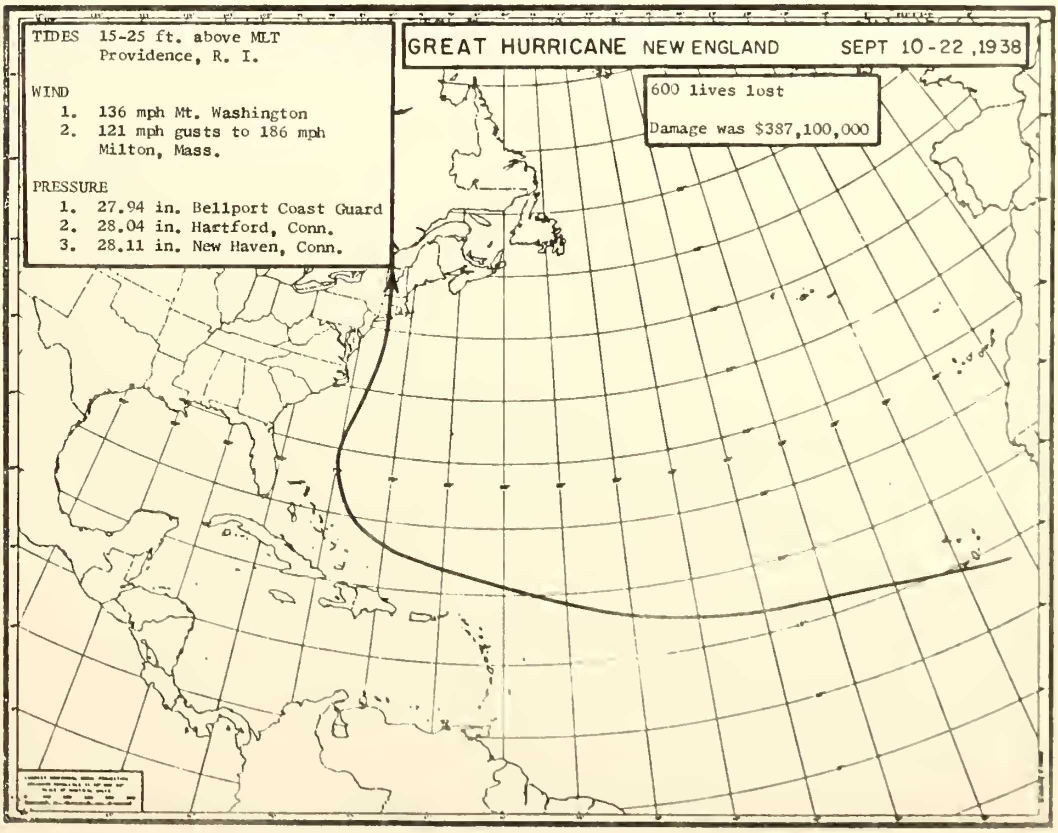

GREAT HURRICANE NEW ENGLAND SEPT 10-22, 1938

TIDES 15-25 ft. above MLT Providence, R. I.

WIND
1. 136 mph Mt. Washington
2. 121 mph gusts to 186 mph Milton, Mass.

PRESSURE
1. 27.94 in. Bellport Coast Guard
2. 28.04 in. Hartford, Conn.
3. 28.11 in. New Haven, Conn.

600 lives lost

Damage was $387,100,000

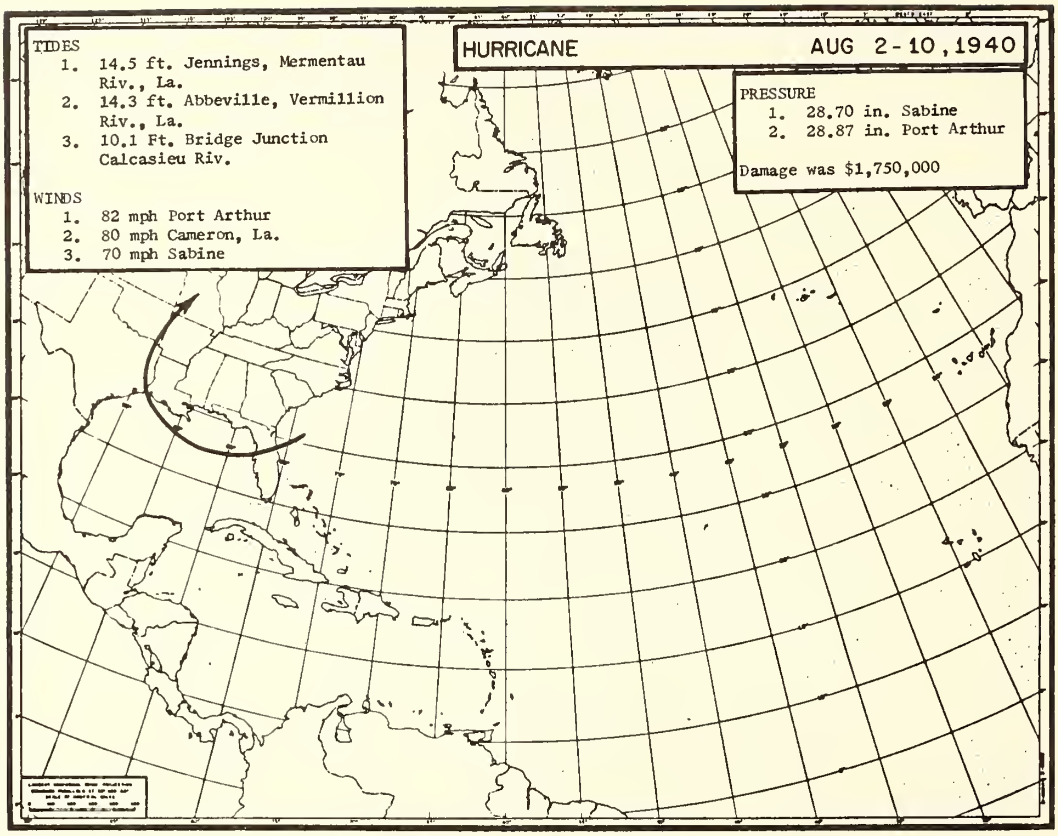

HURRICANE AUG 2-10,1940

TIDES
1. 14.5 ft. Jennings, Mermentau Riv., La.
2. 14.3 ft. Abbeville, Vermillion Riv., La.
3. 10.1 Ft. Bridge Junction Calcasieu Riv.

WINDS
1. 82 mph Port Arthur
2. 80 mph Cameron, La.
3. 70 mph Sabine

PRESSURE
1. 28.70 in. Sabine
2. 28.87 in. Port Arthur

Damage was $1,750,000

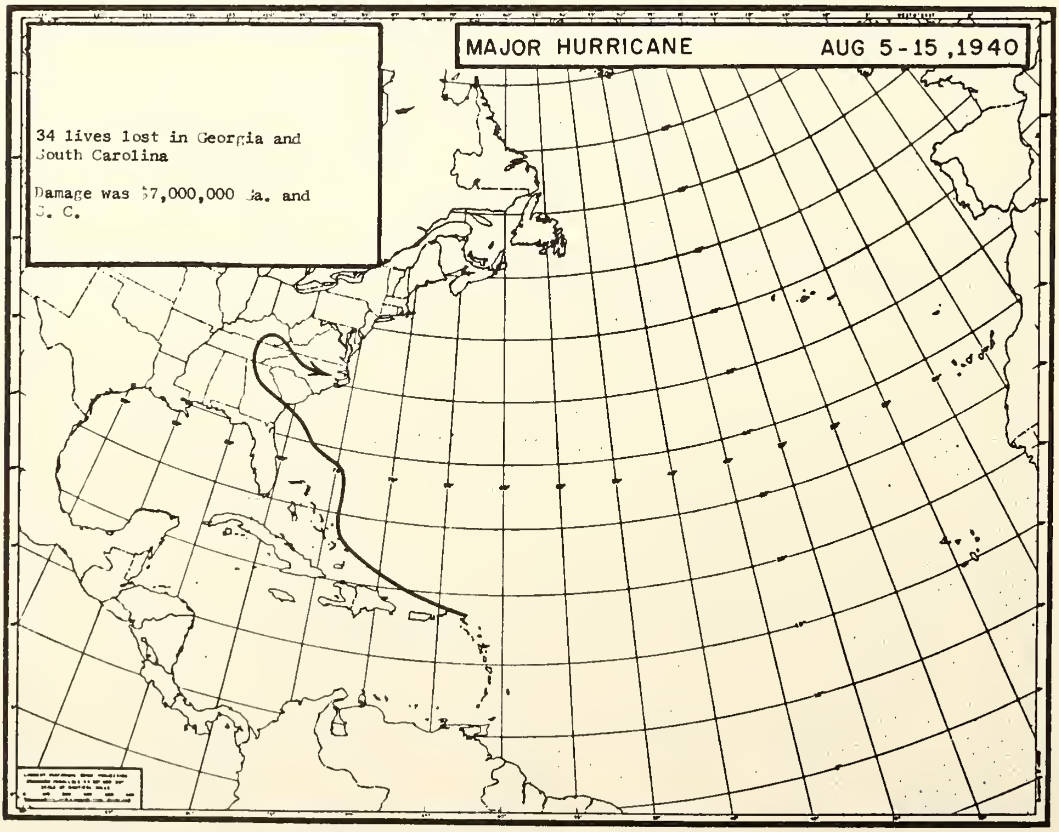

MAJOR HURRICANE AUG 5-15,1940

34 lives lost in Georgia and South Carolina

Damage was $7,000,000 Ga. and S. C.

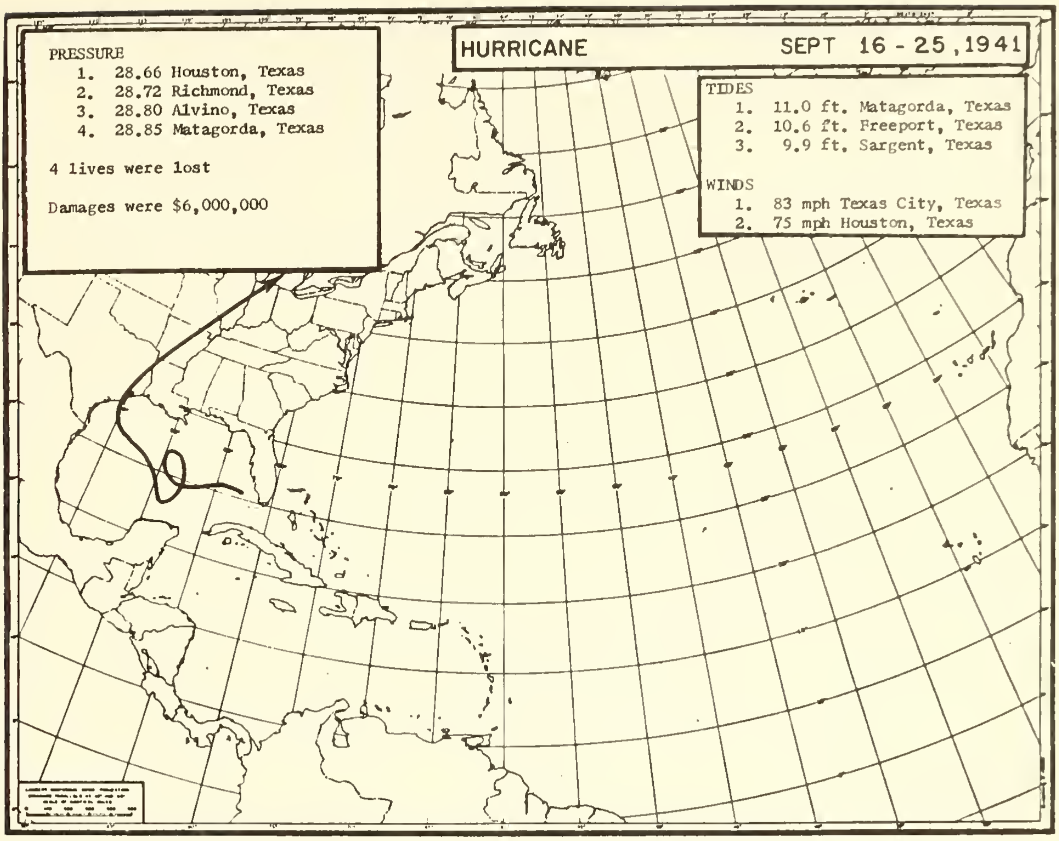

HURRICANE SEPT 16 - 25, 1941

PRESSURE
1. 28.66 Houston, Texas
2. 28.72 Richmond, Texas
3. 28.80 Alvino, Texas
4. 28.85 Matagorda, Texas

4 lives were lost

Damages were $6,000,000

TIDES
1. 11.0 ft. Matagorda, Texas
2. 10.6 ft. Freeport, Texas
3. 9.9 ft. Sargent, Texas

WINDS
1. 83 mph Texas City, Texas
2. 75 mph Houston, Texas

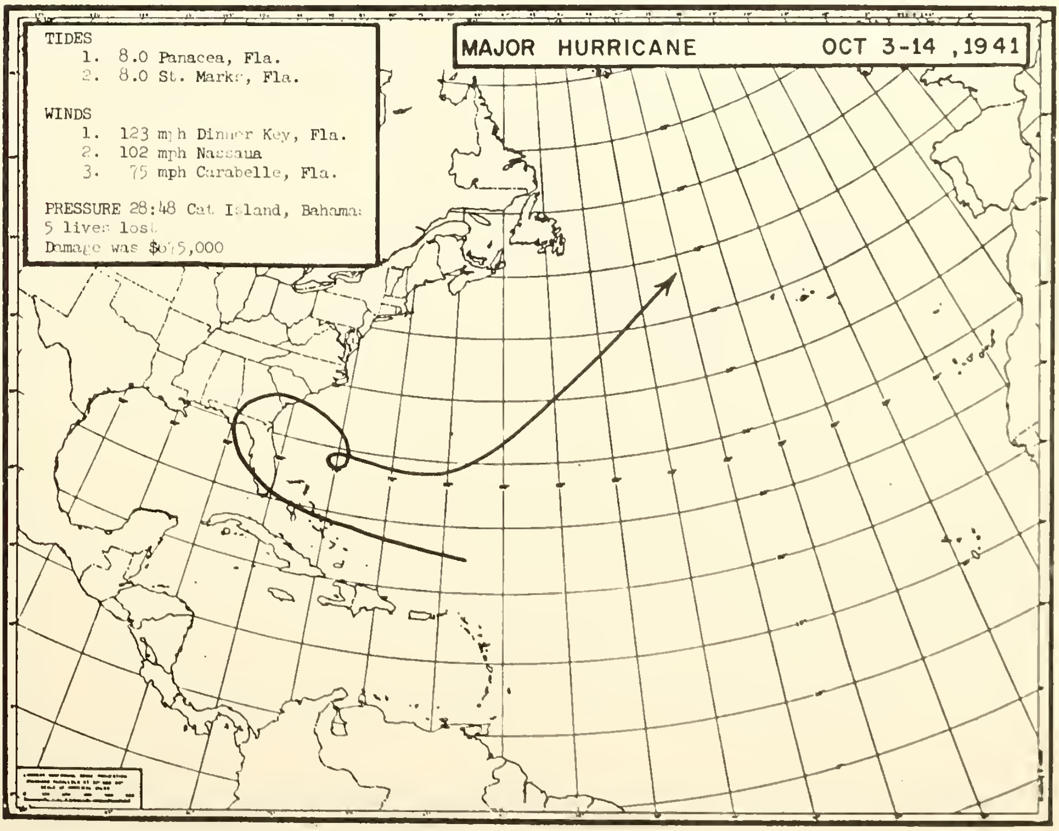

MAJOR HURRICANE OCT 3-14, 1941

TIDES
1. 8.0 Panacea, Fla.
2. 8.0 St. Marks, Fla.

WINDS
1. 123 mph Dinner Key, Fla.
2. 102 mph Nassaua
3. 75 mph Carabelle, Fla.

PRESSURE 28:48 Cat Island, Bahamas
5 lives lost
Damage was $675,000

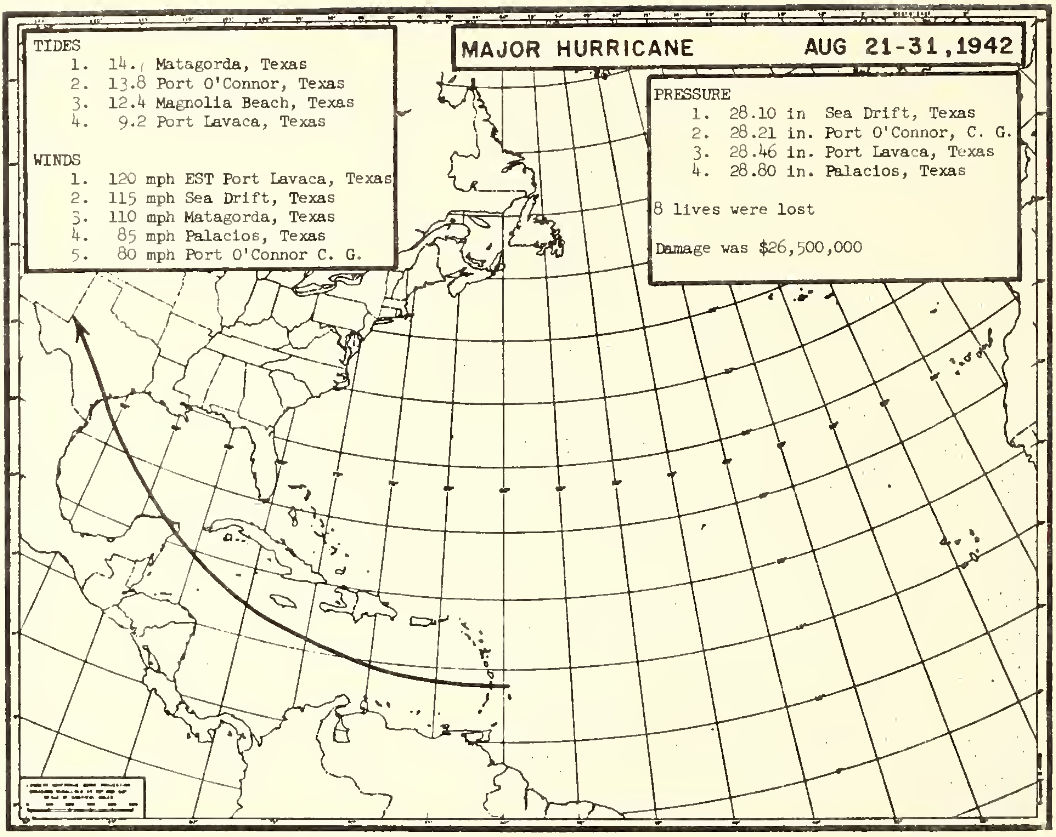

MAJOR HURRICANE AUG 21-31,1942

TIDES
1. 14.7 Matagorda, Texas
2. 13.8 Port O'Connor, Texas
3. 12.4 Magnolia Beach, Texas
4. 9.2 Port Lavaca, Texas

WINDS
1. 120 mph EST Port Lavaca, Texas
2. 115 mph Sea Drift, Texas
3. 110 mph Matagorda, Texas
4. 85 mph Palacios, Texas
5. 80 mph Port O'Connor C. G.

PRESSURE
1. 28.10 in Sea Drift, Texas
2. 28.21 in. Port O'Connor, C. G.
3. 28.46 in. Port Lavaca, Texas
4. 28.80 in. Palacios, Texas

8 lives were lost

Damage was $26,500,000

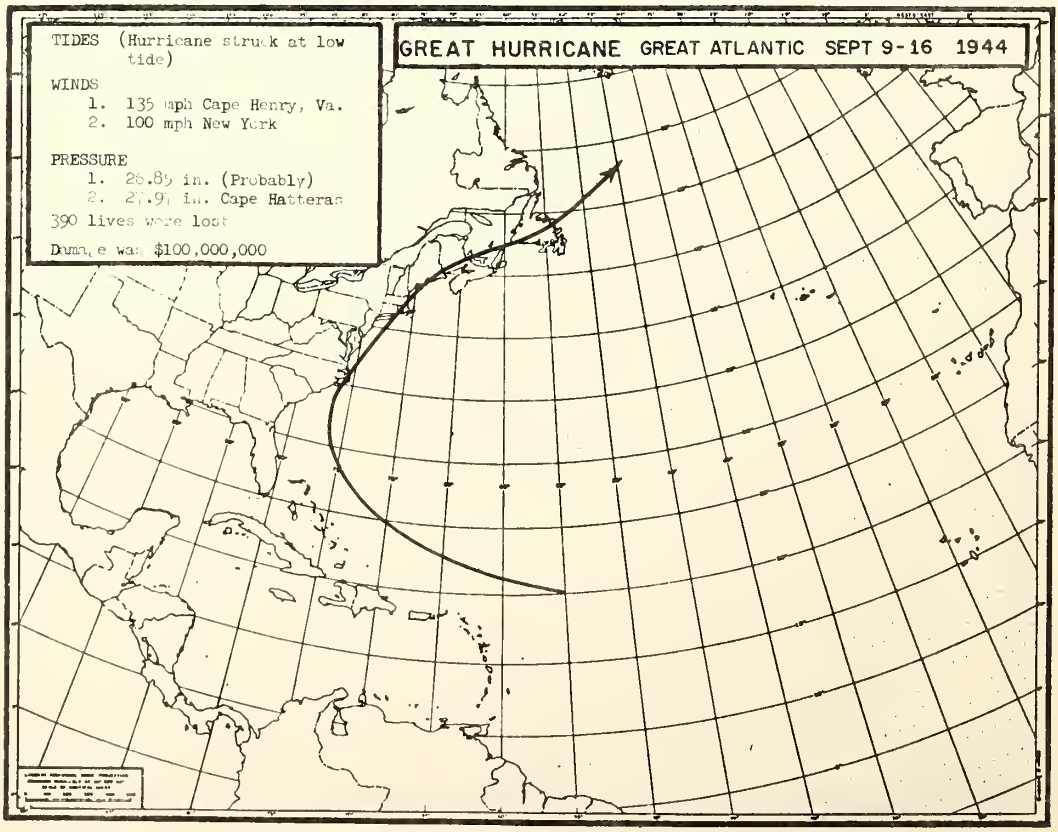

GREAT HURRICANE GREAT ATLANTIC SEPT 9-16 1944

TIDES (Hurricane struck at low tide)

WINDS
1. 135 mph Cape Henry, Va.
2. 100 mph New York

PRESSURE
1. 26.85 in. (Probably)
2. 27.97 in. Cape Hatteras

390 lives were lost

Damage was $100,000,000

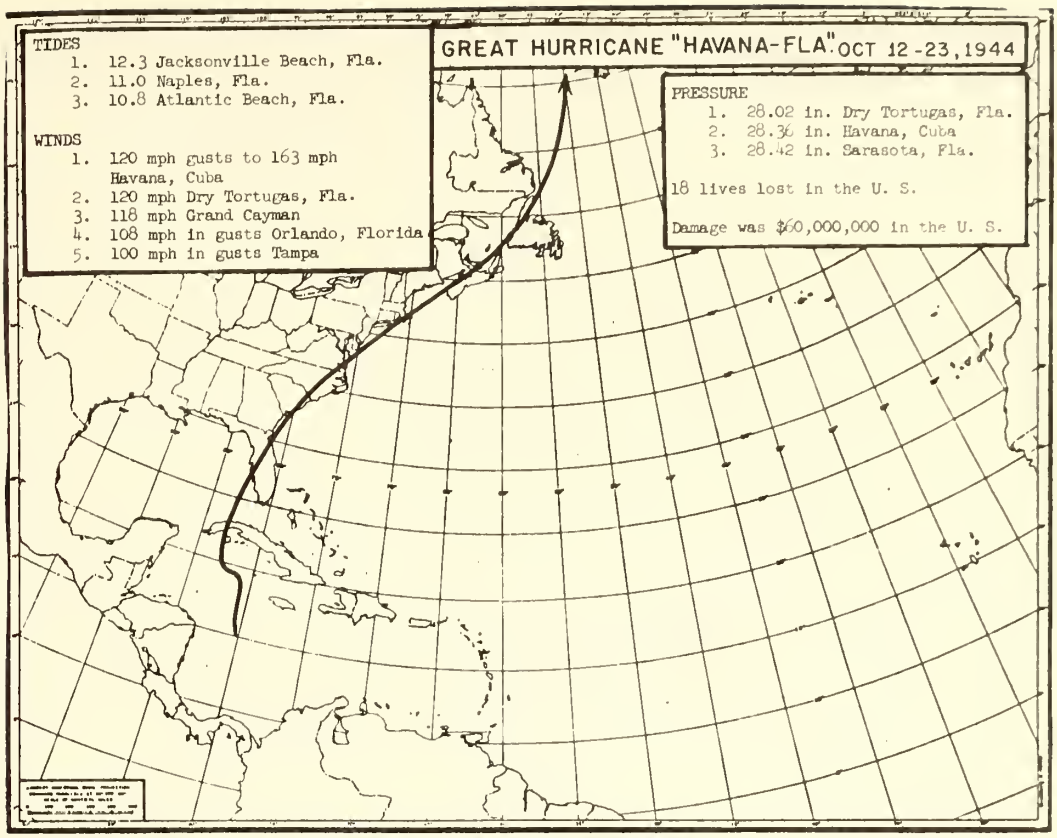

GREAT HURRICANE "HAVANA-FLA" OCT 12-23, 1944

TIDES
1. 12.3 Jacksonville Beach, Fla.
2. 11.0 Naples, Fla.
3. 10.8 Atlantic Beach, Fla.

WINDS
1. 120 mph gusts to 163 mph Havana, Cuba
2. 120 mph Dry Tortugas, Fla.
3. 118 mph Grand Cayman
4. 108 mph in gusts Orlando, Florida
5. 100 mph in gusts Tampa

PRESSURE
1. 28.02 in. Dry Tortugas, Fla.
2. 28.36 in. Havana, Cuba
3. 28.42 in. Sarasota, Fla.

18 lives lost in the U. S.

Damage was $60,000,000 in the U. S.

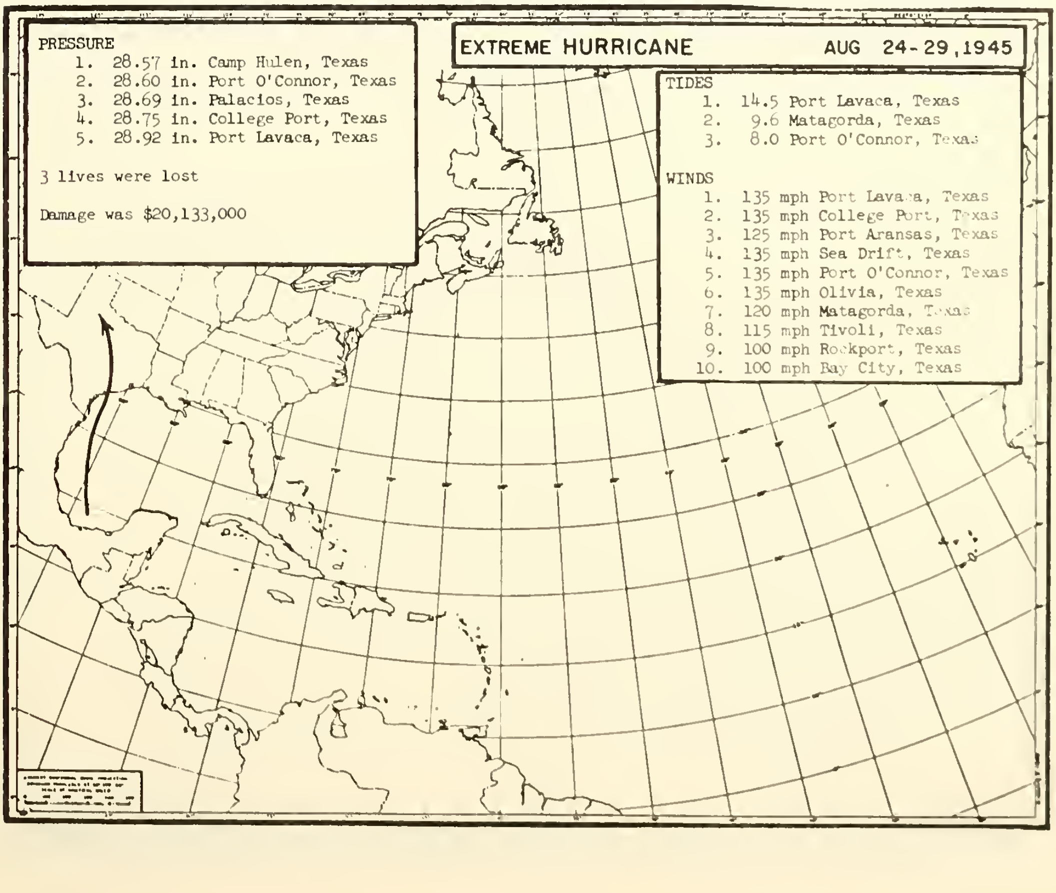

EXTREME HURRICANE AUG 24-29, 1945

PRESSURE
1. 28.57 in. Camp Hulen, Texas
2. 28.60 in. Port O'Connor, Texas
3. 28.69 in. Palacios, Texas
4. 28.75 in. College Port, Texas
5. 28.92 in. Port Lavaca, Texas

3 lives were lost

Damage was $20,133,000

TIDES
1. 14.5 Port Lavaca, Texas
2. 9.6 Matagorda, Texas
3. 8.0 Port O'Connor, Texas

WINDS
1. 135 mph Port Lavaca, Texas
2. 135 mph College Port, Texas
3. 125 mph Port Aransas, Texas
4. 135 mph Sea Drift, Texas
5. 135 mph Port O'Connor, Texas
6. 135 mph Olivia, Texas
7. 120 mph Matagorda, Texas
8. 115 mph Tivoli, Texas
9. 100 mph Rockport, Texas
10. 100 mph Bay City, Texas

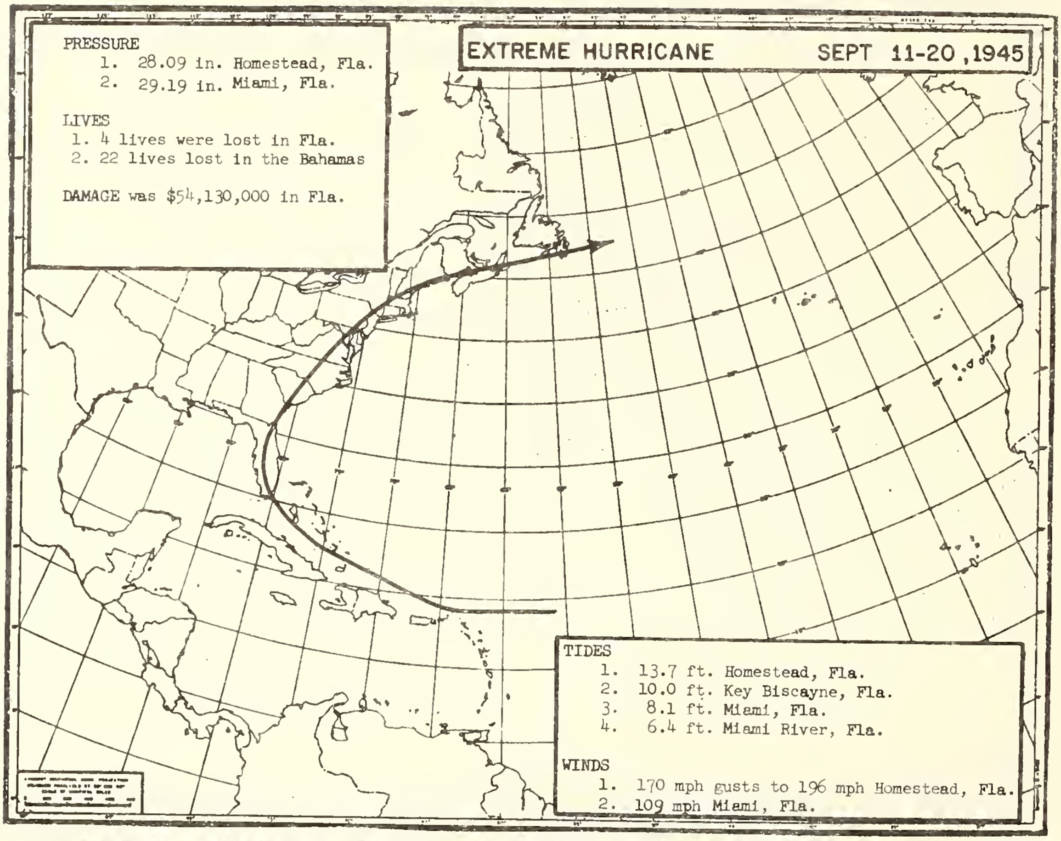

EXTREME HURRICANE SEPT 11-20, 1945

PRESSURE
1. 28.09 in. Homestead, Fla.
2. 29.19 in. Miami, Fla.

LIVES
1. 4 lives were lost in Fla.
2. 22 lives lost in the Bahamas

DAMAGE was $54,130,000 in Fla.

TIDES
1. 13.7 ft. Homestead, Fla.
2. 10.0 ft. Key Biscayne, Fla.
3. 8.1 ft. Miami, Fla.
4. 6.4 ft. Miami River, Fla.

WINDS
1. 170 mph gusts to 196 mph Homestead, Fla.
2. 109 mph Miami, Fla.

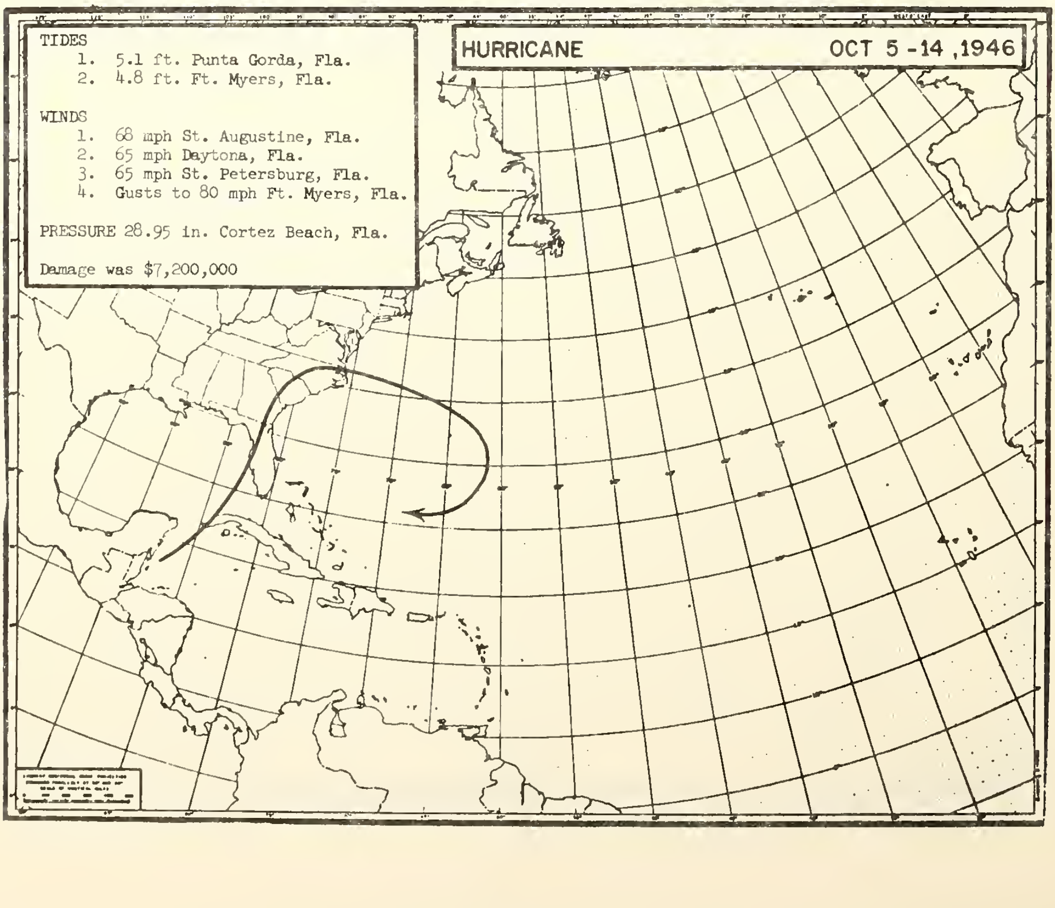

HURRICANE OCT 5 -14, 1946

TIDES
1. 5.1 ft. Punta Gorda, Fla.
2. 4.8 ft. Ft. Myers, Fla.

WINDS
1. 68 mph St. Augustine, Fla.
2. 65 mph Daytona, Fla.
3. 65 mph St. Petersburg, Fla.
4. Gusts to 80 mph Ft. Myers, Fla.

PRESSURE 28.95 in. Cortez Beach, Fla.

Damage was $7,200,000

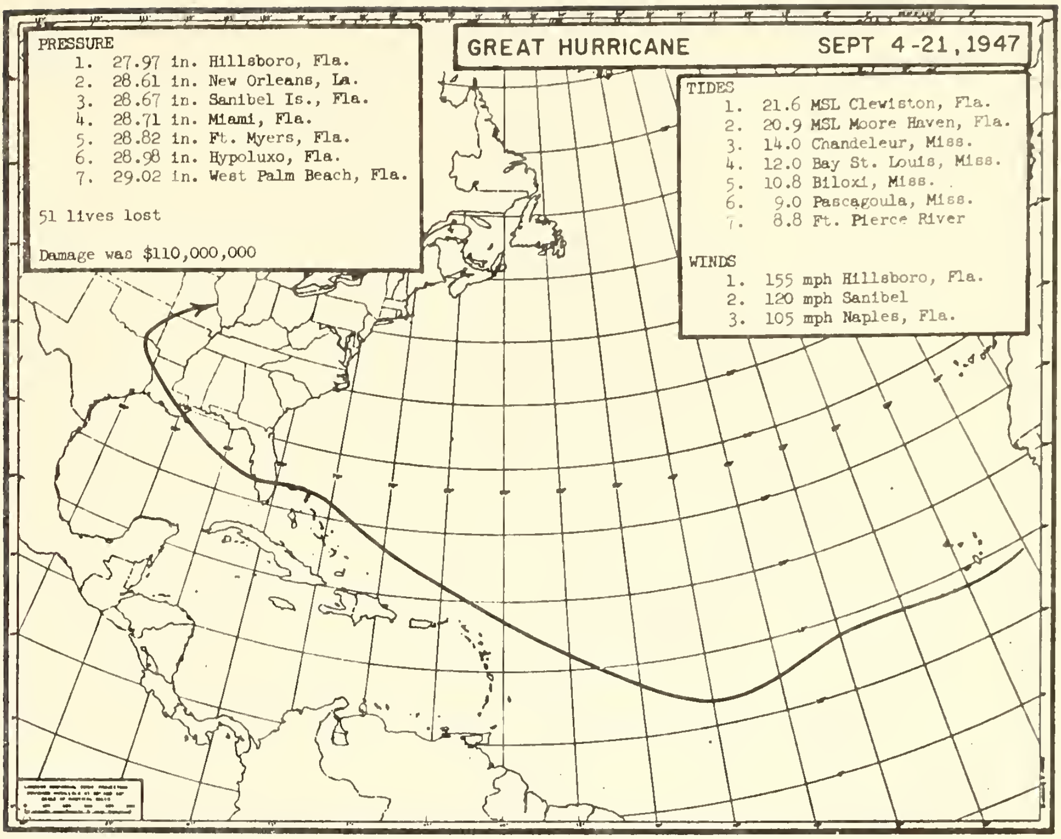

GREAT HURRICANE SEPT 4-21, 1947

PRESSURE
1. 27.97 in. Hillsboro, Fla.
2. 28.61 in. New Orleans, La.
3. 28.67 in. Sanibel Is., Fla.
4. 28.71 in. Miami, Fla.
5. 28.82 in. Ft. Myers, Fla.
6. 28.98 in. Hypoluxo, Fla.
7. 29.02 in. West Palm Beach, Fla.

51 lives lost

Damage was $110,000,000

TIDES
1. 21.6 MSL Clewiston, Fla.
2. 20.9 MSL Moore Haven, Fla.
3. 14.0 Chandeleur, Miss.
4. 12.0 Bay St. Louis, Miss.
5. 10.8 Biloxi, Miss.
6. 9.0 Pascagoula, Miss.
7. 8.8 Ft. Pierce River

WINDS
1. 155 mph Hillsboro, Fla.
2. 120 mph Sanibel
3. 105 mph Naples, Fla.

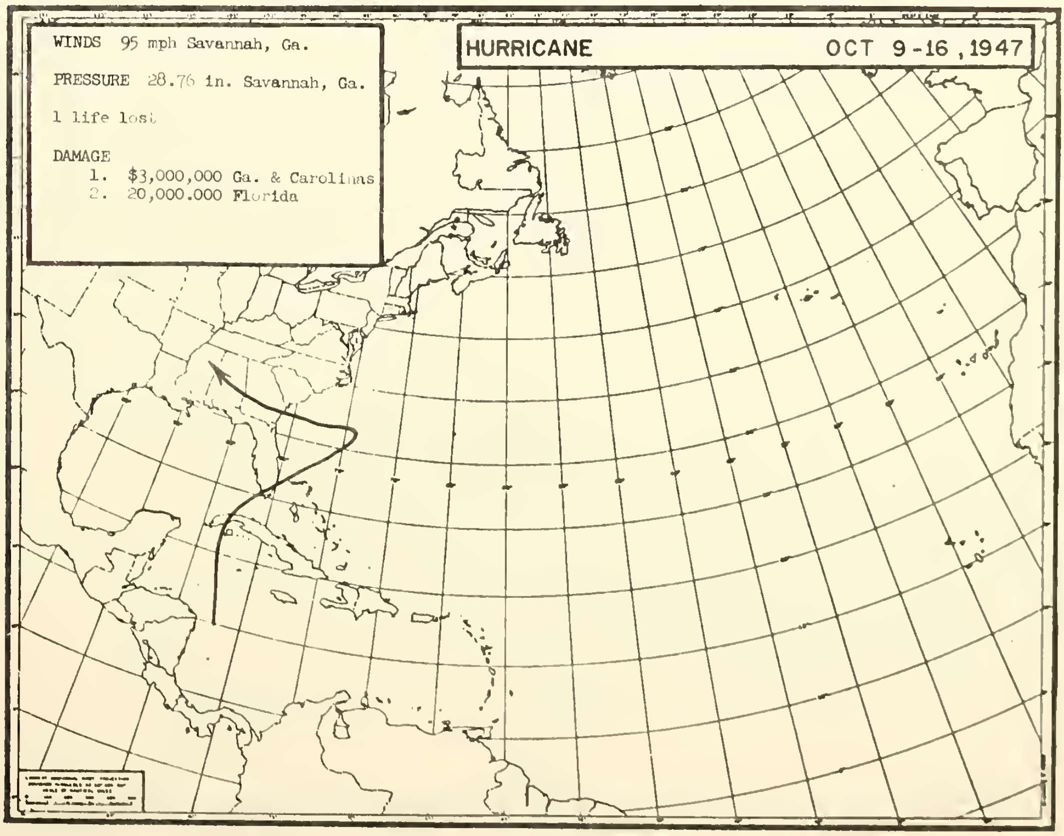

HURRICANE OCT 9-16, 1947

WINDS 95 mph Savannah, Ga.

PRESSURE 28.76 in. Savannah, Ga.

1 life lost

DAMAGE
1. $3,000,000 Ga. & Carolinas
2. 20,000.000 Florida

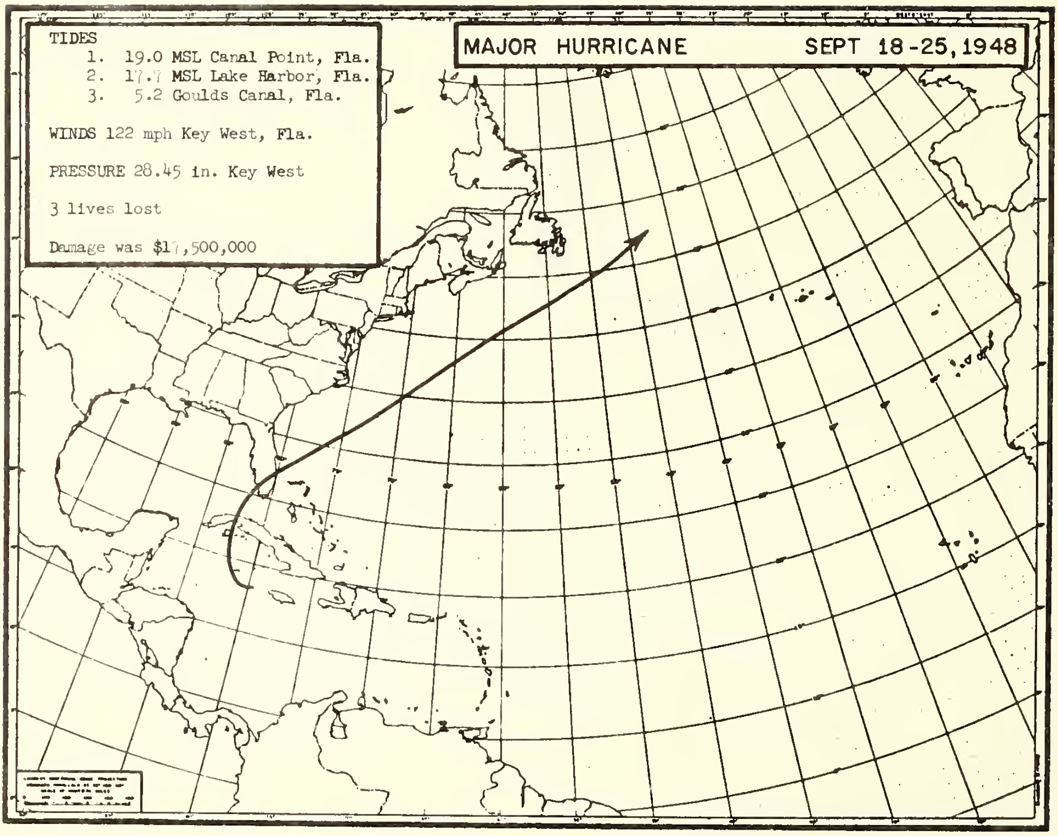

MAJOR HURRICANE SEPT 18-25,1948

TIDES
1. 19.0 MSL Canal Point, Fla.
2. 17.7 MSL Lake Harbor, Fla.
3. 5.2 Goulds Canal, Fla.

WINDS 122 mph Key West, Fla.

PRESSURE 28.45 in. Key West

3 lives lost

Damage was $17,500,000

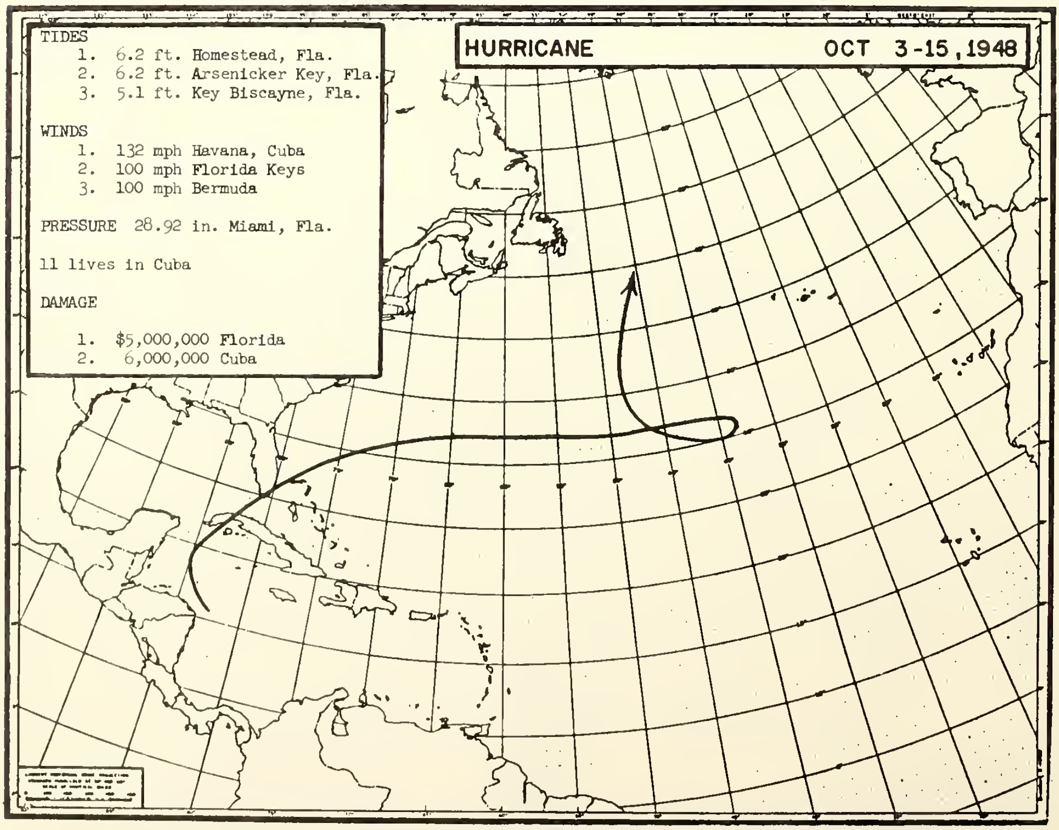

HURRICANE OCT 3-15,1948

TIDES
1. 6.2 ft. Homestead, Fla.
2. 6.2 ft. Arsenicker Key, Fla.
3. 5.1 ft. Key Biscayne, Fla.

WINDS
1. 132 mph Havana, Cuba
2. 100 mph Florida Keys
3. 100 mph Bermuda

PRESSURE 28.92 in. Miami, Fla.

11 lives in Cuba

DAMAGE

1. $5,000,000 Florida
2. 6,000,000 Cuba

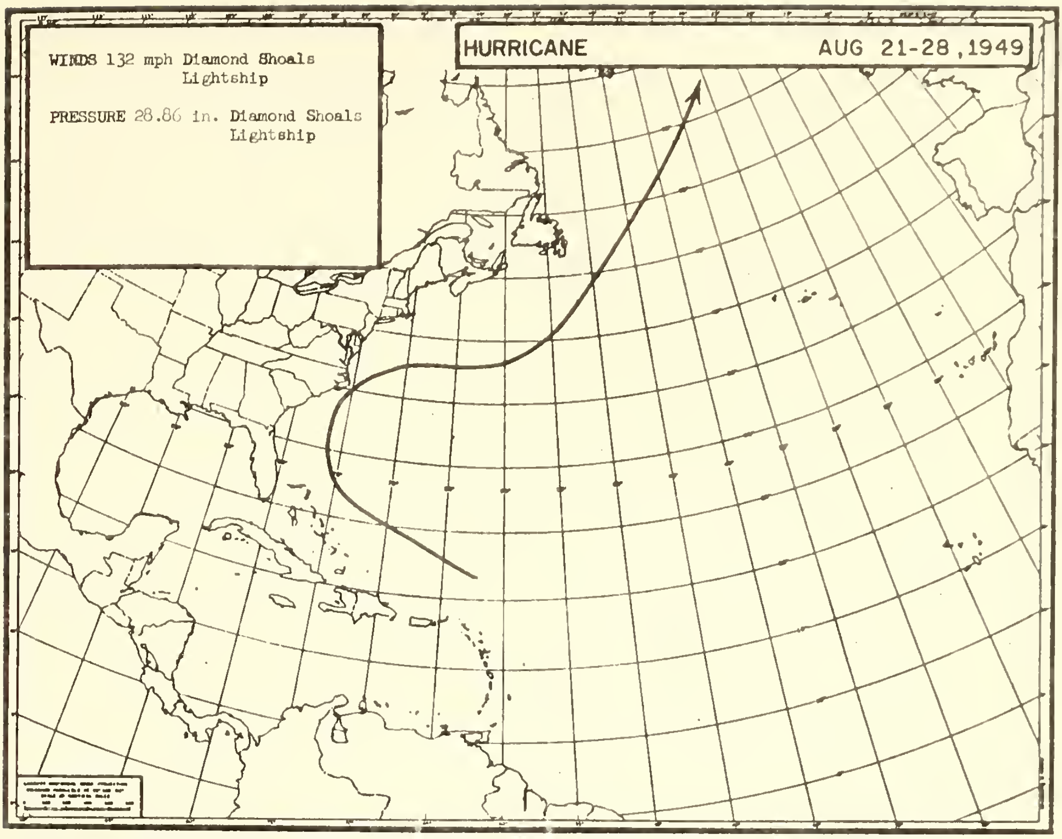

HURRICANE AUG 21-28,1949

WINDS 132 mph Diamond Shoals Lightship

PRESSURE 28.86 in. Diamond Shoals Lightship

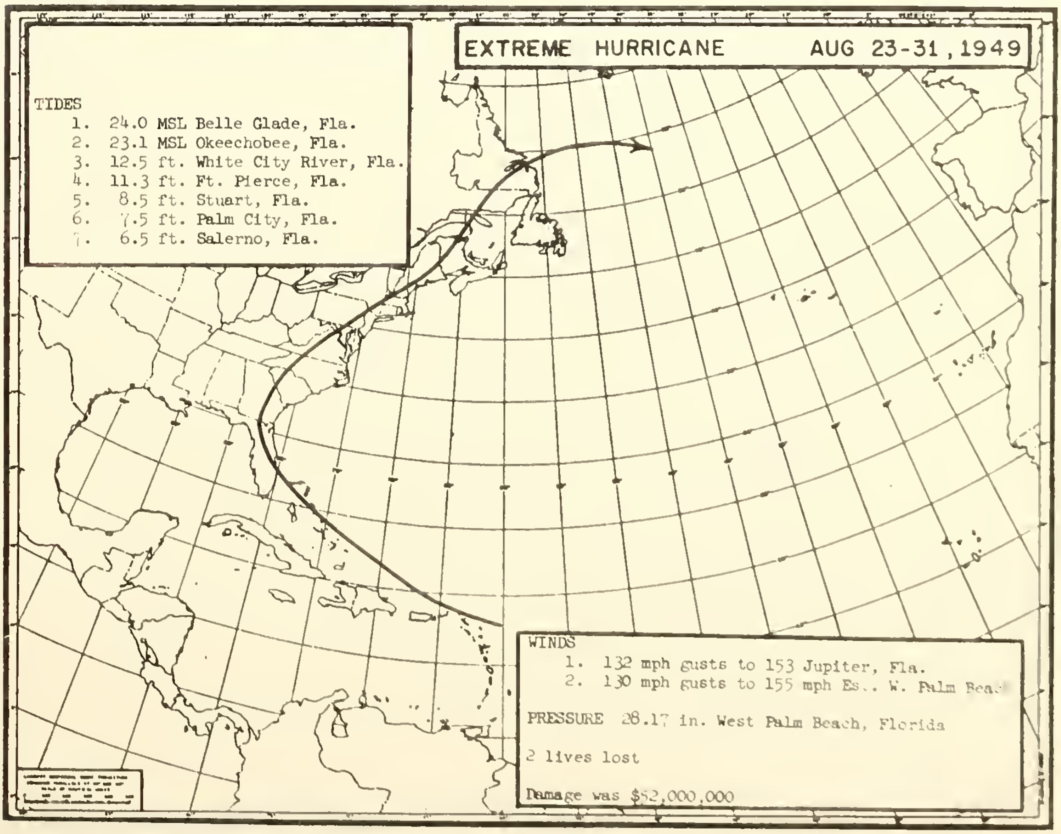

EXTREME HURRICANE AUG 23-31,1949

TIDES
1. 24.0 MSL Belle Glade, Fla.
2. 23.1 MSL Okeechobee, Fla.
3. 12.5 ft. White City River, Fla.
4. 11.3 ft. Ft. Pierce, Fla.
5. 8.5 ft. Stuart, Fla.
6. 7.5 ft. Palm City, Fla.
7. 6.5 ft. Salerno, Fla.

WINDS
1. 132 mph gusts to 153 Jupiter, Fla.
2. 130 mph gusts to 155 mph Es.. W. Palm Bea

PRESSURE 28.17 in. West Palm Beach, Florida

2 lives lost

Damage was $52,000,000

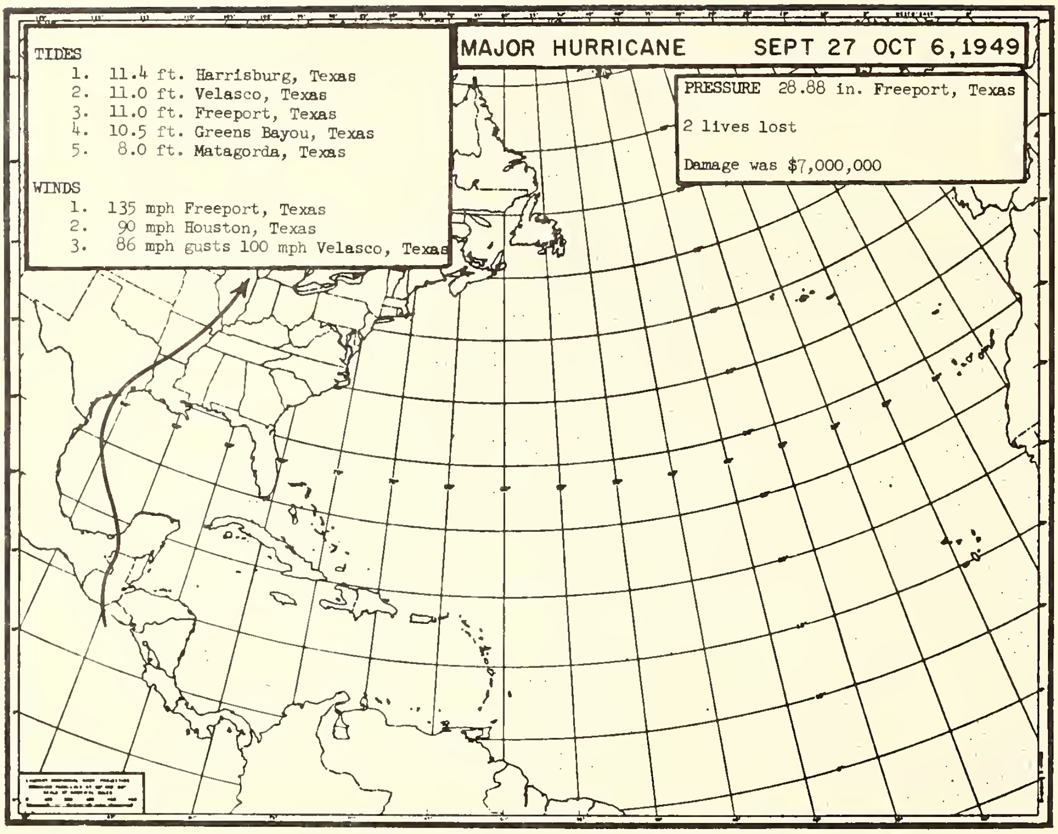

MAJOR HURRICANE SEPT 27 OCT 6,1949

TIDES
1. 11.4 ft. Harrisburg, Texas
2. 11.0 ft. Velasco, Texas
3. 11.0 ft. Freeport, Texas
4. 10.5 ft. Greens Bayou, Texas
5. 8.0 ft. Matagorda, Texas

WINDS
1. 135 mph Freeport, Texas
2. 90 mph Houston, Texas
3. 86 mph gusts 100 mph Velasco, Texas

PRESSURE 28.88 in. Freeport, Texas

2 lives lost

Damage was $7,000,000

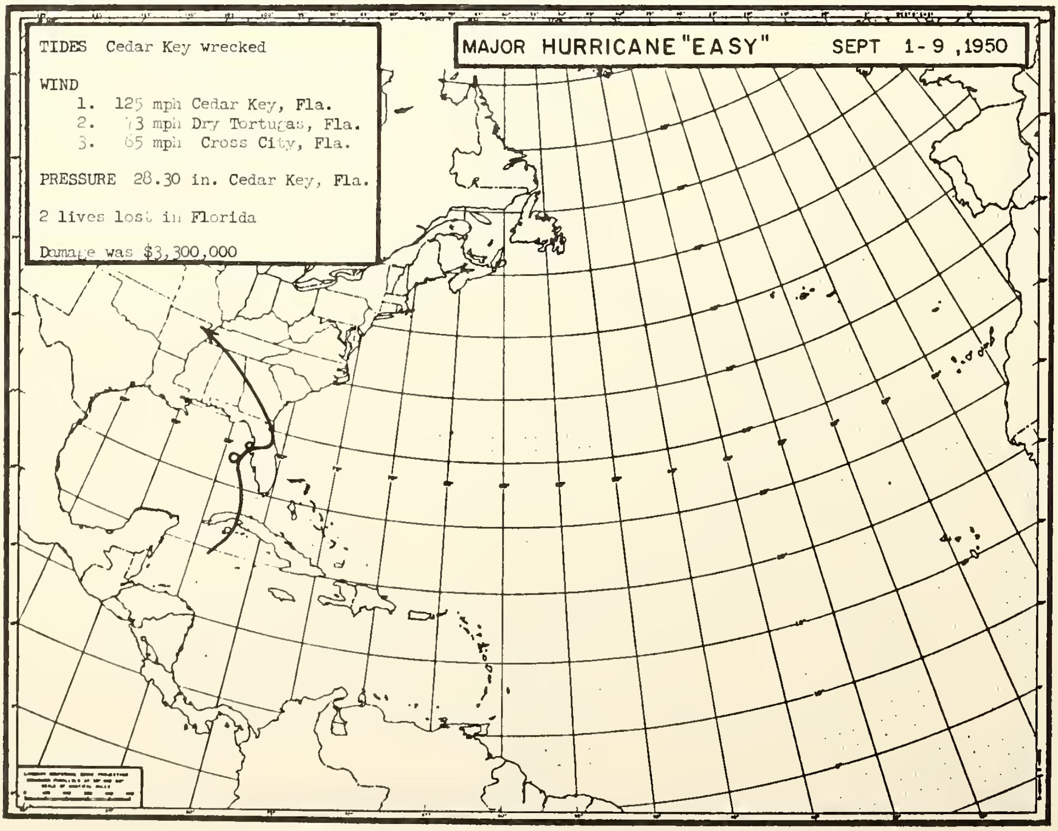

MAJOR HURRICANE "EASY" SEPT 1-9 ,1950

TIDES Cedar Key wrecked

WIND
1. 125 mph Cedar Key, Fla.
2. 73 mph Dry Tortugas, Fla.
3. 65 mph Cross City, Fla.

PRESSURE 28.30 in. Cedar Key, Fla.

2 lives lost in Florida

Damage was $3,300,000

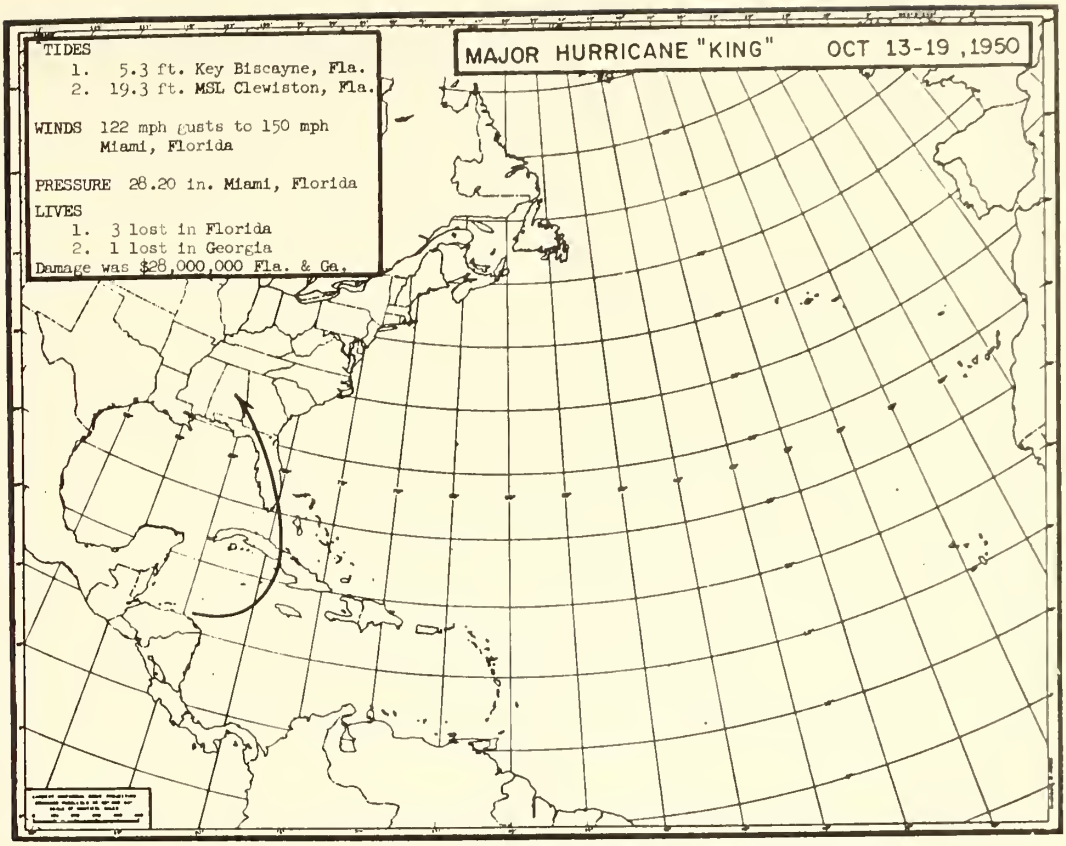

MAJOR HURRICANE "KING" OCT 13-19, 1950

TIDES
1. 5.3 ft. Key Biscayne, Fla.
2. 19.3 ft. MSL Clewiston, Fla.

WINDS 122 mph gusts to 150 mph
Miami, Florida

PRESSURE 28.20 in. Miami, Florida

LIVES
1. 3 lost in Florida
2. 1 lost in Georgia

Damage was $28,000,000 Fla. & Ga.

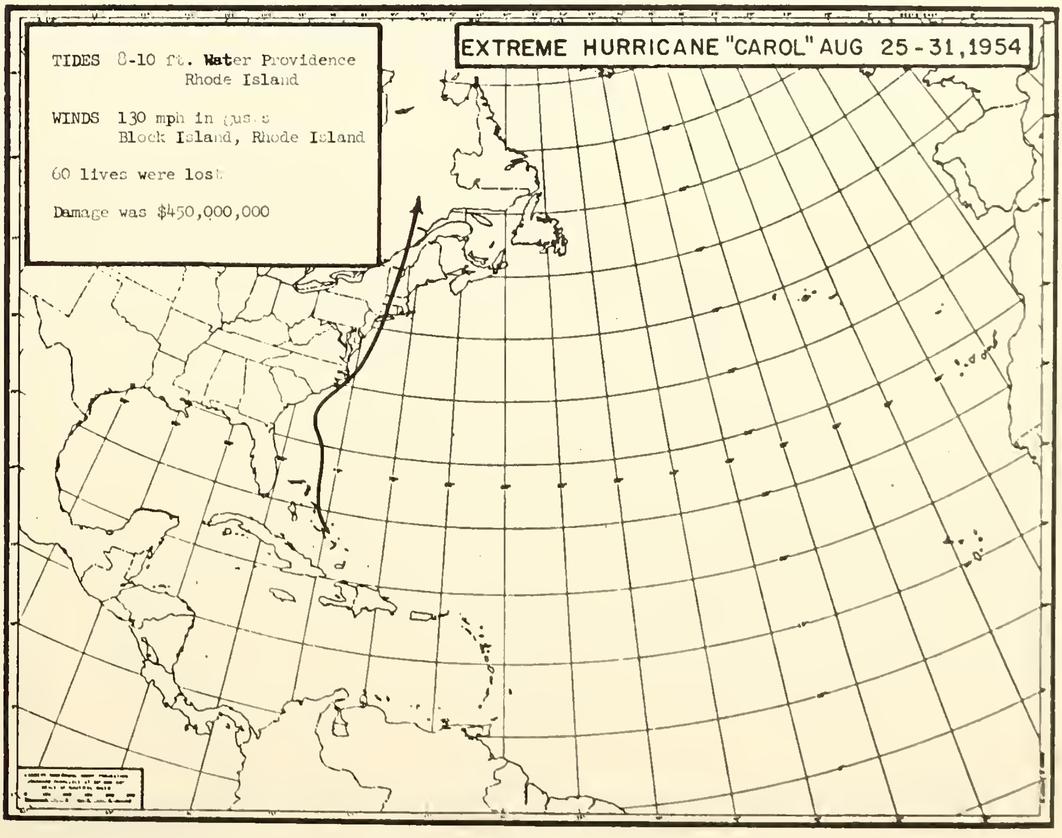

EXTREME HURRICANE "CAROL" AUG 25-31, 1954

TIDES 8-10 ft. **Wat**er Providence
Rhode Island

WINDS 130 mph in gusts
Block Island, Rhode Island

60 lives were lost

Damage was $450,000,000

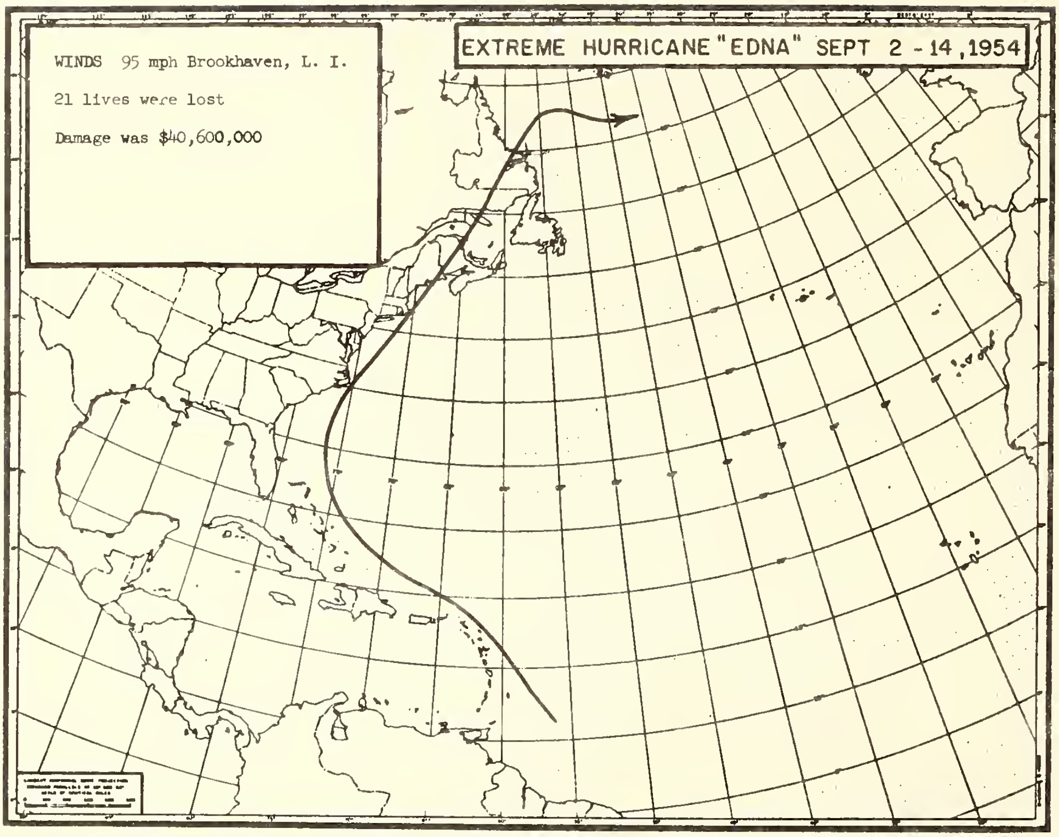

EXTREME HURRICANE "EDNA" SEPT 2 - 14, 1954

WINDS 95 mph Brookhaven, L. I.

21 lives were lost

Damage was $40,600,000

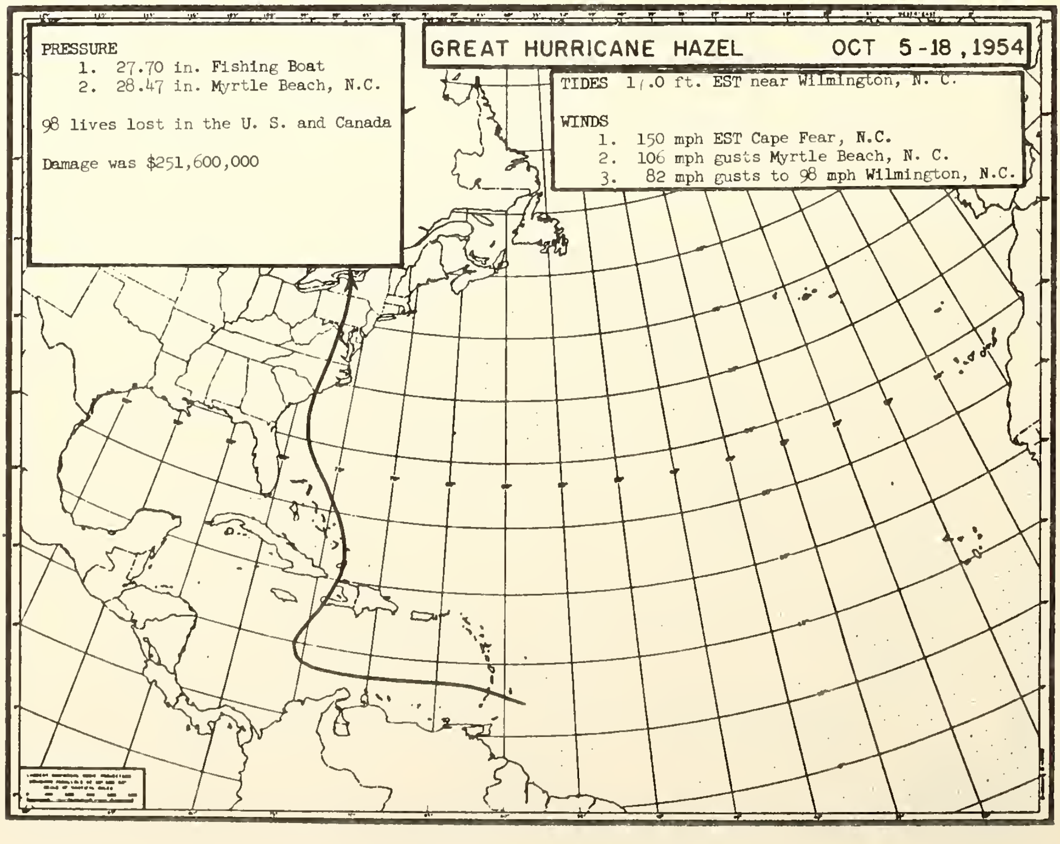

GREAT HURRICANE HAZEL OCT 5-18, 1954

PRESSURE
1. 27.70 in. Fishing Boat
2. 28.47 in. Myrtle Beach, N.C.

98 lives lost in the U. S. and Canada

Damage was $251,600,000

TIDES 17.0 ft. EST near Wilmington, N. C.

WINDS
1. 150 mph EST Cape Fear, N.C.
2. 106 mph gusts Myrtle Beach, N. C.
3. 82 mph gusts to 98 mph Wilmington, N.C.

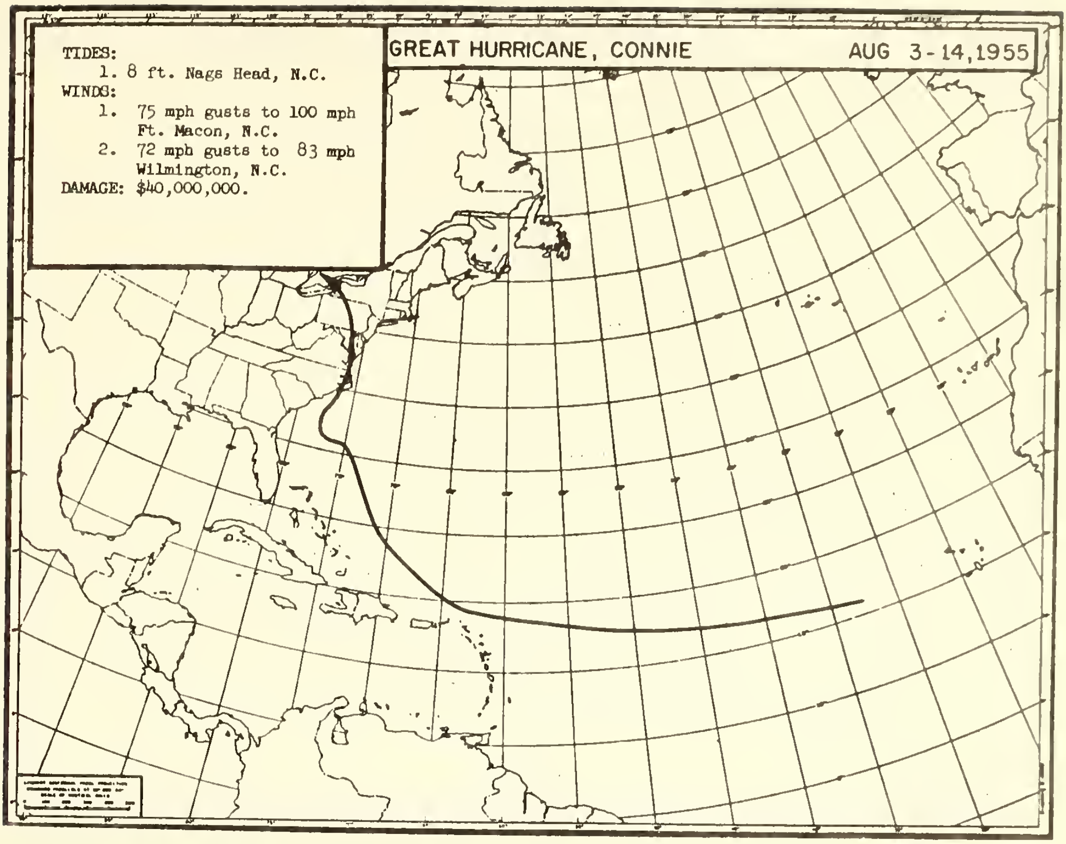

GREAT HURRICANE, CONNIE AUG 3-14,1955

TIDES:
1. 8 ft. Nags Head, N.C.
WINDS:
1. 75 mph gusts to 100 mph Ft. Macon, N.C.
2. 72 mph gusts to 83 mph Wilmington, N.C.
DAMAGE: $40,000,000.

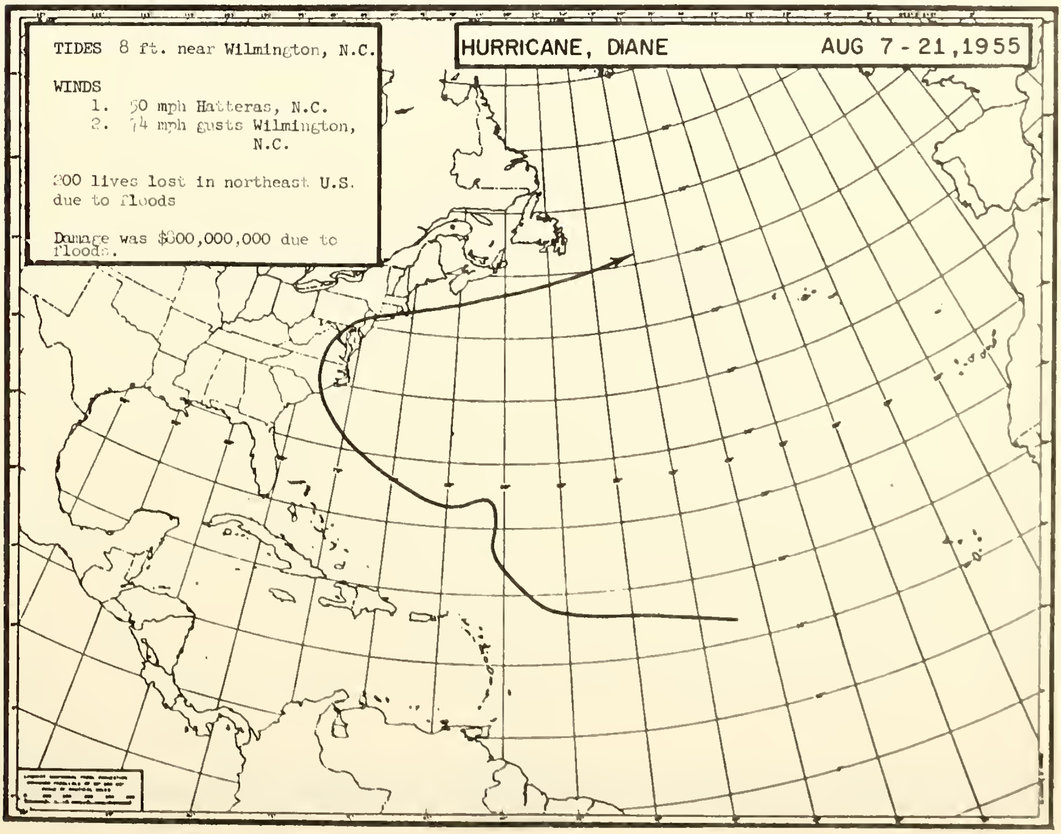

HURRICANE, DIANE AUG 7-21,1955

TIDES 8 ft. near Wilmington, N.C.

WINDS
1. 50 mph Hatteras, N.C.
2. 74 mph gusts Wilmington, N.C.

200 lives lost in northeast U.S. due to floods

Damage was $800,000,000 due to floods.

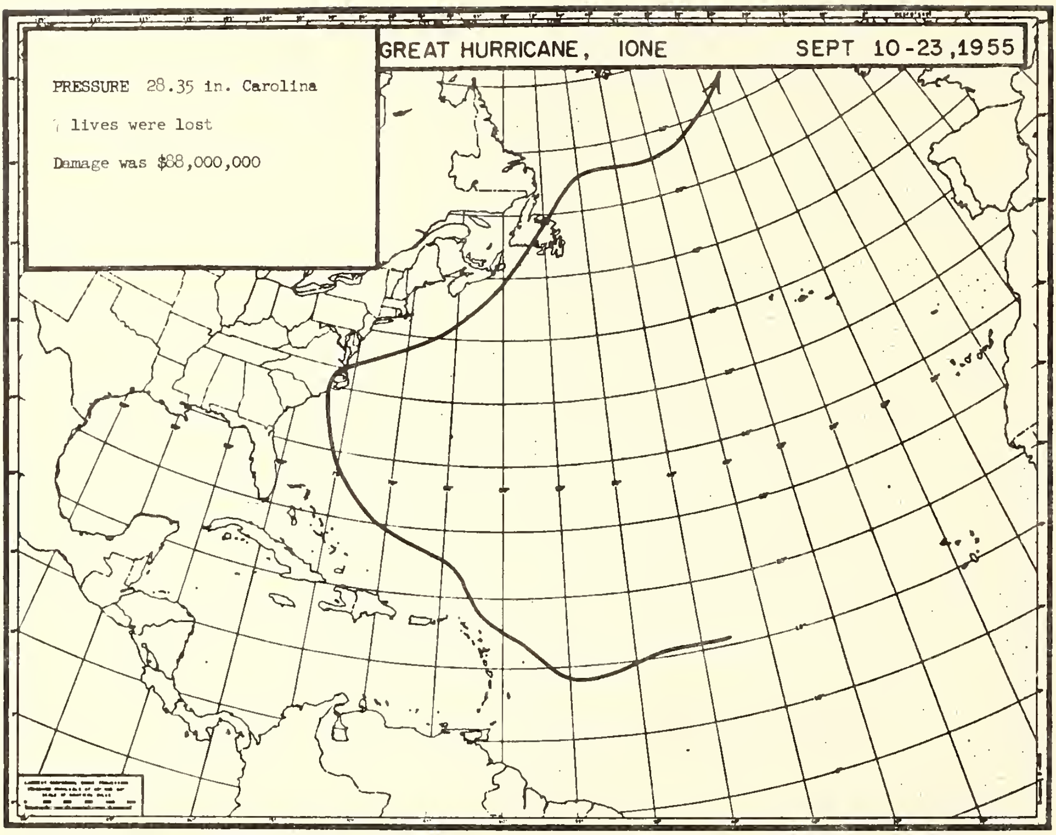

GREAT HURRICANE, IONE SEPT 10-23,1955

PRESSURE 28.35 in. Carolina

7 lives were lost

Damage was $88,000,000

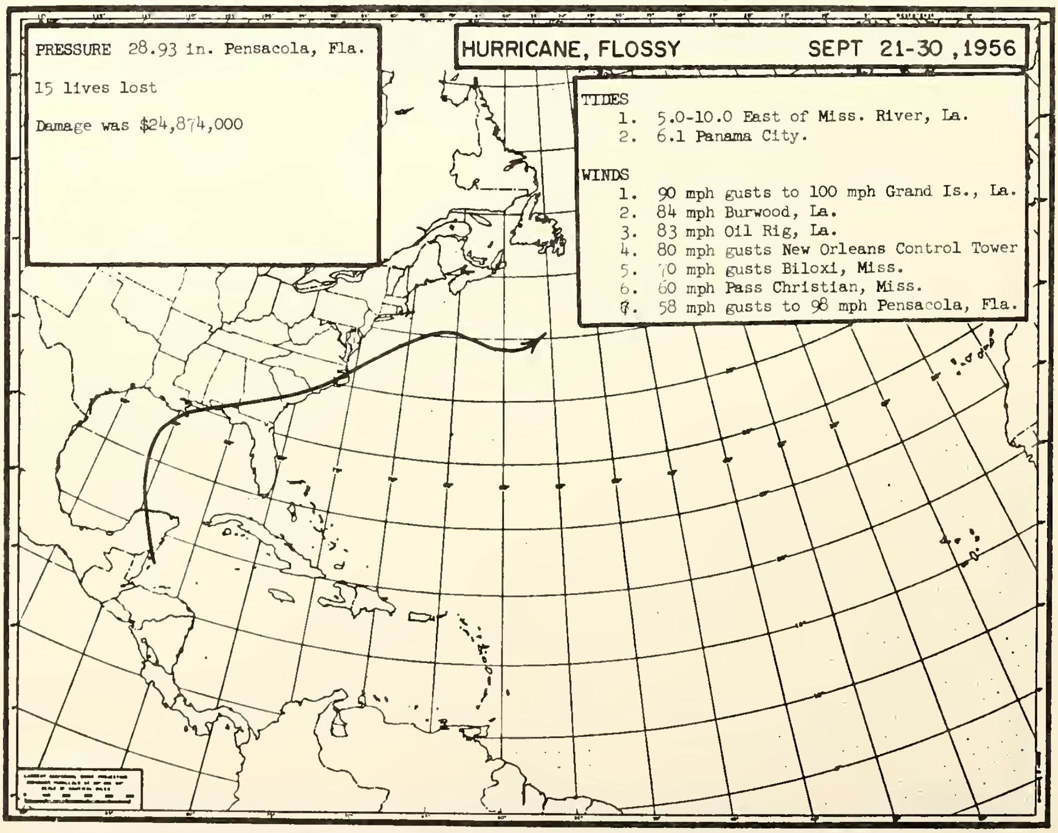

HURRICANE, FLOSSY SEPT 21-30,1956

PRESSURE 28.93 in. Pensacola, Fla.

15 lives lost

Damage was $24,874,000

TIDES
1. 5.0-10.0 East of Miss. River, La.
2. 6.1 Panama City.

WINDS
1. 90 mph gusts to 100 mph Grand Is., La.
2. 84 mph Burwood, La.
3. 83 mph Oil Rig, La.
4. 80 mph gusts New Orleans Control Tower
5. 70 mph gusts Biloxi, Miss.
6. 60 mph Pass Christian, Miss.
7. 58 mph gusts to 98 mph Pensacola, Fla.

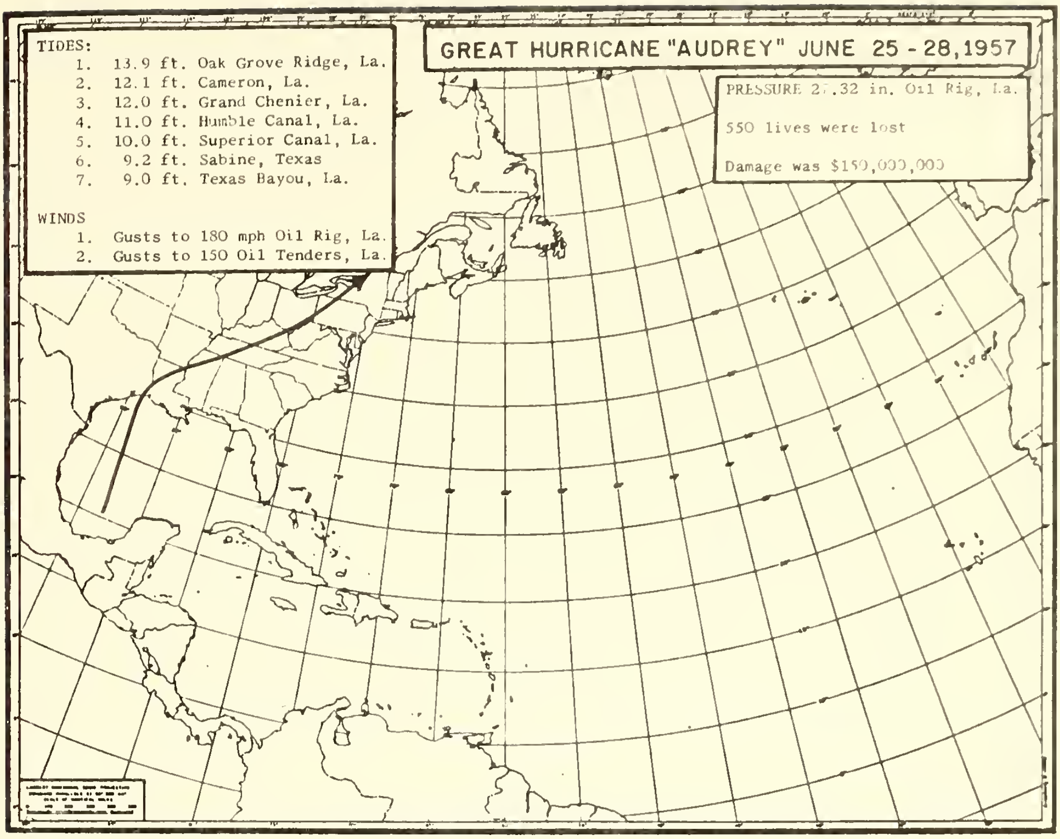

GREAT HURRICANE "AUDREY" JUNE 25 - 28,1957

TIDES:
1. 13.9 ft. Oak Grove Ridge, La.
2. 12.1 ft. Cameron, La.
3. 12.0 ft. Grand Chenier, La.
4. 11.0 ft. Humble Canal, La.
5. 10.0 ft. Superior Canal, La.
6. 9.2 ft. Sabine, Texas
7. 9.0 ft. Texas Bayou, La.

WINDS
1. Gusts to 180 mph Oil Rig, La.
2. Gusts to 150 Oil Tenders, La.

PRESSURE 27.32 in. Oil Rig, La.

550 lives were lost

Damage was $150,000,000

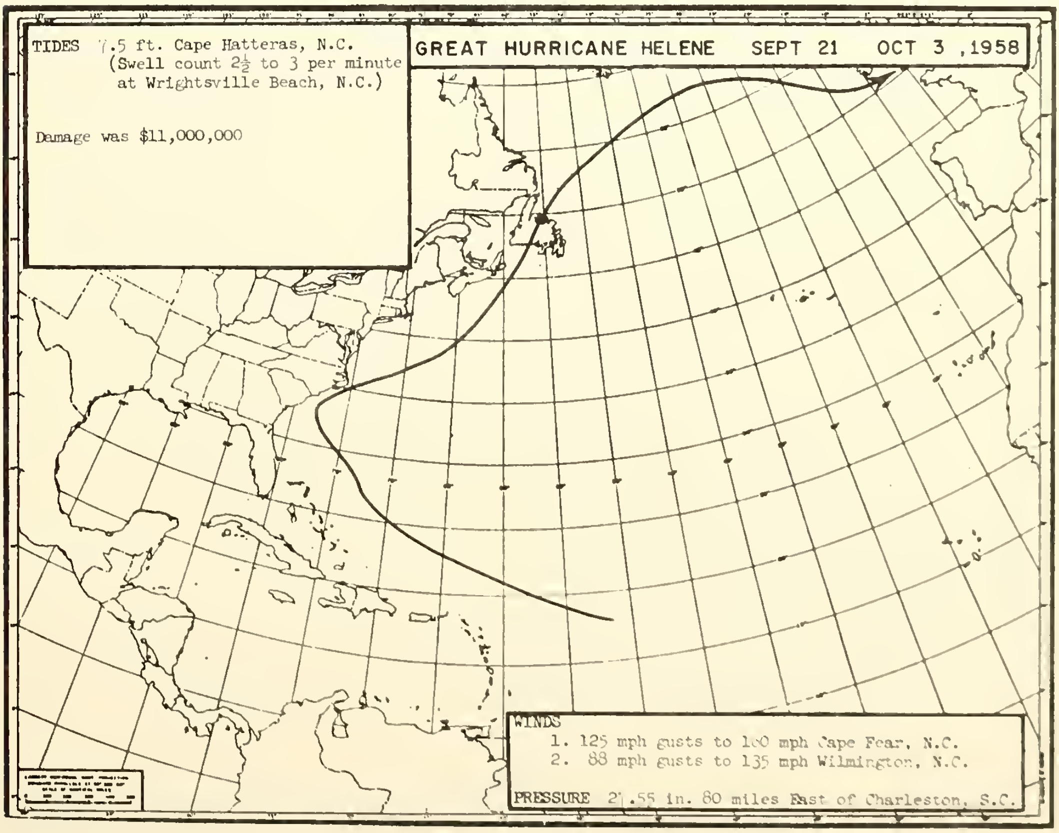

GREAT HURRICANE HELENE SEPT 21 OCT 3 ,1958

TIDES 7.5 ft. Cape Hatteras, N.C.
(Swell count 2½ to 3 per minute
at Wrightsville Beach, N.C.)

Damage was $11,000,000

WINDS
1. 125 mph gusts to 160 mph Cape Fear, N.C.
2. 88 mph gusts to 135 mph Wilmington, N.C.

PRESSURE 27.55 in. 80 miles East of Charleston, S.C.

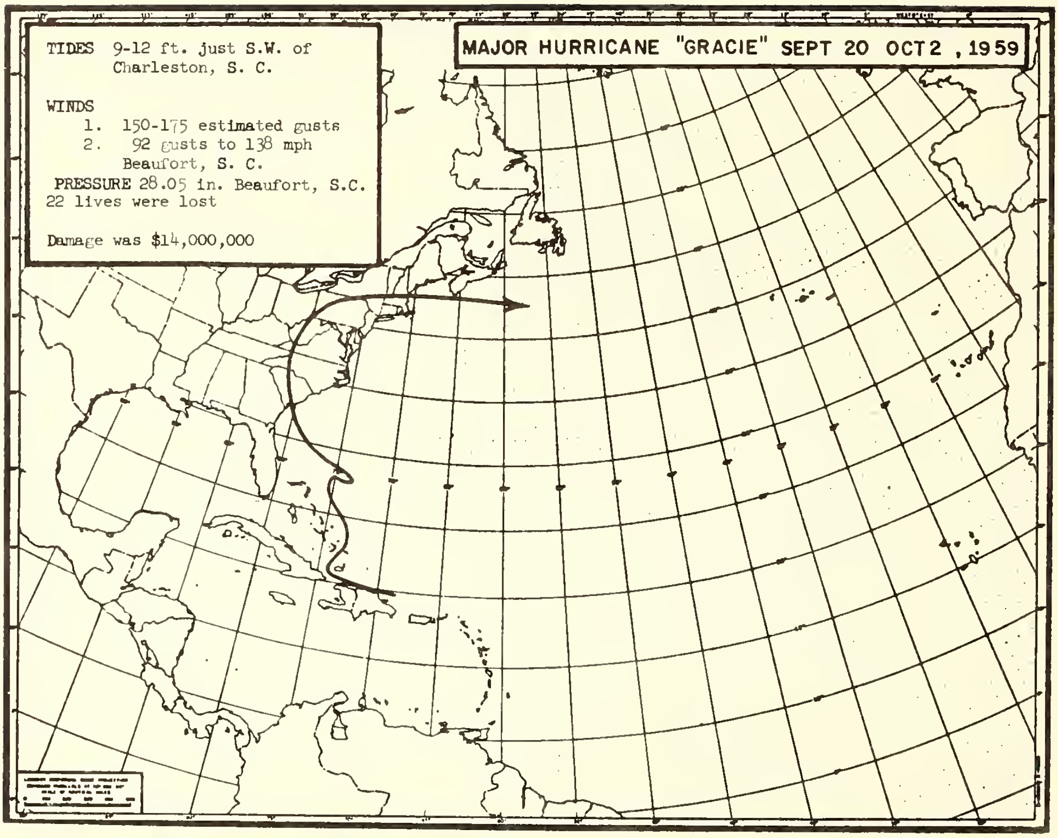

MAJOR HURRICANE "GRACIE" SEPT 20 OCT2 ,1959

TIDES 9-12 ft. just S.W. of Charleston, S. C.

WINDS
1. 150-175 estimated gusts
2. 92 gusts to 138 mph Beaufort, S. C.

PRESSURE 28.05 in. Beaufort, S.C.
22 lives were lost

Damage was $14,000,000

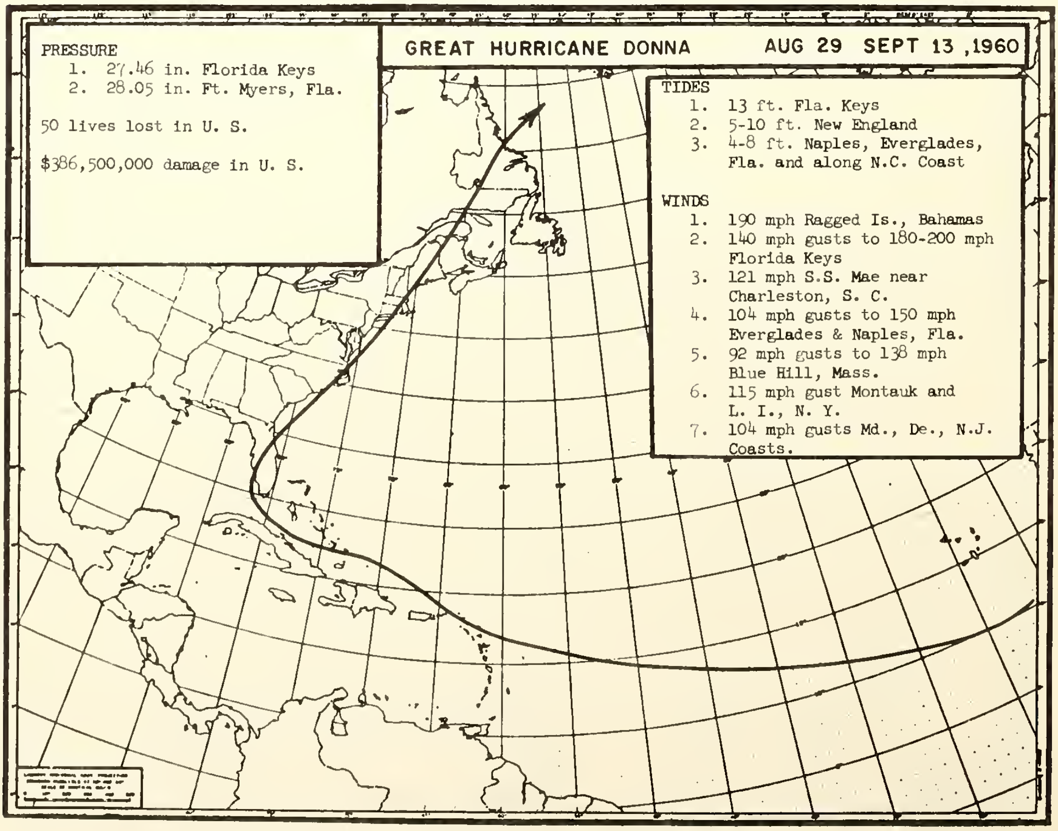

GREAT HURRICANE DONNA AUG 29 SEPT 13 ,1960

PRESSURE
1. 27.46 in. Florida Keys
2. 28.05 in. Ft. Myers, Fla.

50 lives lost in U. S.

$386,500,000 damage in U. S.

TIDES
1. 13 ft. Fla. Keys
2. 5-10 ft. New England
3. 4-8 ft. Naples, Everglades, Fla. and along N.C. Coast

WINDS
1. 190 mph Ragged Is., Bahamas
2. 140 mph gusts to 180-200 mph Florida Keys
3. 121 mph S.S. Mae near Charleston, S. C.
4. 104 mph gusts to 150 mph Everglades & Naples, Fla.
5. 92 mph gusts to 138 mph Blue Hill, Mass.
6. 115 mph gust Montauk and L. I., N. Y.
7. 104 mph gusts Md., De., N.J. Coasts.

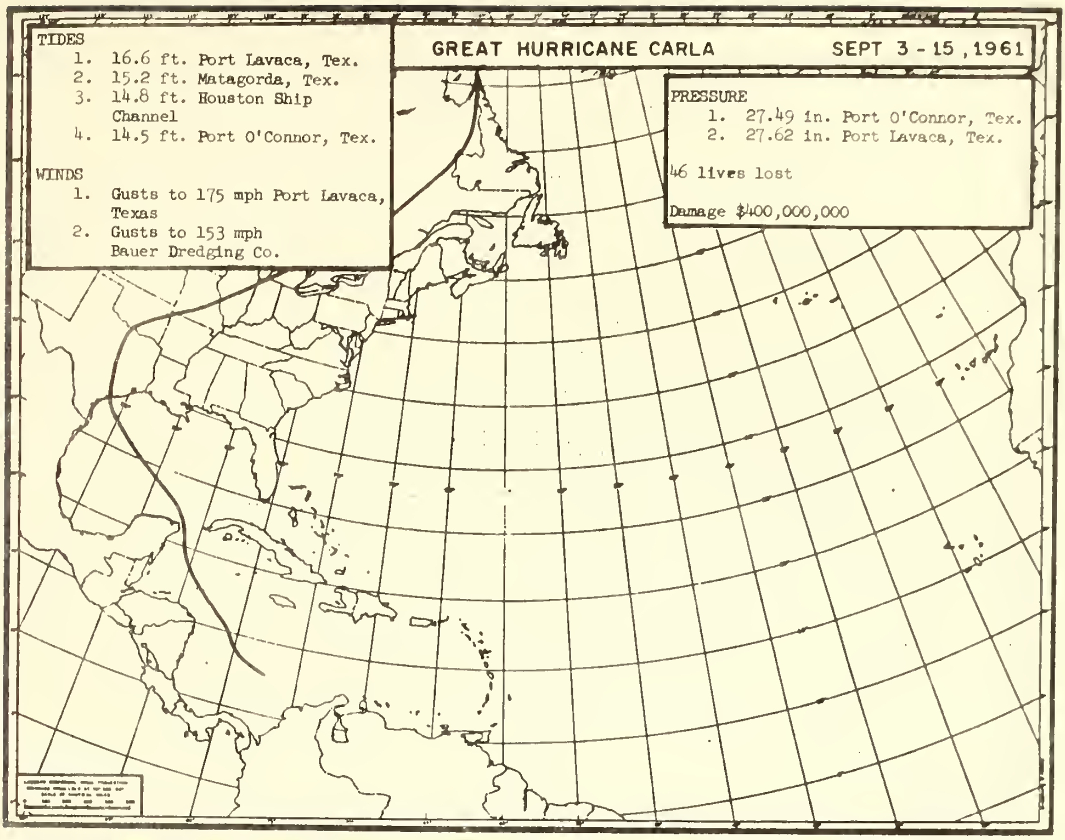

GREAT HURRICANE CARLA SEPT 3 - 15 ,1961

TIDES
1. 16.6 ft. Port Lavaca, Tex.
2. 15.2 ft. Matagorda, Tex.
3. 14.8 ft. Houston Ship Channel
4. 14.5 ft. Port O'Connor, Tex.

WINDS
1. Gusts to 175 mph Port Lavaca, Texas
2. Gusts to 153 mph Bauer Dredging Co.

PRESSURE
1. 27.49 in. Port O'Connor, Tex.
2. 27.62 in. Port Lavaca, Tex.

46 lives lost

Damage $400,000,000

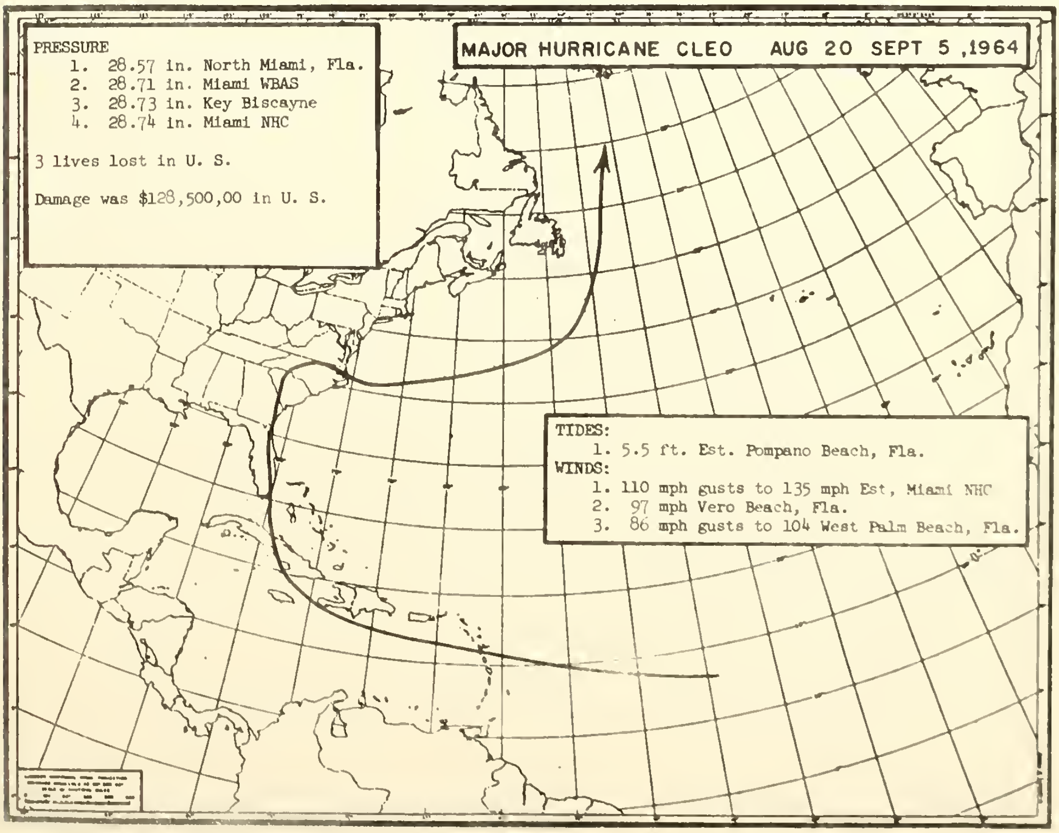

MAJOR HURRICANE CLEO AUG 20 SEPT 5 ,1964

PRESSURE
1. 28.57 in. North Miami, Fla.
2. 28.71 in. Miami WBAS
3. 28.73 in. Key Biscayne
4. 28.74 in. Miami NHC

3 lives lost in U. S.

Damage was $128,500,00 in U. S.

TIDES:
1. 5.5 ft. Est. Pompano Beach, Fla.

WINDS:
1. 110 mph gusts to 135 mph Est, Miami NHC
2. 97 mph Vero Beach, Fla.
3. 86 mph gusts to 104 West Palm Beach, Fla.

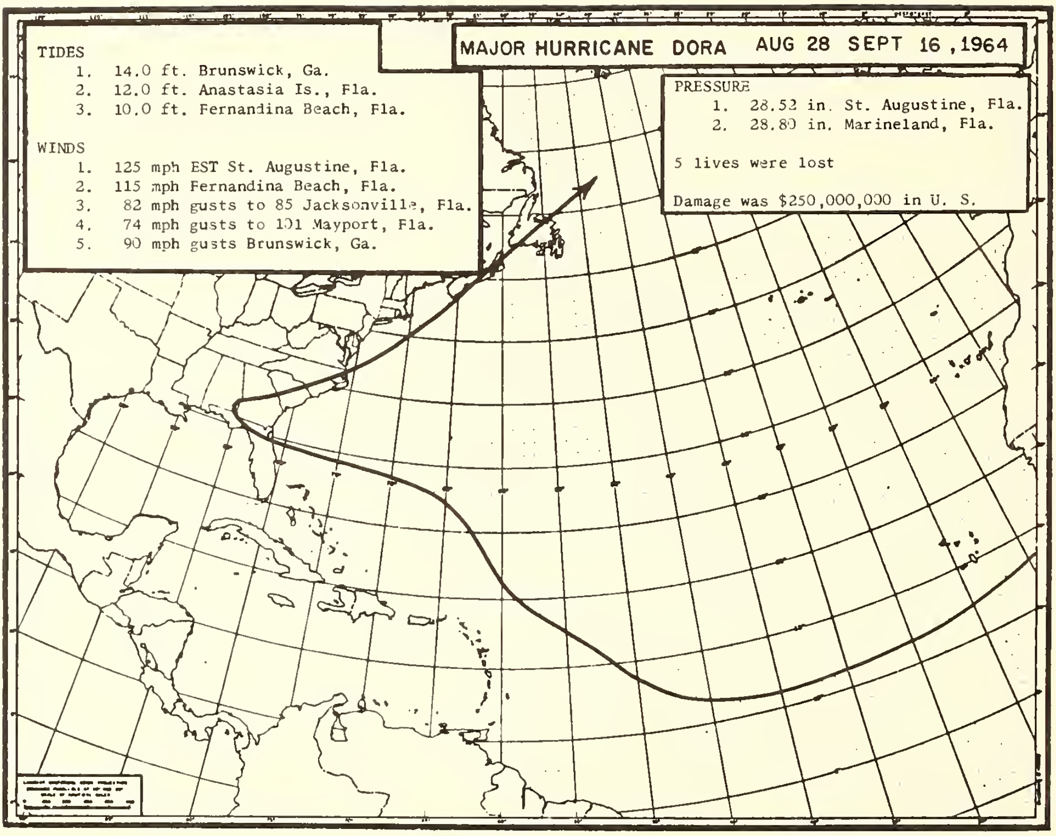

MAJOR HURRICANE DORA AUG 28 SEPT 16 ,1964

TIDES
1. 14.0 ft. Brunswick, Ga.
2. 12.0 ft. Anastasia Is., Fla.
3. 10.0 ft. Fernandina Beach, Fla.

WINDS
1. 125 mph EST St. Augustine, Fla.
2. 115 mph Fernandina Beach, Fla.
3. 82 mph gusts to 85 Jacksonville, Fla.
4. 74 mph gusts to 101 Mayport, Fla.
5. 90 mph gusts Brunswick, Ga.

PRESSURE
1. 28.52 in. St. Augustine, Fla.
2. 28.80 in. Marineland, Fla.

5 lives were lost

Damage was $250,000,000 in U. S.

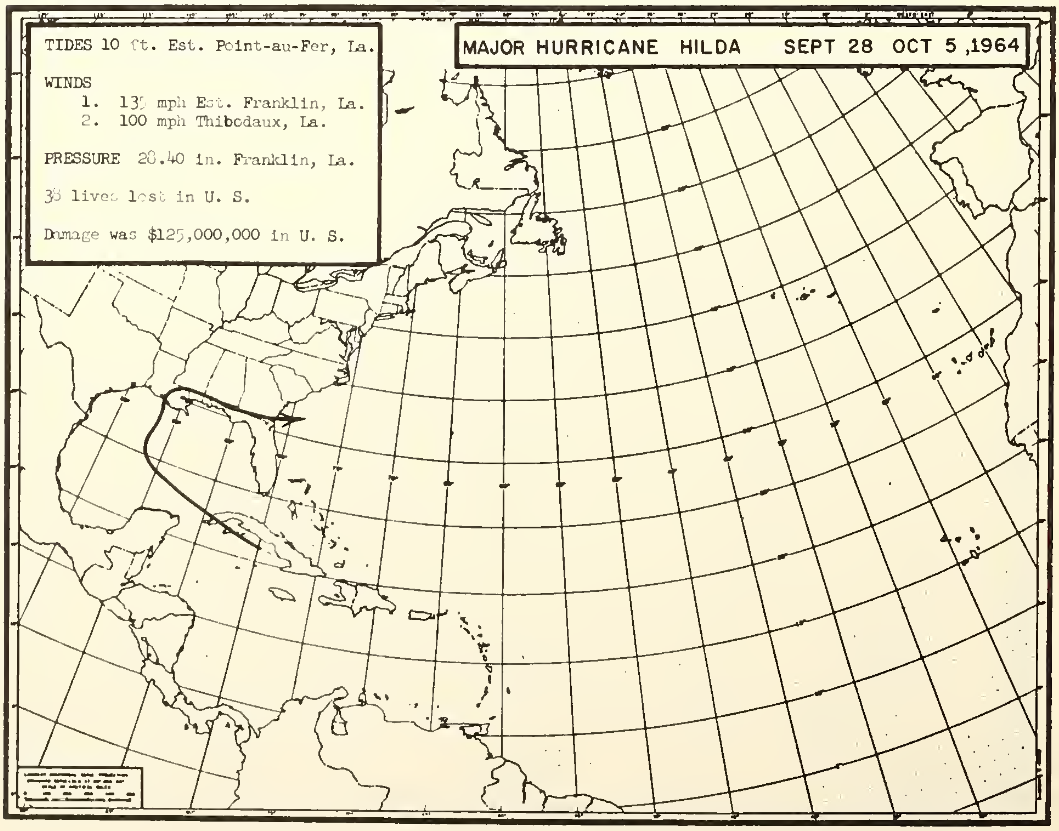

MAJOR HURRICANE HILDA SEPT 28 OCT 5 ,1964

TIDES 10 ft. Est. Point-au-Fer, La.

WINDS
1. 135 mph Est. Franklin, La.
2. 100 mph Thibodaux, La.

PRESSURE 28.40 in. Franklin, La.

38 lives lost in U. S.

Damage was $125,000,000 in U. S.

GREAT HURRICANE BETSY AUG 27 SEPT 12, 1965

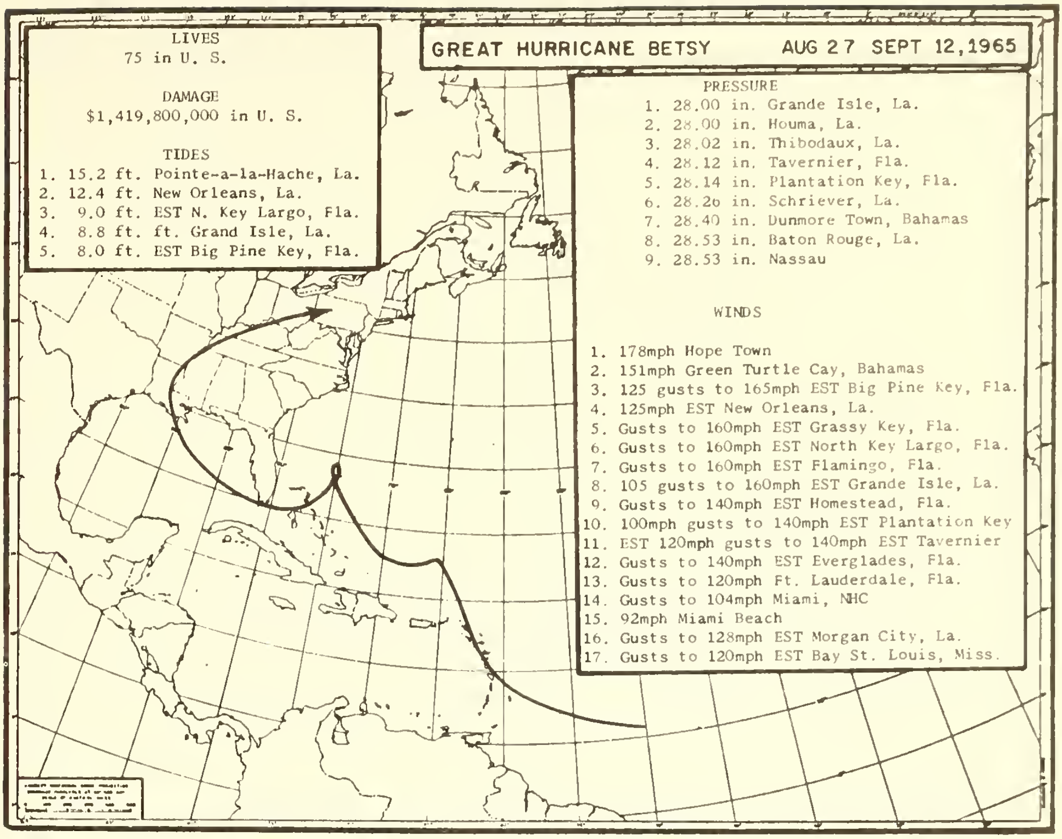

LIVES
75 in U. S.

DAMAGE
$1,419,800,000 in U. S.

TIDES
1. 15.2 ft. Pointe-a-la-Hache, La.
2. 12.4 ft. New Orleans, La.
3. 9.0 ft. EST N. Key Largo, Fla.
4. 8.8 ft. ft. Grand Isle, La.
5. 8.0 ft. EST Big Pine Key, Fla.

PRESSURE
1. 28.00 in. Grande Isle, La.
2. 28.00 in. Houma, La.
3. 28.02 in. Thibodaux, La.
4. 28.12 in. Tavernier, Fla.
5. 28.14 in. Plantation Key, Fla.
6. 28.26 in. Schriever, La.
7. 28.40 in. Dunmore Town, Bahamas
8. 28.53 in. Baton Rouge, La.
9. 28.53 in. Nassau

WINDS
1. 178mph Hope Town
2. 151mph Green Turtle Cay, Bahamas
3. 125 gusts to 165mph EST Big Pine Key, Fla.
4. 125mph EST New Orleans, La.
5. Gusts to 160mph EST Grassy Key, Fla.
6. Gusts to 160mph EST North Key Largo, Fla.
7. Gusts to 160mph EST Flamingo, Fla.
8. 105 gusts to 160mph EST Grande Isle, La.
9. Gusts to 140mph EST Homestead, Fla.
10. 100mph gusts to 140mph EST Plantation Key
11. EST 120mph gusts to 140mph EST Tavernier
12. Gusts to 140mph EST Everglades, Fla.
13. Gusts to 120mph Ft. Lauderdale, Fla.
14. Gusts to 104mph Miami, NHC
15. 92mph Miami Beach
16. Gusts to 128mph EST Morgan City, La.
17. Gusts to 120mph EST Bay St. Louis, Miss.

MAJOR HURRICANE ALMA JUNE 4-14, 1966

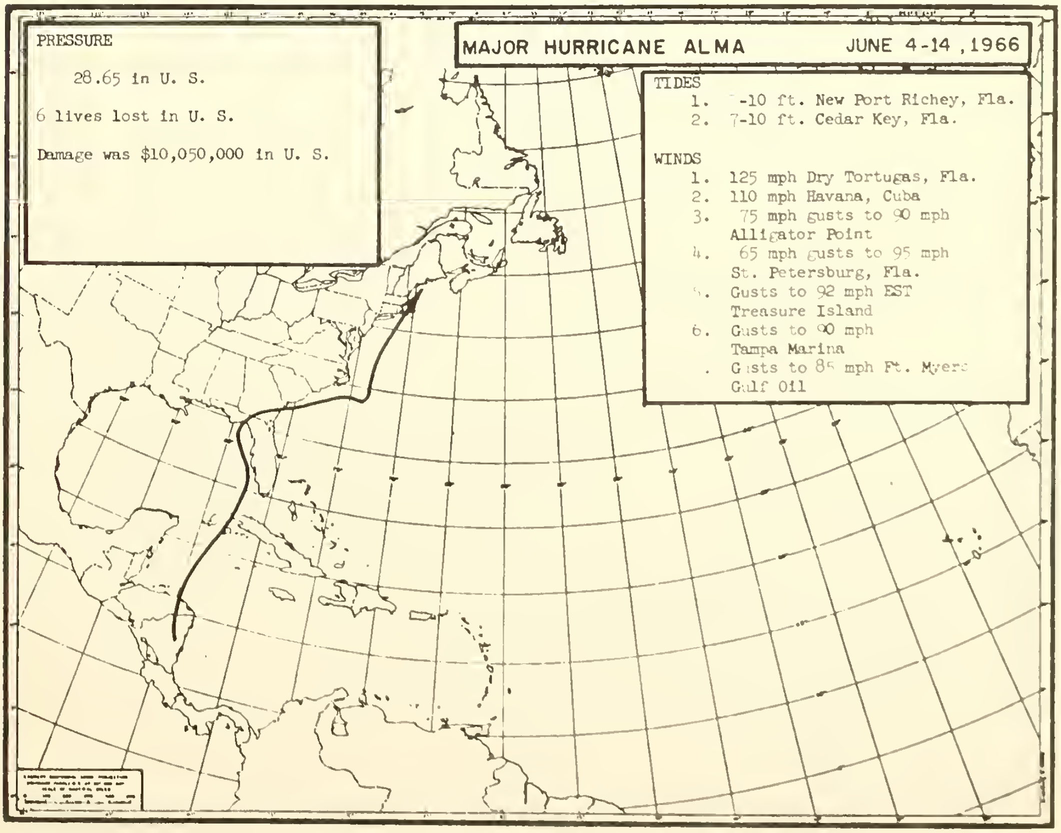

PRESSURE

28.65 in U. S.

6 lives lost in U. S.

Damage was $10,050,000 in U. S.

TIDES
1. -10 ft. New Port Richey, Fla.
2. 7-10 ft. Cedar Key, Fla.

WINDS
1. 125 mph Dry Tortugas, Fla.
2. 110 mph Havana, Cuba
3. 75 mph gusts to 90 mph Alligator Point
4. 65 mph gusts to 95 mph St. Petersburg, Fla.
5. Gusts to 92 mph EST Treasure Island
6. Gusts to 90 mph Tampa Marina
. Gusts to 85 mph Ft. Myers Gulf Oil

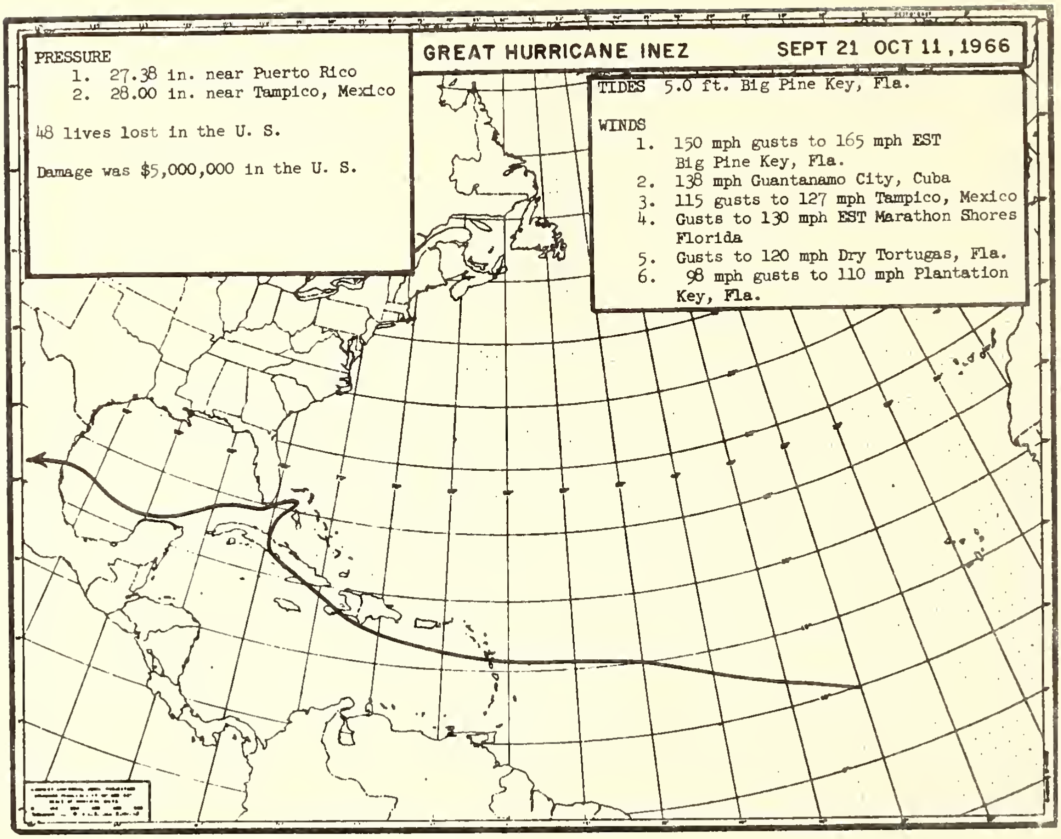

GREAT HURRICANE INEZ SEPT 21 OCT 11, 1966

PRESSURE
1. 27.38 in. near Puerto Rico
2. 28.00 in. near Tampico, Mexico

48 lives lost in the U. S.

Damage was $5,000,000 in the U. S.

TIDES 5.0 ft. Big Pine Key, Fla.

WINDS
1. 150 mph gusts to 165 mph EST Big Pine Key, Fla.
2. 138 mph Guantanamo City, Cuba
3. 115 gusts to 127 mph Tampico, Mexico
4. Gusts to 130 mph EST Marathon Shores Florida
5. Gusts to 120 mph Dry Tortugas, Fla.
6. 98 mph gusts to 110 mph Plantation Key, Fla.

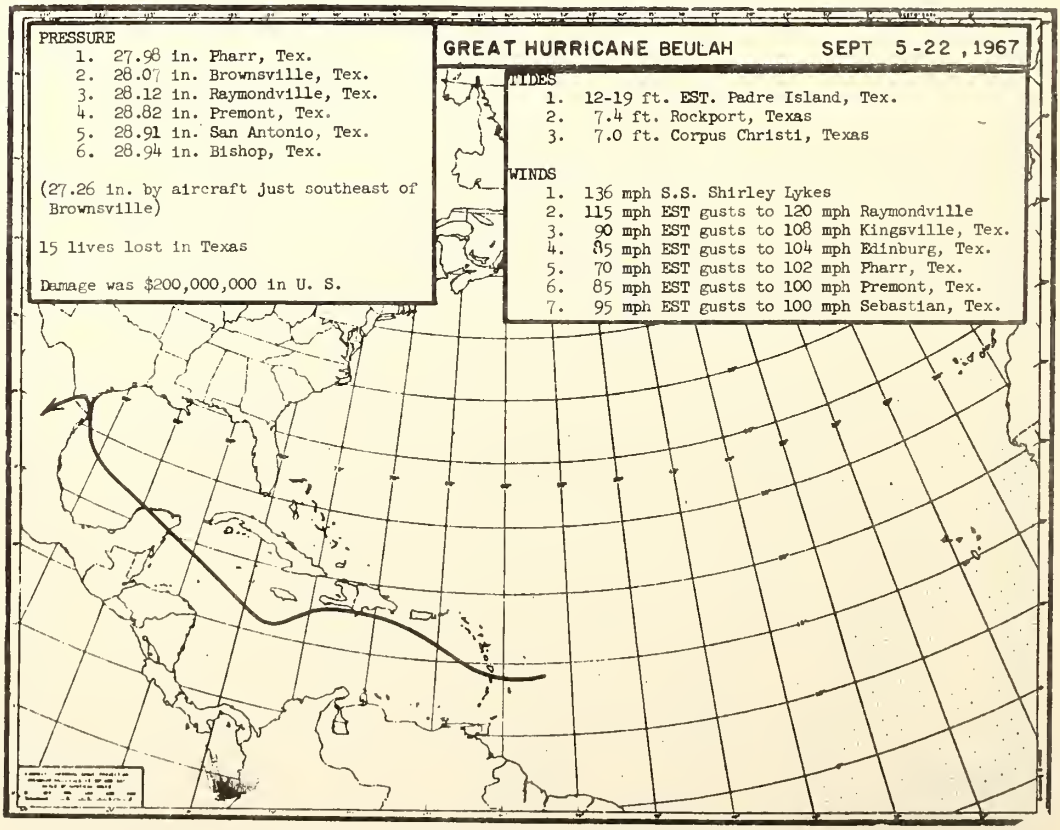

GREAT HURRICANE BEULAH SEPT 5-22, 1967

PRESSURE
1. 27.98 in. Pharr, Tex.
2. 28.07 in. Brownsville, Tex.
3. 28.12 in. Raymondville, Tex.
4. 28.82 in. Premont, Tex.
5. 28.91 in. San Antonio, Tex.
6. 28.94 in. Bishop, Tex.

(27.26 in. by aircraft just southeast of Brownsville)

15 lives lost in Texas

Damage was $200,000,000 in U. S.

TIDES
1. 12-19 ft. EST. Padre Island, Tex.
2. 7.4 ft. Rockport, Texas
3. 7.0 ft. Corpus Christi, Texas

WINDS
1. 136 mph S.S. Shirley Lykes
2. 115 mph EST gusts to 120 mph Raymondville
3. 90 mph EST gusts to 108 mph Kingsville, Tex.
4. 85 mph EST gusts to 104 mph Edinburg, Tex.
5. 70 mph EST gusts to 102 mph Pharr, Tex.
6. 85 mph EST gusts to 100 mph Premont, Tex.
7. 95 mph EST gusts to 100 mph Sebastian, Tex.

.6

U. S. DEPARTMENT OF COMMERCE
Environmental Science Services Administration
Weather Bureau

ESSA Technical Memorandum WBTM SR-46

HEMISPHERIC CIRCULATION AND ANOMALY PATTERNS OBSERVED WHEN TROPICAL STORMS REACH HURRICANE INTENSITY

SOUTHERN REGION HEADQUARTERS
SCIENTIFIC SERVICES DIVISION
FORT WORTH, TEXAS
May 1969

Hemispheric Circulation and Anomaly Patterns Observed when Tropical Storms reach Hurricane Intensity

by

Paul J. Hebert
National Hurricane Center
Weather Bureau
Environmental Science Services Administration
Miami, Florida

and

Banner I. Miller
National Hurricane Research Laboratory
Research Laboratories
Environmental Science Services Administration
Miami, Florida

During the past several years the composite charts prepared by Ballenzweig (2, 3) have been of assistance to hurricane forecasters in identifying circulation patterns which are either favorable or unfavorable to the formation of tropical cyclones. It seems appropriate at this time to bring up to date Ballenzweig's work by making use of several years of additional data which have accumulated since 1955.

Composite charts of the average 700-mb circulation and anomaly patterns for those tropical storms which reached hurricane intensity were prepared for the period 1947-1967. Figure 1 shows the points where tropical cyclones reached hurricane intensity within the designated regions. Figures 2-6 show the average hemispheric circulation and anomaly patterns (units are tens of feet) on D-day (the day that hurricane intensity was reached), and for D-1, and D-2, which are 24 hours and 48 hours prior to the time hurricane status was achieved.

It will be noted that we have departed somewhat from Ballenzweig's approach. The composite charts were obtained by averaging the daily values for each of the three days, regardless of the month in which the hurricane occurred. The anomaly charts are the averages of the departures from the normals, which were obtained by averaging the daily normals for the ten-day period in which the hurricane developed.

The sources of the data used in preparing the composite charts were the 700-mb charts from the Extended Forecast Division's diamond grid, the hurricane tracks published by Cry (1), and the 700-mb normals derived by Lewis (4).

The composite charts are being issued at this time so that they may be available to the hurricane forecasters, and to others who may be interested in seeing these patterns, prior to the 1969 hurricane season. It is anticipated that an expanded version of this study relating the physical and dynamical processes of hurricane formation to these circulation and anomaly patterns will be prepared for publication within the near future. The final paper will also include implications of the patterns for hurricane threat potential in various geographical locations, as well as an attempt to utilize some aspects of this study on an operational basis at the National Hurricane Center during the 1969 season.

Acknowledgements

We are indebted to Mr. Robert L. Carrodus for assistance in drafting and preparing the illustrations, to Mr. Charles H. True for the photographs, to Mrs. Rita Sherrill and Miss Lorraine Kelly who assisted in processing the immense amount of data used in the study. Mr. Billy M. Lewis supplied the initial data.

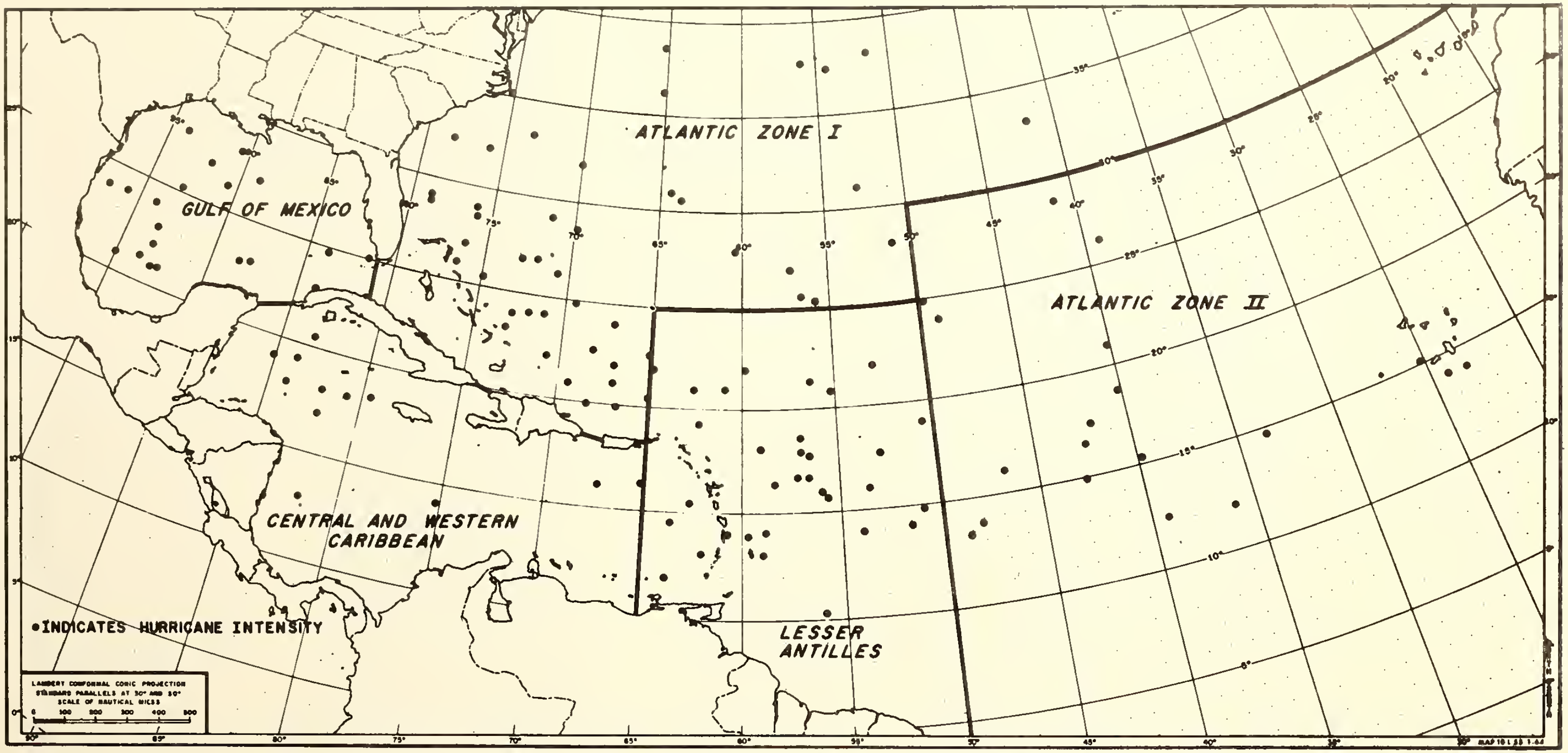

FIGURE. 1 POINTS AT WHICH TROPICAL STORMS REACHED HURRICANE INTENSITY WITHIN THE DESIGNATED REGIONS. (1947 — 1967)

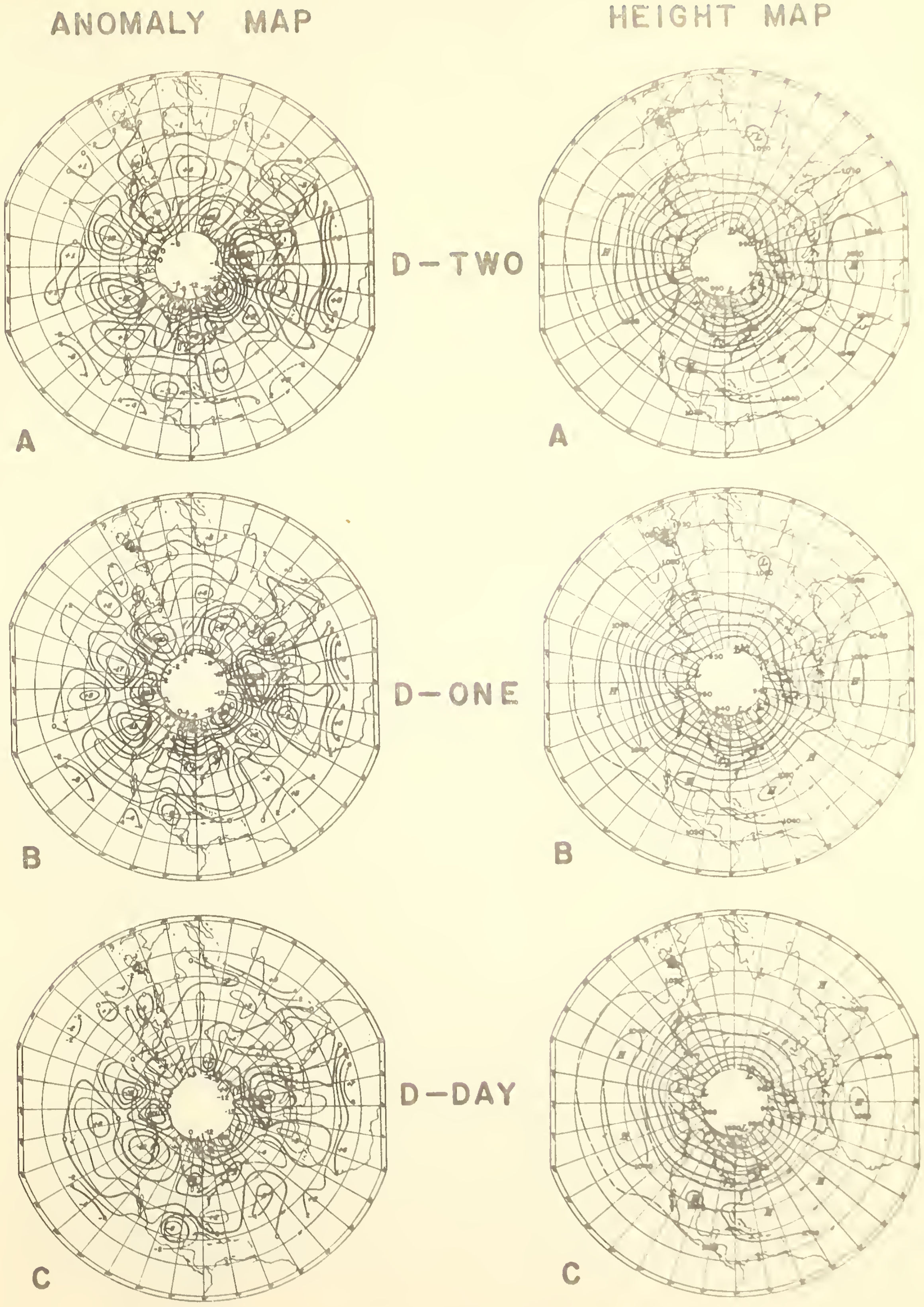

FIGURE. 2 GULF OF MEXICO

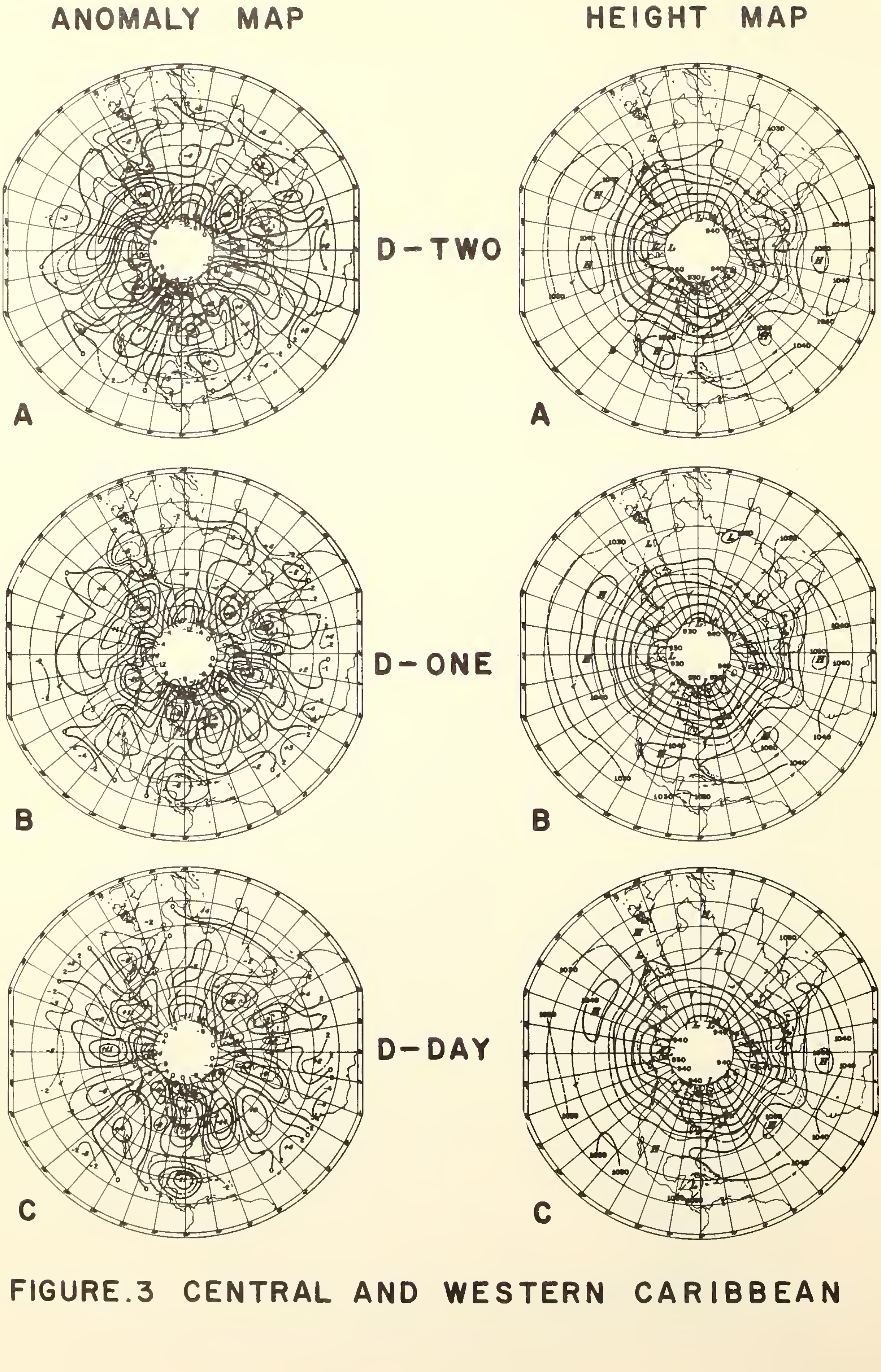

FIGURE.3 CENTRAL AND WESTERN CARIBBEAN

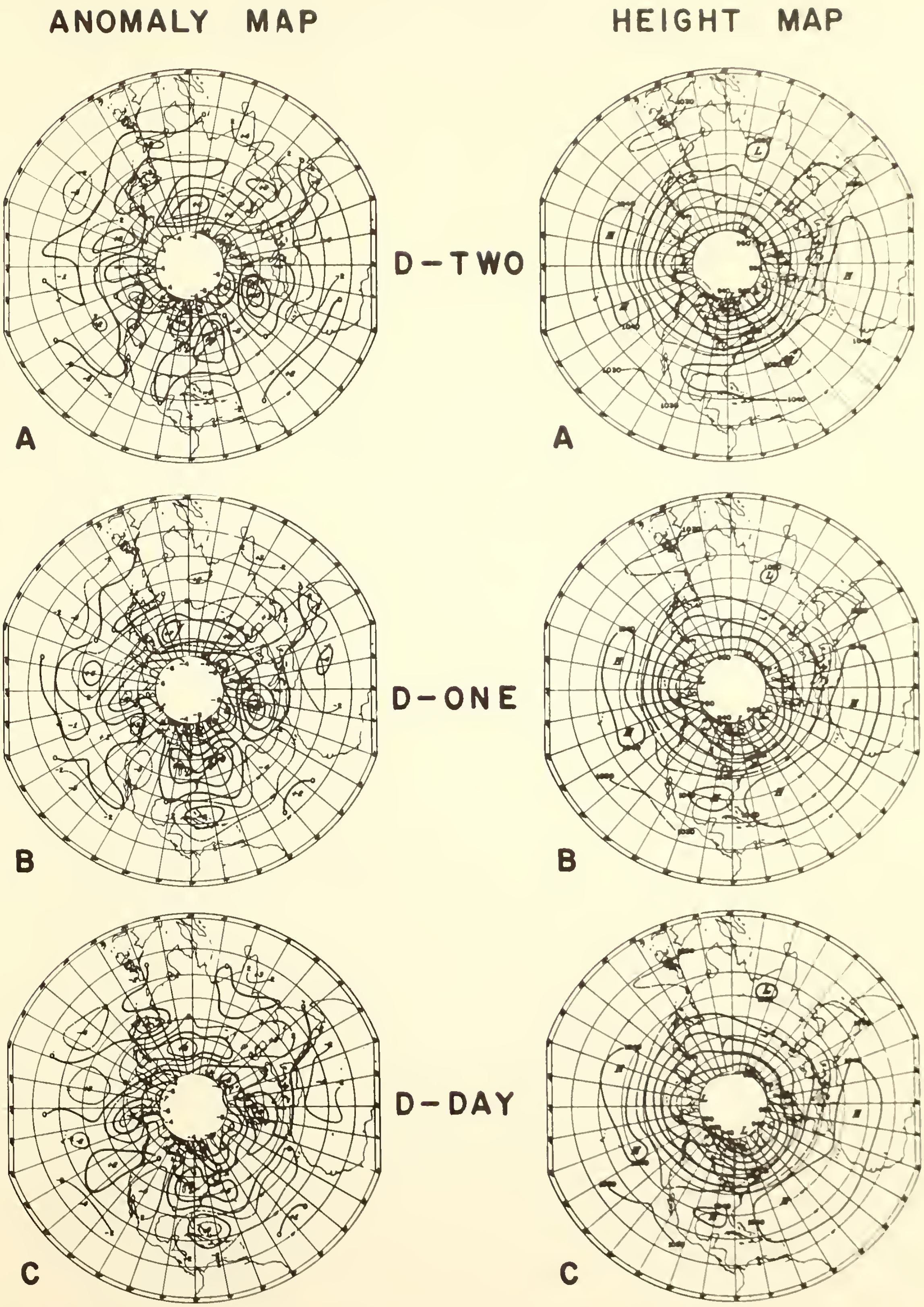

FIGURE. 4 ATLANTIC ZONE I

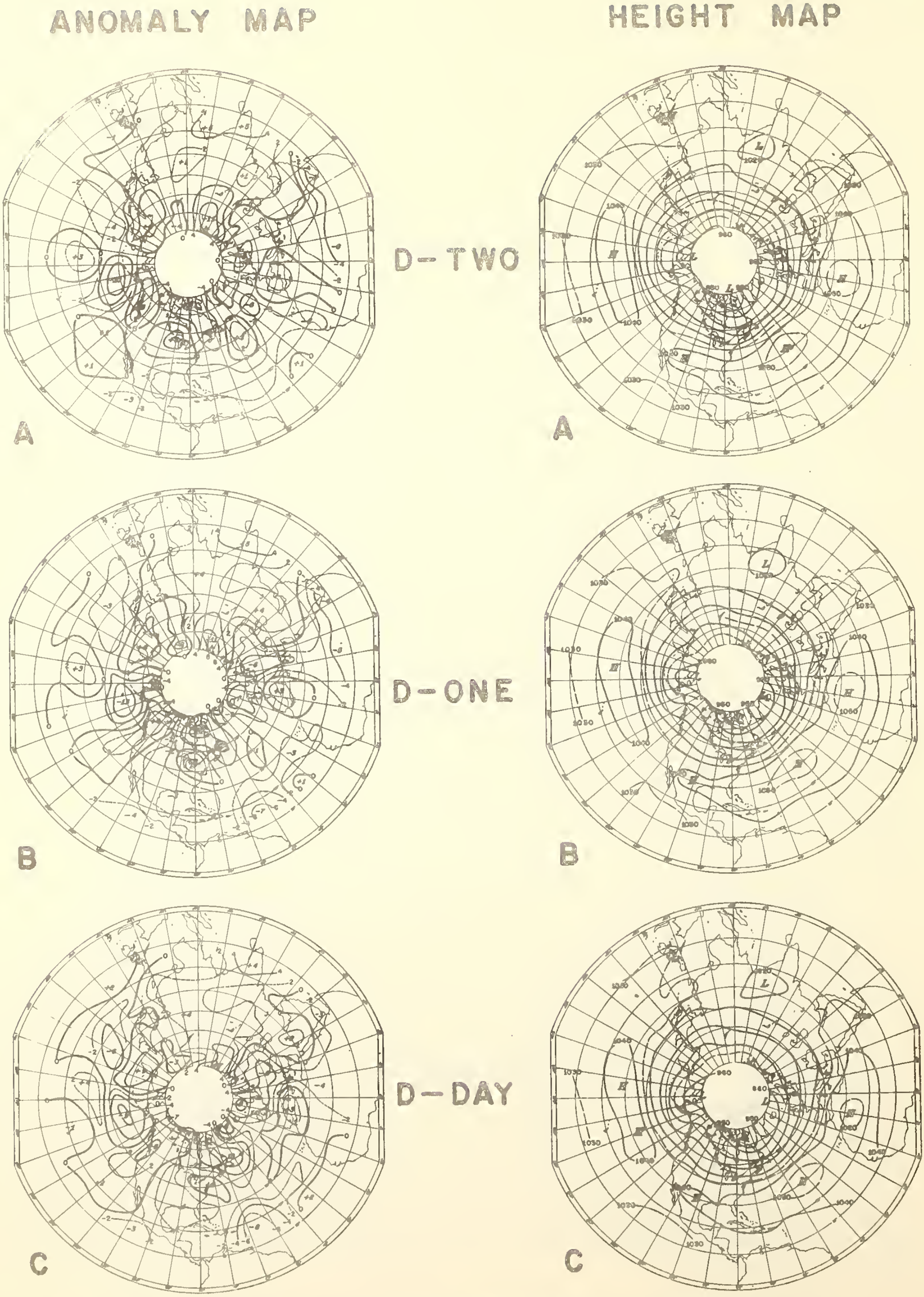

FIGURE. 5 LESSER ANTILLES

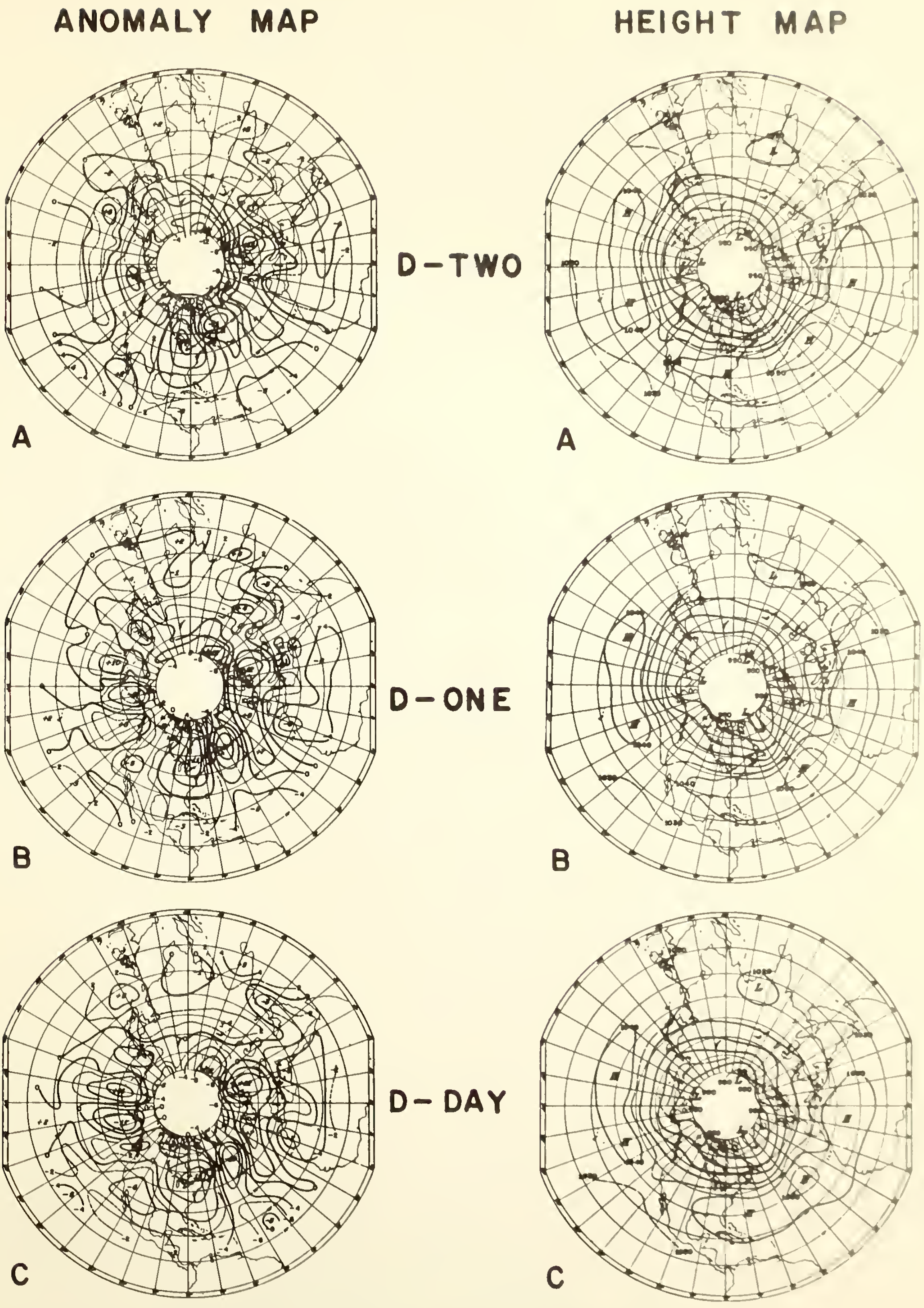

FIGURE. 6 ATLANTIC ZONE II

References

1. George W. Cry, "Tropical Cyclones of the North Atlantic Ocean," Technical Paper No. 55, U. S. Weather Bureau, Washington, D. C., 1965, 148pp.

2. E. M. Ballenzweig, "Seasonal Variations in the Frequency of North Atlantic Tropical Cyclones related to the General Circulation, NHRL Report No. 9, 1957, 32pp.

3. E. M. Ballenzweig, "Formation of Tropical Storms Related to Anomalies of the Long Period Mean Circulation," NHRL Report No. 21, 1958, 16pp.

4. Billy M. Lewis, "Normal 700-mb heights and Sea-level Pressures Obtained by Harmonic Smoothing of Observed Data," Unpublished manuscript, U. S. Weather Bureau, Extended Forecast Division, Washington, D. C., 1964, 36pp.

GPO 830-369

PENN STATE UNIVERSITY LIBRARIES
A000072022306